

A Theory of the Kinetics of Formation of Anode Films at High Fields¹

J. F. DEWALD

Bell Telephone Laboratories, Inc., Murray Hill, New Jersey

ABSTRACT

A theory is presented for the anodic oxidation of metals such as tantalum and aluminum. The theory of Mott and Cabrera has been extended to include effects of space charge on kinetics of the process in the highfield case.

The behavior of these systems is shown to depend critically on a dimensionless factor, δ , which is determined by the lattice and energy parameters and also by the experimental conditions.

For δ very small, corresponding to small space charge, the kinetic equation reduces to that of Mott and Cabrera. For large values of δ a very similar equation results which, however, contains only the parameters of the bulk oxide. For intermediate values of δ , complex behavior is predicted. In particular, the temperature independence of Tafel slope observed for tantalum is shown to be a consequence of the theory for certain reasonable choices of the parameters.

INTRODUCTION

Mott and his coworkers have developed theories for the oxidation of metals, and in a recent paper (1) they derive equations for the rate of growth of "very thin" films. Under this heading they treat the growth of films under electric fields so high that the drift velocity is no longer linear in the applied field. They use the data of Gunterschultze and Betz (2) for aluminum and calculate lattice parameters and activation energies which seem reasonable. Recently, however, Vermilyea (3) has published data covering a range of temperatures, which dispute some of the predictions of the theory of Mott and Cabrera. Their theory predicts a logarithmic increase of forming field with current density (or rate of formation). The rate of this increase [i.e., the Tafel slope ($dE/d\ln i$)] is predicted to be proportional to the absolute temperature. Vermilyea's data indicate the logarithmic increase as predicted, but the rate of increase appears to be temperature independent.

Presented here is an extension of the theory of Mott and Cabrera which was made prior to the publication of Vermilyea's work. Haring (4) has presented a qualitative description of the process, and the present paper puts some of his ideas in quantitative form. The new theory is able to account for all of Vermilyea's data and, in particular, can predict a temperature independent Tafel slope for a wide range of experimental conditions. Two other points of "discrepancy" between theory and experiment were pointed out by Vermilyea. These have been shown (5) to arise from an oversimplified application of the theory.

GENERAL CONSIDERATIONS

The molecular model employed is quite similar to that used by Mott and Cabrera (Fig. 1). Such a potential energy diagram applies to any oxidative process involving the formation of an adherent film. This is true regardless of whether an external voltage is employed (as in the anodic process), regardless of whether the process is a high field or a low field case, and regardless of the detailed mechanism of oxidation.

In the theory of Mott and Cabrera there are four major conditions which affect the rate of oxidation of film-forming metals; two, the activation energy for diffusion of the mobile species (φ) and the jump distance (b), depend only on the nature of the system in question. The other two are the experimentally variable conditions of temperature (T) and electric field (E). The major dependence on these four factors is shown to occur through a term of the form

$$\exp [-(\varphi - Ebq)/kT]$$

where q = the charge of the mobile ion. This factor represents the fraction of ions which have sufficient kinetic energy to surmount the potential energy barrier (φ). A similar term appears in the extension of the theory made below. This fraction is always finite (above 0°K), so the rate of any thermodynamically feasible oxidation will always be finite. However, if the fraction is very small, because of large activation energy or low temperature, the rate may be so small (e.g., 1 Å/century) that the process could be considered as not occurring at all. The dividing line between this condition and the condition of measurable rate is not very sharp, but as an

¹ Manuscript received February 25, 1954.

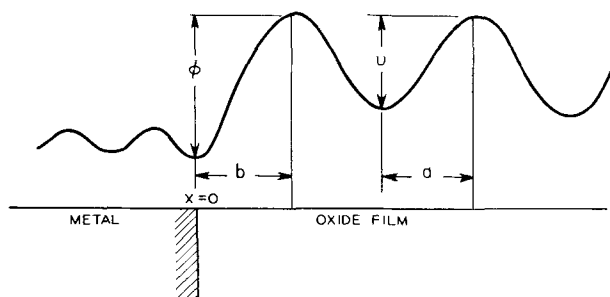


FIG. 1. Schematic potential energy profile of an ion in the high field oxidation process. $x = 0$ is taken as the equilibrium position of the ion on the metal surface.

order of magnitude one calculates (this is implicit in what follows below) that if $\phi - Ebg$ is greater than about $40 kT$ the reaction is essentially at a standstill, while if it is about $20 kT$, reaction will proceed at a very rapid rate.

The high field case of film formation is defined as that in which the field (either inherent in the reaction or applied externally) lowers the potential energy barrier by an amount greater than kT . Thus, if the activation energy is as large as $40 kT$, oxidation can occur *only* by a high field process, for if the barrier were not lowered by the field, the rate of reaction, although finite, would be immeasurably small. Conversely, if ϕ is much less than $20 kT$, only the low field case can be dealt with, for any appreciable lowering of the barrier would induce immeasurably *high* rates of oxidation.

In addition to the above requirements, the film and its immediate environment (particularly the film/electrolyte interface) must be capable of withstanding the high fields without breakdown. If, for example, the field were sufficient to oxidize hydroxide ions at the metal/electrolyte interface before it attained a value sufficient to move the ions through the film, then oxidation of the metal would not occur at all except at the immeasurably small rate discussed above. The metal would then be acting simply as an inert oxygen electrode. The intermediate case would correspond to film formation at reduced efficiency, a condition eventually approached by all metal-oxide systems as the thickness of film is increased without limit. In what follows, the currents employed are forming currents and do not include the current which produces side reactions.

Consider the growth of a partly formed film. The film is considered as an ionic lattice of stoichiometric composition² through which excess metal ions move under the influence of the field. The ions are assumed to move by jumps from one interstitial

position to the next and to be in thermal equilibrium with the lattice at all times.

The assumption that interstitial ions are in thermal equilibrium with the oxide lattice requires some justification. Cabrera and Mott consider that the barrier to ionic motion is at the metal/oxide interface and assume that every ion which escapes from the metal is pulled right across the film. This is not necessarily valid, for when an ion traverses the film it may very well experience deactivating collisions with the lattice and require reactivation before proceeding. Details of this process are quite complex and would require a separate paper for proper consideration. As a first approximation, it is assumed that deactivation occurs immediately after each activation.

Consider first the motion of the ions in the bulk of the film. They obey Boltzmann statistics, so for the number of ions per unit volume capable of moving from x to $x + a$ (i.e., concentration of activated ions),³

$$n^*(x) = \frac{n(x)}{kT} \int_{U-Eaq}^{\infty} e^{-\epsilon/kT d\epsilon}$$

where: $n(x)$ = concentration of interstitial ions at x ; $E = E(x)$ = electric field at x ; U = activation energy for motion between interstitial positions in the absence of the electric field; $2a$ = distance between interstitial positions; and q = the ionic charge.

The number which actually move in unit time from x to $x + a$ may be approximated by saying that once an ion becomes activated it crosses the barrier in one vibration period. The number of ions going from x to $x + a$ in unit time is then given by

$$i_+(x) = \nu n(x) \exp[-(U - Eaq)/kT]$$

where ν is the vibration frequency of the ion in an interstitial position. Similarly the number going from x to $x - a$ in unit time is given by

$$i_-(x) = \nu n(x) \exp[-(U + Eaq)/kT]$$

the only difference being that in this direction the field is retarding the ions; thus a greater activation energy is required. The total current density at x is then given by

$$i(x) = i_+(x) - i_-(x) \\ i(x) = 2\nu n(x) \sinh(Eaq/kT) \exp(-U/kT)$$

So far the treatment is identical with the case of

³ This equation is not exact for the high field case because, in addition to lowering the barrier, the field causes an effective shortening of the jump distance a . This yields an E^2 term in the lower limit of integration. The equations become much more complex if this term is included, so as a first approximation its effect is neglected.

² X-ray studies are somewhat equivocal on this point.

low field conduction, but from here on there is a striking difference. This is readily seen from the argument of the sinh term. Taking a as of atomic order, e.g., 3 Å, and q as the charge of a Ta^{+5} ion, the argument of the sinh term is about $10^{-5} E$ at room temperature (with E in practical v/cm). Then only for fields below about 10^{+5} v/cm is the expansion of the sinh Eaq/kT as Eaq/kT valid. This is the usual approximation yielding a current linear in the field.

$$i = nE\mu \quad (\text{I})$$

where μ , the mobility, is field independent.

For high forming fields the linear expansion is not valid. Instead the negative exponential term may be neglected

$$i = n\mu_o \exp(\beta E) \quad (\text{II})$$

with $\beta = aq/kT$ and $\mu_o = a\nu \exp(-U/kT) =$ constant independent of x and t . Equation (II) relates the forming current density at any point in the film to the concentration of interstitial ions (n) and the electric field (E) at that point.⁴ These quantities may or may not vary with time and position in the film. If the current density does not vary with time or position, the film is considered to be in a condition of steady state.

THE STEADY STATE

This concerns the steady-state properties of a film which has been growing for some time at constant rate. The steady state requires that the concentration of ions at any point remain constant with time,⁵ i.e., that

$$\frac{(\partial n)}{(\partial t)_x} = 0 = - \frac{(\partial i)}{(\partial x)_t} \quad (\text{III})$$

Using (II) and (III) it is found as a condition on E and n ,

$$\frac{(\partial n)}{(\partial x)_t} + n\beta \frac{(\partial E)}{(\partial x)_t} = 0 \quad (\text{IV})$$

but

$$\frac{\partial E}{\partial x} = \frac{4\pi\rho}{K} = \frac{4\pi qn}{K} \quad (\text{V})$$

⁴ For the general nonsteady-state case it is important to distinguish three currents: (a) the ion current *in* the film [$i(x, t)$]; (b) the ion current across the metal-film interface (i_o); and (c) the electron current in the metal (i). These are equal only in steady state.

⁵ This is probably not a completely valid requirement since the film is growing at the expense of the metal; thus the reference point ($x = o$) is not stationary. It can be shown, however, that this is only a minor error which may be neglected.

(where K is dielectric constant of film and ρ is the charge density) so that (IV) becomes

$$\frac{(dn)}{(dx)_{\text{steady state}}} = -\beta\gamma n^2 \quad (\text{VI})$$

with

$$\gamma = \frac{4\pi q}{K}$$

Integrating (VI) gives the dependence of the ion concentration on distance through the film.

$$n = \frac{n_o}{1 + \beta\gamma n_o x} \quad (\text{VII})$$

where $n_o =$ ion concentration at $x = 0$.

Substituting (VII) into (V) and integrating gives for the field at any point x ,

$$E = E_o + \frac{1}{\beta} \ln(1 + \beta\gamma n_o x) \quad (\text{VIII})$$

Equation (VIII) states that the field at any point in the film is composed of two parts, a surface charge contribution (E_o) and a space charge term. The space charge term arises from the fact that the interstitial ions in transit are not compensated electrically under the conditions of high field formation. In an unbiased condition electrons are present to neutralize the excess charge of the interstitial ions, but at high fields these will all be removed from the film, and the lines of force originating on the interstitial ions must pass through the film ending on the negative ions (probably hydroxide ions) waiting at the electrolyte/film interface.

Cabrera and Mott neglect the space charge contribution entirely. This neglect is based on the assumption that the rate-limiting step in the process of film formation is in getting across the metal/oxide interface. At first glance one might conclude that, if the activation energy for diffusive entrance into the film (φ) is larger than the activation energy for diffusion through the film (U), then the rate-limiting process would always be the motion *across* the interface. Such a conclusion might be valid for the low field case but it is not necessarily valid for the high field case. In the first place, activation energies for *high field conduction* are not φ and U but $(\varphi - E_bq)$ and $(U - Eaq)$. Thus, if b is greater than a one might anticipate that at sufficiently high fields the entrance barrier would be reduced enough to be less than the barriers inside the film, even though the entrance barrier were higher than the film barrier in the absence of the field.

Even if φ were greater than U , and a were greater than b , entrance into the film would not necessarily be the rate-limiting process, for by allowing the film thickness to increase without limit under constant

field the increasingly large number of small barriers would eventually predominate over the *single* high entrance barrier (φ) as the rate-determining factor. This treatment makes it possible to predict, for any given set of parameters, at what values of temperature, current density, and film thickness passage through the film becomes rate determining.

The constant E_o in equation (VIII) is given directly by the result of Cabrera and Mott (1) expressed in the form

$$E_o = \frac{kT}{bq} \ln \frac{i_o}{m_s \nu_s} + \frac{\varphi}{bq} \quad (\text{IX})$$

where m_s and ν_s are the surface density of metal ions and their vibration frequency. The constant n_o is obtained by equating the current across the interface, i_o , to the current in the film at $x = 0$.

$$i_o = i(o, t) = n_o a v \exp(-U/kT) \exp(E_o a q / kT) \quad (\text{X})$$

Substituting (IX) into (X) and rearranging for n_o

$$n_o = \frac{(m_s \nu_s)^{a/b}}{a v} i_o^{(1-a/b)} \exp[(U - a/b\varphi)/kT] \quad (\text{XI})$$

At steady state i_o is equal to the external current i so that equations (IX) and (XI) may both be written with i (the directly measurable current) in place of i_o .

Equation (XI) exhibits an interesting dependence of interstitial ion concentration on current density. If the entrance distance, b , is less than the bulk jump distance, a , the steady-state concentration of interstitial ions will decrease as the current density increases. If b is greater than a , increasing current density will cause an increase in the concentration of ions. This behavior is due to the fact that, if the bulk jump distance is greater than the entrance jump distance, an increase in the field will depress the internal barriers more than it depresses the entrance barrier, acting as it does over a larger distance. Thus, a sudden increase in field will cause more ions to leave the film than enter it and, as a consequence, the concentration of ions must decrease with increasing current density. The same argument applies if b is greater than a except that the effect is in the opposite direction.

Finally the average field, \bar{E} , which is the experimentally accessible quantity, is evaluated from

$$\bar{E} = \frac{V}{D} = \frac{1}{D} \int_0^D E dx \quad (\text{XII})$$

where V = voltage drop across the film, and D = film thickness. Substituting (VIII) into (XII), integrating, and replacing n_o by (XI)

$$\bar{E} = E_o + \frac{1}{\beta} \left\{ \left(1 + \frac{1}{\delta}\right) \ln(1 + \delta) - 1 \right\} \quad (\text{XIII})$$

with E_o given by (IX) and δ given by

$$\delta = \beta \gamma n_o D = \left[\frac{4\pi q^2 (m_s \nu_s)^{a/b}}{K k T} \frac{1}{v} \right] \cdot e^{(U - \varphi a / b) / k T} D i^{(1-a/b)} \quad (\text{XIV})$$

Equation (XIII) gives the dependence of the average steady-state field on the three variables: current density (through E_o and n_o); thickness of film D ; and temperature (through E_o , β , and δ). The second term in (XIII) is the space charge contribution to the average field.

The quantity determining the importance of space charge is the dimensionless factor δ . If δ is much less than one, space charge is negligible and the parameters of the metal oxide interface are the rate-determining ones. This is the condition studied by Mott and Cabrera. However, when δ is of the order of one, the neglect of space charge begins to be significant. For δ greater than about 10, the effects of space charge are all important, and the rate of oxidation is determined almost entirely by the bulk properties of the film. This may be seen by approximating the $\ln(1 + \delta)$ term in (XIII) either as

$$\ln(1 + \delta) = \delta - \frac{\delta^2}{2} + \dots$$

for small δ . Or as

$$\begin{aligned} \ln(1 + \delta) &= \ln \delta + \ln(1 + 1/\delta) \\ &= \ln \delta + 1/\delta - 1/2\delta^2 + \dots \end{aligned}$$

for large δ . Dropping the second order terms in these expansions, the two limiting cases are given by

$$\bar{E} \approx \frac{kT}{aq} \ln \frac{4\pi q^2}{K k T e v} D i + U/aq \quad \delta \gg 1 \quad (\text{XV})$$

($e = 2.712 \dots$)

$$\bar{E} \approx E_o = \frac{kT}{bq} \ln \frac{i}{m_s \nu_s} + \frac{\varphi}{bq} \quad \delta \ll 1 \quad (\text{XVI})$$

These equations are of very similar form. For both high and low values of δ the field is logarithmic in current density, and in both cases the *rate* of increase of field with logarithm of current density (the Tafel slope) is proportional to the absolute temperature. For low values of δ the Tafel slope is given by kT/bq , for high values of δ it is given by kT/aq .

Comparison with Experiment

The data of Vermilyea indicate that the Tafel slope is essentially temperature independent over the range from 0° to 80°C. Hence, in this temperature range δ is neither very large nor very small. Therefore the detailed solution with δ of the order of one is required. With reasonable choices of the parameters it is possible to "predict" the existence

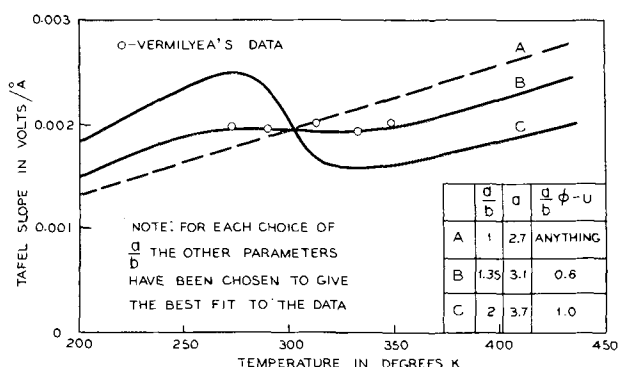


FIG. 2. The variation of Tafel slope with temperature for a 1000 Å film at constant anodizing current density of 100 $\mu\text{a}/\text{cm}^2$. The curves are drawn, using equation (XIV), to give the best fit to the experimental data of Vermilyea.

of a temperature-independent Tafel slope over a fairly wide range of temperature.

The quantity δ depends on film thickness, current density, and on temperature. The first two variations are relatively minor, but the dependence on temperature is quite important. Equation (XIV) shows that the nature of the temperature variation depends upon the sign of the term $[U - a/b\phi]$. If this term is negative, then δ increases with increasing temperature, and high temperature favors large space charge; the opposite effect would be expected if $[U - a/b\phi]$ were positive; in such a case the higher the temperature, the lower the space charge.

The effect of temperature on the Tafel slope may be seen by differentiating equation (XIII)

$$\frac{(\partial \bar{E})}{(\partial \ln i)_T} = \frac{kT}{aq} \left[1 + (a/b - 1) \frac{\ln(1 + \delta)}{\delta} \right] \quad (\text{XVII})$$

= Tafel slope

Temperature affects the Tafel slope in two ways: directly through T , and indirectly through δ . In general, these two effects act in opposite directions, and when δ is of the order of unity they are of the same order of magnitude. Thus it is possible that the Tafel slope may change very little over the temperature range in which δ is approximately 1. However, certain restrictions must be placed on the parameters. The data available at the present time are not sufficient to evaluate these parameters unambiguously. The reason is that the relative magnitudes of a and b are of critical importance in determining the temperature dependence of Tafel slope. It happens that there are two widely different values of the a/b ratio which allow (with judicious selection of the two activation energies and the absolute magnitude of a) a quantitative fit to all the data available. These values are approximately 1.35 and 0.35. Only for these values of a/b is it

possible to achieve a temperature-independent Tafel slope, regardless of the choice of the other parameters. For much different values the Tafel slope either rises continuously with temperature or goes through a maximum and then a minimum before finally rising continuously in the high temperature region.

Using the value 0.35 and determining the other parameters from Vermilyea's data, the resulting value of b places the entrance barrier more than 5 Å away from the equilibrium surface position.⁶ This large value is very difficult to visualize, so the conclusion is reached that the correct a/b ratio is 1.35. Experiments at higher temperature are required to verify this conclusion.

Fig. 2 shows the calculated behavior of the Tafel slope for several ratios of a/b in the neighborhood of 1.35. The data of Vermilyea are also shown. As can be seen from equations (XIV) and (XVII), data on the Tafel slope yield information only on the parameters a , b , and the term $(a/b\phi - U)$. The best fit to the Tafel data are obtained when these parameters have the values 3.1 Å, 2.3 Å, and 0.6 eV, respectively. These values should be viewed as only provisional, since the sensitivity to the parameters is not too large in the plateau region.

The absolute values of ϕ and U calculated from this model may be obtained by the use of equations (XIII), (XIV), and (IX). Knowing a , b , $(a/b\phi - U)$, and the experimental variables, δ may be computed from (XIV) and substituted into (XIII). The average field being known from experiment, E_c is determinable; from equation (IX) ϕ is obtained and thus indirectly U . The values of ϕ and U so computed are 1.5 and 1.4 eV, respectively, for the best fit to the experimental data.

Extended discussion of the parameter values calculated above is hardly merited in view of their highly provisional character. The only value which seems unreasonable is 3.1 Å for the jump distance a . It appears a little high especially since a is the half distance between interstitial sites.

It is not impossible that this large value corresponds to the jump distance from one crystallite to another in the amorphous film. However this may be, it is clear that the data may be empirically represented by the extended theory. The simpler Mott-Cabrera picture cannot do this. The more detailed theory involves two extra parameters, and even though their introduction seems reasonable and was made prior to the experimental observations, further experimental verification would be highly desirable.

⁶ This figure and all the curves and figures presented are based on the assumption of +5 ion charge.

Comments

Equation (XIV) shows that in addition to the temperature variation considered above, δ and thus the average field depends on current density i and film thickness D . The dependence of forming field on film thickness is a relatively minor one. It arises from the space charge term, and even for very high values of space charge ($\delta \gg 1$) corresponds to only about 7% increase in field for tenfold increase in film thickness, while for intermediate space charge ($\delta \approx 1$) the increase is only about 2% per tenfold change in thickness. Methods of estimating film thickness are ambiguous because they involve assumptions regarding the constancy of density, surface roughness, anodizing efficiency, and other effects. The data neither indicate nor preclude a variation of field with thickness of the size predicted above.

The variation of δ with current density is such that at both low and high values of δ the field varies logarithmically with current density [Equations (XV) and (XVI)]. In the intermediate range the Tafel plot of \bar{E} vs. $\ln i$ should not be exactly linear. Equation (XIII) predicts that the Tafel slope should rise with increasing current density

when δ is approximately unity. The effect is not very large, however, and might easily be overlooked, even in the absence of complicating effects, if the precision of the data were not good. A linear approximation would probably be assumed by an experimenter unless his data were of a precision of the order of 1%. Complicating factors introduced by heating and electronic currents make the attainment of such precision difficult.

ACKNOWLEDGMENT

I am indebted to U. B. Thomas and H. E. Haring for many stimulating discussions and also for their continued interest in this work.

Any discussion of this paper will appear in a Discussion Section to be published in the December 1955 JOURNAL.

REFERENCES

1. N. CABRERA AND N. F. MOTT, *Repts. Progr. Phys.*, **12**, 163 (1948-49).
2. A. GUNTERSCHULTZE AND H. BETZ, *Z. Phys.*, **92**, 367 (1934).
3. D. A. VERMILYEA, *Acta Met.*, **1**, 282 (1953).
4. H. E. HARING, *This Journal*, **99**, 30 (1952).
5. J. F. DEWALD, *Acta Met.*, **2**, 340 (1954).

Oxidation of Iron-Molybdenum and Nickel-Molybdenum Alloys¹

S. S. BRENNER

Research Laboratory, General Electric Company, Schenectady, New York

ABSTRACT

Binary alloys of iron and molybdenum (up to 12.5 atomic % Mo) and nickel and molybdenum (up to 19.7 at. % Mo) do not exhibit "catastrophic oxidation" up to 1000°C either in stationary or in flowing atmospheres.

In both systems, MoO₂ and iron molybdate or nickel molybdate are formed in addition to iron oxides or nickel oxide.

Molybdenum significantly decreases the oxidation rate of iron by preventing formation of the cation deficient FeO normally formed on iron above 570°C. The oxidation rate of nickel, however, is affected only to a small extent. Up to 3 at. % molybdenum the rate is slightly increased by the formation of additional vacancies in the nickel oxide, while beyond 12 at. % the oxidation rate is again decreased owing to the densification of the MoO₂ subscale.

INTRODUCTION

In the development of high temperature materials it was hoped that additions of molybdenum would increase the hot strength of heat-resistant alloys. However, molybdenum was found to have a very deleterious effect on the oxidation resistance of such alloys (1-3). Working mainly with the Timken alloy, 16 % chromium, 25 % nickel, and 6 % molybdenum, Leslie and Fontana (1) found that in a static atmosphere at 900°C a 50 g sample would be completely converted to the oxide within 24 hr. This rapid type of oxidation has been termed by them "catastrophic oxidation."

Although there is a difference of opinion as to the exact mechanism of catastrophic oxidation, it is generally agreed that the main cause for this rapid oxidation is the presence of molybdic oxide (MoO₃). The low melting point (795°C) of this oxide and its high vapor pressure (0.25 atm at 1000°C) prevent the formation of the protective oxide which would normally be formed in the absence of MoO₃.

Up to the present, catastrophic oxidation studies have been made mainly on commercial alloys. This paper presents results on the oxidation behavior of laboratory-prepared binary iron-molybdenum and nickel-molybdenum alloys, while the following paper discusses the oxidation behavior of some ternary and quaternary alloys containing nickel or chromium, or both, in addition to iron and molybdenum.

Neither the iron nor the nickel binary alloys exhibited catastrophic oxidation in the temperature range 800° to 1000°C. Maximum molybdenum con-

centrations were 12.5 and 19.7 at. %, respectively. Tests were made both in still air and flowing oxygen.

Oxidation kinetics of the iron-molybdenum and nickel-molybdenum alloys are presented and a mechanism for their oxidation is proposed.

EXPERIMENTAL

Specimen Preparation

The alloys were prepared by melting 100 g charges in a multiple hearth arc furnace. Their compositions are given in Table I. Electrolytic iron, carbonyl nickel, and molybdenum of over 99.9 % purity were used to prepare the melts. Unfortunately, there was considerable tungsten contamination from the tungsten electrode in the preparation of the nickel-molybdenum alloys. However, since tungsten is chemically similar to molybdenum, it is felt that, on an atom to atom basis, tungsten has the same effect as molybdenum. Subsequently all compositions of the nickel-molybdenum alloys are given in atomic per cent of molybdenum plus tungsten.

The 100 g buttons were annealed, ground on two faces, hot rolled, sand blasted, cold rolled, and finally annealed. Final thicknesses were 0.051 cm for iron alloys and 0.064 cm for nickel alloys.

Specimens cut from the rolled strips were cleaned, abraded, and weighed prior to each experiment. In most cases, specimen dimensions were approximately 1.3 x 3.2 cm with an apparent surface area of about 9 cm². Some specimens were electropolished, but no appreciable differences were observed in the experimental results.

Procedure.—Oxidation of the alloys was deter-

¹ Manuscript received March 22, 1954.

TABLE I. Composition of alloys
Iron-molybdenum

Alloy	Mo (at.%)
100	Puron
101	0.64
102	1.83
103	2.61
104	5.29
105	6.16
106	6.51
107	12.5

Nickel-molybdenum

Alloy	Mo (at.%)	W (at.%)	Mo + W (at.%)
900	—	0.32	0.32
902	1.73	0.02	1.75
903	2.87	0.13	3.00
904	6.60	0.20	6.80
905	13.0	<0.17 (spect.)	13.1
906	20.5	<0.18 (spect.)	20.6

mined by continuous weighing. Samples were suspended from a Chain-O-Matic balance into a vertical tube furnace. The sensitivity of the balance was approximately 0.1 mg, while the furnace temperature deviation was less than 2°C.

The sample was inserted into the 1-in. reaction tube while a reducing mixture of hydrogen and helium was being passed through. Construction of the reaction tube insured preheating of the gases. After equilibrium temperature had been reached and the zero time weight had been recorded, the hydrogen flow was interrupted and dried oxygen was introduced. The oxygen flow was maintained at 1 l/min. In a few cases, specimens were oxidized in untreated air both flowing and stationary. Weight measurements were made periodically, in some cases up to 60 hr.

The validity of measuring oxidation rate by following weight increase due to oxygen pickup may be questioned. If volatile MoO₃ is formed by the oxidation reaction, the measured weight increase would not correspond to the amount of oxygen reacted in the oxidation process. To be certain that this factor is not appreciable, metal loss measurements as well as weight gain measurements were made on some of the alloys. Fig. 1 shows such measurements for the Fe-6.16 at. % Mo alloy. After the initial period of formation, the ratio of measured oxygen pickup to amount of metal oxidized ($\Delta m_o/\Delta m_M$) remains at about 0.420.

As shown later, the bulk oxide on this alloy at 1000°C consists primarily of Fe₃O₄ and Fe₂O₃. The ratio of oxygen to metal in these oxides is 0.382 and 0.430, respectively. If there had been an appreciable

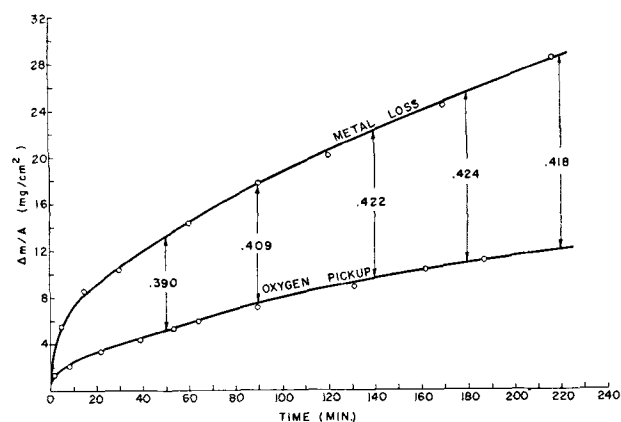


FIG. 1. Comparison between metal loss and oxygen pickup. Fe-6.16 at. % Mo alloy, 1000°C, air flow 3 l/min. Numbers indicate ratio of oxygen pickup to metal loss $\Delta m_o/\Delta m_M$.

amount of volatile MoO₃ formed, $\Delta m_o/\Delta m_M$ would have been significantly lower than 0.420.

To check further the possibility of the formation of volatile MoO₃, three of the iron alloys were first oxidized and then reduced again in H₂. The difference in initial and final weight indicates the amount of molybdenum oxidized to the volatile MoO₃. The following results were obtained at 1000°C:

Atomic % Mo	Oxidation time, min	Metal oxidized, mg/cm ²	Mo lost, mg/cm ²
0.64	120	25.25	nil
6.16	170	24.30	nil
12.5	205	24.70	0.37 (max)

It can be concluded from these results that iron-molybdenum alloys up to 12.5 at. % do not form any appreciable amount of volatile MoO₃ when oxidized at 1000°C. This is in agreement with the early findings of Scheil and Kiwit (4) who reported that iron-molybdenum alloys up to 6.1 at. % molybdenum did not produce any observable amount of MoO₃ when heated to 1200°C. Similar tests with some of the nickel alloys indicated that nickel-molybdenum alloys up to 19.7 at. % Mo also do not form volatile MoO₃ during the oxidation process.

RESULTS

Iron-Molybdenum

Disregarding the initial period of oxide formation, the oxidation of iron and iron-molybdenum alloys up to 12.5 at. % Mo can be described by

$$\frac{\Delta m}{A} = k\sqrt{t} + C \quad (I)$$

where: $\frac{\Delta m}{A}$ = oxygen pickup per unit area of the metal, mg/cm²; k = parabolic rate constant mg/cm² min^{1/2}; t = oxidation time (min); and C = constant.

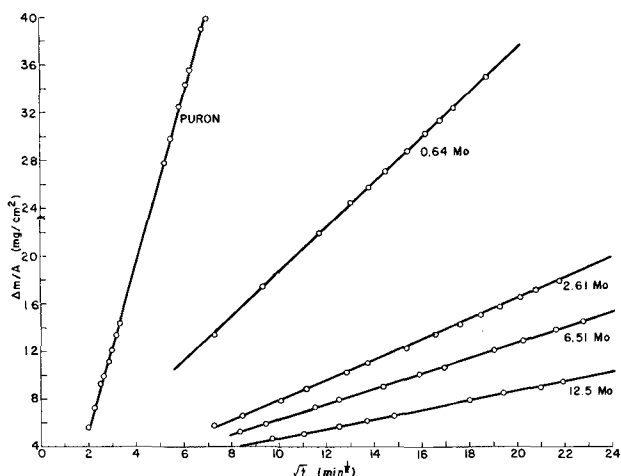


FIG. 2. Oxidation of iron and iron-molybdenum alloys, 1000°C, O₂ flow ~ 1 l/min.

This relation indicates that diffusion of metal ions and oxygen ions through the oxide film is the rate-controlling factor in the oxidation of the alloys as well as of pure iron.

Fig. 2 and 3 show the typical parabolic oxidation of some alloys at 1000°C. Values of the rate constants *k*, in Table II, were obtained from the slopes of these curves. They were determined from single runs of about 8-hr duration. In all cases they are the lowest values of *k* found during this investigation and are considered the most reliable values. Rate constants obtained from duplicate runs vary less than 25% from the values given in Table II.

Samples held in flowing or stationary air oxidized at a slightly faster rate, but there was no evidence of catastrophic oxidation.

There is a significant decrease in the oxidation rate as molybdenum is added with the greatest effect for the first few per cent. This is shown clearly in Figure 4.

Since the parabolic rate constant is directly re-

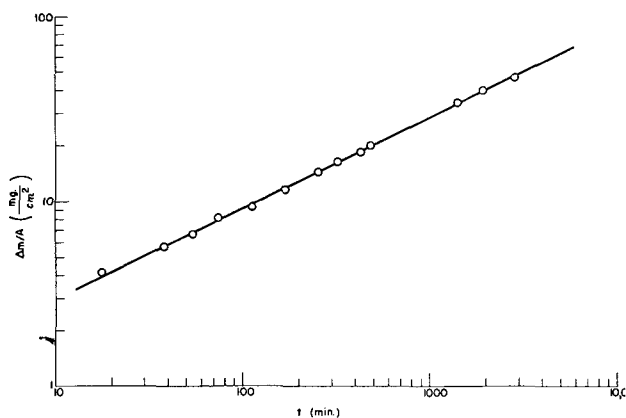


FIG. 3. Oxidation of Fe-6.16 at. % Mo alloy, 1000°C, O₂ flow ~ 1 l/min.

TABLE II. Parabolic rate constants
Iron-molybdenum

Mo (at.%)	Temp, °C	$k \cdot 10^3$ (g/cm ² min ^{1/2})	$k' \cdot 10^8$ (g ² /cm ⁴ sec)
Puron	1000	7.1	80.0
0.64	1000	1.9	5.8
1.83	800	0.11	0.019
	850	0.17	0.048
	900	0.33	0.18
	950	0.67	0.75
	1000	0.98	1.60
	1000	0.86	1.22
2.61	1000	0.66	0.72
	800	0.12	0.23
5.29	850	0.18	0.56
	900	0.30	0.15
	950	0.55	0.50
	1000	0.83	1.15
	1000	0.65	0.66
6.16	800	0.12	0.022
	850	0.18	0.053
	900	0.23	0.087
	950	0.31	0.16
1000	0.40	0.26	

Nickel-molybdenum

Mo + W (at.%)	Temp, °C	$k \cdot 10^3$ (g/cm ² min ^{1/2})	$k' \cdot 10^{10}$ (g ² /cm ⁴ sec)
Carbonyl Ni*	1000	0.119	2.38
0.32	1000	0.182	5.52
1.75	1000	0.195	6.35
3.00	1000	0.214	7.64
6.8	1000	0.219	7.99
	900	0.109	1.98
	800	0.0426	0.302
13.1	1000	0.210	7.33
	904	0.108	1.93
	800	0.0438	0.319
20.6	1000	0.117	2.28

* Value reported by Pfeiffer and Hauffe (8).

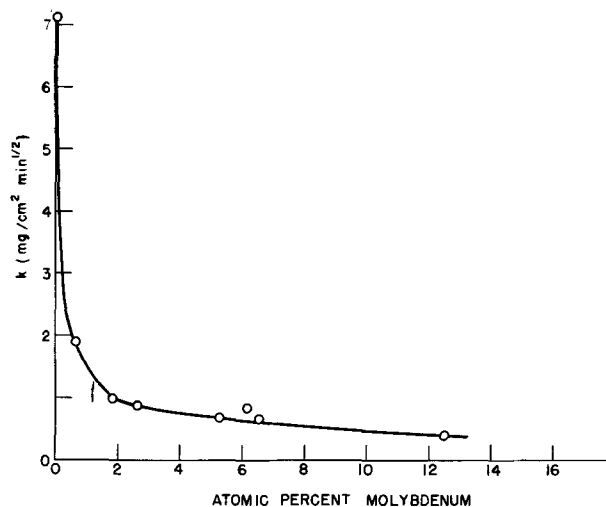


FIG. 4. Parabolic rate constant of iron-molybdenum alloys as a function of composition, 1000°C, O₂ flow ~ 1 l/min.

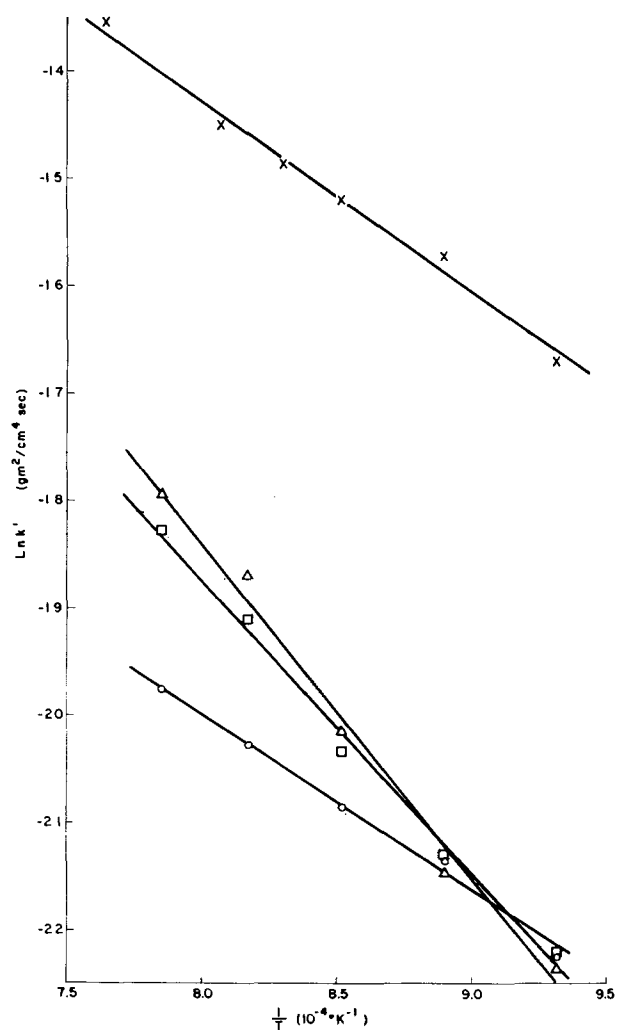


FIG. 5. Temperature dependence of the parabolic rate constant of iron and iron-molybdenum alloys. X, Fe; Δ , 1.83 at. % Mo; \square , 6.16 at. % Mo; \circ , 12.5 at. % Mo. Data for Fe taken from Davies, Simnad, and Birchenall (5).

TABLE III. Values of A and Q

Mo (at.%)	A ($\text{g}^2 \text{cm}^{-2} \text{sec}^{-1}$)	Q (cal/mole)
Iron-molybdenum		
0*	1.2	$36,000 \pm 1000$
1.83	1.0×10^3	$63,000 \pm 3000$
6.16	23.0	$54,000 \pm 2000$
12.5	1.2×10^{-3}	$33,000 \pm 1000$
Nickel-molybdenum		
High purity Ni†	9.6×10^{-1}	41,200
6.8	0.036	$44,500 \pm 1400$
13.1	0.015	$42,600 \pm 1300$

* Obtained from data of Davies, Simnad, and Birchenall (5).

† Gulbransen and Andrew (550°–700°C) (9).

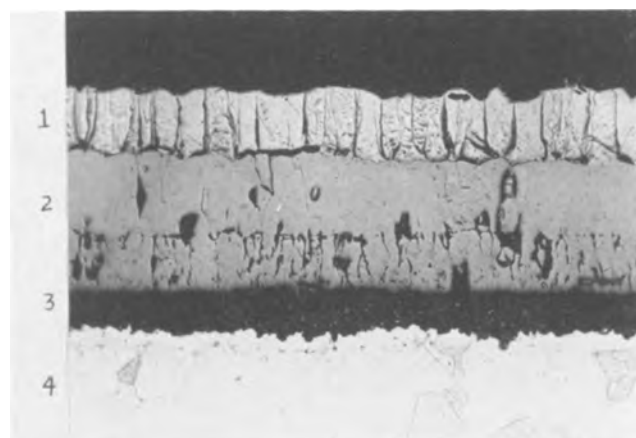


FIG. 6. Oxide layers on Fe-0.64 at. % Mo alloy. Oxidized 350 min at 1000°C. 1— Fe_2O_3 ; 2— Fe_3O_4 ; 3— $\text{MoO}_2 + (\text{Fe}_x\text{Mo}_y)\text{O}$. 4—Alloy. (250 \times before reduction for publication.)

TABLE IV. X-ray diffraction analyses of the innermost oxide layer formed on the Fe-12.5% Mo alloy at 1000°C

d	Phase	hkl
6.32	D.O.*	001
5.00	D.O.	100
3.54	D.O.	110
3.41	MoO_2	
3.15	D.O.	002
2.78	MoO_2	
2.52	D.O.	200
2.50		
2.42	MoO_2	
2.22	D.O.	210
2.11	D.O.	003
2.00	?	
1.72	MoO_2	203
1.71		
1.70		
1.57	D.O.	301
1.48	D.O.	302

* D.O. = double oxide of molybdenum and iron. Possible structure: tetragonal $a_0 = 5.00$; $c_0 = 6.32$.

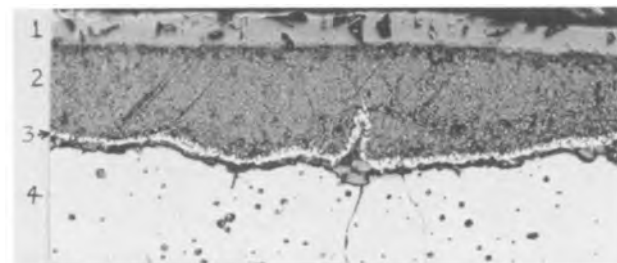


FIG. 7. Oxidation of iron (Puron) at 1000°C. 1— Fe_3O_4 ; 2— $\text{FeO} +$ precipitated Fe_3O_4 ; 3—gold marker; 4—Fe.

lated to the diffusion constant of the ions through the oxide layers, the Arrhenius relationship

$$k' = Ae^{-Q/RT} \quad (k' \text{ in } g^2/cm^4 \text{ sec}) \quad (II)$$

is expected. As Fig. 5 shows, iron-molybdenum alloys do exhibit this relationship although there is some scatter in the data. The temperature dependence of the oxidation of pure iron, as determined by Davies, Simnad, and Birchenall (5), is included as a reference. The values of A and Q computed by the least square method are tabulated in Table III. There is a large variation in both A and Q . Since the oxidation process of these alloys involves the migration of ions through a complex multiple oxide structure, no attempt was made to interpret the mechanism of the oxidation in terms of the A and Q values.

Oxide structure and mechanism of oxidation.—Photomicrographs and x-ray diffraction studies of the oxide revealed three distinct layers (see Fig. 6). The outer layer consists of Fe_2O_3 , the middle layer of Fe_3O_4 , and the inner layer of a mixture of MoO_2 and an unidentified phase presumably a double oxide of molybdenum and iron. X-ray diffraction results of the inner scale on the 12.5 at. % alloy are given in Table IV. Indexing of the “ d ” values corresponding to the double oxide suggests, as one possibility, a tetragonal structure with $a_o = 5.00 \text{ \AA}$ and $c_o = 6.32 \text{ \AA}$. A chemical analysis of the oxide layers on the 12.5% alloy oxidized at $1000^\circ C$ gave the following compositions:

Layer	Mo (at.%)	Fe (at.%)
Bulk oxide ($Fe_3O_4 + Fe_2O_3$ layer)	0.37	44.0
Inner scale [$(MoO_2) + (Fe_xMo_y)O$]	20.4	14.6

Thus, there is a large accumulation of molybdenum in the form of MoO_2 and $(Fe_xMo_y)O$ at the oxide-alloy interface and there is no indication of an FeO layer which would normally constitute the major portion of the oxide formed on pure iron (see Fig. 7).

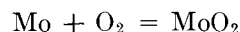
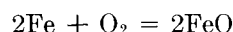
These two phenomena are interrelated. When the specimen is initially exposed to the oxygen, iron oxide forms since the oxygen affinity of iron, as shown in Table V, is larger than that of molybdenum. Since the diffusivities of molybdenum and iron are not infinite, the metal surface soon becomes de-

pleted in iron and enriched in molybdenum. Following Wagner's (6) analysis and assuming ideality, the equilibrium condition for the coexistence of an oxide AO and the alloy A_xB_y is that

$$N_{(i)A}^2 P_{O_2(i)} = \pi_{O_2} \quad (III)$$

where: $N_{(i)A}$ = mole fraction of A in the metal core at the alloy-oxide interface; $P_{O_2(i)}$ = oxygen partial pressure at the interface alloy-oxide; and π_{O_2} = dissociation pressure of AO .

Considering then the two reactions



it is seen that MoO_2 can form at the expense of FeO when

$$\frac{\pi_{FeO_2}}{N_{(i)Fe}^2} = \frac{\pi_{MoO_2}}{1 - N_{(i)Fe}} \quad (IV)$$

Using the calculated dissociation pressures shown in Table V, $\pi_{FeO} = 0.169 \times 10^{-14}$ and $\pi_{MoO_2} = 2.99 \times 10^{-14}$, the mole fraction of iron at which MoO_2 can form (under ideal conditions) is 0.21. As soon as the iron content in the alloy at the alloy-oxide interface falls below this value, MoO_2 can replace FeO along the interface, physically separating the FeO from the metal core. Thermodynamically, FeO is unstable if not in contact with iron and, therefore, converts to Fe_3O_4 .

The fast rate of oxidation of pure iron is a result of the rapid migration of iron ions through the layer of FeO which can exist with a large amount of metal vacancies. If the growth of FeO can be prevented as in the present case, the rate of oxidation will be decreased appreciably. In view of these considerations, it is now understandable why the rate of oxidation of iron is affected most by the addition of the first few per cent molybdenum. As long as the molybdenum content is in excess of that which can be removed by diffusion into the interior, MoO_2 and

TABLE V. Dissociation pressures of some oxides at $1000^\circ C^*$

FeO	1.69×10^{-15}
Fe_3O_4	6.08×10^{-15}
Fe_2O_3	8.77×10^{-14}
MoO_2	2.99×10^{-14}
MoO_3	3.24×10^{-12}
Cr_2O_3	4.84×10^{-24}
NiO	1.67×10^{-10}

* Free energy data from Kubaschewski and Evans (7).

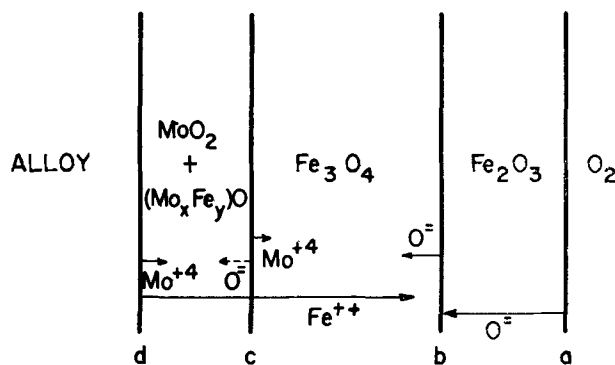


Fig. 8. Growth of oxide layers on iron-molybdenum alloys.

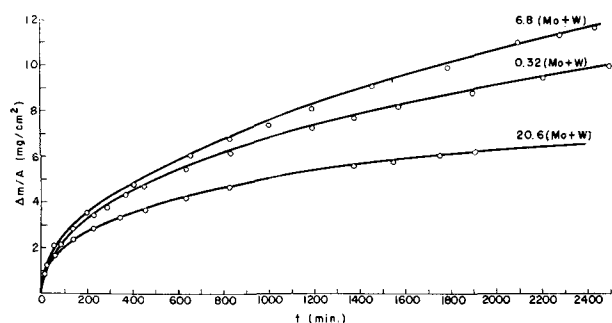


FIG. 9. Oxidation of nickel-molybdenum alloys, 1000°C, O₂ flow ~ 1 l/min.

(Fe_xMo_y)O form, separating the FeO from the metal base. This separation is further facilitated by the formation of the molybdenum-iron double oxide that probably has a still lower dissociation pressure than MoO₂.

The mechanism of the oxide growth on the alloy is postulated to be similar to that on pure iron as described by Davies, Simnad, and Birchenall (5). By means of radioactive tracers, they showed that iron ions migrate through the FeO layer, oxygen ions through the Fe₂O₃ layer, and both iron and oxygen ions migrate through the Fe₃O₄ layer. Oxygen ion migration in the Fe₃O₄ layer, however, is reported to be small in comparison to the iron migration. The oxide growth can be described as shown schematically in Fig. 8. Oxygen ions migrating through the Fe₂O₃ layer and iron ions migrating through the Fe₃O₄ layer react at interface "b" according to



At interface "c," additional Fe₃O₄ can be formed by the direct combination of iron and oxygen ions

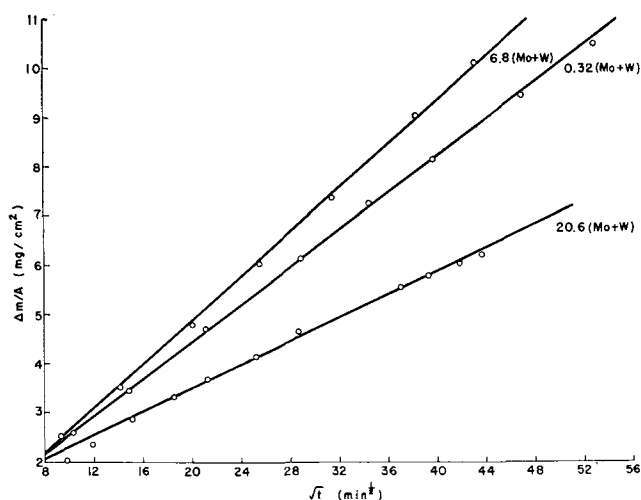


FIG. 10. Oxidation of nickel-molybdenum alloys, 1000°C, O₂ flow ~ 1 l/min.

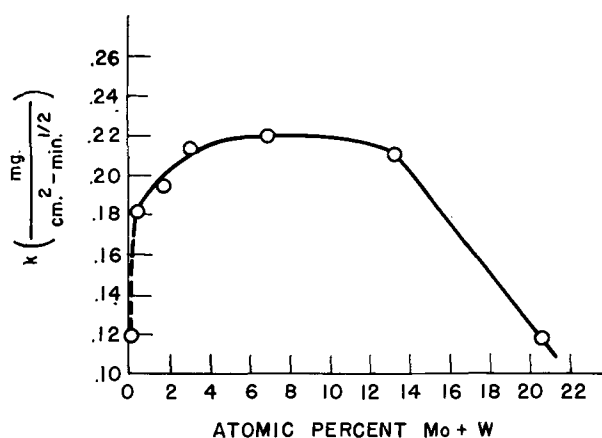


FIG. 11. Effect of composition on the parabolic rate constant of nickel-molybdenum alloys at 1000°C.

The formation of MoO₂ probably occurs at "d," the metal-oxide interface.

Migration of molybdenum ions in the iron oxide at 1000°C is only slight, as the chemical analysis of the bulk oxide indicates. However, at temperatures above 1000°C, the diffusivity of the molybdenum ions and their solubility in the iron oxides becomes great enough for appreciable amounts of molybdenum ions to reach the oxide-oxygen interface where they form the volatile MoO₃.

Nickel-Molybdenum

Fig. 9 shows typical oxidation curves for some of the nickel-molybdenum alloys. Except for the initial period, the oxidation rate is again parabolic and the temperature dependence of the rate constants follow the Arrhenius relationship.

The rate constants k evaluated from curves such as shown in Fig. 10 are summarized in Table II. These constants correspond to single runs of at least 8-hr duration. Duplicate runs indicated a variation in k of less than 10%.

Fig. 11 shows the effect of composition on the parabolic rate constant at 1000°C. The value of k for carbonyl nickel as reported by Pfeiffer and Hauffe (8) is included for reference. As can be observed, the rate increases up to 3 at. % Mo + W, then remains approximately constant up to 12%, beyond which it decreases again. However, the over-all effect of composition is relatively small.

The temperature dependence of k for two of the alloys is shown in Fig. 12. The calculated A and Q values for these two alloys are given in Table III. The values for high purity nickel (550°–700°C) as found by Gulbransen and Andrew (9) are included for comparison. Although there is an appreciable change in A , the heat of activation, Q , for the two alloys varies only by a small amount from that of pure nickel.

Structure of the oxidation product.—Oxidation of the alloys produced three distinct layers, as shown

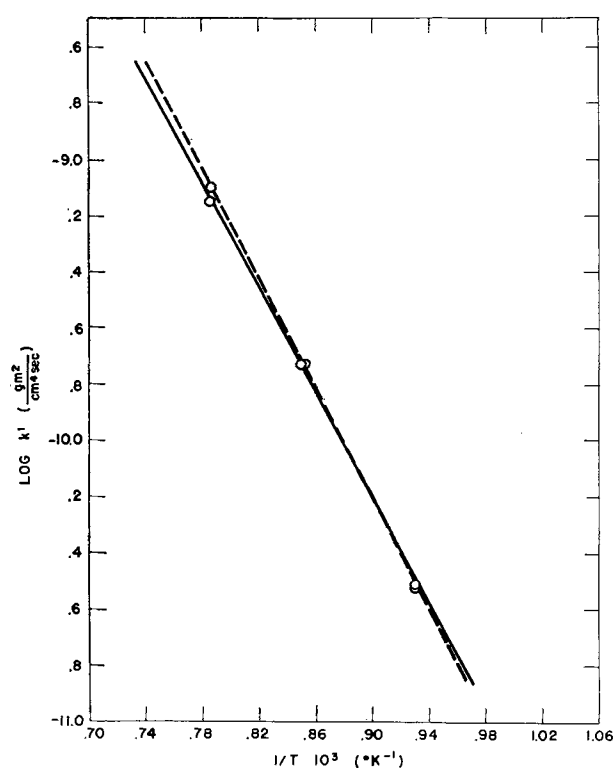


FIG. 12. Temperature dependence of the parabolic rate constant of nickel-molybdenum alloys. ---, 6.8 (Mo + W); —, 13.1 (Mo + W).

schematically in Fig. 13. In addition to the external scale of NiO and NiMoO₄, a subscale of MoO₂ is formed.

Oxides were identified both visually and by x-ray diffraction. By means of a tapered section (10× mechanical magnification), as shown in Fig. 14, the thin layer of NiMoO₄ could be resolved. The subscale region is also clearly evident.

Little is known concerning nickel molybdate. It is soft, light green in color and is readily formed by heating a mixture of NiO and MoO₃ above 500°C. X-ray diffraction from the NiMoO₄ produced by oxidation was identical to that produced synthetically. The "d" values of the major diffraction lines obtained on a Philips x-ray spectrometer are listed

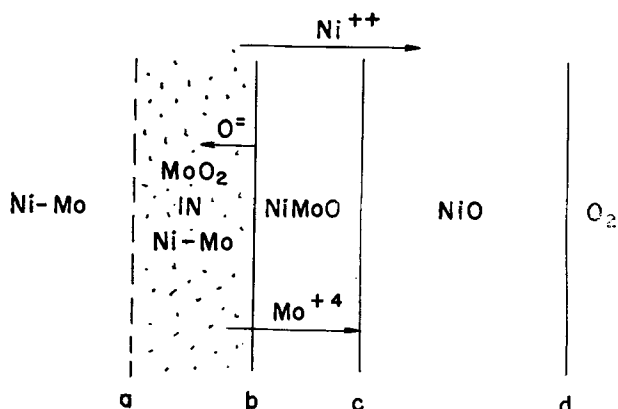


FIG. 13. Oxide growth on nickel-molybdenum alloys

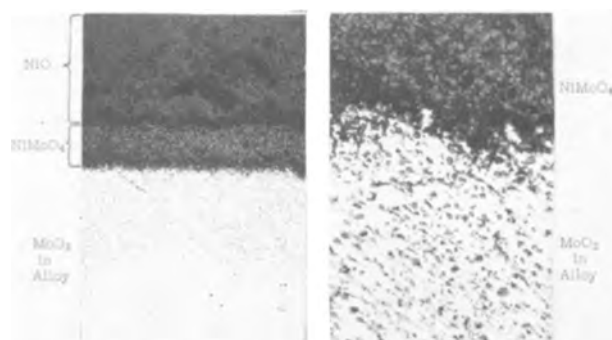


FIG. 14a (left). Alloy 904 (6.8 at. % Mo + W), 63 hr at 1000°C. (1000× before reduction for publication); FIG. 14b (right). Alloy 904 (6.8 at. % Mo + W), 63 hr at 1000°C. (5000× before reduction for publication).

in Table VI. Due to line broadening and distortion, their accuracy is somewhat limited. It was not possible to identify the crystallographic structure, but it seems to fit most closely into the tetragonal system.

NiMoO₄ is stable up to 1150°C, above which it decomposes, releasing MoO₃. As reported by Spretinak and Speiser (10), upon cooling, NiMoO₄ undergoes polymorphic changes causing appreciable volume changes. This behavior is well illustrated by the fact that, upon cooling, the scale on the oxidized alloys shatters off violently from the metal core. It was, therefore, difficult to prepare the specimens for metallographic observation.

Mechanism of oxide growth.—Since the oxidation rate of the molybdenum-containing alloys is not appreciably different from that reported for carbonyl nickel, it can be assumed that the rate-determining factor of the oxidation process is still the diffusivity of the nickel ions in the nickel oxide layer.

It was estimated that the proportion of NiMoO₄ in the bulk oxide increases as a function of molybdenum content from about 2 to 5% in the 3.0% alloy to about 20% in the 20.6% alloy. If the dif-

TABLE VI. Interplanar spacings of NiMoO₄, and relative intensity of diffraction

d	I/I _{max}
6.12	0.61
3.80	0.09
3.48	0.33
3.07	1.00
2.73	0.57
2.31	0.18
2.19	0.20
2.06	0.50
1.91	0.15
1.71	0.15
1.63	0.10
1.60	0.18
1.50	0.25
1.46	0.10

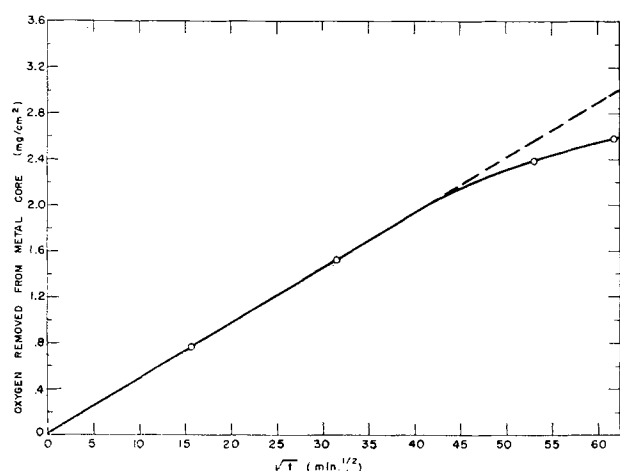


FIG. 15. Growth of the subscale on alloy 904 (6.8 at. % Mo + W), 990°C, O₂ flow ~ 1 l/min.

fusivity of nickel ions in the molybdate were less than that in NiO, an appreciable change in the parabolic rate constant as a function of composition would have been observed. The small variation in the heat of activation, Q , further indicates that the controlling factor, i.e., the diffusion of nickel ions through the NiO, is the same in both nickel and nickel-molybdenum alloys up to 13.1 at. % molybdenum.

Formation of NiMoO₄ and MoO₂ can, therefore, be considered as secondary effects. After reaching stationary equilibrium, the oxide growth continues as shown schematically in Fig. 13. Nickel ions diffuse through the NiMoO₄ and NiO layers to form new NiO at the interface "d." Concurrently, molybdenum ions migrate through the NiMoO₄ layer and react with the NiO at the interface "c" according to



The rate of growth of the NiMoO₄ layer depends on the molybdenum content of the alloy. At the interface "b," oxygen diffuses into the interior, the driving force being the difference between the dissociation pressure of NiMoO₄ and the oxygen partial pressure in the alloy.

Since the decomposition pressure of MoO₂ is much less than that of NiO (3.0×10^{-14} as compared to 1.7×10^{-10} at 1000°C), MoO₂ precipitates in the alloy matrix.

Growth of the subscale is determined by the difference in the rate of formation of the external scale and the diffusion rate of oxygen. A parabolic relationship is therefore expected. This relationship has been confirmed by Rhines (11) and Thomas (12).

The oxygen uptake by the metal core of the 6.8% alloy is plotted as a function of $t^{1/2}$ in Fig. 15. Each point was determined separately by removing the

oxygen with hydrogen after the external scale was removed. Except for deviations at the longer times, a parabolic relationship is observed. Some error is introduced because dissolved oxygen as well as the combined oxygen is removed. Incomplete reduction of the MoO₂ may also have occurred.

Decrease of the oxidation rate of the 20.6% molybdenum alloy may be due to densification of the subscale which hinders migration of nickel ions from the interior. In effect, the contact area between the metal core and the external scale is decreased.

Increase in the oxidation rate of the alloys containing up to 13.1% Mo is probably due to the incorporation of some molybdenum ions in the NiO lattice. Being deficient in cations, ions of higher valency will introduce further metal vacancies in the nickel oxide structure, thus increasing the rate of oxidation. This behavior has been found in the investigations of Wagner and Ziemens (13) and Pfeiffer and Hauffe (8).

As the temperature is increased, the solubility of molybdenum in NiO becomes greater. Some of the molybdenum ions reaching the oxygen interface form MoO₃ which evaporates from the surface. Thus, at 1118°C, the 20.6% Mo alloy formed 0.00062 g/cm² of MoO₃ during 65½ hr of oxidation.

CONCLUSION AND SUMMARY

Molybdenum significantly alters the high temperature oxide structure on iron and nickel. Because of the low solubility of molybdenum in NiO and in the iron oxides, molybdenum-rich oxide layers of MoO₂ and molybdate are formed. The volatile MoO₃, however, is prevented from forming, and catastrophic oxidation does not occur. Molybdenum considerably decreases the oxidation rate of iron. Molybdenum enrichment at the alloy surface during the early part of the oxidation prevents the development of the cation deficient FeO layer normally found on iron above 570°C. The oxidation process is now controlled by the migration of iron and oxygen through the more diffusion-resistant Fe₃O₄ and Fe₂O₃ layers.

The oxidation rate of nickel is affected to a much lesser degree by the addition of molybdenum. Up to 13.1 at. %, the rate is slightly increased by formation of additional vacancies in the NiO lattice due to dissolved molybdenum atoms. Above 13.1%, the MoO₂ subscale becomes dense enough to hinder migration of nickel ions and the rate, therefore, decreases again. It is postulated that the controlling step in the oxidation process is still the migration of nickel ions across the NiO layer. The small change in oxidation rates and in experimental heats of activation of the alloys supports this.

ACKNOWLEDGMENT

The author is grateful to Dr. David Turnbull for his valuable suggestions and criticisms.

Any discussion of this paper will appear in a Discussion Section to be published in the December 1955 JOURNAL.

REFERENCES

1. W. C. LESLIE AND M. G. FONTANA, *Trans. Am. Soc. Metals*, **41**, 1213 (1949).
2. A. DE S. BRASUNAS AND N. J. GRANT, *Iron Age*, 85, Aug. 17, 1950.
3. G. W. RATHENAU AND J. L. MEIJERING, *Metallurgia*, **42**, 167 (1950).
4. E. SCHELL AND K. KIWIT, *Arch. Eisenhüttenw.*, **9**, 405 (1936).
5. M. H. DAVIES, M. T. SIMNAD, AND C. E. BIRCHENALL, *Trans. Am. Inst. Mining Met. Engrs.*, **191**, 889 (1951).
6. C. WAGNER, *This Journal*, **99**, 369 (1952).
7. O. KUBASCHEWSKI AND E. L. EVANS, "Metallurgical Thermochemistry," p. 307, Academic Press, New York (1951).
8. H. PFEIFFER AND K. HAUFFE, *Z. Metallkunde*, **43**, 364 (1952).
9. E. A. GULBRANSEN AND K. F. ANDREW, *This Journal*, **101**, 128 (1954).
10. J. W. SPRETNAK AND R. SPEISER, Report No. 6, NR 039-005, Ohio State University Research Foundation (1953).
11. F. N. RHINES, *Trans. Am. Inst. Mining Met. Engrs.*, **137**, 246 (1940).
12. D. E. THOMAS, *ibid.*, **191**, 926 (1951).
13. C. WAGNER AND K. E. ZIEMENS, *Acta Chem. Scand.*, **1**, 547 (1947).

Catastrophic Oxidation of Some Molybdenum-Containing Alloys¹

S. S. BRENNER

Research Laboratory, General Electric Company, Schenectady, New York

ABSTRACT

When nickel or chromium is added to binary iron-molybdenum alloys, catastrophic oxidation occurs in certain concentration regions. Chromium is more effective than nickel in inducing this rapid type of oxidation.

Catastrophic oxidation occurs because of the formation of liquid MoO₃ along the metal-oxide interface. This is preceded by the cracking of the chromium or nickel-containing oxide.

Catastrophic oxidation does not occur with alloys containing large amounts of nickel.

INTRODUCTION

Catastrophic oxidation of certain alloys containing appreciable amounts of molybdenum has been reported. It is postulated that this rapid type of attack is due to the formation of MoO₃. The presence of other volatile and low melting oxides such as V₂O₅ (670°C), Bi₂O₃ (820°C), PbO (888°C), WO₃ (1473°C), and mixtures of these oxides can also induce this type of attack in the absence of molybdenum (1-4).

While several workers (2-4) are of the opinion that catastrophic oxidation stems from the presence of a liquid oxide layer, none of these postulates how the liquid film is formed and what the oxidation process is, in the case where the liquid oxide is formed by the alloying element.

This paper presents results on the oxidation of some molybdenum-containing materials and proposes a mechanism of catastrophic oxidation. A previous paper (5) showed that binary nickel-molybdenum alloys up to 30% (weight) molybdenum and binary iron-molybdenum alloys up to 20% molybdenum do not oxidize catastrophically at 1000°C. In both cases, MoO₂ and molybdate, in addition to nickel oxide or iron oxide, are formed during oxidation. To induce catastrophic oxidation, additions of nickel or chromium or both were made to binary iron-molybdenum alloys.

EXPERIMENTAL

Specimen preparation.—All alloys were prepared by arc melting in a multiple hearth arc furnace. Their nominal compositions are given in Table I. In most cases, nominal compositions deviate less than 5% from analyzed compositions. Nominal weight percentages are used throughout this paper.

The 100 g alloy buttons were ground on two faces, hot rolled, sand blasted, cold rolled if possible, and

finally annealed. Specimens 0.020 in.-0.040 in. were cut from the rolled strips.

Procedure.—Oxidation of the alloys was determined by measuring the weight loss of the metal. Weighed specimens were placed in covered alundum filtering crucibles which were seated in a 4-in. diameter crucible furnace. The purpose of the alundum crucible was to minimize contamination from the neighboring samples and from the fire brick plug. Oxygen was passed through the crucible furnace at a rate of about 2 l/min to insure against oxygen depletion. The temperature was constant to better than $\pm 5^\circ\text{C}$.

The amount of metal oxidized was determined as follows. After the bulk oxide was removed, the weight of the metal core with the residual oxide remaining on it was determined. The residual oxide was then reduced in hydrogen and its original weight was calculated by assuming that the oxide contained 25% oxygen.

RESULTS

When nickel was substituted for iron in the 20Mo80Fe alloy, the striking and unexpected result shown in Fig. 1 occurred. Up to 10% nickel there is only a small change in the oxidation rate; beyond 15% there is a sudden increase with a maximum at about 25Ni. At this composition the oxidation is about 15 times as fast as with the 20Mo70Fe10Ni alloy. Beyond 25Ni, the oxidation rate again decreases rapidly, approaching that of the 20Mo70Fe-10Ni alloy at 40Ni. An increase to 60Ni gives only a small change in the oxidation rate.

Additions of chromium to the iron-molybdenum alloys initiated rapid oxidation even more readily. Only small amounts of chromium in the order of 5% are sufficient to accelerate attack. Some alloy samples oxidized completely in the 2-hr testing

¹ Manuscript received March 22, 1954.

TABLE I. Loss of metal by oxidation during 2 hr at 1000°C

Alloy	$\Delta m/A$ (mg/cm ²)
20Mo80Fe	16.1
20Mo75Fe5Ni	9.4
20Mo70Fe10Ni	9.9
20Mo65Fe15Ni	27.9
20Mo60Fe20Ni	93.8
20Mo55Fe25Ni	152.5
20Mo50Fe30Ni	46.2
20Mo40Fe40Ni	11.2
20Mo20Fe60Ni	3.7
25Ni75Fe	18.2
25Ni70Fe5Mo	14.1
25Ni65Fe10Mo	23.9 (uneven attack)
25Ni45Fe30Mo	122.5
50Ni20Fe30Mo	4.8
10Mo5Cr85Fe	128.5 (uneven attack)
5Mo15Cr80Fe	112.0 (uneven attack)
15Mo10Cr75Fe	>365.0 (completely oxidized)
25Cr75Fe	1.0
20Mo5Cr75Fe	31.3
15Mo15Cr70Fe	>361.0 (completely oxidized)
20Mo10Cr70Fe	>198.0 (completely oxidized)
5Mo25Cr70Fe	1.0
10Mo25Cr65Fe	58.4 (uneven attack)
30Mo5Cr65Fe	34.3
40Ni20Mo35Fe5Cr	10.3
40Ni20Mo30Fe10Cr	10.5
40Ni20Mo20Fe20Cr	5.7

period. The effect of chromium additions in excess of 25% could not be evaluated because of the difficulty of fabrication of the alloys.

The three quaternary alloys containing 40% nickel did not exhibit catastrophic oxidation even though the chromium and molybdenum content were as high as 20% each.

Table I lists for every alloy the amount of metal oxidized during 2 hr of oxidation at 1000°C. These values are plotted as a function of composition in Fig. 2, the shaded areas indicating the regions of catastrophic oxidation.

The amounts of metal oxidized as given in Table I are single values, not averages. Several duplicate determinations were made on most of the alloy samples, generally giving a reproducibility of within 30% of the reported values. Where oxidation was not uniform, the reproducibility was less satisfactory; however, the relative degree of attack was not altered. Several of the duplicate determinations were made in the absence of other specimens and in different furnaces. In all cases the amount of oxidation was within the normal reproducibility, indicating that contamination of one sample by another was kept to a minimum.

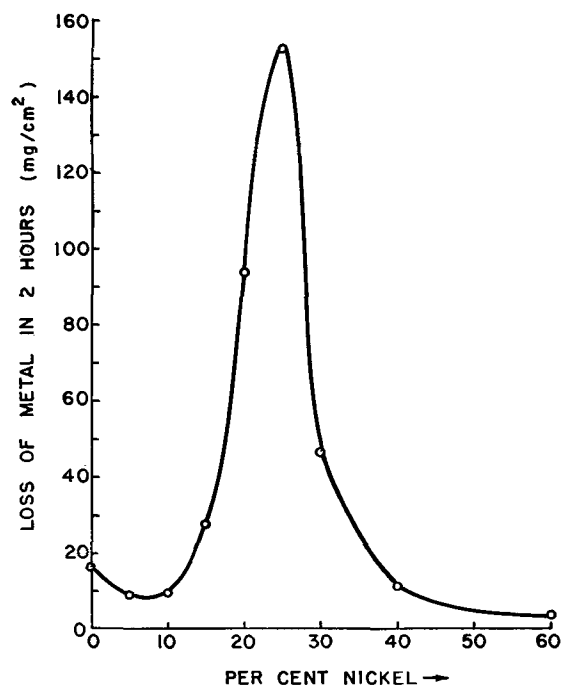


FIG. 1. Oxidation of 20MoFeNi alloys, 1000°C. (Nickel is substituted for iron in the original 20Mo80Fe alloy.)

MECHANISM OF CATASTROPHIC OXIDATION

The results on oxidation of iron-molybdenum alloys and on nickel-molybdenum alloys, as reported previously (5), show that, due to the enrichment of molybdenum, MoO₂ is formed immediately adjacent to the alloy surface. As long as the MoO₂ is prevented from oxidizing to MoO₃, normal oxidation

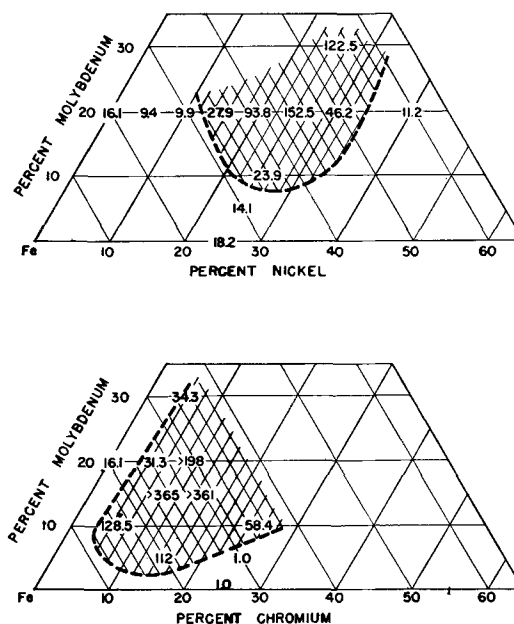


FIG. 2. Oxidation of FeMoNiCr alloys. Numbers indicate weight loss per unit area after 2 hr at 1000°C. Shaded areas indicate regions of rapid oxidation.

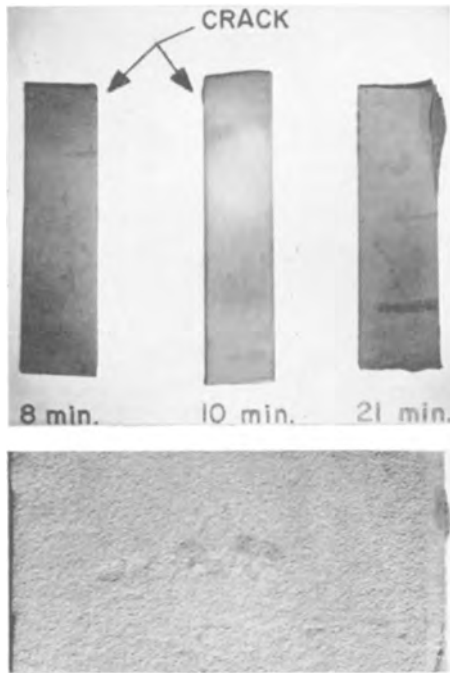
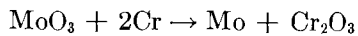
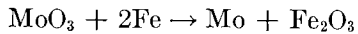


FIG. 3. Crack formation in oxide on 15Mo75Fe10Cr Alloy at 1000°C. Top, crack growth as a function of time. (2X before reduction for publication); bottom, oxidation after 8 min. (10X before reduction for publication.)

occurs. However, as soon as the MoO₂ has access to a large supply of oxygen, the low melting and highly volatile MoO₃ is formed.

The simplest method of supplying the MoO₂ layer with oxygen is by means of a crack or pore in the main oxide. Pore formation does occur with the MoFeCr alloys as shown in Fig. 3. After the initially very rapid formation of the chromium-rich oxide, a crack appears exposing the molybdenum-enriched surface. Molten MoO₃ is formed which penetrates along the metal-oxide interface. Being less noble, the chromium and iron in contact with the MoO₃ constantly reduces the MoO₃ according to



Being an excellent flux, liquid MoO₃ probably dissolves the chromium and iron oxide at the MoO_{3(l)}-metal interface. Fluxing is further facilitated by the

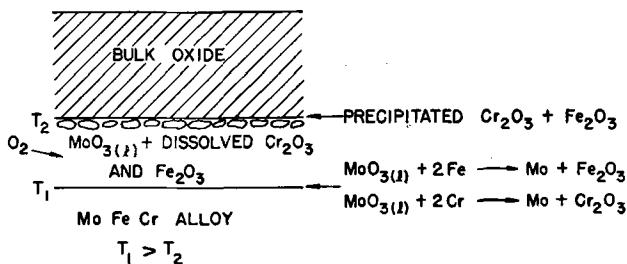


FIG. 4. Mechanism of catastrophic oxidation

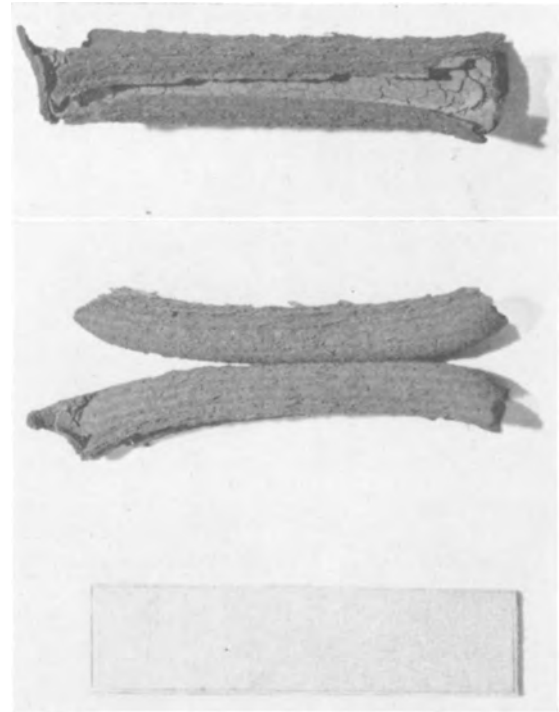


FIG. 5. Oxidation of 15Mo75Fe10Cr alloy, 2 hr at 1000°C. Top, top view of oxidized specimen; center, side view of oxidized specimen; bottom, original alloy specimen. (1½X before reduction for publication.)

released heat of formation of chromium and iron oxide which tends to increase the temperature at the metal-MoO_{3(l)} interface. The dissolved iron and chromium oxide nucleate and precipitate again in

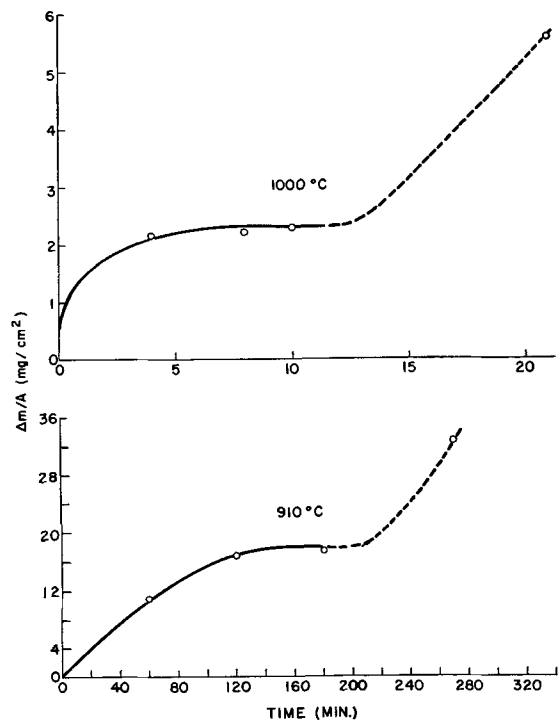


FIG. 6. Oxidation of 15Mo75Fe10Cr alloy

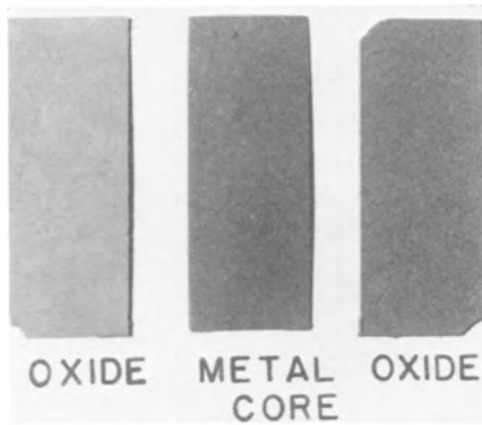


FIG. 7. Oxidation of 20Mo55Fe25Ni alloy, 2 hr at 1000°C. ($1\frac{1}{2}\times$ before reduction for publication.)

the cooler region near the $\text{MoO}_3(\text{l})$ -bulk oxide interface. This process is shown schematically in Fig. 4.

Thus, the original crack or pore is never healed and both MoO_2 and Mo have continual access to the oxygen. As the metal is oxidized along the edges, the oxide curls up until, after complete oxidation, it appears as shown in Fig. 5.

The cracking of the Cr-rich oxide is in agreement with the findings of McCullough, Fontana, and Beck (6). In their investigation on the oxidation of some stainless steels, they found that at 980°C there was an abrupt increase in the oxygen pickup after an initial period ranging from 10 to 45 min. At 925°C the time to rupture increased to about 4 hr.

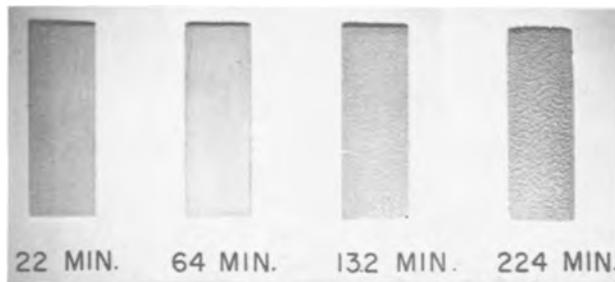


FIG. 8. Surface roughening of the 20Mo55Fe25Ni alloy during oxidation at 910°C. Top, surface roughening as a function of time ($1\times$ before reduction for publication); bottom, surface after 224 min. ($5\times$ before reduction for publication.)

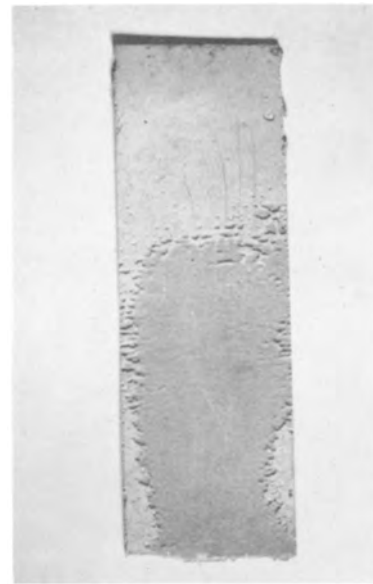


FIG. 9. Nonuniform oxidation of 20Mo55Fe25Ni alloy, 1 hr at 1000°C.

Fig. 6 shows the weight loss of 15Mo10Cr75Fe alloy as a function of time at 1000° and 910°C. The two curves show clearly the abrupt increase of oxidation after about 15 min at 1000°C and $3\frac{1}{2}$ hr at 910°C.

That the crack should appear at the edges is quite reasonable. Presumably the crack formation comes by the stress relieving of the compressed oxide. Since a sharp edge offers little constraint, the oxide tends to pull away from it.

X-ray analysis of the oxide formed on the MoFeCr alloys showed it to consist of a mixture of Fe_2O_3 and Cr_2O_3 . No $\text{Cr}_2\text{O}_3 \cdot \text{FeO}$ could be detected even before the cracking of the oxide occurred.

At first it appeared that the mechanism of the rapid oxidation of the MoFeNi alloys was different from that of the MoFeCr alloys. Oxidation is less violent and more uniform. This behavior is shown

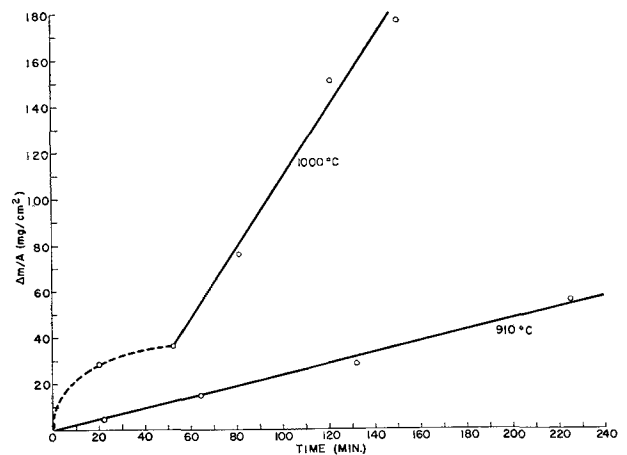


FIG. 10. Oxidation of 20Mo55Fe25Ni alloy

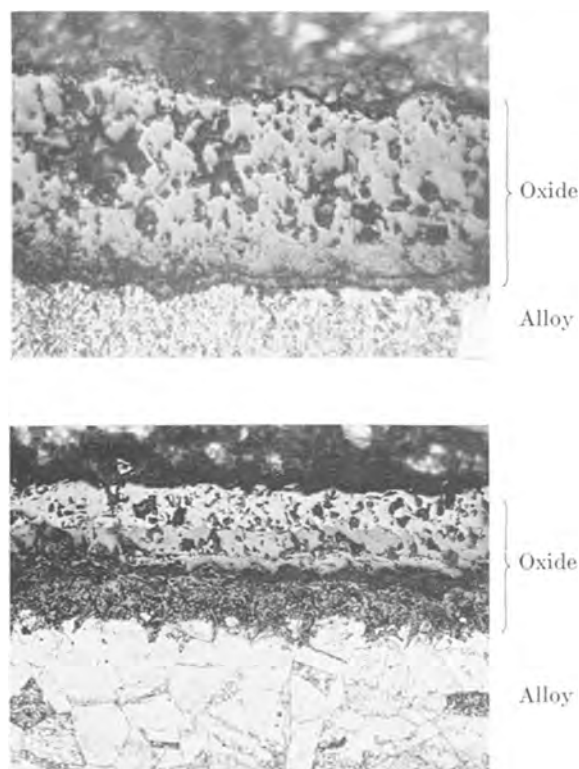


FIG. 11. Top, rapid oxidation, oxide on 30Mo45Fe25Ni alloy, 2 hr at 1000°C; bottom, retarded oxidation, oxide on 5Mo70Fe25Ni alloy, 5 hr at 1000°C. (250 \times before reduction for publication.)

in Fig. 7 which shows the metal core and the two oxide plates removed from the 20Mo55Fe25Ni alloy sample after 2-hr oxidation at 1000°C. However, it was noticed that in many cases the oxide had pulled away slightly from the edges. An investigation of the surface of the 20Mo55Fe25Ni alloy after oxidation for varying periods at 910°C revealed the development of a rough and ridged surface (Fig. 8) suggesting the presence of a liquid phase. It was also observed that at the higher temperature (1000°C) some areas of the specimen were sometimes attacked more severely than others, as shown in Fig. 9.

In view of these facts, it is believed that the oxidation mechanism is similar to that of the MoFeCr alloys. After the metal surface is enriched by molybdenum, oxygen obtains access to the surface and forms liquid MoO₃. The MoO₃ penetrates along the metal-oxide interface, constantly being reduced by the less noble iron and oxidized by the ambient oxygen. Iron oxide is dissolved in the molten MoO₃ and re-precipitated along the bottom surface of the bulk oxide (see Fig. 4). Since nickel is considerably more noble than molybdenum, nickel-rich ridges form on the surface. This process can, therefore, be described as a selective oxidation by a liquid phase. Since the

oxygen affinity of chromium is much larger than that of iron, it can readily be seen that the oxidation of the chromium alloys should be much more violent.

An effort was made to indicate more clearly the cracking or pore formation of the oxide on the 20Mo55Fe25Ni alloy. Oxidation measurements as a function of time were made at both 910° and 1000°C (Fig. 10). Neither of the two measurements definitely shows that cracking occurs, although there is good indication of it at 1000°C. At both temperatures, oxidation is linear with time.

Returning to Fig. 1, it can now be said in view of the foregoing discussion, that in the range of 15–35% nickel, a liquid film of MoO₃ is formed, while with the other compositions molybdenum is prevented from oxidizing to the higher oxide. The difference between the oxide structure of the 45Fe30Mo25Ni alloy exhibiting rapid oxidation and the 5Mo70Fe25Ni alloy exhibiting normal oxidation is pointed out in Fig. 11. The normally oxidized sample exhibits the MoO₂ rich oxide layer adjacent to the alloy surface, while the rapidly oxidized sample shows only one homogeneous layer.

The question remains why there is a critical nickel composition range in which rapid oxidation occurs. It was hoped that x-ray diffraction analysis of the oxides formed on the alloys would give some clue. However, the main oxide on all the MoFeNi alloys beyond 10% nickel consisted primarily of a Fe₃O₄ spinell-type phase. The oxide is undoubtedly (Fe, Ni)O·Fe₂O₃ with nickel ions replacing the ferrous ions as the nickel content is increased.

An analysis of the oxide formed on the 20Mo55Fe25Ni alloy (maximum rate of oxidation) gave the following composition:

	Wt %
Fe	50.0
Ni	22.0
Mo	0.7
O	balance

This indicates that the ratio of nickel to iron is practically the same in the oxide as in the alloy. Furthermore, with this amount of nickel in the oxide, ferrous ions are almost completely replaced by nickelous ions and NiO·Fe₂O₃ is formed exclusively. It is, therefore, hypothesized that (FeNi)O·Fe₃O₄ is more prone to cracking than is the pure FeO·Fe₃O₄. The oxide on the alloys with more than 35% nickel may still crack, but now the alloy surface below the oxide is sufficiently diluted with nickel to prevent the formation of MoO₃. This reasoning is in agreement with results reported previously (5) that nickel-molybdenum alloys containing 30% molybdenum do not exhibit catastrophic oxidation.

Similar analysis is extended to the three MoFeNiCr alloys. If the oxide does crack, there is enough nickel

on the alloy surface to prevent the formation of liquid MoO_3 , and healing of the crack can occur.

SUMMARY AND CONCLUSIONS

When chromium or nickel is added to binary iron-molybdenum alloys which oxidize normally, catastrophic oxidation can occur within certain composition regions. Chromium induces catastrophic oxidation more readily than nickel.

It is postulated that immediately after the initial oxidation, the metal surface becomes enriched in molybdenum. The oxide on the alloy cracks, allowing the formation of liquid MoO_3 along the alloy oxide interface. $\text{MoO}_{3(l)}$ constantly oxidizes the iron and chromium in the alloy to Fe_2O_3 and Cr_2O_3 . Fe_2O_3 and Cr_2O_3 dissolve in the MoO_3 and re-precipitate along the MoO_3 -bulk oxide interface. Healing of the crack cannot, therefore, occur.

When the alloy contains a sufficient amount of nickel, formation of MoO_3 is prevented in a similar manner as in the nickel-rich nickel-molybdenum

alloys. Thus, MoFeNiCr alloys with 40% nickel and 20% molybdenum do not oxidize catastrophically. These alloys may be of industrial use.

ACKNOWLEDGMENT

The author is grateful to Dr. David Turnbull for his valuable suggestions and criticisms.

Any discussion of this paper will appear in a Discussion Section to be published in the December 1955 JOURNAL.

REFERENCES

1. W. C. LESLIE AND M. G. FONTANA, *Trans. Am. Soc. Metals*, **41**, 1213 (1949).
2. A. DE S. BRASUNAS AND N. J. GRANT, *Iron Age*, 85, Aug. 17, 1950.
3. G. W. RATHENAU AND J. L. MEIJERING, *Metallurgia*, **42**, 167 (1950).
4. P. AMGWERD, Eidgenössische Materials prüfungs- und Versuchsanstalt für Industrie, Bauwesen und Gewerbe, Zurich/St. Gallen, Report No. 171, September 1949.
5. S. S. BRENNER, *This Journal*, 102, 7 (1955).
6. H. M. McCULLOUGH, M. G. FONTANA, AND F. H. BECK, *Trans. Am. Soc. Metals*, **43**, 404 (1951).

Controlled Preparation and X-Ray Investigation of Cadmium Sulfide¹

F. SCHOSSBERGER

Armour Research Foundation of Illinois Institute of Technology, Chicago, Illinois

ABSTRACT

A furnace for the controlled preparation of cadmium sulfide (CdS) by the vapor phase method is described. A constant rate of evaporation of the cadmium metal is maintained so that any changes in the ratio of Cd to S, or in the speed of reaction, can be made. Inserts fitted into the reaction tube allow the quick removal of the formed CdS without cooling the furnace. By controlled operation of the reaction furnace, a uniform crystal habit was obtained. X-ray diffraction analysis showed lattice imperfections to be present in CdS and CdSe crystals.

INTRODUCTION

Hexagonal α -CdS, which occurs in nature as the mineral "greenockite," has been grown in the form of crystals by Lorenz (1) by the reaction of Cd vapor with H₂S. Frerichs (2) modified the method by heating Cd metal in a small porcelain boat in a quartz tube to about 800°–1000°C. Cd vapor was driven by a slow stream of H₂ to the zone of the tube where it could react with a stream of H₂S. Yellow hexagonal needles and flat ribbons of photoconducting CdS were obtained.

Replacing H₂ as diluting gas by argon (3), it was found advisable to use baffles in the reaction tube to minimize concentric currents. To grow larger crystals (10 x 5 x 3 mm), CdS powders (4) or the small crystals obtained by the vapor-phase method can be recrystallized (5). This requires a prolonged heat treatment under hydrogen sulfide pressure at temperatures of about 1000°C.

The vapor phase method has the advantage that most impurities are separated by fractionate sublimation (2) so that purification of the Cd metal is not necessary. The light sensitivity of such crystals, however, was found (5–7) to be very different, even for crystals of the same batch. Besides the desirable highly sensitive crystals with high dark resistance up to 10¹³ ohms, crystals with high resistance but low sensitivity were also found. Some crystals show red fluorescence when exposed to ultraviolet light, while others show no evidence of luminescence.

It is conceivable that these differences of the properties of the samples are caused by uncontrolled changes of stoichiometric composition, changes in the impurity content, or possible faults of crystal growth.

With previously described methods of preparing CdS by vapor-phase reaction it is difficult to control

the rate of evaporation of the Cd metal. The evaporation depends not only on the temperature, but also on the continuously changing surface areas of the molten metal in the boat. The first-formed small crystals, therefore, are exposed to vapors of Cd and H₂S in an almost continuously changing ratio. For that reason, an improved reaction furnace was desirable. The features of the new design should lead to a better controlled and more continuous preparation of CdS which would establish the conditions under which certain crystal habits, fine powders, or large uniform crystals can be obtained.

It is comparatively easy to control the temperature of the reaction and the flow of H₂S into the reaction furnace. The problem of operating the furnace at a constant ratio of Cd to S, therefore, is concentrated in the problem of keeping the rate of evaporation of the Cd metal constant.

REACTION FURNACE

The ceramic parts of the furnace are made in the form of two halves between which the glass part can be inserted. To obtain a constant rate of evaporation of the metal, Cd is heated to a temperature slightly above the melting point in a U-shaped Vycor tube (Fig. 1) by a heating coil (F1). The right branch (F2) of the U heats molten Cd up to its boiling point at 767°C. A constant level of the boiling metal surface is maintained by making the left branch (F1) several times larger than the boiler tube (F2). The surface of the molten metal in the left branch must be protected by an inert gas to prevent oxidation. Cd metal can be added to (F1) even during the operation of the furnace through the V-shaped part of the Cd reservoir. A thermocouple placed in the molten metal (Th1) measures and regulates the temperature.

The heating coil for the boiler (F2) covers only a small part of the metal column but all of the gas

¹ Manuscript received April 12, 1954.

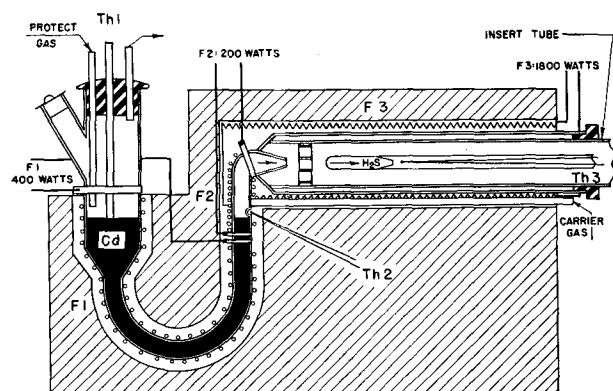


FIG. 1. Reaction furnace

space above it. Above the boiling surface of the metal Cd vapors can be mixed with preheated carrier gases such as N_2 , H_2 , or He. Purified and dried carrier gas enters the furnace through a tube at the extreme right and is heated by the heating elements of the furnace (F3).

The carrier gas serves several purposes. It maintains a constant flow of the vapor in the direction of the reaction zone in (F3) and protects the boiling metal surface so that no H_2S reaches the boiler. It also enables one to change and adjust the amount of Cd entering the reaction tube. The temperature regulation of the boiler (F2) is, of course, very critical, if constant conditions are to be maintained. The hot junction of a thermocouple (Th2) is, therefore, placed in a cavity of the Vycor tube above the boiling metal; the temperature of the boiling metal is controlled by an automatic regulator.

To measure the amount of Cd vapor entering the reaction tube (F3), the following method was adopted. By maintaining a constant temperature in (F2) the level of the boiling metal was kept in coincidence with a mark made on the right branch of the U-shaped Vycor tube. This is possible, if, from time to time during the experiment, solid Cd metal is added to the left branch of the tube. The

TABLE I. Dimensions of the reaction furnace

	Furnace	(F1) Reservoir	(F2) Boiler	Reaction zone (F3)
Length, in.....	22	9	3	15
Width, in.....	10	2	3/8	2
Height, in.....	18			
Heating coil, watts.....		400	200	1800

weight of the metal needed to keep the level in (F2) at a constant height is, of course, equivalent to the amount of Cd entering the reaction tube during the experiment.

A hole drilled into the ceramic insulating material and covered by mica permits observation of the level of liquid Cd (F2) from the outside of the furnace.

The mixture of Cd vapor and carrier gas enters the reaction zone (F3) through a knee and a perforated porcelain plate. The latter serves as a baffle to distribute the gases equally over the space and as an obstacle for the H_2S to avoid blocking of the Cd vapor outlet.

Inside the reaction tube an insert is held tightly by ground glass, whereas outside of the furnace the two tubes are tightened by a rubber ring. The insert tube contains the thermocouple (Th3) for regulating the temperature in (F3) and the H_2S inlet. The length of the H_2S inlet was chosen so that the dried gas already possesses the temperature of (F3) when it enters the reaction zone. The insert tube is used for quick removal of the formed CdS, and several of these inserts are kept in stock.

Formation of CdS can be stopped instantly by cooling the boiling metal at (F2) with cold air, and quick changes of the insert tubes can be made without opening or cooling the furnace. The furnace could be made to work continuously, if a worm screw or a belt is built in to remove the formed material. Some technical data on the furnace are given in Table I.

Depending upon the temperature and the gas

TABLE II. Spectrographic analysis

Elements	Raw material Cd metal for No. 32,33	CdS No. 32 (Table III)	CdS No. 33 (Table III)	Commercial luminescent pigment	Limit of detection
Ca	0.01-0.1	0.001-0.01	0.001-0.01	0.001-0.01	0.0001
Mg	0.001-0.01	0.001-0.01	0.001-0.01	0.001-0.01	0.0001
Si	0.001-0.01	0.001-0.01	0.001-0.01	0.001-0.01	0.0001
Zn	0.001-0.01	—	—	0.05-0.1	0.01
Cu	0.01-0.1	0.0001-0.001	0.0001-0.001	0.0001-0.001	0.0001
Sn	0.01-0.1	—	—	—	0.0001
Ag	0.0001-0.001	*	*	*	0.0001
Fe	0.001-0.01	*	0.0001-0.001	*	0.0001
Ni	0.01-0.1	—	—	—	0.0001
Pb	0.05-0.1	—	—	—	0.0001

* Element may be present at concentrations near the limit of detection.

TABLE III. Preparation conditions and crystal habit

Preparation condition	CdS No. 33	CdS No. 32
Temp, °C		
Melting reservoir (F1)	400	400
Cd boiler (F2)	690	870
Reaction zone (F3)	950	950
Gas flow, mole/min		
Carrier gas N ₂	0.75×10^{-2}	6.4×10^{-2}
Cd vapor	0.668×10^{-3}	17.9×10^{-3}
H ₂ S	0.444	0.018
Mole ratio Cd to S	1:664	1:1.005
Crystal habit	100% type [1] homogeneous needles	85% type [2] 15% type [3], [4], [5] polycrystalline rods

flow maintained, a laboratory furnace of the given dimension yields about 5–200 g CdS/hr.

In fact, the method described for the controlled reaction of vapors might be generally useful for the manufacturing of other substances (ZnS, CdO, PbSe) by vapor-phase reactions.

SPECTROGRAPHIC ANALYSIS, CRYSTAL HABIT, AND X-RAY DIFFRACTION

In Table II, spectrographic analyses of the Cd metal used and the CdS prepared from it in the furnace are compared with the analysis of a commercially available, luminescent CdS obtained by wet chemical preparation methods. The analysis is in accord with Frerichs' (2) observation about purification during the process. It also shows that the vapor-phase method leads to substances which are at least as pure as those obtained by wet chemical methods.

By a morphological investigation of CdS crystals grown by the vapor-phase method, five different "types" were observed and correlation was found (6) between electrical properties and habit. According to this investigation, 500 crystals collected from 15 different batches occurred as needles, ribbons with rectangular and oblique striations, and twins with the following frequencies: type [1] thoroughly homogeneous needles 17%; type [2] ribbons with rectangular striations 18%; type [3] ribbons with oblique striations 25%; type [4] twins of [1]; and type [5] twins of [3]. Relatively poor photoelectric properties were found on crystals of types [4] and [5].

The present experiments, however, performed under controlled conditions, demonstrate that the crystal habit of CdS can be determined by properly chosen preparation conditions. Conditions for obtaining type [1] crystals or a mixture of several types are shown in Table III for two characteristic experiments. With a mole ratio of Cd to S of 1:664 and flow rates of 0.44 moles H₂S/min only single crystal

needles of type [1] were grown with an average needle size of 6 to 15 x 2 x 3 mm. Although some dendritic hollow needles were observed, which is characteristic of rapid crystal growth, the batch was very homogeneous with respect to the crystal habit. By x-ray and optical methods the needle axis was found to be the c-axis of the crystal. Much smaller crystals of all types and microcrystalline rods were obtained with a mole ratio of approximately 1:1 and flow rates of 0.018 H₂S/min. Most of the crystals show dendritic habit and parallel striations in the direction of the c-axis. The twinning of the oblique striated crystals (type [3]) occurs along the by-pyramide face. Spectrographic analysis of the two samples (Table II) does not show significant differences in the impurity content.

The reproducibility for obtaining crystals of type [1] of the same size, purity, and x-ray characteristics was confirmed in several experiments. The uniformity of the crystals within the batch (CdS No. 33 in Table III) was found to be maintained over a length of 7½ in. in the reaction zone of (F3) (Fig. 1), corresponding to the temperature gradient along the furnace.

Grinding of luminescent materials is usually accompanied by a loss of luminescent properties of the material. In the case of hexagonal ZnS, the destruction by pressure was explained (8) by the introduction of lattice defects and the formation of electron traps. The concentration of these imperfections was thought to be so small as to escape detection by routine x-ray and electron diffraction methods.

This is different in the case of α-CdS. If powder x-ray diagrams with Cu-Kα radiation are taken of the unground but sieved CdS crystals, the photograph shows sharp lines up to the highest reflection angles and good resolved α₁-α₂ doublets. Grinding in a mortar, as done for routine x-ray diffraction work, changes the color of the substance from light

TABLE IV. *d*-Values of the low angle lines in CdS and CdSe

α-CdS		α-CdSe	
<i>d</i> in Å	rel. intensity	<i>d</i> in Å	rel. intensity
22	1		
11.5	3		
10.5	7	11.38	5
7.98	3	8.26	1
6.75	5	7.02	3
6.19	4	6.47	3
5.70	4	5.93	3
5.32	—1		
4.92	—1		
4.58	1		
4.11	1		
3.74	1		
3.55 (10T0α-CdS)	8	3.68 (10T0α-CdSe)	6

yellow to brown. At the same time, the x-ray diagram of the ground material shows a loss of intensities and line broadenings with increasing diffraction angles. The intensities of (0002), (10 $\bar{1}$ 2), and (11 $\bar{2}$ 2) are increased. Since the grinding of such substances in a mortar usually does not achieve particle size below 1 μ the line broadening and intensity losses at higher angles are caused solely by mechanical deformation faulting (plastic deformation) (9).

If x-ray diagrams of hexagonal CdS are carefully examined, many of them show additional rings in the low angle region. Rings were found in the powder diagrams of commercial luminescent CdS pigments (Table II), in the ground substance of a commercially available single crystal photocell, in samples prepared by precipitating cadmium chloride solutions or reacting solid cadmium acetate with H₂S, and in many of the vapor-phase prepared crystals. The sharpness of these additional diffraction rings varies, and sometimes diffuse bands are formed. The measured *d*-values of these lines in the low angle region are given in Table IV. It is interesting to note that a similar type of diffuse low angle reflection was found in powder diagrams of vapor-phase grown cadmium selenide (CdSe) of equal purity.

A microscopical investigation of the polycrystalline CdS rods grown by the vapor-phase method under the conditions of experiment CdS No. 32 (Table III), shows small, type [1] crystals grown with their *c*-axis almost perpendicular to the rod axis. A rotation x-ray diagram taken along the rod axis resolved the powder lines of the low angle diffraction into spots of a layer line diagram with an identity period: $I = 22\text{\AA}$.

In Fig. 2 the fiber diagram is shown of the preferential oriented CdS crystallites in the polycrystalline rod with the layer line diagram of the diffuse low angle spots.

The stoichiometric composition of the samples containing the superlattice was investigated by wet chemical analysis. No evidence, however, was found for the existence of another sulfide or polysulfide. The spectrographic analysis of one of the samples is shown in Table II (CdS No. 32).

More instructive were x-ray diffraction diagrams of the different crystal types [1], [2], [3], and [5]. In the powder diagrams of selected single crystals,

low angle lines were observed only on rectangular and oblique striated types [2] and [3] ribbons. The sharpness of low angle rings varied from sample to sample; the broadening, however, seemed to be related to an increase of the diffuse scattering in this area of the photographic film. In diagrams of type [1] crystals, where no low angle lines are detectable, a considerable increase of the scattered intensity could be observed around the incident beam. This indicated the presence of highly dispersed particles (10) in the matrix of hexagonal CdS. If it is assumed, as would seem probable, that it is the same substance which causes low angle diffraction effects, the correlation is immediately evident. The random disorder in type [1] needles appears to be increasingly ordered to a superlattice in the other types.

Single crystal rotation and precession diagrams with exposure times up to 65 hr around the *a*- and *c*-axis of type [2] and [3] striated crystals were made. Photographs showed spots in addition to those due to the hexagonal CdS lattice. However, because of the weak intensity and their small number, it is not possible at this writing to give a satisfactory correlation between the superlattice reflections and the orientation of the hexagonal CdS matrix.

Therefore, only tentative interpretations can be given about x-ray effects. The superlattice could be caused by: (a) an unknown polymorphic modification of CdS; (b) stacking faults (microtwins) (10–13); and (c) mechanical deformation faulting (14–15).

The dimensions of the unit cell of α -CdS were determined by measurements of the high angle reflections of the unground but sieved substance only:

$$\begin{aligned} a_o &= 4.132 \pm 0.001 \text{ \AA} \\ c_o &= 6.734 \pm 0.004 \text{ \AA} \end{aligned}$$

In the limits of the attained accuracy there is no evidence for changes in cell dimensions between samples prepared at different conditions (Table III). The a_o -value confirms the determination of Kröger (17) ($a_o = 4.131 \text{ \AA}$) obtained on a substance of undisclosed origin and purity. The *c*-dimension of Kröger's sample ($c_o = 6.691 \text{ \AA}$) appears, however, to be slightly smaller.

Electrical and photoconducting properties are obviously closely associated with the above described lat-

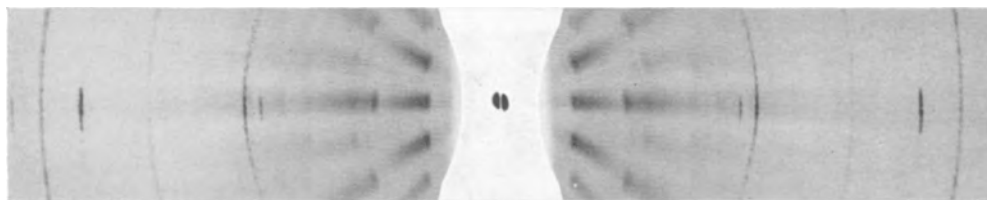


FIG. 2. Fiber diagram of preferential oriented α -CdS crystallites in a polycrystalline rod with the layer lines of the low angle reflections. (Specimen diameter 0.5 mm, rotation along the rod axis, Ni filtered CuK α -radiation.)

tice imperfections of such materials. This and the dependence of the disorder upon the presence of foreign impurities is subject to a further investigation (18).

ACKNOWLEDGMENTS

Acknowledgments are due to the sponsor of the work, the Allen B. DuMont Laboratories, Inc., Passaic, New Jersey, for permission to publish this paper. The author desires to thank G. Costa, I. Corvin, W. C. McCrone, L. V. Azaroff, and W. Oberheim for their discussions and help in performing the experiments.

Any discussion of this paper will appear in a Discussion Section to be published in the December 1955 JOURNAL.

REFERENCES

1. R. LORENZ, *Chem. Ber.*, **24**, 1509 (1891).
2. R. FRERICHS, *Phys. Rev.*, **72**, 594 (1947).
3. M. E. BISHOP AND S. H. LIEBSON, *J. Appl. Phys.*, **24**, 660 (1953).
4. S. J. CZYZAK, D. J. CRAIG, C. E. McCAIN, AND D. C. REYNOLDS, *ibid.*, **23**, 932 (1952).
5. R. CASPARY AND H. MÜSER, *Z. Phys.*, **134**, 101 (1952).
6. L. HERFORTH AND J. KRUMBIEGEL, *Naturwissenschaften*, **40**, 270 (1953).
7. J. E. JACOBS, *Elec. Eng.*, **70**, 667 (1951).
8. I. BROSER AND W. REICHARDT, *Z. Phys.*, **134**, 222 (1953).
9. A. KOCHENDÖRFER, *Z. Krist.*, **105**, 393 (1944).
10. R. GLOCKER, "Materialprüfung mit Röntgenstrahlen, p. 3, A. Springer, Berlin (1949).
11. H. JAGDZINSKY AND F. LAVES, *Schweiz. mineralog. petrogr. Mitt.*, **28**, 456 (1948).
12. H. JAGDZINSKY, *Fortchr. Mineral.*, **28**, 95 (1949).
13. H. MÜLLER, *Neues Jahrb. Mineral. Abhandl.*, **84**, 43 (1952).
14. L. W. STROCK AND V. A. BROPHY, Amer. Cryst. Assoc. Meeting, Ann Arbor, Mich. (1953).
15. C. S. BARRETT, "Imperfections In Nearly Perfect Crystals," John Wiley & Sons, Inc., New York (1952).
16. J. W. CHRISTIAN, *Acta Cryst.*, **7**, 385 (1954).
17. F. A. KRÖGER, *Z. Krist.*, **102**, 132 (1940).
18. Note added in proof: After this work was completed F. A. KRÖGER, H. J. VINK, and J. VAN DEN BOOMGAARD, *Z. Physik. Chem.*, **203**, 1 (1954) reported on the controlled conductivity of CdS crystals.

The Electric Arc as a Circuit Element¹

T. E. BROWNE, JR.

Westinghouse Electric Corporation, Trafford, Pennsylvania

ABSTRACT

Static and dynamic voltage-current characteristics of the electric arc are reviewed, with emphasis on high-current arcs. Typical arc behavior in both d-c and a-c circuits is described with oscillographic examples. The nature and use of some mathematical models for explaining and predicting dynamic behavior of arcs in their connected circuits are considered. Separate contributions to dynamic arc behavior of the arc column and of the electrode regions are discussed.

INTRODUCTION

Since its first scientific study (1) the electric arc has remained an intriguing but rather mysterious phenomenon. The electronic nature of current conduction in the arc was first shown by Weedon (2). Much has been learned since then about the nature of arcs, but they still provide a challenge. Because the theory is incomplete, much of the information about arcs which is available to engineers is necessarily empirical and limited to special cases. Data applicable to higher current arcs are comparatively scarce. This is unfortunate because higher current arcs, which are often of great technical importance, may operate in entirely different regimes with markedly different behavior from arcs with currents near 10 amp, for which the most data are available.

As electrical conductors, arcs exhibit many interesting and often useful properties. These properties may be troublesome, as when they necessitate special stabilizing circuit arrangements for their maintenance in lighting, welding, and furnace applications. Still, their nonlinearity and capacity for rapid change have led to many useful circuit applications in arc oscillators, rectifiers, lightning arresters, and as essential transition elements in power circuit breakers and fuses.

Arcs exist and find important uses in forms and under conditions which are so varied that a general picture is very difficult to present. Even under steady-state conditions, arc behavior depends to a large degree on such factors as electrode material, nature and state of the gas medium, range of current magnitudes, and whether the arc is relatively long or relatively short. Under dynamic conditions, arcs show important additional properties which depend to an essential degree on rates of current change. Often arc behavior is so interrelated with

electrical properties of the connected circuit that it is just as responsive to circuit conditions as it is to the physical state of the arc's surroundings.

EMPIRICAL ARC PROPERTIES

Static Characteristic

Perhaps the most familiar electrical property of an arc under steady conditions is given by its so-called inverse volt-ampere characteristic, illustrated by the curve in Fig. 1. This curve is typical for arcs carrying currents of only a few amperes, a range formerly of much practical interest in connection with arc lamps. A number of equations for this characteristic have been derived from experimental studies. The first and best known such equation is that due to Ayrton (3),

$$V_a = A + BL + \frac{C + DL}{I} \quad [1]$$

expressing the arc voltage, V_a , in terms of the arc length, L , the arc current, I , and the constants A , B , C , and D . This equation was derived primarily for arcs in air with pure carbon electrodes only a few millimeters apart. It was shown by Ayrton and others that arcs with cored carbons, with metal electrodes, or carbon arcs operating in the "hissing" regime occurring at higher currents departed drastically from this relation. Later studies by Nottingham (4, 5) yielded a more generally applicable equation of the same form except that the current was raised to the power n , with n varying according to the anode material from 0.35 for zinc to 1.38 for tungsten. The exponent n was said to vary linearly with the absolute boiling temperature, T , of the anode surface according to the relation

$$n = 2.62 \times 10^{-4} T \quad [2]$$

for arcs in air. For carbon electrodes, n is 1 in agreement with Ayrton. For oxidized copper, n is 0.67. The curve in Fig. 1 has been plotted according to Nottingham's equation, using his values for an arc

¹ Manuscript received March 1, 1954. This paper was prepared for delivery before the Chicago Meeting, May 2 to 6, 1954.

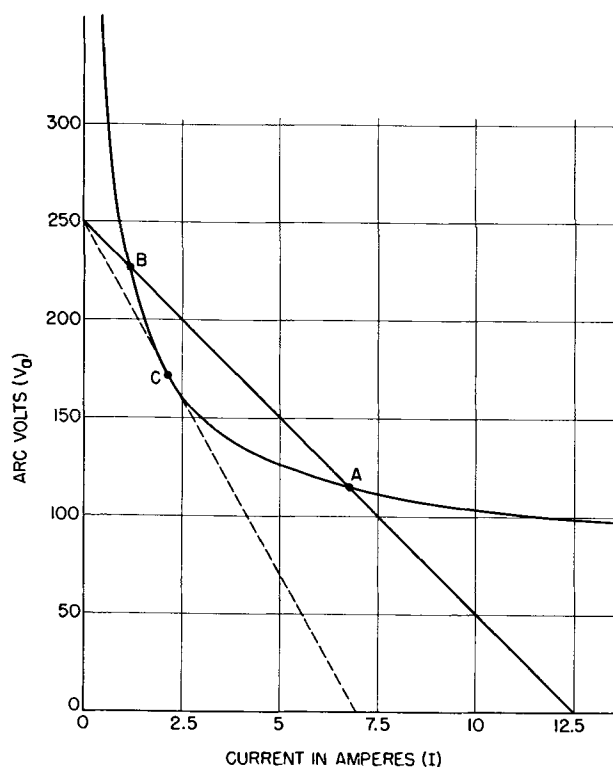


FIG. 1. Static characteristic of a 1.5-in. copper electrode arc in air according to the Nottingham equation.

with oxidized copper electrodes 1.5 in. apart in air. For other gas media, n was different and equation [2] did not apply. The "constant" coefficients in any of the arc equations vary widely with experimental conditions.

Stability requirement.—The first consequence of the falling volt-ampere characteristic is that a steady arc cannot be maintained in a constant emf circuit without a stabilizing series resistance. In Fig. 1 the solid straight line with the equation

$$V_T = 250 - 20 I \text{ volts} \quad [3]$$

gives the available voltage at the terminals of an arc in a 250-volt circuit having a resistance of 20 ohms. Steady arc conditions can exist in this circuit only at the intersection points *A* or *B* where the arc voltage and the available terminal voltages are equal. The arc can operate *stably*, however, only at point *A* where a change in the current would give a voltage unbalance tending to restore the equilibrium. At *B* a current change would give a voltage unbalance tending to further the change, thus prohibiting stable operation at this point. With the conditions illustrated here, lowering the circuit resistance will move the stable operating point *A* to the right, resulting in a higher arc current and a lower arc terminal voltage. The arc current would tend to increase without limit if the circuit resistance were reduced to zero, this being the condition

for a high power "short-circuit." There is also an upper limit for the circuit resistance at this voltage corresponding to the dotted line tangent to the arc characteristic at *C*. As the series resistance is increased from 20 ohms toward the limiting value, about 36 ohms, the stable operating point *A* and the unstable intersection *B* approach each other until they merge at *C*, destroying the condition for stability. When *C* is reached the arc will suddenly "go out," the current dropping to zero and the terminal voltage jumping to the open-circuit value of 250 volts. If there is appreciable inductance in the circuit, the rapid current drop at arc extinction will cause a momentary overvoltage to appear at the arc terminals. With highly inductive circuits this overvoltage may reach dangerous values.

In the opening of direct-current circuits at such voltages and currents that an arc is drawn at the switch contacts, extinction of the arc results generally from *lengthening*, which raises the arc characteristic until it becomes tangent to the fixed V - IR line for the circuit.

Long arcs.—If equation [1] holds over a wide range of the variables, and if L is made sufficiently large, the terms involving A and C may be neglected, and the characteristic equation becomes approximately

$$V_a = L(B + D/I) \quad [4]$$

At small enough currents, the term B in the parentheses may also be neglected, giving

$$V_a = DL/I \quad [5]$$

or

$$V_a I = DL \quad [6]$$

the equation for a rectangular hyperbola with the arc characterized simply by a constant required power per unit length. This limiting approximation is often useful in dealing with long arcs at low currents, as, for example, switch or flash-over arcs in high voltage circuits near the minimum currents at which they may be maintained.

High current arcs.—If in equation [1] the current is sufficiently large, the term containing the current becomes relatively small, and the arc voltage becomes a function only of the arc length according to the equation

$$V_a = A + BL \quad [7]$$

At sufficient lengths the term A may also be neglected, giving an arc voltage proportional only to length,

$$V_a = BL \quad [8]$$

In practice, this assumption is often adequate for representing such arcs as those in high power cir-

cuts under short-circuit conditions, e.g., in power circuit breakers used to clear short circuits.

Under some conditions departure from the assumed arc equation may lead to regimes in which the arc voltage actually rises with arc current. This was observed by Ayrton (3) even at small currents when using cored carbons at short spacings. With long arcs in air at thousands or tens of thousands of amperes, slightly rising volt-ampere characteristics are also observed, due presumably to magnetic effects associated with these currents. Rising characteristics can occur at lower currents also for arcs confined in insulating tubes.

Another noteworthy consequence of the flat or falling volt-ampere characteristic of normal arcs is that such arcs cannot ordinarily be operated in parallel without individual stabilizing resistances.

Nothing has been said so far about the physical basis for the arc characteristic or about numerical values of constants in the arc equations. For short arcs at low currents the observed behavior of these empirical constants is such as to make their theoretical interpretation very difficult, and they vary so much with particular conditions that representative values cannot be stated with any accuracy. For longer arcs, however, some generalizations and some useful values may be noted. For arcs in air at normal pressure and with lengths of a few inches or more, most of the arc voltage exists across the arc column, which has a virtually constant potential gradient. Some 20-40 volts drop (constant A in equation [1]) occurs right at the electrodes and is nearly independent of the arc length. The gradient in the column is almost independent of current magnitude above 50 amp or so and is 12 volts/cm for arcs in the open air (constant B in equation [1]).

Short arcs.—At very short electrode spacings the arc voltage is almost entirely in thin sheaths right at the electrodes and remains virtually constant, being relatively independent of small length variations and of current changes above the range of about 10 amp. The arc characteristic under these conditions is determined principally by the constant A in equation [1]. The constant C always has a relatively small value which may be zero if L is properly measured.

Dynamic Arc Characteristics

With currents changing slowly enough, the voltage drop in an arc follows the static characteristic but, as the current is changed more and more rapidly, hysteresis effects become evident so that the arc voltage departs from the static characteristic by an amount dependent on the rate of current change and the nature and condition of the arc.

This behavior is illustrated schematically in Fig. 2 for an arc with the static characteristic given by the hyperbolic curve AB with dotted extensions. Superimposed on a steady current component i_0 , for which the steady arc voltage is v_0 , is a sinusoidal current oscillation between the limits i_a and i_b . If the frequency of this oscillation, f_1 , is low enough, possibly as low as a few cycles per hour for some arcs, the voltage will retrace the single curve AB , faithfully following the static characteristic. At a somewhat higher frequency, f_2 , current oscillation between the same limits will cause the arc voltage to follow a near-elliptical loop about the single curve AB . With rising current the voltage will be above AB , returning below it for falling current as shown by the arrow points. At a still higher frequency of current oscillation, f_3 , the elliptical curve will change its shape so that its major axis approaches the straight line $A'B'$, while it still retains its clockwise rotation. At a sufficiently high frequency, f_4 , above 100,000 cycles for an arc in air, the arc voltage can be made to follow the single line $A'B'$ very closely. The arc may be said to have an inherent natural frequency of response, f_0 , lying between the values f_2 and f_3 . The extreme fre-

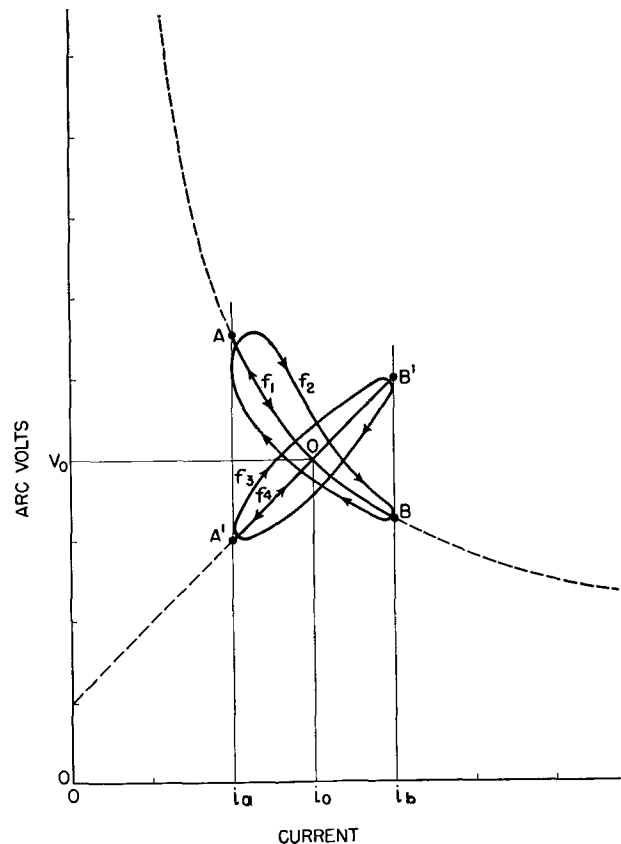


FIG. 2. Dynamic characteristics of arc with current pulsating at successively higher frequencies, $f_1 < f_2 < f_3 < f_4$.

quencies may be characterized by the inequality

$$f_1 \ll f_o \ll f_2 \quad [9]$$

Since the hysteresis effect appears to reside mainly in the arc column, a line through A'B' will not generally pass through the origin. This line represents a constant positive arc column resistance, the value of which is the slope dv/di of the line A'B'. This resistance is in series with relatively constant voltage drops at the electrode surfaces. If for very long arcs electrode drops can be neglected, instantaneous resistance of the arc column at a mean current i_o will be given by the slope of a line from the origin to the point O on the static characteristic. The falling static characteristic clearly results because the arc resistance adjusts itself to the current when the current changes slowly enough. The factors determining the steady burning voltage of the arc column at any given current are complex, but seem to depend mainly on the convective cooling phenomena in and around the column. The dynamic hysteresis appears to be caused by storage in and near the arc column of energy in the form of heat and ionization associated with the column conductance.

Arc oscillator.—If a large value of capacitance is connected in parallel with an arc, it will tend to hold the arc terminal voltage constant, a condition which can lead to instability. This effect is accentuated if the supply circuit has considerable inductance. Such an arrangement employing a smaller inductance in series with the shunting capacitance has been used as a high power oscillator (6). Approximate analysis of this oscillating circuit, shown in Fig. 3, gives the differential equation for the current i in the parallel *LRC* circuit,

$$L \frac{d^2 i}{dt^2} + \left(R + \frac{dV_a}{di} \right) \frac{di}{dt} + \frac{i}{C} = 0 \quad [10]$$

the equation for a damped current oscillation with the effective damping resistance inside the parentheses. The term dV_a/di is the slope of the arc volt-ampere characteristic and is negative for the

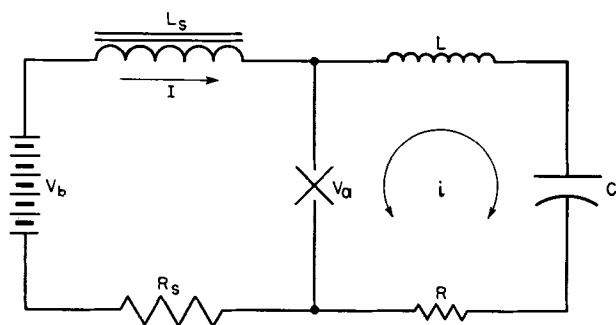


FIG. 3. Circuit of arc oscillator

static characteristic. If the frequency of the superimposed oscillating current i is low enough that the mean slope of the dynamic characteristic, like the loop f_2 in Fig. 2, is negative, the resistance R can be cancelled and the damping brought to zero, giving the necessary condition for a sustained oscillation at the frequency

$$f = \frac{1}{2\pi\sqrt{LC}} \quad [11]$$

By operating the arc in a hydrogen atmosphere and subjecting it to a strong magnetic field, such oscillators can be operated at low radio frequencies.

Alternating-current arcs.—The dynamic volt-ampere characteristics of a-c arcs resemble those for the superimposed oscillation in Fig. 2 except, of course, for the relatively larger amplitude, the symmetry of the oscillation about the zero current axis, and the reversal of polarity of the arc voltage with reversal of the current. At relatively low frequencies, say 60 cycles for an arc in hydrogen, the dynamic characteristic may follow the static characteristic closely except in the immediate vicinity of current zero where the voltage reversal occurs.

Fig. 4 shows a volt-ampere plot from the magnetic oscillogram for one half-cycle of a 60-cycle, 1.5-in. arc in hydrogen with the current limited by inductive reactance plus the arc voltage to about 6.4 rms amperes in a 2300-volt circuit. It is evident that the static characteristic is followed closely except for the peculiar hump just after current zero. This

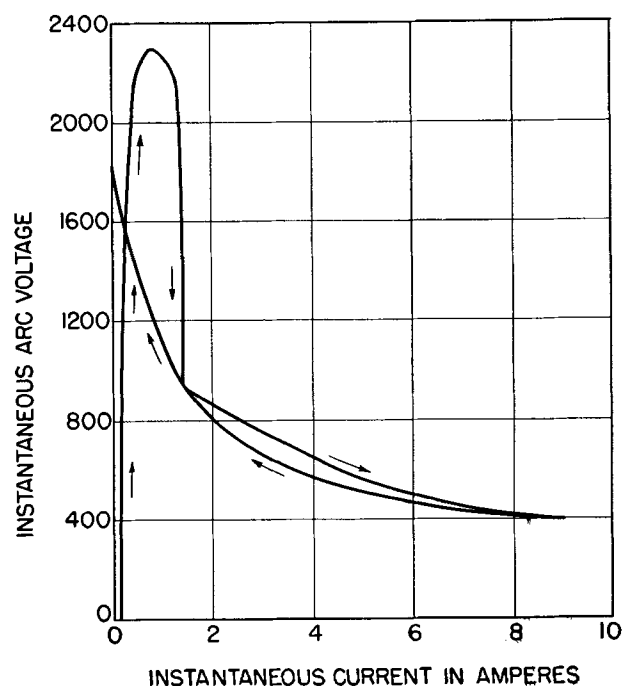


FIG. 4. Volt-ampere cyclogram of 60-cycle arc in hydrogen between copper electrodes 1.5 in. apart.

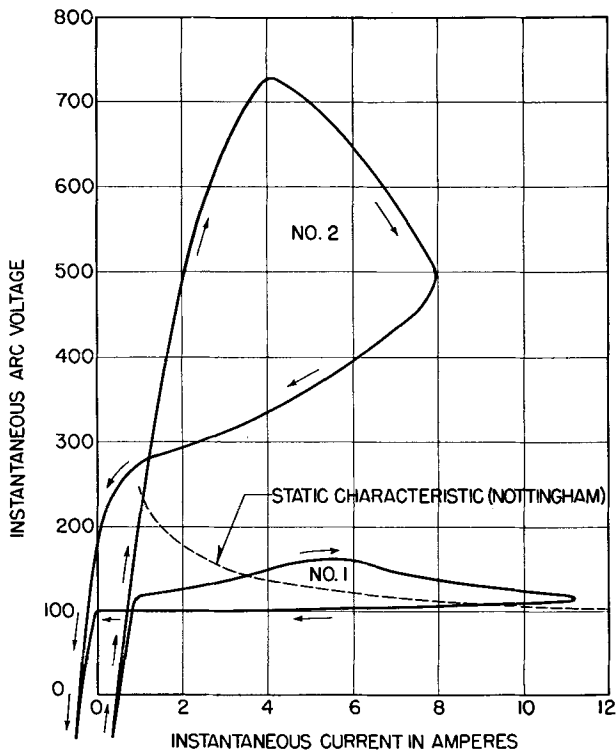


FIG. 5. Volt-ampere cyclograms of 60-cycle arcs in air between copper electrodes 1.5 in. apart. No. 1, arc still about 1.5 in. long; No. 2, arc lengthened by convection almost to breaking point.

hump appears to indicate re-ignition of the arc to a special low-current form which changes to the form normal for higher currents at 1.5 amp. With falling current the arc voltage follows the high-current characteristic right up to current zero. The dynamic volt-ampere characteristic of a similar arc in air is shown in Fig. 5. "No. 1" is for an early half-cycle and "No. 2" is for a half-cycle where the arc had been lengthened by convection almost to the breaking point in a 915-volt reactive circuit. The reversal of the loops near 1 amp in these figures is thought to be due to phase errors in the measuring devices.

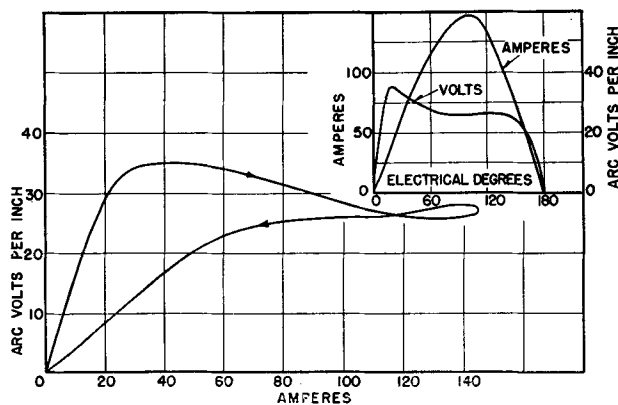


FIG. 6. Volt-ampere cyclogram of vertical 60-cycle arc drawn to a length of 48 in. in a 40-kv circuit in air, 100 amp rms.

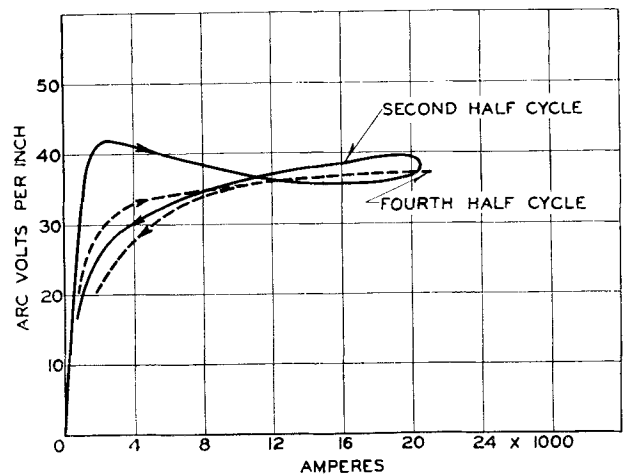


FIG. 7. Volt-ampere cyclograms of vertical 60-cycle arc 12 in. long in air, 15,000 amp rms.

It is evident that 60 cycles is not far from the natural frequency of response of these arcs in still air. The static characteristic shown dotted for comparison is the same as that plotted in Fig. 1.

At 100 amp rms, Fig. 6, taken from a paper by Strom (7), shows a rather similar cyclogram for a 48-in. long vertical 60-cycle arc in air. The time records of current and voltage gradient are shown in the inset. Fig. 7 shows the dynamic characteristics followed in two particular half-cycles by a similar arc 12 in. long carrying 15,000 amp rms. At this high current the upward trend of the arc voltage with current in the 5,000-20,000 amp range is clearly evident. It is believed that the nearly retraced dynamic characteristic should be approximated by equation [8]. On this assumption, the constant B lies between 26 and 38 volts/in.

Fig. 8 shows a cathode-ray volt-ampere cyclo-

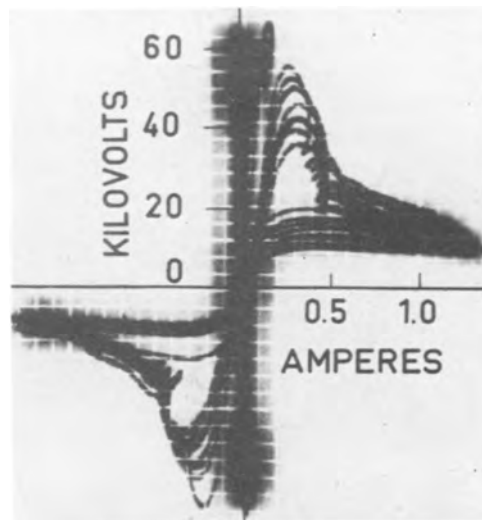


FIG. 8. Cathode-ray volt-ampere cyclogram of vertical 60-cycle arc drawn to a length of 48 in. in a 40-kv circuit in air.

gram of the extinction after somewhat more than one second of a 60-cycle magnetizing current (1.5 amp rms) arc drawn vertically to 48 in. length in a 40 kv circuit. At such a low current the static characteristic should follow the simple hyperbolic equation [6]. The rising (outer) portions of these traces at each polarity do tend to approach rectangular hyperbolas given by $D = 300$ watts/in. in equation [6]. The maintenance requirement for these arcs could be similarly expressed in terms of rms open-circuit volts times short-circuit current as 600 volt-amp/in.

This brief review of a few actual examples of dynamic a-c arc characteristics has shown not only the nature of these characteristics for plain-break arcs carrying 60-cycle currents from 1.5 to 15,000 amp, but also some approximate values applicable to *static* arc characteristic equations over this current range. The above data pertaining to the static open air arc characteristic may be roughly summarized by an equation similar to Ayrton's (3) but neglecting the C term:

$$V_a = 30 (1 + L) + \frac{300 L}{I} \text{ volts} \quad [12]$$

where L is in inches and I in amperes. In using any such equation, however, it must be kept in mind that actual arc voltages are so sensitive to particular conditions that departures from the equation by 100% or more are to be expected. As for the dynamic response of such arcs, it has been shown that they exhibit a great deal of hysteresis with 60-cycle alternating current, indicating that their "natural" response frequency is generally not far above 60 cycles. In hydrogen gas the normal arc form was shown to have a natural response frequency much higher than 60 cycles, but the hydrogen arc may also exist in a different low-current form which appears to have a much lower natural frequency. Very short arcs in which the electrode drops predominate may be expected to have much higher natural frequencies than the relatively long arcs used here as examples. The natural frequency of long arcs can be greatly increased by subjecting them to gas blasts or strong magnetic fields, or by forcing them into intimate contact with cool insulating surfaces.

MATHEMATICAL REPRESENTATION OF DYNAMIC ARC BEHAVIOR

Arc Column

So important are the transient or dynamic properties of arcs in electric circuits that it is worthwhile to try to express these properties mathematically so that they may be included in circuit equations.

Since the electrode regions behave very differently from the column of an arc, the two regions must be considered separately. The following discussion will be limited to the dynamics of the arc *column*.

Development of dynamic arc equations.—The basic assumption upon which mathematical "models" of the arc column are based is that the column conductance per unit length $1/R = I/E$ can be expressed as a prescribed function of the additional stored energy per unit length (often called heat content), Q , associated with the conducting state of the arc column, or

$$\frac{1}{R} = F(Q) = F \left[\int (W - N) dt \right] \text{ mho}, \quad [13]$$

where R = column resistance per unit length, Q = excess energy content per unit length, W = electrical power input, watts per unit length, N = rate of energy loss, watts per unit length, and t = time.

In differential form, this equation is

$$\frac{d}{dt} \left(\frac{1}{R} \right) = (W - N) \frac{\partial F(Q)}{\partial Q} \quad [14]$$

Particular arc model equations depend upon the forms assumed for $F(Q)$ and N . Two workable models have been proposed, each applicable especially to different limiting cases.

Mayr's equation.—The equation proposed and used by Mayr (8, 9) assumes

$$F(Q) = K \exp (Q/Q_0) \quad [15]$$

and

$$N = N_0 \quad [16]$$

where K is an unspecified constant, Q_0 is a constant energy quantity, and N_0 is a constant rate of energy loss, all per unit length of the column. Since in the steady state

$$N = W = EI \quad [17]$$

(E is the column voltage *gradient*), relation [16] defines an arc column with the static characteristic

$$EI = N_0 \quad [18]$$

or

$$V_a I = N_0 L \quad [19]$$

which is the same as equation [6] if N_0 is identified with the constant D . Thus from the static viewpoint this model is best adapted to the low-current range of arc behavior, a range which is important when considering the *extinction* of high-power arcs. The quantity Q_0 is defined by relation [15] as that energy quantity, the loss or gain of which is accompanied by a change in the arc column conductance by the factor e (2.718). This quantity, Q_0 , combined with the rate of energy loss, N_0 , determines the characteristic response frequency, f_0 , of the arc, or inversely the arc's *time constant*, which may be given

the symbol θ and conveniently defined by the relation

$$\theta = Q_0/N_0 \quad [20]$$

Substitution of these three relations in the general equation [14] yields Mayr's arc model differential equation

$$R \frac{d}{dt} \left(\frac{1}{R} \right) = \frac{1}{\theta} \left(\frac{W}{N_0} - 1 \right) \quad [21]$$

If W is expressed as I^2R , this becomes

$$\frac{d}{dt} \left(\frac{1}{R} \right) + \frac{1}{\theta} \left(\frac{1}{R} \right) = \frac{I^2}{\theta N_0} \quad [22]$$

which is a linear first order equation if the current $I = I(t)$ is determined solely by the connected circuit. If, on the other hand, W is written as E^2/R , where E is the column voltage gradient, equation [21] becomes

$$\frac{dR}{dt} - \frac{R}{\theta} = - \frac{E^2}{\theta N_0} \quad [23]$$

which is a linear first order equation in R if the arc column gradient $E = E(t)$, is determined by the connected circuit alone. These equations have been used by Mayr to illustrate the behavior of arcs under a variety of interesting circuit conditions.

Cassie's equation.—A second arc model (10) assumes a column conductance simply proportional to Q , expressible by the relation

$$\frac{1}{R} = \frac{Q}{\theta E_0^2} \quad [24]$$

and a power loss per unit length also proportional to Q according to

$$N = Q/\theta \quad [25]$$

where E_0 is a characteristic voltage gradient. Substituting these relations in the basic equation [14] yields Cassie's differential equation which can be written

$$R \frac{d}{dt} \left(\frac{1}{R} \right) = \frac{1}{\theta} \left[\left(\frac{E}{E_0} \right)^2 - 1 \right] \quad [26]$$

For this equation, the steady-state condition giving the static arc characteristic is

$$E = E_0 \quad [27]$$

or

$$V_a = E_0 L \quad [28]$$

which is the same as equation [8] for a high current arc if E_0 is identified with the constant B . Cassie's equation, then, is most suitable for representing the arc column when its current is relatively large.

As before, linear first order equations may be obtained from [26] for cases where the circuit is an

"infinitely stiff" source of either current or voltage. For impressed *current*, the equation can be written more conveniently

$$\frac{d}{dt} \left(\frac{1}{R^2} \right) + \frac{2}{\theta} \left(\frac{1}{R^2} \right) = \frac{2}{\theta} \left(\frac{I}{E_0} \right)^2 \quad [29]$$

which is linear in $1/R^2$. For impressed *voltage*, the equation may also be slightly simplified to

$$\frac{dR}{dt} = \frac{R}{\theta} \left(1 - \frac{E^2}{E_0^2} \right) \quad [30]$$

which is linear in R .

Uses of arc equations:

Applied voltage.—Simpler uses of the arc models involve only the easily solved linear differential equations [22], [23], [29], and [30]. For E constant, equation [30] can be readily integrated to

$$R = R_0 \exp \left[\left(1 - \frac{E^2}{E_0^2} \right) \frac{t}{\theta} \right] \quad [31]$$

where R_0 is the value of R at $t = 0$. This shows that Cassie's model, like the actual arc, is unstable in a circuit which impresses a fixed voltage gradient, E , since any sustained nonzero value of the exponent will cause the exponential eventually to approach either zero or infinity, for which values the arc is either a short circuit or an open circuit. A similar inspection of the other equations shows that for either model a fixed *voltage* causes instability while conversely a fixed *current* always leads to stable operation. The same is true in general for any forms of rigidly impressed voltage or current varying only with time. For the special case of zero applied voltage Cassie's and Mayr's models both give the same result

$$R = R_0 \exp (t/\theta) \quad [32]$$

showing an arc resistance approaching infinity exponentially with the time constant θ . There is always some critical magnitude of any arbitrarily applied voltage gradient above which the resistance approaches zero instead of infinity. This critical gradient may be considered a breakdown value. Mayr (8) has worked out critical breakdown values and the behavior of arc resistance in terms of the constants of his arc model for various forms of applied voltage as functions of time. These results are significant particularly for the study of extinction or reignition just after current zero of a long a-c arc. The author (11) has extended this study by combining Mayr's model for impressed voltage in the period after current zero with Cassie's model for a large impressed current during the conducting period prior to current zero. The behavior of this composite model can be expressed in terms of the amplitude and frequency of the prior current as

well as the arc conditions, θ and E_o , and the form of the restored voltage.

Applied current.—A solution of Mayr's equation [21] for impressed current which is of special interest is that for a sine-wave alternating current $I = I_1 \sin \omega t$, giving the dynamic characteristic of an a-c arc in a reactive circuit with generated voltage much larger than the arc voltage. This is the usual case for arcs in circuit breakers interrupting a-c short circuits.

For the cyclic steady state (each successive cycle the same) Mayr gives a solution for the arc voltage gradient which leads to

$$E = \frac{2E_1 \sin \omega t}{1 - \frac{\sin(2\omega t + \varphi)}{\sqrt{1 + (2\omega\theta)^2}}} \quad [33]$$

where

$$\varphi = \cot^{-1}(2\omega\theta) \quad [34]$$

and

$$E_1 = N_o/I_1 \quad [35]$$

is the voltage gradient on the static arc characteristic at the peak current, I_1 . For 60-cycle arcs E_1 is very nearly the actual arc gradient at and near the current peak where dI/dt is near zero. Fig. 9 shows a number of a-c volt-ampere cyclograms plotted according to equation [33] for several values of the product $\omega\theta$, which expresses the relation between

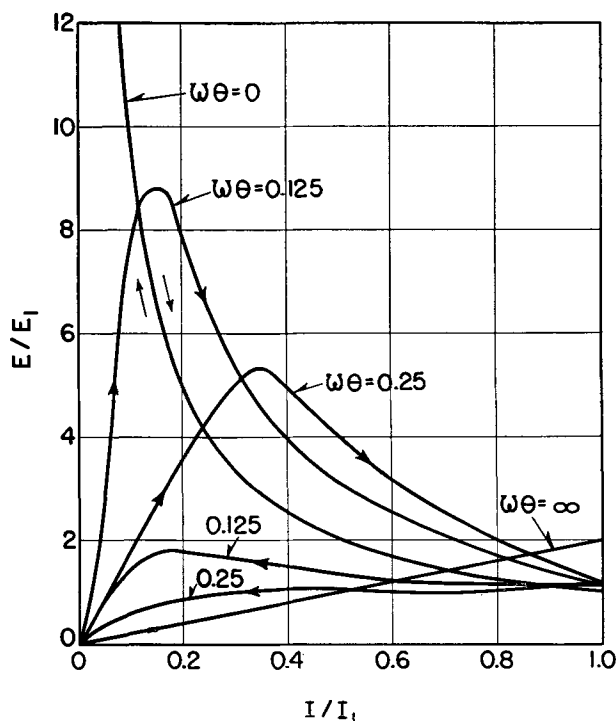


FIG. 9. Dynamic a-c arc characteristics computed by O. Mayr (8) from his arc equation. θ = Arc time constant; ω = angular frequency of arc current; $I = I_1 \sin \omega t$.

the frequency of the current and the natural frequency of response of the model arc column. The general resemblance of some of these curves to the oscillographic traces in Fig. 8 is evident.

A mathematically simple treatment of the arc model behavior near current zero for an a-c arc will be demonstrated for Cassie's model. For the region near current zero where $\omega \ll \pi/2$ the sine wave of current is given with sufficient accuracy by the simple linear expression,

$$I = I_1 \omega t \quad [36]$$

which, when substituted in equation [22], gives an expression for the arc resistance. When multiplied by the current this gives the arc voltage gradient in terms of time for the cyclic steady state,

$$E = \sqrt{2} E_o \frac{t/\theta}{\sqrt{1 - t/\theta + 2(t/\theta)^2}} \quad [37]$$

Fig. 10 shows a plot in dimensionless coordinates of this equation with the negative time portion superimposed on that for positive time to simulate a volt-ampere cyclogram for one half-cycle. As shown, the linear current variation permits interpreting the abscissa units as either t/θ or $I/I_1\omega\theta$, as related through equation [36]. The general resemblance between these curves and the oscillographic records for the long 60-cycle arcs in Fig. 6 and 7 indicate the suitability of Cassie's arc model equation for approximating the dynamic behavior of arcs carrying power-frequency currents of hundreds or thousands of amperes.

By comparing actual dynamic arc characteristics with plots for the appropriate models, one can estimate values of the time constant θ for these arcs. For example, the re-ignition voltage peak occurs in the Cassie model plot, Fig. 10, at $I = I_1\omega\theta$; so $\omega\theta$ should be given by the value of I/I_1 at the ob-

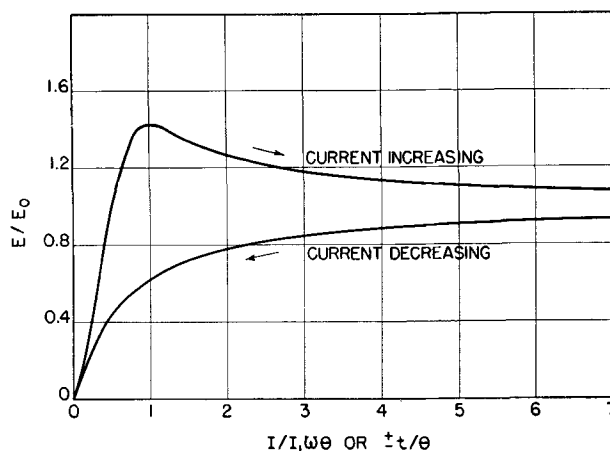


FIG. 10. Dynamic a-c arc characteristic near current zero. Computed from A. M. Cassie's arc equation for higher current arcs. θ = Arc time constant; current: $I = I_1 \omega t$.

served voltage peak for any a-c arc behaving according to Cassie's equation. The estimates of θ by this means for the 60-cycle arcs of Fig. 6 and 7 are about 800 and 300 μsec , respectively, for the second half-cycle. If the curves in Fig. 8 are judged to correspond most nearly to a curve for $\omega\theta = 0.2$ in Fig. 9, the indicated value in Mayr's model for the 1.5 amp arc of Fig. 8 would be about 500 μsec . The fact that these estimated values are all of the same order tends to support a basic assumption underlying the use of these models that θ is a characteristic arc constant not primarily dependent on the current magnitude. In treating the case of a small amplitude current oscillation superimposed on a constant arc current, Mayr shows that the natural response frequency of a model arc column may logically be defined as the frequency for which $\omega\theta = 1$. From this,

$$f_o = \frac{1}{2\pi\theta} \quad [38]$$

giving indicated values of about 200, 500, and 300 cycles/sec, respectively, for the arcs of Fig. 6, 7, and 8.

Interaction of arc with circuit.—Unfortunately, the arc model equations [21] and [26] without restrictions on interaction with the connected circuit are nonlinear and so not amenable to straightforward general solutions. Mayr, however, has shown a graphical method (9) for getting approximate solutions showing the behavior of his arc model in a simple circuit with capacitance directly in parallel with the arc and resistance limiting the current from a constant potential source. The circuit is that of Fig. 3 with all values zero except R_s and C . In general, the graphical solutions gave spirals on the voltage-current diagram either converging to or diverging from a point on the static arc characteristic corresponding to the point A in Fig. 1 for a stable arc in a purely resistive circuit. More or less similar spirals often are observed in actual volt-ampere oscillograms of long arcs re-igniting after a current zero, as for example in Fig. 8.

Another useful approximate method for dealing with the nonlinear arc model equations is that of small variations. For combination with circuit equations it is convenient to express arc resistance or conductance in terms of the current and voltage gradient, giving for Mayr's equation [21]:

$$\frac{1}{I} \frac{dI}{dt} - \frac{1}{E} \frac{dE}{dt} = \frac{1}{\theta} \left(\frac{EI}{N_o} - 1 \right) \quad [39]$$

If $I = I_1 + i$ and $E = E_1 + e$, where I_1 and E_1 are constant values on the static characteristic with $E_1 I_1 = N_o$, $i \ll I_1$, and $e \ll E_1$, neglect of minor

terms gives the linear first order equation in two unknowns,

$$E_1 \frac{di}{dt} - I_1 \frac{de}{dt} = \frac{E_1 i + I_1 e}{\theta} \quad (40)$$

which can be solved in combination with linear equations of the connected circuit by converting the gradients to total voltages for a constant arc length, L . Although these solutions are valid only for small excursions from the steady state, they are useful for investigating *stability* conditions. It is interesting to note that equation [40] for small deviations only can be obtained from Cassie's equation [26] as well as from Mayr's equation [21] if E_1 is taken equal to E_o .

Mayr has shown (8) the mathematical details of these solutions for a number of simple circuit arrangements. One result of great simplicity and also of special interest was obtained for a circuit with capacitance directly in parallel with the arc. The special limitation is that the source resistance or inductance is so high that the total current to the arc and its shunting capacitance is held constant or permitted to change only at a rate small compared with possible rates of variation in arc current. If the steady-state arc resistance (total) is

$$R_s = \frac{E_1 L}{I_1} \quad [41]$$

the limiting condition for arc stability proves to be simply

$$R_s C = \theta \quad [42]$$

or equality between the time constant of the arc and the time constant for discharge of the shunting capacitance through the arc's momentary resistance. For $R_s C < \theta$ any small departure from the steady state tends to disappear; for $R_s C > \theta$, such a departure tends to increase, leading to oscillations of increasing amplitude which may result in arc extinction. If the second inequality is great enough, arc extinction may occur in a simple exponential manner without oscillation.

From a physical viewpoint, one may say that in a circuit where the arc is stabilized by a large source impedance, the presence of capacitance in parallel with the arc may lead to instability if

$$C \gtrsim \theta/R_s \quad [43]$$

In terms of voltage and current, the instability condition is

$$I_1 \leq CV_a/\theta \quad [44]$$

where $V_a = E_1 L = R_s I_1$. This shows that, for a circuit-controlled current approaching zero, some limiting value will be reached at which the residual

capacitance shunting the arc terminals will cause instability, and the arc will "go out" before the actual current zero is reached. This is a common situation with a-c arcs in highly inductive (low power factor) circuits. When arc failure just before a normal current zero occurs at the instantaneous current I_1 in equation [44], the current is diverted into the shunting capacitance, which generally includes the equivalent parallel capacitance associated with the current limiting impedance. The current diversion will occur in a time of the order of θ , which is often so short on the time scale of the normal or circuit-impedance-limited current fall that the diversion may be considered instantaneous. In this case, most of the stored energy associated with the arc failure current I_1 in the circuit inductance must reappear in the shunting capacitance, which will be charged to a peak voltage given approximately by

$$V_p = I_1 \sqrt{L/C} \quad [45]$$

Substituting for I_1 from equation [44]

$$V_p = V_a \sqrt{LC}/\theta \quad [46]$$

showing that the voltage "surge" resulting from arc failure, often called "current chopping," increases with the arc voltage, with the reciprocal of the arc time constant, and also with the product of the circuit inductance *times the shunting capacitance*. This shows the basis for a fact often observed (12) but not always fully appreciated, that the addition of shunting capacitance may actually *accentuate* rather than suppress overvoltage surges resulting from current chopping by a-c arcs.

Electrode regions.—Conditions at anode and cathode terminals of an arc are so incompletely understood that dynamic equations for the voltage drops in these regions are not generally attempted, although it does appear that part of the hysteresis effects in the voltage of relatively short arcs does reside in these regions.

Emanating from both the anode and the cathode of high-current arcs are high-velocity vapor blasts which may markedly affect conditions in the arc column as well as the anode and cathode voltage drops. The effective time constant θ of the cathode drop for a thermionic cathode, which is the normal type when refractory cathode materials like carbon or tungsten are used, might be expected to be much greater than for a so-called "cold" cathode existing on low-boiling metals. The voltage drops at the latter type of cathode and at the anode appear to depend on phenomena taking place in such extremely thin layers of gas at the electrode surfaces that their thermal or electrical inertia is necessarily exceedingly small—very much less than the smallest

values of θ observed for arc *columns*. This is true even for those columns existing in intense gas blasts. That very short time constants are characteristic of these electrode regions is illustrated by sudden jumps in arc voltage often observed near current zero and attributable to transitions between the *arc* cathode with around 10 volts drop and the *glow* cathode with a few hundred volts drop. These short electrode-region time constants help explain, with the aid of equation [44], the relative instability of short metal-electrode arcs. The stabilizing effect of carbon or tungsten electrodes with their slow-responding thermionic cathode spots is similarly explainable.

Short a-c arcs between low-boiling metal electrodes are subject to a special kind of instability sometimes called the rectifying effect, resulting from the loss of the cathode spot when the current passes through zero and tries to reverse. In the absence of electrode temperatures high enough for copious thermionic emission, a new cathode spot must be formed by breakdown of a gaseous space charge layer requiring a few hundred volts minimum (13). Further increase in the required restriking voltage after a current zero results if the circuit natural frequency is such that a few tens or hundreds of microseconds delay occurs in the application of voltage. The rate of this recovery of dielectric strength with time after current zero has been found (14) to be higher for *shorter* electrode separations, for lower boiling temperatures of the electrode surfaces, and for lower 60-cycle current magnitudes.

CONCLUSION

The foregoing discussion of electrical characteristics of arcs, both static and dynamic, has emphasized features believed to be most significant in present-day applications. Some mathematical techniques applicable to calculation of transient conditions in circuits including electric arcs have been outlined. It should be recognized that actual arc behavior is generally so sensitive to small variations in conditions and so incompletely understood in detail that only very approximate calculations can be justified. Nevertheless, it is hoped that this presentation may be of some use as a starting point in attempts by engineers to understand and analyze approximately the behavior of circuits and devices involving arcs.

Any discussion of this paper will appear in a Discussion Section to be published in the December 1955 JOURNAL.

REFERENCES

1. H. DAVY, "Elements of Chemical Philosophy," Vol. I, p. 152, Smith & Elder, London (1812).

2. W. S. WEEDON, *Trans. Amer. Electrochem Soc.*, **5**, 171 (1904).
3. H. AYRTON, "The Electric Arc," *The Electrician*, London (1902).
4. W. B. NOTTINGHAM, *Trans. Am. Inst. Elec. Engrs.*, **42**, 302 (1923).
5. W. B. NOTTINGHAM, *Phys. Rev.*, **23**, 764 (1926).
6. V. POULSEN, *Electrotech. Z.*, **27**, 1040 (1906).
7. A. P. STROM, *Trans. Am. Inst. Elec. Engrs.*, **65**, 113 (1946).
8. O. MAYR, *Arch. Elektrotech.*, **37**, 588 (1943).
9. O. MAYR, *Electrotech. Z.*, **64**, 645 (1943).
10. A. M. CASSIE, "Arc Rupture and Circuit Severity: A New Theory," International Conference on Large Electric High-Tension Systems, Paris, pp. 1-14 (1939).
11. T. E. BROWNE, JR., *Trans. Am. Inst. Elec. Engrs.*, **67**, 141 (1948).
12. H. M. WILCOX AND B. P. BAKER, *Trans. Am. Inst. Elec. Engrs.*, **67**, 154 (1948).
13. F. C. TODD AND T. E. BROWNE, JR., *Phys. Rev.*, **36**, 732 (1930).
14. T. E. BROWNE, JR., *Trans. Am. Inst. Elec. Engrs.*, **50**, 1461 (1931).

Diffusion of Cobalt in Molybdenum¹

E. S. BYRON² AND V. E. LAMBERT

Lamp Division, Westinghouse Electric Corporation, Bloomfield, New Jersey

ABSTRACT

Diffusion coefficients for cobalt in molybdenum were determined at 900°, 1100°, 1275°, 1500°, and 1700°C. In the equation relating diffusion coefficient with temperature, $D = Ae^{-Q/RT}$, the activation energy Q derived was 34,800 cal/mole, and the constant A was 2.82×10^{-6} cm²/sec.

INTRODUCTION

Diffusion coefficients for cobalt in molybdenum were determined in order to estimate minimum sintering times for complete homogenization for powder metallurgy applications. Ruder and Birch- enall (1) report the self diffusion of cobalt as $D = 0.032 \exp(-61,900/RT)$ cm²/sec, and the diffusion of cobalt in nickel as $D = 1.46 \exp(-68,300/RT)$ cm²/sec, but no data were found for diffusion of cobalt in molybdenum.

A small solid solution concentration range is involved in this system, the maximum solubility of cobalt in molybdenum being around 3 wt % at 1620°C according to the phase diagram of Sykes and Graff (2), and decreasing to about half of one per cent at room temperature.

THEORY

It can be shown theoretically that the rate of advance of a zone of concentration is a simple function of the diffusion coefficient, and for linear diffusion, Barrer (3) states the rate is likely to be governed by the equation

$$W^n = 4Dt \quad (I)$$

where W denotes the distance of discontinuity from the origin, D is the diffusion coefficient, t is the time, and $n = 2$.

The theoretical work of Fick was published in 1855 and is still regarded as the descriptive basis of diffusion theory. The diffusion at 1500° and 1700°C was determined by the method outlined by Rhines and Mehl (4) of analyzing chemically the chips machined at increments from the interface and applying Matano's solution of Fick's law,

$$\frac{\partial c}{\partial t} = \frac{\partial}{\partial x} \left(D \frac{\partial c}{\partial x} \right) \quad (II)$$

¹ Manuscript received April 27, 1953. This paper was prepared for delivery before the New York Meeting, April 12 to 16, 1953.

² Present address: Sylvania Electric Products Inc., Towanda, Pa.

which provides for the possibility of a variation of D with concentration c . For constant time t , Rhines and Mehl simplify equation (II) to,

$$D = \frac{1}{2t} \frac{dx}{dc} \int_0^c x dc \quad (III)$$

and this equation was used to solve graphically for D , where dx/dc is the slope of the penetration curve at concentration c , and $\int_0^c x dc$ is the area enclosed by the curve, the interface, and the limits of concentration O and C . The interface used in defining the area $\int_0^c x dc$ is not the original interface, but is defined as the surface through which an equal number of the two kinds of atoms have passed in opposite directions. In using equation (III), the diffusion is considered planar rather than radial.

The universally accepted form of the equation relating D with temperature is,

$$D = Ae^{-Q/RT} \quad (IV)$$

where D , the diffusion coefficient, represents the atomic mobility, and Q , the activation energy, is a measure of the potential barrier that surrounds a diffusing atom. A is a constant, T the absolute temperature, and R the gas constant. In logarithmic form the equation is,

$$\log_e D = \log_e A - Q/RT \quad (V)$$

and when the natural logarithm of D is plotted against the reciprocal of the absolute temperature, the slope is Q/R .

PROCEDURE

900°, 1100°, and 1275°C Runs.—Cobalt-molybdenum couples were prepared by inserting a rod of cobalt into a hollow cylinder of molybdenum and closing the opening with a molybdenum plug. The cobalt inner rod was 0.250 in. in diameter by 1 in. long. The outer cylinder, 0.250 in. I.D. by $\frac{5}{8}$ in. O.D. by 2 in. long, was made from swaged molybdenum rod.

The couples were placed upright in a furnace at room temperature, heated to temperature, and held

for different times in a hydrogen atmosphere. After cooling to room temperature, the specimens were cut at midsection for metallographic examination.

After etching with a solution of 4 parts to 1 by volume of 30% H₂O₂ and 85% H₃PO₄, the widths of the Co-Mo phase were measured directly on the specimens with a Gaertner comparator. Widths were determined also by measuring with a vernier to 0.001 in. on a ground glass screen at 1000× projection, and again by scaling from photomicrographs made at 500× magnification. Neither of the latter two methods appeared to be as reliable as direct measurement with the comparator.

1500° and 1700°C Runs.—The couples for these runs consisted of an inner rod of an alloy of molybdenum and 3.42% cobalt, prepared by powder metallurgy technique, and an outer cylinder of molybdenum with molybdenum plugs at each end. The alloy of 3.42% cobalt was chosen in preference to pure cobalt to eliminate the possibility of melting, and to have a single-phase system. The inner cylinder was 0.375 in. in diameter by 2-3/4 in. long; and the outer cylinder

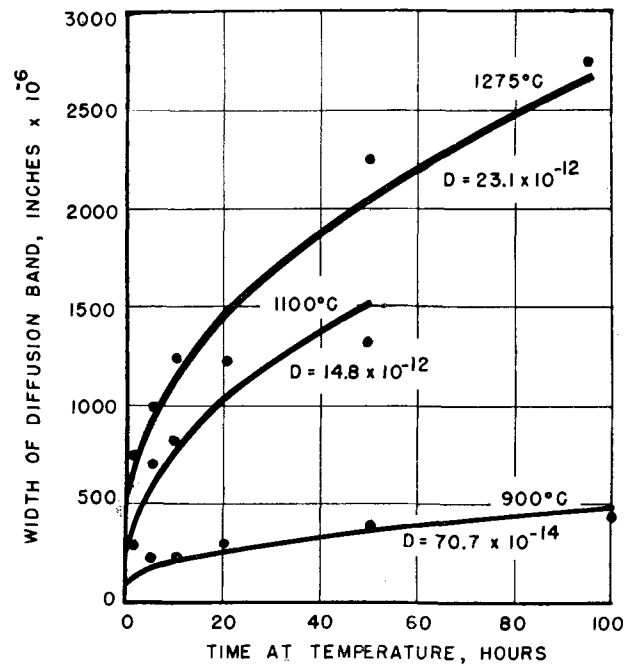


FIG. 1. Width of diffusion band of Co-Mo phase

TABLE I. Width of diffusion band of single-phase Co-Mo for 900°, 1100°, and 1275°C determinations

Diffusion temp, °C	Experimental data		Data using first measured width as starting point		Calculated <i>D</i> using data of (C) and (D) and equation $W^2 = 4 \cdot D \cdot T$ (cm ² /sec)
	Time at temp, hr (A)	Width* of diffusion band, in. × 10 ⁻⁶ (B)	Time, hr (C)	Width in. × 10 ⁻⁶ (D)	
900	0	96†	—	—	—
	1	136	4	92	94.8 × 10 ⁻¹⁴
	5	228	9	120	71.7 × 10 ⁻¹⁴
	10	256	19	183	79.0 × 10 ⁻¹⁴
	20	319	49	266	64.7 × 10 ⁻¹⁴
	50	402	99	309	43.2 × 10 ⁻¹⁴
	100	445	—	—	Avg 70.7 × 10 ⁻¹⁴
1100	0	227†	—	—	—
	1	318	4	392	17.2 × 10 ⁻¹²
	5	710	9	513	13.1 × 10 ⁻¹²
	10	831	19	922	20.0 × 10 ⁻¹²
	20	1240	49	987	8.9 × 10 ⁻¹²
	50	1305	—	—	Avg 14.8 × 10 ⁻¹²
1275	0	465†	—	—	—
	0.5	563	0.5	187	31.3 × 10 ⁻¹²
	1	750	4.5	437	19.0 × 10 ⁻¹²
	5	1000	9.5	687	22.3 × 10 ⁻¹²
	10	1250	19.5	875	17.6 × 10 ⁻¹²
	20	1438	49.5	1687	25.8 × 10 ⁻¹²
	50	2250	94.5	2187	22.7 × 10 ⁻¹²
95	2750	—	—	Avg 23.1 × 10 ⁻¹²	

* Measured on specimen with comparator to 10⁻³ MM.

† Calculated width for time furnace and specimen is coming up to temperature.

was 0.375 in. I.D. by 5/8 in. O.D. by 3-3/4 in. long. The couples were heated for 95 hr at temperature in a hydrogen atmosphere in a refractory lined furnace and then removed for machining of 0.010 in. diameter cuts.

DISCUSSION OF EXPERIMENTAL DATA

The widths of the phase Co-Mo in the 900°, 1100°, and 1275°C runs are listed in Table I and plotted in Fig. 1. Analysis of the data by the method of least squares gave values of *n* = 2.47, 2.22, and 2.07. Using the accepted value of 2 for *n*, values of *D* were computed from the widths of the diffusion band. Photo-

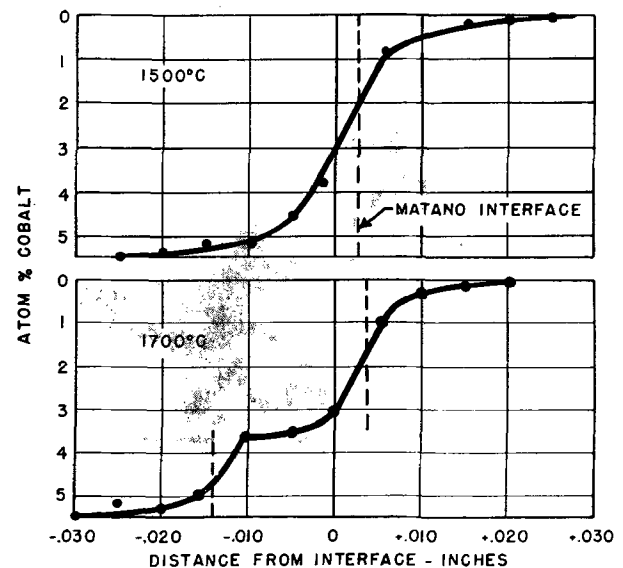


FIG. 2. Concentration-distance curves

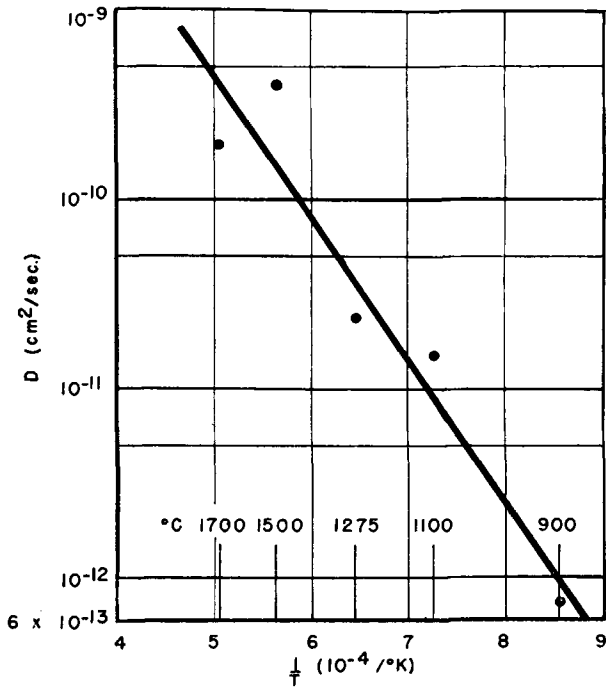


FIG. 3. Temperature dependence of diffusion coefficient

micrographs of the 1- and 50-hr specimens at 900°C are typical of the appearance at the interface and are reproduced in Fig. 4 and 5 at 500× magnification.

The *c-x* data for the 1500° and 1700°C runs are listed in Table II and plotted in Fig. 2. The concentration ratio-distance data are also listed in Table II. When the latter data were plotted on prob-

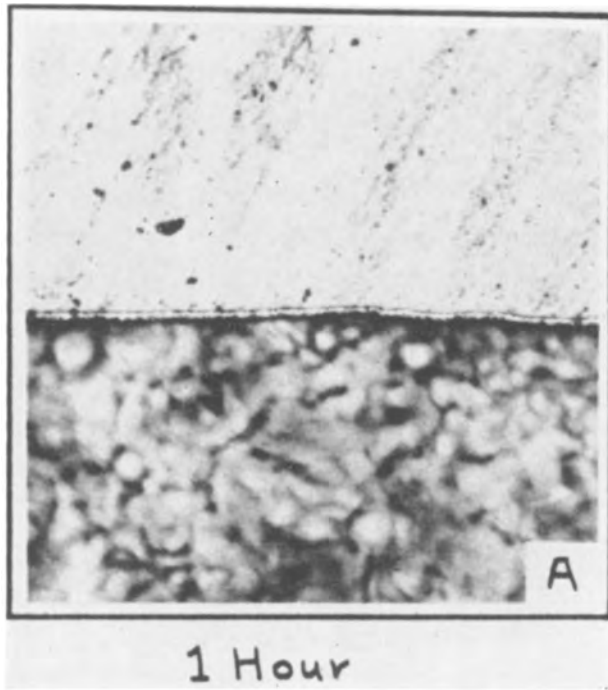


FIG. 4. Co-Mo band after 1 hr at 900°C. Magnification, 500×. Etch, 4:1 H₂O₂:H₃PO₄.

TABLE II. Concentration—distance data for 1500° and 1700°C determinations

Temp, °C	Range of diameter of cut, in.	Distance from interface, in.	Cobalt		C - C ₀ * C ₁ - C ₀
			Wt %	Atom %	
1500	0.430-.420	+0.025	0.010	0.016	0.0029
	0.420-.410	+0.020	0.022	0.036	0.0066
	0.410-.400	+0.015	0.091	0.148	0.0272
	0.400-.375	+0.0063	0.546	0.890	0.163
	0.375-.370	-0.0013	2.37	3.81	0.700
	0.370-.360	-0.005	2.81	4.50	0.825
	0.360-.350	-0.010	3.24	5.17	0.948
	0.350-.340	-0.015	3.23	5.15	0.944
	0.340-.330	-0.020	3.40	5.42	0.995
	0.330-.320	-0.025	3.41	5.44	0.997
1700	0.320-.310	-0.030	3.42	5.45	1.000
	0.430-.420	+0.025	0.003	0.005	0.00092
	0.420-.410	+0.020	0.003	0.005	0.00092
	0.410-.400	+0.015	0.014	0.123	0.0226
	0.400-.390	+0.010	0.111	0.181	0.0332
	0.390-.380	+0.005	0.602	0.978	0.179
	0.380-.370	Interface	1.90	3.03	0.556
	0.370-.360	-0.005	2.18	3.51	0.644
	0.360-.350	-0.010	2.20	3.54	0.650
	0.350-.340	-0.015	3.16	5.05	0.926
0.340-.330	-0.020	3.26	5.19	0.953	
0.330-.320	-0.025	3.24	5.17	0.949	
0.320-.310	-0.030	3.42	5.45	1.000	

* C = Cobalt concentration at distance from interface.
C₀ = Minimum cobalt concentration.
C₁ = Maximum cobalt concentration.

TABLE III. Derived diffusion coefficients from 1500° and 1700°C runs

Temp, °C	Cobalt		D cm ² /sec
	Atom %	Wt %	
1500	0.1	0.062	3.53 × 10 ⁻¹⁰
	0.5	0.300	6.17 × 10 ⁻¹⁰
	1.0	0.650	3.53 × 10 ⁻¹⁰
	2.0	1.25	3.94 × 10 ⁻¹⁰
	3.0	1.90	4.30 × 10 ⁻¹⁰
	4.0	2.50	3.60 × 10 ⁻¹⁰
Avg			4.18 × 10 ⁻¹⁰
1700 (single phase)	0.1	0.062	2.80 × 10 ⁻¹⁰
	0.5	0.300	2.85 × 10 ⁻¹⁰
	1.0	0.650	1.27 × 10 ⁻¹⁰
	2.5	1.55	1.39 × 10 ⁻¹⁰
	3.0	1.90	1.75 × 10 ⁻¹⁰
	3.5	2.20	1.50 × 10 ⁻¹⁰
Avg			1.93 × 10 ⁻¹⁰
1700 (two phase)	4.0	2.50	0.47 × 10 ⁻¹⁰
	4.5	2.80	1.39 × 10 ⁻¹⁰
	5.0	3.15	5.57 × 10 ⁻¹⁰

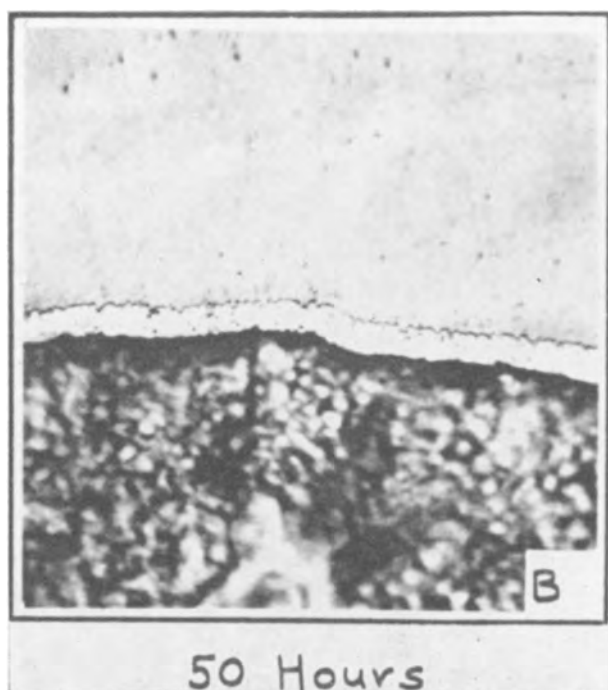


FIG. 5. Co-Mo band after 50 hr at 900°C. Magnification, 500 \times . Etch, 4: 1 H₂O₂:H₂PO₄.

ability paper, either a slightly curved line or a straight line fitted the 1500°C run. The points all fell on a curved line for the 1700°C run. DaSilva and Mehl (5) point out that the plot on probability paper makes it much easier to draw a best fit to eliminate doubtful points. Wells (6) states a curved line indicates a variation of D with C and the Matano method of analysis should be used. The derived diffusion coefficients listed in Table III do not show a consistent variation of D with increasing cobalt but, as previously pointed out, a rather small range of concentration is considered.

The variation of D with temperature has been plotted in Fig. 3.

Values of Q and A were derived from the experimentally determined values of D from runs at the three lower temperatures. Q and A were based on these values of D because 21 specimens were used compared to the 2 specimens for the 1500° and 1700°C runs. It should be noted also that diffusion

coefficients for the latter two temperatures appear to be of the correct order of magnitude, but are of inverse magnitude.

Analysis by the method of least squares of the values of D for all temperatures gives values of $Q = 36,400$ cal/mole and $A = 5.17 \times 10^{-6}$ cm²/sec, but for the reasons given previously, the values of $Q = 34,800$ and $A = 2.82 \times 10^{-6}$ are deemed more likely correct.

SOURCES OF ERROR

Sources of error in the Matano method of analysis are discussed in considerable detail by Rhines and Mehl (4) and their paper should be read for discussion of the precision of this method. The largest source of error in the 1500° and 1700°C runs is probably in the machining of chips for chemical analysis because of brittleness of the metal at the interface. The inversion of the derived diffusion coefficients at these temperatures may be partly attributed to difficulties in operating at the higher temperatures.

ACKNOWLEDGMENT

This paper covers a phase of work sponsored by the Navy Bureau of Ordnance. The authors wish to express their appreciation to the Bureau for permission to publish these results, and to acknowledge the counsel of Dr. W. A. Taebel and J. W. Marden, and the assistance given by the members of the Special Molybdenum Products Division.

Any discussion of this paper will appear in a Discussion Section to be published in the December 1955 JOURNAL.

REFERENCES

1. R. C. RUDER AND E. E. BIRCHENALL, *J. Metals*, **3**, 142, (1951).
2. W. P. SYKES AND H. F. GRAFF, *Trans. Am. Soc. Metals*, **23**, 249 (1935).
3. R. M. BARRER, "Diffusion In and Through Solids," p. 246, Cambridge University Press, London (1941).
4. N. F. RHINES AND R. F. MEHL, *Trans. Am. Inst. Mining Met. Engrs.*, **128**, 185 (1938).
5. L. C. C. DASILVA AND R. F. MEHL, *J. Metals*, **3**, 155 (1951).
6. C. WELLS, "Atom Movements," Chap. 2, American Society for Metals, Cleveland (1951).

Corrosion of Titanium in Fused Chlorides

Formation of Pyrosols¹

C. B. GILL, M. E. STRAUMANIS, AND A. W. SCHLECHTEN

University of Missouri, School of Mines and Metallurgy, Department of Metallurgy, Rolla, Missouri

ABSTRACT

Titanium was severely attacked when immersed in a molten alkali chloride bath in the presence of air. The most severe corrosion of this metal was observed in molten NaCl-NaF mixtures; samples disintegrated completely at temperatures of 850°C in less than 3 hr. Progressively less corrosion occurred in KCl, NaCl, and LiCl melts. In many cases, salt fumes were more corrosive than the molten salt itself, evidently because of the better access of oxygen to the titanium surface. The corrosion rate fluctuated greatly from test to test but was very low in experiments performed in vacuum.

The chief corrosion products were a dispersion of metallic titanium in the molten salt ("pyrosols"), mixed with some titanium oxides. The mixture was dark gray, and colored the solid salt bluish-black. White to yellowish oxides appeared in small amounts on the surface of the salt bath and consisted mainly of TiO₂.

INTRODUCTION

The high corrosion resistance of titanium is frequently emphasized. However, investigations have shown that titanium does not always exhibit excellent properties in this respect. For example, the metal is destroyed quickly by hydrofluoric acid (1), and is readily attacked by the great majority of other acids, strong and weak, if water soluble fluorides are present (2). No references could be found as to the resistance of titanium against the attack of fused salt baths at temperatures above 700°C. Such knowledge is of importance in studies of the electrolytic deposition of titanium from fused salt baths (3). If titanium corrodes to any great extent in fused electrolytes, the difficulty of titanium deposition would be partially explained. The purpose of the present investigation, therefore, was to establish the extent of corrosive attack of various salts on titanium at high temperatures in the presence of air and also in vacuum.

EXPERIMENTAL PROCEDURE

For this study, sodium chloride, potassium chloride, lithium chloride, and sodium fluoride were chosen because they are frequently used for electrolytes. The first two were U.S.P. grade, granular.² The salts were melted in porcelain crucibles in a resistance furnace, the temperature of which was con-

trolled by a variable transformer, and measured by a chromel-alumel thermocouple. Titanium samples were cut from cold rolled and annealed sheet 1.6 mm thick, of 97+ % purity (1).

Titanium samples were first weighed and measured with a micrometer, after which they were submerged in the molten salt bath, held at a constant temperature for the set length of time, and then cooled together with the salt. The salt was dissolved from the sample with hot water, and the samples then washed with cold water, weighed, and measured, so that the percentage loss in weight and the average rate of corrosion could be calculated.

It was found that the titanium samples must be placed in the salt after it is molten, rather than melt the salt with the sample in it; samples must be allowed to cool submerged in the bath, otherwise the metal oxidized at a fast rate during the heating and cooling period. It was necessary to suspend the titanium in the bath so that it would not come in contact with any part of the crucible. A hole was drilled in one end of the sample so that it could be supported either by a platinum wire, or pure iodide titanium hook, hanging from a quartz rod resting across the crucible top.

Tests were also made with only one end of the sample submerged in the molten sodium chloride, while the other end projected out of the crucible into the furnace atmosphere of hot salt fumes, to compare the attack at the two ends. A few tests were made by heating the titanium in air with no salt present.

Other tests were made by placing titanium samples with sodium chloride in a Vycor glass tube; the tube was evacuated, heated to drive off adsorbed moisture,

¹ Manuscript received May 4, 1954. This paper was prepared for delivery before the Chicago Meeting, May 2 to 6, 1954. Based on a portion of work carried out at the Missouri School of Mines and Metallurgy for the Wright Air Development Center under Contract No. AF 33(616)-75.

² LiCl was a purified material obtained from J. T. Baker Chemical Company, and the NaF was "Baker Analyzed" reagent.

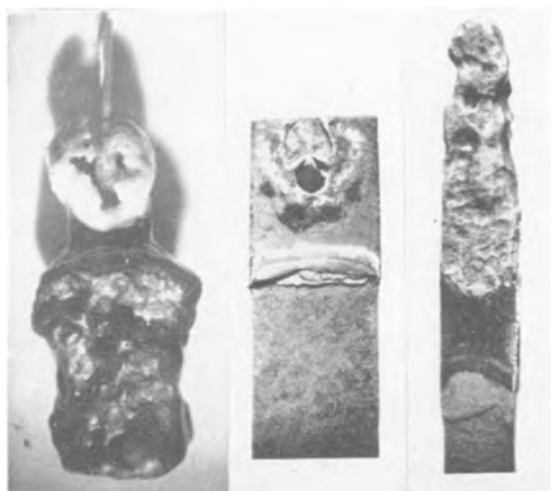


FIG. 1a. (Left) Ti sample removed from the molten NaCl bath where it corroded for 6 hr at 900°C, with corrosion products on its surface; FIG. 1b. (Center) a similar sample with corrosion products washed away; FIG. 1c. (Right) another sample, the end of which is pitted by severe attack of NaCl fumes and oxygen (of the air).

and then sealed while still being evacuated. Samples in the sealed tube were heated in a resistance furnace.

EXPERIMENTAL RESULTS

Attack by sodium chloride.—Titanium samples were strongly attacked by the molten sodium chloride in the presence of air. Fig. 1a shows a sample that was partially immersed, then withdrawn from the molten bath and allowed to cool quickly. The part submerged in the bath was covered with a thick layer of a black material, adhering to the metal, while the part above the liquid salt exposed only to the salt fumes was covered with a white residue. After

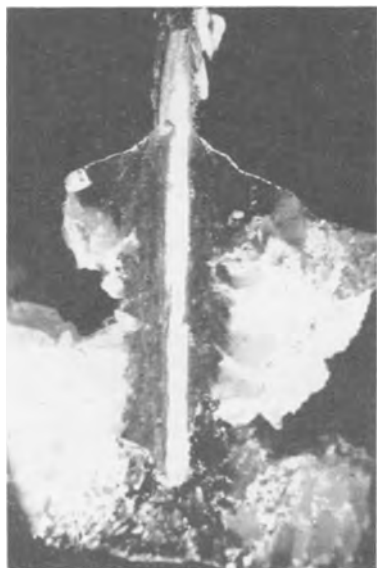


FIG. 2. Cross section through the Ti sample and NaCl, in which the metal corroded for 2 hr at 900°C. Dark corrosion products surround the Ti.

TABLE I. Loss due to corrosion of titanium samples in molten NaCl at 850°C, in 3 hr

Sample No.	Initial wt, g	Final wt, g	Loss in wt, %	Condition of Ti samples
5	0.3160	0.2022	36.0	Suspended by Pt wire
6	0.3986	0.2142	46.3	Suspended by Pt wire
7	0.6735	0.5489	18.5	Suspended by Ti wire
8	1.3270	0.9476	28.6	Half in and half out of NaCl
10	1.0606	0.9824	7.4	Half in and half out of NaCl
9a	0.8459	0.8574	1.36 gain	Heated alone in air
10a	0.8898	0.9157	2.91 gain	Heated alone in air
11	0.6417	0.6374	0.67	In NaCl in vacuum
12	0.5633	0.5535	1.74	In NaCl in vacuum
12a	0.5720	0.5672	0.84	In NaCl in vacuum

the corrosion products were washed off with water, the reduction in size of that part of the sample that was immersed in the bath was very evident (Fig. 1b). In every instance the titanium metal that had been in the corrosive medium was surrounded by a blue-black deposit, which was most dense immediately around the titanium, as seen in Fig. 2, which shows a section through the metal and salt, after they had been cooled slowly in the furnace. Upon dissolving the salt in water, a fine, dark gray powder was collected for identification. The powder dissolved readily in hydrofluoric acid with hydrogen evolution, except for a small residue that proved to be titanium oxide, thus revealing the metallic nature of the corrosion product. X-ray diffraction patterns showed that the powder had a slightly expanded metallic titanium lattice. This demonstrates that solid titanium samples were partially dispersed in molten salt, in the form of a metallic fog or a "pyrosol," according to Lorenz (4). Formation of a metallic fog in the cathodic compartment during the electrolysis of fused salts is a well-known phenomenon. X-ray analysis showed further that the white material on the upper part of the titanium sample contained some titanium dioxide in the form of rutile. The other constituents of the white deposit have not yet been identified. Corrosion of the titanium samples by sodium chloride melts, resulting in pyrosol formation, was heavy and very irregular; the results obtained fluctuated greatly (see Table I). However, in the absence of air (in vacuum) corrosion was much less. Titanium gained in weight if heated in air in the absence of salt, evidently because of the adsorption of oxygen and the formation of an oxide coating. These coatings had a yellowish appearance.

Since the greatest loss in weight was exhibited by samples suspended from a platinum wire, it was thought that this corrosion process might also be electrochemical in nature, accelerated by the

TABLE II. Corrosion rates of titanium samples in molten KCl, LiCl, and KCl-LiCl mixtures

Sample No.	Bath	Temp, °C	Time, hr	Wt loss, %	Corros. rate, mg/cm ² hr	Conditions of Ti samples
14A	KCl	800	3	3.4	3.1	Susp. by Ti wire
18A	KCl	850	3	24.0	19.5	Susp. by Ti wire
18B	KCl	850	3	9.5	7.1	Susp. by Ti wire
19A	KCl	850	3	78.6	50.2*	Half in, half out of KCl
19B	KCl	850	3	88.0	53.5*	Half in, half out of KCl
26A	KCl	850	1	12.4	21.0*	Half in, half out of KCl
26B	KCl	850	2	27.8	25.4*	Half in, half out of KCl
26C	KCl	850	3	60.7	35.0*	Half in, half out of KCl
31	KCl	850	4	2.8	1.38	Vacuum, half out of KCl
32	KCl	850	6	4.3	1.42	Vacuum, half out of KCl
14B	LiCl	625	3	3.2	2.9	Susp. by Ti wire
15	LiCl	625	3	2.3	2.0	Susp. by Ti wire
25B	LiCl	850	3	6.9	4.84	Susp. by Ti wire
16	LiCl	625	3	3.3	2.5	Half in, half out of LiCl
20A	LiCl	850	3	35.8	19.5	Half in, half out of LiCl
20B	LiCl	850	3	20.6	13.7	Half in, half out of LiCl
17A	KCl+ LiCl	375	3	0.4	0.4	Susp. by Ti wire
17B		375	3	1.3	0.8	Half in, half out of LiCl

* Heavy or very heavy attack of the projecting end (Fig. 1c); in all other cases the submerged end was attacked more.

platinum which acted as a cathode. To check this possibility, a short piece of platinum wire was firmly connected to the bottom of a titanium sample, which was suspended on a titanium wire hook in molten sodium chloride for 3 hr. When the salt was washed away there was no evidence of a heavier attack at the point where the platinum wire was connected than on the sample as a whole. This experiment indicates that the heavy corrosion of sample No. 6 (Table I) was accidental and within the range of fluctuations (7-46%) exhibited by similar experiments. Although the parts of the titanium samples which were outside of the salt bath were usually not as heavily corroded as the ends immersed in the bath, in the case of sample 8 (Table I) there was the opposite result; the heavily attacked upper end of the sample is shown in Fig. 1c.

Attack by potassium chloride and lithium chloride.—In these experiments the rate of corrosion in mg/cm² hr was determined. The weight of the samples was between 0.3 and 0.7 g with a surface area between 1.3-3 cm² exposed to the action of the salt bath. For

those samples only half immersed in the bath, so as to study the influence of the hot salt fumes, the two ends were usually unevenly attacked; nevertheless the total loss was determined by weighing, and the rate of corrosion computed on the whole area of the sample. To study the influence of temperature, eutectic mixtures of potassium and lithium chlorides (40-60 mole %) with a melting point of 355°C were used. These mixtures approached in their composition those used in electrolysis of titanium by Cordner and Worner and others (3, 5, 6). Results of these corrosion experiments are summarized in Table II. Again, rates of corrosion fluctuated greatly, and the same dark corrosion product (pyrosol) was formed around the titanium samples in the salt baths, even at the lowest temperatures used (at 375°C, sample 17A and 17B, Table II). The attack was strongest when the samples were only half immersed in the melt, so that fumes could attack the upper part of the sample. These parts were severely corroded, especially in the presence of potassium chloride. Lithium chloride appeared to be less corrosive. The table shows further that rate of corrosion increased with temperature. As before, in vacuum the rate of corrosion was much less than in the presence of air.

Attack by sodium fluoride.—The greatest loss of weight of the titanium samples due to corrosion resulted from immersion in a mixture of approximately 50% of sodium chloride and 50% of sodium fluoride; this bath at 850°C caused the metal to disintegrate completely in 3 hr, leaving a dark gray powder similar in appearance to that obtained in the previous cases. Attempts to heat the sample in the fluoride bath under vacuum were unsuccessful because the melt attacked the silica glass so strongly that air penetrated into the evacuated tubes initiating a severe corrosion of the titanium samples.

DISCUSSION AND CONCLUSION

Although the phenomenon of corrosion of titanium in fused salt baths at elevated temperatures and the formation of pyrosols resembles in many points the pyrosols as described by Lorenz and Eitel (4), and investigated further by Heymann (7), Farquharson (8), and Cubicciotti (9), there are certain differences. The pyrosols described by previous workers were usually prepared by mixing metals of low melting points in molten baths of their own salts. For example, lead in molten lead chloride expels gray clouds which then disappear completely at higher temperatures, probably by forming a true solution with the molten salt. Upon cooling, the gray metallic fog appears again because of aggregation of the lead particles into larger units. With slow cooling the particle size grows larger. In the case of titanium, however, metallic dispersions are formed in fused

alkali salts (salts of titanium itself were not tried), at temperatures far below the melting point of the metal itself. Furthermore, for formation of metallic titanium dispersions, presence of air (oxygen) is necessary, as pyrosol formation in vacuum or under inert gases occurred to a very limited extent. Because of experimental difficulties, no attempt was made to raise the temperatures of the melts above 1000°C, in order to check whether the metallic fog would dissolve completely in the melts, and then crystallize out upon cooling. Nevertheless, the cooled melts with the titanium dispersion resembled salts colored by colloidal dispersed substances (10). The transparent salt near the titanium appeared black to blue, but a part of the metallic dispersion was in the form of coarse powder which settled to the bottom of the crucible (Fig. 2). Regardless of the grain size of these metallic dispersions, the system, molten salt-dispersed titanium, can be called a "pyrosol," and the observed corrosion phenomena are, to a great extent, due to pyrosol formation. The reasons for this kind of corrosion are at present unknown; this action does not seem to be electrochemical in nature, but is related to the oxidation of the titanium in the melt or in salt fumes. It appears that this corrosion is not the same as that observed by Copson (11), who found that electrodes immersed in chloride baths were "pencilled" only during the anodic part of the alternating current cycle.

Results of this study show that corrosion of titanium occurs in molten chloride salt baths in the presence of air even at temperatures as low as 375°C, and that the rate of corrosion increases rapidly with temperature. It is evident that, if titanium could be

electrodeposited from such baths exposed to air, there would be a great tendency for the deposit to corrode and disperse in the bath.

ACKNOWLEDGMENT

The authors are grateful to the Wright Air Development Center for continued support of this work and permission to publish the results obtained.

Any discussion of this paper will appear in a Discussion Section to be published in the December 1955 JOURNAL.

REFERENCES

1. M. E. STRAUMANIS AND P. C. CHEN, *This Journal*, **98**, 234 (1951); *Corrosion*, **7**, 229 (1951); *Metall*, **7**, 85 (1953).
2. M. E. STRAUMANIS AND C. B. GILL, *This Journal*, **101**, 10 (1954).
3. See, for instance, G. D. P. CORDNER AND H. W. WORNER, *Austral. J. Appl. Sc.*, **2**, 365 (1951).
4. R. LORENZ AND W. EITEL, "Pyrosol," Akademische Verlagsges, Leipzig (1926); see also, R. LORENZ, "Pyrosols," in J. Alexander's "Colloid Chemistry," Vol. I, pp. 681-706, Reinhold Publishing Corp., New York (1926).
5. A. BRENNER AND S. SENDEROFF, *This Journal*, **99**, 223C (1952).
6. See also E. J. BRETON, WADC Technical Report 52-232 (1952).
7. E. HEYMANN, *Australian Chem. Inst. J. & Proc.*, **4**, 38 (1937); E. HEYMANN AND E. FRIEDLANDER, *Z. physik. Chem.*, **148A**, 177 (1930).
8. J. FARQUHARSON AND E. HEYMANN, *Trans. Faraday Soc.*, **31**, 1004 (1935).
9. D. CUBICCIOTTI, *J. Am. Chem. Soc.*, **74**, 1198 (1952); *J. Metals*, **5**, 1106 (1953); G. CLEARY AND D. CUBICCIOTTI, *J. Am. Chem. Soc.*, **74**, 1198 (1952).
10. See, for instance, B. JIRGENSONS AND M. E. STRAUMANIS, "A Short Textbook of Colloid Chemistry," p. 400, Pergamon Press, London (1954).
11. H. R. COPSON, *This Journal*, **100**, 257 (1953).

Potentiometric Titrations in Liquid Ammonia

VII. Characteristics of a "Difference Indicator" Electrode System¹

GEORGE W. WATT AND DONALD M. SOWARDS

Department of Chemistry, The University of Texas, Austin, Texas

ABSTRACT

Titration of ammonium bromide with potassium and with potassium amide in liquid ammonia has been followed potentiometrically using a "difference indicator" electrode system. It has been shown that neither the precision with which the end-point is detected nor the magnitude of the corresponding change in potential is appreciably influenced by variation in either the length or diameter of the reference electrode capillary. Data relative to the effect of the concentration of supporting electrolyte and the composition of the solution in the reference electrode compartment are presented and discussed.

INTRODUCTION

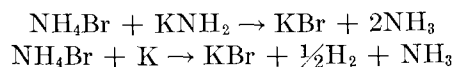
The use of potentiometric titrations to follow the course of reactions in liquid ammonia was first described by Zintl and coworkers (1). They employed an electrode system of the type described by Muller (2) and which is designated by Kortüm and Bockris (3) as a "difference indicator" electrode system. In this titration procedure, one electrode (the indicator electrode) is immersed in the solution to which the titrant is added; the other (reference) electrode is immersed in solution having a composition the same as the initial composition of the solution to be titrated, but isolated from the latter in a separate compartment that is connected to the main body of the solution by a fine capillary tube.²

Following rather extensive modification of Zintl's equipment and procedures (4), this method has been used in these laboratories in the study of a considerable variety of reactions in liquid ammonia in which solutions of alkali metals or alkali metal amides have been used as titrants (5-9). In these studies it has been possible generally to correlate observed changes in potential with either anticipated or reasonable stoichiometry. In a few cases, however, quite anomalous changes in potential have been observed, and it has been suggested that these may be attributable to factors such as changes in composition of the solution in the reference electrode compartment owing to diffusion, concentration of supporting electrolyte, etc. Accordingly, it seemed worth while to investigate the role of such variables and to attempt to establish optimum conditions for the use of this type of electrode system in the study of reaction mechanisms.

¹ Manuscript received May 7, 1954.

² This type of reference electrode has been referred to previously (4) as a differential electrode. There appears to be no sound objection to this term except that, through inadvertence, it is erroneously interpreted as implying a differential titration procedure.

For such purposes it is obvious that the reactions involved in the titrations should be simple, rapid, and quantitative, and that all reactants and products should be ammonia-soluble. These requirements are met by the reactions represented by the equations



which are also representative of simple metathesis and oxidation-reduction reactions, respectively. Attention is also called to the fact that these reactions involve species common to all liquid ammonia solutions, i.e., the ammonium and amide ions.

Equipment

The titrator and its auxiliary equipment consisted of a modification of that described previously (4); major modifications were as follows. The vessel for make-up and storage of standard solutions was replaced by a second buret also connected to the titration vessel as described previously; this modification, of course, necessitates making up the standard solutions directly in the two burets. The other change involved provision for the simultaneous introduction of two or more reference electrodes.

The reference electrode is illustrated by Fig. 1(I). The metallic element is a platinum wire (length, 2 cm; diameter, 0.016 in.) sealed through the top of the electrode compartment and contacting a copper lead-wire via a mercury pool (not shown). The electrode-compartment capillary is of uniform diameter for 1 cm from the tip. The capillary diameter was determined microscopically and, in one case, was checked in terms of the weight of mercury contained in a 35 cm length of capillary tubing having a uniform diameter of 0.8 mm. The uniformity and accuracy of the measurement is estimated to be within 3% of the diameter.

Indicator electrodes are made by sealing platinum

wire (length, 1 cm; diameter, 0.016 in.) in the end of a Pyrex tube; a general purpose indicator electrode was made similarly from platinum rod (length, 1 cm; diameter, 0.05 in.).

Potentials were measured by the null method using a conventional circuit: L&N Type K potentiometer, Certified Weston Standard cell, Rubicon spotlight galvanometer (current sensitivity, 0.011 $\mu\text{a}/\text{mm}$), and an L&N constant-potential lead storage cell.

An alternate reference electrode, the Hg-Hg²⁺ half-cell, is constructed as shown in Fig. 1(II); since it is involved in only minor respects in the work reported below, this electrode will be described in more detail in a later communication.

Materials

Analytical Reagent Grade ammonium bromide and potassium bromide were recrystallized from triple-distilled water, powdered in an agate mortar, and dried at 110°C. Potassium was double-distilled and stored under dry oxygen-free nitrogen in fragile Pyrex glass ampoules by means of techniques to be described elsewhere (10). Potassium amide was prepared *in situ* by the interaction of potassium and liquid ammonia catalyzed by iron wire. Commercial nitrogen (Linde HP Dry) was completely dehydrated and deoxygenated by scrubbing it through a solution of potassium in liquid ammonia at -33.5°C. Commercial anhydrous ammonia was used directly for thermostating purposes, but that used as a solvent and reaction medium was predried over sodium amide and finally passed through a concentrated potassium solution before use in the preparation of standard solutions. The conductivity of this "solvent ammonia" was $<10^{-6}$ ohm⁻¹ cm⁻¹.

PROCEDURE

Scrubber and titration units were cleaned with aqua regia, rinsed with several portions of distilled water, rinsed with ethanol, and dried. Potassium was placed in the scrubber, and the units were assembled (4). The entire system was pumped at 0.03 mm pressure for several hours, filled with "solvent ammonia" gas, re-evacuated, and refilled with ammonia gas just before starting a typical run, which was carried out as follows.

With gaseous ammonia flowing through the system, a bulb containing a known weight of potassium is put into one buret, a weight of ammonium bromide equivalent to the potassium is put into the other buret, and 1.00 g of potassium bromide is placed in the titration vessel. The scrubber is cooled with ammonia, and from 75 to 100 ml of solvent ammonia is condensed therein; this provides a 6-8

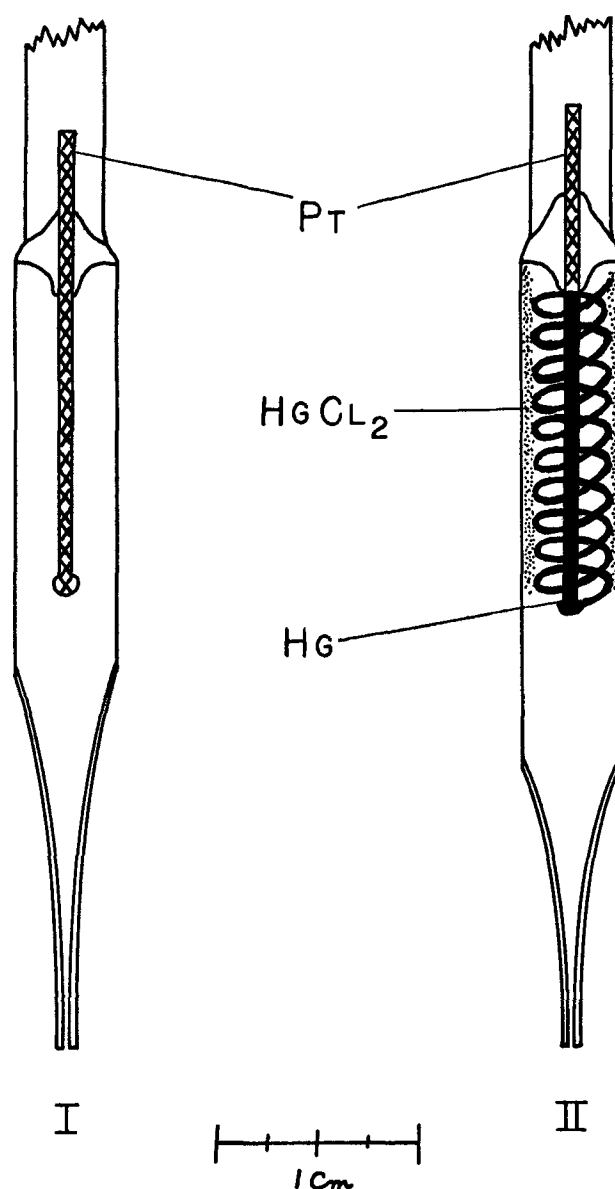


FIG. 1. Reference electrodes. I, The difference indicator electrode; II, the Hg-Hg²⁺ half-cell.

in. head of potassium solution, and all gases entering the titrator pass through this unit. The potassium ampoule in the one buret is crushed, the titrator assembly is cooled with ammonia, and about 30 ml of ammonia is condensed in each buret and in the titration vessel. The reference electrode compartment fills during this operation, and the potential is usually constant after 20 min.

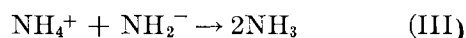
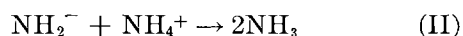
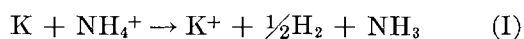
Titration is carried out by adding solution to the titration vessel from one buret, then titrating this with the solution from the other. Enough time is allowed between the additions of titrant for the potential to become constant. A measured excess of titrant may be added beyond the end-point and the resulting solution back-titrated with the solution in

the other buret; this process may be repeated until the supply of one of the solutions is exhausted.

Volume readings are accurate to within 0.05 ml. The accuracy of end-point determinations is about 2%; internal agreement is within 1%. Temperature variations, as indicated by a toluene thermometer, are $<1^\circ$ during the course of a titration; temperatures ranged from -35° to -39° for all of this work. Changes in potential due to temperature changes were less than the precision of potential measurements, which was 5 mv.

RESULTS

Titration involving reference electrodes having different capillary diameters are represented graphically by Fig. 2, 3, and 4; these correspond, respectively, to the titrations:



where the titrant appears first in the equation. Mole ratios shown on the abscissas are calculated from known concentrations of the solutions employed; the points represent the corresponding experimentally measured potentials. The concentration of the titrant varied from 40 to 85 millimolar; that of

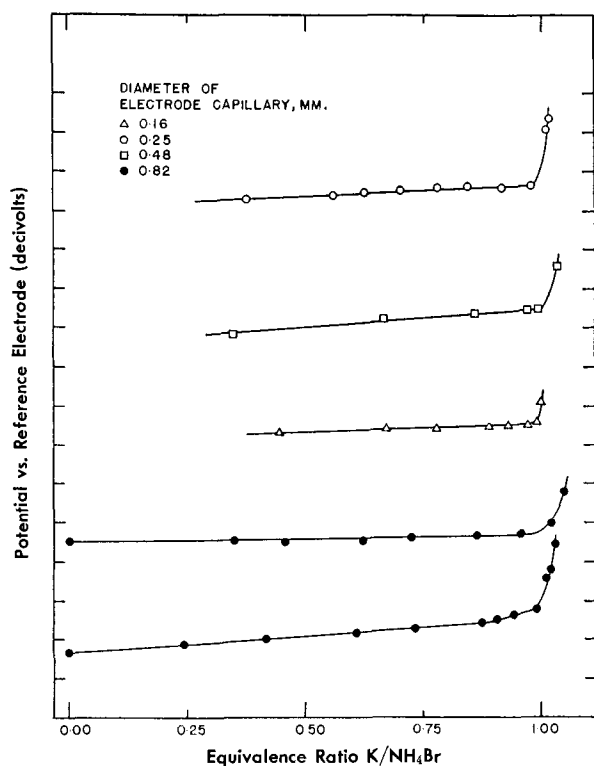


FIG. 2. Potentiometric titrations of NH_4Br with K using difference indicator electrodes having different capillary diameters.

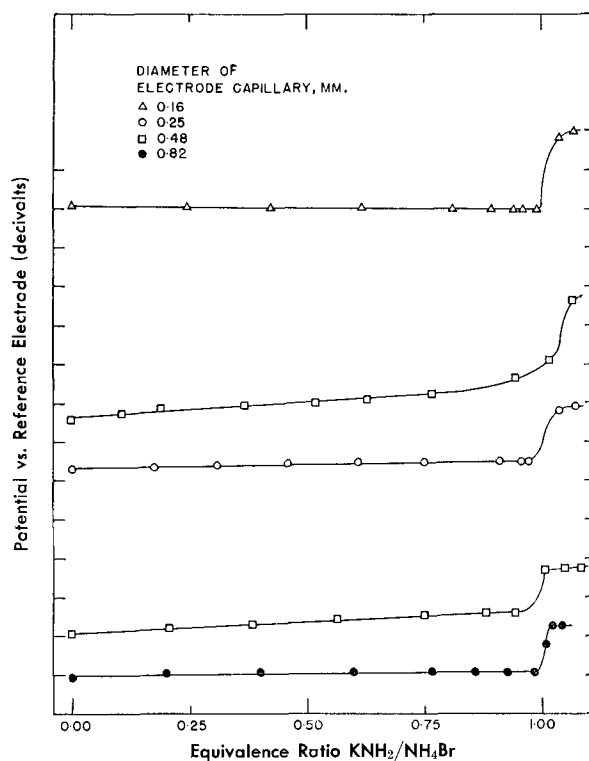


FIG. 3. Potentiometric titrations of NH_4Br with KNH_2 using difference indicator electrodes having different capillary diameters.

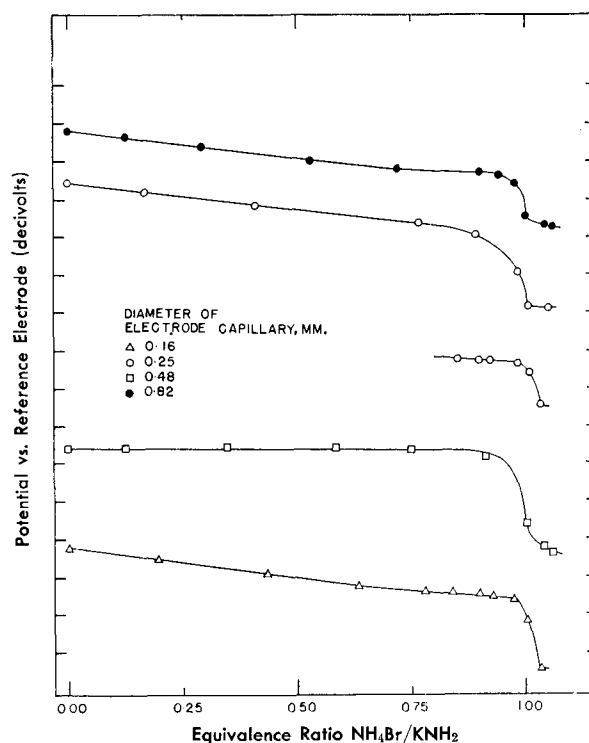


FIG. 4. Potentiometric titrations of KNH_2 with NH_4Br using difference indicator electrodes having different capillary diameters.

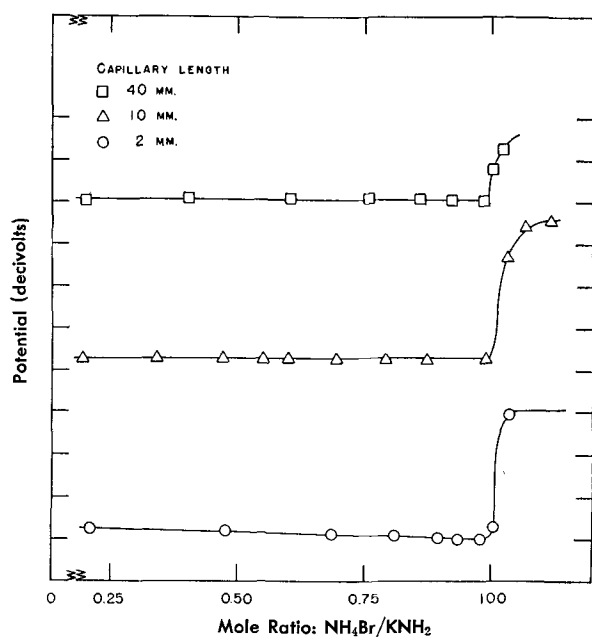


FIG. 5. Potentiometric titrations of KNH_2 with NH_4Br using difference indicator electrodes having different capillary lengths.

the solution being titrated varied from 5 to 20 millimolar. The time required for a single titration was about 2 hr. The potential scale in Fig. 2, 3, and 4 is divided into 0.1 v units, and no attempt is made to relate "absolute potentials" for different titrations. Initial potentials were not reproducible, except for random cases, even when extreme precautions were taken to insure conditions as nearly identical as possible. In some cases, initial potentials varied by as much as 0.6 v; even two indicator electrodes in the same solution would, at times, show a potential difference of 0.4 v. However, the magnitude of the total potential change at the end-point was about the same for the same titration with different reference electrodes.

When the reference electrode contained potassium solution, anomalous results were obtained. These varied from the extremes of a stable reference potential to a rapidly dropping potential accompanied (within 5 min) by a discharge of the blue color characteristic of the potassium solution.

Neutral solutions of supporting electrolyte in the reference electrode sometimes resulted in a titration curve with an anomalous break preceding the correctly indicated end-point. This occurred most frequently in titration (III), for which this break also frequently appeared when acidic or basic solutions were present in the electrode compartment. Otherwise, acidic and basic solutions in the reference electrode gave quite reproducible results, except for the values of the initial potentials.

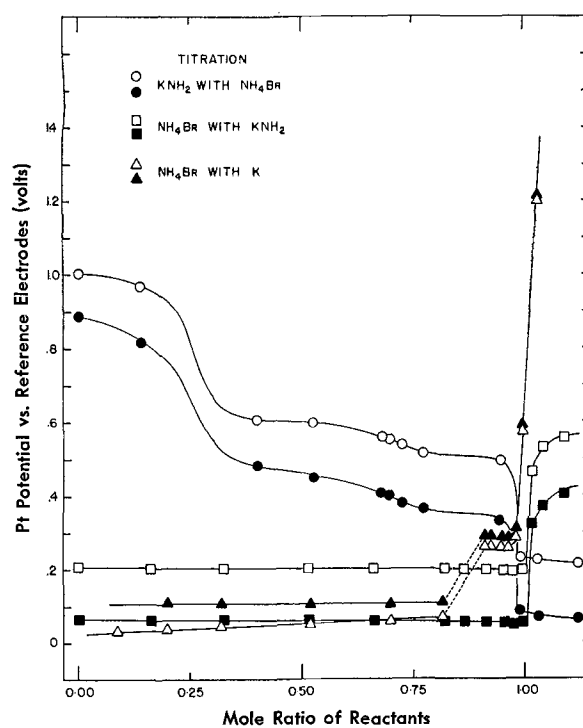


FIG. 6. Potentiometric titrations followed simultaneously with the difference indicator electrode (solid points) and the Hg-Hg^{2+} half-cell (open points).

A reference electrode with a capillary diameter of 0.8 mm was used to investigate the effect of capillary length on the reproducibility of end-point determinations. Results of titrations employing this type of electrode with a capillary of uniform diameter and 2, 10, and 40 mm in length are shown in Fig. 5.

In order to determine the effect of supporting electrolyte concentration on the sensitivity of the potential measurements, titration (III) was followed by means of a reference electrode (capillary diameter, 0.16 mm) in a run without supporting electrolyte. To 25 ml of ammonia was added 8.0 ml of 0.0642*N* potassium amide solution; the electrode was filled, and the solution was titrated with 0.0660*N* ammonium bromide solution. The emf sensitivity was ± 15 mv and the end-point indicated was 8%³ beyond the stoichiometric end-point. To this dilute potassium bromide solution was added 9.0 ml of potassium amide solution, the electrode was refilled, and this solution was titrated with the standard ammonium bromide solution. The emf sensitivity in this case was ± 8 mv, and the titration error was reduced to 6%. The electrode was again refilled after addition of 9.5 ml of the amide solution, and in the ensuing titration the emf sensitivity

³ Estimation of error is made on the basis of the total quantities of the two solutions added; hence, this factor is cumulative.

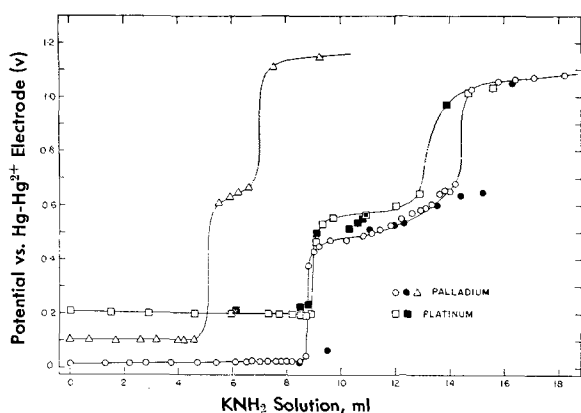


FIG. 7. Indicator electrode behavior in acidic and basic media.

was ± 5 mv, and the end-point was determined to within 1%.

Titrations (I), (II), and (III) were followed simultaneously with a reference electrode having a capillary diameter of 0.25 mm and with the Hg-Hg²⁺ half-cell; results are shown in Fig. 6. The emf sensitivities were ± 10 mv and ± 0.1 mv, respectively. The potential difference of the two reference electrodes could be determined with a precision of ± 10 mv, and it changed at a rate of about 5 mv/hr over a period of several hours.

Since the electrode reactions that occur at the indicator electrode may be expected also to function at the metallic element in the reference electrode compartment, the behavior of the indicator electrode was checked against the Hg-Hg²⁺ half-cell reference potential. Titration (II) was carried out with potassium amide solution additions carried far beyond the stoichiometric end-point, and the resulting solution was back-titrated as in titration (III). Results are shown in Fig. 7, where the open points are for (II) and the solid points correspond to (III); here, again, changes in potential from the lower to the middle plateau are in good agreement with the calculated stoichiometric end-points. Although not shown in Fig. 7, the change from the middle to the upper plateau appears to be sensitive to amide ion concentration, and the potential behavior during the transition is suggestive of a very easily polarizable electrode. Results are quite reproducible if the indicator electrode is exposed *in situ* to a dilute potassium solution prior to the titration; otherwise, the upper plateau may not appear.

DISCUSSION

In designing the experiments reported above, the precision sought has been limited by the lack of data on electrode reactions in liquid ammonia. The half-cells that have been described in the literature were rejected on the grounds that they involve

experimental complexities of an order not compatible with the relatively simple equipment and procedures employed in this work. It is considered sufficient that the present titrations show indicated end-points in quite good agreement with the stoichiometric end-points.

Data of Fig. 2, 3, and 4 show that variation of capillary diameter has no detectable effect upon the accuracy of determination of the end-point using capillaries in this range of length and diameter. With the possible exception of the amide solution, the cell potential is essentially constant with small changes in concentration; only at the end-point, where there is a very large change in the relative ratio of reactants, is there an appreciable abrupt change in potential. The drift in potential in titration (III), Fig. 4, is seen in Fig. 7 (middle plateau⁴) to be attributable to changes in the potential of the indicator electrode. Thus, it may be concluded that the potential of the reference electrode is constant during these titrations.

The variation of capillary length, with the capillary of largest diameter used in any of this work, has no effect on the accuracy of the end-point determination, or the reliability of the reference electrode under the conditions of the titrations illustrated by Fig. 5. It may also be expected that a variation in length between 2 and 20 mm would not have adverse effect on capillaries with a diameter between 0.2 and 0.8 mm.

The composition of the solution in the reference electrode compartment was found to be of importance in only two cases. Despite a reproducible initial cell potential near zero, potassium solutions in this compartment in many instances undergo catalytic decomposition at the platinum electrode element. Although the relative rate of this reaction is low, the volume of this solution is < 0.5 ml, and it undergoes a rather large change in concentration; thus the reference potential changes considerably. Titrations followed with an electrode containing a neutral solution, and in some instances showing a premature change in potential along with a correctly indicated end-point, may be explained on the assumption that the composition of the electrode solution is the same as that of the solution at the transition point between the middle and upper plateaus, as shown in Fig. 7. The actual change is caused presumably by the polarization of the reference electrode; in the cases mentioned, the magnitude of change in potential is in agreement with this explanation. In view of these findings, it is suggested

⁴ As may be seen from Fig. 6 and 7, the potential of this plateau identifies it with the NH₄⁺-H₂ electrode reaction. The potential of the upper plateau is probably that of the NH₂-N₂ half-cell with an appreciable overvoltage (11).

that acidic or basic solutions provide the most suitable reference electrode components.

Results obtained upon variation of the concentration of supporting electrolyte are in keeping with those expected because of low electrical conductivity (12). Comparison of results obtained simultaneously with two different reference electrodes vs. a common indicator electrode (Fig. 6) show that the sluggishness of response in measurements involving the difference indicator electrode may be attributed almost exclusively to that electrode reaction rather than to either the capillary characteristics or the indicator electrode.

ACKNOWLEDGMENTS

This work was supported in part by the Atomic Energy Commission, Contract AT-(40-1)-1639. The liquid ammonia used in these studies was generously supplied by the Polychemicals Department, E. I. du Pont de Nemours and Company.

Any discussion of this paper will appear in a Discussion Section to be published in the December 1955 JOURNAL.

REFERENCES

1. E. ZINTL, J. GOUBEAU, AND W. DULLENKOFF, *Z. physik. Chem.*, **A154**, 1 (1931).
2. E. MULLER, *ibid.*, **135**, 102 (1928).
3. G. KORTUM AND J. O'M. BOCKRIS, "Textbook of Electrochemistry," p. 309, Elsevier Publishing Company, New York (1951).
4. G. W. WATT AND J. B. OTTO, JR., *This Journal*, **98**, 1 (1951).
5. G. W. WATT, J. L. HALL, AND G. R. CHOPPIN, *J. Am. Chem. Soc.*, **73**, 5920 (1951).
6. G. W. WATT, J. L. HALL, AND G. R. CHOPPIN, *J. Phys. Chem.*, **57**, 567 (1953).
7. G. W. WATT, J. L. HALL, G. R. CHOPPIN, AND P. S. GENTILE, *J. Am. Chem. Soc.*, **76**, 373 (1954).
8. G. W. WATT, G. R. CHOPPIN, AND J. L. HALL, *This Journal*, **101**, 229 (1954).
9. G. W. WATT, G. R. CHOPPIN, AND J. L. HALL, *ibid.*, **101**, 235 (1954).
10. G. W. WATT AND D. M. SOWARDS, *J. Am. Chem. Soc.*, **76**, 4742 (1954).
11. V. A. PLESKOV, *Acta Physicochim. (U.R.S.S.)*, **1**, 713 (1935); **20**, 578 (1945).
12. C. A. KRAUS AND V. F. HNIZDA, *J. Am. Chem. Soc.*, **71**, 1572 (1949).

Polarization Studies of Copper, Nickel, Titanium, and Some Copper and Nickel Alloys in Three Per Cent Sodium Chloride¹

H. B. BOMBERGER

Rem-Cru Titanium, Inc., Midland, Pennsylvania

AND

F. H. BECK AND M. G. FONTANA

The Ohio State University, Columbus, Ohio

ABSTRACT

Polarization characteristics were determined for some metals and alloys in flowing salt solutions. Relationships between potential and time, potential and applied current, applied current and corrosion rate, and solution velocity and corrosion rate were considered. Copper and brass anodes dissolved readily. Nickel and copper-nickel alloys exhibited anodic polarization. Titanium anodes resisted dissolution by film growth and extensive polarization.

INTRODUCTION

A study of the polarization properties of an electrode provides information about the type, nature, and rate of the reaction or reactions taking place and is therefore helpful in explaining corrosion phenomena (1-4). In this investigation an attempt was made to explain the behavior of some commercial materials by studying them as individual electrodes and observing their tendency to polarize and corrode.

EXPERIMENTAL PROCEDURE

The test solution was prepared by dissolving 3% by weight of reagent grade sodium chloride in double distilled water. This was held at $30^{\circ} \pm 1^{\circ}\text{C}$ in a 20-l flask and circulated through the test system by means of a Hastelloy C pump. Flow rate was determined with flowmeters, and controlled by stop cocks in the system and an autotransformer in the motor circuit.

Test units, as indicated in Fig. 1, were constructed so that flat test specimens formed part of one side of a rectangular shaped cell through which the solution passed with a minimum of turbulence. Test specimens were 6 in. long and had an effective width of 1 in. They were held $\frac{1}{4}$ in. away from, but parallel to, a platinum electrode of the same size on the opposite side of the tube.

¹ Manuscript received November 4, 1953. This paper was prepared for delivery before the Wrightsville Beach Meeting, September 13 to 16, 1953, and is based on a dissertation presented in partial fulfillment of the requirements for the Ph.D. degree of one of the authors (H.B.B.) at Ohio State University.

Polarization was accomplished by passing a controlled direct current between the platinum and test electrodes. Potentials of the test electrodes were determined periodically by means of an L & N potentiometer and a saturated calomel reference electrode. Tests were continued until the electrode potentials were essentially constant for a few hours, i.e., less than 5 mv/hr variation. In some cases as long as 48 hr were required. For potential measurements the small tip of the calomel electrode was inserted through an opening in the center of the platinum electrode and placed close to the surface of the test electrode to minimize the IR drop. The IR drop across the film was estimated by a method suggested by Pearson (5) and found to be negligibly small for all materials except the titanium anodes.

New specimens and solutions were prepared for each test. For 1 hr before the beginning of each test, solutions were vigorously aerated with air or purified argon. This resulted in 5.15 and 0.05 ml of dissolved oxygen per liter of solution for the air and argon flushed solutions, respectively. Periodic sampling indicated that these values and the $p\text{H}$, between 6 and 7, remained nearly constant during all tests.

Test specimens (Table I) were abraded with No. 240 grit emery cloth and all but the titanium were annealed for 1 hr at 1200°F in purified argon followed by furnace cooling. Before testing, the copper and brasses were swabbed with a 10% solution of potassium cyanide; the other samples were abraded lightly with emery cloth. All were washed in distilled water and acetone and dried in a desiccator until installed in the test cells. Corrosion rates were

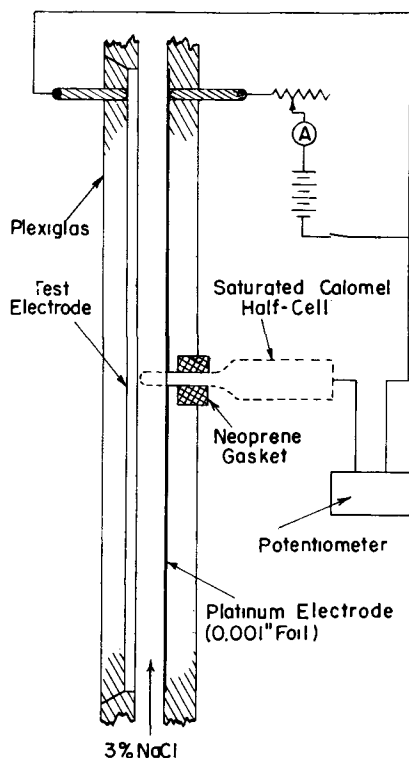


FIG. 1. Schematic diagram of test unit and electrical system.

calculated from the exposed surface area and the loss of weight for the given test periods.

DISCUSSION AND RESULTS

No weight loss or tarnishing was observed on any of these materials when exposed to the argon flushed solutions, indicating little if any local cell action. In view of the energy requirements, corrosion of copper should not occur under these conditions, but nickel, zinc, and titanium should replace hydrogen ions in solution (6). This, however, does not occur readily because of polarization or passivation effects peculiar to these materials. Corrosion rates for these materials exposed to air-saturated solutions for given times are listed in Table II along with corrosion and polarization potentials. Under these conditions, reduction of oxygen, requiring less energy than reduction of hydrogen ions, occurred as the main cathodic reaction, and some corrosion was observed on all materials except nickel and titanium.

In general, cathodic polarization of these materials in the argon flushed solutions was manifested by a change of potential to a greater anodic value (more negative) than observed in the air-saturated solu-

TABLE I. Nominal composition, grain size, and hardness of materials

Material	% Cu	% Zn	% Ni	% Fe	% Mn	% Other elements	A.S.T.M. grain size	Vickers hardness
Deoxidized copper..	99.90	—	—	—	—	0.025P	4	38
Cartridge brass.....	70	30	—	—	—	—	4	50
Red brass.....	85	15	—	—	—	—	5	50
Cupro-nickel.....	70	—	30.0	0.57*	—	—	5	97
Monel.....	30	—	67	1.4	1.0	0.15C 0.1Si	5	97
"A" Nickel.....	0.1	—	99.4	0.15	0.25	0.06C 0.05Si	5	93
Rem-Cru Titanium..	99 + Ti, 0.2C, 0.15N							278

* Determined by analysis.

TABLE II. Steady-state potentials in volts vs. saturated calomel, and corrosion rates in mpy for materials in 3% NaCl flowing at 50 ft/min and 30°C

Materials	Test time, hr	Air-saturated solutions			Argon-flushed solutions*	
		Corrosion rate	Corrosion potential	Max. cathodic polarization	Corrosion potential	Max. cathodic polarization
Copper.....	8	9.0	-0.250	-1.25	-0.260	-1.32
70-30 Brass.....	24	8.8	-0.225	-1.29	-0.320	-1.30
Red brass.....	24	15	-0.193	-1.07	—	—
Nickel.....	24†	0.0	-0.120	-1.29	-0.200	-1.26
70-30 Cu-Ni.....	24†	6.0	-0.191	-1.27	—	—
Monel.....	24†	0.8	-0.10	-1.31	—	—
Titanium.....	7	0.0	-0.10	-1.26	-0.10	-1.40

* No observable corrosion.

† Cathodes tested for 48 hr.

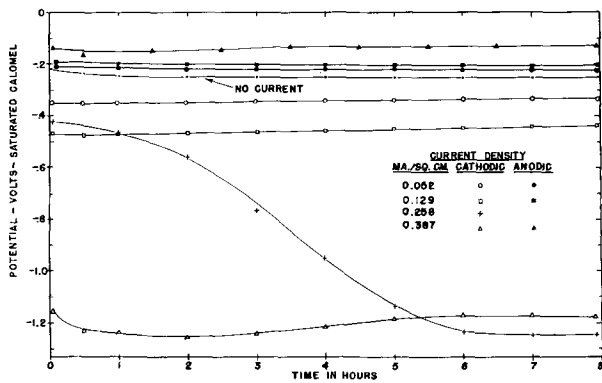


FIG. 2. Polarization of copper in air-saturated 3% NaCl solution (50 ft/min, 30°C).

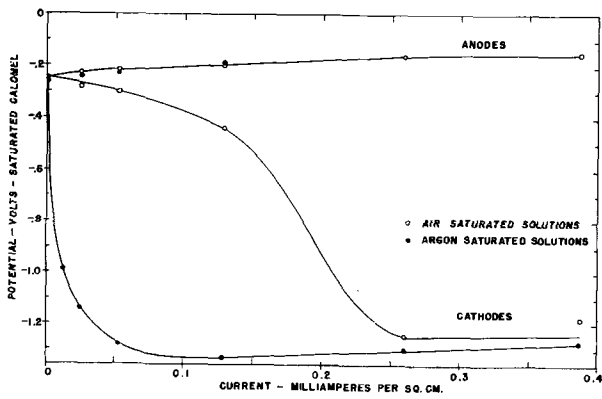


FIG. 3. Polarization of copper in 3% NaCl solutions (50 ft/min, 30°C).

tions, since the main cathodic reaction in this case is the reduction of hydrogen ions. This may be the reason the corrosion potentials are generally more anodic in the air-free solutions (see Table II) since the local cell cathodes are apparently polarized to a greater anodic value and thus displace the corrosion potential to a more anodic value.

Copper.—Typical time-potential curves for copper, given in Fig. 2, show that nearly constant potentials were obtained within 8 hr in 3% NaCl flowing at 50 ft/min. Steady-state potentials are plotted against applied current density in Fig. 3. Copper anodes polarized little with increased current density, suggesting that copper passes readily into solution and that the potential change is due to concentration polarization. Cathodic polarization is a function of current density and oxygen concentration. At low current densities the cathodic reaction is the reduction of oxygen, but at high current densities the rate of oxygen consumption exceeds the rate of supply by diffusion. Thus, the potential changes until the reduction of hydrogen ions also takes place. The apparent decrease in cathodic polarization at the high current densities may have resulted from partial depolarization by chlorine.

Fig. 4 shows that the corrosion rate of copper

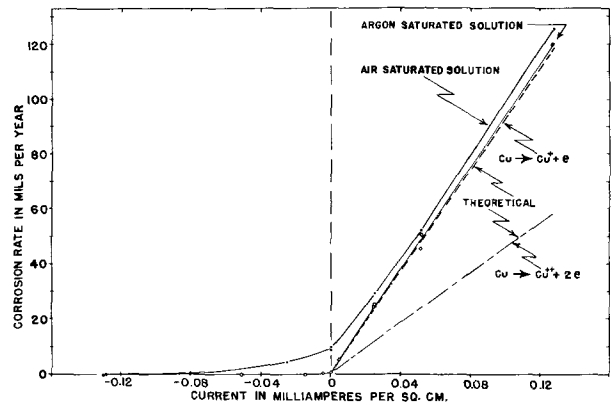


FIG. 4. Corrosion of copper in 3% NaCl solution flowing at 50 ft/min, 30°C.

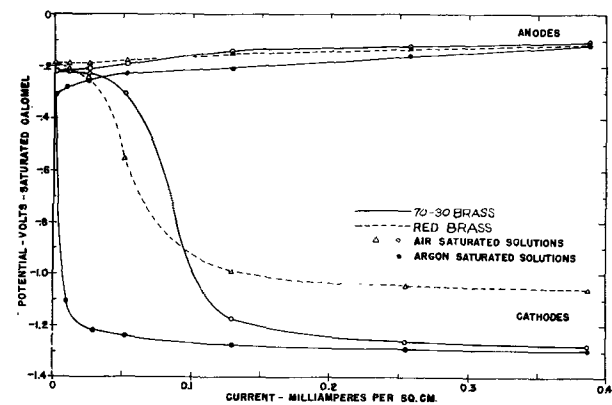


FIG. 5. Polarization of brasses in 3% NaCl solutions (50 ft/min, 30°C).

anodes (based on 8-hr tests) is proportional to the current density and indicates that copper goes into solution as monovalent ions. The corrosion rate in air-saturated solutions is decreased with increased cathodic current until corrosion is almost averted at a current density of -0.08 ma/cm^2 .

The effect of flow rate on the corrosion of copper was studied: Copper corroded almost linearly with solution velocity, from 6 to 78 mils per year, on exposure in air-saturated solutions moving between 10 and 440 ft/min. Cathodes at -0.026 ma/cm^2 corroded at less than 4 mpy until the flow rate increased beyond 150 ft/min where the behavior was almost linear to 48 mpy at 440 ft/min. Anodes at 0.026 ma/cm^2 indicated that corrosion is almost linear with velocity, from 30 to 86 mpy, over the range 50 to 440 ft/min. At 600 ft/min attack was nonuniform and results were inconsistent, presumably because of film erosion by excessive turbulence.

Good correlations between flow rate and electrode potential could not be obtained. In general, however, the potentials appeared to become less anodic with increased flow rate, possibly because of decreased polarization of the local cathodes.

Brasses.—The behavior of 70-30 brass was similar

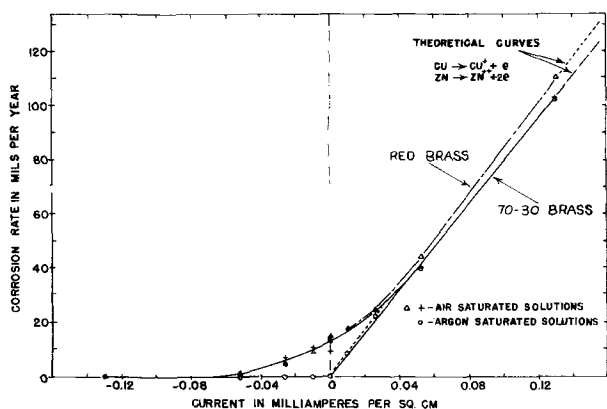


Fig. 6. Corrosion of brasses in 3% NaCl solutions (50 ft/min, 30°C).

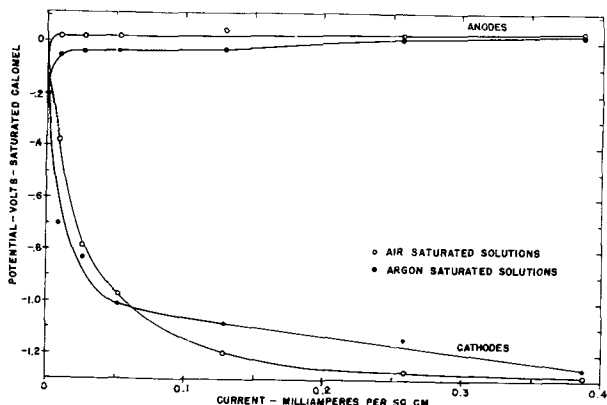


Fig. 7. Polarization of nickel in 3% NaCl solutions (50 ft/min, 30°C).

to that of copper. The potential became quite steady within 8 hr, but the potential of the red brass, in air-saturated solutions flowing at 50 ft/min, varied considerably for almost 24 hr. Fig. 5 indicates that the cathodic polarizations of brasses in air-saturated solutions is more pronounced than that of copper. The curved portions of the anode curves suggest a slight anodic overvoltage, whereas the linear portion is indicative of concentration polarization.

Corrosion rates are plotted against current in Fig. 6 for 70-30 brass and red brass based on 24-hr tests. Cathodic current densities above -0.07 ma/cm^2 appeared to polarize local cathodes sufficiently to prevent corrosion in air-saturated solutions. Since much of the corrosion occurs before appreciable polarization takes place, longer test periods would have resulted in lower average corrosion rates for the cathodes. At an anodic current of about 0.05 ma/cm^2 local anodes polarized to the extent that local action ceased and dissolution was then proportional to the applied current as indicated. Theoretical corrosion rates were calculated from the applied current using the following equation and assuming that the copper went into solution only as monovalent ions; zinc forms only divalent ions:

$$\text{C.R.} = Kit/F [(XM/V)_{\text{Cu}} + (XM/V)_{\text{Zn}}] \quad (I)$$

where X represents mole fractions of the elements in the brass with molecular weights M and valence V , K is a proportionality constant, F is Faraday's constant, and I is the applied current for time t .

Nickel.—Nickel acquired a steady potential in flowing argon-flushed solutions within 24 hr, but cathodes in air-saturated solutions required about 48 hr. Fig. 7 shows an anodic polarization of about 0.15 v in both air- and argon-saturated solutions, by extrapolating the straight portions of the curves to zero current. Because of this anodic polarization, nickel should not be expected to replace hydrogen ions in significant amounts in neutral salt solutions. It is also noteworthy that the cathodic polarization of nickel in air-saturated NaCl appears to be greater at low current densities than that of the other materials under these conditions. According to work by LaQue (7) the metal does not seem to polarize nearly as readily in flowing sea water.

Fig. 8 shows that little or no corrosion was observed in the air- and argon-flushed solutions and that dissolution followed Faraday's law. Corrosion was nonuniform, being of the pitting type.

Although corrosion of the nickel was not observed

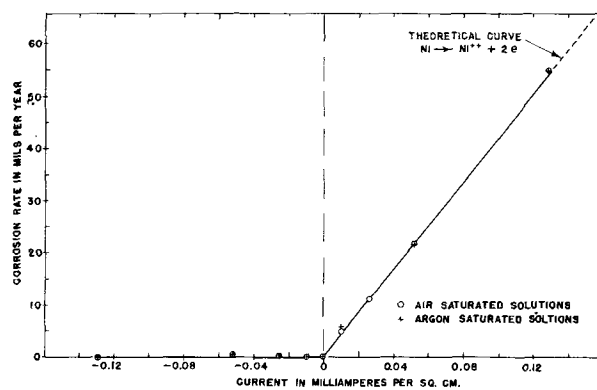


Fig. 8. Corrosion of nickel in 3% NaCl solutions (50 ft/min, 30°C).

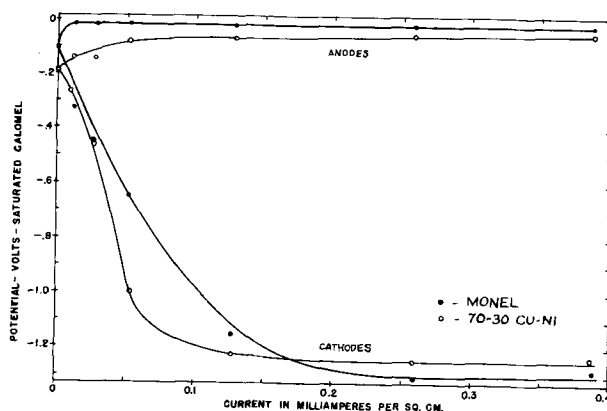


Fig. 9. Polarization of Cu-Ni alloys in air-saturated 3% NaCl solution (50 ft/min, 30°C).

without applied current, the metal dissolved slowly at all low cathodic current densities in flowing 3% NaCl, and the test system repeatedly acquired a black insoluble film. This deposit dissolved readily in potassium cyanide solutions but not in ammonium chloride, thus suggesting that it was Ni_2O_3 and not $Ni(OH)_3$. The maximum cathodic corrosion rate observed was 0.9 mpy at a current density of -0.052 ma/cm^2 . At and above -0.258 ma/cm^2 protection seemed to be complete and no attack was observed. This corrosion is believed to have resulted from the small accumulation of dissolved chlorine.

Copper-nickel alloys.—Monel and 70-30 cupro-nickel and anodes of these materials acquired a steady state in about 24 hr, but the cathodes required about 48 hr in air-saturated solutions. The polarization curves, given in Fig. 9, indicate that anodes of these alloys, like nickel, are characterized by substantial polarization, being about 0.08 and 0.10 v, respectively, at low current densities. Nickel and copper-nickel alloy cathodes appear to polarize more readily and to a greater extent than any of the other materials tested under the given conditions (as indicated in Fig. 12).

Fig. 10 shows that some local cell action does take place on the alloys but that it can be polarized by a small applied current. Unlike nickel, no evidence of induced corrosion was observed with cathodic currents. Anodes dissolved at a slower rate than equation (1) indicated. Apparently in this case, anode reactions are not only the formation of divalent nickel and monovalent copper ions, but may include the formation of divalent copper ions and the discharging of hydroxyl and chloride ions as well.

Titanium.—Titanium and titanium cathodes acquired a steady state in less than 2 hr, but the anodes with more than 0.026 ma/cm^2 changed considerably in potential for almost 7 hr. This was true for both the air- and argon-flushed 3% NaCl flowing at 50 ft/min. The metal without impressed current

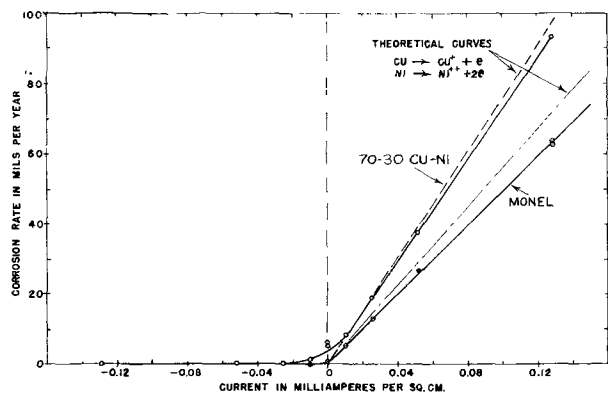


FIG. 10. Corrosion of Cu-Ni alloys in air-saturated 3% NaCl solution (50 ft/min, 30°C).

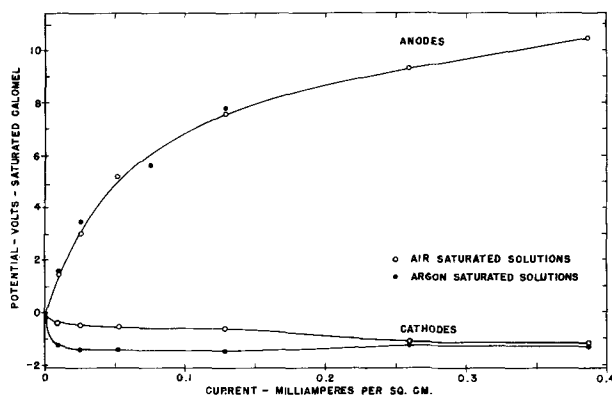


FIG. 11. Polarization of titanium in 3% NaCl solution (50 ft/min, 30°C).

TABLE III. Corrosion of titanium anodes in air-saturated 3% NaCl flowing at 50 ft/min and 30°C for 7 hr

Applied current density in ma/cm ²	Corrosion rate in mpy	Approximate resistance in ohms/cm ²	IR drop, v	Max. anode polarization potential, v (including IR)
0.010	0.0	—	—	1.50
0.026	0.0	2000	0.05	3.00
0.052	0.0	2300	0.10	4.80
0.129	2.2	2000	0.26	7.45
0.258	4.1	2500	0.65	9.35
0.387	94	2700	1.05	10.50

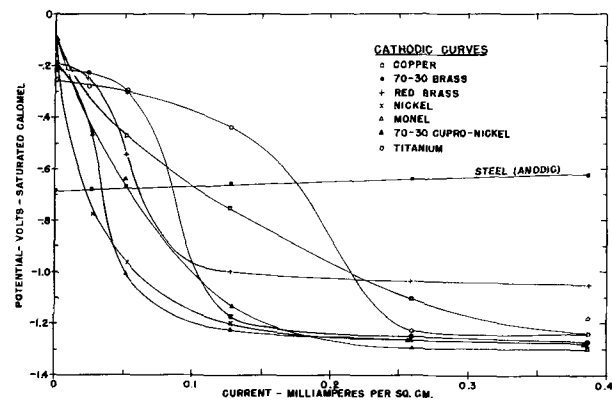


FIG. 12. Anodic polarization of steel and cathodic polarization of other materials in air-saturated 3% NaCl solutions flowing at 50 ft/min, 30°C.

had a potential of -0.10 v . Schlain (8) reported appreciable change in potential with time in air-saturated static 3% NaCl until a potential of 0.44 v was attained after 100 hr. Hackerman and Hall (9) noted slow drifting of the potential in air-saturated 0.5M NaCl for several days until a final potential of 0.17 v was observed. LaQue (7) reported a corrosion potential of -0.10 v for high purity titanium in flowing sea water. Environmental or test variables may account for these differences in results.

The extensive anodic polarization observed in Fig. 11 is believed to be due in part to an adherent in-

soluble film of high ohmic resistance as noted in Table III. Corrosion data are given there also.

At small anodic currents there was no evidence of corrosion until 0.129 ma/cm² was employed which resulted in a slight but nonuniform metal loss and film growth. Identification by electron diffraction of a light golden film, developed at low currents, was not successful. However, data did indicate that the film was crystalline and that it was not TiO, Ti₂O₃, TiCl₂, nor a form of TiO₂. TiH₂ was observed as a reaction product on the cathodes.

The cathodic polarization of titanium is also given in Fig. 12 along with cathode curves for the other materials. LaQue (7) observed similar degrees of polarization of titanium in sea water at current densities of 0.1 and 0.2 ma/cm², but at lower current densities polarization occurred much more readily in sea water than noted in this work.

SUMMARY

Corrosion and polarization studies were made on a number of materials in flowing 3% NaCl. None of the materials showed evidence of corrosion in argon-flushed solutions. Cathodic curves, given in Fig. 12, indicate that nickel and the nickel alloy cathodes polarized more readily than the others tested. LaQue (7) noted that nickel is less readily, and titanium more readily, polarized in sea water than was observed in this work. These differences may be due to environmental factors. Nickel and nickel anodes polarized approximately 0.1 v at low current densities, but the titanium anodes polarized more than 10 v at 0.387 ma/cm².

Mears and Brown (1) and, later, May and LaQue (10) demonstrated that data of this type can also be used for estimating local cell polarization curves by plotting the observed potentials against calculated currents based on a number of assumptions.

According to Wesley (11), curves of this type, plotted with an anodic polarization curve, should be useful in estimating corrosion rates of galvanic couples. For example, the point of intersection of the

steel curve (Fig. 12) with the copper curve should represent the maximum current and, thus, the maximum corrosion rate of such a couple of equal areas, at zero *IR* drop and under the given conditions. An attempt to confirm this was unsuccessful with the closed system employed. Contamination by iron products drastically altered test conditions, preventing detectable polarization of the copper cathode, so that corrosion proceeded at a very rapid rate.

ACKNOWLEDGMENTS

This investigation was conducted under a Fellowship granted by the International Nickel Company, Inc., New York, New York, and under contract N6ori-17, Task Order II, between the Office of Naval Research and the Ohio State University Research Foundation. The interest and support of The International Nickel Company, Inc., and the Office of Naval Research are appreciated.

Any discussion of this paper will appear in a Discussion Section to be published in the December 1955 JOURNAL.

REFERENCES

1. R. B. MEARS AND R. H. BROWN, *This Journal*, **97**, 75 (1950).
2. C. WAGNER AND W. TRAUD, *Z. Elektrochem.*, **44**, 392 (1938).
3. M. POURBAIX, *Corrosion*, **6**, 395 (1950).
4. R. H. BROWN, G. E. ENGLISH, AND R. D. WILLIAMS, *ibid.*, **6**, 186 (1950).
5. J. M. PEARSON, *Trans. Electrochem. Soc.*, **81**, 485 (1942).
6. W. M. LATIMER, "The Oxidation States of the Elements and Their Potentials In Aqueous Solutions," p. 293, Prentice Hall, Inc., New York (1938).
7. F. L. LAQUE, *Proc. Am. Soc. Testing Materials*, **51**, 495 (1951).
8. D. SCHLAIN, *U. S. Bur. Mines Rept. Invest.* 4965, April 1953.
9. N. HACKERMAN AND C. D. HALL, JR., *This Journal*, **101**, 321 (1954).
10. T. P. MAY AND F. L. LAQUE, *Corrosion*, **10**, 91 (1954).
11. W. A. WESLEY, *Proc. Am. Soc. Testing Materials*, **40**, 690 (1940).

Effect of Oxygen, Chlorides, and Calcium Ion on Corrosion Inhibition of Iron by Polyphosphates¹

H. H. UHLIG, D. N. TRIADIS, AND M. STERN

Corrosion Laboratory, Department of Metallurgy, Massachusetts Institute of Technology, Cambridge, Massachusetts

ABSTRACT

Data are presented showing that sodium polyphosphates are effective corrosion inhibitors for steel, provided the dissolved oxygen concentration is above a critical minimum. Presence of calcium ion appreciably improves inhibition under all conditions. In solutions containing less than the critical amount of oxygen (1 ml/l), 60 ppm sodium polyphosphate accelerates corrosion. This is also true when 60 ppm Ca^{++} is added to the polyphosphate solution, although the critical oxygen concentration is now about 0.15 ml/l.

Sixty ppm sodium polyphosphate effectively inhibits against corrosion in solutions containing up to 0.01% NaCl; above this concentration, passivity by dissolved oxygen is lost, and the inhibitor is no longer effective. However, the calcium complex continues to function to some extent even at high chloride ion concentrations.

The foregoing corrosion data combined with polarization and potential studies indicate that sodium polyphosphates inhibit by favoring the passivation of steel by adsorbed oxygen. The hydrous FeO film normally present on iron presumably reacts with polyphosphate to form a soluble complex, permitting higher surface concentrations of oxygen for a given concentration in solution. Corrosion control under these circumstances is mixed, and pitting occurs in presence of chlorides. Calcium salt additions lead to formation on cathode areas of a diffusion barrier film of unknown structure containing both calcium and phosphorus. This film appreciably reduces the corrosion rate, with control of corrosion, however, remaining mixed. Reasons for the need of continuous flow and aeration in practical systems are discussed.

INTRODUCTION

Inhibiting corrosion of iron and steel in water solutions by small additions of sodium polyphosphates, of which sodium metaphosphate is an example, has been described in the literature since 1940 (1-4). Engineering applications have sometimes led to doubtful results (5-7). Laboratory tests show that high concentrations of metaphosphates increase corrosion (3), but smaller additions reduce attack, optimum effects being obtained in the presence of calcium ion (3), together with agitation or continuous flow of inhibited solution, and in presence of dissolved oxygen (4). The mechanism of inhibition has been variously described as being due to adsorption of the metaphosphate or of a complex (1), or to laying down of a calcium carbonate film (8), or to a film of adsorbed oxygen favored by the presence of polyphosphate (9), or to a cathode film or perhaps positively charged colloidal particles laid down by an electrodeposition process (10). Knowledge of the basic factors and mechanism of inhibition, of course, is helpful to the proper application of polyphosphates in practical systems. It appeared worthwhile, therefore, to examine these

proposals in light of additional precise data relating corrosion rates: first, to dissolved oxygen, chloride and calcium concentrations and, second, to anodic and cathodic polarization behavior.

EXPERIMENTAL PROCEDURE

Corrosion Tests

Mild steel (0.06% C, 0.33% Mn, 0.01% P, 0.029% S) samples measuring 5 x 1 x 0.13 in. (12.7 x 2.5 x 0.33 cm) were used for weight loss tests. They were abraded to 00 emery paper, degreased in distilled benzene, and pickled 1 min in 5% HCl-5% H₂SO₄, rinsed in water, followed by acetone and distilled benzene. The specimens, as soon after surface preparation as possible, were suspended in a Pyrex jar containing 4 l of solution, in the center of which was located a glass chimney 1 $\frac{3}{4}$ in. (4.5 cm) in diameter and 7 in. (17.8 cm) high mounted on glass legs. A sintered glass aerator located within the chimney maintained saturation of the solution with gas (flow = 150 ml/min), and also stirred the solution mildly at an estimated rate of 1 in. (2.5 cm)/sec past the specimen surface. Each specimen was suspended from a hole drilled at one end, through which a glass hook was inserted; the latter, in turn, was mounted in a tightly fitting Lucite cover over the jar. A rubber gasket, aided

¹ Manuscript received June 1, 1954. This paper was prepared for delivery before the Boston Meeting, October 3 to 7, 1954.

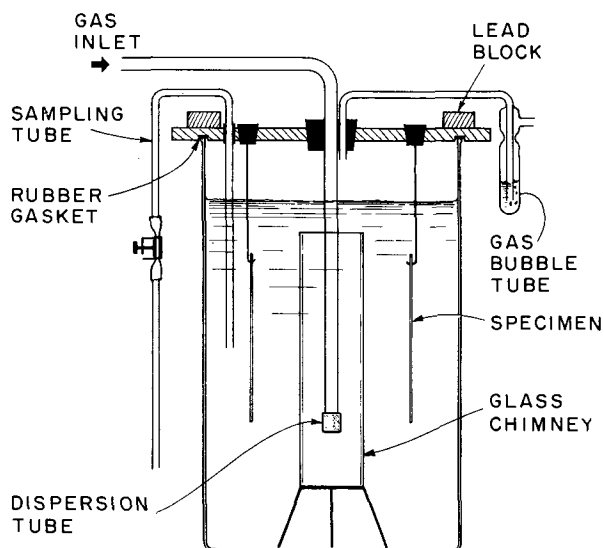


Fig. 1. Sketch of equipment for corrosion tests

by lead weights bearing down on the cover, sealed the jar against leakage of gas into or out of the gas space above the solution (Fig. 1).

The gases used for saturating the solution were bubbled through 10% NaOH to remove carbon dioxide, then through water and a glass-wool filter. Various partial pressures of oxygen were obtained by mixing nitrogen and oxygen in known amounts by use of calibrated flowmeters. Solutions were saturated for several hours or overnight before inserting the specimens. Gas concentrations in solution were calculated from known solubilities using Henry's Law, with several Winkler analyses for dissolved oxygen confirming that this procedure was satisfactory. Solutions free of dissolved oxygen were obtained by bubbling through nitrogen which had first passed over a 4-ft length of copper turnings maintained at 400°C. A sample of the deaerated solution was analyzed before tests to check for complete removal of oxygen. The pH values of the solutions were also measured before and after tests.

Following exposure, specimens were brushed under tap water, immersed in boiling 10% sodium hydroxide containing 10–20 grams of zinc powder/liter, brushed again, immersed in acetone and distilled benzene, and weighed. The polyphosphate inhibitor (Calgon²) was obtained in the form of a glass supplied through the courtesy of Hall Laboratories. This was ground in a mortar and the correct amount added to distilled water just before the tests in order to minimize reversion to the orthophosphate. According to Morgan and Swoope (11), commercial polyphosphate contains about 76% NaPO₃ and 24% Na₄P₂O₇.

² Produced by Calgon, Inc., Pittsburgh, Pennsylvania.

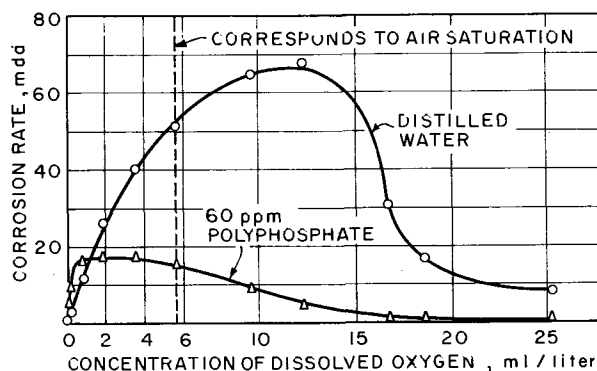


Fig. 2. Effect of partial pressure of oxygen on corrosion of mild steel in slowly moving water and in sodium polyphosphate solutions, 48-hr tests, 25°C.

Some tests were carried out with renewal of the 4l of solution each day, but results were not greatly different from those carried out with the same solution for a period of 7 days. Perhaps this is not unexpected in view of the slow reversion of polyphosphates to orthophosphates in the neutral range of pH at room temperature. Morgan and Swoope (11) found that in distilled water at room temperature, metaphosphate solutions decomposed to the extent of 10% within 30 days, and pyrophosphates were not measurably changed within this time. The majority of corrosion rates herewith reported are for the same solution retained for as long as 7 days.

All corrosion tests and potential measurements were conducted in an air thermostat maintained at $25^\circ \pm 0.5^\circ\text{C}$.

Effect of Dissolved Oxygen and Calcium

Data for mild steel exposed two days to distilled water containing 60 ppm polyphosphate as a function of dissolved oxygen are shown in Fig. 2. Each point represents the average of at least two specimens. Obviously, the polyphosphate is an effective inhibitor in solutions containing more than 2 ml O₂/l, but actually accelerates corrosion when the oxygen concentration is below about 1 ml/l. Similarly shaped curves and comparable corrosion rates, hence identical conclusions, are reached from 7-day exposure tests, data for which were obtained in solutions containing essentially zero up to 5.75 ml O₂/l (12).

Exposures for various times up to 7 days indicate, by and large, a steady rate of attack, with evidence of temporary passivity and corresponding lack of attack in some specimens for perhaps the first few hours, or sometimes the first day or two. Specimens exhibiting irreproducible passivity of this kind either were not included in the final summary of data, or the accepted corrosion rate was obtained

from the slope of weight loss vs. time after such period as the specimens began to corrode.

In absence of dissolved oxygen, mild steel exposed to distilled water suffers an uncertain very small weight loss, the rate being a maximum of 0.2 mdd. This can be compared with about 0.3 mdd obtained by Pryor and Cohen in deaerated water (13). But in presence of 60 ppm polyphosphate, attack becomes considerably greater, the average rate being 5 mdd. Presumably, complexing action of the polyphosphate is sufficient to increase the driving force of the corrosion reaction with consequent liberation of hydrogen. Specimens immersed in deaerated polyphosphate solutions accordingly become covered with an adherent black corrosion product not observed when polyphosphates are absent. The increased corrosion rate in presence of inhibitor at zero oxygen concentration is discernible in Fig. 2, and is presented in greater detail in Fig. 3, together with data on effect of calcium chloride. From data of Fig. 4, and similar data by Hatch and Rice (3), it is obvious that higher concentrations of sodium polyphosphate produce increased attack in both aerated and deaerated solutions.

Rates of attack in deaerated sodium polyphos-

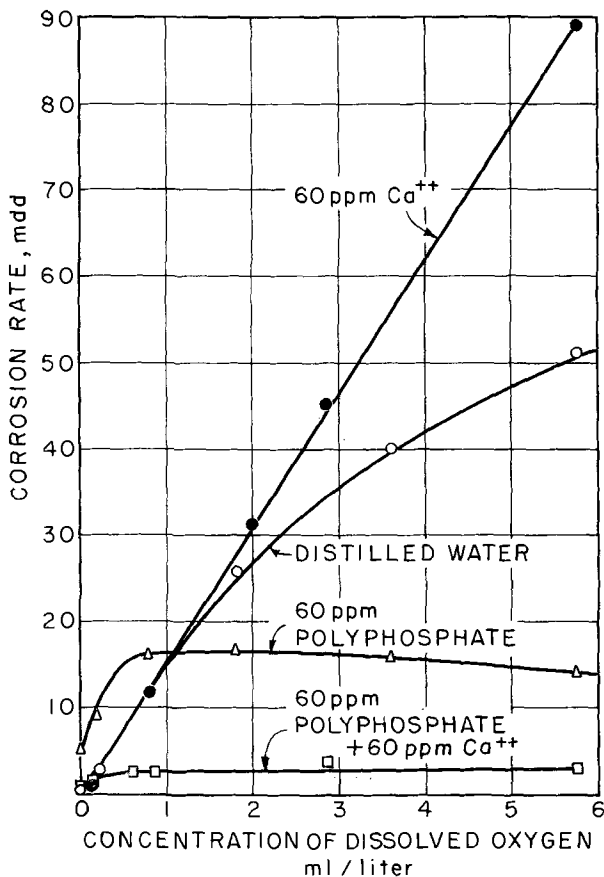


FIG. 3. Effect of CaCl₂ and O₂ on corrosion of mild steel in slowly moving water and in polyphosphate solutions, 48-hr tests, 25°C.

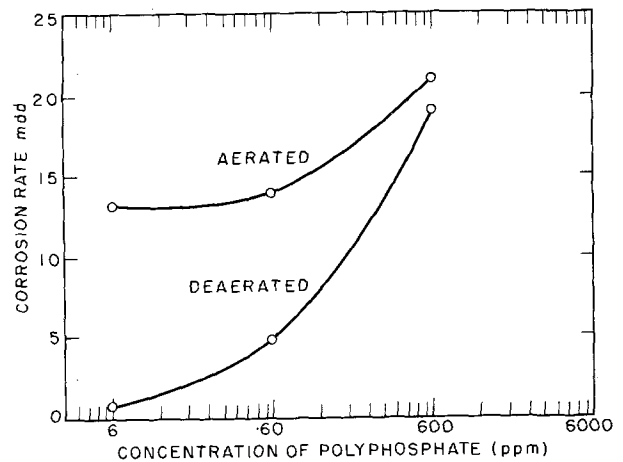


FIG. 4. Effect of sodium polyphosphate concentration on corrosion of mild steel in aerated and deaerated solutions, 48-hr tests, 25°C.

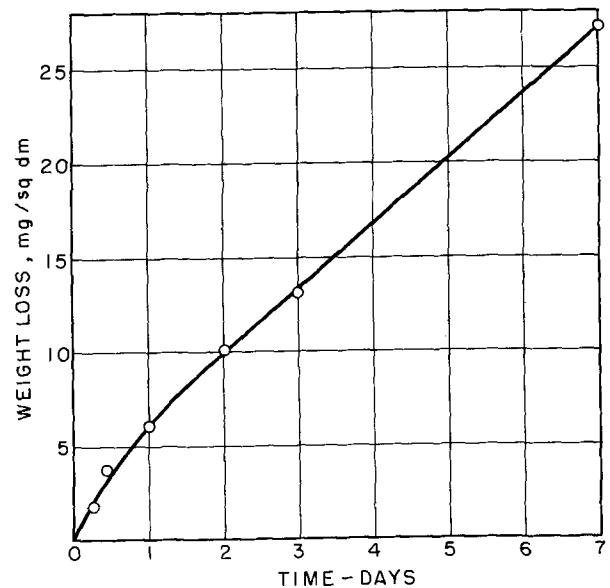


FIG. 5. Weight loss of mild steel vs. time in deaerated 60 ppm sodium polyphosphate solution, 25°C.

phate are initially higher than for final steady state (Fig. 5), probably because the iron polyphosphate complex is less corrosive than the sodium complex.

All solutions were essentially at pH 7 when tests began, and changed no more than a few tenths pH unit in the alkaline direction after exposure for several days in aerated or oxygenated solutions. In deaerated sodium polyphosphate, the pH reached 9.0, suggesting that the corrosion rate would have been still higher had the pH been maintained at 7.

Fig. 2 indicates that oxygen itself is a fair passivator for mild steel when present in high concentrations, but with polyphosphate additions improving matters still further. The inhibiting effect of oxygen alone has been pointed out previously by other investigators (14, 15). A partially passivating effect of oxygen is manifest in Fig. 2, even at low

TABLE I. Corrosion rates of mild steel in deaerated solutions (48-hr exposure; average of 2 or more spec.)

Polyphosphate conc.	Corrosion rate, mdd
0.0	0.2
60 ppm	5.0
60 ppm + 60 ppm Ca ⁺⁺ as CaCl ₂	0.6

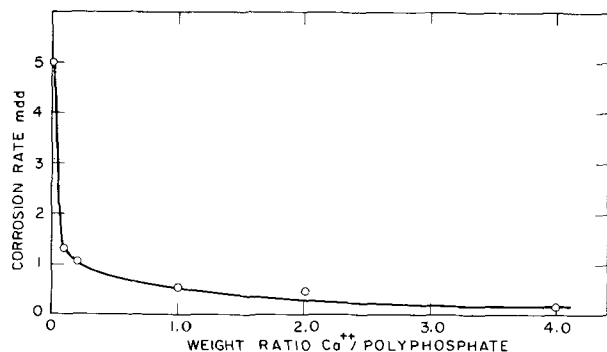


FIG. 6. Effect of weight ratio of calcium (as chloride) to 60 ppm sodium polyphosphate on corrosion rate of mild steel in deaerated solutions, 48-hr tests, 25°C.

oxygen partial pressures, by the curvature of corrosion rate plotted with oxygen concentration. Normally, in natural waters containing dissolved salts, a linear relation is maintained up to oxygen concentrations corresponding to air saturation (approximately 6 ml/l) or above. Accordingly, addition of 165 ppm CaCl₂ to distilled water in the authors' experiments confirmed that the corrosion rate is linear with oxygen concentration (Fig. 3), presumably because chloride ions prevent initiation of passivity within this range of oxygen concentration.

Although CaCl₂ accelerates corrosion of mild steel in distilled water, its presence added arbitrarily in the amount of 60 ppm Ca⁺⁺ (165 ppm CaCl₂), improves inhibition by polyphosphates as Fig. 3 shows, confirming conclusions by Hatch and Rice (3). The corrosion rate in presence of Ca⁺⁺ and above 1 ml O₂/l is on the average only 1/6th that in absence of Ca⁺⁺. However, in complete absence of oxygen, 60 ppm polyphosphate plus 60 ppm Ca⁺⁺ is slightly corrosive to mild steel, although the rate of attack is less for the calcium polyphosphate complex than for the corresponding sodium salt. Data are summarized in Table I. Fig. 6 shows that further addition of CaCl₂ reduces the corrosion rate to a value below 0.6 mdd.

Effect of NaCl

In view of the fact that chloride ions are present in many natural waters and can break down passivity, the behavior of polyphosphates in presence of NaCl has practical interest. Data are summarized

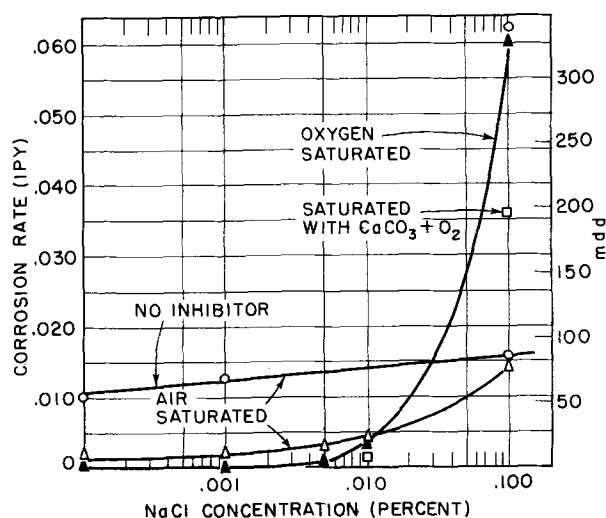


FIG. 7. Effect of sodium chloride concentration on corrosion of mild steel in water and in 60 ppm polyphosphate solutions, 7-day tests, 25°C.

in Fig. 7 for both air- and oxygen-saturated solutions. Polyphosphate present to the extent of 60 ppm is an effective inhibitor up to 0.01% NaCl (100 ppm), and oxygen-saturated solutions corrode mild steel less than do aerated solutions. At higher NaCl concentrations, however, the inhibitor is no longer effective, and high oxygen concentrations corrode steel at a much higher rate than do aerated solutions.

Calcium ion added to sodium polyphosphate appreciably reduces rate of attack, even though the concentration (approximately 3 ppm Ca⁺⁺) corresponds to no more than that resulting from saturation of the solution with CaCO₃. Additional amount of calcium salt would be expected to reduce attack still further.

Pitting attack was typical of specimens immersed in NaCl solutions, the maximum depth of pits in 0.01% NaCl after 7 days reaching several mils in absence of calcium, and several tenths mil in its presence. Pitting was not observed in chloride-free solutions. Formation of soluble or dispersed complexes of iron polyphosphates as a result of corrosion was evident from the transparent light yellow solutions of corrosion products, whereas in absence of polyphosphates insoluble rust flocs formed instead.

Potential and Polarization Measurements

Potentials of mild steel in contact with polyphosphate solutions were carried out to better understand the mechanism of inhibition. Time-potential curves were followed over a period of 48 hr in solutions containing (a) 60 ppm polyphosphate, and (b) the same solution with salts equivalent to 60 ppm Ca⁺⁺, Mg⁺⁺, or Na⁺ added as chlorides. Three representative and convenient concentrations of

dissolved oxygen were selected, namely, deaerated, air-saturated, and oxygen-saturated.

The cell for potential determinations, as well as for subsequent polarization measurements, consisted of three compartments separated from each other by two sintered glass diaphragms. Mild steel specimens were placed in the central 1-liter compartment, and two platinum electrodes in the two outer smaller compartments. This arrangement provided for uniform current density of the mild steel electrode, and avoided contamination of anolyte with catholyte. All three compartments were kept saturated with appropriate gas by bubbling it through sealed-in dispersion tubes at the bottom of each compartment. Potentials were measured with respect to Ag-AgCl in 0.1*N* KCl, which made contact through a salt bridge filled with solution of the same composition as that in contact with mild steel. Because of the high resistance of solution and bridge, an electronic galvanometer was necessary for potential measurements used in conjunction with a precision potentiometer.

The steel electrode, measuring approximately 0.8 x 0.8 x 0.13 in. (2 x 2 x .33 cm), was mounted at the end of a glass tube enclosing a connecting wire. A Teflon washer, separating glass and the electrode, prevented solution coming into contact with metal other than the electrode itself. Surface preparation and composition of the electrode were the same as in the weight loss tests.

Fig. 8 shows that steady-state values of potential are achieved after several hours. Since the half-cell potential of 0.1*N* Ag-AgCl is 0.288 v, the potential of mild steel in deaerated sodium polyphosphate solution, neglecting a small liquid junction potential, is -0.62 on the normal hydrogen scale. This can

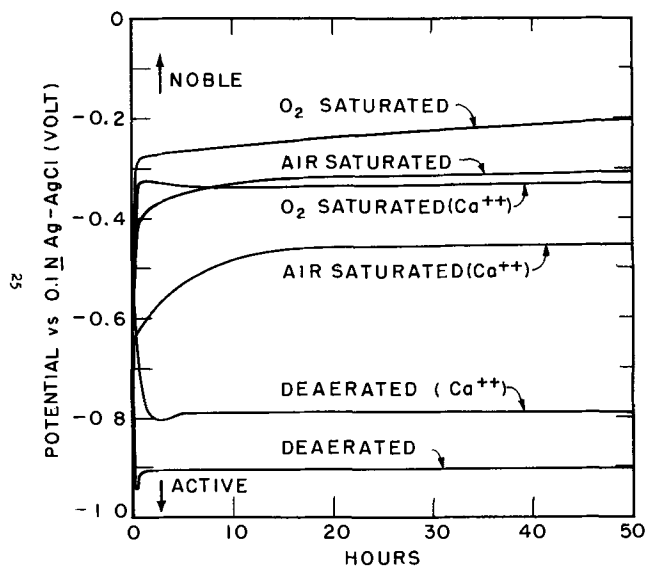


FIG. 8. Potential vs. time for mild steel in 60 ppm polyphosphate solutions in absence and presence of 60 ppm Ca⁺⁺

be compared with -0.54 v for mild steel in deaerated 4% NaCl (16). The difference is ascribable to the complexing action of polyphosphate with iron salts, thereby reducing Fe⁺⁺ activity below the value associated with saturated hydrous ferrous oxide otherwise covering the metal surface. Complexing action shifts the potential in the active direction, in accord with the Nernst equation which expresses the potential of iron as a function of ferrous ion activity. Various soluble complexes of iron with sodium metaphosphate have been described in the literature (17-19).

Addition of calcium salts alters the potential in the noble direction by about 0.1 v, which may be evidence that Fe⁺⁺ is not complexed to the same extent by the calcium polyphosphate solution. Since it is always the corrosion potential that is observed and not the equilibrium potential, interpretation of the actual situation is complicated by change in corrosion rate brought about by Ca⁺⁺ and corresponding change in the anodic and cathodic polarization of local galvanic couples. Chloride ion associated with CaCl₂ is apparently not responsible for the shift in potential, because Ca(NO₃)₂ was found to produce the same shift. By the same token, 60 ppm Na⁺ as NaCl added to 60 ppm polyphosphate reproduced the potential behavior for deaerated polyphosphate solution in absence of Ca⁺⁺. When, however, 60 ppm Mg⁺⁺ was added as chloride, the potential behavior was the same as that produced by Ca⁺⁺ addition.

Oxygen and air produce more noble potentials, the maximum change reaching a value as high as 0.7 v. This can be taken as true indication of passivity by Definition 1, according to the "Corrosion Handbook" (20), with oxygen as the passivator. Calcium ion, this time, alters the potential in the active direction, opposite to its effect in deaerated solutions, indicating increased polarization of the local action cathodes on the iron surface.

Polarization data were obtained with mild steel electrodes previously exposed to either aerated or deaerated solutions for 48 hr. Results are presented in Fig. 9 and 10. Data for oxygenated solutions were almost identical to those in aerated solutions and, hence, are not shown. The majority of measurements represent relatively steady-state values after about 3 to 5 min for each point. For anodic polarization in regions where the potential changed markedly, time to achieve steady state required as long as one hour.

In absence of calcium ions, it is obvious that anodic polarization is much more pronounced than is cathodic polarization, and that the situation reverses itself when calcium chloride is added. Furthermore, anodic polarization is much more pro-

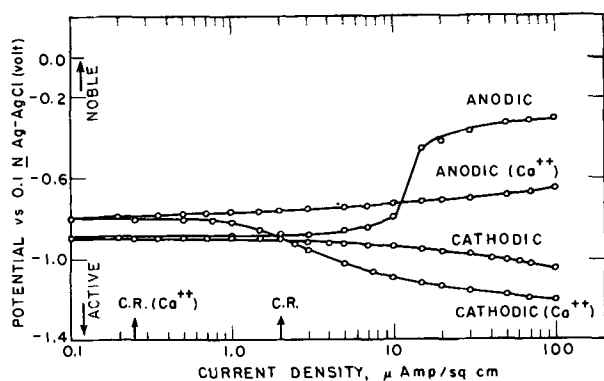


FIG. 9. Polarization curves for mild steel in deaerated 60 ppm polyphosphate solutions in absence and presence of 60 ppm Ca^{++} . C.R. = observed corrosion rate.

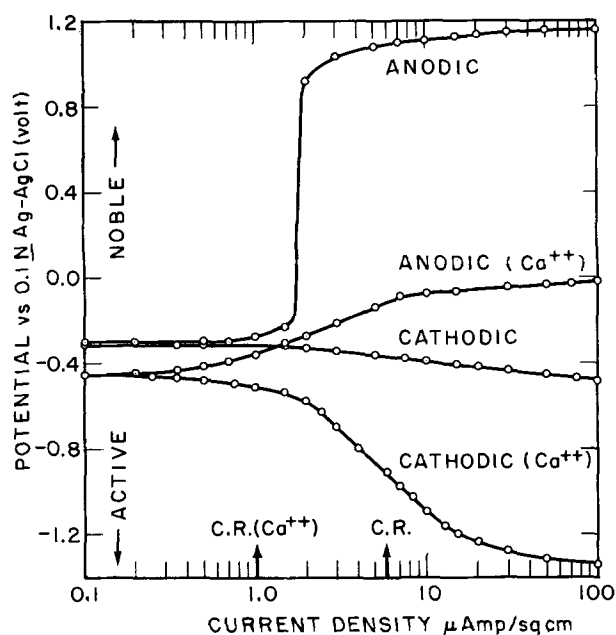


FIG. 10. Polarization curves for mild steel in aerated 60 ppm polyphosphate solutions in absence and presence of 60 ppm Ca^{++} . C.R. = observed corrosion rate.

nounced in presence of oxygen. Although pronounced cathodic polarization in presence of calcium chloride is undoubtedly associated with Ca^{++} , the parallel reduction of anodic polarization is caused instead by Cl^- . This was demonstrated by adding 60 ppm Na^+ as NaCl to 60 ppm sodium polyphosphate and noting a similarly shaped curve. Magnesium chloride additions produced the same polarization curves as calcium chloride additions.

DISCUSSION

The data clearly show that sodium polyphosphates are effective corrosion inhibitors, provided the dissolved oxygen concentration is above a critical minimum. The lowest permissible concentration of oxygen is reduced by presence of calcium ions, and

the effect of dissolved oxygen, in general, is not so marked for solutions containing calcium. In solutions below the critical oxygen concentration, or in deaerated solutions, polyphosphates with or without calcium accelerate attack of steel rather than inhibit corrosion. The rate of attack with 60 ppm Ca^{++} added to deaerated 60 ppm polyphosphate solution is reduced to about $\frac{1}{10}$ th the value for the sodium salt alone.

The beneficial effect of oxygen confirms in part the proposal by one of the authors (9) that inhibition by sodium metaphosphate, or better described as polyphosphates, results from passivation by oxygen. As Fig. 2 shows, oxygen in sufficiently high concentrations passivates iron even in absence of polyphosphates; but at lower concentrations (i.e., air saturation), all oxygen reaching the metal surface is reduced at cathodic areas, and oxygen correspondingly acts as a depolarizer. The corrosion rate for this situation is approximately proportional to oxygen concentration, since the amount of oxygen diffusing through the barrier surface film of hydrous FeO is also proportional to oxygen concentration. However, at high concentrations, more oxygen reaches the iron surface than can be cathodically reduced, whereupon excess oxygen is available to chemisorb on or passivate the metal, with attendant falling off of the corrosion rate and a change of potential in the noble direction. This mechanism of passivity is similar to that postulated for stainless steels (21). One might also hypothesize formation of an oxide film, but this is difficult to visualize in presence of soluble polyphosphate complexes. In fact, it is probably because the naturally formed barrier oxide film on iron is removed by reaction with polyphosphates to form soluble iron complexes that more oxygen can reach the metal surface for a given oxygen concentration in solution, and hence passivity is established at lower oxygen concentrations. This situation for aerated sodium polyphosphate solutions³ accounts for reduced corrosion rates in Fig. 2.

But this model also predicts that, if oxygen concentration is sufficiently low, a value is eventually reached for which surface oxygen again acts as a depolarizer, and the corrosion rate should increase. This prediction is confirmed by the authors' data, and explains why sodium polyphosphates in solutions of low oxygen concentration are accelerators rather

³ Dissolving the film in acid also accomplishes solution of the hydrous FeO film, except that in so doing more acid is brought to the surface, and ample adsorbed hydrogen is produced to react with the increased oxygen supply. With this state of affairs, corrosion always increases. At a neutral pH , as in the case of polyphosphate solutions, the concentration of hydrogen ions is much less.

than inhibitors of corrosion. In deaerated solutions, passivity by oxygen, of course, no longer applies, and corrosion is attended by evolution of hydrogen, the tendency to corrode (i.e., emf of local action cells) being increased by complexing of ferrous ions.

For oxygen concentrations within the region of marked passivity, presence of chloride ion is apt to cause pitting because of the well-known local breakdown of passivity caused by halogen ions. Pitting of stainless steels occurs for similar reasons (22). Local anodes are formed of restricted area where chloride ions competitively displace adsorbed oxygen, such areas being surrounded by broad areas of cathode (passive metal). The combination forms passive-active cells having high emf. Data of Fig. 8 indicate that potential differences inside (low O_2) and outside (high O_2) the pits may amount to about 0.6 v. Calcium ion reduces this potential difference, but does not eliminate it; hence, pitting may also be observed when calcium polyphosphates are used as inhibitors in aerated chloride solutions.

The important part played by calcium ions requires explanation over and above that given above for sodium polyphosphates, since both the present data and previously published observations indicate that the mechanism is quite different. Polarization and potential studies (Fig. 8, 9, 10) show that calcium salts increase cathodic polarization, and, hence, shift greater control of the corrosion rate to the cathode reaction. This fact was also pointed out by Hatch (9). Earlier, Mansa and Szybalski (23) reported that commercial polyphosphates increase polarization of cathodic areas. Experiments by Hatch indicated that relatively thick insoluble phosphate films are electrodeposited by the corrosion process on cathodic areas. The films were stated to contain calcium and to form on any conducting cathode, and not on iron alone. Lamb and Eliassen (24) using radioactive tracers, confirmed that phosphates are deposited on the cathode when current flows. Films so deposited are often thick enough to be visible, and presumably act as diffusion barrier layers impeding access of oxygen to the metal surface. In presence of such a protective barrier, dissolved oxygen has less effect on the over-all corrosion rate; however, oxygen concentration cells can still function, even though the potential difference of such cells is less.

Since there is pronounced inhibition in absence of both calcium salts and carbon dioxide, it is obvious that Raistrick's proposal is not tenable, namely that a protective film of calcium carbonate enters the mechanism of inhibition. Polyphosphates, as a matter of fact, would be expected to dissolve such films rather than to favor their formation.

The practical necessity of continuous flow when using polyphosphate-inhibited solutions is explained by the need to form a continuous protective cathode film over all the metal surface which, in turn, depends on a uniform corrosion rate. If corrosion currents are localized, as would be the tendency in stagnant solutions, obviously the cathode film would form in discontinuous patterns, with consequently lower level of protection. The present investigation indicates, in addition, that high surface oxygen concentrations, which motion of the liquid favors, are desirable from the standpoint of maintaining optimum passivity. Continuous agitation of solution is also necessary to avoid initiation of passive-active cells with attendant pitting. In presence of chlorides corresponding to over 0.01% NaCl, it is essential that calcium ions be present simultaneously, since, in this event, only the cathode diffusion barrier film retards corrosion, and passivity by oxygen is either spotty or does not occur at all. Similarly, adsorption and passivity by oxygen are not expected to function at elevated temperatures. It is the cathodic film that apparently accounts for temporary continuing inhibition in flowing systems after polyphosphate treatment is reduced or discontinued.

In deaerated solutions, the corrosion potential on the normal hydrogen scale (-0.62 v) undoubtedly approximates the open circuit (O.C.) anodic potential (since the anode polarizes less than the cathode), and the cathodic O.C. potential equals -0.0592 pH or -0.41 v. With or without Ca^{++} , therefore, the reaction is cathodically controlled. In aerated solutions, on the other hand, considering the anodic

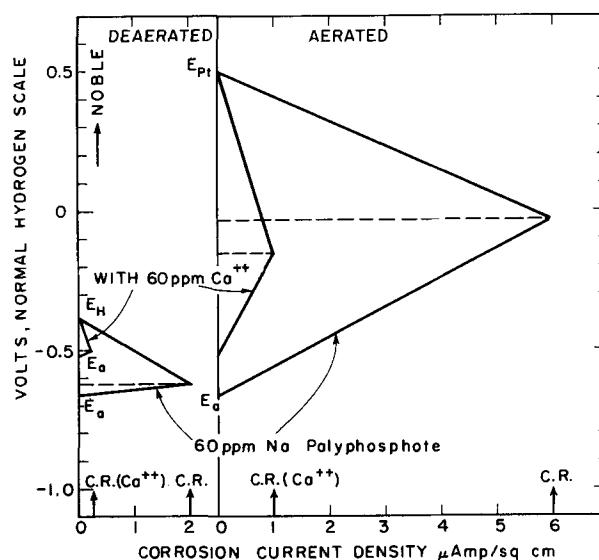


Fig. 11. Schematic polarization curves for equal anodic and cathodic areas on mild steel for deaerated and aerated solutions.

O.C. potential to remain the same, and the cathodic potential, 0.5 v, to be given by the measured potential of a platinum electrode in the same solution (the oxygen reversible potential is 0.81 v), an observed corrosion potential of -0.03 v suggests mixed control (Fig. 11). In presence of calcium, a corrosion potential of -0.16 v shifts control slightly in the anodic direction, but the over-all control is still mixed. Only at such time as the cathodic O.C. potential approaches the hydrogen potential accompanying total loss of passivity through presence of chloride ion or by some other factor, does corrosion control become largely cathodic. Schematic polarization diagrams depicting these relations are given in Fig. 10, with anode and cathode areas assumed equal, for sake of simplicity.

The present investigation, therefore, confirms that the mechanism of inhibition by calcium polyphosphates includes a diffusion barrier film on cathodic areas which increases cathodic polarization. In addition, passivation by dissolved oxygen occurs above a minimum partial pressure of oxygen, with consequent increased polarization of anodic areas. In presence of oxygen, corrosion control is mixed.

ACKNOWLEDGMENT

This research was supported by the Shell Companies of the U. S. to whom the authors express their appreciation. R. C. Lutton carried out valuable preliminary experiments.

Any discussion of this paper will appear in a Discussion Section to be published in the December 1955 JOURNAL.

REFERENCES

1. G. B. HATCH AND O. RICE, *Ind. Eng. Chem.*, **32**, 1572 (1940).
2. *Ibid.*, **37**, 710 (1945).
3. *Ibid.*, **37**, 752 (1945).
4. M. COHEN, *Trans. Electrochem. Soc.*, **89**, 105 (1946).
5. P. PALLO, *J. Am. Water Works Assoc.*, **38**, 499 (1946).
6. O. RICE, *ibid.*, **39**, 552 (1947).
7. "Committee on Water Conditioning Methods to Inhibit Corrosion," *J. Am. Water Works Assoc.*, **34**, 1807 (1942).
8. B. RAISTRICK, *Chemistry & Industry*, **1952**, 408.
9. H. H. UHLIG, *Métaux et corrosion*, **22**, 204 (1947).
10. G. HATCH, *Ind. Eng. Chem.*, **44**, 1774 (1952).
11. R. MORGAN AND R. SWOPE, *ibid.*, **35**, 821 (1943).
12. R. C. LUTTON, M.S. Thesis, Massachusetts Institute of Technology, 1952.
13. M. PRYOR AND M. COHEN, *This Journal*, **100**, 203 (1953).
14. E. GROESBECK AND L. WALDRON, *Proc. Am. Soc. Testing Materials*, Part II, **31**, 279 (1931).
15. G. SCHIKORR, *Z. Elektrochem.*, **39**, 52 (1933).
16. H. H. UHLIG, N. CARR, AND P. SCHNEIDER, *Trans. Electrochem. Soc.*, **79**, 111 (1941).
17. O. SAMULSON, *Svensk. Kem. Tidskr.*, **56**, 277 (1944).
18. D. KANTZER, *Compt. rend.*, **220**, 661 (1945).
19. P. NAVET, *Tech. Eau*, Belgium, June 1947; *C.A.*, **41**, 6003 (1947).
20. H. H. UHLIG (Editor), "Corrosion Handbook," p. 21, John Wiley & Sons, Inc., New York (1948).
21. H. H. UHLIG, *Chem. Eng. News*, **24**, 3154 (1946); *This Journal*, **97**, 215C (1950).
22. H. H. UHLIG (Editor), "Corrosion Handbook," p. 165, John Wiley & Sons, Inc., New York (1948).
23. J. MANSÁ AND W. SZYBALSKI, *Acta Chem. Scand.*, **4**, 1275 (1950).
24. J. C. LAMB AND R. ELIASSEN, *J. Am. Water Works Assoc.*, **46**, 445 (1954).

Solid Dielectric Breakdown Techniques¹

J. J. CHAPMAN, L. J. FRISCO, AND J. S. SMITH

Dielectrics Laboratory, The Johns Hopkins University, Baltimore, Maryland

ABSTRACT

Successful measurement of the breakdown strength of solid insulating materials is greatly dependent on the type of electrodes used. It was found, in studying materials over the frequency range from 60 cps to 100-megacycles/sec, that it was usually necessary to imbed the high voltage electrode.

A method is described that has proved widely applicable and free from compromising effects. Solder may be sprayed from a gun into a properly shaped cavity to form a perfectly imbedded electrode. Specimens that have been conditioned at high humidity may be equipped with such sprayed electrodes within a few minutes after removal from exposure. Tests were made over a temperature range from -55°C to 125°C . The procedure, with minor variations, has been applied successfully to ceramic, laminated thermosetting, molded thermosetting, and rigid thermoplastic materials.

INTRODUCTION

The ever increasing interest in the electrical properties of insulating materials has led to investigation of the dielectric strength of solid materials in the frequency range from 60 cycles to 100 megacycles. Results of these studies have shown that, without exception, the dielectric strength of solids decreases very drastically with increasing frequency.

Fig. 1 illustrates the effect of frequency on the dielectric strength of two commonly used materials. Similar data on many other materials raise interesting questions as to the mechanisms which are involved in the breakdown process. To the designer, however, data of this type are of immediate practical importance, even though the phenomena continues to be a matter of conjecture.

Most of the data on electrical properties of insulating materials which is available to the designer pertains to dielectric constant and dissipation factor as functions of frequency, but dielectric strength is usually stated with no reference to frequency or, at most, a note on the particular 60-cycle test which was applied. The 60-cycle values of dielectric strength not only fail to provide data which are applicable at the higher frequencies, but do not contain information which is required to establish an order of preference when comparing several materials.

In order to enhance the usefulness of high-frequency dielectric strength data it is important to discuss the techniques involved in the collection of such data. Since the usual problems associated with dielectric strength measurements become more critical with increasing frequency, the test methods, which can be used successfully at the higher fre-

quencies, afford improvements in conventional low-frequency techniques. Methods described herein have been used successfully at frequencies ranging from 60 cycles to 100 megacycles on a wide variety of solid materials. Apparatus developed for use in these investigations has been described in other publications (1-3).

REQUIREMENTS OF A DIELECTRIC STRENGTH TEST

The primary requisite of a dielectric strength test is that the destructive effects of the field be limited to a volume within the specimen, bounded on opposite sides by the test electrodes. In other words, when failure occurs, it should not involve the medium in which the sample is immersed, nor should the breakdown path follow the surface of the specimen. This implies that prior to breakdown, as the voltage is being increased, there should be no evidence of incipient glow, or corona, in the immersion medium. Only when these conditions are met does the test indicate the dielectric strength of the specimen material, independent of the properties and the condition of the immersion medium.

In order to study solid breakdown it is necessary to eliminate the compromising effects which are often associated with dielectric strength tests. It is generally known that many spurious effects, such as corona, and accumulation of ionic impurities of the immersion medium in the neighborhood of the high voltage electrode, are time dependent. Therefore, it is always tempting to shorten the duration of a high voltage test and thereby avoid compromising phenomena that are impossible to evaluate.

Impulse studies constitute an important phase of dielectrics research but, in the case of solids, time dependent mechanisms are part of the chemical structure. and proper evaluation by the use of longer

¹ Manuscript received June 28, 1954.

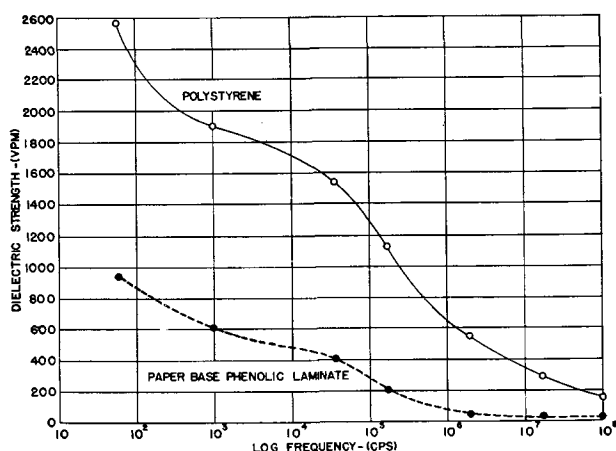


FIG. 1. Variation of dielectric strength with frequency for polystyrene and a paper base phenolic laminate.

time periods is a matter of theoretical and practical interest. To study slow mechanisms means that the specimen-electrode assembly must be electrically stable under longer periods of voltage application so that compromising effects do not enter into the tests. Since there are time-dependent mechanisms involved in the breakdown process, results which are obtained by impulse or pulsing techniques depend on pulse duration. Recourse to these methods has led to higher values of dielectric strength, and consequently has resulted in the use of the term "intrinsic breakdown." Although this may be a useful concept when agreement is reached on its definition and a method for its determination, it should not be implied that a breakdown which is accomplished in a relatively long period of time is not characteristic of the material. A breakdown which is the result of a gradual increase in voltage over a period of 1 min, if properly obtained, is as closely related to the inherent properties of a material, as one obtained with a 0.1 μ sec pulse. Naturally, the values are quite different since the mechanisms involved must necessarily respond in a different manner. The choice of time period depends on the information which is sought and the time-dependent mechanism to be studied.

The longer time period is more difficult experimentally, but ultimately one becomes interested in all mechanisms, even the very slowest, if they are inherent properties of the materials. It is possible to construct a composite dielectric, in a reproducible fashion, which consists of pure compounds. Such a material would exhibit time-dependent phenomena which arise at the interfaces; these phenomena would be inherent to the structure.

To satisfy current interest in the effects of frequency, temperature, moisture absorption, and irradiation on dielectric strength, it is injudicious to ascribe all anomalous behavior to the effect of "heat"

and thereby overlook important factors which influence the behavior of insulating materials. Although the basic structures of many commercial insulating materials appear to be simple, the distribution in chain length, plasticizer action, curing effects, etc., all lead away from precise description; however, these products are sufficiently uniform to be generally reproducible. Since such products represent the only solution to electrical design problems it is essential to evaluate their properties in such a manner that all of the inherent complexities which affect those properties are permitted to exert their influence. Some of the additives in a commercial material, from an electrical viewpoint, are "impurities." However, through them, desirable mechanical and thermal performance is obtained; thus, even from an electrical viewpoint they must be considered inherent to the composition. Tests described herein involve commercial materials which were tested by applying a voltage which was increased from zero to maximum in a period of approximately 40 sec.

Fig. 2 shows a cross-sectional view of the simplest specimen-electrode system, employing conventional electrodes. This arrangement is satisfactory for the very low strength materials at all frequencies up to 100 megacycles. Specimen and electrodes are immersed in transformer oil in order to increase the voltage level at which corona appears in the region around the high voltage electrode, where the electrode meets the surface of the specimen. At 60 cycles it is possible to use larger electrodes of smooth contour and thereby eliminate the troublesome effects of corona in the case of materials of moderate dielectric strength. However, larger electrodes cannot be used at high frequencies because the resulting specimen capacitance would normally be beyond the limit imposed by the requirements of the resonant test circuits which must be employed (1, 2). Moreover, at 60 cycles, recourse to such electrodes will not solve the corona problem for all materials; the very high dielectric strength plastics require a more perfect arrangement.

The limitation of this simple arrangement arises from the fact that often the liquid immersion medium has a lower dielectric strength and a lower dielectric constant than the material which is being tested.

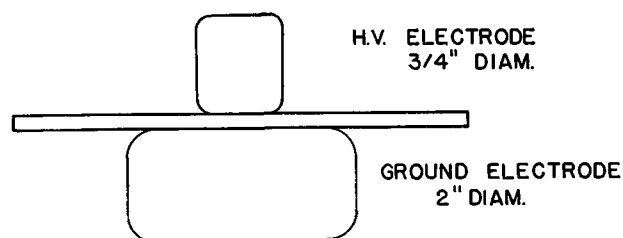


FIG. 2. Conventional electrode arrangement for low-frequency dielectric strength tests.

Two general methods can be used to overcome the difficulty; (a) use a semiconducting surface film in the critical region thus grading the field; and (b) fill the critical region with a material which can withstand the stress to which it will be subjected in the course of the test.

Both methods have been used with considerable success (1), although the former one is restricted to low-frequency investigations. At higher frequencies it proved necessary to use fillets of high dielectric strength material. However, where specimen thickness permitted, the use of recessed cavities to contain the high voltage electrode provided the most homogeneous and certain field configuration. Various types of recessed electrodes have been used by many investigators (1, 2, 4, 5). The fact that the preparation of such cavities for the purpose of careful research is difficult has caused the authors to seek improved techniques that would serve a wide range of practical materials as well as those most promising for theoretical study.

FURTHER DEVELOPMENT OF THE RECESSED BREAKDOWN ELECTRODE

Specimens described below were developed to serve a wide area of investigation involving a large variety of materials which were to be tested at several frequencies, after exposure to various conditions of temperature and humidity.

Fig. 3 shows a cross-sectional view of a specimen which can be drilled or molded in such a way that the cavity conforms to the shape of a $\frac{3}{4}$ in. diameter cylindrical electrode. Intimate contact between the high voltage electrode and the specimen is accomplished by coating the cavity with a metallic film. A 2 in. diameter circular area on the bottom surface of the specimen is also coated to provide intimate contact with the ground electrode.

Commercially available silver paint was tried first (1) and proved satisfactory. However, a recent development is the prime reason for further reporting. It was found possible to apply solder film to the surface of solid insulating bodies in such a manner that the contact is intimate. The solder film has the advantages of no drying period and stability in the presence of solvents.

Various types of metal spray guns are available which can be used with many different metals. Since low melting point metals form excellent electrode surfaces, an inexpensive gun, designed to spray solder, does an excellent job.² The only auxiliary equipment required to operate this type of gun is a source of compressed air.

² The "Emess Hi-Heat Gun," manufactured by the Emess Tool and Chemical Corporation, has been used for this purpose with complete success.

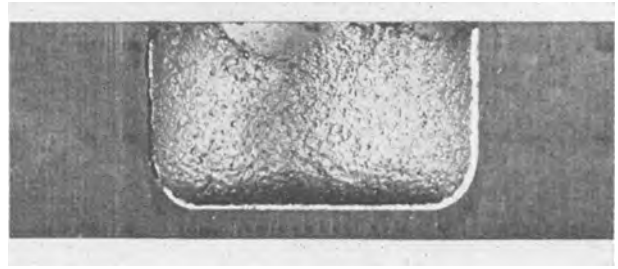


FIG. 3. Cross-sectional view of molded $\frac{3}{4}$ in. diameter cavity coated with solder spray.

A masked sample can be sprayed quickly with the desired thickness of solder film. The solder solidifies immediately and very little heat is transferred to the specimen. The solder film makes perfect contact with the specimen and provides a surface of very high conductivity which the brass electrodes can engage. Since the cavity is coated with a metallic film it is not necessary for the brass electrode to make a perfect fit, because its only function is to engage the solder film. Any voids between the brass electrode and the solder film are in a field-free space, and consequently will not cause any compromising effects.

In order to prepare the surface to be sprayed it is necessary to remove the glaze usually present on most materials. This is accomplished by lightly sandblasting the area just enough to dull the surface finish. A small sandblasting machine³ can be readily adapted to give excellent performance.

The sample shown in Fig. 3 is a cellulose-filled melamine molded material. In this case, the $\frac{3}{4}$ in. diameter cavity was formed by the manufacturer during the molding process. The sample is $\frac{1}{2}$ in. thick and the thickness of material directly under the cavity is approximately 60 mils. The cavity has been sprayed with 50/50 solder. It can be seen that the solder film forms a very rugged conductive surface, which was only slightly damaged in cutting the sample in half. A cavity of this shape can also be formed in most materials by the use of a special drill. In the case of the very hard materials the drill must have a carbide tip.

With some laminates, the mechanical stresses which attend the use of such a flat drill cause delaminations to occur. In order to overcome this difficulty a more practical tapered cavity was introduced, which has proven to have several advantages over the cylindrical cavity of Fig. 3.

Fig. 4 shows a tapered cavity which was drilled in a $\frac{1}{2}$ in. thick glass silicone laminate specimens. A standard $\frac{1}{2}$ in. diameter twist drill is used in this operation. The diameter of the flat section is usually

³ A-C Spark Plug Cleaner, Model K.



FIG. 4. Cross-sectional view of $\frac{1}{2}$ in. diameter tapered cavity drilled in glass silicone laminate.

about twice as great as the thickness of the section directly under the center of the cavity. This configuration results in a very favorable field distribution, as evidenced by results which have been obtained with this type of specimen.

This type has proved successful with many types of materials. A commercially available carbide tipped drill is used with the hard materials. Some of the advantages of this type of specimen are:

(A) No special tools are required for its fabrication.

(B) In drilling the tapered cavity the material is not subjected to severe mechanical stresses which cause delaminations.

(C) The remaining section under the cavity is mechanically stronger than the section under a cylindrical cavity. This reduces the tendency for delamination and deformation during conditioning or handling of specimens.

A depth gauge is used to measure the thickness of the section under the cavity prior to testing. After the test has been completed the specimen is cut open and the breakdown distance is measured with a low power microscope. Assuming a uniform field distribution, the breakdown strength is computed by dividing the breakdown voltage by the distance in mils. Results obtained in this manner yield values of dielectric strength which are, in general, higher than those obtained with other methods. Since the tests are also more reproducible, it is felt that mechanical as well as electrical considerations have eliminated compromising effects.

PERFORMANCE TESTS

The values of dielectric strength shown in Fig. 1 were obtained with the $\frac{1}{2}$ in. diameter tapered cavity. Measurements were made on unconditioned samples which were tested at room temperature. In the case of polystyrene the specimens were subjected to voltages as high as 60 kv, with no evidence of corona around the high voltage electrode. The thickness of the polystyrene section was 20 mils in the breakdown region.

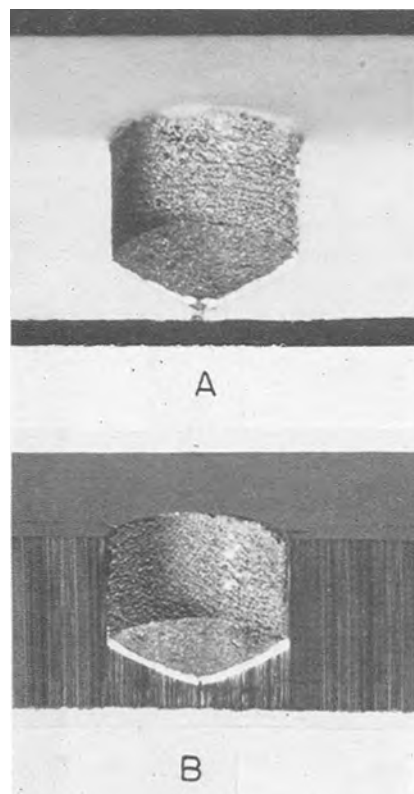


FIG. 5. Cross-sectional view of tapered cavity after 60-cycle breakdown on (A) polytetrafluoroethylene, (B) paper base phenolic laminate.

The solder film performs satisfactorily over the temperature range from -55°C to 125°C on numerous materials. At -55°C , Varsol is used as the immersion medium. Although this liquid has the properties of kerosene, which would make its use at room temperature hazardous, it can be used safely at low temperatures.

Polystyrene is a material that exhibits higher dielectric strength than many others over the wide frequency range explored. Therefore, even with rather thin sections it is necessary to operate at a high voltage level in order to obtain puncture. This critical test on a strong material proved the merits of this type of electrode.

The numerical results obtained are of course the main objective of an investigation, but the descriptive phenomena is also important from the standpoint of both theory and practice.

Fig. 5 shows the typical failures that are obtained at 60 cycles with polytetrafluoroethylene and a paper base phenolic laminate. This pinpoint type of puncture is characteristic of most materials at low frequency. As the frequency is increased, however, the character of the failure changes in the case of some materials. The polytetrafluoroethylene fails in the same sharp manner that it did at low frequency.

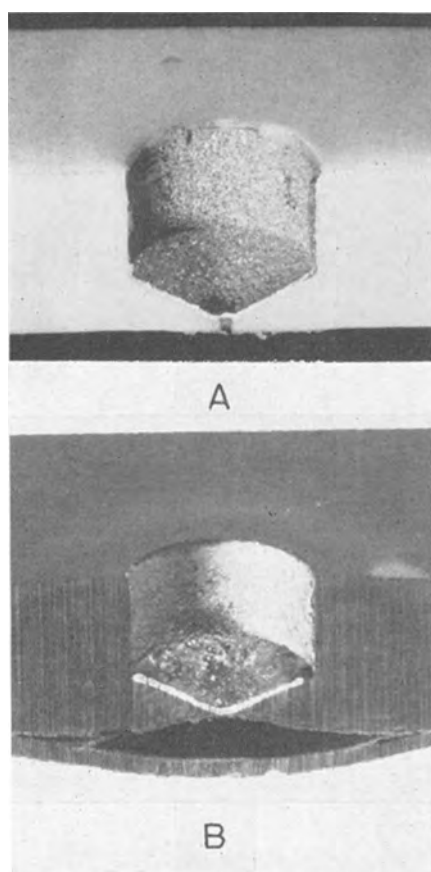


FIG. 6. Cross-sectional view of tapered cavity after 100 megacycle breakdown on (A) polytetrafluoroethylene, (B) paper base phenolic laminate.

The phenolic, however, exhibits a drastic change in behavior.

Polytetrafluoroethylene may be considered as one of the better dielectrics over the frequency range studied. The paper base phenolic laminate drops from a rather high dielectric strength value at low frequency to a quite poor performance at 100 megacycles. At this upper limit, the failure of this material is characterized by the formation of a large internal void, and the entire volume becomes quite hot. It is of further interest that monochlorotrifluoroethylene forms small voids within the failure region at 100 megacycles.

It would be premature to weigh the relative values of quantitative and descriptive observations of breakdown investigations at this time. However it does appear to the authors that, at low frequency, the character of the breakdown is sharp and clear but the numerical results show considerable spread. By contrast the high-frequency upper limit of strength is numerically well defined, but the character of the failure differs widely among materials and, in any particular case, the end point is apt to be decided to an important degree by effects that are not purely electrical.

TABLE I. Comparison tests with three types of electrodes*

Material	Method	Voltage kv	Thickness mils	VPM	Remarks
Polyethylene	A	50.0	125	400	Value incorrect, edge glow
	B	50.0	38	1315	Definite puncture
	C	50.0	37	1350	Definite puncture
Polytetrafluoroethylene	A	70.8	125	566	Value incorrect, edge glow
	B	70.8	118	600	Definite puncture
	C	70.8	118	600	Definite puncture
Polystyrene	A	59.5	125	475	Value incorrect, edge glow
	B	59.5	31	1920	Definite puncture
	C	59.5	32	1860	Definite puncture
Paper base phenolic laminate	A	61.4	125	491	Value incorrect, edge glow
	B	61.4	68	902	Definite puncture
	C	61.4	69	888	Definite puncture
Glass silicone laminate	A	58.5	125	450	Value incorrect, edge glow
	B	58.5	98	587	Definite puncture
	C	58.5	146	400	Value incorrect, some specimens delaminated

Method A, ASTM electrodes.

Method B, $\frac{1}{2}$ in. diameter tapered cavity (See Fig. 4).

Method C, $\frac{3}{4}$ in. diameter cavity (See Fig. 3).

* Tests conducted at 60 cps, voltage raised gradually over approximately 40 sec.

The importance of properly imbedded electrodes is illustrated by Table I. A comparison is made at 60 cycles among three types of electrodes namely, ASTM, $\frac{1}{2}$ in. twist drill cavity, and $\frac{3}{4}$ in. flat bottom cavity. The latter two give nearly identical performance, except that the flat bottom drill causes minute delaminations in materials such as glass silicone laminate. In the case of glass silicone laminate, the resulting low values of breakdown strength from such mechanical imperfections lower the mean value of volts per mil considerably. This mechanical difficulty does not accompany the other four materials listed; however, the flat bottom drill is always slower and less convenient to use than the standard twist drill. Comparison was made at a high level of voltage respective to each material, determined by use of the ASTM electrode and resulting in surface burning and failure. Data from voltage-thickness studies gave comparative points for the other two types of electrodes.

The ASTM tests were performed on $\frac{1}{8}$ in. thick specimens and the values of breakdown strength obtained were all compromised by edge glow in the oil. In fact, unless the immersion oil is kept in excellent condition, the apparent values of breakdown

strength sometimes appear to be 20% lower. By contrast, the same voltage levels could be reached with thinner sections using the $\frac{1}{2}$ in. twist drill cavity. In this case the value of volts per mil were valid and of higher magnitude. In spite of considerable edge glow, polytetrafluoroethylene and glass silicone laminate gave fair performance with the ASTM electrode; these materials are able to withstand considerable heating and arcing. At higher frequencies, corona may result in the dissipation of considerable energy and it is advisable to avoid it by use of an imbedded electrode.

CONCLUSIONS

1. Solder may be sprayed on plastic surfaces to gain intimate contact. Critical tests have proved that the conducting film thus formed is suitable for making breakdown measurements over a wide range of frequency.

2. The film may be applied to specimens that have been conditioned at high humidity. It also proves useful at low temperatures.

3. Results are reproducible under a variety of conditions of temperature, frequency, and choice of materials and may in time provide the synthetic chemist a new viewpoint in the development of materials. Spread in results has been reduced to that inherent to materials rather than method.

4. The performance of the $\frac{1}{2}$ in. diameter cavity

formed with a standard drill is of extreme practical benefit.

5. Considerations of cavity shape and conducting film application are most timely in the large scale evaluation activities necessary to keep pace with new materials.

ACKNOWLEDGMENTS

The research concerning this method of obtaining breakdown has been of value in two contractual investigations. The authors have enjoyed the support of the Bureau of Ships and that of the Components and Materials Branch, Squier Signal Laboratory, SCEL, and therefore express their gratitude to both.

Further acknowledgment is made to Mr. Wilbur G. Baumann and Mr. Richard D. Picard whose careful specimen preparation and testing were an essential factor in the work

Any discussion of this paper will appear in a Discussion Section to be published in the December 1955 JOURNAL.

REFERENCES

1. J. J. CHAPMAN AND L. J. FRISCO, *Elec. Mfg.*, **53**, 136 (1954).
2. J. J. CHAPMAN, J. W. DZIMIANSKI, C. F. MILLER, AND R. K. WITT, *ibid.*, **48**, 107 (1951).
3. L. J. FRISCO AND J. J. CHAPMAN, *Rev. Sci. Instr.*, **25**, 8 (1954).
4. R. BECKER, *Archiv. Electrotech.*, **30**, 411 (1936).
5. A. VON HIPPLE AND R. S. ALGER, *Phys. Rev.*, **76**, 127 (1949).

Nitrides of Chromium and Chromium-Titanium Alloys

New Film-Type Resistance Elements¹

E. R. OLSON, E. H. LAYER, AND A. E. MIDDLETON²

Battelle Memorial Institute, Columbus, Ohio

ABSTRACT

Some electrical properties of nitrided Cr and nitrided Cr-Ti films are presented. Films of chromium and chromium-titanium alloys, deposited on ceramic bases by vacuum-evaporation methods, were nitrided to form electrical resistance elements. By varying thickness and nitriding conditions, the electrical properties of the films can be varied. Materials can be prepared with temperature coefficients of resistance less than 0.01%/°C. Resistors with resistances of from several hundred to several million ohms can be made. Resistance to environmental attack and other properties are also described.

INTRODUCTION

There exists a need for new electrical-resistance materials suitable for high temperature-operating fixed resistors. A research program was undertaken to find and develop materials for such elements. In view of the potentialities of film-type elements, resistance materials in thin film form, which would be tightly adherent to an insulating supporting base, were chosen for study.

Early investigations were conducted by Campbell and coworkers (1) on the vapor-phase deposition of refractory materials. Also, studies of electron conduction in chemical compounds of this nature were made by von Meyer (2) and others (3). These studies prompted evaluation of alloy systems in the classes of materials referred to as nitrides, silicides, and borides.

EXPERIMENTAL DETAILS

Preliminary survey.—A survey program was conducted to screen a large number of materials and to select those showing the most promise. Selection was made on the basis of several requirements which were considered necessary to meet the objectives. These requirements were:

1. Conduction must be electronic rather than ionic.
2. The materials must be of such a nature that they can be applied in thin, adherent, continuous films on a supporting, insulating base.
3. Effects of oxidation and water vapor on the electrical characteristics of the films must be very

¹ Manuscript received April 13, 1953. This paper was prepared for delivery before the New York Meeting, April 12 to 16, 1953.

² Present address: P. R. Mallory and Company, Inc., Indianapolis, Indiana.

small. Good chemical stability between 65° and 200°C was sought.

4. The resistivity must be of such a value that the temperature coefficient of resistance is near zero. This generally excludes materials whose resistivities are above 10⁻² ohm-cm.

5. Resistances in the order of 10 ohms per square³ and 2000–5000 ohms per square should be obtainable with near-zero temperature coefficients of resistance. Specifically, resistances in the range 10 ohms to 10 megohms should be obtainable with temperature coefficients of resistance less than 0.01%/°C.

6. Also required are: low voltage dependence; ability to undergo temporary electrical overload without permanent change; ruggedness to sudden temperature change and to vibration.

Films were prepared by two processes. The first of these employed hydrogen reduction of halide vapors at temperatures high enough that the alloying constituents would codeposit on the ceramic base in adherent, continuous, crystalline films. This is the vapor-phase-decomposition method as described by Campbell (1). Borides and silicides were deposited by this process.

The second method involved thermal evaporation of metals in high vacuum, with subsequent conversion to the desired composition in an atmosphere

³ The normal expression for electrical resistance of a conductor is

$$R = \frac{\rho \times l}{t \times w}$$

where R is resistance in ohms, ρ is resistivity in ohm-cm, l , t , and w are the length, thickness, and width in cm, respectively. The value of the resistance of a film-type conductor of constant thickness, and with length and width equal, is known as the resistance per square. This resistance per square is numerically equal to the resistivity divided by the thickness.

containing the other constituent. This process was used chiefly to produce nitrides, although some silicides and borides were also produced.

From the standpoint of high temperature stability, films exhibiting the best properties were silicides of chromium and molybdenum. Several nitrides had good oxidation properties and could be produced with low temperature coefficients of resistance. In general, borides had poor oxidation resistance. Because film continuity, uniformity, and thickness were difficult to control for silicides and borides it was extremely difficult to obtain reproducible electrical properties in such films. In this respect the nitriding process was much more successful; therefore, most of the effort was concentrated on the systems Cr-N and Cr-Ti-N.

Preparation of Cr-N and Cr-Ti-N films.—Chromium and Cr-Ti alloys in solid form were thermally evaporated at a pressure of about 10^{-4} mm Hg, and condensed on rotating ceramic rods. Mixtures of Cr and Ti powders were also used as the evaporation source. Source-to-rod distances were about 7 cm, and

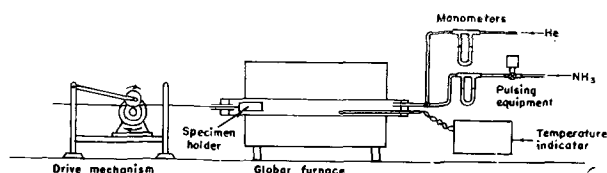


FIG. 1. Schematic diagram of nitriding apparatus

rod-rotation speeds of from 300 to 400 rpm were used. Certain zircons and high-alumina porcelains, detergent washed and rinsed in distilled water, were found to be suitable substrates, the two important properties being smooth, defect-free surfaces, and chemical inertness during the high temperature nitriding process.

The metallic films were nitrided in an ammonia atmosphere for a period of 10 min at various temperatures above 800°C . A schematic diagram of the nitriding apparatus is shown in Fig. 1. Flushing of the nitriding tube prior to introduction of ammonia gas was done with helium, while the metallized ceramic specimens were held in a quartz boat in the cold end of the tube. Either manual feed or mechanical feed was used to introduce the specimens to the hot zone of the nitriding furnace. After nitriding, resistors were cooled in helium at the position shown in the figure, and then removed from the furnace for further processing. Three to five minutes in the cooling zone was adequate.

The $\frac{1}{4}$ -in. cylindrical coated rods were cut to 1-in. lengths and baked silver contact bands applied in $\frac{1}{4}$ -in. widths circumferentially around the ends of the films. To complete the resistor assembly, silver-

plated end caps with tinned copper leads were pressure fitted over the ends of these contact bands.

RESULTS AND DISCUSSION

Electrical and Structural Characteristics of Films in the Cr-N System

Nitriding of chromium can occur at temperatures below 800°C , but Cr-N films with the most suitable electrical properties were formed at temperatures ranging from 950° to 1250°C . Results indicated that film resistivity at room temperature decreased with increasing nitriding temperature over this temperature range. X-ray and chemical analyses were made on powdered chromium samples nitrided at these temperatures. From these studies and published literature (4-6), information was obtained about the formation of the nitrides of chromium. Two known compounds, CrN and Cr_2N , are formed, the CrN having a cubic structure of the NaCl type, and the Cr_2N having the metal atoms arranged in a close-packed hexagonal structure. At the lower temperatures of nitriding 950° to 1000°C , the CrN predominates. At the higher temperatures of nitriding, more of the Cr_2N compound is formed. Decreasing resistivity over this temperature range suggests that Cr_2N has a lower resistivity than CrN.

If the thickness of the Cr films is varied to cover an extended range, the resulting Cr-N films, nitrided at any one temperature, will also exhibit a wide range of resistance per square, resistance decreasing with increasing thickness. The temperature coefficient of resistance of such films varies as a function of resistance per square such that, with increasing resistance (decreasing thickness), the temperature coefficient changes from positive to negative. This change in temperature coefficient from positive to negative occurs at different values of resistance per

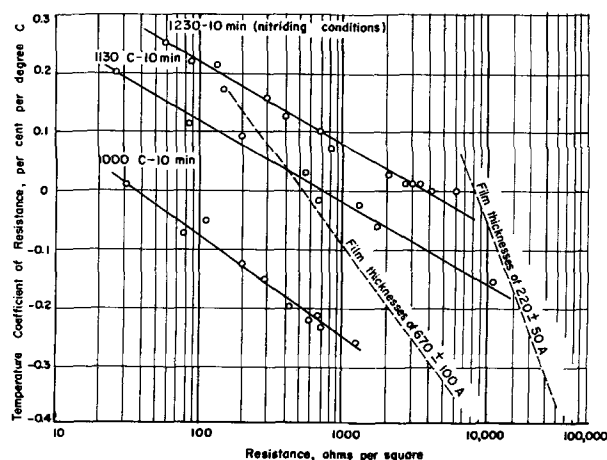


FIG. 2. Relationship between temperature coefficient of resistance and resistance for various values of nitriding and thickness parameters.

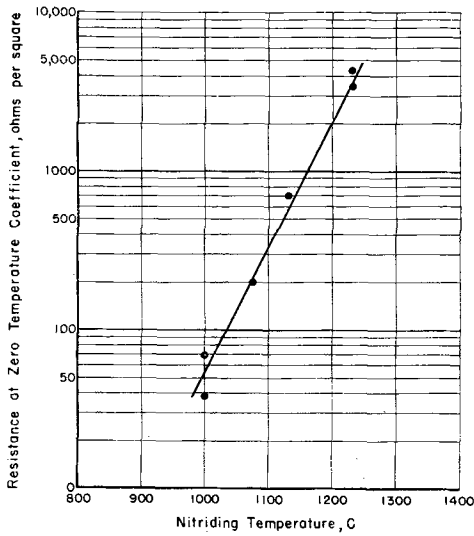


FIG. 3. Relationship between resistance at zero temperature coefficient and nitriding temperature for Cr-N films.

square, the particular value depending on the film thickness and the temperature at which the film is nitrided.

The effect of thickness and nitriding temperature on Cr-N films is shown in Fig. 2. These data were taken on chromium films ranging in thickness from 200 Å to 1500 Å, which were nitrided at temperatures of 1000°, 1130°, and 1230°C. Zircon ceramic was the base used for these films. The temperature coefficient of resistance at room temperature is plotted against resistance per square, the top curve representing results obtained for films nitrided at 1230°C and the lower curve representing the trend for films nitrided at 1000°C. The dotted lines represent approximately constant film thickness for the values indicated.

Resistances at which the temperature coefficients cross through zero are correlated with nitriding temperature in Fig. 3. It can be seen that the resistance at zero temperature coefficient increases with nitriding temperature and extends from about

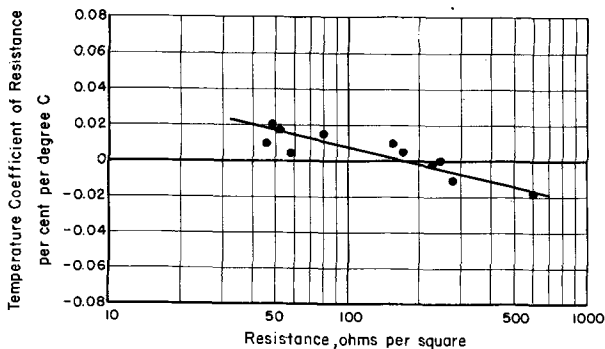


FIG. 4. Relationship between temperature coefficient of resistance and resistance for Cr-Ti-N films produced at 1230°C.

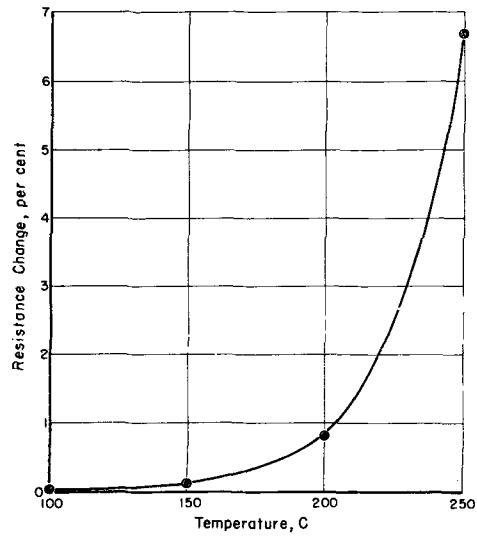


FIG. 5. Average change in resistance with temperature for Cr-Ti-N films heated in air for 200 hr.

50 ohms per square to 4000 ohms per square. This relationship is significant because it indicates essentially that a continuous series of fixed resistances can be produced over a wide resistance range with near-zero temperature coefficients. By altering the geometry of this low temperature coefficient conducting path, an even wider resistance range can be covered. For example, cylindrical resistors ¼ in. in diameter and 1 in. long have been produced over the range from 10 ohms to 10 megohms by employing the common practice of spiralling for extending the length of the conducting path.

Voltage coefficients of resistance of less than 0.02%/v were measured for the Cr-N films.

Electrical Characteristics of Films in the Cr-Ti-N System

Cr-Ti films nitrided in the temperature range 950°-1250°C resulted in Cr-Ti-N films which have electrical properties differing somewhat from those of the Cr-N films.

First, the maximum resistance per square at low temperature coefficient was about 300 ohms per square as compared to 4000 ohms for the Cr-N films. Second, the nitriding temperature did not have

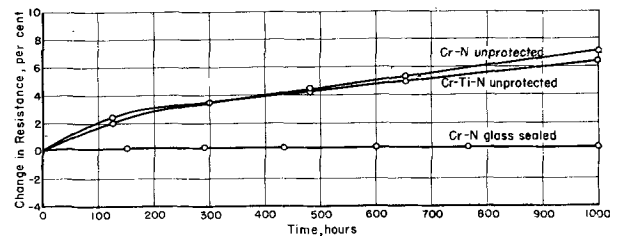


FIG. 6. Change in resistance with time for Cr-N and Cr-Ti-N resistors operating under 1-watt loads at 200°C ambient in air.

nearly so large an effect on the resistivity and temperature coefficient of the Cr-Ti-N films as in the case of the Cr-N films. As a result, small variations or fluctuations in nitriding temperature could be tolerated in the production of low temperature-coefficient Cr-Ti-N films. The third difference was that the temperature coefficient of resistance varied less as a function of resistance per square than in the case of the Cr-N system. This difference gives the Cr-Ti-N films an advantage over the Cr-N films. Fig. 4 shows the temperature coefficient and resistance per square relationship for Cr-Ti-N films produced at 1230°C. The range of resistances for temperature coefficients of less than 0.01 %/°C extended from 80 to 400 ohms per square for the Cr-Ti-N films as compared to the range of 3000 ohms to 5000 ohms per square for films of the Cr-N system nitrided at 1230°C. This meant that in laboratory production much better reproducibility of low temperature-coefficient films could be obtained with the Cr-Ti-N system than with the Cr-N system.

Voltage coefficients of resistance of Cr-Ti-N films were measured to be less than 0.02 %/v.

Stability of Cr-N and Cr-Ti-N Resistors Subjected to Various Environmental Conditions

Like chromium itself, nitrided chromium and nitrided Cr-Ti films exhibited fairly good resistance to oxidation. Fig. 5 shows the average change in resistance of groups of Cr-Ti-N films heated in air at temperatures ranging from 100° to 250°C under no-load conditions. Changes of 0.01 % at 100°C, 0.12 % at 150°C, 0.8 % at 200°C, and 6.7 % at 250°C were noted for 200 hr of test after an initial 150-hr pretreatment at 200°C. These films were exposed directly to the air while under test.

Typical load-life characteristics of Cr-N and Cr-Ti-N resistors are shown in Fig. 6. These resistors were operated for 1000 hr at 200°C ambient, with 1-watt leads. About 6.5 % increase was noted for the

Cr-N and the Cr-Ti-N resistors without protective coverings, as compared to 0.2 % for a glass-sealed Cr-N resistor.

Moisture resistance tests on both types of films, without protective coverings, have generally shown less than 3 % change in 500 hr. These tests were conducted at 95 % relative humidity, 75°C, and with ¼-watt d-c loads cycled 1½ hr on and ½ hr off.

Problems of reproducibility, particularly for the Cr-N resistors, are inherent because of the narrow usable resistance range for near-zero temperature coefficients for any given set of conditions. The necessity of careful control of evaporation conditions is imperative. Also, because of the thinness of the films, the slightest defect in the base can result in faulty performance of the resistor. Good contact termination is also necessary. These problems are still under investigation.

ACKNOWLEDGMENTS

This work was performed under Contract AF 33 (038)-8744 for the Wright Air Development Center. The authors express their appreciation to R. E. Miller of Battelle Memorial Institute for his technical assistance in the determination of the electrical properties of the resistive materials.

Any discussion of this paper will appear in a Discussion Section to be published in the December 1955 JOURNAL.

REFERENCES

1. I. E. CAMPBELL, C. F. POWELL, D. H. NOWICKI, AND B. W. GONSER, *J. (and Trans.) Electrochem. Soc.*, **96**, 318 (1949).
2. W. VON MEYER, *Z. Elektrochem.*, **50**, 274 (1944).
3. C. AGTE AND K. MOERS, *Z. anorg. u. allgem. Chem.*, **198**, 233 (1931).
4. G. HÄGG, *Z. physik. Chem.*, **B12**, 33 (1931); *ibid.*, **B11**, 433 (1930).
5. R. BLIX, *Z. physik. Chem.*, **3**, 229 (1929).
6. K. SANO, *J. Chem. Soc. Japan*, **53**, 931 (1937).

Electrolytic Preparation of Molybdenum from Fused Salts

IV. Preparation of Reduced Molybdenum Chlorides from Molybdenite Concentrate¹

SEYMOUR SENDEROFF AND ROGER J. LABRIE

National Bureau of Standards, Washington, D. C.

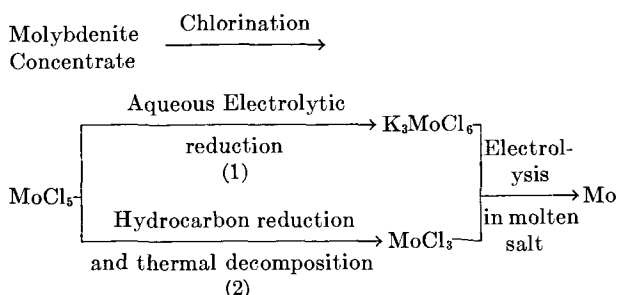
ABSTRACT

Commercial molybdenite concentrates are chlorinated to produce molybdenum pentachloride and sulfur chlorides. Sulfur chlorides are removed and molybdenum pentachloride is reduced either electrolytically in aqueous solution or by reaction with a hydrocarbon in a nonaqueous system. The aqueous reduction product is recovered as potassium hexachloromolybdate (III), K_3MoCl_6 , and the hydrocarbon reduction product is recovered, after heating, as molybdenum trichloride. Either of these salts may be dissolved in alkali halides and electrolyzed to deposit molybdenum metal at the cathode.

INTRODUCTION

In earlier papers of this series, a process was described by which pure molybdenum may be obtained by the electrolytic reduction of a complex trivalent molybdenum halide dissolved in molten alkali halides (1). It was also shown that the presence of oxygen, moisture, and oxygen-containing compounds was harmful to the process (2). The potassium hexachloromolybdate (III), K_3MoCl_6 , used for electrolysis, when prepared by electrolytic reduction of an aqueous molybdate solution (3), was rather difficult to free from the last traces of moisture and oxycompounds.

The present paper describes the preparation of a salt suitable for use in the electrolytic bath by starting from a concentrate of molybdenite, the most commonly occurring ore of molybdenum, and treating it by water-free and "oxygen-free" methods only, in order to obtain the desired reduced molybdenum halide. The process which was developed may be summarized as follows:



Steps 1 and 2 are alternative methods of reduction of the molybdenum pentachloride, but step 2 is

¹ Manuscript received June 11, 1954. This paper was prepared for delivery before the Chicago Meeting, May 2 to 6, 1954.

preferred since it does not require an aqueous system.

The molybdenite concentrate² contained about 80% molybdenum disulfide and about 5% each of water and mineral oil as residues from the flotation operation, with the balance mainly silica. Significant metallic impurities are aluminum, magnesium, calcium, copper, and iron (see Table I).

Molybdenum disulfide is exceedingly inert toward most chemical reagents except strong oxidizing agents and, even with these, elevated temperatures are usually required for reaction to occur at a satisfactory rate. A preliminary study of the common reactions of molybdenum disulfide indicated that the most promising reaction for the authors' purpose might be chlorination.

PREPARATION OF MOLYBDENUM PENTACHLORIDE

It was necessary first to dry the molybdenite concentrate by heating at 300°C in an inert atmosphere for several hours in a large round-bottom flask, the neck of which was tilted downward to drain off oil and water which distilled out. The dried molybdenum disulfide remained as a very fine, free-flowing, dark gray powder similar in appearance and texture to graphite.

The dried molybdenite concentrate was charged into the Pyrex reaction tower shown in Fig. 1. In order to remove air from the tower and thus prevent formation of oxychlorides during chlorination, helium was passed into the system from the bottom of the reaction tube, and heating was begun. When the charge reached a temperature of 550°C, chlorine was passed through the system at a rate of about 0.5 l/min. Chlorine was mixed with about 15% of

² Supplied by Climax Molybdenum Company.

TABLE I. Spectrochemical analysis of molybdenum compounds

Element	Molybdenite concentrate	MoCl ₅	Mo powder from MoCl ₅	K ₂ MoCl ₆	Unreacted residue from chlorination
Ag	VW	—	—	FT	W
Al	M	W	M	VW	S
Ba	T	—	—	—	VW
Bi	W	—	—	—	—
Ca	M	FT	—	VW	M
Cu	W	VW	T	T	M
Fe	W	VW	W	T	W
K	—	—	—	VS	—
Mg	M	VW	T	W	S
Mn	VW	T	—	FT	W
Mo	VS	VS	VS	VS	S
Ni	—	—	VW	—	T
Pb	VW	T	VW	FT	W
Si	S	W	W	W	VS
Sr	T	—	—	—	VW

VS = greater than 10%.

VW = 0.001–0.01%.

S = 1–10%.

T = 0.0001–0.001%.

M = 0.1–1.0%.

FT = less than 0.0001%.

W = 0.01–0.1%.

helium to maintain a sufficient flow of gas through the system so that air would not enter. In order to prevent blocking of the apparatus by the molybdenum pentachloride and sulfur chlorides which were collected in the receiver, the connecting tube between the receiver and reaction tower was wrapped with heating tape and kept at 350°C. When about half of the charge had reacted, the plug at the top of the reaction tube was removed, molybdenite concentrate added, and the plug quickly replaced before an appreciable amount of air could enter.

When the receiver containing the molybdenum pentachloride and the sulfur chlorides was full it was taken off and stoppered quickly. The products were transferred to a distilling flask in an inert atmosphere, and the sulfur chlorides were removed by distillation. Most of the SCl₂ was removed at room temperature by vacuum distillation. The remainder, together with the S₂Cl₂, was then removed by warming the flask under reduced pressure. The mixed sulfur chlorides consisted of about 80% SCl₂ and 20% S₂Cl₂. Molybdenum pentachloride remained as a black powder in the flask.

The process would be more economical with respect to chlorine consumption if more S₂Cl₂ and less SCl₂ were produced. Since SCl₂ is known to dissociate (4), it is possible that other conditions of temperature, flow, etc., and apparatus design may be found which would favor formation of S₂Cl₂.

Seven hundred grams of molybdenum pentachloride was produced during a 20-hr run in which 450 g of dried molybdenite concentrate was added to the reaction tower. Molybdenum pentachloride

produced in this manner is essentially free of the original contaminants of the ore. Most of the silica remained in the reaction tower in the unreacted residue which comprised about 7% of the total charge. Metallic impurities, such as aluminum, magnesium, copper, and iron, also were concentrated in the unreacted residue. In Table I are shown the spectrochemical analyses of the molybdenite concentrate (column 2), the molybdenum pentachloride (column 3), and the unreacted residue (column 6). Comparison of concentrations of impurities in these three materials clearly shows the degree of purification achieved as a result of the chlorination of the ore concentrate. Chemical tests showed, however, that the molybdenum pentachloride contained a trace of sulfur.

Reaction rates at various temperatures were determined by placing porcelain boats containing molybdenum disulfide in a horizontal Vycor tube and heating them for 2 hr under chlorine flowing at 50 ml/min. The weight loss at the end of the run was taken as an indication of the amount of reaction. Approximate relative rates at various temperatures are shown in Table II.

At 1050°C the reaction was nearly quantitative, based on the amount of chlorine passed through. The temperature of 550°C used in the preparation de-

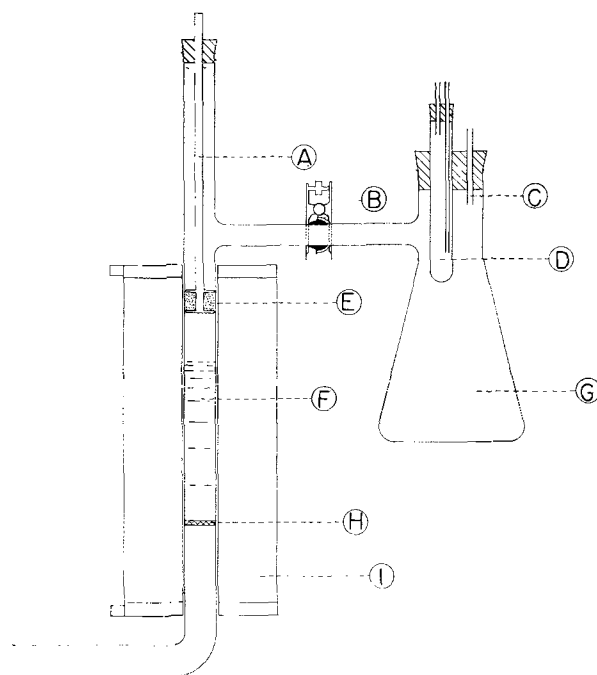


FIG. 1. Apparatus for chlorination of molybdenite concentrate. (A) Glass rod with flanges; (B) 35/20 ball joint with spring clamp; (C) gas outlet tube; (D) water-cooled cold-finger; (E) glass wool plug wound between flanges; (F) molybdenite charge in reaction tower; (G) receiving flask; (H) coarse fritted Pyrex disk sealed in reaction tower; (I) hinged tube furnace.

scribed above was close to the upper limit permissible for the Pyrex equipment that was used. A higher temperature would clearly be desirable when a higher reaction rate is required, and it might also favor the production of S_2Cl_2 rather than SCl_2 . Purification, however, might be less at higher temperatures since it was found that the unreacted residue remaining after exhaustive chlorination at $900^\circ C$ was 5.3% of the total charge, and at $550^\circ C$ it was 6.7% of the total charge.

TABLE II. Rate of chlorination of molybdenum disulfide at various temperatures

Temp, °C	Relative rate
800	1
550	0.3
300	0

PREPARATION OF MOLYBDENUM TRICHLORIDE

In an attempt to find a suitable solvent for the reduction of molybdenum pentachloride it was observed that this compound reacts with cetane and higher paraffin hydrocarbons. Hydrogen chloride is liberated during the reaction, and the reduced molybdenum halide precipitates. Organic products, which might include chloro-alkanes, polymers, or unsaturated products, have not been studied. Because molybdenum compounds are sensitive to moisture, all operations must be performed in an inert atmosphere and all reagents and solvents thoroughly dried. The reaction has been run with cetane and with molten paraffin wax.

About 300 g of paraffin wax (M. P. = 56° – 58°) is heated to $145^\circ C$. About 150 g of molybdenum pentachloride (ground to about No. 80 mesh) is added rapidly and with stirring. Stirring and heating is continued (for about 20 min) until the reddish color disappears and the rate of gas evolution decreases. At this point the level of the liquid drops somewhat and the mixture takes on a green-black color instead of the previous red-brown. The hot mixture is poured onto a coarse fritted glass Buchner funnel and filtered. The solid product is washed further with paraffin wax at about $145^\circ C$. It is then washed with dry benzene and finally with dry petroleum ether, and dried. If cetane is used in place of paraffin wax, this reaction is best carried out at a somewhat higher temperature, about $160^\circ C$.

A representative batch contained 4.1% water-insoluble material, the composition of which was not determined. The Cl:Mo ratio in the water-soluble remainder was 1.55 compared to the calculated value of 1.48 for $MoCl_4$. Unfortunately, this product could not be purified by recrystallization because no suitable solvent could be found.

Preliminary experiments have shown that tungsten hexachloride undergoes a similar reaction at a slightly higher temperature to form, mostly, tungsten pentachloride.

The product of the reaction with the paraffin, the analysis of which corresponds closely to $MoCl_4$, is a very fine black powder that reacts with moist air and must be handled in an inert atmosphere. When heated at $300^\circ C$ in a stream of helium, it disproportionates slowly to form molybdenum trichloride and molybdenum pentachloride; the latter can be recycled in the process. The Cl:Mo ratio in the $MoCl_3$ so produced was 1.11, which agrees, within the limits of accuracy of the analysis, to the calculated value for this compound. The material contained a small amount of carbonaceous residue from the original reaction.

PREPARATION OF POTASSIUM HEXACHLOROMOLYBDATE (III)

Since K_3MoCl_6 has proved useful as an electrolyte for producing molybdenum, its preparation from molybdenum pentachloride obtained by chlorination of the molybdenite concentrate was investigated. The method described previously (3) used the

TABLE III. Reduction of molybdenum pentachloride

Reducing agent	Conditions	Remarks
Na	In bomb above $400^\circ C$	Explosive reaction to produce mixture of reduced halide and fine molybdenum powder.
High surface sodium* (Na dispersed on NaCl)	$180^\circ C$	Smooth reaction to form reduced halides which are difficult to separate from carrier on which Na was dispersed.
H_2	1 atm 350° – $850^\circ C$	Mixtures of halides and Mo metal.
Al powder	(a) $MoCl_5$ and Al powder heated in a sealed tube (b) $MoCl_5$ vapors passed over Al powder at $350^\circ C$	Either incomplete reaction or explosive reaction.
Electrolysis	Sealed cell, $300^\circ C$, with a trace of KF or LiCl.	No reaction observed at cathode.
Thermal decomposition	$MoCl_5$ + helium, $1200^\circ C$, 1 atm.	No visible reaction.

* Described in bulletin entitled "High Surface Sodium," issued in 1953 by U. S. Industrial Chemicals Company, 120 Broadway, New York 5, N. Y.

hexavalent potassium molybdate as a starting material. Electrolytic reduction of the pentachloride, containing pentavalent instead of hexavalent molybdenum, to the trivalent compound would result in a saving of about $\frac{1}{3}$ of the electricity required, and it may have other advantages in cost and solubility.

One hundred and forty g of potassium carbonate and 275 g of molybdenum pentachloride were dissolved in a solution containing 500 ml of concentrated hydrochloric acid and 600 ml of water. A higher acid concentration gave a precipitate of potassium chloride. This solution was electrolyzed as described previously (3), saturated with hydrogen chloride, and the precipitated K_3MoCl_6 was washed and filtered. About 200 g of K_3MoCl_6 was obtained, which represents a yield of 70% based on the $MoCl_5$ used. The spectrochemical analysis of this product is shown in column 5 of Table I, from which it is clear that further removal of impurities from the $MoCl_5$ was accomplished by electrolytic reduction.

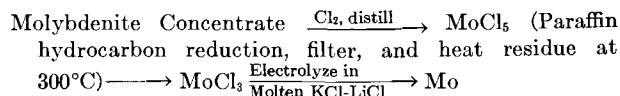
It is interesting to note that molybdenum trichloride prepared by hydrocarbon reduction forms the same trivalent hexachloromolybdate anion when it is added to the eutectic mixture of potassium chloride and lithium chloride and the mixture melted in an inert atmosphere. A 4 mole% solution of molybdenum trichloride in the alkali chlorides was prepared in this manner by heating to 600°C. On cooling, a homogeneous pink melt, having the characteristic appearance of a fused mixture of K_3MoCl_6 and alkali chlorides, was obtained. The molten mixture, $MoCl_3 - KCl - LiCl$, was electrolyzed in a divided cell with a graphite anode and molybdenum deposited at the cathode. The analysis of the molybdenum powder thus produced is shown in column 4 of Table I.

MISCELLANEOUS REDUCTIONS OF MOLYBDENUM PENTACHLORIDE

Other methods of obtaining reduced molybdenum compounds were tried, but were not found to be suitable for the authors' purpose. Results of attempted reductions of $MoCl_5$ are shown in Table III.

SUMMARY

The following procedure for reduction of molybdenite concentrate to molybdenum metal has been shown to be feasible:



Raw materials are molybdenite ore, chlorine, and paraffin hydrocarbon; by-products are sulfur chlorides and anhydrous hydrogen chloride.

Work is now in progress on the electrolysis of the $MoCl_3$ thus produced.

ACKNOWLEDGMENT

The authors express their appreciation to A. Brenner, National Bureau of Standards, for his guidance and suggestions throughout the course of the investigation, and to the Bureau of Ordnance, Department of the Navy, for financial support.

Any discussion of this paper will appear in a Discussion Section to be published in the December 1955 JOURNAL.

REFERENCES

1. S. SENDEROFF AND A. BRENNER, *This Journal*, **101**, 16 (1954).
2. S. SENDEROFF AND A. BRENNER, *ibid.*, **101**, 31 (1954).
3. S. SENDEROFF AND A. BRENNER, *ibid.*, **101**, 28 (1954).
4. J. W. MELLOR, "A Comprehensive Treatise on Inorganic and Theoretical Chemistry," Vol. 10, p. 645, Longmans, Green, London (1930).

Deposition of Titanium Coatings from Pyrosols¹

A. W. SCHLECHTEN, M. E. STRAUMANIS, AND C. B. GILL

Department of Metallurgical Engineering, University of Missouri, School of Mines and Metallurgy, Rolla, Missouri

ABSTRACT

It has been found that titanium dispersed in fused salts can be deposited on other metals, especially on copper and iron. For example, if a piece of copper sheet is placed in close proximity to a titanium sheet (but not in actual contact) and then the whole is immersed into a fused salt, preferably NaCl or KCl, titanium will transfer to the copper sheet. The thickness of the titanium layer on the copper increases with temperature and time, approaching a maximum thickness of 0.001–0.007 in. (0.025–0.178 mm). Titanium forms a coherent layer on the metals mentioned and protects them from corrosion. The substrate can be dissolved from the reverse side (Fe in FeCl₂, Cu in HNO₃); the titanium coating remains.

The mechanism of titanium transfer is thought to consist of, first, a titanium pyrosol formation, and then the deposition of these titanium particles upon the other metals forming a titanium rich alloy. Similar behavior has been observed for other metals.

INTRODUCTION

The excellent resistance of titanium to corrosion, particularly against nitric acid, has given great incentive to the search for a method of coating cheaper metals with titanium. As far as is known by the authors, no successful method exists for electroplating titanium from aqueous or organic solutions. Titanium can be electrodeposited from fused salt baths (1) chiefly in the form of powder and flakes; sometimes a thin diffusion coating of titanium is obtained on the cathode. Fused salt electrolysis requires materials of high purity and a protective atmosphere of helium or argon.

Attempts to obtain titanium coatings by cementation or treatment in TiCl₄ have been summarized by Chapin and Hayward (2); none of these yielded corrosion resistant coatings. Alexander (3) has patented a process which consists of heating titanium hydride on a copper surface; an alloy of eutectic composition is formed which flows and coats the surface. This type of coating is of limited application for corrosion resistance.

The process described in this paper was the outgrowth of previous experiments on corrosion (4) which showed that titanium is severely attacked when immersed in molten chlorides or fluorides exposed to air. The corrosion products, particularly in chloride baths, are to a great extent finely divided titanium and resemble the "metal fogs" or "pyrosols" described by Lorenz and Eitel (5). It was observed

that the walls of the porcelain crucibles used for corrosion tests were covered below the salt level with a layer which was largely titanium. A series of tests were made to determine if such coatings could be obtained on other surfaces.

As a result of these experiments, it was discovered that objects of copper, iron, or other metals, immersed in the salt bath where there was a high concentration of the titanium pyrosol, were covered with a coating of high titanium content.

In order to achieve the necessary high pyrosol concentration, the object to be plated is placed in close proximity to the titanium source which is corroding, but preferably not in contact with it. Thus, flat surfaces may be plated by placing them parallel to sheets of titanium, and irregular objects can be imbedded in titanium powder or cuttings.

The resulting coatings form a coherent layer that protects the underlying metal from corrosion. For example, copper and iron objects coated by this process can be immersed in nitric acid solutions with no evidence of attack.

Experiments are described which demonstrate the variation of the coating process with time and temperature of treatment, composition of bath, and other factors.

EXPERIMENTAL PROCEDURE

Small disks of copper or iron about 2 cm in diameter and 1 mm thick were fastened parallel to pieces of titanium sheet which were slightly larger in diameter; pieces of 0.5 mm wire were used as spacers between the two metals. The assemblage was placed in a small porcelain crucible, covered with salt, and heated in a resistance muffle furnace for several hours at a temperature above the melting point of the salt.

¹ Manuscript received May 4, 1954. This paper was prepared for delivery before the Chicago Meeting, May 2 to 6, 1954, and is based on a portion of the work carried out at the Missouri School of Mines and Metallurgy for the Wright Air Development Center under Contract No. AF 33(616)-75.

After heating, the crucible was removed from the furnace, allowed to cool, and placed in a beaker of water heated to digest the salt. In some experiments, the salt was melted before the object to be plated and the titanium source were placed in the crucible. In other experiments, the assemblage was removed from the molten salt as soon as the crucible was taken from the furnace; there was enough salt adhering to the plated object to prevent any appreciable oxidation of the titanium coating. These variations in procedure had no detectable influence on the results.

After the salt had been dissolved, it was necessary to rub or brush away the dark corrosion residue to expose the metallic titanium coating on the disk.

The weight of the coating was calculated from the increase of weight of the plated disk, or better yet, by dissolving the iron or copper away from the coating, which could then be weighed. The average thickness of the coating was calculated from the weight and density of titanium, and was checked by measuring a cross section under the microscope.

Irregular objects were plated by imbedding them in titanium powder or cuttings on the bottom of the crucible, filling up the crucible with salt, and proceeding as before. Titanium hydride powder was also successfully used in the same way as a source of the titanium pyrosol. Powdered ferrotitanium was tried, but did not give a coating.

A variety of salts were tried for the fused bath; a number of addition agents to regular NaCl or KCl baths were tested. The effect of time and temperature was investigated, as well as the influence of stirring the bath, or applying an external emf.

RESULTS

Metals that can be coated.—Copper, iron, and low carbon steel objects were plated in most of the experiments, but it was found that nickel, cobalt, and nickel-copper alloys were also readily coated with a titanium layer. Medium and high carbon steels, as well as cast iron, were coated only with difficulty, and a relatively thin and patchy titanium layer was observed. Aluminum could not be coated because it was badly corroded in the molten chloride bath.

Arrangement of titanium source and object to be plated.—Flat surfaces to be plated were placed as close as possible to the titanium sheet serving as a source without actually having them touch; usually a 0.5–1 mm diameter wire of chrome-nickel, titanium, or copper was used as a spacer. It is not desirable to have the object and the titanium touch because at the points of contact actual cementation occurs, and when the metals are separated the desired coating may be broken at these points.

If titanium powder is packed around the object to be plated, some small particles of titanium will be cemented to the coating, which will then be rougher than the coating obtained wholly from the pyrosol. Coarse cuttings of titanium, such as come from a hacksaw, give better coatings than powder, because the cuttings do not stick to the plated surface as readily, and seem to allow freer circulation of the pyrosol-bearing molten electrolyte.

Titanium hydride powder, as well as metal powder, served as a source of titanium pyrosol; no particular advantage or disadvantage could be claimed for it.

Tests with a low carbon and a high carbon titanium ferrochrome, containing 24% and 34% titanium, respectively, as a source material, were entirely unsuccessful.

On the theory that plating from the pyrosol is the most desirable method, a piece of titanium metal was heated in a mixture of NaCl and KCl at 850°C for 4 hr. The severely corroded metal was then removed leaving the corrosion products, much of which was the black pyrosol, in the salt in the crucible. Next, a piece of copper was placed in the mixture in the crucible and heated. A very thin and patchy coating was obtained on the copper, indicating that the effectiveness of the pyrosol degenerates rapidly.

In an attempt to plate irregular objects, several experiments were made in which, first, a piece of titanium acting as a source was revolved in the bath with the object to be coated held stationary; next, the object was revolved with the titanium stationary; finally, they were both revolved. Only fragmentary coatings were obtained. This seemed to show that dispersal of the pyrosol by stirring was undesirable.

As mentioned before, coatings obtained from titanium powder are rough, so it was thought that stirring or agitation would be beneficial. However, as the titanium powder partially sinters and agglomerates in the salt bath, all attempts at stirring, agitation, or tumbling of a closed container failed. The powder and the object all moved together as one piece.

Composition of bath.—NaCl, KCl, LiCl, and mixtures of all proportions appeared to be equally effective. Eutectic mixtures of NaCl and KCl had the advantage of a lower melting point. The still lower melting mixtures (around 400°C) using LiCl were not warranted because no coating could be obtained at such low temperature.

Thin unsatisfactory coatings were obtained in K_2TiF_6 , NaOH, and KOH. No coatings were obtained in NaCN, KCN, or a variety of sulfates.

A number of experiments were made in which NaI, KI, NaBr, KBr, K_2TiF_6 , or NaF, were added in amounts varying from 1 to 15% to NaCl or KCl baths. It was thought that these additions would

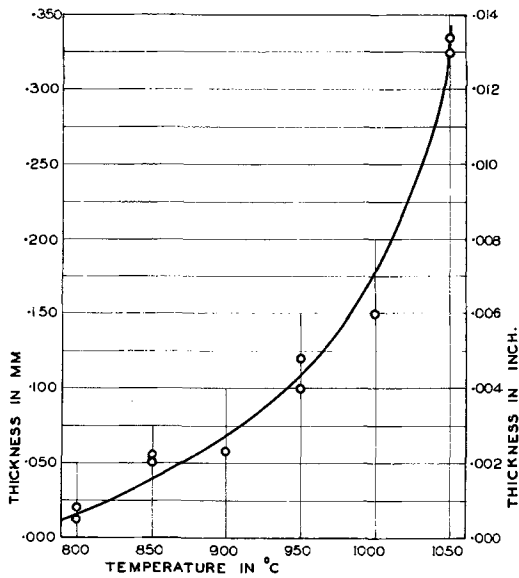


FIG. 1. Thickness of titanium coatings on iron; 7-hr deposition time in a KCl-NaCl bath.

hasten corrosion of the titanium source and, hence, increase the rate of plating. None of the additions was beneficial; the plating obtained with these additions was less than that with baths of only NaCl, KCl, or a mixture of the two. It is evident that for plating purposes it is not only the amount but the nature of titanium corrosion products that must be considered.

Effect of temperature.—Disks of low carbon steel were plated on one side from titanium sheet using a bath of 50-50 mole % of NaCl and KCl, and 7 hr plating time. Iron was then dissolved by heating the sample at 60°-80°C in a saturated solution of ferric chloride. Final traces of iron on the titanium were removed with 1-4 nitric acid. The deposit was washed, dried, weighed, and analyzed for iron and titanium.

Fig. 1 shows how the thickness of the titanium coating increases with the increased temperature of the bath. The thickness was calculated from the weight.

The temperature range for coating copper is more

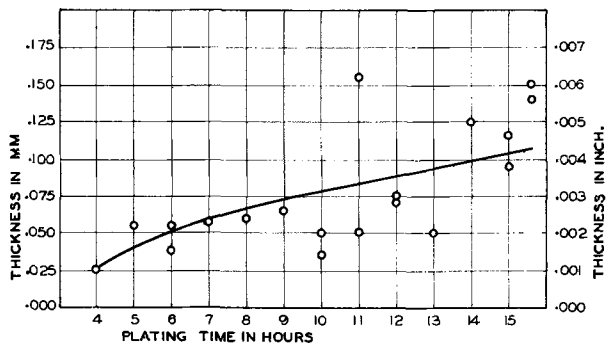


FIG. 2. Thickness of titanium coatings on iron; KCl-NaCl bath at 900°C.

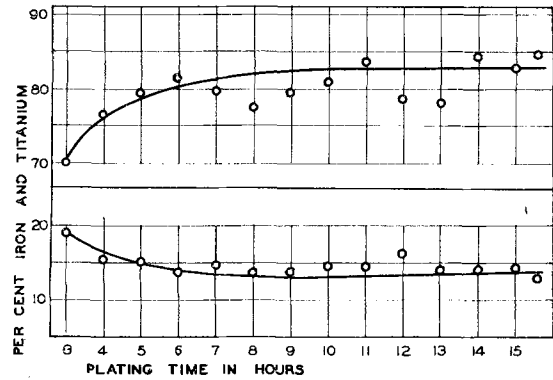


FIG. 3. Titanium and iron contents of titanium coatings vs. coating time; KCl-NaCl bath at 900°C.

limited. Below 800°C very little coating is obtained, and the upper limit is set by the copper-titanium eutectic temperature of about 878°C. If this temperature is exceeded, the sample and the titanium source form a molten alloy. Several tests were made to plate titanium on copper in KCl-LiCl baths at temperatures lower than those reported above. No coating was visible after 4 hr at 450°C and less than 0.0001 in. was obtained at 600°C and 4 hr plating time.

Effect of time.—Using a procedure similar to that described in the previous section, iron samples were coated at 900°C for times varying from 1 to 16 hr. Very little titanium was deposited until after 3 hr plating time. Fig. 2 shows the results of this series of tests.

It can be seen that the thickness of the coating increases with time, but that there is much variation. This lack of reproducibility, especially when longer times are used, is related to the deterioration of the plating power of the bath. Undoubtedly, the pyrosol becomes oxidized in the open crucibles and loses its ability to form a coating, and the rate of oxidation is not the same in successive experiments.

Composition of titanium coatings.—Titanium coatings

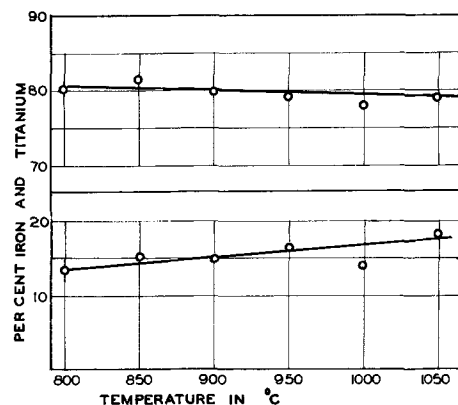


FIG. 4. Titanium and iron contents of titanium coatings vs. temperature; KCl-NaCl bath for 7 hr.

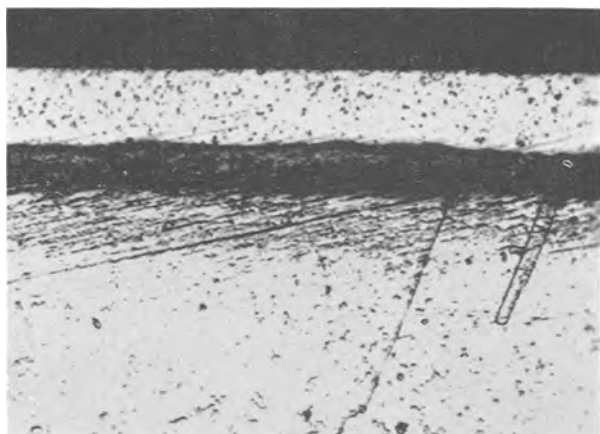


FIG. 5. Titanium coating on copper showing two layers; deposited in KCl at 850°C for 8½ hr; etched in 50% NH₄OH + 50% H₂O + few drops H₂O₂. 500X.

from experiments reported in the previous two sections were analyzed for titanium and iron by colorimetric methods. The determination of titanium was made using hydrogen peroxide as a reagent (Weller's method); iron was determined by the method of Moss and Mellon (6). Results are shown in Fig. 3 and 4.

It can be seen that there is no great variation of composition with time of coating, and only a slight trend toward higher iron content with higher temperatures of treatment. The sum of iron plus titanium is in the neighborhood of 95% for all samples; the remaining 5% is probably oxygen, although this has not been proved by analysis.

Photomicrographs, such as the one shown in Fig. 5, reveal that the coating on copper consists of an outer layer and an intermediate layer of approximately the same thickness which has a dark appearance in the photograph. This same phenomenon has been reported by Steinberg, Sibert, and Wainer (7) for zirconium electrodeposits on copper. Titanium coatings on iron also show two layers, but the intermediate layer, presumably higher in iron, is not more than one tenth the thickness of the outside layer (see Fig. 6).

Application of outside emf.—An experiment was made in which direct current was passed through the salt bath, with a piece of titanium as the anode and a piece of copper as the cathode; no plating was obtained on the cathode. Titanium and copper were in close proximity so that, in the absence of current, a coating would have been obtained on the copper; thus, the current was detrimental in this arrangement. Examination of the bath showed that titanium had gone into the bath as ions of lower valence, giving the salt a purple color. Without the current, the bath would have been gray-black from the finely divided pyrosol.

Several tests were made in which 60-cycle current

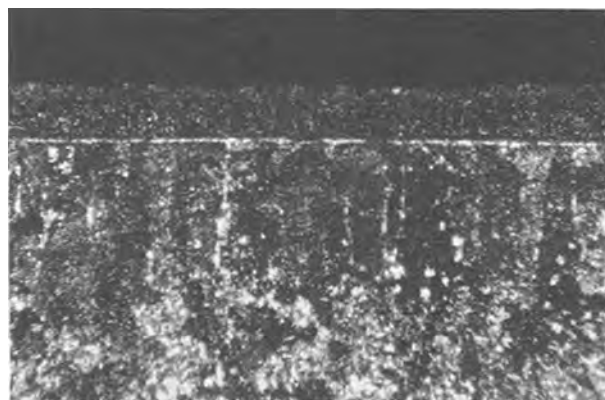


FIG. 6. Titanium coating on iron showing two layers; deposited in NaCl at 950°C for 6 hr. 100X under polarized light.

was passed into the bath through two titanium electrodes. It was hoped that this would hasten the formation of titanium pyrosol, but no advantage could be observed.

DISCUSSION AND CONCLUSIONS

Some aspects of the procedures described in this paper are similar to the process patented by Lauenstein and Ulmer (8) wherein iron castings are packed in powdered ferrochrome or ferromanganese and common salt in a crucible and heated for approximately 3 hr at 1600°–2000°F (871°–1093°C). This procedure results in alloying and coating of the iron surface with chromium or manganese; the inventors claim that the salt is decomposed to yield sodium which acts as a reducing agent for the manganese or chromium chloride formed from the ferroalloy.

The authors' experiments with titanium show that its chief corrosion product in chloride salt baths is in the form of finely divided particles which are not ions (4), and that this material can be used in a practical way to coat iron, copper, and other metal surfaces with a high titanium alloy. Whether this pyrosol acts directly to form a diffusion coating on the base metal, or whether there is an intermediate reaction to form a lower chloride of titanium which

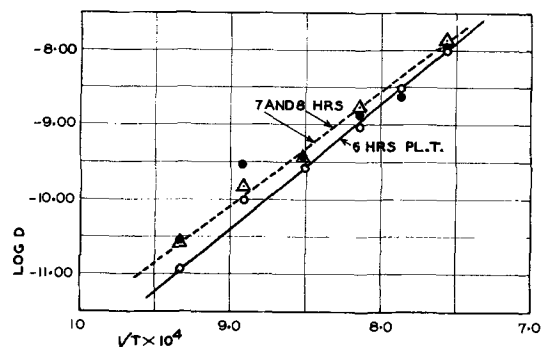


FIG. 7. Log diffusion constant, D , for titanium on iron vs. reciprocal of absolute temperature.

in turn is decomposed to produce the coating is not clear from the present experiments. Analogy with chromizing is not helpful because chromium coatings on iron can be obtained either by packing the iron in metallic chromium powder or by submerging it in salt baths containing chromous chloride.

Using the equation, $x^2/4Dt = K$, where x is the thickness of the coating, t is the time, and K is assumed to be one, values were calculated for D , the diffusion constant, using the data of thickness vs. time and temperature reported in a previous section. The results in Fig. 7 show the expected relationship between D and temperature for a diffusion process.

From a practical standpoint the process will produce a coherent substantial coating high in titanium and suffers only from those drawbacks common to chromizing, siliconizing, and other comparable processes. In a similar fashion coatings have been made of zirconium, hafnium, uranium, and manganese on iron and copper.

ACKNOWLEDGMENTS

The authors are grateful to the Wright Air Development Center for support of this work and permission to publish the results obtained. Valuable

contributions to this investigation have been made by Dr. T. M. Morris, Dr. W. H. Webb, and Professor A. Legsdin.

Any discussion of this paper will appear in a Discussion Section to be published in the December 1955 JOURNAL.

REFERENCES

1. G. D. P. CORDNER AND H. W. WORNER, *Australian J. Appl. Sci.*, **2**, 358 (1951).
2. E. J. CHAPIN AND C. R. HAYWARD, *Trans. Am. Soc. Metals*, **38**, 909 (1947).
3. P. P. ALEXANDER, U. S. Pat. 2,351,798, June 20, 1944; U. S. Pat. 2,512,455, June 20, 1950.
4. C. B. GILL, M. E. STRAUMANIS, AND A. W. SCHLECHTEN, *This Journal*, **102**, 42 (1955).
5. R. LORENZ AND W. EITEL, "Pyrosols," Akad. Verlagsges, Leipzig, (1926); R. LORENZ in J. ALEXANDER'S "Colloid Chemistry," Vol. I, pp. 681-706, Reinhold Publishing Co., New York (1926).
6. M. L. MOSS AND M. G. MELLON, *Ind. Eng. Chem., Anal. Ed.*, **14**, 862 (1942).
7. M. A. STEINBERG, M. E. SIBERT, AND E. WAINER, "Zirconium and Zirconium Alloys," p. 37, American Society for Metals, Cleveland, Ohio (1953). See also, *This Journal*, **101**, 63 (1954).
8. C. F. LAUENSTEIN AND P. F. ULMER, U. S. Pat. 2,046,638, July 7, 1936; U. S. Pat. 2,102,539, Dec. 14, 1937.

The Crystallographic Dependence of the Oxidation Potential of Solid Copper¹

W. E. TRAGERT AND W. D. ROBERTSON

Yale University, New Haven, Connecticut

ABSTRACT

Oxidation potentials of solid copper crystals have been evaluated for the isolated crystallographic planes (111), (110), (100), (210). It has been demonstrated that the only stable surface configuration of atoms is that of the close-packed octahedral plane and, accordingly, only this plane on the electrode surface produces a reversible cell. The significance of potentials obtained with other forms of electrodes has been interpreted on the basis of the observed crystallographic requirement for equilibrium.

INTRODUCTION

The electrochemical anisotropy of crystalline solids has been qualitatively established by several investigators. Following early work on rates of solution of ionic crystals (1-3), studies were made of solution rates and chemical reactivity of metallic single crystals as a function of lattice orientation. Glauner and Glocker (4), working with electrolytic copper crystals, surveyed the basic stereographic triangle with respect to rate of solution in 20 different organic and inorganic solutions. The results they obtained in acetic acid, for example, showed relative solution rates parallel to (111), (100), (110), and (210) directions to be 1.2:1:0.56:0.31, with seven selected orientations completely describing all maxima and minima. Aminoff (5) and Straumanis (6) both observed the stability of the basal plane in zinc relative to the pyramidal and prism planes as indicated by oxidation, vaporization, and solution rates. The latter authors suggested that the stability of a crystal plane could be directly associated with the atomic configuration in that plane, with higher atomic density corresponding to greater stability. More recently, Leidheiser and Gwathmey (7) studied the variation in electrochemical properties of the surface of a copper single crystal as a function of orientation. Their experiments included a measurement of the potential difference between the cube and octahedral planes in an acid CuSO_4 electrolyte; it was determined that the magnitude of the potential difference was dependent on the presence or absence of air in the electrolyte and that the sign of the potential could be reversed by a hydrogen atmosphere anneal of the specimens.

Experimental results cited above indicate that the crystallographic dependence of electrochemical phenomena is real and that specific observations were at least qualitatively reproducible within the rather arbitrary limits of individual experiments. The fact that apparently complementary measurements yielded contradictory results can be directly attributed to the dynamic nature of the experiments. Nonequilibrium conditions, unknown or unrecognized side reactions, chemical impurity and inhomogeneity of the metal crystals, and inadequate control of physical parameters appear to preclude quantitative interpretation of these investigations.

With respect to thermodynamic treatment, the history of the determination of the standard potential of copper may be described in terms of attempts to define a standard form of electrode. Lewis and Lacey (8) attributed the scatter in values obtained from a number of coherently electroplated copper electrodes to surface strains; to eliminate strain they used a copper sponge electrode which they found to be constant and reproducible to 0.0001 v. Neilsen and Brown (9), however, found that values obtained with a copper sponge varied and that reproducibility could only be achieved with a 2-phase copper amalgam electrode. Subsequently, the amalgam electrode was utilized by several other investigators (10-13), all of whom corroborated the experience of Neilsen and Brown. Getman (13) also investigated the potential of an unamalgamated single crystal of copper which he considered to be incapable of supporting significant stress and thus less liable to exhibit the erratic behavior of the massive polycrystalline copper electrodes previously employed. The copper single crystal, in the form of a cylindrical rod of undetermined crystallographic orientation, gave results which were 0.0035 v higher than those obtained with the amalgam but which, in contrast to unamalgamated electrodes previously employed, were re-

¹ Manuscript received July 12, 1954. This paper is taken from a thesis submitted by W. E. Tragert to the Faculty of the School of Engineering, Yale University, in partial fulfillment of the requirements for the degree of Doctor of Engineering.

producibile and constant to 0.0001 v. Recently, Wetmore and Gordon (14) obtained results with amalgam electrodes that agree substantially with those obtained by Nielsen and Brown and with the amalgamated polycrystalline electrodes used by Getman.

It is evident from both equilibrium and non-equilibrium experiments that electrochemical potential measurements involving reactions at a metal surface depend on crystallography. In this connection, two significant and related problems require quantitative evaluation: (a) the magnitude of this crystallographic dependence and its relation to the principal crystallographic directions; and (b) the significance of crystallography with respect to the standard oxidation potential of a metal.

The experiments described below consist of a number of measurements designed to determine the magnitude and significance of potential differences between four low index crystal planes of copper as a function of electrolyte concentration and temperature. The cell chosen for the purpose was Cu; CuSO₄; Hg₂SO₄; Hg. The crystal planes were (111), (110), (100), and (210).

EXPERIMENTAL PROCEDURE

All experiments were conducted in a water thermostat completely covered by a black felt hood. Temperature was controlled to $\pm 0.005^\circ\text{C}$ by high sensitivity mercury switches controlling a small fraction of the required heat input. Temperature was measured with a Beckman thermometer calibrated against a standard platinum resistance thermometer before the series of measurements were made. Potentials were measured with a precision potentiometer in conjunction with a galvanometer of 0.0006 μ amp/mm sensitivity.

All cells were operated under water-pumped nitrogen, deoxidized by passage through a tower containing copper powder at 400°C ; the finely divided powder copper was previously deposited on glass wool by hydrogen reduction of cuprous oxide.

The electrolyte was prepared by dilution of approximately 1.0M stock solution of doubly recrystallized reagent grade copper sulfate. Prior to each run, solutions were deaerated by vigorous boiling and cooling under pure nitrogen; they were then equilibrated with copper chips and reagent grade mercurous sulfate at the temperature of the run for 12 hr. Quantitative determination of concentration was made by standard electrodeposition analysis subsequent to each experiment.

The crystals from which electrodes were cut were grown by the standard Bridgman method in high purity graphite molds from polycrystalline copper rod. Preliminary measurements were made using

crystals of 99.95% Cu (0.04P) and 99.97% Cu (0.02Zn) and final determinations were made with 99.999% copper electrodes. The latter measured 0.30 in. in diameter by 3 in. long; the others were $\frac{1}{2}$ in. by 5 in. The orientation of each crystal was determined by the Laue back reflection technique at two points 90° apart on the circumference and $\frac{1}{2}$ in. from opposite ends. The crystal was then mounted in a goniometer vise with the clamped portion wrapped in a $\frac{1}{16}$ in. thickness of stiff paper to avoid deformation; successive cuts were made with a jeweler's saw running in a steel miter parallel to each of the planes mentioned above. The crystal specimens, each approximately $\frac{3}{4}$ in. long, were etched in 50% HNO₃ until etch pits developed on the cut surfaces. The crystal orientation normal to the end surface, which was to serve as the electrode area on each piece, was then obtained by a back reflection photogram, from which the accuracy of the cut was determined. From the small degree of asteration of the spots on the film the etching operation was judged to be effective in removing the heavily deformed material adjacent to the cut. The surfaces were mechanically abraded on 1/0 emery paper to correct errors in the initial cutting and to bring the desired crystal plane to within 2° of coincidence with the surface. Usually 3 or 4 successive cycles of polishing, etching, and orientation determination were required to produce the desired surface orientation. X-ray photograms of the final test surfaces indicated a lineage of less than $\frac{1}{2}^\circ$.

Final specimen preparation consisted of abrasion on 3/0 and 4/0 emery paper followed by electropolishing for approximately 70 min in a 40% orthophosphoric acid electrolyte at the optimum point on the current-voltage curve as described by Jacquet (15). In order to facilitate handling during the electropolishing operation and subsequently in the cells, a 6-in. length of 18-gauge copper wire was soldered to each specimen at the end opposite the experimental surface. Solder connections and supporting wires were coated with a mixture of 70% beeswax: 30% paraffin after mechanical abrasion had been completed, and the cylindrical surfaces were masked out after 1 hr of electropolishing. Final test surfaces were specular and free from pits. Specimens were electropolished successively and, as each electrode was removed from the polishing cell, it was rinsed thoroughly with deaerated distilled water and allowed to dry in a stream of dry, purified nitrogen. At the same time, a warm copper wire was run along the edge of the masking wax around the test surface to permit the wax to flow over the area which had been undercut in the final 30 min of electropolishing. The specimen was then placed in a nitrogen filled storage flask; the supporting wire was sealed with

wax into a hole previously cut in a large rubber stopper which served to hold the specimens and to seal the flask.

The procedure finally adopted, after the preliminary experiments described below, was the following. When all of the electrodes were in the storage flask, a 50% HgNO_3 solution was introduced under nitrogen pressure to produce simultaneous amalgamation. The order in which electrodes were prepared proved to have no measurable effect on subsequently measured potentials and it was concluded that this technique produced electrodes essentially free from surface films. The assembly of amalgamated specimens in the rubber stopper was removed from the mercurous nitrate solution, rinsed in distilled water and two portions of CuSO_4 solution identical with that in the cell, and then transferred to the cell. Potentiometer leads were immediately soldered to the ends of the electrode support wires. The total time that the wet electrodes were exposed to air during the transfer operation did not exceed 3 or 4 sec and it was estimated that this interval was too short for appreciable oxygen absorption to occur.

Two types of cells were utilized: an H-cell with a fritted glass disk in the connecting arm, and a straight tube cell. Both were equipped with a platinum-in-glass contact for the mercurous half-cell and were sealed with a large, wax coated rubber stopper. Preparation consisted, first, of adding redistilled mercury sufficient to cover the platinum contact and, then, mercurous sulfate which had been thoroughly washed with copper sulfate solution of the same concentration as would subsequently be used in the particular run. Cells were placed in the thermostat, evacuated, flushed with nitrogen, and held under a slow stream of nitrogen for 12 hr prior to introduction of electrodes and the electrolyte. In the case of the H-cell, electrolyte portions for each of the half-cells were separately equilibrated with respect to cupric and mercurous ion, care being taken to maintain a solution head in the copper half-cell during the filling operation to insure exclusion of mercurous ion. Filling was accomplished by transferring the solutions under nitrogen pressure from reservoirs in the water bath. With the straight tube cell this procedure was altered, the electrolyte being siphoned from the equilibration flask. In either case, upon introducing the electrodes the cell was evacuated to boiling of the electrolyte and flushed with nitrogen in order to remove any air carried in with the electrode assembly.

Since the same set of electrodes was used repeatedly during any particular phase of the experiment, it appeared desirable to devise some simple method for removing liquid mercury and the solid phase copper-mercury alloy from test surfaces prior

to reparation of the electrodes between runs. This was accomplished by mounting the electrodes individually in a polishing cell, with a copper wire counter-electrode. Each electrode was first connected as the cathode and a loose copper deposit was formed at low current density on the mercury coated surface. The specimen was removed from the cell and the surface rubbed with tissue paper, causing the deposited copper to amalgamate and thus remove the liquid mercury as the amalgamated sludge was washed away with distilled water. It was usually necessary to repeat this process several times to produce the desired result. The specimen was then connected as the anode and polished for about 1 min at a current density sufficiently high to cause strong anodic gas evolution. This operation served to remove the last traces of amalgam from the surface and left the specimens ready for final preparation in the manner described above.

PRELIMINARY INVESTIGATION

Preliminary measurements were made using an H-cell, unamalgamated crystal electrodes, and an electrolyte concentration of approximately 0.5M. Under these conditions two runs were made, each involving a set of electrodes prepared from one of the two lower purity crystals. In each case, readings were taken over an 8-day period at a temperature of 24.48°C. This arrangement yielded values which fluctuated during a 6-hr interval, then decreased slowly in absolute potential for the remainder of the run. At the beginning of the period of fluctuation, the electrodes maintained relative potential differences of the order of 4.5 mv between the (111) (most noble) and the (110) (least noble) with the (100) value intermediate but closer to (110). The differences decreased proportionately and within minutes settled at about 2 mv maximum after which they diminished very slowly to 1.5 mv at the end of the run. The (210) was not included in these runs. After the first day, the specimens exhibited a photosensitivity which increased with time in an apparently exponential fashion. Upon removal from the cell, specimens were found to be covered with a reddish crystalline deposit, previously discussed by Newbery (16), which was heaviest on the (100) and (110) surfaces. Growth spirals were observed on some of the superficial crystals and a microscopic study of the crystal forms indicated that they were of cubic symmetry. Simple mineralogical tests (fracture, streak, solubility) lead to the tentative identification of the crystalline deposit as cuprite, Cu_2O . On the basis of this assumption, more rigorous precautions were taken to remove and exclude air from the system.

The effectiveness of the exclusion of mercury from

the electrode surface was checked by immersing a polycrystalline copper rod in the cell for one week under operating conditions. Upon removal, approximately 0.005 in. was machined off the surface. The chips were spectrographically analyzed for mercury; none was detected. However, since the electropolished copper surface might be expected to be extremely sensitive to minute quantities of adsorbed substances, it was decided to amalgamate the test surfaces. This arrangement also served to eliminate practical difficulties involved in keeping copper electrodes free of mercury. The amalgamation procedure which was adopted is that described in the previous section.

The amalgamated electrodes, (111), (110), and (100), were mounted in the H-cell and potentials were measured over a period of 20 days. Following an initial interval of transient values, the potentials appeared to stabilize and, in the case of the (110) and (100) planes, remained constant for approximately 9 hr and then tended to approach the (111) value which remained constant to ± 0.00006 v during the period of the run. Upon removal from the cell, the (100) and (110) electrode surfaces were found to be covered in patches with a crystalline deposit having the color of mercury and the physical properties of an intermetallic compound. The (111) surface was free of any film deposit. The electrodes were thoroughly washed and held in a flask open to atmosphere for two weeks. Most of the liquid mercury evaporated and it was then possible to examine the surface and solid residue. The surfaces of the active electrodes, (110) and (100), had been eroded by the development of fine convolutions, and a profusion of superficial crystallites was in evidence. The (111) electrode was relatively unaltered and only one or two microscopic crystallites were present on the surface. In every instance, there was no observable variation in behavior between the two sets of lower purity crystals.

Reference to the copper-mercury phase diagram (17) shows that, at the temperatures here employed, the solubility of copper in liquid mercury is approximately 0.003%, the almost vertical liquidus line giving a very small solubility temperature coefficient. At temperatures below 96°C the liquid solution is in equilibrium with the intermetallic compound CuHg at 50 atom % mercury. On this basis, the crystallites described above were presumed to be CuHg.

Since the necessity for maintaining the surrounding electrolyte free of mercurous ion was eliminated by prior amalgamation of the electrodes, the final preliminary run was conducted with a straight tube cell and electrodes prepared from 99.999% copper. This run was characterized by an

initial period of fluctuation of only 45 min, followed by stable values for a period of 6 hr. At this point, the temperature of the water bath was lowered to 17.2°C and again raised to the reference temperature, 24.48°C. The potentials then measured agreed with those of the stable period to within 0.02 mv. A similar cycle through 34.4°C was performed and identical results were obtained, substantiating the reversible character of the cell.

As a check on the reproducibility of the mercurous sulfate electrodes, a cell was made up of two such electrodes in opposition, and over a period of 3 days the variation from zero potential did not exceed 0.03 mv.

EXPERIMENTAL RESULTS

The final potential values which were obtained are recorded in Table I as a function of crystal surface orientation, electrolyte concentration, and temperature (columns 1-4). Measurements at 25.0°C were corrected from 24.48°C by interpolation based on the observed temperature coefficients for individual concentrations. Each value represents the mean of at least 12 readings taken, in general, at 15-min intervals with an average deviation of 0.04 mv as can be seen in Table II which records a typical run. At the lowest concentration the error in the

TABLE I

M	Temp. °C	Crystal plane	E, v	-log γ	E_{cell}^0 v	$\frac{\Delta E}{v \times 10^{-3}}$	$\frac{dE_{\text{cell}}^0}{dT}$ v $\times 10^{-4}$
0.01447	17.2	111	0.41113	0.445	0.2797	—	8.1
		110	0.41495	—	—	3.8	
		100	0.41483	—	—	3.7	
		210	0.41497	—	—	3.8	
	25.0	111	0.40890	0.455	0.2733	—	
		110	0.41273	—	—	3.8	
		100	0.41262	—	—	3.7	
		210	0.41236	—	—	3.5	
	34.7	111	0.40645	0.467	0.2656	—	
		110	0.41012	—	—	3.7	
		100	0.41002	—	—	3.6	
		210	0.40978	—	—	3.3	
0.05395	25.0	111	0.38835	0.677	0.2733	—	
		110	0.39294	—	—	4.6	
		100	0.39293	—	—	4.6	
		210	0.39287	—	—	4.5	
0.4829	17.2	111	0.36418	1.152	0.2796	—	8.1
		110	0.36847	—	—	4.3	
		100	0.36837	—	—	4.2	
		210	0.36848	—	—	4.3	
	25.0	111	0.36094	1.165	0.2733	—	
		110	0.36491	—	—	4.0	
		100	0.36491	—	—	4.0	
		210	0.36501	—	—	4.1	
	34.7	111	0.35697	1.181	0.2655	—	
		110	0.36056	—	—	3.6	
		100	0.36092	—	—	4.0	
		210	0.36106	—	—	4.1	

TABLE II. $T = 24.48^\circ\text{C}$; $M = 0.4771$

Time $\left\{ \begin{array}{l} \text{hr} \\ \text{min} \end{array} \right\}$	(111)	(110)	(100)	(210)
Cell assembled				
:15	0.36118	0.36562	0.36551	0.36557
:30	0.36121	0.36560	0.36555	0.36563
:45	0.36125	0.36565	0.36559	0.36569
1:00	0.36125	0.36569	0.36559	0.36567
1:15	0.36118	0.36574	0.36560	0.36568
1:30	0.36117	0.36569	0.36559	0.36566
1:45	0.36116	0.36567	0.36561	0.36566
2:00	0.36117	0.36566	0.36559	0.36567
2:15	0.36116	0.36565	0.36561	0.36568
2:30	0.36115	0.36566	0.36555	0.36568
2:45	0.36118	0.36566	0.36563	0.36563
3:00	0.36113	0.36565	0.36551	0.36566
7:00	0.36113	0.36564	0.36553	0.36553
7:15	0.36114	0.36562	0.36550	0.36549

potential values due to the solubility of mercurous sulfate probably does not exceed the limit of uncertainty of the measurement and can accordingly be disregarded.

The standard cell potential was evaluated using the relationship $E = E^0_{\text{cell}} - (\nu RT/nF) \cdot \ln m \gamma$. Because of the inherent unreliability of emf measurements at low electrolyte concentrations, highly dilute solutions were not used in this experiment and the Lewis and Randall (18) method of extrapolating a function of E to infinite dilution to obtain the standard potential was not employed. It appeared that the value of the normal potential could be derived most satisfactorily from freezing point depression measurements (19), and relative partial molar heat content values (20) in the manner outlined by Wetmore and Gordon (21). The assumption was made that a function which empirically represented the freezing point data, $j = Amx$, where $x = 0.423$ and $A = 1.718$, could be extended without significant error to include 0.01447M, the lowest concentration. The corresponding $\ln \gamma$ was calculated and then corrected to 298.2°K using the appropriate \bar{L}_2 and considering $(\bar{C}_{P2} - \bar{C}^0_{P2})$ to be negligible (22). The result of this calculation, $\log \gamma = -0.455$, permitted the direct evaluation of E^0_{cell} for the (111) electrode in the most dilute electrolyte. This choice of electrode surface was made because of typical stability of the (111) potential with time in every cell which was observed. Potential differences, listed in column 7, Table I, are thus simply the arithmetic differences in measured potential relative to the standard, (111). Taking the normal potential of the mercurous sulfate electrode (23) as -0.6152 at 25°C , the standard potential of the amalgamated copper crystal electrode is -0.3419 v. Activity coefficients at two other temperatures, 17.2° and 34.7°C , were calculated from the activity coefficient at the freezing point and the value of \bar{L}_2 , and cor-

responding E^0_{cell} values were obtained directly. These results are entered in Table I, columns 5 and 6. At other electrolyte concentrations the value of the activity coefficient was similarly based upon the E^0_{cell} corresponding to the (111) electrode.

Since a single set of high purity crystal electrodes was used throughout the final measurements, it appeared desirable to establish the fact that strain had not been anisotropically introduced during the original cutting operation. Although the maximum residual stress remaining in any one specimen would not be expected, on a bulk thermodynamic basis, to affect the potential within the limits of the present experimental error, strain might conceivably exert a disproportionate influence on surface properties, thus constituting the source of the potential differences. Specimens were prepared, accordingly, as for a potential run, then stripped of wax and solder and heated in vacuo at the rate of $10^\circ\text{C}/\text{hr}$ to 250°C , and furnace cooled. There was no visual evidence of recrystallization after brief etching in 25% HNO_3 . Test surfaces were repolished electrolytically and the specimens mounted in a 0.01447M cell. Observed potential differences were identical with those previously obtained.

To facilitate direct comparison of the single crystal electrodes with a polycrystalline electrode, an annealed 0.25-in. diameter rod of 99.999% copper having a small grain size was electropolished, amalgamated, and placed in a 0.4829M cell. The measured potential, which initially remained constant for 6 hr at 0.05 mv below the value of the (110) electrode in the same cell, decreased continuously for about 40 hr and finally stabilized at a value 0.5 mv higher than the (111). At this point the surface was examined microscopically. Nonuniform surface alteration was observed, certain grains having been deeply eroded, others less, and some apparently not at all. Grain boundaries were similarly affected, the extent of erosion presumably being a function of boundary angle. CuHg crystallites were in evidence on the surface; apparently their distribution was related directly to the extent of localized erosion.

To determine the rate of precipitation of CuHg from a homogeneous solution of copper in mercury, a 5% copper amalgam was prepared electrolytically and stored under an acidified CuSO_4 solution for one week. The presence of solid phase CuHg in detectable amounts was not observed until the second day. After the third day, the volume of CuHg appeared to remain constant, indicating that phase equilibrium had been established within two days.

DISCUSSION

Data and calculated values obtained in the present investigation are in substantial agreement with those

in the literature. A direct comparison of the authors' data with that obtained by Wetmore and Gordon (14), Getman (13), and Neilsen and Brown (9) is shown in Fig. 1 where the quantity $E^{0'}$, defined by the relationship

$$E^{0'} \equiv E + \frac{\nu RT}{nF} \ln m = E^0 - \frac{\nu RT}{nF} \ln \gamma$$

is plotted against $m^{1/2}$. It can be seen that values derived from saturated amalgam electrodes, with and without massive copper present, approximate a curve which defines the lower limit of all data represented. The curve which represents Getman's single crystal data is roughly 3.5 mv above the lower curve, while a third curve, about 5 mv above the amalgam curve, contains potential values typical of the authors' most active crystal plane electrodes. The positive drift in their values at the lowest concentration is ascribed to chemical factors associated with more dilute solutions, since the potential differences are consistent with those observed at other concentrations.

A comparison of the authors' values for $\log \gamma$, based on E (111), with those of Wetmore and Gordon shows a definite deviation. This is related to the deviation in observed E mentioned above. Inasmuch as the same extrapolation function of the freezing point data of Hovorka and Rodebush (19) was used in both instances, identical values of $\log \gamma$ are obtained up to the limits of the extrapolation. At 0.01447M the observed E yields a value of E^0 (0.2733 v) approximately 3 mv higher than Wetmore and Gordon's value (0.2702 v) at 0.02024M. Correspondingly, at 0.05395M and 0.4289M, the authors' E^0 and the observed potentials give $\log \gamma$ values greater than those calculated by the above investigators in the same concentration range. If $E^0 = 0.2702$ v is assumed to be consistent with solutions

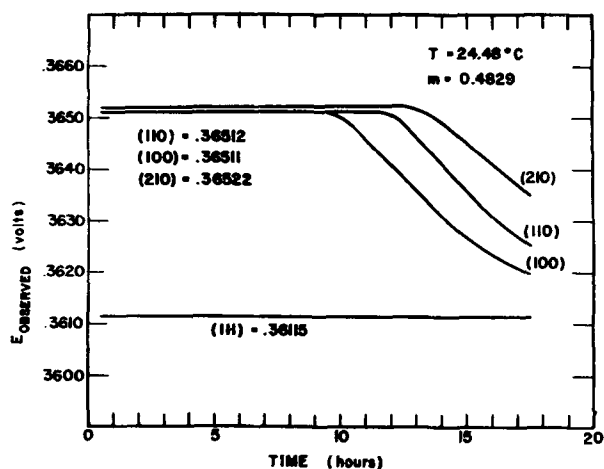


FIG. 1. Potentials of single crystal plane electrodes recorded during a typical determination.

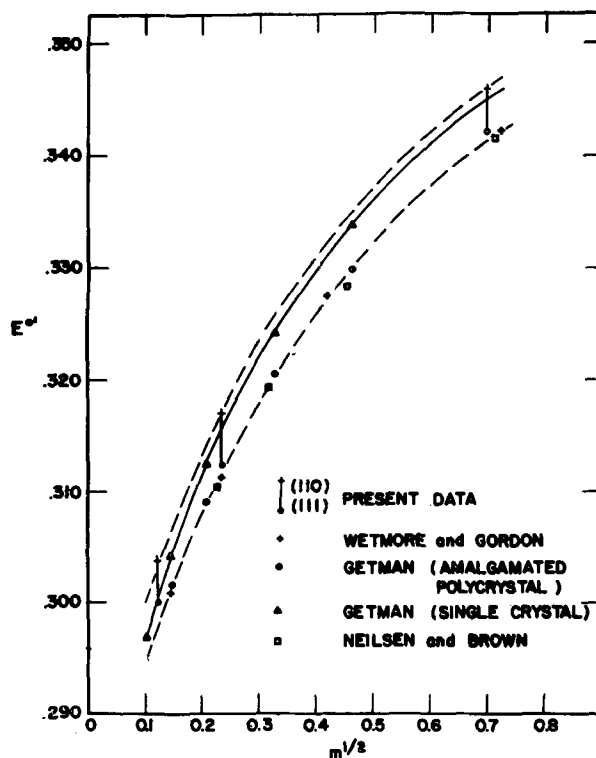


FIG. 2. Crystal plane potentials plotted together with other electrode values.

more concentrated than approximately 0.02M, and is accordingly used with the authors' observed potentials, the resulting values for $\log \gamma$ are in good agreement with those of Wetmore and Gordon. In fact, using this E^0 , the activity coefficients do not differ significantly when calculated from any of the data that define the amalgam curve (Fig 2).

The absolute value of E^0 thus appears to be susceptible to evaluation from data obtained either with an equilibrium two-phase amalgam or with a critically oriented single crystal surface as is discussed presently. It is immediately apparent, however, that considerable difficulty is involved in the experimental realization of the crystal electrode with respect to both preparation and prevention of surface film formation. On this basis, the electrolytic amalgam appears to offer the most convenient form of reversible electrode.

Single crystal electrodes having a given lattice plane lying in the surface exhibit potentials which may be classified as stable and metastable, constancy in time being the criterion for such designation. The (111) surface appears to yield the stable potential in the system under consideration. Metastable surfaces yield potentials approximately 4.5 mv above the value characteristic of the (111) plane. In copper sulfate solutions, using unamalgamated electrodes, this potential difference deteriorates within minutes to about 2 mv, then more slowly to

1.5 mv at the end of eight days. Amalgamated crystal electrodes, however, give cell potentials which retain the initial 4.5 mv differences for 10–15 hr and approach the (111) value as shown in Fig. 1. In neither case can potential differences be considered quantitative in the sense of providing a direct measure of variation of surface activity with orientation because a reversible cell is obtained only with the (111) electrode.

The single crystal potential values reported by Getman and plotted in Fig. 2 may be interpreted as representing metastable potentials intermediate to values derived in this investigation. Since the crystal was utilized without regard to crystallographic orientation, it must, of necessity, have presented a variety of surface configurations to the electrolyte. In the absence of mercury on the surface (the crystal was unamalgamated), any surface alteration toward a stable configuration was rendered impossible, at least in the time required for the potential measurements.

Behavior of amalgamated crystal electrodes may be interpreted in terms of the following facts: all surfaces except (111) show attack and deposited CuHg; a finite time of the order observed for constant potential difference is required to nucleate and form solid CuHg from supersaturated liquid solution (24). Upon amalgamation, the mercury covering the metastable faces becomes supersaturated with the copper removed from these faces in an attempt to reach a stable crystallographic configuration by the development of etch facets. On the other hand, copper is removed from the stable (111) face to saturate liquid mercury at a concentration consistent with the activity of copper in the close-packed face and without crystallographically altering the exposed face except possibly to the extent required by inaccuracies of preparation. In fact, no macroscopic changes of the surface of this electrode were ever observed and the potential is definite and constant for prolonged periods of time, the equilibrium value having been recorded for 17 days in one instance.

Observed, initial, potential differences between planes represent potentials corresponding to different concentrations of copper homogeneously dissolved in mercury. The small differences between the metastable planes may be attributed to the fact that the amount of copper removed from the different planes to approximate a (111) configuration does not vary greatly between the low index planes. The higher potential associated with supersaturated mercury persists during the induction period characteristic of the nucleation of CuHg, after which the growth of CuHg depletes the solution of excess copper and the potential approaches the value of the

amalgam in equilibrium with the stable (111) surface.

If the electrode is prepared by the amalgamation of massive polycrystalline copper, the initial potential is characteristic of the degree of supersaturation of copper in mercury as derived from those copper crystallites whose surface orientations represent other than the most stable atomic configuration. In time, the potential decreases with the progressive formation of CuHg. The final surface is comprised of regions defined by areas of individual crystallites which have been more or less altered, depending on their initial orientation. The final potential is very nearly (0.5 mv) that of the electrolytic amalgam or the stable (111) amalgamated face; a small disparity is to be expected as a result of the continued presence of higher activity surface areas and grain boundaries which mark the lines of geometric transition between stable regions. If a sufficient volume of liquid mercury is not available for the equilibrating process to proceed to completion, the terminal emf would be expected to be somewhat above the proposed most stable value. That Getman's amalgamated polycrystal values are in good agreement with the electrolytic amalgam data would appear to be a consequence of the above described process having been completed while the electrode was stored for some considerable time under liquid mercury prior to immersion in the cell. The position of the authors' most stable crystal potentials, generally above the amalgam curve, is attributable to a slight convexity of the test area resulting from electropolishing, and to the small change in surface orientation attendant to the preparation of electrodes for successive runs. These factors would not be expected to influence seriously the behavior of the more active electrodes if one considers the observed potential to vary rather slowly as a function of orientation except near the (111) surface configuration. On this basis, surface convexity and error in gross orientation of the (111) electrode would serve to alter its potential rather sharply and in the more active direction, as indicated in Fig. 2. The relatively small scatter of values about the amalgam curve may, in general, be attributed to the varying degree of control of physical and chemical parameters in the several investigations considered.

Reference to Table I, column 7, shows that the potential differences between crystal electrodes varied in successive runs by about 0.5 mv. Since measurements were first made at the highest electrolyte concentration and then, in turn, at the intermediate and lowest concentrations, the variation appears not to be systematic but rather a function of surface preparation between runs. Accordingly,

potential differences are probably characteristic of the amalgamated copper crystals and are independent of the electrolyte concentration.

Variation of potential differences with temperature is, on the other hand, not indicative of any intrinsic property of the crystal faces, but is probably related to the differing proportions of copper in the four amalgams. The temperature-potential relationship was determined by making the measurements at 17.2°, 24.48°, and 34.7°C in that order, followed by return to 24.48°C. In terms of the phase diagram, such temperature changes require an increased equilibrium concentration of copper in liquid mercury. On the basis of the previously stated mechanism, metastable electrode amalgams contain an excess of copper relative to the equilibrium concentration at any of these temperatures and so would not be expected to dissolve additional copper from the crystal surfaces upon temperature increase. The (111) amalgam, however, would become progressively richer in copper in accordance with the requirements of phase equilibrium and its potential would thus approach those of the metastable electrodes. This process would lead to a diminution of potential differences upon increasing temperature, which is, in fact, indicated by present data. Presence of the minute quantity of CuHg which has been observed on the amalgamated (111) surface may, in part, be attributed to the slight supersaturation which resulted from the return of the electrode to 24.48°C subsequent to the 34.7°C measurements.

The temperature coefficient of the cell, -8.1×10^{-4} , again calculated for the (111) electrode, is slightly greater than the value of -7.6×10^{-4} obtained by Wetmore and Gordon. It may be pointed out, however, that the higher value is in better agreement with the temperature coefficient of the cell as calculated from available entropy data (25). Unfortunately, the greatest uncertainty among the individual entropy values employed exists for the oxidation of copper to cupric ion, the reaction pertinent to this discussion. The authors' temperature coefficient yields a calculated entropy for cupric ion of -22.6 eu, the dE/dT value of -7.6×10^{-4} yields an entropy of -20.4 eu, and the reference literature value is -25.9 ± 3 eu:

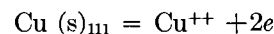
Oku (26) has measured the potential between a saturated electrolytic amalgam and an electrodeposited copper sludge and reports a value of 5 mv which can also be considered to define the difference between the lowest and highest curves of Fig. 2.

The 5 mv difference measured by Oku can be explained in the following manner. The electrodeposited copper sludge consisted of extremely small copper crystals, whose predominating surfaces were

different from the (111) orientation. The potential of this electrode would thus be less noble than the equilibrium amalgam and would constitute a compromise value for the higher activity crystal faces exposed on the surfaces of the particles. In addition, the size of particles may have given rise to a second contribution to the potential on the basis of the increase of solubility with decrease in radius, as defined by the Gibbs adsorption equation. Since the size of the particles which comprised the sludge is not known, it is impossible to evaluate the latter factor. It appears, then, that Oku's value for copper, relative to the amalgam, does not represent a reversible potential and, consequently, should not be added to amalgam values to obtain the oxidation potential of crystalline copper.

SUMMARY

1. The oxidation potential of solid copper, and presumably other metals, is dependent on the crystallographic configuration of atoms in the surface.
2. The only stable plane of the face-centered cubic system is the close-packed octahedral plane and, accordingly, only this plane produces a reversible cell. The electrode reaction may thus be written



3. All other crystal plane surfaces are metastable and approach the (111) configuration in time.
4. Polycrystalline electrodes approach the stable state providing sufficient time is allowed for the establishment of the stable crystallographic configuration.

ACKNOWLEDGMENTS

The authors wish to express their thanks to the Office of Naval Research for financial support of these experiments under Contract Nonr 305(00), and to the American Smelting and Refining Company for supplying the high purity copper.

Any discussion of this paper will appear in a Discussion Section to be published in the December 1955 JOURNAL.

REFERENCES

1. D. N. ARTEMIEV, *Z. Krist.*, **48**, 415 (1910).
2. W. SCHNORR, *ibid.*, **54**, 289 (1914).
3. W. SCHNORR, *ibid.*, **68**, 1 (1928).
4. H. GLAUNER AND R. GLOCKER, *ibid.*, **80**, 377 (1931).
5. G. AMINOFF, *ibid.*, **65**, 23 (1927).
6. M. STRAUMANIS, *Z. physik. Chem.*, **147**, 161 (1930).
7. H. LEIDHEISER, JR., AND A. T. GWATHMEY, *Trans. Electrochem. Soc.*, **91**, 97 (1947).
8. G. N. LEWIS AND W. LACEY, *J. Am. Chem. Soc.*, **36**, 804 (1914).
9. R. NIELSEN AND D. BROWN, *ibid.*, **49**, 2423 (1927).

10. E. COHEN, F. CHATTAWAY, AND W. TOMBROCK, *Z. physik. Chem.*, **60**, 706 (1907).
11. M. OBATA, *Proc. Phys. Math. Soc. Japan*, **2**, 223 (1920).
12. M. QUINTIN, *Compt. rend.*, **196**, 473, 538 (1933).
13. F. GETMAN, *J. Phys. Chem.*, **34**, 1454 (1930).
14. F. WETMORE AND A. GORDON, *J. Chem. Phys.*, **5**, 60 (1937).
15. P. JACQUET, *Metal Finishing*, **47**, (5), 48 (1949).
16. E. NEWBERRY, *J. Am. Chem. Soc.*, **51**, 1315 (1929).
17. M. HANSEN, "Der Aufbau der Zweistofflegierungen," p. 565, Springer, Berlin (1936).
18. G. N. LEWIS AND M. RANDALL, "Thermodynamics," p. 286, McGraw-Hill Book Co., New York (1923).
19. F. HOVORKA AND W. RODEBUSH, *J. Am. Chem. Soc.*, **47**, 1614 (1925).
20. E. LANGE, J. MONHEIM, AND A. ROBINSON, *ibid.*, **55**, 4733 (1933).
21. F. WETMORE AND A. GORDON, *loc. cit.*
22. *International Critical Tables*, Vol. V, p. 122.
23. H. S. HARNED AND B. B. OWEN, "The Physical Chemistry of Electrolytic Solutions," p. 439, Reinhold Publishing Corp., New York (1950).
24. H. TERREY AND C. WRIGHT, *Phil. Mag.*, *Bd. 6*, 1055 (1928).
25. K. K. KELLEY, *U. S. Bur. Mines Bulletin* 477.
26. M. OKU, *Sci. Rep. Tohoku Imp. Univ.*, **22**, 288 (1933).

Polarographic Investigation of Organic and Inorganic Compounds in an Ammonia-Ammonium Nitrate Solvent¹

GUY WILLIAM LEONARD, JR., AND DOUGLAS E. SELLERS

Department of Chemistry, Kansas State College, Manhattan, Kansas

ABSTRACT

Precision polarography is applied to the study of organic and inorganic compounds in Divers' solution. The lead-lead nitrate cell serves satisfactorily in Divers' solution as a reference electrode. Although the measured half-wave potentials are shown to be shifted by the addition of water to the solvent, values for the half-wave potential reproducible within ± 0.003 v can be obtained. Well formed polarograms are obtained for which the diffusion current is proportional to the concentration, and the half-wave potential is dependent on the species being reduced.

INTRODUCTION

During recent years an increasing number of polarographic studies have been carried out in non-aqueous solvents. Among the solvents studied, the ammonia-ammonium nitrate system (1) appears to have a distinct advantage over other nonaqueous solvents, for no supporting electrolyte is needed since the solvent is an excellent conductor. This solvent (2), which is often called Divers' solution, is formed by passing anhydrous ammonia gas over ammonium nitrate at 0°C. Ammonium nitrate takes up sufficient ammonia gas to form a saturated solution whose ammonia vapor pressure is reduced to such an extent that the solution can exist at room temperature.

Since the chief difficulties encountered in the use of organic solvents are the high resistance of the solution and the necessity of finding a suitable supporting electrolyte, the present investigation was undertaken to determine the possible use of Divers' solution for the polarographic study of organic compounds as well as to extend the investigation of the polarographic behavior of inorganic compounds in this solvent.

EXPERIMENTAL

Chemicals.—Reagent grade chemicals were used without further purification except for certain salts which were prepared in this laboratory. The anhydrous ammonia was purchased in 50 lb tanks from Armour.

Apparatus.—A Sargent-Heyrovsky Polarograph Model XII was used with a wave spreader (3). A Rubicon Portable Potentiometer was used to measure the applied potential at the beginning and at the

end of the polarogram. Calibration points were marked on the photographic record by adjusting the galvanometer to 20 and opening the shutter at each point. The reference electrode was a lead-lead nitrate electrode (4). The electrolysis cell was of the H-type. The resistance of the cell circuit as measured by an Industrial Instruments Conductivity Bridge Model RC was 31 ohms.

Procedure.—A weighed amount of previously dried ammonium nitrate was placed in one arm of the H-cell and an approximately equal amount was placed in the other half of the cell. The cell was then placed in a constant temperature bath maintained at 0°C by melting ice. Anhydrous ammonia was simultaneously passed through each cell until the system reached vapor pressure equilibrium with 1 atm ammonia at 0°C. The obtaining of equilibrium was indicated by the total dissolution of ammonium nitrate. Under these conditions, the resulting solution contained approximately three moles of ammonia per mole of ammonium nitrate. After equilibrium was established, the reference cell was saturated with lead nitrate, the lead electrode placed in the solution, and a weighed amount of sample placed in the sample compartment. Ammonia was again bubbled through both cells for about ten minutes to insure thorough mixing. The polarograms were then taken with a span of 0.2 v.

RESULTS AND DISCUSSION

A preliminary investigation, using a mercury pool as the reference electrode, revealed that the potential of the reference electrode was dependent on the length of time the mercury had been in contact with the solution. Since equilibrium conditions could not be obtained readily, and since reproducible measurements of half-wave potentials could not be obtained,

¹ Manuscript received July 12, 1954.

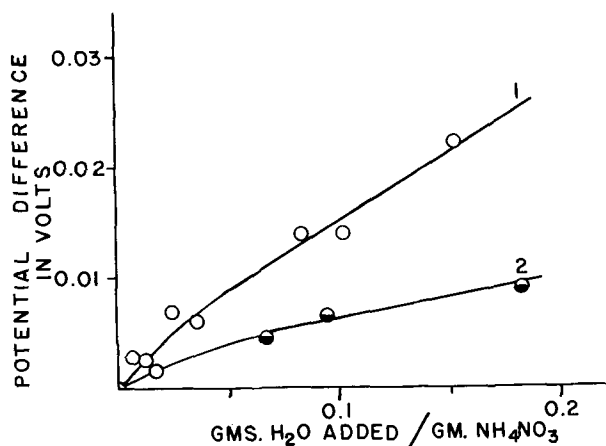


FIG. 1. Effect of moisture content upon half-wave potentials. Curve 1, change of half-wave potential for the lead system; curve 2, change of half-wave potential for the diphenyl thiocarbazon system. Potential difference = $E_{1/2}$ without added water - $E_{1/2}$ with given amount of water added.

the mercury pool was replaced with the lead-lead nitrate reference cell. The lead-lead nitrate reference cell gave results which could be reproduced within ± 0.003 v. The polarographic investigation of a sample could be completed before detectable amounts of lead diffused from the reference cell into the working cell.

The influence of moisture contamination upon the half-wave potential is shown in Fig. 1. The half-wave potential of the $Pb^{++} + 2e^- = Pb$ couple was shifted toward more positive potentials as the amount of water contamination was increased in the working cell. No water was added to the reference cell. A similar dependency upon moisture content was found for the half-wave potentials of diphenyl thiocarbazon (curve 2, Fig. 1); however, the shift in the half-wave potentials was much less than that for the lead couple. Although there is a change in the half-wave potential accompanying a change in the water content, as is shown in Fig. 1, reproducible results for the half-wave potentials could be obtained.

Table I shows the typical compounds that were

TABLE I. Inorganic and organic compounds which are soluble in Divers' solution at 0°C

As ₂ O ₃	Hg(SCN) ₂	Nicotinic acid
BaO	CdSO ₄	Aspartic acid
HgO	Cu(NH ₃) ₄ (SCN) ₂	Thiourea
PbO	Co(NH ₃) ₆ (NO ₃) ₂	Maleic anhydride
PbBr ₂	<i>m</i> -Nitroaniline	Benzil
PbI ₂	Diphenyl thiocarbazon	Azobenzene
Pb(NO ₃) ₂	Benzoic acid	1 Naphthol-5-sulfonic acid
AgSCN		

TABLE II. Inorganic and organic compounds which are insoluble in Divers' solution at 0°C

Al ₂ O ₃	TeO ₂	Ni(CN) ₂
CuO	TiO ₂	<i>p</i> -Hydroxybenzophenone
Fe ₂ O ₃	Co(CN) ₂	Phenyl- α -chloroisobutyrate
MgO	Ni(NH ₃) ₆ Br ₂	Benzoyl peroxide
Sb ₂ O ₅	Benzophenone	Phthalic anhydride
SeO ₂		

found to be soluble in Divers' solution, while Table II shows those that were found to be insoluble. Not all of the compounds shown in Table I gave polarographic waves falling within the useable voltage span of the ammonia-ammonium nitrate electrolyte against the lead-lead nitrate reference cell, i.e., + 0.4 to -0.8 volt. Table III lists the compounds that gave well-defined polarographic waves. Copper, cobalt, and cadmium compounds were prepared and purified according to recommended procedures (5-7). A plot of $\log [i/(i_d - i)]$ against E gave straight lines with very little scatter of points. Slopes of the plots for lead, cadmium, and cobalt were, respectively, 0.0289, 0.031, 0.105, indicating that lead and cadmium gave reversible reactions corresponding to a two-electron change, while the cobalt reduction was irreversible. The copper compound formed two reversible waves each representing a one-electron change which corresponds to the reduction of cupric to cuprous and then cuprous to copper as indicated by a slope of 0.0562 and 0.068. Some of the compounds formed a maximum in the polarogram, but the maximum was easily suppressed by the addition of gelatin. Since gelatin is just slightly soluble in Divers' solution, a saturated solution was prepared by adding a few grains of gelatin to the solution and bubbling ammonia through it for five minutes to assure thorough mixing. The diffusion current was found to be propor-

TABLE III. Half-wave potentials and diffusion current constants for various inorganic and organic compounds

Compound	$E_{1/2}$ in volts vs. the lead-lead nitrate reference electrode	$\frac{i_d}{cm^{2/3} t^{1/6}}$
PbO	+0.019	10.9
Cu(NH ₃) ₄ (SCN) ₂ *	+0.185	4.04
Cu(NH ₃) ₄ (SCN) ₂ *	-0.026	4.04
Co(NH ₃) ₆ (NO ₃) ₂	+0.191	†
CdSO ₄	-0.387	14.9
<i>m</i> -Nitroaniline*	-0.034	48.8
Diphenyl thiocarbazon	+0.173	0.536
Benzil*	+0.088	†
Azobenzene	+0.196	†

* Gelatin added to suppress the maximum.

† Low solubility.

m 2/3 *t* 1/6 equaled 1.97 a at potential of 0.4769 vs. the lead-lead nitrate electrode. *c* is expressed in mg/g of NH₄NO₃.

tional to the concentration of reducible material, and the half-wave potential was found to be dependent upon the species present.

Any discussion of this paper will appear in a Discussion Section to be published in the December 1955 JOURNAL.

REFERENCES

1. E. VECCHI, *Atti accad. Nazl. Lincei, Rend., Classe sci. fis., mat. e nat.*, **14**, 290 (1953).
2. E. DIVERS, *Proc. Roy. Soc.*, **21**, 109 (1875).
3. D. N. HUME AND T. W. GILBERT, *Anal. Chem.*, **24**, 431 (1952).
4. V. A. PLESKOV AND A. M. MONOSSON, *J. Phys. Chem. (U.S.S.R.)*, **4**, 696 (1933).
5. T. W. RICHARDS AND B. S. MERIGOLD, *Z. anorg. Chem.*, **17**, 245 (1898).
6. W. C. FERNELIUS, Editor, "Inorganic Syntheses," 1st ed., Vol. II, p. 218, McGraw-Hill Book Co., New York (1946).
7. A. DE SCHULTEN, *Compt. rend.*, **107**, 405 (1888).

Resistance and Polarization in a Storage Battery¹

E. WILLIHNGANZ

Gould National Batteries, Depew, New York

ABSTRACT

The electrical resistance of one cell of a 100 amp-hr automobile type storage battery has been studied by the a-c bridge method at 30–16,000 cycles. Results can be explained by considering the battery as a source of potential in series with a resistance, a capacitance, and an inductance. The inductance is only a fraction of a microhenry. Apparent values of the resistance and capacitance vary with frequency. At 1000–3000 cycles the apparent resistance is about one milliohm, but at 60 cycles it is 10–20% higher. The apparent capacitance is 15–20 Farads at 60 cycles and becomes too small for measurement at 1000 cycles. Attempts to explain these results show a step in the electrochemical reaction which has not been recognized previously and which requires further study.

INTRODUCTION

The high rate performance of a battery depends to a large extent on its internal resistance. This resistance is particularly important when a voice frequency is passed through a battery in a telephone exchange, or when a short pulse of current is used to operate a switch in a central power station.

Earlier work (1) indicated that the resistance could be measured by a bridge using 3000 cycle alternating current. This high frequency was chosen to eliminate polarization, that is, to prevent chemical effects from building up a counter emf which could be confused with that due to electrical resistance. In subsequent work it was observed that there was polarization in measurements at lower frequencies. The bridge was modified, therefore, to study this polarization.

Bridge measurements of lead batteries have been made by Kluck (2) and resistance measurements using pulses of direct current have been made by Lander (3). These workers were interested in the electrical resistance, rather than polarization. The general problem of electrode polarization has been reviewed by Grahame (4, 5) and pertinent studies of the lead electrode have been made by Baars (6) and by Falk and Lange (7).

EXPERIMENTAL

The battery used for this work was a single cell from a 100 amp-hr automobile cranking battery of conventional construction. The bridge was similar to that used previously (1) except for the presence of an adjustable condenser in series with the adjustable resistor of the bridge arm adjacent to the battery being tested. The null indicator was a cathode ray oscillograph. This gave excellent sen-

sitivity at high and low frequencies and permitted the unbalanced portion of the battery output voltage to be photographed and studied.

Exploratory tests showed that the bridge balance was practically complete at each frequency, and was independent of current in the range 0.1–5 amp. At frequencies of 3000–16,000 cycles results appear unreliable. Effects of stray capacitance and inductance were clearly evident, and it also appeared possible that inductive effects caused the current distribution to be nonuniform within the cell. Therefore, only the low frequency results are discussed. In this range of frequencies, the apparent inductance was constant and equal to that of a copper rod about 4 in. long. Since this is very nearly the distance between cell terminals, it is considered to have no chemical significance.

When both electrodes were lead dioxide, the apparent resistance was independent of the frequency, and no capacitance was needed in the bridge to get a good balance. However, when sponge lead electrodes were used, there was a considerable variation with frequency of both the measured resistance and capacitance (see Fig. 1). It is concluded, therefore, that in an ordinary battery, the variation with frequency occurs exclusively at the lead-acid interface, and not at the lead dioxide surface.

The electrochemistry of the lead-acid interface was also studied by passing short pulses of direct current through the bridge circuit after removing all condensers from the current path. The current pulse was obtained by putting a half wave rectifier in series with a 60 cycle current source and connecting enough batteries in opposition to block all but the current peaks. The bridge was balanced to eliminate the first portion of the battery voltage pulse, and the residual voltage delivered by the bridge circuit was photographed. Fig. 2A shows a current pulse of 1.75 amp peak, Fig. 2B shows the battery output

¹ Manuscript received September 10, 1954. This paper was prepared for delivery before the Boston Meeting, October 3 to 7, 1954.

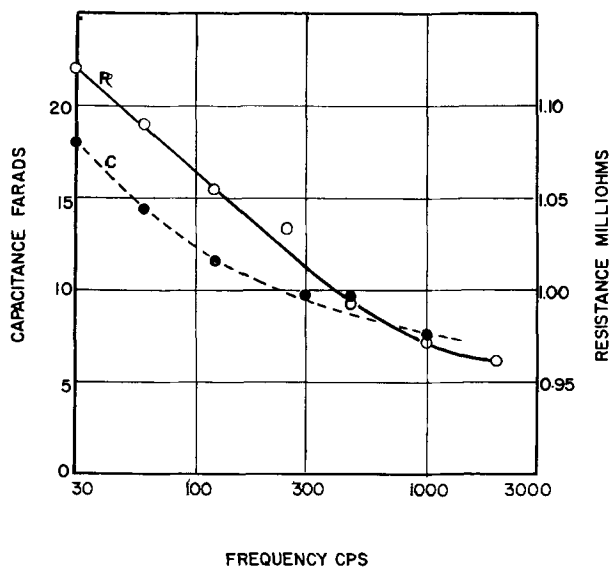


FIG. 1. Typical bridge results

voltage pulse of approximately 1.75 millivolts peak, while Fig. 2C shows the bridge output of approximately 0.2 millivolts which corresponds to a battery voltage of 0.5 millivolts.

This pulse was next studied by varying the concentration of lead ions in solution. This was done by superimposing a steady direct current bias on the pulsed current passing through the bridge. The effect of this bias on a charge pulse is shown in Fig. 2D, 2E, and 2F for bias values of 2.5, 0, and -25 amp. Similar results for a discharge pulse are shown in Fig. 2G, 2H, and 2I. In each of these figures three separate lines are shown. There is the voltage across the battery to show the size and position of the current pulse; there is the bridge output at a

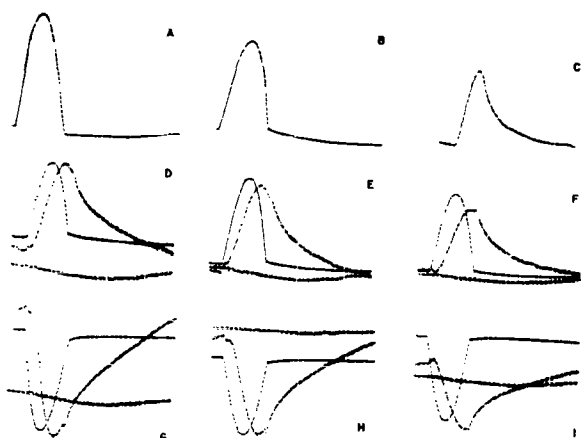


FIG. 2. Oscillograms using 60 cycle pulsed d.c. A, current; B, battery voltage; C, bridge output voltage (nonohmic overpotential); D, charge pulse and 2.5 amp d-c charge; E, charge pulse, no steady d.c.; F, charge pulse, 25 amp d-c discharge; G, discharge pulse, 2.5 amp d-c charge; H, discharge pulse, no steady d.c.; I, discharge pulse, 25 amp d-c discharge.

sensitivity 10 times as great; finally there is the residual hum. Fig. 2B and Fig. 2C can be used to identify the battery voltage and bridge output in these patterns.

The battery used for this test was first kept for one week on a low rate charge to remove all soluble lead compounds. This charge was continued while Fig. 2D and 2G were prepared. It is assumed that the lead-acid interface was free of lead ions.

The battery was then given a 25 amp discharge for 5 min and allowed to stand on open circuit for several hours. Fig. 2E and 2H were then made. It is assumed that during this test the acid at the interface was practically saturated with lead sulfate.

Finally the battery was discharged at 25 amp while Fig. 2F and 2I were made. It is assumed that during this test the electrolyte was supersaturated with lead sulfate.

DISCUSSION

The lead ion concentration during these tests can be calculated using the Nernst equation. The 0.1 v polarization during charge and the -0.1 v polarization during discharge indicate a difference in lead ion activity of more than one million times, but the difference in the voltage pulse is barely measurable. This is difficult to explain unless the primary battery reaction does not involve lead ions. Normal battery operation is difficult to explain without involving lead ions, so that battery reactions apparently consist of two steps, the first of which does not involve lead ions at the sponge lead surface.

Another aspect of this reaction is indicated by using the data of Falk and Lange (7) who observed that in sulfuric acid at 1000 cycles lead has a capacitance of 12 microfarads/cm². Under the same conditions, the battery used here had a capacitance of 6 Farads and, therefore, should have an interfacial area of 500,000 cm². This number appears consistent with the particle size of sponge lead observed under the microscope. The current pulse of 1.25 amp average for 0.0044 sec gives a charge of 0.005 amp-sec or 0.01 microcoulombs/cm². To deposit a monolayer of hydrogen with a spacing of 5°A would require 64 microcoulombs/cm². Consequently, the test pulse corresponds to only a small fraction of a monolayer, and probably only a small fraction of the charge of the double layer. There is considerable uncertainty in the estimated area of the interface, but this should not invalidate the conclusion that the current pulse causes only a minor disturbance to the composition of the double layer.

The decay process explains, electrically at least, the results of the a-c bridge measurements. At 60 cycles the measured capacitance includes a considerable amount of pseudocapacitance as defined

by Grahame (5), while the high apparent resistance is clearly the result of energy dissipated by the decay process, and is believed to correspond to his polarization resistance.

There is no evidence for an activation overpotential in these measurements. Such an effect could be present and pass unnoticed if this potential were proportional to the current in the range studied. It would thus show up electrically as an additional resistance on the lead surface. Such a film was not mentioned by Falk and Lange (7) whose experimental apparatus should have shown it had it been present.

Accordingly, it is concluded that the nonohmic overpotential produced during these tests involves only a change in the composition of the double layer and its subsequent decay. The nature of this decay reaction requires further study.

Resistance values assigned to a battery depend

on the contribution of the decay process to the bridge readings at the test frequency. At 1000 cycles it is estimated that the error amounts to about 1%. However, to avoid ambiguity it is desirable to specify the test frequency whenever a battery resistance is mentioned.

Any discussion of this paper will appear in a Discussion Section to be published in the December 1955 JOURNAL.

REFERENCES

1. E. WILLIHNGANZ, *Trans Electrochem. Soc.*, **79**, 253 (1941).
2. J. H. KLUCK, Naval Research Laboratory Report 3839 (1951).
3. J. J. LANDER AND E. E. NELSON, Naval Research Laboratory Report 4347 (1954).
4. D. C. GRAHAME, *Chem. Revs.*, **41**, 441 (1947).
5. D. C. GRAHAME, *J. Electrochem. Soc.*, **99**, 370C (1952).
6. E. BAARS, *Sitzber. Ges. Beförder. Naturw. Marburg*, **63**, 214 (1928).
7. G. FALK AND E. LANGE, *Z. Naturforsch.*, **1**, 388 (1946).

Galvanic Corrosion Behavior of Titanium and Zirconium in Sulfuric Acid Solutions¹

DAVID SCHLAIN, CHARLES B. KENAHAN, AND DORIS V. STEELE

Metallurgical Division, U. S. Bureau of Mines, Region VIII, College Park, Maryland

ABSTRACT

Aluminum alloys are the anodic members of titanium-aluminum alloy couples in dilute sulfuric acid solutions in the presence of air. In stronger acid solutions, particularly when air is absent, aluminum alloys are anodic only at the beginning of the immersion period. After an induction period titanium becomes anodic. Aluminum alloys are always anodic in zirconium-aluminum alloy couples immersed in sulfuric acid solutions. The rate of galvanic attack increases with the supply of air. The direction of flow of the galvanic current is always in agreement with the relative values for the electrode potentials of the single metal specimens. Little, if any, galvanic corrosion occurs in couples of titanium or zirconium with stainless steel, although there are generally sizeable differences of potential between single specimens of these metals. In solutions in which single specimens of titanium are inert and cathodic with respect to aluminum alloys, contact with these alloys may cause titanium to corrode. This is attributed to activation of titanium surfaces by the hydrogen evolved. Contact with stainless steel in solutions in which titanium is the anodic member of the couple results in marked decreases in corrosion rates of titanium because of anodic polarization of titanium surfaces.

INTRODUCTION

A knowledge of the galvanic corrosion properties of titanium and zirconium is essential because of the growing industrial importance of these metals and the probability that they will be used in structural contact with other metals under corrosive conditions. The present investigation includes a study of the behavior of titanium and zirconium in contact with aluminum alloys or 18-8 stainless steel in several concentrations of sulfuric acid. These alloys are not only common structural materials but, upon dissolution, may form cations known to have pronounced effects on the electrode potentials and corrosion rates of titanium in acid solutions (1, 2). Since titanium surfaces are passivated by the presence of air (3, 4), various types of aeration were used in these experiments.

EXPERIMENTAL METHOD

All experiments were done at 35°C, and generally lasted 15 days. Some were carried out in stoppered bottles with a constant flow of air or helium, others in loosely covered vessels with no forced gas flow. In stoppered-bottle tests, gas was passed through the solution for about 1 hr before immersion of the metal specimens and continuously throughout the experiment. Rates of flow, measured with rotameters, were approximately 50 ml/min. Helium was passed

through a water bottle and several spray traps before entering the experimental train. Air was passed through an additional bottle containing sodium hydroxide solution. When acid was consumed rapidly as a result of the corrosion process, the solution was replaced with fresh solution at suitable intervals. Evaporation from loosely covered vessels was compensated for by adding distilled water. The acid concentration was generally maintained within a range of 0-20% of the nominal value.

Table I gives the composition of titanium and zirconium specimens; other metals used were standard commercial products. All specimens were given a preliminary polish with wet silicon carbide paper on a mechanical polisher. Just prior to immersion they were surfaced by hand with dry 3/0 emery cloth, rubbed with wet pumice, washed with water, dried with acetone, and weighed. Specimens were never reused. C. P. chemicals, distilled water, and Grade A helium (99.9 + % pure) were used. The number of experiments carried out for each set of conditions varied from one to six.

Two types of galvanic-couple experiments were used. One, the "open" couple, is a modification of one described by Fraser and his coworkers (5). Fig. 1 shows the apparatus used in experiments with stoppered bottles. The large bottle contained two specimens of each of the two metals involved in the experiment and approximately 550 ml of solution. The metal specimens were 0.13 cm thick, 0.64 cm

¹ Manuscript received June 8, 1954. This paper was prepared for delivery before the Wrightsville Beach Meeting, September 13 to 16, 1953.

TABLE I. Analysis of titanium and zirconium

	C	N ₂	O ₂	Fe	Mg	Mn	Cr	Ni	W	Cu	Si	Cl	Hf
Titanium ^a	0.044	0.027	0.1 ^c	0.13	0.013	0.076			0.02 ^c max		0.04 ^c max		
Zirconium, high purity ^a	0.02	0.04	0.09	0.05					0.001	0.005			0.20
Zirconium, low purity ^b	0.38	0.045	0.1 ^c	0.74	<0.01		0.042	<0.01			0.03	0.02	1.65

^a Consolidated by arc-melting, 20% cold rolled.

^b Annealed in vacuum at 800°C for 2 hr.

^c Nominal value, not based on an actual analysis of the metal used.

wide, and 15.3 cm long. The upper portion of each specimen was insulated with plastic cement, leaving 7.6 cm of length exposed to the solution (area, 0.12 dm²). Galvanic currents flowing through the couple were determined by measuring voltage drops across the 1 ohm ($\pm 1\%$) resistance with a millivoltmeter or a potentiometer and by applying Ohm's law. Galvanic corrosion rates were calculated from average galvanic currents by applying Faraday's law. Weight losses of coupled and uncoupled metal specimens were determined. Electrode potentials of each uncoupled specimen and of the couple were measured with an L & N type K-2 potentiometer, a saturated calomel electrode, and a saturated potassium chloride bridge. The apparatus was arranged to measure the potential of the whole specimen surface rather than that for a particular point. The potentials are good to ± 0.010 v and are on the saturated calomel electrode scale. Experiments with natural aeration of solution were carried out

in loosely covered vessels, with the use of essentially the same experimental method described above. The volumes of solution used in these experiments were either 750 ml or 2500 ml, depending on rate of acid consumption.

The second type of galvanic couple experiment was a simple weight loss test carried out with two metal specimens maintained in face-to-face contact either by means of a small rubber band at each end or by a rivet. Specimens were 0.13 cm thick, 0.64 cm wide, and 7.6 cm long (area, 0.12 dm²) and were arranged in such a manner that each member of the couple extended 1.3 cm beyond the other at one end. The volume of solution used was approximately 500 ml, and two replicates were placed in each bottle. Chemical corrosion rates for the various metals were based upon tests in which two pieces of the same metal were fastened together as described above. Total specimen areas were always used in converting weight losses to corrosion rates in mils per year. Corrosion rates, summarized under "Increase caused by contact," were obtained by subtracting values for chemical corrosion (single metal) from the value for total corrosion (bimetallic). Chemical corrosion rates are not included in the tables for the sake of brevity.

SINGLE ELECTRODE POTENTIALS

A summary of the electrode potentials of titanium, zirconium, aluminum, and stainless steel in sulfuric acid solutions appears in Table II. These values are for single (uncoupled) specimens after immersion for approximately 15 days in vessels containing couples. Electrode potentials were almost constant after 15 days' immersion with the exception of those for stainless steel in 2*N* acid in the presence of air and those for zirconium in 2*N* acid with all types of aeration. The electrode potentials of titanium varied with immersion time, generally becoming more cathodic (electropositive) with time in the presence of air and more anodic (electronegative) in the absence of air. At any acid concentration, the steady-state values were always most cathodic

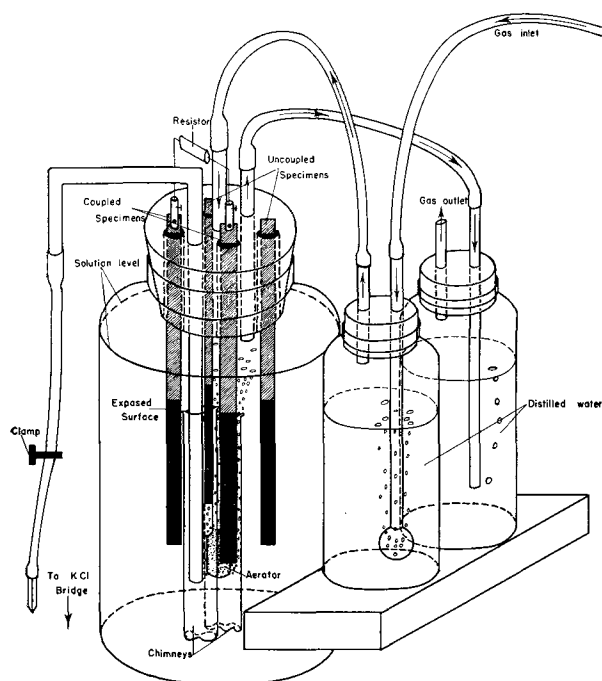


FIG. 1. Apparatus used in open couple experiments

TABLE II. Single electrode potentials of metals in sulfuric acid solutions, 35°C

Metal	Electrode potential, volts (referred to saturated calomel electrode)		
	Flow of air	Natural aeration	Flow of helium
0.025N H ₂ SO ₄			
Titanium.....		0.26	-0.55
Zirconium.....			-0.23
Aluminum 2 S-O		-0.54	-0.66
0.10N H ₂ SO ₄			
Titanium ^b	0.19	0.10	-0.70
Zirconium.....	0.31	0.24	-0.28
Aluminum 2			
S-O ^a	-0.43	-0.57	-0.64
Stainless steel, type 302.....		0.21	-0.41
1.0N H ₂ SO ₄			
Titanium ^b	0.04	-0.56	-0.67
Zirconium.....	0.09	0.26	-0.33
Aluminum 2			
S-O.....	-0.47	-0.43	-0.65
Stainless steel, type 302.....	-0.12-0.20	0.23	-0.35
2.0N H ₂ SO ₄			
Titanium ^c	-0.57-0.07	-0.61	-0.67
Zirconium.....	-0.20-0.05	-0.14-0.05	-0.15-0.25
Stainless steel, type 302.....	-0.14-0.30	-0.14-0.27	-0.35

^a Values for aluminum alloys 24 S-O, 61 S T6, and 3 S H14 varied less than 0.1 v from these values.

^b These values were taken from experiments with aluminum alloy 2 S-O. More positive values were sometimes obtained in experiments with stainless steel, such as: 0.18 v in 0.1N H₂SO₄ with flow of helium, 0.40 v in 1.0N H₂SO₄ with flow of air, and 0.07 v in 1.0N H₂SO₄ with natural aeration.

^c These values were taken from experiments with stainless steel. Electrode potentials were always electronegative during the first 8 or 9 days of immersion in 2N H₂SO₄ with a flow of air but sometimes became more positive later in the experiment.

with a flow of air, most anodic in the absence of air (flow of helium), and intermediate with a limited supply of air (natural aeration). In the absence of air, acid concentration had little effect on the electrode potentials of titanium, but with air present the values became more anodic with increasing concentration. Electrode potential values for titanium obtained during experiments with stainless steel in the presence of air were sometimes more cathodic than those obtained in experiments with commercially pure aluminum because of the passivating effect of the ferric ions. However, ions formed from the alloying elements present in the various aluminum alloys did not appear to affect

the potential of titanium. The electrode potentials of zirconium usually became more noble with time, but there were no significant changes in the potentials of aluminum or stainless steel with immersion time. Electrode potential values for the two grades of zirconium were essentially the same. Potentials of aluminum and stainless steel did not vary greatly with changes in acid concentration, but these metals were more noble in the presence of air. Ranges of electrode potential values are given in Table II for titanium, zirconium, and stainless steel in those solutions in which the measurements were erratic. Electrode potentials of aluminum alloys 24 S-O, 61 S T6, and 3 S H14 varied only slightly from those of commercially pure aluminum (2 S-O). Hence, electrode potential data for 2 S-O in Table II may be used in interpreting corrosion data for the other aluminum alloys.

COUPLES WITH ALUMINUM ALLOYS

Corrosion data obtained in titanium-aluminum alloy open-type couple experiments are summarized in Tables III and IV. The direction of the galvanic currents shows that aluminum alloys are the anodic (electronegative or corroding) members of titanium-aluminum alloy couples immersed in 0.1N sulfuric acid either with a flow of air or with natural aeration. In the absence of air, aluminum alloys are anodic only during the first 2½-9 days of the experiment. Then the galvanic current begins to flow in the opposite direction, indicating that titanium is anodic. Available data show that these reversals in the direction of the galvanic currents occur more readily in higher acid concentrations. In 0.025N sulfuric acid, for example, commercially pure aluminum (2 S-O) was anodic with respect to titanium throughout the experiment even in the complete absence of air, while a reversal in the direction of current flow took place in 1N acid with natural aeration. Relative positions of the time-potential curves for uncoupled specimens of titanium and aluminum alloys are consistent with the direction of the galvanic currents in these experiments (Fig. 2 and 3). A shift in the relative positions of the time-potential curves occurs with reversals in the direction of the currents. Only sample curves are included, but the steady-state electrode potential values in Table II show this consistency. The size of the galvanic current generated in titanium-aluminum couples apparently is not affected by acid concentration but is affected by type of aeration, being smallest with a flow of helium and largest with a flow of air. This may be attributed to the greater potential differences between the two metals in presence of air and perhaps also to the de-

TABLE III. Corrosion of titanium-aluminum alloy open couples in 0.1N sulfuric acid solutions, 35°C, 15 days

Aluminum alloy	Anodic metal	Galvanic corrosion, ^d mpy (calculated from current)	Corrosion rate, mpy (based on weight loss)			
			Titanium		Aluminum alloy	
			Coupled	Un-coupled	Coupled	Un-coupled
Flow of air						
2 S-O ^a	Al	23.5	0.8	0.1	47.3	43.0
24 S-O	Al	40.5	0.4	0.2	102.0	85.1
61 S T6	Al	29.0	1.3	0.0	71.7	59.5
3 S H14	Al	36.5	0.8	0.0	58.5	49.9
Natural aeration ^b						
2 S-O	Al	12.5	4.7	0.0	30.7	26.9
24 S-O	Al	9.0	5.1	0.0	74.9	72.0
61 S T6	Al	12.0	6.3	0.0	50.7	47.8
3 S H14	Al	14.0	6.3	0.0	37.4	33.2
Flow of helium ^c						
2 S-O	Al, Ti	4.0, 1.5	5.4	4.9	29.4	30.6
24 S-O	Al, Ti	0.5, 2.5	3.8	3.8	54.5	54.5
61 S T6 ^b	Al, Ti	4.0, 2.5	5.5	3.2	45.0	44.5
3 S H14 ^b	Al, Ti	5.0, 1.5	4.5	4.8	34.1	29.4

^a Number of replicates 4.^b Number of replicates 2.^c Aluminum alloy was anodic during first 2½ to 9 days of experiment, titanium was anodic remainder of time.^d Equivalent weights used in calculating galvanic corrosion from galvanic current:

Ti	15.97
Al 2 S-O	8.99
24 S-O	10.16
61 S T6	9.06
3 S H14	9.20

polarizing action of air on the cathodic areas of the couple.

Weight loss corrosion data for single (uncoupled) specimens of titanium are consistent with published data (6). Rates for single specimens of titanium indicate that the presence of air inhibits the initiation of chemical corrosion, presumably because of the formation of oxides or layers of adsorbed oxygen. Once corrosion starts, however, air appears to increase the rate, probably because of improved depolarization. Chemical corrosion of aluminum alloys was somewhat more rapid in the presence of air and in higher acid concentrations. Alloys of aluminum studied in this investigation all show the same general behavior in couples with titanium, although individual corrosion rates and electrode potentials do show variations. For both titanium and aluminum alloys, the sum of the corrosion rate of the uncoupled specimen and the galvanic corrosion rate of the coupled specimen is usually greater than the total corrosion rate of the coupled

specimen as determined by weight loss measurements. This tendency toward a negative difference effect is much less pronounced for titanium than for aluminum. Both titanium and aluminum specimens corroded uniformly in these experiments. Multicolored interference films were sometimes formed on titanium surfaces when no weight losses of titanium specimens were observed. Copper and possibly other constituents of the aluminum alloys frequently appeared on the immersed surfaces of the specimens in the form of loosely adhering, spongy deposits. Corrosion rates and electrode potentials of titanium in experiments with those aluminum alloys containing considerable amounts of copper (24 S-O and 61 S T6) were not appreciably different from those obtained with other aluminum alloys. Apparently, the continuous reduction of copper ions to metallic copper on the electronegative surfaces of the aluminum alloys and the titanium-aluminum alloy couples kept the concentration of copper ions below the level required for the passivation of titanium.

Titanium specimens lost weight and acquired the "corroded" appearance in certain environments as a result of coupling with aluminum alloys, in spite of the fact that the direction of the current flow through the couples and the pertinent electrode potential

TABLE IV. Effect of sulfuric acid concentration on corrosion of titanium-aluminum (2 S-O) open couples, 35°C, 15 days

Normality	Anodic metal	Galvanic corrosion, mpy (calculated from current)	Corrosion rate, mpy (based on weight loss)			
			Titanium		Aluminum	
			Coupled	Un-coupled	Coupled	Un-coupled
Flow of air						
0.1 ^a	Al	23.5	0.8	0.1	47.3	43.0
1.0 ^b	Al	8.5	25.6	0.1	69.2	62.6
Natural aeration ^b						
0.025 ^c	Al	10.0	0.0	0.0	25.9	19.1
0.1	Al	12.5	4.7	0.0	30.7	26.9
1.0 ^d	Al, Ti	16.5, 16.0	35.4	26.4	71.0	67.7
Flow of helium						
0.025	Al	3.5	1.7	0.2	21.3	21.6
0.1 ^e	Al, Ti	1.5, 4.0	5.4	4.9	29.4	30.6
1.0 ^f	Al, Ti	5.0, 3.5	14.3	13.6	35.7	36.4

^a Number of replicates 4.^b Number of replicates 2.^c Experiment was 7 days long.^d Aluminum was anodic during first 2 days of experiment, titanium was anodic remainder of time.^e Aluminum was anodic during first 4½ days of experiment, titanium was anodic remainder of time.^f Experiment was 19 days long. Aluminum was anodic during first 7 days of experiment, titanium was anodic remainder of time.

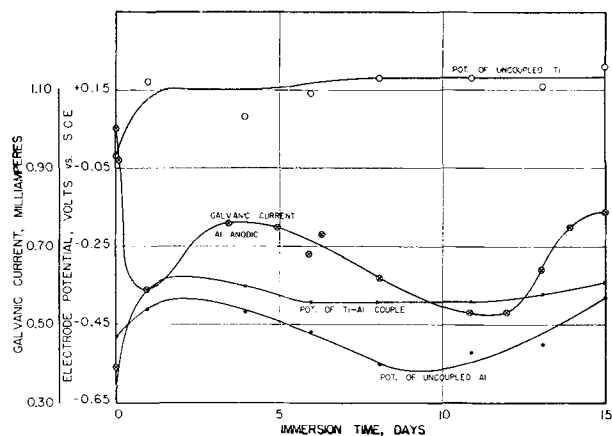


FIG. 2. Titanium-aluminum (2S-O) couple in 0.1N sulfuric acid with flow of air.

values show that titanium was cathodic with respect to aluminum alloys. This type of attack was rapid in 1N sulfuric acid with flow of air and much less so in 0.1N acid with flow of air. It also occurred in 0.1N acid with natural aeration and in 0.025N acid with a flow of helium. Single specimens of titanium were inert in all of these solutions. It is believed that the flow of current through the titanium-aluminum couples results in evolution of active hydrogen on titanium surfaces which, in turn, destroys the oxide film that ordinarily protects titanium in these solutions. Mears and Brown (7) explained the corrosion of stainless steel as a result of contact with aluminum in 0.5% sulfuric acid in the same manner. The term "cathodic corrosion" has been applied to this phenomenon (8). In the case of titanium, a greater supply of air decreases the tendency for this reaction to occur because the protective film is repaired more readily. Higher acid concentrations aid in the destruction of the protective film and hence promote the reaction. The effectiveness of active hydrogen in destroying passivity was demonstrated by electrolyzing sulfuric

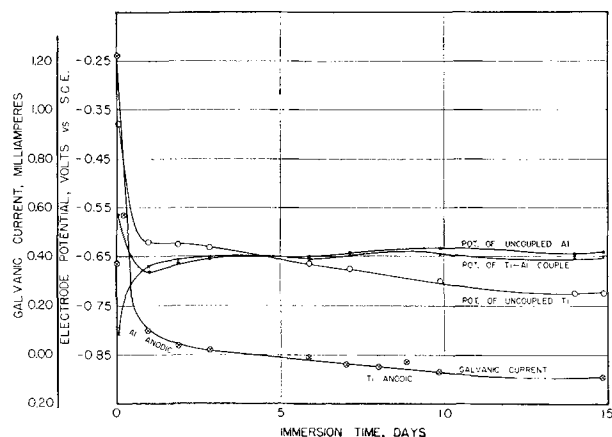


FIG. 3. Titanium-aluminum (2S-O) couple in 0.1N sulfuric acid with flow of helium.

TABLE V. Corrosion of titanium-aluminum alloy face-to-face contact couples in 0.1N sulfuric acid solutions, 35°C, 15 days

Aluminum alloy	Corrosion rate, mpy			
	Total corrosion		Increase caused by contact	
	Ti ^a	Al	Ti ^a	Al
Flow of air				
2 S-O ^b	1.1 ^c	38.2	1.1	9.5
3 S H14	3.9	38.1	3.9	1.8
Natural aeration				
2 S-O ^b	4.9 ^c	28.5	4.9	1.6
24 S-O	2.7	62.7	2.7	2.1
61 S T6	4.4	42.9	4.4	2.0
3 S H14 ^b	4.2	31.3	4.2	2.5
Flow of helium				
2 S-O	3.9 ^c	23.9	-1.2	0.8
24 S-O	3.6	58.3	-1.5	8.9
3 S H14	3.0	25.9	-2.1	-2.8

^a To correct for uncorroded areas multiply corrosion rates obtained with flow of air and natural aeration by 1.25; with flow of helium by 1.10.

^b Number of replicates 4.

^c Values obtained in experiments in which a rivet replaced the rubber bands are as follows: flow of air (2 replicates) Ti 2.8, Al 36.2; natural aeration (5 replicates) 5.3, 29.0; flow of helium (2 replicates) 4.8, 28.0.

acid solutions using a platinum anode and a titanium cathode with a cathode current density of 4 ma/dm². In 1N sulfuric acid with a flow of air the titanium cathode corroded at the rate of 27.4 mpy during a 5-day test while another titanium specimen immersed in the same solution without an external current lost weight at the rate of only 0.5 mpy. Corresponding values for 0.1N acid with natural aeration were 4.9 and 0.0 mpy.

Table V shows that titanium corrodes at moderate rates as a result of face-to-face contact with aluminum alloys in 0.1N sulfuric acid in the presence of air, although two pieces of titanium in contact under the same conditions are inert. For all conditions of aeration, "total corrosion" rates for titanium and aluminum alloys in face-to-face contact are in general agreement with corrosion rates for "coupled" specimens in open type couples (Table III). This is also true for "increase caused by contact" and the difference in corrosion rates between "coupled" and "uncoupled" specimens. Corrosion of titanium specimens appeared to be uniform except for some uncorroded areas on the contact sides which were not "wetted." These uncorroded areas averaged about 20% of the total specimen area in the presence of air and 10% in the absence of air. Corrosion rates in Table V are based upon total specimen area,

TABLE VI. Corrosion of zirconium^a-aluminum alloy open couples in 0.1N sulfuric acid solutions, 35°C, 15 days

Aluminum alloy	Anodic metal	Galvanic corrosion, ^d mpy (calculated from current)	Corrosion rate, mpy (based on weight loss)			
			Zirconium		Aluminum	
			Coupled	Un-coupled	Coupled	Un-coupled
Flow of air						
2 S-O	Al	12.5	0.08	0.0	44.2	42.3
24 S-O	Al	22.5	0.1	0.0	82.9	78.0
61 S T6	Al	11.5	0.1	0.04	68.0	60.1
3 S H14	Al	17.5	0.1	0.0	50.8	47.0
Natural aeration ^b						
2 S-O ^c	Al	9.0	0.1	0.04	32.2	26.8
61 S T6	Al	10.5	0.07	0.02	39.3	38.1
Flow of helium						
2 S-O	Al	2.5	0.04	0.03	34.4	32.0
24 S-O	Al	1.0	0.07	0.03	60.6	59.1
61 S T6	Al	2.0	0.04	0.0	54.4	50.9
3 S H14	Al	2.5	0.1	0.0	30.8	33.6

^a Low purity zirconium.^b Number of replicates 2.^c Experiment was 11 days long.^d Equivalent weight used in calculating galvanic corrosion from galvanic current: Zr 30.41.

but estimated correction factors appear in a footnote. Aluminum specimens appeared uniformly corroded at the end of the test period and were covered with loosely adhering red or dark deposits. Substitution of an aluminum rivet for the rubber bands did not substantially change the corrosion rates (Table V, footnote c).

Table VI includes corrosion data for zirconium (low purity), aluminum alloys, and zirconium-aluminum alloy open-type couples in 0.1N sulfuric acid solutions. Both the direction of flow of the galvanic currents and the electrode potentials of uncoupled specimens of the metals (Table II) show that the aluminum alloys are always the anodic or corroding members of the couple. Galvanic corrosion of aluminum alloys was always appreciable and was much greater in the presence of air. Corrosion rates for aluminum alloys and the negative difference effect of aluminum in the presence of air are in agreement with the data for titanium-aluminum alloy couples. Weight losses for zirconium specimens, single or coupled with aluminum alloys, were negligible in these solutions. However, the surfaces of zirconium specimens in contact with aluminum alloys frequently became dull or blistered, and x-ray determinations show high concentrations of zirconium hydride on these surfaces. In another series of experiments, contact with aluminum alloys in 1 and 2N acid solutions caused zirconium to

undergo slight weight losses (equivalent to 0.3 mpy) and pronounced hydride formation. Uncoupled specimens of zirconium were inert in these solutions and remained unchanged in both appearance and weight. Zirconium of high purity in contact with commercially pure aluminum did not lose weight or change in appearance. Data for zirconium and aluminum in face-to-face contact experiments are in general agreement with these results.

COUPLES WITH STAINLESS STEEL

The curves in Fig. 4 represent a typical open-type couple experiment with titanium and type 302 stainless steel in 2N sulfuric acid with a flow of helium. The electrode potential of the coupled titanium specimen (and of the couple) became the same as that of the single stainless steel specimen soon after coupling, showing that titanium is readily polarized in this environment. When the couple was disconnected, the "coupled" titanium specimen quickly acquired the same electrode potential as the single specimen (within 0.02 v in 3 to 7 min). The specimen was polarized again within 1/2 min after reconnecting the couple. Time-potential curves for the uncoupled stainless steel specimen and for the couple in 2N sulfuric acid with a flow of air are somewhat farther apart and more erratic than the curves in Fig. 4. In the presence of air the titanium specimen was polarized as described above but was not readily depolarized. In this environment the "coupled" specimen was still noble a day or more after breaking the couple.

Data for titanium-stainless steel open-type couples summarized in Table VII show that galvanic currents in sulfuric acid solutions were small or negligible in size in spite of the large differences between the electrode potentials of the two metals

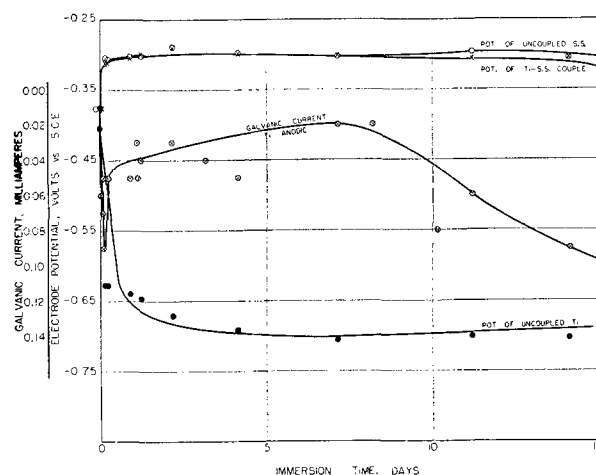


FIG. 4. Titanium-stainless steel couple in 2N sulfuric acid with flow of helium.

TABLE VII. Corrosion of titanium-stainless steel (type 302) open couples in sulfuric acid solutions, 35°C, 15 days

Normality	Anodic metal	Galvanic corrosion, ^g mpy (calculated from current)	Corrosion rate, mpy (based on weight loss)			
			Titanium		Stainless steel	
			Coupled	Un-coupled	Coupled	Un-coupled
Flow of air						
1.0	S.S. ^d	1.5	0.7	0.2		
2.0 ^a	Ti	0.5	0.2	40.8	4.1 ^e	0.1
Natural aeration						
0.1 ^b	Ti	0.0	0.0	0.0	0.0	0.0
1.0 ^c	Ti	0.0	0.1	22.2	0.2	0.1
2.0 ^b	Ti	0.0	0.2	43.1 ^f	1.0 ^f	0.6
Flow of helium						
0.1 ^{a, g}	Ti ^h	0.0	0.05	1.7	2.1	3.1
1.0	Ti	0.5	1.3	13.7	11.2	13.4
2.0 ^{a, g}	Ti	3.0	4.5	19.8	24.1	23.9

^a Number of replicates 3.

^b Number of replicates 4.

^c Number of replicates 2.

^d Corrosion rates for stainless steel were 3 to 5 mpy but most of corrosion occurred above the stopper because of a leak. No galvanic corrosion was detected before the second day or after the twelfth day.

^e Values were 10.7, 1.6, 0.2 mpy.

^f Rate for titanium is made up of 3 values, the fourth, 10.4 mpy, was omitted. Rate for stainless steel is made up of 3 values, the fourth, 9.2 mpy, was omitted.

^g Lengths of experiments varied from 13.9 to 19.0 days.

^h Titanium was cathodic in one of these experiments.

ⁱ Equivalent weight used in calculating galvanic corrosion from galvanic current: stainless steel 26.14.

(Table II, Fig. 4). The direction of the current flow indicated that titanium was anodic with respect to stainless steel in all environments studied except 1*N* sulfuric acid with flow of air. This is in agreement with the electrode potential values in Table II. Weight loss corrosion data for uncoupled specimens of titanium were consistent with data from other sources (6). Coupling with stainless steel in solutions in which titanium normally undergoes chemical corrosion and is less noble than stainless steel causes large decreases in the chemical corrosion rates of titanium. This is evidently caused by anodic polarization of titanium. Since uncoupled specimens of titanium present in the same vessels corroded at the normal rates, this relative inertness of the coupled specimens cannot be ascribed to the presence of the ferric ion. Corrosion of stainless steel in these environments was quite erratic and, apparently, was not affected by contact with titanium.

Corrosion rates obtained for titanium in face-to-face contact with stainless steel are in good agree-

ment with the values for open-type couples (Table VII). For example, the following corrosion rates were obtained for titanium in face-to-face contact with stainless steel in 2*N* sulfuric acid: flow of air 1 mpy, natural aeration 2 mpy, flow of helium 6 mpy.

Zirconium-stainless steel couples generated only small galvanic currents (equivalent to 1 mpy or less) in 2*N* sulfuric acid with the three types of aeration and in 0.1 and 1*N* acid with a flow of helium, even though electrode potential measurements (Table II) generally show zirconium to be less noble than stainless steel. Furthermore, the direction of the tiny currents frequently did not correspond to the relative values of the potentials. Coupled or uncoupled, the low purity zirconium corroded slowly in 2*N* sulfuric acid (up to 0.3 mpy in the absence of air). The high purity zirconium did not show appreciable weight losses. Both zirconium and stainless steel were unaffected by contact with each other. Data obtained in face-to-face contact experiments were in agreement with those for the open-type couples.

CONCLUSIONS

Contact between titanium and aluminum alloys in sulfuric acid solutions (0.025–1*N*) causes galvanic corrosion. The aluminum alloy tends to be the anodic (corroding) member of the couple in lower acid concentrations and in the presence of air. In stronger acid solutions, especially when air is absent or in limited supply, a reversal in the direction of the current flow takes place after a number of days' immersion and titanium becomes anodic. Contact between zirconium and aluminum alloys in these solutions always results in galvanic corrosion of the latter. Zirconium of high purity is inert in these environments. On the other hand, surfaces of low purity zirconium specimens acquire a dull and blistered appearance and a high concentration of zirconium hydride, although weight losses are small. The severity of galvanic attack in these couples increases with air supply at the metal surfaces. The direction of flow of the galvanic current is consistent with the relative values of the electrode potentials of the single metal specimens.

Contact between titanium and stainless steel (type 302) in sulfuric acid solutions (0.1–2*N*) causes little or no galvanic corrosion, although electrode potential measurements show titanium to be much less noble than stainless steel. This is the result of the ease with which titanium undergoes anodic polarization. Little, if any, galvanic corrosion occurred in zirconium-stainless steel couples, although stainless steel was generally anodic according to electrode potential measurements.

Corrosion rates obtained for uncoupled titanium specimens are in good agreement with published data for chemical corrosion of titanium. However, contact with other metals sometimes produced important changes in the chemical corrosion properties of titanium. Contact with aluminum alloys in certain solutions in which titanium is ordinarily inert and cathodic (noble) with respect to the aluminum alloys causes titanium to corrode. This is believed to be the result of the destruction of the protective oxide film by the active hydrogen evolved at the cathode surfaces. Contact with stainless steel in solutions in which titanium is anodic decreases the chemical corrosion rates of titanium because of anodic polarization of titanium surfaces.

The results of experiments in which metals were merely in electrical contact are in substantial agreement with those of experiments in which the metal

specimens were maintained in actual face-to-face contact with rubber bands or rivets.

Any discussion of this paper will appear in a Discussion Section to be published in the December 1955 JOURNAL.

REFERENCES

1. J. R. COBB AND H. H. UHLIG, *This Journal*, **99**, 13 (1952).
2. D. SCHLAIN AND J. S. SMATKO, *ibid.*, **99**, 417 (1952).
3. M. E. STRAUMANIS AND P. C. CHEN, *Corrosion*, **7**, 229 (1951).
4. D. SCHLAIN, *U. S. Bur. Mines, Rept. Invest.* 4965 (1953).
5. O. B. FRASER, D. E. ACKERMAN, AND J. W. SANDS, *Ind. Eng. Chem.*, **19**, 332 (1927).
6. E. A. GEE, L. B. GOLDEN, AND W. E. LUSBY, JR., *ibid.*, **41**, 1668 (1949).
7. R. B. MEARS AND R. H. BROWN, *Trans. Electrochem. Soc.*, **81**, 519 (1942).
8. W. A. WESLEY AND R. H. BROWN, "Corrosion Handbook," (H. H. Uhlig, Editor), p. 482, John Wiley & Sons, Inc., New York (1948).

Electrodeposition of Cellulose¹

C. L. MANTELL AND FRANK COZZARELLI²

Department of Chemical Engineering, Newark College of Engineering, Newark, New Jersey

ABSTRACT

Cellulose has been plated at the anode from solutions containing approximately 1% cellulose, where the solvent is an alkaline sodium zincate modified by additions of urea.

INTRODUCTION

Some time ago the senior author (1) investigated cellulose solubility in alkaline solutions and found that the solvency power of sodium zincate solutions is markedly improved by the addition of specific amounts of urea or related materials. Sodium zincate solutions alone have a restricted field of application, exhibiting solvency power for only a limited number of cellulose materials and being ineffective for others. This is true below 5°C, which is the required maximum temperature at which sodium zincate exerts solvency power on cellulose. As the cellulosic content of sodium zincate solutions increases, viscosities become enormous. Some relief may be achieved by the use of excessive amounts of sodium zincate, but this introduces other difficulties.

In the case of the sodium zincate-urea solvents, it is particularly noticeable that an increased number and variety of forms of regenerated cellulose may be treated. These embrace a wide variety of paper mill and factory wastes which can be put in solution at room temperatures or above without the necessity of cooling or exact temperature control.

The basic thought which led to this investigation was that mill scraps and other factory wastes could be dissolved and then electroplated to a useful form. There is a possibility of electroplating on wire to form an insulating cover, or plating on wire screen to form a protective coating, or simply to make a fine grade paper. Upon careful consideration, many more applications could be found.

The solvent is commonly prepared by mixing together either an alkaline aqueous solution of sodium zincate and urea or by the addition of urea and zinc oxide to an aqueous solution of sodium or potassium hydroxide. It is interesting to note that composition ranges are reasonably limited. Urea is effective at about 4 to 10% by weight of solution,

and preferably from 6 to 10%. Below this range the solvency power of the solution is decreased, while little worth-while improvement results at urea concentrations above 10%. The zinc oxide percentages may vary from a minimum of 2 to the saturation value, while the NaOH varies from 7 to 15%. Solvency power is adversely affected by concentrations of zinc oxide and caustic below the minimum, while above the maximum little advantage is gained and some difficulties might be experienced. A typical effective solvent is one composed of 4.5% zinc oxide, 10% caustic, 10% urea, and the balance water. Chemicals such as cyanamid, guanidine, and guanyleurea, for example, which hydrolyze with alkalies or zincates to form urea, may be employed in amounts equivalent to the urea.

It appears that amphoteric metals forming hydroxides and salts or ammonia complexes might be employed in place of zinc oxide. Experimental work over a wide range with copper, nickel, and cobalt oxides and hydroxides showed that their solubility in caustic and urea combinations was low and compounds were not formed which showed cellulose solvency at room temperatures. In the case of the amphoteric metals such as aluminum and tin, aluminates offered little encouragement but stannates with urea gave useful effects. Solutions of 8-15% NaOH and 1-5% sodium stannate were found to dissolve on rayon and related materials at low temperature. A minimum of 10% NaOH was necessary with 2-3 g stannate/100 cc solvent. Clear solutions were obtained up to 5% regenerated cellulose content after a few minutes of constant stirring. However, after approximately 15 min the solution gelled and within an hour was converted to a stiff clear gel. Addition of urea reduced the viscosity to approximately 20% of the viscosity of the solution with no urea.

From solvents such as the above, with control of viscosity, electrodeposition of cellulose was investigated.

EXPERIMENTAL

Solvent preparation.—The solvent was prepared by the addition of urea and zinc oxide to an aqueous solution of sodium hydroxide.

¹ Manuscript received January 15, 1954. This paper was prepared for delivery before the Wrightsville Beach Meeting, September 13 to 16, 1953. The paper was submitted as a partial requirement for the M.S. degree from the Graduate School, Newark College of Engineering.

² Present address: Bakelite Corporation, Bound Brook, New Jersey.

Solvent

Zinc oxide.....	4.5% by weight
Caustic.....	10% by weight
Urea.....	10% by weight
Water.....	75.5% by weight

Electroplating solution.—A series of cellulose solutions were made as follows:

Electroplating Solution

Concentration of cellulose material (% by weight)	Consistency of bath
0.5	Very thin
1.0	Thin
1.5	Thin
2.0	Gels after standing several hours
2.5	Gels after standing several hours

It is apparent that the 2.0 and 2.5% solutions must be used before they gel. The 1% solution was used for electrodeposition experiments.

The plating bath was contained in glass beakers into which the electrodes were immersed. Each electrode was supported by a copper conductor bar. A selenium rectifier of 75 amp/0–15 v or 150 amp/0–7.5 v was utilized.

Test of electrodes

Electrode material	Current density 0.2 amp/ft ²	Current density 1.0 amp/ft ²
Stainless steel....	—	Zinc deposited at cathode
Zinc plated steel..	—	Zinc deposited at cathode
Tin plate.....	—	Zinc deposited at cathode
Bronze.....	Compound deposited at anode	Zinc deposited at cathode
Copper.....	Compound deposited at anode	Zinc deposited at cathode
Lead.....	Compound deposited at anode	Zinc deposited at cathode

Chemical testing of the film.—In order to prove that the substance plated was cellulose, the plated material was scraped off the electrode and dissolved in concentrated sulfuric acid and diluted in water. This solution was refluxed for several hours to hydrolyze the cellulose to glucose. The refluxed liquid contained a sugar as indicated by Fehling's solution. The dried plated material was also tested for insolubility in hot water and solubility in Schweizer's reagent (cuprammonium reagent). The results of these tests showed the plated material to be cellulose and it was concluded that cellulose can be plated from a solution of sodium zincate and urea onto a copper, bronze, or lead anode. Copper was arbitrarily chosen as the electrode material for use in the remainder of the experiments.

Electroplating range.—The conditions necessary

for the electrodeposition of cellulose were determined by conducting a series of depositions for 10 min at constant current density. Seven trials at an electrode spacing of one inch were made and the required conditions were found to be:

Electroplating Range

Current range.....	20–120 milliamp
Voltage range.....	1.10–1.28 v
Current density range.....	0.137–1.11 amp/ft ²

Above the upper limit of current density, zinc was plated at the cathode. With a considerable increase in current density (80 amp/ft²) spongy zinc deposited at the cathode and cellulose migrated toward the anode, but did not adhere. It appears that the cellulose was coagulated but not deposited under these conditions.

Estimate of current efficiency.—Cellulose is not a substance possessing molecular homogeneity. Molecules widely varying in weight are present in a solution. It was necessary to deal with averages, such as average molecular weights and average chain lengths. Current efficiencies calculated on the assumption of a molecular weight of 50,000 and a valence change equivalent to 2 are low. Increasing the cellulose concentration improved the efficiency, but this was limited by the point at which the solution gelled. Current efficiency increased as current density decreased.

Current Efficiency

% Cellulose	Current density	Average current efficiency
	amp/ft ²	%
1	0.320	3.30
	0.513	2.38
	0.641	1.99
2	0.575	2.98

Results.—When the anode was sufficiently covered to insulate it, the deposition of cellulose ceased. Several platings could be made from the same bath.

An attempt was made to increase the amount of material deposited and improve the film characteristics. This was done by doubling the cathode area and keeping the same anode area; thus, the anode current density was doubled and the cathode current density remained the same. The voltage was 1.28 v in both instances but the current increased from 150 to 300 milliamp. The only noticeable effect was a slight increase in material deposited.

In order to strip the cellulose film from the anode, it was necessary to allow the plated cellulose to air dry. The anode was immersed in methyl alcohol to facilitate the drying operation. After drying, the unit was washed with 6*N* HCl to dissolve any metallic salts or hydroxides transported with the cellulose during the plating operation. Following

this treatment, the film was easily removed and then allowed to dry. The film was like a soft tissue paper and was about 0.006 in. in thickness and quite fragile.

In order to improve the characteristics of the plated material, various plasticizers were incorporated in the baths as additives. The examination was only cursory, since the primary point of interest was the determination of the necessary plating conditions. Among the plasticizers incorporated in the solution were shellac, ammonia casein, glycerine, methyl abietate, all without success. It is believed further experimentation should include glycol derivatives and other compounds such as alkaline soluble resins to impart wet strength to the film.

Platings were also made on wire screen, wire, and on other irregular objects, but the film could not be stripped.

CONCLUSIONS

The electrolyte for a typical plating bath would have the following weight-per cent composition: cellulose, 1.0; zinc oxide, 4.5; sodium hydroxide, 10.0; urea, 10.0; water, 74.5. Typical plating conditions call for an anode current density of 0.137–1.11 amp/ft², cell voltage, 1.10–1.28 v, average current efficiency, 1.99–3.30 %, average deposition rate, 3.30–5.46 g/amp-min.

A suitable solution contains 1–2.5% by weight of cellulose and, when plating, the current density must be closely controlled to prevent the deposition of zinc at the cathode.

Any discussion of this paper will appear in a Discussion Section to be published in the December 1955 JOURNAL.

REFERENCE

1. C. L. MANTELL, *Textile Research J.*, **16**, 481 (1946).

The Electrolytic Reduction of Isobutyraldehyde in Acid Solution¹

SHERLOCK SWANN, JR., E. I. ONSTOTT,² AND F. H. BAASTAD³

Division of Chemical Engineering, University of Illinois, Urbana, Illinois

ABSTRACT

The electrolytic reduction of isobutyraldehyde has been carried out at cathodes of cadmium, zinc, mercury, and lead. The influence of the physical condition of the cathode has been studied. Preparation of the surface has been shown to have a marked effect on the products obtained at lead and zinc.

INTRODUCTION

This study was undertaken to show the influence of the cathode material on the electrolytic reduction of an aliphatic aldehyde having a branched chain adjacent to the carbonyl group. It has been previously shown that straight chain aliphatic aldehydes are reduced to the primary alcohol as main product at cathodes of cadmium, mercury, and lead (1-3). The yield of hydrocarbon was found to increase with temperature (1). The only simple branched chain aldehyde which has been reduced is isobutyraldehyde. Hibbert and Read (2) found that it behaved similarly to the straight chain aldehydes in being reduced to isobutyl alcohol as the main product at a lead cathode. Since its behavior at other cathodes had not been studied, isobutyraldehyde was chosen for the present investigation.

APPARATUS AND PROCEDURE

The apparatus and general procedure was the same as that described in previous communications (4-6). Only cathodes of zinc, cadmium, mercury, and lead were used in this investigation because they had been shown to be the most active in the reduction of aliphatic carbonyl compounds (3).

Pure isobutyraldehyde (bp 63°C) was obtained from a crude starting material by fractionation in a high precision column.

RECOVERY OF PRODUCTS

Isobutane and isobutene.—In the first experiments the calcium chloride tube originally used (3) was replaced by a U-tube cooled in an ice salt bath to remove the isobutyraldehyde carried over in the gas stream. A very small amount of aldehyde was

found in the dry ice-isopropyl alcohol trap along with the hydrocarbons. In later experiments a tube containing an alkaline solution of hydroxylamine hydrochloride was inserted in the train before the ice-salt trap and a calcium chloride tube before the dry ice-isopropyl alcohol trap. In this way the hydrocarbons were obtained uncontaminated.

At certain cathodes some isobutene was formed along with the isobutane. It was determined in some typical experiments by analysis of the gases formed by allowing the liquid hydrocarbons to vaporize.

Products in the catholyte.—After completion of the runs the catholyte together with the washings of the porous cup and cathode were poured into a distilling flask and the isobutyl alcohol and unreduced aldehyde removed by distillation. In certain experiments a heavy oil, which turned out to be paraisobutyraldehyde, was found. This was separated from the diluted catholyte before distillation. The distillate was then fractionated in a high precision column. The efficiency of the separation was determined by fractionating known mixtures of isobutyraldehyde isobutyl alcohol, and water. It was found that over 95% of the aldehyde distilled at 60°-63°C. The temperature then rose rapidly to 88°C at which the constant boiling mixture of isobutyl alcohol and water distilled. It was decided to make the cut at 77°-80°C. There was no loss on account of hold up in the column, as water started to come over immediately after the isobutyl alcohol-water fraction.

The isobutyl alcohol-water fraction was dried with anhydrous potassium carbonate, redistilled, and weighed. Water content was determined by refractive index and found to be very small.

Small quantities of solid paraisobutyraldehyde (MP 59°-60°C) were sometimes found in the tube cooled in the ice salt mixture.

The solid metal cathodes were cast in a cold mold, and at 50°C under their melting points. Besides the usual anodization of zinc and cadmium

¹ Manuscript received June 1, 1954. This paper was prepared for delivery before the New York Meeting, April 12 to 16, 1953.

² Present address: University of California, Los Alamos Scientific Laboratory, Los Alamos, New Mexico.

³ Present address: Grandeveien 5, Bygdøy, Oslo, Norway. Fellow of the Royal Norwegian Council, 1952-53.

in sulfuric acid and preparation of the lead by the Tafel procedure (7) the metals were etched in nitric acid and lead was anodized in perchloric acid. All of the solid metals were studied in electropolished condition also. The baths for polishing were as follows: ethyl alcohol-phosphoric acid for zinc (8) and cadmium and perchloric acid-acetic anhydride for lead (9). Unless otherwise noted, cathodes of zinc were dipped in dilute nitric acid, those of cadmium anodized in sulfuric acid, and those of lead given a "Tafel" preparation.

Only 5 g of isobutyraldehyde per 100 cc of catholyte was used in each run on account of its low solubility. The use of a blending agent was undesirable on account of the difficulties it might cause in separating the products. In the recovery of products from runs with all cathodes except mercury, four runs were combined. In some of the experiments two cells were connected in series.

DISCUSSION OF RESULTS

The effect of experimental conditions on the electrolytic reduction of isobutyraldehyde is shown in the following tables and discussion.

It may be seen in Table I that the temperature of the catholyte has a marked effect not only on the total yield but also on the type of product. At the lower temperature the zinc cathode was practically inactive, while the yields of alcohol were much higher with yields of hydrocarbon correspondingly lower at cathodes of cadmium and lead. The behavior of mercury was exceptional. No hydrocarbon was found under any conditions. There were found considerable amounts of a heavy oil, which turned out to be paraisobutyraldehyde. As in the case of cadmium and lead the lower temperature was favorable to the formation of the alcohol.

Effect of acid concentration.—It was found that lowering the acid concentration in the catholyte from 30 to 10% had little effect on the yield of hydrocarbon at any cathode. The yields of alcohol, however, were about 10–15% higher than those shown in Table I at temperatures of 58°–61°. Considerable amounts of paraisobutyraldehyde were found in the catholyte of 10% sulfuric acid with the mercury cathode.

Effect of current density.—Lowering the current density from 0.05 amp/cm² to 0.02 amp/cm² had no beneficial effect. In fact, some of the yields were decreased.

Effect of physical structure of cathode.—Several interesting points are illustrated in Table II. In the first place, zinc cathodes are much more active after being treated with nitric acid than after the usual anodization. The higher yields of alcohol obtained at the same type of cathode were due to

TABLE I. Influence of temperature

Anode: lead cylinder; anolyte: 10% sulfuric acid; catholyte: 100 cc of 30% sulfuric acid with 5 g of isobutyraldehyde; cathode area: 100 cm²; amp: 5; current density: 0.05 amp/cm²; duration of run: 1½ hr (theoretical for reduction of isobutyraldehyde to isobutane).

Products of four runs combined

Cathode material	Temp, °C	Grams of isobutane	% yield of isobutane	Grams of isobutyl alcohol	% yield of isobutyl alcohol
Zinc, 370	58-61	3.6	23.0	2.8	13.7
Same	58-61	3.6	23.0	3.2	15.1
Same	58-60	3.4	21.1	3.5	17.0
Same	18-21	0.1	0.6	1.4	6.8
Same	18-21	0.1	0.6	1.1	5.3
Cadmium, 270	58-60	4.9	30.4	3.9	19.0
	58-60	4.7	29.1	3.8	18.5
Same	58-60	5.2	32.3	4.4	21.2
Same	59-61	5.3	32.9	4.5	21.8
Same	19-22	3.1	19.3	6.6	32.1
Same	18-21	3.3	20.5	7.2	35.0
Mercury*	58-61	0	0	1.5	7.2
Same*	58-61	0	0	1.9	9.6
Same*	18-21	0	0	10.2	49.6
Same*	18-21	0	0	12.1	59.0
Same	19-21	0	0	12.4	60.1
Lead, RT	58-61	3.8	23.5	5.8	28.3
Same	58-60	4.0	24.8	6.4	31.1
Same	58-61	4.0	24.8	6.2	30.2
Same	19-21	1.6	10.0	9.0	43.6
Same	18-21	1.5	9.3	8.7	42.3

* Catholyte: 20 g of isobutyraldehyde in 400 cc of 30% sulfuric acid; duration of run: 6 hr. Numbers following the names of the cathodes are the mold temperatures of the cast. RT signifies room temperature.

longer treatments with nitric acid. Treating a machined cadmium surface similarly raised the yield of alcohol, but had no effect on that of the hydrocarbon. The effect on a lead cathode was to increase the amount of hydrocarbon at the expense of the alcohol.

The effect of electropolishing on zinc was to make it less active for hydrocarbon and alcohol formation. The activities of cathodes of cadmium and lead were practically unchanged.

The temperature at which the electrodes were cast was an important factor with zinc and cadmium but not with lead. Higher yields of the alcohol were obtained at cathodes cast at the lower temperature.

It is possible that differences in behavior of the two types of cathodes may be due to crystal orientation. The orientation in the metal cast at room temperature would be random with small grain size, while preferred orientation would be increased by the formation of large columnar crystals resulting from casting the metal 50°C under its melting point. Similarly, the effects of etching with nitric acid could be ascribed to an increase in preferred orientation.

TABLE II. *Effect of physical structure of cathode*
Temp, 52°-61°. All other conditions as in Table I.

Cathode material	Grams of isobutane	% yield of isobutane	Grams of isobutyl alcohol	% yield of isobutyl alcohol	Treatment of cathode
Zinc, RT, 2 sets	2.8	17.5	4.8	23.3	Dil. HNO ₃
	3.5	21.7	5.8	28.2	Dil. HNO ₃
Zinc, RT, set 1	2.1	13.0	1.7	8.5	Anod. H ₂ SO ₄
	1.2	7.5	1.3	6.3	Anod. H ₂ SO ₄
Same	3.7	23.0	6.9	33.0	Dil. HNO ₃
Same	3.7	23.0	6.1	30.0	Dil. HNO ₃
Zinc, RT, set 2	0.8	5.0	1.0	5.0	Anod. H ₂ SO ₄
	0.6	3.6	1.3	6.3	Anod. H ₂ SO ₄
Same	3.7	23.0	6.9	33.5	Dil. HNO ₃
Same	3.6	22.5	6.7	32.5	Dil. HNO ₃
Same	2.5	15.4	1.0	5	Pol., electropol.
Same	2.2	13.6	1.1	5.5	Pol., electropol.
Zinc, 370, 2 sets	3.6	23.0	2.8	13.7	Dil. HNO ₃
	3.6	23.0	3.2	15.1	Dil. HNO ₃
	3.4	21.1	3.5	17.0	Dil. HNO ₃
Zinc, 370, set 1	3.4	21.0	5.8	28.0	Dil. HNO ₃
	2.2	13.6	5.3	25.5	Dil. HNO ₃
Same	2.4	15.0	4.5	22	Anod. H ₂ SO ₄
Same	5.0	31	6.2	30.5	Dil. HNO ₃ each run
Zinc, 370, set 2	2.3	14.2	5.3	25.5	Dil. HNO ₃
	3.0	18.7	5.3	25.5	Anod. H ₂ SO ₄
Cadmium, RT, set 1	5.3	32.8	6.0	29.0	Anod. H ₂ SO ₄
	5.2	32.1	6.4	31.0	Anod. H ₂ SO ₄
Cadmium, RT, set 2	5.0	31.0	6.5	32.0	Anod. H ₂ SO ₄
	5.3	32.8	5.8	28.0	Anod. H ₂ SO ₄
Cadmium, 270, set 1	5.8	36	5.3	26	Anod. H ₂ SO ₄
	3.9	24	5.3	26	Anod. H ₂ SO ₄
Cadmium, 270, 2 sets	4.9	30.4	3.9	19	Anod. H ₂ SO ₄
	4.7	29.1	3.8	18.5	Anod. H ₂ SO ₄
Same	5.2	32.3	4.4	21.2	Anod. H ₂ SO ₄
Same	5.3	32.8	4.5	21.8	Anod. H ₂ SO ₄
Cadmium, 270, mach. 2 sets	5.5	34.2	4.0	19.5	Anod. H ₂ SO ₄
	5.2	32.3	3.8	18.5	Anod. H ₂ SO ₄
	5.2	32.3	3.8	18.5	Anod. H ₂ SO ₄
	5.2	32.3	4.2	20.4	Anod. H ₂ SO ₄
Cadmium, 270, mach. set 1	5.7	35.5	4.7	23.0	Pol. electropol.
	5.9	36.5	5.5	26.5	Pol. electropol.
	5.1	31.5	6.2	30.5	1:1 HNO ₃
	5.3	32.7	6.1	29.5	1:1 HNO ₃
Lead, RT, 2 sets	3.8	23.5	5.8	28.3	Tafel prep.
	4.0	24.8	6.4	31.1	Tafel prep.
	4.0	24.8	6.2	30.2	Tafel prep.
Lead, RT, set 1	4.3	26.5			Tafel prep.
	3.9	24.0			Tafel prep.
	2.9	18.0	5.1	25	Tafel prep.

TABLE II—Continued

Cathode material	Grams of isobutane	% yield of isobutane	Grams of isobutyl alcohol	% yield of isobutyl alcohol	Treatment of cathode
Same	2.4	14.6	6.5	31.5	Tafel prep., 2 C.D.
Same	2.9	18.0	5.4	26.5	Anod. HClO ₄
Same	3.0	18.5	5.3	26.0	Anod. HClO ₄ , Tafel prep.
Same	3.3	20.5	4.8	23.5	1:1 HNO ₃ , Tafel prep.
Lead, RT, set 2	3.4	21.5	5.2	25.5	Tafel prep.
	4.8	29.5	5.0	24.5	Tafel prep.
	3.6	22.3	6.3	30.0	Tafel prep.
Same	3.9	24.0	6.0	29.0	Tafel prep.
Same	3.8	23.5	6.5	32.0	Tafel prep.
Lead, Rt, set 3	3.4	21.0	5.7	28.0	Tafel prep.
	2.8	17.2	6.7	33.0	Tafel prep.
	6.2	38.0	4.1	20.0	3 hr, 1:1 HNO ₃
Same	6.4	40.0	5.3	26.0	1½ hr., 1:1 HNO ₃
Lead, 270, 2 sets	3.8	23.6	5.8	28.2	Tafel prep.
	4.3	26.7	6.1	29.6	Tafel prep.
	4.1	25.5	6.4	31.1	Tafel prep.
Same	4.1	25.5	6.9	33.4	Tafel prep.
Lead, 207, set 1	2.8	17.2	6.4	31.3	Tafel prep.
	5.8	36.5	5.0	24.5	4 hr, 1:1 HNO ₃
Lead, 270, set 2	4.5	28.0	6.3	30	Tafel prep.
	4.3	27.0	6.3	30	Tafel prep.
Lead, mach.	3.3	20.5	5.7	28	Electropol.
	3.5	21.5	6.0	29	Electropol.
Same	5.0	31.0	6.5	31.5	Electropol., Tafel prep.
Same	3.1	19.0	6.2	30.5	Pol., electropol.
Same	4.0	24.5	5.5	27.0	Tafel prep.

Mach. after cathode: surface smoothed by machining. Two sets: runs from 2 sets of cathodes combined. Dil. HNO₃: dipped in dilute nitric acid. Anod. H₂SO₄: anodized in 20% sulfuric acid. Pol.: polished. Electropol.: electropolished. Tafel prep.: Tafel preparation. Anod. HClO₄: anodized in 20% HClO₄. 2 C.D.: double the usual current density.

After many Tafel preparations the yield of hydrocarbon decreased at one set of lead cathodes cast at room temperature. Small amounts of paraisobutyraldehyde were found as in the case of mercury.

Formation of olefine.—At all cathodes except mercury the isobutane was found to contain small amounts of unsaturated material, presumably, 2-methylpropene. As much as 13% was found from the reduction in the total hydrocarbon at the zinc cathode cast at 370°C.

GENERAL CONCLUSIONS

Isobutyraldehyde has been reduced electrolytically to isobutane, isobutene, and isobutyl alcohol. The highest yield of hydrocarbon, 40%, was obtained at a lead cathode which had been allowed to stand in strong nitric acid for several hours. The highest yield of the alcohol, 60.1%, was obtained at a mercury cathode. No hydrocarbon at all was found at the mercury cathode.

Decreasing the temperature of the catholyte caused a lowering of the activity of cathodes of zinc and an increase in the yield of the alcohol at cathodes of cadmium, mercury, and lead.

In all cases, decreasing the acid concentration led to an increase in the yield of the alcohol and hence to an over-all increased conversion of the aldehyde.

Lowering the current density either had no effect or resulted in lower conversions.

The change of structure of the cathode due to its casting temperature was important with cathodes of zinc and cadmium. A higher yield of the alcohol was obtained at the low temperature cast.

In general, electropolished surfaces were less active than others.

Highly active surfaces were obtained by treatment of the cathodes with nitric acid. Machined cadmium was affected the least. Renewal of the surface of the electrodes was found to be very important.

Results obtained with isobutyraldehyde were very

similar to those found with straight chain aldehydes by other investigators in that at room temperature the alcohol was the main product and that formation of hydrocarbon increased with the temperature.

ACKNOWLEDGMENTS

Acknowledgments of gifts of metals for electrodes and for their casting have been made in previous papers.

The infrared spectral analysis of paraisobutyraldehyde was carried out and interpreted by Miss Helen Miklas.

Any discussion of this paper will appear in a Discussion Section to be published in the December 1955 JOURNAL.

REFERENCES

1. W. SCHEPSS, *Ber.*, **46**, 2564 (1913).
2. H. HIBBERT AND R. R. READ, *J. Am. Chem. Soc.*, **46**, 983 (1924).
3. S. SWANN, JR., AND E. W. FIELD, *Trans. Electrochem. Soc.*, **72**, 327 (1937).
4. S. SWANN, JR., *ibid.*, **62**, 153 (1932).
5. S. SWANN, JR., R. W. BENOLIEL, L. R. LYONS, AND W. H. PAHL, *ibid.*, **79**, 83 (1941).
6. S. SWANN, JR., "Electrolytic Reactions" in "Technique of Organic Reactions," A. Weissberger, Editor, Vol. II, Fig., p. 155, Interscience Publishers, Inc., New York (1948).
7. *Ibid.*, p. 171.
8. P. A. JACQUET, *Rev. gen. elec.*, **54**, 239 (1945).
9. P. A. JACQUET, *Bull. soc. chim.*, **5**, **3**, 705 (1936).

Determination of Hydrogen in Titanium¹

T. D. MCKINLEY

Pigments Department, Chemical Division, E. I. du Pont de Nemours & Company, Newport, Delaware

ABSTRACT

A simple, rapid, precise method for determination of hydrogen in titanium is described. It is based on measurement of the equilibrium pressure of hydrogen over the metal in a closed system under predetermined conditions. Construction, calibration, and operation of the analytical equipment are described. Hydrogen can be determined in the range 0.001–0.33 wt % with a probable error of about 5%. The physical form of specimens is unimportant. Twenty analyses can be made in an 8-hr period.

INTRODUCTION

The chemical constitution and phase relationships of the titanium-hydrogen system at high temperatures have received attention from several investigators (1, 3–5, 8–10). Recently, McQuillan (6, 7) determined in great detail the pressure-temperature-concentration relationships for the titanium-hydrogen system in the range 450°–975°C. McQuillan's data indicate a continuous single phase in the condensed system where α or β titanium exists alone. Extrapolation of his curves would indicate very high solubility of hydrogen in titanium at room temperature. However, it was found (2) that solubility of hydrogen in titanium decreases markedly at temperatures below 200°C. Hydrogen in excess of the solubility limit precipitates, presumably as a hydride. The hydride precipitate in titanium or titanium-rich alloys seriously lowers the impact strength of the metal. Hence, control of the hydrogen level is of major importance in the manufacture, melting, fabrication, and subsequent use of titanium. Simultaneously it becomes highly desirable to have a simple, rapid, precise method for determination of hydrogen in titanium.

Available Analytical Methods

The most widely used techniques for determining hydrogen in titanium are the vacuum fusion method (11) and modifications involving temperatures short of fusion. In these methods hydrogen is quantitatively removed from the specimen by evacuation at high temperatures with subsequent analysis of the gases, usually in an integrated closed system. While such methods are capable of adequate precision, the apparatus required is rather elaborate and considerable time is required to outgas the furnace assembly either to a reproducible or to a negligible blank. Moreover, if gases other than hy-

drogen are evolved from the specimen, separation and analysis of the gases are necessary.

Another approach to hydrogen determination is via combustion in dry oxygen and gravimetric determination of the hydrogen as water. This method has shortcomings of a practical nature in that combustion is difficult to control and results generally lack the reproducibility and precision desired.

Principle of the Method

McQuillan's data indicate that, in single phase titanium under equilibrium conditions, dissolved hydrogen behaves as an ideal liquid, i.e., a linear relationship exists between the logarithm of the equilibrium pressure and reciprocal absolute temperature when the hydrogen concentration in the metal is held constant. Likewise, a plot of the logarithm of equilibrium pressure vs. the logarithm of concentration of hydrogen in the metal is linear under isothermal conditions. In regions where α and β titanium coexist, equilibrium pressure is independent of the hydrogen concentration in the metal as would be predicted from phase rule considerations. It has been established that hydrogen is the only common gas that, once dissolved in the metal, can be extracted to any measurable extent by temperature and pressure manipulation alone. Thus, determination of the equilibrium hydrogen pressure over a specimen of single phase titanium at a predetermined temperature for which the pressure-concentration relationship is known and in an apparatus of known volume affords data from which the hydrogen content of the metal can be readily calculated.

From a practical standpoint it is highly desirable to make these determinations in the β region for the following reasons.

1. The system is sluggish in attaining equilibrium conditions at low temperatures, whereas equilibrium is established very rapidly above the transition point (882°C).
2. The higher the temperature the higher the

¹ Manuscript received Aug. 11, 1954. This paper was prepared for delivery before the Boston Meeting, October 3 to 7, 1954.

equilibrium pressure, increasing the relative precision with which pressure measurements can be made. It is true that the equilibrium pressure over α -titanium just below the transition point is greater than the equilibrium pressure over β -titanium at, say, 1000°C, concentration being constant. However, regions immediately in the vicinity of the transition point should be avoided for titanium specimens other than those of very high purity.

3. Many impurities stabilize a portion of the β structure well below the transition point. Hydrogen itself is a β -stabilizer. Therefore, the existence of single phase metal below the transition point cannot be universally assumed. On the other hand, the common α -stabilizers (oxygen, nitrogen, aluminum, and tin) must be present in much larger amounts than ordinarily found to effect any α -stabilization at 100°C above the normal transition temperature.

APPARATUS

All parts of the apparatus (Fig. 1) other than the sample tubes and heating sleeves are fabricated from borosilicate glass. Pressure is measured by means of the Todd Universal Gauge (A), a three-scale mercury gauge with a range of 0.0001 to 25 mm mercury. Bulb (B) is of approximately 250 ml capacity and is carefully calibrated for volume between stopcocks before attachment to the manifold. Tapered joint (C) permits attachment of other equipment to the bulb. Silica sample tubes (D) are connected to the manifold through 4 mm high vacuum stopcocks. Heating sleeve (E) is supplied with power by a 500 watt combination of a constant voltage transformer and variable transformer in tandem (F). Temperature is measured by means of a 20 gauge chromel-alumel thermocouple (G) and potentiometer (H). Evacuation is effected by means of a single stage mercury diffusion pump (I) with conventional mechanical forepump. Power to the heater of the diffusion pump is controlled by a 5 amp variable transformer (J); 4 mm stopcocks (K) and (L) permit isolation of the manifold from

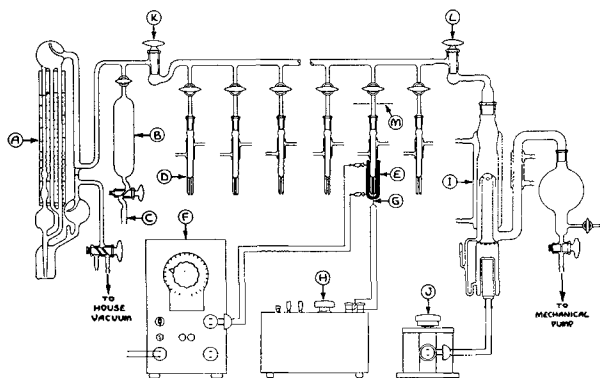


FIG. 1. Apparatus

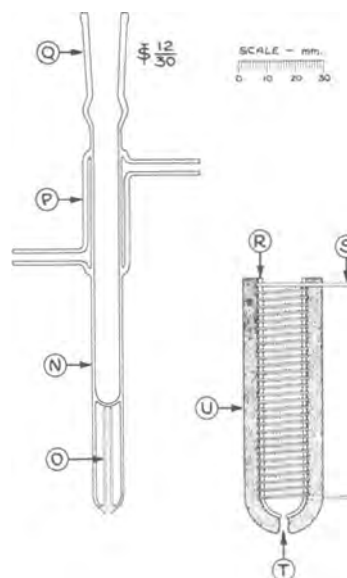


FIG. 2. Details of sample tube and heating sleeve

the gauge and from the pumping system. All stopcocks and tapered joints are hand-lapped to a fine finish. Stopcocks are lubricated with a highly refined vacuum grease with low thermal coefficient of viscosity, such as Apiezon N, and joints sealed with nongassing hard wax. Removable asbestos paper shields (M) protect the stopcocks from heat of the gas flame used in sealing and unsealing the hard waxed joints.

Details of a silica sample tube and heating sleeve are shown in Fig. 2. Sample tubes are fabricated entirely from transparent silica. The titanium sample rests on the bottom of the sample tube chamber (N). Sleeve (O) acts as a guide for the thermocouple, the hot junction of which touches the bottom of the furnace chamber. Thus the sample is separated from the thermocouple by only about 1 mm of silica. Chamber (P) provides for water cooling so that joint (Q) is kept at approximately room temperature. The water-cooled chambers of adjacent sample tubes are connected by short lengths of rubber tubing permitting in-line flow of cooling water. The heating sleeve consists of a silica shell (R) covered with thin asbestos paper and wound with 6 ft of $\frac{1}{32} \times 0.0035$ in. nichrome ribbon. The ends of the heating ribbon are joined to short lengths of heavy nichrome ribbon (S) which protrude from the shell to form lugs for connection to the power source through small battery clamps. A small opening (T) at the bottom of the sleeve provides access for the thermocouple. The wound sleeve is covered with a thermal insulating layer of macerated asbestos paper (U) $\frac{3}{16}$ in. in thickness. After bakeout, the exterior of the sleeve is painted with heat resistant aluminum paint. The inner diameter of the silica shell of the sleeve is approximately 1 mm greater than the outer

diameter of the sample tubes. A sample tube with heating sleeve in place is shown in Fig. 1. Approximately 2 ml of the sample tube volume is heated by the sleeve.

CALIBRATION

The purpose of the calibrated bulb (B) in Fig. 1 is to provide a means for determining the volume of the equipment. The procedure consists of partial evacuation of the system with the lower stopcock of the bulb closed, the upper stopcock open, and the stopcock to one sample tube open. Stopcock (L) is then closed and pressure measured by the gauge. The upper stopcock of the bulb is then closed, stopcock (L) is opened, and the system evacuated to a low pressure. This leaves a known volume of gas under a known pressure in the bulb. Stopcock (L) is then closed and the gas in the bulb is expanded to the evacuated system. Pressure is again determined. The volume of the apparatus (without the bulb which is normally not a part of the working volume) is then:

$$V_a = V_b \frac{P_1 - P_2}{P_2}$$

where V_a = volume of apparatus, V_b = volume of bulb, P_1 = initial pressure, and P_2 = final pressure (temperature assumed constant). This determination is then repeated at several pressure levels. The volume of the apparatus can be quickly determined with a probable error of less than 0.5%. The working volume of the apparatus is 400 ± 100 ml, depending on the number of sample tube connections and minor differences in construction details.

As previously discussed, it is highly preferable to operate in the β region. The operating temperature is ideally the highest readily attainable. However, this is moderated by several practical considerations. A temperature of 1000°C was selected as a compromise since: (A) It is sufficiently elevated above the normal transition temperature to guarantee single phase (β) titanium. (B) Reaction of titanium with the silica sample tube in the few minutes required at temperature is superficial, introducing negligible error due to contamination, and allowing reasonable sample tube life. It was found that the sample tubes remain operable for several hundred analyses. (C) Operating lifetime of nichrome heaters is reasonable. (D) Loss of hydrogen by diffusion through the silica is negligible in the short time required to attain equilibrium.

Determination of the equilibrium pressure-concentration relationship was made in the same apparatus later used for analyses. A few grams of titanium hydride was placed in a silica sample tube

and surmounted by a small plug of glass wool to prevent dusting. The tube was attached to the apparatus at joint (C) by hard wax. The hydride was thoroughly outgassed at room temperature, followed by heating to a moderate temperature where evolution of a minor amount of hydrogen helped to sweep out any remaining gases. After outgassing, the tube was never exposed to air during the equilibrium determinations. A 0.500 gram sample of commercially pure titanium sponge was placed in a sample tube which was hard waxed to the manifold. The titanium specimen was outgassed by heating at 1000°C and a pressure of approximately 10^{-5} . Outgassing under these conditions reduces the hydrogen content of the titanium to less than 3 ppm in 60 min. After outgassing, the sample tube was allowed to return to room temperature. Stopcock (L) was closed, isolating the system from the pumps and, with both stopcocks on bulb (B) open, the hydride tube was heated to generate hydrogen. When the desired hydrogen pressure had been attained, the upper stopcock on the bulb was closed and heating was discontinued. Hydrogen pressure and room temperature were observed. The titanium specimen was then heated to 1000°C and, when the system had attained equilibrium (less than 10 min over-all), room temperature and hydrogen pressure were again observed. From these observations and the known volume of the apparatus, one point of the equilibrium curve can be calculated:

$$\begin{aligned} H_o &= 2.02 \times \frac{P_1}{760} \times \frac{273}{T_1} \times \frac{V}{22,400} \\ &= 3.23 \times 10^{-5} \frac{P_1 V}{T_1} \end{aligned}$$

$$\begin{aligned} H_G &= 2.02 \times \frac{P_E}{760} \times \frac{273}{T_E} \times \frac{V}{22,400} \\ &= 3.23 \times 10^{-5} \frac{P_E V}{T_E} \end{aligned}$$

$$H_T = H_o - H_G$$

$$C_E = \frac{H_T}{S} \times 100$$

where: H_o = hydrogen introduced, grams; H_G = gaseous hydrogen at equilibrium, grams; H_T = hydrogen in the titanium sample at equilibrium, grams; C_E = concentration of hydrogen in titanium at equilibrium, wt %; P_1 = initial hydrogen pressure, mm Hg; T_1 = room temperature, $^\circ\text{K}$, at P_1 ; P_E = equilibrium hydrogen pressure, mm Hg; T_E = room temperature, $^\circ\text{K}$, at P_E ; V = volume of apparatus, ml; and S = weight of titanium specimen, grams.

The titanium was then outgassed and the cycle

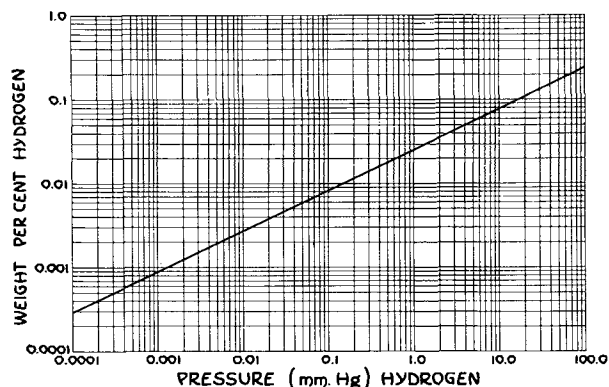


FIG. 3. Equilibrium curve for titanium-hydrogen at 1000°C.

repeated at 12 levels of equilibrium hydrogen pressure in the range 0.001–10 mm Hg. A plot of the equilibrium pressure vs. concentration at 1000°C is shown in Fig. 3. The mean deviation of points from the curves is less than 2%. Repeat measurements with ingot and sheet of commercial purity showed that equilibrium values for these materials fell on the same curve. Impurities within the commercial range of concentration do not materially affect the equilibrium. The slight deviation from the theoretical slope of $\frac{1}{2}$ is believed to be a systematic error.

ANALYTICAL PROCEDURE

Specimens to be analyzed should be in the range 0.4–0.6 gram and are weighed to ± 0.01 gram. The physical form of samples is relatively immaterial; samples may be in the form of sponge, solid pieces of ingot or sheet, drillings, turnings, shavings, or finely divided metal. Bulky samples, i.e., fine turnings, should be compacted by pressing. Samples are placed in individual sample tubes which are attached to the manifold with hard wax. If less than a full complement of sample tubes is attached to the manifold, it is advisable to cap off the remaining joints to minimize the possibility of leaks. The system is evacuated at room temperature to an ultimate pressure of about 10^{-4} . The pressure in the system is observed and, with all stopcocks to sample tube open, stopcock (L) is closed. After 10 min the pressure is again observed. If the final pressure is 5×10^{-4} or lower, the error introduced by leaks will be negligible if the hydrogen content of samples is above 20 ppm. All stopcocks to the sample tubes are then closed with the exception of #1 tube. With heater and thermocouple in place, the tube is heated to 1000°C in 6–7 min and held to $\pm 2^\circ\text{C}$ to the end of 10 min from start of heating. Room temperature and hydrogen pressure are then observed. Heating is discontinued, the stopcock to #1 tube closed and #2 opened. The system is evacuated to about 10^{-4} and the analytical cycle repeated for the second specimen. Successive samples are treated in the

same fashion. Equilibrium pressures can be determined in a single apparatus at the rate of four per hour.

Calculation of the hydrogen content of a specimen involves, for the general case: (a) estimation of the equilibrium hydrogen concentration, C_E , from the curve (Fig. 3); (b) calculation of the hydrogen in the gas phase at equilibrium from observed pressure and room temperature and known volume of the apparatus; (c) summation of the hydrogen in the gaseous and condensed phases and conversion to per cent hydrogen in the original specimen:

$$\begin{aligned} \%H &= C_E + 2.02 \times \frac{P_E}{760} \times \frac{273}{T_E} \times \frac{V}{22,400} \times \frac{100}{S} \\ &= C_E + 3.23 \times 10^{-3} V \frac{P_E}{T_E S} \\ &= C_E + K \frac{P_E}{T_E S}, \quad \text{where } K = 3.23 \times 10^{-3} V \end{aligned}$$

An estimation of the probable errors in the various factors and their influence on the accuracy of the analysis indicates their relative importance and points out some justifiable short-cuts when ultimate accuracy is not required. The values for maximum error in Table I were derived with the following assumptions of accuracy of measurement of the individual factors: (A) Specimen temperature at equilibrium is $1000 \pm 2^\circ\text{C}$. (B) Values of C_E as derived from P_E (Fig. 3) are $\pm 1\%$. (C) Equilibrium pressure is measurable to within one scale division. This amounts to $\pm 20\%$ at 0.001 mm, $\pm 0.4\%$ at 25 mm. (D) The volume of the apparatus is known to $\pm 1\%$. (E) Room temperature is measured to $\pm 1^\circ\text{C}$. (F) The weight of the titanium specimen is known to 0.01 gram.

Nominal values used in the calculations are $V = 400$ ml, $T_E = 300^\circ\text{K}$, and $S = 0.50$ gram.

The greatest individual source of error is the uncertainty in the measurement of P_E . It is also apparent that for low hydrogen concentrations the hydrogen in the gas phase at equilibrium may be generally regarded as negligible. Per cent H = C_E may be assumed up to concentrations of 0.0030% with an error of 0.0001% or less, i.e., about equal to the error introduced by uncertainty in the value of P_E .

TABLE I

P_E	% H	C_E	$K \frac{P_E}{T_E S}$	Error, % H	% Error
0.001	0.000873	0.000864	0.000009	0.000094	10.8
0.01	0.00269	0.00260	0.00009	0.00016	5.9
0.1	0.00888	0.00801	0.00087	0.00035	3.9
1	0.0331	0.0244	0.0087	0.0014	4.2
10	0.1609	0.0741	0.0868	0.0046	2.9
25	0.331	0.116	0.215	0.010	3.0

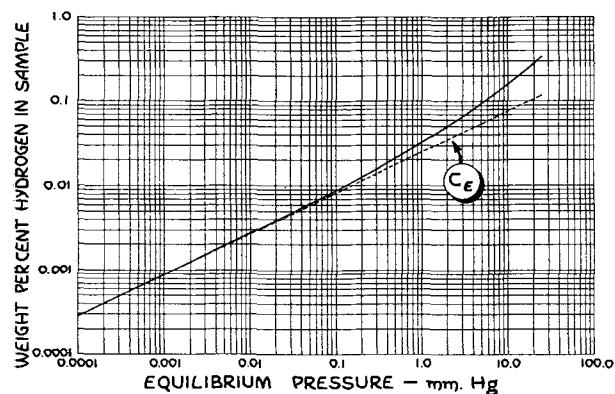


FIG. 4. % H vs. P_E at 1000°C. $V = 400$ ml; $T_E = 300^\circ\text{K}$; and $S = 0.50$ g.

If the sample weight and room temperature are held constant, the per cent hydrogen in the sample will be a function of the equilibrium pressure alone. Small variations in T_E introduce negligible error. Therefore, if S is held constant, T_E varies only a few degrees, and V is known, it is possible to draw a curve interrelating % H with P_E . The curve allows estimation of % H directly from the equilibrium pressure reading with an expected error of less than 10%. A family of such curves permits interpolation for variations in sample weight. A plot of % H vs.

TABLE II. Comparative results by equilibrium and vacuum fusion methods

Sample No.	Equilibrium method	Vacuum fusion method	Difference
1	0.0017	0.0015	+0.0002
2	0.0037	0.0042	-0.0005
3	0.0047	0.0049	-0.0002
4	0.0071	0.0067	+0.0004
5	0.0098	0.0101	-0.0003
6	0.0103	0.0106	-0.0003
7	0.0242	0.0234	+0.0008
8	0.0402	0.0387	+0.0015
9	0.0861	0.0840	+0.0021
10	0.182	0.183	-0.001
11	0.304	0.316	-0.012

P_E is shown in Fig. 4 in which nominal values of $T_E = 300^\circ\text{K}$ and $S = 0.50$ gram are used.

After analyses have been completed, sample tubes are removed from the manifold, the titanium specimens discarded, and the tubes cleaned by digestion in warm 10% HCl. After rinsing with water and methanol and oven drying, the tubes are ready for reuse.

ACCURACY AND REPRODUCIBILITY

Several samples of closely sized titanium sponge covering a wide range of hydrogen contents were prepared by exposing the sponge to hydrogen at about 400°C. After the desired amount of hydrogen had been added, samples were heated in a closed system at 600°C for several hours to promote homogeneity. Samples of the sponge were then analyzed for hydrogen by the equilibrium method and by the vacuum fusion technique as a reference method, each analysis being made in triplicate. Average results are shown in Table II.

Another set of sponge samples, similarly prepared, was subjected to multiple analyses by the equilibrium method to ascertain the reproducibility of the method. Results are given in Table III.

These results indicate the reliability of the method in regard to accuracy and reproducibility. Equilibrium method results are in good agreement with those obtained by vacuum fusion. The average deviation is 3.3% when the hydrogen content is above 0.005%. Random interchange of direction of difference indicates continuity of basic agreement between the two methods within the range investigated. Results in general follow the pattern of error calculations presented in Table I although the most deviant results indicate the possibility of somewhat greater error in single determinations. Reproducibility results may be looked upon as "minimum reproducibility" since deviations may be partially due to minor inhomogeneity in the sponge. Consideration of results of the two sets of tests indicates

TABLE III. Reproducibility of results by the equilibrium method

	Sample #1	Sample #2	Sample #3	Sample #4	Sample #5	Sample #6
	0.0016	0.0027	0.0100	0.0254	0.0397	0.340
	0.0015	0.0032	0.0102	0.0241	0.0402	0.308
	0.0019	0.0027	0.0108	0.0220	0.0412	0.316
	0.0020	0.0029	0.0101	0.0248	0.0396	0.337
	0.0018	0.0032	0.0105	0.0236	0.0407	0.306
	0.0018	0.0030	0.0102	0.0239	—	0.301
	0.0020	0.0028	0.0110	0.0242	—	0.322
	0.0016	0.0028	0.0106	0.0255	—	0.325
	0.0014	0.0031	0.0107	0.0243	—	—
	0.0018	0.0030	0.0104	0.0247	—	—
Avg.	0.00174	0.00294	0.01045	0.02425	0.0403	0.319
M.D.	0.00017	0.00016	0.00027	0.00070	0.00054	0.0116
%M.D.	10	5.4	2.6	2.9	1.3	2.8

TABLE IV. Probable errors of single hydrogen determinations

Hydrogen level	Probable error
0.001-0.01	0.0003
0.01-0.02	0.0006
0.02-0.05	0.0012
0.05-0.1	0.0025
0.1-0.2	0.005
0.2-0.3	0.01

the approximate pattern of probable errors in single determinations by the equilibrium method as shown in Table IV.

From this the probable per cent error in a single determination is 5% or less, provided the hydrogen content is above 0.006%. At lower hydrogen levels the probable per cent error increases to about 30% at 0.001% hydrogen.

These tests were made on specially homogenized sponge but, in actual analyses, the hydrogen usually is less uniformly dispersed. This is particularly true of fabricated metal where it is not uncommon to find 20% variations in hydrogen content, depending on the site of sampling.

In obtaining the data presented in Table II it was found that the reproducibility of the equilibrium method is about double that of the vacuum fusion technique even when extraordinary care is used in applying the latter method. This has been substantiated by subsequent comparative analyses on ingot and sheet samples of commercially pure titanium.

ANALYSIS OF TITANIUM-RICH ALLOYS

Tests have shown that this method can be applied to the determination of hydrogen in titanium-rich alloys. Specimens of 4% Mn-4% Al and of 7% Mn commercial titanium alloy sheet were prepared with a number of hydrogen concentration levels by introducing or removing hydrogen by heating specimens under hydrogen or in vacuum. Samples of each specimen so prepared were analyzed in triplicate by vacuum fusion and by the equilibrium method using C_E values established for commercially pure titanium. Results are shown in Fig. 5 and 6. The linearity of comparative results obtained by the two methods indicates that, at least within the hydrogen concentration range investigated, the equilibrium method is adapted to the determination of hydrogen in these two alloys. It is necessary, when using equilibrium data for commercial titanium, only to multiply the result by factors of 0.89 and 0.76, respectively, to obtain per cent hydrogen in the alloys. Since the conversion factors are close to unity, minor changes in the percentage constitution of the alloy introduce little error. Of course, C_E vs. P_E and % H vs. P_E curves could be established for alloys as for the commercially pure metal. It

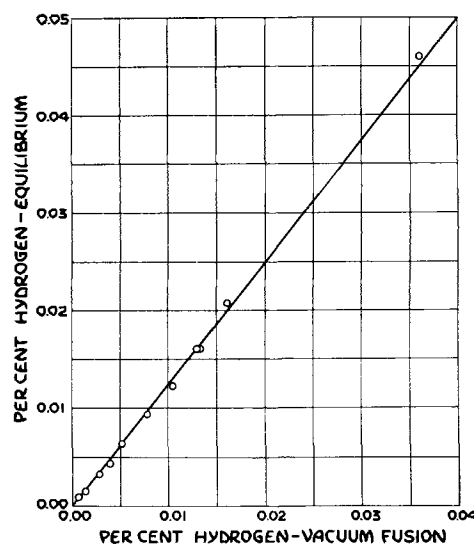


FIG. 5. Hydrogen analysis of 4% Mn-4% Al alloy

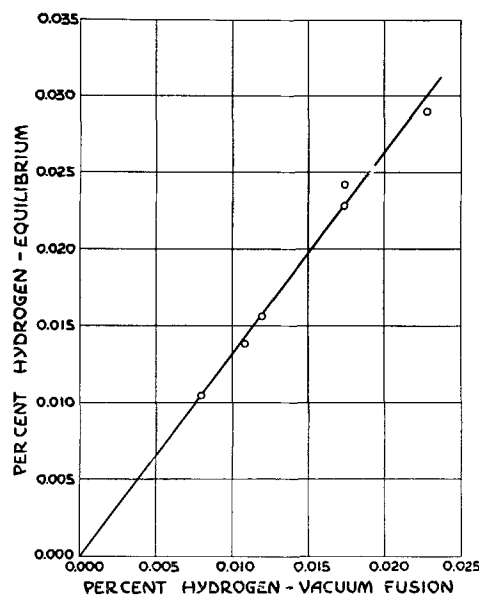


FIG. 6. Hydrogen analysis of 7% Mn alloy

is probable that most titanium-rich alloys can be treated in the same manner.²

DISCUSSION

The analytical apparatus described has a large number of vacuum stopcocks. Stopcocks were used in setting up the apparatus for trial with the expectation of replacing them with mercury cut-offs if the method proved successful. However, it was found that by careful lapping and greasing, the stopcocks provide adequate sealing and no trouble is encountered by outgassing of the lubricant in the pressure range for which the method is adapted.

² This method may also be applied to 5% Sn-2.5% Al alloy, using a factor of 0.60. Thus the method is applicable to the determination of hydrogen in the three general alloy systems: α - β , α -strengthened α - β , and α -stabilized.

The theoretical range of the method as described is 0.0003–0.33% hydrogen. Samples have been analyzed in the range 0.0008–0.31% hydrogen. Lower hydrogen concentrations down to about 0.00001% hydrogen can be determined by replacing the Todd gauge with a sensitive McLeod gauge. However, this would almost certainly also involve replacement of the stopcocks with mercury cut-offs and recourse to much more complete outgassing of the equipment before determination of the equilibrium pressure. Concentrations higher than about 0.3% can be determined by replacing the gauge with a manometer. Determination of the equilibrium curve for equilibrium concentrations greater than 0.15% hydrogen would have to be determined since the curve ceases to be linear.

The sample size has no practical bearing on the accuracy of the analysis provided equilibrium conditions are maintained. Therefore, there is little to gain by using a large specimen other than the possibility of obtaining a more representative sample. Sample size selection is guided, therefore, by the optimum size of silica sample tubes for ease of fabrication with vacuum-tight welds. The specification of 0.5 ± 0.1 gram samples is made in the interest of maintaining a fairly constant geometric relationship between sample and sample tube.

Errors due to outgassing of the equipment have proved to be no problem. Normally the pressure rise, due to outgassing and leaks, in a 10-min period at room temperature is less than 0.5μ . Thus it appears that adsorbed gas remaining after evacuation of the glassware is tightly enough bound to preclude any considerable outgassing in the short analytical period. Blank determinations with empty sample tubes give a pressure rise of less than 1μ . This is due almost entirely to outgassing of the heated section of the sample tubes. A 1μ pressure rise corresponds to approximately 50 monolayers of adsorbed water on the walls of the sample tube. In an actual determination, the hot specimen getters a portion of any desorbed oxygen or nitrogen. The error introduced by desorption of water from the walls of the sample tube is of the order of 0.00015% hydrogen at the 0.0010% hydrogen level, 0.00005% at the 0.0025% level, and is entirely negligible at higher levels.

The determination as described is a measure of the hydrogen content of the metal plus any hydrogen retained as water after evacuation. Adsorbed water that cannot be removed by evacuation is negligible unless the sample has very high surface. Water associated with residual salts in sponge is another possible hydrogen reservoir but has been found to be negligible if the sponge has been properly vacuum distilled during manufacture.

Sample tubes can be heated to 1000°C in 6–7 min.

Establishment of equilibrium is very rapid. A total heating time of 10 min, i.e., 3–4 min at 1000°C, is specified to insure reproducible thermal conditions in the heated sample tube. Specimens held at temperature for times up to 30 min showed no drift in the equilibrium pressure.

It is important that the equilibrium pressure of samples be measured under the same thermal conditions for which the equilibrium curve was established.

The portion of the sample tube that is heated to 1000°C represents only about 0.5% of the total volume of the apparatus. Treating the apparatus as an isothermal unit for mathematical purposes is justified since the error introduced in doing so is very small.

The sample tube connections on the manifold may be any number between 1 and 20, depending on the volume of analyses to be performed.

Whether analytical results should be calculated by summation of $C_E + K (P_E/T_E S)$ or read directly from a % H vs. P_E plot (Fig. 4) is dependent on the uniformity of samples and the precision desired. For samples of low hydrogen content the relationship % H = C_E is valid within the accuracy of the method.

Experience has shown that an analyst familiar with the method can perform twenty analyses per day on a routine basis with a single apparatus.

This method is applicable to analysis of other metals for which an equilibrium hydrogen concentration-pressure relationship can be established.

ACKNOWLEDGMENT

The author wishes to thank Cortland Warrington of this laboratory who performed most of the equilibrium analyses and Frederick Walls, also of this laboratory, who performed the vacuum fusion analyses and prepared the line drawings.

Any discussion of this paper will appear in a Discussion Section to be published in the December 1955 JOURNAL.

REFERENCES

1. P. P. ALEXANDER, *Metals & Alloys*, **9**, 45 (1938).
2. C. M. CRAIGHEAD, G. A. LENNING, AND R. I. JAFFEE, *J. Metals*, **4**, 1317 (1952).
3. G. HAGG, *Z. physik. Chem.*, **B11**, 433 (1931).
4. H. HUBER, L. KIRSCHFELD, AND A. SIEVERTS, *Ber.*, **59**, 2891 (1926).
5. L. KIRSCHFELD AND A. SIEVERTS, *Z. physik. Chem.*, **A145**, 227 (1929).
6. A. D. MCQUILLAN, *Proc. Roy. Soc. (London)*, **204A**, 309 (1950).
7. A. D. MCQUILLAN, *J. Inst. Metals*, **79**, 371 (1951).
8. E. A. SCHNEIDER, *Z. anorg. Chem.*, **8**, 81 (1895).
9. C. WINKLER, *Ber.*, **23**, 2642 (1890).
10. C. WINKLER, *ibid.*, **24**, 873 (1891).
11. R. A. YEATON, *Vacuum*, **2**, 115 (1952), (published in 1953).

Influence of Impurities in the Electrolyte in Chlorine-Caustic Electrolysis by the Mercury Cell Process

IV. Investigation of the Influence of Metals on the Cathodic Current Efficiency¹

GÖSTA ANGEL, TAGE LUNDÉN, STIG DAHLERUS, AND ROLF BRÄNNLAND

Division of Applied Electrochemistry, Royal Institute of Technology, Stockholm, Sweden

ABSTRACT

An electrolysis cell for laboratory use with circulating brine and mercury was constructed. With this cell the effect of a number of metals upon cathodic current efficiency was studied, among which vanadium, molybdenum, chromium, and titanium proved to be the most harmful ones.

INTRODUCTION

In previous papers (1-3) results were reported from a number of experiments with NaCl solution contaminated with various metal salts and shaken with sodium amalgam. The purpose of those experiments was to investigate the influence of impurities on the amalgam decomposition rate. Results were expected to be of great value for predicting the effect of contaminations in a mercury cell with sodium amalgam cathode, even though conditions are quite different in the two cases.

However, results from amalgam decomposition experiments had to be confirmed by electrolysis experiments in order to provide the chlorine caustic industry with reliable information concerning the influence of various impurities. Thus, a mercury cell suited for laboratory scale electrolysis experiments had to be constructed. The laboratory cell, made by Walker and Paterson (4), was considered unsuitable because it used noncirculating mercury as cathode.

The object was to reproduce the construction and working properties of the industrial mercury cell as well as possible on a smaller scale. Consequently, the cell had to be long and the mercury layer comparatively thin. Calculations showed that, if the proper scale was used, the depth of mercury should be only 0.2 mm with 300 mm cell length, in order to give the same mercury flow rate as in full size. So thin a film is quite impossible to obtain in a glass apparatus; it is even difficult to obtain a coherent mercury layer thinner than 1-1.5 mm.

Furthermore, the cell temperature had to be about 70°C, corresponding to normal working temperature in industrial practice. Preparatory experiments in a cell consisting of a 400 mm glass tube showed that the heat generated by the cell resistance is far from sufficient to maintain this

temperature, so a preheater for the brine was provided.

DESCRIPTION OF CELL

The cell construction was unrestricted except that circulating mercury had to be used to obtain interpretable results, and for continuous operation it was necessary to supply fresh concentrated brine to the cell.

A basin-shaped glass cell (Fig. 1) was supplied with inflow tubes for mercury and brine. Mercury left the cell through a centrally placed overflow pipe. This was extended below the cell and there formed a lock, which prevented the brine from running off with the mercury.

Current was supplied to the mercury by a platinum wire. The anode consisted of a circular platinum sheet provided with a number of holes to facilitate escape of the chlorine. The cell could also be operated with a graphite anode to test various graphite properties.

The cell was closed by a rubber stopper which also carried the anode. Chlorine and spent brine left the cell through an outlet tube which opened at the lower surface of the stopper. There was also space for a thermometer and capillaries for polarization measurements.

The cell was safe in operation and extremely easily cleaned, which was of great importance in experiments with contaminated salt solutions. These experiments were often of comparatively short duration and required an exceedingly careful cleaning after each experiment to give reproducible results.

Auxiliary Equipment

A sketch of the complete apparatus is given in Fig. 2. Mercury ran from storage bottle A to a level

¹ Manuscript received May 12, 1952.

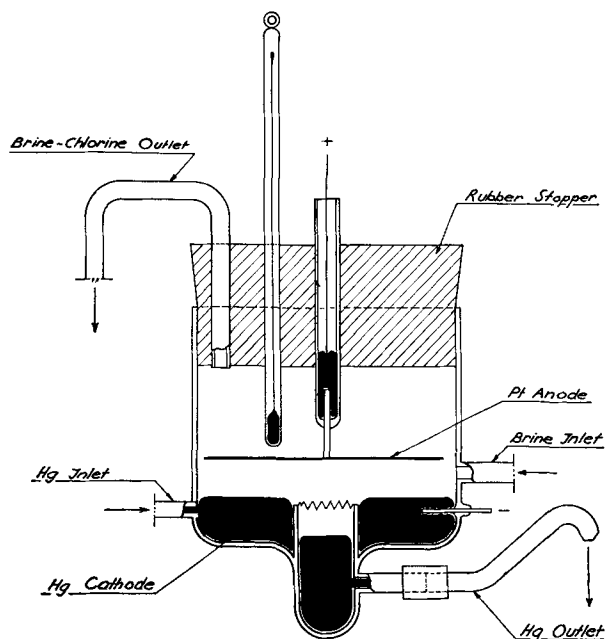


FIG. 1. Sketch of electrolysis cell

control B, and C regulated the flow of mercury to cell D. Because of the overflow pipe, the mercury column remained constant; hence mercury flow through the cell was also constant. The amalgam passed through the lock C and descended into the amalgam decomposer E, which was filled with about 2-mm pieces of graphite. Water was supplied through a glass tube to the lowest part of the graphite filled column and then ascended counter current to the mercury. Hydrogen and sodium hydroxide formed by the amalgam decomposition left the decomposer through a separate tube. The pure mercury passed through a tube F, was collected in a vessel, and covered with water. A mixture of mercury and water was pumped to storage bottle A, where excess water was removed by suction. This water treatment washed the mercury free from graphite particles from the decomposer. It was advantageous to add the water just in front of the pump, which emulsified the mercury in water, and the removal of graphite was complete.

The simple practical pump consisted of a rubber hose and a brass rotor, provided with four elastic rollers, also made of brass. Two rollers always pressed the hose, and in that way the pump effect was obtained. Consequently, the hose was made of thick, oil-resistant, synthetic material. It usually worked for about 100 hr, provided it was well lubricated with thick oil.

The brine ran from storage bottle G to the level control H, constructed on conventional principles. Brine flow to the cell was regulated by I, and constant flow was maintained by the control H, independent of the volume of solution in G.

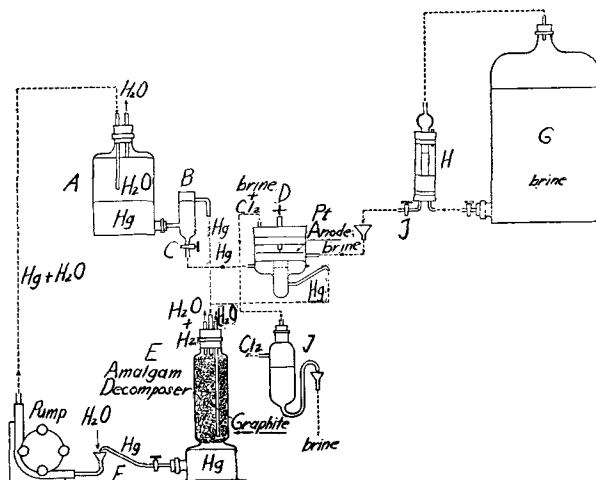


FIG. 2. Sketch of complete electrolysis apparatus

The spent brine and gases formed in the cell were removed together, then separated in the glass vessel J, which could be connected to a gas testing apparatus. The spent brine is not reused.

EXPERIMENTAL

In all experiments saturated brine (Merck's Analytical Reagent) was used, and small quantities of the substance to be investigated, i.e., 0.1–25 mg/l were added. The flow rate of brine was regulated so that about 15% of the salt was decomposed in the electrolysis cell, corresponding to 7.5 ml brine/min.

The flow rate of mercury was also kept constant at 8–10 ml/min, corresponding to a sodium content in the departing mercury of 0.13–0.10% at a current density of 25 amp/dm². This value was the usual one and corresponded to a cell current of 10 amp.

In most cases, the cell temperature was not externally regulated so, under the operating conditions mentioned above, a constant temperature of 38°–42°C was reached within 30 min. In some cases, however, when cathodic current efficiency was low, the equilibrium temperature was considerably higher.

Current efficiency was calculated from analyses of mercury departing from the cell and, in certain cases, from estimations of the hydrogen volume evolved per unit time.

The mercury analysis consisted of an addition of excess 0.1N sulfuric acid to 5 ml amalgam. When hydrogen evolution ceased, the solution was back titrated with 0.1N sodium hydroxide. The reaction could be conveniently accelerated by addition of a few drops of vanadate solution.

Cathodic current efficiency was estimated from analyses of the cell gas only when hydrogen evolution was small, i.e., when the current efficiency exceeded 95%. The calculation was made under the

assumption that hydrogen evolution was the only loss reaction at the cathode, which is probably the case at high current efficiencies. The two methods for determining current efficiency gave coinciding results, except for experiments with low current efficiencies, in which the gas analysis method gave values which seemed to be a little too high.

For analysis of the cell gas, a volume corresponding to about one minute of electrolysis was collected in concentrated sodium hydroxide in a gas burette. Finally, the volume of the hydrogen gas was recorded. In order to avoid errors due to varying brine volume in the cell, the brine circulation was interrupted during the analysis period. The mercury was, however, circulated continuously.

Before an experiment was started, the storage bottle was charged with 2–4 l saturated, filtered brine, which had been mixed with the impurity to be studied. After the cell was filled with brine and the correct flow rate reached, the current was switched on.

During the experiment the mercury and brine flow were repeatedly controlled. The analysis of departing mercury was made at suitable intervals. By observation of gas evolution at the cathode surface current efficiency could be approximately estimated. When it was seen that the current efficiency was changing rapidly, the amalgam or cell gas was analyzed as frequently as possible while, in other cases, analyses were performed at longer intervals.

After each experiment the apparatus was carefully cleaned and the electrolysis cell washed with concentrated hydrochloric acid and rinsed with distilled water.

The mercury was purified when it had been polluted with certain noble metals by shaking with soft paper. The polluting metals were oxidized and absorbed by the paper, after which it was filtered through a punctured paper cone. When this procedure had been repeated two or three times, the mercury was pure enough to be used again in electrolysis experiments.

The investigation included experiments with vanadium, molybdenum, chromium, titanium, magnesium, calcium, barium, aluminum, iron, nickel, copper, zinc, lead, arsenic, and manganese. These were assumed to occur, ordinarily or exceptionally, in industrial brines.

In order to test the apparatus, a great number of experiments with pure sodium chloride solutions were performed, giving an average current efficiency of 98.5–99.2%.

Vanadium.—Previously (1–3) vanadium proved to be one of the most harmful metals; hence it was more thoroughly investigated than other impurities.

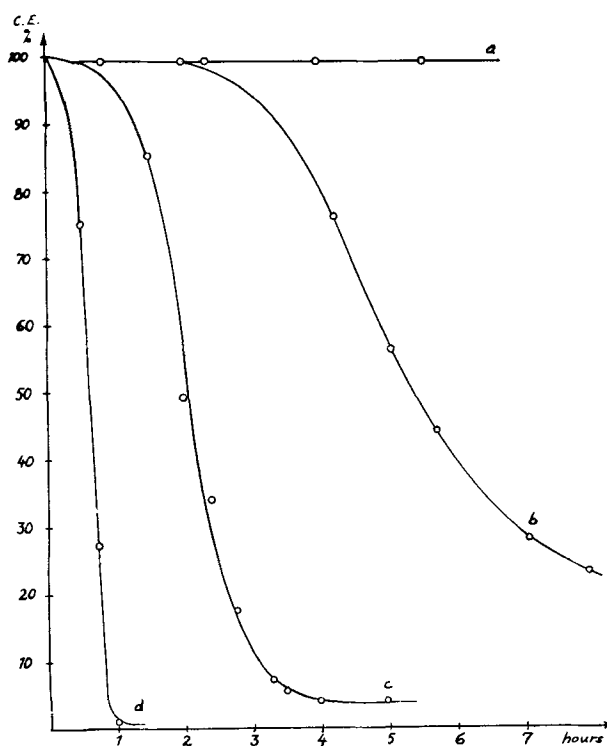


FIG. 3. Current efficiency in presence of vanadium. Curve a, 0.1 mg/l V; curve b, 0.25 mg/l V; curve c, 0.5 mg/l V; curve d, 1.7 mg/l V.

Reproducibility of these experiments was not so good, and many of them had to be repeated several times. Fig. 3 shows some representative current efficiency curves from experiments with vanadium concentrations, ranging from 1.7 to 0.1 mg/l in the brine supplied.

In all of these experiments the mercury surface was partly covered with a "gas spot," from which the gas emanated. The size of this spot grew as the current efficiency decreased, and finally covered the cathode completely. (The current efficiency had then usually decreased to 4–5%.)

In most experiments, part of the spot occasionally flaked off and departed from the cell with the mercury. This may explain the lack of reproducibility.

The experiments show that vanadium greatly reduces cathodic current efficiency. The higher the vanadium concentration, the greater the decrease. With 1.7 mg/l vanadium practically only hydrogen gas is formed, whereas with 0.1 mg/l vanadium no decrease in the current efficiency can be observed even after 7 hr.

A few additional experiments with a single (non-recurrent) addition of a certain quantity of vanadium (as sodium metavanadate solution) to the pure brine were performed in order to make clear whether the action of a certain quantity of vanadium was

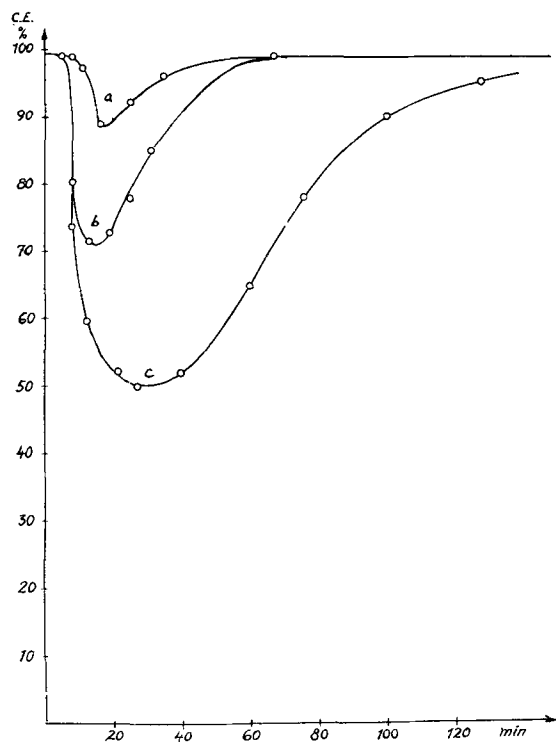


FIG. 4. Current efficiency after addition of a certain quantity of vanadium. Curve a, 0.05 mg V; curve b, 0.1 mg V; curve c, 0.2 mg V.

permanent or if it ceased when the supply of vanadium to the cell was cut off.

Results of these experiments are demonstrated by curves in Fig. 4 and show that vanadium does not remain very long in the electrolysis cell. The problem of whether its removal can be performed by successive replacement of vanadium-containing brine with pure brine or by deposition of metallic vanadium at the mercury surface cannot be definitely solved by these experiments, but will be discussed later.

There is, however, some evidence that the "gas spots," mentioned previously, consist of interfering metals in the reduced form and that vanadium is thus removed from the cell with the mercury. In the latter experiments, the mercury circulation rate was about 3.5 times the usual one, i.e., 28 ml/min, in order to facilitate any possible mechanical removal of vanadium. The brine supply rate was maintained at 7.5 ml/min.

Molybdenum.—In industrial brines molybdenum will probably not occur ordinarily, but as a complement of the amalgam decomposition experiments, this metal was also investigated. Results are represented in Fig. 5.

The curves show that molybdenum also caused a considerable hydrogen evolution in the electrolysis experiments.

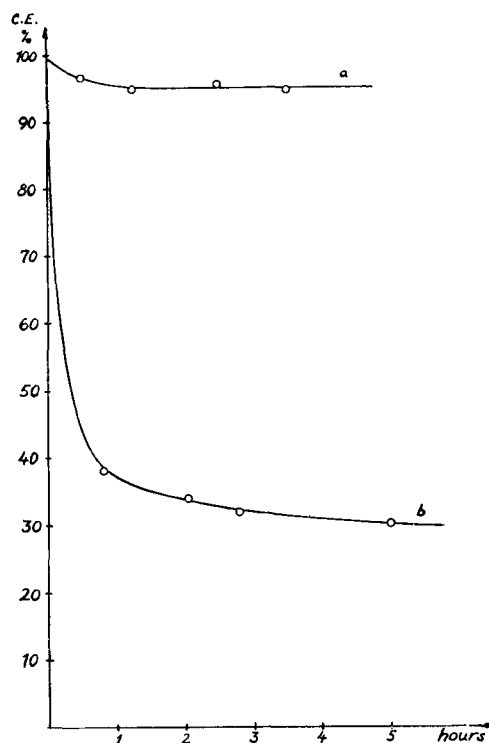


FIG. 5. Current efficiency in presence of molybdenum. Curve a, 0.5 mg/l Mo; curve b, 1.5 mg/l Mo.

In these experiments also gas evolution was found to take place at one spot on the mercury surface.

Chromium.—In the previous amalgam decomposition experiments, it was found that chromium belongs to the same group of harmful metals as vanadium but that its influence depends on the pH. In alkaline solutions chromium is very harmful, while in acid solutions the influence is moderate. It may be expected, therefore, that chromium causes comparatively small gas evolution at first, when the brine is slightly acid, but that the influence is greater with pH increase of hydrogen ion deposition.

Chromium was added as chromium sulfate. Results are represented in Fig. 6. The curves show that chromium strongly decreases the cathodic current efficiency, and that even 0.25 mg/l Cr has a considerable influence.

So it may be concluded that vanadium, chromium, and molybdenum cause a very great reduction of the cathodic current efficiency. Thus, results gained from the amalgam decomposition experiments are fully verified by the electrolysis experiments. It is also remarkable that all of these metals, at least in moderate concentrations, cause hydrogen evolution from only a limited part of the cathode surface.

Titanium.—In the amalgam decomposition experiments (1-3), titanium caused a somewhat increased decomposition rate. In the electrolysis experiments this metal behaved very remarkably.

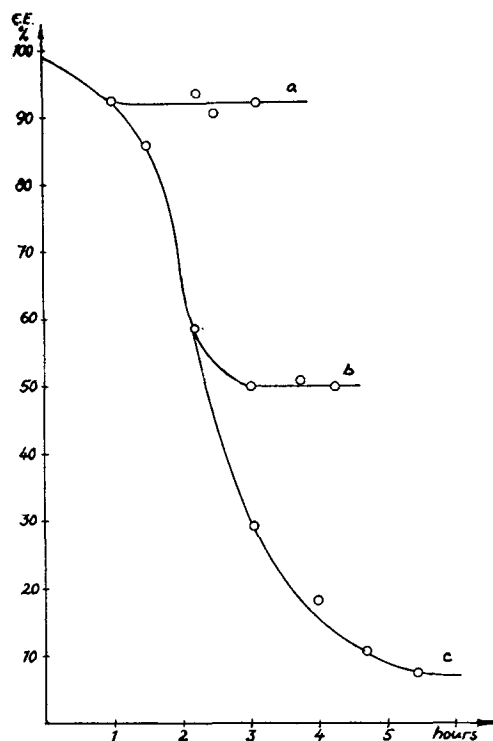


FIG. 6. Current efficiency in presence of chromium. Curve a, 0.25 mg/l Cr, curve b, 0.5 mg/l Cr; curve c, 1.5 mg/l Cr.

As soon as the current was switched on, the cathode was covered with small gas bubbles. With higher concentrations of titanium, a dark spot was formed at which the gas evolution took place. After a few minutes the spot diminished in size, and after about 15 min of electrolysis the cathode was quite bright again and current efficiency had been restored to 98–99%. Current efficiency curves for 0.1, 1, and 5 mg/l Ti are shown in Fig. 7.

Titanium in concentrations of 1–5 mg/l caused still another effect. When the brine flow rate was increased ten times, a dark spot appeared in a few minutes. The surface was soon completely covered simultaneously with a decrease of the current efficiency to about 30%. When the normal brine circulation rate was restored, the spot disappeared, and the cathode was again bright in a few minutes.

This effect was not obtained with vanadium (0.1 mg/l) or aluminum (5 mg/l).

Magnesium.—In concentrations below 25 mg/l magnesium did not interfere with amalgam decomposition (1–3), but in the electrolysis experiments some interesting observations were made. In the presence of magnesium at concentrations above 5 mg/l, current efficiency was slightly decreased from about 98.7% to about 97.1%. During electrolysis, a thin layer of hydroxide or possibly a mixture of hydroxide and magnesium amalgam was formed at the cathode surface. In this case, hydrogen

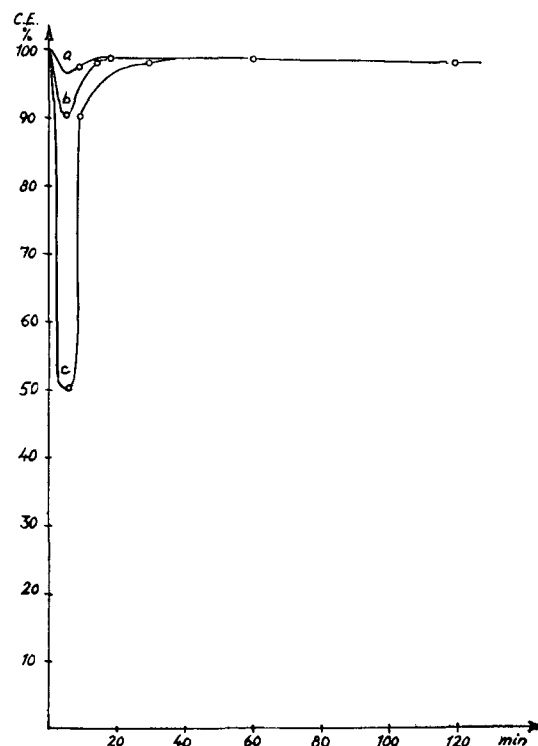


FIG. 7. Current efficiency in presence of titanium. Curve a, 0.1 mg/l Ti; curve b, 1.0 mg/l Ti; curve c, 5.0 mg/l Ti.

evolution did not occur at a single spot, but was distributed over the whole of the mercury surface.

Furthermore, mercury circulation was, in many cases, disturbed in such a way that amalgam accumulated in the cell, thus giving a seemingly strong decrease of the current efficiency. After a certain time the film was partly destroyed and removed from the cell. Current efficiency then seemed to be greater than 100%. Fig. 8 shows a typical current efficiency curve which is based on amalgam analyses. The cell gas analyses, however, showed an approximately constant value of about 97%.

Calcium.—In amalgam decomposition experiments, calcium had no influence at concentrations up to 25 mg/l. Electrolysis experiments confirmed this result, and 10 mg/l Ca in the brine caused no decrease of current efficiency within 3 hr.

Barium.—With barium the same result was obtained; 10 mg/l Ba did not affect current efficiency.

Aluminum.—It was found that aluminum accelerated amalgam decomposition (1–3). Also, in electrolysis experiments, hydrogen gas evolution occurred, and immediately after the start of an experiment, small gas bubbles were formed all over the mercury surface. A few minutes later a dark spot appeared, at which the gas evolution was concentrated. The spot grew very quickly and soon covered the whole cathode surface. However, after about 15 min of electrolysis gas evolution decreased again, and after half an hour it had ceased com-

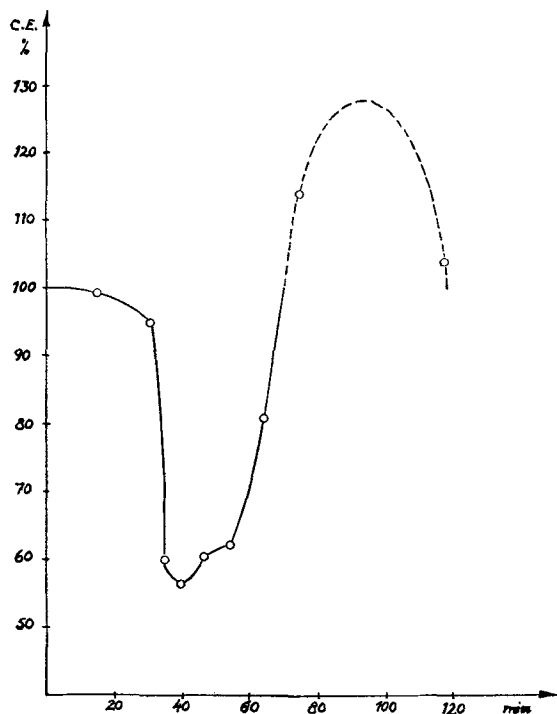


FIG. 8. Current efficiency in presence of 5 mg/l magnesium as indicated by amalgam analyses.

pletely. The mercury cathode was then quite bright, and the current efficiency was 98–99%.

The same cycle was repeated about 15 min later, as shown in Fig. 9. Reproducibility was not very good, but the tendency is quite clear. The experiments show that current efficiency is decreased by aluminum in concentrations greater than 1 mg/l. Thus the metal must be regarded as harmful, although not belonging to the same class as vanadium.

Iron.—In amalgam decomposition experiments, iron was found to affect the decomposition rate very slightly. Electrolysis experiments also showed that iron has no influence on cathodic current efficiency when the iron concentration does not exceed 10 mg/l.

Nickel.—In concentrations below 25 mg/l this metal had no influence on current efficiency.

Copper.—In concentrations below 10 mg/l, copper proved to have no effect on cathodic current efficiency in electrolysis experiments of normal duration. However, the metal was not oxidized in the amalgam decomposition tower, but was accumulated in the mercury system, thus giving rise to disturbances when the comparatively low solubility limit had been reached and pure copper was deposited at the cathode.

Zinc.—With 25 mg/l Zn in the brine the current efficiency was 98.9–99.3%, which is in good agreement with amalgam decomposition experiments.

Lead.—In concentrations below 25 mg/l, this

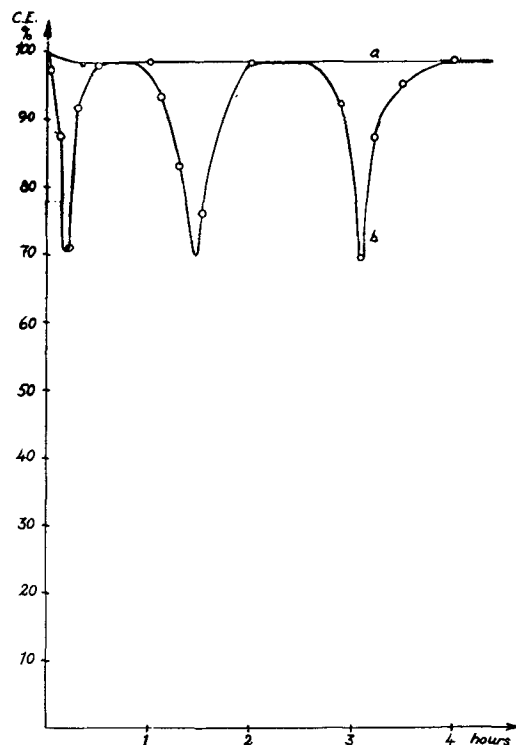


FIG. 9. Current efficiency in presence of aluminum. Curve a, 1 mg/l Al; curve b, 25 mg/l Al.

metal had no direct influence on current efficiency. It should be noted, however, that lead salts are able to precipitate certain harmful metals, such as vanadium, molybdenum, and chromium, and may therefore be used for purification of brines containing these metals (5).

Arsenic.—The influence of arsenic was studied in concentrations up to 25 mg/l. No decrease of the current efficiency was observed, although this metal had previously been proved to interfere with the amalgam decomposition.

Manganese.—With sodium chloride solutions containing 5–25 mg/l manganese, current efficiency was even somewhat higher than normal, 99.3–99.8%. In the electrolysis, Mn^{2+} was oxidized to MnO_2 which was deposited at the anode and increased the cell voltage.

SUMMARY

A mercury cell with circulating brine and circulating mercury is described, and results from a series of experiments with this cell are reported. It has been shown that:

1. Vanadium, molybdenum, chromium, and titanium cause very strong hydrogen gas evolution and thus decrease cathodic current efficiency considerably.

2. Magnesium and aluminum interfere with

cathodic reactions and may decrease current efficiency.

3. Calcium, barium, iron, nickel, copper, zinc, lead, arsenic, and manganese have no influence upon the cathodic current efficiency when they are in low concentrations and not mixed with other metals.

ACKNOWLEDGMENTS

This investigation was promoted by a grant from Elektrokemiska AB, Bohus; Mo och Domsjö AB, Örnsköldsvik; Svenska Cellulosa AB, Sundsvall;

and Uddeholms AB, Skoghall, for which the authors wish to express their deep appreciation.

Any discussion of this paper will appear in a Discussion Section to be published in the December 1955 JOURNAL.

REFERENCES

1. G. ANGEL AND T. LUNDÉN, *This Journal*, **99**, 435 (1952).
2. G. ANGEL AND R. BRÄNNLAND, *ibid.*, **99**, 442 (1952).
3. G. ANGEL, T. LUNDÉN, AND R. BRÄNNLAND, *ibid.*, **100**, 39 (1953).
4. J. W. WALKER AND C. S. PATERSON, *Trans. Am. Electrochem. Soc.*, **3**, 185 (1903).
5. G. ANGEL AND T. LUNDÉN, Swedish Pat. 133,866, Dec. 11, 1951.

Electrochemical Behavior of a Titanium-Fused Salt-Platinum Cell¹

M. E. STRAUMANIS AND A. W. SCHLECHTEN

Department of Metallurgical Engineering, University of Missouri, School of Mines and Metallurgy, Rolla, Missouri

ABSTRACT

The cell, Ti/NaCl or KCl fused/Pt at temperatures above 800°C and in air, displays a substantial open-circuit potential difference of 1.40–1.53 v. In vacuum or under an inert gas the difference is approximately 0.5 v, and the current that can be drawn from such a cell is low. Air, oxygen, and water vapor act as cathodic depolarizers, maintaining a positive potential of the cathode and an appreciable current if the cell is short circuited. The reaction occurring in the cell is $\text{Ti} + 4\text{NaCl} + \text{O}_2 = \text{TiCl}_4 + 2\text{Na}_2\text{O}$. Alkali oxides are produced on the cathode if a salt containing Ti ions is electrolyzed in presence of air. Under an inert gas the discharge of alkali ions hampers the deposition of Ti, which is then produced in the form of a powder, and possibly as the result of a secondary reaction wherein it is reduced by the alkali metals.

INTRODUCTION

It is well known that it is extremely difficult to deposit titanium even from molten salt baths with an external current; the metal may be deposited under an inert atmosphere in the form of powder, flakes, or as a very thin layer (1), but no deposition is observed if air (oxygen) is present to any appreciable extent.

It would be of value to know the reasons for this behavior, and to determine the action of air and moisture during electrolysis. Such knowledge might furnish clues to the successful solution of the problems of the electrodeposition of titanium.

One of the obstacles to the electrodeposition of titanium in the presence of air is the high susceptibility of this metal to oxidation, and to corrosion in molten salts at elevated temperatures (2). Titanium, if deposited on the cathode, may disperse in the molten salt because of pyrosol formation, thus retarding the deposition process. However, it is doubtful if pyrosol formation is the chief deterrent to the deposition of the metal, especially if the cathode is capable of forming a solid solution with titanium. The fact that, in the presence of air or moisture, no titanium is cathodically deposited points toward other electrochemical or chemical events which hamper electrodeposition.

The behavior of the cell Ti/fused salt/Pt in various gases and in the presence of water vapor gives some answers to the problems of deposition.

¹ Manuscript received May 4, 1954. This paper was prepared for delivery before the Chicago Meeting, May 2 to 6, 1954. This paper is based on a portion of the work carried out at the Missouri School of Mines and Metallurgy for the Wright Air Development Center under Contract No. AF 33(616)-75.

EXPERIMENTAL PROCEDURE

A preliminary experiment showed that a cell consisting of titanium and platinum electrodes immersed in molten sodium chloride produced a fairly strong current if the electrodes were short circuited through a milliammeter. The direction of the current indicated that titanium went into solution acting as an anode with the platinum as the cathode.

In order to explore this phenomenon in detail a cell was constructed which made it possible to accumulate separately the anodic and cathodic reaction products for subsequent analysis. Copper tubing was also provided for introducing gases and steam into the cathodic compartment. The arrangement is shown in Fig. 1. Air had access to the crucible in the furnace, although a loose cover was made from a piece of fire resistant brick.

To determine the influence of air (oxygen), arrangement was made to heat the crucible C (Fig. 1) in vacuum or in an inert gas, and simultaneously to measure the emf of the open cell or the current delivered by a closed cell. This was accomplished by placing the crucible together with the electrodes and salt in a quartz glass tube, as shown in Fig. 2. The lower part, C, of this apparatus was placed into the furnace (Fig. 1).

The operating procedure was as follows: the temperature of the furnace was raised to 880°C or higher to melt completely the salts, and then lowered to the working temperature of 850° or 800°C, which is above the melting point of the 50–50 mole per cent KCl–NaCl mixture. Some runs were made in pure sodium chloride and some in pure potassium chloride. Measurements of the emf of the Ti/molten salt/Pt cell were continued until this force became approximately constant. Then the switch, S, (Fig. 1)

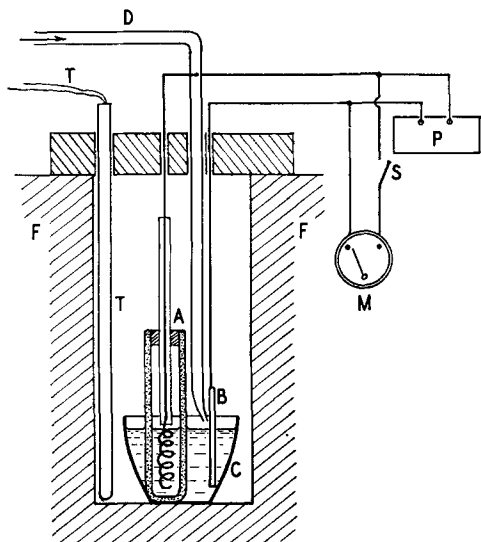


FIG. 1. Arrangement of the Ti/salt/Pt cell for emf and current measurements. (A) Ti wire anode in a porous Al_2O_3 thimble with the top open or closed; (B) Pt cathode (3 cm^2); (C) porcelain crucible containing alkali salt or mixture of salts; (D) copper tubing for gas introduction; (F) resistance furnace; (M) milliammeter; (P) potentiometer; (S) switch; (T) thermocouple.

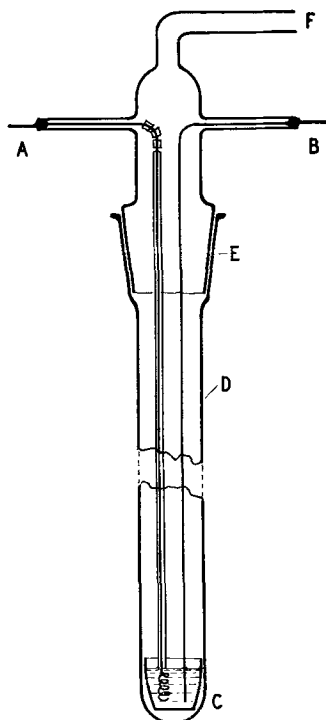


FIG. 2. Arrangements of the Ti/fused salt/Pt cell for emf and current measurements under a protective atmosphere. (A, B) Leads to potentiometer or milliammeter; (C) crucible with salt bath; (D) tube of quartz glass; (E) joint; (F) connection to vacuum and gas supply.

was closed, and the current produced by the cell was registered. After the cell had operated for several hours, the circuit was disconnected, the thimble, A (anodic compartment, Fig. 1), removed from C,

and the furnace cooled down. The salts of the anodic and cathodic compartments were separately dissolved in water and the solutions were analyzed as to their content of acid and of base. Methyl orange was used as indicator.

For experiments with inert gas atmospheres, such as hydrogen, nitrogen, and helium, the air was first pumped out of the tube (Fig. 2) and then the commercially pure inert gas was admitted. Moisture was removed from all of the gases, but the traces of residual oxygen were removed only from the hydrogen by means of a catalyst.

RESULTS

Electromotive force of the cell.—Measurements of the potential difference (emf) of the cell Ti/molten KCl/Pt were made in air and continued until this difference became approximately constant. Then the temperature was changed in order to establish the relation between the emf and the temperature. Some of the runs are listed in Table I. The table shows that the cell displays an emf of about 1.48 v at 900°C . The potential fluctuated during all of the experiments, but finally a fairly constant value (actually slowly decreasing) was established at a given temperature. There seems to be no relation between temperature and emf; usually the emf increased slowly from the beginning of the experiment up to a maximum value and then decreased slowly.

The values for the emf in a 50-50 mole per cent mixture of sodium and potassium chloride were approximately the same, reading about 1.48 v at 800°C . In pure sodium chloride they were somewhat lower, approaching 1.46 v at 950°C . All of these potential measurements represent open-circuit

TABLE I. Potential differences as shown by the cell Ti-Pt (open circuit) in molten KCl in presence of air

Time, min	Run No. I		Run No. III		Run No. V	
	Temp, $^\circ\text{C}$	Emf in v	Temp, $^\circ\text{C}$	Emf in v	Temp, $^\circ\text{C}$	Emf in v
0	900	—	1000	1.516	850	1.39
10	900	1.42	1000	1.518	—	—
20	900	1.45	1000	1.521	870	1.43
30	900	1.49	1000	1.520	—	—
40	900	1.48	950	1.527	900	1.44
50	920	1.48	950	1.524	—	—
60	900	1.48	950	1.522	—	—
70	900	1.49	950	1.521	—	—
80	900	1.49	950	1.517	—	—
100	—	—	950	1.515	910	1.48
160	—	—	950	1.484	900	1.47
180	—	—	850	1.496	—	—
200	—	—	850	1.468	—	—
220	—	—	850	1.453	900	1.48
270	—	—	850	1.441	—	—
280	—	—	800	1.403	900	1.45
325	—	—	800	1.301	—	—

TABLE II. Potential difference produced by the cell Ti/KCl, NaCl (molten)/Pt at 800°C in nitrogen and vacuum. Open-circuit values

Time, min	Gas	Emf in v
0	N ₂	0.42
5	N ₂	0.60
10	N ₂	0.58
15	N ₂	0.57
20	Vacuum	0.59
25	Vacuum	0.63
30	Vacuum	0.62
35	Vacuum	0.49
40	N ₂	0.55
50	N ₂	0.45

values. If a current was drawn from the cell, the emf dropped immediately (measured after opening the circuit), but started to increase slowly as long as the circuit was open and the temperature was constant, finally in several hours attaining the values mentioned above.

The emf as developed by the cell in an inert atmosphere or vacuum was much lower (Table II), and fluctuated between 0.45 and 0.60 v. Experiments in vacuum could not be continued for very long because the salt evaporated quickly from the crucible. Therefore, the remaining experiments were made using nitrogen under slight pressure (about 100 mm Hg); the cell developed approximately the same emf as listed in Table II. Replacing the nitrogen with helium or hydrogen gave essentially the same results. In the case of helium a greater emf was developed by the cell; evidently the helium contained some oxygen which was not removed prior to the experiments. The lowest emf of the cell, 0.35–0.50 v, was observed using hydrogen from which the oxygen had been removed. All of this indicates that the presence of air (oxygen) was necessary for the emf to appear. However, traces of water present in the salts can also cause an emf, as shown below.

Current produced by the cell. As soon as the switch S (Fig. 1) of the Ti/molten salt/Pt cell was closed, such a strong current was developed in the first moments that it usually could not be measured by the instruments in the circuit. In a few seconds the current dropped abruptly, and slowly approached a fairly constant value, although it always fluctuated somewhat (Fig. 3). The sudden drop of the current is, of course, typical for a cell displaying polarization phenomena at the electrodes.

After the cell had been operating for a certain time, the circuit was opened and the furnace cooled. The salt from the anodic and cathodic compartments was removed, and separately dissolved in water. Qualitative tests showed that the solution obtained from the salt of the anodic compartment was strongly acidic, while that of the cathodic compartment was

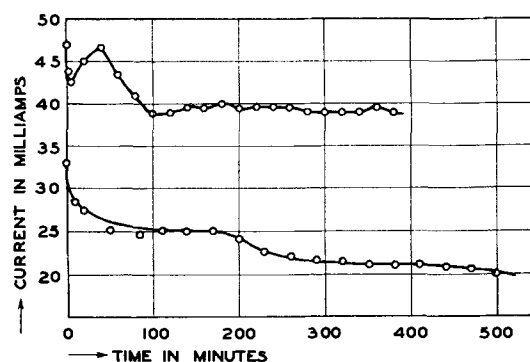


FIG. 3. Current developed by the cell Ti/molten NaCl, KCl/Pt vs. time at 800°C. Upper curve, Pt crucible as cathode; lower curve, a Pt sheet of 2 cm² as a cathode, electrode distance approximately 1 cm.

basic. A series of quantitative determinations was made in order to establish the amount of acid and base produced by the working cell.

The number of milliamperere minutes delivered by the cell were determined from graphs such as shown in Fig. 3, and from this were calculated the equivalents of metal going into solution in the anodic compartment as well as the deposition in the cathodic compartment. Because the electrolyte was usually a mixture of sodium and potassium chloride, only the equivalents or milliequivalents produced could be calculated (1608 ma min to correspond to one millieq.). The amount of acid and base produced by the working cell was determined by titration of the aqueous solutions of the salts of the separate compartments, and was compared with the calculated results based on the milliamperere minutes which flowed through the circuit. Results are summarized in Table III.

Table III shows clearly that acid and base are formed in appreciable amounts in the anodic and cathodic compartments, varying from 44 to 74% of the value as calculated from the current of the cell. The fact that the base and acid generated is appreciably lower than the theoretical value can be attributed to diffusion of reaction products through the porous alundum diaphragm so that partial neutralization occurred and, as a consequence, a smaller amount of base and acid was titrated. The fact that the amount of acid or base (Table III) is not equal is discussed later.

A series of qualitative experiments were made to determine the mechanism responsible for production of potential and current in the cell. It was found that the magnitude of the current obtained was dependent upon the presence of oxygen, similar to the results shown in Table II for emf of the open-circuit cell. At 800°C the cell delivered 35–40 ma; if the quartz tube containing the cell was evacuated, the current dropped to 0.27 ma or less. Upon ad-

TABLE III. Acid and base produced by the working Ti/molten salt/Pt cell in millieq.

Run No.	Salt	Millieq. calc. (from current)	Acid in millieq. anodic comp.	Base in millieq. cathodic comp.	Ratio of millieq. titrated to millieq. calculated
II	NaCl-KCl	1.18	0.37	0.51	0.51/1.18 = 0.44
Ia	NaCl-KCl	3.5	—	1.76	0.50
III	NaCl-KCl	7.35	3.45	5.05	5.05/7.35 = 0.69
IV	NaCl-KCl	9.55	5.24	6.0	6.0/9.55 = 0.63
6	KCl	4.65	1.91	2.81	2.81/4.65 = 0.60
7	KCl	2.29	1.12	1.68	1.68/2.29 = 0.74
9	NaCl	3.14	0.87	1.46	1.46/3.14 = 0.47

mission of air, again the current increased by a factor of 100 or more. This cycle could be repeated only a limited number of times, because the salt evaporated from the crucible when the vacuum was applied. However, alternate cycles of air and nitrogen gave, respectively, high and low currents for many repetitions. It seemed quite evident that oxygen acted as a depolarizer, maintaining by its presence the emf of the working cell. The action of other neutral gases was similar to that of nitrogen; they all decreased the current produced by the cell as soon as they displaced the air. However, in a hydrogen atmosphere the cell showed (at 800°C) a potential difference of only 0.35–0.50 v, but the current produced was somewhat higher than in nitrogen or vacuum; it fluctuated around 4 ma, but sometimes dropped to zero and became negative, which indicated that platinum went into solution. It may be that this behavior of titanium in a hydrogen atmosphere has some relation to the formation of titanium hydrides. The titanium was brittle after the experiments.

To check once more the depolarizing action of oxygen, it was introduced through a Vycor glass tube into the furnace (Fig. 1) so that the gas stream impinged on the platinum cathode. Immediately a current was observed with up to 4 times the value observed in air, indicating a pronounced depolarizing effect. Upon decreasing the oxygen stream, the current decreased also. However, it was necessary to prove whether the strong current observed on introducing oxygen was actually due to the depolarizing action at the cathode, or simply the result of stirring the electrolyte with the gas stream. If stirring caused the increase of current, then it could be expected that a nitrogen stream introduced near the cathode would also increase the strength of the current delivered by the cell. However, a nitrogen stream on the cathode caused a decrease of the current until it became even less than it was in air. Therefore, the effect of stirring of the bath was far below the effect caused by the chemical action of oxygen. In experiments with the nitrogen stream the

current did not drop to values as low as those observed in the experiments using inert gas atmospheres because of the oxygen still present. In the furnace (Fig. 1), the oxygen was only diluted by the nitrogen stream, but not completely displaced.

Many chemical reactions are influenced by water vapor even when only traces of vapor are present. To check this possibility, water vapor was introduced into the crucible of Fig. 1 through the tubing, D. The effect of the water vapor was quite impressive and resulted in currents which sometimes exceeded those generated in the presence of oxygen. Water vapor acted as a strong depolarizer.

In all experiments in which the current produced by the cell or the potential difference of the open cell was measured, it was impossible to say where the polarization or depolarization of the working cell occurred, whether on the anode or cathode, or on both electrodes simultaneously. Because of experimental difficulties and the lack of good reference electrodes (3) for temperatures close to 900°C, no attempts were made to measure the single potentials of the electrodes. However, an attempt was made to get an answer in an indirect way. For this purpose the titanium anode was completely encased in an alundum thimble by sealing its top with alundum cement and asbestos wool. Thus, the oxygen access to the anode was very limited. Oxygen, nitrogen, and steam were admitted alternately into the furnace (Fig. 1) near the cathode and the milliam-

TABLE IV. Depolarizing effect of oxygen and steam on the Ti/NaCl/Pt cell at 900°C

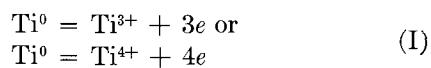
Ti anode was encased in a coarse grained alundum thimble. Time indicates the period after closing the circuit, and the moments at which the operations indicated are performed.

Time, min	Gas admitted	Current, ma
20	Air	85
25	N ₂ in	25
27	N ₂ off	85
30	O ₂ in	150
33	O ₂ off	120
39	N ₂ in	75
41	N ₂ off	110
45	O ₂ in	150
47	O ₂ off	120
49	N ₂ in	90
51	N ₂	80
53	N ₂ off	107
60	Steam in	170
61	Steam off	150 to 130
66	N ₂ in	100
68	N ₂ off	135
69	O ₂ in	150
70	O ₂ off	125
71	N ₂ in	90
76	Steam in and so on	150

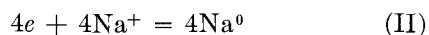
meter readings were observed. The qualitative results obtained are shown in Table IV. It should be remembered that in such an experiment the current with admitted nitrogen never dropped to zero because the nitrogen only diluted the oxygen present in the furnace, as already mentioned. Nevertheless the experiment showed quite well the influence of the steam and oxygen. Table IV shows that a remarkably strong current can be drawn from the small cell for a period of several hours. The effect of oxygen, steam, or nitrogen on the current is decisive and appears immediately. For example, if the nitrogen stream is discontinued, the current increases immediately because of the action of the oxygen still present in the furnace. The same effects were produced with a titanium anode encased in a fine grained thimble, except that the current delivered by the cell was smaller because of the resistance of the alundum thimble walls. A comparison of these results with those obtained with an open anodic compartment shows that there was no difference in the general behavior of the cell, except that the current produced was more regular than with an open thimble (Fig. 3) and there was less titanium pyrosol in the closed thimble. Therefore, polarization and depolarization occurred mainly on the platinum cathode, and with a high speed.

DISCUSSION

There seems to be only one way to explain the behavior of the Ti/fused salt/Pt cell without contradictions. It has to be assumed that the titanium anode going into solution in the fused salt bath as Ti^{3+} or Ti^{4+} ions (in the presence of oxygen at the high temperature the oxidation of Ti^{3+} to Ti^{4+} would occur anyway) is the source of energy. Therefore, the anodic process is (4):



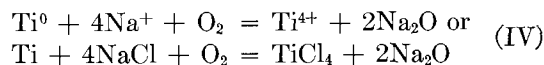
The electrons liberated pass into the platinum cathode, and attract the positive ions, which can only be the sodium or potassium ions. However, these ions can be discharged only in a limited amount to form a very thin alkali metal layer on the platinum cathode because the potential of the titanium is insufficient for a continuous reduction of alkali ions. Formation of such layers has been discussed previously (5). Under these conditions, only an insignificant fem is developed by the cell. The situation changes as soon as oxygen has access to the cathode; the electrons at the cathode can now be discharged at a fast rate by



because another cathodic energy delivering process is occurring:



Sodium peroxide may be also formed. The final process occurring in the cell during its operation is the sum of (I), (II), and (III):



Titanium displaces the sodium from the sodium chloride melt, and the sodium is oxidized by the oxygen of the air. Of course, a still better cathodic depolarizer is pure oxygen or water vapor; the latter reacts violently with the sodium with liberation of hydrogen. However, the presence of hydrogen could not be proved because of the high temperature; the platinum cathode would act as a catalyst in burning the hydrogen to water. Thus, oxygen or water vapor further the rate of reaction (II) and consequently increase the emf and the current of the cell. The reaction products, Na_2O and $TiCl_4$, dissolve in the salt of the cathodic and anodic compartments. No increase in weight of the platinum cathode after the experiments was observed, but it suffered from corrosion, especially in baths containing potassium chloride.

Thermodynamic calculations are difficult to apply, because the electrodes of the cell are not in equilibrium with the salt melt. However, very approximate estimations, taking into account the high concentration of the salt in the bath and the fact that at least in the beginning of the experiment the concentration of titanium ions is nearly zero, showed that reaction (IV) is thermodynamically possible.

Upon dissolution of the salt of the anodic and cathodic compartments separately in water, the titanium chloride hydrolyzes in water to give an acidic reaction, while the sodium oxide of the cathodic compartment gives the basic one. It follows from $Ti^{4+} + 4H_2O = Ti(OH)_4 + 4H^+$ and reactions (I) and (II) that the amounts of acid and base produced should be equal, regardless of whether Ti^{3+} or Ti^{4+} ions are formed. The lesser amount of hydrochloric acid actually obtained (Table III) can be explained by the partial evaporation of $TiCl_4$ during the experiment. Diffusion of the acidic and basic reaction products through the wall of the thimble during the runs and mutual neutralization after the dissolution in water explain the lesser amount of base or acid obtained as calculated from the current.

Encasing the anode did not influence the effects observed. So oxygen, steam, and nitrogen affect only the processes occurring on the cathode. No

attempt was made to determine the degree of anodic or cathodic polarization by direct determinations (3).

CONCLUSIONS

The experiments showed that in the presence of air, alkali oxides were produced on the cathode of a galvanic cell Ti/fused salt/ Pt by the emf of the titanium itself. If the same cell is now used for electrolysis by applying an external current and with titanium as the anode, alkali oxides will be formed on the cathode. This will happen even in the presence of titanium cations, because the formation of alkali oxides occurs at a lower potential than required for the discharge of Ti^{4+} , as shown by the cell experiment. Hence no titanium can be deposited on the cathode because of this reason (other reasons are mentioned in the introduction).

Discharge of alkali cations on the cathode may also occur under an inert gas atmosphere, especially when the concentration of the titanium salt in the bath is low. Hence the discharging alkali ions will hamper deposition of titanium in the regular growth of the deposit, and formation of titanium powder will be favored. Furthermore, it may be that formation of titanium powder is also due to reduction of titanium ions by the electrolytic alkali metal formed (6). The possibility that titanium powder is formed through secondary reactions such as $Ti^{4+} + 4Na = Ti^0 + 4Na^+$ is supported by observations on deposition of aluminum from cryolyte baths where, if the current is too strong (the voltage applied is too high, or the concentration of Al_2O_3 in the bath is too

low), alkali metals are discharged together with aluminum.

If the concentration of metallic titanium particles in the interface of the cathode during the electrolysis and the temperature is high enough, alloy formation with the cathode by direct contact of the particles may occur, as discussed in another article (7).

Of course, direct cathodic deposition of titanium is not excluded if the concentration of titanium salt in the bath is sufficiently high.

ACKNOWLEDGMENT

The authors are grateful to the Wright Air Development Center for continued support of this work and permission to publish the results obtained. Acknowledgment must be made to Dr. S. T. Shih for assistance on this particular phase of the project.

Any discussion of this paper will appear in a Discussion Section to be published in the December 1955 JOURNAL.

REFERENCES

1. G. D. P. CORDNER AND H. W. WORNER, *Australian J. Appl. Sci.*, **2**, 365 (1951).
2. C. B. GILL, M. E. STRAUMANIS, AND A. W. SCHLECHTEN, *This Journal*, **102**, 42 (1955).
3. See, for instance, A. ÖLANDER, *Z. physik. Chem. A.* **163**, 107 (1933); **164**, 428 (1933).
4. M. E. STRAUMANIS AND P. C. CHEN, *This Journal*, **98**, 234 (1951).
5. M. E. STRAUMANIS AND C. C. FANG, *ibid.*, **98**, 9 (1951).
6. P. DROSSBACH, *Z. Elektrochem.*, **57**, 548, 557, 558 (1953).
7. A. W. SCHLECHTEN, M. E. STRAUMANIS, AND C. B. GILL, *This Journal*, **102**, 81 (1955).

The Extractive Metallurgy of Zirconium By the Electrolysis of Fused Salts

III. Expanded Scale Process Development of the Electrolytic Production of Zirconium from K_2ZrF_6 ¹

BERTRAM C. RAYNES, EDWARD L. THELLMANN, MORRIS A. STEINBERG, AND EUGENE WAINER

Horizons Incorporated, Cleveland, Ohio

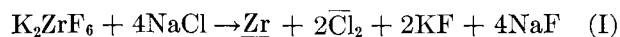
ABSTRACT

The electrolysis of K_2ZrF_6 in an electrolyte of NaCl to produce ductile zirconium metal has been expanded from the laboratory scale into a larger scale operation. An electrolytic cell capable of producing 3-4 lb of zirconium metal per run was designed and operated. Following successful operation of this unit, a cell capable of producing 30-40 lb of zirconium metal per run was used to evaluate the process on a scale 50 to 60 times the laboratory scale.

Electrolytic zirconium powder of high purity has been reproducibly obtained in good yields and at commercially acceptable current efficiencies. Upon consolidation, the metal shows fabricating properties comparable to those exhibited by Kroll sponge zirconium. The present larger electrolytic cell produces zirconium metal at a rate approaching that of the original commercial Kroll sponge producing reactors. Further expansion to larger scale operation should be entirely feasible.

INTRODUCTION

Two preceding papers (1, 2) on the extractive metallurgy of zirconium by the electrolysis of fused salts have discussed historical and theoretical aspects of this process, operational procedures, operational variables affecting the production of zirconium metal by the electrolysis of the double fluoride of zirconium, and the application of this process in producing high quality zirconium metal powder. The process can be summarized as being the electrolysis of fused potassium zirconium fluoride in molten sodium chloride in a purified argon atmosphere. The zirconium is deposited as dendritic crystalline metal in a matrix of salts from which it can be separated readily by water leaching. The over-all cell reaction is



In this paper, the expansion of the process from a laboratory unit capable of producing 200 g of zirconium per run to a cell in which 3-4 lb (1.3-1.8 kg) of zirconium metal per run can be made is described. This paper also describes the further expansion from this 3-4 lb cell, to a cell capable of producing 30-40 lb (13.5-18.0 kg) of zirconium metal per cathode at a rate of 4-6 lb/hr (1.3-2.7 kg/hr).

¹ Manuscript received July 6, 1954. This paper was prepared for delivery before the Chicago Meeting, May 2 to 6, 1954 and is based on a portion of the work carried out by Horizons Incorporated for the New York Office of the Atomic Energy Commission under contract No. AT (30-1)-1144.

The zirconium metal produced in this expanded scale equipment has been evaluated by chemical analysis and by physical metallurgical procedures, and the results are presented.

FOUR POUND PRODUCING UNIT

Experimental Work

Equipment.—An electrolytic cell capable of producing 3-4 lb of zirconium in one 8-hour day by the electrolysis of K_2ZrF_6 in NaCl was designed and constructed at Horizons Incorporated. This cell represents approximately a tenfold increase in productive capacity over the laboratory cells previously described (2). It resembles the smaller cell in materials of construction and consists essentially of a graphite crucible and anode, a thermally insulated shell in which an inert atmosphere of argon can be maintained, and an operating head through which solid cathodes can be inserted into the molten bath. The cell is heated by a graphite resistance element. The cathode is comprised of a nickel rod to which a steel cathode is welded. The nickel rod is protected by a graphite sleeve within the cell and at the bath surface.

Normal operation consists of a charge melting period, a pre-electrolytic period, and the electrolysis. The cell and cathodic deposit are allowed to cool overnight to room temperature, and a 1-hr period at the beginning of the next cycle is used to remove the cathode and the crucible and to prepare for the subsequent run.

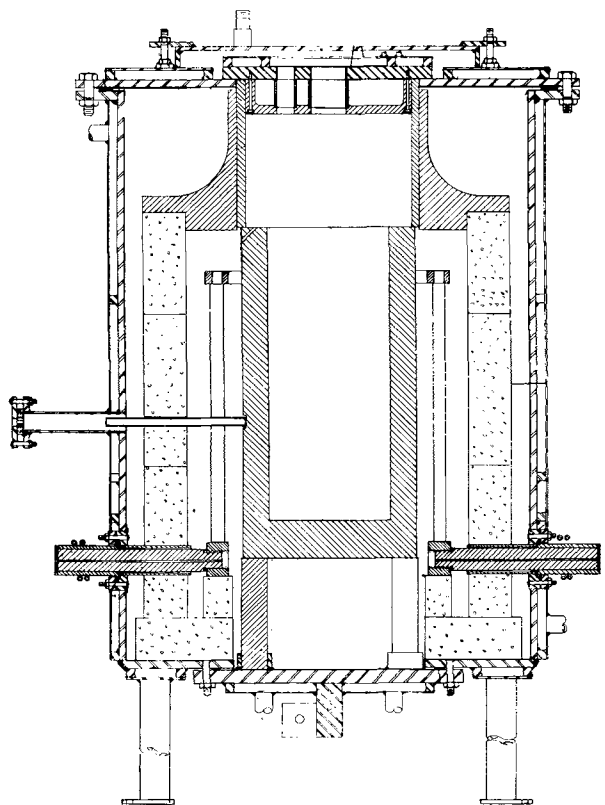
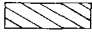
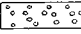



FIG. 1. Electrolytic cell.  graphite;  K-28 firebrick;  steel, nickel sheathed.

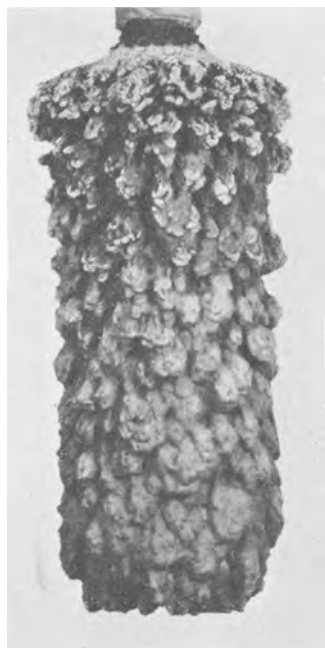


FIG. 2. Typical zirconium "carrot" on removal from electrolytic cell. $\frac{1}{2}$ normal size before reduction for publication.

Cell Operation

The electrolytic cell is cleaned and assembled as shown in Fig. 1, and the crucible is charged with granular sodium chloride. The salt is melted under

an argon atmosphere in about 2 hr with an a-c power input of about 24 kw. Dry potassium fluozirconate is then added to the molten sodium chloride through the charging hole and is rapidly melted. A normal starting charge is 10 lb of K_2ZrF_6 and 20 lb of NaCl. The bath temperature is controlled at 830°–850°C. A graphite cathode is immersed in the bath and a low voltage pre-electrolysis bath purification is performed. A small direct current starting at 1.5–1.8 v is passed through the bath for about 30 min, during which time the voltage increases to 2.8 v indicating removal of metallic impurities and water. At this voltage zirconium begins to deposit on the cathode and chlorine is evolved at the anode. The pre-electrolysis is continued for another 30 min at 2.8 to 3.1 v d.c. as a precautionary measure. A small amount of zirconium metal deposits out on the graphite rod. After this pre-electrolytic purification step, the bath is ready to be electrolyzed.

Upon removal of the pre-electrolytic cathode, a steel cathode is then immersed completely in the fused salt bath with a small d-c voltage impressed upon it. When the cathode reaches bath temperature (in about 5 min), the voltage is increased to 5 to 6 v d.c. to pass enough current to establish the initial current density at 300 to 400 amp/dm². When the cell polarizes, additional K_2ZrF_6 and NaCl are charged into the crucible. By this means, production of zirconium can be maintained at a consistently high rate.

When the predetermined number of ampere hours has been put through the electrolyte, the cathode is raised from the bath. The cathode is held above the bath, but in the argon atmosphere, and the entire unit is allowed to cool to room temperature.

Fig. 2 shows a typical cathode and cathode deposit after removal from the cell. Fig. 3 shows the deposit broken open to reveal the zirconium metal and the customary outer salt-metal layer.

Both crucibles and cathodes are reused; normal life for a crucible is 20 electrolyses or more and for a cathode, 100 runs. Cathodes are protected at the bath interface and in the chlorine atmosphere above the bath by graphite sleeves. These sleeves are replaced after each run.

Materials.—The cell, after any maintenance work or an extended shut-down, is made anhydrous by evacuation at 900°C at 50–100 μ . The K_2ZrF_6 is vacuum dried at 90°C and 150 μ for 2 hr before being charged into the cell. The sodium chloride used in this large unit is AR granular grade NaCl, supplied in 100-lb drums, and is used after drying in air at 120°C overnight. Melting the salts is carried out under a purified argon atmosphere.

In this work, three grades of potassium fluozirconate have been used: a C.P. grade K_2ZrF_6 , 99+ % in

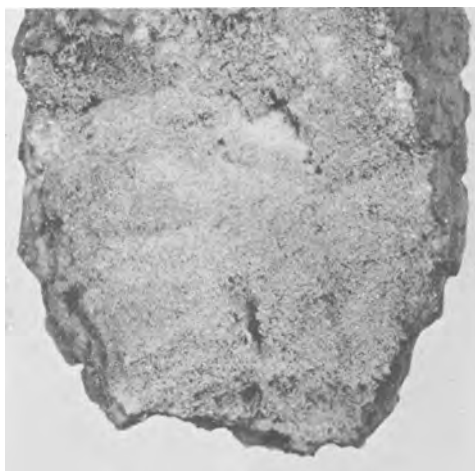


FIG. 3. Zirconium cathode "carrot" after breaking away part of the deposit showing the coarse zirconium powder, as deposited during electrolysis, and the outer salt layer.

purity, available commercially; double recrystallized K_2ZrF_6 , an anhydrous salt available commercially; and double recrystallized K_2ZrF_6 produced in the authors' laboratory from commercial grade K_2ZrF_6 .

Double recrystallized K_2ZrF_6 is required as the proper starting raw material for the production of low hardness zirconium metal. However, workable zirconium metal can be produced from commercial grade potassium zirconium fluoride. These conclusions are justified by the results of runs made in this unit. These results are shown in the tabulation of typical experimental runs given below.

Table I is a summary of a number of electrolyses in this larger scale unit. Three runs from each grade of K_2ZrF_6 used are summarized. All runs were made using a starting composition of 33% by weight of the fluozirconate and 67% by weight of sodium chloride.

In Table I, runs 1, 2, and 3 are typical of 29 electrolytic runs made with commercial grade K_2ZrF_6 . Zirconium produced with this material ranged in hardness from Rockwell A 57 to Rockwell

A 64 (Brinell 205 to 275). Current efficiencies are good, averaging 55–60%, but extremely wide variations were found in the chemical analysis, particularly in oxygen contents. The product is washed with more difficulty than that obtained from purer starting materials and, upon melting, fumes appreciably.

Per cent yield figures in runs 3–9 are lower than those obtained in strictly batch operations because of a change in operational procedure. Excess K_2ZrF_6 was added to the salt bath as the predetermined number of ampere hours were approached to keep the concentration of zirconium salt high. This cell ran for a predetermined number of ampere hours and the bath was not depleted of available zirconium.

Runs 4, 5, and 6 represent 17 runs made in the 4-lb cell using K_2ZrF_6 recrystallized in the laboratory and vacuum dried at 150°C. Consistently good quality zirconium, low in oxygen content, can be made with this salt as a starting material. The current efficiencies obtained in the electrolyses are somewhat lower, 45–55%, as are the over-all yields. The hardness of the zirconium is consistent at R_A 50–52 (Brinell 150–170). Oxygen contents of zirconium produced from this material range from 0.06 to 0.10%.

Runs 7, 8, and 9 represent 12 electrolytic experiments in which commercial anhydrous double recrystallized K_2ZrF_6 was used as the zirconium raw material. The electrolysis of this fluozirconate produces zirconium metal with Rockwell hardnesses from R_A 47 to R_A 51 (Brinell 145 to 170). Current efficiencies average 55–65%. The purity of the zirconium metal made in these experiments is very high. Oxygen contents range from 0.03 to 0.07% and carbon from 0.02 to 0.03%. Nitrogen contents, in nearly every run in this cell, average about 0.0035%.

Conditions of bath temperature and initial current

TABLE I. Summary of runs made in 3–4 lb zirconium cell

Run	Reference No.	Grade of K_2ZrF_6	Bath temp, °C	Current density amp/dm ²	Current efficiency	% yield	As-cast Rockwell hardness	Analysis		
								% O	% N	% C
1	92-69	Commercial CP	850	370	70	78.5	R_A 62	0.22	0.0027	0.037
2	92-77	Commercial CP	850	390	65	85.0	R_A 58	0.130	0.0031	0.051
3	92-103	Commercial CP	850	330	62	52.5	R_A 58	0.229	0.0028	0.056
4	92-121	Commercial CP Horizons recrystallized	850	325	47	59.0	R_A 52	0.080	—	0.017
5	92-123	Commercial CP Horizons recrystallized	850	340	45	44	R_A 52	0.088	0.0034	0.062
6	92-171	Commercial CP Horizons recrystallized	840	370	59	58	R_A 51	0.062	0.0099	0.028
7	92-173	Commercial double recrystallized	830	340	53	62	R_A 51	0.035	0.0008	0.024
8	92-177	Commercial double recrystallized	830	330	70	49	R_A 49	0.034	—	0.026
9	92-179	Commercial double recrystallized	835	370	61	56.5	R_A 48	0.042	—	0.025

TABLE II. *Typical screen analyses of electrolytic zirconium powder*

(USS Tyler Standard Sieves)

Run No.	+35	-35 +100	-100 +150	-150 +200	-200 +325	-325
92-96	0.4	30.2	24.0	18.2	20.2	7.0
92-103	1.0	15.8	12.2	20.4	34.2	16.4
92-123	7.8	17.8	12.4	17.2	27.8	17.0
92-177	0.2	20.2	14.8	26.4	25.6	12.8
92-179	0.2	31.4	14.4	29.8	18.0	6.2

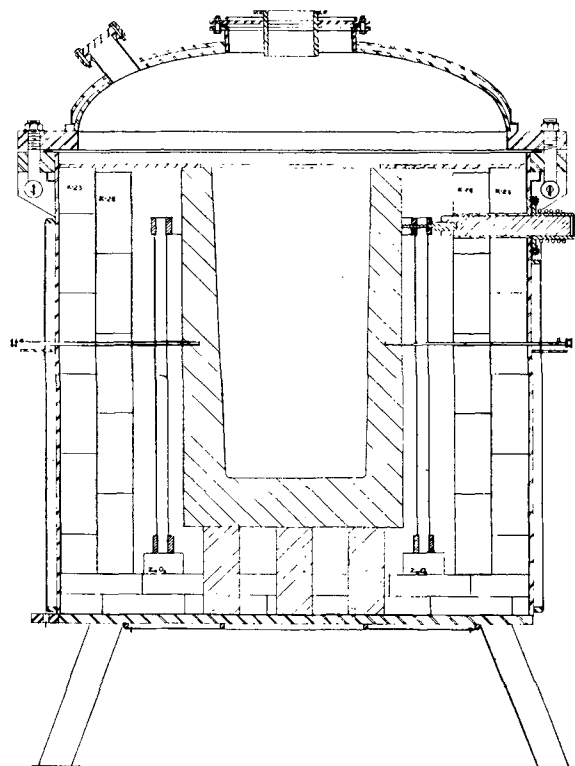

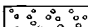



FIG. 4. Large scale electrolytic cell.  graphite;  K-28 firebrick;  steel, nickel sheathed.

density used in the 9 runs summarized in Table I have been established as the most desirable ones, not only in this larger scale equipment, but also in the small scale work previously reported (1, 2). In this 4-lb/run electrolytic cell, the electrolyses differ from the small scale operation in that additions of K_2ZrF_6 and NaCl were made during the electrolysis in order to avoid polarization and to keep the concentration of zirconium salts nearly constant in order to assure a supply of available zirconium. This cell is run, therefore, for a specified number of ampere hours. Hence, current efficiencies remain high, averaging about 55%, and are comparable to results obtained in the 200 gram cells with similar raw materials. However, the material yields are lower since this particular unit was operated as a batch unit and the bath was never run to exhaustion.

Yields reported in Table I should be considered in the light of this explanation.

Table II shows typical particle size distributions of the zirconium produced in this large laboratory electrolytic cell. No specific correlation has been made between particle size distribution and hardness for the zirconium powder, but, as a generalization, the coarser deposits tend to result in slightly softer metal upon melting. In some runs, the finer material has been found to result in harder ingots, but in other runs there has been no difference in the hardness of the consolidated metal. Coarse powder is preferable, however, since its recovery from the cathode deposit is easier and there is less loss in handling and in leaching. The metal is recovered by water leaching followed by air drying.

FORTY POUND PRODUCING UNIT

Experimental Work with 40-lb per Run Electrolytic Cell

Equipment.—A large scale electrolytic cell was designed (Fig. 4) to produce 30–40 lb of zirconium metal per run.² The design was based upon the laboratory electrolytic cell and the larger unit discussed above, with some modifications. Additional design features were incorporated, because of the increased physical size, in order to provide flexibility of operation, although it was not the intention to arrive at a prototype of a commercial cell.

This unit consists of a nickel-sheathed mild steel shell and is constructed on the interior much like the smaller units. It is completely water jacketed and is heated with a sectioned graphite heating element. The unit is insulated with refractory insulating brick on its sides and bottom. A machined graphite piece is both crucible and anode and can accommodate a 250–350 lb charge of molten salts. The cathode consists of jointed steel and graphite sections, the section upon which the zirconium metal is electrodeposited being mild steel. This section is threaded into a solid graphite rod which extends out of the cell through a nickel-sheathed operating head. The cell can carry up to 5000 amp direct current if desired. The unit operates in an argon atmosphere.

Cell operation.—Prior to its initial run, this unit was evacuated for eight hours at 900°C at a pressure of 35–125 μ . If any extended shut-down for maintenance or observation takes place between runs, the cell is again evacuated at a lower temperature before subsequent use. For these subsequent evacuations, a temperature of 200°C is adequate.

The crucible is brought up to 830°–850°C operating temperature in about five hours, at which time the sodium chloride, about 170 lb, is charged. Analytical

² This cell was designed and built on ONR Contract No. Nonr-394 (01).

Reagent grade NaCl is used without predrying. Double recrystallized potassium zirconium fluoride, about 50 lb, is then added to the molten sodium chloride and is rapidly melted.

No pre-electrolysis is carried out in this large unit.

The steel cathode (including an additional 2-3 in. of graphite) is completely immersed in the fused salt bath with a small d-c voltage impressed upon it. The current is slowly increased until a current density of 260-300 amp/dm² is established on the cathode. When the bath polarizes, additional K₂ZrF₆ and NaCl are charged into the bath. Normally, a 50-50 mixture of K₂ZrF₆ and NaCl is used for the charge. By this means, the initial high production rate of zirconium metal can be maintained.

When a predetermined number of ampere hours has been passed through the electrolyte, the cathode is raised from the bath. The cathode is suspended above the bath, but in the argon atmosphere, and the entire unit is allowed to cool to room temperature.

Typical cathode deposits are shown in Fig. 5 and 6.

Some difficulty was experienced in this cell with crucible leakage and cathode breakage. Other graphite and nickel-clad parts appear to be satisfactory for reasonable service; that is, no gross attack has been observed in eight complete electrolytic cycles.

Table III is a summary of the runs made in this unit. As in the smaller unit, all runs were made using a starting composition of 33% by weight of the fluozirconate in the sodium chloride.

Metal recovery of electrolytic deposits.—Electrolytic deposits from the electrolysis of K₂ZrF₆ in fused sodium chloride average about 30% by weight of zirconium metal, the remainder being a mixture of soluble zirconium and sodium halides. The cold deposit is chipped away from the steel cathode by an air hammer and is then jaw crushed to about ¼ in. sized chunks. These lumps are then pulverized to about -80 mesh powder.

The crushed and pulverized cathode deposit is then leached in a continuous cone washer in which the metal is fluidized by an upward movement of water as the soluble salts are leached away and removed in the overflow. This unit represents, therefore, an approach to a continuous counter-current leaching operation.

When the zirconium metal is free of all soluble salts, it is removed from the water, filtered, and air dried.

PROPERTIES OF ELECTROLYTIC ZIRCONIUM

Physical Properties

The electrolytically deposited zirconium metal, in the form of dendritic crystals, is consolidated first by pressing into dense compacts 1 in. in diameter

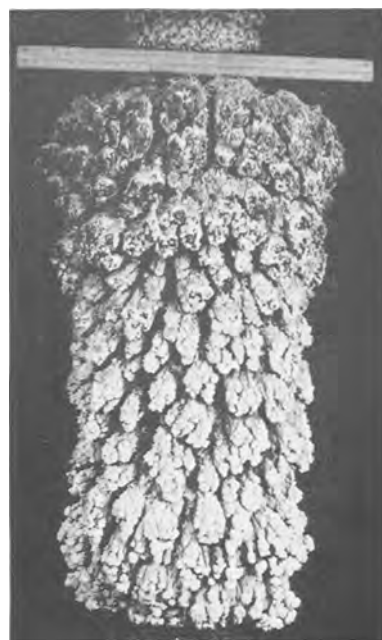


FIG. 5. Typical zirconium cathode deposit produced in the large scale electrolytic cell.



FIG. 6. Zirconium cathode deposit compared with typical mild steel cathode.

and ¼ in. to ¾ in. in height. These compacts are then arc melted in a tungsten-arc, water-cooled, copper hearth furnace under a quarter of an atmosphere of argon. Fig. 7 shows typical zirconium metal dendritic crystals as produced in the large scale electrolytic cell. Fig. 8 shows uncompact electrolytic zirconium, a compact of 20 grams of this powder, and an arc melted compact.

TABLE III. Summary of electrolytic runs made in large scale electrolytic cell

Run No.	Bath temp, °C	Initial current density, amp/dm ² on cathode	Current density amp/dm ² on anode	Current efficiency	Rate of production, lb Zr/hr of electrolysis	As-cast Rockwell hardness	Remarks
1	835	330	55	62	5.0	R _A 61	O ₂ = 0.320%; C = 0.015%
2	870	330	45	67	5.5	R _B 90	O ₂ = 0.108%; C = 0.045%
3	870	290	40	60	5.0	R _B 91	O ₂ = 0.061; C = 0.067%
4	820	330	45	65	5.3	R _B 87	
5	855	370	50	64	5.3	R _B 93	
6	840	270	37	53	3.8	R _B 88	

All runs made with starting concentration 33% K₂ZrF₆ by weight. Salt additions made during electrolysis, at bath polarizations.



FIG. 7. Typical zirconium metal dendritic crystals

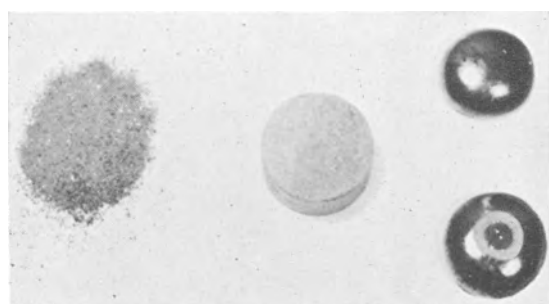


FIG. 8. Recovered zirconium powder, compacted zirconium powder, and small arc-melted zirconium ingots.

The arc furnace uses a tungsten electrode mounted in a water-cooled copper tube which is flexibly mounted in a copper head through a bellows assembly. The hearth is water-cooled copper, to take advantage of the fact that molten zirconium does not wet cold copper. The outer shell of this furnace is a cylindrical piece of Pyrex glass. Auxiliary equipment consists of an argon purification train of P₂O₅ and heated titanium sponge, a vacuum pump and cold trap, a manometer, and a 400 amp d-c Hobart

welder for the power source. It is similar to many which have been described in the literature.

Metal Evaluation

Rockwell hardnesses are taken on these arc melted pellets and this hardness becomes the primary means of product evaluation. Although hardnesses are customarily determined on the Rockwell B scale, a conversion from Rockwell A to Rockwell B scale was made since the hardness of zirconium alloys cannot always be made in the Rockwell B scale. This conversion between Rockwell A, Rockwell B, and Brinell is shown in Fig. 9.

Various melted pellets of 20–60 g and ingots of 100–150 g have been hot and cold reduced by rolling to determine the workability of the electrolytic zirconium. All of the metal produced can be hot worked to strip at 700°–800°C. Zirconium as-cast ingots or pellets, Rockwell B 85–92, can be cold rolled but are more successfully worked with successive anneals at 850°C (in air) after moderate

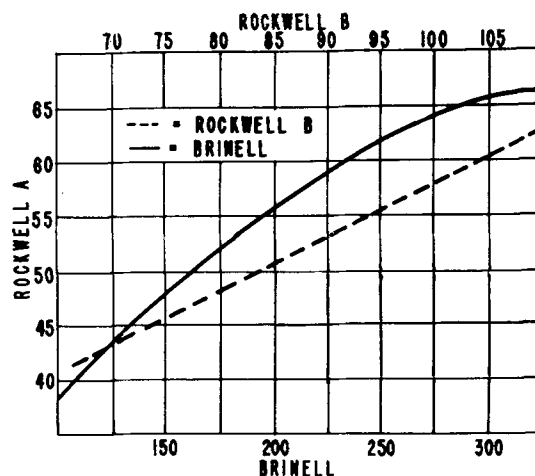


FIG. 9. Conversion from Rockwell "A" to Rockwell "B" and Brinell for zirconium.

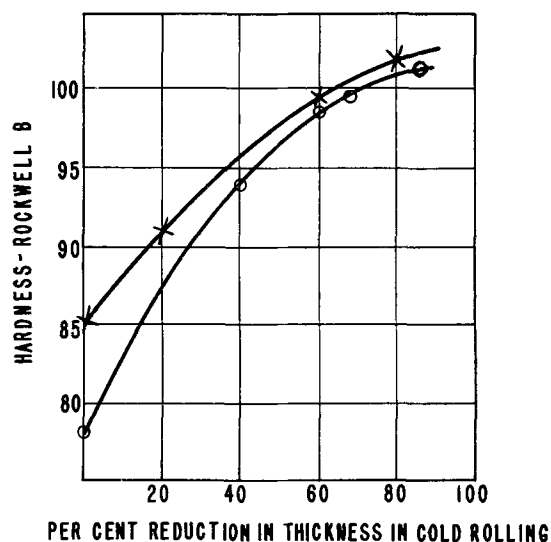


FIG. 10. Effect of cold rolling on the hardness of electrolytic zirconium.

TABLE IV. Spectrographic analyses of typical electrolytic zirconium powder and of rolled arc melted zirconium made from this powder

	Powder	Strip
Zr	Major	Major
Si	0.003	0.002
Fe	0.01	0.03
Al	0.01	0.007
Hf	1.5	1.5
Cu	0.0005*	0.0007
Ti	0.05	0.05
Ca	0.005*	0.005*
Mg	0.001*	0.001*
Mn	0.001*	0.001*
Pb	0.001*	0.001*
Mo	0.001*	0.001*
Ni	0.004	0.003
Cr	0.003	0.002
Sn	0.001*	0.001*
W	—	—

* Less than.

(20–40%) cold working. Fig. 10 illustrates typical hardness change with per cent reduction in thickness obtained in cold rolling of electrolytic zirconium. It can be seen that the hardness approaches R_B 100 during cold rolling before edge cracking, regardless of the initial as-cast hardness.

Spectrographic analyses of typical electrolytic zirconium powder as produced in the two electrolytic cells described above and of arc melted buttons made from this powder are given in Table IV. Typical oxygen analyses of such powder range from 0.06 to 0.09%, nitrogen from 0.003 to 0.009%, and carbons from 0.02 to 0.06% (see Table I).

CONCLUSIONS

The process development of the electrolysis of potassium fluozirconate in sodium chloride has been successfully expanded from the laboratory bench scale through a development-sized electrolytic cell capable of producing 3–4 lb to an electrolytic unit capable of producing 30–40 lb of zirconium metal per run. The process has been demonstrated to operate at commercially acceptable current efficiencies and yields and to produce good quality zirconium metal at a rate of about 4–6 lb/hr, which is equivalent to the production rate of the original Kroll sponge reactor. Results indicate that further expansion of the scale of operation will present no unsurmountable technical difficulties.

The zirconium metal, produced at this near-commercial rate of 4–6 lb/hr, has been evaluated, as as-cast metal, to have a hardness of Rockwell B 80 to Rockwell B 83 (Brinell Hardness Number 150 to 165), if recrystallized potassium zirconium fluoride is used as starting material. Such K_2ZrF_6 is readily available from commercial manufacturers.

Zirconium metal produced by the process, consolidated by arc melting, can be either hot or cold worked to sheet, foil, or wire. The oxygen content of this metal ranged from 0.06 to 0.09%; nitrogen averages 0.003%; and carbon 0.02 to 0.06%.

Comparison with Kroll Process

The operating schedule to produce 220 lb of zirconium by the Kroll magnesium reduction process (magnesium reacted with zirconium tetrachloride) is 41 hr and 30 min. The vacuum distillation of the yield of the reduction requires 42 hr and 10 min (3). Thus the 220 lb of zirconium are produced in 83 hr and 40 min. This is an over-all production rate of 2.6 lb of zirconium per hour for the Kroll process.

The electrolytic process time schedule, as obtained in the operation of its largest scale unit, is as follows for the production of 135 lb of zirconium: heat-up and melting of salt charge, 11 hr; electrolysis, 30 hr; metal recovery, 13 hr; total time, 54 hr. This is an over-all production rate of 2.5 lb of zirconium per hour, comparing favorably with the production rate obtained with the magnesium reduction process.

Another comparison between the two processes is possible. Excluding vacuum distillation time, the Kroll process requires 5.3 hr to produce 1 lb of zirconium. The electrolytic process produces zirconium at the rate of 3.3 lb of zirconium per hour, including cell heat-up time. However, more than one run can be made in a cell which is equipped with facilities for cathode removals without cooling-down

periods. If the initial 11-hr cell heat-up period is excluded, therefore, a production rate of 5.5 lb of zirconium per hour is achieved.

ACKNOWLEDGMENTS

The authors wish to make special acknowledgment to S. Z. Cardon, D. F. Gollwitzer, R. M. Ferryman, F. C. Wagner, E. D. Fisher, and J. A. DaMico, all of whom are or were members of the staff at Horizons Incorporated, for their assistance in carrying out this work. This work was carried out under Contract No. AT(30-1)-1144 for the Atomic Energy Com-

mission, to whom gratitude is expressed for permission to publish this paper.

Any discussion of this paper will appear in a Discussion Section to be published in the December 1955 JOURNAL.

REFERENCES

1. M. A. STEINBERG, M. E. SIBERT, AND E. WAINER, in "Zirconium and Zirconium Alloys," American Society of Metals, Cleveland (1953).
2. M. A. STEINBERG, M. E. SIBERT, AND E. WAINER, *This Journal*, **101**, 63 (1954).
3. S. M. SHELTON AND E. D. DILLING, in "Zirconium and Zirconium Alloys," American Society of Metals, Cleveland (1953).

Conductances, Viscosities, and Densities of Solutions of Potassium Thiocyanate in Methanol at Temperatures within the Range 25° to -50°C¹

PAUL G. SEARS, RICHARD R. HOLMES, AND LYLE R. DAWSON

Department of Chemistry, University of Kentucky, Lexington, Kentucky

ABSTRACT

Conductances, viscosities, and densities have been determined for solutions of potassium thiocyanate in methanol at nine temperatures within the range 25° to -50°C. Concentrations of potassium thiocyanate ranged from 4×10^{-4} to 1.75*N*. Good agreement exists between the observed behavior and the theoretical Onsager relationship for dilute solutions at all temperatures used in this study. The variation of conductances and viscosities of the more concentrated solutions is discussed with respect to both concentration and temperature.

INTRODUCTION

With the possible exception of certain ammoniacal systems, studies of electrolytic solutions at low temperatures are rather limited. The investigation summarized here represents part of a program intended to accumulate comprehensive data which may be useful in furthering the understanding of conducting nonaqueous solutions at low temperatures.

Potassium thiocyanate was selected for investigation because it is an inorganic salt which is not only quite soluble but also highly conducting in methanol, one of the few solvents for which dielectric constant data are available for low temperatures. According to the literature, the conductance of potassium thiocyanate in dilute methanol solutions has been investigated previously by Kreider and Jones (1) at 25° and 0°C (however, their data are uncorrected for the conductance of the solvent) and by Hartley and his associates (2) at 25°C. Inasmuch as little is known about this system except for conductance data for extremely dilute solutions at 25°C, it appeared to be quite worthwhile to investigate the conductance of potassium thiocyanate in methanol at lower temperatures and over a greater concentration range as well as to determine the corresponding viscosities of solutions in which the viscosity differs appreciably from that of the solvent.

EXPERIMENTAL

Absolute methanol was purified using the procedure described by Evers and Knox (3). Conductivities of the retained middle fractions were approximately 10^{-7} ohm⁻¹ cm⁻¹. Reagent grade potassium thiocyanate was rendered anhydrous by the

method of Kolthoff and Lingane (4) and used without further purification. Concentrated solutions were prepared by adding a weighed quantity of methanol to a known weight of potassium thiocyanate, whereas the dilute solutions were prepared by the weight dilution of stock solutions. Sufficient amounts of the concentrated solutions were prepared to permit separate portions of a solution to be used for measuring the conductance, viscosity, and density. Necessary buoyancy corrections were applied to all weights. Weight-based concentrations were converted to a volume basis through utilization of the proper density data. All transfers were made in a dry box.

A Jones bridge (manufactured by the Leeds and Northrup Company) was used to measure resistances of the solutions contained in the conductance cells. For larger resistances, 30,000 ohms of the bridge resistance was shunted in parallel with the cell and the series cell resistance was computed from the measured parallel resistance. The constants (ranging from 0.2502 to 31.99 cm⁻¹) of the Jones and Bollinger cells (5) having electrodes platinized by the standard procedure (6) were determined using standard 0.01 *demal* aqueous potassium chloride solutions according to the method of Jones and Bradshaw (7) or by intercomparison of resistances with cells having known constants. Resistances of solutions measured at 500, 1000, and 2000 cycles were found to have no significant frequency dependence. Conductance of the potassium thiocyanate was obtained by subtracting the conductance of the solvent from that of the solution. In no case did the solvent correction exceed 2%.

Two size-50 Ostwald-Cannon-Fenske viscometers were used in measuring efflux times of the solutions. Calibrations of the viscometers were based on the

¹ Manuscript received July 19, 1954. Based on research performed under contract No. DA 36-039-sc-42581 for the U. S. Army Signal Corps.

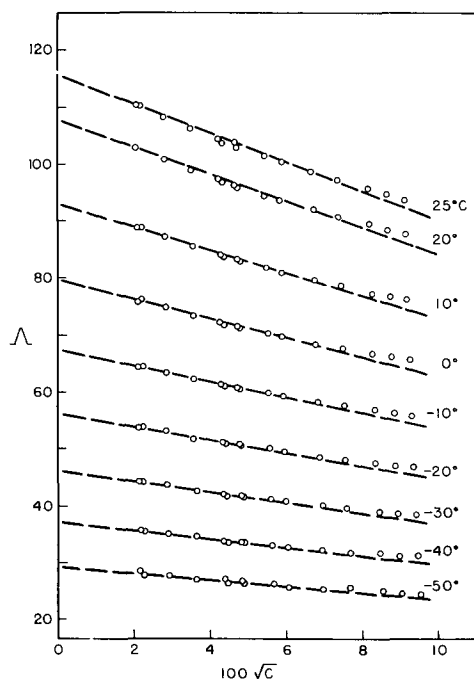


FIG. 1. Kohlrausch plots for potassium thiocyanate at low concentrations in methanol.

TABLE I. Some physical properties of methanol

°C	Density (g/ml)	Viscosity (millipoises)	Dielectric constant (11, 12)
25	0.7866	5.42	32.6
20	0.7916	5.81	33.7
10	0.8010	6.76	35.6
0	0.8102	7.94	37.5
-10	0.8200	9.41	39.6
-20	0.8296	11.3	41.8
-30	0.8390	13.8	44.0
-40	0.8485	17.2	46.2
-50	0.8580	21.9	48.5

TABLE II. Test of Onsager's equation for solutions of potassium thiocyanate in methanol at temperatures within the range 25° to -50°C

°C	Limiting equivalent conductance	Observed slope (S_E)	Theoretical slope (S_T)	$\frac{(S_E - S_T)}{S_T} \cdot 100$
25	115.7	-259	-253	3
20	108.0	-240	-233	3
10	93.3	-205	-197	4
0	79.8	-171	-166	3
-10	67.4	-139	-138	1
-20	56.0	-110	-110	0
-30	46.0	-91	-92	-1
-40	37.0	-72	-73	-1
-50	29.3	-58	-57	2

efflux times of water and two National Bureau of Standards viscosity oils (D-8 and H-8) at 20°C. Viscometer constants at temperatures other than the calibration temperature were calculated using

the equation introduced by Cannon and Fenske (8). Calibrated timers reading directly to 0.2 sec were employed to measure efflux times of the solutions through the viscometers. The viscometer arms were vented to the atmosphere through drying tubes containing anhydrous calcium chloride and Ascarite. Appropriate kinetic energy corrections were applied in the calculation of viscosities. All viscosity data are referred to the viscosity of water, 1.002 centipoise at 20°C (9).

Densities of the solutions were determined using two Pyrex pycnometers of 22.3 and 22.4 ml capacities. Each pycnometer consisted of a spherical bulb to which was sealed a small-bore graduated stem closed at the other end with a ground-glass cap. Calibrations of the pycnometers were made at 20°C using distilled water. Applying the necessary corrections for cubical contraction of Pyrex glass, the pycnometer volumes were calculated at ten-degree intervals over the temperature range from 20° to -50°C.

All measurements were carried out in a manually controlled thermostat consisting of a five-gallon Dewar flask containing impure ethanol cooled by adding powdered dry ice. Vigorous agitation of the bath liquid was obtained through the use of a mechanical stirrer having three sets of propellers. Temperatures in all cases were observed by the use of alcohol-filled thermometers which were periodically compared with two thermometers calibrated by the National Bureau of Standards. Emergent stem corrections were unnecessary inasmuch as thermometers were totally immersed in the bath liquid. Measurements were made at 25°, 20°, 10°, 0°, -10°, -20°, -30°, -40°, and -50°C. In each case the temperature could be controlled well within 0.2°.

RESULTS AND DISCUSSION

Plots of the equivalent conductance, Λ , of potassium thiocyanate in methanol at various temperatures against the square root of concentration are shown in Fig. 1. The dashed line in each case represents the theoretical behavior predicted by the Onsager equation (10) which may be written as follows for a uni-univalent electrolyte:

$$\Lambda = \Lambda_0 - [A + B]\sqrt{C}$$

where

$$A = \frac{82.42}{(DT)^{1/2}\eta}$$

$$B = \frac{8.203 \times 10^5}{(DT)^{3/2}}$$

in which D and η are the dielectric constant and viscosity of the solvent, respectively.

TABLE III. Limiting equivalent conductances and dissociation constants determined by Shedlovsky method and conductance-viscosity products for potassium thiocyanate in methanol

	Λ_0	K	$\Lambda_0\eta$
°C			
25	115.7	0.09	0.627
20	107.8	0.09	0.626
10	93.1	0.09	0.629
0	79.7	0.10	0.633
-10	67.4	0.13	0.634
-20	56.0	0.11	0.633
-30	46.0	0.20	0.635
-40	36.9	0.59	0.633
-50	29.2	0.35	0.638

Viscosity and dielectric constant data used in the calculation of the theoretical slope, $-[A + B\Lambda_0]$, may be found in Table I. A summary of the limiting equivalent conductances, obtained by extrapolation, and the observed and theoretical limiting slopes is given in Table II. It may be noted that good agreement exists between observed and theoretical slopes; however, the observed slope generally is slightly more negative than the theoretical slope which may be evidence of incomplete dissociation of the solute. The equivalent conductance data were analyzed, therefore, by the Shedlovsky method (13) which permits simultaneous evaluation of the limiting equivalent conductance and the dissociation constant. The resulting data obtained from the intercepts, evaluated by the method of least squares, and slopes of plots of $S\Lambda$ vs. $Cf_{\pm}^2S^2\Lambda^2$ may be found in Table III. The dissociation constants indicate that potassium thiocyanate is very highly dissociated in methanol and that its dissociation becomes even more pronounced at lower temperatures. The corresponding Λ_0 values listed in Tables II and III agree within experimental and extrapolation errors. The limiting equivalent conductance value of 115.7 $\text{ohm}^{-1} \text{cm}^2$ for potassium thiocyanate in methanol at 25°C is approximately 1% greater than that reported by Hartley and his associates (2).

Fig. 2 shows that a plot of the logarithm of the limiting equivalent conductance of potassium thiocyanate in methanol vs. the reciprocal of the absolute temperature is linear over the temperature range studied. Consequently, for the system under consideration it is possible to regard conductance as a rate process (14) in which case the relation between Λ_0 and T can be written in the form, $\Lambda_0 = A \exp(-E/RT)$, where A and E are constants, E being the energy of activation for the process of ionic transport through the solution. E amounts to 2.42 kcal for potassium thiocyanate in methanol, whereas it is approximately 3.60 kcal for most normal electrolytes in water. Fig. 2 also shows that the logarithm of the viscosity of methanol vs. $1/T$

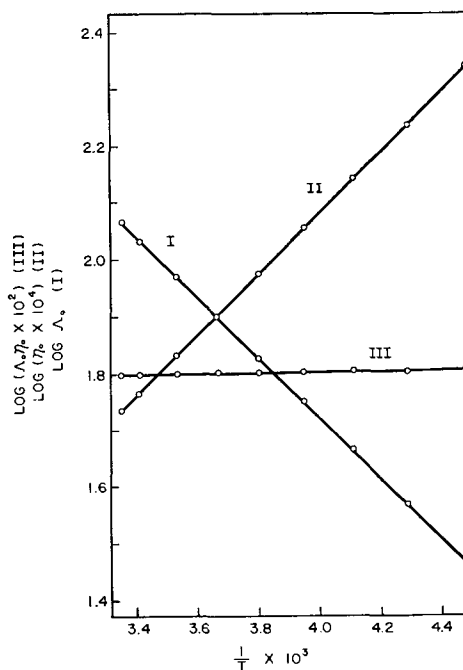


FIG. 2. Logarithms of the limiting equivalent conductance, viscosity of the solvent, and the product of these values, as functions of the reciprocal of the absolute temperature.

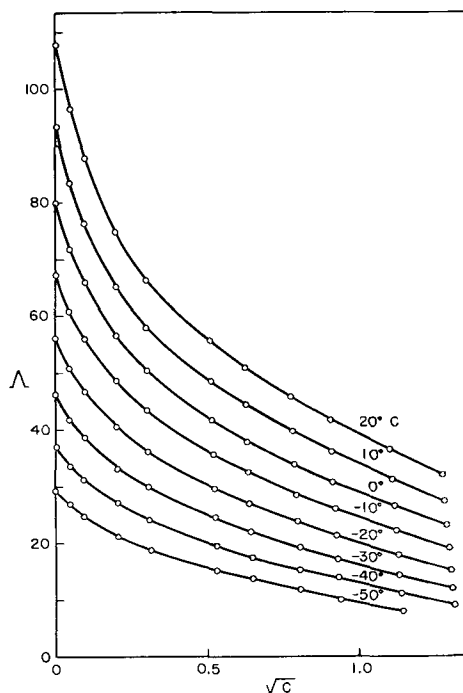


FIG. 3. Kohlrausch plots extending to higher concentrations of potassium thiocyanate in methanol.

is linear, indicating that the relation between η_0 and T may be written in a similar form, $\eta_0 = B \exp(E'/RT)$, where B and E' are constants, E' being the activation energy of viscous flow. For methanol E' equals 2.47 kcal. Combining the logarithmic expressions of the two equations given above, the expression $\log_{10}(\Lambda_0\eta_0) = \text{constant} +$

$(E' - E)/2.303 R 1/T$ may be obtained. Hence, a plot of $\log(\Lambda_0\eta_0)$ vs. $1/T$ should be linear, and the slope should be a function of the difference of the activation energies of the conductance and viscous flow processes. A combined plot of this nature for potassium thiocyanate in methanol may be seen in Fig. 2. If the activation energies were equal, the

equation would reduce to Walden's rule, $\Lambda_0\eta_0 = \text{constant}$. Quite aside from any question related to mechanistic processes, however, equality of the so-called activation energies means simply that the positive conductance temperature coefficient is approximately equal to the negative viscosity temperature coefficient. Hence, the product of the limiting

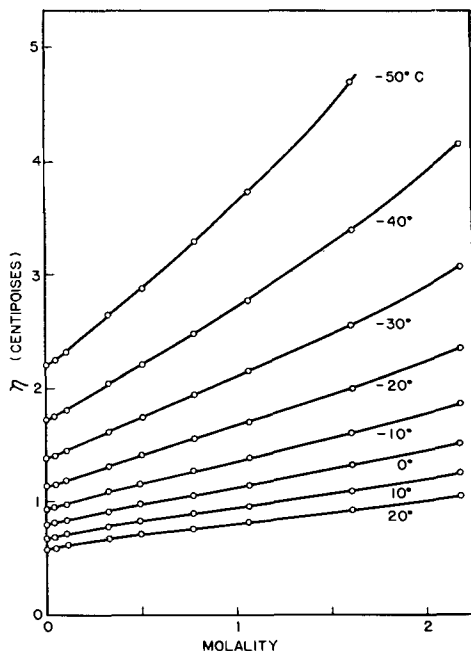


FIG. 4. Concentration dependence of the viscosity of solutions of potassium thiocyanate in methanol.

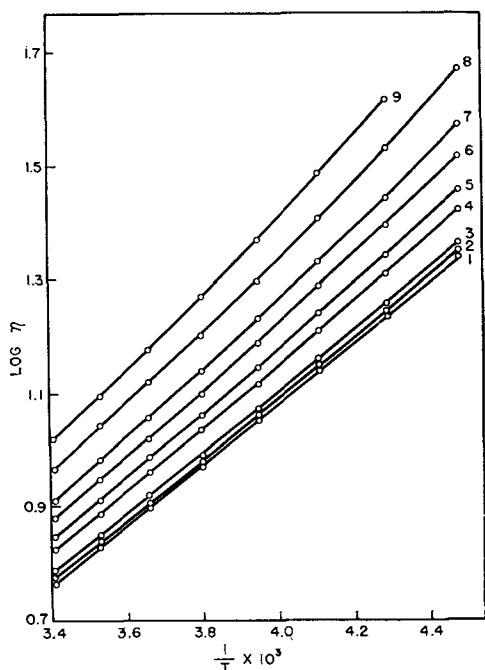


FIG. 5. Temperature dependence of the logarithm of the viscosity of solutions of potassium thiocyanate in methanol. (1) solvent; (2) 0.0482M; (3) 0.111M; (4) 0.329M; (5) 0.498M; (6) 0.777M; (7) 1.065M; (8) 1.604M; (9) 2.183M.

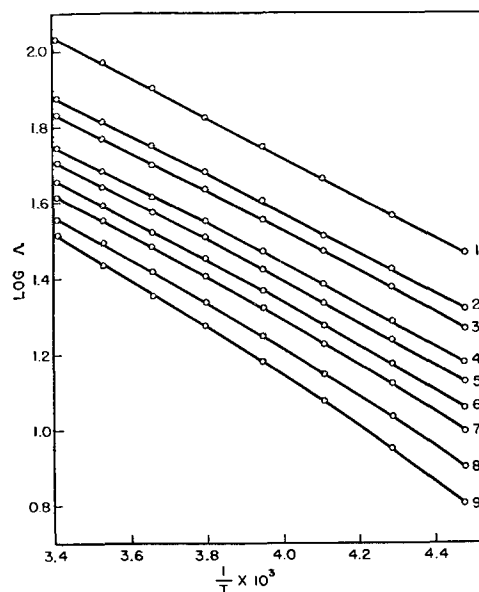


FIG. 6. Temperature dependence of the logarithm of the equivalent conductance of potassium thiocyanate in methanol. (1) Λ_0 values; (2) 0.0482M; (3) 0.111M; (4) 0.329M; (5) 0.498M; (6) 0.777M; (7) 1.065M; (8) 1.604M; (9) 2.183M.

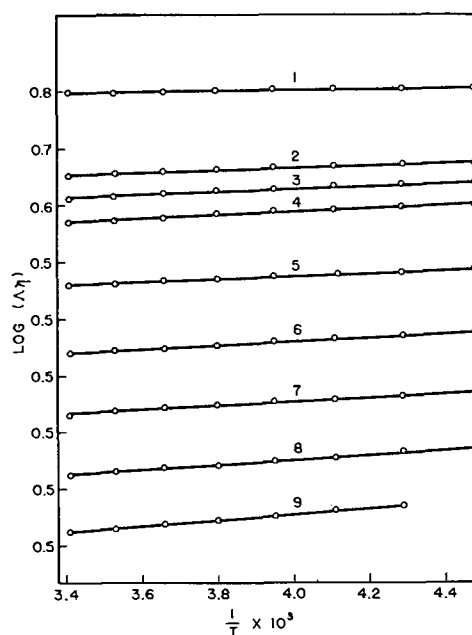


FIG. 7. Logarithm of the product of the equivalent conductance and the viscosity of the solutions as a function of the reciprocal of the absolute temperature. (1) 0.00M; (2) 0.048M; (3) 0.111M; (4) 0.329M; (5) 0.498M; (6) 0.777M; (7) 1.065M; (8) 1.604M; (9) 2.183M.

equivalent conductance and the viscosity of the solvent should be approximately constant. The values of this product for potassium thiocyanate in methanol at various temperatures are listed in Table III.

Fig. 3 shows Kohlrausch plots for potassium thiocyanate in methanol covering the entire concentration range studied. Plots for the various temperatures are similar in shape and differ principally only in the magnitude of displacement along the ordinate. The variation of viscosity with molality for solutions of potassium thiocyanate in methanol at various temperatures is shown in Fig. 4. Curvature of the plots becomes more pronounced at lower temperatures. Density plots have not been included because the following equation describes within 1 mg/ml the densities of this system within the temperature range from 20° to -50°C for concentrations up to 2.183*m*:

$$d = 0.7916 - (0.000943 - 0.000044m)(t - 20) + 0.530m - 0.00095m^3$$

where *d* = density in g/ml, *m* = molality, and *t* = temperature in °C.

Plots of the logarithm of the viscosity vs. 1/*T* for various molal concentrations of potassium thiocyanate in methanol appear in Fig. 5. It may be observed that the graphs become more curved as molality increases. Fig. 6 presents corresponding plots of the equivalent conductance vs. 1/*T* for the same molal concentrations. If plots for various molar concentrations were constructed, the over-all picture would not be changed appreciably. Nevertheless, these graphs become more curved with increasing molality in the same manner as the viscosity plots in Fig. 5. The logarithm of the conductance-viscosity product, at the same molal concentrations, as a function of the reciprocal of the absolute temperature is shown in Fig. 7. In this figure the ordinate

value has been displaced 0.1 logarithm unit for each of the five most concentrated solutions to prevent superposition of the curves. The plots are linear and have slopes which increase with increasing molality. Whether the linearity results from fortuitous cancelling effects or depends upon a constant difference in the activation energies of conductance and viscous flow or other factors is unknown. However, for the system potassium thiocyanate in methanol, the conductance-viscosity product is not a constant over the temperature range 20° to -50°C, but can be expressed empirically by an equation of the form, $\Delta\eta = A \exp(B/RT)$, where *A* and *B* are constants characteristic of a particular molal concentration.

Any discussion of this paper will appear in a Discussion Section to be published in the December 1955 JOURNAL.

REFERENCES

1. H. R. KREIDER AND H. C. JONES, *Am. Chem. J.*, **46**, 574 (1911).
2. A. UNMACK, E. BULLOCK, D. A. MURRAY-RUST, AND H. HARTLEY, *Proc. Roy. Soc. (London)*, **A132**, 427 (1931).
3. E. C. EVERS AND A. G. KNOX, *J. Am. Chem. Soc.*, **73**, 1739 (1951).
4. I. M. KOLTHOFF AND J. J. LINGANE, *ibid.*, **57**, 2126 (1935).
5. G. JONES AND G. M. BOLLINGER, *ibid.*, **53**, 411 (1931).
6. G. JONES AND G. M. BOLLINGER, *ibid.*, **57**, 280 (1935).
7. G. JONES AND B. C. BRADSHAW, *ibid.*, **55**, 1780 (1933).
8. M. R. CANNON AND M. R. FENSKE, *Ind. Eng. Chem., Anal. Ed.*, **10**, 297 (1938).
9. J. F. SWINDELLS, J. R. COE, AND T. B. GODFREY, *J. Research Natl. Bur. Standards*, **48**, 1 (1952).
10. L. ONSAGER, *Physik. Z.*, **28**, 277 (1927).
11. A. A. MARYOTT AND E. R. SMITH, National Bureau of Standards Circular 514, August 10, 1951.
12. "International Critical Tables", Vol. VI, p. 83.
13. T. SHEDLOVSKY, *J. Franklin Inst.*, **225**, 739 (1938).
14. A. E. STEARN AND H. EYRING, *J. Chem. Phys.*, **5**, 113 (1937).

A Further Study of Electrodeposited Manganese Dioxide Electrodes¹

W. C. VOSBURGH, RICHARD S. JOHNSON, JOHN S. REISER, AND DOUGLAS R. ALLENSON

Duke University Durham North Carolina

ABSTRACT

Manganese dioxide electrodes prepared by electrodeposition on graphite rods were discharged in ammonium chloride electrolyte of pH 7.2 to 7.5. Two discharge products were identified and measured, an oxide with a composition of about $\text{MnO}_{1.6}$, and manganese (II) ion which appeared in the solution. The electrical output was accounted for satisfactorily by these two products. Atmospheric oxygen had only a small effect on the discharge.

Electrodes of the same type decreased slowly in potential on standing in ammonium salt electrolyte. The decrease continued for many months and its rate was independent of the anion present and of the presence or absence of oxygen. Similar electrodes on platinum instead of carbon decreased appreciably faster. Analyses and discharges of electrodes that had stood in electrolyte showed a loss of available oxygen.

INTRODUCTION

Some aspects of the behavior of manganese dioxide electrodes prepared by electrodeposition on graphite rods were left unexplained in the work of Ferrell and Vosburgh (1). Such electrodes in ammonium chloride electrolyte of pH 7 were not very reproducible and decreased in potential with time on open circuit. Discharge sometimes gave a capacity more than that calculated on the basis of reduction to the oxyhydroxide, MnOOH . It was suggested that reduction below the trivalent state might have taken place. However, reaction of oxygen from air, which was not excluded, would also give an apparent excess capacity. This reaction has been considered to play a part in the discharge of manganese dioxide electrodes (2-4).

It has been found that the excess discharge capacity is mainly the result of reduction of part of the dioxide to manganese (II) ion in agreement with Cahoon (5). The reaction of atmospheric oxygen was relatively unimportant. The decrease in open-circuit potential is at least partly the result of a slow decrease in available oxygen on long standing in ammonium salt electrolyte.

EXPERIMENTAL

Preparation, Measurement, and Discharge of Electrodes

Most of the manganese dioxide electrodes were prepared as described by Ferrell and Vosburgh (1). Briefly, graphite rods of highest purity were sealed in glass tubes so that 8 cm² of surface was exposed.

¹ Manuscript received May 3, 1954. This paper was prepared for delivery before the Boston Meeting, October 3 to 7, 1954.

Manganese dioxide was deposited electrolytically on this surface from an acid manganese (II) sulfate bath at about 80°C by means of a current of 25 ma (3.1 ma/cm²) for either 15 or 30 min. The longer time is to be assumed unless otherwise indicated.

Treatment of the graphite rods before they were plated was found to be of some importance. The usual treatment was to immerse the rod in water while the water was boiled and then cooled. This seemed to give more uniform results than did no treatment.

Two other treatments were used. In what will be called the oxygen treatment, the rod was made the anode in the electrolysis of dilute sulfuric acid. In the hydrogen treatment, the rod was made the cathode in a similar electrolysis.

It was found necessary to wash the manganese dioxide electrodes thoroughly as the final step in their preparation. They were allowed to stand in frequently changed distilled water until no more acid was washed out and then kept in distilled water until used. If not thoroughly washed, manganese (II) ion from the plating bath was retained as well as acid.

When open-circuit electrode potentials only were to be measured, four or more electrodes were mounted in a rubber stopper fitting a vessel of about 200 ml capacity. In the vessel was placed about 180 ml of electrolyte, or enough to cover the manganese dioxide. A hole in the stopper allowed insertion of a bridge to a reference electrode, which was either a saturated calomel electrode or a silver chloride electrode which had been checked against a calomel electrode. The electrode potentials are given as measured against the calomel electrode.

The electrolyte was 2M NH_4Cl with enough

ammonia added to bring the pH to 7.2 to 7.5, except as otherwise noted. The pH was measured by means of a glass electrode and Beckman pH meter.

When electrodes were to be discharged they were transferred singly to a vessel holding about 250 ml of the electrolyte. A large cylindrical silver electrode was used as the anode. The electrode to be discharged was mounted in the center of the vessel and centrally with respect to the anode by means of a rubber stopper, which also bore a reference electrode and gas-inlet and outlet tubes. Either air or nitrogen was passed through the solution continuously during the discharge. Current from three dry cells in series was passed through a variable resistance, a calibrated milliammeter, and the cell composed of the experimental manganese dioxide electrode and the silver anode. The initial current was adjusted to 0.1 ma/cm² and fell to about 0.09 ma/cm² at the end of the discharge. The current and the potential difference between the manganese dioxide electrode and reference saturated calomel electrode were measured frequently. The discharge capacity was taken as the summation of current in milliamperes times time in minutes to the time when the potential difference had fallen to zero from an initial value of 350 to 450 millivolts. The fall in potential from about 100 mv to zero was rapid, indicating approximate completion of the discharge.

All measurements were made at room temperature, which was never far from 25°C. The change of electrode potential with temperature in the vicinity of 25°C was found to be -0.0006 v/degree, and temperature errors were seldom more than a millivolt.

Analytical Methods

A number of electrodes were analyzed either as prepared, or after standing in electrolyte, or after discharge. Without weighing, one or more electrodes

TABLE I. Analytical results for some representative electrodes

No. of electrodes	Reducing solution	Mn, total per electrode m-moles	O available per electrode m-moles	x in MnO_x
2 ^a	0.1N H_3AsO_3	0.223 ^a	0.201 ^a	1.90
1 ^a	0.1N H_3AsO_3	0.220 ^a	0.180 ^a	1.82
1 ^b	0.1N H_3AsO_3	0.216	0.186	1.86
6	0.025N H_3AsO_3	0.209	0.137	1.65
2 ^c	0.025N H_3AsO_3	0.213	0.114	1.53
4	0.02N $FeSO_4$	0.212	0.185	1.88
1	0.02N $FeSO_4$	0.172	0.142	1.83

^a Each sample consisted of four 15-min electrodes each. The manganese and available oxygen were calculated on the basis of a two-electrode sample.

^b Two 30-min electrodes analyzed as one sample.

^c These electrodes were placed in 1M ammonia solution for an hour before analysis.

were digested on a steam bath with a measured volume of 0.025 or 0.1N arsenious acid solution to which some sulfuric acid had been added. When the oxide was dissolved and the graphite rod thoroughly washed, the excess arsenious acid was titrated with permanganate. The total manganese was then determined in the same solution after addition of pyrophosphate by potentiometric titration with permanganate (6). This method proved to be defective when applied to electrolytic manganese dioxide on graphite rods, though it has given good results for precipitated manganese dioxide. However, even for the electrolytic oxide it gives fairly reproducible results under a given set of conditions and, because of this, some useful information can be gained from the analytical data.

Some typical results on freshly prepared electrodes are given in Table I. For the data in the first three rows, the standard solution for the available oxygen determination was 0.1N arsenious acid while, for the data in the fourth and fifth rows, the solution was 0.025N. This apparently minor change in procedure led to a large decrease in the apparent x -value in the formula MnO_x . This suggests that the x -value 1.90 may be too small. The data in the last two rows of the table were obtained with a 0.020N iron (II) ammonium sulfate solution substituted for the arsenious acid solution. In this case it was necessary to protect from oxygen while dissolving the manganese dioxide as well as during the final titration. The iron method agrees fairly well with the 0.1N arsenious acid method.

Comparison of the fourth and fifth rows shows another source of error in the arsenite method. Manganese dioxide adsorbs ammonia or ammonium ion, and electrodes treated with an ammonia solution can be expected to retain some ammonia (7). Such electrodes give lower x -values than untreated ones, the retained ammonia apparently affecting the results.

The reproducibility of the electrodes was shown by the analytical data. There is probably little error in the total manganese determination. Of 13 electrodes similarly prepared, two were abnormally low in total manganese, one of them being the single electrode in the last line. If these two are excluded, the average total manganese was 0.213 millimole with a standard deviation of 0.006 millimole, or 3%. The average apparent x -value for the group of six electrodes, 1.65, had a standard deviation of 0.05.

Discharge Experiments

Discharges were made in air and nitrogen atmospheres for checking the effect of oxidation by air. Provision was made for examination of the reduction products. Cahoon (5) found that reduction in the

presence of a large volume of electrolyte gave only manganese (II) ion. At the much higher pH of the present investigation this product is less probable, judging from equilibrium measurements of McMurdie, Craig, and Vinal (8), but it was found in considerable quantity in the electrolyte after discharge. The quantity was determined by potentiometric titration with permanganate in the presence of pyrophosphate (9). The manganese oxide remaining on the electrode after discharge to zero potential against the saturated calomel electrode was analyzed for available oxygen and total manganese with the use of 0.025*N* arsenious acid solution. Data for eight discharges are given in Table II.

The first four electrodes were given the oxygen treatment prior to electrodeposition of the manganese dioxide, and the other four the boiling treatment. The only difference in these experiments that can be ascribed to the treatment of the graphite is that the total manganese (sum of columns 3 and 4) in the oxygen group was 6% less on the average than that of the others. A similar difference was noticed in the total manganese of the two kinds of electrodes when they were analyzed undischarged. For 15-min electrodes with a more severe oxygen treatment the difference was larger, 0.112 millimoles of manganese for normal electrodes and 0.081 millimoles for oxygen-treated.

The electrical outputs varied rather widely. The amount of manganese (II) ion in solution was fairly uniform and was almost half of the total manganese. The oxide remaining on the electrode after discharge to a potential of zero against the saturated calomel electrode varied from $MnO_{1.48}$ to $MnO_{1.58}$. It made little difference whether a current of air or a current of nitrogen was passed through the solution before and during discharge. As indicated in the sixth column, half of the discharges were made one way and half the other. In the last column are given the ratios of oxygen to manganese in the original oxides as calculated from the discharge data. These values are much less variable than any of the other data and are appreciably higher than the original electrode compositions as found by analysis. They are based on the assumption that part of the original oxide was reduced to the oxide remaining on the electrode after discharge and the remainder to the manganese (II) ion found in solution. The calculated original oxide of the four air discharges is somewhat richer in oxygen than that of the nitrogen discharges. This indicates a small oxidizing effect of atmospheric oxygen during the discharge. Another minor effect of the atmospheric oxygen may be on the amount of manganese (II) ion formed, which was in all cases smaller in the air discharges than in the nitrogen discharges.

TABLE II. Discharge data

Electrode No.	Output ma-min	Mn ⁺⁺ in solution m-moles	Mn on electrode m-moles	O available, electrode m-moles	Gas present	Original oxide x in MnO_x
25	336	0.079	0.095	0.055	air	1.92
26	367	0.086	0.100	0.054	N ₂	1.91
28	352	0.077	0.107	0.061	air	1.92
29	354	0.082	0.083	0.040	N ₂	1.91
47	386	0.081	0.105	0.051	N ₂	1.92
48	426	0.077	0.121	0.059	air	1.97
49	404	0.081	0.115	0.060	N ₂	1.93
50	378	0.075	0.097	0.051	air	1.98

There were two sources of error in the data from which the original compositions in the last column of Table II were calculated. One was the separation of a small amount of oxide from the electrode during discharge. The total manganese found on the electrodes and in solution after discharge was one to two milligrams less per electrode than the total manganese on undischarged electrodes according to Table I. The separated oxide could be observed, but was small enough to escape detection unless sought. If this oxide were lower oxide, the x -values would be too high; if it were dioxide, there would be little error. The other source of error was in the available oxygen determination, for which the method was questionable, and would lead to low x -values. The two errors might compensate or the second might predominate. It seems probable that the average x -value for the discharges in nitrogen, 1.92, represents a minimum for the original oxide in spite of the lower analytical values for undischarged electrodes as shown in Table I.

To check the hypothesis that the composition given above for the discharged electrodes is too low, additional electrodes were discharged and analyzed. Five electrodes analyzed using 0.1*N* iron (II) sulfate as the reducing agent gave an average x -value of 1.58 with a range from 1.55 to 1.61. The eight electrodes of Table II averaged 1.53 with a range from 1.48 to 1.58. The difference is not large in view of the variation of the electrodes, but is in the expected direction, since the iron sulfate method gave more nearly correct results than the dilute arsenious acid method for freshly prepared electrodes.

In addition, the oxide was scraped from four discharged electrodes and analyzed without the presence of the graphite rod. The electrodes were discharged with a current density of 0.4 ma/cm², and it is possible that, because of the high current density, the oxide might be a little too high in available oxygen, although there is no evidence for this at present. By 0.025*M* iron sulfate two samples gave 1.61 and 1.61, and by 0.025 arsenious acid two others 1.62 and 1.63 for x . Both methods give correct results for precipitated manganese dioxide. Therefore, it is

probable that the values for available oxygen in Table II are somewhat too low, and that the oxide resulting from the discharge of manganese dioxide under the conditions of the present work is richer in available oxygen than $\text{MnO}_{1.5}$. Feitknecht and Marti (10) showed that the ratio of oxygen to manganese in manganese oxyhydroxide can vary.

*Change in Electrode Potential on Standing
in Electrolyte*

The results of most of the experiments on the change in electrode potential on standing in electrolyte are given in Fig. 1. All of the electrodes were prepared by electrodeposition for 15 min. Each point on or near curves B and C represents the average potential of four electrodes in the same solution. The points on curve A represent the average of three such groups.

The region between the two dashed curves represents seven different groups of four electrodes each, all of which decreased in potential at about the same rate. Curve B is drawn through the average values for three closely agreeing groups, but the points are omitted to avoid confusion; the points shown on curve B belong to a fourth group.

The three groups of curve B had air, oxygen, and nitrogen atmospheres, respectively, with the electrolytes saturated with these gases. No significant differences could be detected. This was true also of the three groups represented by curve A in which the manganese dioxide was deposited on platinum instead of graphite, and in which the electrolytes were saturated with air, oxygen, and nitrogen. The electrodes on platinum decreased at a greater rate than similar electrodes on carbon.

There are three sets of points between the dashed lines representative of electrodes in 2M ammonium bromide, 2M ammonium fluoride, and 1M ammonium perchlorate with enough ammonia in each case

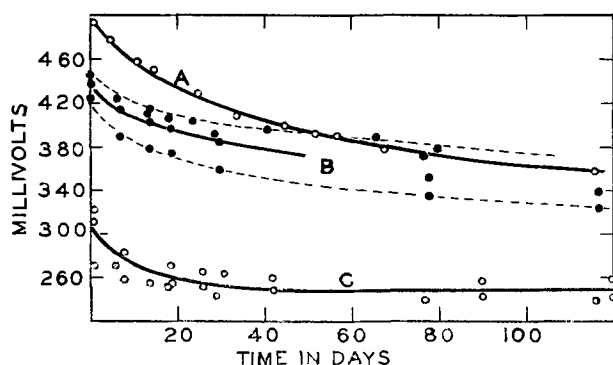


FIG. 1. Change in electrode potential on standing in ammonium salt electrolyte. Curve A represents electrodes of manganese dioxide on platinum, curve B and the region between dotted lines, electrodes on graphite, and curve C, electrodes on oxygen-treated graphite.

to give an initial $p\text{H}$ of from 7.2 to 7.5. Finally, one group is included for ammonium chloride and the hydrogen treatment of the graphite prior to the electrodeposition of the manganese dioxide. The changes on standing are independent of the anion present.

Changes in electrolyte $p\text{H}$, measured after the period of observation, up to 0.25 units had occurred, some in one direction and some in the other. Correction for these would not alter the conclusions, and were not made.

Different groups of electrodes had somewhat different initial potentials, and the differences were maintained for the most part throughout the period of observation; the changes were more consistent than the electrode potentials. The decrease in electrode potential with time is characteristic of all groups represented by curves A and B. For some of the groups it continued for 100 days beyond the period shown in Fig. 1.

The three groups of electrodes represented by curve C were those in which the electrodeposition had followed an oxygen treatment of the graphite. The potentials were much lower than those of the other groups and nearly constant, after an initial decrease. They averaged 0.25 v at $p\text{H}$ 7.5 after more than 200 days, with changes of only a few millivolts after the first month.

That the oxygen treatment gives lower electrode potentials than the normal treatment has been verified in later experiments. The effect varies inversely with the thickness of the oxide layer. For 30-min electrodes no difference is noticed at first but, on standing in electrolyte, the oxygen-treated electrodes decrease faster in potential than the others, falling to a lower value in a short time.

The decrease in electrode potential might have been the result of ion exchange with the electrolyte (7), or of slow loss of available oxygen (11), or it might have been a change from a less stable to a more stable crystal form, or a combination of the

TABLE III. Discharge data for electrodes that had stood in electrolyte more than two years

Electrode No.	Storage electrolyte	Output ma-min	Mn ⁺⁺ in solution m-moles	Mn on electrode m-moles	O available, electrode m-moles	Original oxide x in MnO _x
79	NH ₄ Cl	149	0.0501	0.0330	0.0192	1.79
80	NH ₄ Cl	104	0.0328	0.0245	0.0154	1.84
81	NH ₄ Cl	115	0.0376	0.0387	0.0183	1.71
82	NH ₄ Cl	120	0.0427	0.0327	0.0200	1.76
59	NH ₄ Br	186	0.0641	0.0533	0.0332	1.78
60	NH ₄ Br	165	0.0398	0.0632	0.0442	1.92
62	NH ₄ F	176	0.0602	0.0498	0.0286	1.76
63	NH ₄ F	199	0.0696	0.0440	0.0267	1.78
73	NH ₄ ClO ₄	146	0.0359	0.0243	0.0186	2.06
74	NH ₄ ClO ₄	156	0.0574	0.0325	0.0208	1.77

three. Analyses indicating a loss of available oxygen were found later to be untrustworthy because of the interference of ammonium ion as illustrated in Table I and confirmed by later experience.

Some of the electrodes not used for analysis were observed for a period of over two years. The potentials continued to decrease and at the end of this time were 0.28, 0.27, and 0.25 v (corrected to pH 7.5) for three groups made with ammonium bromide, ammonium fluoride, and ammonium perchlorate electrolytes, respectively. A fourth group, not previously described, of 12 electrodes in chloride electrolyte fell to 0.25 v during this time. Electrodes from each of these four groups were discharged to determine their composition after the long standing in electrolyte. Discharges were made as described above, with analysis of the products and calculation of the composition before discharge as for the experiments of Table II. In the analyses of the discharged electrodes 0.025*N* iron (II) sulfate was used for the available oxygen determination except that 0.025*N* arsenious acid was used for electrodes 79, 80, and 82. Results are shown in Table III.

All discharges made are reported in Table III. The one leading to an original x -value of 2.06 must have been in error, although no source of error was recognized. In most cases, the calculated original ratio of oxygen to manganese (in terms of x in MnO_x) is so much less than the similar values given in Table II for fresh electrodes that it must be concluded that some of the available oxygen has been lost.

The decrease in electrode potential on standing can be explained as the result of the loss of available oxygen. A rough estimate of the capacity loss on standing can be made from the change in electrode

potential, with the help of an appropriate open-circuit discharge curve (1). The loss estimated in this way is in as good agreement as could be expected with that estimated from the data of Table III.

ACKNOWLEDGMENTS

The authors are indebted to A. M. Chreitzberg, Jr., and Stanley Hills for their aid in checking some of the results.

Part of this work was carried out under Contracts N6ori-107 and Nonr-1016(00) with the Office of Naval Research and part on fellowships supported by the American Cyanamid Company and the National Science Foundation.

Any discussion of this paper will appear in a Discussion Section to be published in the December 1955 JOURNAL.

REFERENCES

1. D. T. FERRELL, JR., AND W. C. VOSBURGH, *This Journal*, **98**, 334 (1951).
2. K. ARNDT, H. WALTER, AND E. ZENDER, *Z. angew. Chem.*, **39**, 1426 (1926).
3. C. DROTSCHMANN, "Trockenbatterien," 3d ed., p. 10, Becker and Erler Kom.-Ges., Leipzig (1945).
4. R. C. KIRK, P. F. GEORGE, AND A. B. FRY, *This Journal*, **99**, 323 (1952).
5. N. C. CAHOON, *ibid.*, **99**, 343 (1952).
6. R. F. STALZER AND W. C. VOSBURGH, *Anal. Chem.*, **23**, 1880 (1951).
7. R. S. JOHNSON AND W. C. VOSBURGH, *This Journal*, **99**, 317 (1952).
8. H. F. McMURDIE, D. N. CRAIG, AND G. W. VINAL, *Trans. Electrochem. Soc.*, **90**, 509 (1946).
9. J. J. LINGANE AND R. KARPLUS, *Anal. Chem.*, **18**, 191 (1946).
10. W. FEITKNECHT AND W. MARTI, *Helv. Chim. Acta*, **28**, 129 (1945).
11. R. S. JOHNSON AND W. C. VOSBURGH, *This Journal*, **100**, 471 (1953).

The Anodic Treatment of Aluminum in Sulfuric Acid Solutions¹

ROY C. SPOONER

Aluminium Laboratories Limited, Kingston, Ontario, Canada

ABSTRACT

High purity aluminum was anodized in sulfuric acid solutions at various concentrations (5 – 50%), temperatures (10° – 50°C), time periods (2 – 60 min), and current densities (1.7 – 6.2 amp/dm²). The coating weight, metal loss, coating ratio, sealing weight gain, dyed color, density, and coating chemical dissolution rate were determined.

INTRODUCTION

The sulfuric acid anodizing process for aluminum and its alloys has been adopted widely in industry. By this technique the thickness of the natural oxide film on aluminum can be greatly increased, thus either strengthening many of the oxide film's inherent properties, such as its high corrosion resistance, or contributing new characteristics, such as the ability to become colored by organic dye adsorption.

Early quantitative studies (1) of anodic processes dealt with the metal dissolution and coating formation and determined the current efficiency with respect to these two processes. Later, Anderson (2) presented a theoretical analysis of the mechanism of anodic coating formation. He employed the term "efficiency ratio," defined as the coating weight per gram of metal consumed with a maximum value of 1.89. Anderson's theory indicated that, in sulfuric acid type electrolytes, the highest efficiency ratio would be considerably below this value since part of the aluminum dissolved by anodic reaction diffuses into the electrolyte without forming oxide.

Mason and Slunder (3) presented the results of a broad and detailed quantitative study of the anodic reactions of aluminum in sulfuric acid solutions and their variation with anodizing time, alloy composition, electrolyte concentration, and temperature, etc. The effect of these variables on the efficiency ratio, now termed "coating ratio," was discussed. A similar but less extensive paper was published later by Chanda (4). Kronsbein (5), and Bradshaw and Clarke (6) have continued this study. Their evaluation of the extent of other anodic reactions is of special interest. A recent paper by Mason and Fowle (7) discussed the variation of coating ratio during anodizing under various current densities and at temperatures between 1° and 21°C.

The present investigation employed sulfuric acid solutions and used the technique of Mason and Slunder but extended the range of the several variables studied, noting their effect, not only on metal loss, coating weight, and coating ratio, but also on the weight gain with water sealing, the depth of dyed color, and the apparent density of the anodic film.

EXPERIMENTAL PROCEDURE

High purity aluminum sheet, 0.5 mm thick, having the following percentage composition, was employed:

Fe 0.09, Si 0.04, Cu < 0.01, Mn < 0.01, Al 99.87
(by diff.)

Sets of four panels, each 5 x 15 cm with a small hole drilled at one end, were bolted about 3.5 cm apart and parallel to each other on an aluminum anodizing rack. A glass battery jar (16 x 20 x 26 cm) contained the electrolyte. The cathode, a U-shaped lead sheet, hung from the two opposite sides of the jar. Air agitation and water cooling were provided by glass and lead coils immersed in the solution. The jar was set in a large water bath with air agitation and water cooling coils, and with a thermoregulator - controlled electric immersion heater. The electrolyte temperature was maintained to within $\pm 0.1^\circ\text{C}$ of the set value.

Series of experiments were carried out anodizing in sulfuric acid solutions of 5, 15, 30, and 50% by weight at 10.1, 21.1, 30.4, and 50.2°C² for periods of 2, 5, 10, 30, and 60 min at 1.7 amp/dm² with a moderate degree of air agitation. A duplicate 30 min set was prepared for determination of the dissolution rate of the oxide coating. Another series measured the effect of air agitation under one set of conditions.

Panels were cleaned and oxide stripped (ASTM B-137-45) prior to weighing (W_1). Electroplating

² For convenience designated as 10°, 21°, 30°, and 50° in further references.

¹ Manuscript received October 16, 1953. This paper was prepared for delivery before the Boston Meeting, October 2 to 7, 1954.

stopoff tape was applied before and removed after anodizing to expose 1 dm² of surface. Current connection was made to the rack prior to immersion and disconnected after removal from the electrolyte. Panels were weighed after anodizing (W_2). One panel from each set was immersed in a dye solution (National Alizarine Sapphire SE, 4 g/l, 65°C, pH 6.5) for 5, 5, 10, 10, and 20 min for the 2, 5, 10, 30, and 60 min anodized panels, respectively. These periods were long enough to produce relatively complete dye take-up. The colored panels were sealed in boiling de-ionized water (pH 6.0 \pm 0.2) for a period equal to the anodizing time and then weighed (W_4). Dyed panels were mutually compared and assigned a color rating ranging from 0, no color to 8, heavy color. Panels were oxide stripped, with customary confirmation of complete oxide removal and weighed (W_3).

The oxide film thickness was determined by standard metallographic technique on a thin strip cut from across the middle of one of the dyed 30 min anodized panels. The coating weights per square centimeter in the upper and lower sections were noted by weighing (W_4), oxide stripping, and reweighing (W_3). Apparent film density for the sealed coating was calculated.

The dissolution rate of the oxide coating in the electrolyte was determined by weighing (W_2) the panels from the duplicate 30 min sets and re-immersion in the electrolyte in which they had been anodized under the conditions that had prevailed during anodizing. Individual panels were removed after different immersion periods and weighed (W_5), stripped, and reweighed (W_3). The coating weight and metal loss with this set confirmed the values of the other set but were not included in the results recorded below.

The time of the shortest period of immersion decreased with rise in electrolyte temperature and, to a lesser extent, concentration. The first panels were removed after 5, 2, and 1 min from the electrolytes at 10° and 21°, 30° and 50°C, respectively. The time was reduced to 10 sec with the 30 and 50% acid at 50°C.

The effect of current density was examined in a second series of experiments, employing the procedure listed above, and anodizing in 15% by weight sulfuric acid solution at 21°, 30°, and 50°C at current densities of 0.5, 1.7, 3.6, and 6.2 amp/dm² for periods of 2, 5, 10, and 30 min. At the two higher current densities the panel size was proportionately reduced to permit anodizing with the current employed at 1.7 amp/dm² and so avoid an increased heating effect. Attempts to use 12 amp/dm² produced nonuniform growth of the anodic film with "burning" at points and edges, and results obtained are not recorded. A brief series was done with

5, 30, and 50% acid at 21°C and 3.6 amp/dm². Results obtained with the 5% solution are not listed because of the "burning" encountered.

The following values were determined as indicated:

Metal loss	$W_1 - W_3$
Coating weight	$W_2 - W_3$
Coating ratio	Coating weight/metal loss
Sealing weight gain*	$W_4 - W_2$
Unit sealing	$1000 \times \text{Sealing weight gain/coating weight}$
Coating dissolved by electrolyte	$W_2 - W_5$
Apparent density	$\frac{\text{Coating weight (mg/cm}^2) \times 10}{\text{Film thickness } (\mu)}$

* Includes the relatively small weight gain on dyeing.

Adequate cold water rinses were provided after all solution treatments. No allowance was made for water, sulfuric acid, metal constituents, or aluminum salts in the coating. Under all conditions the bath voltage remained approximately constant during the anodizing period. Values reported are the average for the four panels of each set, except with the 30 min anodized series where they are based on three panels only. Individual panel results generally showed good agreement; otherwise the work was repeated. Values for dyed color, sealing weight gain, and density are based on single panel results.

EXPERIMENTAL RESULTS

Appearance of anodic coatings.—A wide variety of coatings was produced with broad differences in their thickness and other characteristics. The two extremes were (a) a patchy "burnt" coating produced at 10°C with 5% acid, and (b) heavy chalking found at 30° and 50°C. Anodizing under the former conditions quickly formed a thin film with, it is believed, relatively high resistance over the entire surface. This was accompanied by the growth of a thicker film of a different type at many scattered points which were usually close to the bottom and lower side edges of the panel. Current density at such points was higher than elsewhere, affecting the local electrolyte temperature, and resulting in uneven and irregular coating formation. With continued anodizing these points grew together and finally spread over much of the surface. Dyed panels from this series became colored only in the areas with heavier deposit. Microscopic examination showed two distinct layers in the coating. Numerous pit-like points were visible in many of these patches with a center depression surrounded by concentric circles due to crazing. The pit depths were estimated as high as 10 μ . Current densities over 6.2 amp/dm² tended to produce even more pronounced "burning" at particular points or areas.

Air agitation.—Increased air agitation produced a slight rise in the coating weight and coating ratio due to its effect in lowering the electrolyte temperature at the coating-solution interface, and thus decreasing the loss of oxide by chemical dissolution.

Metal loss.—Metal loss values were approximately constant for passage of constant electric charge, regardless of variations in electrolyte temperature, concentration, or current density, and agreed closely with the calculated values.

Tosterud and Mason (8) found that anodizing in a 15% sulfuric acid bath at 27°–32°C takes place with an anodic metal dissolution efficiency of close to 100%, but suggested that at higher bath temperatures the aluminum may react by chemical, in addition to electrochemical, action so increasing the apparent efficiency to over 100%. Results indicate that with the high purity aluminum employed there is no significant chemical solution of the metal or anodic liberation of oxygen during anodizing with 5 to 50% sulfuric acid over the 10°–50°C range with current densities up to 6.2 amp/dm².

Coating weight.—Coating weight increases with anodizing time to a maximum value, which then remains approximately constant. The time required

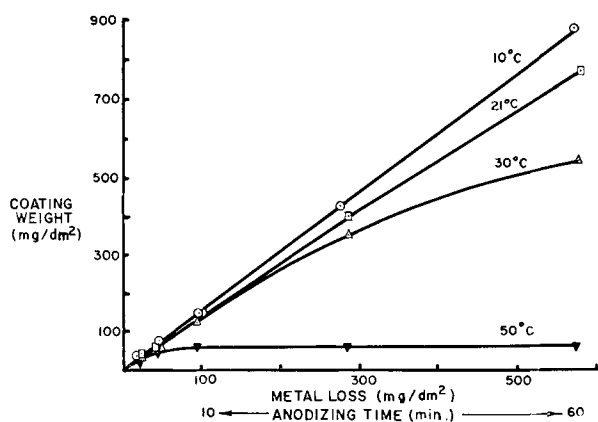


FIG. 1. Coating weight-metal loss relationship at various electrolyte temperatures (15% sulfuric acid, 1.7 amp/dm²).

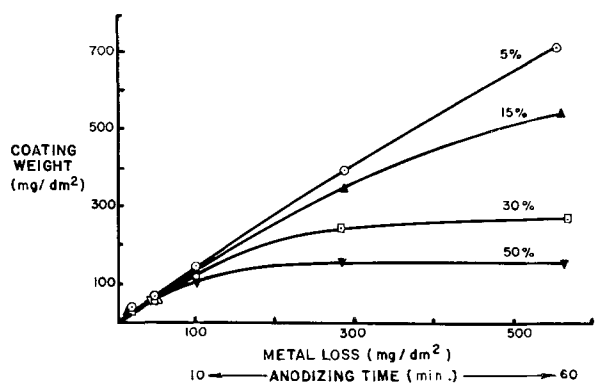


FIG. 2. Coating weight-metal loss relationship at various sulfuric acid concentrations (30°C, 1.7 amp/dm²).

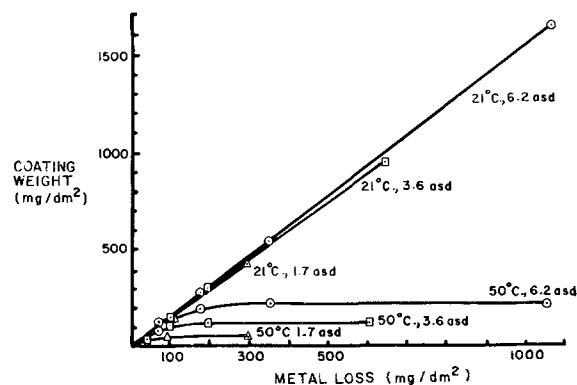


FIG. 3. Coating weight-metal loss relationship at various current densities and temperatures (15% sulfuric acid).

to attain this maximum is lowered by higher electrolyte concentration, increased electrolyte temperature, and lowered current density, as illustrated in Fig. 1, 2, and 3. Choice of suitably low temperature and concentration provides linear growth of coating weight for anodizing periods of 60 min or longer.

Increased current density (Fig. 3) raises the coating weight, but the effect is less striking than that of lowered electrolyte temperature or decreased electrolyte concentration, particularly the former between 21° and 30°C.

The great influence of anodizing conditions is illustrated by the broad range of coating weights and thicknesses obtained. For instance, the 30 min coatings vary from 10 mg/dm² or 0.6 μ thickness (50% acid, 50°C, and 1.7 amp/dm²) to 1622 mg/dm² or 66 μ thickness (15% acid, 21°C, and 6.2 amp/dm²).

Coating ratio.—Under the conditions employed the coating ratio decreases with increased anodizing time, greater electrolyte concentration, higher electrolyte temperature, and lowered anodizing current density. This is illustrated by Fig. 4 and 5, showing the fall in coating ratio with increased metal loss (i.e., prolonged anodizing) under various conditions at 21° and 50°C. These effects are due, as has been pointed out (3), to changes in the dissolution rates of the oxide film, produced by an increase in the surface area exposed to attack, a rise in the dissolving power of the electrolyte at higher concentrations and temperatures, or a slower formation rate, and thus a relatively greater degree of attack. The influence of these factors on coating ratio is much larger at higher electrolyte concentrations and temperatures.

Under some conditions of higher current density and lower temperature (Fig. 5) the coating ratio, after an initial fall, remains almost constant during further anodizing. In no case was there a rise in coating ratio as reported (7) for more extreme conditions.

The coating ratios varied from 0.01 (60 min, 50%

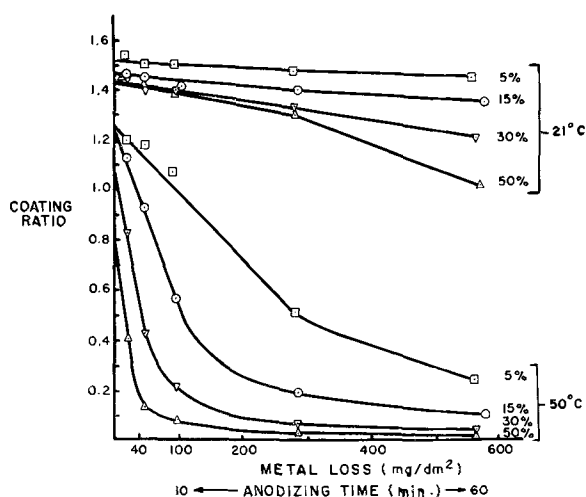


FIG. 4. Coating ratio vs. metal loss at various electrolyte concentrations and temperatures (1.7 amp/dm²).

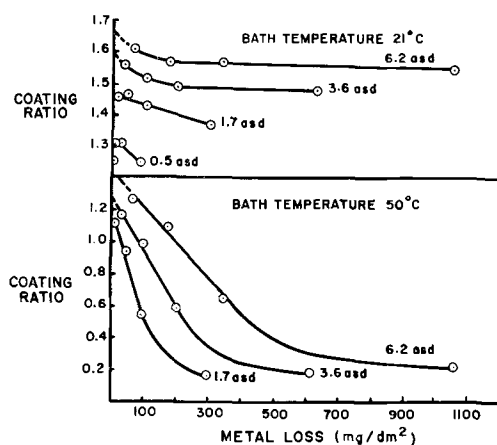


FIG. 5. Coating ratio vs. metal loss at various current densities and electrolyte temperatures (15% sulfuric acid).

acid, 50°C, and 1.7 amp/dm²) to 1.61³ (2 min, 15% acid, 21°C, at 6.2 amp/dm²). The highest value reported by Mason and Slunder was approximately 1.51. Values as high as 1.90 have been secured by Mason and Fowle (7) by anodizing in 15% sulfuric acid at low temperature and high current density (1.1°C, 7.8 amp/dm²). The coating ratio increased with prolonged anodizing under these extreme conditions.

Chemical dissolution of the anodic coating.—Under all conditions the weight loss increased with longer immersion times but at a decreasing rate due to the reduction in the area of coating exposed to electrolyte attack. Dissolution of the thin coatings formed at 50°C, particularly in the more concentrated acid,

³ A special attempt was made to obtain a high coating ratio. A 5% acid solution chilled to 6°C was employed with a current density of 5.4 amp/dm². The current flow concentrated on the two lower edges, and thus produced a non-uniform coating. The coating ratio, in spite of high current density and decreased dissolution rate, was only 1.68.

was very rapid. For instance, the 50% acid coating was removed completely in 30 sec.

The initial dissolution rates (Fig. 6), determined under conditions prevailing during anodizing except for the absence of current, may be taken as an approximation to the coating dissolution rate during anodizing. Values rise with higher bath temperature and acid concentration and range from 0.6 to 30 mg/dm²/min, an increase of fiftyfold in the dissolution rate. This difference explains the wide variations in coating weights and other film properties with anodizing conditions. Calculation of the specific dissolution rates (rates per gram of coating weight) gave a 3000-fold range of values, indicating the wide choice in electrolyte conditions possible.

Sealing weight gain.—The sealing weight gain rose with increased anodizing time at electrolyte temperatures of 10°, 21°, and 30°C. At 50°C gains were more constant in value due to the smaller and less regular effect of continued anodizing on the coating weight. The sealing weight gain would be expected to increase with heavier coatings and/or with an increase in their porosity.

Unit sealing values are dependent in large degree only on porosity. Values increased with greater coating weights. The effect was more pronounced at higher electrolyte temperatures (9) (Fig. 7) and lower current densities (Fig. 8).

Color rating of dyed panels.—The color of the dyed panels covered a wide range extending from ab-

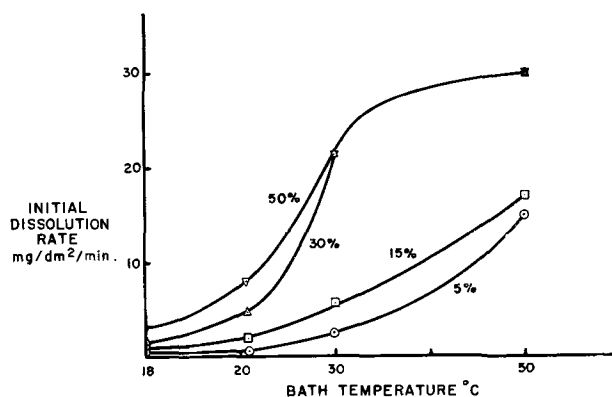


FIG. 6. Dissolution rates of anodic coatings in sulfuric acid electrolyte (panels anodized for 30 min).

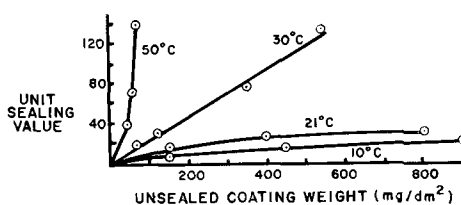


FIG. 7. Unit sealing values vs. unsealed coating weights at various electrolyte temperatures (15% sulfuric acid, 1.7 amp/dm²).

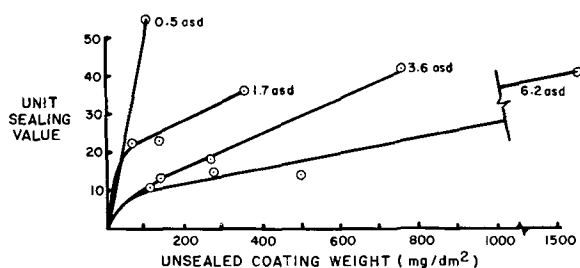


FIG. 8. Unit sealing values vs. unsealed coating weights at various current densities (15% sulfuric acid, 21°C).

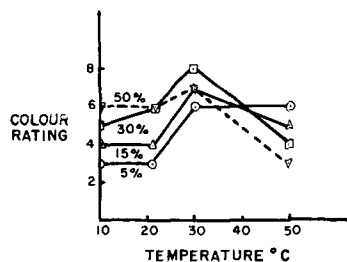


FIG. 9. Effect of electrolyte temperature on the color of dyed anodic coatings (panels anodized for 30 min at 1.7 amp/dm²).

sence of color to a very heavy blue black. The color rating (like the unit sealing values) in general rose with prolonged anodizing, higher acid temperatures, and concentrations. An increase in the temperature (Fig. 9) from 21° to 30°C produced a much darker color. At higher temperatures, the color became lighter. The color rating increased, but only slightly with higher current density.

The following typical example illustrates the qualitative relationships between coating weight, unit sealing value, and color ratings for panels anodized for 10 min in the four electrolyte concentrations at 30°C.

Acid concentration	5%	15%	30%	50%
Color rating	3	4	5	6
Coating weight (mg/dm ²)	137	127	117	109
Unit sealing value	13	31	45	144

The color rating steadily increased, accompanied by a large gain in unit sealing due to increased coating porosity. This was in spite of the lowering in coating weight which would tend to lower the color rating.

Apparent coating density.—The apparent coating density decreased with increased acid concentration and higher temperature (Table I). The effect was more marked at higher concentrations and temperatures. Density fell with higher current densities rather than rising as would be expected. This was due probably to the much greater coating thickness produced as the current density increased. The influence of this variable was not determined. The

TABLE I. Apparent density of sealed anodic coatings (30 min anodized panels)

Sulfuric acid electrolyte		Current density, amp/dm ²	Film thickness, μ	Apparent density
Temp, °C	Conc, % by wt			
10	15	1.7	18.1	2.54
	30		16.8	2.53
	50		19.0	2.39
21	5	1.7	16.3	2.66
	15		16.5	2.64
	30		17.1	2.36
	50		18.7	2.08
30	5	1.7	15.6	2.68
	15		15.0	2.53
	30		15.6	2.04
	50		10.0	1.93
50	5	1.7	9.7	1.9
	15		3.4	1.8
			1.5	1.5
21	15	0.5	4.1	2.8
		1.7	14.0	2.68
		3.6	29.7	2.66
		6.2	66.0	2.46
30	15	1.7	14.9	2.50
		3.6	30.5	2.41
		6.2	58.5	2.18
50	15	1.7	2.5	2.1
		3.6	6.5	2.1
		6.2	12.3	2.1

density of the sealed films varied from 2.68 to 1.5 due to differences in the characteristics, particularly the porosity of the anodic coatings.

DISCUSSION

Anodic Film Growth

The growth rate of the anodic film on high purity aluminum in sulfuric acid solutions is the resultant of two opposing factors: the electrochemical growth of aluminum oxide and the chemical dissolution of the film. The former depends upon current density and anodizing time, but is influenced by changes in anodizing conditions. The dissolution of the coating is affected by the electrolyte composition and concentration, bath temperature, degree of air agitation, and the extent of oxide surface present. With continued anodizing, the dissolution rate rises finally to equal the growth rate. From this point the coating weight remains constant (Fig. 2, 30 and 50% acid curves).

However, this picture is oversimplified and does not include the effect of possible variations in film structure, film composition, and anodic reactions

with changes in anodizing conditions. It also neglects the mutual dependence of some of the anodizing variables. For instance, current density affects not only the rate of film formation, but also the temperature of the liquid film in the pores and on the external surface of the anodic coating (10). A great part of the anode-to-cathode electrical resistance is in the pores, particularly at their base where the so-called "barrier layer" is formed. This layer is believed to be nonporous and thus possesses high resistance. The heating effect at this point should be considerable and will increase with the square of the current. This heat can be dissipated only slowly and, thus, the local temperature will be expected to be considerably higher than the bath temperature. Any increase in current density will consequently increase the local temperature and raise the rate of chemical dissolution in addition to its other effects. Under certain extreme anodizing conditions increased current density may reduce the rate of chemical dissolution of the oxide at the base of the pores due, it is claimed (7), to the build-up of solution products. This has been suggested to explain the rise in coating ratio with prolonged anodizing at low temperatures (1°–10°C) and high current densities (3.9–7.8 amp/dm²).

Coatings can be obtained with a wide range of film properties by a choice of anodizing variables. Many anodic films of given thickness and porosity can be produced by several different combinations of anodizing conditions. Changes in electrolyte temperature have a relatively greater effect on film properties than variations in other conditions, particularly as the temperature rises above 25°C.

Anodic Reactions

The reactions that may take place during anodic treatment of high purity aluminum in sulfuric acid are as follows: (a) electrochemical dissolution of aluminum and formation of oxide; (b) electrochemical dissolution of aluminum and formation of soluble aluminum salts; (c) electrochemical formation and evolution of oxygen; (d) chemical dissolution of oxide by the electrolyte; (e) chemical dissolution of aluminum and liberation of hydrogen.

It has been shown that under the wide range of anodizing conditions studied the metal loss is constant and approximates the theoretical value. This proves that reactions (c) and (e) do not occur to any significant extent under these conditions. Thus, the anodic formation of the oxide coating includes reaction (a) to form the oxide, (d) to form the pores which permit continued anodizing, and (b) which, if present, reduces the coating formation efficiency and the coating ratio. The possibility of (b) has been

mentioned by others (2, 3, 5) but not verified experimentally.

The coating ratio may be represented as follows:

$$\text{Coating ratio} = \frac{\text{Weight of coating formed} - \text{Weight of coating dissolved}}{\text{Metal loss}}$$

The ratio at the moment of initiating anodizing is of special interest. At this point chemical dissolution of the film is just beginning and has its minimum effect on the coating weight. If the dissolution were negligible, the coating ratio would approach the following value.

$$\text{Coating ratio} = \frac{\text{Weight of coating formed}}{\text{Metal loss}}$$

that is, the actual ratio of two processes, the formation of oxide and the accompanying dissolution of aluminum.

Mason and Slunder (3) employed simple extrapolation of the coating ratio-metal loss curves to zero metal loss to yield a value which they employed to calculate the weight of the coating dissolved in the electrolyte during anodizing. This value has been determined for the various anodizing conditions reported above and designated the "CR₀" value, the "coating ratio at zero metal loss."

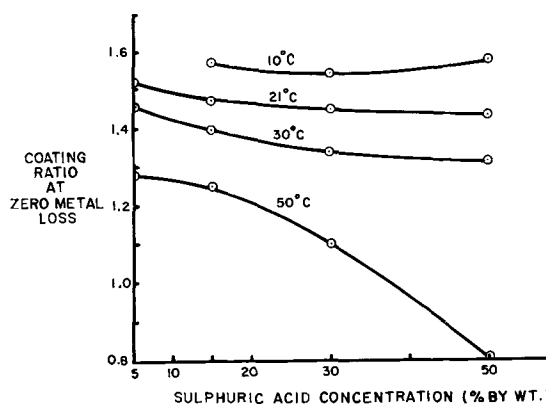


FIG. 10. Effect of electrolyte concentration on coating ratios at zero metal loss at various temperatures (1.7 amp/dm²).

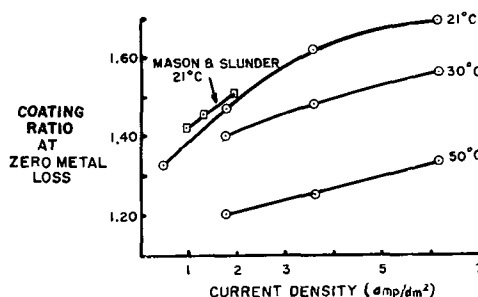


FIG. 11. Effect of current density on coating ratios at zero metal loss at various temperatures (15% sulfuric acid).

The CR_0 values obtained are plotted in Fig. 10 and 11 as functions of electrolyte concentration and current density, respectively. The former has a relatively small effect on the CR_0 at the three lower temperatures, but at 50°C the value drops severely with higher concentration.

As expected, the CR_0 value rises with increased current density (Fig. 11). At 21°C the rate of increase lessens as a current density of 6.2 amp/dm² is approached, and suggests that still higher current densities probably would cause only a slight further increase. Three CR_0 values taken from Mason and Slunder (3) are plotted in Fig. 11, and show good agreement with the other results particularly in view of the slightly different anodizing conditions employed.

The CR_0 values range from 0.80 to 1.67. Even the highest figure is considerably below the maximum theoretical value of 1.89 which is based on the premise that the sole anodic reaction is the electrochemical conversion of aluminum into aluminum oxide. This figure should be increased if allowance is made for the sulfate or water contained therein. Mason and Fowle (7) have mentioned a value of 2.2, but the figure will vary with anodizing conditions due to variations in the sulfate and/or water content.

The effect of chemical dissolution of the oxide film on the CR_0 values will vary with the anodizing conditions, but probably is far from negligible and, under some conditions, quite appreciable. This will lower these values and affect the accuracy of calculated weights of the coating chemically dissolved at various anodizing periods based on such values.

Dissolution rates derived from such calculations should be comparable with initial dissolution rates measured as described above at several anodizing periods. If agreement is lacking the CR_0 value may be varied until such is secured. The modified CR_0 value may be a more accurate measure of the coating ratio at zero metal loss than the extrapolated figure. The initial dissolution rates listed above were obtained only on the 30 min coatings and so permitted checking at this one point only. This technique was applied to one set of conditions and gave fair agreement at 21° and 30°C and poor agreement at 50°C.

Any discussion of this paper will appear in a Discussion Section to be published in the December 1955 JOURNAL.

REFERENCES

1. J. D. EDWARDS AND F. KELLER, *Trans. Electrochem. Soc.*, **79**, 135 (1940).
2. S. ANDERSON, *J. Appl. Phys.*, **15**, 477 (1944).
3. R. B. MASON AND C. J. SLUNDER, *Ind. Eng. Chem.*, **39**, 1602 (1947).
4. B. CHANDA, *Trans. Indian Inst. Chem. Eng.*, **1**, 67 (1949).
5. J. KRONSBELN, *J. (and Trans.) Electrochem. Soc.*, **94**, 353 (1948).
6. W. N. BRADSHAW AND S. G. CLARKE, *J. Electrodepositors' Tech. Soc.*, **24**, 147 (1949).
7. R. B. MASON AND P. E. FOWLE, *This Journal*, **101**, 53 (1954).
8. M. TOSTERUD AND R. B. MASON, *Trans. Electrochem. Soc.*, **90**, 221 (1946).
9. M. SCHENK, "Der Eigenschaften der anodischen Oxydschichten," p. 667, A. Francke Ag. Verlag, Bern (1948).
10. R. C. SPOONER, *Metal Ind.*, **81**, 248 (1952).

An Interpretation of the Significance of the Potentials of Passive Iron¹

M. J. PRYOR

Department of Metallurgical Research, Kaiser Aluminum and Chemical Corporation, Spokane, Washington

ABSTRACT

The steady-state value of the passive potential of iron in anodic inhibitors forming hydrated oxide corrosion products with ferrous ions becomes less noble with increasing pH and with increasing inhibitor concentration. Values of passive potentials in phosphate solutions become more noble with increasing pH. The effect of surface pretreatment and of the addition of small amounts of chloride on the passive potentials is more pronounced at high pH values. Increasing the oxygen concentration of the solutions results in a shift in the steady-state values of the passive potentials in the more noble direction. An explanation of these effects, based on the oxide film theory of anodic inhibition, is advanced.

INTRODUCTION

The electrode potential of iron has long been considered to give some approximate indication of its behavior toward aqueous solutions. For instance, when iron is corroding freely in an aqueous solution, its potential is often of the order of -0.4 to -0.5 v;² when corrosion is inhibited by an efficient anodic inhibitor the potential of iron usually will be of the order of zero volts or more noble. In this connection the ennobled potentials of passive iron are frequently referred to as "passive potentials."

Passive potentials are encountered on iron exposed to solutions of efficient anodic inhibitors. Any interpretation of these potentials depends to a considerable extent on which of the several theories of anodic inhibitors is adopted. Supporters of the precipitation theory (1) have attributed the noble values of the passive potentials to the high degree of anodic polarization resulting from the precipitation of insoluble iron corrosion products at anodic areas or to an increase in the internal resistance of the local corrosion cells for the same reason (2). Until recently, supporters of other theories of anodic inhibition have made no comparable attempt to interpret passive potentials. Recently, however, Uhlig and Geary (3) measured the potentials of electrolytic iron in distilled water containing between 0 and 2.5×10^{-3} moles/liter of chromate. On plotting change in potential against chromate concentration, a curve, similar in form to a Langmuir isotherm, was obtained. The authors, using the electrostatic theory of potential, suggested that

the change in potential was directly proportional to the amount of chromate adsorbed and that the maximum or most noble value of potential measured was proportional to the maximum amount of chromate adsorbed.

However, the main purpose of this article is not to argue the relative merits of different theories of anodic inhibition but to determine how an extension of the oxide-film theory of anodic inhibition (4-11) can account, at least in a semiquantitative manner, for passive potentials and their variation with different conditions in solution.

Values of the passive potentials would appear from the literature to be rather irreproducible and few definite trends have been reported previously for iron. Corrosion investigators have long been interested in the theoretical aspects of corrosion potentials, and Müller and others (12-14) derived equations relating the corrosion potential to the potentials of the local anodes and cathodes, the resistance of the surface oxide film, and that of the pores in its film. It was shown that increasing the resistance of the pores in the oxide film by some type of film repair process (either precipitation of corrosion product or formation of oxide) resulted in a shift in potential in the positive (more noble) direction. At the time these equations were derived, however, the chemistry of the reactions taking place between iron and anodic inhibitors was not well understood and this prevented the investigators from carrying their calculations further.

Recently it has been found possible to determine passive potentials of iron in solutions of anodic inhibitors in a reasonably reproducible manner (8). It was found that, with a very few exceptions, the steady values of the passive potentials became more negative (active) with increasing pH in anodic in-

¹ Manuscript received August 23, 1954. This paper was prepared for delivery before the Boston Meeting, October 2 to 7, 1954.

² All potentials in this paper are expressed on the standard hydrogen scale.

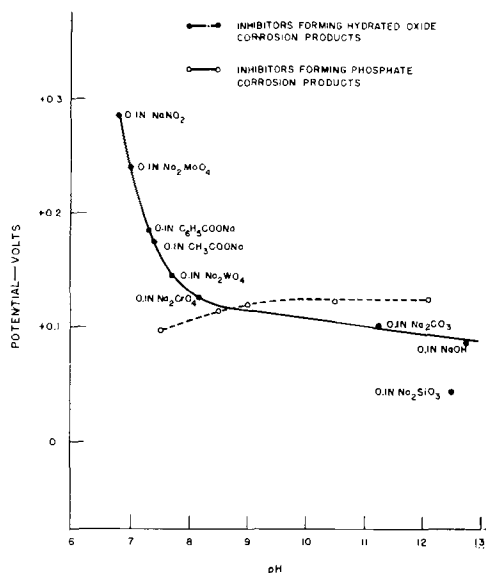


FIG. 1. Relationship between passive potentials and pH . ●—●, Inhibitors forming hydrated oxide corrosion products; ○—○, inhibitors forming phosphate corrosion products.

inhibitors which can form hydrated iron oxide corrosion products, but that they became more positive with increasing dilution of the same inhibitor solution (8). This paper describes an extension of these studies to include such variables as the surface condition of the iron, the oxygen content of the solution, and the addition of chloride ions. An attempt is also made to explain these well-defined trends in the passive potential and also to account for the exceptions to these trends.

EXPERIMENTAL

Materials and methods.—The iron used was in the form of annealed sheet 0.02 cm thick; its analysis was described previously (6). Specimens cut from this sheet were degreased with benzene and cut to size so that an area 2.5 cm x 0.5 cm was exposed to the solution under examination. All solutions were made up with C.P. chemicals and distilled water. The apparatus used for the potential determinations and the experimental method were described in a previous paper (8).

Results

Potential-time curves³ were determined previously (8) on iron specimens freshly abraded with 3/0 emery paper in 0.1*N* solutions of sodium nitrite, molybdate, tungstate, benzoate, acetate, chromate, carbonate, hydroxide, and silicate. These inhibitors are of the type that, at a concentration of 0.1*N*, form hydrated oxide corrosion products on reaction with ferrous ions.

³ All potential-time curves were determined in triplicate.

In this investigation, potential-time curves were determined on iron immersed in five 0.1*M* phosphate solutions having pH values within the range 7.5–12.1. These solutions at a concentration of 0.1*M* form corrosion products of ferrous or ferric phosphate.

Fig. 1 summarizes the relation between the steady-state values of the passive potentials and the pH values of the nine 0.1*N* inhibitor solutions and those of the five 0.1*M* phosphate solutions. The steady value is the value of the potential after five days and changes little with increasing time.

Fig. 2 shows the relation between passive potential and concentration of sodium nitrite, acetate, and chromate. In all cases the potential becomes more noble with increasing dilution, provided passivity is maintained.

Experiments were next carried out to determine the effect of surface treatment on the passive potential. The surface treatments investigated were as follows.

(A) The air-formed oxide films were destroyed by immersing degreased specimens in 0.1*N* hydrochloric acid for 1 min (15); specimens were then washed rapidly in distilled water and immediately exposed to the passivating solution.

(B) Specimens were abraded with 3/0 emery paper and then swabbed with benzene, dried in acetone, and exposed to the passivating solution.

These two surface treatments were selected because they gave consistently the most reproducible results. The effect of these surface treatments was investigated in decinormal solutions of sodium hydroxide, benzoate, and disodium phosphate. The results (Fig. 3) show that iron in the comparatively

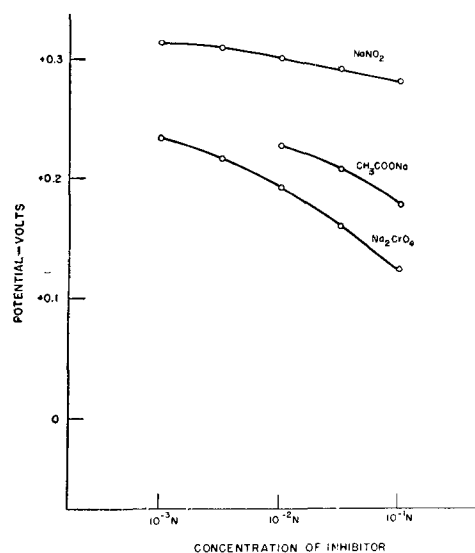


FIG. 2. Relationship between passive potentials and concentration of sodium nitrate, sodium chromate, and sodium acetate.

"film-free" condition, i.e., after treatment with hydrochloric acid, consistently gives lower values of potential than when it carries an imperfect oxide film as after abrasion and that the difference in potential increases with increasing pH .

Experiments were also carried out to determine the effect of adding 10 ppm of chloride ion in the form of potassium chloride to decinormal sodium hydroxide, sodium benzoate, and disodium phosphate. The results (Fig. 4) show that the addition of chloride to disodium phosphate and sodium hydroxide causes a shift in potential in the negative direction and that the effect increases with a rise in pH .

Since the access of air to the solution is influenced by the ratio of surface area of the solution to its volume, experiments were carried out to determine the effect of the area of surface at constant volume of solution on the passive potential in 0.1N sodium hydroxide using specimens having a surface area of 2.5 cm². In the normal method of carrying out these experiments, the ratio of surface area of the solution to its volume is 33:300. Two additional tests were carried out under conditions of free access of the

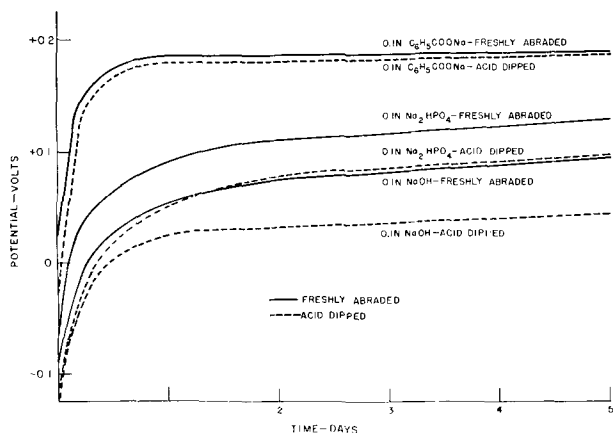


FIG. 3. Effect of surface pretreatment on passive potentials.

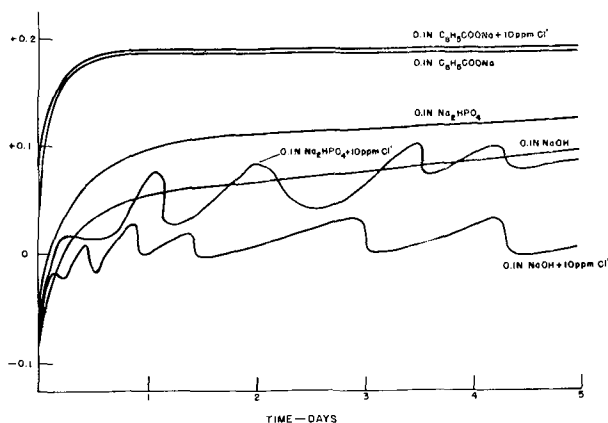


FIG. 4. Effect of chloride ion on passive potentials

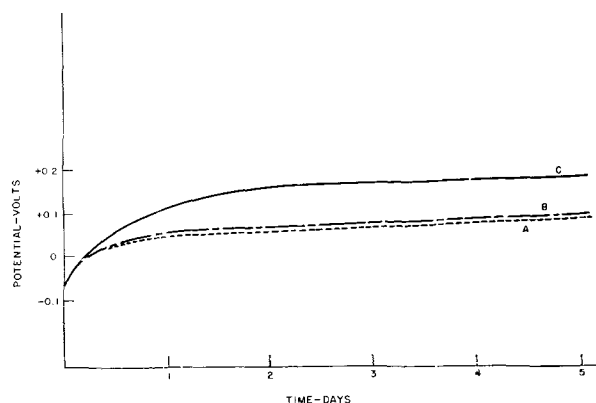


FIG. 5. Effect of surface area of the solution on passive potentials. Curve A, surface area of solution: volume = 33:300; curve B, surface area of solution: volume = 44:300; curve C, surface area of solution: volume = 229:300.

atmosphere to the solution. Ratios of surface area of the solution to volume were 44:300 and 229:300. The area of specimens exposed to the solution was the same (2.5 cm²) in each experiment. However, in experiments with a surface area of 229 cm², specimens were exposed with their short axes vertical rather than their long axes as in all previous experiments. Results are shown in Fig. 5 from which it may be seen that increasing the ratio of surface area of the solution to the volume results in a shift in potential in the positive, more noble, direction.

DISCUSSION

The anodic inhibitors investigated above may be divided into two classes, viz.: (a) those inhibitors which at a concentration of 0.1N form hydrated iron oxides when reacted with ferrous ions and oxygen; and (b) those inhibitors which at a concentration of 0.1M form ferrous or ferric phosphate when reacted with ferrous ions and oxygen.

With inhibitors of the first class, values of the passive potentials of iron become progressively less noble with increasing pH of the inhibitor (Fig. 1) with the exception of sodium silicate.

With inhibitors of the second class the steady-state value of the passive potentials became progressively more noble with increasing pH (Fig. 1), exactly the opposite trend observed in inhibitors forming hydrated oxide corrosion products with ferrous ions. However, over the same pH range, change in potential was less than with inhibitors of the first class.

It is believed that the mechanism of inhibition for the inhibitors studied in this investigation is essentially similar (8). Inhibition is believed to be associated with oxygen dissolved in solution. The oxygen is believed first to adsorb on the iron surface and then to take part in a direct reaction with sur-

face iron ions to form a thin film of $\gamma\text{-Fe}_2\text{O}_3$ which is considered to grow to an equilibrium thickness in a manner similar to that by which oxide films grow on iron in dry air. Rate of growth is probably controlled by the rate of diffusion of iron ions and electrons through the film to the film/solution interface. The film is considered to prevent corrosion by stopping iron ions leaving the metal lattice and passing into solution. However, the formation of a protective film of $\gamma\text{-Fe}_2\text{O}_3$ is not instantaneous and, at discontinuities initially present in the film, very slow corrosion occurs. This corrosion is believed to be subject to a high degree of anodic polarization due to the small size of the discontinuities (anodic areas) in the oxide film.

In inhibitor solutions originally free from iron ions, iron can pass into solution as soluble ions. During this period, the oxide film is considered to be not only thickening, but also to be extending laterally and thus further reducing the size of the anodic areas. However, all inhibitor solutions considered here eventually react with a sufficiently high concentration of ferrous or ferric ion to form insoluble corrosion products, either of hydrated iron oxide or of hydrated iron phosphate. Thus, insoluble corrosion products will ultimately be formed at the discontinuities in the oxide film. The corrosion product is believed to greatly assist the achievement of a passive state by further reducing the rate at which iron ions pass into solution. However, these inclusions of corrosion product are not absolutely necessary for passivity since inhibition can be obtained in sodium cyanide and tartrate which prevent precipitation of corrosion product. The time taken for precipitation depends on the solubility product of the corrosion product, the rate of corrosion of the iron at discontinuities in the film, the pH of the solution and, in phosphates, the phosphate content of the solution. It has been suggested that the precipitation of corrosion products at discontinuities in the passivity film not only increases the anodic polarization, but also interferes with the lateral film growth of the oxide film (8). Thus, the time at which precipitation of corrosion product occurs should determine the size of the inclusions of corrosion product in the oxide film. Their permeability to the outward diffusion of hydrated ferrous ions will determine their final thickness, which appears to be greater than that of the oxide film (5).

For purposes of interpreting passive potentials, it is assumed that formation of oxide by direct interaction of dissolved oxygen with surface iron atoms makes no direct contribution to the potential of the specimen as normally measured. Thus, the passive potential is believed to be the potential of the very slow corrosion reaction leading to the formation of

small inclusions of corrosion product in the passivity film. Therefore, the contribution of the oxide film on the passive potential is indirect in that it influences the size of the anodic areas and the size of the inclusions of corrosion product. The anodic reaction of this corrosion process is believed to be the passage of ferrous ions into solution at discontinuities in the oxide film and the cathodic reaction is primarily the reduction of dissolved oxygen at the surface of the oxide film. Since the anodic areas, even initially, are small, the cathodic area should be essentially constant. The passive potential is a mixed potential since both the anodic and cathodic polarization are appreciable.

The two main reactions taking place during the passivation of iron in anodic inhibitors are thus: (a) formation of a thin film of $\gamma\text{-Fe}_2\text{O}_3$ by direct interaction of the iron surface with dissolved oxygen; and (b) corrosion at initial discontinuities in the $\gamma\text{-Fe}_2\text{O}_3$ film leading eventually to the formation of small and relatively thick inclusions of corrosion-product (7).⁴

Reaction (a), the formation of the oxide film by dissolved oxygen, should be largely independent of pH and should depend only on the concentration of oxygen in solution and on the active mass of the iron. The rate of reaction (b), however, should be controlled largely by the environment surrounding the specimen.

Müller (14) has derived a general relationship for the potential of a metal partly covered with a protective oxide film. This relationship is

$$E = E_A(1 - K) + E_cK \quad (\text{I})$$

where E_A and E_c are the true potentials of the anode and cathode, respectively, E the measured compromise potential, and

$$K = \frac{R_p}{R_p + R_f} \quad (\text{II})$$

where R_f and R_p are the resistances of the film and of pores in the film, respectively. It can be seen that, as the resistance of the pores increases, the fraction K tends to unity and the potential moves in the cathodic direction. When R_p is infinitely large,

$$E = E_c \quad (\text{III})$$

Since the size of discontinuities in the oxide film is initially small, the film resistance and the cathodic

⁴ Oxidizing inhibitors such as chromate, nitrate, tungstate, and molybdate are believed to have the ability to form some oxide at discontinuities in $\gamma\text{-Fe}_2\text{O}_3$ film (8) which accounts for their superior inhibitive powers. The great majority of oxide film is, however, believed to be formed by dissolved oxygen.

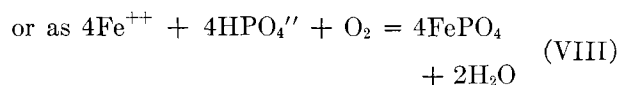
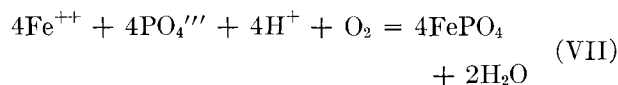
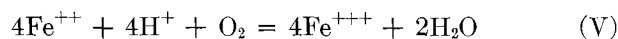
area can be considered to be constant. In the period before precipitation takes place in the pores

$$R_p = \frac{R_o L}{A} \quad (\text{IV})$$

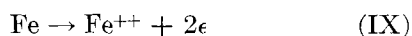
where R_o is the specific resistance of the electrolyte, L equals the length of the pore in the film (approximately the thickness of the film), and A is the cross-sectional area. As film growth proceeds in the absence of precipitation, the lateral extension of the oxide film decreases the value of A and increases R_p . Thus, a relatively rapid initial increase in potential with time is observed for all anodic inhibitors (8). Later, corrosion products become precipitated in the pores, essentially fixing the size of the anodic areas, as suggested above. Equation (IV) shows that the smaller the size of the anodic areas the higher is the value of R_p and that of the potential. Of course, precipitation of corrosion product further increases the resistance of the pores and makes it more difficult for iron ions to pass into solution at these areas. The further gradual increase in the potential with time (6, 8) probably reflects the very slow thickening of the inclusions of corrosion product.

In the case of phosphate solutions, it has been shown that inclusions composed mainly of strengite ($\text{FePO}_4 \cdot 2\text{H}_2\text{O}$) are formed in the passivity films (10). The size of the inclusions (10) and the quantity of ferric phosphate (7) are less in trisodium phosphate (0.2×10^{-3} mg/cm² at $p\text{H} = 12.1$) than in disodium phosphate (0.6×10^{-3} mg/cm² at $p\text{H} = 9.0$). Evidently in these phosphate solutions ferric phosphate is more insoluble than lepidocrocite.

The formation of ferric phosphate can be expressed in equation form as follows



It is assumed in the following arguments that the ferrous ion concentration in solution determines the unpolarized potential of the anode (16, 17) and that the ferrous ion concentration is controlled by the precipitation of ferric phosphate. Accordingly, the basic anodic reaction is:



The initial iron content of the solution is proportional to the rate at which the iron corrodes at discontinuities in the oxide film. According to

Abbott and Bray (18) the $[\text{PO}_4''']$ concentration in aqueous solutions is given by the relationship

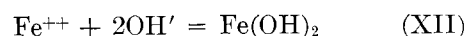
$$[\text{PO}_4'''] = \frac{K_1[\text{HPO}_4'']}{[\text{H}^+]} \quad (\text{X})$$

where $K_1 = 3.6 \times 10^{-13}$. Evidently $[\text{PO}_4''']$ ions are present only in minor quantities in a 0.1M solution of so-called trisodium phosphate ($p\text{H} = 12.1$). This is supported by the absence of an inflection in the neutralization curve of phosphoric acid at a $p\text{H}$ value of 12.1 (6). The solubility product of ferric phosphate is given by the product of the concentrations of $[\text{Fe}^{+++}]$ and $[\text{PO}_4''']$ ions in equilibrium with solid ferric phosphate. From equations (VII) and (X), the solubility product of ferric phosphate can be expressed in terms of concentrations of $[\text{Fe}^{++}]$, $[\text{HPO}_4'']$, and oxygen as follows

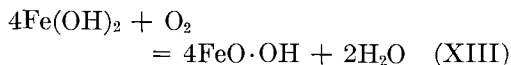
$$S_{\text{FePO}_4} = K_1 K_2 [\text{Fe}^{++}] [\text{HPO}_4''] [\text{O}_2]^{1/4} \quad (\text{XI})$$

where K_2 is the equilibrium constant of equation (V). Since, in the solutions under examination, $[\text{HPO}_4'']$ is approximately constant at 10^{-1}M , the time taken to reach the solubility product of ferric phosphate at constant oxygen concentration depends only on the rate of corrosion of the iron at discontinuities in the oxide film. The rate of corrosion should decrease with increasing $p\text{H}$ of the bulk solution, and so the time elapsing before precipitation of ferric phosphate occurs should increase with increasing $p\text{H}$ of the solution. Since it has been assumed that the formation of insoluble precipitates interferes with the lateral growth of the oxide film, this indicates that the size of the inclusion of corrosion product should decrease and that the anodic polarization and the value of the passive potential should increase with increasing $p\text{H}$ in 0.1M phosphate solutions. This is demonstrated experimentally in Fig. 1. The solubility product relationship shown in equation (XI) is complicated at the lower $p\text{H}$ values by the presence of $\text{H}_2\text{PO}_4'$ ions. However, at $p\text{H}$ value of 7.5 only about 14% of the total phosphate is present as $\text{H}_2\text{PO}_4'$ ions and at a $p\text{H}$ value of 8.5, the fraction is only about 1.4%. The concentration of this ion is, therefore, small and does not invalidate the reasoning outlined above.

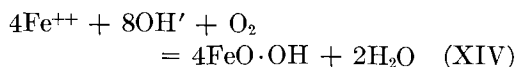
In inhibitors capable of forming hydrated oxide products of reaction with ferrous ions, the passive potential decreases with increasing $p\text{H}$ (Fig. 1), the opposite trend observed in phosphate solutions. In this case, however, the first step in the formation of hydrated-oxide corrosion product, usually lepidocrocite $\gamma\text{-Fe} \cdot \text{O} \cdot \text{OH}$ (10), is probably the precipitation of ferrous hydroxide



Although the exact mechanism of formation of lepidocrocite is not known, Schikorr (19) has suggested that it is formed by the slow oxidation of ferrous hydroxide by air, probably according to a reaction such as:



The over-all reaction may be written as follows



It was suggested above that the rate of corrosion of iron at discontinuities in the passivity film decreased with increasing $p\text{H}$ of the bulk solution. However,

$$S_{\text{FeO}\cdot\text{OH}} = K[\text{Fe}^{++}][\text{OH}]^2[\text{O}_2]^{1/4} \quad (\text{XV})$$

and per unit increase in $p\text{H}$, $[\text{OH}]^2$ increases by a factor of 100. This large increase should easily outweigh the decrease in the rate of dissolution of the iron with increasing $p\text{H}$. The solubility product of lepidocrocite should, therefore, be exceeded more rapidly at higher $p\text{H}$ values and the size of the inclusions of corrosion product should increase. Consequently the resistance of the pores, and also the value of the passive potential, should decrease with increasing $p\text{H}$ of the inhibitor solution (Fig. 1). It is interesting to note that inclusions of lepidocrocite found in passivity films formed in sodium hydroxide were quite large, being of the order of 1–2 microns in diameter (5). Electron microscopic examination of films formed in sodium borate solution which has a much lower $p\text{H}$ did not yield as clear cut results (10). Well-defined rings characteristic of $\gamma\text{-Fe}_2\text{O}_3$ were observed together with a few weak spots which might indicate the presence of a very small amount of second phase. This observation would be in accord with the reasoning outlined above although Mayne (20, 21) considers it possible that ferrous hydroxide can oxidize directly to $\gamma\text{-Fe}_2\text{O}_3$ or to magnetite, and that the presence of these compounds in passivity films does not necessarily imply that the film is formed by direct interaction of dissolved oxygen with the iron surface. However, the balance of the electron diffraction/electron microscope evidence supports the view outlined above.

The one exception to this behavior is that of sodium silicate solutions in which iron exhibits anomalously low values of passive potential (Fig. 1). Sodium silicate is believed to contain negatively charged colloidal silica particles (22) and these would be expected to be attracted to the anodic areas even before precipitation of corrosion product occurs. This would result in interference with the

lateral growth of the oxide and would thus yield larger anodic areas of lower resistance and thus low values of the passive potential.

When solutions of sodium chromate, sodium nitrite, and sodium acetate were diluted, the steady-state value of the passive potential invariably became more noble. Similar behavior was observed on all inhibitors used in this investigation. The relationship between passive potential and inhibitor concentration is shown in Fig. 2. It is believed that the increase in passive potential accompanying the dilution of these inhibitors is due to (a) a decrease in $p\text{H}$ of the solution, and (b) a possible small increase in oxygen concentration of the solution.

The first factor, which has been observed experimentally to be sufficient to account for the greater portion of the change in potential, increases the potential according to the reasoning outlined previously. The second factor, oxygen concentration, is important since it affects the rate of formation of the oxide film. At higher oxygen contents the rate of film growth, and hence the rate of lateral extension of the oxide, would be faster. If the corrosion rate of the iron at the anodic areas were essentially unchanged, then the final size of the inclusions of corrosion product would be smaller and the value of the potential higher. This point is considered in more detail later.

Potentials in phosphate solutions also become more noble with increasing dilution. Although the reduction in $p\text{H}$ accompanying dilution would tend to shift the potential in the less noble direction (Fig. 1), dilution also decreases the concentration of $[\text{HPO}_4^-]$ ions which has a major effect on the solubility product of ferric phosphate (equation XI). Since the effect of $p\text{H}$ on passive potentials in phosphate solutions is relatively small (Fig. 1), the effect of decreasing the $[\text{HPO}_4^-]$ ion concentration is more important. Thus, at lower concentrations of $[\text{HPO}_4^-]$ ions, more ferrous ions must pass into solution to exceed the solubility product of ferric phosphate. Consequently, a large period of time elapses before precipitation, dimensions of anodic areas decrease, and the passive potential becomes more noble.

Since it is believed that the final size of the inclusions of corrosion products determines the values of the passive potentials, it would appear likely that these potentials would be affected by surface pretreatment of the iron. Preparation involving immersion in hydrochloric acid results in a surface carrying less oxide than one that has been abraded with fine emery paper. Of course, the intervening brief exposure to air results in the formation of some oxide, but the areas available for initial anodic reaction should be larger on the acid-washed speci-

mens. Fig. 3 shows that the largest effect of surface pretreatment is observed at the highest pH values. It was suggested earlier that precipitation at discontinuities in the passivity film took place quickly in sodium hydroxide solution. In this solution, the oxide film has only a short period in which it can extend laterally. Consequently, it would be expected that, in this solution, the final size of the anodic areas should be quite highly dependent on the magnitude of their initial size. As the pH of the solution decreases it has been indicated that the time required for precipitation increases and so the effect of initial size of the anodic areas should decrease with decreasing pH.

The effect of the addition of 10 ppm of chloride ion to sodium benzoate, sodium hydroxide, and disodium phosphate solutions is more pronounced at high pH values than at low pH values (Fig. 4), and irregular form of the potential-time curves in sodium hydroxide and disodium phosphate suggests an alternate process of film breakdown and repair. Previous work (23) has shown that the addition of small amounts of chloride greatly reduces the internal resistance of corrosion cells, and that a large part of this reduction of internal resistance was due to the relative ease with which chloride ions can migrate through hydrated oxide corrosion products (23). Thus, at pH values where precipitation occurs earliest, the effect of chloride in reducing anodic polarization might be expected to be greatest (Fig. 4).

In sodium benzoate solutions the potential in the presence of chloride is steady and some 15 mv more positive than in the absence of chloride. This is probably due to a decrease of 0.15 pH units on addition of the chloride. The absence of fluctuation in potential of iron in sodium benzoate-potassium chloride solution is surprising and is not at present understood.

Fig. 5 demonstrates that, as the ease of access of air to the solution is increased, the value of the passive potential becomes more noble. Similar results have been obtained by Uhlig and Geary (3) using different oxygen concentrations. As the access of air, hence the oxygen concentration in solution, is increased, the rate of formation of γ -Fe₂O₃ and, consequently, its rate of lateral growth, should increase. If the rate of the corrosion process at discontinuities in the oxide film is not markedly changed, the size of the corrosion product inclusions should progressively decrease with increasing oxygen

concentration. Accordingly, with increasing oxygen concentration, the anodic polarization and thus the value of the passive potential should increase as shown in Fig. 5. In the absence of oxygen the iron is no longer passive and the potential is of the order of -0.7 v (5).

Actually, the concentration of oxygen influences the solubility product relationships shown in equations (XI) and (XV) in the opposite direction to that considered above. However, oxygen concentration only enters these equations as the $\frac{1}{4}$ power and so its effect is comparatively small.

ACKNOWLEDGMENTS

The author wishes to thank Dr. U. R. Evans, Dr. F. J. Bowen, and Dr. J. F. Murphy for their valuable criticisms and suggestions.

Any discussion of this paper will appear in a Discussion Section to be published in the December 1955 JOURNAL.

REFERENCES

1. U. R. EVANS, "Metallic Corrosion Passivity and Protection," p. 24, Arnold, London (1945).
2. U. R. EVANS, "An Introduction to Metallic Corrosion," p. 73, Arnold, London (1948).
3. H. H. UHLIG AND A. GEARY, *This Journal*, **101**, 215 (1954).
4. J. E. O. MAYNE AND M. J. PRYOR, *J. Chem. Soc.*, **1949**, 1831.
5. J. E. O. MAYNE, J. W. MENTER, AND M. J. PRYOR, *ibid.*, **1950**, 3229.
6. M. J. PRYOR AND M. COHEN, *This Journal*, **98**, 263 (1951).
7. M. J. PRYOR, M. COHEN, AND F. BROWN, *ibid.*, **99**, 542 (1952).
8. M. J. PRYOR AND M. COHEN, *ibid.*, **100**, 203 (1953).
9. M. J. PRYOR, *ibid.*, **101**, 141 (1954).
10. J. E. O. MAYNE AND J. W. MENTER, *J. Chem. Soc.*, **1954**, 103.
11. M. COHEN, *J. Phys. Chem.*, **56**, 451 (1952).
12. W. J. MULLER, *Korr. u. Metallschutz*, **13**, 145 (1937).
13. V. CÜPR, *Z. Elektrochem.*, **45**, 297 (1939).
14. W. J. MÜLLER, *Trans. Electrochem. Soc.*, **76**, 167 (1939).
15. M. J. PRYOR AND U. R. EVANS, *J. Chem. Soc.*, **1950**, 1259.
16. M. COHEN, *Corrosion*, **9**, 372 (1953).
17. W. M. LATIMER, "Oxidation Potentials," p. 210, Prentice Hall, Inc., New York (1938).
18. C. A. ABBOTT AND W. C. BRAY, *J. Am. Chem. Soc.*, **31**, 729 (1909).
19. G. SCHIKORR, *Z. anorg. Chem.*, **191**, 322 (1930).
20. J. E. O. MAYNE, *J. Chem. Soc.*, **1953**, 129.
21. J. E. O. MAYNE AND J. W. MENTER, *ibid.*, **1954**, 99.
22. L. LEHRMAN AND H. L. SHULDENER, *J. Am. Water Works Assoc.*, **43**, 175 (1951).
23. M. J. PRYOR, *Corrosion*, **9**, 467 (1953).

Transformer Oil: Properties of Naphthenic and Aromatic Fractions¹

R. NICHOLS HAZELWOOD,² RAYMOND M. FREY, AND JOANNE B. BROECKER

Line Material Company (A McGraw Electric Company Division), South Milwaukee, Wisconsin

ABSTRACT

Transformer oil can be separated into naphthenic and aromatic fractions by percolation through silica gel. The following properties of the fractions have been determined: d-c conductivity, viscosity, viscosity index, interfacial tension, acid number, steam emulsion number, refractive dispersion, and molecular type. The behavior of these fractions in an arc is discussed with reference to the formation of gases, the production of carbon, and the structural changes of the molecules of the fractions.

INTRODUCTION

One of the more useful techniques for studying the constitution of petroleum-derived materials is selective adsorption. Based on the principles discovered by Tswett, the method is generally known as "chromatography." A technique developed by Mair and coworkers (1), called "displacement development," is particularly useful for the study of electrical insulating oil, the so-called transformer oil.

When a charge of transformer oil is allowed to flow into a column packed with silica gel, adsorption occurs. If the oil is then displaced from the column by a solvent more strongly adsorbed than any of the oil components, the displaced material is found to be separated into two principal groups. Normally, a water soluble alcohol is used for displacement. This permits extraction of the solvent with water. The raffinate oil is readily dried.

The two principal groups of components obtained from transformer oil differ greatly. The first group obtained is a water-white oil which appears to have no unsaturated carbon-carbon linkages. It has a relatively flat viscosity-temperature curve and a low pour point. This is called the naphthenic portion.

Following the naphthenic portion, a yellow oil is obtained. This oil shows characteristic reactions of aromatic compounds, has a steep viscosity-temperature curve, and may contain small quantities of oxygen, nitrogen, and sulfur. This oil is called the aromatic portion.

The types of hydrocarbon molecules normally occurring in petroleum fall into three major classes: paraffinic, naphthenic, and aromatic. The paraffins

and naphthenes are concentrated together by the displacement development technique. The transformer oil used in this work did not appear to contain any paraffins. This was expected from the properties of the base-stock crude and the refining techniques used.

The distinction between an aromatic and a naphthenic molecule is rather precise: if the molecule contains an aromatic ring, it is classified as aromatic regardless of the other structures present. Compounds containing only cycloalkyl rings are known as naphthenes (2).

The available evidence about hydrocarbon types above the gasoline range in petroleum does not permit accurate location of side chains on either aromatic or naphthenic rings. There is good evidence, however, that when more than one ring is present in a compound, it is present in a fused ring system. The typical ring structures are Kata-condensed, rather than peri-condensed, or isolated (2). Strong evidence has been advanced to indicate that aromatic rings usually occur fused with naphthenic rings (3, 4). Structures having isolated rings may also occur (5), although more evidence is needed. For simplicity, only six-membered rings are used in these representations, although cyclopentyl rings may be present (2).³

The behavior of various molecular types when subjected to high voltage discharge (6), cathode rays (7), and capacitance sparks (8) indicates that naphthenic molecules produce large amounts of gas compared to aromatics, and that aromatics tend to have an inhibiting effect on gas production. Work on insulating oils (cable oils) under high voltage discharges (9) and arcs (10, 11) indicates that a similar trend might occur. The situation is complicated, however, by the effect of interrupter design (12). The aromatics also seem to promote forma-

³ A more thorough discussion of molecular structure may be found in reference (2), particularly pages XX and 94.

¹ Manuscript received June 28, 1954. This paper was prepared for delivery before the Chicago Meeting, May 2 to 6, 1954.

² Present address: Donner Laboratory, University of California, Berkeley 4, California.

tion of carbon or "coke" (6, 9, 10). There is little data on the type of gas produced by the various molecular types upon arcing.

Aromatic types have higher viscosities and a lower viscosity index than naphthenic types of similar molecular weight. From the structure, one would expect aromatics, which are more polar molecules, to have a higher density, refractive dispersion, conductivity, and lower interfacial tension (against water); aromatics would be adsorbed more strongly than naphthenes on silica gel (2).

EXPERIMENTAL

Preparation of concentrates.—Twenty liters of uninhibited transformer oil were taken from a newly received tank car. This material was stored at room temperature in a sealed, opaque container. A Pyrex column 5 x 120 cm, packed with silica gel (Davison #922), was charged with 500 ml of transformer oil. A layer (2–4 cm) of silica gel was added on top of the column and reagent grade methanol was added from a reservoir under pressure (ca. $\frac{3}{4}$ kg/cm²). Effluent oils were collected, freed of methanol by washing with distilled water, dried, and stored in sealed glass containers. Approximately 10 l of oil were fractionated in this manner. The oil had a final yield of 82.5% (volume) naphthenic molecules. The losses in the column and due to subsequent manipulations were ca. 10% of the original volume.

Conductivity measurements.—Conductivity was measured using a calibrated cell of cylindrical shape. The cell was approximately 9 x 10 cm and had an electrode spacing of approximately 0.75 cm. The cell constant was 9.73×10^{-3} cm⁻¹.

Interfacial tension.—The procedure followed ASTM D971-50.

Viscosity and viscosity index.—The procedure followed ASTM D445-53 and D567-53.

Steam emulsion number.—The procedure followed ASTM D157-52.

Total acid number.—The procedure followed ASTM D664-49.

Physical properties.—Density, refractive index, refractive dispersion, and carbon content were measured as described previously (13).

Arcing tests.—A plexiglas test cup was used in the arcing tests. It was cylindrical, 4.5 cm I.D. and 14 cm high, and contained tellurium copper contacts which were arranged to give a variable gap space, fixed at 0.25 cm for this work. A 0.038 mm diameter nichrome fuse wire bridged the gap. Application of load melts the fuse and arcing proceeds until the circuit is broken by a manually controlled oil switch. The load was applied from a 4.8 kv source, with a potential transformer of 2875:110 ratio connected across the gap, and a current transformer

of 50:5 ratio in series with the gap. A magnetic oscillograph containing voltage, current, and watt elements was used to record the conditions of each run.

The 220 ml test cup was fitted with a cover sealed by a neoprene gasket, and clamped down. An opening in the side of the cup below the contact level was connected to a standpipe to permit escape of oil as the gases were formed by the arc.

From the calibration data, the arc energy in kilowatt seconds could be determined by planimeter integration of the oscillograph record. The procedure eliminates the necessity of accurate measurement of the effective arc column length; it also simplifies the adjustment of the contact gap, because only a low order of accuracy is necessary.

Molecular type analysis.—The molecular structures of the concentrates were determined by correlations with physical properties. The naphthenes were analyzed using the *n-d-M* correlations described by Van Nes and Van Westen (2), and the aromatics by the Hazelwood method (14). These correlations express the composition of an oil in terms of the average number of aromatic rings, R_A , and the average number of naphthenic rings, R_N , per molecule. These correlations can also be used to express the average number of paraffinic carbon atoms present as side chains on the ring, C_P (14).

RESULTS AND DISCUSSION

Fig. 1 is a plot of current density vs. field intensity for the naphthenic and aromatic concentrates. Fig. 2 is a plot of conductivity vs. time for the concentrates, at a field strength of 20 kv/cm. These curves are similar to those obtained for hydrocarbons (15).

Table I summarizes the results of all the other tests on the aromatic and naphthenic concentrates. The polar nature of the aromatic concentrate is

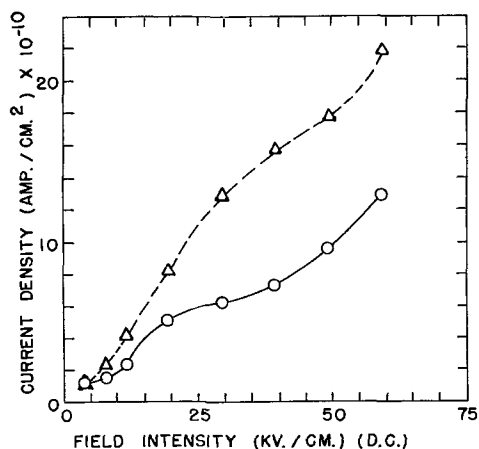


FIG. 1. Current density vs. field intensity d-c measurement. —○— Naphthenic concentrate; --△-- aromatic concentrate.

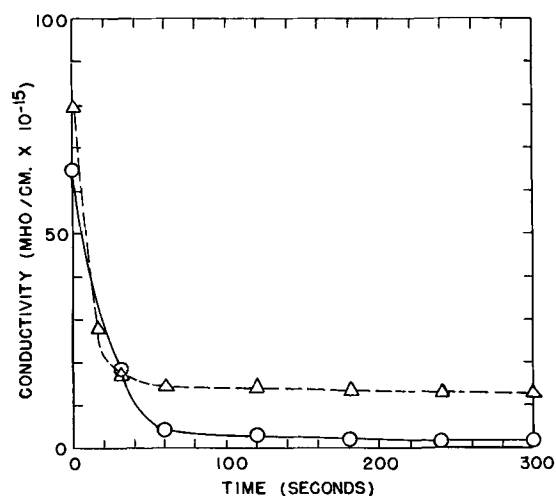


FIG. 2. D-C conductivity vs. time. Potential 20 kv/cm. —○— Naphthenic concentrate; - -△- - aromatic concentrate.

evident from the values of interfacial tension, conductivity, and refractive dispersion.

When a mixture of compounds, such as oil, is percolated through silica gel, fractionation occurs. The least polar compounds, being least strongly held by the adsorbent, move at the greatest rate and are eluted first. In the case of the transformer oil used in this work, the first compounds eluted are the naphthenes with the longest side chains. The aromatics follow the various naphthenes and, as a rule, the aromatics are separated on the basis of the number of aromatic rings present. Thus, the benzene type aromatic systems precede the naphthalene types, etc. Finally, after the aromatics, the oxygenated compounds, and the sulfur and nitrogen compounds, if any, are eluted (2).

TABLE I. Properties of isolated oil concentrates

	Naphthenes	Aromatics	Typical values for original oil
D.C. Conductivity (mho/cm).....	1.9×10^{-15}	1.2×10^{-14}	—
Viscosity 100°F (centistokes).....	7.96	11.32	9.3
Viscosity index.....	84	7.5	60
Interfacial tension (dyne/cm ⁻¹) (vs. H ₂ O).....	45.2	29.2	44
Steam emulsion number (sec).....	29	50	30
Total acid number (mg KOH/g).....	0.003	0.018	0.010
Refractive dispersion ($n_p - n_c$) $\times 10^4$	77	127	83
Number of aromatic rings.....	0.00	0.93	0.40
Number of naphthenic rings.....	1.92	1.19	1.75
Number of paraffinic carbon atoms.....	9.2	7.7	8.8

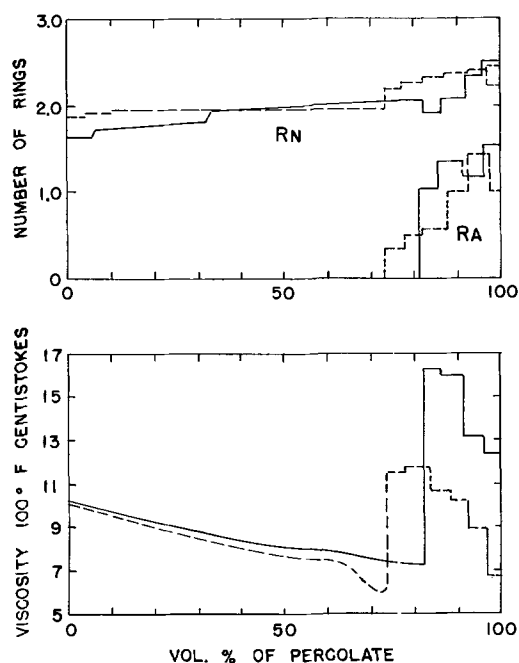


FIG. 3. Fractionation of transformer oil on silica gel. - - -Original oil; —oil after arcing 60 times at 7.2 kv, 490 amp, 30% p.f. [See Reference (13)].

Fig. 3 shows percolation curves for a transformer oil before and after arcing in an oil circuit recloser (13). Table II lists the properties of the aromatics concentrated from these samples. The method of determining ring content, aromatic content, and number of paraffinic carbon atoms is based on that of Kurtz and Martin (16). The data indicate that there is a shift toward a higher molecular weight, a decrease in the amount of aromatic compounds present, and an increase in the number of paraffinic carbons. This agrees with the idea that the lighter fractions of the oil are decomposed, and that some aromatic rings are hydrogenated. Such fractionations, however, do not give conclusive information about processes involved in arcing.

Various studies on arcing in oil indicate that the primary reaction is to break down the oil molecules to hydrogen and hydrocarbon gases. Some carbon is formed as well. This carbon may be elemental carbon or highly cross-linked hydrocarbon polymers. The gases formed are approximately 70% hydrogen, 10–25% acetylene, and smaller amounts of methane, ethylene, and aromatics (11, 17, 18). The volume of

TABLE II. Aromatic concentrate from original and arced oil

	Before arcing	After arcing
Vol. % aromatics.....	17.5%	16.5%
Mol. weight.....	270	285
No. aromatic rings.....	1.16	1.18
No. naphthenic rings.....	1.35	1.30
No. paraffinic carbon atoms.....	7.5	8.6

gas produced per kilowatt second of arc energy is estimated to range from 35 cc (12) to 70 cc (11) for plain break contacts. Investigations of pure compounds indicate that naphthenes are somewhat decomposed, but that some fraction is converted to olefins and polymerized (6). Paraffins seem to be more susceptible to polymerization, and aromatics are readily condensed (6). In oil, some lighter fractions may be formed (17), and these are thought to promote gas formation (9).

Aromatic content of oils seems to be related to carbon formation (9). Condensation of aromatics could promote this (6), and the type of refining, which is related to the aromatic type, has an influence (10). Oura (19) showed that arcing produced approximately one-half as much carbon in a so-called "over-refined" transformer oil as in a normally processed oil.

This work did not demonstrate any marked difference in the volume of gas produced per kilowatt second in the naphthenic and aromatic concentrates (Fig. 4). The gas volume produced by the aromatic concentrate was only slightly less than that produced by the naphthenic concentrate. The difference, on only three samples, was not significant. The average for all samples is 55 cc gas/kw sec at S.T.P., in good agreement with other work. Kesselring (20) found 60 cc/kw sec, Magrini (21) found 53 cc/kw sec, Schrottke (22) found 56 cc/kw sec, and Muller (23) found 60 cc/kw sec. Todd and Thompson (12) suggest 60 cc/kw sec as reasonable for high currents, i.e., above 400 amp. In Fig. 5, which is a portion of an oscillograph tracing of arcing in the naphthenic concentrate, the arc current is 27 amp (rms). For low currents, Todd and Thompson (12) suggest a value of 35 cc/kw sec.

The oscillograph record shown in Fig. 5 is typical of runs on both naphthenic and aromatic concentrates. The upper trace is the arc watts. Periodic

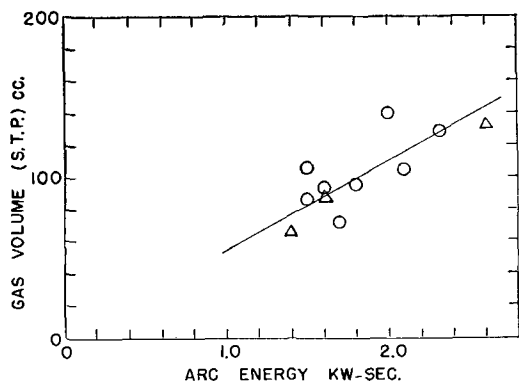


FIG. 4. Gas volume at S.T.P. vs. arc energy in kw-sec. O = Naphthenic concentrate; Δ = aromatic concentrate. Average = 55 cc gas/kw sec; average deviation = 7.2 cc/kw sec; maximum deviation = 15 cc/kw-sec; standard deviation = 9.4 cc/kw sec.

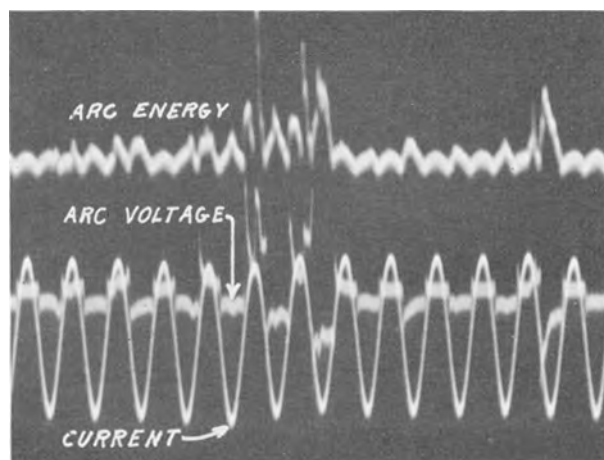


FIG. 5. Portion of oscillograph record of arcing in naphthenic concentrate.

bursts of energy were found in all cases. The sine curve is the current, and the other lower curve is the instantaneous arc voltage.

Fig. 6 is a diagram of the variations in the carbon contents of the samples. While there is a wide range of values, it appears that the aromatic concentrate generally produces much more carbon for a given amount of energy than the naphthenic concentrate. The aromatic concentrate averages approximately three times as much carbon per kilowatt second, in agreement with earlier work.

Oil samples from the various tests were filtered to remove the carbon. Refractive index, dispersion, density, and viscosities at 37.8°C (100°F) and 98.9°C (210°F) were determined. Molecular weight was calculated from the viscosity data (24). The percentage of aromatic molecules present (as opposed to the aromatic rings) was estimated from specific dispersion measurements (25).

Table III shows some of the results from selected runs. With the naphthenic concentrate, the percentage of aromatic molecules present increased.

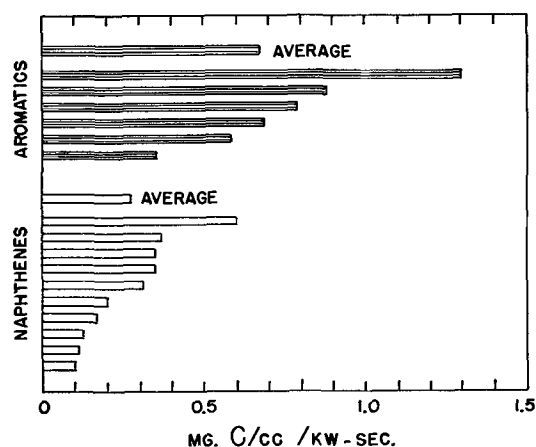


FIG. 6. Carbon content/kw sec for all samples

TABLE III. Arcing tests of naphthenic and aromatic concentrates

Material	M	V.I.	R_N	$\%C_P$	AR%	Arc energy
Original naphthenic...	267	84	1.92	9.2	0.0	—
Naphthenic #1.....	274	86	1.97	9.5	3.3	5.4
Naphthenic #11.....	261	74	1.90	8.9	4.3	8.1
Original aromatic....	253	7.5	1.19	7.7	85	—
Aromatic #10.....	270	46	1.23	8.7	85	1.4

M = molecular weight calculated from two viscosities.

V.I. = viscosity index.

R_N = number of naphthenic rings.

$\%C_P$ = number of paraffinic carbon atoms.

$\%AR$ = percentage aromatic molecules, estimated from specific dispersions.

Arc energy = kw sec.

The general behavior was a decrease in molecular weight, viscosity index, and number of paraffinic carbon atoms. A very few cases, however, showed a pattern such as naphthenic run No. 1 in Table III.

The aromatics showed an increase in molecular weight, viscosity index, and number of paraffinic carbon atoms, and no change in the per cent of aromatic molecules present. There was evidence that the gases formed by arcing the aromatics contained considerably more acetylene than the gases from the naphthenes. Complete data are not available on this matter.

In a previous discussion of the mechanisms of arcing breakdown in transformer oil (13), the analogy to thermal cracking was cited. With the evidence obtained from work on the aromatic and naphthenic concentrates, this analogy becomes clearer. In thermal cracking, naphthenes tend to dehydrogenate their rings rather than to open them (26). Thus, in Fig. 7, reaction I is more probable than reaction II. In this figure, the nature and orientation of the alkyl side chains is not specified. There is some evidence to support a concept of a

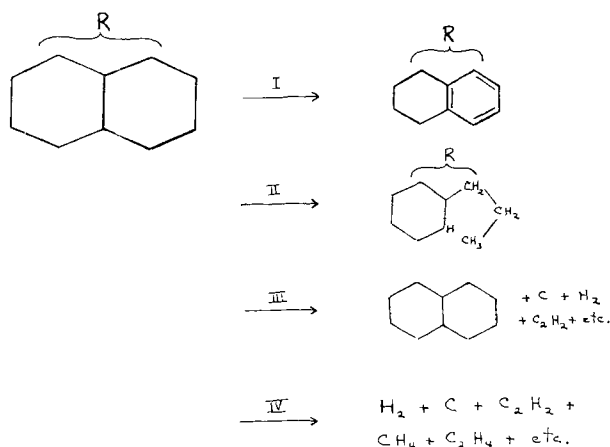


FIG. 7. Reactions of naphthenic molecules in an arc

number of short side chains rather than one long side chain (2, 27). While the ring system is shown as a decalin ring, there are undoubtedly some compounds present with one or three naphthene rings as well. The decalin ring represents an average composition of the concentrate.

Thermal cracking of naphthenes also causes a random splitting of side chains (26); this is represented by reaction III of Fig. 7. Finally, some decomposition to the elements and to light hydrocarbon gases occurs (reaction IV of Fig. 7). A further possibility is polymerization of the naphthenes (not shown).

If all of the reactions suggested are of equal probability, one could expect the mixture to have a lower molecular weight, an increase in aromatic content, a smaller number of paraffinic carbon atoms, and a lower viscosity index. If the polymerization reaction and selective decomposition of the lower molecular weight compounds occurs, there should be a shift toward higher molecular weight, increased naphthenic rings, higher viscosity index, and increased number of paraffinic carbon atoms. Forma-

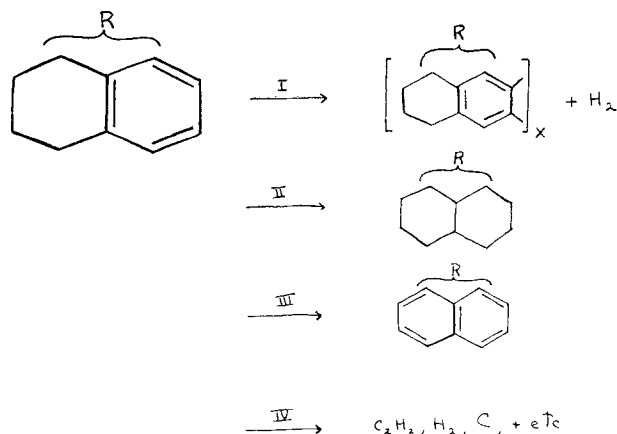


FIG. 8. Reactions of aromatic molecules in an arc

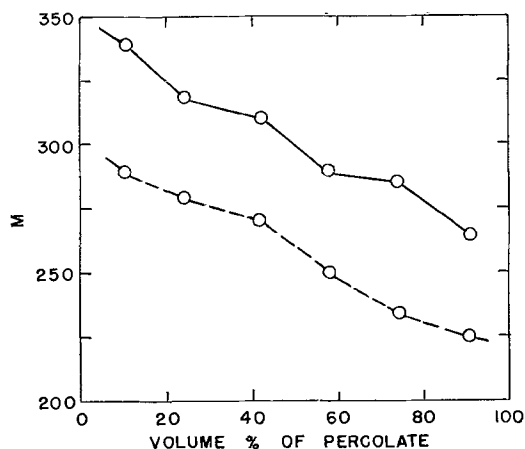


FIG. 9. Silica gel fractionation of arced and original aromatic concentrates. --Original; —arced.

tion of aromatic rings should also occur. The authors have not been able to find good evidence for such a selective reaction pattern.

Fig. 8 shows some of the probable cracking reactions of the aromatic concentrate. An important feature of thermal cracking of aromatics is condensation of nuclei by elimination of hydrogen (26) (reaction I). This is similar to results found with high voltage discharges on pure aromatic compounds (6). Fig. 9 shows the results of silica gel fractionation of an aromatic concentrate before and after arcing. It can be seen that an appreciable number of higher molecular weight condensation products have been formed.

Further possibilities are hydrogenation of rings to naphthenic structures (reaction II), dehydrogenation of naphthenic rings to condensed aromatic systems like naphthalene (reaction III), and decomposition (IV). Reactions I, II, and IV of Fig. 8 are considered to be the predominant ones. It is unlikely that an appreciable quantity of aromatic rings is formed. The experimental data in Table III indicate that a significant increase in paraffinic carbons occurs, as well as an increase in naphthenic rings which might be significant. These would account for the increased viscosity index (2). It is possible that ring-opening is also a factor in the reactions.

The reactions of the molecular types can be summarized:

(A) The principal reaction caused by arcing of either molecular type in oil is decomposition to hydrogen, carbon and coke, and light hydrocarbon gases. Evidence presented indicates that the amount of gas produced is approximately the same for either molecular type for a given amount of arc energy; that the composition of the gases from naphthenic types and aromatic types may differ; and that aromatic types produce approximately three times as much carbon for a given amount of arc energy as do naphthenes.

(B) Secondary reactions of naphthenes yield aromatic molecules, and often involve a decrease in molecular weight as well as a decrease in side chain length. Little ring opening or condensation is involved.

(C) Secondary reactions of aromatic molecules yield condensation products by elimination of hydrogen and show side chain cleavage. A general shift to a higher molecular weight occurs, indicating the importance of condensation reactions.

ACKNOWLEDGMENTS

The authors wish to thank Dr. C. M. Cheng and Mr. R. E. Riebs for their help in devising the arcing

apparatus and tests, and for their help in performing the arcing experiments. Thanks are also extended to Mr. L. R. Larson for assistance in making the conductivity measurements and to Messrs. A. Van Ryan, L. A. Peppey, and L. C. Westphal for helpful discussions.

Any discussion of this paper will appear in a Discussion Section to be published in the December 1955 JOURNAL.

REFERENCES

1. B. J. MAIR, A. J. SWEETMAN, AND F. D. ROSSINI, *Ind. Eng. Chem.*, **41**, 2224 (1949); B. J. MAIR AND J. D. WHITE, *J. Research, Natl. Bur. Standards*, **15**, 51 (1935).
2. K. VAN NES AND H. A. VAN WESTEN, "Aspects of the Constitution of Mineral Oils," Elsevier Publishing Co., New York (1951).
3. K. VAN NES, H. I. WATERMAN, H. A. VAN WESTEN, AND H. VAN KRANEN, *J. Inst. Petroleum*, **38**, 998 (1952).
4. B. J. MAIR, C. B. WILLINGHAM, AND A. J. STREIFF, *J. Research, Natl. Bur. Standards*, **21**, 581 (1938).
5. M. R. LIPKIN AND C. C. MARTIN, *Ind. Eng. Chem., Anal. Ed.*, **19**, 183 (1947).
6. H. BECKER, *Wiss. Veröff. Siemens-Konzern*, **8**(2), 199 (1929); *ibid.*, **5**(1), 160 (1926).
7. C. S. SCHOEPFLE AND L. H. CONNELL, *Ind. Eng. Chem.*, **21**, 529 (1929); C. S. SCHOEPFLE AND C. H. FELLOWS, *ibid.*, **23**, 1396 (1931).
8. H. F. CHALCOTE, C. A. GREGORY, JR., C. M. BARNETT, AND R. B. GILMER, *Ind. Eng. Chem.*, **44**, 2656 (1952).
9. G. W. NEDERBRAGT, *J. Inst. Elec. Engrs.*, **79**, 282 (1936).
10. A. W. THOMPSON AND J. C. WOOD-MALLOCK, *J. Inst. Elec. Engrs.*, **90**(II), 35 (1943).
11. E. B. WEDMORE, W. B. WHITNEY, AND C. E. R. BRUCE, *J. Inst. Elec. Engrs.*, **67**, 557 (1929).
12. R. W. TODD AND W. H. THOMPSON, "Outdoor High Voltage Switchgear," Pitman & Sons, Ltd., London (1937).
13. R. N. HAZELWOOD, K. OURA, AND R. M. FREY, *This Journal*, **101**, 185 (1954).
14. R. N. HAZELWOOD, *Anal. Chem.*, **26**, 1073 (1954).
15. A. GEMANT, "Physical Chemistry of Hydrocarbons," **1**, 215, Academic Press, Inc., New York (1950).
16. S. S. KURTZ, JR., AND C. C. MARTIN, *India Rubber World*, **126**, 495 (1952).
17. W. F. COOPER, *J. Inst. Elec. Engrs.*, **90**(II), 23 (1943).
18. C. E. R. BRUCE, *J. Inst. Elec. Engrs.*, **69**, 557 (1930).
19. K. OURA, Unpublished data, Line Material Co. Laboratory (1948).
20. F. KESSELRING, *Elektrotech. Z.*, **48**, 1278 (1927).
21. L. MAGRINI, "Contributo all Studia della Formazione dell 'arco nell' alio," Bergamo, Italy (1927).
22. F. SCHROTTKE, *Elektrotech. Z.*, **40**, 625 (1919).
23. A. L. MULLER, *Ark. Elektrotech.*, **24**, 503 (1930).
24. A. E. HIRSCHLER, *J. Inst. Petroleum*, **32**, 133 (1946).
25. A. V. GROSSE AND R. C. WACKER, *Ind. Eng. Chem., Anal. Ed.*, **11**, 614 (1939); S. GROENINGS, *ibid.*, **17**, 361 (1945).
26. R. C. HANSFORD, "Physical Chemistry of Hydrocarbons," **2**, 188, Academic Press, Inc., New York (1953).
27. C. C. MARTIN AND A. SANKIN, *Anal. Chem.*, **25**, 206 (1953).

Relation of Color to Certain Characteristics of Anodic Tantalum Films¹

A. F. TORRISI²

General Electric Company, Hudson Falls, New York

ABSTRACT

Anodic oxidations of tantalum have been conducted over a range of formation voltages and temperatures. The thickness of the resultant film has been measured by several methods and related to the capacitance per unit area. The product of the voltage of formation, E , and the temperature of formation, T , (in °K) was found to be a constant for a specific film thickness. The gravimetric method of measuring film thickness was used to estimate a density lower than 8.7 commonly used for Ta₂O₅. Electrical losses of the Ta₂O₅ film are lower if the formation is carried out at higher temperatures. The color of the anodic film defines the voltage and temperature conditions of formation, which, in turn, determine the initial capacity and the expected capacity changes with time, temperature, and voltage stresses on accelerated life tests.

INTRODUCTION

The practical objective of this work was to produce an anodic film on tantalum which was as thin as possible and which resisted changes in thickness and electrical resistance under accelerated conditions of capacitor life test (usually rated d-c voltage at 85°C).

The studies were concerned with measuring film thicknesses obtained by known methods of anodic formation where formation voltage comprised the usual variable. The general procedure was to connect the tantalum to the positive terminal of a voltage supply and form to a given voltage at a given temperature. An estimate of film thickness was indirectly obtained by measuring the capacitance of the oxidized foil on a suitable capacitance bridge. The capacity in microfarads/in.², C , was known to vary inversely with the formation voltage, E . Since capacitance was also known to vary inversely with the thickness of the dielectric, then the thickness of the tantalum oxide varied directly with the formation voltage. Guntherschulze (1) shows that the thickness of a tantalum oxide film is 21 Å/v at 20°C. This statement, accurate as it may be, requires closer scrutiny, when formations are carried out not only at different voltages but different temperatures. It has been observed by the author that tantalum formed to a constant voltage at widely different temperatures varied greatly in capacity, inferring, therefore, wide differences in the film thickness. These suspicions were subsequently verified.

¹ Manuscript received July 1, 1953. This paper was prepared for delivery before the New York Meeting, April 12 to 16, 1953.

² Present address: Ohmite Manufacturing Company, Skokie, Illinois.

Four methods of measuring film thickness were selected. Two of these methods, namely, weight measurements and the use of the photoelectric spectrophotometer, have been reported also by Waber and coworkers (2) in their studies of the air oxidation of tantalum. The two other methods are a direct comparison with a standard color gauge, described by Blodgett (3) such as barium stearate interference colors, and the observance of maximum extinction points when examined with a sodium lamp.

EXPERIMENTAL PROCEDURE

Tantalum of high purity, 10 mils in thickness, was rolled down in a Sendzimir mill to a thickness of ½ mil. Samples for anodizing were cleaned and thoroughly rinsed.

The sheet was then suspended in a forming electrolyte of the type commonly used and described by Deeley (4). Tantalum was connected to the positive terminal of the d-c power supply and a metal beaker served to complete the circuit. An on-off switch, a voltmeter, ammeter, and rheostat were also included in the circuit. The beaker may be heated with a Glas-col mantle or placed in a constant temperature bath. Temperature was kept to ±3°C. Anodizing for these experiments was performed at a current density of 20 ma/in.² until terminal voltage was reached, after which constant voltage was applied for 1 hr.

After the oxide film was deposited, the tantalum sample was washed in distilled water, acetone dipped, and air dried prior to weighing or color comparison.

Specimens were anodized from 5 to 500 v and temperatures from 0° to 200°C. The capacitance, per cent dissipation factor, and electrical leakage

measurements of the foil were made as a guide of expected performance in a capacitor. Some of these foils, or comparable ones, were used in a practical electrolytic capacitor and placed on accelerated life test. In addition to these tests, thickness measurements of the oxide film were made.

GRAVIMETRIC RESULTS OF OXIDE THICKNESS

The procedure used to obtain the film thickness of anodized tantalum by the gravimetric method was to weigh the tantalum before and after anodizing on an analytical balance. The density of anodic Ta_2O_5 is assumed equal to that of the crystalline form. The oxide surface is assumed smooth and the area of the oxide assumed to be equal to the area of the tantalum sheet. When tantalum sheet deviates from smoothness, as it can be made to by suitable etching, then final results of thickness by this method will be in error by an order of magnitude equal to the etch ratio. The inherent roughness of tantalum is neglected in the nonetched sheets.

The thickness of the oxide film is calculated from the density, weight of film area, and formation voltage. The oxide film is assumed to be Ta_2O_5 as identified by x-ray diffraction techniques here. No other lines have been identified, although Waber and co-workers (2) in their studies of air oxidation of tantalum report that a phase other than Ta and Ta_2O_5 is present in oxidation products formed at 300°C and below.

Table I shows typical data obtained by the gravimetric procedure for 0.0005 in. tantalum which has been anodically oxidized to indicated voltage at 95°C. An estimated residual oxide thickness of 360 Å before formation if used as a blank would decrease the spread in results for T in respect to E .

BARIUM STEARATE STEP GAUGE RESULTS FOR OXIDE THICKNESS

The step gauge reported by Blodgett (3) measures thickness of thin films by comparing the interference colors of the unknown film with the colors of the step gauge. Barium stearate film is constructed on special glass so that steps 2–16 μ in. thick are shown (additional ranges are available). Each thickness reflects a characteristic color which is used as a standard.

TABLE I. Gravimetric data for oxide thickness

Sample area in cm^2 A	Formation voltage E	Weight change in grams $W_1 - W_2$	Thickness in Å/v T
90.3	100	0.00545	19.7
90.3	200	0.01036	18.4
90.3	300	0.01498	17.7
90.3	400	0.01781	15.8
90.3	500	0.02122	15.0

Laws governing the interference of light rays reflected by thin films are fairly well established and detailed in standard texts in physical optics, and in Blodgett's report on the barium stearate step gauge. When light is reflected by a thin film of a transparent substance, part of the light is reflected at the upper boundary of the film and part at the lower boundary. Two rays may then travel together after reflection. Since one ray travels a longer distance they will, in general, have a phase difference as they emerge at the upper boundary. If the two rays are in phase, maximum intensity of light is reflected; if they are out of phase, less intensity is reflected. The intensity of the reflected light varies with film thickness. A plot of the intensity against film thickness results in a cosine curve. The "dark" series would correspond to the minima at thicknesses.

$\lambda/4n, 3\lambda/4n \dots$ where n = refractive index of the film. The "bright" series would correspond to the minima at thicknesses $0, \lambda/2n, \lambda/n \dots$

In the barium stearate step gauge, colors reflected by steps 2–8 are called the "first order" colors. Each of the first 3 orders starts with a yellow or yellow-brown, followed by dark blue, medium blue, etc.

Step 4 corresponds to the color of tantalum anodically oxidized at 20 v d.c. and 95°C for 1 hr. A 20 v, 95°C formation is then 4 μ in. thick if the tantalum oxide refractive index were comparable to that of the barium stearate (1.491). While the refractive index for anodic Ta_2O_5 is not available, the geometric mean refractive index of the orthorhombic tantalum pentoxide and its optical dispersion can be represented by the Cauchy formula (2)

$$n = 2.033 + 8.74 \times \frac{10^6}{\lambda^2}$$

where n is the refractive index at λ wave length.

For sodium light of 5893 Å the refractive index of 2.275 can be used. This gives a calculated value of 2.62 μ in. for the thickness of a 20 v film formed at 95°C or 33 Å/v. Step 12 of the barium stearate step gauge corresponds to the color of tantalum formed to 75 v d.c. at 95°C for 1 hr, or 27 Å/v. It would seem that similar to the gravimetric procedure there appears to be a blank which if taken into account would result in more constant value of Angstrom units per volt.

MAXIMUM EXTINCTION RESULTS

Aside from the direct comparison with the step gauge, if a series of tantalum foils is formed from 5 v to 100 v d.c. for 1 hr at 95°C and then placed behind a source of sodium light, it will be observed that the 20 v film and the 75 v film are the darkest. Since they are, respectively, first and second order

minima, they may be calculated respectively $T_1 = \lambda/4n$ and $T_2 = 3\lambda/4n$: substituting the 5893 Å for the wave length of sodium light and the refractive index of 2.275 and dividing by the respective voltages, then 33 and 26 Å are obtained for thickness which compare favorably with step gauge results.

RECORDING PHOTOELECTRIC SPECTROPHOTOMETRIC RESULTS

With a recording spectrophotometer measurements can be made of the color of reflecting materials such as the Ta_2O_5 interference colors. Any two colors that have the same spectrophotometric curve appear identical to the normal eye under any lighting conditions. In short, these color curves are the signatures of the different colors. The spectrophotometer used consists of a light source which radiates all wave lengths of the visible and near infrared spectrum, a monochromator for selecting monochromatic light as the spectrum, a monochromator for selecting monochromatic light as the spectrum is scanned, a flicker system for shining the light alternately on the sample and on a standard, a phototube and associated amplifier circuits, and a recorder. The monochromator is a double prism type which passes a constant wave-length band of

10 μ throughout the entire visible spectrum from 400 to 700 μ . Since the colors of the anodic Ta_2O_5 are a function of the oxide thickness, then a spectrophotometric curve could be used for the determination of thickness wholly independent of the human eye.

The minima and maxima points are easily read off the per cent reflectance vs. wave-length curve (4000–7000 Å). When a series of curves is plotted for anodized tantalum foils formed from very low voltage to high voltage, the minima and maxima points not only serve for thickness calculation but depict the order as well.

$$T \text{ minimum} = \lambda/4n, 3\lambda/4n, 5\lambda/4n \dots$$

$$T \text{ maximum} = 0, \lambda/2n, \lambda/n, 3\lambda/2n$$

where T equals oxide thickness in Å for the first order, second order, etc., λ = wave length where minima or maxima occurs, and n = refractive index at corresponding wave length.

A plot of the minima and maxima points of a series of anodically oxidized foils vs. the formation voltage can be used to set up calibration curves (Fig. 1). By comparing the maxima and minima points of an unknown sample to the calibration curves, a good estimate of thickness and formation conditions can be obtained.

COMPARISON OF RESULTS OBTAINED

The three optical methods are considered in excellent agreement for this type of measurement and can be brought much closer by optical considerations of a phase shift in the wave length of light upon reflection from a metallic surface and the use of micro techniques. Considerations of surface oxide of the tantalum before anodizing have been recognized, but left uncorrected. Efforts to obtain a pattern by electron diffraction techniques of the tantalum metal before anodizing have been unsuccessful because of the rapid protective air oxide formation. An air-formed oxide is present on tantalum to a thickness of about 300 Å as determined by electron diffraction studies; this value may vary with the method of cleaning and the elapsed time between cleaning and anodizing.

The lower values of thickness obtained by the gravimetric procedure can be explained by postulating the presence of a gaseous constituent in the film. If enough oxygen were a part of the film structure to lower the density to 6.4, then the gravimetric results would agree with the optical data. The possibility also exists that the optical results have a constant error because of phase reversal considerations which have not been evaluated.

While it is not known by the author that the "gase-

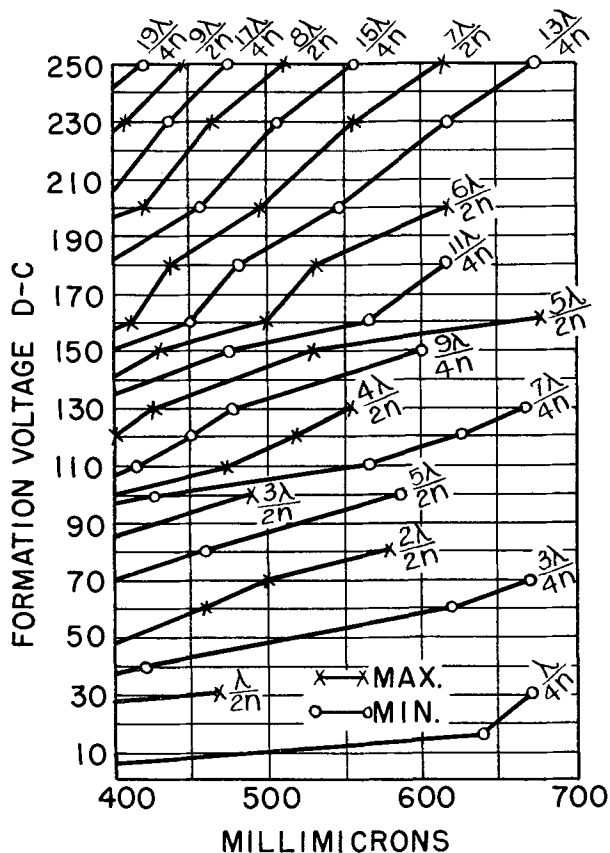


FIG. 1. Maximum and minima of designated formation voltages.

TABLE II. Film thickness of formed tantalum in Å/v at indicated temperatures

Method of measurement	Temperature of formation			
	0°C	25°C	95°C	195°C
Gravimetric results.....	13	16	20	25
Step gauge results.....	17	21	26	32
Spectrophotometric results.....	18	22	28	35

ous film" theory has been advanced for tantalum oxide films, it has been suggested by experimenters considering anodic aluminum oxide. Dieckmann (5) states that unused oxygen is driven into the pores of aluminum oxide film under high electrostatic pressure which tends to diffuse back into the electrolyte at increased temperatures and during shelf life.

Oxygen gas, which may be a part of the tantalum oxide film, would differ from aluminum in the direction of diffusion at increased temperatures. It is likely that there is a migration of oxygen at increased temperatures in the direction of the tantalum metal. The getter properties of tantalum and the less soluble oxide could account for the difference in behavior to that of the aluminum. Temperatures of several hundred degrees centigrade have been applied to anodically oxidized tantalum with no observed change in weight before and after air heat treating. However, a large increase in capacitance, leakage current, and per cent dissipation accompanies this treatment.

Table II summarizes the oxide thickness data by the various methods at various temperatures. Data nearest the 100 v anodic formation were arbitrarily selected as a compromise between the high results caused by "phase jumps" at the lower voltages and questionable uniformity of formation at higher voltages where "scintillation effects" can occur.

ELECTROLYTIC CELL PERFORMANCE

If the data on oxide thickness are at least relatively correct, then it would be expected that a film formed on tantalum at 200 v and 95°C would have the same thickness as a film formed at 160 v and 195°C. It would be expected that a capacity reading in microfarads per square inch would be the same for the two formed foils although there is a 40 v difference in formation. This is exactly the case (Fig. 2). The same, of course, is true over a much wider range limited mainly by the proper choice of electrolytes to avoid dull films which are connected with dielectric breakdown, a specialized subject not discussed here.

When two tantalum sheets have been anodically formed to the same oxide thickness but at widely

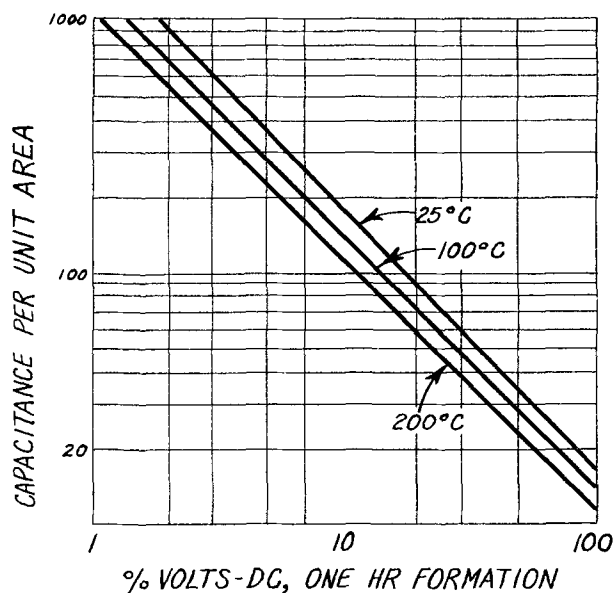


FIG. 2. Capacitance per unit area with voltage and temperature of formation of 0.0005 in. tantalum.

different temperatures and voltages, it has been observed that the sheet which has been anodized to the higher temperature exhibits lower electrical losses. The oxide film allows fewer electrons to penetrate to the tantalum metal, consequently the current flow is reduced. The author believes that in forming to a higher temperature more oxygen is driven into the film toward the tantalum metal underneath. This oxygen acts as a barrier and inhibits the current flow.

It is not the intent of the author to offer a mechanism for the formation of anodic tantalum oxide. Cabrera and Mott (6) have proposed a theory of the oxidation of metals where the metal ion is said to move through the metal oxide layer and combine with oxygen. Vermilyea (7) has supplemented this study and discussed the logarithmic growth law of Cabrera and Mott. In order to explain all of the results reported in this paper it would appear to the author that an additional effect of oxygen migration through the oxide film occurs at least under special conditions as well as the tantalum ion migration.

SUMMARY

The anodic oxidation of tantalum from 0° to 200°C and up to several hundred volts d.c. has been studied by gravimetric, optical, and electrical measurements. The correlation of thickness results with voltage and temperature are reproducible and constant in trend. The higher temperature at fixed voltages produces a thicker anodic film which is additionally borne out by capacity measurements. The product of the forming voltage, E , and the absolute temperature, T , are a constant for a given capacitance per square inch so that $E_1T_1 = E_2T_2$.

The gravimetric procedure gives lower results and lends support to a lower density for anodic tantalum oxide films and an "oxygen film" theory. This gaseous layer is used to explain the lower leakage currents obtained on high temperature films.

ACKNOWLEDGMENT

The author wishes to express his appreciation to Mr. B. S. Pritchard for his work on the recording spectrophotometer, to Dr. K. B. Blodgett for conferences on the step gauge results, and to fellow members of the research team on the development of the tantalytic capacitor for their valuable criticisms and suggestions, in particular Messrs. F. W. Grahame, D. H. Stephenson, A. L. Jenny, and R. A. Ruschetta. The cooperation and assistance of the Engineering Staff is also gratefully acknowledged and of Tom Gore of the Squier Signal Corps Laboratories. Data in this report were obtained in con-

junction with Signal Corps Contract DA 36-039-sc-15423.

Any discussion of this paper will appear in a Discussion Section to be published in the December 1955 JOURNAL.

REFERENCES

1. A. GUNTHERSCHULZE AND H. BETZ, "Electrolyt-Kondensatoren," p. 122. Technischer Verlag Herbert Cram-Berlin W 35 (1952).
2. J. T. WABER, G. E. STURDY, E. M. WISE, AND C. R. TIPTON, JR., *This Journal*, **86**, 121 (1952).
3. K. B. BLODGETT, "Barium Stearate Stepgauge," Instructions GEJ-2324, General Electric Co., Schenectady, N. Y., October (1950).
4. P. M. DEELEY, "Electrolytic Capacitors," p. 55, Recorder Press, Plainfield, N. J. (1938).
5. G. DIECKMANN, *J. Funk-Technik*, 210, Sonderdruck ans Heft 8, Jahrgang (1951).
6. N. CABRERA AND N. F. MOTT, *Repts. Progr. Phys.*, **12**, 163 (1948-49).
7. D. VERMILYEA, *Acta Met.*, **1**, 282 (1953).

Chloride and Sulfate Ion Contamination of Zinc Sulfide Precipitates¹

DOMINIC T. PALUMBO AND ALBERT K. LEVINE²

Physics Laboratories, Sylvania Electric Products Inc., Bayside, New York

ABSTRACT

Data are presented to show that zinc sulfide precipitated from chloride or sulfate solutions retains from 0.2 to over 2% chloride or sulfate ion after thorough washing. Ion displacement experiments show that sulfate contamination is mainly or entirely a surface phenomenon; results with chloride are not as conclusive; there seems to be both surface and volume contamination. The exchange is mainly anionic; only small quantities of zinc and hydrogen ions are displaced. Digestion of anion contaminated sulfides for periods up to 500 hr in water at 70°C removes only a fraction of the contaminating anions; for example, only 7% of chloride ion is removed after 212 hr, and 16% of the sulfate after 228 hr.

INTRODUCTION

Many investigations have been carried out on the physical properties, particularly luminescence, of zinc sulfide. In most cases scant attention has been paid to the purity of the material, and, in those instances where the investigators have been purity conscious, their interest has, with few exceptions, been restricted to contamination by heavy metals. Work and Odell (1), Rothschild (2), and Smith (3) indicate that precipitated zinc sulfide can be contaminated with the anion of the zinc salt used in the precipitation. Recent investigations in this laboratory have shown that all zinc sulfide derived via aqueous precipitation is contaminated with substantial quantities of sorbed water³ (removable only at temperatures above 400°C), sulfate, and frequently chloride. Zinc sulfide which contains sulfate must be presumed on firing to become contaminated with zinc oxide (5). The fate of contaminating chloride on firing is not yet clear; after firing the quantity left behind may be undetectable by ordinary chemical means yet, before it is expelled, it may play a crucial role in the formation of luminescent centers. The contaminating chloride and sulfate cannot be ascribed to insufficient washing. Typical values for washed zinc sulfide⁴ are: chloride, 0.72%; sulfate, 0.34%.

The occurrence of sulfate or chloride in the

¹ Manuscript received July 16, 1954. This paper was prepared for delivery before the Chicago Meeting, May 2 to 6, 1954.

² Chemistry Department, Brooklyn College, Brooklyn, New York; Consultant, Physics Laboratories, Sylvania Electric Products Inc.

³ Becker and Grassman (4) have shown that this bound water is not water of hydration.

⁴ As evidenced by the absence of those anions in the washings.

washed precipitate is due to precipitation of the zinc sulfide from zinc sulfate or zinc chloride solution, respectively. Generally, no matter what anion is present in the precipitating solution, one must expect that anion to be a contaminant of the zinc sulfide.

EXPERIMENTAL

The experimental procedures used to determine the nature of the anionic contamination of precipitated zinc sulfide were as follows:

A. Digestion experiments.—Precipitated zinc sulfide was digested in distilled water at 70°C and the amount of anionic contamination retained by the precipitate as a function of the time of digestion was determined.

B. Precipitation experiments.—Zinc sulfide was precipitated from mixtures of zinc chloride and zinc sulfate solutions and the washed⁵ precipitate investigated for the amount of retained anions (chloride and sulfate).

C. Ion displacement experiments.—Contaminated precipitates were leached⁵ with solutions of chloride or sulfate salts to replace, respectively, the original sulfate or chloride contaminant in washed zinc sulfide precipitates.

Samples of zinc sulfide were prepared from both zinc chloride and zinc sulfate solutions by precipitation with tank hydrogen sulfide. Two to three liters of 0.5M solution were adjusted to pH 2.5 at the start by addition of hydrochloric or sulfuric acid, respectively. The temperature of the solution was

⁵ Washing refers to the treatment of a zinc sulfide precipitate with distilled water to remove contaminants; "leaching" to the treatment of the zinc sulfide with a salt solution (usually sodium chloride or sodium sulfate) to replace the original contaminant with a different species.

TABLE I. Analyses of unfired, unactivated ZnS

Sample No.* %	1	2	3	4	5	6	7	8
SO ₄ ²⁻	2.65	0.56	0.73	0.34	0.46	0.41	1.81	1.90
Cl ⁻	0.98	0.53	0.82	0.72	0.00	0.00	0.00	0.00
NH ₄ ⁺	0.55	0.03	0.04	—	—	—	—	—
H ₂ O	0.81	1.08	1.43	—	—	—	—	—

* Numbers 1-6 are commercial samples; 7-8 are laboratory preparations.

70-75°C, and the hydrogen sulfide was maintained at a gauge pressure of 5 in. of water. The time of precipitation was from one to three hours. During precipitation the formation of hydrochloric or sulfuric acid caused the pH to drop; generally the final pH was 1.0 to 1.2.

Where precipitation was from mixtures of the chloride and sulfate, the mole ratio of chloride to sulfate was varied from 0.05 to 0.50 keeping the zinc molarity constant at 0.5M.

The precipitate obtained was filtered immediately, washed with distilled water at 70°C until three successive washings showed no chloride or sulfate, then dried at 110°C for 24 hr. Filtration was accomplished on fritted glass filters. Samples difficult to filter were centrifuged. The volume of wash water was approximately 10 milliliters per gram of solid per wash. The number of washings required before the filtrate was free of chloride and sulfate varied with the particular sample. Chloride precipitates were the most difficult to wash. Fifteen to twenty washes were usually required for precipitates from sulfate solutions.

1. *Analysis for impurities in zinc sulfide.*—Analytical data are presented on an oven dry (110°C) basis. For the determination of chloride and sulfate the procedure was to dissolve the sample in hot 4N nitric and hydrochloric acid, respectively, boil gently to expel all the hydrogen sulfide, and then neutralize with aqueous ammonia.⁶ Chloride and sulfate were determined by standard gravimetric methods, the former as silver chloride, the latter as barium sulfate. Duplicate runs were made on each sample. Ammonium ion was determined by the Kjeldahl method. Analyses of commercial samples and those prepared at this laboratory are given in Table I.

2. *Digestion of zinc sulfide.*—Since thoroughly washed zinc sulfide contains substantial quantities of sulfate and/or chloride (see Table I), it was decided to determine whether these anionic impurities are retained (a) by coprecipitation, that is, by entrapment in the forming lattice during precipitation,

⁶ The evolved gases were checked for entrained or volatile chlorides in several determinations. No chloride was found.

TABLE II. Digestion of ZnS, Cl⁻ in H₂O at 70°C. (Initial Cl⁻ content = 0.72%)

Hours	% Cl ⁻ in solution	% Cl ⁻ remaining in ZnS	Total
27	0.043	0.67	0.71
27	0.041	0.70	0.74
75	0.047	0.67	0.72
75	0.047	0.67	0.72
116	0.051	0.68	0.73
116	0.051	0.68	0.73
212	0.053	—	—
212	0.053	—	—

TABLE III. Digestion of ZnS, SO₄²⁻ in H₂O at 70°C. (Initial sulfate content = 1.86%)

Hours	% SO ₄ ²⁻ in solution	% SO ₄ ²⁻ remaining in ZnS	Total	Increase in SO ₄ ²⁻
4	0.36	1.54	1.90	0.04
4	0.36	1.54	1.90	0.04
21	0.41	1.52	1.93	0.07
21	0.41	1.52	1.93	0.07
48	0.45	1.55	2.00	0.14
48	0.45	1.55	2.00	0.14
141	0.58	1.55	2.13	0.17
141	0.59	1.55	2.14	0.18
288	0.86	1.57	2.43	0.57
288	0.90	1.55	2.45	0.59
528	1.13	1.60	2.73	0.87
528	1.15	1.59	2.74	0.88

or (b) by adsorption. Two methods, digestion and ion displacement, were employed. The former method might liberate a portion of the contaminant if it were in the lattice; the latter method would be confined to the surface of the zinc sulfide crystallites.

Weighed samples of washed and dried zinc sulfide, prepared from chloride solutions, were digested with 200 milliliters of distilled water at 70°C for from 27 to 212 hr. During digestion the samples were stirred every four hours. After digestion the samples were filtered and washed, and the chloride content of the filtrate determined. Table II shows that there is a definite increase in the amount of chloride released

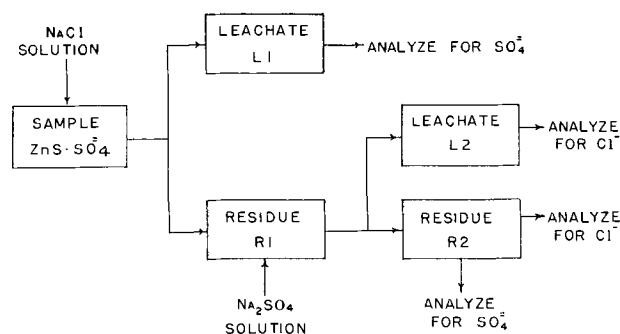


FIG. 1. Flow diagram of ion displacement procedure

TABLE IV. *Effect of ion displacement of SO₄²⁻ and Cl⁻ from ZnS*

Run	Sample, g	Initial sulfate		Displaced SO ₄ ²⁻		% Displaced	Leached with
		%	g	g	meq/g		
1	10.267	0.31	0.0318	0.0204	0.0414	64.1	1N NaCl
	11.571	0.31	0.0359	0.0203	0.0365	56.5	
2	10.978	0.31	0.0340	0.0227	0.0431	66.8	2N NaCl
	7.869	0.31	0.0244	0.0186	0.0492	76.2	
3	5.133	1.99	0.1021	0.0950	0.386	93.0	2N NaCl
	5.145	1.99	0.1024	0.0957	0.388	93.5	
4	3.697	1.99	0.0736	0.0747	0.421	101.5	2N NaCl
	3.702	1.99	0.0737	0.0740	0.416	100.4	
5	4.544	1.82	0.0827	0.0668	0.306	80.8	2N K ₂ S
	4.365	1.82	0.0794	0.0637	0.304	80.2	
		Initial Chloride		Displaced Cl ⁻			
		%	g	g	meq/g		
6	4.504	2.32	0.1045	0.0195	0.122	18.7	2N MgSO ₄
	4.502	2.32	0.1044	0.0196	0.123	18.8	
7	4.557	1.17	0.0533	0.00756	0.0468	14.2	2N Na ₂ SO ₄
	4.919	1.17	0.0576	0.00807	0.0463	14.0	

TABLE V. *Effect of cyclical displacement of Cl⁻ and SO₄²⁻ on ZnS*

Run No.	Sample, g	Initial SO ₄ ²⁻ meq/g	L ₁ , SO ₄ ²⁻ removed meq/g	R ₁ , SO ₄ ²⁻ remaining meq/g	L ₂ , Cl ⁻ removed meq/g	R ₂ , Cl ⁻ remaining meq/g	R ₂ , SO ₄ ²⁻ remaining meq/g
1	3.697	0.415	0.421	0.00*	0.280	—	0.318
	3.702	0.415	0.416	0.00*	0.344	0.00	—
2	4.122	0.379	0.316	0.063*	0.0789	0.0034	—
	4.184	0.379	0.316	0.063*	0.0789	0.0034	—
3	10.978	0.0645	0.0431	0.0214*	—	—	0.0473
	7.869	0.0646	0.0492	0.0154*	—	—	0.0466
		Initial chloride meq/g	Cl ⁻ removed meq/g	Cl ⁻ remaining meq/g	SO ₄ ²⁻ removed meq/g	SO ₄ ²⁻ Remaining meq/g	Cl ⁻ remaining meq/g
4	4.504	0.654	0.122	0.532*	0.0777	—	0.542
	4.502	0.655	0.123	0.532*	0.0717	—	0.539

* Calculated value = initial value - amount removed.

as the digestion becomes longer, but that the amount is small compared with the chloride remaining in the solid phase.

A similar experiment was performed with zinc sulfide prepared from sulfate solution. Results are presented in Table III, which shows that the sulfate content of the solid phase is relatively unchanged, while that of the solution increases. The enrichment in sulfate must be attributed to oxidation of zinc sulfide during digestion.

3. *Ion displacement on zinc sulfide.*—Freshly precipitated zinc sulfide has a large surface to volume ratio.⁷ If part or all of the anionic contamination is due to adsorption, that contamination should be replaceable by leaching with a solution of a different anion. Accordingly, samples of zinc sulfide

⁷ Gas adsorption measurements and electron microscope examination show that precipitated zinc sulfide particles are 100 to 1000 Å in diameter.

prepared from zinc sulfate solution were weighed and placed into fine fritted glass funnels and 25 milliliters of 1N or 2N sodium chloride (at 70°C) added. The solution and precipitate were left in contact, with stirring. After fifteen minutes the chloride solution was filtered off by applying vacuum and a fresh 25 milliliter portion added. The process was repeated until 300 milliliters had been contacted with the zinc sulfide. The leachings were analyzed for sulfate.

To determine whether displacement is reversible the samples, which had been leached with sodium chloride, were washed until the filtrate was chloride free, then leached with 1N or 2N sodium sulfate. The leachings were analyzed for chloride. Similarly, zinc sulfide samples with initial chloride contamination were leached first with 1N or 2N sodium sulfate at 70°C, then with water until the filtrate was sulfate free, and finally with 1N or 2N sodium chlo-

TABLE VI. Ion displacement on zinc sulfide with initial chloride and sulfate contamination

Mole ratio $\text{Cl}^-/\text{SO}_4^{2-}$ in precipitating solution	0.05	0.10	0.50
% Initial chloride in ZnS	0.89	1.15	1.47
% Initial sulfate in ZnS	1.49	1.58	1.39
% Initial chloride displaced by 2N Na_2SO_4	15.7	11.3	13.6
% Initial sulfate displaced by 2N NaCl	91.9	81.5	92.7
	91.9	81.0	92.0

TABLE VII. Cation and anion displacement in ZnS precipitated from sulfate solution

Weight of sample g	Initial SO_4^{2-} , meq.	Meq. removed by 2N KCl		
		Zn^{++}	H^+	SO_4^{2-}
1. 4.135	1.567	0.0896	0.060	1.317
2. 4.135	1.567	0.0784	0.048	1.291
3. 5.172	2.144	0.0841	0.044	1.923
4. 5.173	2.144	0.0841	0.052	1.923

* The observed Zn^{++} displacement is only slightly greater than the normal solubility of ZnS in water.

ride.⁸ A flow diagram of the procedure is shown in Fig. 1; results are given in Tables IV and V.

With zinc sulfide samples prepared from mixed chloride and sulfate solutions, separate samples from each run were leached with 2N sodium chloride and 2N sodium sulfate at 70°C and the leachings analyzed for sulfate and chloride, respectively. Results are given in Table VI.

The results are summarized as follows.

1. With chloride-contaminated sulfides the displacement takes place to a considerably lesser extent than with sulfate-contaminated precipitates (Table V, columns 3 and 4). For sulfides contaminated with both chloride and sulfate the chloride is displaced to a considerably lesser extent than is the sulfate (Table VI).

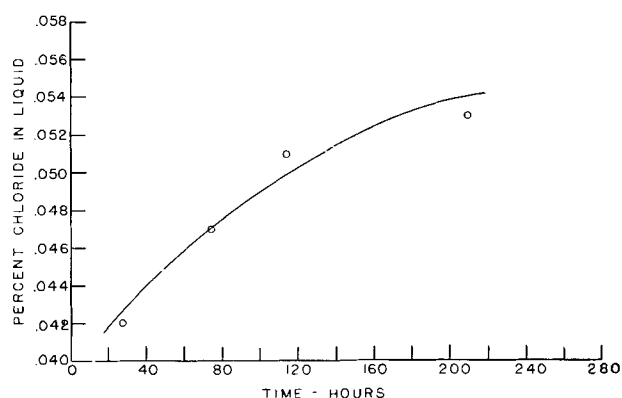
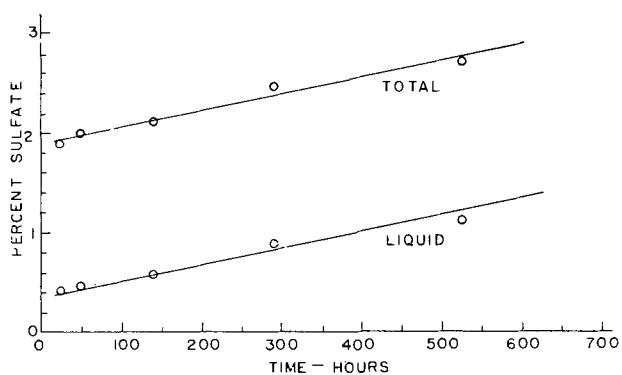
2. When chloride displaces the sulfate of a sulfate-contaminated precipitate, the chloride can be removed by subsequent leaching with sodium sulfate solution (Table V, run 1, columns 6 and 7).

3. In all cases it was found that the displacement was nonstoichiometric, i.e., milliequivalents of sulfate removed from the precipitate were greater than the milliequivalents of chloride added to the precipitate.⁹

Ion displacement experiments were extended to

⁸ Several runs were made using 2N potassium sulfide. These solutions were extremely difficult to filter through the zinc sulfide bed and their use was discontinued. A typical run using potassium sulfide is shown in Table IV.

⁹ If a portion of the adsorption attributed to sulfate is actually bisulfate the number of milliequivalents of adsorbed ions is smaller. However, on the basis of the amount of titratable hydrogen displaced (Table VII), it appears that little bisulfate is present.

FIG. 2. Digestion of ZnS, Cl^- in H_2O at 70°C; initial $\text{Cl}^- = 0.72\%$.FIG. 3. Digestion of ZnS, SO_4^{2-} in H_2O at 70°C; initial $\text{SO}_4^{2-} = 1.86\%$.

determine whether appreciable cation exchange occurred. Samples of sulfate-contaminated precipitates were leached with 2N sodium chloride and 2N potassium chloride. The leachate was divided in half, zinc and hydrogen ions were determined in one half and sulfate in the other. Zinc was determined as the sulfide and hydrogen ion by titration with sodium hydroxide. The results are shown in Table VII. In all cases the sum of the milliequivalents of zinc and hydrogen ion was much less than the milliequivalents of sulfate exchanged.

DISCUSSION

When zinc sulfide contaminated with chloride or sulfate is digested it is seen (Tables II and III, Fig. 2 and 3) that a small percentage of the contaminant is extracted. This release could conceivably be from the interior of crystallites by a process in which small crystallites dissolve in the aqueous digestion medium yielding zinc and sulfide ions and simultaneously precipitate on existing larger crystallites. In such a process the occluded contaminant released does not tend to become reoccluded because (a) its concentration in the solvent is now very small, and (b) the growing crystallite is adding zinc and sulfide ions under thermodynamically reversible conditions, a

situation leading toward crystal perfection. The small quantity of contaminating anions released after long digestion, about 7% in the case of chloride and 16% in the case of sulfate, indicates that this solution process (i.e., the growth of large crystallites at the expense of the small ones) occurs to a limited extent, if at all.

The release of contaminant during digestion may be explained on the basis of a "regularization" of the precipitated crystallites. In the technique which the authors employed (and which is practically universally employed) the zinc sulfide is precipitated under thermodynamically irreversible conditions. Consequently the crystallites formed do not have a minimum surface energy, and are irregular (6). As the crystallites are permitted to digest they tend to minimize their surface energy by becoming more regular. If contaminating anions are held by surface forces, a decrease in the specific surface by the regularization of the crystallites will release them, and the amount of anions released will be roughly proportional to the decrease in surface. That this is the mechanism by which anions are released during digestion is indicated by the experiments involving ion displacement.

In the ion displacement experiments when sulfate-contaminated zinc sulfide was leached with sodium chloride solution 56% to 100% of the sulfate was readily displaced. Furthermore, as the ratio of mass of chloride to mass of zinc sulfide was increased, so was the percentage of sulfate displaced also increased. Since the leaching solution has access only to the surface, it must be presumed that the sulfate removed was situated on the surface. In the instance where complete sulfate removal was achieved by displacement with chloride, all the sulfate contaminating the zinc sulfide (1.99%) must have been on crystallite surfaces.

Concomitant with the anion exchange there occurs a small amount of cation exchange (Table VII). One would expect a material to show one or the other of these displacement phenomena, but not both. Under the conditions of precipitation, i.e., excess zinc (from zinc sulfate or zinc chloride), the zinc sulfide formed is positively charged and will adsorb negative ions (sulfate, chloride, etc.) from the solution to compensate for this excess charge.¹⁰ These negative ions will be held loosely compared to the positive ions initially taken up by the zinc sulfide and are, therefore, easily displaced by a high concentration of a different anion. Experimental data support this hypothesis. In fact, in the case of the sulfate exchange, the ratio of milliequivalents of cation ex-

¹⁰ Kolthoff indicates that precipitated zinc sulfide is positively charged (7).

TABLE VIII. Tetrahedral* and ionic radii in Å

Atom	Tetrahedral radii	Ionic radii
Zn	1.31	0.74 (+2)
S	1.04†	1.84 (-2)
Cl	0.99	1.81 (-1)
O	0.66†	1.40 (-2)

* Derived from interatomic distances in crystals where the atoms form four tetrahedral bonds, e.g., ZnS.

† On this basis the tetrahedral SO_4^- ion would have a radius sum of 1.70 Å. Observed values of the S-O distance are ~ 1.50 Å. The sphere circumscribing the SO_4^- ion is, therefore, $1.50 + 0.66 = 2.16$ Å. A substitution of SO_4^- for S^{2-} corresponds to replacement by an ion 107% larger than the S^{2-} , i.e.,

$$\frac{2.16 - 1.04}{1.04} \times 100 = 107\%$$

changed to milliequivalents of anion exchanged in the four experimental runs is less than 0.11.

The results on the removal of chloride from zinc sulfide were different from those obtained in the case of sulfate. Leaching a sample of high chloride contamination with 300 ml of 2N sodium sulfate resulted in replacement of only 19% of the chloride; in other cases 14% was replaced.

The data (Table V, run 1) also show that chloride introduced on the surface of a zinc sulfide sample (by exchanging the original sulfate contamination with chloride) can be completely removed by subsequent washing with sodium sulfate solution. However, samples of zinc sulfide initially contaminated with chloride show that only a small fraction (ca. 10-19%) of the total chloride can be displaced.

Similar results obtain for sulfide samples with both initial chloride and sulfate contamination. Here a maximum of 15.7% of chloride could be displaced with 2N sodium sulfate. For the same sample 91.9% of the sulfate contamination was removed with 2N sodium chloride.

From comparison with the results of displacement with sulfate-contaminated precipitates, it is indicated that chloride exists both in the interior and on the surface of the zinc sulfide crystallites.

Table VIII lists the ionic radii and the tetrahedral "covalent" radii¹¹ of the atoms of interest in the preparation of ZnS from aqueous solutions containing the chloride and sulfate salts. On the assumption that zinc sulfide is covalent, substitution of chlorine for sulfur atom involves the exchange of atoms of comparable size. Replacement by sulfate, however, requires the substitution of an ion that is about 107% larger than the sulfur atom.¹² Similarly, if

¹¹ Derived from interatomic distances in crystals where the atoms form four tetrahedral bonds, e.g., ZnS (8).

¹² The sulfate ion is assumed to act as a sphere of radius equal to the observed S-O distance plus the radius of the O atom.

zinc sulfide is assumed to be an ionic crystal,¹³ the replacement of sulfur by sulfate requires the exchange with an ion about 58% larger than sulfur. From considerations of ionic size alone it would appear that the formation of a solid solution of zinc sulfide and zinc chloride is possible, while a solid solution of zinc sulfide and zinc sulfate is not.

ACKNOWLEDGMENTS

Thanks are due Mr. S. Faria for his assistance with the experimental work, and Mr. R. Bastian of Sylvania's Product Development Laboratories for his help in performing analyses of various samples.

¹³ Born indicates that zinc sulfide is partly covalent (9).

Any discussion of this paper will appear in a Discussion Section to be published in the December 1955 JOURNAL.

REFERENCES

1. L. T. WORK AND I. H. ODELL, *Ind. Eng. Chem.*, **25**, 411, 543 (1933).
2. S. ROTHSCHILD, *Trans. Faraday Soc.*, **42**, 635 (1946).
3. A. L. SMITH, J. (and Trans.) *Electrochem. Soc.*, **96**, 75 (1949).
4. E. A. BECKER AND W. GRASSMAN, *Farben, Lacke, Anstrichstoffe*, **2**, 139 (1948).
5. J. R. PARTINGTON, "Textbook of Inorganic Chemistry," p. 846, Macmillan and Co., New York (1939).
6. H. W. LEVERENZ, *Science*, **109**, No. 2826, 183 (1949).
7. I. M. KOLTHOFF, *Pharm. Weekblad*, **57**, 1510 (1920).
8. A. F. WELLS, "Structural Inorganic Chemistry," p. 49, Oxford University Press, Oxford, England (1950).
9. M. BORN AND E. BORMANN, *Ber. deut. physik. Ges.*, **21**, 735 (1919).

Production of Zirconium Alloys by Consumable Electrode Arc Melting¹

R. A. BEALL, J. O. BORG, AND H. L. GILBERT²

Bureau of Mines, U. S. Department of the Interior, Albany, Oregon

ABSTRACT

The technique and advantages of consumable electrode arc melting and remelting in the production of zirconium alloys are discussed. Descriptions of the equipment and conditions of operation involved in double melting are given. Discussion of homogeneity, purity, and effective yield is included.

INTRODUCTION

Zirconium metal poses many special problems in melting operations because of its high melting point and its great chemical reactivity which prevents the use of known refractories and melting techniques (1). While several methods have been developed which are relatively successful in producing ingots of zirconium (and titanium), most of these cause considerable contamination. More serious immediate problems occur in the production of alloys where lack of homogeneity and rather high scrap loss are encountered. Consumable electrode arc melting is particularly effective in controlling these two problems, and makes possible the production of alloys more economically by greatly increasing the actual amount of metal available for effective use (2).

EXPERIMENTAL

The basic design of a furnace for experimental melting of consumable electrodes has been described (3) as has a production model of such a furnace (4). It is the alloy products of this type of furnace that are discussed. The furnace makes use of 2 in. x 2 in. x 20 in. electrodes pressed from zirconium sponge and operates under atmospheric pressure of an inert gas (see Fig. 1).

Electrodes (A) are placed in a guide clamp (B) by use of rubber gloves (C) sealed into the furnace wall. A small tungsten electrode welding arc (D) is used to join the electrode sections into the melting electrode which passes through steel drive rolls (E) and water-cooled copper rolls (F) which apply the melting current. The electrode is advanced until it strikes a pad of zirconium turnings in the bottom of the water-cooled copper melting cup (G) whereupon melting is initiated. Additional electrode

sections are joined continuously to the top of the melting electrode until the desired ingot is melted. Additional features of the furnace are the alloy adding device (H) and the control field coil (J). This furnace was quite successful in turning out zirconium ingots of high quality.

Power for melting is produced by banks of standard dual 400 amp selenium welding rectifiers. These machines balance the load on the 3 phase 440 v main power line and provide very flexible and convenient energy for melting. They furnish 60% of their rated output continuously. Arc current stability is excellent in that voltage recovery requires only one-half cycle.

The pressed sponge electrodes employed are pressed at 50 tons/in.² which gives them a density 87% that of metallic zirconium. The bars weigh 7.5 kg each and have an electrical resistivity of 1.6×10^2 microhms/cm³. Breaking strength of the electrodes in tension for various conditions of pressing is as follows:

Pressure (tons/in. ²)	10	20	30	40	50
Breaking strength, 2 in. x 2 in. bar (lb)	115	850	2200	2610	6900

A standard 2 in. x 2 in. pressed sponge electrode operates satisfactorily while carrying up to 5000 amp at 40 v in producing a 10 in. diameter ingot. As a 10 in. ingot is as large as is usually used for remelting purposes, tests beyond this point have not been made.

A few simple changes permit alloy ingots to be produced. Powder, shot, or wire of the appropriate alloying agent were added centrally in the sponge bar at the time of pressing. Several problems which resulted from the rigid specifications of the finished ingots are worthy of discussion.

Most commercial metal powders are relatively expensive and impure, (particularly in regard to oxygen and nitrogen contamination). An alternate choice is to produce a master alloy of some suitable

¹ Manuscript received August 27, 1954. This paper was prepared for delivery before the Chicago Meeting, May 2 to 6, 1954.

² Present address: Harvey Aluminum, Torrance, Calif.

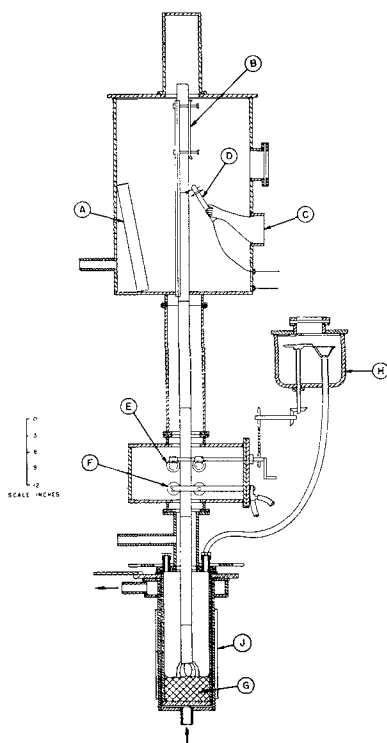


FIG. 1

composition which can be powdered for ease of distribution in the electrode pressing step. Most such brittle master alloys are very strong in compression and create a great problem in crushing. Use of the sharp, hard alloy particles also causes considerable increase in die wear during electrode pressing.

With metals which could be drawn or extruded to dimension, wires formed a very satisfactory form for addition. Dimension of the wire was controlled so that one, two, or three die lengths provided the exact amount desired. Shot was less desirable than wire as uniform distribution in the electrode was more of a problem.

All bar additions suffered certain drawbacks in operation, foremost of which was the formation of a low-melting eutectic in the hot electrode several inches above the point of melting, and consequent irregular "bleeding" of this alloy out of the bar. This resulted in a "banded" ingot of alternate layers of high and low alloy content. Further trouble occurred when the run was completed and the furnace opened for cleaning. The end of the electrode, for a distance of 6 in. back from the tip, was impregnated with heterogeneous alloys and intermetallic compounds which often were very pyrophoric or underwent rapid decomposition and oxidation, with the result that the routine operation often involved removal and rejection of this section of the electrode. In an attempt to avoid this, a series of tests on screw-feeders was made to determine the suitability of these devices for adding alloying powder to the

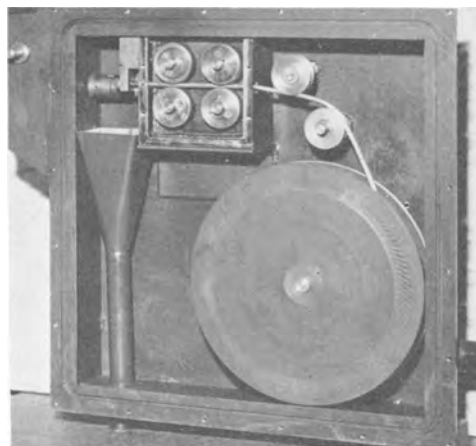


FIG. 2

molten pool. Due to an arc blast, "flotation" of powder with subsequent segregation, the nonavailability of some pure metal powders, and the high ingot specification, screw feeders were abandoned.

A particularly difficult problem arose in making additions of tin in the range of 1–5% to a series of ingots. This was solved by a mechanical wire feeding device as shown in Fig. 2. Extruded tin wire, $\frac{1}{4}$ in. in diameter, was loaded into the device on a large spool from which feed rolls delivered it to a revolving cutter. From the cutter the sections approximately $\frac{1}{4}$ in. long were fed directly to the molten metal pool in the melting furnace. By connecting the arc melting electrode drive to the tin cutting device through a timing arrangement, satisfactory proportioning was obtained.

A very effective means of alloy addition when satisfactory powders of the desired alloying agent can be obtained, is a pill feeding device. The powder, or blend of various powders, is fed to an automatic rotary tablet press which produces the compacts about 1 cm in diameter and $\frac{1}{2}$ cm thick at a rate of 200/min with a deviation in weight of less than 0.05 g per 10 tablets weighing 20 g or 0.25% error. These are loaded in batch lots into a circular vibrating feeder which feeds individual tablets to a metering gear as shown in Fig. 3. The entire device is sealed in the melting furnace or an auxiliary box where it feeds the tablets to the molten pool at a rate proportional to electrode consumption. This alloy addition system has given the best results to date.

A further difficulty, while due in part perhaps to peculiarities of the zirconium-tin system, has been encountered in enough other metals to be a serious problem. Ingots made by means of the tin wire cutting device had an excellent appearance when machined, and, although external analyses were quite satisfactory, sections cut from the ingots showed inclusions of almost pure tin as indicated by the arrows in Fig. 4, caused by gravity segregation.

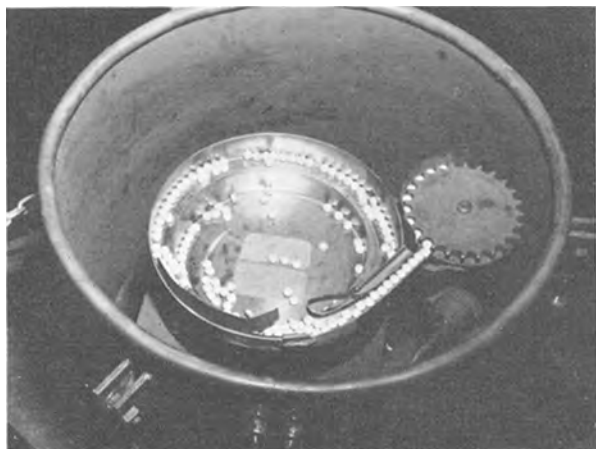


FIG. 3

These defective ingots were forged and rolled into 2 in. x 2 in. x 20 in. bars and fed through the furnace for remelting. Three tons of metal were produced by this method with considerable loss in forging and rolling due primarily to the inhomogeneities present in the core of the ingots. The yield of finished metal from sponge was in the order of 56%. In all cases the forging and rolling caused a hardening due to oxygen pickup as reported by Van Thyne and coworkers (5). Usual hardness increase in the tin alloy was 13 BHN.

In an effort to improve the unsatisfactory yield, the furnace was modified through the use of a d-c magnetic field created about the melting area by covering the entire water jacket from top to bottom with 3 layers of number 20 copper magnet wire (see Fig. 1). This device has been employed elsewhere for a somewhat different purpose (6). Here it was found that application of a small amount of direct current to the coil would cause the pool of molten metal inside the furnace to spin and mix. In this specific instance about 0.2 amp input was sufficient to give excellent stirring without centrifuging. Use of 1.4 amp on the coil caused heavy segregation of alloy particles in the outer surface of the ingot. Another effect of the stirring coil, perhaps as important in view of later developments as the stirring itself, is the arc control effect. Without a magnetic field applied the arc wanders at will and frequently localizes momentarily near one side of the crucible. The arc may later leave this spot so suddenly that it becomes deflected to the copper wall, with the result that the latter is instantly perforated and cooling water rushes in terminating the run. The magnetic field tends to center the arc, decreasing the possibility of ingot loss.

A slight improvement in yield was realized through the use of magnetic stirring of the metal pool, followed by rolling and remelting, and immediate needs

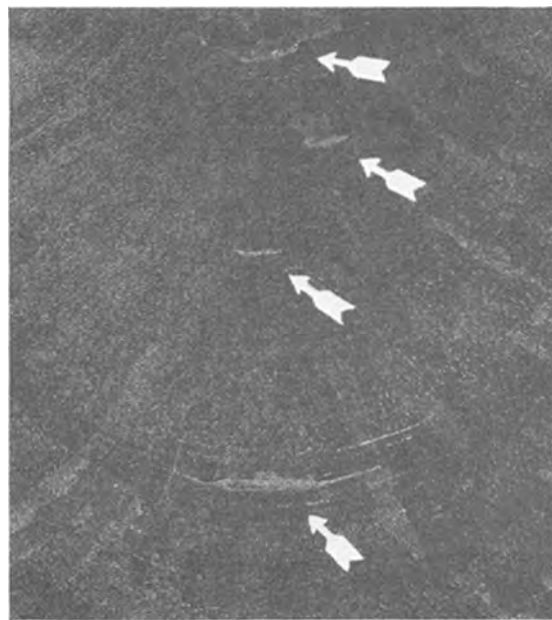


FIG. 4

for alloy were met. However, increase in hardness, due to oxidation during these steps, plus losses mentioned in the forging and rolling, led to further efforts in the remelting work.

An obvious improvement was to produce an ingot in the first melting step which would serve as the electrode for remelting without forging and rolling. Such a system involving tungsten electrode melting has been described by Herres (7), but was not useful here since tungsten contamination was excessive.

The problem was solved by production of 6-in. diameter ingots in the first furnace and the remelting of these forms into an 8-in. final ingot. Addition of continuous ingot extraction as practiced by Gilbert and coworkers (8) has permitted production of single ingots long enough to provide the desired weight for remelting.

Design of the remelting furnace is identical with the first-melting furnace except for power application to the electrode. A typical furnace is shown in Fig. 5. The consumable electrode (A), made up in this case by nipping together several 6 in. diameter ingots, is supported by a water-cooled copper pipe (B). This assembly is lowered into the furnace by a geared winch (C). The entrance of the pipe into the furnace is sealed by a greased rubber "O" ring and packing gland (D). All other furnace parts are similarly sealed by rubber "O" rings permitting vacuum melting if this should be desirable. The furnace previously described cannot be operated under vacuum because of the various manipulations carried out by means of the rubber gloves which would stand, at best, only a few ounces of pressure differential.

In many cases vacuum melting is important since the zirconium sponge metal or the alloying agent may contain sufficient hydrogen to cause "rimming" or bubbling in the last portion of the ingot to freeze. Reduction of furnace pressure to 4 cm or less eliminates rimming, generally without causing other undesirable effects. Recent analyses indicate that ingots produced using a reduced pressure final melting

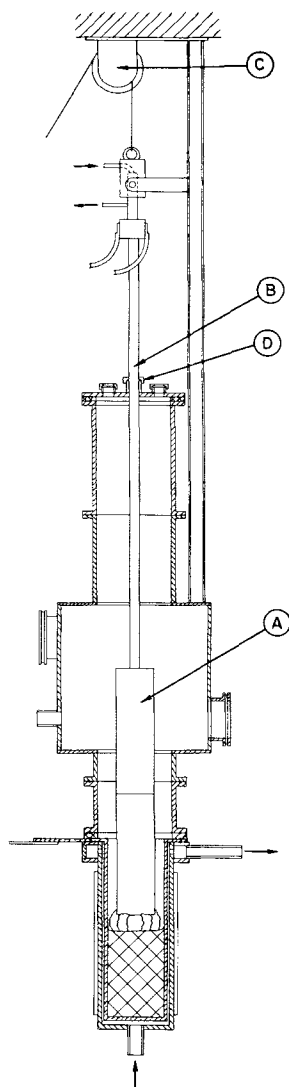


FIG. 5

step have a hydrogen content on the order of 15 ppm. A single stage mechanical vacuum pump having a free air rating of 110 ft³/min provides adequate vacuum for successful remelting and at the same time does not pump down under normal operation into the "glow discharge" range, which must be avoided for uniform results. This furnace can produce double melted ingots from 8 to 14 in. diameter.

Satisfactory ingots are produced using the following power inputs:

Ingot, diameter in.....	2	3	4	5	6	7	8	9	10	14
Volts.....	25	28	30	38	40	40	40	40	40	40
Amperes.....	800	1000	1800	2500	3500	4000	4500	5000	5500	6000
Kilowatts.....	20	28	54	85	140	160	180	200	220	240

Energy input above this level is desirable only in an effort to reach maximum production rates per furnace operation hour. Use of as high as 160 kw (40 v—4000 Å) in the production of 5-in. diameter ingots has caused no difficulty.

Rate of melting and furnace efficiency vary slightly with different types of sponge metal and alloying agents, but under production conditions the rate of melting depends directly upon the power applied. Average power consumption for melting zirconium is about 0.25 kwhr/lb. This is based on the use of direct current, the electrode being cathodic. Employing the latest value for the heat content of zirconium at the melting point as furnished by Kelley (9) the above figure shows the furnace to have an electrical efficiency of about 50%. This is possible only because the heat is generated within the metal mass being melted.

Water consumption is variable, the quantity of water used being that required to carry off residual energy and to prevent steam pocket formation. Convenient practice is to circulate water from a cooling sump, thus permitting use of high flow rates which eliminate steam pocket formation. No effect upon furnace efficiency or ingot wall imperfections has been found possible by water control over the discharge temperature range of 37°–100°C. Usual rate employed for routine melting of a 10-in. ingot is 120 gal/min.

PURITY AND HOMOGENEITY

Ingots are machined on the surface to remove visible flaws and are then checked by means of a Sperry Ultrasonic Reflectoscope for shrinkage cavities or other internal flaws.

There are few steps that can be taken with an active metal like zirconium that do not add some contamination. While consumable electrode arc melting does not add carbon or tungsten, usually encountered in arc melting work, it does raise oxygen and nitrogen contamination. Oxygen is contributed by moisture often present in hygroscopic salts carried over in the sponge metal from the manufacturing process. Extensive exposure of sponge to moisture or use of sponge containing excessive residual chlorides must be avoided if low-oxygen metal is required. Further, experiments have shown that it is futile to attempt to dry zirconium sponge, once it has become damp, without expecting a significant increase in hardness. This is due partly to the hygro-

scopic nature of the entrapped magnesium chloride, and partly to the highly reactive surface of sponge zirconium which forms oxide and hydrogen from water at room temperature. Nitrogen contamination is due generally to atmospheric contamination during melting. Helium and argon employed in inert atmosphere melting do not contribute significant contamination since only one furnace filling of these gases is employed for each ingot.

Oxygen content of Kroll process zirconium ingot produced at the Bureau of Mines is now averaging around 1100 ppm. Procedures for determination of oxygen in zirconium metal are not highly accurate at present so contamination is reported in terms of nitrogen. Routine double melted 500-lb ingots gain 0.001% (10 ppm) nitrogen in processing from sponge to final form, indicating moderately good furnace technique. It may be inferred that very little oxygen is added by furnace operation since, under operating conditions, no selectivity for oxygen or nitrogen is considered likely.

The homogeneity of the ingots is illustrated by the case of tin, a most difficult metal to alloy properly with zirconium. Production analyses are made by a recording spectrograph which is arranged to make tests at 1-in. intervals down the side of the ingot, two passes being made at 90° to each other (10). The accuracy of the process was checked by sawing numerous ingots in half vertically and analyzing them internally also. Under certain circumstances tin was specified at 2.5%. Acceptability of the ingots was based on the range of tin values and the standard deviation, σ defined by

$$\sigma = \sqrt{\frac{\sum(\Delta)^2}{\eta}}$$

where Δ is the individual deviation from average and η is the number of analyses considered.

The first ingot in a series of ten to be discussed had the following analyses:

Position	Tin, %	Position	Tin, %
1	2.49	9	2.51
2	2.51	10	2.51
3	2.48	11	2.46
4	2.49	12	2.51
5	2.51	13	2.51
6	2.50	14	2.50
7	2.50	15	2.49
8	2.50		

This is admittedly a very good ingot having a standard deviation of only 0.01. The next nine ingots produced had standard deviations ranging from 0.02% to 0.08%.

Homogeneity of this degree compares favorably with other industrial techniques.

EFFECTIVE RECOVERY AND ECONOMICS

Production of pure zirconium ingots by a single melting operation gives 85% recovery of the sponge in the form of finished ingot, free of flaws. These ingots and all alloy ingots can be remelted economically since the effective recovery is increased to an average of 95% by this process due to an improved sidewall. This automatic increase in useful metal is important since the value of one pound of metal is equivalent to the electrical energy required to melt 4 tons of ingot. First benefit of consumable electrode double melting is thus that very little ingot scrap is produced.

Second advantage is found in the homogeneity of the small amount of turnings that are produced. It has been possible to clean these chips and combine them in later runs without any decrease in quality or change in analysis. A distinct effort must be made in the machine shop to cut a smooth, heavy chip that can be salvaged.

Finally, ingots without segregation and internal flaws seldom fail in forging and rolling and no "head crop" is necessary. The decrease in this type of scrap is quite important in the effective metal yield obtained by consumable electrode double melting.

CONCLUSIONS

It is felt that from the above information the following statements are in order in regard to the consumable electrode double melting technique.

1. There is no "electrode" contamination of carbon or tungsten.
2. The method produces homogeneity comparable to the best attainable commercially.
3. Scrap recovery is high in that only a small amount of scrap is produced and this is easily recovered.
4. Increase in effective metal recovery and decreased forging and rolling loss more than pays for remelting.
5. Simplicity of design, flexibility of the furnaces, and absence of specialized hard-to-get components makes possible the erection of such melting equipment at very low cost.

ACKNOWLEDGMENTS

The work reported herein was carried out through the cooperation of The Naval Reactors Division of the Bureau of Ships on contract NPO 19905. The assistance of E. T. Hayes in the field of metallography and physical testing in conjunction with the work has been of great assistance. Recognition is made of the services of Floyd Wood, Physicist, and Lambert Woudenberg and Frank Wagyu, plant foremen in this work.

Any discussion of this paper will appear in a Discussion Section to be published in the December 1955 JOURNAL.

REFERENCES

1. W. J. KROLL AND H. L. GILBERT, *J. (and Trans.) Electrochem. Soc.*, **96**, 158 (1949).
2. R. A. BEALL, F. CAPUTO, AND E. T. HAYES, "Homogeneous Alloy Ingots Produced by Consumable Arc Melting", presented at Brookhaven AEC Metallurgical Conference, April, 1953.
3. R. M. PARKE AND J. L. HAM, *Trans. Am. Inst. Mining Met. Engrs.*, **171**, 416 (1941).
4. W. W. STEPHENS, H. L. GILBERT, AND R. A. BEALL, *Trans. Am. Soc. Metals*, **45**, 862 (1953).
5. R. J. VAN THYNE, D. H. TURNER, AND H. D. KESSLER, *Iron Age*, **172**, 146 (Aug. 6, 1953).
6. W. J. HURFORD, Private communication.
7. S. A. HERRES, U. S. Pat. 2,541,764.
8. H. L. GILBERT, W. A. ASCHOFF, AND W. E. BRENNAN, *This Journal*, **99**, 191 (1952).
9. K. K. KELLEY, Private communication.
10. D. M. MORTIMORE, "Application of the Quantometer in Determining Minor Constituents in Zirconium Ingots," presented at Fifth Pittsburgh Conference on Analytical Chemistry and Applied Spectroscopy, March 5, 1954.

Concentration Polarization and Overvoltage¹

CECIL V. KING

Department of Chemistry, New York University, New York, New York

ABSTRACT

Concentration gradients exist at the electrodes in every electrolysis. This paper discusses the magnitude of concentration polarization to be expected in the measurement of hydrogen overvoltage, and demonstrates the use of the Nernst-Fick equation to calculate its effect, in acid, alkaline, and buffered solutions.

THEORETICAL ASPECTS

Theories of overvoltage deal with the chemical or electrochemical ("activation") polarization at an electrode surface. In any electrolysis, or other process at a solid-liquid interface, concentration gradients exist near the solid surface. Whether or not they are important in determining the rate of the process depends on the relative rates of reaction and of convective-diffusive transport at the surface. Theory and experiment have been thoroughly reviewed, with respect to both dissolution rates (1) and electrode processes (2). It is especially important to avoid, or recognize and correct for, concentration polarization in overvoltage measurements.

The rate of diffusive transport to or from an electrode surface may be expressed by the Nernst equation

$$\dot{n} = D\Delta c/\delta \quad (\text{I})$$

where \dot{n} designates equivalents transported per second per cm^2 , D is the diffusion coefficient in cm^2/sec , Δc is the difference in surface and bulk concentrations in equiv/cm^3 , and δ is the "effective thickness" of the boundary layer (thickness it would have if the gradient were linear with distance). D varies with reagent concentration and other factors, δ is highly dependent on stirring speed and to the $1/5$ to $1/3$ power of D (1).

This equation may be applied very simply to calculate surface concentrations in polarization experiments, provided the solution composition is suitable and precautions are taken to insure constancy of D and δ . It may be written as follows:

$$\Delta C = 10^3 \frac{\delta i}{D F} \quad (\text{II})$$

where i = current density in amp/cm^2 , F is the faraday, and C is now concentration in $\text{equiv}/\text{liter}$. For calculations it is necessary to know δ and D under the particular conditions employed, and

these may be measured by supplementary experiments.

Many hydrogen and oxygen overvoltage measurements have been made with stirring by gas bubbles and at a total electrolyte concentration of 0.1N–1.0N. The approximate value of δ has been determined under these conditions, at room temperature, as follows.² The rate of dissolution of strips of zinc of 13 cm^2 area was measured, in 50 cm^3 of solution containing (a) 0.0200M HCl, 0.06M KNO_3 , 0.50M NaCl; (b) 0.0229N H_2SO_4 , 0.06M KNO_3 , 0.50N Na_2SO_4 . The solutions were stirred with nitrogen, the dissolution rate increasing with the speed of bubbling. At the highest practical bubbling rate, solution (a) dissolved an average of 16.9 mg in 4 min, solution (b) an average of 13.3 mg in 4 min. This is a first order, diffusion-controlled process, and δ is calculated from the integrated Nernst equation:

$$\frac{D}{\delta} = \frac{2.3V}{At} \log \frac{a}{a-x} \quad (\text{III})$$

where A = area, V = solution volume in cm^3 , a = total dissolving capacity (29.7 and 34.0 mg, respectively, by experiment), and x = amount dissolved at time t .

Values of D used in these and other calculations below are listed in Table I (3, 4). The above experiments give $\delta = 0.0048$ and 0.0044 cm; 0.005 cm has been used in the calculations below, with $F = 10^5$ coulombs. Neither D nor δ varies much with reasonable changes in concentration of acid, base, salt, or buffer, and no attempt has been made to secure exact values for any particular case. Gas evolution at the electrode surface probably has little effect on δ in the current range considered here.

Gas bubbling is a rather ineffective means of stirring. With a metal cylinder rotating at a peripheral speed of 160,000 cm/min , with baffles to prevent cavitation and splashing, δ is reduced to about 1.5×10^{-4} cm (5). With a thin wire mounted near a grooved 2 cm shaft rotating at 4000 rpm, δ is 6 or 7×10^{-4} cm (6). It has been claimed (7) that

¹ Manuscript received September 9, 1954.

² Experiments by Eric Rau.

TABLE I. Some values of D , the diffusion coefficient, at 25°C

0.05N HCl	3×10^{-5} cm ² /sec
0.05N HCl + 0.5N NaCl	6.5×10^{-5}
Dil. NaOH	2×10^{-5}
Dil. NaOH + 0.5N NaCl	4×10^{-5}
Dil. H ₂ SO ₄	2×10^{-5}
Dil. H ₂ SO ₄ + 0.1N MgSO ₄	3.3×10^{-5}
Dil. H ₂ SO ₄ + 0.5N MgSO ₄	3.5×10^{-5}
0.05N acetic acid + 0.1N Mg(C ₂ H ₃ O ₂) ₂	1.25×10^{-5}

TABLE II. Surface C_{H^+} as function of current density for 0.1N H₂SO₄, assuming $D = 3.3 \times 10^{-5}$ cm²/sec, $\delta = 5 \times 10^{-3}$ cm

i , amp/cm ²	ΔC_{H^+} , mol/l	ΔpH	ΔE_{rev} , volt
10^{-3}	1.5×10^{-3}	0.01	0.001
10^{-2}	1.5×10^{-2}	0.07	0.004
2.5×10^{-2}	3.75×10^{-2}	0.20	0.011
5×10^{-2}	7.5×10^{-2}	0.40	0.035
7.5×10^{-2}	>0.1	>6	>0.41

the boundary layer is reduced to negligible thickness at a small rotating platinum wire mounted near a glass bladed stirrer also rotating at 600–1100 rpm. This claim seems improbable; limiting currents given by the authors suggest a thickness of about 10^{-3} cm.

Neutral salt solutions.—Imagine a salt solution like 0.5N NaCl, in pure water and quite neutral, so that $C_{H^+} = C_{OH^-} \cong 1.4 \times 10^{-7}$ moles/l [for the ionization of water in salt solutions see reference (8)]. An inert cathode is introduced and the solution is stirred by gas bubbling. Most of the current is carried by other ions, and OH⁻ ions produced leave the cathode surface by diffusion (i.e., the transference number $t_{OH^-} \rightarrow 0$). Numerical values may be inserted in equation (II):

$$\Delta C_{OH^-} = 10^3 \frac{5 \times 10^{-3}}{4 \times 10^{-5}} \frac{i}{10^5} = 1.25i$$

This equation is not valid at $i < 10^{-6}$ amp/cm² because of the slight buffering action of water, but when $i > 10^{-5}$ amp/cm² this effect will be negligible. It is assumed that the volume of solution is large or that current is passed too briefly to affect the bulk pH.

Each tenfold increase in current density, above $i = 10^{-6}$, will increase the surface pH by one unit, and the reversible emf of a hydrogen electrode (E_{rev}) will change by 0.059 v (the activity coefficients of H⁺ and OH⁻ are independent of concentration in this "swamping" salt solution, and junction potential between the surface and the bulk of solution is negligible). A "Tafel plot" with slope of 0.059 would be obtained with no "activation polarization" whatsoever.

If a weak base should be present in the salt solution, it will have very little buffer capacity toward OH⁻ ions and similar concentration polarization will result. The slope will approach 0.059 at a slightly higher pH.

Acid solutions.—It is obvious that for each acid solution a sharp rise in surface pH occurs when ΔC_{acid} approaches the original C_{acid} —as the "limiting current" is approached. This is illustrated in Table II and with several curves in Fig. 1, where ΔE_{rev} is plotted vs. log i .

If the current is increased beyond the acid diffusion current, the cathode surface becomes alkaline, and the curve continues as shown in Fig. 2 for 0.001M HCl in 0.5M NaCl. In this particular case equation (II) can be applied up to $i = 1.3 \times 10^{-3}$,

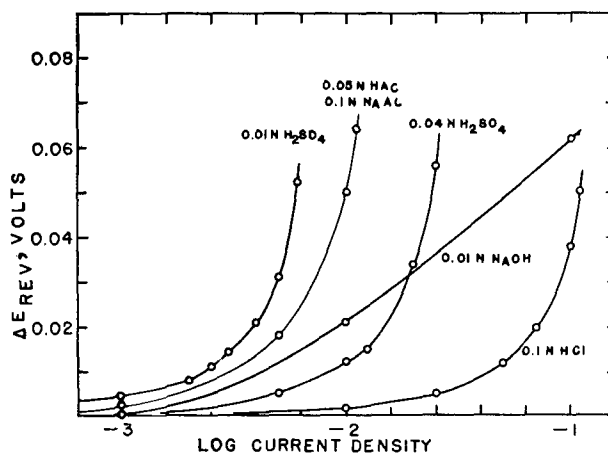


FIG. 1. Concentration polarization in various solutions. Sulfuric acid solutions to contain 0.5N sulfate; HCl and NaOH solutions to contain 0.5N NaCl. Circles are calculated points.

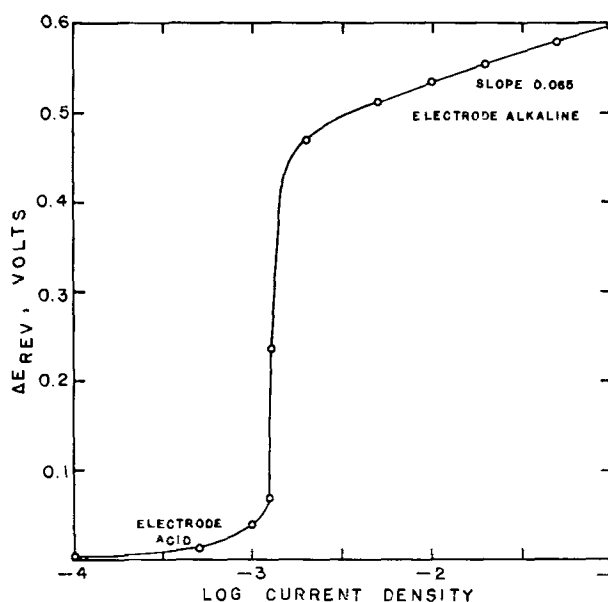


FIG. 2. Concentration polarization in 0.001M HCl, 0.5M NaCl. Circles are calculated values.

when the surface pH rises to 7. At higher current density OH⁻ ion is produced in excess and, as it diffuses outward, it is met and neutralized by the acid, at a plane within the boundary layer which we may say is $y\delta$ distant from the surface. Equation (I) may be modified as follows (3), since acid and base diffuse in equivalent amounts:

$$\dot{n} = \frac{D_{\text{OH}^-} c_{\text{OH}^-}}{y\delta} = \frac{D_{\text{H}^+} c_{\text{H}^+}}{(1-y)\delta} \quad (\text{IV})$$

When $10^3 c_{\text{OH}^-}$ and $10^3 c_{\text{H}^+}$ are $\gg 1.4 \times 10^{-7} M$ they are equivalent to the previous ΔC 's.

For calculation of the surface C_{OH^-} and E_{rev} , y may be eliminated and i/F substituted for \dot{n} :

$$C_{\text{OH}^-} = \frac{i/F - 10^{-3} D_{\text{H}^+} C_{\text{H}^+}}{10^{-3} D_{\text{OH}^-}} \quad (\text{V})$$

where the C 's are in moles/liter. With a high concentration of supporting electrolyte, changes in activity coefficients, and junction potential, may again be neglected.

Since in the alkaline surface range a reversible hydrogen electrode, if placed immediately at the cathode surface, would show a potential of 0.5 v or more with respect to one in the bulk of the solution, apparent overvoltage should be corrected accordingly.³ Curves similar to that of Fig. 2 would be obtained with weak acid or acid buffers. All the curves for acids in Fig. 1 would be similar at higher current densities. The curve in the alkaline region in Fig. 2 is nearly, though not quite, linear with an average slope of 0.065. The more acid in the solution, the higher this slope will be.

Buffer solutions.—With a buffer consisting of a weak acid and its salt, appreciable concentration polarization is found at a lower current density than with the same concentration of strong acid, as shown for an acetate buffer in Fig. 1. This is because pH depends on the ratio acid/salt, and as surface C_{acid} decreases, surface C_{salt} increases by an equal amount. Equation (II) may be employed for calculation except at extreme acid/salt ratios. Alkaline buffers consisting of an acid molecule and its reciprocal base may be treated in the same way, provided the cathode reaction remains simple neutralization of the acid component. If hydroxyl ion is produced in excess at the surface this becomes an interdiffusion problem as described above.

Strong base solution.—Fig. 1 shows the concentration polarization curve to be expected if the starting solution is 0.01N NaOH in 0.5N NaCl. The slope is smaller than 0.059 v/unit log i , approaching this value at sufficiently high current density.

³ Note, however, that the remaining curve would refer to a surface solution whose composition varies with current density.

Acid alone.—If no indifferent salt (supporting electrolyte) is present, the fraction t_{H^+} of the cathode current is carried by ion migration, and only $(1 - t_{\text{H}^+})$ by diffusion. Equation (II) should be modified:

$$\Delta C_{\text{H}^+} = (1 - t_{\text{H}^+}) 10^3 \frac{\delta i}{D F} \quad (\text{VI})$$

where t_{H^+} is the transference number. Concentration polarization becomes appreciable at a somewhat higher current density. In 0.1N H₂SO₄, 0.5N MgSO₄, with $\delta = 5 \times 10^{-3}$ cm

$$\Delta C = 1.43 i$$

In 0.1N H₂SO₄ alone, with $t_{\text{H}^+} = 0.82$ (8)

$$\Delta C = 0.45 i$$

Over a wide range of ΔC , the change in t_{H^+} with concentration should be considered.

In solutions of acid alone, concentration polarization measurements may also be extended beyond the acid diffusion (and migration) current; Coates (9), using an interrupter method to separate the concentration effect from true overvoltage, has shown that the curves look much like Fig. 2, with even larger increases in potential. If actually no positive ions except H⁺ are present, an equilibrium pH above 7 seems impossible. Coates postulates an excess of OH⁻ ions, and lack of electroneutrality at the cathode surface, forced by the current flow; a very small excess C_{OH^-} in the abnormal electrical double layer would account for an apparent pH of 20 or more. This is neither normal concentration polarization nor activation polarization in the usual sense.

DISCUSSION

Breaks in hydrogen overvoltage curves from Tafel slopes of about 0.03 to slopes of about 0.1 have been found in acid and buffer solutions by Schuldiner (10). These breaks appear at current densities where equation (II) predicts the existence of appreciable concentration polarization. Current densities plotted by Schuldiner are based on electrode roughness factors of about 2, and in comparing with the present treatment i must be based on apparent area, since δ is not much affected by very small surface irregularities. The breaks to higher slopes follow regularly with increasing acid concentration, and are predicted rather closely with δ a little smaller than 0.005 cm. Adequate correction of the curves requires a more precise value of D and a knowledge of whether δ is affected by gas evolution in addition to the stirring by hydrogen bubbling. In the meantime, changes in slope can be given

little significance. In only one case did Schuldiner continue measurements to high enough currents to obtain a curve like Fig. 2.

Uniform overvoltage curves were found by Bockris and Azzam (11), in 5*N* HCl, to current densities of the order of 100 amp/cm². These authors were well aware of the danger of including concentration polarization in the measurements, and attempted to calculate the current at which it would be appreciable. While their method of calculation was not well suited to the experimental conditions, and the value (0.01 cm) chosen for δ was certainly incorrect, they were probably correct in assigning another reason for the breaks in slope found at the highest current densities. Equation (VI) could be applied directly; D and t_{H^+} can be sufficiently well estimated, but δ would have to be found, since the intense hydrogen evolution at very high current densities would certainly decrease its value below 0.005 cm.

Cathodic polarization measurements on titanium and zirconium electrodes in sodium chloride solutions have been made by Hackerman and his students (12, 13). While these were not intended as precise overvoltage measurements, they illustrate the uncertainty of interpretation. The solutions perhaps had a small buffer capacity, and at small currents the cathode potential remained low because of oxygen reduction, even though the surface solution became alkaline. The sharp rises observed were due, as the authors state, to limiting oxygen diffusion currents. In the hydrogen evolution region the authors give the equations for E vs. the saturated calomel cell

$$E = -1.93 - 0.154 \log i \text{ titanium}$$

$$E = -1.47 - 0.15 \log i \text{ zirconium}$$

Provided δ does not vary with current, both slopes should be corrected by about 0.06. Correction of the constants is less certain; if surface $pH = 7$ when $\log i = -6$, then 1.01 v is found, including the calomel cell potential. The overvoltage equations become—for alkaline solutions of varying composition—:

$$\eta = 0.92 + 0.094 \log i \text{ titanium}$$

$$\eta = 0.46 + 0.09 \log i \text{ zirconium}$$

For the case of a single diffusing species whose concentration can fall to zero at the electrode surface, the method described above is equivalent to use of the well-known relation

$$E_{rev} = \frac{RT}{nF} \ln \frac{i_d - i}{i_d} \quad (\text{VII})$$

where i_d is the diffusion or limiting current density. This equation is derived on the same premises as equation (II), but assumes D and δ to be constant, while different values can be inserted in equation (II) for each current density, if required. Coates (9) shows that, with no stirring except cathodic hydrogen evolution, experimental concentration polarization is greater than equation (VII) predicts, simply because δ decreases with increasing current density. This is equivalent, in equation (VII), to an increase in i_d for each increase in i .

With auxiliary stirring, does gas evolution at the electrode cause δ to decrease with current density? At relatively high stirring speeds, hydrogen evolution when magnesium dissolves in acids does not appear to affect δ much (4). In the present case, the same is probably true until stirring by gas evolution alone approaches the auxiliary stirring alone. Comparison with magnesium dissolution indicates that this would occur (i. e., $\delta = 0.005$ cm) at a current density somewhat above 0.1 amp/cm² (14). At lower currents δ is probably constant, but this should be tested by experiment.

Not all investigators can agree with Coates that forced electrolysis in a solution of pure acid leads to lack of electroneutrality at the cathode surface, or that his measured potentials in this region have been interpreted correctly. However, could not a smaller degree of charge separation be present in every electrolysis, and vitiate any calculation of concentration polarization? There is no experimental evidence to suggest such an effect for ordinary solutions. With sufficient supporting electrolyte, or with current densities low compared to total concentration, the Nernst emf equation can be employed with confidence.

What recommendations can be made concerning the composition of solutions to be used in hydrogen overpotential measurements? It seems better to avoid corrections for concentration polarization so far as possible, since these entail some uncertainty at best. Further, it is desirable to measure overvoltage as a function of both current density and composition of solution, and it is obviously preferable to change these variables separately. No difficulties are encountered in concentrated strong acid or base solutions, except at very high current densities. With neutral salts, correction is almost unavoidable. Reliable measurements are highly desirable in dilute acid and base solutions and in buffers around the neutral point. There is no doubt a change in Tafel slope in acid and alkaline solutions, and it would be useful to know just how and where this occurs. In this region concentration polarization is sure to be present except at the lowest current densities and, if it is undesirable to

make direct corrections for it, at least its magnitude can be calculated and its effect studied.

In this paper no assumptions have been made concerning the mechanism of hydrogen discharge, or the nature and magnitude of "activation" overpotential; indeed, such assumptions were quite unnecessary for the purpose. Concentration polarization is directly related to current density and the other factors considered, but of course has nothing to do with the discharge mechanism.

Similar treatment can naturally be applied to anodic oxygen evolution, to metal deposition, to oxidation-reduction processes at inert electrodes, etc. More thorough and elegant treatment of some of these cases has been made by Petrocelli (15) and by Eisenberg, Tobias, and Wilke (16).

ACKNOWLEDGMENTS

The author wishes to acknowledge helpful discussion with C. Wagner, H. H. Uhlig, and B. R. Sundheim.

Any discussion of this paper will appear in a Discussion Section to be published in the December 1955 JOURNAL.

REFERENCES

1. L. L. BIRCUMSHAW AND A. C. RIDDIFORD, *Quarterly Revs. London*, **6**, 157 (1952).
2. C. W. TOBIAS, M. EISENBERG, AND C. R. WILKE, *This Journal*, **99**, 359C (1952).
3. C. V. KING AND W. H. CATHCART, *J. Am. Chem. Soc.*, **58**, 1639 (1936).
4. C. V. KING AND W. H. CATHCART, *ibid.*, **59**, 63 (1937).
5. C. V. KING AND M. SCHACK, *ibid.*, **57**, 1212 (1935).
6. C. V. KING AND P. L. HOWARD, *Ind. Eng. Chem.*, **29**, 75 (1937).
7. I. M. KOLTHOFF AND J. JORDAN, *J. Am. Chem. Soc.*, **75**, 4869 (1953); **76**, 3843 (1954).
8. H. S. HARNED AND B. B. OWEN, "The Physical Chemistry of Electrolytic Solutions," p. 578, Reinhold Publishing Corp., New York (1943).
9. G. E. COATES, *J. Chem. Soc.*, **1945**, 484.
10. S. SCHULDINER, *This Journal*, **99**, 488 (1952); **101**, 426 (1954).
11. J. O'M. BOCKRIS AND A. AZZAM, *Trans. Faraday Soc.*, **48**, 145 (1952).
12. N. HACKERMAN AND C. D. HALL, *This Journal*, **101**, 321 (1954).
13. N. HACKERMAN AND O. B. CECIL, *ibid.*, **101**, 419 (1954).
14. B. ROALD AND W. BECK, *ibid.*, **98**, 277 (1951).
15. J. V. PETROCELLI, *ibid.*, **98**, 187 (1951).
16. M. EISENBERG, C. W. TOBIAS, AND C. R. WILKE, *ibid.*, **101**, 306 (1954).

A Theoretical Basis for a New Method of Investigating Corrosion Inhibition¹

JAMES G. JEWELL

Gulf Research & Development Company, Pittsburgh, Pennsylvania

ABSTRACT

An inequality has been derived that bounds the derivative of the corrosion current with respect to the concentration of a strictly cathodic inhibitor:

$$\left| \frac{\partial I_1}{\partial x} \right| \leq \frac{\left| \frac{\partial \Gamma}{\partial x} \right|}{\left| \frac{\partial \Gamma}{\partial I_3} + W \right|}$$

(See text for definition of terms.)

In special cases the inequality is a direct consequence of Cupr's generalization of Müller's electrochemical model of corrosion. In the general case it is necessary to invoke a statistical assumption to obtain the same result. The upper bound of the derivative can be calculated from measurements of the potential difference between a corroding electrode and a reference half-cell at different concentrations of the inhibitor and at different densities of an externally applied current. If the upper bound is small, the agent under investigation is definitely not a good cathodic inhibitor, although it may or may not be a good anodic one. If the upper bound is large, no conclusion can be drawn; some other method must be employed to determine whether the agent is an effective inhibitor. Therefore, what the theory provides is a rapid method for screening cathodic inhibitors to eliminate from further consideration certain ones that can be shown ineffective. If the Müller-Cupr model is a valid one, there is no obvious way of accomplishing more than this by means of potential measurements alone.

INTRODUCTION

Mears (1) has shown that the direction of potential shift of a corroding metal surface following adsorption of a chemical additive is not a dependable indication of whether the additive is functioning as an inhibitor. Furthermore, the magnitude of the shift is not necessarily a measure of the effectiveness of the additive in those cases in which a known inhibitor alters the potential to a more noble value. Unfortunately these observations imply that the once much-used technique of screening inhibitors by means of potential measurements is not a trustworthy one. Mears' conclusions, based implicitly on Müller's (2) electrochemical model of corrosion and on its generalization by Cupr (3), apply to potential measurements of metals in inhibited solutions when no external current is imposed across the metal-solution interface. This paper shows that there is a theoretical basis for screening cathodic inhibitors by means of a function that may be determined by potential measurements when an external current is applied.

¹ Manuscript received July 9, 1954. This paper was prepared for delivery before the Boston Meeting, October 3 to 7, 1954.

The conclusions to be drawn here, like those of Mears, are based on Cupr's concept of a corroding metal surface. Before examining this matter in detail it is worth while to list some of the conventions that have been adopted in this paper. In the preceding paragraph the word *potential* was used in its electrochemical sense. From here on it refers to the work required to bring a unit electrical charge to a point. A potential E_o will be assigned arbitrarily to some point, α , in the system under consideration. Then, at any other point, β , to which a potential is assigned the potential is E_o plus a potential difference between α and β defined in the usual way. Current flows from a point of higher (more positive) to a point of lower (less positive) potential in any region not containing points of discontinuity of potential, regardless of whether the current is electronic or ionic. As an exception to this rule, small ohmic potential drops in metals are neglected, i.e., a metal may be assumed to be at constant potential even though it carries a small current. Points of discontinuity of potential in a circuit are denoted by the usual symbol (a) illustrated in Fig. 1. Current may flow in either direction across such a point. However, if the point of discontinuity is the only source of

electromotive force in a closed circuit, the direction of current flow is that shown by the arrow in Fig. 1 regardless of whether the current is ionic or electronic. At the risk of some confusion the expression *half-cell potential* will be given an electrochemical meaning different from the meaning of *potential* just discussed. Specifically, if there is no current flowing across the interface between a solution and a reference half-cell or in the lead wire to the half cell, and if $V(\alpha)$ is the potential at an arbitrary point, α , of the (equipotential) lead wire and $V(\beta)$ is the potential at an arbitrary point, β , of the (equipotential) interface, then $\Theta = V(\beta) - V(\alpha)$ will be defined to be the half-cell potential.

THEORY

According to Cupr a metal electrode corroding in an electrolyte may be represented symbolically by the network of Fig. 2 in which N local cells are arranged in parallel between two equipotential surfaces. One of these is the metal-solution interface and the other is the electrode boundary, the significance of which is discussed by Cupr and by Pearson (4). The interface to be discussed here is roughly plane and the electrode boundary is approximately a plane located in the electrolyte "parallel" to the interface at a distance from it that may be determined experimentally. The electrolyte outside the electrode boundary is assumed to be homogeneous; hence, if an external current is made to flow from a remote source through the electrolyte to the boundary, the lines of flow outside the boundary will be perpendicular to it and the equipotentials will be planes parallel to it. The current density outside the boundary is, of course, constant.

Consider a j^{th} arbitrary local cell in Fig. 2. The local anode components are R_{1j} , a resistance, and E_{1j} , a point discontinuity in potential that constitutes the "driving force" for the corrosion current in this j^{th} local cell. Similarly, the cathode components are R_{2j} and E_{2j} . E_{2j} represents the solution pressure and back emf of polarization at the j^{th} cathode. The phenomenon of anode polarization is taken into account by making E_{1j} and R_{1j} variables. I_{1j} is the current in the anode branch of the j^{th} cell, and I_{2j} is the current in the cathode branch. If no external current is applied to the j^{th} cell, I_{1j} and I_{2j} are equal, are not zero, and flow in the directions indicated by the arrows in the figure. The component of the external current that enters the j^{th} cell is I_{3j} . For sufficiently large values of I_{3j} (note direction in Fig. 2), the direction of I_{1j} may be reversed. If, when this happens, I_{1j} is defined to be a negative quantity, and if I_{2j} and I_{3j} are always taken to be positive or zero, all of the equations that follow remain valid

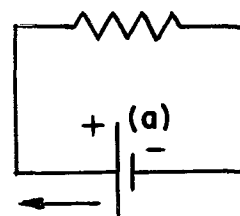


FIG. 1. Potential discontinuity; direction of current flow

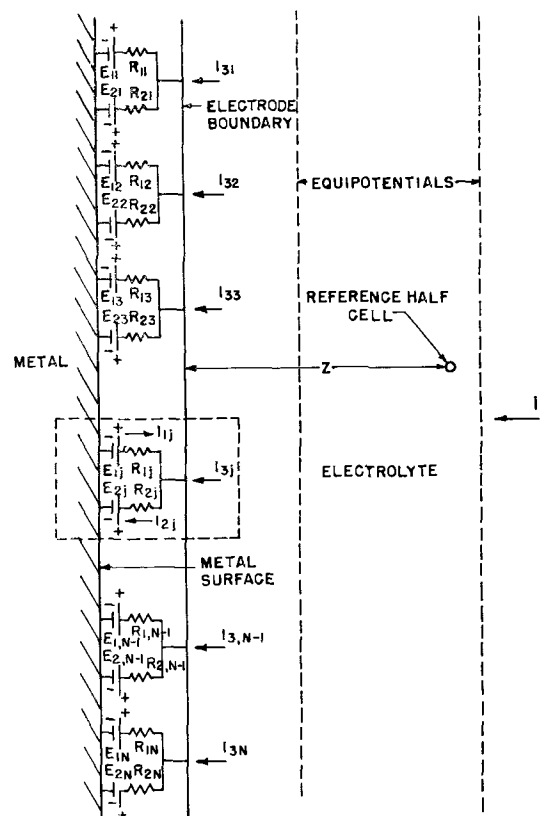


FIG. 2. The Müller-Cupr model

regardless of the direction of the currents at the local anodes.²

In order not to complicate the problem unnecessarily the resistivity, ρ , of the electrolyte is considered to be constant, although in fact it might depend to a small extent on the concentration, x , of an inhibitor. This is not a crucial point; corrections for variations in ρ can be made if necessary. Because of the convention stated above concerning current directions N , the number of local cells, is a constant. The total anode current in the N cells is

$$I_1 = \sum_{j=1}^N I_{1j} \quad [1]$$

² In general, it should be noted that the second subscript following a symbol identifies the local cell to which the symbol pertains. The range of this subscript is 1 to N . The first subscript will always be a 1, 2, or 3; 1 indicates an anode component, 2 a cathode component, and 3 (used always with I) an externally applied current.

Faraday's law implies that I_1 is directly proportional to the rate of corrosion of the metal under test. The total external current applied is

$$I_3 = \sum_{j=1}^N I_{3j} \quad [2]$$

If A is the area of the metal surface and z is the distance between the electrode boundary and a reference half-cell located outside the electrode boundary (see Fig. 2), the resistance between the boundary and the half-cell is:

$$W = \frac{\rho z}{A} \quad [3]$$

It is assumed that the resistive and emf components of each local cell are functions of the in-

$$dI_{1j} = \frac{\left[dE_{1j} - dE_{2j} + \frac{(-E_{1j} + E_{2j} + R_{2j}I_{3j})dR_{1j}}{R_{1j} + R_{2j}} + \frac{(-E_{1j} + E_{2j} - R_{1j}I_{3j})dR_{2j} - R_{2j}dI_{3j}}{R_{1j} + R_{2j}} \right]}{(R_{1j} + R_{2j})}$$

hibitor concentration and the current through the component. That is, for each j :

$$\begin{aligned} E_{1j} &= E_{1j}(x, I_{1j}) \\ E_{2j} &= E_{2j}(x, I_{2j}) \\ R_{1j} &= R_{1j}(x, I_{1j}) \\ R_{2j} &= R_{2j}(x, I_{2j}) \end{aligned} \quad [4]$$

This is a natural, but by no means inevitable, assumption. It would not hold over a long period of time because of the accumulation of corrosion products on the metal surface and because of gradual changes in location of the active centers of corrosion. Nor would it hold, for example, in the case of an inhibitor for which the extent of adsorption depends on whether the inhibitor is added before or after an external current is applied.

The half-cell potential of the reference half-cell is called Θ . If α is an arbitrary point in the lead wire to the half-cell, a potentiometer connected to the lead wire and to the corroding metal measures a potential difference, Γ :

$$\Gamma = E_o - V(\alpha)$$

where E_o is the potential arbitrarily assigned to the metal and $V(\alpha)$ is the potential at α . If β is a point on the interface between the half-cell and the solution:

$$\Theta = V(\beta) - V(\alpha)$$

Also from Ohm's and Kirchoff's laws for each j :

$$V(\beta) = E_o + E_{1j} - I_{1j}R_{1j} + I_3W$$

Combining these last three equations:

$$\Gamma = \Theta - E_{1j} + I_{1j}R_{1j} - I_3W \quad [5]$$

Of course when Θ and I_3 are zero, and I_{1j} vanishes for every j , $-\Gamma$ becomes the thermodynamic half-cell potential of the metal. Application of the principle of superposition of currents and Kirchoff's laws to the j^{th} cell yields the well-known equations [see reference (4) for example]:

$$I_{1j} = \frac{E_{1j} - E_{2j}}{R_{1j} + R_{2j}} - \frac{R_{2j}I_{3j}}{R_{1j} + R_{2j}} = \phi_1(E_{1j}, E_{2j}, R_{1j}, R_{2j}, I_{3j}) \quad [6]$$

$$I_{2j} = \frac{E_{1j} - E_{2j}}{R_{1j} + R_{2j}} + \frac{R_{1j}I_{3j}}{R_{1j} + R_{2j}} = \phi_2(E_{1j}, E_{2j}, R_{1j}, R_{2j}, I_{3j}) \quad [7]$$

Differentiation of [6] yields

Or in view of [6] and [7],

$$dI_{1j} = \frac{(dE_{1j} - dE_{2j} - I_{1j}dR_{1j} - I_{2j}dR_{2j} - R_{2j}dI_{3j})}{(R_{1j} + R_{2j})} \quad [8]$$

On differentiating the equations [4],

$$\begin{aligned} dE_{1j} &= \frac{\partial E_{1j}}{\partial x} dx + \frac{\partial E_{1j}}{\partial I_{1j}} dI_{1j} \\ dE_{2j} &= \frac{\partial E_{2j}}{\partial x} dx + \frac{\partial E_{2j}}{\partial I_{2j}} dI_{2j} \\ dR_{1j} &= \frac{\partial R_{1j}}{\partial x} dx + \frac{\partial R_{1j}}{\partial I_{1j}} dI_{1j} \\ dR_{2j} &= \frac{\partial R_{2j}}{\partial x} dx + \frac{\partial R_{2j}}{\partial I_{2j}} dI_{2j} \end{aligned} \quad [9]$$

Substitution of the values of dE_{1j} , dE_{2j} , dR_{1j} , and dR_{2j} given by [9] in equation [8] yields after rearrangement:

$$\begin{aligned} dI_{1j} \left(R_{1j} + R_{2j} - \frac{\partial E_{1j}}{\partial I_{1j}} + I_{1j} \frac{\partial R_{1j}}{\partial I_{1j}} \right) &= \left(\frac{\partial E_{1j}}{\partial x} - \frac{\partial E_{2j}}{\partial x} - I_{1j} \frac{\partial R_{1j}}{\partial x} - I_{2j} \frac{\partial R_{2j}}{\partial x} \right) dx \\ &\quad - \left(\frac{\partial E_{2j}}{\partial I_{2j}} + I_{2j} \frac{\partial R_{2j}}{\partial I_{2j}} \right) dI_{2j} - R_{2j}dI_{3j} \end{aligned} \quad [10]$$

Kirchoff's laws imply that for every j ,

$$I_{2j} = I_{1j} + I_{3j} \quad [11]$$

Therefore

$$dI_{2j} = dI_{1j} + dI_{3j}$$

On substituting this value of dI_{2j} in [10]

dI_{1j}

$$\begin{aligned} & \left(R_{1j} + R_{2j} - \frac{\partial E_{1j}}{\partial I_{1j}} + I_{1j} \frac{\partial R_{1j}}{\partial I_{1j}} + \frac{\partial E_{2j}}{\partial I_{2j}} + I_{2j} \frac{\partial R_{2j}}{\partial I_{2j}} \right) \\ & = \left(\frac{\partial E_{1j}}{\partial x} - \frac{\partial E_{2j}}{\partial x} - I_{1j} \frac{\partial R_{1j}}{\partial x} - I_{2j} \frac{\partial R_{2j}}{\partial x} \right) [12] \\ & \cdot dx - \left(\frac{\partial E_{2j}}{\partial I_{2j}} + I_{2j} \frac{\partial R_{2j}}{\partial I_{2j}} + R_{2j} \right) dI_{3j} \end{aligned}$$

For reasons that will become apparent later it is useful to define

$$\begin{aligned} \lambda_j &= R_{1j} - \frac{\partial E_{1j}}{\partial I_{1j}} + I_{1j} \frac{\partial R_{1j}}{\partial I_{1j}} \\ \mu_j &= R_{2j} + \frac{\partial E_{2j}}{\partial I_{2j}} + I_{2j} \frac{\partial R_{2j}}{\partial I_{2j}} \\ \Delta_j &= \frac{\mu_j}{\lambda_j + \mu_j} \text{ (provided } \lambda_j + \mu_j \neq 0) \\ \psi_j &= \frac{\partial E_{1j}}{\partial x} - I_{1j} \frac{\partial R_{1j}}{\partial x} \end{aligned} [13]$$

The coefficient of dI_{1j} in equation [12] is $(\lambda_j + \mu_j)$, and the coefficient of dI_{3j} is μ_j . Therefore,

$$\frac{\partial I_{1j}}{\partial I_{3j}} = -\Delta_j [14]$$

$$\frac{\partial I_{1j}}{\partial x} = \frac{\left(\psi_j - \frac{\partial E_{2j}}{\partial x} - I_{2j} \frac{\partial R_{2j}}{\partial x} \right)}{\lambda_j + \mu_j} [15]$$

After elimination of E_{1j} , E_{2j} , R_{1j} , R_{2j} , and I_{2j} among equation [6], the four equations [4], and equation [11], I_{1j} may be expressed as a function of x and I_{3j} only as is implicit in [12], [14], and [15]. Then:

$$dI_{1j} = \frac{\partial I_{1j}}{\partial x} dx + \frac{\partial I_{1j}}{\partial I_{3j}} dI_{3j} [16]$$

Substituting [14] in [16]:

$$dI_{1j} = \frac{\partial I_{1j}}{\partial x} dx - \Delta_j dI_{3j} [17]$$

From Kirchoff's laws and the principle of superposition of currents it is easily deduced that

$$I_{3j} = I_j I_3 [18]$$

$$\frac{\partial I_{1j}}{\partial x} = \frac{\Delta_j \left[\left(\frac{\partial \Gamma}{\partial I_3} + W \right) I_3 \frac{\partial I_j}{\partial x} - \left(\frac{\partial \Gamma}{\partial x} + \psi_j \right) \left(I_j + I_3 \frac{\partial I_j}{\partial I_3} \right) \right]}{\left(\frac{\partial \Gamma}{\partial I_3} + W \right)} [27]$$

where

$$I_j = \frac{\left(\frac{1}{R_{1j}} + \frac{1}{R_{2j}} \right)}{\sum_{k=1}^N \left(\frac{1}{R_{1k}} + \frac{1}{R_{2k}} \right)} [19]$$

Summation of [19] on j from 1 to N yields

$$\sum_{j=1}^N H_j = \frac{\sum_{j=1}^N \left(\frac{1}{R_{1j}} + \frac{1}{R_{2j}} \right)}{\sum_{k=1}^N \left(\frac{1}{R_{1k}} + \frac{1}{R_{2k}} \right)} = 1; [20]$$

and differentiating [20]

$$\sum_{j=1}^N dH_j = 0 [21]$$

Since Θ and W are constants it follows from [5] that for each j ,

$$d\Gamma = -dE_{1j} + I_{1j} dR_{1j} + R_{1j} dI_{1j} - W dI_3$$

Combining this last equation with [9], [13], and [17]:

$$d\Gamma = \left(\lambda_j \frac{\partial I_{1j}}{\partial x} - \psi_j \right) dx - \lambda_j \Delta_j dI_{3j} - W dI_3 [22]$$

From [18],

$$dI_{3j} = H_j dI_3 + I_3 dH_j [23]$$

Combining [22] and [23],

$$\begin{aligned} d\Gamma &= \left(\lambda_j \frac{\partial I_{1j}}{\partial x} - \psi_j \right) dx - (\Delta_j \lambda_j H_j + W) \\ &\cdot dI_3 - \Delta_j \lambda_j I_3 dH_j \end{aligned} [24]$$

Since I_3 and x may be varied independently,

$$\frac{\partial x}{\partial I_3} \equiv \frac{\partial I_3}{\partial x} \equiv 0$$

However H_j is a complicated function of both I_3 and x so that in general,

$$\frac{\partial H_j}{\partial x} \neq 0$$

$$\frac{\partial H_j}{\partial I_3} \neq 0$$

Therefore,

$$\frac{\partial \Gamma}{\partial x} = \left(\lambda_j \frac{\partial I_{1j}}{\partial x} - \psi_j \right) - \lambda_j \Delta_j I_3 \frac{\partial H_j}{\partial x} [25]$$

$$\frac{\partial \Gamma}{\partial I_3} = -\lambda_j \Delta_j \left(H_j + I_3 \frac{\partial H_j}{\partial I_3} \right) - W [26]$$

By solving [26] for λ_j , substituting the expression so obtained in [25] and solving for $\partial I_{1j}/\partial x$ one finds:

Advantage may be taken of the monotonic nature of anode and cathode "polarization curves" to prove that for every j ,

$$\begin{aligned} \lambda_j &\geq 0 \\ \mu_j &\geq 0 \end{aligned} [28]$$

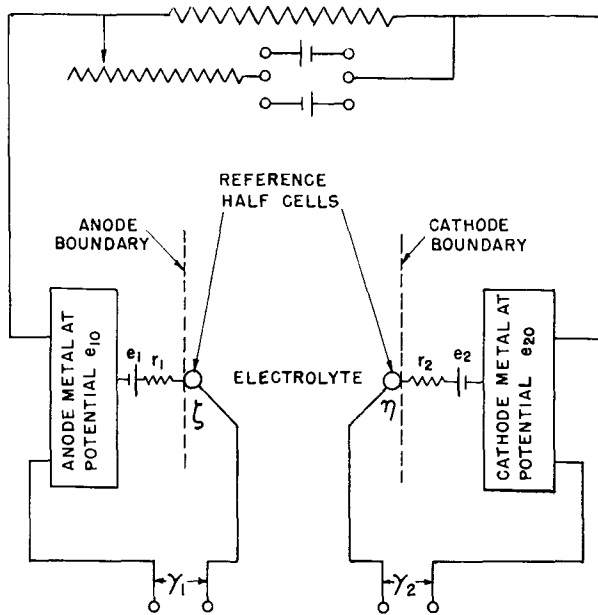


FIG. 3. Polarization of isolated anode and cathode

The argument is as follows. Under certain conditions single anodes and cathodes may be isolated that are large enough to study experimentally. In Fig. 3 an isolated anode and cathode in an electrolyte are represented schematically. An electric circuit is so arranged that an arbitrary external current may be imposed in either direction between the anode and cathode. Close to each electrode surface (ideally on the electrode boundary) so as to avoid ohmic drops in the solution is placed a salt bridge to a reference half-cell with half-cell potential θ . The potential difference between the anode metal and the lead wire to the half cell is γ_1 ; between the lead wire and the cathode metal, γ_2 . The salt bridge on the anode boundary is located at the point ζ and the one on the cathode boundary is at η . $V(\zeta)$ and $V(\eta)$ are the potentials at ζ and η , respectively. The current flowing in the solution between the electrode boundaries is i and is positive if the direction of flow is from anode to cathode, and negative otherwise. The "half-cell potential" of the anode is P_1 and that of the cathode P_2 ; the potential in the metal phase at the anode is e_{10} and at the cathode e_{20} . By definition

$$P_1 = V(\zeta) - e_{10} \quad [29]$$

$$P_2 = V(\eta) - e_{20} \quad [30]$$

Consider first the anode polarization in terms of the notation of Fig. 3. Kirchoff's law requires:

$$V(\zeta) = e_{10} + e_1 - ir_1$$

When $V(\zeta) - e_{10}$ has been eliminated between this and [29] and the resulting equation differentiated with respect to i there results:

$$\frac{dP_1}{di} = \frac{de_1}{di} - i \frac{dr_1}{di} - r_1 \quad [31]$$

Since r_1 is always nonnegative, in the simple case when e_1 and r_1 are constants:

$$\frac{dP_1}{di} = -r_1 < 0 \quad [32]$$

That is, the anode polarization curve is strictly decreasing. As a matter of fact it is one of the fundamental assumptions of corrosion theory that regardless of whether e_1 and r_1 are constant or not, the anode polarization curve is monotonic decreasing; although in general it is not linear as in the simple case described by equation [34]. Furthermore the assumption is usually made (and is made here) that the polarization curves of microscopic anodes, as well as of anodes large enough to be isolated, are monotone decreasing. Monotonicity implies

$$\frac{dP_1}{di} \leq 0$$

Therefore equation [31] implies

$$\frac{de_1}{di} - i \frac{dr_1}{di} - r_1 \leq 0 \quad [33]$$

Consider next the cathode polarization:

$$V(\eta) = e_{20} + e_2 + ir_2$$

Elimination of $V(\eta) - e_{20}$ between this equation and [30], and differentiation with respect to i yields,

$$\frac{dP_2}{di} = \frac{de_2}{di} + i \frac{dr_2}{di} + r_2 \quad [34]$$

When e_2 and r_2 are constants

$$\frac{dP_2}{di} = r_2 \geq 0$$

Then by analogy with the anode case the proper assumption is that the cathode polarization curve is monotone increasing, regardless of whether e_2 and r_2 are constants. Therefore,

$$\frac{de_2}{di} + i \frac{dr_2}{di} + r_2 \geq 0 \quad [35]$$

The sign conventions here are consistent with those adopted earlier in connection with the Müller-Cupr model of corrosion. Therefore in that model postulates [33] and [35] become,

$$\frac{\partial E_{1j}}{\partial I_{1j}} - I_{1j} \frac{\partial R_{1j}}{\partial I_{1j}} - R_{1j} \leq 0 \quad [36]$$

$$\frac{\partial E_{2j}}{\partial I_{2j}} + I_{2j} \frac{\partial R_{2j}}{\partial I_{2j}} + R_{2j} \geq 0 \quad [37]$$

These inequalities apply for each j . The subscripts 1 and 2 appear here with I because unlike the case when the anode and cathode may be separated,

$$I_{1j} \neq I_{2j}$$

In view of equation [13], [37] may be rewritten $\mu_j \geq 0$. On multiplication of equation [36] by -1 and reversal of its sense there results

$$\lambda_j \geq 0$$

Thus the inequalities [28] have been verified. An immediate consequence of [28] and [13] is

$$0 \leq \Delta_j \leq 1 \tag{38}$$

except in the singular case when λ_j and μ_j both vanish, which need not be considered here.

Differentiation of equation [1] with respect to x and substitution of [27] in the equation for the derivative yields,

$$\begin{aligned} \frac{\partial I_1}{\partial x} = & \left(\frac{1}{\frac{\partial \Gamma}{\partial I_3} + W} \right) \left[- \frac{\partial \Gamma}{\partial x} \sum_{j=1}^N \Delta_j H_j \right. \\ & - I_3 \frac{\partial \Gamma}{\partial x} \sum_{j=1}^N \Delta_j \frac{\partial H_j}{\partial I_3} + I_3 \left(\frac{\partial \Gamma}{\partial I_3} + W \right) \sum_{j=1}^N \Delta_j \frac{\partial H_j}{\partial x} \tag{39} \\ & \left. - \sum_{j=1}^N \Delta_j \psi_j H_j - I_3 \sum_{j=1}^N \Delta_j \psi_j \frac{\partial H_j}{\partial I_3} \right] \end{aligned}$$

In order to obtain an important result in as simple a manner as possible the local cells are assumed identical, as a special case. Then the same result will be proved in a more general case by means of a statistical argument. If all the cells are identical, the Δ_j are all equal to some Δ and the ψ_j to some ψ . Then:

$$\begin{aligned} \sum_{j=1}^N \Delta_j \frac{\partial H_j}{\partial I_3} &= \Delta \sum_{j=1}^N \frac{\partial H_j}{\partial I_3} \\ \sum_{j=1}^N \Delta_j \frac{\partial H_j}{\partial x} &= \Delta \sum_{j=1}^N \frac{\partial H_j}{\partial x} \\ \sum_{j=1}^N \Delta_j \psi_j \frac{\partial H_j}{\partial I_3} &= \Delta \psi \sum_{j=1}^N \frac{\partial H_j}{\partial I_3} \end{aligned}$$

But [21] implies

$$\sum_{j=1}^N \frac{\partial H_j}{\partial I_3} = \sum_{j=1}^N \frac{\partial H_j}{\partial x} = 0$$

Therefore [39] reduces to

$$\frac{\partial I_1}{\partial x} = \frac{\left(- \frac{\partial \Gamma}{\partial x} \sum_{j=1}^N \Delta_j H_j - \sum_{j=1}^N \Delta_j \psi_j H_j \right)}{\frac{\partial \Gamma}{\partial I_3} + W} \tag{40}$$

To remove the restriction that the local cells be identical in the derivation of [40] consider the terms in [39] containing the expressions

$$\sum_{j=1}^N \Delta_j \frac{\partial H_j}{\partial I_3}; \quad \sum_{j=1}^N \Delta_j \frac{\partial H_j}{\partial x}; \quad \text{and} \quad \sum_{j=1}^N \Delta_j \psi_j \frac{\partial H_j}{\partial I_3} \tag{41}$$

Equations [13] and [19] imply that the Δ_j and ψ_j are partly but not entirely independent of the

$\partial H_j / \partial x$ and $\partial H_j / \partial I_3$. However, the partial functional relationships linking these two sets of quantities are extremely complicated in nature, being unknown solutions of a set of differential equations. In order to reduce the problem to manageable proportions it is necessary to invoke a statistical assumption, i.e., that the complicated partial relationships associate the Δ_j and ψ_j with the $\partial H_j / \partial I_3$ and $\partial H_j / \partial x$ in a random manner. More specifically, the Δ_j and ψ_j are distributed in some way about their respective means. It will be assumed that these distributions are independent of the distributions of the $\partial H_j / \partial I_3$ and $\partial H_j / \partial x$ for every value of I_3 and x . It should be noted that this assumption is somewhat more plausible when the corroding surface is macroscopically homogeneous than when unevenly pitted.

Define G to be the statistical expected-value function. If f is the distribution function of the Δ_j define

$$M = G(\Delta_j) = \int_{-\infty}^{\infty} \Delta_j f(\Delta_j) d\Delta_j$$

In view of the constancy of the $\frac{\partial H_j}{\partial I_3}$ and $\frac{\partial H_j}{\partial x}$ for fixed I_3 and x , and the assumed independence of the Δ_j ,

$$\begin{aligned} G \left(\sum_{j=1}^N \Delta_j \frac{\partial H_j}{\partial I_3} \right) &= \int_{-\infty}^{\infty} \cdots \int_{-\infty}^{\infty} \sum_{j=1}^N \Delta_j \frac{\partial H_j}{\partial I_3} \prod_{k=1}^N f(\Delta_k) d\Delta_k \\ &= \sum_{j=1}^N \frac{\partial H_j}{\partial I_3} \int_{-\infty}^{\infty} \cdots \int_{-\infty}^{\infty} \Delta_j \prod_{k=1}^N f(\Delta_k) d\Delta_k \\ &= \sum_{j=1}^N \frac{\partial H_j}{\partial I_3} \int_{-\infty}^{\infty} \Delta_j f(\Delta_j) d\Delta_j \\ &= \sum_{j=1}^N \frac{\partial H_j}{\partial I_3} G(\Delta_j) = M \sum_{j=1}^N \frac{\partial H_j}{\partial I_3} = 0 \end{aligned}$$

Similarly,

$$G \left(\sum_{j=1}^N \Delta_j \frac{\partial H_j}{\partial x} \right) = 0$$

and

$$G \left(\sum_{j=1}^N \Delta_j \psi_j \frac{\partial H_j}{\partial I_3} \right) = 0$$

On replacing the expressions, [41] by their expected values (i.e., by zero) in [39], that equation is reduced to [40] in the general case.

Since the absolute value of a sum never exceeds the corresponding sum of absolute values equations [20], [38], and [40] imply

$$\left| \frac{\partial I_1}{\partial x} \right| \leq \frac{\left| \frac{\partial \Gamma}{\partial x} \right| + \left| \sum_{j=1}^N \psi_j H_j \right|}{\left| \frac{\partial \Gamma}{\partial I_3} + W \right|} \tag{42}$$

The inequality [42] provides a measure of the ability of a chemical agent to inhibit corrosion by polarizing local cathodes, but yields no direct information regarding anodic inhibition. To see why this is so consider the case of a strictly cathodic additive, i.e., a chemical agent that may alter the polarization of local cathodes, but which has no effect on local anodes. If such an agent is present in solution at concentration, x , then the R_{2j} and E_{2j} are the functions of x and I_{2j} defined by [4]. However, R_{1j} and E_{1j} are independent of x by hypothesis, although they are functions of the current densities at the local anodes. That is,

$$E_{1j} = R_{1j}(I_{1j})$$

$$R_{1j} = R_{1j}(I_{1j})$$

$$W_1 = \frac{\left(\frac{\partial \Gamma}{\partial x}\right)_1 \left(\frac{\partial \Gamma}{\partial I_3}\right)_2 - \left(\frac{\partial \Gamma}{\partial x}\right)_2 \left(\frac{\partial \Gamma}{\partial I_3}\right)_1 + \left(\frac{\partial \Gamma}{\partial x}\right)_1 (W_2 - W_1)}{\left(\frac{\partial \Gamma}{\partial x}\right)_2 - \left(\frac{\partial \Gamma}{\partial x}\right)_1} \quad [45]$$

Hence [13] implies that $\psi_j = 0$ for every j . Therefore, in the case of a strictly cathodic inhibitor, [42] simplifies to

$$\left| \frac{\partial I_1}{\partial x} \right| \leq \frac{\left| \frac{\partial \Gamma}{\partial x} \right|}{\left| \frac{\partial \Gamma}{\partial I_3} + W \right|} \quad [43]$$

Note that the left-hand member of equation [43] is a measure of the effectiveness of the inhibitor under investigation. If $\partial I_1/\partial x$ can be determined at several concentrations of the inhibitor ranging from zero to x_0 , the maximum concentration of interest, and at zero external current, the area under the graph of $\partial I_1/\partial x$ vs. x from 0 to x_0 is

$$\int_0^{x_0} \frac{\partial I_1}{\partial x} dx = I_1(x_0) - I_1(0) \quad [44]$$

This is just the decrease in corrosion current brought about by increasing the inhibitor concentration from 0 to x_0 , which is proportional by Faraday's law to the change in corrosion rate effected by the inhibitor. Thus, if $\partial I_1/\partial x$ is negative and large in absolute magnitude on the interval $0 - x_0$, the inhibitor is a good one. Otherwise it is not.

Observe next that the three quantities in the right-hand member of inequality [43] may be measured experimentally. If the inhibitor concentration is fixed and observations of Γ are made at several values of I_3 , the slope of the graph of Γ vs. I_3 at any value of I_3 is $\partial \Gamma/\partial I_3$ at that value. Of course, the value of I_3 of greatest interest is zero since it is usually desired to determine the effectiveness of

inhibitors in the absence of any external current.

Similarly $\frac{\partial \Gamma}{\partial x}$ may be measured at $I_3 = 0$. In some instances W may be computed from [3] by taking z to be the distance from the reference half-cell to the metal surface. If this estimate of z is not good enough, W may be determined by one of the methods suggested by Pearson (4). Or measurements of $\partial \Gamma/\partial x$ and $\partial \Gamma/\partial I_3$ with two half-cells at different distances from the metal surface may be substituted in equation [40] with the ψ_j all zero since $\partial I_1/\partial x$, and $\sum_{j=1}^N \Delta_j H_j$ are independent of the location of the reference half-cell. Specifically, if W_1 and W_2 are the values of W for two different positions of the reference half-cell, $(W_2 - W_1)$ can be measured easily. Then

Since all of the terms in the right-hand member of this equation can be measured, W_1 may be computed.

CONCLUSIONS

The right-hand member of [43] determines an upper bound for $|\partial I_1/\partial x|$ whose value can be found experimentally. If the upper bound is small over the entire concentration range of interest, then $|\partial I_1/\partial x|$ is small over the same range and [44] implies that the inhibitor is not very effective. On the other hand, if the upper bound is large, no conclusion can be drawn. The inhibitor may be a good one or it may not. Some other technique must be used to decide ultimately whether agents for which $\left| \frac{\partial \Gamma}{\partial x} \right| / \left| \frac{\partial \Gamma}{\partial I_3} + W \right|$ is large are good inhibitors. What the method described here does provide is a rapid screening method that eliminates from further consideration materials that certainly are not good cathodic inhibitors.

In the general case when the chemical agent is not a strictly cathodic inhibitor equation [42] implies that [43] may be in error by as much as Q , where

$$Q = \frac{\left| \sum_{j=1}^N \Delta_j \psi_j H_j \right|}{\left| \frac{\partial \Gamma}{\partial I_3} + W \right|}$$

Unfortunately, Q cannot be measured directly. Note, however, that its value, for all practical purposes, depends only on the effectiveness of the chemical

agent in polarizing (or depolarizing) the local anodes. Hence equation [43] remains valid provided $\partial I_1/\partial x$ is interpreted as the component of the derivative of the corrosion current with respect to concentration that results from the polarization or depolarization of the local cathodes by the agent. That is, equation [43] provides a method for screening chemical agents as cathodic inhibitors regardless of whether the agents also function as anode polarizers or depolarizers. The inequality, however, provides no information regarding anode polarization. In principle, it is possible to calculate Q as well as $\partial I_1/\partial x$ and $\sum_{j=1}^N \Delta_j H_j$ from four measurements of $\partial \Gamma/\partial x$ and $\partial \Gamma/\partial I_3$ by the same procedure that was used to derive equation [45]. It is very unlikely, however, that the method would be feasible experimentally. Although the author intends soon to undertake an experimental verification of [43] no measurements have yet been made. Experiments should shed light on the question of whether the electrochemical theory of corrosion can be applied quantitatively to inhibitor studies.

It is interesting to note that, if the agent added to the system under investigation is a cathode polarizer, equation [43] may be written,

$$0 < -\frac{\partial I_1}{\partial x} \leq \frac{\partial \Gamma/\partial x}{\frac{\partial \Gamma}{\partial I_3} + W} \quad [46]$$

Equation [26] implies

$$\frac{\partial \Gamma}{\partial I_3} \sum_{j=1}^N \frac{1}{\lambda_j} = -\sum_{j=1}^N \Delta_j H_j - I_3 \sum_{j=1}^N \Delta_j \frac{\partial H_j}{\partial I_3} - W \sum_{j=1}^N \frac{1}{\lambda_j}$$

Or since the statistical expectation of the second term on the right is zero

$$\frac{\partial \Gamma}{\partial I_3} = \frac{-\sum_{j=1}^N \Delta_j H_j}{\sum_{j=1}^N \frac{1}{\lambda_j}} - W$$

In the first term on the right of this last equation Δ_j , H_j , and λ_j are positive for every j . Therefore, the first term is negative. Since W is positive the second term is also negative, which implies that is negative. Therefore

$$\left| \frac{\partial \Gamma}{\partial I_3} \right| = -\frac{\partial \Gamma}{\partial I_3}$$

It can be shown similarly that

$$\left| \frac{\partial \Gamma}{\partial I_3} + W \right| = -\frac{\partial \Gamma}{\partial I_3} - W$$

and that for cathode polarizers

$$\left| \frac{\partial \Gamma}{\partial x} \right| = -\frac{\partial \Gamma}{\partial x}$$

Substitution of these values in [43] yields [46].

Any discussion of this paper will appear in a Discussion Section to be published in the December 1955 JOURNAL.

REFERENCES

1. R. B. MEARS, *J. (and Trans.) Electrochem. Soc.*, **95**, 1 (1949).
2. W. J. MÜLLER, *Trans. Electrochem. Soc.*, **76**, 167 (1939).
3. V. CUPR, *Z. Elektrochem.*, **45**, 297 (1939).
4. J. M. PEARSON, *Trans. Electrochem. Soc.*, **81**, 485 (1942).

The Crystallization of Anodic Tantalum Oxide Films in the Presence of a Strong Electric Field¹

D. A. VERMILYEA

Research Laboratory, General Electric Company, Schenectady, New York

ABSTRACT

Crystallization of amorphous anodic oxide films on tantalum may be accomplished by holding at temperatures in the neighborhood of room temperature provided a strong electric field is present in the film. This results in crystalline areas consisting of pie-shaped polycrystalline segments surrounded by coiled-up cylinders of the replaced amorphous phase. Factors affecting the nucleation and growth of these areas are discussed, and a mechanism of growth is proposed. The nucleation of the areas is not understood at present.

INTRODUCTION

There are at least two processes by which an amorphous anodic tantalum oxide film may be crystallized. It may be done simply by heating at 800°C (1). Recent experiments by Hillig (2) have shown that crystallization proceeds rapidly at temperatures as low as 650°C. This *thermal crystallization* apparently proceeds by the nucleation of a crystal and its growth into the amorphous phase.

The second process by which such films may be crystallized consists of holding them at temperatures from 0° to 100°C while a strong electric field is applied across the film. This paper presents the results of a study of crystallization by the second process, which will be referred to as *field crystallization*.

EXPERIMENTAL

The constant voltage power supply and constant temperature bath used in these experiments have been described previously (1). Measurements of amorphous and crystalline film thickness were made by comparison with the optical step gauge described in the previous paper (1). The growth of crystals was observed with a microscope using polarized light, and some electron micrographs were made using nitrocellulose replicas shadowed at 10° with chromium. Time-lapse motion picture studies were also made of some of the growing crystals.

THE PROCESS

Before discussing in detail the factors affecting the nucleation and growth of crystals in field crystallization, an example will be given to describe the over-all process. Consider an amorphous film being formed at 110 v in 2% HNO₃ at 99°C. Up to about 400 sec there is no crystallization, but the amorphous film grows in thickness and the current flowing

through the cell decreases as shown in Fig. 1. At about 350 sec the current starts to decrease less rapidly and, at the same time, examination with a microscope reveals a few very small crystals in the amorphous film. As time goes on these crystals grow, more crystals appear, and the current stops decreasing and begins to increase. Eventually the growing crystals impinge, the current reaches a maximum and then decreases again, and finally the entire oxide film has become crystalline. An electron diffraction pattern taken from a completely crystallized film by Alessandrini² showed that the crystals formed were Ta₂O₅.

NATURE OF THE CRYSTALS AND MECHANISM OF THEIR GROWTH

Fig. 2 and 3 show crystals formed on specimens held 2350 and 5500 sec under the conditions for which Fig. 1 was obtained. The individual crystals are irregular polygons with as few as 5 and as many as 11 sides, the average number being between 6 and 8. These polygons will be referred to as "crystalline areas" since they are not single crystals but consist of many smaller crystals as discussed below. On the top surfaces of the crystalline areas are a number of fine lines parallel to the sides and irregularly spaced. There is a broad out-of-focus region which looks like a cylinder outside of each side of the areas. These cylinders are above the plane of focus and frequently become detached as may be seen at a few places in Fig. 2. If the specimen is rubbed between the fingers this material in the cylinders is removed leaving only the crystalline areas as shown in Fig. 4. At the same time the appearance of the specimen to the naked eye changes from gray and dull to colored and shiny. It is believed that the presence of the material outside the crystals and raised above the surface

² Miss E. I. Alessandrini is associated with the General Electric Company, Schenectady, New York.

¹ Manuscript received September 17, 1954.

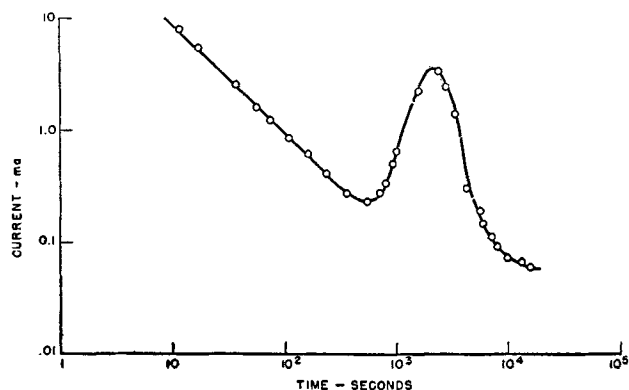


FIG. 1. Behavior of cell current during crystallization

simply diffuses light reflected from the surface causing a dull gray appearance.

The rolled-up material outside the crystalline areas is apparently the amorphous film which is pushed back and rolled up as the area grows. In other words, crystallization does not occur by consumption of the amorphous phase but by the replacement of it. The behavior of the cell current during crystallization provides support for the belief that an entirely new crystalline film is formed. For the run shown in Fig. 1 the total number of coulombs passed between 350 sec (when crystallization started) and 450 sec (when the entire film was crystalline) was 6.4. If Ta_2O_5 of normal density was the product, this electrical energy would produce 4900 Å of oxide film on the 6.6 cm² specimen. The thickness of the crystalline film was estimated by comparison with the optical step gauge to be about 4200 Å. This estimate of thickness assumes that the refractive indexes of the amorphous and crystalline films are the same. While this may not be exactly true, a

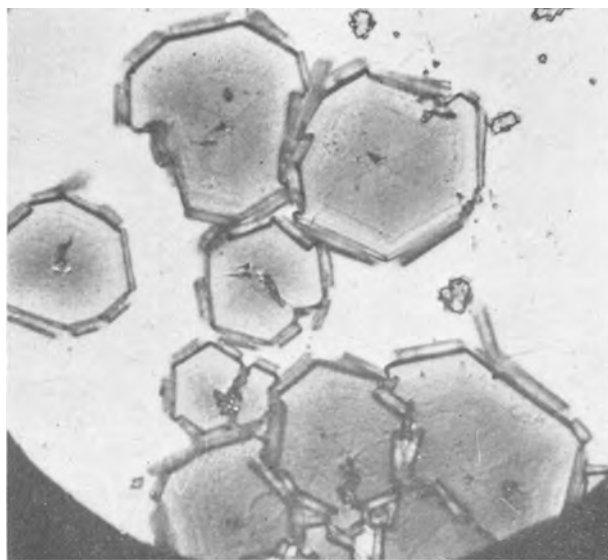


FIG. 2. Crystalline areas formed in 2350 sec. 500× before reduction for publication. Unetched.

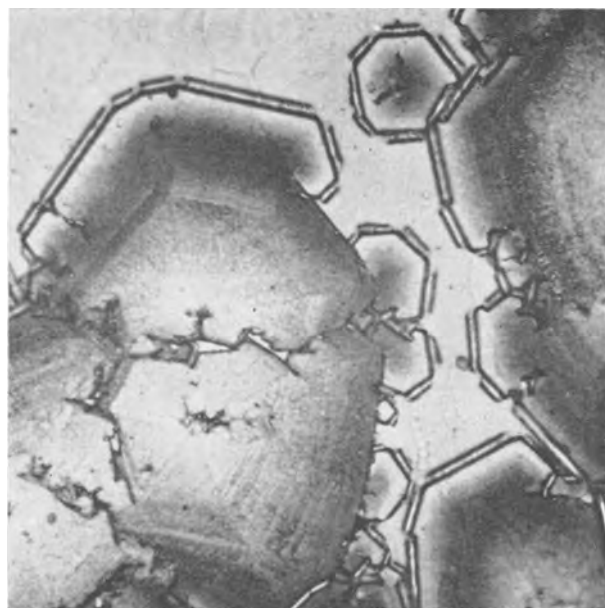


FIG. 3. Crystalline areas formed in 5500 sec. 500× before reduction for publication. Unetched.

comparison of the refractive index determined for the amorphous films with that for crystals of Ta_2O_5 shows that the two are probably within 10% of each other [see reference (1)]. At any rate, it appears that more than enough coulombs have passed through the cell to completely replace the amorphous film with a crystalline one of the observed thickness.

When the crystalline areas are examined using polarized light, it is found that they are not single crystals but that each one consists of several pie-shaped segments. Fig. 5, of the same area illustrated in Fig. 3, shows that there is one segment for each

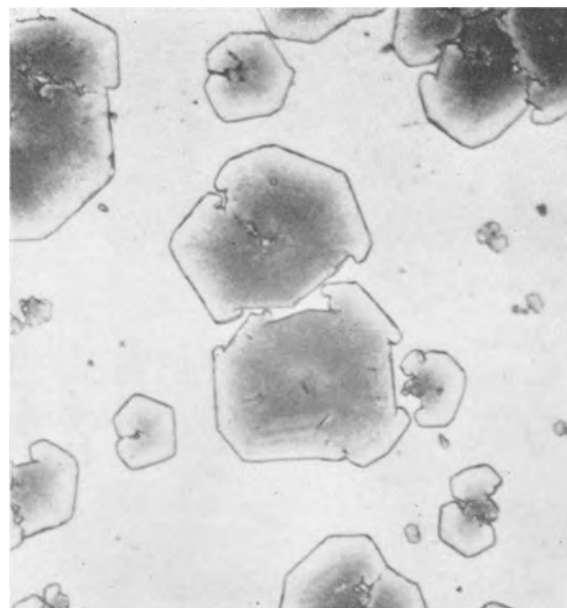


FIG. 4. Specimen after light rubbing to remove amorphous oxide. 500× before reduction for publication. Unetched.

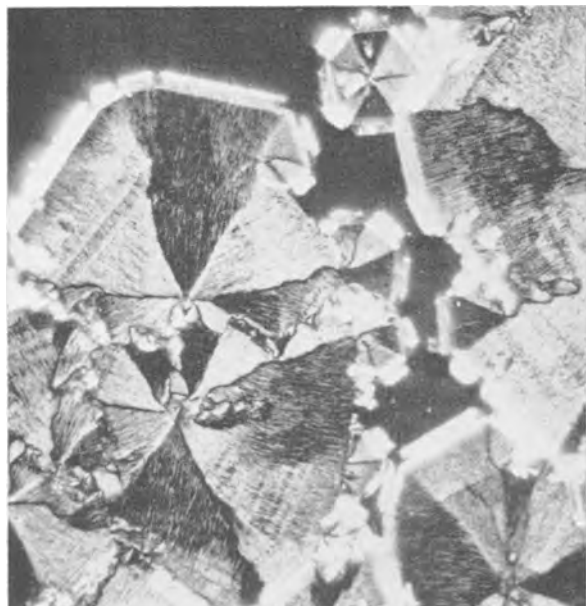


FIG. 5. Same area as Fig. 3, polarized light. 500 \times before reduction for publication.

side of the crystal. Each of the segments is itself apparently not a single crystal, but is composed of smaller crystallites which appear to be elongated in the radial direction. The boundaries of the pie-shaped segments are generally jagged and uneven and not straight. Also, as impingement has occurred, or as interfaces have become stopped in their growth for other reasons, new small crystals have started at the stopped face and grown outward in all directions.

The electron microscope has been of great help in revealing the nature of the fine details of the crystalline films. The first observed indication of crystallization is a cracking of the amorphous oxide as shown in Fig. 6. From these cracked regions there next develops a crystalline area consisting of one or two segments as shown in Fig. 7. The impression of "flow lines" in the segments is obtained from subsequent figures. Cracks appear in the amorphous film at the intersections of the faces of the crystals. Fig. 8 shows larger crystalline areas which are beginning to assume a nearly equi-axial shape. The crystals usually start on one side of some region in the amorphous oxide and grow around it, although areas have been observed which were approximately equi-axial initially.

Only one of the crystalline areas shown in Fig. 6-8 exhibits any of the fine lines parallel to the crystal sides which were visible in Fig. 2 and 3. Fig. 9, taken of areas on a specimen which had an almost completely crystalline film, shows many such lines and also shows the manner in which the crystals have grown together. The fine lines apparently are produced more frequently after the crystals have become larger. The boundary between the segments of

the area becomes very jagged, with changes of direction occurring at positions where the fine lines meet the boundary. In Fig. 6-8, on the other hand, the boundaries are much less jagged and either straight or gently curved.

Observations on the nature of the crystalline areas suggest that growth occurs in the following manner. A nucleus forms beneath the amorphous film and starts to grow, producing a crack in the amorphous film. As the nucleus thickens, it pushes the amorphous film up off the metal, extending the original cracks, and producing more cracks. As the amorphous film is pushed off the metal the crystalline area grows radially, following the receding amorphous film. It is apparently often easier to strip back the amorphous film on one side of the nucleus than on the other, so that one or two wedge-shaped segments grow out first on one side of the nucleus and later others grow from these and, finally, completely surround the nucleus with crystalline material.

The number of segments in a crystalline area produced by such a process would be controlled by the number of cracks formed in the amorphous film, which might in turn depend on the surface condition of the metal, the presence of inclusions in the metal, and other factors which govern adherence of the



FIG. 6. Start of crystallization. 15,000 \times



FIG. 7. Crystalline area with 2 segments. 15,000 \times

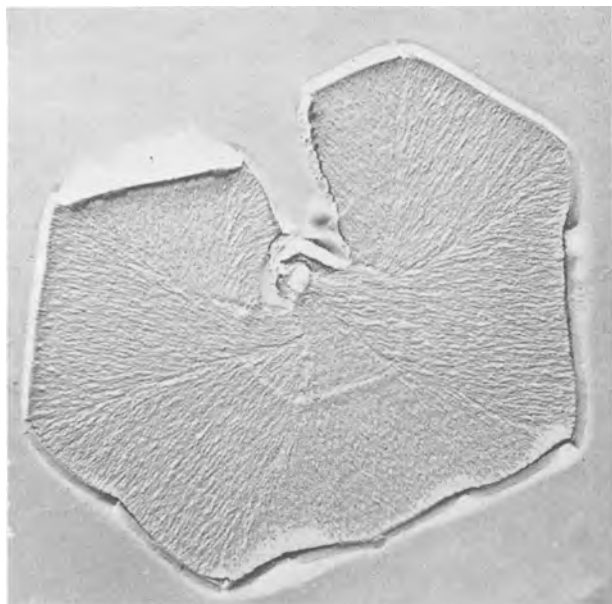


FIG. 8. Crystalline area nearly equi-axial. 5000 \times

oxide to the metal. It would be expected, therefore, that the number of segments would not be the same in all crystalline areas, in agreement with the experimental findings.

Each segment appears to consist of very small crystals elongated in the radial direction. Apparently when the amorphous film is pushed back many small crystals nucleate and grow, following the receding amorphous film. If there is a preferred growth direction, then those small crystals which are favorably oriented will grow most rapidly and crowd out the others. Each segment should thus consist not of a single crystal but of a number of small crystals with nearly the same orientation elongated in the radial direction, as observed. Such a preferred growth direction would result in the same orientation for most of the small crystals in each parallel segment of any crystalline area in the specimen. Fig. 5 shows that all parallel segments have the same appearance under polarized light, indicating that they have the same orientation. The growth of these small crystals with a long axis perpendicular to the advancing interface explains the appearance of flow lines in Fig. 6 through 8.

The forces acting on the amorphous film at the advancing crystal interface are those exerted by the crystal tending to push the film upward and the adhesion of the film to the metal. These forces tend to bend the amorphous film at its point of departure from the metal. Since the ions are mobile in the film due to the high electric field, presumably they move under the influence of the mechanical stresses in such a way that the stresses are relieved. In other words, the amorphous film becomes permanently curved. As the crystal grows, producing more curved

amorphous film, a cylinder of rolled up amorphous film is formed at the advancing interface, as shown in Fig. 2 and 3.

Crystalline areas growing by the mechanism suggested should show erratic growth rates, varying from place to place on the specimen as the ease of stripping the amorphous film varied. Time-lapse motion pictures have shown that the individual faces of the crystalline areas grow rapidly at some times and apparently stop at others. The fine lines visible in Fig. 2 and 3 are probably places where the crystal grew very slowly, or stopped altogether. The jagged boundaries between segments result when one segment stops or slows down while the other, growing more rapidly, attempts to grow around the stopped segment.

The rate of radial growth varies from place to place on the specimen, as might be expected on the basis of the proposed mechanism. Fig. 10 shows curves of diameter vs. time for crystalline areas growing simultaneously on one specimen. Not only are the growth rates different for the two areas, but they are not constant. This behavior is typical of radial growth and, while the growth rate usually decreases with time, in a few instances it has increased with time.

If the electric field is removed, growth ceases since no thickening of the crystals occurs and hence no further stripping of the amorphous film. If the field is reduced, the radial growth rate is decreased because the rate of thickening decreases, while increasing the field increases the radial growth rate. For a given formation voltage radial growth is also more rapid at high temperatures, as might be ex-



FIG. 9. Intersections of crystalline areas on a specimen almost completely crystallized. 5000 \times .

pected because the rate of thickening is greater at higher temperatures.

The rate of growth depends on the nature of the solution in which the film is formed as seen by Fig. 11. Fig. 12 shows that the number of crystals formed at a given time is about the same in both solutions. Average growth rates, however, were 1.13×10^{-6} cm/sec for H_2SO_4 and 2×10^{-6} cm/sec for KCl, so that the crystallization was completed sooner in KCl. Growth rates as low as 3.3×10^{-8} cm/sec have been measured for solutions of $Na_2B_4O_7$ at $99^\circ C$.

The difference in radial growth rates of crystalline areas formed in different solutions is believed to be the result of a difference in the rate of growth of the crystals in thickness. The thickness of the crystalline

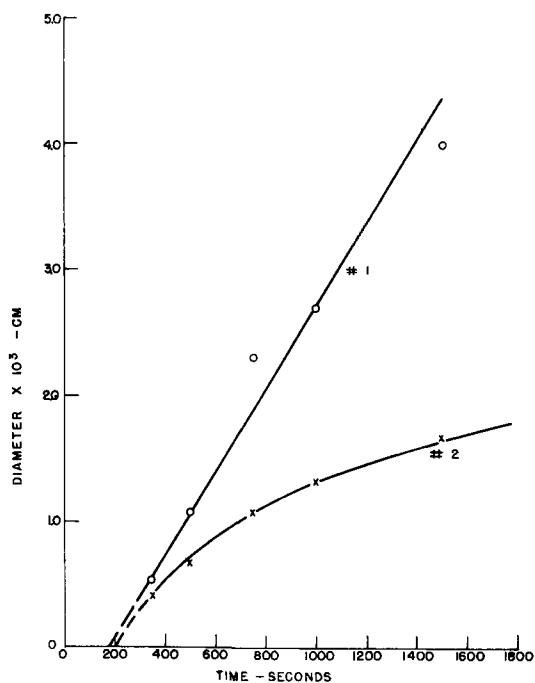


FIG. 10. Growth of crystalline areas being formed simultaneously on the same specimen.

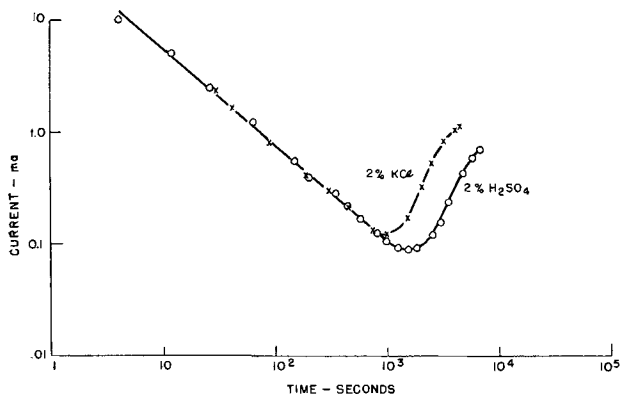


FIG. 11. Cell current in two electrolytic solutions each at $99^\circ C$ with formation voltage of 100 v.

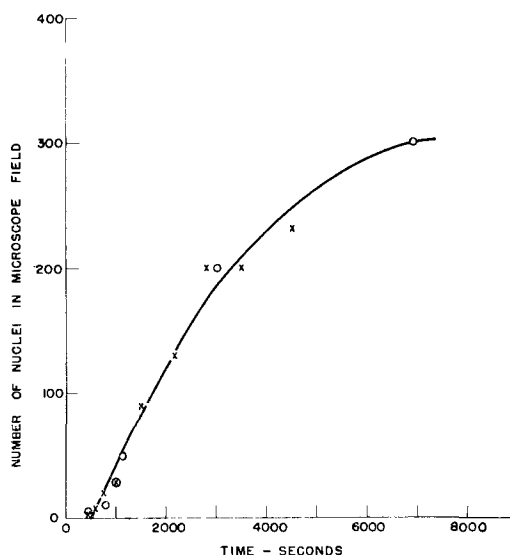


FIG. 12. Nucleation frequency in two solutions; $\circ = 2\% H_2SO_4$; $\times = 2\% KCl$.

areas formed in 66,000 sec at $99^\circ C$, 100 v, was 4650 \AA in 2% KCl, 4500 \AA in 2% H_2SO_4 , and 3900 \AA in 2% $Na_2B_4O_7$. If radial growth occurs only as the crystals thicken and push back the amorphous film, these differences in thickness growth rate can explain qualitatively the difference in radial growth rate. Quantitative comparisons would require a greater knowledge of the stripping process and of the change in growth rate of the crystals with time.

The reason why the rate of thickness growth of the crystals depends on the solution in which they are formed is not known. The effect of solution composition is apparently associated with the oxide-electrolyte interface, however, because the rate of crystal growth changes immediately upon changing the electrolyte. For example, Fig. 13 shows a current-time curve for a specimen which was formed in 2% HNO_3 to 300 sec and in 2% $Na_2B_4O_7$ thereafter. When the electrolyte was changed, the growth of the crystals was drastically reduced and, since most of the current passing through the cell is used to form new crystalline material, the current fell to about 20% of its value in 2% HNO_3 .

One further experiment supports the hypothesis that radial growth occurs only as the amorphous film is pushed back. If an amorphous film is formed in a solution containing a small amount of HF, the resulting film may be very easily stripped from the metal. When such a film is formed at 100 v in 2% HNO_3 at $99^\circ C$, no crystals of the type described in this paper are formed. Instead, at about 400 sec (the time at which crystals form in normal Ta_2O_5 films not easily stripped) there appear regions in the film where the amorphous film has been stripped away over a considerable area and is no longer in contact

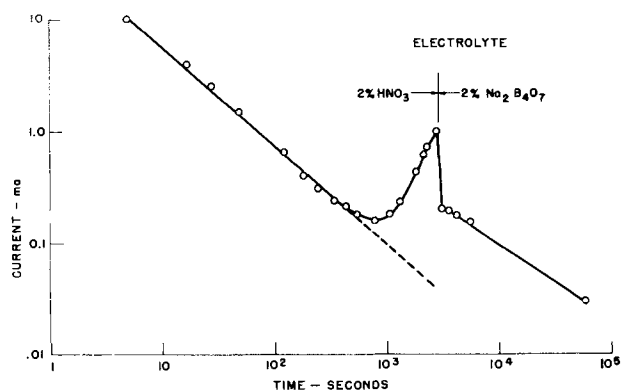


FIG. 13. Effect of changing solution composition on the progress of crystallization.

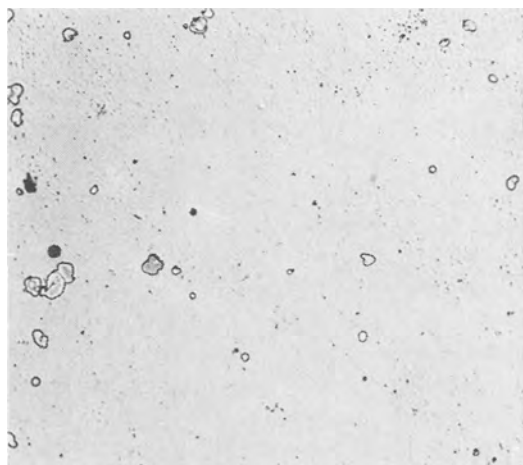


FIG. 14. Areas where amorphous film was stripped from the metal on a specimen with an easily stripped film. 100X. Unetched.

with the metal. Fig. 14 shows some of these areas. These regions are not crystalline, although very small crystals may be seen inside the areas. Presumably a crystal nucleates as usual but, instead of cracking, the amorphous film simply lifts the film off the specimen for a considerable distance. No further growth of the crystal, now buried beneath the stripped area, can occur.

Field crystallization thus produces crystalline areas composed of multicrystalline pie-shaped segments. These areas grow laterally by pushing the amorphous film aside, producing a coiled cylinder of amorphous film outside of each advancing side of the area. The remainder of this paper is concerned with the results of a study of the factors which affect the nucleation of these areas.

NUCLEATION OF CRYSTALLINE AREAS

The amount of time which elapses between the application of the voltage and the appearance of the first crystals has been found to be influenced by the temperature, the applied voltage, and the condition of the metal surface.

The effect of the metal surface.—The effect of surface condition of the tantalum sheet was investigated using as-rolled sheet, electropolished sheet, chemically polished sheet, and chemically polished sheet etched 30 sec in HF. These different surface treatments caused the nucleation time to vary between 150 and 600 sec, the shortest time being observed for as-rolled sheet and the longest for electropolished sheet. In addition, variations in the lot of tantalum used with one surface treatment caused the nucleation time to vary from 150 to 400 sec.

These observations indicate that inclusions or impurities present in the metal may play an important role in the nucleation process, and further support for this idea is found in the fact that, when time-lapse motion pictures are run in reverse, spots, presumably inclusions, are observed at places where the crystals disappeared. Since the surface treatment also influences nucleation, it is very important when evaluating the influence of other factors on crystallization to make certain that the material used is from the same lot and is prepared in the same manner. In the remainder of this work specimens from the same lot of material were chemically polished and then etched 30 sec in HF, since this treatment gave the most reproducible results.

Effect of formation voltage.—The influence of formation voltage on the nucleation rate was determined by holding specimens at 99°C in 2% HNO₃ at various voltages and examining them periodically to determine whether any crystals had formed. Data obtained are given in Table I and plotted in Fig. 15 and 16. It may be seen that the time to start crystals is greater at lower voltages and that the field at the start of nucleation is less the lower the forming voltage. A lower forming voltage necessarily means a smaller film thickness.

Effect of temperature.—The effect of temperature on the time of nucleation was determined by holding specimens at 100 v in 2% HNO₃ at various temperatures. Results are given in Table II. As the temperature decreases, nucleation time increases, the field in the amorphous film at nucleation increases, and

TABLE I. Field crystallization in 2% HNO₃ at 99°C

Formation voltage	Nucleation time, sec	Thickness of amorphous film, Å	Electric field, v/Å
41	4800	909	0.0452
61	2270	1305	0.0467
81	800	1640	0.0495
100	400	1960	0.0512
131	100	2435	0.0538
141	48	2574	0.0548
161	20	2830	0.0569

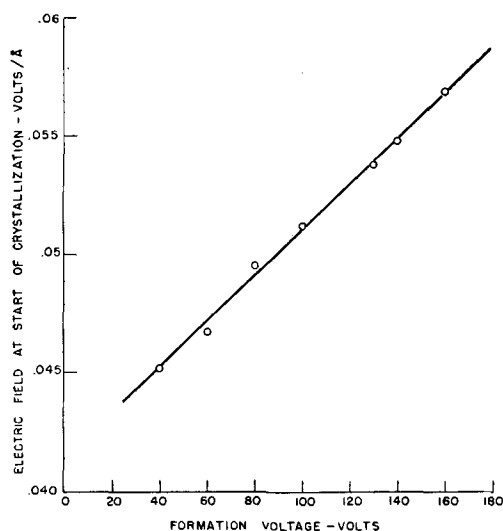


FIG. 15. Effect of formation voltage on the electric field at the start of crystallization.

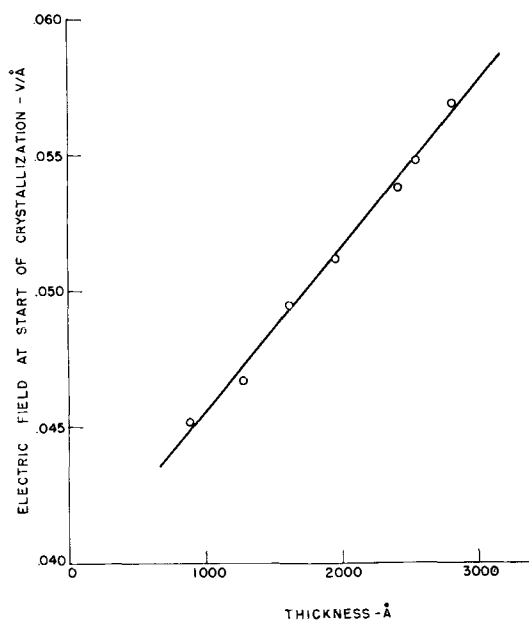


FIG. 16. Effect of thickness on the electric field at the start of crystallization.

the rate of amorphous film growth at nucleation decreases.

Effects of history, rate of amorphous film growth, and electrical breakdown.—Experiments in which the history of a film was varied indicate that at a particular voltage and temperature there is a critical thickness below which nucleation does not occur. For example, at 100 v, 99°C, nucleation was observed on holding for 400 sec, at which time the film thickness was 1960 Å. When a film was formed rapidly at a low temperature to a thickness greater than 1960 Å and subsequently etched in HF to below that thickness, nucleation occurred at 1960 Å when the film was subsequently held at 100 v, 99°C. In another

TABLE II. Effect of temperature on nucleation, 100 v

Temp, °C	Nucleation time, sec	Electric field in amorphous film, v/Å	Thickness, Å	Rate of growth of amorphous film, Å/sec
19	500×10^2	0.0554	1805	0.94×10^{-3}
29	250	0.0547	1830	1.95
40	150	0.0537	1866	3.5
49.5	70	0.0533	1875	7.78
60	40	0.0527	1900	14.5
73	20	0.0518	1930	30.9
86	10	0.0513	1950	66.0
99	4	0.0509	1965	166.0

experiment a film was formed for 300 sec at 100 v, 99°C, and the film was then corroded in HF to the starting thickness. The process was repeated four times, making a total of 1200 sec; no nuclei were observed. When the specimen was then held 100 sec longer at 100 v, nuclei appeared, and the film thickness was 1960 Å. Nucleation of crystals occurs at the same thickness regardless of the number of interruptions for the purpose of observing the film and of the temperature and rate of formation to the starting conditions.

If an amorphous film is formed at a low temperature to a thickness greater than the critical thickness but so great that on subsequent application of the test voltage the growth rate of the amorphous film is very low, crystal formation is greatly retarded. For example, at 100 v and 99°C nuclei are normally observed at 1960 Å, and growth of the amorphous film is extremely slow at thicknesses greater than 2300 Å. A film formed to 2525 Å at room temperature and then held at 100 v and 99°C showed no crystals after 3350 sec. It was calculated from other data that the rate of amorphous film growth would be 2.3×10^{-4} Å/sec. When the specimen was etched in HF to 2105 Å, however, where the rate of growth should have been about 0.02 Å/sec, nuclei were observed after holding at 100 v for an additional 750 sec. These experiments suggest that some ion movement in the amorphous film may be necessary for nucleus formation.

Crystals of Ta_2O_5 powder in contact with the outer surface of the oxide film do not hasten crystal formation. This fact supports the idea that nuclei are formed at the oxide-metal interface. Only one phenomenon is known which is a direct cause of crystal formation. When a film which has been formed under conditions which produce electrical breakdown is subsequently held under conditions where crystallization is possible, the regions where breakdown has occurred are found to be nucleation sites. The question arises whether all crystals start from electrical breakdowns in the film. If such were the case, it would be expected that nucleation would

occur at the greatest applied field strength, that is, as soon as voltage was applied. Also, it would be expected that, if the film thickness were reduced by a factor of two, the field necessary to cause breakdown would be increased tremendously, but in fact the field necessary for nucleation is smaller as shown in Fig. 16. These facts seem to make electrical breakdown unattractive as an explanation of the origin of crystal nuclei.

At the present time no satisfactory interpretation of the effects of voltage and temperature on nucleation has been discovered. Fig. 15 and 16, along with the evidence that at any temperature there is a voltage dependent critical thickness below which nucleation will not occur, suggest an influence of the electric field on the nucleation of crystals under those conditions. On the other hand, since the rate of growth of the amorphous film at any temperature is determined by the field, it may be that a critical growth rate is required for nucleation, and that the critical rate depends on the film thickness.

In either case it is surprising that at one temperature there should be such a marked variation of nucleation time with the thickness of the amorphous film. Further work will be directed toward an understanding of the mechanism of nucleation under these conditions.

DISCUSSION

It is interesting to inquire why the initial low temperature film which forms on tantalum, and on other metals such as aluminum, is amorphous rather than crystalline. When one of the films which has been partly or completely crystallized by field crystallization is anodized further the new film formed on top of the crystalline film is also crystalline. The maximum growth rate for which this observation has been made was only about 100 Å/sec, however, which is low compared to the rate of forming the first few layers of oxide when a clean specimen is exposed to air. It may be that at extremely rapid rates the molecules which are forming the new oxide do not have time to arrange themselves in the lattice structure of the crystalline phase.

It is also interesting that the field required to cause appreciable ionic movement at a given temperature is only about half as great for the crystalline as for the amorphous film. This fact and the fact that the thickness growth rate is a function of the solution composition indicate that interesting results might

be obtained from a study of the kinetics of growth of the crystalline film.

CONCLUSIONS

1. Amorphous tantalum oxide films crystallize at temperatures between 0° and 100°C provided a strong electric field is present in the film. The result of such crystallization is crystalline areas consisting of pie-shaped polycrystalline segments surrounded by coiled-up cylinders of the replaced amorphous film. In each segment the individual crystallites have a preferred growth direction perpendicular to the edge of the segment.

2. The crystalline areas grow by pushing back the amorphous film, and this only occurs when the crystals thicken. Any reduction in the rate of thickness growth of the crystals, such as is produced by lower temperature or lower field, decreases the radial growth rate as well. The rate of growth of the crystals is also slightly different in different solutions.

3. Nucleation of the crystals occurs only below a critical electric field strength in the amorphous film. This critical field depends on the temperature of formation, the surface condition and impurity content of the metal, and the thickness of the amorphous film, but does not depend on the history of the film. At fields far below the critical field nucleation is greatly retarded. Nucleation apparently occurs at the oxide-metal interface.

4. Once a crystalline film has been formed subsequent growth in thickness is always crystalline.

5. The thickness of a crystalline film formed at a given voltage and temperature is about twice as great as that of an amorphous film formed under the same conditions.

ACKNOWLEDGMENTS

The author is indebted to R. Smith for the electron micrographs and to R. L. Fullman for the time-lapse motion pictures. He acknowledges with thanks the helpful criticisms of the manuscript by D. Turnbull, and the many valuable discussions with R. L. Fullman and W. B. Hillig.

Any discussion of this paper will appear in a Discussion Section to be published in the December 1955 JOURNAL.

REFERENCES

1. D. A. VERMILYEA, *Acta Met.*, **1**, 282 (1953).
2. W. B. HILLIG, Private communication.
3. D. A. VERMILYEA, *Acta Met.*, In press.

Results of Some Marine-Atmosphere Corrosion Tests on Magnesium-Lithium Alloys¹

P. D. FROST, F. W. FINK, H. A. PRAY, AND J. H. JACKSON

Battelle Memorial Institute, Columbus, Ohio

ABSTRACT

Magnesium-lithium binary alloys which contain just enough lithium (about 11 wt %) to produce a single-phase, body-centered cubic structure have shown surprisingly good resistance to corrosion in 3% salt solution. High-strength alloys having about 9% lithium and various quantities of aluminum, zinc, and other elements have a mixed hexagonal-plus-body-centered cubic structure. Such alloys generally have poorer corrosion resistance than the single-phase binaries. Three of the high-strength alloys were exposed for 32 months to the sea-coast atmosphere near Daytona Beach, Florida. For comparison purposes, samples of commercial AZ31A-H24 alloy were exposed at the same time. All alloys were in the form of 4 × 6 × 0.064 in. panels. The AZ31A sheet had corrosion resistance only slightly superior to that of an alloy containing Mg-8.7% Li-5% Al-8% Zn. The other two alloys, Mg-8.8% Li-7% Al-0.05% Sn-1% Mn and Mg-8.8% Li-7% Al-1% Sn, had much poorer corrosion resistance.

INTRODUCTION

Results of extensive research programs conducted in this country on magnesium-lithium-base alloys have been published in earlier papers (1-4). In addition to the work done in this country, investigations on magnesium-lithium alloys were carried out in England (5, 6) and in Russia (7).

The primary objective of the research in this country during the 1940's was to develop ultralight, high-strength alloys for structural applications. Although many alloys having high strength and good ductility were developed, their properties were not stable at temperatures above about 150°F. This instability, characteristic of all magnesium-lithium-base alloys, has prevented their use for structural purposes.

This paper describes the results of corrosion tests begun in June 1950, on several experimental structural-type alloys.

CORROSION TESTS

Lithium forms a series of solid solutions with magnesium. Alpha alloys, containing from 0 to 5.7% lithium, have a hexagonal close-packed structure; beta alloys, containing 10.3% or more lithium, are body-centered cubic. Between 5.7 and 10.3% lithium, a mixture of the alpha and beta phases exists.

Contrary to expectations, certain magnesium-lithium-base compositions have surprisingly good resistance to corrosion in 3% NaCl solution. Table I and Fig. 1 compare the relative corrosion resistance of several binary magnesium-lithium and ternary

magnesium-lithium-zinc alloys with that of a commercial magnesium-manganese composition in salt solution (1). The magnesium-manganese alloy corresponds to ASTM Alloy M1A, which is one of the more corrosion resistant commercial magnesium alloys. In this experiment the single-phase, beta Mg-11%Li alloy suffered the smallest weight loss and the least pitting attack of all the alloys tested. Thus, a magnesium-lithium alloy can have reasonably good corrosion resistance.

The marine-atmosphere corrosion tests, which comprise the main topic of this paper, were conducted on three high-strength magnesium-lithium-base alloys and the high-strength commercial Alloy AZ31A.² The alloys had the following nominal compositions:

Heat No.	Composition	Specific gravity
2611	Mg-8.8% Li-7% Al-1% Sn	1.56
2613	Mg-8.8% Li-7% Al-0.05% Sn-1% Mn	1.53
2615	Mg-8.7% Li-5% Al-8% Zn	1.65
AZ31A	Mg-3% Al-1% Zn-0.3% Mn	1.77

The three experimental alloys are of the alpha-beta type, containing appreciable quantities of the hexagonal phase. These were melted as 18-lb heats into ingots about 5 x 5 x 8 in. The ingots were homogenized 3½ hr at 720°F, scalped, and press forged.³ The ingots were preheated 4 hr at 500°F and raised to 675°F for 1 hr prior to forging. They were upset and cross worked considerably and finally pressed into slabs approximately 1¼ x 6 x 21 in. These were scalped at Battelle and rolled into the sheet product at a temperature of about 625°-700°F. The panels

² Formerly designated as AZ31X.

³ At Wyman-Gordon Co., Worcester, Mass.

¹ Manuscript received July 31, 1953. This paper was prepared for delivery before the Wrightsville Beach Meeting, September 13 to 16, 1953.

TABLE I. Relative corrosion resistance of several magnesium-lithium-base alloys in 3% NaCl solution at 95°F for 8 days*

Heat No.	Nominal composition, %				Average wt loss, mg/cm ² /day
	Zn	Mn	Li	Mg	
875	4	—	10.6	Bal	2.83
690	4	—	9.0	Bal	2.81
874	—	—	11.0	Bal	0.57
873	—	—	9.3	Bal	0.77
872	—	—	4.0	Bal	4.44
871	—	—	2.0	Bal	4.92
251	—	1.26	—	Bal	0.62

* Alternate immersion test, 1/2-min immersion, 2-min emersion. Solutions were changed after 4 days. Specimens were tested as extruded and were approximately 6 x 1 x 1/4 in. in size.

were exposed to the sea-coast atmosphere in the hot-rolled condition. In this condition, these alloys have a yield strength of about 28,000 psi. The commercial-alloy panels were all taken from the same sheet. They were exposed, as received, in the hard-rolled (H24) condition. The yield strength of this material, as hard rolled, is about 32,000 psi.

All specimens were in the form of sheet panels, 4 x 6 x 0.064 in. in size and weighing between 38

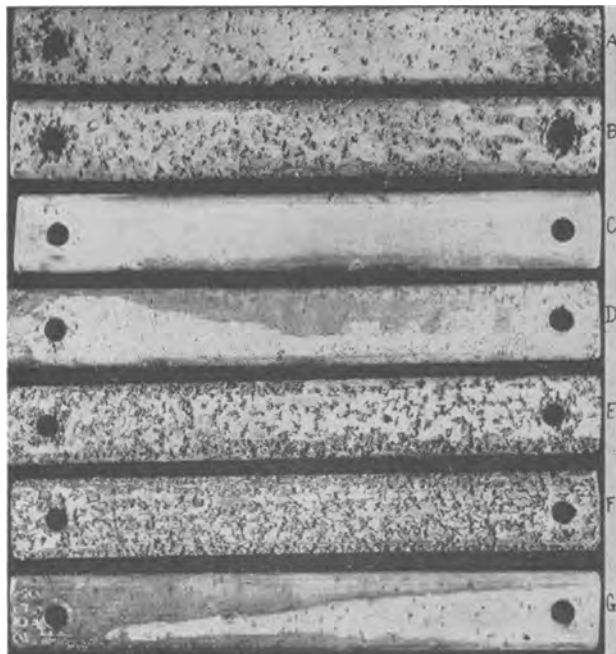


FIG. 1. Specimens of Mg-Li alloys compared with a commercial Mg-1.26%Mn alloy following cyclic immersion corrosion test in 3% NaCl at 95°F for 8 days. A—Heat No. 875, Mg-10.6%Li-4%Zn, lattice structure β ; B—Heat No. 690, Mg-9%Li-4%Zn, lattice structure β ; C—Heat No. 874, Mg-11%Li, lattice structure β ; D—Heat No. 873, Mg-9.3%Li, lattice structure α - β ; E—Heat No. 872, Mg-4%Li, lattice structure α ; F—Heat No. 871, Mg-2%Li, lattice structure α ; G—Heat No. 251, Mg-1.26%Mn, M1A alloy, lattice structure α .

and 46 g, depending on the alloy. After abrading with emery cloth to remove scale and degreasing, the panels were exposed, at the Battelle exposure station located about 12 miles south of Daytona Beach, Florida. This site is approximately 500 ft inland from the mean high tide line. At this point, the shoreline runs approximately northeast-southwest. The corrosion racks face south. The racks are dew coated about 9 out of 10 nights. The relative humidity in this area averages 82% and heavy fog occurs about 10% of the time. Thus, the panels were frequently wet.

Standard ASTM stainless steel corrosion racks were used. The panels were inclined 30 degrees from the horizontal and were supported at four points by porcelain insulators.

Ten panels of each alloy were exposed. Two panels of each were removed after intervals of 2, 4, 8, 16, and 32 months. The results of the tests are summarized graphically in Fig. 2. As might be expected, all four alloys corroded more rapidly during the early months of exposure. The corrosion rate reached a maximum in the Mg-Li-Al-Sn and Mg-Li-Al-Sn-Mn alloys after four months, whereas in the Mg-Li-Al-Zn and Mg-Al-Mn alloys the maximum occurred around two months or shortly thereafter. The commercial AZ31A alloy had the best corrosion resistance and the Mg-Li-Al-Zn alloy behaved very

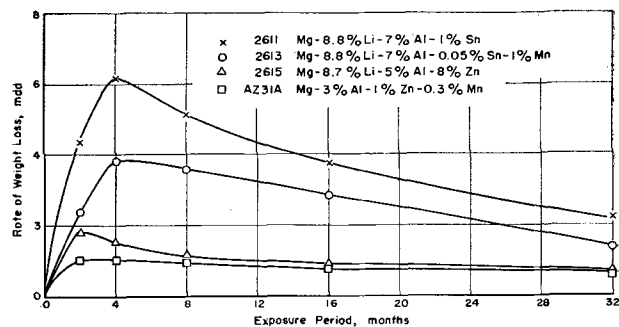


FIG. 2. Corrosion rate, expressed as weight loss, of experimental magnesium-lithium base alloys compared with commercial AZ31A alloy.

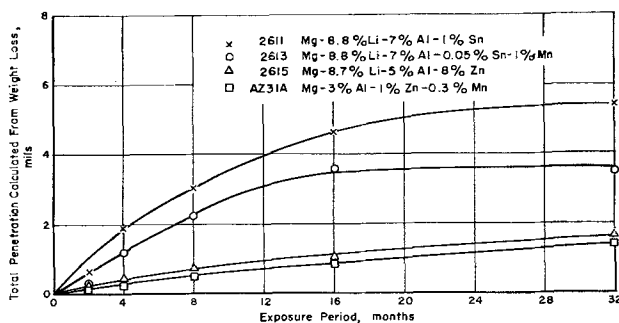


FIG. 3. Total penetration, calculated from weight loss, in experimental magnesium-lithium base alloys compared with commercial AZ31A alloy.

similarly. The Mg-Li-Al-Sn-Mn alloy had considerably poorer resistance; the Mg-Li-Al-Sn alloy had the highest corrosion rate of the four alloys.

Corrosion rates of the two more resistant alloys remained nearly constant after about eight months' exposure, whereas those of the two least resistant alloys decreased continuously during the same period. The trend is shown more strikingly when total penetration rather than penetration rate is plotted against the time abscissa, as in Fig. 3. Thus, the slopes of the corrosion curves for the Mg-8.7%Li-5%Al-8%Zn and Mg-3%Al-1%Zn-0.3%Mn alloys are essentially equal and constant between 8 and 32 months, but for the other two alloys the slopes decrease. This suggests that the two alloys which had the poorer corrosion characteristics in this experiment might appear to somewhat better advantage after exposures considerably longer than 32 months.

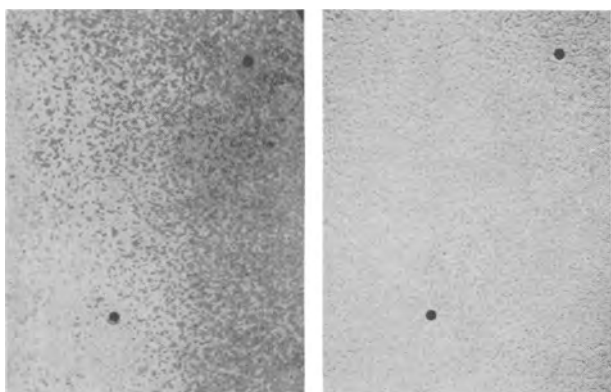


FIG. 4 (left). Underside of panel of the Mg-8.8%Li-7%Al-1%Sn alloy after 16 months' exposure; actual size before reduction for publication.

FIG. 5 (right). Same panel after removal of corrosion products.

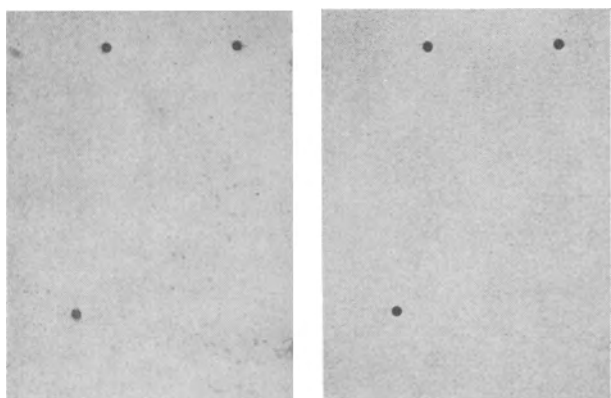


FIG. 6 (left). Underside of panel of the Mg-8.8%Li-7%Al-0.05%Sn-1%Mn alloy after 16 months' exposure; actual size before reduction for publication.

FIG. 7 (right). Same panel after removal of corrosion products.

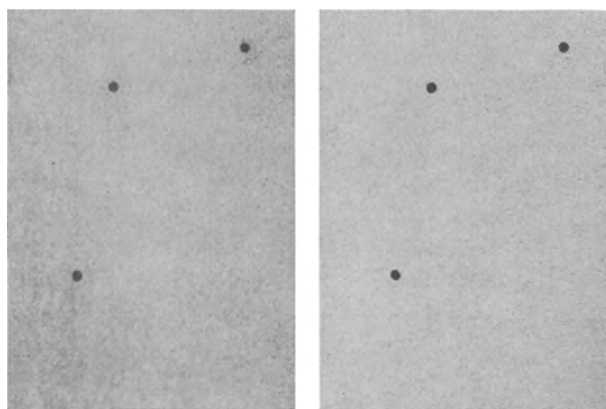


FIG. 8 (left). Underside of panel of the Mg-8.7%Li-5%Al-8%Zn alloy after 16 months' exposure; actual size before reduction for publication.

FIG. 9 (right). Same panel after removal of corrosion products.

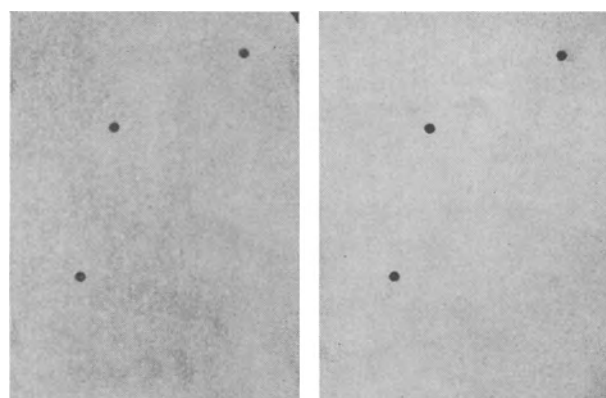


FIG. 10 (left). Underside of panel of the Mg-3%Al-1%Zn-0.3%Mn alloy after 16 months' exposure; actual size before reduction for publication.

FIG. 11 (right). Same panel after removal of corrosion products.

Photographs were taken of the underside of the panels exposed 16 months. These are shown in Fig. 4 through 11 before and after the corrosion products were removed.⁴ The extent of the attack was invariably greatest on the underside of the panels throughout the entire experiment.

The appearance of the panels reflects the results shown by the graphical data. All panels were pitted, the first two alloys more severely than the last two. The commercial AZ31A alloy showed the least amount of attack. However, there was little difference in the appearance of this alloy and the Mg-8.7%Li-5%Al-8%Zn alloy. It might be added that unprotected carbon steel panels of the same thickness

⁴ Corrosion products were removed by immersing the panel for 1 min in a water solution of 232.6 g/l CrO₃ and 11.7 g/l AgNO₃ maintained at the boiling temperature.

exposed under similar conditions at the same site tend to disintegrate in less than 24 months.

ACKNOWLEDGMENTS

This investigation was part of a research program sponsored by the Department of the Navy, Bureau of Aeronautics, and the Mathieson Chemical Corporation. The authors wish to express their appreciation to these organizations for permission to publish this work.

Mr. R. Glenn Fuller was responsible for the panels during their exposure at the Florida Station, and Mrs. Patricia Dent processed the exposed plates in the Battelle laboratories. The authors are grateful for the careful assistance of these people. They also wish to thank Dr. C. H. Lorig, of Battelle, for his suggestions and help on the project, and Mr. A. C. Loonam, of Deutsch and Loonam, New York, N. Y., for his contribution to this paper.

Any discussion of this paper will appear in a Discussion Section to be published in the December 1955 JOURNAL.

REFERENCES

1. J. H. JACKSON, P. D. FROST, A. C. LOONAM, L. W. EASTWOOD, AND C. H. LORIG, *J. Metals*, **185**, 149 (1949).
2. P. D. FROST, J. G. KURA, AND L. W. EASTWOOD, *J. Metals*, **188**, 1277 (1950).
3. P. D. FROST, J. H. JACKSON, A. C. LOONAM, AND C. H. LORIG, *ibid.*, **188**, 1171 (1950).
4. R. S. BUSK, D. L. LEMAN, AND J. J. CASEY, *ibid.*, **188**, 945 (1950).
5. W. HUME-ROTHERY, G. V. RAYNOR, AND E. BUTCHERS, *J. Inst. Metals*, **71**, 589 (1945).
6. Unpublished discussions and communications with Prof. A. J. Murphy, Chairman Industrial Metallurgy Department, University of Birmingham, Birmingham, England.
7. F. L. SHAMRAI, *Bull. acad. sci. U.S.S.R.*, Section of Chemical Sciences, Part I, No. 6, 606 (1947); Part II, No. 1, 83 (1948); Part III, No. 3, 290 (1948).
8. G. GRUBE, H. VON ZEPPELIN, AND H. BUMM, *Z. Elektrochem.*, **40**, 160 (1934).

On The Nature of Lead Surfaces Passivated in Sulfuric Acid¹

E. J. CASEY AND K. N. CAMPNEY

Defence Research Chemical Laboratories, Ottawa, Canada

ABSTRACT

Experimental results are presented which show that the rate of ennoblement of the electrochemical potential of lead which is passivating in sulfuric acid is markedly dependent on the concentration of hydrogen peroxide, whether formed by irradiation or added directly to the system. A study of factors which affect the ennobled potential of the sulfated or passivated lead is presented, as is a study of the conditions under which the sulfated lead shows rectifying properties. Results are interpreted in terms of the suggested presence of oxygen atoms sorbed into the lead sulfate layer.

INTRODUCTION

Considerable practical as well as theoretical importance attaches to the passivation of lead in sulfuric acid. In this paper are presented the results of some chemical, electrochemical, and electrical experiments which shed further light on the nature of the surface processes which give rise to the various observed phenomena. In particular, electrochemical effects observed during passivation by Müller (1), Haring and Thomas (2), and others have been puzzling. Thus, Müller has noted that lead pieces autocorroding in sulfuric acid show an electrochemical potential usually within 3 mv of the Pb/PbSO₄ reversible potential, but that when passivated they will exhibit a potential 0.50–0.65 v more noble than the Pb/PbSO₄ reversible potential. Müller has described this phenomenon in terms of a covering layer-pore theory (3), in which the ennobled potentials are described in terms of the electrolytic iR drop thought to exist in the pores in the film of PbSO₄. The potentials exhibited by such passivated electrodes, in terms of this theory, would be those measured between the metallic lead and the bulk electrolyte at the end of the pores, and would thus be (a) the potential of the local anode, the Pb/PbSO₄ electrode at the base of the pore, plus $i_L R_a$, where i_L is the local corrosion current and R_a is the electrolytic resistance of the pore; or (b) the potential of the local cathode, the nature of which is undetermined, but whose site is considered to be the whole PbSO₄-electrolyte interface; the local cathode is connected to metallic lead by the lead sulfate layer.

This theory leads to some difficulties. For instance, the theory does not adequately interpret the local cathode: what is the source of the driving energy for the maintenance of a local current of such a magnitude through such a high pore resist-

ance? If $R_a + R_c$ is so large that i_L is so small that no appreciable change in pore size occurs during local action, then, if $R_a \cong R_c$, any measurement made with a common potentiometer circuit would be insensitive because of high film resistances in the circuit; such is not the experimental observation. On the other hand, if $R_a \gg R_c$, say, the potentiometric measurement would be that of the local cathode which could not be sensibly polarized by the local current because the local current density through the cathode would be so small. Yet the potentials exhibited by the passivated pieces do not correspond to any of the common, known, redox systems. If, on the other hand, the local cathode is truly a strongly oxidizing electrode polarized down to the 0.50–0.65 v potential, then the implication in the Müller theory that unsealed pores exist on the passivated electrode is untenable.

The alternative argument, that pores do seal over while others are being formed by stress cracking of the surface film, to maintain open pores always of constant number and size, formed on different specimens which contain films of different thicknesses formed in different ways, which would have to be the case in order that the potential be reproducible, does not seem to be very likely either.

Haring and Thomas (2) considered the passivated lead to be completely covered with a layer of sulfate, and they considered the ennobled potential to be that of "an oxygen-depolarized hydrogen electrode," presumably a mixed potential of hydrogen and oxygen electrodes, both highly polarized, active at the lead sulfate-electrolyte interface. A detailed mechanism is not offered, however, for the formation and maintenance of the potential observed.

Experiments reported in the present paper have led to a new interpretation of the nature of the sulfated lead surface.

It is after the ennoblement of potential that the metal piece is defined, in the present paper, as passivated. This is perhaps a narrower definition of

¹ Manuscript received February 24, 1954. Issued as DRCL Report No. 129.

passivation than is used by Pourbaix (4), but is the one used by Müller and his associates with reference to the type of electrochemical information herein reported.

EXPERIMENTAL RESULTS AND DISCUSSION

Lead samples were cut from Baker & Adamson lead metal sheet, which analyzed for: silver, 0.008%; bismuth, <0.001%; arsenic, <0.001%; copper, 0.06%; antimony, <0.005%. Surface preparation was effected by scraping the lead surface down to the bright metal by means of a glass edge, usually a microscope slide. The sulfuric acid and other chemicals were reagent grade.

Potential measurements were made with a Leeds & Northrup Type K potentiometer and with a General Radio type 715-A d-c amplifier plus Esterline-Angus recording milliammeter. Inverted lead-lead sulfate-sulfuric acid reference electrodes were made simply by covering the submerged, freshly prepared lead surface with lead sulfate crystals. Mercury-mercurous sulfate reference standards were prepared by a variation of the electro-oxidation method used by Harned and Hamer (5).

Rate of passivation.—Although lead sulfate, a good insulator, is formed on the surface of lead autocorroding in sulfuric acid, it is formed as small crystals. To a magnification of about 500 times the only apparent physical difference between an unpassivated and a passivated lead piece is the number and depth of the crystals (Fig. 1). The low current d-c resistance has increased markedly with passivation, but the electrode is by no means electrically insulated from the electrolyte by the lead sulfate layer, otherwise measurement would be impossible.

Fig. 2 shows a typical potential-time plot obtained with lead pieces allowed to autocorrode in 1.223 s.g. sulfuric acid. Potentials were measured against a Pb/PbSO₄ reference electrode, which was

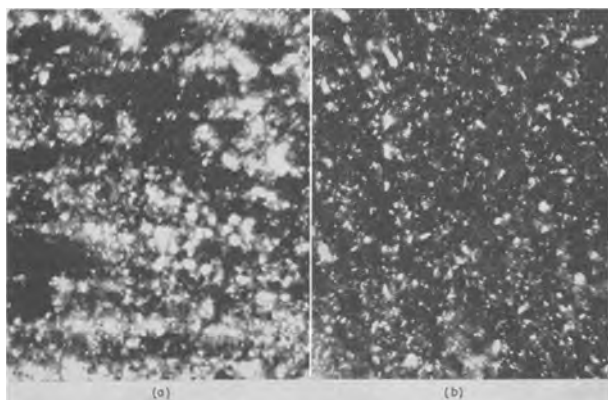


FIG. 1. Photomicrograph ($\times 500$, approx) of lead surfaces: (a) unpassivated; (b) passivated.

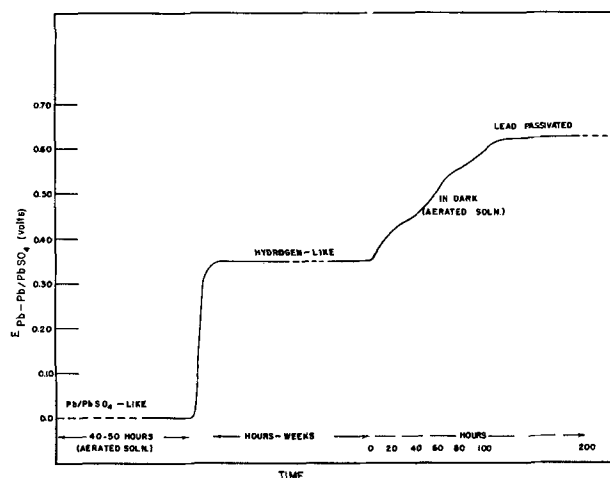


FIG. 2. Potential-time plot of lead pieces autocorroding in sulfuric acid.

frequently standardized against a Hg/Hg₂SO₄ reference electrode. Three distinct sections are noted in Fig. 2: (a) the time as a Pb/PbSO₄ electrode, when the corrosion is under cathodic control, before sulfation; (b) the time as a hydrogen-like electrode, when the rate may be anodically controlled by the covering layer of lead sulfate; and (c) the subsequent time as a fully passivated lead electrode, the nature of which was the subject of this investigation. The sulfation time, or the rate of attainment of sulfation, has been found previously by Müller and by Haring and Thomas to be transport-controlled, and the rate increases with increasing concentration of oxygen. Removal of the electrolyte-lead-air interface was found by Thomas (6) to reduce the sulfation time. It was concluded by Müller that diffusion of oxygen through the electrolyte toward the electrode controls sulfation. However, the existence of hydrogen-like electrodes on lead does not seem to have been noted previously.

After the electrodes have exhibited the hydrogen potential (0.35 v) for some time, the potential begins to rise slowly, and ultimately attains a value in the vicinity of 0.627 v more noble than the lead-lead-sulfate reference. Fig. 3 shows the general trend of the effects of irradiation (Hanovia, Type 30600, 140 w, mercury arc) on the rate of the passivation from 0.35 v toward 0.627 v. The stronger and more intense the radiation the faster is the rate of rise toward 0.627 v. If the radiation is very intense, the potential-time curve goes through a maximum; this perhaps indicates that some photochemical decomposition of the species which gives rise to the 0.627-v potential is occurring, or perhaps that photoconduction in the film exists. The bulk temperature of the electrolyte did not change appreciably during irradiation in these experiments. Pre-irradiation of the electrolyte before the immer-

sion of the 0.35-v electrode also increased the rate of the passivation to 0.627 v.

Since hydrogen peroxide is produced quite easily photochemically in many systems in the presence of certain sensitizers (7), and since possible sensitizers, such as iron, are commonly present in small amounts in sulfuric acid, analyses of the irradiated solutions for hydrogen peroxide were made. By the development of the characteristic color (absorption maximum at 4200 Å) of the titanium ion complex (8), it was established spectrophotometrically that in these irradiated solutions, whether or not a lead electrode was present, hydrogen peroxide was produced photochemically. It was found, further, that hydrogen peroxide was produced in greater quantity by irradiation of the air-electrolyte interface than by irradiation of a closed but aerated system through a quartz window. In the latter case, the production of a species which is not hydrogen peroxide and whose long wave-length absorption limit, about 3000 Å, is not different from that of persulfate ion (9), was evident. However, photochemical production of the $SO_4^-S_2O_8^-SO_5^-H_2O_2$ system was not studied beyond these qualitative observations.

When hydrogen peroxide was added directly to even a freshly prepared lead piece, passivation time was reduced to nearly zero, and the hydrogen-like step was eliminated. Fig. 4 shows the effects on the potential of adding hydrogen peroxide directly to fresh lead pieces in sulfuric acid. Within a matter of seconds a transparent, glassy layer builds up on the lead surface. X-ray diffraction patterns of crystals taken from this surface layer were characteristic of pure lead sulfate. After some minutes this glassy layer becomes covered with a second, whitish lead

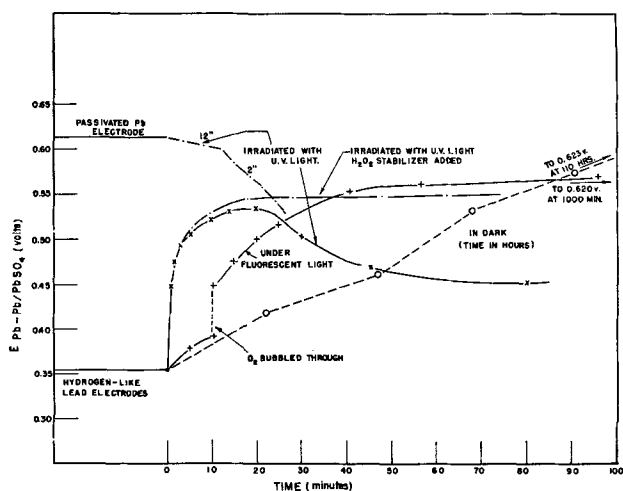


FIG. 3. Effects of irradiation on the rate of passivation. 12" and 2": electrode 12" and 2", respectively, from u.v. source.

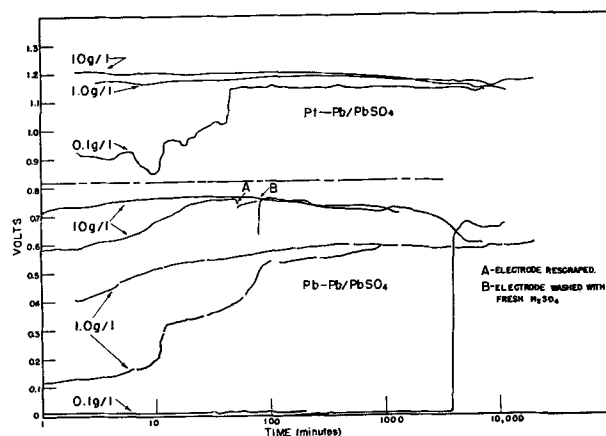


FIG. 4. Rate of ennoblement of potential as a function of H_2O_2 concentration.

sulfate layer, the second layer bound only loosely to the first.

It was found that neither oxygen nor ozone has this effect on the rate of ennobling of the potential. This may be simply a question of rate of reaction or, alternatively, it may be a concentration effect, since O_2 and O_3 are gases with limited solubility in sulfuric acid solutions, while the liquid hydrogen peroxide is completely miscible and readily available to the surface. Although there existed spectrophotometric indication that $S_2O_8^-$ was present after irradiation, direct addition of $K_2S_2O_8$ to a sulfuric acid solution containing a fresh lead specimen did not result in the immediate passivation of lead to the 0.6-v potential, as did the addition of H_2O_2 .

Factors which affect the potential of passivated surfaces.—The presence of oxygen (Fig. 2) or hydrogen peroxide (Fig. 4) seems to be a sufficient condition for the ennobled 0.6-v potential to be initiated. Therefore, the effects of oxygen concentration and hydrogen peroxide concentration were determined independently. Oxygen gas was bubbled into an electrolyte containing a 0.6-v lead electrode; then N_2 ; but other than Müller's "motor-electric" effect no change in the potential of the passivated lead was noted with changes in partial pressure of oxygen. In Table I are contained results which show that the passive potential is pressure independent and essentially temperature independent from 0°–55°C and from 40–760 mm mercury. This information seems to eliminate the possibility that O_2 species itself gives rise directly, even in part, to the potential measured. Platinum pieces in the same electrolyte, showing presumably the redox potentials of the electrolyte, were within a few millivolts of the O_2/H_2O_2 electrode, but the pressure and temperature independence of the potentials shown by both the platinum and passivated lead pieces seem to eliminate the possibility that O_2/H_2O_2 could be

TABLE I. Dependence of potential of passivated lead on temperature and on air pressure; also, results on Pt pieces under same conditions

Pressure (mm)	$E_{Pb_{pass}-Pb/PbSO_4}$			$E_{Pt-Pb/PbSO_4}$	
	0°C	25°C	50°C	25°C	50°C
760	a	0.628 ± 0.008	0.627 ± 0.002	c	1.039 ± 0.006
	b		0.613 ± 0.004	d	1.000 ± 0.005
				e	0.789 ± 0.005
380	a	0.626 ± 0.002	0.627 ± 0.002	c	1.037 ± 0.002
	b	0.613 ± 0.004			
100	a	0.627 ± 0.001	0.626 ± 0.004	c	1.036 ± 0.006
	b	0.615 ± 0.005		d	1.018 ± 0.007
				e	0.809 ± 0.009
40	a				
	b	0.610 ± 0.005			

Note: The limits assigned to each value express the range in which the electrode potential, as measured, drifted up and down during a time interval usually not less than 1-2 hr. *a*, *b*, etc., refer to experiments done at different times with different electrodes. Values read simultaneously against Hg/Hg₂SO₄ electrodes simply verified the above results and are not given.

the cathode of the Müller-type of local cell on the sulfated lead electrode.

Fig. 4 shows how the potential of a freshly prepared lead piece during passivation builds up in the presence of different concentrations of hydrogen peroxide. The peroxide was decomposing as the runs were made, so much so that at 10,000 min peroxide concentrations were all reduced to a common value. It was then established that the steady potential of the completely passivated lead becomes more noble with increasing hydrogen peroxide concentration. Typical results are contained in Table II; these figures are measurements made on several passivated pieces, each passed repeatedly and in random sequence into sulfuric acid solutions containing hydrogen peroxide of different concentrations. A plot of $E_{Pb_{pass}}$ vs. $[H_2O_2]$ is sigmoidal after the manner of an adsorption curve. Peroxide breakdown with the evolution of oxygen begins at concentrations about 5 g/l in 30% acid. Results given in Table III show that the final potential, $E_{Pb_{pass}}$ (hydrogen scale), of lead pieces passivated in sulfuric acid containing hydrogen peroxide becomes more noble also with increasing concentration of sulfuric acid. The dependence of the passivated potential on $[H_2O_2]$ and upon $[H_2SO_4]$ is discussed in the last section of the paper.

That the passivated lead does not behave as an inert metal electrode (e.g., platinum) and exhibit the redox potential of the electrolyte was shown by the fact that in ferrous-ferric sulfate solutions in sulfuric acid the passivated lead did not exhibit the same potential values as did platinum pieces: thus, when E_{Pt} was 0.86 v more noble than the Pb/PbSO₄ reference, $E_{Pb_{pass}}$ was ~0.60 v, and when E_{Pt} was 1.14 v, $E_{Pb_{pass}}$ was ~0.61 v. Thus the passivated

TABLE II. Dependence of potential of passivated lead upon H₂O₂ concentration
H₂SO₄ sp gr 1.223 (4.35M, 7.7N)

Conc. (g/l)	Mean $E_{Pb_{pass}}^*$ (v)	Prob. error† of mean (v)
0.10	0.502	0.016
0.25	0.576	0.004
0.50	0.565	0.015
1.0	0.590	0.003
2.0	0.584	0.010
2.5	0.599	0.002
5.0	0.609	0.003
7.5	0.665	0.005
10.0	0.688	0.012
15.0	0.783	0.008

* Measured against Pb/PbSO₄/H₂SO₄ (7.7N) electrode.

† By Bessel's method (10).

lead is its own electrical buffer against changes in redox potential of the electrolyte. However, since the electrode responds to changes in concentration of H₂SO₄ and H₂O₂, the implication is strong that the surface of the passivated electrode is somewhat specific in the type of molecules or ions which can exchange electrons at the lead sulfate electrolyte interface.

In the presence of a passivated lead electrode the electrolyte was reduced cathodically, under nitrogen, on an auxiliary platinum cathode in a Pyrex system in which the anode and cathode compartments were separated by a closed, moist, ungreased stop-cock. Reduction at a cathode current density of 200 μ a/cm² and voltage, with respect to Pb/PbSO₄, of about +0.07 v failed to alter the 0.627-v potential of the passivated lead. It was found, too, that passivated lead could be moved

TABLE III. Dependence of potential of passivated lead on H_2SO_4 concentration

% H_2SO_4	(Molality)	$a_{H_2SO_4}$ (activity)	$E_{Pb_{pass}}$ measured (v)	$E_{Pb_{pass}}$ reduced (v)	Probable error
1.0	0.103	0.028	0.372	0.062	0.011
15.0	1.80	0.22	0.495	0.158	0.007
30.0	4.35	0.78	0.584	0.232	0.010
36.6	5.74	1.5	0.688	0.327	0.009
50.0	10.2	(6.0)*	0.735	(0.37)	0.04

* From an extrapolation of the activity coefficient data.

The values given for $E_{Pb_{pass}}$ are mean values, of not less than seven independent experiments. Measurements were made against a $Pb/PbSO_4/H_2SO_4$ (m) electrode, and reduced to the hydrogen scale by means of the Nernst equation and the activity information of Harned and Hamer (11).

into successive fresh sulfuric acid electrolytes without any marked change in potential occurring. From these experiments it is inferred that the seat of the potential must be either (a) in or on the surface, the potential-determining species being very difficult to remove, or (b) in the solution, supplied continuously, if needed, by dissolution from the surface. In this latter case the rate of dissolution from the surface must be large enough to build up rapidly and thereafter maintain a saturation concentration of the potential-determining species. Thus, the electrode would exhibit behavior similar to that of a silver-silver chloride electrode placed in a chloride-free electrolyte.

Cathodic reduction, under nitrogen, of the passivated lead surface itself at $0.25 \mu a cm^{-2}$ resulted in no permanent alteration of the potential. But at $40 \mu a cm^{-2}$ the passage of the same number of coulombs did result in a temporary activation (that is, lessening of the potential to below 0.627 v). After some hours of idle stand, still under nitrogen, the potential had drifted upward again to 0.63 v. Hence, once the passivated potential is shown by a specimen, the presence of oxygen or hydrogen peroxide is not necessary for the re-ennoblement after the partial reduction of the surface: the unreduced surface resupplies the species needed to repassivate the reduced surface.

Rectification phenomena.—A striking fact is that for different specimens of passivated lead, all of which exhibited the passivated potential, the apparent electrical resistance, as determined from the voltage drop effected by the passing of $0.25 d.c. \mu a cm^{-2}$, was found to vary over fiftyfold. It was also found that the apparent resistance measured when the passivated lead was made positive (oxidized) was two to three times higher than that measured when the lead piece was made negative (reduced). Thus the passivated lead surface in sulfuric acid

exhibits modified rectifying properties. With 60 cycles/sec alternating current a small ($\sim 10\%$) rectification of the current was observed on an oscilloscope when set up in the manner indicated in Fig. 5. The direction of the rectification of the current was found to be the same as that in an aluminum rectifier. The voltage across the passivated lead piece was also distorted in the same direction as that across the standard aluminum rectifier. Calibrations of the circuit were made on pure resistances and sufficient variations in cell construction made to eliminate the possibility that any factor other than the passivated lead surface was responsible for the observed rectification effects.

It was noted that, although the passivated potential of a lead piece would be established very soon (see Fig. 4) after the addition of H_2O_2 to the sulfuric acid electrolyte, the current rectification property developed very slowly, and was at its maximum value (5–10%) only after 24–36 hr. This suggests that the process responsible for the establishment of the passivated potential and the process responsible for the establishment of the properties of a rectifier are not identical. However, that the two processes must be related is shown by the facts that the appearance of the ennobled potential is a sufficient condition for the establishment of a rectifier, and that the rectifying property was never detected until the lead had become passivated. It was noted further that if hydrogen peroxide was added in excess (to concentration greater than 5 g/l) to the electrolyte which contained a rectifying electrode, peroxide breakdown accompanied by oxygen evolution occurred on the lead surface, and the rectification which formerly was exhibited by the passivated lead surface was thereby destroyed.

In contrast with the behavior of aluminum rectifiers, at the higher currents (~ 0.8 – $1.0 ma cm^{-2}$) and higher impressed voltages, the rectification of

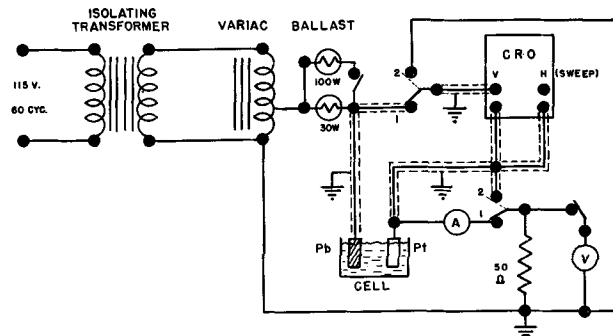


FIG. 5. Electrical circuit used to follow rectifying properties. With the switches closed to positions marked "1" the voltage variations of the electrode are displayed. Closed to positions "2", the current through the cell is displayed.

the passivated lead piece decreased and disappeared within about one minute after the current was turned on. This loss of the rectifying power was found usually to be not permanent, and would return by an idle stand of some minutes or hours.

DISCUSSION

It would seem that penetration of current carriers through thick layers of lead sulfate on the surface would be highly unlikely. Suppose that even at the bottom of the cracks, pores, or holes in the lead sulfate layer the lead surface was converted to lead sulfate by local action until the pores had sealed over completely. The authors assume that it is lead sulfate at the bottom of the pore because PbO is neutralized rather quickly by H_2SO_4 and because the presence of H_2O_2 (shown above to be a sufficient constituent for the establishment of the ennobled potential of Pb in H_2SO_4) has been found in this laboratory to accelerate greatly the rate of conversion of any of the lead oxides into lead sulfate. The increase in potential of the passivated lead as the concentrations of H_2O_2 and/or H_2SO_4 increase only serves to emphasize the possible reaction products, persulfate ($S_2O_8^{2-}$) and monopersulfate (SO_5^-) ions. It is reasonable to suppose, then, that the outer part of the surface of the sulfated electrode is oxidized sulfate, containing SO_5^- , perhaps, or the stoichiometric equivalent, $SO_4^- + O$. It would thus seem possible for oxygen atoms to be absorbed into the lead sulfate surface and thence perhaps to penetrate further into the lead sulfate lattice by diffusion. These impurity centers in the lead sulfate would make the lead sulfate a defect-type semiconductor (12). This layer of oxygen atoms in the lead sulfate layer at or near the electrolyte-lead sulfate interface (see Fig. 6) is pictured as being the negative analog of the Schottky-type barrier layer which exists in semiconductor materials near the metal-semi-

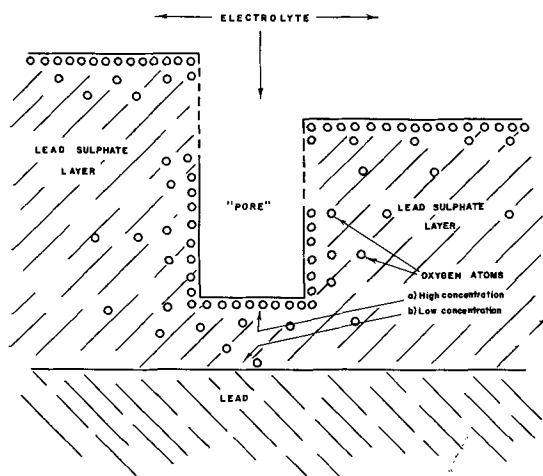


FIG. 6. Idealized model of passivated lead surface

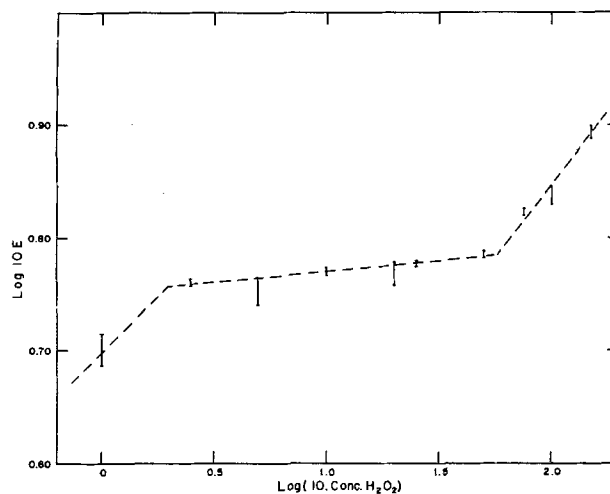


FIG. 7. Freundlich-type plot of potential of passivated lead as a function of H_2O_2 concentration.

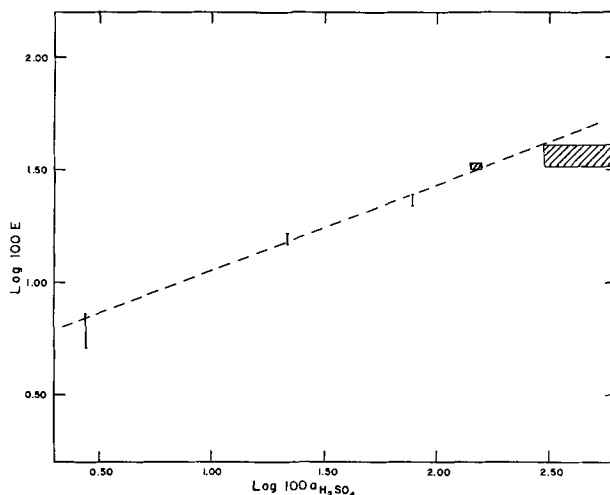


FIG. 8. Freundlich-type plot of potential of passivated lead as a function of activity of H_2SO_4 .

conductor interface. A detailed consideration of the oxygen atom layer reveals properties which are strikingly analogous to the properties of the Schottky-type barrier. Thus the highest concentration of positive charge in the Schottky-type barrier is near the metal semiconductor interface, and falls off rapidly into the semiconductor. The highest concentration of negative charge of the oxygen barrier is near the lead sulfate-electrolyte interface, and falls off rapidly into the lead sulfate. Thus the direction of the rectification effects should be the same for both cases, as was found experimentally.

The oxygen barrier layer differs from the Schottky-type in the strength with which the barrier layer is held by the surface. Strong reduction of the electrolyte on an auxiliary cathode and even mild direct reduction of the passivated surface fail to disturb the potentials exhibited; however, the layer

is disturbed by strong reduction of the surface, by H_2O_2 breakdown accompanied by oxygen gas evolution at the surface if the concentration of H_2O_2 is made too high, or by high alternating currents.

Further evidence of adsorption of oxygen atoms during passivation is provided from a study of the dependence of potential upon concentration of H_2O_2 and upon concentration of H_2SO_4 . As noted earlier, results in Table II show that the dependence of potential upon $[\text{H}_2\text{O}_2]$ is sigmoidal. If one assumes that the potential measured during the passivated state is a measurement of the amount of oxygen atoms adsorbed, then the Freundlich adsorption isotherm should be applicable. Fig. 7 shows a plot of $\log 10E$ vs. $\log 10 [\text{H}_2\text{O}_2]$. Three distinct regions are noted. Above 5 g/l, H_2O_2 increases the thickness of the adsorbed layer beyond the stability limit, and oxygen gas is released. Below about 0.25 g/l, not enough H_2O_2 is present to mend the cracks which occur due to strains in the film during short-term experiments. Between 0.25 and 5.0 g/l the Freundlich equation describes adequately the results found, although the variation of potential with concentration is so slight that the surface must be nearly saturated over this range of concentration.

A remarkable fact is the strong dependence of potential on activity of sulfuric acid. The experimental points are not described even remotely by the Nernst equation when applied to any of the known lead redox systems (13) or the known oxygen or hydrogen peroxide systems (14). In terms of the Freundlich expression, Fig. 8 shows $\log 100 E_{\text{Pb pass-hyd}}$ vs. $\log 100 a_{\text{H}_2\text{SO}_4}$. Linearity within the limits of the probable error, and the strong dependence of potential upon concentration suggest the adsorption of a second potential-determining species, perhaps SO_4^- , whose adsorption in the range of concentrations studied was considerably below saturation. Thus it seems reasonable to conclude that the passivated potentials observed are those of one of the equilibria of the SO_4^- - $\text{S}_2\text{O}_8^{2-}$ - SO_5^- - H_2O_2 system, about which very little thermodynamic information at present exists.

The response of the passivated surface to changes in concentration of H_2O_2 and of H_2SO_4 , and the lack of response to wide changes in the redox potential of the electrolyte (produced by changes in the

Fe^{++} - Fe^{+++} additions) warrant a further comment. This behavior suggests that the electrical response of the surface is specific to those redox species which can, for steric reasons, be preferentially sorbed into the surface. In a metal-electrolyte system the source or sink of electrons is pictured as being right at the interface; but in the semiconductor-electrolyte system an electron transfer must be made at a defect center. Thus, in the present case, the potential-determining species must be able to penetrate right into the oxygenated sulfate of the surface. Hence the steric factor may well be quite critical.

ACKNOWLEDGMENTS

The thanks of the authors are expressed to Mr. L. G. Wilson, of these Laboratories, for identification of the surface films by x-ray diffraction techniques, and to the Department of Mines and Technical Surveys for the analysis of the lead used.

Any discussion of this paper will appear in a Discussion Section to be published in the December 1955 JOURNAL.

REFERENCES

1. W. J. MULLER, *Kolloid-Z.*, **86**, 150 (1939).
2. H. E. HARING AND U. B. THOMAS, *Trans. Electrochem. Soc.*, **48**, 293 (1935).
3. W. J. MULLER AND W. MACHU, *Korrosion u. Metall-schutz*, **16**, 187 (1940).
4. M. POURBAIX, "Thermodynamics of Dilute Aqueous Solutions," Edward Arnold & Co., London (1949).
5. H. S. HARNED AND W. J. HAMER, *J. Am. Chem. Soc.*, **57**, 31 (1935).
6. U. B. THOMAS, Private communication, April 1953.
7. See, e.g., E. BAUR AND C. NEUWEILER, *Helv. Chim. Acta*, **10**, 901 (1927); M. C. MARKHAM AND K. J. LAIDLER, *J. Phys. Chem.*, **57**, 363 (1953).
8. See, e.g., F. G. PALILLA, N. ADLER, AND C. F. HISKEY, *Anal. Chem.*, **25**, 926 (1953).
9. J. L. R. MORGAN AND R. H. CRIST, *J. Am. Chem. Soc.*, **49**, 338 (1927).
10. W. N. BOND, "Probability and Random Errors," E. Arnold & Co., London (1935).
11. H. S. HARNED AND W. J. HAMER, *J. Am. Chem. Soc.*, **57**, 27 (1935).
12. N. F. MOTT AND R. W. GURNEY, "Electronic Processes in Ionic Crystals," 2nd ed., Oxford University Press, New York (1948).
13. P. DELAHAY, M. POURBAIX, AND P. VAN RYSELBERGHE, *This Journal*, **98**, 57 (1951); J. J. LANDER, *ibid.*, **98**, 213 (1951).
14. W. K. LATIMER, "The Oxidation States of the Elements and Their Potentials in Aqueous Solutions," 2nd ed., Prentice-Hall, Inc., New York (1952).

Stress During the Electrodeposition of Copper on Copper Substrate¹

HUSSEIN SADEK, M. HALFAWY, AND S. G. ABDU

Chemistry Department and Institute of Industrial Chemistry, Alexandria University, Alexandria, Egypt

ABSTRACT

The stress in electrodeposits of copper on a copper substrate was investigated. Copper strips, coated on one side by petroleum jelly wax mixtures, were used as cathodes and the deflection they suffered during electrodeposition was measured. Maximum deflection was obtained at a current density of 2 amp/dm² using 60% wax coating. The deflection does not vary linearly with the time during electrodeposition but becomes linear during anodic attack.

INTRODUCTION

Electrodeposition of metals is widely used to provide the substrate metal with a more corrosion-resistant or a better wearing surface. Most metals are normally electrodeposited in a state of stress. Not only does stress occur during electrodeposition, but it often increases on standing (1). An understanding of the various factors that cause and control stress in electrodeposited metals is of both theoretical and technical importance.

Various authors (1-3) have studied the stress of several electrodeposited metals using different substrates, various bath conditions, and addition agents. Results obtained, however, differ among the different authors. It is believed that the type of solution is a factor more important than the operating conditions in determining the physical properties of the deposits (4). However, no adequate explanation of the causes of the stress has yet been given. The present paper is one of a series which summarizes work undertaken to elucidate the nature of the phenomenon.

EXPERIMENTAL

Electrolytic copper strips² were used as substrates. They were 10 mm wide, 0.3 mm thick, and were bent at an angle of 90° at one end so as to leave a length of 10 cm for electrodeposition. Before electrodeposition, the strips were annealed for ½ hr at 500°C, dipped in dilute nitric acid (1:1) for 3 sec, thoroughly rinsed with water and alcohol, dried between filter paper, checked for weight and modulus of elasticity, and finally bent and waxed on one side. The modulus of elasticity was checked by clamping the strip firmly at one end in a horizontal position and measuring the deflection produced on hanging a weight of one gram at the other end. Only strips which gave the same deflection (within 2%) were chosen for the stress measurements. Following the procedure of Van der Sommen (3), wax

was applied by a warm spatula to produce a fairly thin and uniform coating. After being waxed, the strip was etched in 3% solution of KCN, rinsed, immersed in dilute HCl (1:20), and rerinsed. The strip was then weighed after standing for ½ hr in a desiccator. To insure uniform thickness of the wax on each strip, differences in weight before and after waxing were always compared. They showed a deviation of the order of 1% which was considered quite satisfactory. A light-weight glass fiber about 4 cm long was fixed at the extreme free end of the strip by gently warming the wax locally. This fiber served as a pointer whose movement could be followed easily by a vernier microscope, accurate to 0.01 mm. The same pointer was used throughout the whole series of measurements.

The electrolytic cell was a shallow porcelain vessel of about 600 cc capacity. The plating bath containing 150 g/l of CuSO₄·5H₂O and 50 g/l of concentrated sulfuric acid was prepared from analytically pure reagents. The effect of the very small amounts of impurities could not be of primary importance in comparing the stress values, since the same bath was used throughout.

The strip was held in a horizontal position by a clamp with the unwaxed side facing the copper anode made of electrolytic copper. The tip of the pointer was always above the wall of the cell and its deflection (Δ) was followed by the travelling microscope. Plating was carried out at room temperature 25° ± 2°C for 18 min.

RESULTS

In all cases it was observed that, when the strips were coated electrolytically, they contract and become concave on the coated side. Comparison of the deflection (Δ) of the strip rather than the calculated stress was made since all substrate strips were exactly the same, and the deposit and substrate were of the same metal. The variation of the deflection as a function of time of deposition at various current densities is shown in Fig. 1. It is obvious that the

¹ Manuscript received October 6, 1953.

² Provided by the Egyptian Copper Works Company.

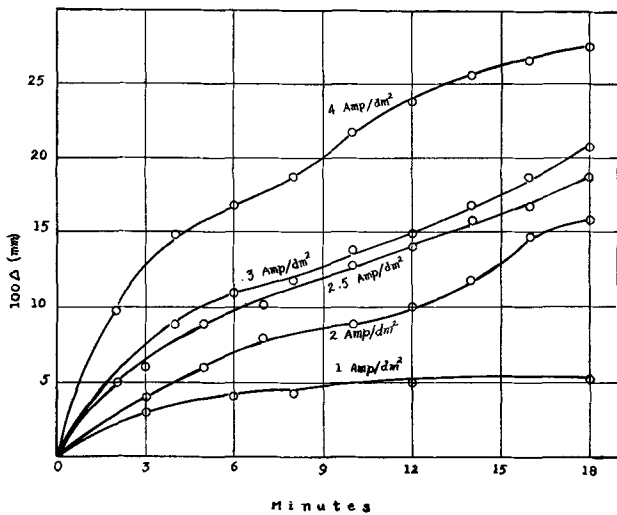


FIG. 1. Variation of the deflection (Δ) with time at several current densities.

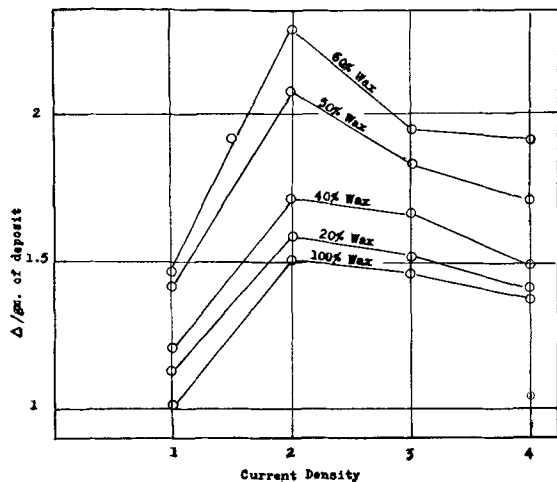


FIG. 2. Dependence of specific deflection on the composition of coating.

deflection after a given time is greater the greater the current density. All the curves are almost linear in the early stages of deposition.

The deflection at a given current density, after 18 min of deposition, varies with the composition and, hence, with the mechanical properties of the coating material. The highest deflection was obtained when a coating of 60% wax and 40% petroleum jelly was applied (Fig. 2). This coating (mp, 48°C) was used throughout the work. It will be noticed that the highest specific deflection (Δ/g Cu deposited) for any one coating is obtained at a current density of 2 amp/dm².

Although the total deflection of the strip after 18 min of deposition was greater at higher current density, the relation was not linear, as can be seen from Fig. 3. The weight of copper deposited at each current density is also shown in the same figure, and is seen to vary linearly with current density as required by Faraday's laws. Similar results, using other coatings of the wax-petroleum jelly mixtures,

were obtained. The cathode efficiency was found to be $100 \pm 0.1\%$.

Anodic attack of the deposit in the same bath resulted in a linear decrease of the deflection with time of attack, as shown in Fig. 4. In this case, the strip was first coated on one side with a copper deposit at 5.5 amp/dm² for 18 min, weighed, and then made anode in the same bath and attacked at the same current density. The deflection and weight of the

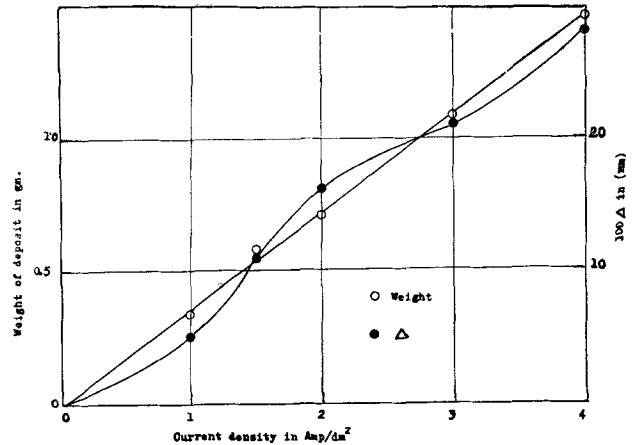


FIG. 3. Variation of weight of deposit and of deflection with current density.

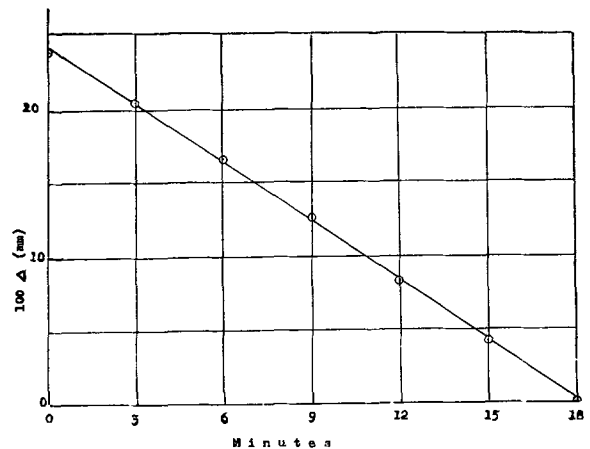


FIG. 4. Plot of deflection against time during anodic attack.

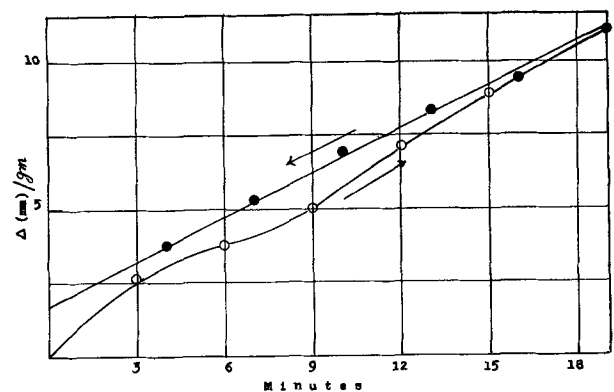


FIG. 5. Variation of (Δ/g) during deposition and anodic attack with time.

strip were determined every 3 min. The linearity of the anodic attack curve as compared to the non-linearity during cathodic deposition indicates hysteresis in the phenomenon. This result is clearly shown in Fig. 5 by plotting the specific deflection for each 3-min interval for both deposition and attack. This result has been repeatedly confirmed and cannot be attributed to experimental error. The anode efficiency in this case was found to be $99.8 \pm 0.1\%$. Work in progress in this laboratory has indicated that this hysteresis phenomenon is even more pronounced when zinc is electrodeposited on a copper substrate and then anodically attacked.

DISCUSSION

Jacquet (2) investigated the effect of very small but variable concentrations of addition agents, such as gelatin, on the amount of stress in electrodeposited copper. He found that such addition agents affected the stress in varying degrees according to their nature and concentration. These agents are known to produce fine-grained deposits probably because they are adsorbed on the crystal nuclei and thus prevent their growth. The consequent discharge of ions must lead, therefore, to the formation of new nuclei. Piontelli (5) showed that, during deposition of a metal on the same metal, the formation of new nuclei implies changes of configuration and of energy of the base metal. The former change involves disappearance of a portion of the original and formation of a new surface between nuclei and liquid. The latter change involves sublimation energy of the deposited metal (when an incomplete lattice plane is formed) and adsorption as well as interfacial energies (when two-dimensional nuclei are formed). Moreover, deformation of metallic crystal faces usually takes place when subjected to a stress (6). Furthermore, Yang (7) has proved by electron diffraction studies that the stress is in no way connected with a favored orientation of the crystals of the deposit on the substrate surface. Such a view was previously held by Bozorth (8) and Wyllie (9).

In the present case of deposition of copper on copper substrate it cannot be argued that the stress is in any way connected with the difference in lattice constants between deposit and substrate. The explanation that seems most reasonable is that the observed tensile stress is due to the forces of attraction parallel to the surface between adjacent crystallites. Fig. 2 shows that tensile stress increases with increase in current density up to 2 amp/dm². This result may be explained as being due to an increase in the density of the deposit as it grows in thickness, and hence the attractive forces between crystallites increase. Such attractive forces are responsible for sintering in metals, which is largely due to increase in particle size. On this basis one can explain the

readiness with which condensed nickel atoms on glass surfaces sinter at 100°C (10). The decrease in the tensile stress above a current density of 2 amp/dm² may be attributed to a decrease in the density of the deposit and, hence, to a fall in the attractive forces. The effect may be linked to a decrease in density of a cold-rolled metal (11). The same sort of effect occurs when a bag of sand which has been well shaken is compressed. The grains are disturbed from their equilibrium positions and the net effect is to increase the volume they occupy and thus reduce the density.

The kinetics of electrode processes at metal surfaces has been discussed by Lorenz (12) from the standpoint of the theory of crystal growth. He distinguishes electrolytic crystal growth from growth out of the gas phase or from melts in that, in the former, separations of electrically charged particles depend on the moving electric field forming within the electrolyte. A clear understanding of the cathodic process of crystal growth and of the nature of the bonding between deposit and substrate might throw more light on the nature of the interatomic forces in the deposit.

The hysteresis phenomenon shown in Fig. 5 may be explained by the heterogeneity of metallic surfaces (13). The last crystals to grow by cathodic deposition are not necessarily the first to be attacked anodically. It has been shown by tracer technique that the surface layer of electrodeposited copper includes sulfur as SO₄²⁻ which could be bound either electrostatically or by adsorption, causing favorable orientation of crystallites (14).

Any discussion of this paper will appear in a Discussion Section to be published in the December 1955 JOURNAL.

REFERENCES

1. A. W. HOTHERSALL, *J. Inst. Metals*, Reprint 1082, 107 (1947); *C.A.*, **42**, 465 (1948).
2. P. A. JACQUET, *Compt. rend.*, **194**, 456, 870 (1932).
3. J. VAN DER SOMMEN, *Proc. 3rd Intern. Electrodep. Conference*, London, 195 (1947).
4. A. BRENNER, V. ZENTNER, AND C. W. JENNINGS, *Plating*, **39**, 865 (1952).
5. R. PIONTELLI, *Proc. 3rd Intern. Electrodep. Conference*, London, 157 (1947).
6. A. T. STEER, *Proc. 3rd Intern. Electrodep. Conference*, London, 165 (1947).
7. L. YANG, Ph.D. Thesis, London University, London (1948).
8. R. M. BOZORTH, *Phys. Rev.*, **26**, 390 (1925).
9. M. R. J. WYLLIE, *J. Chem. Phys.*, **16**, 52 (1948).
10. O. BEECK, A. E. SMITH, AND A. WHEELER, *Proc. Roy. Soc. London*, **177A**, 162 (1940).
11. A. TAYLOR, "An Introduction to X-ray Metallography," p. 233, Chapman and Hall, London (1947).
12. W. LORENZ, *Z. physik. Chem.*, **202**, 275 (1953).
13. H. SADEK AND H. S. TAYLOR, *J. Am. Chem. Soc.*, **72**, 1168 (1950).
14. F. G. HOUTERMANS, D. VICENT, AND G. WAGNER, *Z. Elektrochem.*, **56**, 944 (1952).

On the Behavior of Rapidly Diffusing Acceptors in Germanium¹

F. VAN DER MAESEN AND J. A. BRENKMAN

Philips Research Laboratories, N. V. Philips' Gloeilampenfabrieken, Eindhoven, Netherlands

ABSTRACT

The acceptor activity of Cu and Ni and their diffusion in germanium have been investigated. Their acting as acceptors as well as recombination centers gives reason to believe that impurity atoms are placed substitutionally in the lattice. However, the value of 10^{-5} cm²/sec of the diffusion constant makes it likely that the diffusion goes interstitially. This leads to the concept of an equilibrium existing between substitutional and interstitial atoms. The fact that the diffusivity is dependent on the range of diffusion can be explained qualitatively on the basis of the picture given above.

INTRODUCTION

A number of investigations have been made recently on the influence of impurities such as copper, nickel, and elements other than 3rd or 5th column elements, on the properties of germanium. Investigations by Theuerer and Scaff (1) on "thermal conversion," experiments by Fuller and Struthers on acceptor activity and on the saturation concentration and diffusion of copper in germanium (2), as well as the authors' work on these subjects (3) are mentioned. Investigations on the influence of Cu and Ni on the lifetime of holes and electrons have been reported recently (4).

Experiments with Ni in the authors' laboratory have shown that Ni behaves similarly to Cu. The saturation concentration of Ni in germanium at high temperatures (800°C) is about one-tenth of the value for Cu at the same temperature and the diffusivity is of the same order of magnitude.

Prolonged heating of samples saturated with Ni or Cu at 500°C restores the original resistivity; there is also evidence that the lifetime is then increased (5).

Diffusion experiments show that the diffusion coefficient D of Cu and Ni is not simply a constant; D increases from the beginning toward the end of the diffusion range in all cases.

In this paper the authors propose that copper and nickel may be present at both normal and interstitial lattice positions. These two forms are in a thermodynamic equilibrium. They will explain how the diffusion experiments can be understood by assuming different diffusion constants for substitutional and interstitial atoms.

EFFECT OF HEAT TREATMENTS

It is well known that copper produces in Ge an acceptor level with an activation energy of 0.04 ev

¹ Manuscript received October 20, 1954. This paper was prepared for delivery before the Chicago Meeting, May 2 to 6, 1954.

(6). According to Burton (4), one should ascribe to Cu also an acceptor level with a rather high activation energy of 0.25 ev which also acts as recombination center (7). The acceptor properties of Cu and the fact that a negative Cu ion in itself would be too large for an interstice suggest that the Cu concerned is placed *substitutionally* in the lattice.

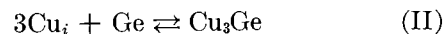
On the other hand, copper has a remarkably high diffusion constant of 10^{-5} cm²/sec at 800°C (8) (for normal donors and acceptors this value is about 10^{-12} cm²/sec). These facts give strong support to the idea that the diffusion proceeds *interstitially*.

The above considerations lead to the concept that both substitutional (Cu_s) and interstitial (Cu_i) atoms are present. The two forms will be in a temperature dependent equilibrium:²



One assumes that only the substitutional atoms will show an electrical (i.e., acceptor) activity.³

Prolonged heating at 500°C for 48 hr nearly restores the original resistivity. In view of the phase diagram Cu—Ge it is likely that the excess of Cu is precipitated, presumably as Cu₃Ge:



² Just before the completion of our work, an extended article appeared by Fuller et al. from Bell Telephone Laboratories (9). Comparing the total saturation concentrations (Cu_i + Cu_s) determined *with radioactive Cu with the concentration* (Cu_s) *derived from direct resistivity measurements from figure 5 of their paper, it is clear that at 600°C these two quantities have nearly the same value, whereas at 800°C Cu_i + Cu_s is about twice Cu_s. This can be explained by a shift of the equilibrium toward an increase of interstitial Cu at higher temperatures. At the same time the direction of the shift should indicate that the thermochemically denoted Q has a positive sign.*

³ It is possible that the situation is more complicated; e.g., one might think of Cu_i as a donor. The general idea however will not be affected.

TABLE I. Cu

Time (<i>t</i>) min	12			15			20		
	x (mm)	$\lambda = x/\sqrt{t}$, $10^{-3} \frac{\text{cm}}{\text{sec}^{1/2}}$	C_{Cu} , $10^{14} \frac{\text{at}}{\text{cm}^3}$	D , $10^{-5} \frac{\text{cm}^2}{\text{sec}}$	$\lambda = x/\sqrt{t}$, $10^{-3} \frac{\text{cm}}{\text{sec}^{1/2}}$	C_{Cu} , $10^{14} \frac{\text{at}}{\text{cm}^3}$	D , $10^{-5} \frac{\text{cm}^2}{\text{sec}}$	$\lambda = x/\sqrt{t}$, $10^{-3} \frac{\text{cm}}{\text{sec}^{1/2}}$	C_{Cu} , $10^{14} \frac{\text{at}}{\text{cm}^3}$
0.00	0	140.0	0.5	0	140.0	1.0	0	140.0	2.0
0.50	1.9	50.6	3.1	1.7	58.1	4.1	1.4	68.8	3.7
1.00	3.7	40.6	3.3	3.3	43.5	4.5	2.9	56.8	3.9
1.50	5.6	33.6	3.5	5.0	37.0	4.7	4.3	49.3	4.1
1.75									
2.00	7.4	27.5	3.6	6.7	28.9	4.9	5.8	40.5	4.2
2.38	8.7	17.4	3.9						
2.50	9.3	12.9	4.0	8.3	21.5	5.2	7.2	35.5	4.3
2.88							8.3	27.2	4.5
3.00	11.1	12.2	4.1	10.0	16.8	5.3	8.7	23.2	4.6
3.50	13.0	9.3	4.2	11.7	15.0	5.5	10.1	19.4	4.7
3.90				13.0	10.9	5.6			
4.00	14.8	5.8	4.3	13.3	7.6	5.7	11.5	16.6	4.6
4.50	16.7	3.3	4.5	15.0	7.1	5.8	13.0	12.3	4.8
5.00	18.5	0.5	4.8	16.7	6.1	5.7	14.4	8.1	4.9
5.50				18.3	4.9	5.9	15.9	4.6	5.1
6.00				20.0	3.9	6.0	17.3	2.7	5.2
6.50							18.8	1.0	5.3
7.00							20.2	0.2	5.5
		0.0	6.2		0.0	8.3		0.0	6.5

In equation (II) the symbol Cu_i is used in order to show that the compound will be formed mainly from interstitial Cu atoms, because they can move easily through the lattice. After heat treatment the compound Cu_3Ge will be distributed throughout the germanium in a dispersed phase. The two equations describe the general behavior of copper in germanium. Annealing at 500°C causes reaction (II) to go to the right, and therefore reaction (I) shifts to the left: the acceptor activity disappears and the lifetime increases. On the other hand, reheating at 800°C of such an annealed piece of germanium will restore the Cu_s concentration quite quickly throughout the whole crystal, a fact which is confirmed by experiment: after reheating only two minutes, followed by quenching, a sample was *p*-type throughout the whole crystal (3, 9). One can repeat this cycle of annealing and restoring the acceptor activity.

DIFFUSION

The diffusivity D of Cu does not seem to be a constant along the range of diffusion. A comparison of the measurements of Fuller and Struthers (2) with those of Fuller, Theuerer, and van Roosbroeck (8) shows that the D value computed from measurements at short diffusion times is 8 times smaller than the D value found from an experiment with a long diffusion time.

It is to be noted that the latter authors can fit their data on the diffusion-penetration curve with a

constant D of $8 \times 10^{-5} \text{ cm}^2/\text{sec}$, but with an effective starting concentration of one-tenth the saturation concentration of Cu at the given temperature. Furthermore, the work of Esaki (10) on the diffusion of thermal acceptors is of interest. He gives the value of 37,000 cal/mole for the activation energy, which is large compared to the value 12,000 cal/mole found by Fuller, Theuerer, and van Roosbroeck (8).⁴

A number of experiments were carried out by the authors to investigate these phenomena. Penetration curves (concentration C vs. depth x) of Cu and Ni diffusing in germanium at 800°C at different diffusing times were obtained from resistivity measurements. In making the experiments, samples were first thoroughly cleaned with pure HNO_3 in a soxhlet in the manner described earlier (3), then covered with copper on one side and heated. The cleaning step is necessary in order to avoid copper diffusion from side and rear surfaces. In later work a solution of Complexon III was used. Results for copper are given in Table I. Here it is assumed that each acceptor gives one hole in the valence band.⁵

⁴ According to a more recent paper by Fuller and co-workers (9) this value should not exceed 4500 cal/mole.

⁵ This does not have to be necessarily true if each Cu atom provides a second acceptor level with a rather high activation energy. In that case the number of acceptors will be dependent on the position of the Fermi level. In

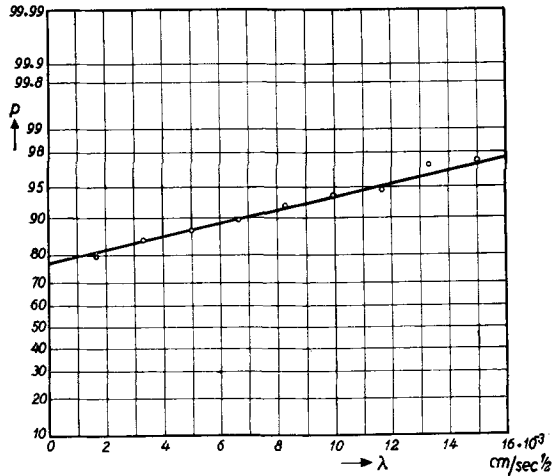


FIG. 1. Copper diffusion in germanium at 800°C during 15 min. $p = 50(2 - C/C_0)$ as a function of $\lambda = x/\sqrt{t}$.

Ordinary diffusion processes are governed by Fick's second law. In this case

$$\frac{\partial C}{\partial t} = \frac{\partial}{\partial x} \left(D \frac{\partial C}{\partial x} \right) \quad (\text{III})$$

or, for constant D ,

$$\frac{\partial C}{\partial t} = D \frac{\partial^2 C}{\partial x^2} \quad (\text{IV})$$

The experimental conditions are that at $x = 0$, the concentration is equal to the saturation concentration C_0 for all times, and the internal concentration C is equal to zero at $t = 0$. In that case the solution of (IV) can be written as

$$\frac{C}{C_0} = 1 - \operatorname{erf} \frac{x}{2\sqrt{Dt}} \equiv 1 - \operatorname{erf} \tau = \operatorname{erfc} \tau \quad (\text{V})$$

$$\operatorname{erf} \tau = \frac{2}{\sqrt{\pi}} \int_0^\tau e^{-z^2} dz \quad \tau = \frac{x}{2\sqrt{Dt}}$$

Introducing $\frac{x}{\sqrt{t}} = \lambda$, (V) can be rewritten as

$$\frac{C}{C_0} = 1 - \operatorname{erf} h\lambda = \operatorname{erfc} h\lambda \text{ and } h = \frac{1}{2\sqrt{Dt}} \quad (\text{VI})$$

When the experimental concentration C is plotted as a function of λ , the curves do not seem to follow the ordinary error function denoted by (VI). This indicates that D is not simply a constant.

It was shown by Boltzmann that, in case D is a function of C , the solution of Fick's law under the same initial conditions as given above is still of the

experiments with Ni this is taken into account by calculation (Table II). Experiments with Cu have shown that the number of acceptors for a given concentration of Cu is, to a large extent, independent of the position of the Fermi level. (To be published in *Physica*.) This holds also in the case of the diffusion experiments.

form $C = C \left(\frac{x}{\sqrt{t}} \right)$. Then D at various C can be found by integration of (III) leading to (11)

$$D = -\frac{1}{2} \frac{d\lambda}{dC} \int_0^C \lambda dC \quad (\text{VII})$$

An expedient method of computing D has recently been reported by Hall (12). One can plot C/C_0 on probability paper and see whether one obtains a straight line. In all cases for Cu and Ni the authors found that the greatest part of the penetration curve plotted in this way gives a straight line; an example is given in Fig. 1: the values of Table I for $t = 15'$ are used.

The straight line can be expressed as:

$$C/C_0 = \operatorname{erfc}(h\lambda + k) = \operatorname{erfc} u \quad (\text{VIII})$$

Applying (VII) to (VIII) leads to

$$D = \frac{1}{4h^2} - \frac{k\sqrt{\pi}}{4h^2} e^{u^2} \operatorname{erfc} u \quad (\text{IX})$$

the constants h and k are the slope and intercept, respectively, of the straight line in Fig. 1 and $k = 0$ gives the ordinary error function (VI) with a constant D . The values of D in Table I are those calculated from (IX). D varies appreciably.⁶

Results on Ni diffusion are listed in Table II. According to the authors' measurements of the resistivity and Hall effect of Ni-saturated samples, Ni atoms produce one acceptor level lying 0.23 eV above the valence band. This is in agreement with values of 0.25–0.30 eV given by Burton (4).

In calculating the values of C from the resistivity measurements it has been taken into account that acceptors with such a high energy are not completely exhausted. The fraction α of the acceptors which give free holes is given in the table.

The question arises as to whether C is a function of $\frac{x}{\sqrt{t}} = \lambda$ or not. Fig. 2 and 3 show penetration curves for various diffusion times for Cu and for Ni, respectively; C is plotted as a function of λ . It is apparent that the curves do not coincide; this is very clear in the case of Ni. The curves show a shift downward when t decreases; hence C is not a function of λ alone.

It should be mentioned that if C is not a function of λ alone, D is not a function of C alone. Therefore, D calculated from (VII) is not a real diffusivity but

⁶ According to Fuller and coworkers (9) equation (IV) is obeyed, and D , therefore, should be a constant. With respect to this it should be noted that the C_0 values the authors used are taken from direct resistivity measurements of the interior of saturated samples. Fuller and collaborators use C_0 values obtained by extrapolation of the diffusion experiments.

TABLE II. Ni

Time (<i>t</i>) (min)	10.5					15				
	$\lambda = x/\sqrt{t}$, $10^{-3} \frac{\text{cm}}{\text{sec}^{1/2}}$	$(p - n + N_d)$ $10^{14} \frac{\text{at}}{\text{cm}^3}$	α	C_{Ni} , $10^{14} \frac{\text{at}}{\text{cm}^3}$	D , $10^{-5} \frac{\text{cm}^2}{\text{sec}}$	$\lambda = x/\sqrt{t}$, $10^{-3} \frac{\text{cm}}{\text{sec}^{1/2}}$	$(p - n + N_d)$ $10^{14} \frac{\text{at}}{\text{cm}^3}$	α	C_{Ni} , $10^{14} \frac{\text{at}}{\text{cm}^3}$	D , $10^{-5} \frac{\text{cm}^2}{\text{sec}}$
0				15.95					15.95	0.4
0.25	1.0	2.72	0.970	2.80	2.8	0.8	5.96	0.921	6.47	3.5
0.50	2.0	2.67	0.971	2.75	2.8	1.7	5.49	0.929	5.91	3.6
0.75	3.0	2.40	0.975	2.46	3.0	2.5	5.08	0.935	5.44	3.8
1.00	4.0	2.18	0.979	2.23	3.0	3.3	4.80	0.940	5.10	3.9
1.25	5.0	2.14	0.979	2.18	3.1	4.1	4.51	0.944	4.78	3.9
1.50	6.0	2.04	0.981	2.08	3.1	5.0	4.23	0.949	4.45	4.0
1.75	7.0	1.94	0.982	1.98	3.2	5.8	3.90	0.954	4.09	4.1
2.00	8.0	1.87	0.983	1.90	3.2	6.7	3.40	0.962	3.53	4.2
2.20	8.8	0.93	1.00	0.93	3.9					
2.25	9.0	0.58	1.00	0.58	4.2	7.5	3.14	0.966	3.25	4.3
2.50	10.0	0.55	1.00	0.55	4.3	8.3	2.81	0.971	2.89	4.4
2.75	11.0	0.51	1.00	0.51	4.3	9.2	2.41	0.977	2.47	4.6
3.00	12.0	0.48	1.00	0.48	4.3	10.0	2.21	0.980	2.26	4.6
3.25	13.0	0.43	1.00	0.43	4.4	10.8	2.08	0.982	2.12	4.7
3.50	14.0	0.34	1.00	0.34	4.5	11.7	1.95	0.984	1.98	4.7
3.75	15.0	0.29	1.00	0.29	4.5	12.5	1.80	0.988	1.82	4.8
3.90						13.0	1.07	1.00	1.07	5.0
4.00	16.0	0.21	1.00	0.21	4.7	13.3	0.81	1.00	0.81	5.1
4.25	17.0	0.20	1.00	0.20	4.8	14.1	0.78	1.00	0.78	5.1
4.50	18.0	0.11	1.00	0.11	4.9	15.0	0.72	1.00	0.72	5.1
4.75	19.0	0.08	1.00	0.08	5.1	15.8	0.62	1.00	0.62	5.3
5.00	20.0	0.07	1.00	0.07	5.1	16.7	0.52	1.00	0.52	5.3
5.25						17.5	0.47	1.00	0.47	5.3
5.50						18.3	0.41	1.00	0.41	5.4
5.75						19.2	0.37	1.00	0.37	5.4
6.00						20.0	0.33	1.00	0.33	5.6
∞					8.1					7.6

an apparent one. The variation of the apparent D with λ calculated according to (IX) shows in all cases the same behavior and is represented for Cu and Ni in Fig. 4, the values being taken from the tables at $t = 900$ sec.

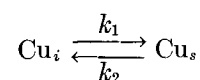
The experimental facts just presented indicate that the diffusion process is more complicated than one would expect.

For an ordinary diffusion process of one kind of particles one would not expect any influence of the concentration upon D because this quantity is very small. It is quite possible, however, that diffusion of just one kind of particles does not occur in this case, and that a diffusion of two species, namely, Cu_i and Cu_s , must be considered. Moreover, if these two can interchange, it is clear that application of Fick's second law as given in (III) is not permissible.

Giving these considerations a more strict form one arrives at the following picture which makes it possible to understand a variation of the apparent D regardless of the small concentration of the impurities.

1. Cu_s and Cu_i atoms have different constants D_s and D_i , where it is likely that $D_s < D_i$

2. During diffusion, the Cu_s and Cu_i atoms are subjected to the reactions



where k_1 and k_2 are reaction constants.

Accordingly, the concentrations N_s and N_i of Cu_s and Cu_i have to obey the following equations:

$$\frac{\partial N_s}{\partial t} = D_s \frac{\partial^2 N_s}{\partial x^2} + k_1 N_i - k_2 N_s$$

$$\frac{\partial N_i}{\partial t} = D_i \frac{\partial^2 N_i}{\partial x^2} - k_1 N_i + k_2 N_s$$

In the following, two extreme cases will be considered: (a) k_1 and k_2 very large; (b) k_1 and k_2 very small.

(a) If the rate of exchange between Cu_i and Cu_s is very large (k_1 and $k_2 \rightarrow \infty$), the ratio of N_i and N_s is equal to k_2/k_1 for every x and t . In that case

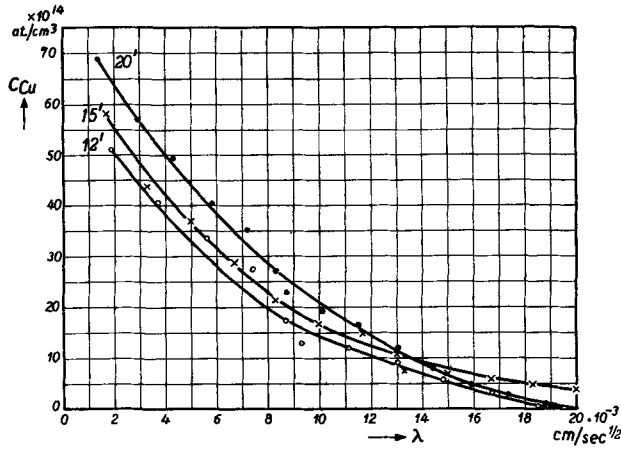


FIG. 2. Copper concentration as a function of $\lambda = x/\sqrt{t}$ at different times.

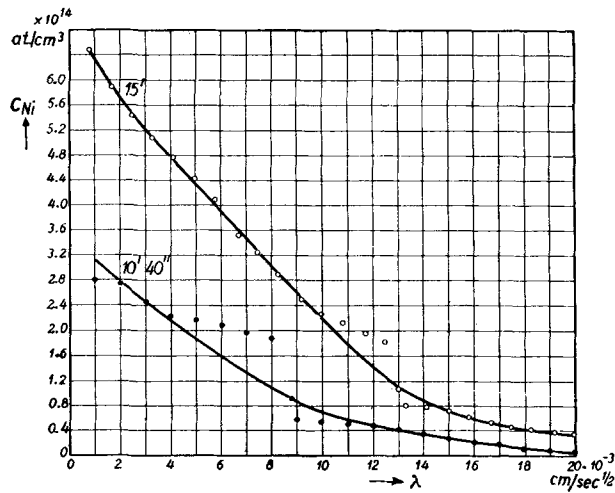


FIG. 3. Nickel concentration as a function of $\lambda = x/\sqrt{t}$ at different times.

solutions for the total concentration N_{tot} and the concentrations N_i and N_s are error functions:

$$N_{tot} = N_0 \operatorname{erfc} \tau$$

$$N_i = \frac{k_2}{k_1 + k_2} N_0 \operatorname{erfc} \tau, N_s = \frac{k_1}{k_1 + k_2} N_0 \operatorname{erfc} \tau \quad (\text{XI})$$

N_0 is the total concentration at $x = 0$, which is supposed to be constant for all t , furthermore

$$\tau = \frac{x}{2\sqrt{Dt}} D = \frac{k_2 D_i + k_1 D_s}{k_1 + k_2} = \text{constant}$$

(b) An approximate solution for small reaction constants k_1 and k_2 can be written as

$$N_s = \frac{k_1}{k_1 + k_2} N_0 \operatorname{erfc} \tau_s + \frac{k_1 k_2 N_0 t}{k_1 + k_2} \frac{1}{1 - \gamma^2}$$

$$\left[\frac{2}{\sqrt{\pi}} \gamma^2 \tau_s e^{-\tau_s^2} + (1 + 2\tau_s^2)(\operatorname{erf} \tau_s - \operatorname{erf} \tau_i) - \frac{2}{\sqrt{\pi}} \tau_i e^{-\tau_i^2} \right] \quad (\text{XII})$$

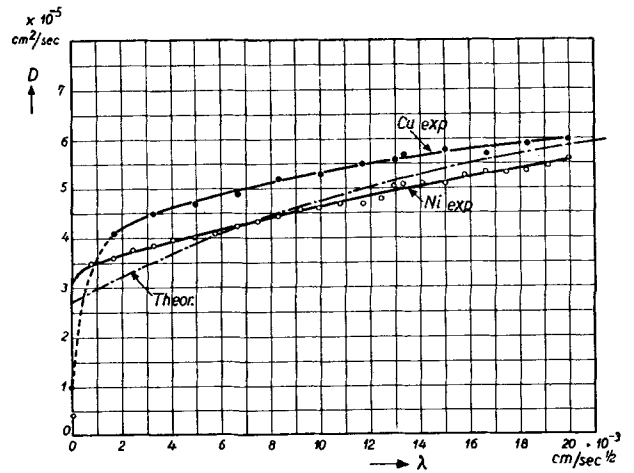


FIG. 4. The diffusion coefficient D for Cu and Ni at 800°C as a function of $\lambda = x/\sqrt{t}$.

where

$$\tau_s = \frac{x}{2\sqrt{D_s t}} \quad \tau_i = \frac{x}{2\sqrt{D_i t}} \quad \gamma = \sqrt{\frac{D_s}{D_i}}$$

At $x = 0$, the quotient $N_s/N_i = k_1/k_2$ is supposed to be a constant.

When $D_s \ll D_i$, i.e., $\gamma \rightarrow 0$, τ_i will be small compared to τ_s . For a given time (XII) can be simplified to

$$N_s = \text{const.} \left[(1 + 2\tau_i^2) \operatorname{erfc} \tau_i - \frac{2}{\sqrt{\pi}} \tau_i e^{-\tau_i^2} \right] \quad (\text{XIII})$$

$$= \text{const.} i^2 \operatorname{erfc} \tau_i$$

$i^n \operatorname{erfc} \tau_i$ denotes the n times integrated error function. One can replace (XII) by (XIII) except for very small x .

With (VII) D can be calculated from (XIII) as a function of τ_i . The result is

$$\frac{D}{D_i} = \frac{1}{3} \frac{4\tau_i^3 \operatorname{erfc} \tau_i + (1 - 2\tau_i^2) \frac{2}{\sqrt{\pi}} e^{-\tau_i^2}}{2i^2 \operatorname{erfc} \tau_i} \quad (\text{XIV})$$

If one assumes D_i to be a certain value, say, $8.1 \cdot 10^{-5}$ cm\$^2\$/sec, D can be calculated from (XIV) as a function of λ . For τ_i or $\lambda = 0$, $D/D_i = 1/3$; for τ_i or $\lambda = \infty$, $D/D_i \rightarrow 1$. D as a function of λ is plotted in Fig. 4 (theoretical curve).

The experimental and theoretical curves show an agreement; it must be pointed out, however, that validity of (XII) can only be expected when the k_2 value is small, that is, of the order of 10^{-3} sec\$^{-1}\$. In this way the diffusion experiments give support to the general picture given above.

ACKNOWLEDGMENT

The authors are indebted to Mr. F. H. Stieltjes for his help in the solution of the differential equations and especially for his valuable discussions.

Any discussion of this paper will appear in a Discussion Section to be published in the December 1955 JOURNAL.

REFERENCES

1. H. C. THEUERER AND J. H. SCAFF, *J. Metals*, **191**, 59 (1951).
2. C. S. FULLER AND J. D. STRUTHERS, *Phys. Rev.*, **87**, 526 (1952).
3. F. V.D. MAESEN, P. PENNING, AND A. V. WIERINGEN, *Philips Research Repts.*, **8**, 241 (1953); F. V.D. MAESEN AND J. A. BREKMAN, *ibid.*, **9**, 225 (1954).
4. J. A. BURTON, G. W. HULL, F. J. MORIN, AND J. C. SEVERIENS, *J. phys. Chem.*, **57**, 853 (1953).
5. D. NAVON, R. BRAY, AND H. Y. FAN, *Proc. I.R.E.*, **40**, 1342 (1952).
6. F. J. MORIN AND J. P. MAITA, *Bull. Am. Phys. Soc.*, **28**, 8 (1953).
7. W. SHOCKLEY AND W. T. READ, *Phys. Rev.*, **87**, 835 (1952).
8. C. S. FULLER, H. C. THEUERER, AND W. VAN ROOSBROECK, *Phys. Rev.*, **85**, 678 (1952); W. C. DUNLAP, JR., *ibid.*, **94**, 1531 (1954).
9. C. S. FULLER, J. D. STRUTHERS, J. A. DITZENBERGER, AND K. B. WOLFSTIRN, *ibid.*, **93**, 1182 (1954).
10. L. ESAKI, *ibid.*, **89**, 1026 (1953).
11. C. MATANO, *J. Phys. (Japan)*, **8**, 109 (1933); "Atom Movements," Chicago (1950).
12. L. D. HALL, *J. Chem. Phys.*, **21**, 87 (1953).

Polarographic Studies in Acetonitrile and Dimethylformamide

II. Behavior of Aromatic Olefins and Hydrocarbons¹

S. WAWZONEK, E. W. BLAHA,²

R. BERKEY,² AND M. E. RUNNER³

Department of Chemistry, State University of Iowa, Iowa City, Iowa

ABSTRACT

Stilbene, anthracene, and 9-anisylidene-fluorene are reduced stepwise polarographically in anhydrous acetonitrile and in dimethylformamide. Triphenylethylene, tetraphenylethylene, styrene, and 1,1-diphenylethylene give only one reduction wave. Large-scale electrolytic reductions in these solvents indicate that carbanion intermediates exist for a short period of time. 1,2,3,4-Tetraphenylbutane and *meso*-diphenylsuccinic acid have been prepared electrolytically from stilbene in dimethylformamide.

INTRODUCTION

Previous work on the polarographic behavior of inorganic salts in acetonitrile (1) has indicated that this solvent is suitable for studies in this field. The work has now been extended to the study of aromatic olefins and hydrocarbons, examples of irreversible organic systems. Since the results in dimethylformamide were quite similar to those obtained in acetonitrile, data obtained in both solvents are treated together.

EXPERIMENTAL

Polarograms were obtained in a manner similar to that described previously (1). Characteristics for the dropping mercury electrode used in acetonitrile were the same as given before (1). The dropping mercury electrode for the studies in dimethylformamide was used at 60 cm pressure and had a drop time of 3.91 sec (open circuit). The $m^{2/3} t^{1/6}$ value was $1.77 \text{ mg}^{2/3} \text{ sec}^{-1/2}$. The resistance of the electrolysis cell using dimethylformamide as a solvent with 0.2M tetrabutylammonium iodide as the supporting electrolyte was found to be 500 ohms.

Materials

Dimethylformamide was purified in the following manner. A sample dried over anhydrous potassium carbonate for several days was distilled through an 80 cm Fenske column. The first 200 ml of the distillate was discarded and the fraction boiling at

151.5°–153°C collected. Tetrabutylammonium iodide was prepared according to directions in the literature (2). Tetrabutylammonium bromide was prepared by a variation of the directions of Hager and Marvel (3). A solution of tri-*n*-butylamine (156 g) and *n*-butyl bromide (116 g) in anhydrous ethyl acetate (400 ml) was refluxed for 48 hr. The resulting solution on cooling gave crystalline tetra-*n*-butylammonium bromide. Several recrystallizations from anhydrous ethyl acetate gave a product (64 g) melting at 115°–116°C.

The acetonitrile was purified in a similar fashion to that reported previously (1).

Experimental Techniques of Electrolyses

Electrolyses were carried out in a cell similar in construction to that used by Lingane (4) with a 7 mm tube fitted with a stopcock connecting the two flasks at their mid-points. The purpose of this additional tube was to counteract the electrical osmosis which occurred during the electrolyses; the solution flowed from the anode to the cathode compartment. Purified nitrogen was passed through both compartments for an hour to remove the dissolved oxygen. The mercury pool used as a cathode had an area of approximately 50 cm². The anode was either a stirred mercury pool or a platinum electrode with an area of 65 cm². The direct current obtained from an 85 v generator was not controlled. Electrolyses were carried out with stirring and with cooling by an ice bath to prevent loss of the solvent; otherwise, heat was usually generated in a run and caused the solvent to boil. Analysis of gases given off during the electrolysis was accomplished by an absorption train attached to the cell, consisting of an ice trap, a 10% hydrochloric acid trap, an ascarite tube, an anhydrone tube, and a dry ice trap. The effluent

¹ Manuscript received August 13, 1954. The greater part of this research was done under A.E.C. Contract AT(11-1)-72, Project No. 6.

² Abstracted in part from the Ph.D. Theses of E. W. Blaha (1954) and R. Berkey (1955).

³ National Institute of Health Postdoctorate Fellow 1949–50. Present address: Department of Chemistry, Illinois Institute of Technology, Chicago, Illinois.

gases were then passed through a column of iodine pentoxide at 155°. Iodine, formed from the oxidation of hydrogen and carbon monoxide liberated in the electrolysis, was condensed in an air-cooled tube and the resulting water and carbon dioxide collected in anhydrous and ascarite tubes, respectively, after purification by passing over a plug of silver wool at 350°C to remove any traces of iodine carried over.

Electrolyses in Dimethylformamide

Following is a typical electrolysis in dimethylformamide. To the reduction cell containing a stirred mercury pool cathode and a platinum anode was added a solution of stilbene (10 g) in dimethylformamide (350 ml) which was 0.155*M* with respect to tetrabutylammonium iodide. The solution in both compartments was deaerated with nitrogen for one hour. Direct current was passed through the cell for 22 hr starting with a value of 0.42 amp and gradually decreasing to 0.17 amp at the end of the electrolysis. During the electrolysis a violet-black color streamed from the sintered glass disk into the catholyte. This color varied with the compound reduced and the inert electrolyte used.

After the electrolysis, anolyte and catholyte were combined and distilled under reduced pressure to remove the dimethylformamide and other volatile substances. From this distillate there could be isolated tri-*n*-butylamine (3.4–5.7 g) by acidifying with dilute hydrochloric acid, removing the dimethylformamide under reduced pressure, and neutralizing the residue with alkali. Identification was made by forming tri-*n*-butylmethylammonium iodide, mp 178°C (5).

The residue from the distillation was steam distilled and the distillate extracted with ether. The ether solution gave, after removal of traces of tri-*n*-butylamine with acid, pure bibenzyl (6.37 g), mp 52°C. The residue from steam distillation when extracted with ether gave 1,2,3,4-tetraphenylbutane and, occasionally, stilbene. Separation of the two hydrocarbons was accomplished by reducing the stilbene to bibenzyl with sodium (23.0 g) in absolute ethanol (200 ml) and steam distilling. The nonvolatile 1,2,3,4-tetraphenylbutane, after one recrystallization from ethanol, melted at 86° and proved identical with the lower melting isomer obtained by the sodium-alcohol reduction of 2,3,4,5-tetraphenylthiophene (6).

The steam distillation residue left after the ether extraction of the hydrocarbons proved to be a mixture of ditetrabutylammonium tetraiodomercurate, tetrabutylammonium iodide, and tetrabutylammonium triiodide (1.8 g). Separation was effected by dissolving the residue in hot ethanol. The ditetrabutylammonium tetraiodomercurate (2–6 g)

crystallized and melted at 132°C. The alcohol filtrate gave tetrabutylammonium iodide when treated with an excess of ether. Removal of the solvent from the filtrate gave tetrabutylammonium triiodide (1.8 g) which melted at 69°C after one crystallization from ethyl acetate (7).

The liquid (0.5–0.8 g) collected in the dry ice trap proved to be a mixture of butene-1 and *n*-butane. The butene-1 was identified by conversion to 1,2-dibromobutane. Presence of *n*-butane was demonstrated by combustion in an Orsat gas analyzer after removal of the butene-1 with concentrated sulfuric acid.

Carbon monoxide and hydrogen were determined by oxidation with iodine pentoxide to carbon dioxide and water and collecting these substances.

meso-Diphenylsuccinic acid.—A solution (200 ml) of 0.155*M* tetrabutylammonium iodide in dimethylformamide containing stilbene (3.0 g) was electrolyzed, using a stirred mercury cathode and a platinum anode. For one hour prior to electrolysis and during the electrolysis, carbon dioxide was passed through the solution. The electrolysis was carried out for 19 hr using a current of 0.32 amp. The catholyte remained colorless throughout this period. Removal of the solvent under reduced pressure was followed by the addition of 10% sodium hydroxide (100 ml) and steam distillation. From the distillate a small amount of bibenzyl (0.1 g) was obtained. The solution left in the distillation flask was filtered from the precipitated tetrabutylammonium iodide and ditetrabutylammonium tetraiodomercurate and acidified with excess dilute hydrochloric acid. Crystals obtained after one crystallization from methanol melted at 229°C and proved to be *meso*-diphenylsuccinic acid by comparison with an authentic sample (8), yield, 4.1 g (92%).

1,1,2-Triphenylethane.—Triphenylethylene (3.0 g) in a dimethylformamide solution (280 ml) of 0.193*M* tetrabutylammonium iodide was reduced electrolytically for 19 hr in a cell similar to that described for the reduction of stilbene. The current, which was 0.53 amp at the beginning, gradually decreased to 0.36 amp at the end of the electrolysis. The catholyte assumed a bright violet color during this period.

Removal of the solvent under reduced pressure gave a brown residue (22.9 g) which was extracted with ether. The ether extract after removal of tri-*n*-butylamine with dilute acid gave 1,1,2-triphenylethane (2.8 g). Recrystallization from ethanol gave a sample melting at 53°–54°C (9).

Electrolyses in Acetonitrile

The following procedure was used for the reduction of stilbene and triphenylethylene. Stilbene

(5.0 g) was reduced electrolytically in acetonitrile (300 ml) which was 0.45*M* in tetrabutylammonium iodide. The current, which was passed through the cell for 10 hr, started at 0.52 amp and gradually decreased to 0.34 amp. The catholyte turned a bright green; if the current was turned off, the green changed to red which then faded to a light yellow. Removal of the solvent from the combined catholyte and anolyte gave a brown residue which was steam distilled. The distillate yielded bibenzyl (4.0 g), mp 51°–52°C. The residue from the steam distillation when dissolved in hot ethanol gave, on cooling, ditetrabutylammonium tetraiodomercurate (11 g), mp 131°–132°C. The alcohol filtrate upon removal of the solvent gave a solid, from which 4-amino-2,6-dimethylpyrimidine (0.02 g) sublimed when heated at 200°C under reduced pressure (1 mm). A mixture of this compound with an authentic sample (10) melted at the same point.

Electrolysis of a similar solution without stilbene gave ditetrabutylammonium tetraiodomercurate, 4-amino-2,6-dimethylpyrimidine, and tri-*n*-butylamine. No hydrogen butane or 1-butene were detected.

Substitution of a mercury anode for the platinum anode in the reduction of stilbene gave a comparable yield of bibenzyl.

Use of tetrabutylammonium bromide as the inert electrolyte in the reduction of stilbene gave only bibenzyl and 4-amino-2,6-dimethylpyrimidine.

1,1,2,2-Tetraphenylethane.—A suspension of tetraphenylethylene (5.0 g) in acetonitrile (250 ml) which was 0.175*M* in tetrabutylammonium iodide, was electrolyzed for 23.5 hr. The current was 0.5 amp at the beginning and gradually decreased to 0.12 amp at the end. During this time, a dark violet color was produced in the cathode compartment. The resulting solution was filtered from the unchanged tetraphenylethylene (0.4 g) and gave, after removal of the solvent, a brown residue (25.4 g). Treatment of this material with hot ethanol (100 ml) gave the insoluble 1,1,2,2-tetraphenylethane which was recrystallized from a benzene-ethanol mixture; yield, 2.4 g; mp 204°–206°C. The alcohol filtrate upon cooling gave ditetrabutylammonium tetraiodomercurate (1.8 g). Removal of alcohol, followed by steam distillation, gave diphenylmethane (2.0 g), mp 25°–26°C. The melting point was not depressed when this compound was mixed with an authentic sample (11).

1,2-Diphenylbutane.—A solution of stilbene (5 g) and ethyl iodide (23 ml) in acetonitrile (250 ml), which was 0.175*M* in tetrabutylammonium iodide, was electrolyzed for 19 hr. The current which started at 0.64 amp gradually decreased to 0.02 amp at the end of the run. Removal of the solvent gave a brown residue (20 g) which was taken up in ether and washed with dilute hydrochloric acid. The residue obtained after removing the ether was subjected to fractional distillation under reduced pres-

TABLE I. Half-wave potentials, diffusion currents, and diffusion current constants of various compounds in solutions indicated

Compound	Conc. millimoles/liter	$i_d, \mu a$		I_d^*		$E_{1/2}$ (v) vs. Hg pool		0.059/ n^{**}	
		1st wave	2nd wave	1st wave	2nd wave	1st wave	2nd wave	1st wave	2nd wave
Acetonitrile—0.1 <i>M</i> tetrabutylammonium bromide									
$(C_6H_5)_2C=C(C_6H_5)_2$	1.0	6.56	—	4.31	—	–1.62	—	0.028	—
$(C_6H_5)_2C=CHC_6H_5$	1.0	7.36	—	4.84	—	–1.67	—	0.089	—
$(C_6H_5)_2C=CH_2$	1.0	8.65	—	5.69	—	–1.92	—	0.032	—
$C_6H_5CH=CHC_6H_5$ (trans)....	1.0	4.67	2.68	3.07	1.76	–1.73	–2.06	0.078	0.086
$C_6H_5CH=CHC_6H_5$ (cis).....	1.0	5.57	2.29	3.66	1.50	–1.81	–2.11	0.025	0.095
Anthracene.....	1.0	4.77	2.88	3.14	1.89	–1.48	–2.06	0.073	0.078
Ethyl iodide.....	8.28	88.0	—	6.15	—	–1.85	—	—	—
Dimethylformamide—0.2 <i>M</i> Tetrabutylammonium iodide									
$C_6H_5CH=CH_2$	2.31	13.1	—	3.21	—	–1.96	—	0.145	—
$C_6H_5CH=CHC_6H_5$ (trans)....	1.20	4.10	3.21	1.92	1.51	–1.61	–2.02	0.069	0.075
$C_6H_5CH=CHC_6H_5$ (trans)†...	1.20	3.55	2.67	—	—	–1.64	–2.02	0.068	0.075
9- <i>p</i> - $CH_3OC_6H_4CH=CC_{12}H_8$ ‡...	1.20	3.40	3.02	1.64	1.42	–1.17	–1.56	0.057	0.050
CO ₂ §.....	—	—	—	—	—	–2.05	—	—	—

$$* I_d = \frac{i_d}{C_m^{2/3} t^{1/6}}$$

** From current-voltage curve analysis.

† Hg height = 40 cm instead of 60 cm.

‡ *p*-Anisylideneffluorene.

§ Concentration not known.

TABLE II. Effect of proton donors on the polarographic behavior of hydrocarbons in acetonitrile—0.175M tetrabutylammonium bromide

Compound ^a	Water added to 20 ml soln (ml)	$i_{d\mu a}$		$E_{1/2}(v)$ vs. Hg pool		$0.059/n^b$	
		1st wave	2nd wave	1st wave	2nd wave	1st wave	2nd wave
Anthracene	0	4.77	2.88	-1.48	-2.06	0.073	0.078
	0.1	4.97	3.78	-1.49	-2.06	0.062	0.098
	0.2	5.27	3.28	-1.54	-2.10	0.043	0.095
	0.5	5.87	2.58	-1.58	-2.13	0.076	0.085
	1.0	7.36	1.0 ^c	-1.63	-2.2 ^c	0.060	— ^c
Stilbene (trans)	0	4.67	2.68	-1.73	-2.06	0.078	0.086
	0.2	7.26	1.5 ^c	-1.80	-2.2 ^c	0.069	— ^c
	0.5	8.75	—	-1.81	—	0.033	—
Stilbene (cis)	0	5.57	2.29	-1.81	-2.11	0.025	0.095
	0.1	7.95	1.2 ^c	-1.80	-2.1 ^c	0.056	— ^c
	0.5	8.65	—	-1.84	—	0.038	—
<i>p</i> -Anisylidenefluorene ^d	0	2.91	2.52	-1.17	-1.56	0.057	0.050
Benzoic acid ^{d, e}	0	6.74	—	-1.58	—	—	—
<i>p</i> -Anisylidenefluorene and benzoic acid ^{d, f}	0	4.76	—	-1.11	—	— ^g	—

^a 0.001M solutions.^b From current-voltage curve analysis.^c Supporting electrolyte discharge interferes.^d In dimethylformamide containing 0.2M (C₄H₉)₄NI.^e 0.003M solution.^f 0.985 Millimoles of *p*-anisylidene fluorene and 3.32 millimoles of benzoic acid.^g Maximum present.

TABLE III. Large-scale electrolytic reductions of hydrocarbons in acetonitrile and dimethylformamide

Amount of hydrocarbon	Electrolyte	Anode	Colors observed	Current used amp		Time of electrolysis (hr)	Products formed
				Start	Finish		
5.0 g Stilbene	CH ₃ CN - 0.145M (C ₄ H ₉) ₄ NI (300 ml)	Pt	Green-red-yellow	0.5	0.05	22	C ₆ H ₅ CH ₂ CH ₂ C ₆ H ₅ (3.9 g) C ₆ H ₅ CH=CH ₂ C ₆ H ₅ (0.8 g)
3.0 g Stilbene	CH ₃ CN - 0.175M (C ₄ H ₉) ₄ NI (200 ml)	Hg	Greenish-black	0.5	0	24	C ₆ H ₅ CH ₂ CH ₂ C ₆ H ₅ (2.5 g)
5.0 g Triphenylethylene	CH ₃ CN - 0.154M (C ₄ H ₉) ₄ NI (300 ml)	Pt	Bright violet	0.5	0.12	22	(C ₆ H ₅) ₂ CHCH ₂ C ₆ H ₅ (5.0 g)
3.0 g Triphenylethylene	HCON(CH ₃) ₂ - 0.193M (C ₄ H ₉) ₄ NI (280 ml)	Pt	Bright violet	0.53	0.36	19	(C ₆ H ₅) ₂ CHCH ₂ C ₆ H ₅ (2.8 g)
5.0 g Tetraphenylethylene (partially insoluble)	CH ₃ CN - 0.175M (C ₄ H ₉) ₄ NI (250 ml)	Pt	Dark violet	0.40	0.12	23.5	(C ₆ H ₅) ₂ CHCH(C ₆ H ₅) ₂ (2.4 g) (C ₆ H ₅) ₂ CH ₂ (2.0 g) (C ₆ H ₅) ₂ C=C(C ₆ H ₅) ₂ (0.4 g)

sure and fractional crystallization. The lower boiling fraction upon steam distillation gave an oil which, after two distillations at atmospheric pressure, had the physical properties of 1,2-diphenylbutane, bp 288°C, n_D^{20} 1.554 (12).

Anal. calc'd for C₁₆H₁₈: C, 91.37; H, 8.63

Found: C, 91.21; H, 8.64

The amount isolated was insufficient to make a solid derivative.

*Ditetra-*n*-butylammonium tetraiodomercurate*.—Mercuric iodide (2.0 g) and tetra-*n*-butylammonium iodide (3.2 g) were refluxed in 50% ethanol (50 ml) until the mercuric iodide turned white. More ethanol (25 ml) was added and the solution heated

TABLE IV. *Electrolyses products from stilbene in dimethylformamide—0.155M (C₄H₉)₄NI in millimoles*

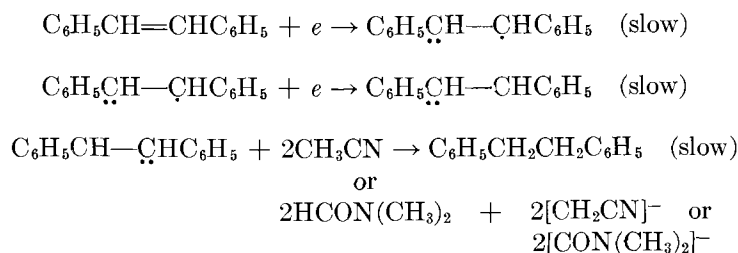
Stilbene used	Bi-benzyl formed	1,2,3,4-Tetra phenyl-butane Formed	H ₂ re-quired for stilbene reduction	CO obtained	H ₂ obtained	CO due to stilbene reduction	H ₂ due to stilbene reduction
0	0	0	0	6.4	13.0	0	0
13.9	12.6	0.8	13.4	23.5	46.4	17.1	33.0
27.8	24.7	1.4	26.1	33.5	69.9	27.1	56.9
55.6	13.2	6.4	19.6	25.5	51.0	19.1	38.0
55.6	35.6	8.8	44.4	35.5	71.0	29.1	58.0

to reflux. Cooling gave a white curdy precipitate which was recrystallized from ethyl acetate, yield, 4.9 g, mp 131°–132°C.

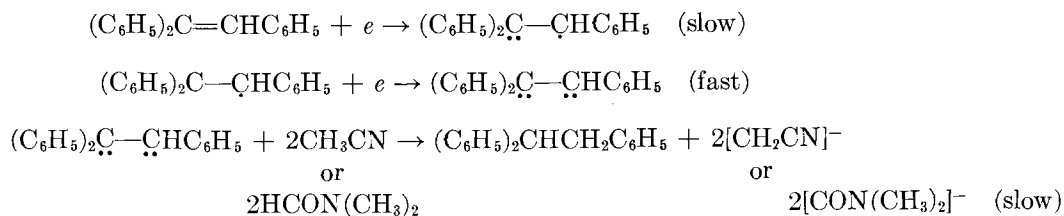
Anal. calc'd for C₃₂H₇₂N₂HgI₄: C, 32.25; H, 6.05; N, 2.35.
Found: C, 32.23; H, 5.93; N, 2.40

Results

Polarographic data obtained for the various hydrocarbons in acetonitrile and dimethylformamide containing tetrabutylammonium iodide and bromide are given in Table I. The waves in all cases were well defined. Since the availability of protons in these solvents is very poor, the effect of water and benzoic acid upon the polarographic waves was studied and is given in Table II.



To help formulate electrode reactions, large-scale reductions of the various hydrocarbons were carried out in acetonitrile and dimethylformamide, and the products are summarized in Table III. In the electrolyses in dimethylformamide, hydrogen and carbon monoxide were obtained as by-products. The amounts of these obtained in the reduction of varying amounts of stilbene are given in Table IV.



DISCUSSION OF RESULTS

Examination of results in Table I indicates that the polarographic behavior of aromatic olefins and hydrocarbons in acetonitrile and dimethylformamide is similar to that observed in 75% dioxane (3, 13) except for the behavior of three compounds. Stilbene, 9-anisylidene-fluorene, and anthracene are reduced stepwise and give two polarographic waves. The sum total of the two waves, however, is approximately equal to the height of the one wave observed with triphenylethylene which shows a normal behavior.

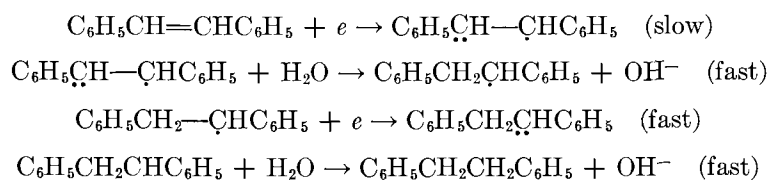
The two waves for these compounds are markedly affected by the addition of small amounts of water or benzoic acid as is shown in Table II. At a high enough concentration (2.44%) of water, the two waves for stilbene are replaced by one wave with a height equal approximately to the combined heights of the two waves obtained in anhydrous media. Benzoic acid exerts its effect on the waves of *p*-anisylidene-fluorene at a much lower concentration. This behavior is in agreement with the more acidic nature of benzoic acid. It was not possible to use this proton donor with stilbene because the discharge of hydrogen ions occurred before the reduction of the olefin.

These results indicate that the following mechanism of reduction, using stilbene as an example, applies to these three compounds:

Analyses of the current-voltage curves were not consistent; the majority of the values, however, approximated 0.059. Varying the height of the mercury reservoir for stilbene indicated that the currents for both waves were diffusion-controlled.

The reduction of the other hydrocarbons, which show only one polarographic wave, must differ from the above in that the second step, illustrated with triphenylethylene, is a rapid reaction.

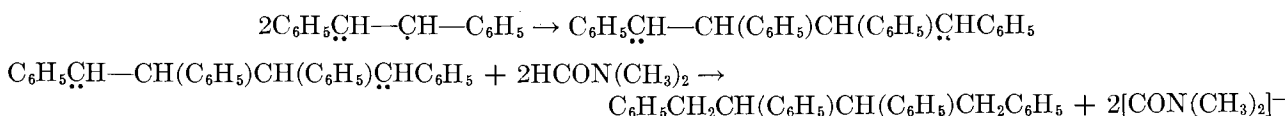
In the presence of water or other acidic materials the mechanism of reduction must be the following:



The second step under these conditions involves a rapid reaction with water to give a free radical which is reduced immediately. These steps must

formamide, however, it was possible to isolate, in addition to the bibenzyl, up to a 30% yield of the

lower melting isomer of 1,2,3,4-tetraphenylbutane (6). This product would arise from a dimerization of the intermediate anion-free radical postulated

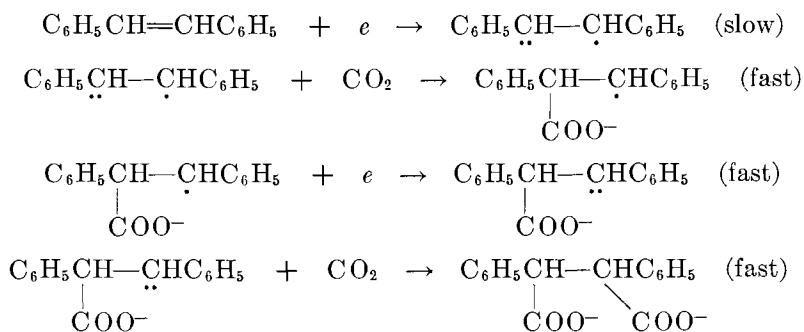


also occur in the reduction of the hydrocarbons in 75% dioxane solution rather than those previously suggested (2).

Reaction between the anion-free radical and either acetonitrile or dimethylformamide must occur to a certain extent and form the free radical which is reduced immediately since the two waves obtained are not of equal heights. At the first wave, which is the higher of the two, some anion-free radical would diffuse away from the electrode and

The formation of this dimer solely in dimethylformamide is made possible no doubt by the fact that dimethylformamide is a weaker acid than acetonitrile.

Further evidence for the stable anion intermediates proposed is the formation of *meso*-diphenylsuccinic acid from the reduction of stilbene in dimethylformamide in the presence of carbon dioxide. The reaction under these conditions probably goes by a step-wise addition of electrons and carbon dioxide.



some would react with the solvent and be immediately reduced further. The difference in the two wave heights found in dimethylformamide is smaller than that found in acetonitrile and indicates that dimethylformamide is less acidic than acetonitrile. This behavior is in accord with the structure of these two solvents.

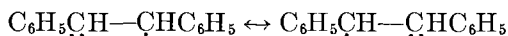
Evidence for the mechanisms proposed is the nature of the products isolated in the large-scale reductions of these hydrocarbons and the colors observed during the large-scale electrolysis. Triphenylethylene gave, in both acetonitrile and dimethylformamide, using tetra-*n*-butylammonium iodide as the inert electrolyte, 1,1,2-triphenylethane as the sole product. Stilbene in acetonitrile under similar conditions gave bibenzyl. In dimethyl-

More, but less conclusive, evidence for anion intermediates is the formation of 1,2-diphenylbutane in a poor yield in the electrolysis of stilbene in acetonitrile in the presence of ethyl iodide. In this example ethyl iodide is reduced at only a slightly more negative potential than stilbene and the possibility therefore exists that the resulting product, an ethyl free radical or anion, may add to the stilbene and give the same product as would be obtained by alkylating the stilbene anion-free radical with ethyl iodide. In the previous example cited carbon dioxide does not have this disadvantage since it is reduced at a more negative potential than stilbene.

Colors observed (Table III) for the intermediates formed during the electrolyses were dependent on

the hydrocarbon and the solvent used. In general, colors were lighter than those reported for disodium derivatives of the hydrocarbons in ether (14).

A possible explanation for the different polarographic behaviors observed for the hydrocarbons is that the group, which gives a two-step reduction, with the exception of *p*-anisylidene-fluorene, is symmetrical in structure. The other examples, which give only one wave, are unsymmetrical in structure with the exception of tetraphenylethylene. The symmetry present in stilbene and anthracene allows a greater resonance stabilization of the intermediate anion-free radical since the forms are equivalent.



p-Anisylidene-fluorene does not have such a symmetrical structure but contains groups which may help stabilize free radicals.

Symmetry is apparently not the only factor necessary for a two-step reduction. The ability of the intermediate to assume a planar arrangement is also important. Tetraphenylethylene is an excellent

phenylethyl from the disodium derivative of tetraphenylethylene and triphenylmethyl chloride (16).

The availability of protons in acetonitrile is indicated by the isolation of 4-amino-2,6-dimethyl pyrimidine. This compound is usually made by treating acetonitrile with strong base (10) and points to the formation of the carbanion $[\text{CH}_2\text{CN}]^-$ in the electrolysis.

The role of the solvent in the electrolytic reductions in dimethylformamide is not clear. Inspection of Table IV indicates that approximately one mole of carbon monoxide and two moles of hydrogen are liberated for each mole of hydrogen consumed in the reduction. Participation of the inert electrolyte in the reaction is indicated by the formation of butene-1 and *n*-butane. These hydrocarbons may be formed both by deposition of the tetrabutylammonium ion and by interaction of this ion with carbanions formed in the electrolysis. Possible reactions, which would explain the formation of the carbon monoxide and hydrogen but not the ratios of these found, are the following:

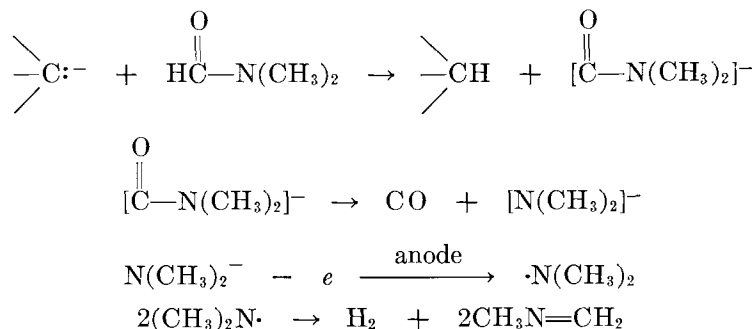
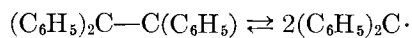


illustration of this point since it is symmetrical but is reduced in a single two-electron step. The intermediate anion-free radical, because of the four bulky phenyl groups, cannot assume the planar arrangement necessary for resonance stabilization and is, therefore, reduced further and rapidly to a dianion. Evidence for this mechanism is the large-scale reduction of tetraphenylethylene to 1,1,2,2-tetraphenylethane and diphenylmethane. The last hydrocarbon apparently arises from the dissociation of the intermediate dianion into an anion free radical followed by a reaction of the latter with the solvent.



This dissociation is no doubt due to the highly arylated structure and the electrostatic repulsion of the two negative charges present in the molecule. Such an equilibrium may also be the basis for the cleavage of 1,1,2,2-tetraphenylethane with sodium-potassium alloy (15) and for the formation of penta-

The tetrabutylammonium tetraiodomercurate and tetrabutylammonium triiodide isolated are products of the reactions of tetrabutylammonium iodide with the mercuric iodide and iodine formed in the electrolysis.

The demonstration of the carbanion intermediates in anhydrous dimethylformamide and acetonitrile indicates that direct electron addition to organic compounds occurs in electrolytic reductions. A similar mechanism is indicated for aromatic olefins and hydrocarbons in solutions containing water since the differences in half-wave potentials for the various hydrocarbons are similar to those observed in anhydrous media.

Any discussion of this paper will appear in a Discussion Section to be published in the December 1955 JOURNAL.

REFERENCES

1. S. WAWZONEK AND M. E. RUNNER, *This Journal*, **99**, 457 (1952).
2. H. A. LAITINEN AND S. WAWZONEK, *J. Am. Chem. Soc.*, **64**, 1765 (1942).

3. F. D. HAGER AND C. S. MARVEL, *ibid.*, **48**, 2689 (1926).
4. J. J. LINGANE, C. G. SWAIN, AND M. FIELDS, *ibid.*, **65**, 1348 (1943).
5. G. S. FORBES AND C. E. NORTON, *ibid.*, **48**, 2278 (1926).
6. E. BERGMANN, *J. Chem. Soc.*, **1936**, 505.
7. R. E. BUCKLES AND J. P. YUK, *J. Am. Chem. Soc.*, **75**, 5048 (1953).
8. A. LAPWORTH AND J. A. McRAE, *J. Chem. Soc.*, **121**, 1699 (1922).
9. A. KLAGES AND S. HELLMANN, *Ber.*, **37**, 1433 (1904).
10. A. R. RONZIO AND W. B. COOK, *Org. Syntheses*, **24**, 6 (1944).
11. T. ZINCKE, *Ann.*, **159**, 367 (1871).
12. V. N. IPATIEFF, H. PINES, AND R. E. SCHAAD, *J. Am. Chem. Soc.*, **66**, 816 (1944).
13. S. WAWZONEK AND H. A. LAITINEN, *ibid.*, **64**, 2365 (1942).
14. W. SCHLENK AND E. BERGMANN, *Ann.*, **463**, 1 (1928).
15. J. B. CONANT AND B. S. GARVEY, JR., *J. Am. Chem. Soc.*, **49**, 2599 (1927).
16. W. SCHLENK AND H. MARK, *Ber.*, **55**, 2285 (1922).

Preliminary Investigation of Hafnium Metal by the Kroll Process¹

H. L. GILBERT² AND M. M. BARR

Northwest Electrodevelopment Laboratory, U. S. Bureau of Mines, Albany, Oregon

ABSTRACT

Several hundred pounds of hafnium metal of better than 98% purity have been produced by the Kroll process of magnesium reduction of the tetrachloride. A discussion of the process from oxide to metal stages is given with thermodynamic values for chlorination and reduction. Metal produced to date is hot malleable but not cold ductile.

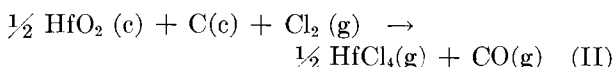
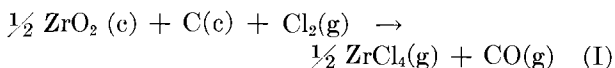
PRELIMINARY INVESTIGATION

The Kroll process (1) has been employed in the production of titanium and zirconium metals with great success (2-4). While application of the process to the production of other metals may be postulated, recent production of several hundred pounds of relatively pure hafnium metal is of particular interest due in part to the rarity of this element in the pure state.

Hafnium is normally associated with zirconium ores to the extent of about 2%, and while as common as beryllium, germanium, and uranium, and more plentiful than mercury, tantalum, niobium (columbium), and silver (5), it is far more unusual in the pure form because of the great difficulty encountered in separating it from zirconium. It has been reported that the separation may be accomplished through fractionation of mixtures of hafnium-zirconium chloride-phosphorous oxychloride addition compounds (6) and by fractional crystallization of the mixed zirconium-hafnium fluoride-potassium fluoride double salts. Selective precipitation (7), ion exchange, and liquid-liquid exchange (8) are known to give reasonable separations, but no method is without disadvantages.

The material employed in this work was prepared by the Oak Ridge National Laboratory Materials Chemistry Division through methods employed in isotopic separations (9).

The thermodynamics involved in converting hafnium oxide to the metal may be compared with zirconium on a relative basis by the following calculations of Kelley (10):



¹ Manuscript received August 20, 1954. This paper was prepared for delivery before the Cincinnati Meeting, May 1 to 5, 1955.

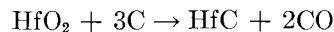
² Present address: Harvey Aluminum Company, 19200 South Western Avenue, Torrance, California.

	ΔH 1200	ΔF° 1200
Zirconium	1700	-32,600
Hafnium	-9700	-43,100
$\frac{1}{2} \text{ZrCl}_4 (\text{g}) + \text{Mg} (\text{l}) \rightarrow \frac{1}{2} \text{Zr} (\text{c}) + \text{MgCl}_2 (\text{l}) \quad (\text{III})$		
$\frac{1}{2} \text{HfCl}_4 (\text{g}) + \text{Mg} (\text{l}) \rightarrow \frac{1}{2} \text{Hf} (\text{c}) + \text{MgCl}_2 (\text{l}) \quad (\text{IV})$		
	ΔH 1150	ΔF° 1150
Zirconium	-39,300	-26,600
Hafnium	-26,200	-14,700

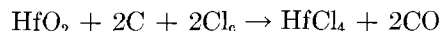
Free energy values favor reaction (II) over reaction (I) and reaction (III) over (IV), meaning that hafnium oxide is more readily chlorinated than is zirconium oxide, but the tetrachloride formed is less efficiently reduced by magnesium than is the tetrachloride of zirconium. Both of these predictions were borne out by reaction behavior in the plant runs.

EXPERIMENTAL

The hafnium material received was first calcined at 800°C to assure the conversion of any compounds present to the oxide. Tests showed that carbiding of the oxide by the reaction



proceeded satisfactorily, but formation of a dense crystalline material so familiar with zirconium (11) could not be attained readily in the case of the hafnium carbide, due perhaps to the higher melting point of the latter material. Since chlorination of a noncrystalline material is difficult, hafnium oxide was chlorinated directly according to the reaction.

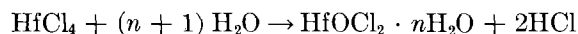


It must be noted that other products, particularly carbon dioxide and phosgene, also are formed, showing that the reaction probably is more complicated than indicated (12).

A chlorination mixture was prepared as follows: hafnium oxide, 81.5%; carbon black, 9.5%; dextrine, 4.5%; water, 4.5%.

This mixture was blended in a ribbon mixer and then stored for 24 hr to allow the moisture to become diffused throughout the mass. Briquetting was accomplished in a Belgian roll type machine which produced very hard, dense briquets about $1\frac{3}{8} \times 1 \times \frac{3}{4}$ in. These were dried at 140°C and chlorinated at 900°C in an experimental 12-in. diameter shaft chlorinator previously described (12).

Crude hafnium tetrachloride as produced was a buff-colored powder which sublimed at 317°C and was sensitive to oxidation and hydrolysis, fuming when exposed to the atmosphere, even at room temperature. By the time this fluffy mass had been transferred to the purification furnace considerable oxidation and hydrolysis had taken place, partly because of the finely divided state of the material. The more troublesome reaction is the hydrolysis to form hafnyl chloride:



Prior to reduction, this material must be removed from the tetrachloride since much of the success of the entire process depends upon the extent of its removal. Best results were found with a combination of thermal decomposition and vacuum treatment to remove the water liberated:



Under parallel circumstances in the zirconium process rather complete elimination of volatile oxide-bearing compounds is effected, but with hafnium it would appear that the oxychloride has sufficient stability in the anhydrous form (HfOCl_2) to permit some carry-over in subsequent sublimation. Attempts to establish the existence of a volatile oxychloride were not successful, in part because of difficulties encountered in the analysis for oxygen.

By careful heating and evacuation, the bulk of the moisture was removed from the raw hafnium tetrachloride at an ultimate temperature of 200°C . The furnace was then filled with helium and the crude tetrachloride transferred by sublimation to a water-cooled coil where it collected in a dense massive form.

The purified tetrachloride was transferred to a reduction furnace and there sublimed under helium into molten magnesium. The effect of the lower free energy of the reaction coupled with apparent insolubility of the hafnium metal in molten magnesium required a magnesium excess of 40% over the stoichiometric amount. Operating temperature during reduction was 850°C .

Separation of the hafnium formed from the excess magnesium and by-product magnesium chloride was accomplished in the standard vacuum distillation furnace employed in processing zirconium.

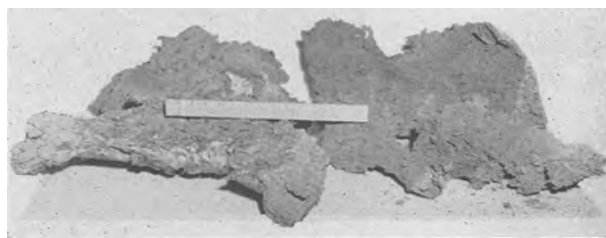


FIG. 1. Hafnium sponge after vacuum distillation step

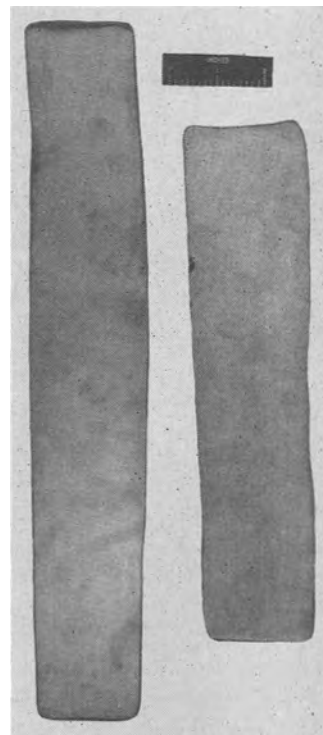


FIG. 2. Hafnium sheet hot rolled from arc melted ingot

The sponge metal shown in Fig. 1 was very heavy, since hafnium has a density of 13.3, but did not appear to have coalesced to the extent that is found with zirconium. Several observations tend to show a very low comparative solubility of hafnium in magnesium which could impede crystal growth, and the considerably higher transformation temperature of hafnium (1550° vs. 861°C) might also contribute to the crystalline form.

The physical state of the hafnium sponge made it rather reactive when exposed to air. Initial exposure was to an air-helium mixture which prevented actual ignition of the sponge while allowing the more pyrophoric materials to oxidize slowly to such an extent that the furnace could be opened and the sponge removed without loss. Handling, cutting, and cleaning of the sponge was done in a helium atmosphere box.

Hafnium sponge was melted by consumable electrode arc methods and the ingots forged and rolled to sheet as shown in Fig. 2. All metal had a

hardness of Rockwell C 20 to 25 which is indicative of oxygen contamination. At such hardnesses the metal may not be considered cold ductile. The sponge can be purified by the iodide dissociation method to give metal having a reported hardness of Rockwell B 78 (5).

Analysis of three test lots of sponge metal was as follows:

Sample No.	$\frac{Zr}{Hf + Zr}$		Analysis ppm						
			O ₂	Fe	N ₂	Cl	Al	Cu	Pb
1	1.4		650	400	10	150	30	100	30
2	1.4		850	400	20	100	30	100	30
3	1.3		950	400	30	200	50	50	20
	Zn	Cr	Co	Mn	Ni	Si	Ti	V	Mo
1	5	100	10	30	5	100	50	20	10
2	5	100	10	30	5	100	50	20	10
3	50	5	10	30	5	20	50	20	10

All residues and metal scrap were burned in large porcelain dishes to hafnium oxide for recycling in the process.

Several modifications in the process are under consideration, and it is hoped that by means of these and the exercise of extreme care throughout the process the hardness of the metal may be reduced to more satisfactory levels.

CONCLUSIONS

Hafnium metal may be produced in zirconium plant equipment without modification. Greater sensitivity of hafnium tetrachloride to atmospheric moisture and higher stability of hafnyl chloride required some additional care and effort in chloride purification. Magnesium in the amount of 40% over stoichiometric is employed in reducing the

chloride. Magnesium chloride by-product and excess magnesium were removed by vacuum distillation. Sponge metal was somewhat reactive in air. Metal ingots had a hardness of Rc 20 to 25 but could be hot forged and rolled to sheet.

ACKNOWLEDGMENT

This paper is a report of one of the investigations carried out by the Rare Metals Branch, Bureau of Mines, Region II, Albany, Oregon, under the supervision of S. M. Shelton, Regional Director. The authors wish to make special acknowledgment of the services of C. Q. Morrison and I. J. Groce who carried out the preliminary phases of this work.

Any discussion of this paper will appear in a Discussion Section to be published in the December 1955 JOURNAL.

REFERENCES

1. W. J. KROLL, U. S. Pat. 2,205,854.
2. H. C. FULLER, D. H. BAKER, AND F. S. WARTMAN, U. S. Bur. Mines Rept. Investigation 4879, June 1952.
3. S. M. SHELTON AND E. DON DILLING, "Zirconium and Zirconium Alloys," p. 82, American Society for Metals, Cleveland (1953).
4. D. I. BROWN, *Iron Age*, **170**, 260 (1952) et seq.
5. F. B. LITTON, *This Journal*, **98**, 488 (1951).
6. D. M. GRUEN AND J. J. KATZ, *J. Am. Chem. Soc.*, **71**, 3843 (1949).
7. H. H. WILLARD AND H. FREUND, *Ind. Eng. Chem. (Anal. Ed.)*, **18**, 195 (1946).
8. E. H. HUFFMAN AND L. J. BEAUFAIT, U. S. Pat. 2,566,665.
9. E. C. MILLER, "Zirconium and Zirconium Alloys," p. 337, American Society for Metals, Cleveland (1953).
10. K. K. KELLEY, Private communication.
11. W. J. KROLL, W. W. STEPHENS, AND J. P. WALSTAD, *Trans. Am. Inst. Mining Met. Engrs.*, **188**, 1394 (1950).
12. W. W. STEPHENS AND H. L. GILBERT, *J. Metals*, **4**, 733 (1952).
13. A. E. VAN ARKEL AND J. H. DE BOER, *Z. anorg. u. allgem. Chem.*, **141**, 289 (1924).

The Influence of Impurities in the Electrolyte in Chlorine-Caustic Electrolysis by the Mercury Cell Process

V. Further Investigation of the Influence of Metals on the Cathodic Current Efficiency¹

GÖSTA ANGEL, TAGE LUNDÉN, STIG DAHLERUS, AND ROLF BRÄNNLAND

Division of Applied Electrochemistry, Royal Institute of Technology, Stockholm, Sweden

ABSTRACT

In a number of electrolysis experiments the influence of mixtures of certain common metals, such as vanadium, magnesium, and aluminum, was investigated. A theory is developed for the action of those metals which have previously been shown to interfere with electrolysis in mercury cells.

INTRODUCTION

A number of metals have been examined with respect to their influence on the cathodic current efficiency in mercury cells (1), but in each experiment only one metal was added. Certain amalgam decomposition experiments indicated, however, that two metals may interfere in an unexpected manner; therefore, another series of experiments was made with extraneous metals combined in groups of two.

The experiments were performed in the same way as those previously described (1); the current was 10 amp (25 amp/dm²), the brine flow rate 7.5 ml/min, the mercury flow rate 8–10 ml/min, and the temperature generally 38°–42°C.

EXPERIMENTAL

Vanadium and iron.—As previously reported (2), amalgam decomposition experiments showed that the influence of vanadium on decomposition rate was promoted very much by comparatively small quantities of iron. Since vanadium, and iron above all, may be present in industrial brines, this pair of metals was thoroughly investigated by electrolysis experiments.

The somewhat surprising results of these experiments are reproduced in Fig. 1. In the presence of comparatively large quantities of iron, the influence of vanadium was very much reduced, contrary to what might be predicted from the amalgam decomposition experiments.

During the experiments, the mercury surface was bright, and all the hydrogen evolution was concentrated at the glass wall and the mercury lock. In the presence of only 1–2.5 mg/l iron, a gas "spot"

¹ Manuscript received June 14, 1954. This paper was prepared for delivery before the Cincinnati Meeting, May 1 to 5, 1955.

was formed after some time at the cathode surface, and the current efficiency began to decrease markedly.

In a special series of experiments it was found that, after it had once started, hydrogen evolution due to vanadium could not be nullified by addition of iron-containing brine. It was also observed that ferric hydroxide was precipitated in the cell during electrolysis; this phenomenon may explain why vanadium was de-activated by iron under conditions prevailing in a mercury cell.

Experiments with magnesium as one constituent.—With magnesium mixed with a number of other metals, a series of experiments was performed as shown by the table below:

	Ti	Al	Cu	Fe	Ni	Mn	Ca
Mg	+	+	+	+	+	+	○

"+" means that the influence of both metals together is stronger than that of any of them alone; "○" means that no increased influence was observed.

In the experiments with brine containing 5 mg/l magnesium and 5 mg/l titanium, hydrogen gas evolution occurred within 2 min, and after 15 min the current efficiency had decreased to about 30%. This result does not agree with those obtained from brines containing a titanium salt alone.

With 2.5 mg/l magnesium and 5 mg/l aluminum simultaneously present in the brine, the cathodic reaction was similarly affected; hydrogen gas evolution started within 1 min and current efficiency was 29% in 20 min.

Using 5 mg/l magnesium and 5 mg/l copper, cathodic current efficiency was 47% after 20 min.

Experiments were made with magnesium and iron simultaneously present in varying concentrations. The results of typical runs with 10 mg/l iron mixed with 10 and 25 mg/l magnesium, respectively, are demonstrated in Fig. 2. Although

neither iron nor magnesium was able to cause any hydrogen evolution separately, they decreased the current efficiency considerably when present together. In the experiments it was also observed that the mercury surface was completely covered by a thick layer of iron and magnesium hydroxide, possibly mixed with some amalgam.

With 5 mg/l magnesium and 5 mg/l nickel a similar phenomenon occurred; in 10 min the current efficiency had decreased to about 40%. With the same quantities of magnesium and manganese the same result was obtained, and after 15 min the current efficiency was only 50%.

In the simultaneous presence of magnesium and calcium, however, no interference with the cathodic current efficiency was observed.

Experiments with aluminum as one constituent.—

Results of the experiments with aluminum as one constituent are given in the following table:

	V	Ti	Cu	Fe	Ni	Mn	Ca
Al	+	+	+	○	○	○	○

“+” means that the influence of both metals together is stronger than that of any of them alone; “○” means that no increased influence was observed.

With 12.5 mg/l aluminum and 0.5 mg/l vanadium the influence was considerably greater than with vanadium alone. Thus the current efficiency decreased to 4% in 1 hr, and it is therefore clear that vanadium is not de-activated by the formation of aluminum hydroxide.

With 5 mg/l aluminum and 0.3 mg/l titanium, hydrogen evolution occurred immediately after the start of the experiment and after 10 min the current efficiency had decreased to 76%.

With 5 mg/l aluminum and 5 mg/l copper, the hydrogen evolution started after about 2 min of electrolysis, then the current efficiency decreased to 20% in 18 min. After the experiment was finished, a reddish brown film was observed on the mercury surface.

With 5 mg/l aluminum and either 5 mg/l iron, 5 mg/l nickel, 50 mg/l manganese, or 50 mg/l calcium, no effect was observed.

Experiments with copper as one constituent.—

As well as the previously described combination experiments with copper mixed with either magnesium or aluminum, experiments on mixtures of copper with the following metals were carried out:

	Ti	Fe	Ni	Mn	Ca
Cu	+	○	○	○	○

“+” means that the influence of both metals together is stronger than that of any of them alone; “○” means that no increased influence was observed.

With 0.5 mg/l copper and 5 mg/l titanium,

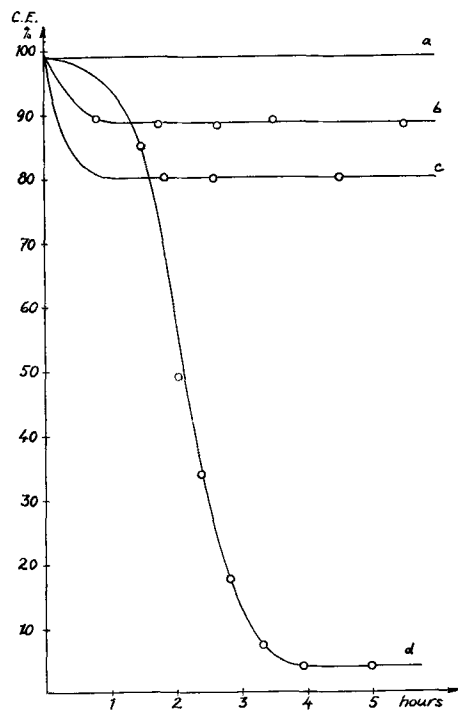


FIG. 1. Current efficiency in presence of vanadium and iron. Curve a, 12.5 mg/l Fe; curve b, 0.5 mg/l V + 12.5 mg/l Fe; curve c, 1.0 mg/l V + 12.5 mg/l Fe; curve d, 0.5 mg/l V.

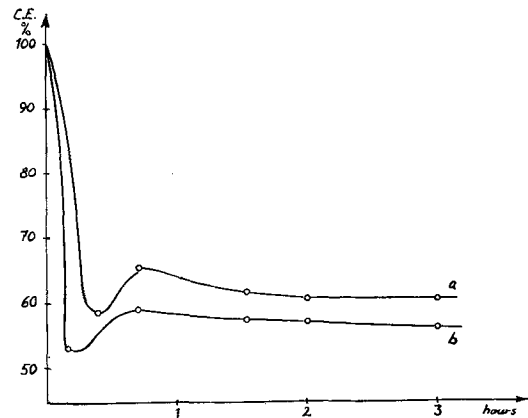


FIG. 2. Current efficiency in presence of magnesium and iron. Curve a, 10 mg/l Mg + 10 mg/l Fe; curve b, 25 mg/l Mg + 10 mg/l Fe.

hydrogen evolution occurred a few seconds after the start of electrolysis. After 13 min the current efficiency had decreased to 0%. Also in this case a reddish brown film was found at the cathode surface after the experiment.

With the other metals in the table no interference with the cathode reaction was obtained.

Experiments with sodium silicate.—In a previous paper (3) it was reported that sodium silicate or silicic acid had a strongly de-activating influence on vanadium and molybdenum in the amalgam decomposition experiments. The influence of silicate

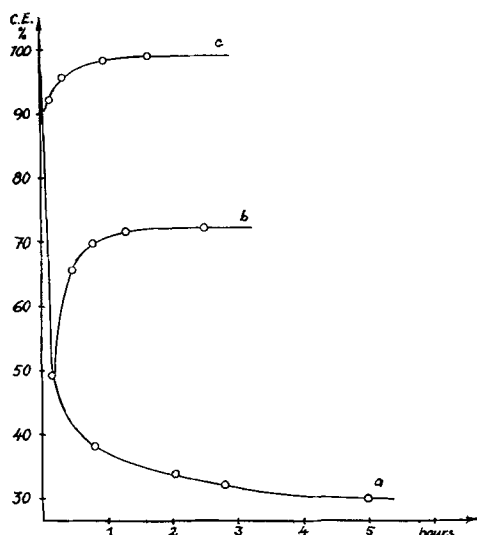


FIG. 3. Current efficiency in presence of silicate and molybdenum. Curve a, 1.5 mg/l Mo; curve b, 1.5 mg/l Mo + 25 mg/l Si; curve c, 1.5 mg/l Mo + 100 mg/l Si.

with respect to certain interfering metals was also investigated by electrolysis experiments, typical results of which are presented in Fig. 3.

The experiments show that 25 mg/l silicon is sufficient to de-activate 0.5 mg/l vanadium or the same concentration of chromium. With 1.5 mg/l molybdenum and 25 mg/l silicon the current efficiency was, however, decreased to 49% in 8 min, and 100 mg/l silicon was needed in order to de-activate this quantity of molybdenum.

The effect of silicate addition to brine containing 10 mg/l iron and 25 mg/l magnesium was also investigated, but in this case the current efficiency still decreased to about 57%.

In the electrolysis experiments with silicate some observations were made which are of great importance for an explanation of the reaction mechanism and for the possible use of silicate as de-activator of vanadium.

It was found that silicate had no effect on metals belonging to the vanadium group, if the silicate was added when gas evolution had once started at the cathode. This indicates that vanadium ions may be absorbed by silicic acid and thus removed from solution.

Experiments with silicate show that comparatively large quantities are required to de-activate completely the interfering metals, 25–40 times the concentration of the metal in question. But experiments with large concentrations of silicic acid have also shown that the mercury cathode may be covered with a film of silicic acid, which acts as a diaphragm and impedes the sodium ion transport to the cathode, thus causing hydrogen gas evolution and a decrease of current efficiency. With 30 mg/l

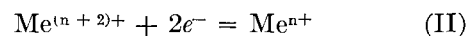
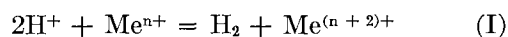
silicon a maximum hydrogen content of 30% was obtained.

However, if silicate-treated brine was allowed to stand for a few hours before the electrolysis, no disturbance was observed, and brines with 100 mg/l silicon could then be electrolyzed without any film formation. The phenomenon is probably caused by cataphoretic deposition of colloidal silicic acid at the cathode. If on the other hand the brine is allowed to stand, the silicic acid flocculates and cannot move in the electric field.

DISCUSSION

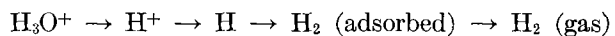
Metals investigated may be arranged with respect to their influence on cathodic current efficiency into two groups: one of strong influence (vanadium, molybdenum, chromium, titanium), and one of slight or no influence (magnesium, calcium, barium, iron, etc.).

With regard to the strong effect of the vanadium group, the polyvalent character of these metals is striking. It might be assumed that, under certain conditions, hydrogen ions could be reduced by metal ions of low valency, which were then reduced again at the cathode, according to the formulas:



In that case, reaction (I) would take place in the cathode film and reaction (II) at the mercury surface. However, most of the active metals were added as anions, and, although the same reactions would take place, the ions would have to be transported to the cathode by diffusion alone. On account of the violent gas evolution, which makes the concentrating of active metals in the cathode film difficult, and because of certain observations accounted for below, this explanation seems improbable.

Of course, it is very convenient to characterize the action of the vanadium group as catalysis. According to this hypothesis, the active metal ions should lower the hydrogen overvoltage on mercury by catalyzing one of the steps in the reaction chain:

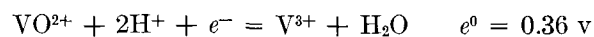


However, experiments described later show that the hypothesis cannot be correct in this form, but must be modified to an assumption of deposition of the metal in question on the mercury surface. In this case, the reaction no longer involves hydrogen overvoltage on mercury but on the deposited metal.

This theory thus presumes that: the active metal can be electrochemically deposited at the actual cathode potential; the deposited metal remains at

the mercury surface and is not amalgamated, dissolved, or dispersed; the hydrogen overvoltage upon the deposited metal is lower than that upon mercury.

Cathode potentials.—According to Latimer (4) the following standard potentials apply to the metals discussed. For vanadium,



These equations may be combined according to Luther's rule:



With $a_{\text{VO}^{2+}} = 10^{-6}$ and $p\text{H} 12$, the reversible cathode potential at 50°C is -1.2 v .

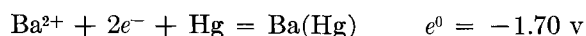
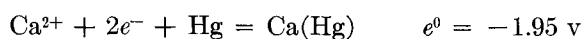
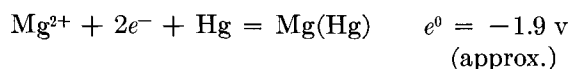
For molybdenum, $\text{H}_2\text{MoO}_4 + 6\text{H}^+ + 6e^- = \text{Mo} + 4\text{H}_2\text{O}$ $e^0 = 0.0 \text{ v}$ (approx). With $a_{\text{H}_2\text{MoO}_4} = 10^{-6}$ and $p\text{H} 12$, the reversible cathode potential at 50°C is about -0.9 v .

For chromium, $\text{Cr}^{3+} + 3e^- = \text{Cr}$ $e^0 = -0.74 \text{ v}$
With $a_{\text{Cr}^{3+}} = 10^{-6}$, the reversible potential at 50°C is -0.87 v .

For titanium, $\text{TiO}^{2+} + 2\text{H}^+ + 4e^- = \text{Ti} + \text{H}_2\text{O}$
 $e^0 = -0.88 \text{ v}$

With $a_{\text{TiO}^{2+}} = 10^{-6}$ and $p\text{H} 12$, the reversible potential at 50°C is approximately -1.4 v .

For magnesium, calcium, barium, and iron, the standard potentials are below -2 v , but the reduction is depolarized by amalgam formation and, according to Kolthoff and Lingane (5), the actual standard potentials are:



De Nora (6) reported that the cathode potential is about -1.75 v in industrial electrolysis of saturated NaCl solutions with mercury cathode. Thus most of the metals mentioned above may be electrochemically deposited even if they occur in concentrations of $1 \text{ } \gamma/\text{l}$.

Solubility in mercury.—Irving and Russel (7) studied the solubility of vanadium, molybdenum, and chromium in mercury and found that they were practically insoluble: vanadium, $5 \times 10^{-5}\%$; molybdenum, $2 \times 10^{-5}\%$; chromium, $5 \times 10^{-5}\%$; titanium, $10^{-5}\%$.

The solubility of amalgams formed by magnesium, calcium, and barium is comparatively high (8–10).

The solubility of iron in mercury has been studied very extensively, but the results are partly contradictory. The general opinion is that iron is quite insoluble and merely forms a suspension in the mercury (11). Thus the iron particles in a mercury suspension are influenced by a magnetic field (12). Katoh (13) examined an iron "amalgam" by x-ray analysis and found that the iron particles consisted of α -iron. The iron concentration in mercury may be so high that a solid mixture is formed (amalgam butter), corresponding to an iron content of more than 2%.

Hydrogen overvoltage.—According to investigations by Thiel and Hammerschmidt (14) the minimum hydrogen overvoltage is: mercury 0.570 v , vanadium 0.135 v , molybdenum 0.157 v , chromium 0.182 v , titanium 0.236 v .

Important Observations for Establishing the Reaction Mechanism Theory

In the electrolysis experiments, some observations were made which must be taken into consideration when the hypotheses given above are discussed.

1. The addition of absorbing substances, such as silicic acid and ferric hydroxide, has no effect if they are added when gas evolution, caused by vanadium, for example, has once occurred. This phenomenon indicates that the active metal is no longer present in the solution, but precipitated at the electrode surface.

2. In the presence of moderate quantities of vanadium, molybdenum, or chromium, the gas evolution is concentrated to only a part of the cathode surface (gas spot). If the electrolysis is interrupted and this gas spot is removed by suction together with some mercury, gas evolution will not occur again when the electrolysis is continued. It is probable that, if a metal, insoluble in mercury, is deposited at the cathode, the metal forms a coherent film owing to the surface forces, the area of which increases with the quantity of metal deposited and at which the gas evolution is located.

3. If the electrolysis of a salt solution polluted with vanadium, molybdenum, or chromium is interrupted, the brine carefully sucked off, and the cell rinsed with distilled water, then a violent gas evolution nevertheless occurs when fresh pure brine is supplied and the electrolysis is continued.

4. In experiments with about 5 g/l vanadium, a dark, tough film was obtained at the cathode after a few minutes of electrolysis.

In addition to the electrolysis experiments described above, some amalgam decomposition experiments were performed in order to show that vanadium is removed from the solution with the amalgam. The experiments included shaking the

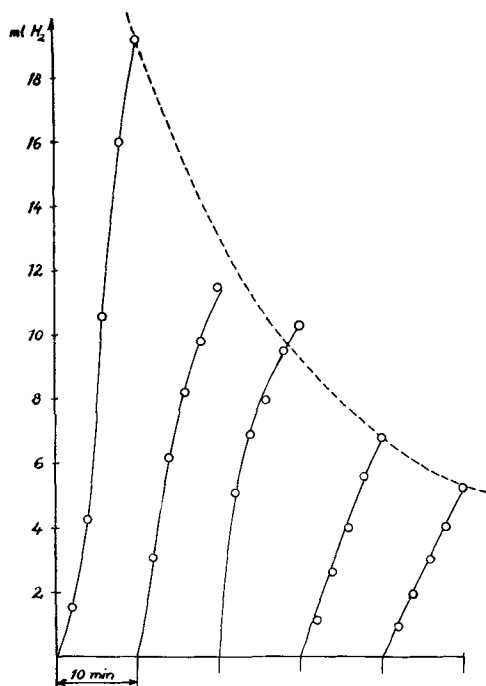


FIG. 4. Amalgam decomposition experiment with vanadium-containing brine and addition of fresh amalgam at 10 min intervals.

polluted salt solution with sodium amalgam for 10 min. The solution was then decanted, acidified with hydrochloric acid to pH 6.5, and again shaken with a quantity of fresh amalgam for 10 min, etc. This was repeated 5 times, and in the course of the experiment the gas evolution decreased steadily (cf Fig. 4). The experiment shows that vanadium is removed from the solution to a considerable extent and presumably deposited at the amalgam surface.

CONCLUSIONS

Theoretical considerations show that the electrochemical reduction of vanadium, molybdenum, and chromium to the metallic state is possible. The deposited metals are not soluble in mercury but remain at the cathode surface and, since the hydrogen overpotential is lower on these metals than on mercury, hydrogen evolution is promoted.

As to the action of magnesium, this metal is probably reduced to some extent and amalgamated but, more important, the hydroxide is precipitated in the alkaline cathode film and forms a diaphragm there, which makes the passage of sodium ions difficult while the smaller hydrogen ions migrate more easily and are discharged at the cathode. The diaphragm is further reinforced if other hydroxides are coprecipitated.

The observations accounted for above support the assumption that certain mercury-insoluble metals are deposited in small quantities at the cathode and

form there active spots where hydrogen ions exclusively are discharged.

As to mixtures of interfering metals, experiments have shown that interaction between, e.g., magnesium and metals of the vanadium group, may very well occur, so that the cathode film is rendered more alkaline by the hydrogen ion discharge, more hydroxide is precipitated, the sodium ion migration is made still more difficult, etc.

Yet, the literature (15) shows that two metals may interfere in the mercury phase so that their solubility in mercury is considerably decreased. A film of the interfering metal is then formed at the cathode, and hydrogen evolution is promoted.

Results of the electrolysis experiments are directly applicable to the industrial chlorine-caustic electrolysis in mercury cells. Thus, vanadium has been proved to be the most dangerous of the impurities examined, and the vanadium influence is greater in brine purer with respect to certain other substances, such as ferric iron and silicic acid, which decrease the influence of vanadium to a considerable extent. Therefore, the previously mentioned, serious interruptions in 1949 at two Swedish chlorine plants were no doubt caused by vanadium dissolved from the graphite anodes employed (2). The less serious disturbances at other chlorine plants may be explained by the assumption that the brine in those cases contained certain impurities which have been shown to inhibit vanadium influence.

SUMMARY

A number of electrolysis experiments are described, in which the influence of mixtures of certain metals was investigated under normal operating conditions: current density 25 amp/dm², brine depletion 15%, and amalgam concentration 0.14%. In each experiment the brine was polluted with salts of two metals so that the combined effect of these metals could be studied. It is shown that:

1. Magnesium interferes with the cathode reaction when iron, nickel, titanium, copper, aluminum, or manganese is simultaneously present.
2. Aluminum promotes hydrogen ion discharge when either titanium or copper is also present in the brine.
3. Silicate or silicic acid in adequate quantities reacts with vanadium, molybdenum, and chromium, so that these metals are de-activated and sodium ion discharge proceeds undisturbed.

A theory is developed for the action of metals belonging to the vanadium group and for other metals. The former are assumed to be electrochemically deposited and to remain at the surface, thus decreasing hydrogen overvoltage and promoting

the discharge of these ions. Magnesium, on the contrary, is supposed to act quite mechanically by the formation of a hydroxide diaphragm reinforced by other metal hydroxides, which makes the sodium ion migration difficult.

ACKNOWLEDGMENT

The authors wish to express their deep appreciation for generous financial support from Elektrokemiska AB, Bohus; Mo & Domsjö AB, Örnsköldsvik; Svenska Cellulosa AB, Sundsvall; and Uddeholms AB, Skoghall.

Any discussion of this paper will appear in a Discussion Section, to be published in the December 1955 JOURNAL

REFERENCES

1. G. ANGEL, T. LUNDÉN, S. DAHLERUS, AND R. BRÄNNLAND, *This Journal*, **102**, 124 (1955).
2. G. ANGEL AND T. LUNDÉN, *This Journal*, **99**, 435 (1952).
3. G. ANGEL, T. LUNDÉN, AND R. BRÄNNLAND, *ibid.*, **100**, 39 (1953).
4. W. M. LATIMER, "The Oxidation States of the Elements and Their Potentials in Aqueous Solutions," Prentice-Hall, New York (1952).
5. I. M. KOLTHOFF AND J. J. LINGANE, "Polarography," Interscience Publishers, New York (1952).
6. V. DE NORA, *This Journal*, **97**, 346 (1950).
7. N. M. IRVIN AND A. S. RUSSEL, *J. Chem. Soc. London*, **1932**, 891.
8. A. SMITS AND R. P. BECK, *Proc. Acad. Amsterdam*, **23**, 975 (1921).
9. H. MOISSAN AND G. CHAVONNE, *Compt. rend.*, **140**, 125 (1905).
10. A. SCHÖLLER, *Z. Elektrochem.*, **5**, 259 (1898).
11. T. W. RICHARDS AND R. N. GARROD-THOMAS, *Z. phys. Chem.*, **72**, 181 (1910).
12. M. RABINOWITSCH AND P. B. ZYWOTINSKI, *Koll.-Z.*, **52**, 31 (1930).
13. N. KATOH, *J. Chem. Soc. Japan*, **64**, 1079 (1943).
14. A. THIEL AND W. HAMMERSCHMIDT, *Z. anorg. u. allgem. Chem.*, **132**, 15 (1923).
15. H. HOHN, *Österr. Chem.-Ztg.*, **49**, 15 (1948).

Electrolytic Reduction of Titanium Monoxide¹

M. E. SIBERT, Q. H. MCKENNA, M. A. STEINBERG, AND E. WAINER

Horizons Incorporated, Cleveland, Ohio

ABSTRACT

An electrolytic method for preparation of titanium metal from titanium monoxide is described. The process is carried out in alkaline earth halide melts under an inert atmosphere. The inert atmosphere cell and its operation are described. Methods for preparation of reduced titanium oxides are also discussed. These include reactions of titanium carbide with ZnO or MgO, carbon reduction of TiO₂, and electrolytic reduction of TiO₂. Electrolytic titanium prepared from TiO is deposited as a crystalline metal powder in a salt matrix and is recovered by aqueous techniques. Although metal so prepared has not generally been acceptable from a purity standpoint, revision in cell design and procedure could offer improvement in this respect.

INTRODUCTION

Considerable effort has been expended on the development of new processes for titanium metal preparation, much of this effort toward electrolytic processes.

Probably the biggest problem is that of a source electrolyte. Such a material should preferably be obtainable as an ore or be readily processed, be stable under normal conditions, and lend itself readily to electrolysis. The most logical material is TiO₂ since naturally occurring rutile, anatase, and ilmenite are easily converted to pure TiO₂. However, there is no known single stage reductant capable of producing metal from the dioxide even by thermal reaction. Thus, it was decided to investigate methods of preparing the lower oxides and their electrolysis.

Four methods were developed for production of the monoxide or sesquioxide. Since a one-step reduction (Ti II to Ti) is preferable to a two-step (Ti III to Ti II to Ti), and since the monoxide is about as easy to prepare as the sesquioxide, the electrolytic effort was concentrated on the monoxide.

An electrolytic method for reduction of the monoxide to metal was subsequently developed. The procedure entails a high temperature electrolysis of TiO in a melt of an alkaline earth halide. For most of the work anhydrous CaCl₂ has been employed.

A protective atmosphere of argon or helium is a requirement of the process, both for protection of produced titanium metal and the TiO in the bath.

With this process titanium up to 99% purity has been produced. The metal can be arc melted and hot worked although, in general, it does not meet commercial specifications at this stage of the

development. The only significant impurities present are oxygen and carbon.

Titanium Metal Preparation

A review of the literature on the electrolytic preparation of titanium reveals a varied array of attempts, but little in the way of substantial results. A number of these have been carried out in aqueous solution, but it is improbable that pure titanium can ever be isolated in this manner.

Titanium films of 1 μ thickness on copper were deposited from sulfanilic acid—Ti(OH)₄ solutions (1) as were thin black films of titanium on lead, zinc, and antimony by electrolysis of TiO₂ in H₂SO₄—Na₂SO₄—10H₂O solutions (2), or from Ti₂(SO₄)₃ solutions (3).

There are patents on electroplating titanium from strongly alkaline solutions of TiO₂ or Ti(OH)₄ on iron or copper (4) and for treatment of base metals by anodization in baths containing colloidal suspensions of Si, Al, Zr, or a "rare earth oxide" (including TiO₂) and a conducting salt or acid (5). An anion must be present to form an insoluble salt of the metal being treated.

Titanium plating has been reported from Ti(C₄H₄O₆)₂ solutions at room temperature (6). Electrolysis of titanium salicylates have been attempted (7) where titanium apparently formed an anionic complex. Negative results are reported using solutions of TiCl₄ in CH₃OH, C₂H₅OH, pyridine, and other organic solvents (6).

Deposition of titanium and other reactive metals on mercury by shaking with an acidified salt of the metal has been claimed (8). Another use of a mercury cathode was reported as an analytical method for quantitative determination of titanium in silica-aluminum by electrolysis (9). An unsuccessful attempt was made to plate titanium from aqueous solution as well as a number of other high dielectric constant electrolytes (10). The metal

¹ Manuscript received July 6, 1954. This paper was prepared for delivery before the Chicago Meeting, May 2 to 6, 1954, and is based on a portion of the work carried out by Horizons Incorporated for the Office of Naval Research under Contract Nos. Nonr-394(00) and 394(01).

could only be plated from highly ionized complexes as opposed to the simple salts employed in the work described. It has been claimed that titanium can be electroplated from solutions of complex organic titanium salts where the concentration was 35 g Ti/l or more (11). Titanium was said to have been plated on Hg from a solution of TiCl_2 in 2N HCl (12).

A number of summaries of attempts to produce titanium electrolytically have been written. Andrieux (13, 14) considered the fused salt field. Others, covering varying aspects of the whole field, include those by Keeney (15) and Spence (16).

Attempts have been made to produce the metal directly by electrolysis of ores, e.g., titaniferrous ores (17) or the aluminum by-product "red mud" as an electrolytic feed material (18).

Others have produced alloys successfully by electrolytic methods. A patent entailing electrolysis of a fused mixture of alkali, alkaline earth, and titanium halides and employing the cathode as alloying metal has been obtained (19).

Binary and ternary alloys have been prepared (1) using baths of AlCl_3 —NaCl and NaCl—NaF with TiO_2 as a source electrolyte. The alloying metal was derived from the anode in most cases; Zn—Ti was commonly used.

There are numerous reports of titanium preparation by fused salt electrolysis. A reasonably pure product was claimed from electrolysis of TiO_2 in CaCl_2 (20). Electrolysis of pure rutile later failed (21). The use of 1 mole of TiO_2 in 10 moles of K_2SiF_6 produced only TiSi_2 and Ti_2O_3 (22). Only lower oxides were obtained with TiO_2 in a variety of fused salts and salt mixtures and with K_2TiF_6 in a mixture of NaCl—KCl (23).

A process for producing Ti by electrolysis of TiCl_4 in one or more of NaCl, KCl, CaCl_2 , and MgCl_2 using a cell of special design has been described recently (24). Dendritic powder has been formed from TiCl_3 dissolved in a mixture of LiCl and KCl at 550°C under a hydrogen atmosphere (25) and Ti powder has been prepared from baths of K_2TiF_6 —NaCl—KCl, TiCl_3 —NaCl—KCl, and TiF_3 —NaCl—KCl at 850°–900°C under an inert atmosphere (26). A further process involving electrolysis of TiCl_4 in a LiCl—KCl mixture at 400°C has been reported (27).

The present authors have reported on the electrolysis of K_2TiF_6 in NaCl producing a very pure titanium powder (28). A major difference in this work and that of earlier investigation (23) was the use of a controlled inert atmosphere.

TiO Preparation

Claims for the formation of TiO by reduction of TiO_2 by carbon (29–31), by Zn (32, 33), by Mg (34), and by Na (35) have been made. The possibility of

TiO in slags from the smelting of titaniferrous ores has been described (36).

In all of these studies the TiO was generally not pure; some (33, 32) found it to have an indigo-blue color, while another obtained it as a black crystalline mass prepared by heating the TiO_2 with carbon in the electric arc furnace. Newberry and Pring (37) found that under a pressure of 150 atm hydrogen reduces titanous acid at 2000°C to the monoxide.

One mole of TiO_2 was reacted with two moles of Mg powder at a red heat in a current of hydrogen, the reduction taking place with incandescence (38). The product was cooled in an atmosphere of hydrogen, washed in glacial acetic acid, dried at a moderate heat, then completely dried in a current of hydrogen at 150°C. A brown powder was obtained which contained no metallic material but a lower oxide of the metal, mixed with magnesium in the form of magnesium titanate. From the quantity of oxygen taken up on heating the reduction product, it appears that the reduction takes place according to the equation $2\text{TiO}_2 + \text{Mg} = \text{TiO} + \text{MgTiO}_3$. When sodium vapor is passed over heated TiO_2 , the product is a mixture of TiO and Ti_2O_3 (35).

TiO was obtained as a brown powder by heating an intimate mixture of TiO_2 and metallic Ti (38), but no information was given regarding the properties of TiO. Carstens (36) prepared TiO as described above. X-ray analysis (39) of TiO prepared this way (36) showed that it belongs to the cubic system (NaCl type) with the cube edge $a_0 = 4.235 \text{ \AA}$. The calculated specific gravity lies between 5 and 6.

Others (40) prepared TiO in a like manner, but were unable to confirm the formation of TiO as a solid phase by the reduction of TiO_2 with carbon. Junker (41) also assumed that the reduction of TiO_2 with carbon merely yields mixtures of Ti_2O_3 and TiC.

Dawihl and Shroeter (42) also prepared TiO by reaction of Ti and TiO_2 . The mole for mole mixture was pressed into rods and heated in a vacuum of 1×10^{-3} mm Hg at 1700°–1750°C. It was later found that 1550°C was high enough. These rods were golden yellow in color, and broke with a coarsely crystalline fracture. X-ray analysis showed it to have an NaCl structure with $a_0 = 4.154 \text{ \AA}$ (see above).

Metallographic examination revealed that the TiO rods were porous but consisted of a homogeneous yellow coarsely crystalline phase, as is confirmed by x-ray examination.

TiO dissolves slowly in dilute H_2SO_4 and in HCl with evolution of H_2 . It does not dissolve in HNO_3 , but is rapidly oxidized to TiO_2 in the boiling acid.

When finely powdered and heated in air for one hour at 400°C, it is converted, with about 1% weight increase, into a dark-blue crystalline material; when heated one hour at 600°C, it becomes gray-green in

color, with about 5% weight increase; above 800°C oxidation to TiO₂ proceeds rapidly.

Determination of the specific gravity of finely powdered TiO samples shows a value of 4.93, considerably lower than that calculated from the edge length of the elementary unit or by x-ray analysis (39). The melting point of TiO, determined by the Pirani-Alterthelm bore-hole method (43) was found to be 1750°C. The electrical conductivity at room temperature averages 2490 reciprocal ohm cm.

Many of the literature references to TiO are in error. Observations of color alone illustrate this. It has been reported to be blue, green, black, violet, and golden. Pure TiO is a stable golden yellow compound and is essentially inert to most chemical attack (38, 42). This is borne out by the work described herein.

EQUIPMENT

Thermal reactions.—High temperature thermal reactions were initially carried out in high temperature Pyrex glass furnaces. The units were modifications of a design of Guldner and Beach (44). The unit is essentially a 3 in. Pyrex glass envelope fitted with a vacuum side arm, sight glass window, and a side arm magnetic crucible loading device. A fused clear quartz tube 2 in. in diameter is supported on glass hooks inside the Pyrex tube by platinum wire. A 3/4 in. ID x 3 in. graphite crucible is inserted inside this tube surrounded by graphite filings for insulation. Pelleted reaction mixtures are dropped in the crucible from the side arm above.

The furnace unit is heated by a 3 1/8 in. ID induction coil powered by a 6 kw Ajax converter. A flat glass plate on the furnace bottom is removable for loading. A large Pyrex funnel fits over the bottom of the furnace; an air jet blows through this for cooling.

The furnace is connected through a dry ice-acetone cold trap to an Eimac oil diffusion pump (HVI). A Cenco Megavac is used as forepump. Ionization and thermocouple gauges are in the line between the trap and diffusion pump. The system is capable of attaining a vacuum of 10⁻⁴ mm of mercury at 1500°C. Temperatures in excess of 2000°C are possible.

This equipment was employed for sintering or melting of small titanium samples as well as for thermal reactions.

When larger amounts of monoxide were required, the vacuum thermal reactor was scaled up to produce TiO in 100 g lots. The components were the same, except that the diffusion pump was eliminated. A quartz tube furnace with lampblack insulation was used. The graphite crucible was 1 3/4 in. ID by 7 in. high and was molybdenum-lined to eliminate TiC formation. The rest of the vacuum line was composed

of welded steel fittings. An ultimate vacuum of 10–15μ was used and temperatures to 2500°C were possible.

Electrolytic Cells

Two sizes of cells have been utilized in this work, but both are of similar design. One has a 100 g salt capacity and the other a 2250 g capacity. The cell has several specific functions: (a) be capable of temperatures to 1000°C; (b) provide an inert air free atmosphere; (c) be resistant to chlorine and salt corrosion; and (d) provide for d-c electrodes.

Graphite is the principle material of construction being used for the entire interior of the cell including a crucible container for the melt. A steel outer shell is used but this is protected against chlorine by an insulating layer of calcined lampblack. A graphite retaining inner shell holds the lampblack in place. A machined graphite resistance heating element is located just inside this shell. Water cooled external copper leads are employed to feed alternating current to the element. The graphite crucible fits inside the element, and rests on a graphite pedestal. This pedestal in turn rests on a nickel post welded through the bottom of the steel shell. This enables the crucible to serve as an anode. The top of the furnace is fitted with a removable head allowing insertion of the crucible. Holes are provided for admission of the cathode, charging of the salts, and observation. These are normally closed with graphite plugs. Argon is admitted through the bottom of the cell. A.C. power is supplied by a 7.5 kva transformer coupled with a variable voltage transformer. D-C power is furnished by a 400 amp motor generator. Argon used was 99.9% pure, but was further purified by passing through a P₂O₅ tower and a hot titanium sponge tower.

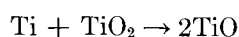
Cells of this type have been further described in a previous article (45).

Arc melting furnace.—A small arc melting unit was constructed in order to consolidate the metal powders produced for evaluation. A water cooled copper hearth anode is used with a water cooled tungsten tipped cathode. A Pyrex cylinder encloses the unit and is sealed against the copper with neoprene gaskets. A 400 amp motor generator powers the unit which can melt up to 50 g of titanium per melt. The cathode is silver soldered to a copper head through a bellows arrangement allowing flexibility; vacuum and argon inlets are also made through this head. Melting is done under about 200 mm of argon pressure.

PREPARATION OF TiO

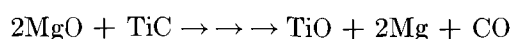
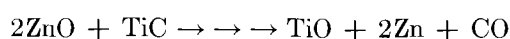
Initially, TiO was prepared by a 1200–1400°C solid-state reaction between the metal and dioxide.

This produces a very pure monoxide when the reaction is carried out under vacuum or argon.

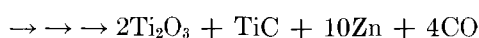
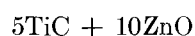


After the process fundamentals were established other methods of preparation were investigated. Three successful reactions were found. It was prepared from titanium carbide by reaction with zinc or magnesium oxide and by direct carbon reduction of the dioxide. All were run under high vacuum to enable removal of by-product gases as rapidly as formed to prevent recombination with titanium. In all cases, reactants were mixed by micropulverizing and ball milling, and then compressed into pellets. Reactions were carried out in molybdenum-lined graphite vessels.

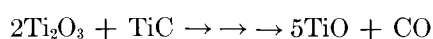
Zinc oxide and magnesium oxide react with the carbide nearly identically according to the reactions,



Zinc or magnesium starts to come off at about 900°C. The metal is collected in a special condensing trap between the furnace and pump. Evolution of metal and CO is complete at 1350°–1400°C. The reaction is stepwise, first going to Ti_2O_3 . The first stage of the reaction accomplishes removal of all of the Zn or Mg and most of the CO.



A temperature of 1730°–1740°C is required for the sintering operation to insure complete reaction of the Ti_2O_3 in the second stage of the reaction.



The TiO as produced by this method is a uniform golden yellow in color with a near lustrous characteristic of the crystals. Typical TiO ingots are illustrated in Fig. 1. It has a melting point of slightly more than 1775°C. When touched to a grinder, orange yellow sparks are emitted. A small amount of Ti_2O_3 present greatly reduces this sparking.

The exact pressure maintained in the system is not critical as long as it is substantially reduced and the atmosphere is free of air and moisture. Successful runs have been made where the pressure was never less than 1000 μ .

The mixtures employed were not strictly stoichiometric. Extra ZnO was added, e.g., to allow for its moisture content and to compensate for free carbon in the TiC. The TiC as received contains several per cent of iron. This is leached out with acid or ferrofiltered prior to mixing with the oxides.

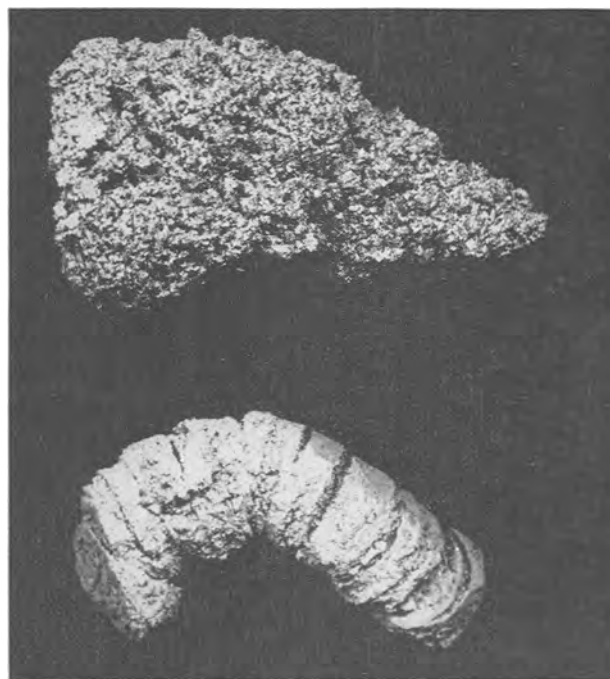
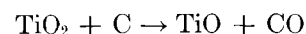


Fig. 1. Typical TiO ingots. Above, from tamped ZnO-TiC mix; below, pressed from ZnO-TiC mix

The sesquioxide may be prepared in like manner using a 2:5 ratio of TiC to ZnO or MgO.

These reactions are particularly attractive since only the product oxide remains in the crucible. Products so formed are of near theoretical composition, and low in all impurities.

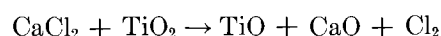
The alternative thermal method is more direct, since the intermediate TiC formation is unnecessary.



This reaction is carried out in the same manner and in the same equipment as the oxide-carbide reactions. It is run just under the melting point of TiO which is about 1750°C. This is also a stepwise reduction going through the Ti_2O_3 stage. High vacuum is essential to prevent reversal of the reaction.

Typical data for preparation of TiO by thermal reactions involving the reaction of TiC with zinc or magnesium oxides and reduction of TiO_2 with carbon is given in Table I.

A further alternative method for TiO preparation is attractive in light of the process for metal preparation. This is an electrolytic procedure involving electrolysis of TiO_2 dissolved in CaCl_2 under an inert atmosphere. At 1000°–1100°C, under 4–5 v, TiO is deposited cathodically from such a melt per the reaction



Melts consisting of 80% CaCl_2 and 20% TiO_2 have been used. The TiO deposits as a golden yellow crystalline mass interspersed with salts. It is re-

TABLE I. Preparation of TiO by thermal reaction

Run No.	Furnace charge	Temp, °C	Time, min	Pressure		Yield TiO %	Remarks
				Min	Max		
4447-1	28.3 g TiC 41.5 g MgO*	1400-1700	90	10 μ	600 μ	98.5	No Mg evolved after 45 min
4476-1	47 g TiC 41.5 g MgO*	1500-1700	90	10	700	98	
83-17	198 g TiC 256 g ZnO	RT-780	43	150	790	ND†	P break 862°-heavy Zn reaction over 142 min
		862-1100	142	3800	>5000		
		1175-1200	138	760	2800	ND†	Sintering step
		RT-1590	52	100	>5000		
83-36	198 g TiC 256 g ZnO	1600-1730	39	5500	>5000	ND†	P break <965°-heavy Zn
		RT-750	35	160	1500		
		965-1075+	140	5000	>5000	ND†	Sintering step
		RT-1160	39	90	570		
83-82	5900 g TiO ₂ 890 g C	1160-1720	45	1900	>5000	ND†	Heavy gassing
		RT-1115	57	170	1700		
		1165-1540	206	1500	>5000	84	Shrinkage noted
		RT-1160	92	150	150		
83-103	6000 g TiO ₂ 900 g C	1160-1750	285	150	1000	74	P break 925°, 99 min
		RT-1145	203	80	4800		
		1150-1400	170	1900	>5000		
		RT-950	100	50	170		
		1145-1520	220	40	1300		

* 91.8% MgO.

† Not determined.

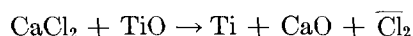
TABLE II. Electrolytic preparation of TiO

Run No.	Electrolyte composition	Temp, °C	Time, min	E volts	Current density amp/dm ²	Total amp hr	Current efficiency %	Total yield %
2286-D1	80% CaCl ₂ 20% TiO ₂	975-1050	45	5.0	200	20	48	97
2273-B1	80% CaCl ₂ 20% TiO ₂	1200-1250	15	7.5	400	12	ND	ND
2273-B2	80% CaCl ₂ 20% TiO ₂	1150-1200	30	6.5	300	20	46	95

covered by crushing the mass and washing in hot water and dilute HCl. The latter wash serves to remove any occluded CaO. Data for TiO₂ electrolysis are shown in Table II.

PREPARATION OF TITANIUM METAL

Titanium metal is produced from the monoxide by electrolysis in molten anhydrous CaCl₂. The over-all cell reaction is



The exact mechanism of the process has not been conclusively demonstrated, but a number of facts and observations can be listed.

TiO is soluble only to about 0.5% in CaCl₂, at 850°C. However, this would be sufficient to satisfy a reaction mechanism dependent upon the solubility factor. It is reasonably certain that the TiO solubility is a factor in this process, either chemically or electrically. As the process is carried out, the CaCl₂ is first melted and the TiO charged on top of the

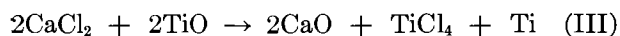
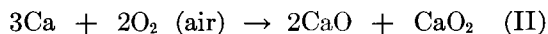
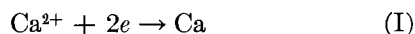
melt. The bulk of the TiO settles to the bottom becoming part of the anode.

A purification electrolysis is usually run prior to addition of TiO to further purify the CaCl₂. A graphite cathode is employed for this purpose. Any deposit is discarded.

The main electrolysis is carried out using a rod cathode of steel, molybdenum, titanium, or zirconium. The portion of the cathode above the bath level is protected from chlorine by a graphite sleeve. Electrolysis is run under 3–5 v at 850°–900°C using a current density of 200–500 amp/dm². A concentration of 5–10 wt % TiO is generally employed.

It is possible that the reaction is a two-step procedure, TiO going into solution as an ion, probably TiO²⁺, and migrating to the cathode where it interacts with calcium metal produced there, which in turn reduces the titanium ion to metal. This explanation is somewhat justified by the following.

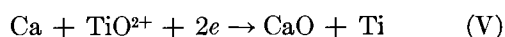
At the start of the electrolysis, a great deal of fuming takes place. This is largely CaO (from Ca metal vapor) with some CaO₂ and TiCl₄. Calcium is formed and floats on the bath surface, some of it volatilizing and oxidizing as it leaves the cell.



After 10–15 min of electrolysis the process proceeds quietly and fuming ceases. If TiO is oxidized anodically, it can migrate to the cathode as an ion:



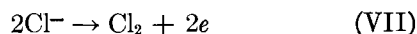
Calcium liberated at the cathode according to (I) can then reduce this ion.



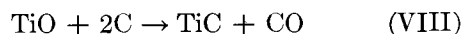
The lime so formed is not too soluble in CaCl₂ and much of this would precipitate out; such is found on the bath surface. As solubility permits, some is added to the electrolyte and broken down in preference to CaCl₂. Any oxygen so evolved would be liberated as CO at the anode.



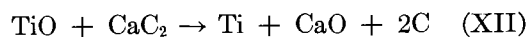
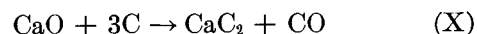
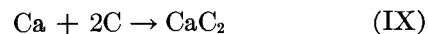
Chlorine must also evolve at the anode if Ca is produced.



Certain side reactions take place to some extent causing some contamination. The most serious of these are carbide formation and liberation of free carbon.



Lime or calcium may react with carbon to form CaC₂. Titanium oxide then can react with this CaC₂ producing further TiC impurity, or perhaps elemental carbon.



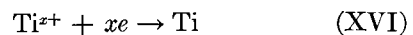
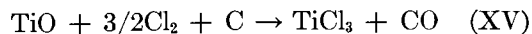
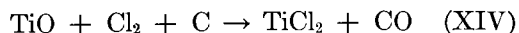
Calcium metal can also reduce CO, and this may occur to some extent.



Any rechlorination of calcium or titanium will, of course, reduce the efficiency of the process.

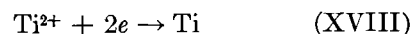
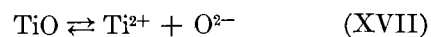
If this sort of mechanism prevails, then titanium is actually produced from a +4 valence change. All efficiencies are calculated on the basis of a divalent change however (0.8935 g/amp-hr).

It is frequently observed, particularly above 900°C, that very little chlorine is evolved from the cell for the amount of metal produced. This suggests that the above mechanism is not valid and that a straight electrolytic mechanism would prevail. This could involve a chlorination of the TiO at the anode to TiCl₂, TiCl₃, or both which is subsequently broken down electrolytically.



This would then account for the excess Ca formed and subsequent CaC₂ and also the lack of chlorine evolution in many runs; it would also explain the formation of some TiCl₄ early in the run.

A third mechanism might involve ionization of TiO and a direct electrolysis to yield CO and Ti.



CO is evolved from the cell, but such a mechanism has little other evidence in its favor. The chlorination and Ca reduction mechanisms appear the most likely possibilities at present.

When the salt bath is exhausted of Ti, a voltage rise and current drop occur. A red flame is then detected at the cell vent indicating heavy calcium production. The cathode is withdrawn from the bath and the power shut down. The cathode is allowed to cool in the argon atmosphere and subsequently removed from the cell.

TABLE III. *Electrolysis of TiO in CaCl₂*

Run No.	TiO %	Pre-electrolysis		Electrolysis					Yield %	BHN arc-melted ingot	Remarks
		Volts	Amp hr	Temp, °C	Volts	Current density amp/dm ²	Amp hr	Current efficiency %			
61-23	8	1-2	9	880	4-6	200-450	288	51	88	—	
74-151	3.2	1.4-2	10	900	5.2-6.3	150-450	95	33	51	362	Run to end of fuming
75-182	4.2	1.3-1.8	1	885	7.3-6.4	250-300	166	40	79	382	
93-125	4.2	1.2-1.7	9	820	7.4-6.2	300	165	22	43	—	Low temperature

The cathode deposit is a cylindrical shaped mass of metal and salt particles. It is sponge-like in character and loosely adherent to the metal cathode rod. The deposit is gray in color and contains many metal agglomerates, but no well-defined large crystals. Such deposits are from 40-60% metal.

The deposits are mechanically broken off the rod, crushed to -40 mesh, and washed in warm water to remove excess salts. An acid treatment in dilute HCl or HCOOH removes CaO. Final water washing removes the acid.

Typical data for the electrolysis of TiO—CaCl₂ baths are shown in Table III including power and efficiency figures. Fig. 2 illustrates the type of cathode deposit obtained.

As-recovered metal powder is largely +150 mesh.



FIG. 2. Typical cathode deposit. Titanium produced by electrolysis of TiO in CaCl₂.

The material analyzes up to 99% titanium, the balance being principally oxygen and carbon.

Consolidated arc melted pellets have shown a hardness range of 200-900 Vickers. They have averaged 300-400 Vickers which is outside the range of commercial titanium. The high hardness values are due principally to carbon and residual oxygen.

Decomposition Potentials of Titanium Oxides

As a supplement to this program, decomposition potentials of TiO and TiO₂ were determined in CaCl₂. This entailed a series of current-voltage curves using standard salt baths of TiO and TiO₂ in CaCl₂ as employed in the electrolytic TiO and metal preparations.

A small, 100 g inert atmosphere graphite resistance furnace was used as the cell. A selenium rectifier was coupled with a current voltage control for use as a d-c source. This unit can be set for a given current or voltage and will maintain such a setting on the cell regardless of resistance changes. A recorder is included in the circuit to plot temperature, current, or voltage. Measurements were made with AGR graphite electrodes. The regulator was set at voltages from 1-5 progressively. Currents corresponding to these settings are then recorded. On plotting such data as current density vs. voltage

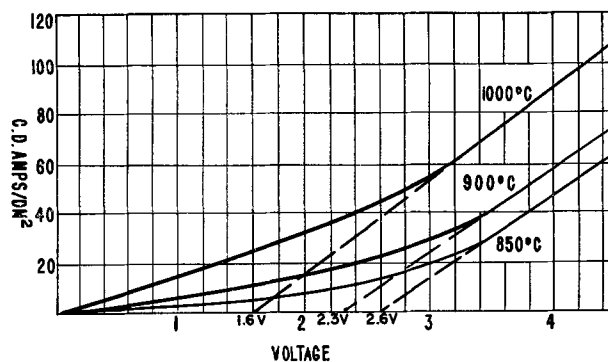


FIG. 3. Decomposition potential measurements; 15% TiO in CaCl₂.

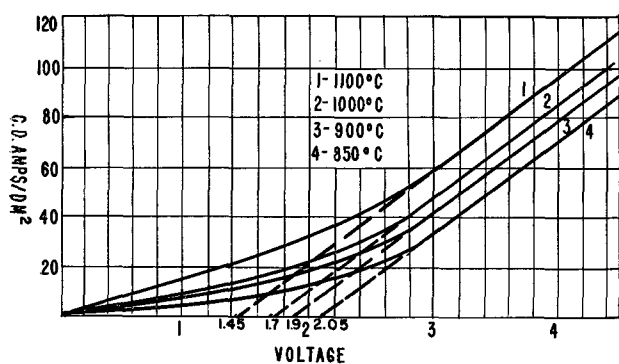


FIG. 4. Decomposition potential measurement; 20% TiO_2 in CaCl_2 .

and extrapolation to zero current, an approximate value of the decomposition voltage is obtained. Measurements were made using baths of 15% TiO and 20% TiO_2 at 850°, 900°, 1000°, and 1100°C. Results are shown in Fig. 3 and 4.

DISCUSSION

The effects of various factors on operation of and results from the process have been largely ascertained and are discussed below.

Reagents.—It has been demonstrated that high purity chemical reagents lead to better over-all results. It is not difficult to obtain high purity TiO , but the CaCl_2 is difficult to obtain in a pure dry state. Thus this material is thoroughly air-dried at 110°C for long periods prior to charging to the cell. Water is deleterious to the process since oxygen is anodically liberated on electrolysis, causing oxidation of the TiO . Small amounts of CaO are not harmful, since this is normally produced as a by-product in the electrolysis.

Despite oven drying of the CaCl_2 , a low voltage pre-electrolysis of the molten salt gives off large amounts of H_2 and CO . This has been carried out routinely through all the work to obtain as anhydrous a bath as possible. In general, this pre-electrolytic cycle is run at 1–2 v for approximately 10 amp-hr. Gas evolution is noted at both electrodes; the effluent gases are primarily CO and H_2 .

The use of the CaCl_2 electrolyte is reasonably specific for the process. A series of runs with varying bath compositions are reported in Table IV. In no case has an alkali metal halide resulted in a satisfactory run. The CaCl_2 bath may be mixed with LiCl up to 50 wt % and be run with reasonable success [74–16]. Similarly, KCl may be used up to 20–25% [74–20]. Presumably, other alkaline earth chlorides may be used if they are sufficiently anhydrous. Successful runs have been made with a good grade of BaCl_2 in 30–35% concentration with CaCl_2 , but even BaCl_2 seems to have a deleterious

TABLE IV. *Electrolyte composition*

Run No.	Electrolyte composition %	Current efficiency	Yield %	Remarks
74-16	55% CaCl_2 45% LiCl	22	50	Bath vacuum melted
75-44	28% CaCl_2 72% LiCl	—	—	No deposit
93-131	80% CaCl_2 20% LiCl	10	16	
74-20	80% CaCl_2 20% KCl	20	45	Bath vacuum melted
93-140	80% CaCl_2 20% KCl	7	9	Bath vacuum melted
74-36	80% CaCl_2 20% MgCl_2	—	—	No deposit
74-40	50% NaF 50% KF	—	—	Only Na produced
74-44	40% MgF_2 60% CaF_2	—	—	Small deposit—not recovered
75-16	100% NaCl	—	—	No deposit— TiO not soluble
75-37	84% NaCl 16% CaCl_2	—	—	No deposit—many polarizations
75-40	65% CaCl_2 35% NaCl	—	—	No deposit
75-199	90% CaCl_2 10% CaF_2	7	14	Very poor deposit
93-17	55% CaCl_2 45% BaCl_2	2	4	
93-128	68% CaCl_2 32% BaCl_2	35	67	
93-27	60% CaCl_2 40% Na_2CO_3	—	—	Na_2TiO_3 produced 131 g

effect if this concentration is exceeded (runs 93–17, 93–128). It is thought that MgCl_2 could be used if it were sufficiently pure; the grade used [74–36] was high in oxide and moisture content.

In no case has a successful run been obtained with fluoride present. Even the addition of 10% CaF_2 resulted in a gross reduction in efficiency and metal quality [75–199].

When alkali halides (NaCl , KCl) are substituted for CaCl_2 as an electrolyte, only the alkali metal is

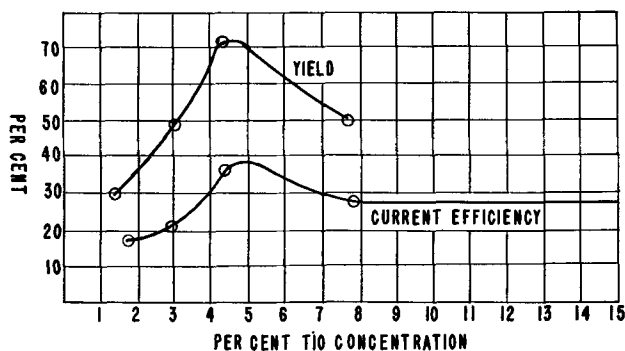


FIG. 5. Effect of TiO concentration

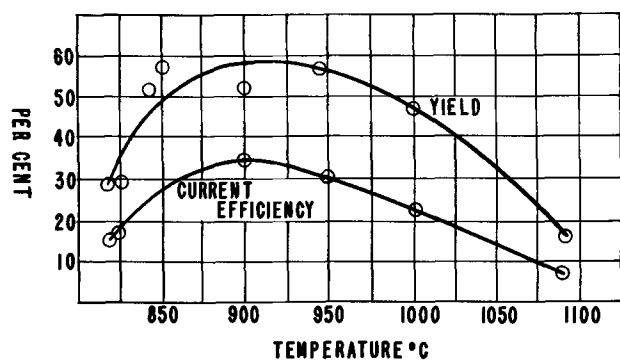


FIG. 6. Effect of temperature on current efficiency and yield.

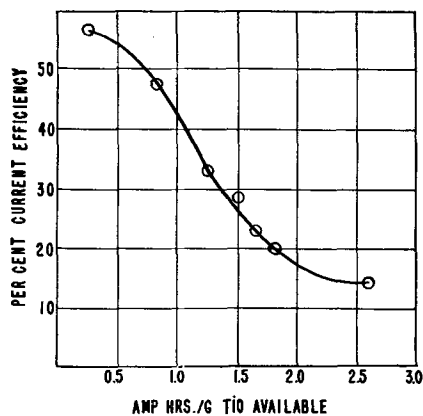


FIG. 7. Change in current efficiency with time of electrolysis.

produced. The TiO remains inert and has been recovered in its original form after such runs.

Concentration of TiO.—TiO concentration has a profound effect on operation or efficiency of the electrolytic cell. Low concentrations of the order of 1–2 wt% are undesirable and result in lower efficiencies. There is apparently an optimum concentration of 4–5% TiO where maximum efficiency and recovery are obtained. At higher concentrations the total yield is reduced, possibly due to a cyclic reaction whereby metal produced reacts with available TiO or a halide intermediate.

TABLE V. Variation of cathode current density $900^{\circ} \pm 25^{\circ}\text{C}$; 3.2% TiO bath

Run No.	Current density amp/dm ²	Volts <i>E</i>	Current efficiency	Yield %	Remarks
74-14	600	10	—	—	Poor results
75-182	260-300	7.3-6.4	40	79	BHN 382
74-130	200	6.8-5.9	18	45	BHN 509
74-109	200	7.9-7	21	51	
74-104	120-130	5.4	8	18	

The rate of reaction is apparently governed largely by solubility of TiO in the melt and/or its interaction with the melt rather than initial concentration. The concentration effect is illustrated by Fig. 5.

Temperature.—The optimum salt bath temperature has been found to be about 900°C for the CaCl_2 -TiO melt. At this point efficiency and metal recovery are at a maximum. The process is not operable at less than 800°C or above 1100°C . Runs of varying temperature are plotted as Fig. 6.

Time of electrolysis.—Reduction efficiency is at a maximum in the initial stages of a run. It falls off quite rapidly after about one-half the TiO has been utilized (5–6% bath). Thus, it is preferable to charge more TiO after a run is about half done rather than to attempt to exhaust the bath. The effect of time is demonstrated in Fig. 7 where current efficiency is plotted as a function of ampere hours/gram TiO input current. It is noted that this curve falls off rapidly after about 1 amp-hr/g.

Current density.—Current density and voltage may be varied to some extent and still yield satisfactory results. However, maximum efficiencies are obtained at about 300 amp/dm². Runs made at less than 150 or more than 500 amp/dm² are generally poor with respect to current efficiency. Voltages of 4–8 yield satisfactory results. Typical runs showing this variation are listed in Table V.

Metal Evaluation

As previously stated, titanium metal produced by electrolysis of TiO in CaCl_2 has not generally been acceptable by present purity standards. Its oxygen content is somewhat high and the carbon content is excessive. This is evidenced by the typical structures in Fig. 8 and 9. These are arc melted 10 g ingots electrolytically polished. The lattice-like structure is typical of high oxygen titanium and a large amount of carbide precipitation is evident at the grain boundaries. Carbon is a more serious contaminant than oxygen despite the nature of the source material.

The hardness of metal produced was generally in the range BHN 250–400. Arc melted ingots have been successfully hot rolled, but the sheet produced is

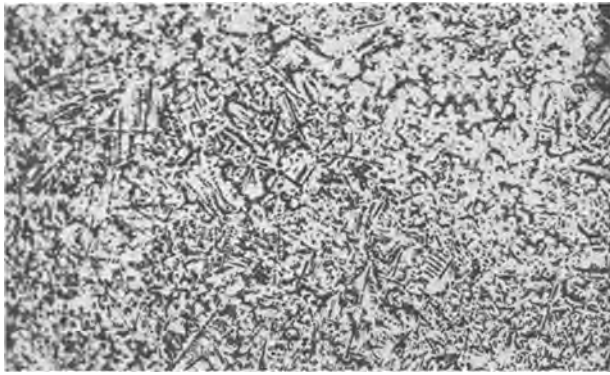


FIG. 8. As-cast titanium, showing dendritic structure of carbide phase. Lattice-like typical high oxygen titanium structure. Unetched. 100X before reduction for publication.

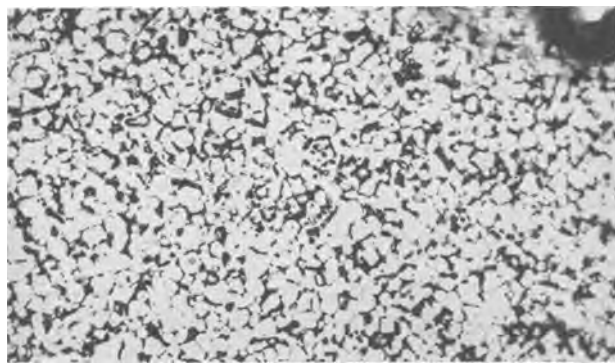


FIG. 9. Same as Fig. 8, but at 250X before reduction for publication, showing carbide precipitation at grain boundaries in detail.

TABLE VI. Spectrographic analyses

	Ti Metal 75-178	TiO 83-44
ZrO ₂	0.07	0.20
TiO ₂	Major	Major
SiO ₂	0.50	0.35
Fe ₂ O ₃	0.20	0.10
MgO	0.05	0.002
MnO	0.05	0.001
HfO ₂		
Al ₂ O ₃	0.15	0.20
Cb ₂ O ₅	0.05	0.05
MoO ₃	0.001	0.003
V ₂ O ₅	0.60	0.60
CaO	1.5	0.05
CuO	0.003	0.005
NiO	0.001	0.001
PbO	0.001*	0.001*
K ₂ O	0.001*	0.001*
Cr ₂ O ₃	0.07	0.03
Na ₂ O	0.001*	0.001*
Li ₂ O	0.001*	0.001*
P ₂ O ₅	0.02	0.02

* Less than.

Not detected: Co, B, Sb, As, Cd, Sn.

brittle. The metal in general runs from 96–98% titanium, 0.1–0.3% oxygen, and 1.5–3% carbon. Nitrogen and hydrogen contents are quite low, both <0.05%. Other impurities of some significance are Si, Fe, Al, V, and Ca. Of these, all but Ca presumably have their major source in the TiO and could be reduced by improvement in the purity of the TiO. Table VI shows spectrographic analyses of a lot of TiO and metal prepared from it. The relationship and carry-over of impurities is quite evident.

CONCLUSIONS

A process has been developed whereby titanium metal of moderate purity may be electrolytically produced from its monoxide. The process at present is not suitable for preparation of commercially pure titanium, but suitable modifications in cell design and operational procedures may enable further improvement in the process.

The exact mechanism by which the reduction proceeds is not known. It is known that TiO is soluble in CaCl₂ to a small extent, whereas it is not soluble in NaCl which likewise will not function as an electrolyte. Thus, the process apparently depends on this factor at least to some extent.

The loosely packed sponge-like cathode deposits suggest that the titanium may be the result of a secondary reaction, i.e., reduction of a titanium ion by calcium metal. Calcium metal has been found in deposits and salt baths on occasion. The production of CaC₂ as a side reaction is also suggestive of this type of mechanism. The fact that process efficiency is essentially nil above 1100°C is further evidence, since calcium boils at about 1200°C.

Alternatively, the process may be electrolytic in nature whereby Ti²⁺ ions are cathodically reduced. The fact that titanium is found in a cathode mass and not dispersed throughout the bath seems to indicate this. Calcium metal is liquid at the operating temperature and is found in areas of the cell other than the cathode. The fact that very little Cl₂ is produced at higher temperatures is also support for this mechanism. Gas evolution is primarily CO under these conditions.

The most complete phase of this work is in the methods developed for producing TiO. Any of the four methods described, with the possible exception of the electrolytic procedure, are well defined and could be commercially adapted to production of TiO in pure form. The reaction mechanism and operating characteristics of the thermal reactions are well worked out.

Even though pure titanium has not been produced from TiO, it has been shown that minimum oxygen products can be produced. A revised cell type to overcome the carbon contamination prob-

lem conceivably could enable the successful validation of this process.

ACKNOWLEDGMENT

The authors are indebted to the Office of Naval Research for their continued support of this research effort, and permission to publish this work. Credit is also given to a number of staff members who assisted in the carrying out of this work: electrolysis program, E. Thellmann and A. Topinka; materials preparation, B. C. Raynes, S. Carlton, and J. K. Abbott; evaluation, E. D. Fisher and J. Wick; analysis, R. R. Britton, S. Leber, and M. Rose.

Any discussion of this paper will appear in a Discussion Section to be published in the December 1955 JOURNAL.

REFERENCES

1. N. N. GRATSIANSKII AND A. P. VOVKOGON, *Zapiski Inst. Khim. Akad. Nauk U.R.S.R.*, **7**, 173 (1940).
2. M. HAISSINSKY AND H. EMMANUEL-ZAVIZZIANO, *Compt. rend.*, **204**, 759 (1937).
3. M. HAISSINSKY AND H. EMMANUEL-ZAVIZZIANO, *J. chim phys.*, **34**, 641 (1937).
4. E. POKORNY AND K. SCHNEIDER (I. G. Farbenind, A.-G.), German Pat. 582,528, April 22, 1934; 605,551, Nov. 13, 1934.
5. R. H. LEUTZ, German Pat. 741,670, Sept. 30, 1943.
6. G. J. MOUNDRITCH, "Contribution to the Study of the Coating of Iron with Titanium," Part II, ScD. Thesis, University of Nancy, France (1931).
7. B. DIETHELM AND F. FORSTER, *Z. physik. Chem.*, **62**, 129 (1908).
8. A. S. RUSSELL, *Nature*, **127**, 273 (1931).
9. H. BOZON AND A. BOZON, *Bull. Soc. Chim.*, **18**, 917 (1951).
10. D. B. KEYES AND S. SWANN, *Univ. Illinois Bull. Eng. Exp. Station Bull. Ser.*, No. 206, **23**, 13 (1930).
11. A. TRAVERS, *Chimie & industrie*, Special No. 347 (1932).
12. R. GROVES AND A. S. RUSSELL, *J. Chem. Soc.*, **1931**, 2805.
13. J. L. ANDRIEUX, *J. four elec.*, **57**, 26 (1948).
14. J. L. ANDRIEUX, *Rev. met.*, **45**, 49 (1948).
15. R. KEENEY, *Elec. J.*, **17**, 206 (1920).
16. N. S. SPENCE, *Canadian Mining Met. Bull.*, **44**, 21 (1951).
17. G. GIN, *Trans. Am. Electrochem. Soc.*, **11**, 291 (1907).
18. Y. HAYAKAWA, *J. Electrochem. Assoc. Japan*, **15**, 64 (1947).
19. H. FISCHER AND K. DORSCH (Siemens and Halske, A.-G.), German Pat. 615,951, July 16, 1935.
20. W. HUPPERTZ, *Electrochem. and Met. Ind.*, **3**, 35 (1905).
21. J. KONIGSBERG AND J. SHILLER, *Physik. Z.*, **9**, 347 (1908).
22. M. DODERO, *Compt. rend.*, **208**, 799 (1939).
23. S. I. SKLYARENKO, Y. M. LIPKES, et al., *Zhur. Priklad. Khim.*, **13**, 51 (1940).
24. Shawinigan Water and Power Co., British Pat. 678,807, May 11, 1951.
25. G. D. P. CORDNER AND H. W. WORNER, *Australian J. Appl. Sci.*, **2**, 358 (1951).
26. A. BRENNER AND S. SENDEROFF, *This Journal*, **99**, 223C (1952).
27. Electrolytic Titanium, *Chem. Eng.*, **59**, 103 (1952).
28. M. A. STEINBERG, M. E. SIBERT, S. S. CARLTON, AND E. WAINER, to be published in this Journal.
29. P. BERTHIER, *Ann. chim. et phys.*, **7**, 84 (1843).
30. A. LAUGIER, *ibid.*, **89**, 306, 317 (1814).
31. H. MOISSAN, *Compt. rend.*, **120**, 290 (1895); **115**, 1034 (1892); *Ann. chim. et phys.*, **9**, 229 (1896); **4**, 136 (1895); *Bull. Soc. Chim.*, **9**, 957 (1892).
32. C. M. KERSTEN, *Pogg. Ann.*, **50**, 313 (1840); *J. Prakt. Chem.*, **20**, 373 (1840).
33. H. ROSE, *Pogg. Ann.*, **61**, 513 (1844).
34. C. WINKLER, *Ber.*, **23**, 2642 (1890).
35. T. KOENIG AND O. VON DER PFORDTEN, *ibid.*, **22**, 1485 (1889).
36. C. W. CARSTENS, *Z. Krist.*, **67**, 260 (1928); Kongelige Norske Videnskabers Selskabs, Det. Forhandlinger, 1926-28, No. 20, **56** (1929).
37. E. NEWBERRY AND J. N. PRING, *Proc. Roy. Soc.*, **A92**, 276 (1916).
38. M. BILLY, *Ann. chim. Paris*, **16**, 5 (1921).
39. H. BRÄKKEN, *Z. Krist.*, **67**, 547 (1928).
40. L. R. BRANTLEY AND A. O. BECKMANN, *J. Am. Chem. Soc.*, **52**, 3956 (1930).
41. E. JUNKER, *Z. anorg. u. allgem. Chem.*, **228**, 97 (1936).
42. W. DAWIHL AND K. SCHROETER, *ibid.*, **233**, 178 (1937).
43. Gmelin's Handbuch der Anorganischen Chemie, Vol. 8, p. 220, Verlag. Chemie, GMBH, Weinheim/Bergstrasse (1951).
44. W. G. GULDNER AND A. L. BEACH, *Ind. Eng. Chem., Anal. Ed.*, **22**, 366 (1950).
45. M. A. STEINBERG, M. E. SIBERT, AND E. WAINER, *This Journal*, **101**, 63 (1954).

The Electrochemistry of Some Nonaqueous Solutions of Alkali Metal Salts¹

HARRY C. MANDELL, JR.,² WALLACE M. MCNABB, AND J. FRED HAZEL

Department of Chemistry, University of Pennsylvania, Philadelphia, Pennsylvania

ABSTRACT

Conductivities of lithium chloride and bromide and potassium iodide and thiocyanate in pyridine have been redetermined and results are in good agreement with literature values. Previously unreported conductivities of lithium iodide dihydrate in pyridine, lithium chloride, bromide, and iodide dihydrate in quinoline, and lithium iodide dihydrate and potassium iodide and bromide in nitrobenzene have been determined.

The decomposition potential of lithium chloride in pyridine has been redetermined in agreement with an earlier worker. Original determinations were made of decomposition potentials of lithium bromide and iodide dihydrate in pyridine and in quinoline, and of potassium iodide and lithium iodide dihydrate in nitrobenzene. The decomposition potential of potassium thiocyanate in pyridine was found to be different than that recorded in the literature. The decomposition potential of potassium iodide in pyridine was not reproducible.

Using a platinum cathode, it was shown that it is possible to electrodeposit lithium from its bromide and iodide dihydrate in pyridine and quinoline and from its iodide dihydrate in nitrobenzene. In contradiction to results published by others, deposition of potassium from its iodide and thiocyanate in pyridine was accomplished. Metal deposits were all amorphous in gross appearance and were probably impure. These methods hold little promise of value as commercial means for alkali metal production.

INTRODUCTION

As early as 1897 conductances of lithium chloride, potassium iodide, and potassium thiocyanate in pyridine were studied. Laszczynski and Gorski (1) deposited lithium in a black crust from this solvent. A gray deposit from the potassium thiocyanate solution seemed to be potassium mixed with potassium sulfide. No decomposition potentials were given for this work. Kahlenberg (2) reported the plating out of lithium from its chloride in pyridine. Patten and Mott (3) gave the decomposition potential for this system as 4.0 v. Lithium has also been deposited from its iodide in pyridine (4).

Muller and coworkers (5) plated lithium from lithium chloride in pyridine above 4.05 v and from the nitrate above 5.0 v. Solutions of sodium iodide, nitrate, and potassium thiocyanate in pyridine were said to deposit the metals only when a mercury cathode was used. Potassium thiocyanate had decomposition potentials of 1.8 and 2.6 v on platinum. With regard to the electrolysis of potassium thiocyanate in pyridine, there is disagreement between the results of Laszczynski and Muller.

Lithium, sodium, and potassium have been deposited from solutions of their halides plus aluminum halides in nitrobenzene (6-8). There is no report of the electrolysis of alkali halides alone in nitrobenzene. The only recorded deposition of a metal from quinoline solution is silver from silver nitrate (9).

EXPERIMENTAL

Apparatus

The cell (Fig. 1) was 1¼ in. in diameter and 3 in. high. A loose fitting Plexiglass cover carried removable electrodes used for electrolyses and fixed electrodes for conductance measurements. All electrodes and connecting wires were of bright platinum. The area of the electrodes was 1 cm² each.

A glass encased stirring bar was used in the cell. The magnetic stirring motor was enclosed in a water-tight can, and the entire assembly was immersed in a constant temperature bath held at 25° ± 0.05°C.

The cell constant was determined using 0.001, 0.010, and 0.100*N* potassium chloride solutions. It was found to be 0.400 ± 0.001. There was no appreciable polarization effect on the bright platinum electrodes up to specific conductance values of 1.6 millimhos.

The power sources were 6 v wet storage batteries and a 125 v d-c line. Potentiometers were used to

¹ Manuscript received July 16, 1954. This paper was prepared for delivery before the Chicago Meeting, May 2 to 6, 1954.

² Present address: Research and Development Laboratories, Pennsylvania Salt Manufacturing Company, Philadelphia, Pa.

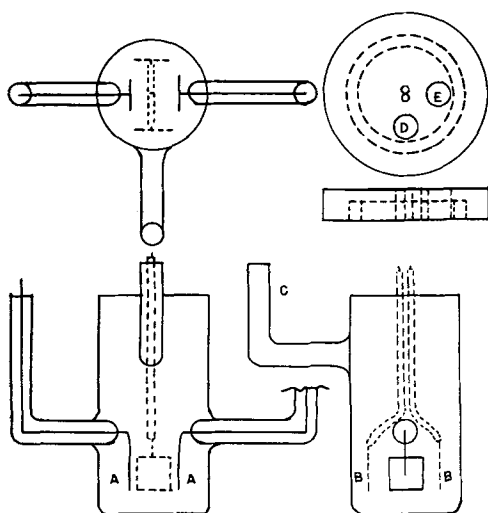


FIG. 1. Electrolysis cell and cover. (A) Fixed conductance electrodes; (B) removable electrolysis electrodes; (C) gas admission side arm; (D) burette tip admission hole; (E) thermometer admission hole.

obtain intermediate values of voltage. The current was measured with the 1.2 and 12 μ a ranges of a Triplett multimeter. Voltages were determined with a 0–15 v Simpson meter which had three extended ranges made by placing empirically cut resistances in series with it.

Conductances were determined with a Serfass RCM 15 model bridge. By placing a one megohm precision resistor in parallel with the test leads of the bridge, its range was extended from 10^6 to 10^8 ohms.

Reagents

Nitrobenzene.—Eastman Kodak White label nitrobenzene was stored over anhydrous potassium carbonate for one week. It was decanted and distilled under dry nitrogen, a 1.5° fraction being collected. This was redistilled in vacuo, the fraction boiling 55° – 57° C at 0.5 mm of mercury being collected. The specific conductivity was 4×10^{-8} mho.

Other portions of nitrobenzene were stored over phosphorus pentoxide for two weeks. These were distilled twice under dry nitrogen at atmospheric pressure. Fractions collected boiled over 0.5° to 1.0° C ranges. The specific conductivity was also 4×10^{-8} mho.

Pyridine.—Baker and Adamson reagent pyridine was stored over pellet potassium hydroxide for ten weeks. This was decanted and distilled under dry nitrogen. A central fraction boiling over 1.5° C was collected and redistilled under nitrogen. A portion boiling 114.5° – 115.5° C was kept and found to have a specific conductivity of 4×10^{-7} mho.

Quinoline.—Paragon Division (Matheson Company) quinoline was dried and distilled in the same

manner as was pyridine. From the second distillation a 2° C fraction was collected and found to have a specific conductivity of 2×10^{-8} mho.

Potassium bromide, potassium iodide, lithium chloride.—These Baker analytical reagents were pulverized and stored at 140° C.

Lithium bromide monohydrate.—Merck N.F. salt was recrystallized from water then heated to 175° C. The salt melted and then solidified. The solid was pulverized and stored at 175° C. According to Mellor (10) this salt is anhydrous above 159° C.

Lithium iodide trihydrate.—Merck. The salt was recrystallized from water. Attempted dehydration by simple heating led to obvious decomposition. The salt was stored over phosphorus pentoxide in a vacuum desiccator for two months. A sample of the resulting material was weighed out and treated with excess sulfuric acid. Evaporation and ignition converted it to the sulfate. Calculation from the weight of sulfate produced indicated that the salt resulting after desiccation was lithium iodide dihydrate.

Potassium thiocyanate.—Baker reagent salt was recrystallized from absolute alcohol and dried 18 hr at 95° C. It was stored over phosphorus pentoxide in a vacuum desiccator.

Procedure

The thoroughly dried cell and cover were placed in the constant temperature bath. Nitrogen was dried by passing it through saturated potassium hydroxide solution, anhydrous magnesium perchlorate, and phosphorus pentoxide. A brisk stream of the dry gas was passed through the side arm of the cell for at least 15 min. The salt to be studied was added swiftly from a weighed vial while the cover of the cell was raised. A measured volume (about 30 ml) of solvent was added from a buret through a hole in the cover.

The electrolysis electrodes were raised from the solution and the conductance was determined with the fixed conductance electrodes. The electrolysis electrodes were returned to their normal position and connected to the power supply. Five minutes after the voltage was applied, the current passing was noted, and a new, higher voltage was applied. In most cases, 0.5 v steps were taken. After a sufficiently complete polarization curve had been obtained, prolonged electrolysis was carried out to obtain a characteristic cathode deposit.

RESULTS

Results are presented in Tables I to III. The straight portion of the current vs. voltage curve for each system was extrapolated to zero current and

TABLE I. *Electrochemical studies in pyridine at 25°C*

Run	Solute	Conc. m/l	Spec. cond. $\times 10^6$ mho	Molar cond.	Dec. pot. v	Cathode current density amp/dm ²	Cathode product
1	LiBr	0.178	372.0	2.09	4.00	0.33	Lithium
2	LiCl	0.284	99.6	0.351	4.00	0.17	Yellow slime
3	LiI·2H ₂ O	0.534	6520.0	12.2	3.90	0.50	Lithium
4	KI	Sat.	181.0	—	5.40	0.50	Pot. and sludge
5	KI	Sat.	186.0	—	1.95	0.93	Pot. and sludge
6	KI	Sat.	210.0	—	1.90	0.44	Pot. and sludge
7	KI	Sat.	206.0	—	5.40	—	Brown sludge
8	KI	Sat.	208.0	—	1.50	0.43	Brown sludge
9	KCNS	0.2185	1440.0	6.59	1.50	0.29	Potassium
10	KCNS	0.205	1344.0	6.56	3.70	0.32	Potassium
11a	KCNS	0.1132	840.0	7.42	3.65	0.84	Potassium
11b	KCNS	0.1132	876.0	7.73	3.70	0.58	Potassium
12	KCNS	0.1327	944.0	7.12	3.70	0.59	Potassium
					3.65	0.54	Potassium

TABLE II. *Electrochemical studies in quinoline at 25°C*

Run	Solute	Conc. m/l	Spec. cond. $\times 10^6$ mho	Molar cond.	Dec. pot. v	Cathode current density amp/dm ²	Cathode product
13	LiBr	Sat.	5.20	—	3.4	0.038	Lithium
14	LiI·2H ₂ O	Sat.	588.0	—	3.45	0.10	Lithium
15	LiCl	Sat.	0.40	—	—	—	—
15a	LiCl	Sat.	—	—	—	—	—
	LiI·2H ₂ O	ca 0.1	184.0	—	3.40	0.22	Lithium

TABLE III. *Electrochemical studies in nitrobenzene at 25°C*

Run	Solute	Conc. m/l	Spec. cond. $\times 10^6$ mho	Molar cond.	Dec. pot., v	Cathode current density amp/dm ²	Cathode product
16	KBr	Sat.	0.36	—	—	—	—
17	KI	Sat.	6.80	—	1.80	0.11	Brown sludge
18	LiI·2H ₂ O	Sat.	88.0	—	2.50	0.34	Lithium

the corresponding voltage was taken as the decomposition potential.

Concentrations are expressed in moles of solute per liter of solvent. For dilute solutions this is almost identical to molarity, and these concentration values were used in computing molar conductances.

The current density at which prolonged electrolysis was carried out was calculated using the apparent cathode area of 2 cm² (both sides of the electrode). The voltages necessary to obtain these currents were, of course, mostly a function of the resistance of the solution. For systems of low conductivity, up to 115 v were applied.

Lithium deposits were all smooth and dull and ranged from dark gray to black in color. The potassium deposits were light gray in color and were characterized by extensive treeing and nugget formation on the edges of the cathode. All deposits appeared amorphous and were probably impure. There was never any discernible crystalline nature.

Deposits of both metals were completely adherent and did not peel or flake off the cathode.

Lithium and potassium deposited from pyridine were quickly and completely converted to metal oxide (or hydroxide) upon exposure to the air. In a few cases, the potassium reacted rapidly enough as the solvent (pyridine) evaporated to produce a small burst of flame.

Lithium and potassium produced by electrolysis were identified by the fact that the deposits dissolved vigorously in water with gas evolution. In some cases, an explosive flash of flame was observed. Characteristic flame tests were obtained with a platinum wire dipped in the water solution of the deposit. These tests were negative when no cathode product was observed.

The specific conductivity of lithium bromide was in good agreement with the value 375 micromhos which is obtained for that concentration by the authors' interpolation in Anderson's work (11).

The specific conductivity of lithium chloride

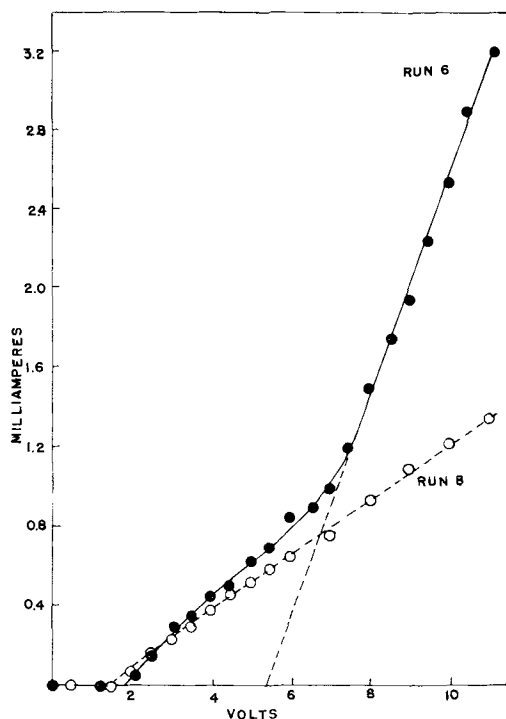


FIG. 2. Decomposition curve for KI in pyridine. Curve A, Run 6, Table I; Curve B, Run 8, Table I.

compared only fairly well with the value 88×10^{-6} mhos obtained by interpolation in the literature values of Anderson (11). The decomposition potential found was identical to that reported by others. Since only small currents were passed, it is reasonable to assume that the failure to deposit lithium was due to its reacting with the solvent as it deposited slowly. Emmert (12) has described the reaction of lithium with pyridine.

The iodide dihydrate of lithium was employed since it was the lowest hydrate of the iodide readily obtainable. The deposition of the metal from this system containing, molewise, twice as much water as lithium ion, was an unexpected result. The implication is that the extreme precautions taken to insure anhydrous conditions may not be necessary for the deposition of lithium. Others who have worked with lithium iodide in pyridine do not give the details of solute preparation. Anderson dried lithium iodide trihydrate by "constant heating." Since the hydrate he used is unknown, comparison of conductivities is not very meaningful. Von Hevesy (4) reported depositing lithium from its "iodide" in pyridine, but gave no decomposition potential or details concerning the solute.

The literature value for the conductivity of a saturated solution of potassium iodide in pyridine is 210×10^{-6} mhos (13). In runs 4 and 5 where the observed values were significantly lower, the fault was undoubtedly in allowing insufficient time for

solubility equilibrium. The solubility of potassium iodide in pyridine is 0.25 g/100 ml of solution at 10°C (17).

As is seen from Table I there was difficulty in reproducing the electrolysis of potassium iodide in pyridine. In runs 4, 5, and 6 the cathode products were gray nuggets mixed with brown sludge. These deposits dissolved explosively in water with a burst of flame and certainly seemed to contain metallic potassium. The polarization curves for runs 4-6 varied in shape for the region 2-6 v giving breaks at 1.9 and/or 5.4 v. Fig. 2 compares polarization curves for runs 6 (typical of runs 4-6) and 8 (typical of 7 and 8). Note that they were essentially the same up to 7 applied volts, whereupon run 6 displayed a rise in potential and potassium nuggets began to appear on the cathode. The cathodic product in runs 7 and 8 was only a brown sludge appearing after prolonged electrolysis. The same results were obtained by Patten and Mott (3). Part of the difficulty here was probably due to the relatively low conductivity of the system. Such a solution would be expected to be proportionately more sensitive to the effects of traces of impurities. This may not be the full reason for the lack of reproducibility.

The values of conductances for potassium thiocyanate in pyridine in runs 9 and 10 were in agreement with a smooth extrapolation of the data of Anderson (11). The values for runs 11 and 12 agreed

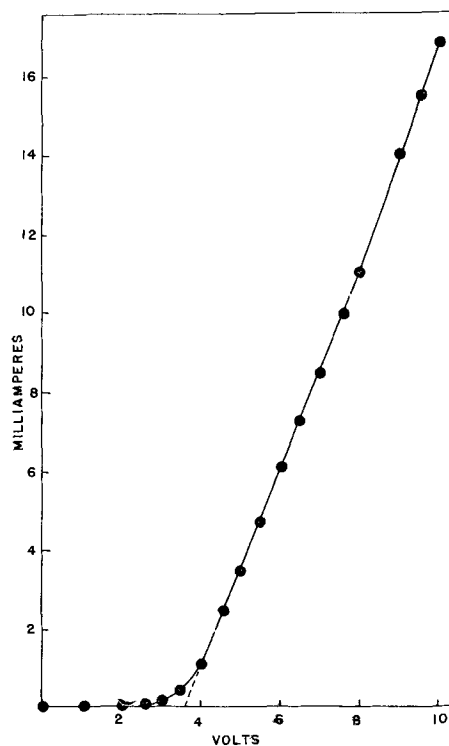


FIG. 3. Decomposition curve for KCNS in pyridine

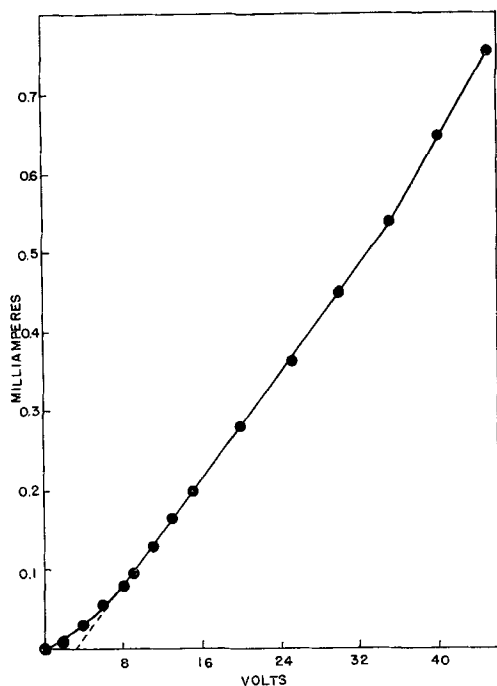


Fig. 4. Decomposition curve for LiBr in quinoline

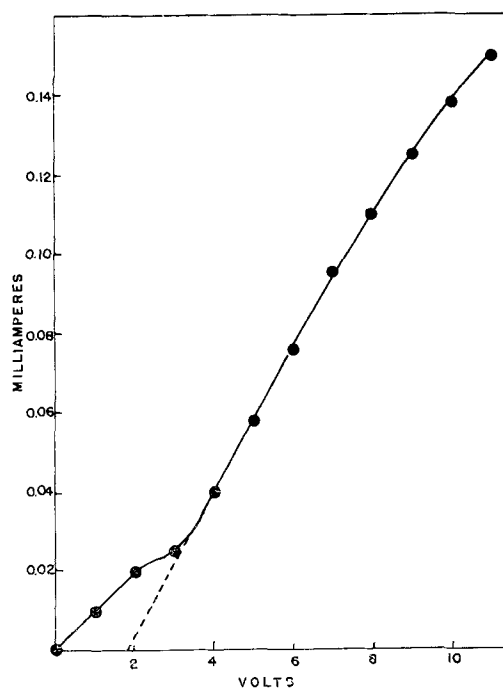


Fig. 5. Decomposition curve for KI in nitrobenzene

well with the values 840 and 950×10^{-6} mhos obtained by interpolation in Anderson's work.

The deposition of potassium on a platinum cathode confirms the observation of early workers (4, 15). The decomposition potential (Fig. 3) and the deposition of potassium observed are contradictory to the results presented by Muller (5).

The conductivity of lithium bromide in quinoline (Table II and Fig. 4) was so low that it was necessary to carry out electrolysis at 115 v for an hour to obtain an appreciable deposit. The concentration of saturated lithium iodide dihydrate in quinoline was about 0.26M.

Although the solubility of lithium chloride in quinoline is reported to be appreciable [0.3538 g/100 g quinoline (16)], the conductivity was too low to carry out electrolysis.

The conductivity of potassium bromide in nitrobenzene was too low to carry out electrolysis.

In run 17 (Fig. 5) a trace only of brown deposit appeared on the cathode. It dissolved in water, but the amount was too small to permit identification. Walden (14) reported the solubility of potassium iodide in nitrobenzene as 0.0019 g/100 ml solvent at 25°C.

Dawson and Jackson (18) report forming polyiodides of potassium in nitrobenzene by simple mixing of potassium iodide and iodine. These were more soluble and much more highly dissociated than the simple iodide. Therefore, as the electrolysis of potassium iodide proceeded and free iodine (presumably) was liberated at the anode, a great increase

in conductivity was anticipated. This was observed. After one hour of electrolysis at 120 v, the specific conductivity rose from 6.8 to 41.2 micromhos.

The solution in run 18 was pale yellow immediately upon mixing, suggesting a chemical reaction. It has been reported (19) that the compound lithium iodide:nitrobenzene exists as yellow crystals, and this may have been the source of the color. The deposit on the cathode above 2.5 v was black in color. Above 11 v it became lighter gray.

DISCUSSION

The salts employed in all runs were weighed to the nearest 0.2 mg, liquids measured to the nearest 0.02 ml. Thus, concentrations were known with better than 1% accuracy. The error inherent in the conductance measuring system was 1%. Conductivity values, then, were known to $\pm 1\%$.

The voltmeter used in finding decomposition potentials was accurate to 2%. It was read to the nearest 0.05 v. The ammeter also was accurate to 2%. For most cases, the 0–12 ma scale was used and readings were to the nearest 0.05 ma. In poorly conducting systems the 0–1.2 ma scale was used, and it was read to 0.005 ma.

Since the accuracy and precision of the ammeter and voltmeter used were constant, there was greater precision of decomposition potential determination in systems of higher conductivity. When the conductivity was high, the break in the polarization curve at the decomposition potential was a sharper one.

Another factor may have decreased the accuracy and precision of conductance and polarization measurements in solutions of low conductivity. Traces of impurity in the solute and solvent would have greater effect on the observed results when the initial conductivity was low.

As an estimate of precision, the standard deviation of the decomposition potential was calculated for a typical well conducting system. Results of 5 separate determinations of decomposition potential were used. It must be remembered that for cases of lower conductivity the standard deviation was undoubtedly greater.

For potassium thiocyanate in pyridine $\sigma = 0.024$ v.

Standard Deviation

$$\sigma = \sqrt{\frac{\sum d_a^2}{n}}$$

Where $d_a = x - a$ and $a = \frac{\sum x}{n}$ (20).

Any discussion of this paper will appear in a Discussion Section to be published in the December 1955 JOURNAL.

REFERENCES

1. ST. V. LASZCZYNSKI AND ST. V. GORSKI, *Z. Elektrochem.*, **4**, 290 (1897).
2. L. KAHLENBERG, *J. Phys. Chem.*, **3**, 602 (1899).
3. H. E. PATTEN AND W. R. MOTT, *J. Phys. Chem.*, **12**, 49 (1908).
4. G. VON HEVESY, *Z. Elektrochem.*, **16**, 672 (1910).
5. R. MULLER, F. HOLZL, A. PONTONI, AND O. WINTERSTEINER, *Monatsh.*, **43**, 419 (1922).
6. V. A. PLOTNIKOV AND E. YA. GORENBEIN, *J. Gen. Chem. (U.S.S.R.)*, **7**, 372 (1937).
7. S. I. YAKUBSON, *J. Phys. Chem. (U.S.S.R.)*, **21**, 343 (1947).
8. S. I. YAKUBSON AND M. A. ABRAMOVA, *C.A.*, **47**, 7348 (1953); *Ukrain. Khim. Zhur.*, **15**, 362 (1949).
9. R. MULLER, E. PINTER, AND K. PRETT, *Monatsh.*, **45**, 525 (1925).
10. J. W. MELLOR, "Comprehensive Treatise on Inorganic and Theoretical Chemistry," Vol. II, p. 582, Longmans, Green and Co., London (1922).
11. E. X. ANDERSON, *J. Phys. Chem.*, **19**, 753 (1915).
12. B. EMMERT, *Ber.*, **49**, 1060 (1916).
13. L. F. AUDRIETH AND J. KLEINBERG, "Non-Aqueous Solvents," p. 125, J. Wiley & Sons, Inc., New York (1953).
14. P. WALDEN, *Z. phys. Chem.*, **55**, 709 (1906).
15. M. G. LEVI AND M. VOGHERA, *Gazz. Chim. Ital.*, **35**, 277 (1905).
16. J. H. WALTON AND C. R. WISE, *J. Am. Chem. Soc.*, **44**, 103 (1922).
17. P. WALDEN, "Electrochemie Nichtwasseriger Losungen," p. 470, J. A. Barth (1924).
18. H. M. DAWSON AND C. G. JACKSON, *J. Chem. Soc.*, **93**, 2063 (1908).
19. H. M. DAWSON AND E. E. GOODSON, *ibid.*, **85**, 796 (1904).
20. T. B. CRUMPLER AND J. H. YOE, "Chemical Computations and Errors," p. 132, J. Wiley & Sons, Inc., New York (1940).

Conductance of Lithium Bromide at Low Concentrations in Methanol within the Temperature Range 20° to -50°C¹

PAUL G. SEARS, ROBERT L. McNEER,² AND LYLE R. DAWSON

Department of Chemistry, University of Kentucky, Lexington, Kentucky

ABSTRACT

The conductance of lithium bromide in methanol has been determined over the temperature range 20° to -50°C for several concentrations ranging from 4×10^{-4} to $1 \times 10^{-1}N$. Limiting equivalent conductances were obtained by extrapolation of Λ_0' vs. C plots. Fair agreement was found to exist between the experimental and the theoretical conductance behavior of lithium bromide in dilute methanol solutions. A plot of the logarithm of the limiting equivalent conductance in methanol as a function of the reciprocal of the absolute temperature over the range 20° to -50°C was found to be linear and to have the same slope as several corresponding plots constructed from experimental data for low concentrations.

INTRODUCTION

This investigation represents a part of a broad program, being carried out in this laboratory, concerned with the conductance of nonaqueous solutions at low temperatures. The objective of the investigation reported here has been to determine the conductance behavior of lithium bromide in dilute methanol solutions and to compare the observed behavior with that theoretically predicted by the Onsager equation (1). Methanol is a low-freezing hydroxylic solvent for which dielectric constant data are available at low temperatures. Lithium bromide was selected primarily because of its pronounced solubility in this solvent.

EXPERIMENTAL

Absolute methanol ("Baker Analyzed" reagent) was refluxed several hours over calcium oxide prior to fractionation through an efficient column. The middle fractions, which were retained, had conductivities of approximately 1×10^{-6} ohm⁻¹ cm⁻¹. Anhydrous lithium bromide was obtained from A. D. Mackay, Inc. Triplicate potentiometric titrations performed on a Fisher titrimeter using a standardized silver nitrate solution showed the lithium bromide to be 99.3% pure. Because of a trace of material (assumed to be lithium oxide) in the lithium bromide which was insoluble in methanol, the weight of the salt used was multiplied by 0.993 to determine the actual quantity of lithium bromide. Solutions were prepared by the weight dilution of concentrated stock solutions. Appro-

appropriate buoyancy corrections were applied. All transfers were made in a dry box and other precautions were observed throughout the experimental procedure in an attempt to ensure that the solutions remained anhydrous.

The resistances of the solutions contained in the conductance cells were measured with a Jones bridge (2) manufactured by the Leeds and Northrup Company. Resistances greater than 30,000 ohms were measured in parallel with 30,000 ohms of shunted bridge resistance, and the series cell resistance was computed from the measured parallel resistance. Confirmatory determinations by independent workers using the Jones and Bradshaw method (3) showed the two Washburn conductance cells employed to have constants of 2.075 and 2.206 cm⁻¹ at 25°C. It was assumed that the change in a cell constant is negligible over the temperature range studied. This assumption is supported by calculations of changes in cell measurements expected to result from temperature changes.

The temperature of solutions in the conductance cells was maintained constant to within 0.3 degree during determinations by a manually controlled thermostat consisting of a clear 1 gal Dewar flask filled with denatured alcohol. The bath liquid was cooled by the addition of powdered Dry Ice and agitated effectively by a motor-driven stirrer. Temperatures in all cases were measured with total-immersion thermometers which are periodically compared with thermometers calibrated by the National Bureau of Standards. The estimated uncertainties of the conductance data range from 0.5% at 20° to 1.0% at -50°C. The conductivity of the lithium bromide was obtained by subtracting the conductivity of the solvent from that of the solution.

¹ Manuscript received July 30, 1954. This paper is based on research performed under Contract No. DA-36-039-sc-5398 for the U. S. Army Signal Corps.

² Present address: Carbide and Carbon Chemical Company, Charleston, West Virginia.

TABLE I. Equivalent conductance of lithium bromide in methanol

(a) 20°C		(b) 10°C		(c) 0°C		(d) -10°C		(e) -20°C		(f) -30°C		(g) -40°C		(h) -50°C	
$C \times 10^4$	Λ	$C \times 10^4$	Λ	$C \times 10^4$	Λ	$C \times 10^4$	Λ	$C \times 10^4$	Λ	$C \times 10^4$	Λ	$C \times 10^4$	Λ	$C \times 10^4$	Λ
918	50.3	929	43.8	940	37.8	951	32.2	962	26.9	973	22.1	984	17.8	995	14.0
382	60.2	387	51.9	391	44.6	396	38.1	401	31.9	405	26.3	410	21.3	414	16.8
197	65.2	199	56.7	202	48.7	204	41.6	207	34.8	209	28.7	211	23.2	214	18.3
91.8	70.8	92.9	61.5	94.0	52.8	95.1	44.9	96.2	37.7	97.3	31.1	98.4	25.1	99.5	20.1
57.5	73.8	58.2	63.9	58.8	54.8	59.5	46.6	60.2	39.1	60.9	32.2	61.6	26.0	62.3	20.4
37.0	75.5	37.4	65.3	37.9	56.1	38.3	47.7	38.7	39.8	39.2	32.8	39.6	26.5	40.1	21.0
8.98	82.1	9.09	70.8	9.20	60.6	9.31	51.6	9.42	43.0	9.52	35.7	9.63	28.5	9.74	22.5
6.39	83.1	6.46	71.7	6.54	61.6	6.62	52.5	6.69	43.7	6.77	36.2	6.85	29.0	6.92	22.9
4.09	84.7	4.14	73.2	4.19	62.6	4.24	53.2	4.29	44.4	4.34	36.4	4.39	29.3	4.44	23.2

RESULTS

Values of the equivalent conductance, Λ , and the concentration in gram equivalents of lithium bromide per liter of methanol solution, C , are presented in Table I.

DISCUSSION

Plots of the equivalent conductance of lithium bromide in methanol vs. the square root of the concentration may be found in Fig. 1. Owing to the curvature of these plots at low concentrations, accurate extrapolations to infinite dilution were unobtainable. Hence, recourse to another method for determining Λ_0 was necessary.

The Onsager equation, which may be written in the following form for a uni-univalent electrolyte,

$$\Lambda = \Lambda_0 - [A + B\Lambda_0]\sqrt{C}$$

where

$$A = \frac{82.42}{(DT)^{1/2}\eta}$$

$$B = \frac{8.203 \times 10^5}{(DT)^{3/2}}$$

in which D and η are the dielectric constant and viscosity of the solvent, can be rearranged into the form suggested by Shedlovsky (4)

$$\Lambda_0 = \frac{\Lambda + A\sqrt{C}}{1 - B\sqrt{C}}$$

which permits the computation of Λ_0 directly from the Λ values and the Onsager constants, A and B . Λ_0 values calculated by this method are usually designated as Λ'_0 to differentiate them from the true limiting conductance. In the concentration range in which Onsager's equation holds, Λ'_0 is equal to Λ_0 ; under other conditions Λ'_0 varies with concentration. Shedlovsky found that for many salts Λ'_0 varied linearly with concentration, or

$$\Lambda'_0 = \Lambda_0 + aC$$

where a is a constant. This equation describes the conductance of many strong uni-univalent electrolytes in water to 0.1*N*. Fig. 2 shows plots of

Λ'_0 vs. C for lithium bromide in methanol at various temperatures. It may be observed that all of the graphs are very similar and appear to be merely displaced at various magnitudes along the ordinate. While these plots are not exactly linear and cannot be analytically extrapolated, smooth-curve extrapolations across a short distance should yield fairly accurate values for the limiting equivalent conductance. According to Baker and Kraus (5), $\Lambda'_0 - C$ plots which show a slight minimum are rather common and the conductance of such systems can be expressed by an equation of the form proposed by Onsager and Fuoss (6),

$$\Lambda_0 = \Lambda'_0 + aC + bC \log C$$

where a and b are constants. The concentration at which the minimum occurs may be designated as C_{\min} and another concentration, C^* , which is equal to $2.7 C_{\min}$, represents the concentration at which the terms aC and $bC \log C$ are of equal magnitude

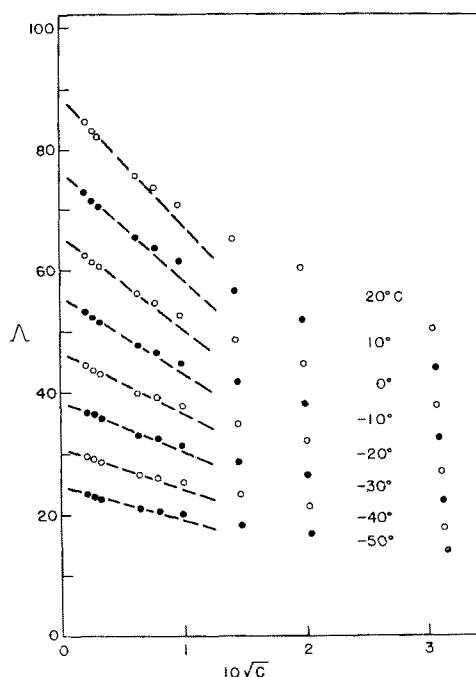


FIG. 1. Kohlrausch plots for lithium bromide in methanol. Dashed lines represent theoretical slopes.

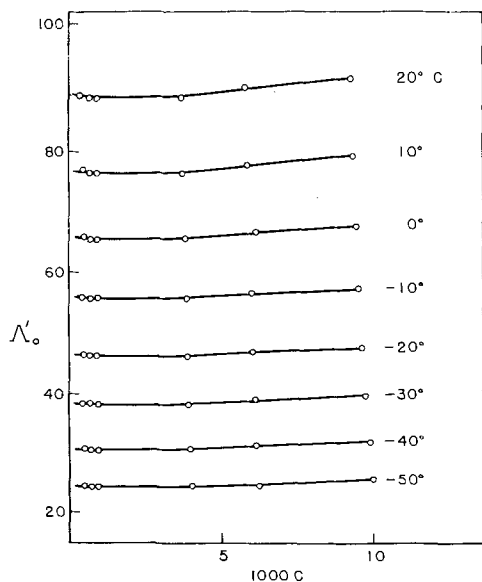


FIG. 2. Plots of Λ'_0 as a function of concentration of lithium bromide.

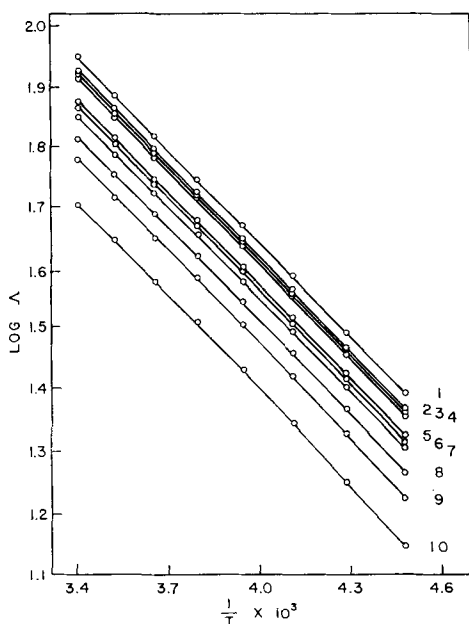


FIG. 3. Temperature dependence of the logarithm of the equivalent conductance of lithium bromide at concentrations expressed as molality $\times 10^4$. (1) 0.00; (2) 5.17; (3) 8.07; (4) 11.3; (5) 46.7; (6) 72.6; (7) 116; (8) 249; (9) 483; (10) 1160.

but of opposite sign, making Λ'_0 equal to Λ_0 . In Fig. 2, C_{min} appears between 0.0015 and 0.0020*N*, and the Λ'_0 values at approximately 0.005*N* are very nearly equal to the corresponding extrapolated Λ_0 values. Limiting equivalent conductances obtained from these graphs are listed in Table II. Listed also in Table II are dielectric constant and viscosity data used in the calculation of the Onsager constants and the Walden products, that is, the products of the limiting equivalent conductance and the viscosity of the solvent. The approximate constancy of the Walden products indicates that conductance and

TABLE II. Dielectric constant (7, 8) and viscosity (9) data for methanol and the limiting equivalent conductance and Walden product for lithium bromide in methanol at temperatures with the range 20° to -50°C

°C	<i>D</i>	$\eta \times 10^3$ (poise)	Λ_0 (ohm ⁻¹ cm ²)	$\Delta\sigma\eta_0$
20	33.7	5.81	89.1	0.518
10	35.6	6.76	76.9	0.520
0	37.5	7.94	65.9	0.523
-10	39.6	9.41	56.0	0.527
-20	41.8	11.31	46.7	0.528
-30	44.0	13.81	38.6	0.533
-40	46.2	17.17	30.9	0.531
-50	48.5	21.89	24.6	0.538

viscosity are probably very closely related in this system; however, the general trend of the product which decreases with increasing temperature is evidence that the temperature coefficient of viscosity is decreasing more rapidly than the temperature coefficient of conductance is increasing.

Utilizing the Λ_0 values in Table II, theoretical slopes at the various temperatures were calculated and drawn in Fig. 1. It may be observed from this figure that in dilute solutions the experimental points coincide very well with the theoretical slope.

Fig. 3 shows plots of the logarithm of the equivalent conductance vs. the reciprocal of the absolute temperature for various molal concentrations of lithium bromide in methanol. Examination of this figure reveals that all of the plots have identical slopes within experimental error. Points on plot 1 represent the Λ_0 values which are listed in Table II. An extrapolation of plot 1 in Fig. 3 to the $1/T$ value for 25°C permits the estimation of a Λ_0 value for lithium bromide in methanol which may be compared with existing data in the literature for that temperature. The authors' value of 96.0 ohm⁻¹ cm² obtained in this manner compares favorably with 96.4 ohm⁻¹ cm² which is the sum of the ionic conductances of the lithium and the bromide ions at 25°C reported by Gordon (10).

Any discussion of this paper will appear in a Discussion Section to be published in the December 1955 JOURNAL.

REFERENCES

1. L. ONSAGER, *Physik. Z.*, **27**, 388 (1926); **28**, 277 (1927).
2. P. H. DIKE, *Rev. Sci. Instruments*, **2**, 379 (1931).
3. G. JONES AND B. C. BRADSHAW, *J. Am. Chem. Soc.*, **55**, 1780 (1933).
4. T. SHEDLOVSKY, *ibid.*, **54**, 1405 (1932).
5. E. G. BAKER AND C. A. KRAUS, *Proc. Nat. Acad. Sci.*, **37**, 726 (1951).
6. L. ONSAGER AND R. M. FUOSS, *J. Phys. Chem.*, **36**, 2689 (1932).
7. A. A. MARYOTT AND E. R. SMITH, National Bureau of Standards Circular 514, August 10, 1951.
8. "International Critical Tables," Vol. VI, p. 83.
9. P. G. SEARS, F. J. SHELL, AND L. W. DAWSON, Unpublished data.
10. R. E. JERVIS, D. R. MUIR, J. P. BUTLER, AND A. R. GORDON, *J. Am. Chem. Soc.*, **75**, 2855 (1953).

Technical Note



Potentiometric Study of Bimetallic Electrodes in Corrosive Solutions¹

M. G. FOUAD

Department of Chemical Technology, Faculty of Engineering, Alexandria University, Alexandria, Egypt

Potentials of zinc, zinc-copper composite electrodes and amalgamated zinc electrodes dissolving in hydrochloric acid solutions of zinc chloride were measured. Zinc-copper composite electrodes were made by plating copper on a portion of the zinc surface. The results shown below can be explained on the basis of the electrochemical theory of corrosion (1).

The reducing potential (e) of each system was calculated by subtracting the observed emf, E' , of the cell $H_2/HCl(M)$, Hg_2Cl_2/Hg . Values of E' were obtained by interpolation of the results of various authors (2). The rate of dissolution of amalgamated zinc in acids is extremely small (3) and as the emf of systems of the type Zn-Hg $ZnCl_2$, HCl were found to be reproducible within 1 mv and independent of stirring, it is reasonable to suppose that emf values measured in such systems are reversible values (4).

RESULTS

Zinc-Copper Composite Electrodes

I. $[ZnCl_2]$ constant

Ratio of areas Zn:Cu 10:1

(a) $N-HCl-0.2M-ZnCl_2$

	$E.v.$	$E'v.$	$(e)v.$
Zinc	1.055	0.278	-0.777
Copper	1.053	0.278	-0.775

(b) $0.3N-HCl-0.2M-ZnCl_2$

Zinc	1.086	0.342	-0.744
Copper	1.085	0.342	-0.743

(c) $0.1N-HCl-0.2M-ZnCl_2$

Zinc	1.109	0.396	-0.713
Copper	1.108	0.396	-0.712

II. Change of $[ZnCl_2]$

$0.3N-HCl-0.02M-ZnCl_2$

Zinc	1.086	0.342	-0.744
Copper	1.085	0.342	-0.743

III. Change of areas of copper

$0.3 N-HCl-0.2M-ZnCl_2$

	$E.v.$	$E'v.$	$(e)v.$
(a) Zn:Cu 2:3			
Zinc	1.078	0.342	-0.736
Copper	1.067	0.342	-0.725
(b) Zn:Cu 2:1			
Zinc	1.078	0.342	-0.736
Copper	1.067	0.342	-0.729
(c) Zn:Cu ∞ :1			
Zinc	1.082	0.342	-0.740
Copper	1.081	0.342	-0.739

Pure and Amalgamated Zinc

(a) $N-HCl-0.2M-ZnCl_2$

(Zinc in the composite electrode)

Pure zinc	1.062	0.278	-0.784
Amalgamated zinc	1.075	0.278	-0.797

(b) $0.3 N-HCl-0.2M-ZnCl_2$

(Zinc in the composite electrode)

Pure zinc	1.086	0.342	-0.744
Amalgamated zinc	1.096	0.342	-0.754

All emf values recorded were independent of rate of stirring.

Any discussion of this paper will appear in a Discussion Section to be published in the December 1955 JOURNAL.

REFERENCES

- cf. U. R. EVANS, "Metallic Corrosion, Passivity and Protection", p. 5, 8, 256, etc., Edward Arnold Co., London (1946).
- J. H. ELLIS, *J. Am. Chem. Soc.*, **33**, 737 (1916); G. A. LINHART, *ibid.*, **39**, 2601 (1917); M. RANDALL AND G. F. BRECKENRIDGE, *ibid.*, **49**, 1435 (1927).
- R. VONDRACEK AND J. ISAK-KRIZKO, *Rec. trav. Chim.*, **44**, 376 (1925).
- R. LUTHER, quoted in *Chem. Rev.*, **1**, 394 (1925).

¹ Manuscript received April 20, 1954.

Resistance Studies on Various Types of Dry Cells¹

RICHARD GLICKSMAN AND C. K. MOREHOUSE

RCA Laboratories, Radio Corporation of America, Princeton, New Jersey

ABSTRACT

A direct current method has been devised for measuring the internal resistance of dry cells. Data are presented which show that the internal resistance of a Leclanché type of dry cell is greater when measured at low current drains than at high current drains. This difference is believed to be due to a film formation on the zinc anode. It is also shown that during discharge the drop in terminal voltage of a dry cell owing to an increase in internal resistance is small. It is believed that pH changes of the electrolyte at the electrode surfaces and the change in the composition of the surface of the manganese dioxide electrode account for most of the potential drop when a Leclanché cell is discharged.

Studies made on magnesium-manganese dioxide cells show that these cells undergo greater instantaneous voltage fluctuation than the conventional Leclanché cells. This voltage fluctuation is due to a high resistance coating on the magnesium anode. The direct current method for measuring internal resistances of dry cells described in this paper could be useful in the study of film formation on the surface of magnesium electrodes.

INTRODUCTION

Resistance of cell components and departure of half-cell potentials from their reversible electrode potentials are some of the factors which determine the rate at which electrical energy can be withdrawn from any electrochemical cell.

The mercuric oxide-zinc type of dry cell has a constant voltage curve when discharged over a wide range of current drains, whereas the voltage of the Leclanché (manganese dioxide-zinc) type of cell decreases with time, especially at high discharge rates. It has been the opinion of many that the increase in internal resistance is an appreciable factor in causing this drop in terminal voltage of the Leclanché cell during discharge.

Several alternating and direct current methods for measuring the internal resistance of batteries have been proposed (1-4). It is essential that the effect of electrode polarization be eliminated when making resistance measurements by either of these two methods. Direct current measurements, unless they are made in short time intervals, include some polarization effects.

A direct current method has been devised, whereby pulses of current on the order of $\frac{1}{5}$ th of a second duration are withdrawn from the cell and the instantaneous IR drop measured. This instantaneous IR drop represents the voltage drop due to the resistance of cell components.

Measurements have been made on several types of dry cells using this method to determine the

change of resistance as the cells are discharged and the effect of resistance on cell performance.

EXPERIMENTAL APPARATUS

The apparatus designed for making the resistance measurements consists of (a) an RCA WO-27A D-C oscilloscope with a P-7 screen that retains the image for a few seconds; (b) a discharge circuit containing a variable resistance and a booster battery for maintaining a constant current; and (c) a potentiometer circuit to balance out the voltage of the cell under test allowing potential changes to be read on the oscilloscope.

A circuit diagram of the apparatus is shown in Fig. 1. A and C designate the anode and cathode of the cell being tested, and T is a reference saturated calomel electrode used for single electrode studies. Cell electrodes are connected to the oscilloscope and potentiometer circuit by means of two switches. Switches S_1 and S_2 in the position shown connect the anode and cathode to the oscilloscope. If S_1 is moved to position T, the half-cell readings of either electrode can be made depending on the position of switch S_2 . Current drawn from the test cell by the oscilloscope and potentiometer circuit is negligible, being less than $1 \mu\text{a}$.

The discharge circuit consists of a series of micro-switches, S_3 , S_4 , S_5 , and S_6 , for opening and closing the discharge circuit at controlled time intervals, a milliammeter, MA, a variable resistance, R_L , and a booster battery, B_2 , connected in series with the test cell A-C.

The potentiometer circuit consists of a variable resistance, R_p , and a battery, B_1 . The voltage of the

¹ Manuscript received August 20, 1954. This paper was prepared for delivery before the Boston Meeting, October 3 to 7, 1954.

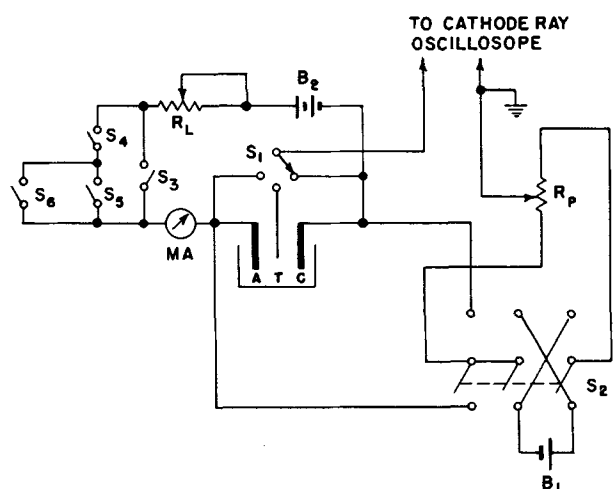


FIG. 1. Schematic diagram of apparatus used for d.c. resistance measurements of galvanic cells.

potentiometer circuit is adjusted to equal and oppose that of the test cell when on open circuit.

Two procedures, (a) the potential-decay, and (b) the potential-recovery, for measuring the resistances of cells have been used in this work.

Potential-decay method.—If switch S_3 is left open, switches S_4 and S_5 must be closed in order to draw current from the cell. Switches S_4 and S_5 are operated by cams mounted on slow speed shafts driven by fractional horsepower motors. They continually make and break the circuit, S_4 once every second and S_5 once every nine seconds; therefore, current flows through the experimental cell every ninth second when both S_4 and S_5 are closed. The time interval of any one discharge is one-fifth of a second. This setup was included so as not to discharge the cell at too fast a rate while making measurements. However, if switch S_6 is closed, the current that flows through the experimental cell is controlled by S_4 alone, and the cell will be discharged for one-fifth of a second every second.

In this method, the cell is on open circuit and a pulse of current is withdrawn from it. There is an instantaneous drop in potential, which manifests itself as a vertical drop on the oscilloscope, followed by a more gradual drop in potential due to polarization of cell electrodes. Resistance can then be calculated from a measurement of the instantaneous IR drop and the current flowing. This is termed the potential-decay method of measuring the resistance. **Potential-recovery method.**—An alternate method of measuring resistance is to measure the instantaneous IR recovery when the load is taken off the cell. This measurement can be controlled simply by closing and opening switch S_3 , and thereby causing the battery to go from a closed circuit to an open circuit condition, with the accompanying increase in voltage.

Measurements by these two methods are made 10^{-3} – 10^{-4} sec after the current has been switched on or off. This would preclude any change in potential due to polarization effects which are negligible during this short time interval.

VARIATION OF INTERNAL RESISTANCE WITH CURRENT DRAIN IN DRY CELLS

Experimental

Resistances of various size Leclanché and alkaline RM-1 cells were measured at various current drains by the potential-decay method. Short pulses ($\frac{1}{5}$ sec duration) of current ranging from 5 to 800 ma were withdrawn from the cell and the resistance computed from the instantaneous IR drop as measured on the oscilloscope.

Results obtained are shown in Fig. 2; each point represents the average of 2–4 measurements.

It should be noted from these data that the resistance of the Leclanché cell decreases as the current drain is increased, whereas the resistance of the RM-1 alkaline cells was nearly constant over the discharge current range of 5–200 ma.

Additional Leclanché cells were tested by the same potential-decay method as used above, only the cells were discharged 10–20 times at pulses of $\frac{1}{5}$ th sec duration before the actual IR drop was measured. Data as presented in Table I show that under these conditions the measured resistance is more nearly constant as the current drain is increased from 25 ma to 400 ma.

A third set of results was gathered on D size Leclanché cells, using the potential-recovery method previously described. The cells were discharged continuously for 5 min after which the current was interrupted and the instantaneous increase in potential was measured on the oscilloscope. Results presented

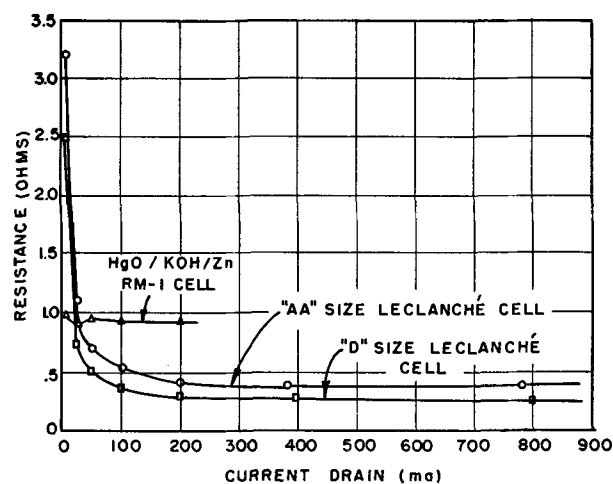


FIG. 2 Effect of current drain on the internal resistance of dry cells.

TABLE I. Internal resistance (ohms) of size D Leclanché dry cells measured at various current drains

Current drain (ma)	Potential-decay method			Potential-recovery method	
	No. 5	No. 6	No. 7	No. 8	No. 9
25	0.28	0.28	0.33	0.22	0.19
50	0.25	0.31	0.30	0.22	0.19
100	0.23	0.28	0.27	0.22	0.18
200	0.22	0.21	0.23	0.20	0.18
400	0.20	0.23	—	—	—

in Table I are in agreement with those obtained by the second procedure, but are not in agreement, at low current drains, with data gathered by the first technique.

In order to determine which electrode of the Leclanché cell was causing a variation of resistance with current drain, a cell was constructed in a beaker using the same size electrodes as found in the conventional D size Leclanché type dry cell. A saturated calomel reference electrode was used to measure the change of potential at the two respective electrodes as the current drain was varied. It was found qualitatively that the resistance between the manganese dioxide and the reference electrode was constant by the potential-decay method over the current drain range 25–200 ma. The resistance between the reference electrode and the zinc electrode, however, decreased as the current drain was increased in the manner shown in Fig. 2. These data, while qualitative, show that the zinc electrode is the electrode which causes a variation in resistance when measured under certain conditions.

Discussion

Vinal (1) has pointed out that, as far back as 1885, Preece found that the resistance of a cell was greater when measured at high current drains than when measured at low current drains. This has been observed by several subsequent experimenters (1, 2), and appears to be true for primary and secondary batteries.

Since resistances of the electrolyte, electrodes, and separator are definite physical quantities independent of the current flowing through the cell, there must be another resistance factor which varies with current drain. Chaney (5) investigated the performance of dry cells and concluded that there is a contact resistance in dry cells due to the formation of a hydrogen layer or film on the zinc as a product of the zinc corrosion reaction. It is Chaney's opinion that this film is considerably altered as the current drain is varied, being removed at high current densities.

Data presented in this paper support Chaney's

findings, namely, that the resistance of a dry cell is less when the current drain is greater. The variation of resistance is believed to be due to a film formed over the surface of the zinc electrode, the nature of which varies as the cell is subjected to varying current drains. The present experiments have not identified the existence or the nature of the film, but it is believed that a film does exist and that this film is either a hydrogen layer or an oxide type of coating. Constant resistance values can be obtained providing the cell is discharged a sufficient amount to remove the film.

EFFECT OF DISCHARGE ON THE INTERNAL RESISTANCE OF DRY CELLS

The Leclanché and the alkaline RM type cells differ in their discharge characteristics, especially at high discharge rates. The RM cell has a constant voltage discharge curve, whereas the voltage of the Leclanché cell decreases gradually with time. Many observers believed that this difference is due to a large extent to an increase in the internal resistance of the Leclanché cell, caused by the formation of high resistant products such as $Mn_2O_3 \cdot H_2O$, $ZnO \cdot Mn_2O_3$, $Zn(NH_3)_2Cl_2$, or $ZnCl_2 \cdot 4Zn(OH)_2$, whereas a more conductive discharge product, metallic mercury, is formed in the alkaline mercuric oxide cell.

Leclanché and RM dry cells were discharged continuously at 200, 100, and 50 ma constant current drains and the internal resistance measured by interrupting the flow of current at various time intervals of discharge. The instantaneous increase in potential was measured on the oscilloscope and the resistance calculated.

The change in cell voltage with time for a D size Leclanché cell discharged continuously at 200 ma constant current is presented in Fig. 3. Also included is a curve showing the potential (IR) drop with time

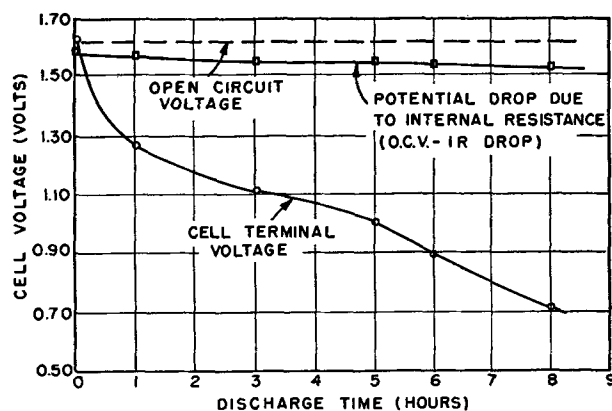


FIG. 3 Change in potential drop due to internal resistance of a size D Leclanché dry cell discharged continuously at 200 ma constant current drain.

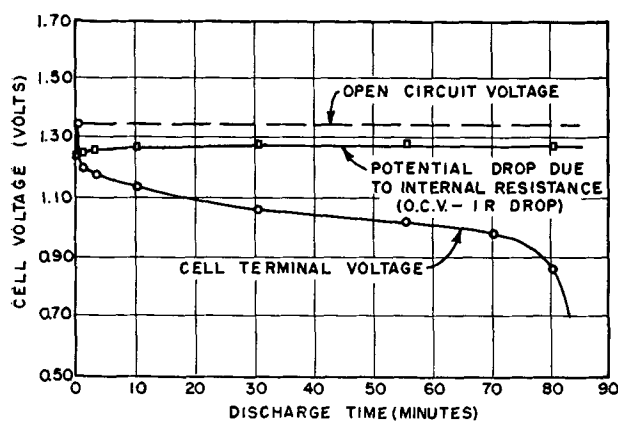


FIG. 4 Change in potential drop due to internal resistance of an alkaline-mercuric oxide RM-1 dry cell discharged continuously at 100 ma constant current drain.

as a result of the change in resistance as the cell is discharged. The potential loss due to internal resistance is small, varying from approximately 0.04 to 0.08 during cell discharge. This corresponds to an increase in resistance from 0.20 to 0.41 ohm as the cell voltage decreases from 1.62 to 0.72. Even when the cell is discharged for 24 hr to a voltage of 0.07, the resistance increases only to 0.74 ohm. These data show that the voltage drop owing to a change in internal resistance is negligible compared to the total drop in cell voltage.

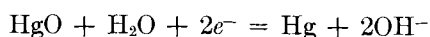
Comparable results obtained on mercuric oxide RM-1 cells are shown in Fig. 4.

These data show that the internal resistance of the mercuric oxide cell does decrease slightly, but this change is a minor factor in causing a change in cell voltage as the cell is discharged.

Discussion

It has been shown by others that the manganese dioxide is the limiting electrode of a Leclanché dry cell. This paper shows that the potential decrease or increase due to a change of internal resistance is small as the Leclanché or the alkaline RM type cells are discharged. A more important factor than resistance which probably contributes to the gradual drop in potential is a change of pH of the electrolyte at the electrode surface due to the cell reaction.

The cathodic reaction for the Ruben-Mallory cell can be expressed by the following equation:



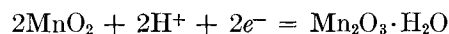
Applying the Nernst equation to the reaction, the following expression is obtained:

$$E = E^0 - \frac{0.059}{2} \log a_{\text{OH}^-}^2$$

Since E^0 is a constant, the potential E of the half-cell reaction is dependent on the concentration of

the hydroxide ion, i.e., it is a function of pH . Since the electrolyte in this cell is strongly basic (35–40% KOH), it would be expected that formation of hydroxyl ions during discharge would have little or no effect on the pH of the electrolyte and, therefore, the electrode potential. The fact that the system has a fairly constant discharge potential is probably due to the direct reduction of mercuric oxide to mercury without intermediate products, along with a constant pH during discharge.

The cathodic reaction for the Leclanché cell can be written:



and applying the Nernst equation, it is seen that this electrode is pH dependent:

$$E = E^0 - 0.059 pH$$

Cahoon (6) and McMurdie, Craig, and Vinal (7) investigated the effect of pH on the manganese dioxide potential. The latter showed that in acid solutions the change in potential of the manganese dioxide electrode is 0.12 v per unit change of pH , while in basic solution the change in potential is 0.06 v per unit of pH . Cahoon and Heise (8) reported that as a D size Leclanché cell is discharged through a 4 ohm resistance, the pH of the paste layer changes from 4.7 to 3.8, while the innermost portion of the manganese dioxide cathode mix changes from 5.8 to 10.1. On the basis of these data, change in pH can account for approximately 30% of the total potential drop from a 1.50 voltage level to the 0.75 v end point. It has also been shown by Herbert (9) that the manganese dioxide electrode polarizes to an appreciable extent when discharged in a strongly alkaline solution. Thus, while the effect of pH on the manganese dioxide electrode is a factor in causing the Leclanché cell to polarize on discharge, there must be other factors which play a major role.

Ferrell and Vosburgh (10) assumed that a solid solution is formed between the manganese dioxide and a lower oxide of manganese, and that the oxidation potential is dependent on the composition of the solid solution. Johnson and Vosburgh (11) found that electrodes made with mixtures of precipitated manganese dioxide and manganese oxyhydroxide have potentials varying linearly with the logarithm of the ratio of the two oxides.

It is concluded from a survey of the literature and data presented in this paper that polarization of the manganese dioxide electrode is due to a change in pH of the electrolyte and electrode composition at the electrode surface, which results in a lower electrode potential. It is also recognized that, depending on the rate of discharge, a variation in

electrode potential can be caused by diffusion effects at the electrode surface. This is shown by the difference in performance of a Leclanché cell when it is discharged at high and low current drains and on continuous and intermittent types of tests. Change in internal resistance accounts for only a small percentage of the total voltage drop as the cell is discharged.

APPLICATION OF PRESENT METHODS TO A STUDY OF MAGNESIUM-MANGANESE DIOXIDE TYPE DRY CELLS

Magnesium-manganese dioxide dry cells of the type described by Kirk, Fry, and George (12, 13) were studied with the apparatus shown in Fig. 1. The cells were of the conventional construction and contained magnesium alloys, AZ10A and AZ31A, as anodes, an African manganese dioxide cathode blended with acetylene black and barium chromate, an absorbent paper separator, and a magnesium bromide electrolyte. Data obtained on magnesium and zinc-manganese dioxide AA size dry cells discharged intermittently at current drains of either 10 or 50 ma are plotted in Fig. 5. The discharge cycle as shown is approximately $\frac{1}{2}$ sec duration followed by 1 sec open circuit.

The data presented show changes in terminal voltage of the cell after the discharge cycle had been repeated approximately five to ten times.

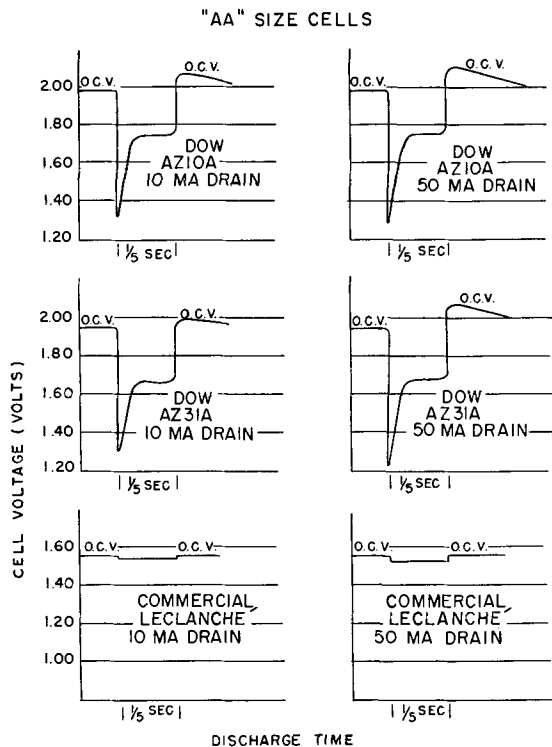


FIG. 5 Oscillographic measurements of change in voltage of AA size magnesium and zinc Leclanché type cells, subjected to 10 and 50 ma constant current drains.

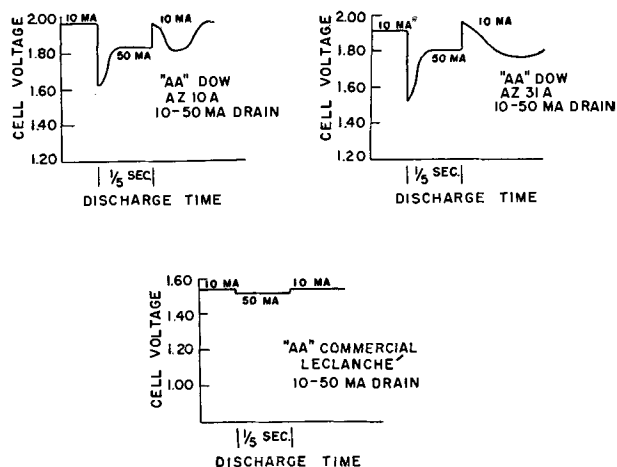


FIG. 6 Oscillographic measurements of change in voltage of AA size magnesium and zinc Leclanché type cells when subjected to a change in constant current drains from 10 to 50 ma.

The large initial drop is due to the resistance of the oxide or chromate type film on the magnesium, the voltage rising as the oxide layer is removed reaching a more steady state. When the circuit is opened the cell voltage rises above the original open circuit value and then gradually returns to its original value. This is primarily due to the reformation of the oxide coating on the surface of the magnesium.

The apparatus shown in Fig. 1 was modified to measure voltage fluctuations of cells discharged intermittently for 1 sec on a 10 ma drain followed by a $\frac{1}{2}$ sec discharge at a 50 ma drain. This represents a condition which might be encountered in a transistor-operated radio receiver utilizing a class B amplifier circuit. Results obtained on AA size magnesium and zinc-type cells are shown in Fig. 6. It is seen that the magnesium cells, while operating at a higher voltage level than the Leclanché cell, have a larger potential drop as the load is changed from 10-50 ma. This is because of the existence of a high resistance film on the magnesium anode.

Data presented in this section show that, because of the coating on the magnesium anode, the voltage of the magnesium dry cell undergoes greater fluctuation than the Leclanché cell. This method of study is suggested as a means of studying the "delayed action" as encountered in magnesium dry cells.

ACKNOWLEDGMENT

The authors wish to express their appreciation to Dr. Ross E. Shrader for assistance in designing and constructing the equipment for making the d-c resistance measurements.

Any discussion of this paper will appear in a Discussion Section to be published in the December 1955 JOURNAL.

REFERENCES

1. G. W. VINAL, "Storage Batteries," 3rd ed., Chap. VII, John Wiley & Sons, Inc., New York (1940).
2. E. F. NORTHRUP, "Methods of Measuring Electrical Resistance," Chap. XI, McGraw-Hill Book Co., New York (1912).
3. N. C. CAHOON, *Trans. Electrochem. Soc.*, **92**, 159 (1947).
4. W. HEUBNER, *Elektrotech. Z.*, **61**, 149 (1940).
5. N. K. CHANEY, *Trans. Am. Electrochem. Soc.*, **29**, 183 (1916).
6. N. C. CAHOON, *Trans. Electrochem. Soc.*, **68**, 177 (1935).
7. H. F. McMURDIE, D. N. CRAIG, AND G. W. VINAL, *ibid.*, **90**, 509 (1946).
8. N. C. CAHOON AND G. W. HEISE, *J. (and Trans.) Electrochem. Soc.*, **94**, 214 (1948).
9. W. S. HERBERT, *This Journal*, **99**, 190C (1952).
10. D. T. FERRELL, JR., AND W. C. VOSBURGH, *ibid.*, **98**, 334 (1951).
11. R. S. JOHNSON AND W. C. VOSBURGH, *ibid.*, **100**, 471 (1953).
12. R. C. KIRK AND A. B. FRY, *J. (and Trans.) Electrochem. Soc.*, **94**, 277 (1948).
13. R. C. KIRK, P. F. GEORGE, AND A. B. FRY, *This Journal*, **99**, 323 (1952).

Investigation of Storage Battery Failure by a Method of Plastic Impregnation¹

A. C. SIMON AND E. L. JONES

Naval Research Laboratory, Washington, D. C.

ABSTRACT

Electrolytic cells may be prepared for microscopic examination by replacement of the electrolyte with liquid epoxy resin, which later hardens. The cell containing the hardened plastic may then be cut into sections and the cell elements examined in detail after suitable grinding and polishing. Growth and buckling of plates may be observed and measured and the rate of corrosion determined from the area of the remaining metal in the grid cross section if the area of the original is known. Modified chemical microscopy, spot testing, and physical measurements offer possibilities for identification of products of reaction and corrosion.

INTRODUCTION

In any post-mortem examination of the lead-acid storage battery, the fragile condition of the remaining grid structure and the tendency of the active materials to shed makes the task more difficult. The plates tend to disintegrate after disassembly of the elements so that the original physical relationship of the various parts becomes uncertain and the cause of failure may evade detection.

Just as metallography has immeasurably increased the knowledge of the structure of metals so likewise do well-prepared cross sections of battery elements offer equal possibilities for increased knowledge of battery processes. An attempt to prepare such specimens was first reported by Buckle and Hanemann (1), who impregnated individual battery plates with carnauba wax and subjected them to microscopic examination after suitable polishing. Sections of plates have also been imbedded in the thermoplastic resins used for mounting metallurgical specimens. These methods are not suitable for the impregnation of an entire cell and, in addition, require the use of heat or pressure that may produce changes in the active material.

The present description is based on the use of an epoxy resin that may be introduced into the cell as a liquid and then left to harden by catalytic action. The solid cell may then be sectioned, polished, and the resulting cross section of the battery element studied for both macro- and microstructure (Fig. 1).

Although the method herein described offers no microscopic technique that could be considered new, the application of an impregnating and sectioning technique to the study of cell processes appears to offer unusual possibilities for investigation. In this

paper the authors have attempted to give examples of possible applications rather than a report on a specific use. The method, however, has been applied with considerable success to a study of the mechanism of grid corrosion, the results of which will be subsequently reported. The procedure described is by no means perfected, but produces results encouraging enough to justify further investigation.

EXPERIMENTAL PROCEDURE

The procedure outlined below has been applied to many types of batteries without difficulty. Experience has shown, however, that a plastic suitable for impregnating a storage battery cell should possess the following characteristics: (a) the plastic or any contained solvents should not react with any cell unit such as case, separators, or active material; (b) the plastic in the liquid condition should possess a low viscosity; (c) the period of setting should be long enough to allow penetration of the plastic to all parts of the cell and into the various porous portions; (d) the plastic should have good adherence to all cell constituents; (e) the plastic should not shrink to any great extent in the solidification process; (f) the solidification process should take place without the liberation of excessive heat.

A plastic that completely meets these requirements has not as yet been found. Of all the plastics tried, an epoxy resin has been used most extensively.^{2, 3}

The described method is based upon the use of the epoxy in the impregnation of the cell as a unit. The

² The specific material used was Coil Seal No. 11, National Engineering Products, Inc., Washington, D. C.

³ Another material used successfully was Scotch Cast No. 3, Minnesota Mining and Manufacturing Company, Minneapolis, Minn. It has a low viscosity and long pot life so that penetration is excellent; it has the further advantage that little heat is generated in setting.

¹ Manuscript received October 14, 1954. This paper was prepared for delivery before the Boston Meeting, October 3 to 7, 1954.

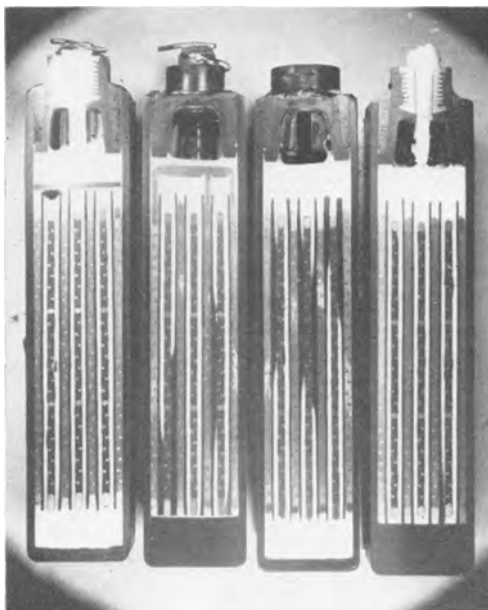


FIG. 1. Cross sections of storage battery cell after impregnation with plastic. $\frac{1}{2}$ actual size before reduction for publication.

same method, modified to individual requirements, can be used with other plastics and for mounting or impregnating individual cell constituents or other substances of a porous nature.

Impregnation of the Cell

For satisfactory impregnation with plastic the cell must be washed free of acid and dried. The acid is not emptied by inverting the cell. Instead, a small hole is made at the bottom while a stream of water is run in at the top. In this way the acid may be slowly replaced by water without unduly heating the electrolyte or plates and with minimum disturbance to sediment and loose corrosion products. The washing is continued until the water gives no acid test.

After washing, the cell is drained and dried by passing a stream of warm air through it. After drying, the cell is evacuated of air and any residual water vapor. A length of tubing is extended from the cell to a position outside of the vacuum system, and the plastic mix is forced into the cell by atmospheric pressure. After the plastic has been introduced, atmospheric pressure is restored on the cell and the plastic is allowed to harden.

Caution is required in the use of this plastic in lead-lead acid batteries. It is important that no more than 400 ml of the plastic be mixed and used at one time and, if more than this amount is required, that each batch harden before adding the next. The solidification reaction is exothermic and is accelerated by heat. So much heat can be generated in large masses of the plastic that an almost explosive reaction takes place with the lead oxides of the plates. In addition, heat-

ing accelerates the hardening process and causes difficulty in proper impregnation even if the reaction with the lead oxides is not initiated. Large cells can be filled with successive portions of the plastic mix, and hardening and cooling of each mix will occur without any sign of the successive layers being visible in the section.

Cutting, Grinding, and Polishing the Section

The abrasive action of the lead oxides has been found to be destructive to cutting tools. A narrow-bladed skip-tooth band saw is used for the preliminary sectioning. Excessive friction at the cutting edge may cause ignition of the section, so a sharp saw, a slow saw speed, and a light feed should be employed. Use of a water coolant is advisable, but an alkali soap type of coolant should be avoided since it will corrode the specimen.

After sectioning, the sample is brought to a smooth condition by hand grinding under a stream of water. Garnet Number 80 waterproof paper is used for rough grinding the specimen to a flat surface and silicon carbide waterproof papers, grades 240 and 400 mesh, are used for intermediate grinding. Fine grinding is accomplished with grade 600 gritcloth.⁴ When this technique is used, grinding is rapid, the paper does not become clogged by lead particles, and no hazard is caused by the fine lead and lead oxide dust produced in polishing.

A final hand polishing is given the specimen on a wet, tightly stretched surface of airplane wing fabric. A paste of polishing powder type A-5175⁵ is used as the polishing agent.

APPLICATIONS

Since the plastic is an excellent insulating material, a current path is furnished only by those conducting portions of the section that were in actual contact before impregnation took place. The section may thus be tested with a good ohmmeter or similar device for such conditions as shorts between positive and negative plates, separation of active material from the grid, and broken grid sections. By progressive sectioning and testing, the source of such conditions may be located and subjected to microscopic examination (Fig. 2).

Growth of plates, distortion of grids, breakage of separators, and "treeing" can be detected in the macro section. The universal measuring microscope can be used to measure distortion and growth in the section with a high degree of precision. A contour-measuring projector can also be used for direct visual

⁴ Bay State Abrasive Products Company, Westboro, Mass.

⁵ Linde Air Products Company, New York, N. Y.

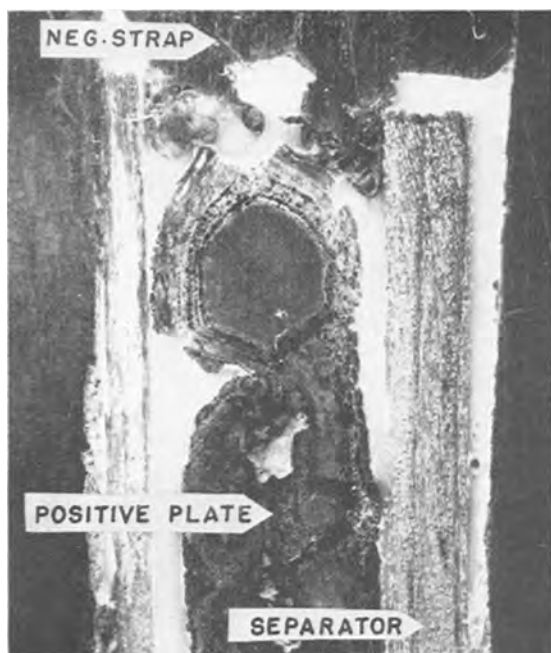


FIG. 2. Short circuit, between positive plate (center) and negative plate connecting strap (top), located by electrical conductance test and progressive sectioning. Short occurred because of growth of positive plate and "treeing" from negative plate connecting strap. 4X before reduction for publication.

comparison of sections from newly assembled and used cells.

Higher magnification reveals the structure of the active material and its relation to the products of grid corrosion. The harder parts of the corrosion product, portions of the positive active material, sponge lead, lead sulfate crystals, the metal of the grid, and the plastic material used for impregnation are capable of a high polish, and the section can be observed by bright-field vertical illumination (Fig. 3). By this means the boundaries between metal, corrosion product, and active material are usually sharply defined, but much detail is lacking. A better idea of the actual appearance and colors of the various constituents can be obtained through the use of dark-field illumination. With at least one type of illuminator⁶ the over-all appearance of the specimen can be much improved if observed by dark-field illumination through a cover glass attached to the surface by immersion oil (Fig. 4).

Careful polishing reveals the microstructure of the metal as well as that of the corrosion product, but with dark-field illumination the brightness of the metal is relatively so much greater than that of the corrosion product that the detail in both, visible to the eye, is difficult to reproduce in a single photographic print.

⁶ Trivert illuminator, Bausch and Lomb Optical Company, New York, N. Y.

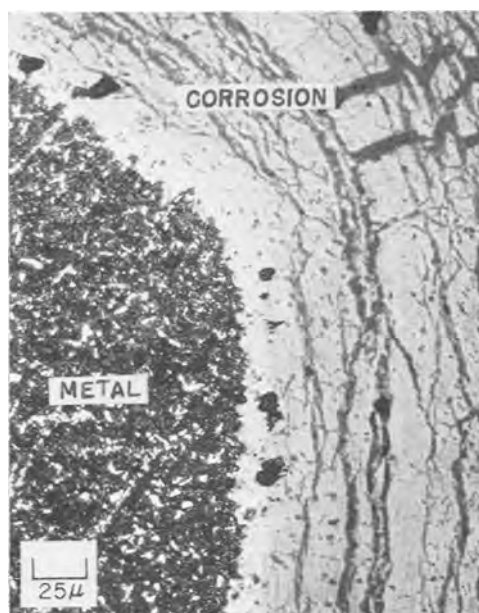


FIG. 3. Positive plate photographed under bright-field illumination. Portion of grid member appears at left and a portion of the corrosion ring at right. Section has been rubbed with dry polishing powder to subdue reflectivity of the lead. The bright particles in the grid member are segregated antimony. 400X before reduction for publication.



FIG. 4. Positive plate corrosion photographed under dark-field illumination through cover glass and immersion oil. Section was ground on number 600 gritcloth but not polished. Direction of grinding is indicated by metal smear across dark corrosion product. Such smears and surface dirt can be removed with Scotch tape. 100X before reduction for publication.

The high reflectivity of the various polished surfaces is misleading, and the use of polarized light has been found helpful in differentiating polished crystal surfaces from metal surfaces. This is particu-

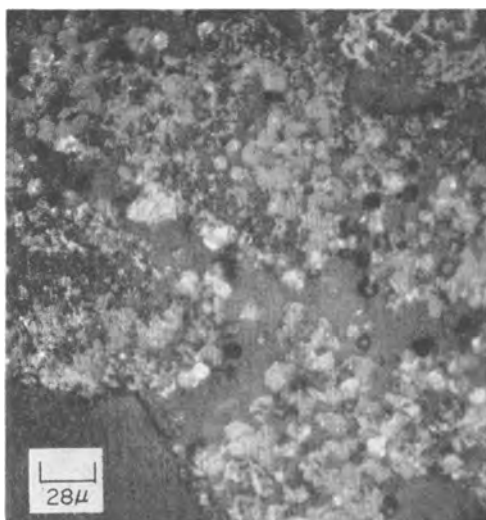


FIG. 5. Section of negative plate photographed under bright-field illumination. The bright areas of apparent metal are revealed as sulfate crystals when examined under polarized light (Fig. 6). 350 \times before reduction for publication.

larly useful in the examination of the negative plate (Fig. 5 and 6).

A planimeter or a grid laid out on transparent material may be used to measure the relative areas of corrosion product and the remaining grid metal either indirectly from a photographic negative or directly from a projected image of the corroded grid member. Comparison of the remaining metal with that present before corrosion began gives the corrosion rate. However, as a result of variable casting conditions, the actual grid sections of a new grid vary in shape and area to a considerable extent. For this reason it is necessary to use the average of a number of observations to obtain a reliable figure. In a study of the

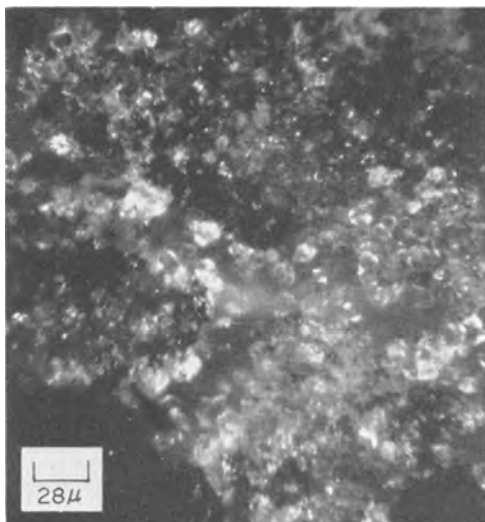


FIG. 6. Section of negative grid (same area as in Fig. 5) photographed by polarized light. 350 \times before reduction for publication.

corrosion of 25 different batteries, for example, twelve individual measurements were taken at random positions on a cross section of each battery. The area of both remaining grid metal and corrosion product was recorded and the results averaged. When the planimeter was used, individual measurements at any one position were found reproducible with an accuracy of 1% or better. However, the deviation, or the amount that single independent measurements at different positions on the section differed from the most probable value, was as high as 10%. This figure represents the reliability of a single measurement. The average deviation, which is a measure of the reliability of the average value (twelve measurements), did not exceed 3% in any section and in the majority of sections was less than 1%. Variations in grid cross section introduced greater uncertainty than the method of measurement or variations in corrosion penetration. The area of corrosion product, in general, was remarkably uniform throughout the section and independent of the original grid area.

Under varied operating conditions differences in the active material, corrosion product, and metal are easily detected. For example, the appearance of the negative active material is quite different before and after cycling. The dendritic lead structure of the newly formed negative plate changes gradually to a mass of crystals, presumably lead sulfate (Fig. 6).

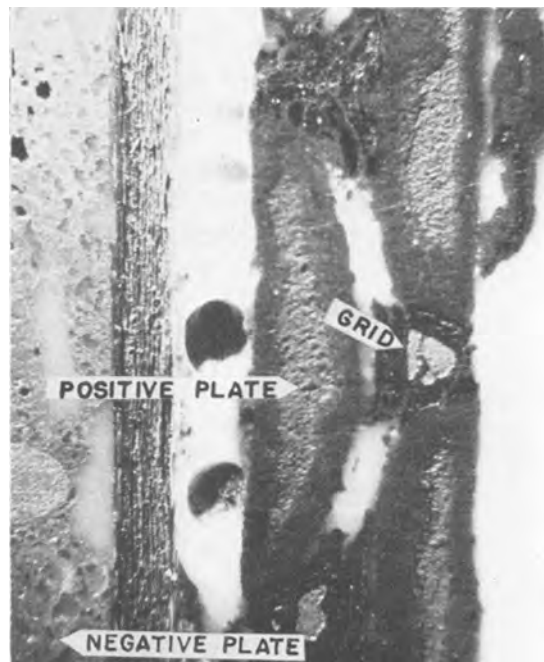


FIG. 7. Positive plate in cross section, showing manner in which splitting of the active material (dislodgment of pellets) takes place along the center line of the plate. Grainy appearance of surface was caused by incomplete impregnation with plastic. 5 \times before reduction for publication.

The positive plate in cross section appears to be split down the center after a few charge cycles (Fig. 7). This might be attributed to the pressure set up by the change from lead to oxides or sulfates of greater volume during corrosion. Apparently other factors are at work, however, since under different operating conditions the corrosion layer can become quite thick without causing any splitting of the active material.

It may be possible to determine the constituents of the active material and the chemical composition of the various layers in the corrosion product that surrounds the grid members. There are, first of all, definite color differences among the various products, and these show up beautifully in color photography. The hardness, as determined with the Eberbach micro hardness tester, varies considerably and consistently among the various constituents that are otherwise distinguishable. The various parts of the section also show some differences under polarized light. These purely physical differences may be supplemented by chemical tests. As in the case of metal surfaces, various parts of the section react differently to chemical reagents, and the plastic impregnating material usually remains inert. The resulting reaction products often remain as crystals of different shape and color. Comparison of such reactions for unknown corrosion products and known lead oxides or sulfates may offer a definite clue to identity.

As an example, a solution of ammonium acetate applied to the surface of the section changes the corrosion ring next to the metal surface of the positive grid from black to white (Fig. 8) without producing any effect on other parts of the corrosion product. Tests on various lead oxides show that ammonium acetate produces this effect with lead oxide (PbO), which indicates that the layer next to the metal surface may be lead oxide.

Results of such tests must be confirmed by other means, however, since the possibility of an electrochemical reaction must also be considered. Ammonium acetate or acetic acid, for example, shows a rapid and pronounced attack on the metal of the positive grid, but has an inappreciable effect on the metal of the negative. No such attack is observed on cross sections of the same positive grid, however, when the active material and corrosion products have been scraped off. This indicates that the corrosion by ammonium acetate had an electrochemical origin. Thus, a determination of weight loss by stripping the corrosion product with ammonium acetate would produce a serious error due to metal corrosion, although tests on bare metal with the same solution would indicate that attack on the grid metal was negligible.

In order to use chemical tests as a means of identi-

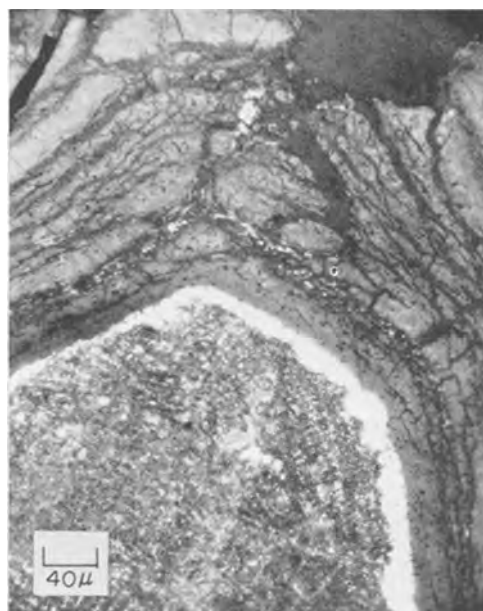


FIG. 8. White ring formed in positive grid corrosion product adjoining metal surface by the use of an ammonium acetate etch. Compare this with Fig. 3, a similar section prior to etching. 250 \times before reduction for publication.

fication, it is advisable to use known oxides in making up artificial sections that contain the same electrochemical couples as those suspected and then compare chemical reactions against these known standards.

There is also the possibility that microdrilling (2) or sampling methods can be used to remove portions of the material on a selective basis so that x-ray or electron diffraction studies can be made.

DISCUSSION AND CONCLUSIONS

The ideal method of investigating battery processes from the standpoint of microscopic inspection would be one by which the actual processes could be watched as they occur. Although this may eventually be possible, present methods of attaining this goal leave much to be desired.

By microscopic examination of impregnated sections removed from a series of cells that have operated under various conditions, an approximation can be made of the changes that occur. The permanent nature of the specimens makes possible a large number of manipulations and measurements and a direct comparison of different characteristics at any future time.

Unfortunately, the plastic cannot be added to the operating cell to seal it at once against any further change. The necessary washing and drying operations undoubtedly produce some changes from operating conditions. The sponge lead of the negative will be oxidized to some extent, some lead sulfate and oxide will be dissolved, sediment may be washed out or

disturbed, wood separators may split, and so forth. The entrance of the plastic may also cause a slight washing action at exposed surfaces, and displacement of material and the heat evolved in setting up of the plastic may also cause some changes.

Fortunately, these effects do not appear to have a large order of magnitude. Lead sulfate and the lead oxides have a low solubility in water and solution is slight during washing. Reprecipitation of lead salt crystals also appears to occur only slightly during the drying process. The oxidation of sponge lead is a surface effect and, since examination is made of the cross section, it can be discounted. As far as comparison is possible, little difference is observed in microstructure or appearance between cross sections obtained from impregnated cells and sections examined immediately after removal from the electrolyte.

Although physical changes do occur, they may be considered to have a low order of magnitude. Cells

of similar construction and operated in the same manner show reproducibly the same microstructure in the impregnated section even though this microstructure may not be exactly that which would be observed in the operating cell immediately before impregnation. If the separate cells of a similar series, therefore, are operated under different conditions and variations are found in the observed microstructure of the individual cells after impregnation, then these differences in observed microstructure may be attributed safely to differences in cell operation and so evaluated.

Any discussion of this paper will appear in a Discussion Section to be published in the December 1955 JOURNAL.

REFERENCES

1. H. BUCKLE AND H. HANEMANN, *Z. Metallkunde*, **32**, 120 (1940).
2. F. R. BRYAN AND C. H. NEVEU, *Metal Progr.* **64**, No. 6, 83 (1953).

The Effect of Cobalt on the High Temperature Oxidation of Nickel¹

S. F. FREDERICK² AND I. CORNET

University of California, Berkeley, California

ABSTRACT

Nickel-cobalt alloys of high purity, in sheet form, were oxidized in air at temperatures ranging from 800° to 1400°C. The oxidation rate of high purity carbonyl nickel was found to be lower than previously reported in the literature. The oxidation rate increased with increasing cobalt content, but the effect was small until over 11% cobalt had been added. The activation energy for oxidation decreased with increasing cobalt content from a value of 51 kcal/mole for pure nickel to about 28.8 kcal/mole for pure cobalt.

INTRODUCTION

Nickel and cobalt are frequently used as basis metals or as alloying constituents for oxidation resistant alloys for relatively high temperature applications. There have been many studies of the oxidation behavior of pure nickel (1-3) and of pure cobalt (1, 4, 5), generally because of their intrinsic importance, but relatively little information is available on the effect of cobalt on the rate of oxidation of nickel (1, 6).

While determining the heat of formation of nickel oxide, Kelley and Humphrey (7) reported that high purity nickel could be ignited only with difficulty, and when ignited did not react completely. Addition of a small amount of cobalt, however, promoted ignition and assured a complete reaction. This experimental report seemed sufficient reason for re-examining the effect of cobalt on the oxidation of nickel.

EXPERIMENTAL

Materials

High purity carbonyl nickel powder was graciously supplied by the International Nickel Company. Spectrographically pure cobalt sponge was purchased from Johnson, Matthey and Company, Ltd. All test samples were prepared from these two materials, for which analyses are presented in Tables I and II.

Approximately 10 g of sample of the desired composition was melted in a crucible in a hydrogen atmosphere using an induction heated carbon block as the heat source. Pure cobalt was melted in a ZrO₂

crucible (Norton sintered ZrO₂, no binder). Pure nickel and all nickel-cobalt alloys were melted in MgO crucibles.

The melting procedure was to place the crucible with the charge in the carbon block in the induction furnace and evacuate the chamber to a pressure of less than 5×10^{-3} mm mercury with a Welch Duo Seal vacuum pump. With an Ajax-Northrup 40 kw high frequency converter, the temperature was raised in about 10 min to 1100°-1200°C, as measured with an optical pyrometer. Hydrogen was introduced. The charge was then melted and heated to the range 1550°-1600°C. The system was evacuated again and a fresh supply of hydrogen introduced. After one minute the system was again evacuated and the metal allowed to freeze and cool under vacuum. The metal charge was in the molten state for approximately 5-7 min.

Except for the 78% cobalt alloy and the pure cobalt, samples were prepared as follows. Ingots were cold rolled in multiple passes, with no intermediate anneals, to sheet about 0.3 mm thick. Rectangular specimens of 2-10 cm² total area, including edges, were cut from the sheets. Specimens were drilled, and then polished with 3/0 emery paper. Dimensions were measured with a micrometer stage on a metallurgical microscope to the nearest 0.1 mm. Specimens were then washed with soap and water and rinsed in alcohol, dried, and weighed with an analytical balance to the nearest 0.1 mg. They were then either tested immediately or placed in a desiccator until testing.

An attempt was made to cold roll the 78% cobalt alloy and the pure cobalt, but they proved to be too brittle. Therefore, small chips were broken from the ingots; each chip was placed in an ordinary metallurgical mounting press, heated to 240°C, and pressure applied. With the small chip size used, specimens were thus hot forged with pressures, based on chip

¹ Manuscript received August 27, 1954. From a thesis submitted by S. F. Frederick to the Graduate School of the University of California in partial fulfillment of the requirements for the degree of Master of Science.

² Present address: Douglas Aircraft Company, Santa Monica, California.

TABLE I. Analysis of carbonyl nickel

Element	Spectrographic estimate of quantity present
	%
Silicon	Trace (0.001)
Iron	0.003
Copper	0.0005
Magnesium	0.0001
Chromium	Less than 0.001
Manganese	N.D.—less than 0.002

Other elements were not detected.

Spectrographic analysis provided through the courtesy of G. M. Gordon.

TABLE II. Analysis of cobalt sponge

Element	Spectrographic estimate of quantity present
	%
Silicon	0.002 (average value)
Magnesium	0.0005
Aluminum	0.0002
Manganese	0.0001
Calcium	—

The following elements were only detected by the total combustion method: iron, less than 0.001%; nickel, 0.0005%.

No lines of the following elements were observed: Ag, As, Au, Be, Bi, Cd, Cr, K, Li, Mo, Na, Pb, Rb, Sb, Sn, Ti, V, W, Zn, Zr.

Analysis furnished by Johnson, Matthey and Company, Limited.

area, of approximately 200,000 psi. Instead of trying to cut these specimens into shapes convenient for measuring, thereby reducing the already small areas, the areas of these specimens were measured by making contact prints of them. The prints were cut out, weighed, and compared with a weighed and measured area of print. Subsequent surface preparation was the same as for the other alloy specimens.

Testing Procedure

The specimen was suspended by a platinum wire in a Burrell vertical tube Glo-bar furnace. The 1 in. diameter tube was vented at the top and bottom, allowing an air flow due to convection currents through the furnace, thus preventing any oxygen depletion during the test. Preliminary tests with specimens of different areas also showed that oxygen depletion was not a factor. Temperatures in the test zone were maintained within $\pm 5^\circ\text{C}$ by a Leeds & Northrup Micromax temperature controller. The original plan was to weigh the specimen continuously during the testing period, and an automatic recording balance of the type developed by the National Bureau of Standards was constructed for that pur-

pose (8). Unfortunately, the convection currents in the furnace tube prevented establishing the initial zero point with any precision, and the weight-time records could not be considered reliable enough to detect deviations from the parabolic rate. Therefore, a parabolic rate was *assumed* for all tests and independent measurements of the weight change together with the total time were used to calculate the *parabolic rate constant* K_p by the relation

$$K_p = \frac{(W_f - W_o)^2}{A^2 t}$$

where W_o is the initial weight of the specimen, W_f is the final weight of the specimen, A is the total surface area of the specimen (including the edges), and t is the total time of testing.

Tests varied in duration from a minimum of 13 min for 100% cobalt at 1405°C to a maximum of 1638 min for 100% nickel at 806°C . For a given alloy, however, the test duration varied widely, 84–1638 min for pure nickel, 13–1464 min for pure cobalt, for example. Despite the wide variation in duration of tests, results were quite self-consistent. Thus, for pure nickel at 1405°C , for times of 84, 88, and 558 minutes, K_p values were 5.82, 6.17, and 5.79×10^{-9} , respectively.

Results

In Fig. 1, the logarithm of the parabolic rate constant for each alloy is plotted as a function of the reciprocal of the absolute temperature. From the

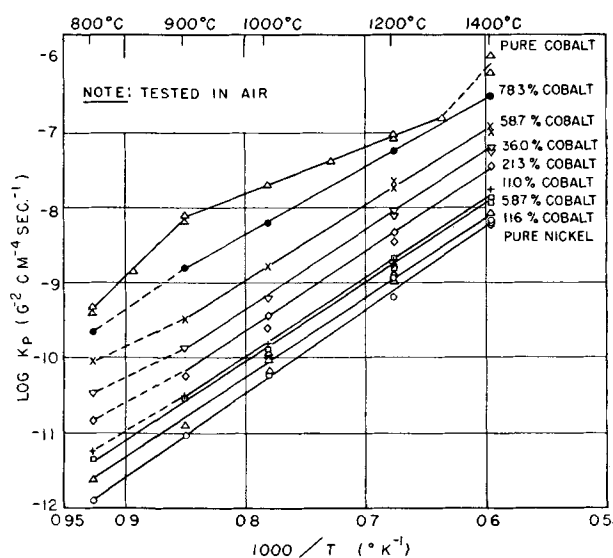


FIG. 1. Effect of temperature on the oxidation rate on nickel-cobalt alloys. K_p = oxidation rate assuming a parabolic law of oxidation is followed.

curves in Fig. 1, the activation energy E for oxidation was calculated using the relation

$$E = -R \left\{ \frac{\ln K_p}{1/T} \right\} = -2.3Rs$$

where R is the gas constant and s is the slope of the curve. In Fig. 2, the activation energy for oxidation is shown as a function of cobalt content. Fig. 3-8 show rate constants for the indicated temperatures as a function of cobalt content. In drawing these curves, Fig. 1 was arbitrarily selected as the primary curve and the curves on Fig. 3 through 8 were drawn to be consistent with Fig. 1. Fig. 9 shows photomicrographs of the cross section of some of the oxidized samples.

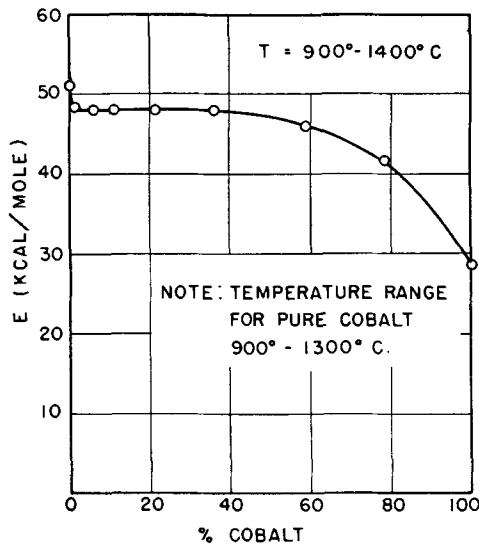


FIG. 2. Activation energy for oxidation of nickel-cobalt alloys.

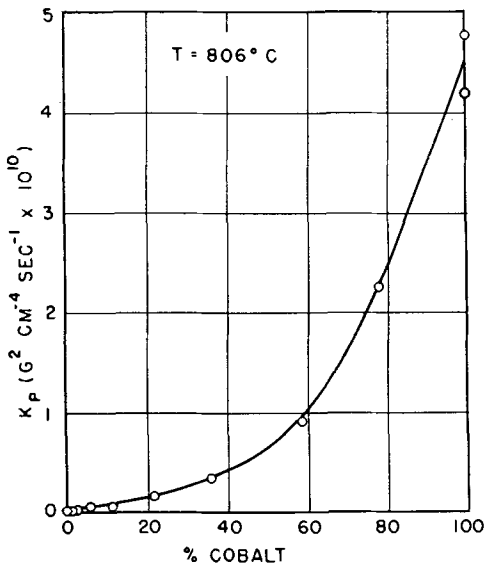


FIG. 3. Oxidation rate of nickel-cobalt alloys

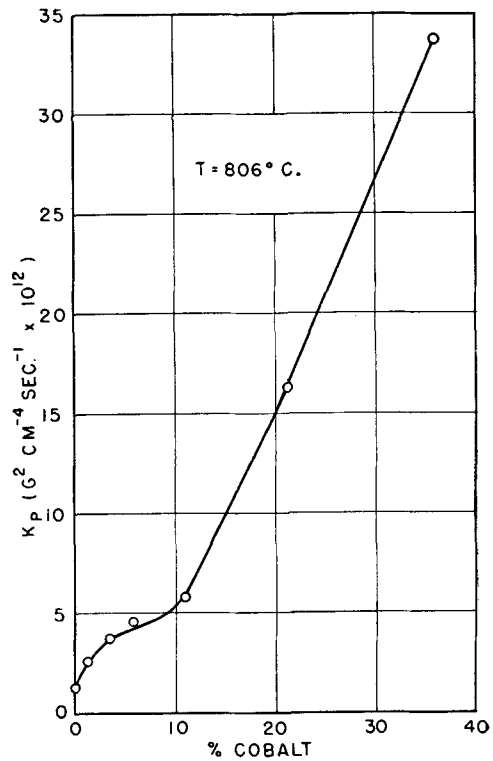


FIG. 4. Oxidation rate of nickel-cobalt alloys

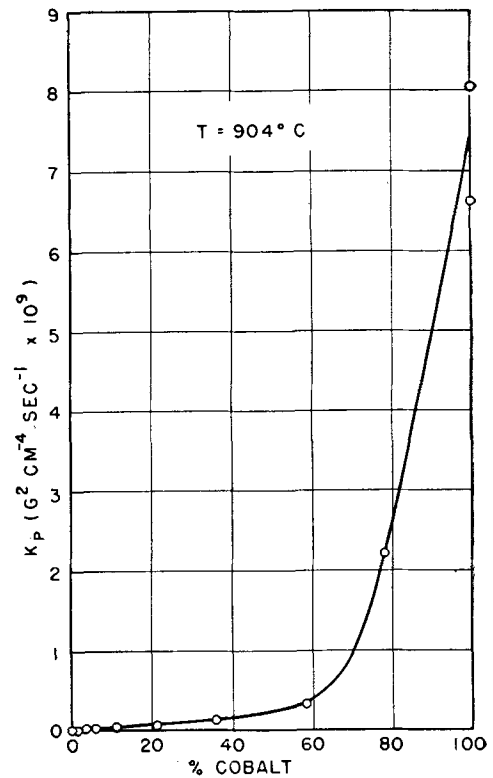


FIG. 5. Oxidation rate of nickel-cobalt alloys

Data are reported for 80 individual tests, for nickel alloys containing (nominally) 0, 1, 3, 6, 11, 21, 36, 59, 78% cobalt, and for 100% cobalt. Many duplicate tests at a given temperature for a given alloy gave rate constants so close that the points coincide on the scale of presentation used. Thus in Fig. 7,

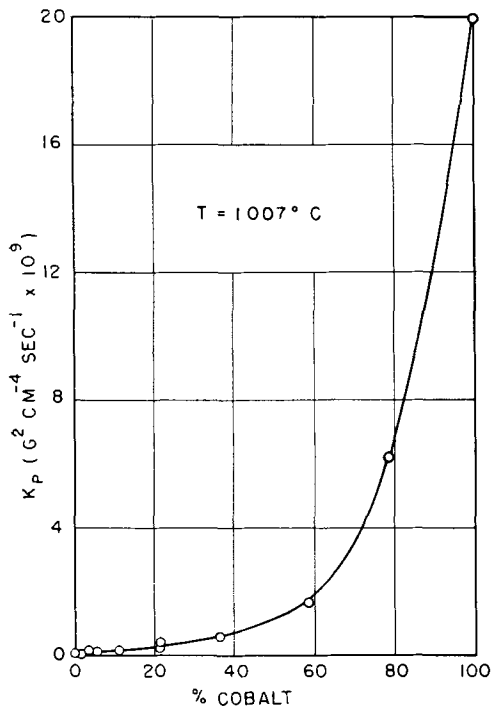


FIG. 6. Oxidation rate of nickel-cobalt alloys

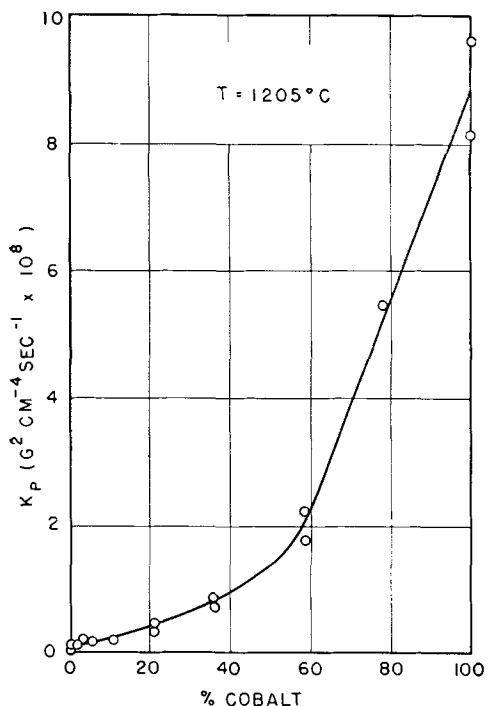


FIG. 7. Oxidation rate of nickel-cobalt alloys

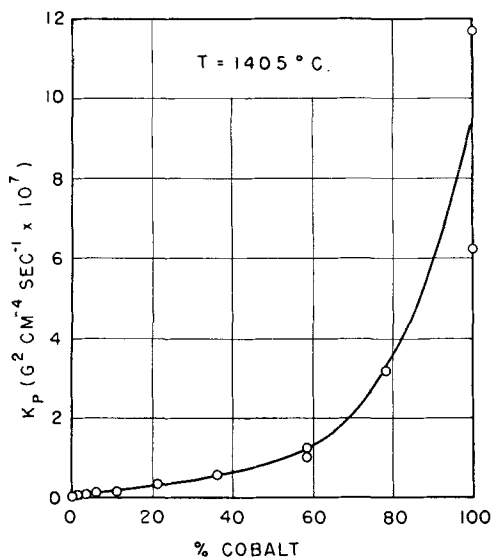


FIG. 8. Oxidation rate of nickel-cobalt alloys

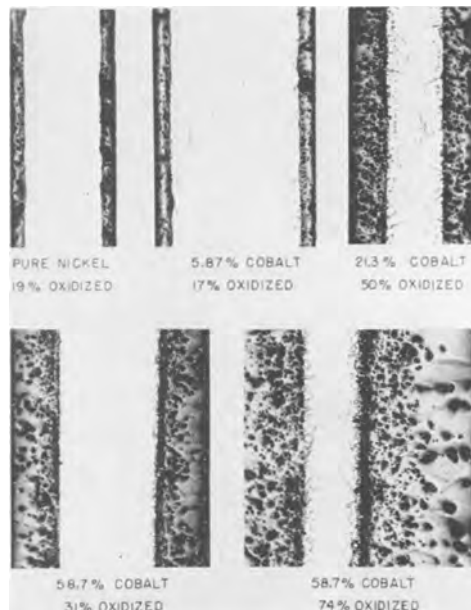


FIG. 9. Cross sections of samples tested at 1205°C. Un-etched. 150X

at 1205°C there are coincident experimental points for nickel alloys containing 0, 1.16, 3.42, 5.87, and 11.0% cobalt.

Besides the 80 tests reported above, some data were obtained initially for alloys containing 0.1, 0.2, 0.4, and 0.6% cobalt, since it was thought that a very small amount of cobalt might greatly affect the oxidation rate of nickel. For these concentrations of 0.1–0.6% cobalt, rates were the same as for 1.16% cobalt alloy. Data for these 0.1–0.6% cobalt alloys, therefore, were not shown.

DISCUSSION

Oxidation of Pure Nickel

Nickel oxide is a *p*-type semiconductor. From the observations that NiO has a NaCl type structure with an excess of oxygen compared to the stoichiometric composition (9), and from the variations of electrical conductivity when ions of higher or lower valency are added, a model of the oxide film has been proposed (1) as shown in Fig. 10. In this model there are occasional vacancies in place of nickel ions. Concentration of vacancies is highest at the oxide-atmosphere interface and lowest at the oxide-metal interface. There are also trivalent nickel ions or "electron holes" to maintain electrical neutrality. Oxidation of nickel proceeds predominantly by diffusion of nickel ions and electrons through the oxide film to the oxide-atmosphere interface where the reaction $\text{Ni}^{++} + 2e^- + \frac{1}{2}\text{O}_2 = \text{NiO}$ occurs. Diffusion of nickel ions is the rate-controlling process.

Over a wide range of temperatures nickel obeys the parabolic law of oxidation (1), derived experimentally by Tammann (10) and by Pilling and Bedworth (11), and derived on the basis of electrochemical theory by Wagner (1, 12). As with other kinetic processes the rate of oxidation is temperature dependent and follows Arrhenius' equation

$$K_p = A \exp^{-E/RT}$$

where K_p is the parabolic rate constant, A is a constant, E is the activation energy for oxidation, R is the universal gas constant, and T is the absolute temperature.

Qualitatively, therefore, the oxidation of nickel is well understood. Quantitatively, however, some problems remain. The theoretical determination of the oxidation rate of nickel, based on semiconductor theory, is hampered by the fact that measurements of the electrical conductivity of nickel oxide have

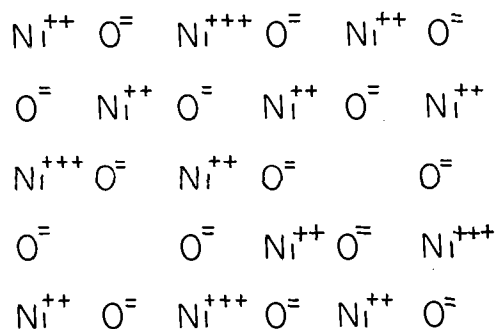


FIG. 10. Model of nickel-oxide film showing cation vacancies and corresponding trivalent nickel ions or "electron holes."

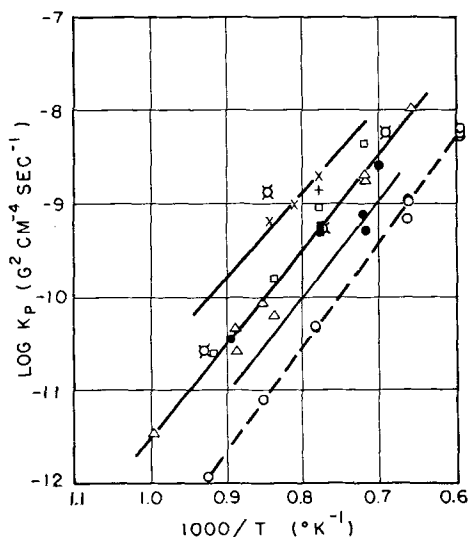


FIG. 11. Oxidation rate of nickel of different purities [cf. Kubaschewsky and Hopkins (1)]. \times , Nickel 'A', 98.88% Ni, 0.48% Fe, 0.18% Mn, 0.17% Si; \square , electrolytic nickel, 99.67% Ni, 0.25% Fe, 0.03% C, 0.04% Si, trace Mn; \boxtimes , carbonyl nickel, 0.04% C, 0.12% Fe, 0.09% O, nil S; $+$, nickel, 0.5–1.0% Mn, some Fe, nil Mg; Δ , 'Rein-nickel,' 0.07% Si, 0.07% Cu, 0.27% Fe, 0.20% Co, 0.01% Cr, 0.01% Al, nil Mn; \blacktriangle , electrolytic nickel remelted in vacuo; \bullet , carbonyl nickel remelted in vacuo; \circ — — — \circ , present investigation.

been made on samples of highly impure or incompletely stated composition (2).

There are problems also in the experimental determination of the oxidation of nickel. Rates are particularly influenced, even by a factor of tenfold, by small quantities of impurities in the metal (1) (cf. Fig. 11). It is difficult to compare results of various investigations because of differences in metal composition, specimen preparation, method of measurement—thickness of film or weight gain, oxidizing atmosphere, and other variables. However, the results of the present investigation are in good agreement with rate constants previously reported (Fig. 11), although E is 51,000 cal/mole as compared to 45,000 cal/mole, and rate constants are somewhat lower than previously reported by Kubaschewski and Hopkins (1).

Moore and Lee (2, 4), using a nickel foil of purity comparable to the present material, reported a slightly lower rate constant, $(1.71 \pm 0.30) \times 10^{-12}$ ($\text{g}^2/\text{cm}^4\text{sec}$) at 900°C , and $(5.86 \pm 0.20) \times 10^{-13}$ ($\text{g}^2/\text{cm}^4\text{sec}$) at 800°C ; but they found $E = 38.4$ kcal/mole. However, the study of Moore and Lee was performed at 10 cm pressure of oxygen and based on measurements of film thickness rather than weight gain. The effect of oxygen pressure may not be important, since it has been reported that there is no change in the oxidation rate of pure

nickel for pressures of 1 atm to 500 psi (13). However, data of Wagner and Grunewald at 1000°C have indicated that the rate constant varied as $P_{O_2}^{1/5.3}$ (2), and other data have shown the conductivity of nickel oxide to vary as $P_{O_2}^{1/4}$ above 350°C (2).

Data of Gulbransen and Andrew (3) on the oxidation of high purity nickel yield a heat of activation of 41.2 kcal/mole compared to 51.0 kcal/mole for the present study. Data of Gulbransen and Andrew (3) on extrapolation to 1000°C yield parabolic rate constants similar to those obtained in the present study. However, Gulbransen and Andrew performed their experiments in oxygen at 0.1 atm, and limited oxidation to relatively thin films.

Oxidation of Nickel-Cobalt Alloys

Small additions of many metals have been shown to increase the oxidation rate of nickel (1). This may be explained by considering the effect of adding chromium. Since chromium forms a trivalent ion, two chromium ions and a vacancy are equal to three nickel ions. Therefore, addition of chromium to nickel should increase the concentration of vacancies in the oxide film, thereby increasing the diffusion rate of nickel ions, giving a higher oxidation rate. Experiments confirm this picture; the oxidation rate of nickel-chromium alloys increases up to about 6% chromium, then the rate decreases to a minimum at 40% chromium, the decrease being attributed to the formation of the spinel $NiO \cdot Cr_2O_3$.

Nickel and cobalt form a continuous solid solution (14) and there is evidence that their oxides are mutually soluble. Unlike nickel, which forms only the one stable oxide NiO , cobalt may form Co_3O_4 and CoO below 900°C, but only CoO is stable above that temperature. At temperatures where an appreciable quantity of trivalent cobalt ions are formed, cobalt would be expected to affect oxidation rates much as does chromium. However, at higher temperatures, where cobalt forms stable divalent ions only, it should not greatly accelerate formation of nickel oxide. NiO and CoO have the same crystal structure and almost the same lattice parameter (4.17 Å for NiO and 4.25 Å for CoO). The activation energy for oxidation of cobalt at high temperature is reported to be only slightly lower than E for nickel, but cobalt oxidizes about 25 times faster than nickel (1). In nickel alloys containing small concentrations of cobalt, formation of CoO in the oxide layer may be expected, with a corresponding increase in oxidation rate, assuming that no double oxide is formed.

Experimental results obtained are quite consistent with the foregoing theory. Additions of up to 11% cobalt have only small effect on the oxidation rate

of nickel. This would indicate that probably nickel oxide is formed with cobalt present substitutionally. The external appearance of the oxide film tends to support this view. The color of the oxide changes from the green of nickel oxide to the blue-black of cobalt oxide by the time the cobalt content has reached 11%. The oxide on the 3% alloy is almost as dark as on the 11% alloy, while oxide on the 1% alloy is still quite green. As the cobalt content is increased over 11% (Fig. 4), there is a rapid increase in the oxidation rate, with an even more rapid increase over about 60%, possibly indicating that cobalt oxide is becoming the predominant constituent of the oxide film.

Although there is a fair amount of scatter in the data, particularly at the higher temperatures, the photomicrographs of Fig. 9 show that this may be expected as internal oxidation is present. Internal oxidation would indicate that there are some deviations from the parabolic rate law.

Preece and Lucas (6) have reported on the oxidation of nickel, cobalt, and cobalt + 40% Ni in the temperature range 800°–1200°C. Their results are not directly comparable with data of the present investigation because they used materials of commercial purity and specimens cut from vacuum melted ingot without further treatment. Furthermore, they appear to have used a 24 hr oxidation test, regardless of temperature, and they did observe some internal oxidation above 1000°C.

Oxidation of Pure Cobalt

The hot-press-forged cobalt sheet used in this investigation had some edge fissures, introducing an uncertainty in the determination of surface area and possibly introducing some deviations from parabolic oxidation rates. Oxidation rates of pure cobalt in the range 800°–1200°C given by Preece and Lucas (6) are greater than rates of the present investigation by factors up to tenfold; this would be expected because Preece and Lucas used material of commercial purity.

Activation Energy for Oxidation

The rate data obtained permit determination of the activation energy for oxidation of nickel-cobalt alloys. For pure nickel, E is approximately 51,000 cal/mole. E drops to 48,000 cal/mole with the addition of small quantities of cobalt; beyond 40% Co, E decreases rapidly to 28,800 cal/mole for pure cobalt.

CONCLUSIONS

With the assumption that nickel-cobalt alloys oxidize according to the parabolic rate law, it was

found that additions of up to 11% cobalt had only a small effect on the oxidation rate of nickel. More than 11% cobalt caused a rapid increase in the rate of oxidation, while more than 60% cobalt caused an even more rapid increase in the rate. The absolute value of the oxidation rate of pure nickel was found to be below the values previously reported in the literature for the temperatures investigated.

The activation energy for oxidation of pure nickel in the temperature range 800°–1400°C was found to be 51,000 cal/mole compared to 45,000 cal/mole reported in the literature. The activation energy for the oxidation of pure cobalt was found to vary; a value of 28,800 cal/mole was found for the temperature range 900°–1300°C. The activation energy for oxidation of nickel-cobalt alloys was found to decrease with increasing cobalt content in the temperature range 900°–1400°C.

ACKNOWLEDGMENTS

The authors express their appreciation of the assistance of T. Hazlett and Paul Langstrom in preparing the high purity alloys.

Any discussion of this paper will appear in a Discussion Section to be published in the December 1955 JOURNAL.

REFERENCES

1. O. KUBASCHEWSKI AND B. E. HOPKINS, "Oxidation of Metals and Alloys," pp. 31–32, 44, 68–69, 120–125, 162–163, 176–177, 197–199, Academic Press, Inc., New York (1953).
2. W. J. MOORE AND J. K. LEE, *Trans. Faraday Soc.*, **48**, 916 (1952).
3. E. A. GULBRANSEN AND K. F. ANDREW, *This Journal*, **101**, 128 (1954).
4. W. J. MOORE AND J. K. LEE, *J. Chem. Phys.*, **19**, 255 (1951).
5. C. R. JOHNS AND W. M. BALDWIN, *J. Metals*, **1**, 720 (1949).
6. A. PREECE AND G. LUCAS, *J. Inst. Metals*, **20**, 219 (1952).
7. K. K. KELLEY AND G. L. HUMPHREY, Private communication.
8. ANON., *Natl. Bur. Standards Tech. News Bull.*, **37**, 86 (1953).
9. J. S. ANDERSON, *Ann. Repts. Progr. Chem. (Chem. Soc. London)*, **43**, 104 (1946).
10. G. TAMMANN, *Z. anorg. Chem.*, **111**, 78 (1920).
11. N. B. PILLING AND R. E. BEDWORTH, *J. Inst. Metals*, **29**, 529 (1923).
12. C. WAGNER, "Diffusion and High Temperature Oxidation of Metals," in "Atom Movements," pp. 153–173, American Society for Metals, Cleveland (1951).
13. W. M. FASSELL, JR., R. C. PETERSON, D. W. BRIDGES, AND J. P. BAUER, "The High Pressure Oxidation of Metals," paper presented by W. M. Fassell, Jr., at AIME Pacific Northwest Metals and Minerals Conference (May 1, 1954).
14. C. E. LACY, "Metals Handbook," p. 1192, American Society for Metals, Cleveland (1948).

Reaction of Nitrogen with Uranium¹

M. W. MALLETT AND A. F. GERDS

Battelle Memorial Institute, Columbus, Ohio

ABSTRACT

Rates of reaction of nitrogen with uranium were determined by volumetric measurements in the temperature range 550°–900°C at atmospheric pressure. The reactions were found to follow a parabolic rate law with some deviations initially and also after the period of parabolic reaction. Surface reaction products formed in the temperature range 550°–750°C were identified by x-ray diffraction studies to consist principally of UN₂ with slight evidence of U₂N₃ in some cases. Between 775° and 900°C the three nitrides UN, U₂N₃, and UN₂ were found in the surface reaction product. The parabolic rate constant for the reaction between 550° and 750°C was found to be $k = 202 \exp(-25,500/RT)$ (ml/cm²)²/sec. The activation energy, 25,500 cal/mole, has a probable error of ± 1800 cal/mole. Between 775° and 900°C the parabolic rate constant is $k = 3.95 \exp(-15,100/RT)$ (ml/cm²)²/sec, where $15,100 \pm 2000$ cal/mole is the energy of activation. It has not been determined if the change in rate constant near the temperature of the beta to gamma transformation in uranium has any special significance.

INTRODUCTION

This investigation was made to obtain fundamental information on the kinetics of reaction of nitrogen with uranium. Surface reactions of massive uranium with nitrogen were studied in the temperature range 550°–900°C at a pressure of 1 atm. No information concerning this subject was found in the literature.

Three nitrides of uranium are reported in the literature (1, 2). The mononitride, UN, has a face-centered cubic structure, $a_0 = 4.880$ Å, and has 4 molecules in a unit cell. The sesquinitride, U₂N₃, has a body-centered cubic structure of the Mn₂O₃ type with 16 molecules per unit cell and lattice constant of 10.678 Å. The dinitride, UN₂, has a face-centered cubic, fluorite-type structure with 4 molecules per unit cell and $a_0 = 5.31$ Å. The dinitride is reported to form only at high nitrogen pressures.

MATERIALS

The uranium rod used in this study was fabricated from a 1 $\frac{1}{8}$ -in. square bar sawed from an ingot of good purity. After heating to 600°C in a helium atmosphere, the square section was rolled to 1 $\frac{1}{16}$ -in. round rod. The surface of the rod was vapor blasted to remove contamination, reheated to 600°C in helium, and rolled to $\frac{7}{16}$ -in. round rod. After again vapor blasting and pickling, the rod was cold swaged to approximately $\frac{3}{8}$ -in. diameter. Test specimens, each about 1 $\frac{1}{2}$ -in. long and 1 $\frac{1}{32}$ -in. diameter, were machined from the rod.

The uranium was analyzed for impurities by means of chemical, spectrographic, and vacuum-fusion methods. The total of all measured impurities

in the metal was only about 400 ppm and each detected impurity was present in a concentration of less than 100 ppm. The following elements were detected as impurities: aluminum, calcium, carbon, chromium, copper, iron, magnesium, manganese, molybdenum, nickel, nitrogen, oxygen, silicon, and vanadium.

Nitrogen used in this study was prepared by passing Matheson prepurified tank nitrogen over zirconium turnings heated at 850°C. The gas was dried by passing through a dry ice-acetone cold trap. A sample of the purified gas was analyzed by means of a mass spectrometer and found to contain 99.8 vol % nitrogen and 0.2 vol % argon.

PROCEDURE

Apparatus and sample preparation.—The reaction rate of nitrogen with uranium was determined by volumetric measurement of the rate of gas consumption by the metal specimen at elevated temperatures. A Sieverts-type apparatus, slightly modified from that described (3, 4) previously, was used. In this work, the uranium specimen was supported on a Vycor stool within the Vycor reaction tube. A platinum-platinum + 10% rhodium thermocouple was spot welded to the top of the specimen. The thermocouple was calibrated (3) against a standardized optical pyrometer. A Vycor tube sealed at both ends was used to reduce the dead volume of the reaction system. Specimens were heated by induction, power being supplied by a 4-kw tungsten-gap-type converter. Temperatures were maintained to $\pm 10^\circ\text{C}$.

Uranium specimens were abraded through 600-grit silicon carbide papers soaked in kerosene. Specimens were then rinsed with naphtha, ethyl

¹ Manuscript received September 23, 1954. Work performed under AEC Contract W-7405-eng-92.

ether, and cp acetone. After determining the dimensions of the specimen with a micrometer, the thermocouple was attached. The specimen, together with the thermocouple, reaction tube, and dead volume reducer, was placed in a dry-box which was flushed with argon for 1 hr to displace the air. The dry-box also contained trays of magnesium perchlorate desiccant to remove moisture from the argon. The specimen was lightly abraded in the dry-box with dry 600-grit silicon carbide paper to remove surface oxidation, after which it was mounted in the reaction tube inside the dry-box. A rubber stopper was placed in the ground glass joint by which the reaction tube was attached to the Sieverts apparatus. The assembled tube was then removed from the dry-box, attached to the Sieverts apparatus, and immediately evacuated. Because of the rapid surface oxidation of uranium, the final dry abrading of the uranium specimens in the argon atmosphere was deemed necessary. The customary rinse in an organic solvent was avoided since no solvent was found which did not accelerate atmospheric oxidation or otherwise contaminate the uranium surface.

Degassing.—Since uranium exists in three allotropic forms, it was desirable to degas specimens in the modification in which the reaction was to be studied to avoid changing the grain size of the metal. Specimens were degassed at a pressure of less than 10^{-4} mm mercury according to the following schedule: (a) for reaction rate studies in the alpha phase (below 665°C) specimens were heated for 1 hr at 650°C; (b) for reactions in the beta, specimens were heated for 1 hr at 750°C; (c) for reactions in the gamma, specimens were held for 1 hr at the operating temperatures prior to reacting.

Reaction rate studies.—Nitrogen was added in measured quantities from a 50-ml gas buret to the reaction system containing the uranium specimen heated to the desired temperature. Progress of the reaction was followed by observing pressure changes in the closed system with an open-end mercury manometer. Measured amounts of nitrogen were added from time to time to maintain the pressure between $\frac{3}{4}$ and 1 atm. The system was evacuated and the specimen was cooled to room temperature in the evacuated system after the reaction had proceeded for the desired period of time.

Individual points in a reaction rate experiment were determined by calculating the amount of gas remaining in the gas phase at any time and subtracting this amount from the total gas addition. The difference (measured to 0.04 ml STP) is a measure of the nitrogen consumed by the uranium specimen. The quantity of gas reacted per unit area was computed by using the original dimensions of the specimens.

RESULTS AND DISCUSSION

Quality of uranium metal.—It is customary to express surface reaction rates in terms of the gas consumed per unit of surface area based on geometric measurements, even though the true surface area is known to be greater than these measurements indicate. The roughness factor of carefully polished specimens is around 2 to $2\frac{1}{2}$. If the method of abrasion is kept uniform from specimen to specimen, the roughness factor will be very nearly the same for all specimens.

During the early stages of this study, it was difficult to obtain uranium rod free of cracks and other surface defects. Because of this, the ratio of true area to geometric area varied erratically and this was reflected in the calculated reaction rates. Later the uranium was carefully selected from the best available metal. Occasionally even this metal contained some surface defects.

Fig. 1 shows the microstructure at the surface of the cross section of a uranium specimen reacted with nitrogen for 3 hr at 800°C. This specimen was etched electrolytically in a 10% citric acid solution at a potential of 10 v d.c. on the open circuit to remove the worked surface of the metal. Presence of the nitride reaction product at the surface of the metal is evident. Nitrogen also appears to have penetrated into the uranium and reacted with the metal to form nitride at the site of a defect in the metal surface. All specimens used in reaction rate studies were sectioned and examined metallographically after reaction to determine if they were free of surface defects. Data obtained on specimens showing defects were discarded.

Surface-reaction product.—The rate of surface reaction of nitrogen with massive uranium was studied in the temperature range 550°–900°C at atmospheric pressure. Specimens reacted with nitrogen between 775° and 900°C produced a tightly

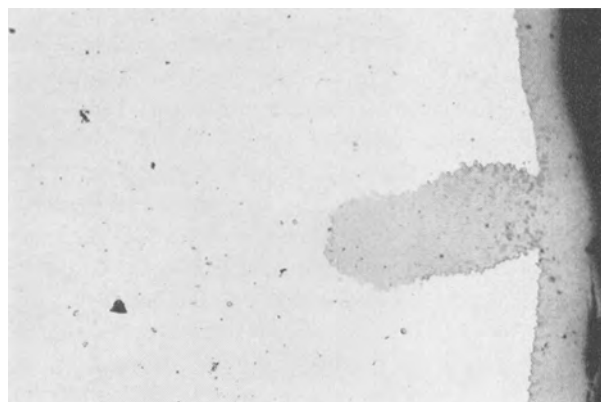


FIG. 1. Uranium reacted with nitrogen at 800°C for 3 hr. Note nitride at site of defect. Citric acid etch. 100X before reduction for publication.

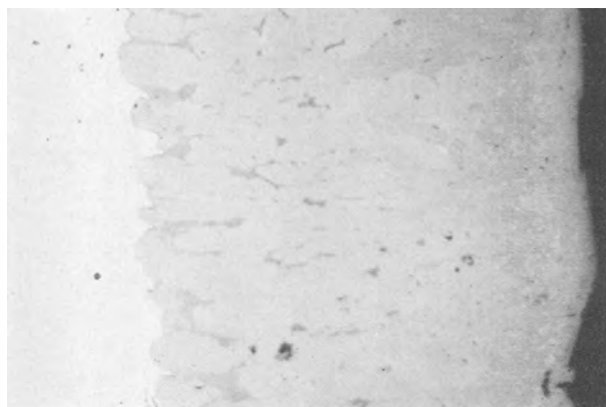


FIG. 2. Uranium reacted with nitrogen at 900°C for 4½ hr. Citric acid etch. 500× before reduction for publication.



FIG. 3. Uranium reacted with nitrogen at 600°C for 5 hr. Citric acid etch. 500× before reduction for publication.

adherent surface film which appeared roughened at the surface exposed to nitrogen. This roughened surface tended to powder off slightly on exposure to the atmosphere at room temperature. The microstructure at the surface of the cross section of a uranium specimen reacted with nitrogen at 900°C for 4½ hr is shown in Fig. 2. Three nitrides were identified in the surface reaction product by means of x-ray diffraction studies and metallographic examination. These nitrides all appear gray in the photomicrograph. UN₂, the outermost, lightest gray phase was found at the nitride-gas surface. It is likely that the compound showing the UN₂ crystal structure is deficient in nitrogen since the literature reports that stoichiometric UN₂ is obtained only at high nitrogen pressure (1, 2). This compound was also the principal constituent of the loose powder found in the vial in which the specimen was stored. The darkest gray (actually tan-gray) phase, at the metal-nitride interface and in the apparent grain boundaries of the thick, intermediate-gray U₂N₃² was identified as

² X-ray diffraction studies of the surface reaction products showed a phase having a hexagonal structure iso-

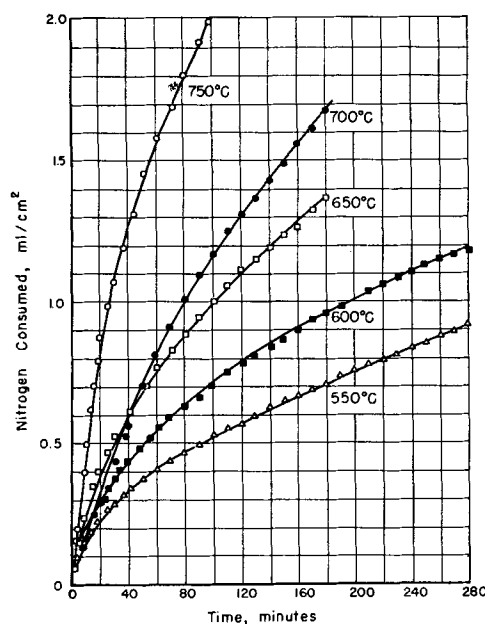


FIG. 4. Uranium-nitrogen reaction at 550°-750°C

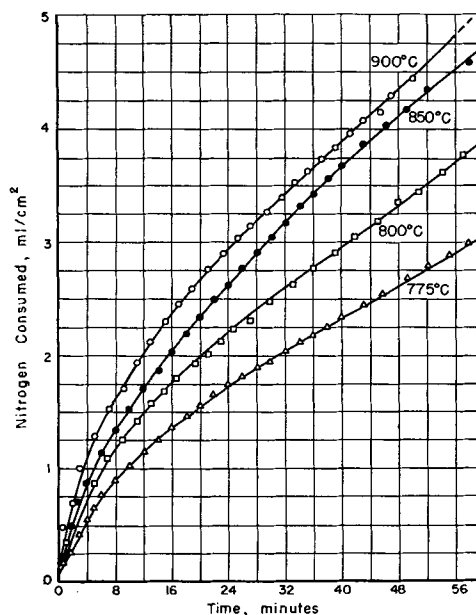


FIG. 5. Uranium-nitrogen reaction at 775°-900°C

UN. U₂N₃ which lies between the UN and UN₂ was the phase present in greatest quantity in the surface reaction product.

Specimens reacted with nitrogen between 550° and 750°C also produced tightly adherent surface films, but these films were much less rough on the exposed surface than those produced at higher temperatures. The microstructure at the surface of a specimen

morphous with Th₂N₃. This new uranium nitride is assumed to be U₂N₃ on the basis of its structure. No evidence of the body-centered cubic U₂N₃ (1) was found in the present study.

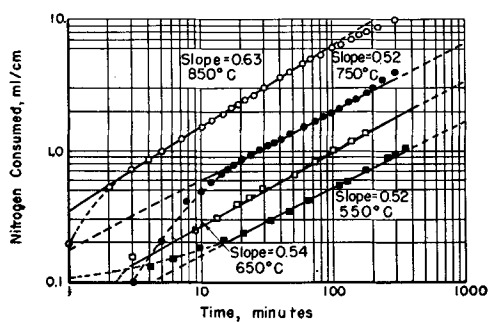


FIG. 6. Typical log-log plots for uranium-nitrogen reaction in the range 550°-850°C.

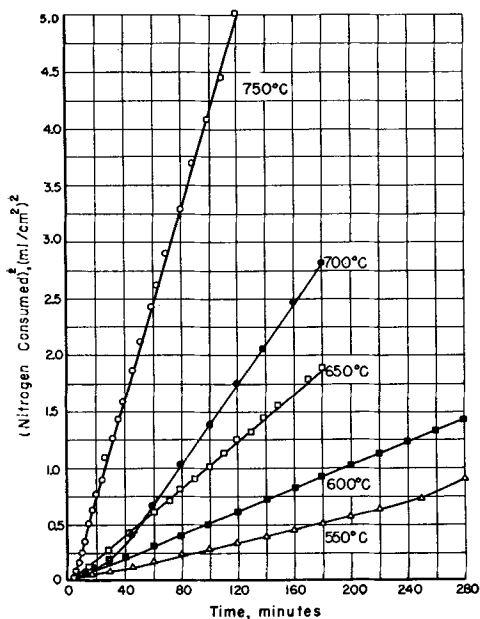


FIG. 7. Uranium-nitrogen reaction at 550°-750°C

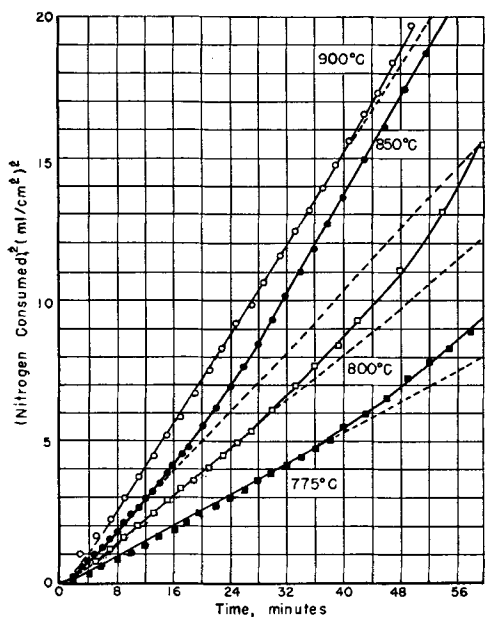


FIG. 8. Uranium-nitrogen reaction at 775°-900°C

TABLE I. Rate constants, k , determined at various temperatures for the reaction of nitrogen with uranium

Temp, °C	$k \times 10^4$, (ml/cm ²) ² /sec	Slope of log-log plot
550	0.463	0.52
600	0.542	0.54
600	0.855	0.52
650	1.76	0.54
700	2.90	0.62
750	7.06	0.52
750	9.70	0.55
775	23.6	0.58
800	34.9	0.57
800	40.0	0.57
850	43.5	0.63
900	54.7	0.60
900	65.5	0.53

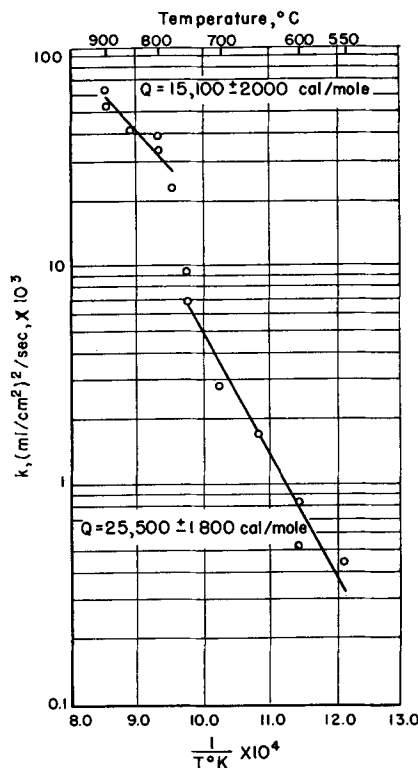


FIG. 9. Uranium-nitrogen reaction; variation of parabolic rate constant with temperature.

reacted with nitrogen at 600°C for 5 hr is shown in Fig. 3. The surface film appears to contain only one phase. The outermost surface reaction product on these specimens powdered off on storing. This powder was identified as face-centered-cubic UN₂. UN₂ also was the chief constituent in the adherent surface films where some evidence for U₂N₃ was found in some of the x-ray diffraction patterns. No UN was found in any of the surface films of specimens reacted with nitrogen below 750°C.

Hardness traverses of specimen cross sections revealed no evidence of solution of nitrogen in the

metal. This is what one would expect since the solubility of nitrogen in uranium is very low (<100 ppm) over the entire range 550°–900°C.

Reaction rates.—The reaction of nitrogen with uranium was found to follow a parabolic rate law over the entire range of temperatures 550°–900°C. Reactions were continued for times up to 6 hr. Reactions showed initial induction periods ranging from about 1 min to as long as 15 min. Since uranium metal oxidizes readily in air at room temperature, it is likely that during these induction periods, the reaction of nitrogen is hindered by a thin oxide film already on the uranium. However, after the initial nitride film has formed, further reaction (film thickening) proceeds in a parabolic manner.

Some deviations from parabolic behavior also were noted after a considerable amount of nitrogen had been reacted. These deviations generally were in the direction of rates faster than parabolic and occurred over the entire temperature range studied. Deviations became apparent in shorter times at the higher temperatures. This may indicate that these deviations are caused by cracking of the surface films at some limiting thicknesses.

Several typical plots of the amounts of gas consumed vs. time are shown in Fig. 4 and 5. The crossing of some of the lines in the vicinity of the origin is evidence of the varying lengths of the initial induction periods of nonparabolic behavior. Only the first 60 min of the reactions at 775°–900°C are plotted in Fig. 5 since the behavior became extremely erratic after this period.

If the logarithm of the amount of nitrogen consumed is plotted against the logarithm of time, a straight line with a slope of 0.5 results if the parabolic rate law is obeyed. Typical plots, as seen in Fig. 6, show both initial deviations from parabolic behavior and also deviations after a considerable amount of nitrogen has been reacted.

In Fig. 7 and 8, the square of the amount of nitrogen consumed per unit surface is plotted against time. These plots show the periods of time over which parabolic behavior was observed. The induction period for the reaction at 700°C is especially noticeable. The break from parabolic behavior to a faster rate for the reaction at 550°C also is evident.

The dashed line extensions of the straight line portions of the curves of Fig. 8 show the extent of the deviations from the initial period of parabolic reaction. All of the reactions in this temperature range have very short, almost negligible, induction periods and show deviations to faster rates following the period of parabolic reaction. Parabolic rate constants were calculated for each reaction by determining the slope of the straight line portions of the curves in Fig. 7 and 8. Rate constants calculated in

this manner and slopes of the log-log plots are listed in Table I.

An Arrhenius plot of the rate constants is shown in Fig. 9. It can be seen that the experimental points appear to fall on two straight lines, the one covering the range from 550° to 750°C and the other, the range from 775° to 900°C. The Arrhenius-type equation, $k = A \exp(-\Delta H/RT)$, was determined for each line by the method of least squares. At 550°–750°C the parabolic rate constant is $k = 202 \exp(-25,500/RT)$ (ml/cm²)²/sec where $25,500 \pm 1800$ cal/mole is the activation energy and the probable error³ in a calculated k is $\pm 20\%$. At higher temperatures, 775°–900°C, the parabolic rate constant is $k = 3.95 \exp(-15,100/RT)$ (ml/cm²)²/sec. The activation energy is $15,100 \pm 2000$ cal/mole and the probable error in k is $\pm 10\%$. It is not known whether it is significant that the apparent change in activation energy occurs at about the beta to gamma transformation in uranium (770°C).

CONCLUSIONS

Nitrogen was found to react with uranium in a parabolic manner in the temperature range 550°–900°C. The surface reaction product formed below 750°C consisted principally of UN₂ with some evidence of U₂N₃. Between 775° and 900°C, the compounds UN, U₂N₃, and UN₂ were found in the films. An apparent change in activation energy for the reaction occurs between 750° and 775°C.

ACKNOWLEDGMENTS

The experimental reaction rate experiments were performed by Mr. B. G. Koehl. X-ray diffraction studies of the surface reaction products were carried out by Mr. D. A. Vaughan. Specimens were prepared for metallographic examination by Miss Betty J. Hannahs.

Any discussion of this paper will appear in a Discussion Section to be published in the December 1955 JOURNAL.

REFERENCES

1. R. E. RUNDLE, N. C. BAENZIGER, A. S. WILSON, AND R. A. McDONALD, *J. Am. Chem. Soc.*, **70**, 99 (1948).
2. J. J. KATZ AND E. RABINOWITZ, "The Chemistry of Uranium," p. 235, McGraw-Hill Book Co., Inc., New York (1951).
3. M. W. MALLETT, J. BELLE, AND B. B. CLELAND, *This Journal*, **101**, 1, (1954).
4. A. F. GERDS AND M. W. MALLETT, *ibid.*, **101**, 4, (1954).

³ From the least square calculation, the probable error in k can be calculated by the equation $k = A \exp(-\Delta H/RT) \exp \pm PE_k$. The probable error in $\log k$ is $PE_k = 0.6745 \sqrt{\Sigma d^2/n^2}$ where Σd^2 is the summation of the squares of the differences between the least square calculated values of $\log k$ and the experimental values of k , and n is the number of experimental values of $\log k$ used. For this work the approximation is used that $\exp \pm PE_k = 1 \pm PE_k$.

Kinetics of Surface Reactions of Metals

I. Iron¹

DONALD M. SOWARDS AND NORMAN HACKERMAN

Department of Chemistry, The University of Texas, Austin, Texas

ABSTRACT

The reaction of iron with dilute, aqueous acetic acid was studied in a closed system with a nitrogen atmosphere at 34°C. The solution was sprayed on the metal continuously for periods up to 24 hr. The extent of reaction, determined gravimetrically, was found to be directly proportional to exposure time. The reaction rate was a function of acidity, flow rate, gaseous atmosphere composition, temperature, and nature of the adherent reaction products. Total activity and type of local activity changed with exposure conditions. This can be explained in terms of the defect structure of the film on the metal. Identity and properties of the films check with those described by others. It was concluded that ferrous acetate, ferrous carbonate, monobasic ferric acetate, and dibasic ferric acetate protect the underlying metal when formed as adherent, continuous films on the surface.

INTRODUCTION

Corrosion studies are usually classed in one or two categories: dry oxidation of metals by gases, and wet corrosion of metals by liquids. However, in terms of the role of the solid reaction products, the two may be quite similar.

Experimental dry oxidation rate curves which can be described by linear, parabolic, cubic, logarithmic, or asymptotic equations are quite common. Satisfactory theoretical expressions for rate constants for the second, third, and fifth type have been derived (1, 2). Theory requires a defect lattice and a sustained electric field in which ions without excessive kinetic energy may migrate. In these polyphase systems, a potential gradient and an electrical double layer contribute to the electric field in varying amounts according to scale thickness; thus, theoretical applications are restricted to specific cases of film thickness where field strengths are calculable. There is little doubt of the conceptual correctness of the theory because of successful verifications in several cases (3).

Evans (4) suggests a direct connection between dry oxidation and wet corrosion wherein metal ions, emerging from thin oxide film on the metal, are incorporated in the film on reacting with oxide ions at the film-solution interface. Oxide ions are presumed to form from environmental oxygen and electrons from the metal by way of the film. Thus,

with poor circulation, the oxygen supply is insufficient for good oxide coverage, and metal ions escape into solution, thereby increasing the corrosion rate. This is found, for example, with iron or zinc in distilled water, showing the importance of films in wet corrosion. These films may form in several ways.

Atmospheric oxygen is consumed rapidly by iron (5), producing an oxide film that is difficult to remove, even by exposure to hydrogen at elevated temperatures (6, 7). When iron is immersed in dilute acid, the initial dissolution rate decreases rapidly during the first few minutes (8, 9). The initially high rate is attributable to exposure of metal either by cathodic reduction of oxide film in the cell, Fe/electrolyte/oxide/Fe (10, 11), or by film rupture (12). Decrease in reaction rate under these conditions involves only inorganic substances, and as Hoar (12) and Hackerman (13) indicate, may be attributable to film formation or repair. Although there is insufficient evidence for determining which of these predominates (12), strict repair should be limited to continuation of the existing lattice, thus limiting the number of metal oxides to those of a structure compatible with that of the protecting oxides.

The expected behavior of iron oxide in wet corrosion reactions has been determined (14, 15), and recently an experimental system yielding results which are expressible in terms of the laws of film growth was described (16). It was believed that investigation of corrosion in such a system would provide information about the initial conditions of film formation and subsequent behavior in a corrosive medium. In view of the earlier work (16), the present effort was arrived at determining: (a) rate and mechanism of the reaction of iron

¹ Manuscript received August 26, 1954. This paper was prepared for delivery before the Wrightsville Beach Meeting, September 13 to 16, 1953, and is based in part on a dissertation by Donald M. Sowards, submitted to the faculty of the Graduate School of the University of Texas in partial fulfillment of the requirements of the degree of Doctor of Philosophy.

coupons exposed in a weak acid spray system; (b) dependence of reaction rate on solution composition, conditions of exposure, and physical nature of the products; (c) identification of the solid, adherent reaction products; (d) temperature coefficient of the reaction.

MATERIALS AND PROCEDURE

Iron coupons² ($2 \times 5 \times 0.15$ cm) were polished on No. 2 emery, No. 2/0 emery, and ferric oxide on worn No. 2/0 emery. This gave a mirror-bright surface visually free from scratches and pits.

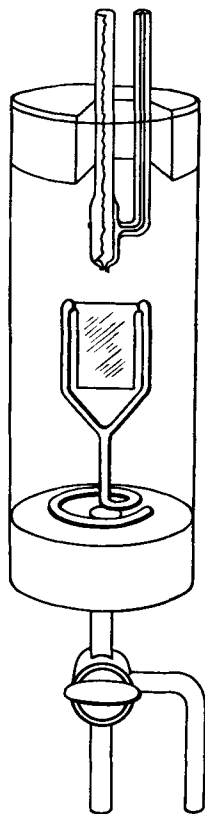


FIG. 1. Spray chamber showing spray unit, coupon, and coupon holder.

They were reduced and annealed in hydrogen (950°C for 2 hr), cooled slowly, and pumped for 8 hr at 0.05 mm Hg.

Deaerated distilled water was used for solution preparation and for cleaning the system.

C. P. Bakers Analyzed grade acetic acid in sealed, $\frac{1}{4}$ -lb bottles was used.

Reagent grade acetone was dried over anhydrous potassium carbonate for five months (17) and distilled in an all-glass still, the fraction distilling at

² All cut from the same sheet of Armco Ingot iron and certified by the supplier, Armco Steel Company, Middletown, Ohio, to contain: 0.010% C, 0.010% Mn, 0.005% P, 0.012% S, 0.002% Si, and 0.040% Cu.

$56.2 \pm 0.1^\circ\text{C}$ and 756 mm Hg (18) being collected for wash liquid.

Water-pumped nitrogen was scrubbed in an acidic solution of vanadyl sulfate over lightly amalgamated zinc (19), then concentrated sodium hydroxide, saturated lead nitrate, and finally moist glass wool. The flow rate was less than 500 ml/min.

Tank hydrogen was passed through a palladium catalytic deoxygenator and a 15-in. column of anhydrous magnesium perchlorate.

The spray chamber with coupon and holder is shown in Fig. 1. All parts were Pyrex glass except the top and bottom which were neoprene. The spray unit was of one-piece construction and required 5 l/min gas flow with a 150 mm Hg pressure drop across the unit for normal operation. Pressure fluctuation in the chamber was less than 10 mm Hg. The Y-shape coupon holders were of Pyrex glass.

The entire system was made of Pyrex and Tygon housed in an air thermostat. Details of the system are available elsewhere (20). Before a run, the system was rinsed with six 7–14 l portions of water and flushed with nitrogen; the solution and gas were then circulated at thermostated temperature for 8 hr while 90 l of nitrogen swept through the system.

On removal, coupons were rinsed with acetone, vacuum dried, and weighed. Next, they were descaled for 5 min in 10% sulfuric acid containing 150 ppm inhibitor³ while cathodically protected (3 v, 0.6 amp). The final weight was then taken.

Most runs were made at $34 \pm 0.1^\circ\text{C}$, but some were also made at 20.0° and 41°C in order to obtain the temperature coefficient of the reaction.

Iron coupons were continuously sprayed with dilute acetic acid in a closed system for periods up to 24 hr. They were placed about 4 cm directly below the spray nozzle.

Nitrogen, pure or containing 1% or less of air, was circulated at a constant velocity of about 5 l/min in each of the spray units.

The acetic acid volume was 10–14 l, and the concentration 0–1000 ppm. Acidity changed with time, observations being made over the range pH 3.4–7.0. The ratio of solution volume to metal surface varied because of the necessity of removing coupons during the run; therefore, pH vs. time relations were not amenable to quantitative interpretation.

The liquid circulation rate varied from coupon to coupon, but was usually constant for a single coupon. In cases of variation, the weighted average rate was used. Flow rates are expressed in terms of the number of drops per minute leaving the coupon.

³ Rodine No. 77, American Paint Company.

The volume of a drop was determined to be reproducibly 0.13 ml.

There were two distinct flow regions on all coupons; an active region directly below the spray nozzle and a stagnant region on other parts. The flow rate in the stagnant region was about one-tenth of that in the active region. The coupons were located so that active and stagnant regions were about equal in area.

RESULTS

Initial film formation.—When coupons were first exposed to the spray, they remained bright for about five minutes if air was absent, but for only a few seconds if air was present. In either case a very thin, black, transparent film then appeared, covering the entire surface within 3–5 sec; it remained for about 10 sec, then, within 1–2 sec, it disappeared in the region of active flow. The re-exposed surface was as bright as the initial surface; in fact, if there was a pre-exposure film, the surface was now mirror bright.

In the stagnant region, the black film thickened rapidly and became opaque. After about 30 min with traces of air or 2–3 hr in its absence, a faint tan film formed in patches over the black film. There was always black scale between the tan film and metal unless at least one volume per cent of air was present, in which case tan rust appeared everywhere. Several attempts to identify the black film material by x-ray analysis failed.

Post-exposure observations.—Scale characteristics were also affected by flow rate and acidity. In nitrogen with flow rates of 5–100 drops/min, up to 1 mg/day of adherent scale was formed on each coupon if the initial pH was greater than 4; 5–15 mg/day formed at lower initial pH. At other flow rates or with air present, more scale was formed, about 20–30 mg/day under optimum scaling conditions.

The descaled coupon was abraded on No. 2 emery, and relative metal loss from different regions was determined by the amount of abrasion required to remove the etch marks. Under certain exposure conditions more metal was lost in the stagnant region; under different ones, more metal was lost in the active region. There were still other exposure conditions such that the metal was lost uniformly from the entire surface. The region of metal loss was a function of relative flow rate and was independent of the absolute flow rate.

With initial pH less than 4, major metal loss was in the stagnant region. The region of active flow remained smooth except for microgrooves parallel to the direction of flow. These were very shallow, ranging up to 2 cm in length. They increased

in number and were closer together with decreasing initial pH. Below pH 3.5, the region of active flow was uniformly etched, but greater attack was noted underneath the scale.

More metal was lost from the active flow region if the initial pH exceeded 4.5. The stagnant region scale, although limited in quantity, was more adherent, and the metal remained smooth except for an occasional rough spot. In the intermediate range, pH 4.0–4.5, the metal was lost uniformly from the entire coupon surface, although scattered etched patches under the scale sometimes occurred in the stagnant region.

Reaction rate.—Results of runs in solutions with an initial pH of 4.4–3.5 are shown in Fig. 2. The zero time and weight loss point has been chosen as common to all curves, although there was an initially rapid, irregular reaction. However, the errors are no

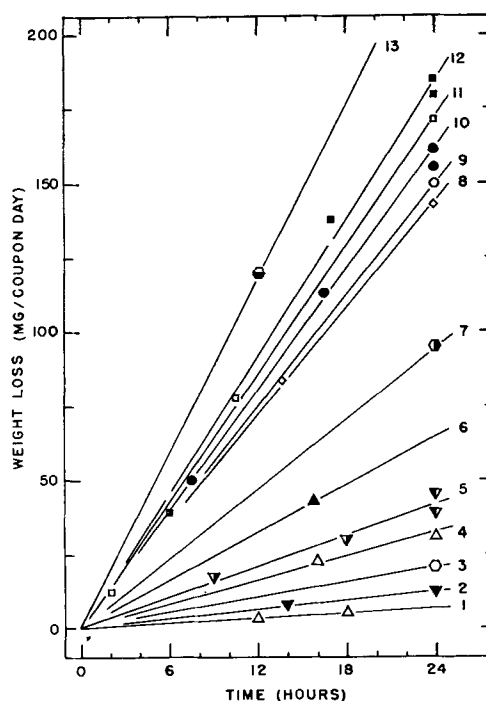


FIG. 2. Weight loss of iron coupons in acetic acid at comparable solution flow rates as a function of time.

Curve	Conc (ppm)	Slope
1	15	0.29
2	25	0.52
3	—	0.87
4	95	1.35
5	140	1.75
6	150	2.70
7	200	3.92
8	285	6.00
9	385	6.25
10	600	6.75
11	1000	7.17
12	375 (41°C)	7.62 _s
13	385	10.3

(Approx. 1% air)

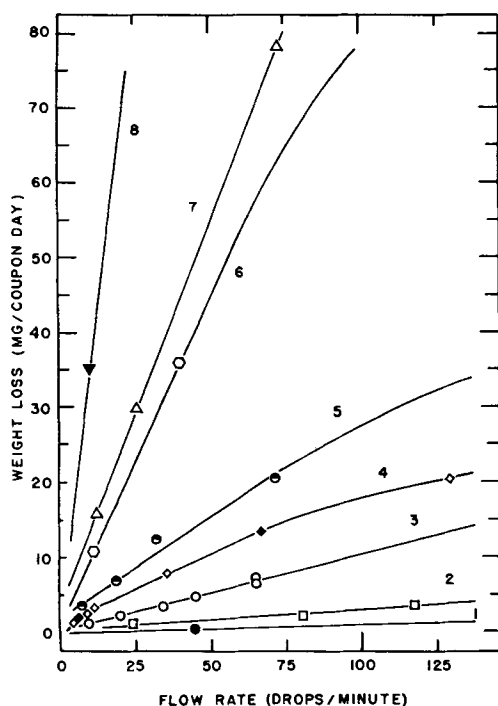


FIG. 3. Weight loss of iron coupons for one-day exposures in dilute acetic acid solutions as a function of liquid flow rate.

Curve	HAc conc (ppm)	Initial pH
1	0	7.0
2	0	5.0
3	0	4.6
4 (open pts.)	0	4.4 _s
4 (solid pts.)	15	4.4 _s
5	25	4.3
6	0	4.0
7	95	3.9
8	150	3.8

greater than 5% after the first hour. Duplicate time points were taken at the end of 24 hr to illustrate the effect on weight loss obtained by doubling the flow rate. Some curves have been drawn to conform to the trend of the entire group. The reaction rates are given in the figure caption as the slopes. Aside from curve 13, determined with air present, and curve 12, representing a run at 41°C, solution acidity was essentially the only variable in these experiments.

The effect of flow rate on weight loss is illustrated in Fig. 3. These curves all approach a maximum weight loss value, although this is not evident in the figure. An approach to a constant value also appears in the pH vs. time curves in Fig. 4. (The high degree of reproducibility is apparent.) This value is between pH 4.9–5.0 and is also reached by solutions with an initial pH greater than 5 (not shown). This is approximately the pH of a solution saturated with ferric hydroxide.

Electrical conductivities.—Specific conductivities

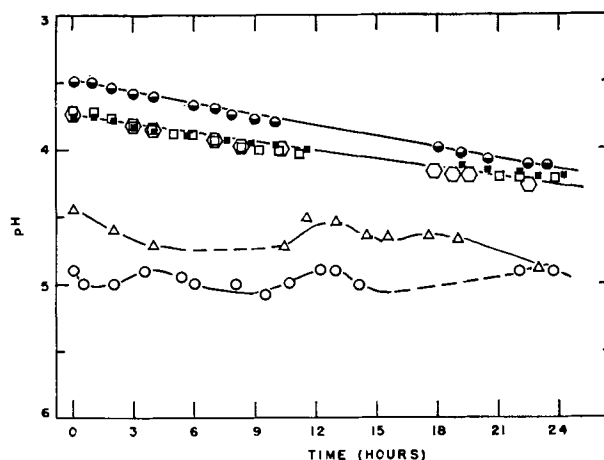


FIG. 4. Solution pH as a function of time

of several powdered salts prepared in the course of this work were measured but are good only to an order of magnitude.

Ferrous carbonate	$(2) \times 10^{-9}$	$(\text{ohm-cm})^{-1}$ at 26°C
Ferrous acetate	$(5) \times 10^{-7}$	25°C
Monobasic ferric acetate	$(1) \times 10^{-7}$	25°C
Dibasic ferric acetate	$(2) \times 10^{-7}$	25°C

Coefficients are given only for comparative purposes. Compounds show an increase in conductivity with increasing temperature at about room temperature. All of them are considered to be electronic conductors (21).

DISCUSSION

The reproducible behavior observed during initial film formation and in curves of Fig. 4 are indicative of the reliability of the experimental method employed in these experiments.

The electrochemical nature of the reaction under study has been well established, and although no potential measurements were made in the course of this study,⁴ results are interpreted in terms of current corrosion theory. (All potentials refer to the standard hydrogen potential.) When the potential of iron in an acid solution increases to about -0.3 v (i.e., changes from more negative values), a black, nonprotecting film appears and hydrogen evolution decreases. Further increase in potential is accompanied by a transformation of this film to a brown film, the change apparently originating at the region of highest current density. At still more positive

⁴ Separate studies in this laboratory showed that while forming similar films fully immersed in 2500 ppm acetic acid, the open circuit potential of these same coupons is about -0.3 v. The polarization curves are linear, at least at low current densities, with a potential of -0.2 v at 4 ma/cm² applied anodic current, and -0.5 v at 4 ma/cm² applied cathodic current.

potentials, the brown film disappears, leaving a bright metallic surface (21, 22).

Identification of the films was based on reports of similar films (14, 15, 21, 22). The black film was magnetite and is nonprotective on the basis of previous reports and observation here of its behavior in the descaling process. This is implied also by linearity of the rate curves. The thin, flaky brown film was ferric oxide as reported for other air-free systems [(15); see also (14, 21, 22)]; it may form a protective film when deposited in direct contact with the surface.

When the coupons were first exposed in the present system the active metal underwent anodic polarization. The time required for appearance of the magnetite film corresponded to that required for the potential to reach about -0.3 v. Film formation reduced the cathodic reaction rate either by lengthening the diffusion path or by altering the over-all diffusion mechanism. The cathodic process was either hydrogen evolution or oxygen reduction depending on exposure conditions. The initial rapid reaction depended on cathodic depolarization by oxygen adsorbed when coupons were weighed.

Nitrogen-air atmosphere.—Only a few runs were made with traces of air present. These were made in order to determine the effect of oxygen on the appearance of the scale and the reaction rate in general so that, in the absence of a direct test for the presence of oxygen, its presence might be suspected. The abundance of red ferric oxide formed under these conditions, along with traces of green magnetite, was considered to be evidence of the presence of traces of air in the system; otherwise, it was considered to be absent. The reaction rate was greater with oxygen present (compare curves 9 and 12 of Fig. 2); however, the linear law was followed for only about 20 hr when the rate began to decrease rapidly because of the type of film formed.

Nitrogen atmosphere.—With film formation, the differential flow regions began to affect subsequent behavior. Because of the higher solution replenishment rate, the active flow region became the place of major cathodic activity. The potential in this region became more positive, and the magnetite film disappeared. Location of the anodic site as indicated by the region of metal loss depended on acidity and, to some extent, on the relative flow rate. The sensitivity of anodic activity to changes in acidity and flow rate is shown in Fig. 5.

Above pH 5, the anodic region was restricted to the region of active flow because of low electrical conductivity of the solution and low degree of cathodic activity elsewhere, i.e., low rate of replenish-

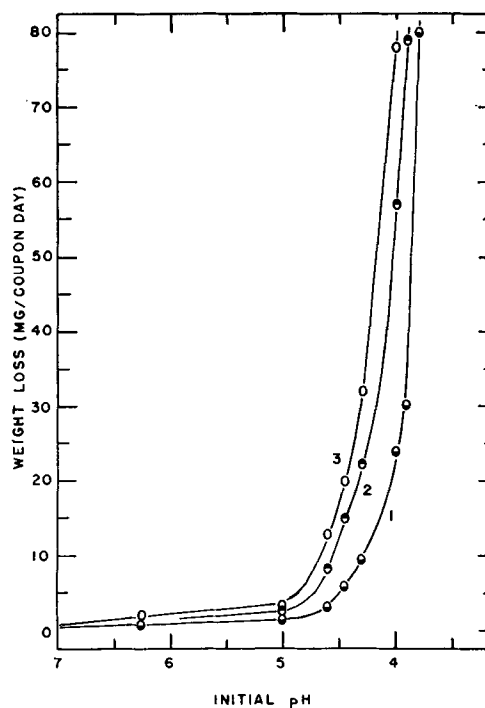


FIG. 5. Weight loss of iron coupons for one-day exposures in dilute acetic acid solutions at constant flow rates as a function of initial solution pH.

Curve	Flow rate (drops/min)
1	25
2	75
3	125

ment of hydrogen ion for the cathodic reaction. There appears to be a semiprotective, invisible film present in this pH range⁵ because of the dependence of reaction rate on flow rate and because the pH changes to a constant value of 5, suggesting a buffered system. The nonprotective nature of this film is shown by the fact that on starting at pH 7, the slowest reaction condition in this work, the rate curve was linear for at least 48 hr. During this time the pH changed to 5 in 26 hr and was constant thereafter.

Below pH 4, the anodic region was the region of stagnant flow, but there was an increasing amount of anodic activity in the active flow region as the acidity increased. This was indicated by the microgrooves. In this pH range, the reaction rate was under anodic control. As pH decreased and the rate of hydrogen evolution increased, there was an increasing amount of anodic activity in the active flow (cathodic) region because the high degree of anodic polarization forced an expansion of the anodic area

⁵ Above pH 6, the initial film is gray rather than black, but this is probably due to the small amount of film material formed.

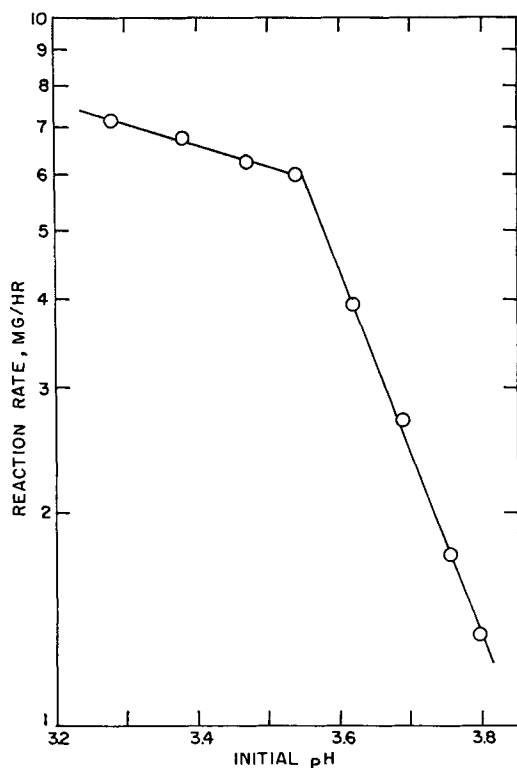


FIG. 6. Logarithm of reaction rate of iron coupons for one-day exposures at comparable flow rates as a function of initial solution pH.

from the stagnant into the active flow region. It should be noted that this movement of anodic into cathodic area had a twofold effect in keeping the total anodic and cathodic activity in balance; it simultaneously increased total anodic activity and lowered total cathodic activity. This is graphically illustrated in Fig. 6 and 7 where it may be seen that there was an abrupt decrease in reaction rate at pH 3.5 with increasing pH. As previously mentioned, the active flow region was uniformly etched with microgrooves below pH 3.5. The fact that most of the metal loss occurred in the stagnant flow region under these conditions suggests that the major effect of microgroove formation was to lessen total cathodic activity, i.e., reduce the total effective cathodic area.

It is interesting to note the similarity of Fig. 7 with previously reported results for mild steel immersed in oxygen-containing solutions of varying pH (23). The present work shows that the pH at which the film dissolves, as indicated by an abrupt increase in reaction rate with decreasing pH, is a function of other exposure conditions as well as of the specific acid present (see Fig. 5 also), and that this behavior is not restricted to systems containing oxygen.

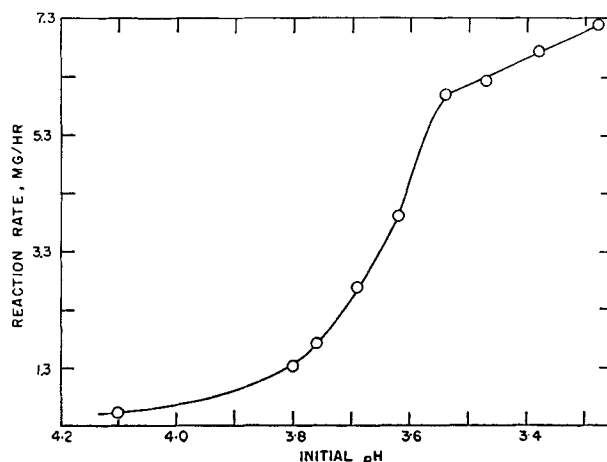


FIG. 7. Reaction rates of iron coupons for one-day exposures at comparable flow rates as a function of initial solution pH.

In the intermediate range, pH 4-5, the reaction was under mixed control in view of the uniform loss of metal from the entire surface regardless of relative flow rate. There was probably a nearly homogeneous distribution of physically small active sites which became polarized and were forced to migrate, thereby covering the entire surface during the time of measurement.

The source of the films formed in these experiments is not known. In the high pH range, the buffering agent was probably ferric hydroxide because of the approach to pH 5. Also, the time required for this pH to be reached was in keeping with the time necessary for the reaction to generate the appropriate amount of iron as ferric ion. Its semiprotecting properties were in keeping with those expected for a slightly insufficient amount of film material. The abrupt increase in reaction rate in Fig. 5 was at the pH expected for film solubility. This could also have been the cause of the linear reaction rate observed for both changing and constant pH in the runs with initial pH 7. The pH at the coupon should be the same and constant after the first minutes of the reaction, thus affording a constant supply of hydrogen ion to the cathode. It is possible that the half-cell reaction $\text{Fe}/\text{Fe}(\text{OH})_3$, with a potential⁶ just -0.25 v vs. a hydrogen electrode in a solution of the same pH and a partial pressure of hydrogen

⁶ Using a pH-independent potential difference of -0.3 , as this implies, a value of 1000 ohms/cm (for approximately 350 ppm acid), and 0.6 ma (calculated from rate curve and area), an active distance between local anodes and cathodes of 2 cm may be calculated from Ohm's law. This is the maximum distance for interaction of local elements, and is sufficient to allow the cathodic active flow region to stimulate the stagnant anodic region.

$= 10^{-7}$ (21) could have been the source. Likewise, Fe/Fe₃O₄ may have a potential of -0.3 v with the same conditions of reference (21), thus indicating a source for this material also. The high degree of anodic polarization which has been suggested for this system makes these possibilities even more attractive. The thin flaky, brown ferric oxide overlying the magnetite was probably produced electrically by the conversion of magnetite, as noted above, at electrical leaks with high current flow through the nonprotecting magnetite. They should be more adherent and less restricted in location if deposited from solution.

Reaction rates indicated by the slopes of curves 9 and 12, Fig. 2, were used to calculate a temperature coefficient for reactions under these supposedly similar conditions. A value of 5 kcal/°C/g atom was found. Similar conditions for curve 13 and a run at 20°C (not shown) with about 1% air present gave a value of 3 kcal/°C/g atom. Both of these values indicated diffusion control in the rate-determining step of the reactions. It is not prudent, however, to attach too much significance to these values.

The linear relation of log hydrogen ion activity to time which is found in Fig. 4 is suggestive of a first order dependence of rate on hydrogen ion activity.

The slope of that portion of the curve between pH 3.5 and 3.8 in Fig. 6 is -0.4 which is in exact agreement with the value predicted for an air-free system by Gatty and Spooner (24). It is postulated here that the break in the curve at pH 3.5 is a function of relative and absolute flow rates, as well as of the ratio of stagnant flow to active flow region. These factors probably affect the comparison of the different curves of Fig. 2-6, since this comparison should be made with these factors held constant. This has been considered with the present results when possible.

From the resistivities and nature of the current carriers in the solids prepared for resistance measurements in this work, it is concluded that they would protect the underlying metal if they formed adherent, continuous films on the surface.

ACKNOWLEDGMENT

Financial support of this project by the Office of Ordnance Research under Contract DA-23-072-ORD-216 is gratefully acknowledged.

Any discussion of this paper will appear in a Discussion Section to be published in the December 1955 JOURNAL.

REFERENCES

1. C. WAGNER, *Z. physik. Chem.*, **21B**, 25 (1933).
2. N. CABRERA AND N. F. MOTT, *Repts. Progr. Phys.*, **12**, 163 (1948).
3. O. KUBASCHEWSKI AND B. E. HOPKINS, "Oxidation of Metals and Alloys," pp. 119-142, Academic Press Inc., New York (1953).
4. U. R. EVANS, *Nature*, **168**, 853 (1951).
5. H. H. UHLIG, *This Journal*, **97**, 215C (1950).
6. E. J. CAULE AND M. COHEN, *Can. J. Chem.*, **31**, 237 (1953).
7. F. C. TOMPKINS, *Z. Elektrochem.*, **56**, 360 (1952).
8. R. V. COMEAUX, *Corrosion*, **8**, 305 (1952).
9. V. D. YAKHONTOV, *J. Appl. Chem. (U.S.S.R.)*, **19**, 761 (1946).
10. W. SCHWARZ, *Z. Elektrochem.*, **55**, 170 (1951).
11. U. R. EVANS AND I. D. G. BERWICK, *J. Chem. Soc. (London)*, **1952**, 3432.
12. T. P. HOAR, *Trans. Faraday Soc.*, **45**, 683 (1949).
13. N. HACKERMAN, *Corrosion*, **4**, 45 (1948).
14. H. O. FORREST, B. E. ROETHEL, AND R. H. BROWN, *Ind. Eng. Chem.*, **23**, 650 (1931); G. L. COX AND B. E. ROETHEL, *ibid.*, **23**, 1015 (1931).
15. M. G. FONTANA AND W. A. LUCE, *Corrosion*, **5**, 189 (1949).
16. E. E. GLENN AND N. HACKERMAN, *This Journal*, **100**, 339 (1953).
17. C. F. H. ALLEN, Editor, "Organic Syntheses," **20**, p. 7, John Wiley and Sons, Inc., New York (1950).
18. J. TIMMERMANS, "Physico-Chemical Constants of Pure Organic Compounds," p. 354, Elsevier Publishing Co., Inc., New York (1950).
19. L. MEITES AND T. MEITES, *Anal. Chem.*, **20**, 984 (1948).
20. D. M. SOWARDS AND N. HACKERMAN, Technical Report, Office of Ordnance Research Contract No. DA-23-072-ORD-216, University of Texas, February 10, 1953; *ibid.*, July 1, 1953.
21. M. POURBAIX, *Corrosion*, **5**, 121 (1949).
22. J. H. BARTLETT AND L. STEPHENSON, *This Journal*, **99**, 504 (1952).
23. H. H. UHLIG, Editor, "The Corrosion Handbook," pp. 128, 129, John Wiley & Sons, Inc., New York (1948).
24. O. GATTY AND E. C. R. SPOONER, "The Electrode Potential Behavior of Corroding Metals in Aqueous Solutions," p. 279, The Clarendon Press, Oxford (1938).

The Difference Effect on Aluminum Dissolving in Hydrofluoric and Hydrochloric Acids¹

M. E. STRAUMANIS AND Y. N. WANG

Department of Metallurgy, University of Missouri School of Mines and Metallurgy, Rolla, Missouri

ABSTRACT

The positive difference effect was observed during dissolution of high purity aluminum coupled with platinum in 0.05, 0.1, 0.25, 0.5, 0.75, 1.0, and 2.0 hydrofluoric acid at 25°C. The effect was directly proportional to the galvanic current up to 60 ma/cm², being nearly independent of the concentration of the acid. The proportionality constant, *K*, was 5.34, corresponding to a polarizability of 77% for the aluminum in hydrofluoric acid.

Positive as well as negative difference effects were observed under the same conditions while aluminum was dissolving in 0.1, 0.25, 0.5, 0.75, 1, and 2*N* hydrochloric acid. Points for the positive effect at low current densities, as well as those for the negative effect at higher current densities up to 200 ma/cm², lay along a downward exponential curve. The effect was independent of the concentration of the acid.

The positive effect is explained by the anodic polarization of aluminum by the additional current, and the negative one, which actually represents an overlapping of both effects, by the breakdown of the surface film because of the same current. A theoretical treatment of both effects is given. The term "polarizability" in per cent (*P* %) is introduced. The dissolution of aluminum in hydrofluoric acid is an electrochemical process.

INTRODUCTION

Even purest aluminum dissolves readily in hydrofluoric acid, and at a much higher rate than in hydrochloric acid. So it was important to know whether one of the symptoms of the electrochemical mechanism of reaction (1), the difference effect, still occurs while aluminum is dissolving in hydrofluoric acid. On the other hand, it was also important to study the effect on the same metal dissolving with a much slower rate in hydrochloric acid, because the comparison of both effects might give some clue to the mechanism of dissolution and the surface condition of aluminum in the two acids.

The difference effect is established by comparing the rate, V_1 , of hydrogen evolution of a metal dissolving in an acid or base, with that, V_2 , observed during anodic polarization of the metal at a current density, I . Usually these two rates are not equal, and the difference Δ , known as "difference effect" (2) is

$$V_1 - V_2 = \Delta \quad (I)$$

If $V_2 < V_1$ the effect is "positive" and shows how much has to be added to the lower rate, V_2 , to restore the previous rate, V_1 . This effect has been studied on: aluminum in sodium hydroxide (2, 3); zinc in sulfuric acid (2, 4); and titanium in hydro-

fluoric acid (1). If $V_2 > V_1$, the effect is "negative" because Δ has to be subtracted from V_2 , to get V_1 . This type of effect was observed on magnesium corroding in sodium chloride (5), and on aluminum dissolving in hydrochloric acid (5). However, only one concentration of the acid was used in the latter case.

EXPERIMENTAL PROCEDURE AND MATERIALS USED

The experimental procedure was the same as described previously (1). Some improvements were made by using glass tubes and joints, wherever possible, to reduce the loss of hydrogen by diffusion through the rubber parts. Potential measurements of the dissolving metal were not made during these experiments, but were made separately.

The dissolving electrode (anode) with a surface of one cm² exposed to the acid was made of an aluminum sheet.² It was cold rolled to a final thickness of 1 mm. The analysis supplied with this material claimed the following impurities: Si, 0.0015; Fe, 0.0007; Cu, 0.0004; and Mg, 0.0007% by weight. It showed a much higher dissolution rate in 2*N* hydrochloric acid than the 99.998% French aluminum³ used in previous experiments (7). From the point of view of local cells the aluminum of this investigation was of lower purity. The acids used were of the highest purity commercially obtainable.

² Obtained from The Aluminum Company of America, designated H-18 temper.

³ Compagnie Alais, Froges et Camargue, France.

¹ This paper was prepared for delivery before the Boston Meeting, October 3 to 7, 1954 and is based on a thesis submitted by Y. N. Wang in partial fulfillment of the requirements for the Ph.D. degree to the Graduate School of the University of Missouri.

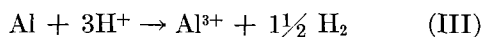
The method of calculation of the results was the same as pointed out previously (1). The difference effect [Equation (I)] expressed in $\text{mm}^3\text{cm}^{-2}\text{min}^{-1}$ was calculated by the equation:

$$\Delta = V_1 + 6.97I - V_t \quad (\text{II})$$

where V_t is the total rate of hydrogen evolution from the anode and platinum cathode while the current I was flowing through the circuit. The factor 6.97 converts the milliamperes passing the cathode for one minute into mm^3 of hydrogen.

RESULTS

Aluminum in hydrofluoric acid.—The velocity of dissolution of this aluminum is comparable to that of titanium in 0.02 to 10*N* hydrofluoric acid (6), although aluminum shows a lower rate, especially at concentrations of 4 to 8*N*. The dissolution reaction is



and AlF_3 is formed which does not completely dissolve in the acid. In a porous state it partially sticks to the dissolving plate, especially in the corners. However, this salt does not have the property of

TABLE I. Positive difference effect on Al in 2*N* HF, 25°C. Hydrogen volumes reduced to normal conditions

Time <i>min</i>	V_1 mm^3/cm^2 <i>min</i>	I <i>ma/cm}^2</i>	$6.97I$ mm^3/cm^2 <i>min</i>	V_t mm^3/cm^2 <i>min</i>	Δ mm^3/cm^2 <i>min</i>	K mm^3/ma <i>min</i>
0	0	—	—	—	—	—
5	262.6	0	—	—	0	—
10	377.5	0	—	—	0	—
15	443.2 ¹	0	—	—	0	—
20	492.2 ²	0	—	—	0	—
25	—	5.1	35.5	525.4	23.0	4.51
30	—	5.1		525.4		
35	558.0 ³	0	71.1	541.8	87.3	8.55
40	—	10.2		541.8		
45	—	10.2	104.6	525.4	104.4	6.95
50	558.0	0		591.0		
55	—	15.0	139.4	558.2	139.2	6.96
60	—	15.0		558.2		
65	558.0	0	254.4	607.4	188.7	5.17
70	—	20.0		723.8		
75	—	20.0	390.3	689.6	267.1	4.77
80	558.2 ⁴	0		689.4		
85	—	35.0	404.3	623.8	314.0	5.41
90	—	38.0		771.6		
95	541.6 ⁵	0	—	—	—	—
100	—	58.0		—		
105	—	54.0	—	—	—	—
110	591.0 ⁶	0	—	—	—	—
115	—	58.0	—	—	—	—
120	—	58.0	—	—	—	—
125	623.8 ⁷	0	—	—	—	—

Average values for V_1 : ¹, ², and ³: 512.9; ⁴ and ⁵: 549.9; ⁶ and ⁷: 607.4.

some oxide layers or protective films which adhere firmly to the surface of the metal, inactivating the local cathodes, and stopping the dissolution reaction. Aluminum fluoride specks on the aluminum surface do not prevent dissolution of the metal but they slow down the rate of reaction, as could be concluded from special experiments.

The difference effect was determined in seven concentrations of hydrofluoric acid at 25°C: 0.05, 0.1, 0.25, 0.5, 0.75, 1, and 2*N*. All measurements showed that a positive effect results [equation (I)], as shown in Table I. The approximate constancy of the K value [equation (IV)] in the last column of the table indicates that the difference effect is proportional to the anodic current passing the aluminum surface, as found by other investigators (1–6). The empirical equation (II)

$$\Delta = KI \quad (\text{IV})$$

combined with equation (II), gives an expression for K :

$$K = 6.97 + \frac{V_1 - V_t}{I} \quad (\text{V})$$

In the positive effect V_t must be larger than V_1 so K is always smaller than 6.97. However, sometimes larger values are found, e.g., 8.55 in Table I. It is believed that this comes from experimental difficulties and inaccuracies, from a breakdown of part of a protective scale possibly present on the surface, or from a sudden increase in the rate of self-dissolution V_1 of the metal. A reverse effect, producing too low K -values, would originate from a sudden decrease of V_1 .

The constants K obtained in all concentrations of

TABLE II. Slope constant K of the positive difference effect, equation (IV), obtained with Al in various concentrations of HF at different current densities I .

I <i>ma/cm}^2</i>	Concentration of HF in <i>N</i>							K avg mm^3/ma <i>min</i>
	0.05	0.1	0.25	0.5	0.75	1.0	2.0	
2.5	5.35	5.29	5.31	—	—	—	—	5.32
3.6	5.83	—	—	—	—	—	—	5.83
5.1	—	2.96	6.96	2.88	2.63	9.07	4.51	4.84
7.0	—	3.80	6.41	—	—	—	—	5.11
10.2	—	—	5.73	6.53	6.58	7.81	8.55	7.04
15.0	—	—	4.03	5.86	5.91	6.69	6.95	5.89
20.0	—	—	—	—	—	6.18	6.96	6.57
28.0	—	—	—	—	5.49	—	—	5.49
30.0	—	—	—	—	5.04	—	—	5.04
33.5	—	—	—	—	—	3.70	—	3.70
36.5	—	—	—	—	—	2.88	5.17	4.03
56.0	—	—	—	—	—	—	4.77	4.77
58.0	—	—	—	—	—	—	5.41	5.41
K avg	5.59	4.01	5.69	5.09	5.13	6.06	6.05	5.34

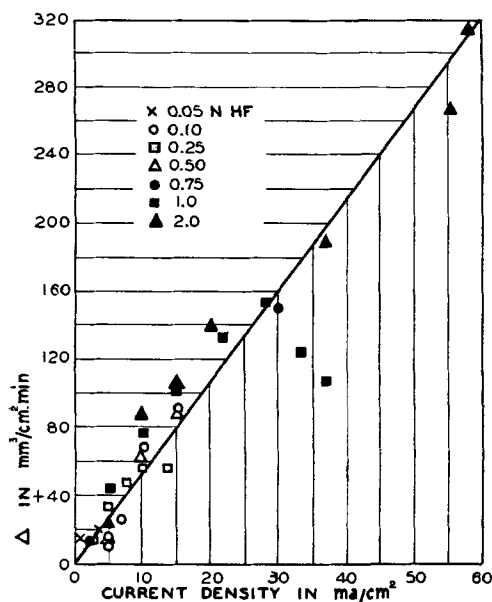


FIG. 1. Positive difference effect on aluminum in 7 hydrofluoric acid concentrations vs. current density. The ordinate shows the rate of hydrogen evolution to be added to the rate observed under current to obtain the initial rate V_1 .

hydrofluoric acid at different current densities are summarized in Table II.

The scattering of the K values is the consequence of the difficulty of reproduction of Δ -measurements, as already pointed out. The scattering can be even better seen from the difference effect current density plot (Fig. 1). Nevertheless, a straight line can be drawn through the accumulation of the experimental points with a slope constant $K = 5.34$. However, it seems that at lower acid concentrations straight lines with a slightly larger K can be drawn through experimental points. Inserting the value 5.34 for K in equation (V) gives

$$V_t - V_1 = (6.97 - 5.34)I = 1.63I \quad (VI)$$

This means that instead of 6.97 mm³ of hydrogen as a total result only 1.63 mm³/ma/cm² of anodic surface are developed by the couple. Approximately 77% of the current went to overcome the difference effect and only 23% of it contributed to the increase of the rate of dissolution of the anodically polarized aluminum.

Potential of aluminum in hydrofluoric acid.—For the explanation of the difference effect some knowledge of the electrochemical behavior of aluminum in hydrofluoric acid is necessary. No published potential measurements of aluminum in hydrofluoric acid were found. The potential difference of the chain

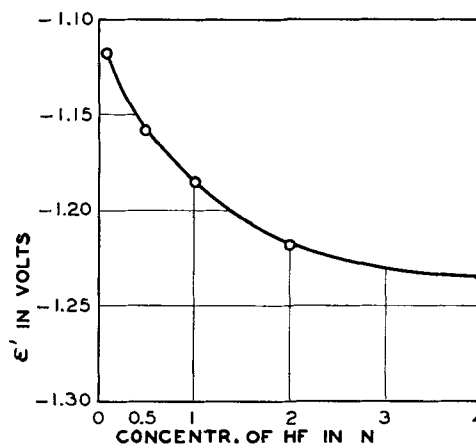
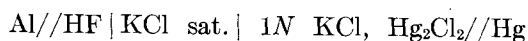


FIG. 2. Dissolution potential ϵ' of Al in HF vs. concentration of the acid. Hydrogen scale.

was measured, and the values obtained were reduced to the potential of the normal hydrogen electrode. As the metal dissolved in the acid, the measured potentials were dissolution potentials ϵ' . The tip of a Luggin capillary was pressed against the clean surface of the aluminum electrode under the acid.

After immersion of the electrode in the acid, the potential drops suddenly, then it becomes slowly less negative, and after a few hours a fairly steady potential is established. This potential is plotted against the concentration of the acid in Fig. 2, which clearly shows that the potential of aluminum decreases with the concentration, reaching values as low as -1.23 v in 4N acid. This very negative potential exceeds that of -1.209 v measured on amalgamated aluminum in 0.1N hydrochloric acid (9), and approaches that of -1.38 to -1.4 v obtained in a 1N sodium hydroxide solution (8). The equilibrium potential of aluminum calculated from the thermal data of the dissolution reaction is -1.69 v (10).

For potential measurements under anodic current, the aluminum electrode of the aforementioned chain was connected with a platinum electrode 1 cm away from the aluminum. Both electrodes had an area of 2 x 2 cm exposed to the electrolyte, and their construction has been described previously (11). By means of a rheostat and a milliammeter in the aluminum-platinum chain, a given current density could be obtained.

Results are shown in Fig. 3. It follows from this figure that in each case the increase of current density is associated with the shifting of the potential of the dissolving aluminum toward more positive values, as it was also found in the cases of titanium, zinc, and other metals (1, 12-17). The irregularity of the curves in Fig. 3 is explained by the fact that the rate of self-dissolution of the aluminum

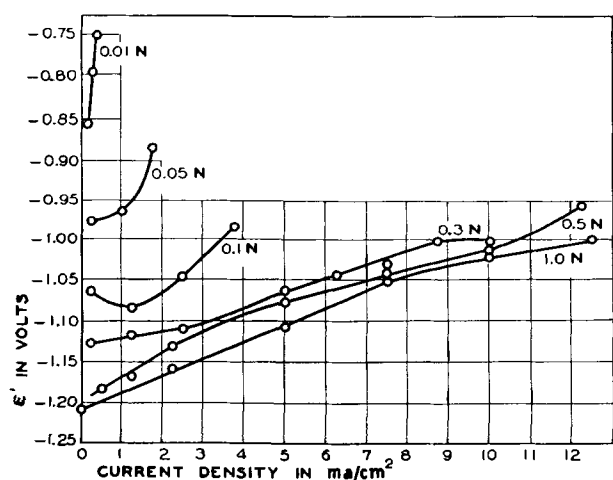


FIG. 3. Electrode potential e' of Al vs. current density in various concentrations of HF.

electrode was not included in the current density given. This rate may influence the potential of the metal (12).

Aluminum in hydrochloric acid.—The fairly noble potential of -0.577 for aluminum in $1N$ hydrochloric acid (18), as compared with that in hydrofluoric acid, shows that surface conditions of the dissolving metal are quite different in both cases. The less negative potential indicates that there is a film or a scale on aluminum in hydrochloric acid, which probably is less porous, less soluble in the acid, and which sticks better to the metal than that at equilibrium on aluminum in hydrofluoric acid. Hence, another kind of difference effect was to be expected on aluminum in hydrochloric acid. Measurements, carried out in one concentration of the acid by other workers, showed that the effect was negative (5).

The experiments were repeated here using the following acid concentrations: 0.1 , 0.25 , 0.5 , 0.75 , 1 , and $2N$. The experimental procedure and the calculation [equation (II)] were the same as already demonstrated in the case of the positive effect. An example of the negative effect is shown in Table III obtained in $1N$ hydrochloric acid. The table shows two features that were not observed previously: (a) at small current densities the difference effect is positive, which turned out to be true also with other concentrations of the acid; and (b) K values show that experimental points do not lie on a straight line, but on an irregular curve. However, if all the experimental points obtained in the other concentrations of the hydrochloric acid are plotted against the current density, a quite regular curve can be drawn through the accumulations of the points, as shown in Fig. 4. Thus, the couple Al/HCl/Pt develops more hydrogen than expected from the initial rate of

TABLE III. Negative difference effect on Al dissolving in $1N$ HCl, $25^\circ C$; hydrogen volumes reduced to normal conditions

Time	V_1	I	$6.97I$	V_t	Δ	K
min	mm^3/cm^2 min	ma/cm^2	mm^3/cm^2 min	mm^3/cm^2 min	mm^3/cm^2 min	mm^3/ma min
0	0	0	—	—	—	—
20	0	0	—	—	—	—
30	—	5}	34.9	24.7}	+14.2	+2.84
40	—	5}	—	33.1}	—	—
50	16.5	0	—	—	—	—
60	—	10}	—	74.3}	+7.8	+0.78
70	—	10}	69.7	82.6}	—	—
80	16.6 ¹	0	—	—	—	—
90	—	15.5}	—	132.1}	-10.4	-0.68
100	—	14.9}	105.2	140.4}	—	—
110	24.8 ²	0	—	—	—	—
120	—	20.0}	—	173.4}	-16.2	-0.82
130	—	19.2}	136.6	173.5}	—	—
140	16.5 ³	0	—	—	—	—
150	—	30.0}	—	247.8}	-29.2	-1.00
160	—	28.0}	202.1	247.8}	—	—
170	16.5	0	—	—	—	—
180	—	48.0}	—	363.4}	-35.0	-0.71
190	—	51.0}	345.0	429.5}	—	—
200	16.5	0	—	—	—	—
210	—	81.0}	—	716.6}	-117.5	-1.44
220	—	82.0}	568.1	685.6}	—	—
230	16.5 ⁴	0	—	—	—	—
240	—	116.0}	—	908.5}	-79.1	-0.77
250	—	90.0}	717.9	710.3}	—	—
260	8.3 ⁵	0	—	—	—	—

Average values for V_1 : ¹ and ²: 20.7; ² and ³: 20.65; ⁴ and ⁵: 12.4.

dissolution of aluminum and the current produced by the cell.

THEORY OF THE DIFFERENCE EFFECT

The fact that the negative difference effect also shows as a positive one at low current densities (Fig. 4) can be explained by the assumption that every difference effect appears as the result of an overlapping of both positive and negative effects. Hence, the correct expression for the difference effect observed should be:

$$\Delta = V_1 - (V_2 + V_4) \quad (\text{VII})$$

V_4 is the increase of hydrogen evolution due to the negative difference effect, which is also a function of anodic current density. Thus, under conditions where there is no appreciable film on the metallic surface, for instance aluminum in hydrofluoric acid, or amalgamated aluminum in hydrochloric acid (14), the term V_4 can be neglected, and a pure positive effect results. But if there is a film on the surface of the metal (aluminum in hydrochloric acid), the breakdown of the film as a result of applied or self-generated anodic current (see below), causes the additional rate V_4 . It is clear then that at low current

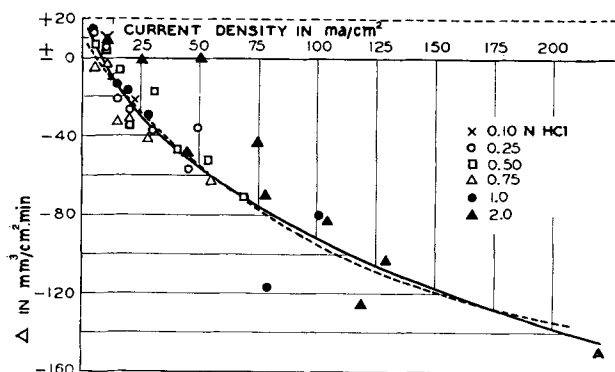


FIG. 4. Solid curve: difference effect on Al in HCl: positive at small current densities, negative at larger ones. The negative effect shows the rate of hydrogen evolution that has to be subtracted from the one observed under current to obtain the initial rate V_1 . Dashed line: theoretical curve.

densities $V_1 > (V_2 + V_4)$, and the positive effect is still observed. With increasing current density $V_2 + V_4$ may become equal to V_1 , and no effect appears, $\Delta = 0$ (see Fig. 4). Finally, at still higher current densities, V_1 is overbalanced by $V_2 + V_4$, and the negative effect shows up.

Attempts have never been made to derive the curve for the negative difference effect theoretically, although the positive one was successfully explained by Straumanis (1, 4, 13). In the following an expression for both effects is derived on the basis of equation (VII) and using the concept of local currents in a form proposed by Straumanis (4, 19).

The rate V_1 is given by

$$V_1 = \frac{\Delta v}{\Delta t A} = k_1 z' \frac{\eta - \epsilon'}{r} \quad (\text{VIII})$$

where Δv is the volume of hydrogen evolved in the time Δt on the surface area A , η is the hydrogen overpotential of the local cathodes (its value is negative), z' the number of active local cathodes (cells) per unit area, ϵ' the dissolution potential of the base metal, and r the average resistance of a local cell. k_1 is a constant converting the current into volume units of hydrogen (20).

Polarizing the same metal surface anodically with a current density I , ϵ' changes to a more noble value (ϵ'_2). But the values of the variables η and r cannot change appreciably: the first because the local cathodes are polarized to a maximum according to the logarithmic Tafel's rule, and small changes in the local current, due to $\epsilon' \rightarrow \epsilon'_2$, do not alter η ; the second because the resistance of the electrolyte in the interface, around the local cathodes, does not change much with the polarizing current. Therefore, the expression for V_2 is

$$V_2 = k_1 z' \left(\frac{\eta - \epsilon'_2}{r} \right) \quad (\text{IX})$$

Simultaneously the polarizing current breaks down one part of the protective film on the metal, and a number of new active local cathodes, z'' , starts to work

$$V_4 = k_1 z'' \left(\frac{\eta - \epsilon'_2}{r} \right) \quad (\text{X})$$

Substituting in equation (VII) the values for V_1 , V_2 , and V_4 [equations (VIII), (IX), (X)] and simplifying

$$\Delta = \frac{k_1}{r} [z'(\eta - \epsilon') - (z' + z'')(\eta - \epsilon'_2)] \quad (\text{XI})$$

Now, the question is, how does z'' increase with the current density. According to Evans (14), Kroenig and Uspenskaja (5), and the authors' observations, parts of a film are stripped down from the surface of aluminum if the metal immersed in hydrochloric acid is touched by a platinum wire under the acid. Simultaneously the rate of hydrogen evolution increases on the surface of the aluminum. Evidently the discharge of electrons on the platinum surface forces Al^{3+} to leave the compact metal. But as it is covered largely by a dense protective film, the latter partially breaks down upon the impact of the Al^{3+} leaving the metal. The breakdown uncovers a number of new local cathodes (z'') which immediately start to act. The situation is then as shown in Fig. 5. It is quite clear that the film will not adhere equally to the whole surface of the metal. The weakest spots of the film will break down at first, then with increasing current density those which adhere slightly better follow, and so on. It can be assumed that the breakdown of parts of the film, or the uncovering of new active cathodes, z''_1 , with

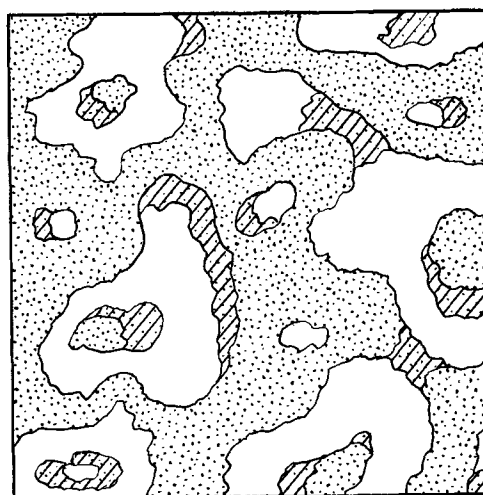


FIG. 5. Increase of z'' with current I . White areas: protective film per surface area unit. Dotted: areas producing the rate V_1 and V_2 (after anodic polarization); number of local cathodes z' . Striped and dotted: areas with the film broken down while current I is flowing, producing the rate V_4 , number of local cathodes z'' .

increasing current density i is proportional to the number of cathodes still under the protective film:

$$\frac{dz_1''}{di} = k_3[z - z'] - z_1''$$

or

$$\int_0^i di = \frac{1}{k_3} \int_0^{z''} \frac{dz_1''}{D - z_1''} \quad (\text{XII})$$

where z is the total number of local cathodes on the dissolving metal surface, while z' is the number of active cathodes present in the pores before passing the current I . Therefore, z_1'' can increase according to (XII) from 0 to z'' ; $z - z' = D$. The solution of this well-known type of equation (XII) gives for I :

$$I = \frac{1}{k_3} \ln \frac{D}{D - z''},$$

and for z'' :

$$z'' = D(1 - e^{-k_3 I}) \quad (\text{XIII})$$

Substituting (XIII) for z'' in equation (XI) and rearranging:

$$\Delta = \frac{k_1}{r} [z'(\epsilon'_2 - \epsilon') - D(\eta - \epsilon'_2)(1 - e^{-k_3 I})] \quad (\text{XIV})$$

This is the general equation for the difference effect, the positive as well as the negative.

For aluminum dissolving in hydrofluoric acid or in strong bases, the formation of new local cathodes z'' , due to the film stripping effect by the polarizing current, can be neglected as already mentioned. Thus, z'' becomes zero if k_3 of equation (XIII) is zero. Substituting 0 for k_3 in equation (XIV), the second term of this equation vanishes. ϵ'_2 in the rest of the equation can be replaced by

$$\epsilon'_2 = \epsilon' + k_2 I \quad (\text{XV})$$

because the potential ϵ' of an anodically polarized metal, also of aluminum in hydrofluoric acid (Fig. 3), frequently increases linearly with current density (12, 14-17). k_2 is the slope constant. Under such conditions equation (XIV) converts into

$$\Delta = \frac{k_1 k_2 z' I}{r} = KI \quad (\text{XVI})$$

as all the four constants can be joined into a new one K , if the effect is observed in one concentration of the acid. However, if the concentration of the acid is changed, e.g., decreased, then, as shown by Fig. 3, the constant k_2 increases. Simultaneously, the average resistance, r , of a local cell increases also. Hence, the effect of changed concentrations of the acid may nearly cancel out. Equation (XVI) for the positive difference effect reveals that the effect is proportional to the current density, I , is independent of the nature of the dissolving metal, and may be nearly independent of the concentration of the

corrosive agent used. This is shown by difference effect measurements on titanium (1) and aluminum (Fig. 1) in hydrofluoric acid.

To derive the curve for the negative effect one has to assume that the values of ϵ'_2 and η [equation (XIV)] are independent of the current density because: (a) with increase of current a part of the film breaks down and the actual current density, at least in the beginning of the process, remains approximately the same (21); and (b) if it is assumed that ϵ'_2 changes according to equation (XV) also during the breakdown of the film, the curve obtained goes through a minimum in contradiction to experimental results (Fig. 4). The constancy of η has already been discussed. Under such conditions a curve is calculated, the course of which agrees quite well with experiment (Fig. 4).

The discussion of this chapter shows that both effects, the positive and the negative one, can be well explained quantitatively using the concept of local currents.

CONCLUSION

The appearance of the difference effect and its theoretical treatment confirms again the assumption previously made by other authors (14) that the presence of the negative effect is a consequence of tight protective films on a metal which dissolves in a certain corrosive electrolyte. For instance, because there are no such films on aluminum dissolving in strong bases (3, 22), or in hydrofluoric acid, the positive effect appears, but, since there are films on this metal dissolving in hydrochloric acid, the negative effect shows up. The presence of a film is indicated by the comparatively noble potential of the metal, or its absence by a very negative potential.

The positive difference effect gives information about the polarizability of a metal. It is well known that metals are not equally polarized by an anodic current of the same strength. Some show slight potential shifts toward more positive values, and others larger shifts under the same conditions. However, potential measurements on working electrodes are not always reliable. The positive difference effect, according to the theory developed, is caused by the shift just mentioned and is independent of potential measurements. Constant K of equation (IV) shows directly the mm³ of hydrogen by which

TABLE IV. Polarizability of some metals in per cent

Metal	K	Electrolyte	$P\%$
Zn	2.5	H ₂ SO ₄	36
Al	5.34	HF	77
Ti	5.7	HF	84

the rate of dissolution (per cm² and minute) of a common metal is decreased per each milliampere of the current discharged through the platinum cathode. Furthermore, it was shown that the maximum value for K is 6.97, meaning there is no hydrogen evolution on the dissolving metal when connected to a platinum anode (1). Therefore, the anodic metal is totally polarized (100%) as the hydrogen produced by the current is completely subdued by the difference effect. On the other hand, if $K = 0$, there is no difference effect at all, and no anodic polarization (0%). In between are the K values for different metals, and their polarizability in per cent ($P\%$) can be expressed as follows:

$$P\% = \frac{100K}{6.97} = 14.35K \quad (\text{XVII})$$

Table IV shows the polarizability of some elements, for which K was determined in the units used above.

This shows that titanium and aluminum are polarized much more strongly than zinc by the same current density. The polarizability of a metal exhibits its ability to deliver electrons for the local cathodes and to expel anions into the respective corrosive agent; if the rate of both processes is high, the polarizability is low and vice versa.

ACKNOWLEDGMENTS

Sincere thanks are given to Dr. J. A. Nock, Jr., Assistant Chief of the Physical Metallurgy Division, Aluminum Research Laboratories, Aluminum Company of America, for the donation of the aluminum sheet used for this investigation, and to Dr. C. B. Gill for the correction of the English of the manuscript.

Any discussion of this paper will appear in a Discussion Section to be published in the December 1955 JOURNAL.

REFERENCES

1. M. E. STRAUMANIS AND P. C. CHEN, *This Journal*, **98**, 351 (1951).
2. A. THIEL AND J. ECKELL, *Z. Elektrochem.*, **33**, 370 (1927).
3. M. A. STREICHER, *J. (and Trans.) Electrochem. Soc.*, **93**, 304 (1948).
4. M. STRAUMANIS, *Z. physik. Chem. A*, **148**, 349 (1930).
5. W. O. KROENIG AND V. N. USPENSKAJA, *Korrosion u. Metallschutz*, **11**, 10 (1935); **12**, 123 (1936).
6. M. E. STRAUMANIS AND P. C. CHEN, *This Journal*, **98**, 234 (1951).
7. M. STRAUMANIS, *Korrosion u. Metallschutz*, **14**, 1 (1938).
8. L. KAHLBERG AND J. A. MONTGOMERY, *Trans. Am. Electrochem. Soc.*, **36**, 285 (1919).
9. J. HEYROVSKÝ, *J. Chem. Soc.*, **117**, 32 (1920).
10. W. M. LATIMER AND B. S. GREENSFELDER, *J. Am. Chem. Soc.*, **50**, 2202 (1928).
11. M. E. STRAUMANIS AND P. C. CHEN, *Corrosion*, **7**, 229 (1951).
12. M. STRAUMANIS, *Z. physik. Chem. A*, **147**, 161 (1930).
13. M. STRAUMANIS, *Korrosion u. Metallschutz*, **14**, 67 (1938).
14. U. R. EVANS, "Metallic Corrosion, Passivity and Protection," p. 34, difference effect p. 220, Longmans, Green & Co., New York (1948); see also U. R. EVANS AND T. P. HOAR, *Proc. Roy. Soc. (A)*, **137**, 343 (1932).
15. R. B. MEARS, *J. (and Trans.) Electrochem. Soc.*, **95**, 1 (1949); R. B. MEARS AND R. H. BROWN, *This Journal*, **97**, 75 (1950).
16. R. H. BROWN, G. C. ENGLISH, AND R. D. WILLIAMS, *Corrosion*, **6**, 186 (1950).
17. M. A. STREICHER, *J. (and Trans.) Electrochem. Soc.*, **96**, 170 (1949).
18. C. J. DE GRUYTER, *Rec. trav. chim.*, **44**, 960 (1925).
19. M. STRAUMANIS, *Korrosion u. Metallschutz*, **9**, 1, 29 (1933).
20. M. E. STRAUMANIS AND C. B. GILL, *This Journal*, **101**, 10 (1954).
21. U. R. EVANS AND T. P. HOAR, *Trans. Faraday Soc.*, **30**, 424 (1934).
22. M. E. STRAUMANIS AND N. BRAKŠS, *J. (and Trans.) Electrochem. Soc.*, **95**, 98 (1949); **96**, 21 (1949); **96**, 310 (1949).

Recent Innovations in the Control and Operation of Zirconium Reduction Furnaces¹

F. E. BLOCK AND A. D. ABRAHAM

U. S. Department of the Interior, Bureau of Mines, Albany, Oregon

ABSTRACT

A general outline of the Kroll process for production of zirconium sponge is presented. Recent trends in automatic furnace control and instrumentation are reported. Modification of furnace operations to streamline production are discussed in terms of sponge quality.

INTRODUCTION

The Kroll process for producing zirconium by magnesium reduction of zirconium chloride under a helium atmosphere is the primary method for its manufacture today. Development of this process has been the subject of several articles (1-5). Although much effort has been devoted to developing a continuous process, no successful approach is evident. The most noteworthy accomplishments to date have been directed toward increasing efficiency through better utilization of existing plant equipment and by streamlining production operations. This paper covers recent experimental studies made in an effort to develop an automatically controlled reduction furnace and methods for increasing production quality and efficiency.

The Kroll process in its earliest form consisted of a purification step in which crude zirconium chloride was sublimed in a hydrogen atmosphere and condensed on water-cooled coils suspended from a cover that floated in a molten lead-alloy seal. The solid block of dense chloride that resulted was free from contaminating oxides and iron. In the reduction step that followed, the chloride was resublimed in a helium atmosphere and reduced in a crucible containing molten magnesium. The reaction product consisted of fine zirconium crystals surrounded by magnesium and covered by a layer of magnesium chloride. The mixture was subjected to vacuum distillation to remove magnesium and magnesium chloride and resulted in a sponge-like product of sintered zirconium crystals.

Recently it has been demonstrated that the purification step can be eliminated by allowing crude zirconium chloride to outgas at reduced pressure below 331°C, the sublimation temperature of the chloride (5, 7). Since this combined purification-

reduction step is carried out in a single furnace, a considerable reduction in the amount of equipment and handling was realized.

During the reduction step careful furnace control is necessary to maintain the reaction rate in balance with the rate of zirconium chloride sublimation. Efforts to control the furnace automatically require regulation of temperature, pressure, and gas phase composition.

The bulk of the volume of the reduction crucible is actually employed to contain the by-product magnesium chloride, and only a relatively small amount of zirconium sponge remains after this salt is removed by distillation; therefore, a means for tapping the salt from the crucible and adding more magnesium in order to continue the reaction is desirable (6, 7). Another approach toward better utilization of distillation furnace capacity is the use inside the reduction crucible of expendable liners which can be stripped from the reaction products after the reduction, allowing two or more metallic reguli to be combined for a single distillation.

EXPERIMENTAL

Automatic furnace control.—A conventional zirconium reduction furnace was used in this work (Fig. 1). It consisted of a stainless steel retort 28 in. in diameter and 72 in. deep, heated in a Nichrome wound pit furnace. An annular trough attached to the upper edge of the retort contained molten lead-antimony alloy which served to seal the retort from the atmosphere while allowing the retort top to rise or descend as the gas volume changed. Suspended from the top were steel coils through which air or water was passed to cool the retort atmosphere or condense excess zirconium chloride. Gas valves were incorporated in the top to bleed vapors or add helium to the retort. A chromium iron reaction crucible was placed in the bottom of the crucible and an Inconel charge vessel above it. Independently controlled heating zones were employed for the

¹ Manuscript received July 30, 1954. This paper was prepared for delivery before the Chicago Meeting, May 2 to 6, 1954.

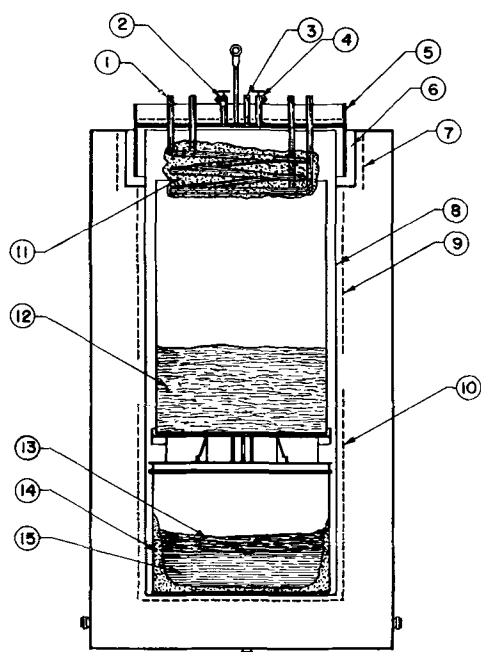


FIG. 1. Zirconium reduction furnace. 1, Condensing coils; 2, retort bleeder valve; 3, evacuation tube; 4, gas inlet valve; 5, floating retort top; 6, lead alloy seal; 7, lead seal heating element; 8, retort shell; 9, chloride zone heating element; 10, reduction zone heating element; 11, condensed zirconium chloride; 12, zirconium chloride charge; 13, unreacted magnesium; 14, zirconium; 15, magnesium chloride.

reaction crucible, charge can, retort top, and lead seal.

The rate at which zirconium chloride reacted was measured by suspending the charge vessel from the retort top. By measuring the pressure required to float the entire assembly at various time intervals, the rate of sublimation, hence the rate of reaction, could be calculated. Reaction rates varying from 4 to 80 lb zirconium chloride per hour were found to be common during an efficient reduction run. During the first 5-7 hr of the reaction, the rate was found to fluctuate rapidly, and it was during this period of increased activity that maximum rates were observed. Although it is difficult to determine the composition of gases in the retort with any degree of accuracy, a composition corresponding to approximately 30% helium and 70% zirconium chloride at the start of the reaction was found to result in a maximum reaction rate of 80 lb/hr. By following a rigid schedule for adding helium or bleeding gases from the system, this composition could be maintained and the reaction made to progress at a predetermined rate. Having established these conditions, the process could be started and stopped on a time schedule and controlled by some form of instrumentation.

During manual operation the floating retort top functions to prevent rapid pressure changes within the retort and allows an opportunity to correct

for changes in reaction rate. By maintaining an immobilized top, pressure fluctuations could be used as a means for compensating automatically for the changing reaction rate. Although various devices were tested for measuring the retort pressure, best results were obtained when using a diaphragm type of element operating from a remote position. In order to prevent condensation of zirconium chloride in the pressure sensing line, a helium purge flow of 0.1-0.2 ft³/hr was employed.

Automatic control was achieved by modifying a Forboro Model 40 Hyper-Reset controller to operate a pneumatic proportioning valve and six electrical relays within the pressure range 0-2.5 psi gauge. In operation the control cycle was as follows: when the retort pressure was in the range 0.5-1.3 psi the furnace operated satisfactorily and no control action occurred in this neutral range. If the reaction rate fell below the chloride sublimation rate and the pressure began to rise, compressed air was metered to the retort condensing coils through the pressure controlled proportioning valve. If the pressure could not be controlled by condensation of zirconium chloride alone, a relay actuated a pneumatically operated valve which bled gases from the retort and reduced the pressure to the neutral range. An audible alarm was employed as a warning in the event of an excessive pressure rise due to mechanical failures. If, instead, the reaction rate exceeded the chloride sublimation rate and the pressure began to decrease, additional heat was applied to that section of the retort containing the charge, and zirconium chloride was sublimed at an increased rate. If the pressure continued to fall because of an excessive reaction rate, a second pneumatically operated valve admitted helium to the retort to return the pressure to the neutral range. Addition of helium also tended to moderate the reaction by reducing the concentration of gaseous zirconium chloride in the retort. This entire sequence of operations was carried out at pressures above atmospheric to prevent air contamination through minor leaks in the apparatus. It was necessary to freeze the retort top into the lead-alloy seal during these tests in order to maintain the retort at a constant volume and allow the pressure to reflect changes in reaction rate.

Previous experience with retort bleeder valves has demonstrated that they must operate above 331°C to prevent fouling by condensation of zirconium chloride between the moving parts. Because of the corrosive nature of the gases being handled, auxiliary electric heaters have not been successful. A valve, consisting of a stem machined to a taper at its lower portion and ground to fit into a tapered seat in the retort top, was used for this work. The stem was moved in and out of its seat by a diaphragm air motor

TABLE I. Average analytical values for zirconium sponge produced during plant operation and by various operational modifications

Analysis No.	Description	Analysis, ppm				
		O ₂	Al	Pb	Fe	Si
1	Average for plant production	980	37	41	444	56
2	Automatically controlled reduction furnace	833	39	15	568	83
3	Drain crucible tests	992	69	59	530	45
4	Two crucible tests	836	30	29	616	78
5	Lined crucible tests	740	22	26	278	55

linked to the stem through a lever arm. By insulating the valve to reduce heat losses it was heated sufficiently through conduction from the retort.

The valve employed to admit helium to the retort was similar in design except that its stem was sealed from the atmosphere with high temperature packing.

Table I, analysis No. 2, is an average analysis for sponge produced during an automatically controlled reduction cycle, and analysis No. 1 is an average for normal production quality sponge produced during the same operating period. Because the retort was sealed and operated at a slight positive pressure throughout the cycle, air contamination was completely eliminated. This probably accounts for the reduction of approximately 150 ppm in the oxygen content of sponge produced in these tests.

Oxygen determinations reported were made by the hydrogen chloride method (8). Metallic elements were determined by quantitative spectrographic analyses.

Operational innovations.—Early attempts to tap molten salt from the reduction crucible before adding more magnesium demonstrated that back reaction occurred between the zirconium chloride vapors and the exposed zirconium metal (7). Since the lower chlorides were pyrophoric and were not reduced during the subsequent reaction, metal losses often resulted. To minimize this effect experiments were performed in which a sufficient depth of salt was maintained in the crucible to cover the reduced zirconium, while excess salt was drained continuously. A furnace modified to hold a retort almost twice the normal length and having a third independently controlled heating zone was used (Fig. 2). The furnace was loaded with 1000 lb zirconium chloride positioned in the upper heating zone. The middle heating zone was occupied by a normal size crucible fitted with a centrally located overflow drain pipe and charged with 220 lb magnesium. A cowl-like cover surrounded the drain pipe to within 2 in. from the bottom. Occupying the lowest heating zone and supporting the crucible was a steel container of sufficient volume to receive the material drained

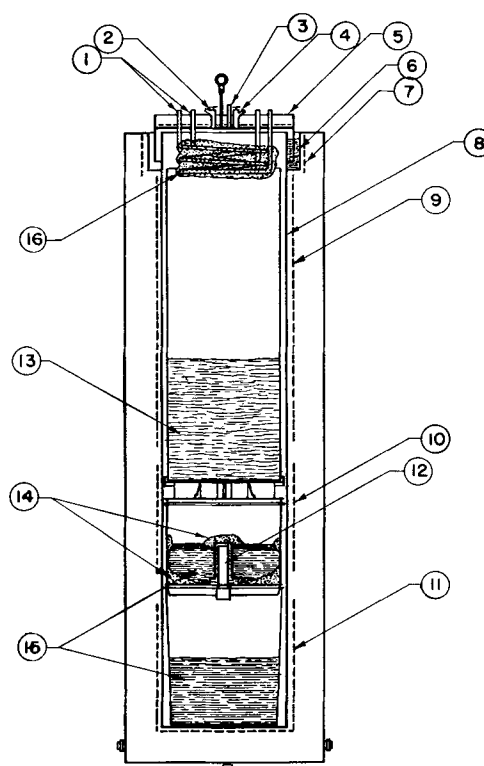


FIG. 2. Drain crucible retort. 1, Condensing coils; 2, retort bleeder valve; 3, evacuation tube; 4, gas inlet valve; 5, floating retort top; 6, lead alloy seal; 7, lead seal heating element; 8, retort shell; 9, chloride zone heating element; 10, reduction zone heating element; 11, lower zone heating element; 12, drain pipe assembly; 13, zirconium chloride charge; 14, zirconium; 15, magnesium chloride; 16, condensed zirconium chloride.

from the crucible. After the chloride charge had been heat conditioned at reduced pressure, the crucible was heated to melt the magnesium and promote the reaction in the usual manner. As the reaction progressed, metallic zirconium formed in the bottom of the crucible while a layer of magnesium chloride formed beneath the molten magnesium. When the liquid level reached the height of the drain pipe, molten salt was drained from the crucible as rapidly as it was formed. A small amount of magnesium was inadvertently trapped in the annular space between the drain pipe and its cover and was drained from the crucible. This amount was small, however, since the magnesium layer rose above the lower lip of the drain pipe cover rapidly and prevented further entrance of magnesium.

Single batches of zirconium containing up to 350 lb, twice the normal amount, could be made in this apparatus in approximately 70% of the time required to produce an equivalent amount in a conventional furnace. Analysis No. 3 in Table I is an average analysis for zirconium sponge produced in these tests. Neither the quality of the sponge nor the efficiency of the reaction had suffered; however, separation of

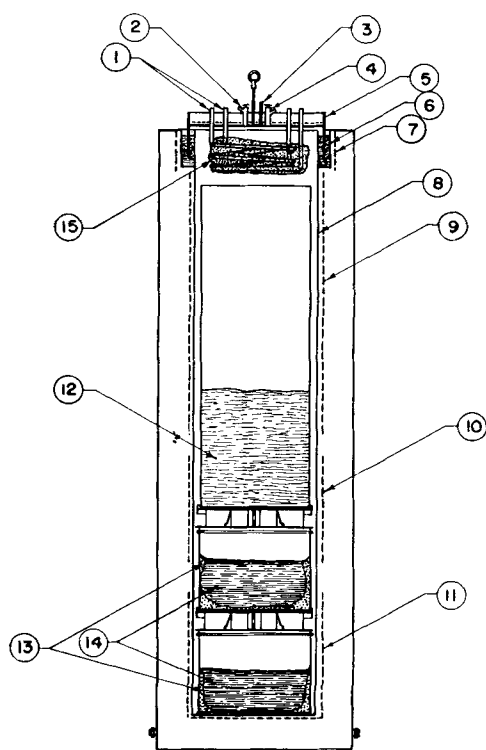


FIG. 3. Two crucible retort. 1, Condensing coils; 2, retort bleeder valve; 3, evacuation tube; 4, gas inlet valve; 5, floating retort top; 6, lead alloy seal; 7, lead seal heating element; 8, retort shell; 9, chloride zone heating element; 10, upper reduction zone heating element; 11, lower reduction zone heating element; 12, zirconium chloride charge; 13, zirconium; 14, magnesium chloride; 15, condensed zirconium chloride.

the sponge from the crucible and its components was more difficult.

The above equipment was modified to allow use of two conventional crucibles as depicted in Fig. 3. In these experiments the furnace was charged with 1000 lb zirconium chloride and 120 lb magnesium in each crucible. After the reaction had been initiated in the upper crucible and was approximately one-fifth completed, the magnesium in the lower crucible was melted and the reaction was initiated in this crucible. A yield of approximately 165 lb zirconium sponge, which is equal to the amount produced in a conventional reactor, was obtained in each of the crucibles. In terms of production capacity, only 75% of the normal furnace time was required to produce an equivalent amount of sponge. Analytical data for the sponge produced in these tests are tabulated in Table I, analysis No. 4. No significant variation in the impurity content from the normal production sponge was observed. Because the automatic furnace controller described previously was employed in these tests, a reduction in the level of oxygen contamination was achieved. A comparison of sponge quality between the upper and lower crucibles did not indicate a significant difference.

This same apparatus was tested using a single crucible twice the depth of a conventional type in order that double the amount of sponge could be formed in it. Because only half as much of the liquid surface was exposed to the retort atmosphere, a slightly higher yield of recoverable metal was obtained.

Operations involving the lined reduction crucible were performed in the conventional reduction furnaces illustrated in Fig. 1. Liners were fabricated from 0.025-in. type AISI 1095 carbon steel sheet by autogenous oxyacetylene welding. No deviation from the normal furnace operation was made during the reduction step. After reduction, the liner and its contents were removed from the reduction crucible by inverting it. The liner subsequently was handled in a low-humidity room maintained at a dew point of -15°C . After the liner was cut down one side, it could be peeled from the reduction mass with little difficulty. After removal of the liner, approximately 90% of the magnesium chloride could be split away from the metallic regulus by separating the layers with a chisel.

The regulus, which normally weighs 190–200 lb and is formed in the shape of a ring, was chucked in a lathe and the outer surface on both the sides and the bottom was scalped to a depth of approximately $\frac{1}{4}$ in. The material removed represented approximately

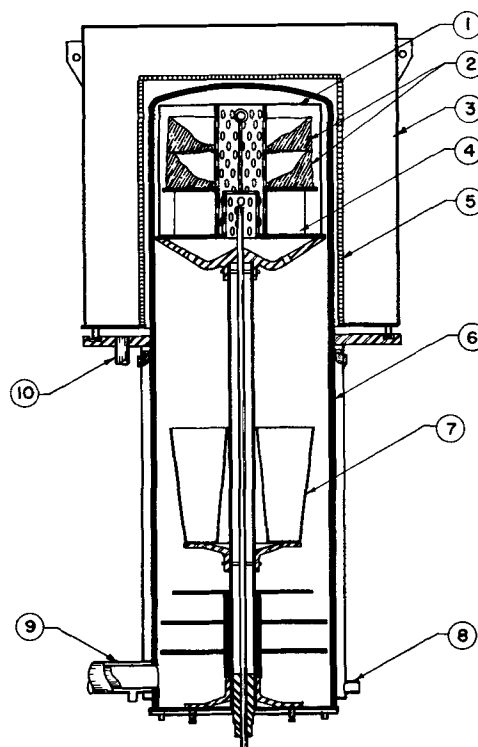


FIG. 4. Distillation retort. 1, Distillation crucible; 2, zirconium sponge; 3, furnace; 4, baffle; 5, heating element; 6, retort shell; 7, salt collector; 8, cooling water inlet; 9, retort evacuation tube; 10, furnace evacuation tube. ¶

10 lb or 5% of the original weight of metal. Two or three reguli were combined in a single crucible and distilled in the apparatus shown in Fig. 4. The metal was distilled by heating for 24 hr at a temperature setting of 1000°C and at an absolute pressure below one micron. After distillation the metallic sponge could be removed from the crucible easily for crushing and blending.

Table I, analysis No. 5, lists the average analysis for sponge produced by the lined crucible technique. A general reduction in each of the metallic impurities is apparent because the portion of the sponge previously in contact with the reduction crucible liner had been removed prior to distillation. The most significant benefit, however, is the decrease in oxygen contamination of over 200 ppm. This reduction may be due to the presence of 2-3 times the normal amount of zirconium sponge in the distillation retort, resulting in a correspondingly lower degree of contamination per unit sponge weight during the high temperature distillation. A reduction in manpower normally required to break the pyrophoric sponge from the crucible by hand methods is also achieved.

ACKNOWLEDGMENTS

This investigation was conducted under a project sponsored jointly by the U. S. Bureau of Mines and

the Navy, Bureau of Ships, under AEC contract No. At-(11-1-140). The authors wish to acknowledge the leadership and guidance offered by S. M. Shelton, A. H. Roberson, and H. L. Gilbert and the cooperation extended by the staff of the Zirconium Production plant in which this investigation was made.

Any discussion of this paper will appear in a Discussion Section to be published in the December 1955 JOURNAL.

REFERENCES

1. W. J. KROLL, A. W. SCHLECHTEN, AND L. A. YERKES, *Trans. Electrochem. Soc.*, **89**, 263 (1946).
2. W. J. KROLL, A. W. SCHLECHTEN, W. R. CARMODY, L. A. YERKES, H. P. HOLMES, AND H. L. GILBERT, *ibid.*, **92**, 99 (1947).
3. W. J. KROLL, C. T. ANDERSON, H. P. HOLMES, L. A. YERKES, AND H. L. GILBERT, *ibid.*, **94**, 1 (1948).
4. W. J. KROLL, W. W. STEPHENS, AND H. P. HOLMES, *Trans. Am. Inst. Mining Met. Engrs.*, **188**, 1445 (1950).
5. S. M. SHELTON AND E. D. DILLING, "The Production of Zirconium Sponge," chapter in "Zirconium and Zirconium Alloys", p. 82, ASM, Cleveland (1953).
6. W. J. KROLL, W. F. HERGERT, AND L. A. YERKES, *This Journal*, **97**, 305 (1950).
7. H. L. GILBERT AND C. Q. MORRISON, "Variations and Modifications of the Kroll Process for the Production of Zirconium," a paper presented before the Washington, D.C., meeting of the A. I. Ch. E., March 1954.
8. E. B. READ AND L. P. ZOPATTI, "Determination of Oxygen in Zirconium Metal," U. S. Atomic Energy Commission AECD-2798, declassified February 14, 1950.

A Metallurgical Evaluation of Iodide Chromium¹

D. J. MAYKUTH, W. D. KLOPP, R. I. JAFFEE, AND H. B. GOODWIN

Battelle Memorial Institute, Columbus, Ohio

ABSTRACT

Both the physical condition and the purity of chromium are important factors in its ductility. By proper fabrication techniques, iodide chromium sheet having an average ductile-to-brittle bend-transition temperature below 0°C has been obtained. Small quantities of oxygen, nitrogen, iron, molybdenum, tungsten, and silicon have little effect on the bend ductility of chromium. However, nickel, carbon, or sulfur adversely affect both the hot and cold ductility.

INTRODUCTION

While chromium finds widespread use in electroplated form and as an alloying addition to other metals, the cold brittleness of commercially available grades of the metal has thus far precluded any direct applications of it in massive form. Recent work at various laboratories, however, has furnished strong evidence that pure chromium is actually a ductile metal.

The first report of any ductility in chromium was that given by Kroll (1). By utilizing various reduction processes, he obtained chromium granules of "better than 99 per cent purity" which, although brittle when cold, could withstand deformation by forging when red hot. In later work (2), Kroll and his associates prepared chromium powder which analyzed 99.9% pure by the reduction of chromic chloride with magnesium and subsequent deoxidation with pure, dry hydrogen. Sheet prepared from this product by powder metallurgical processes was ductile at temperatures above 500°C but brittle at temperatures below 500°C.

At about this same time, Greiner (3) showed that chromium could be deformed in compression at room temperature. Additional evidence of the ductility of chromium in cold compression was obtained in exploratory work at Battelle (4).

In 1952, Hayes (5) and Gilbert (6) reported that arc melting of hydrogen-treated chromium had been accomplished and that successful forging, rolling, and swaging of this material had been carried out. A representative analysis (7) of the hydrogen-reduced arc-melted chromium showed that 0.001% iron, 0.05% silicon, 0.003% oxygen, 0.002% nitrogen, and 0.005% hydrogen were present. In regard to all other metallic impurities, the metal was described as pure as the best spectrographic standards available. The workability of this chromium was shown by the ability to drill, saw, grind, tap, turn, and file in the

cold state, and to spot weld chromium to either chromium or iron. The metal could not be bent cold, but did withstand a free bend at 325°C.

Recently, Sully and coworkers (8), using sintered compacts of hydrogen-reduced electrolytic chromium, showed that chromium undergoes a sharp transition in bend tests from brittleness to appreciable ductility over the range of a few degrees of temperature. The lowest temperature at which he found substantial ductility in bend tests was 50°C. In a study of the influence of impurities on this transition temperature, Sully observed that oxygen in the range 0.001–0.9% has hardly any influence on the transition temperature. He stated that elements in solid solution show a marked effect in raising the transition temperature, the extent being roughly proportional to the amount of solid solution hardening. Thus, the addition of 1% nickel raised the transition temperature to over 400°C. Copper and aluminum were also reported to have similar effects. In short-time, elevated temperature tensile tests, none of the sintered chromium samples showed any significant ductility at temperatures up through 900°C.

The present research was carried out to further identify the compositional factors that affect the ductility of chromium. This problem was approached by preparing chromium of the highest purity possible and by studying the effects of deliberate additions of various impurity elements on the properties of this chromium.

EXPERIMENTAL METHODS

Materials

Information available at the time this research was started indicated that, among the various contaminants normally present, oxygen was particularly deleterious to the ductility of chromium. Since one of the chief virtues of the "iodide" process is the removal of nonmetallic contaminant elements, it was selected as being most likely to yield pure chromium metal. A detailed description of the work leading to the successful adaptation of the iodide purification

¹ Manuscript received September 9, 1954. This paper was prepared for delivery before the Chicago Meeting, May 2 to 6, 1954.

process for chromium is beyond the scope of this paper. For this reason, only a brief description of the processes and equipment used is given at this time.

Dehydrogenated, electrolytic chromium was used as the primary chromium source for all of the material prepared in this work. After iodination, the thermal decomposition of the chromous iodide was effected by either of two deposition units especially evolved for this work. The first of these, hereafter referred to as the "metal" unit, consisted of a molybdenum-lined Hastelloy B reaction bulb in which deposition of the chromium occurred on an electrically-heated filament wire. The other deposition unit, hereafter called the "Vycor" unit, resembled the conventional Van Arkel-de Boer deposition chamber, excepting that a heated, re-entrant Vycor tube was used for the deposition surface in place of a metal filament.

Representative analyses for iodide chromium and the electrolytic chromium from which it was produced are given in Table I. Both the metal and Vycor units were capable of producing chromium of this quality. However, since both of these operations are batch processes, compositions of the various chromium lots produced by both methods were subject to significant departures from the values listed in Table I.

Chromium prepared in the metal unit suffered one major disadvantage in that metallic contamination was necessarily introduced, during arc melting, from the filament material. For this purpose, tungsten and molybdenum wires of a 3-mil diameter were the only satisfactory materials available. Attempts were made to remove as much of the filament as possible by breaking the chromium crystals free and physically separating the dissimilar metals. Despite these efforts, a tungsten or molybdenum pickup in amounts from 0.03 to 0.56% was incurred during arc melting of the crushed, metal-unit chromium.

In order to isolate the effects of the various major contaminant elements on the structure and properties of iodide chromium, alloys containing deliberate binary additions of oxygen, nitrogen, carbon, sulfur, nickel, iron, silicon, and tungsten were prepared using the following materials:

Element	Material form
Oxygen	cp Cr ₂ O ₃
Nitrogen	gaseous, tank nitrogen
Carbon	spectrographic rod
Sulfur	99% pure Cr ₂ S ₃
Nickel	cp shot
Iron	cp powder
Silicon	97.6% pure lump
Tungsten	99 + % pure wire

For alloying purposes, master alloys for oxygen, carbon, nickel, iron, and silicon were prepared by

TABLE I. Representative analyses for feed chromium and as-deposited chromium from which it was prepared

Element	Composition, wt %	
	Electrolytic feed material	As-deposited†
O	0.38	0.0044
N	0.006	0.0013
H	0.0056‡	0.00008
C	0.004	0.002
S	0.019	0.011
Al	0.005	ND*
Ca	0.001	0.005
Cu	0.002	<0.001
Fe	ND	0.003
Mg	0.002	0.002
Mn	ND	—
Mo	0.01	0.005
Ni	0.003	ND*
Si	0.01	<0.005

* ND designates not detected.

† Prepared in Vycor unit.

‡ After degassing.

encapsulating the alloy additions in a small, unalloyed, iodide chromium ingot and arc melting. A nitrogen master alloy was made by arc melting iodide chromium under a nitrogen atmosphere. Alloys with tungsten and sulfur were made by direct melting charges of iodide chromium with tungsten wire and Cr₂S₃, respectively.

Procedures

Analyses.—Two methods of chemical analysis for the oxygen content of chromium have been mentioned in the literature. These are the method of Adcock (9) and the use of vacuum fusion (10). Sully (11) has shown that both methods are in good agreement at oxygen levels down to about 0.02%, although, as Sully points out, special treatment must be given to chromium analyzed using Adcock's method in order to prevent the loss of some oxide. However, the use of Adcock's method at lower oxygen concentrations than 0.02% is not so reliable since no means is provided for separating other impurities from the oxide. These and other limitations of Adcock's procedure have been adequately described elsewhere (2, 5, 6).

In the present work, the vacuum-fusion method of oxygen analyses was used. Basically, this consists of using carbon to reduce the chromium oxide to form carbon monoxide, which is then collected, analyzed, and converted to a weight percentage of oxygen. Examination of the thermodynamics of the reaction indicated that a temperature of 1500°–1600°C would be sufficient to insure complete reduction of the oxide by carbon. Experimental work showed that no significant gettering of the carbon monoxide occurred by the chromium during the reaction. An important

factor in the technique is to add the chromium to the iron bath at a rather low temperature, such as 1200°C. When this procedure was used, the vacuum-fusion method gave reproducible results for oxygen content with an accuracy of about ± 4 ppm. The nitrogen and hydrogen contents of the chromium samples were determined concurrently during the vacuum-fusion analysis for oxygen.

Carbon and sulfur analyses were carried out by using ignition methods in a Leco Carbon Determinator and Leco Sulfur Determinator, respectively. In the adaptation of these processes to chromium, it was found essential to use a finely divided sample and to provide suitable fluxes so that complete oxidation of the sample would occur. For fluxing, an iron-lead bath in the carbon determination and an iron-tin bath in the sulfur determination were found to be satisfactory.

Metallic impurities in chromium were determined by the spectrographic method. In the early part of the work, analyses were carried out by direct metal arcing on a 10-mg sample. Later, two other modifications of the spectrographic method were tried in order to increase the sensitivity of the method. These modifications may be briefly described as follows.

(A) CrSO_4 solution method. Both standards and the samples are dissolved in sulfuric acid and dried by baking at 500°C. The sample and standard are arced separately, and their spectra recorded on the same film. A densitometer is employed to determine the relative intensities of the spectrum lines, and the analysis is calculated from the densitometer readings.

(B) Concentration method. The sample is dissolved in hydrochloric acid and then perchloric acid is added. Chromium is evaporated off as chromyl chloride, concentrating the impurities in the residue which is redissolved in a hydrochloric-nitric acid solution. Standards are also prepared by dissolving chromium containing known amounts of impurities in the hydrochloric-nitric acid mixture. The spectra of the sample and standards are photographed on the same film.

Use of the concentration method significantly lowered the detection limits for metallic elements. However, both the CrSO_4 solution and concentration methods were in excellent agreement down to the lower limits of the direct-metal-arc method. The accuracy of the direct-metal-arc method is believed to be about ± 25 relative %, and that of the concentration method is somewhat better.

Melting.—All of the evaluation work was carried out with 8-g ingots prepared from individual runs of iodide chromium by arc melting under an atmosphere of argon gas of 99.95% purity on a water-cooled copper hearth. A description of the furnace used has been given previously in the literature (12).

Prior to melting, two charges of iodide chromium and one titanium gettering ingot were placed in three shallow receptacles provided on the copper hearth. Melting was conducted by directing the arc first to the titanium getter button and then, in succession, to each of the chromium charges. In order to insure homogeneity, each ingot was given a minimum of three melts, with the ingot being inverted prior to each succeeding melt.

Bend testing.—The principal means of evaluating the ductility of chromium was the determination of the bend-transition temperature of sheet samples. For this purpose, a small stainless steel jig was constructed. This consisted of a female die, containing a 75° V-notch, enclosed in a perforated sleeve. This assembly was inserted either into a furnace or a refrigerating bath, depending on the test temperature desired. The male die consisted simply of a stainless steel plunger whose lower end was finished with $\frac{1}{16}$ -in. round radius.

In operation, a sample was placed across the notch in the female die and the plunger lowered through a guide block onto the center of the sample. In all cases, the bending stress was applied at a constant deflection rate of 0.05 in./min by lowering the cross-head of a tensile testing machine onto the top of the plunger. Vertical travel of the plunger was followed by means of a dial gauge in contact with the cross-head.

All bend-test samples were cut to approximately 0.4 in. long by 0.2 in. wide, using a water-cooled, abrasive, cut-off wheel. Except where otherwise indicated, the sample direction was oriented so that its longitudinal axis was parallel to the rolling direction of the sheet from which it was prepared. Prior to testing, all samples were finish ground by hand along both the edges and the flat surfaces, using 600X abrasive paper. Here, the final direction of polishing was oriented parallel to the longitudinal sample axis, to minimize any notch effects. The final thickness of all samples tested ranged between 0.015 and 0.030 in.

Two types of bend test were carried out using this equipment. In one type, called the "one-shot" method, a sample was bent through the total allowable vertical deflection (approximately 0.120 in.) of the jig at a single test temperature. Mating a 0.030-in. specimen to a $\frac{1}{16}$ -in. radius corresponds to 20% elongation in the outer fibers.² Because the amount of sample material from some runs of iodide chro-

² Calculated from the expression:

$$\text{Elongation, \%} = \frac{t/2}{R + t/2} \times 100$$

where t is the thickness of the specimens and R is the bend-die radius.

mium was limited, use was also made of a second test method, called the "progressive" bend-test method. In this procedure, each sample was subjected to a vertical deflection of only 30 mils at a given test temperature. If the sample withstood this bending, the temperature was reduced and an additional deflection increment of 30 mils was applied. The temperature and also the deflection at which fracture occurred were noted. Subsequent examination of a large number of samples broken in the progressive bend test showed that, in every instance where fracture occurred at 25 mils or greater, some permanent set (i.e., plastic deformation) had occurred. Samples which failed at a total deflection of less than 25 mils generally showed no evidence of ductile behavior.

As shown in Fig. 1, a fairly good correlation was obtained between the two test methods on wrought samples taken from the same piece of chromium sheet. Both types of test indicated an average ductile-to-brittle transition range of -20° to 0°C for this material. As indicated in the figure, many of the samples tested by the one-shot method showed varying degrees of ductility (greater deflection than 25 mils), even though they fractured before taking a complete bend. For the purpose of determining the transition temperature, these samples were labeled "ductile." Although many of the one-shot samples tested above the transition range took the full bend, none of the one-shot samples tested below the transition range showed evidence of ductility.

However, it was later found that annealed samples were subject to rheotropic recovery, i.e., bending above the transition temperature enabled ductility to be retained below the transition temperature. Thus, the correlation between one-shot and partial bend methods does not hold for annealed samples. Consequently, bend-transition temperatures for annealed chromium sheet were determined by one-shot bend tests.

For the purposes of comparison and discussion, bend data on individual samples from each chromium sheet were summarized and are reported in the two following categories:

(A) *Transition range.*—This was defined as the range extending from the highest temperature at which any of the individual bend-test samples was brittle (i.e., broke at a deflection of less than 25 mils with no permanent set) to the lowest temperature at which any of the individual samples was ductile (i.e., withstood a deflection greater than 25 mils and showed evidence of plastic deformation).

(B) *Average bend-transition temperature.*—This was taken for each chromium sheet as a statistical average based on the number of individual samples

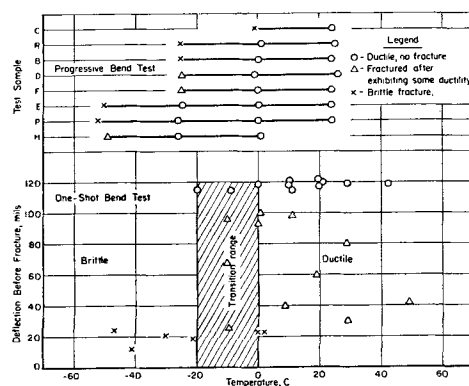


FIG. 1. Correlation of bend-test procedures carried out on wrought chromium strip.

tested and the lowest test temperature at which bend ductility was observed in each sample.

Tensile testing.—Tensile-test samples were prepared by clamping the chromium sheets between mild steel plates and grinding in a reduced section $\frac{1}{4}$ -in. wide over a 1-in. gauge length. During the first attempt at edge grinding two chromium sheets, both samples failed as a result of cracks that developed at several points on each sample. This brittle behavior was apparently caused by the development of fine surface cracks as a result of heat checking or fatigue. Before grinding the balance of the tensile samples, the jig containing the blanks was dipped into a room-temperature-setting plastic to eliminate sample vibration within the jig during grinding. All of these samples were edge ground successfully.

Tensile testing was carried out with a Baldwin Southwark tensile-testing machine, at a constant strain rate of 0.01 in./min. Elastic extensions of the samples during testing were measured by means of an SR-4 resistance-type strain gauge glued to one side of the reduced section of the samples.

EXPERIMENTAL RESULTS WITH UNALLOYED IODIDE CHROMIUM

Melting

Despite the use of a titanium gettering melt, the unalloyed chromium ingots picked up an average of about 25 ppm of oxygen during arc melting. Neither the nitrogen nor hydrogen content, both of which were usually less than 10 ppm, was altered significantly during melting. Spectrographic analysis showed that no significant metallic contamination occurred from either the copper hearth or the tungsten electrode.

After triple-inversion arc melting, the hardness of the iodide chromium prepared in the Vycor unit increased from an average of 136 VHN in the as-deposited condition to an average value of 141 VHN, an increase of only 5 VHN. Although the average as-deposited hardness of chromium prepared in

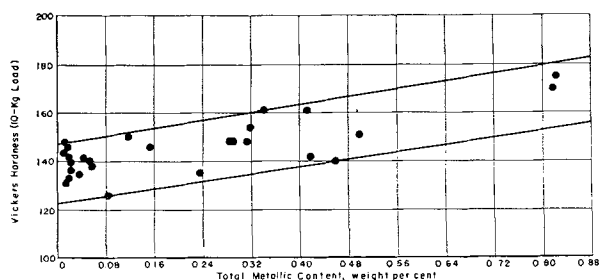


FIG. 2. Correlation of metallic contaminant elements in arc-melted iodide chromium with as-cast hardness.

metal apparatus was somewhat lower than that of chromium prepared in the Vycor unit (128 VHN, as compared with 136 VHN), ingots made from metal-unit chromium had an average increase of 17 VHN points after triple arc melting. The slightly greater hardness increase occurring in these ingots during melting was attributed to solid-solution hardening from the residual molybdenum or tungsten filament wires contained in the chromium made in the metal unit.

Comparison of cast hardnesses with compositions of various chromium samples did not show that any one contaminant element had a greater hardening effect than any of the others, although several samples contained from 0.1 to 0.5% of either nickel, iron, and/or molybdenum or tungsten. As shown in Fig. 2, a rather broad correlation was found when the cast hardnesses were plotted against the total metallic-impurity content. This would indicate that metallic contaminants, at the levels encountered, have only a small, equivalent, additive effect on the hardness. No correlation of the quantity of carbon or sulfur with cast hardness was possible with the data available. Also, rather wide variations of total oxygen content (from 70 to 160 ppm) and total nitrogen content (from 10 to 50 ppm) appeared to have no effect on hardness.

Fabrication

Hot rolling.—Hot rolling of the unprotected ingots in air proved to be the most expedient method of fabrication. Experiments with a large number of ingots from different lots of iodide chromium indicated that the optimum preheating temperature was in the range of 700°–800°C. Increasing the temperature to 850° or 900°C resulted in a high incidence of failure as a result of hot shortness.

Straight rolling of the ingots to 30-mil sheet at 600°C produced sheet with severe edge cracks as a result of excessive hot-cold work. However, it was shown that iodide chromium can be rolled to satisfactory sheet at temperatures as low as 500°C, so long as appropriate annealing treatments are provided.

In this work, 700°C was used as the rolling temperature for most of the material evaluated. Direct rolling of the ingots to sheet at 700°C elongates, but does not otherwise refine, the large, as-cast grain structure. Also, sheet prepared in this manner tended to show a spread in hardness. For these reasons, an intermediate annealing treatment of 1 hr in argon at 1000°C was incorporated as part of the standard fabrication procedure. After annealing, rolling was resumed at 700°C and continued to a final reduction of 80%.

Vacuum-fusion analyses showed that an oxygen pickup of from 10 to 35 ppm occurred during fabrication when the procedure outlined above was used. Some slight increase in the nitrogen and hydrogen contents of some of the chromium ingots also occurred as a result of working in air at 700°C. Generally, however, concentrations of nitrogen and hydrogen in the fabricated iodide chromium sheets rarely exceeded 30 and 3 ppm, respectively.

Forging and swaging.—Attempts were made to forge several good-quality ingots by directing hammer blows to the edges of the ingots in a direction transverse to the columnar grain structure. Forging was tried using preheating temperatures of both 700° and 800°C, but in neither case could cracking be avoided. Although the ingot worked at 800°C seemed more amenable to plastic deformation, fine transcrystalline cracks developed on the ingot surface, despite the facts that (a) forging was carried out using light hammer blows, and (b) the ingot was reheated frequently between forging operations. These findings are consistent with early work on arc-melted chromium done at the Bureau of Mines (6).

On the other hand, working in a direction perpendicular to the usual rolling direction was accomplished by encasing an ingot in an iron sheath and swaging at 700°C. A chromium rod approximately 0.05 in. in diameter by 6 in. long was prepared by using this procedure.

Effect of contaminant elements on fabricability.—A small number of ingots from some of the first lots³ of the iodide chromium prepared cracked up during attempted rolling by the standard procedure. Fabrication data for these lots are given in Table II along with similar data for material which fabricated satisfactorily.

Most of the ingots that failed to fabricate contained nickel in quantities of 0.27% or greater. This

³ Most of these were prepared in a Hastelloy B reaction bulb and contained appreciable quantities of nickel that had transferred to the chromium from the Hastelloy B during deposition. This transfer of nickel was subsequently eliminated by inserting a molybdenum-sheet liner in the reaction chamber.

TABLE II. Fabrication data for representative arc-melted unalloyed iodide chromium ingots rolled in air at 700°C

Ingot	Composition, wt %						Vickers hardness		Final reduction, %	Quality of sheet
	O	N	C	S	Ni	Total Metallics	As-cast	As-fab.		
R27-1	0.0013*	0.0004*	0.002*	0.005*	0.1	0.460	140	236	80	Good
R28-1	0.0090	<0.0030	—	—	0.2	0.819	170	308	88	Poor
R29-1	—	—	—	—	0.3	<0.318*	154	—	15	No good
R30-1	—	—	—	—	0.3	<0.340*	161	—	18	No good
R31-1	—	—	—	—	0.27	<0.286*	148	—	19	No good
R33-1	—	—	—	—	0.4	<0.412*	139	—	35	No good
R34-1	—	—	—	—	0.09	0.512	123	226	80	Good
R39-1	—	—	—	—	0.33	0.419	142	—	25	No good
R42-1	—	—	0.004	—	0.001*	<0.014*	131	—	37	No good
R44-1	—	—	0.002	0.013	0.008*	<0.082*	126	—	37	No good
R45-1	—	—	0.005	0.011	0.003*	0.153*	146	—	47	No good
R46-1	—	—	0.007	0.009*	0.003	0.036	134	223	80	Good
R35-1	0.0160	0.0050	—	—	<0.001	0.044	141	218	80	Good
R36-1	0.0042*	0.0013*	0.002*	0.011*	0.0005	0.118	150	218	80	Good
R37-1	0.0042*	0.0005*	—	—	0.005	0.059	138	221	80	Good
R38-1	0.0190*	<0.0050*	0.002*	0.015*	ND*†	0.010*	143	210	80	Good
R40-1	0.0100	0.0030	0.001	—	ND*†	0.020*	133	213	80	Good
R41-1	0.0074	<0.0007	0.007	—	ND*†	0.021*	140	205	80	Good
R43-1	0.0140*	<0.0003*	—	—	ND*†	0.011*	148	211	80	Good
R49-1	0.0073	0.0010	0.002*	0.002*	0.001	0.020	141	215	80	Good
R50-1	0.0120*	0.0012*	0.002*	0.017*	0.0005*	0.017*	161	—	80	Poor

* Analysis on the as-deposited form of the metal.

† ND means "not detected."

indicates that the fabricability tolerance for nickel is slightly less than 0.2%. On the other hand, several ingots (R27-1 and R34-1) containing 0.3 and 0.4% molybdenum and one other containing 0.2% tungsten rolled to satisfactory strip. The highest contaminant levels encountered for iron and silicon were 0.1 and 0.016%, respectively, and ingots containing these amounts of either element also fabricated successfully. The data also indicate that oxygen in amounts up to 0.019% does not affect the fabricability of chromium adversely.

Other work, described in a later section of this paper, showed that the presence of either carbon or sulfur in relatively small quantities is definitely deleterious to the ductility of chromium. Thus, chromium containing above 0.016% carbon or about 0.02% sulfur cannot be fabricated to sound sheet. Since several ingots, listed in Table II, made from chromium containing up to 150 ppm of sulfur rolled to good sheet, the tolerance for sulfur is probably at least this great. However, it seems possible that the poor fabricability of Ingot R50-1 (made from chromium low in all impurities except oxygen and sulfur) can be attributed to its sulfur content, which was determined by analysis to be 170 ppm. This suggests that an increase in the sulfur content from 150 ppm to 170 ppm produces a sharp decrease in the fabricability of chromium.

Although complete analytical data were not obtained on all of the material tested, the data available for Ingots R44-1, R45-1, R46-1, R36-1, R38-1,

R49-1, and R50-1 suggest that the ductility of chromium is closely related to the total amounts of carbon, sulfur, and metallic-impurity elements, as well. The limited data for these alloys in Table II indicate that, if the total amount of carbon and sulfur exceeds 150 ppm and the total metallic content exceeds about 500 ppm, the chromium is not amenable to rolling at 700°C.

Recrystallization Behavior

Softening curves were determined on 30-mil chromium sheet prepared by straight rolling at 600°, 700°, and 900°C. These data, given in Fig. 3, show that the hardness started to drop after 1 hr at 800°C. After 1 hr at temperatures above 900°C, the hardness is reduced to about the same level as for the as-cast condition.

Metallographic examination of the samples used to construct Fig. 3 showed that recrystallization be-

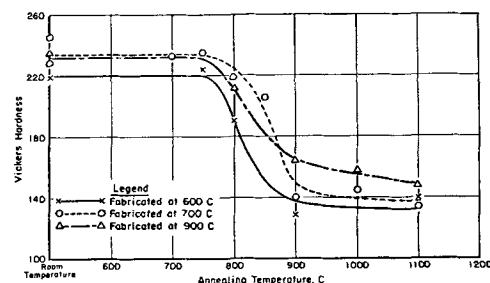


FIG. 3. Softening curves for iodide-chromium sheet fabricated at various temperatures after 1-hr annealing treatments.



FIG. 4. Longitudinal fibered grain structure of iodide-chromium sheet rolled at 700°C. Oxygen content of 0.0093%; electrolytic etch in 10% oxalic acid. 250X.



FIG. 5. Recrystallized grain structure of iodide-chromium sheet fabricated at 700°C and annealed 1 hr at 1000°C. Oxygen content of 0.0074%; note the rounded, gray, oxide inclusions; electrolytic etch in 10% oxalic acid. 500X.

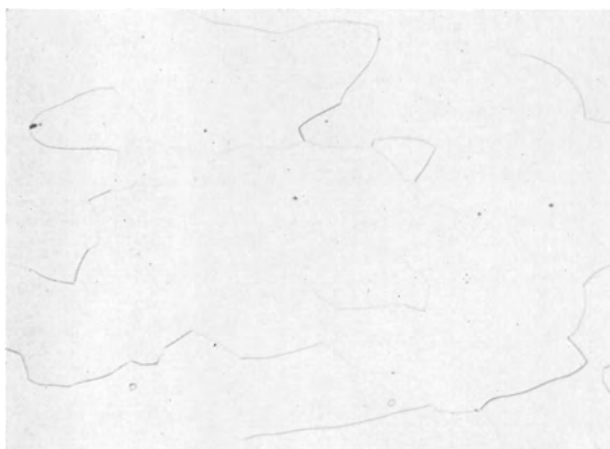


FIG. 6. Equiaxed iodide-chromium sheet containing 0.001% carbon. Note the round, light-colored carbide particles in the lower part of the photograph; electrolytic etch in 10% oxalic acid. 500X.

gan on all samples after 1 hr at 800°C. Sheet fabricated at 600°C was completely recrystallized after 1 hr at 900°C, whereas complete recrystallization in sheet fabricated at 700° and 900°C required 1 hr at 1000°C. Fig. 4 and 5, respectively, illustrate typical wrought and recrystallized structures observed in these samples. The grain size in the crystallized samples usually ranged between 0.03-mm and 0.05-mm average grain diameter. No gross differences in grain growth for any of these samples were noticed over the time and temperature intervals investigated.

Metallography

All of the annealed sheet samples examined contained varying amounts of Cr_2O_3 . At the oxygen contents normally encountered (i.e., less than 200 ppm), the oxides generally appeared as small, rounded, gray inclusions, illustrated in Fig. 5, randomly distributed in the grain structure. Only a very few oxide particles were observed in a sample from R40-2, which had the lowest analyzed oxygen content (60 ppm). Since so few oxide particles were noted in this specimen, the solubility limit of chromium for oxygen is probably only slightly below 60 ppm. Other work on chromium-carbon alloys described in a later section of this paper indicated that, in the presence of excess carbide, the oxygen-solubility limit actually was located between 20 and 40 ppm.

It was observed later that sulfur in chromium also forms a compound very similar in appearance to the oxide. Available data indicate that sulfur, in the quantities normally observed (i.e., less than 0.015%), is soluble in chromium. Nevertheless, since the sulfur content was not determined on most of the chromium samples, it is possible that, in some instances, small quantities of the sulfide phase coexisted with the oxide phase.

Similarly, most of the annealed-sheet samples also contained a few small, light-colored, rounded particles tentatively identified as a carbide of chromium. Since none of these samples contained an appreciable number of carbides, visible detection and identification of this phase in the unalloyed iodide chromium was sometimes difficult. However, as shown in Fig. 6, a few widely scattered carbides were observed in chromium samples which had analyzed carbon contents of 0.001 and 0.002%, respectively. These data, therefore, suggest that the solid solubility of carbon in chromium is very low.

Bend Ductility

Effects of fabrication variables and annealing treatments.—In an evaluation of the hot malleability of iodide chromium, several ingots were initially rolled to a 50% reduction at 700°C, annealed, then rolled

at progressively lowering finishing temperatures of 600°, 550°, and 500°C, respectively. Bend data from these sheets, given in Table III, show that variations in rolling temperature between 500° and 700°C have little effect on the ductile-to-brittle bend transition range of the as-fabricated chromium sheet.

In another experiment, five ingots prepared from the same lot of iodide chromium were used to study the effects of increasing amounts of hot-cold work on the bend ductility. All five ingots were fabricated first to varying thicknesses by rolling at 700°C and annealed for 1 hr at 1000°C. These billets were then rolled to the same final thickness of 30 mils at 700°C, and tested for bend ductility in the as-fabricated condition. The reductions given during the final rolling operations ranged from 25 to 90%.

As shown in Fig. 7, the hardness of the as-fabricated sheets increased from 200 to 222 VHN as the final reduction was increased from 25 to 90%. Fig. 7 also shows that all of the bend samples from each of these sheets had a brittle-to-ductile transition temperature of about 0°C. This shows that variations from 25 to 90% in the final reduction after intermediate annealing have no significant effect on the bend-transition temperature. On the other hand, recrystallized samples from these same chromium sheets showed significantly higher average transition temperatures, ranging from 65° to 150°C. These data are also shown in Fig. 7. It is apparent from these data that optimum bend ductility in the iodide chromium sheet is associated with a fibered grain structure.

The effect of stress-relief annealing treatments in the recovery range on the bend ductility of as-fabricated chromium sheet was investigated. This work indicated that 1-hr stress-relief anneals at 500° and 600°C increase the transition temperature by about 60°C, whereas treatment at 700°C apparently has no effect.

Rheotropic recovery of annealed chromium.—Early in this research, considerable scatter in the bend ductility of annealed, recrystallized chromium was noticed when the progressive bend test was used. The scatter was found to be the result of rheotropic recovery. This phenomenon appears in metals crystallizing in other than the face-centered-cubic lattice that show a sharp ductile-to-brittle transition (13). By prestraining annealed samples of a metal which exhibits this behavior at a temperature above the transition temperature, ductility can be retained at temperatures considerably below the transition temperature. This ductility is termed "rheotropic recovery," since rheotropy is related to flow or strain.

Since chromium is subject to this phenomenon, the progressive bend test is invalid for determining

TABLE III. Effect of variations in rolling temperature on the bend ductility of iodide chromium sheet

Ingot	Fabrication-temp range, °C		Vickers hardness	Bend ductility		
	Start	Finish		Transition range, °C		Transition temp, °C
				Highest brittle	Lowest ductile	
R41-1	700*	700*	205	-25	-25	-25
R41-5	700	600	219	0	-25	0
R41-4	700	550	224	25	0	25
R41-2	700	500	228	0	-25	0

* Standard fabrication procedure.

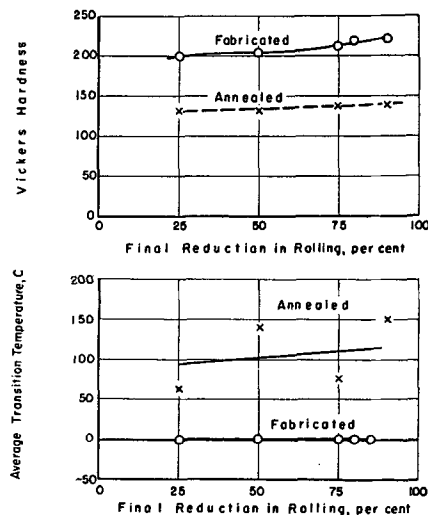


FIG. 7. Effect of reduction in rolling on the hardness and bend-transition temperature of iodide-chromium sheet.

the transition temperature of annealed bend-test samples. Partial bending above the transition temperature strains the sample enough to allow it to be bent below this temperature. By reappraisal of progressive bend data for annealed samples, a sharp, well-defined transition temperature was obtained when only the results of the first bending temperature were considered. Fig. 8 illustrates a typical bend-transition temperature curve obtained on recrystallized chromium sheet.

There is no evidence of rheotropic recovery in wrought samples, evidently because they are already highly strained from the hot-cold work resulting from rolling at 700°C.

Bend anisotropy.—In a study of the anisotropy of wrought chromium sheet, two groups of bend-test samples were prepared from a single sheet. One group was cut so the longitudinal axes of the samples were parallel to the rolling direction; this was the procedure normally used for all bend samples. The other bend-test samples were cut with their longitudinal axes perpendicular to the rolling direction. Bend-transition temperatures were determined on

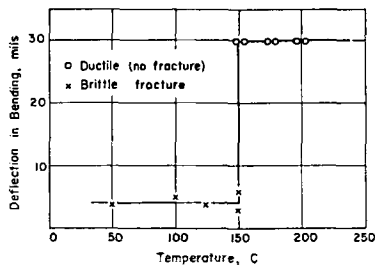


FIG. 8. A typical bend-transition temperature curve for recrystallized iodide-chromium sheet.

TABLE IV. Effect of machining on the bend ductility of iodide chromium sheet fabricated using the standard procedure at 700°C

Ingot	Method of finishing to size	Vickers hardness	Bend ductility		
			Transition range, °C		Avg transition temp, °C
			Highest brittle	Lowest ductile	
R38-2	Abrasive cut-off wheel*	218	-25	-25	0
	Edge ground, transverse to rolling direction	220	50	0	15
	Edge milled, transverse to rolling direction	216	50	25	30
R41-1	Abrasive cut-off wheel*	205	-25	-25	-25
	Edge ground, parallel to rolling direction	205	100	75	85

* Standard procedure.

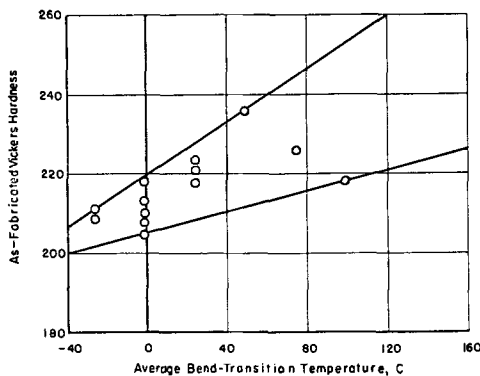


FIG. 9. Relationship between as-fabricated hardness and average bend-transition temperature for iodide-chromium sheet, made using the standard fabrication procedure. Each point represents a separate lot of iodide chromium.

samples from the two groups, both in the as-fabricated condition and after a recrystallizing anneal.

Transition temperatures of samples cut parallel to the rolling direction from the wrought sheet were the lowest (about 75°C) of any for the four test conditions. Conversely, transition temperatures for transverse samples from the wrought sheet were the highest (about 300°C). After a recrystallizing anneal, average transition temperatures of both longitudinal and transverse bend-test samples were about the

same, the values being intermediate to those obtained in the wrought longitudinal and transverse specimens. Thus, recrystallization tends to overcome the bend anisotropy shown by the as-fabricated sheet, but at the expense of the excellent longitudinal-bend-transition temperature of the wrought material.

Effect of machining on bend ductility.—As a result of the ill effects experienced in the grinding of sheet chromium (described in an earlier paragraph of this paper), it was decided to investigate the effect of machining on the bend-transition temperature. Three groups of samples were prepared from the same sheet after hand grinding the surface with 600X abrasive paper. One group was edge ground (transverse to the rolling direction) to size, another was edge milled (transverse to the rolling direction) to size, and the third group was cut to size using a cut-off wheel. One out of seven samples failed during milling, and two out of seven failed during grinding. Bend data on the balance of these samples, given in Table IV, indicated transition temperatures of about 15° and 30°C, respectively, for ground and milled samples, as compared with 0°C for samples prepared using the cut-off wheel.

Additional bend samples were made from a second sheet of chromium. One group was edge ground parallel to the rolling direction, and a control group was made using the cut-off wheel. Again, as shown in Table IV, machine-ground samples showed a much higher average bend-transition temperature.

This work shows that machining by grinding or milling is definitely detrimental to the bend ductility of chromium. This would appear to be associated with a notch effect caused by these machining operations. If macronotches were the reason for the apparent brittle behavior, one should expect that orienting the scratches parallel to the rolling direction would minimize this effect. However, the bend-test data do not support this point of view. It seems plausible that, if neither machine grinding nor milling generates either micro- or macrocracks directly, these operations actually may work harden a thin surface layer of the metal to a point where further action of the fiber stress in bending accelerates fracture of the surface layer. This would lead to an early fracture in bend testing. Whatever the true mechanism responsible for the deleterious effects of machining on bend ductility may be, this is further evidence that the ductility of chromium is very sensitive to surface effects.

Correlation of Bend Ductility and Hardness

A plot of the as-fabricated hardnesses vs. average bend-transition temperatures shown for a number of lots of unalloyed iodide chromium is shown in Fig. 9.

This plot shows that a rough correlation between these properties exists. Thus, those chromium sheets which had higher as-fabricated hardnesses generally showed higher transition temperatures. The wide spread in fabricated hardness is probably the result of compositional differences within these samples, which caused differences in the rate of strain hardening.

The bend-ductility data for each lot of unalloyed iodide chromium were also compared with its composition. Results of this work are more conveniently discussed in the following section of this paper.

Tensile Properties

Several sheet tensile-test samples were prepared from lots of iodide chromium that had shown ductile-to-brittle transitions in bending at temperatures well below room temperature. All samples were tensile tested at room temperature in the as-fabricated condition. After grinding to shape, each sample was hand polished on both the flat surfaces and edges with 600X abrasive paper, taking care to polish in a direction parallel to the longitudinal axis of the specimen.

Despite the precautions taken in their preparation, all of the tensile samples failed by brittle fractures in the reduced sections at stresses between 15,000 psi and 62,000 psi. None of the samples showed any measurable permanent elongation or reduction in area. The best values obtained for the tensile properties of wrought iodide chromium sheet are:

Proportional limit, psi.....	33,000
0.1% offset yield strength, psi.....	58,000
Maximum load, psi.....	62,000
Modulus of elasticity, psi.....	45,000,000
Per cent elongation in 1 in.....	0

Examination of broken samples indicated that fracture was initiated by formation of fine cracks which developed along the edges of the sheets during application of the load. Bend tests on samples prepared from both stressed and unstressed tensile samples showed consistently higher transition temperatures than did samples taken from other portions of the original wrought sheets. This and the fact that several bend-ductile chromium sheets failed in grinding suggests that the tensile ductility as well as the bend ductility of chromium is extremely sensitive to surface effects.

EVALUATION OF EFFECTS OF IMPURITY ELEMENTS IN CHROMIUM

Hardness and Fabricability of Chromium-Impurity Alloys

Compositions, hardnesses, and fabrication data for all alloys investigated are listed in Table V, which

also includes data for the unalloyed iodide chromium lots from which the majority of these alloys were prepared.

Oxygen (up through 0.18%), iron (up through 0.25%), silicon (up through 0.15%), and tungsten (nominally up through 0.2%) have no deleterious effects on the fabrication of chromium by rolling at 700°C. Similarly, none of these alloy additions showed any significant effect on the hardness of the chromium from which they were prepared. Master alloy data, also given in Table V, show that increasing the quantity of oxygen up through 0.57% or iron up through 1% (nominal) still has no significant effect on the hardness.

Nickel, carbon, and sulfur, on the other hand, are definitely detrimental to the fabricability of chromium. Thus, chromium which contains nickel in excess of 0.2%, or carbon and/or sulfur above about 0.015%, cannot be fabricated to sound strip by rolling at 700°C. Neither nickel nor carbon in quantities up through 0.2% has any effect on the cast hardness of the chromium used as a base. However, increasing the quantity of either of these elements to about 1% results in a hardness increase of about 100 Vickers points. The addition of 0.2% sulfur appears to increase the hardness only slightly.

Because of insufficient material, no attempts were made to fabricate the only two nitrogen alloys prepared. Hardness data on these alloys showed that additions of up to 0.124% nitrogen have relatively little effect on the hardness of chromium.

Metallography

Oxygen-addition alloys.—As mentioned in an earlier paragraph, most of the unalloyed chromium samples examined contained varying amounts of small, rounded, gray inclusions of chromium oxide. Fig. 5 and 10 illustrate typical structures at increasing levels of oxygen content.

Actually, the lowest oxygen contents of all the arc-melted metal examined were obtained in the carbon alloys. This is understandable, since carbon, in the quantities added, acts as a deoxidizer. Examination of the two lowest oxygen-content carbon alloys showed that only a very few, small, scattered oxides were present at 0.004% oxygen. No oxides were observed in the carbon alloy containing 0.002% oxygen. On the other hand, two unalloyed ingots prepared from the same lot of chromium contained a significantly larger number of oxide particles in proportion to their analyzed oxygen contents of 0.006 and 0.010%, respectively. These data indicate, therefore, that the solubility limit of oxygen in chromium is slightly below 0.004%.

Carbon-addition alloys.—Work on unalloyed chromium samples showed that the solubility limit of

TABLE V. Compositions, hardnesses, and fabrication data for contaminant alloys in an iodide chromium base

Ingot	Analyzed composition, wt %								Quality of sheet as-rolled at 700°C	Vickers Hardness		
	O	N	C	S	Ni	Fe	Si	W		As- cast	As- fabri- cated	As-an- nealed at 1000°C
<i>Unalloyed controls</i>												
R40-2	0.0060	<0.0020	—	—	<0.001	0.002	0.015	—	Good	139	213	138
R40-1	0.0100	0.0030	0.001	—	<0.001	0.002	0.01	—	Good	133	209	134
R38-3	0.0190*	<0.0050*	0.002*	0.015*	ND*	0.001*	0.003*	—	Good	142	222	140
R43-1	0.0140*	<0.0003*	—	—	ND*	0.002*	<0.005*	—	Good	148	211	—
<i>Oxygen alloys</i>												
R40-X1	0.012	0.002	0.007	—	<0.001	0.008	0.007	—	Good	146	204	147
C3	0.015	<0.002	—	—	—	—	—	—	—	150	—	141
R40-X2	0.051	<0.002	—	—	—	—	—	—	Good	141	210	152
R40-X3	0.075	<0.002	—	—	—	—	—	—	Good	138	207	154
C4	0.096	<0.002	—	—	—	—	—	—	—	155	—	161
R40-X4	0.180	<0.003	0.005	—	0.002	0.015	0.007	—	Good	145	212	156
R43-M4	0.57	<0.01	—	—	—	—	—	—	—	148	—	—
<i>Nitrogen alloys</i>												
C5	0.052	0.069	—	—	—	—	—	—	—	154	—	147
C6	0.059	0.124	—	—	—	—	—	—	—	174	—	158
<i>Carbon alloys</i>												
R40-C5	0.0040	0.002	0.011	—	—	—	—	—	Good	147	214	—
R40-C1	0.0020	<0.002	0.016	—	—	—	—	—	Poor	140	232	161
C1	0.049	<0.004	0.04	—	—	—	—	—	—	159	—	154
R40-C2	—	—	0.052	—	—	—	—	—	Did not roll	138	—	—
C2	0.008	—	0.09	—	—	—	—	—	—	146	—	144
R40-C3	—	—	0.1†	—	—	—	—	—	Did not roll	144	—	—
R40-C4	—	—	0.2†	—	—	—	—	—	Did not roll	160	—	—
R43-M5	—	—	1.0†	—	—	—	—	—	—	228	—	—
<i>Sulfur alloys</i>												
R38-S1	—	—	—	0.02†	0.007	0.003	0.005	—	Did not roll	136	—	—
R38-S2	—	—	0.010	0.22†	0.007	0.003	0.002	—	Did not roll	161	—	—
<i>Nickel alloys</i>												
R40-N1	—	—	—	—	0.01†	—	—	—	Good	138	214	—
R40-N2	—	—	—	—	0.055	0.002	0.01	—	Good	126	222	127
R40-N3	—	—	—	—	0.101	0.003	0.01	—	Good	128	224	129
R40-N4	—	—	—	—	0.199	0.005	0.005	—	Poor	140	241	151
R43-M2	—	—	—	—	1.0†	—	—	—	—	230	—	—
<i>Iron alloys</i>												
R40-F1	—	—	—	—	<0.001	0.016	0.01	—	Good	139	216	138
R40-F2	—	—	—	—	<0.001	0.058	0.01	—	Good	135	204	131
R40-F3	—	—	—	—	0.001	0.117	0.003	—	Good	132	214	132
R40-F4	—	—	—	—	0.001	0.246	0.003	—	Good	130	219	133
R43-M1	—	—	—	—	—	1.0†	—	—	—	151	—	—
<i>Silicon alloys</i>												
R40-S1	—	—	—	—	<0.001	0.002	0.03	—	Good	144	206	144
R40-S2	—	—	—	—	<0.001	0.003	0.07	—	Good	142	217	141
R40-S3	—	—	—	—	<0.001	0.005	0.07	—	Good	136	217	144
R40-S4	—	—	—	—	<0.001	0.01	0.15	—	Good	133	243	145
R43-M3	—	—	—	—	—	—	1.0†	—	—	166	—	—
<i>Tungsten alloys</i>												
R38-W1	—	—	—	—	—	—	—	0.05	Good	141	224	156
R38-W2	—	—	—	—	—	—	—	0.2†	Good	145	217	148

* From analysis on as-deposited chromium used for this ingot.

† Nominal composition.

ND means "not detected."

carbon in chromium is less than 0.001%. As illustrated in Fig. 6 and 11, increasing the quantity of carbon from 0.001 to 0.016% results in an increasing amount of the carbide, which, in the annealed sam-

ples, generally assumes the form of spheroids. Examination of a cast 0.04% carbon alloy showed that, in this condition, some carbides also assumed the form of rods or platelets. This would indicate that

some carbide precipitated from the chromium during cooling, and suggests that the terminal solid solution of chromium shows a decreasing solubility for carbon with decreasing temperature. At levels of 0.09% carbon and above, the carbide phase also occurs, in the cast structures, in an interdendritic filler pattern as an almost continuous phase. Examination of the nominal 0.2% carbon alloy, after attempted fabrication and annealing, showed that many of the interdendritic carbide patches contained fine particles of another microconstituent, which was identified tentatively as eutectic particles of carbon-rich chromium.

These observations are consistent with the partial chromium-carbon equilibrium diagram given on page 1181 in the 1948 Edition of the *ASM Metals Handbook*. This diagram shows that chromium containing "probably less than 0.1 per cent" carbon undergoes a eutectic reaction at 1475°C with a carbon-rich phase containing about 5% carbon. This same source lists the eutectic composition at 4.5% carbon and identifies the carbon-rich phase as Cr_4C or Cr_{23}C_6 , which has a cubic structure having an a_0 value of 10.64kx units.

Nitrogen-addition alloys.—The structure of the cast 0.069% nitrogen alloy contained many short rods or plates of a Widmanstätten-type precipitate, similar in color to the chromium matrix. As in the case of the chromium-carbon alloys, the Widmanstätten form indicates that the nitrogen-rich phase shows a decreasing solubility in the chromium terminal solid solution with decreasing temperature. This is illustrated more clearly in the 0.124% nitrogen alloy structure shown in Fig. 12. Here, the nitrogen-rich phase occurs in appreciably larger plates and also at the grain boundaries. A heat treatment of 24 hr at 1000°C followed by water quenching had no significant effect on either the quantity or the mode of occurrence of these Widmanstätten structures. This suggests that there is relatively little change in the solubility of this phase in chromium at temperatures up to 1000°C.

Aside from these two alloys, none of the arc-melted chromium samples examined contained any recognizable quantity of the nitrogen-rich phase. The highest analyzed nitrogen content in any sample to which nitrogen was not added deliberately was 0.032% (for an arc-melted sample of as-received electrolytic chromium). On this basis, the solubility limit of nitrogen in chromium was placed tentatively between 0.032 and 0.069%.

Sulfur addition alloys.—Of the two sulfur-addition alloys prepared, the one containing nominally 0.022% sulfur did not contain any second phase which could be associated with sulfur. However, the nominal 0.22% sulfur alloy definitely contained an

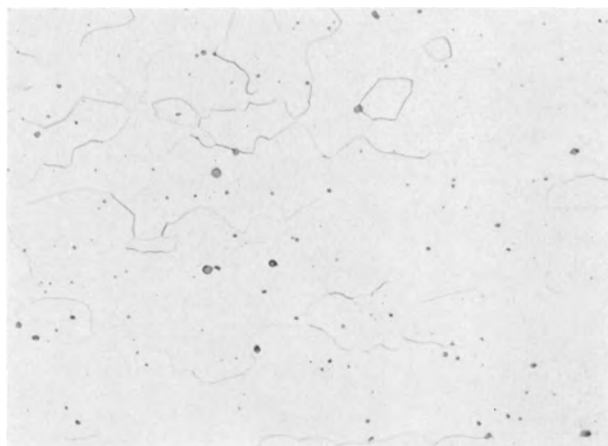


FIG. 10. Oxide inclusions in chromium containing 0.051% oxygen; electrolytic etch in 10% oxalic acid. 500X.

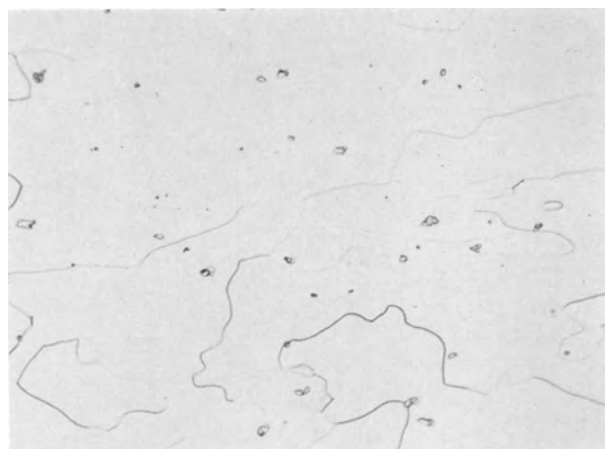


FIG. 11. Carbides in chromium containing 0.016% carbon; electrolytic etch in 10% oxalic acid. 500X.



FIG. 12. As-cast structure of chromium containing 0.124% nitrogen and 0.059% oxygen. Large, light-colored Widmanstätten rods and grain boundary precipitate of nitrogen-rich phase plus gray-colored oxide inclusions; electrolytic etch in 10% oxalic acid. 500X.

inclusion phase characteristic of the sulfur addition. As shown in Fig. 13, these particles appear very similar to the oxide phase. Under direct illumination, however, the large sulfide particles have a brown color after electrolytic etching with oxalic acid, as opposed to the slate-gray color always shown by the oxide. Admittedly, visual differentiation between these phases, where either or both exist in small particle sizes or quantities, would be very difficult. However, this work indicates that the solubility of sulfur in chromium extends beyond 0.02%.

Nickel-, iron-, silicon-, and tungsten-addition alloys.—Nickel (up through 0.2%), iron (up through 0.25%), silicon (up through 0.15%), and tungsten (nominally up through 0.2%) all appeared to be soluble in chromium.

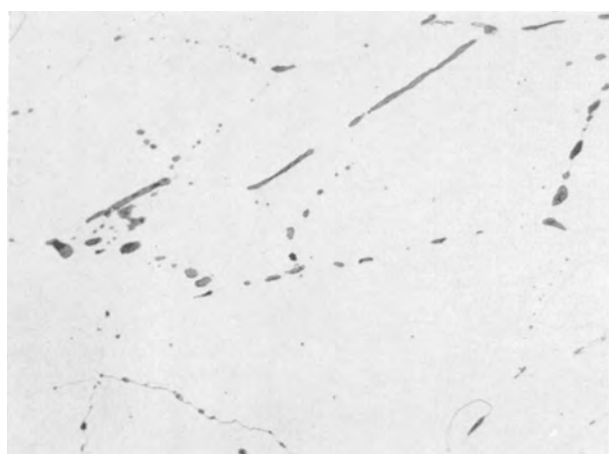


FIG. 13. Annealed structure of chromium containing, nominally, 0.22% sulfur and 0.019% oxygen. Large particles of a brown sulfur-rich phase plus small particles of oxide; electrolytic etch in 10% oxalic acid. 500X.

Correlation of Bend Ductility and Impurity Content of Chromium

All the chromium-plus-impurity element alloys which were successfully fabricated to sheet were bend tested by using the same procedure as used for bend testing the unalloyed iodide chromium. Since the impurity content of the unalloyed chromium was determined in many cases, the two sets of bend-test data together give a good idea of the effects of a number of impurity elements on the bend ductility of chromium.

Transition temperatures in both the as-fabricated and the annealed conditions and the compositions of the various lots of unalloyed chromium tested are shown in Table VI. The same information is given in Table VII for the alloys containing the deliberate impurity additions. The latter table also gives bend data for unalloyed sheet prepared from the same chromium as used for making the alloys.

From Table VI (unalloyed chromium), it appears that increasing the amounts of total metallic impurities generally increases the average transition temperature of wrought chromium sheet. Here, as in the correlation of composition with as-cast hardness, the effects of the individual metallic contaminant elements appeared equivalent and additive. The total metallic-impurity content appears to have less effect on the ductility of annealed chromium. Good bend ductility in wrought chromium can be obtained at relatively high oxygen levels. For example, the sample from Ingot R38-3, containing 190 ppm of oxygen, showed an average bend-transition temperature of 0°C. The effects of carbon, nitrogen, and sulfur are not apparent from these data on unalloyed chromium.

TABLE VI. Composition and bend-test data for representative iodide chromium sheet samples prepared using the standard fabrication procedure

Ingot	Composition, wt %						Fabricated bend ductility				Annealed bend ductility			
	O	N	C	S	Total metallics	Total purity	Vickers hardness	Transition range, °C		Avg transition temp, °C	Vickers hardness	Transition range, °C		Avg transition temp, °C
								Highest brittle	Lowest ductile			Highest brittle	Lowest ductile	
R38-3	0.0190*	<0.0050*	0.002*	0.015*	0.0100*	99.95	222	-25	-25	0	140	150	150	150
R43-1	0.0140*	<0.0003	—	—	0.0112	<99.97	211	-25	-50	-25	—	—	—	—
R49-1	0.0073	0.0010	0.002*	0.002*	0.020*	99.97	215	-25	0	0	—	—	—	—
R40-2	0.0060	<0.0020	—	—	0.020*	<99.97	209	-25	-50	-25	134	200	175	175-200
R40-1	0.0100	0.0030	0.001	—	0.020*	<99.97	213	25	0	0	138	200	225	215
R41-1	0.0074	<0.0007	0.007	—	0.021*	<99.97	205	0	-25	0	—	—	—	—
R47-1	—	—	0.005	—	0.022	<99.97	208	25	-25	0	—	—	—	—
R46-1	—	—	0.007	0.009*	0.036	<99.95	223	0	0	25	—	—	—	—
R35-1	0.0160	0.0050	—	—	0.044	<99.93	218	25	0	25	—	—	—	—
R48-1	—	—	0.005	—	0.054	<99.94	263	25	0	0-125	—	—	—	—
R37-1	0.0042*	0.0005*	—	—	0.059	<99.94	221	50	0	25	—	—	—	—
R36-1	0.0042*	0.0013*	0.002	0.011*	0.118	99.86	218	125	50	100	124	175	175	175
R27-1	0.0013*	0.0004*	0.002	0.005	0.460	99.53	236	75	25	50	—	—	—	—
R34-1	—	—	—	—	0.512	<99.49	226	100	0	75	129	200	200	200

* Analyses were taken from as-deposited chromium from which these ingots were prepared.

TABLE VII. Bend-test data on chromium-plus-impurity base alloys

Ingot	Alloyed Composition*, wt %	Fabricated condition				Annealed condition			
		Vickers hardness	Bend ductility			Vickers hardness	Bend ductility		
			Transition range, °C		Avg transition temp, °C		Transition range, °C		Avg transition temp, °C
			Highest brittle	Lowest ductile			Highest brittle	Lowest ductile	
R40-1	Unalloyed	213	25	0	0	138	200	225	212
R40-2	Unalloyed	209	-25	-50	-25	134	200	175	187
R40-X1	0.012 O	204	0	-50	-20	147	200	200	200
R40-X2	0.051 O	210	-50	-50	-37	152	225	250	237
R40-X3	0.075 O	207	-50	-50	-16	154	300	300	300
R40-X4	0.180 O	212	-50	-25	-30	156	275	300	287
R40-C5	0.011 C	214	50	50	60	—	—	—	—
R40-C1	0.016 C	232	50	25	55	161	200	200	200
R40-F1	0.016 Fe	216	-25	-25	-25	138	—	—	—
R40-F2	0.058 Fe	204	-25	0	0	131	—	—	—
R40-F3	0.117 Fe	214	-25	0	0	132	—	—	—
R40-F4	0.246 Fe	219	-25	-50	-25	133	—	—	—
R40-N1	0.01† Ni	214	25	25	25	—	—	—	—
R40-N2	0.055 Ni	222	0	-25	0	127	—	—	—
R40-N3	0.101 Ni	224	75	25	50	129	—	—	—
R40-N4	0.199 Ni	241	50	50	55	151	—	—	—
R40-S1	0.03 Si	206	25	0	15	144	150	150	150
R40-S2	0.07 Si	217	-50	-25	-40	141	150	175	163
R40-S3	0.07 Si	217	-50	-25	-25	144	175	200	187
R40-S4	0.15 Si	243	0	0	15	145	50	100	75
R38-3	Unalloyed	222	-25	-25	0	140	150	25	110
R38-W1	0.05† W	—	0	0	0	156	—	—	—
R38-W2	0.2† W	—	0	0	0	148	—	—	—

* See Table V for more complete analytical data on these alloys.

† Nominal compositions; all others by analysis.

The data of Table VII (chromium-plus-impurity alloys) have been plotted graphically in Fig. 14 to facilitate their interpretation. From Table VII and Fig. 14, it appears that binary additions of oxygen (up through 0.18%), iron (up through 0.246%), tungsten (nominally, up through 0.2%), and silicon (up through 0.15%) have no significant effect on the average bend-transition temperature of wrought chromium. At levels of 0.1% and above, nickel increases the bend-transition temperature by about 50°C.

Bend data on the chromium-carbon alloys show that carbon has a greater effect on ductility than any single metallic impurity. The presence of as little as 0.011% carbon results in about the same increase in transition temperature as does about 0.2% nickel for sheet tested in the as-fabricated condition.

The nitrogen level in all unalloyed chromium samples was usually less than 50 ppm, and variations in nitrogen content around this concentration could not be correlated with any properties of the metal. However, results of bend tests on a few samples of arc-melted electrolytic chromium suggest that nitrogen in the range from around 50 to 300 ppm has relatively little effect on ductility.

It was not possible to roll the ingots with sulfur additions (0.02 and 0.22% nominal), so they could

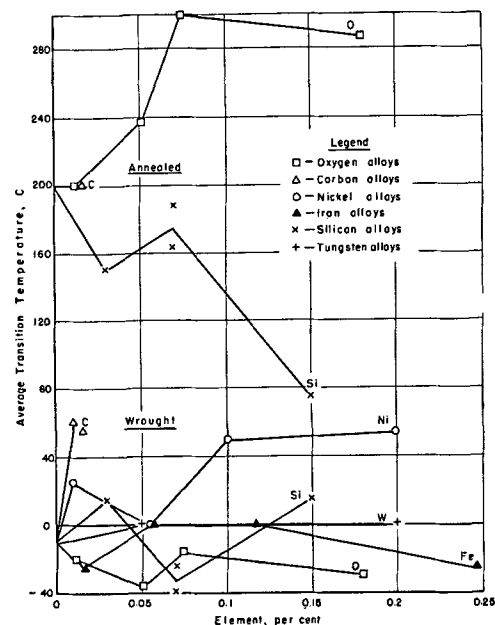


FIG. 14. Effect of various alloy additions on the bend-transition temperature of wrought and annealed iodide-chromium sheet.

not be bend tested. However, the extremely deleterious effect of sulfur on fabricability suggests that small amounts of sulfur may also be damaging to bend ductility.

Bend-test data on recrystallized samples of the oxygen alloys showed that the addition of 0.2% oxygen raised the transition temperature by about 100°C. This is in contrast to bend data on these same alloys in the wrought condition, where the oxygen content did not appear related to the transition temperature. Carbon in amounts up to 0.016% has no effect on the transition temperature of annealed chromium, in contrast to its adverse effect on the bend transition of wrought chromium. On the other hand, presence of silicon is beneficial to the ductility of annealed chromium, although it has little effect in wrought chromium. The 0.15% silicon alloy, in the annealed condition, showed the lowest average transition temperature (75°C) obtained in all of the bend tests on the recrystallized alloyed chromium samples.

SUMMARY

This investigation has shown that both the purity and the physical condition of chromium are important factors in determining the degree of ductility at temperatures near room temperature.

By fabrication in a temperature range just below the recrystallization temperature, chromium sheet having an average ductile-to-brittle bend transition at temperatures well below room temperature can be obtained. When arc-melted iodide chromium was used, the lowest bend-transition temperature of -25°C was found for metal which contained 0.006% oxygen, less than 0.002% nitrogen, and a total of approximately 0.02% metallic elements. Carbon and sulfur analyses were not available for these specimens, but should run well below 0.015 and 0.02%, respectively. Increasing amounts of nickel (up to 0.1%) or molybdenum (up to 0.5%) above the levels normally found for these elements in the iodide chromium generally increased the bend-transition temperature. In this respect, the effects of the individual metallic contaminants present in unalloyed iodide chromium could be taken to be equivalent and additive.

Work with a number of impurity-addition alloys showed that iron (up through 0.25%), silicon (up through 0.15%), and tungsten (up through 0.2%, nominal) have no significant effect on the average bend-transition temperature of wrought chromium sheet. At levels of 0.1% and above, nickel increases the bend-transition temperature to about 50°C. Chromium containing nickel in amounts above 0.2% cannot be fabricated to sound sheet by using the procedures devised in this research.

Oxygen in amounts from 0.006 to 0.37% does not have any significant effect on the bend-transition temperature of wrought chromium. Similarly, changes in nitrogen content from 0.001 to 0.032%

have no apparent effect on bend ductility. On the other hand, carbon and sulfur are both very detrimental to the hot and cold ductility of chromium. Chromium containing above about 0.015% carbon or 0.02% of sulfur cannot be rolled to sound strip. Although some small tolerance for both of these elements is indicated, chromium containing carbon in excess of 0.01% or sulfur in excess of 0.015% will not be bend ductile at room temperature.

Wrought chromium sheet exhibits marked anisotropy in its bend properties. Samples bent around an axis parallel to the rolling direction show ductile-to-brittle transition temperatures on the order of 200°C higher than do samples bent around an axis perpendicular to their rolling direction. Recrystallization tends to overcome the bend anisotropy, but invariably results in an increase in the average bend-transition temperature over that obtained on samples cut longitudinally from the wrought sheet.

Chromium in the wrought condition is extremely sensitive to notch effects. Minute surface irregularities produced by normal machine grinding or milling the edges of bend-test samples, in directions parallel to or transverse to the rolling direction, increase the transition temperature by about 50°C.

Several wrought-sheet tensile samples from material which had bend-transition temperatures well below room temperature all showed brittle fractures at stresses of 62,000 psi or less. The reason for this brittle behavior is not understood clearly, although, in view of the good bend ductility, it seems likely that this behavior is associated with a surface effect derived from machine grinding of the samples.

ACKNOWLEDGMENTS

The authors are grateful to the Air Research and Development Command of the U. S. Air Force at Wright-Patterson Air Force Base, Ohio, for permission to publish the results of this work which was done at Battelle Memorial Institute under their sponsorship. They also wish to acknowledge the assistance of I. E. Campbell and J. M. Blocher, Jr., who directed the research on the preparation of iodide chromium, and of M. W. Mallett, C. B. Griffith, W. M. Henry, E. K. Blosser, H. R. Harris, D. P. Leiter, Jr., and F. E. Huber, Jr., of the Battelle Analytical Laboratory Staff for their invaluable contributions to this work.

Any discussion of this paper will appear in a Discussion Section to be published in the December 1955 JOURNAL.

REFERENCES

1. W. KROLL, *Z. anorg. u. allgem. Chem.*, **226**, 23 (1935-6).
2. W. KROLL, W. F. HERGERT, AND L. A. YERKES, *This Journal*, **97**, 258 (1950).
3. E. S. GREINER, *Trans. Am. Inst. Mining Met. Engrs.*, **188**, (6), 891 (1950).

4. H. B. GOODWIN, R. A. GILBERT, C. M. SCHWARTZ, AND C. T. GREENIDGE, *This Journal*, **100**, 152 (1953).
5. E. T. HAYES, WADC Tech. Rept. 52-54, Wright-Patterson Air Force Base, Ohio (March 1952).
6. H. L. GILBERT, H. A. JOHANSEN, AND R. G. NELSON, U. S. Bur. Mines, Rept. Invest. No. 4905 (September 1952).
7. H. L. GILBERT, H. A. JOHANSEN, AND R. G. NELSON, *Trans. Am. Inst. Mining Met. Engrs.*, **5**, 63 (1953).
8. A. H. SULLY, E. A. BRANDES, AND K. W. MITCHELL, *J. Inst. Metals*, **81**, 585 (1953).
9. F. ADCOCK, *J. Iron Steel Inst. (London)*, **115**, 369 (1927).
10. A. BRENNER, P. BURKHEAD, AND C. JENNINGS, *J. Research Natl. Bur. Standards*, **40**, No. 1, R. P. 1854, 31 (1948).
11. A. H. SULLY, E. H. BRANDES, AND A. G. PROVAN, *J. Inst. Metals*, **81**, 569 (1953).
12. R. I. JAFFEE, L. W. EASTWOOD, D. J. MAYKUTH, R. M. GOLDHOFF, H. R. OGDEN, J. W. HALLADAY, AND J. G. KURA, AF Tech. Rept. No. 6515, Part 1, Wright-Patterson Air Force Base, Ohio (June 1951).
13. E. J. RIPLING, *ASTM Bull.*, No. 186, 37 (December 1952).

Preparation of Titanium by Fluoride Electrolysis¹

M. A. STEINBERG, S. S. CARLTON, M. E. SIBERT, AND E. WAINER

Horizons Incorporated, Cleveland, Ohio

ABSTRACT

Preparation of commercially pure titanium metal powder by electrolysis of K_2TiF_6 in molten NaCl is described. The process is carried out under an inert atmosphere in an all-graphite cell. Operating conditions of the electrolysis and their effect upon the metal so produced are discussed. Preparation of the K_2TiF_6 and the electrolytic procedure are completely described. The process is capable of producing metal of high purity which may be consolidated and fabricated by standard techniques as applied to metal powders. The metal is recovered by aqueous washing techniques. It may be prepared either as coarsely crystalline metal or as coarse thin metal flakes.

INTRODUCTION

One of the more conspicuous current research efforts is the attempt to develop new processes for production of titanium metal in a more economical and straightforward fashion. A large amount of this effort is concerned with electrochemical processes. One such development is described in this paper.

Three general approaches have been made to the extractive metallurgy of titanium: (a) thermal reduction by active metals; (b) thermal dissociation; and (c) electrolytic processes. The first of these approaches, as exemplified by the Kroll process, is limited economically by the cost of magnesium metal and $TiCl_4$ and the fact that such processes are, of necessity, batch processes. The second approach is even more severely limited by costs of materials and equipment. Notable in this respect is the Van-Arkel deBoer hot wire dissociation of the tetraiodide. Although considerable effort has been expended on refinements and improvements of existing methods, a very large portion of the research effort has gone into development of electrolytic processes. These offer prospects of inexpensive materials and continuous or semicontinuous operation.

Consideration of possible electrolytic methods and the properties of titanium metal and its salts essentially eliminates all but fused salt methods. Titanium is among those metals which are highly oxyphilic in character. Where oxygen is available, it forms an oxytitanium ion in preference to a simple metal ion. Efforts to isolate the metal from aqueous or other oxygen-containing media have produced only titanium oxides.

This particular process concerns the electrolysis of potassium fluotitanate in a melt of an alkali or

alkaline earth halide. This salt of titanium is employed as the source electrolyte because it is one of the few ionic titanium salts which is stable at elevated temperature and can be obtained in an anhydrous form. Electrolysis is carried out in special cells providing an inert atmosphere to prevent oxidation of the source electrolyte and deposited titanium metal. Metal is obtained as coarse crystalline granules or as thin flakes up to $1\frac{1}{2}$ in. long. Cathode deposits are recovered by aqueous techniques and consolidated by conventional powder metallurgical methods.

Ample reviews of the background of the electrolytic preparation of titanium have already been given (1-5). Of specific interest with respect to this process are previous attempts to produce pure titanium from K_2TiF_6 .

Deposition of bright titanium from an electrolytic bath of K_2TiF_6 , Na_2SO_4 , and H_2SO_4 has been reported (6). This claim is quite doubtful, however. Electrolysis of K_2TiF_6 in a fused NaCl and KCl medium gave cathode deposits consisting essentially of reduced oxides, with only sparse evidence of a few metallic particles (7). No protective atmosphere was employed. K_2TiF_6 has been electrolyzed in a mixture of NaCl and KCl, yielding dendritic titanium crystals of undisclosed purity (8). Electrolysis was carried out at 850°C under 30-100 amp/dm² current density. This cell employed an inert atmosphere. Similar results were obtained using $TiCl_3$ and TiF_3 as the source electrolyte. Similar deposition was reported for LiCl-KCl- K_2TiF_6 at 700°C (9). This work was done in an admittedly contaminated glass system, however. A patent has been granted utilizing a bath of $TiCl_4$ in an alkali chloride, alkaline earth chloride, or mixture thereof (10). The cell is of a closed type operating at 675°C, and $TiCl_4$ is continuously added to the electrolyte. Crystalline titanium was deposited from a bath of $TiCl_3$ in

¹ Manuscript received July 6, 1954. This paper was prepared for delivery before the Chicago Meeting, May 2 to 6, 1954. It is based on a portion of the work carried out by Horizons Incorporated for the Office of Naval Research under Contract Numbers Nonr-394 (00) and 394 (01).

KCl-LiCl at 550°C (11) under hydrogen, at 1–2 v and about 6 amp/dm².

Equipment

Experimental work was carried out in inert atmosphere cells of graphite interior construction. Graphite crucibles also served as anodes. A graphite resistance element surrounding the crucible served as a heating source. The unit was essentially closed, with only a cathode entrance and charging opening being provided in the removable head. Purified argon gas was used as a cell atmosphere. Each cell took a charge of 5 lb of salts and produced up to 100 g of titanium per run. Cells of this type have been described in detail in previous papers (5, 12).

Preparation of High Purity K₂TiF₆

K₂TiF₆ may be prepared from a good grade of TiO₂ by dissolution in HF, followed by precipitation with pure K₂CO₃. Such material is subsequently water recrystallized by the following procedure.

In most cases a commercial grade of K₂TiF₆ has been obtained and only the purification step carried out.

The crude K₂TiF₆ from either source was dissolved in about 1½ gal of water/lb of K₂TiF₆ at 90–100°C with agitation using rubber coated equipment. The solution was then filtered through Nibri-cel into a neoprene lined trough equipped with a cooling jacket.

After cooling and crystallization took place, the crystals were filtered in a polyethylene funnel or suitable filter press and the mother liquor recycled. The product, K₂TiF₆, was then vacuum dried at 85–90°C under 2–5 cm pressure for 24–30 hr and stored in airtight containers.

This procedure enables the removal of residual TiO₂, iron, aluminum, and other minor metallic impurities. The material, as charged to the cell, contains <0.01% H₂O and <0.01% insolubles (TiO₂).

Decomposition Voltage of K₂TiF₆

An attempt was made to determine the decomposition voltage of K₂TiF₆. A small 100 g electrolytic cell coupled with an accurate current-voltage control and recorder was used for this work. Graphite electrodes were used. Voltage readings were measured as a function of current density. Extrapolation of the straight line portion of the curve to zero current gave an approximate E_D value, the exact point being determined by the point of inflection.

Results indicate a value of 1.8–2.0 at 800°C which has been experimentally verified. This curve is shown in Fig. 1.

Electrolytic Procedure

This process is essentially a straightforward fused salt electrolysis, but the elements of bath purity and exclusion of oxygen and nitrogen from both the salt bath and atmosphere determine the relative success of the process with respect to the type of metal produced. Operating variables affect the efficiency and recovery to a great extent as will be shown later.

The most satisfactory melt has been found to be a mixture of K₂TiF₆ in NaCl, and most of the work has involved this system. A typical run is carried out as follows.

A clean cell is thoroughly purged with argon gas with the crucible containing the NaCl in position. If the cell is in any manner contaminated, it is first hot evacuated until a pressure of 10–25μ is obtained and all residues are removed. This is followed by a flushing cycle with argon gas.

NaCl is then melted at 850–900°C. After a short period to allow for volatilization of any moisture, K₂TiF₆ is charged and melted.

A pre-electrolysis is then carried out by low voltage electrolysis under the decomposition voltage of K₂TiF₆. This step removes residual moisture, iron, and perhaps other impurities. The procedure requires 5–20 amp-hr/lb of bath and is judged by a series of voltage rises which take place. When the voltage reaches 2.5–3.0 v, the procedure is terminated. Steel or graphite cathodes may be employed, but steel is preferred. The small deposits obtained are discarded. They contain appreciable amounts of iron and oxygen.

The electrolysis proper is carried out using a steel cathode supported by a steel or, preferably, a nickel shaft covered with a graphite tube. The nickel and graphite minimize corrosion due to chlorine gas.

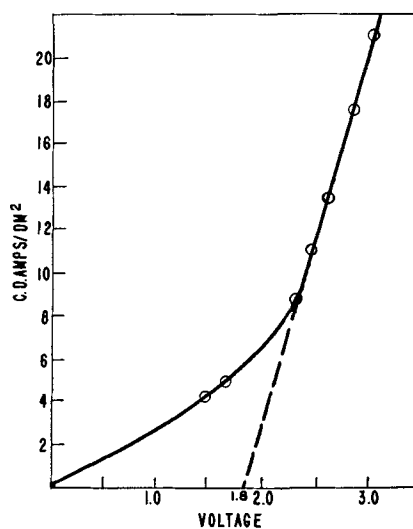


FIG. 1. Decomposition potential of K₂TiF₆, temp, 800°C, 4 runs, average value, 1.8 v.

Cathodes of cylindrical or truncated cone shape are generally employed. The steel cathode is lowered with a small voltage on it to prevent any solution of the steel in the melt. The bath temperature meanwhile is lowered to 740°–760°C. Electrolysis is then initiated at 4–6 v and 200 amp, equivalent to 400–550 amp/dm². Generally, 1 or 2 polarizations are encountered during a run requiring about a 25% cut-back in current. Electrolysis is carried out for 240–260 amp-hr on this particular cell. Chlorine

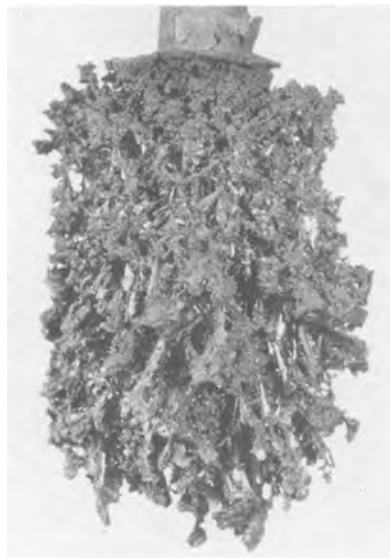


FIG. 2. Typical titanium flake cathode deposit obtained from electrolysis of K_2TiF_6 .

gas is evolved throughout the process. The end of the run is ascertained by a voltage rise of 0.2–0.5 v when the titanium has been essentially exhausted. If the run is prolonged, sodium is produced, complicating recovery of the titanium metal.

The deposit is withdrawn from the melt under low voltage and allowed to cool either above the melt or in a sealed water-cooled chamber which may be attached to the cell.

When below 200°C, the deposit is removed. Such deposits appear as ragged salt metal agglomerates, the outer layer consisting of very coarse thin titanium flakes. Deposits contain from 40–60% metal. The interior of the deposit is coarsely crystalline metal embedded in a salt matrix. The larger flake material is essentially salt-free. A typical deposit is illustrated in Fig. 2.

The deposit is chipped from the cathode, crushed to about 20 mesh, and recovered by washing in warm water. It is then filtered and oven-dried at 40°–50°C.

Several washing steps are required to remove all salts from the metal deposits. Since the deposits contain some lower titanium halides, pH control is necessary to prevent precipitation of titanium hydrates which would seriously contaminate the metal powder. A final acetone or alcohol rinse is generally used to facilitate drying.

Operating and recovery data for several typical runs are given in Table I.

TABLE I. *Electrolysis of K_2TiF_6 in NaCl*

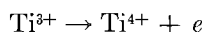
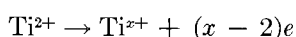
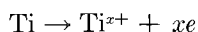
Run No.	Bath composition	Temp	E^*	I	Amp-hr of pre-electrolysis	Total amp-hr	Yield	Current efficiency	Remarks
		°C	v	amp			%	%	
61-68	78% NaCl 22% K_2TiF_6	715	—	150	44	330	46.2	26.9	Coarse crystals
61-73	83% NaCl 17% K_2TiF_6	730	—	200	39	295	87.5	45.0	
61-85	75% NaCl 25% K_2TiF_6	740	6.0	150	162	465	53.8	22.4	Very coarse crystals
				200					
				100					
61-109	84% NaCl 16% K_2TiF_6	755	8.0	200	92	255	87.0	51	Some crystals and platelets
				150					
				100					
61-113	85% NaCl 15% K_2TiF_6	725	5.6	100	52	315	76	37	Coarse platelets. Used residual salt from above run.
				100					
				100					
61-116	84% NaCl 16% K_2TiF_6	740	7.5	200	45	445	—	35	—
				150					
				100					
61-120	84% NaCl 16% K_2TiF_6	755	7.4	200	49	235	89	58	—
				150					
				100					
61-124	85% NaCl 15% K_2TiF_6	750	7.8	250	61	245	82	51	Very coarse platelets
				150					
				100					
61-127	84% NaCl 16% K_2TiF_6	800	5.8	100	33	243	59	37	Used residual salt from above run.
				100					
				100					

* Includes resistance of cell to crucible anode.

PROCESS VARIABLES

Aside from the purity of the salt bath and requirement of an inert atmosphere, process variables are also of considerable importance to the efficient operation of the fluoride process. These include K_2TiF_6 concentration, temperature, voltage, current density, and bath composition. These factors are discussed individually below.

K_2TiF_6 concentration.—The concentration of K_2TiF_6 in the electrolyte is one of the major contributing factors to the efficiency of the process. The amount of K_2TiF_6 present seems to determine the extent to which back reactions can interfere with deposition of titanium as metal. This may be due to the Ti-F ions, Ti^{x+} ions, or the simple F^- ion. Such reactions must fall into three general types.



The optimum concentration for the cell used in this work has been empirically determined as 15–17 wt %. This is equivalent to a molar ratio of 1:20–23:: K_2TiF_6 :NaCl.

The effect of higher concentration on efficiency of the process is apparent from the data in Table I (runs 61–68 and 61–85), where a 22 and 25 % concentration was used.

Electrolyte composition.—A survey of possible electrolytes was made to determine the most suitable bath composition. This included principally alkali and alkaline earth chlorides and fluorides, since a number of these could satisfy the requirement for an anhydrous oxygen-free salt medium. Initially pure K_2TiF_6 was subjected to electrolysis, but current efficiency was extremely poor as would be expected from the behavior of the K_2TiF_6 concentration variable.

Pure sodium chloride is the most satisfactory diluent from the standpoint of purity, availability, and behavior on electrolysis. This has been employed as the electrolyte in all work reported.

Alkaline earth halides are generally unsatisfactory due to the difficulty in maintaining them in anhydrous form. These are, in general, hydrates and must be vacuum dried for effective use in a process of this type. Fluorides are generally not suitable due to their relative insolubility and resultant difficulty of removal from the metal deposits. Other alkali chlorides may be used if in sufficiently pure and anhydrous form, but there is no apparent advantage to justify the higher cost of such materials over NaCl.

Various eutectic mixtures have been tried but, again, these offer no significant advantages.

Temperature.—The prime effect of temperature change is on the characteristics of the metal crystals produced. This is primarily governed by the transformation temperature of titanium (882°C). Normally an HCP structure is observed, but, above the transformation temperature, a BCC structure results. In this electrolytic procedure, electrolysis is usually carried out at 740°–760°C, whereby a hexagonal structure results. Deposits contain large hexagonal platelets and smaller hexagonal crystallites. If the temperature of the bath is greater than 830°–840°C, these large platelets do not form at all and the deposits consist essentially of a distorted cubic type of crystal. The BCC structure is not stable at normal temperatures and crystals invert to an HCP form. The fact that the change in crystal type occurs at less than 882°C is indicative that cathodes run hotter than the salt bath itself.

At bath temperatures above 800°C the current efficiency falls off, due in part to loss of titanium from the bath by $TiCl_4$ formation. At temperatures below 700°C the bath is too viscous for efficient operation. Effects of temperature on operation of the cell are illustrated by Fig. 3.

Time of electrolysis.—The time required for completion of a run is determined primarily by the starting current. This is customarily adjusted to give a current density of 400–600 amp/dm². A run on the 5 lb cell requires about 260 amp-hr to complete, or about 90 min time. Normally, 1–3 polarizations are encountered in a given run, necessitating periodic reduction in the current passed.

As would be anticipated, the least pure metal is deposited first. The average metal hardness thus decreases somewhat with the length of a given run.

Voltage.—Applied voltage is important only insofar as it is above the decomposition voltage of K_2TiF_6 , about 1.8 v. With overvoltage and drop through the cell considered, a minimum voltage of about 2.6 is required to produce titanium metal.

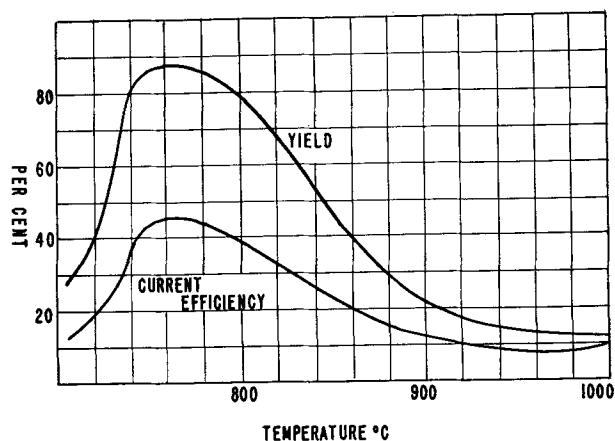
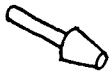



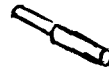





FIG. 3. Effect of temperature on efficiency and yield

TABLE II. Current efficiency vs. cathode shape (current density)

Run No.	Cathode shape	Cathode dimensions	Wt ratio NaCl to K ₂ TiF ₆	Temp, °C	Amp range	Avg current density in amp/dm ²	Amp-hr	% Current efficiency
64-195		Trunc. cone, 1/2 in. dia. × 1 in. dia. × 2 in. long	84-16	750	200-150	545-415	260	52
64-177		Bar, 1 in. × 3 in. × 1/8 in.	84-16	750	200-150	450-340	256	47
75-113		Inverse of 64-195	84-16	750	200-150	545-415	260	46
64-185		Disk, 1/4 in. × 2 1/2 in. on rod 1/2 in. × 2 1/4 in.	84-16	750	200-150	200-150	260	44
83-9		Rod 1/2 in. dia. × 2 1/2 in. long	84-16	750	200-150	750-560	260	43
64-183		Inverse of 64-185	84-16	750	200-150	200-150	260	39
64-187		Cylinder, 3 in. dia. × 3 in. long	84-16	750	150	57	181	34
83-11		Cylinder, 1 1/2 in. dia. × 2 3/4 in. long; hole 1/2 in. dia. × 1/4 in. deep	84-16	750	200-150	190-140	267	30

All cathodes are steel on steel rods with graphite sleeves. Where more than one run was made on any type (as is the case with all), efficiencies reported are the highest of the set.

Optimum C.D. seems to range from 200-700 amp/dm² and is best from 350-550.

TABLE III. Chemical analysis

Sample No.	Total Ti	Carbon	Nitrogen
	%	%	%
64-183	99.8	0.102	—
64-187	99.6	0.066	—
64-191	99.8	0.06	—
75-74	99.5	—	0.004
75-80	99.5	—	0.002
75-110	99.6	0.13	0.017
75-137	99.7	0.03	—

Very high voltages of the order of 10 v are undesirable because some concurrent production of sodium metal is obtained. The decomposition voltage of NaCl is 3.15 v at 750°C, and there is no interference at nominal voltages if the bath titanium concentration is above 0.5%.

Current density and cathode geometry.—The starting current densities used varied from 50 to 750 amp/dm². There is no reliable means of determining current density once deposition starts. Also, current density is not uniform over a given cathode but depends on the particular cathode shape and resistive path through the salt bath.

A variety of cathode types has been employed consisting of cylinders, cones, disks, and strips. These were all run using uniform currents, voltages, temperatures, and bath compositions. Thus, a large

range of current density resulted. It was found that higher current densities resulted in higher current efficiencies. Optimum current density seems to be in the range of 350-550 amp/dm². This is evident from Table II.

Cathode geometry is also a factor in current efficiency apart from the current density. Table II shows that the inverted truncated cone is superior to all types. An upright truncated cone did not behave as well under like conditions, presumably due to an inferior current density distribution. Strip cathodes, small cylinders, and a cylinder with disk above it behaved essentially the same. Larger cylinders gave decidedly inferior efficiencies at low current densities. Even under higher currents they do not give results equivalent to the cone cathode.

METAL EVALUATION

A complete evaluation of the electrolytic titanium produced accompanied the process development.

Analysis.—Chemical analyses for titanium, carbon, and nitrogen were carried out for a large number of electrolytic titanium samples (see Table III).

Total titanium values were obtained by the Jones reductor method whereby tetravalent titanium in solution is reduced by zinc to the trivalent state and then back titrated with a ferric sulfate solution. Nitrogen was checked by the standard Micro-

Kjeldahl method, and carbon values were obtained by combustion in oxygen at 2400°F. A standard Leco Carbon Determinator was employed.

Oxygen data are not included since work to date has been done with the HCl volatilization method which has not been found to be reliable in the case of titanium. Oxygen contents are indicated to range from 0.05 to 0.10%, however. This is verified by the hardness data.

Spectrographic analyses were run on the various types of electrolytic titanium crystals. These include large flakes, coarse crystals, and impure fines which resulted from improperly controlled runs and are listed as Table IV. The only significant impurities in coarse and flake materials are iron and zirconium. Most of the iron can be eliminated by careful control in the electrolytic and recovery steps. In the case of the fine crystals, no purification electrolysis was included in the procedure accounting for the high values for Fe, Al, Mo, and V.

Screen analysis.—A large number of samples were subjected to particle size analysis. Most runs average 60–80% + 80 mesh with only 5% or less –325 mesh. Any impurities drastically reduce average particle size. Also, indications are that very high or very low current densities (>750 < 300 amp/dm²) tend to reduce particle size. Typical analyses are given in Table V.

Physical testing and metallography.—Electrolytic titanium produced by the fluoride process was continuously consolidated and arc melted to produce small ingots (usually 10 g) for physical testing. The hardness of such specimens ranges from Brinell 110–160. This corresponds to the best commercial sponge metal produced.

Hardness measurements were also carried out on a series of large flake crystals using a Tukon Hardness Tester with a 25 g load. Vickers hardness numbers of 50–70 VHN have been obtained with an average of about 55. This value is in line with values obtained for iodide titanium and is indicative of very low oxygen, nitrogen, and carbon contents.

Arc melted samples were cold rolled to varying degrees of reduction in order to determine the workability and effects on hardness and tensile strength. Edge cracking is generally first detected at 50–60% reduction. Hardness and tensile strength increase is comparable to that obtained with commercial titanium (Fig. 4). Annealing, of course, alters these curves drastically.

Some arc melted ingots were examined metallographically. Fig. 5 illustrates the typical basket weave structure of arc melted, rapidly cooled titanium. Fig. 6 is a twice arc melted specimen showing large coarse as-cast grains. Fig. 7 is a typical Widmanstätten structure with some carbide evident

TABLE IV. Spectrographic analysis (in per cent)

Element	Flake titanium +10 mesh	Coarse crystals -10, +80 mesh	Fine crystals -80, +325 mesh
Ti.....	Major	Major	Major
Si.....	0.001	0.002	0.001
Fe.....	0.005	0.05	0.15
Mg.....	0.001*	0.001*	0.001*
Mn.....	0.001*	0.001*	0.001*
Al.....	0.007	0.007	0.03
Mo.....	0.001*	0.001*	0.14
V.....	0.001*	0.001*	0.20
Cu.....	0.005*	0.0005	0.0008
Zr.....	0.01	0.01	0.01
Ni.....	0.001*	0.001	0.02
Pb.....	0.001*	0.001*	0.001*
Ca.....	0.002*	0.002*	0.002*
Cr.....	—	0.001*	0.001*
Total.....	0.0315%	0.0785%	0.5678%
Ratio.....	1	2.5	18

Trace amounts of Co, Cb, Ta, W, Bi, Zn.

* Less than.

TABLE V. Particle size analysis

Sample No.	+35	+80 -35	+100 -80	+150 -100	+200 -150	+325 -200	-325
	%	%	%	%	%	%	%
64-191	42.8	30.6	8.2	8.9	4.6	3.6	1.3
75-130	23.4	33.8	9.2	12.2	8.6	7.8	5.0
83-11	31.8	36.3	9.1	10.6	6.1	4.5	1.5
64-179	21.1	48.5	10.3	10.0	5.7	3.2	1.2

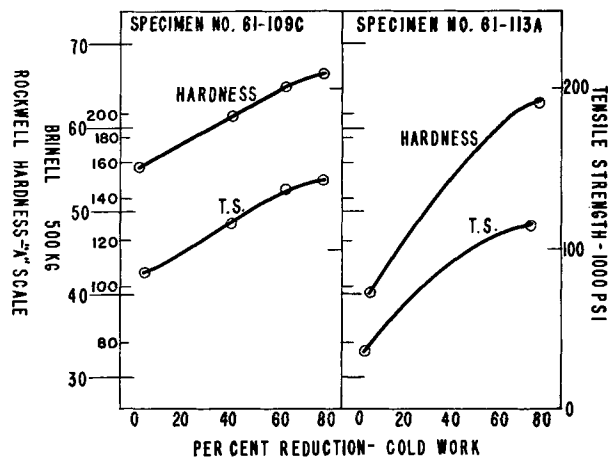


FIG. 4. Hardness and tensile strength as a function of cold reduction for two specimens of electrolytically produced titanium.

at the grain boundaries and dispersed in the structure. Fig. 8–11 illustrate the effect of annealing for various times on a 90% cold reduced ingot.

A preliminary analysis of the mechanism of this crystal growth has been done by metallographic and x-ray methods. These large platelets do not seem to have any preferential direction of growth in regard to lines of current flow. Thus, this growth must be a

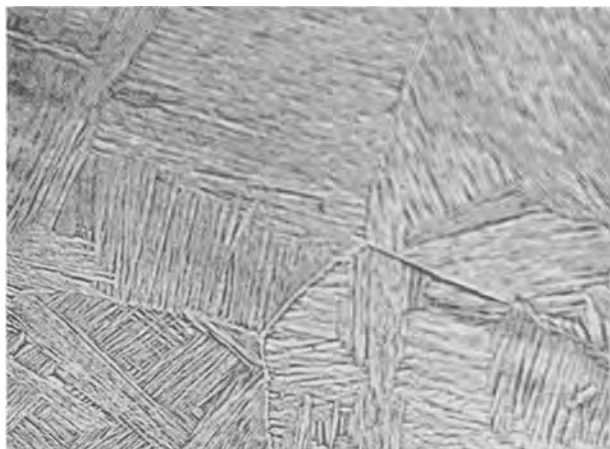


FIG. 5. Electrolytic arc melted as-cast titanium structure showing basket-weave pattern.



FIG. 8. Cold rolled and annealed structure of electrolytic titanium, 90% reduction, top view.



FIG. 6. Twice arc melted electrolytic titanium as-cast structure showing large coarse grains of high purity metal.

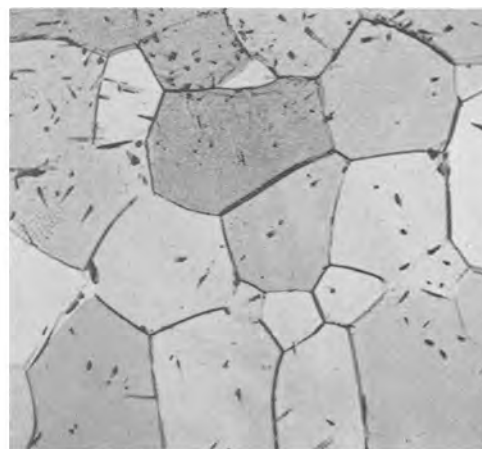


FIG. 9. Cold rolled and annealed structure of electrolytic titanium, 90% reduction, annealed at 800°C 15 min, air-cooled.



FIG. 7. Arc melted as-cast titanium surface, Widmanstatten structure. Electrolytically polished and etched.



FIG. 10. Cold rolled and annealed structure of electrolytic titanium, 90% reduction, annealed at 800°C, 30 min, air-cooled.

function of the concentration gradient of Ti ions and probably also of the current density at a particular growth point.

Growth of an individual crystal, however, is determined by the specific habits of titanium. Fig.

12 illustrates some typical recovered plate crystals and the two general types found. One type has a ridge down the center parallel to the plates. In the other case, the ridge is the trace of a twin plane and

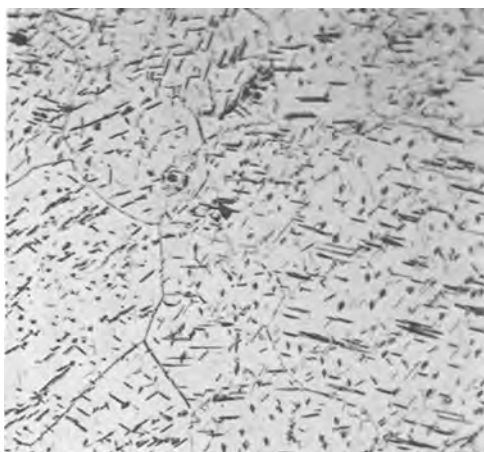


FIG. 11. Cold rolled and annealed structure of electrolytic titanium, 90% reduction, annealed at 800°C in argon atmosphere 2 hr, air-cooled.

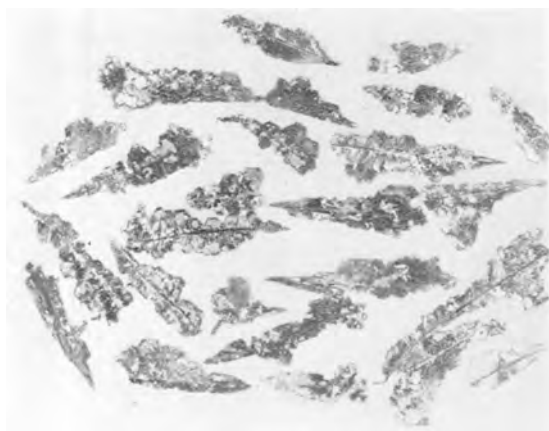


FIG. 12. Leaf-like flakes of electrolytic titanium metal showing characteristic shapes obtained. Growth twins and ribs are shown in some of the crystals.

the crystals grow as a twin with a specific angle between the two principal surfaces. All of these crystals form with their 0001 surfaces exposed, so there is no evidence of slip bands; only twins would be in evidence if deformation occurs by basal plane slip only.

The direction of crystal growth was determined by x-ray methods using Laue transmission and back reflection techniques. Molybdenum radiation at 40 kw and 20 ma was used with 2 hr exposures.

The crystals grow so that their wide surfaces are the 0001 planes; these are the minimum growth surfaces. The direction of growth from the orientation of crystals in the x-ray holder is of necessity a 2110 direction, the direction of most rapid growth.

Fig. 13 and 14 show that the large surfaces are basal plane surfaces. Growth of the layers and stacking of basal planes is clearly evident. The crystals must grow by having atoms from the electrolyte attach themselves to exposed corners in the electrolyte such that the basal plane is always

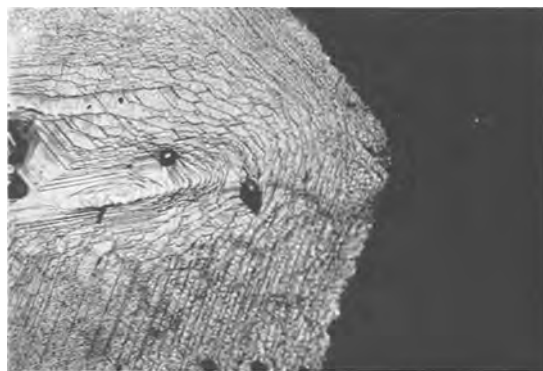


FIG. 13. Photomicrograph of electrolytic titanium crystal showing layer structure.

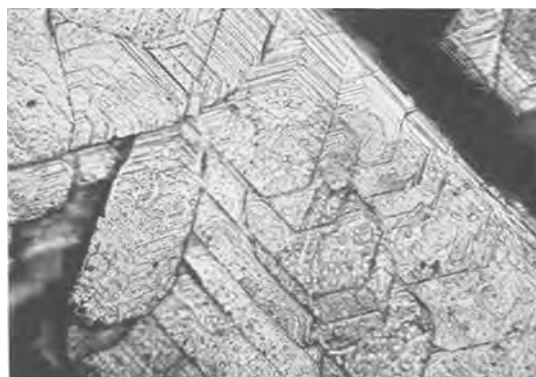


FIG. 14. Enlarged view of electrolytic titanium crystal showing well-defined layer structure and growth lines.

the surface plane. Fig. 14 illustrates the growth lines and layer structure.

DISCUSSION

A fused salt electrolytic process has been developed which is capable of yielding titanium metal of purity equivalent to commercial titanium. The process entails an electrolysis of a melt of K_2TiF_6 and NaCl under a protective inert atmosphere in closed cells. Major criteria for successful operation of the procedure include high purity reagents and elimination of container and atmosphere contamination.

Metal is obtained as a crystalline material in a salt matrix, and is recovered by carefully controlled aqueous procedures. The crystals are of three general types: (a) narrow flat platelets up to $1\frac{1}{2}$ in. long of hexagonal structure; (b) coarsely crystalline hexagonal crystals of +100 mesh or greater; and (c) fine, less pure crystals. The latter are in very small amount under properly controlled conditions. If the temperature of operation exceeds 830°-840°C, the large platelets do not form, and deposits consist essentially of coarse crystals and dendrites of a distorted cubic structure. It is preferable from a purity standpoint to use lower temperatures.

Deposits do not consist of one crystal type alone,

although relative amounts of a given type may be controlled by adjustments of temperature, current density, and purity of the bath. The fine material is normally found adjacent to the steel cathode surface and is the least pure portion of the deposit. The large plates then grow from this crystal bed.

If significant amounts of impurities such as oxides are present, large plates do not form. The presence of even small amounts of iron as FeCl_3 or FeCl_2 is intolerable. Efficiencies are grossly reduced by a reoxidation of reduced titanium species by Fe^{3+} . Since FeCl_3 is volatile at the operating temperature, any iron exposed to the chlorine atmosphere can result in a continuous oxidation-reduction recycling.

It has been demonstrated that a purification electrolysis is a requisite in order to obtain maximum efficiency and purity of product. Such an electrolysis is normally carried out at 1–2 v using a graphite rod cathode. A total of 20–30 amp-hr is required for a 5 lb bath of good starting purity. When impurities, principally moisture, have been eliminated, a characteristic voltage rise occurs. A small amount of titanium plates out, but the deposit is principally iron and lower Ti oxides. A satisfactory pre-electrolysis cathode is uniformly coated with a thin layer of deposit, whereas, if a bath is severely contaminated, only the tip becomes coated.

The electrolysis is made using a steel cathode. A variety of shapes has been used, but an inverted truncated cone has been most satisfactory with respect to current efficiency and uniformity of deposit. This is presumably due to a more nearly ideal current density distribution.

Electrolysis is preferably carried out at 350–550 amp/dm² under 4–5 v. Very high current densities tend to decrease particle size, and lower currents offer no advantages, only slowing down the electrolysis. A temperature of 740°–760°C is preferred to give a fluid bath, maximum efficiency, and minimum tendency for impurity pick-up by metal produced. The over-all voltage must exceed 2.8 to produce metal, otherwise there is no operating limit up to the point where sodium is simultaneously liberated.

Baths may be recharged with K_2TiF_6 and run repeatedly up to a limit. There is a gradual buildup of KF and NaF in the melt and, eventually, the bath becomes sufficiently refractory and less conductive such that it is undesirable for electrolysis

from a time standpoint. In addition, some of the fluorides are withdrawn with the deposit and present an extraction problem in recovery of the metal.

The process could be operated as a semicontinuous procedure, and as such would offer some advantage over existent batch processes. Materials required are readily prepared in a pure state by standard chemical techniques. The electrolysis is straightforward and, although requiring special closed cells, the design is not complicated or extremely costly. Titanium produced by this method is equivalent to or superior to present commercially available material with respect to purity and physical properties.

ACKNOWLEDGMENTS

The authors appreciate the support of the Office of Naval Research in this work and their permission to publish these results. Acknowledgment is also made of the help given by the following individuals, who are or were members of the staff of Horizons Incorporated, in carrying out this program: process development, A. A. Topinka, Q. H. McKenna, B. C. Raynes; materials preparation, S. Cardon and D. Gollwitzer; metallography, S. Kulchar; metal recovery and evaluation, J. Wick and E. D. Fisher; photography, W. Sargent.

Any discussion of this paper will appear in a Discussion Section to be published in the December 1955 JOURNAL.

REFERENCES

1. J. BARKSDALE, "Titanium," p. 41–101, Ronald Press Co., New York (1947).
2. J. J. BERZELIUS, *Pogg. Ann.*, **4**, 1 (1825).
3. W. KROLL, *Trans. Electrochem. Soc.*, **78**, 35 (1940).
4. J. W. MELLOR, "A Comprehensive Treatise on Inorganic and Theoretical Chemistry," Vol. 7, pp. 50–89, Longmans Green and Co., London (1927).
5. M. E. SIBERT, Q. H. MCKENNA, M. A. STEINBERG, AND E. WAINER, *This Journal*, **102**, 252 (1955).
6. J. DEBUSSY, *Compt. rend.*, **36**, 540 (1853).
7. S. I. SKLYLARENKO AND J. LIPKES, *Zhur. Priklad. Khim.*, **13**, 51 (1940).
8. A. BRENNER AND S. SENDEROFF, *This Journal*, **99**, 223C (1952).
9. P. DROSSBACH, *Z. Elektrochem.*, **57**, No. 7, 548 (1953).
10. Shawinigan Water and Power Co., British Pat. 678,807, May 11, 1951.
11. G. D. P. CORDNER AND H. W. WORNER, *Australian J. Appl. Sci.*, **2**, 358 (1951).
12. M. A. STEINBERG, M. E. SIBERT, AND E. WAINER, *This Journal*, **101**, 63 (1954).

Conductimetric and Viscometric Behavior of Lithium Bromide in 50–50 Weight Per Cent Methanol-Acetone at Temperatures within the Range 20° to –50°C¹

LYLE R. DAWSON, RICHARD A. HAGSTROM,² AND PAUL G. SEARS

Department of Chemistry, University of Kentucky, Lexington, Kentucky

ABSTRACT

Conductances, viscosities, and densities, at temperatures within the range 20° to –50°C, have been determined for solutions of lithium bromide in 50–50 wt % methanol-acetone over a wide concentration range. An indirect method has been used to evaluate the limiting equivalent conductance at temperatures other than 20°C. The logarithm of the conductance-viscosity product has been found to be a linear function of the reciprocal of the absolute temperature for all solutions studied. A linear relationship has been found also between the logarithm of the equivalent conductance and the logarithm of the viscosity for all of the solutions over the temperature range studied.

INTRODUCTION

Mixed solvents frequently have some properties which are more desirable in certain respects than those of the pure constituents. Such is the case for a mixture of methanol and acetone. The mixed solvent is less viscous than methanol, thereby permitting increased ionic mobilities; it has greater dissolving power for electrolytes, and is less volatile than acetone. Since mixtures of methanol and acetone should be similar to those of methanol and methyl ethyl ketone (1), the mixed solvent furthermore should have a greater dissociating power for electrolytes than that exhibited by either methanol or acetone.

In this investigation, the conductimetric and viscometric behavior of lithium bromide in 50–50 methanol-acetone has been determined at eight temperatures within the range 20° to –50°C for eighteen solutions having molal concentrations ranging from 418×10^{-4} to 4.14. Densities of the solutions were determined also for use in the conversion of molalities to molarities and for the calculation of absolute viscosities.

EXPERIMENTAL

The anhydrous lithium bromide used in the preparation of the solutions for this investigation was a portion of that described previously (2). Both methanol and acetone were prepared by fractional distillation of 'Baker Analyzed' products

¹ Manuscript received September 24, 1954. This paper was prepared for delivery before the Cincinnati Meeting, May 1 to 5, 1955. Based on research performed under a contract with the U. S. Army Signal Corps.

² Present address: Standard Oil Company, Whiting, Indiana.

after each had been refluxed for 12 hr over calcium oxide. The middle fractions, which were retained, had conductivities of 4.0×10^{-7} and 1.8×10^{-7} , respectively. The solutions were prepared by dissolving in methanol a weighed quantity of anhydrous lithium bromide contained in a tared flask. After dissolution was complete and the solution had cooled, the weight of methanol was determined and an equal weight of acetone was added to make a 50–50 solvent mixture. It was not practicable to use an initially prepared mixed solvent because the heat of solution of the lithium bromide was sufficient to cause appreciable loss of the solvent by vaporization.

Experimental procedures for measurements of the conductances, viscosities, and densities have been described adequately in previous papers (2, 3).

RESULTS

All experimental data except densities are incorporated in figures presented in this paper. Inasmuch as the tabulation of the data would be quite extensive, it has been omitted.³

DISCUSSION

The equivalent conductance of lithium bromide at low concentrations in 50–50 methanol-acetone is shown in Fig. 1 as a function of the square root of the concentration. Analysis of conductance data for dilute solutions at 20°C by the Shedlovsky extrapolation method (4) yielded $117.5 \text{ ohm}^{-1} \text{ cm}^2$ and 4.8×10^{-2} for the limiting equivalent conductance and

³ For tables summarizing data pertinent to the conductances, viscosities, and densities for the solutions studied, contact the Department of Chemistry, University of Kentucky.

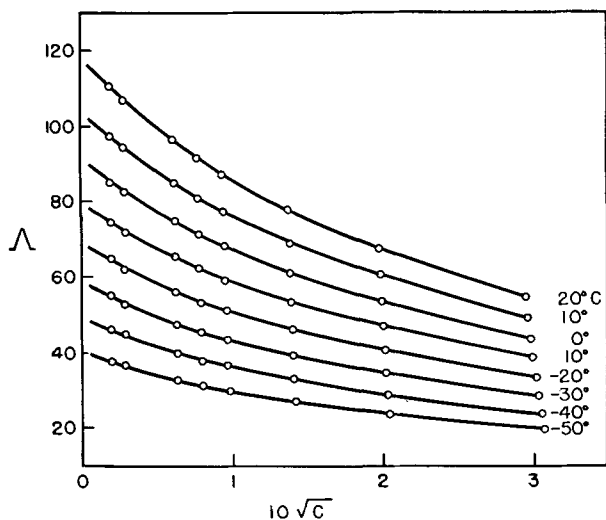


FIG. 1. Equivalent conductance of lithium bromide in 50-50 methanol-acetone.

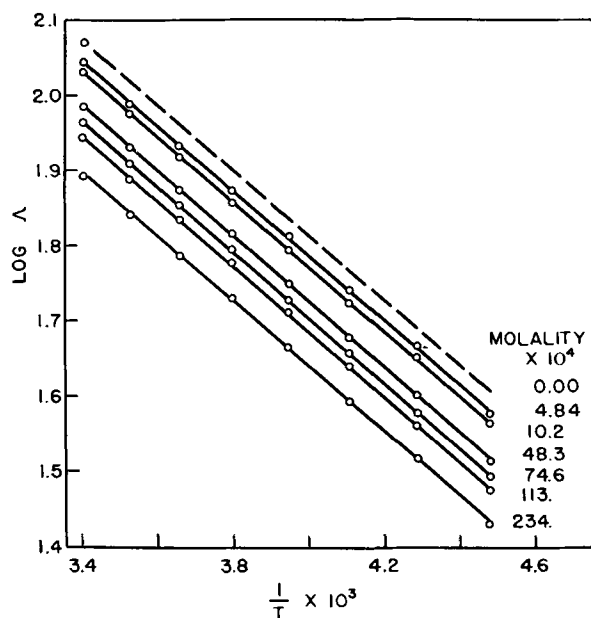


FIG. 2. Temperature dependence of the logarithm of the equivalent conductance of lithium bromide at low concentrations in 50-50 methanol-acetone.

TABLE I. The limiting equivalent conductance and the conductance-viscosity product for lithium bromide in 50-50 methanol-acetone at temperatures within the range 20° to -50°C

$t^{\circ}\text{C}$	$\Lambda_0(\text{ohm}^{-1}\text{ cm}^2)$	$\eta_0(\text{poise} \times 10^3)$	$\Lambda_0\eta_0$
20	117.5	3.95	0.465
10	104.1	4.50	0.469
0	91.5	5.14	0.470
-10	79.7	5.93	0.473
-20	68.7	6.91	0.475
-30	58.3	8.16	0.477
-40	49.0	9.76	0.478
-50	40.3	11.95	0.482

dissociation constant, respectively, of lithium bromide in this mixed solvent. Owing to a lack of dielectric constant data, the Shedlovsky method could not be applied at other temperatures.

Plots of the logarithm of the equivalent conductance of the salt in several dilute solutions vs. the reciprocal of the absolute temperature are shown in Fig. 2. The graphs for the five lowest concentrations are linear and have equal slopes. In accordance with results reported in an earlier paper (2), it seemed reasonable to assume that a corresponding plot of the limiting equivalent conductance of lithium bromide in 50-50 methanol-acetone also would be linear and its slope would be identical with that of similar plots in the dilute range. Having available the values of Λ_0 at 20°C and the slope of the plots for dilute solutions, the point-slope method was utilized to construct a large plot of the logarithm of Λ_0 against $1/T$, from which the appropriate information was taken to calculate the limiting conductance data which appear in Table I. Conductance-viscosity products also listed in Table I are approximately constant, although an apparent trend of the product slightly decreasing with increasing temperature may be noted. Such a trend occurs when the limiting equivalent conductance increases at a slower rate than the viscosity decreases as the temperature becomes higher. The relative magnitude of the product, which is approximately 11% less for lithium bromide in 50-50 methanol-acetone than in pure methanol, is evidence that the effective size of the conducting species is greater in the mixed solvent.

The logarithm of the equivalent conductance of solutions of lithium bromide at higher concentrations in 50-50 methanol-acetone is shown in Fig. 3 as a function of the reciprocal of the absolute temperature. It may be observed that the deviation of the plots from linearity increases with increasing concentration. For comparison purposes, corresponding plots involving the viscosity instead of the conductance have been incorporated in Fig. 4. Deviation of these plots from linearity similarly becomes more pronounced with increasing concentration. Owing perhaps to cancelling effects, however, the logarithm of the equivalent conductance-viscosity product is a linear function of the reciprocal of the absolute temperature for all concentrations studied. This may be expressed mathematically as follows:

$$\log(\Lambda\eta) = A + B\left(\frac{1}{T}\right) \quad (\text{I})$$

where A and B are constants for a given solution representing the intercept and slope, respectively, of a plot of $\log(\Lambda\eta)$ vs. $1/T$. Although graphs of this nature have not been included, data pertinent to

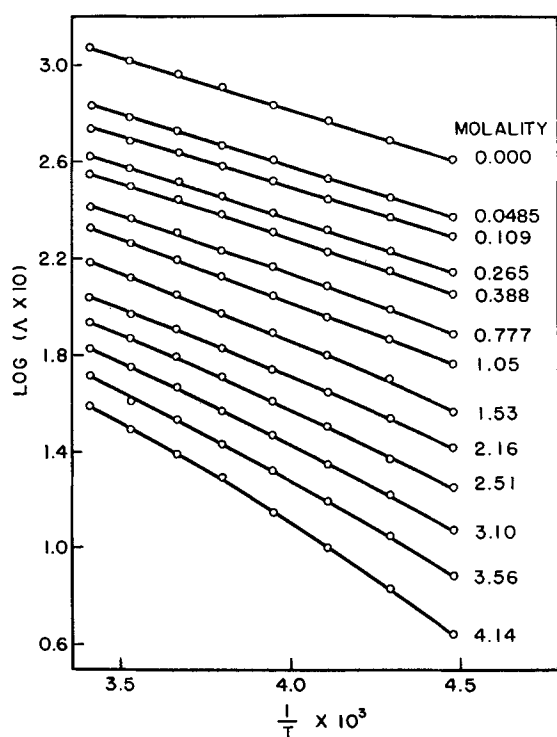


FIG. 3. Temperature dependence of the logarithm of the equivalent conductance of more concentrated solutions of lithium bromide in 50-50 methanol-acetone.

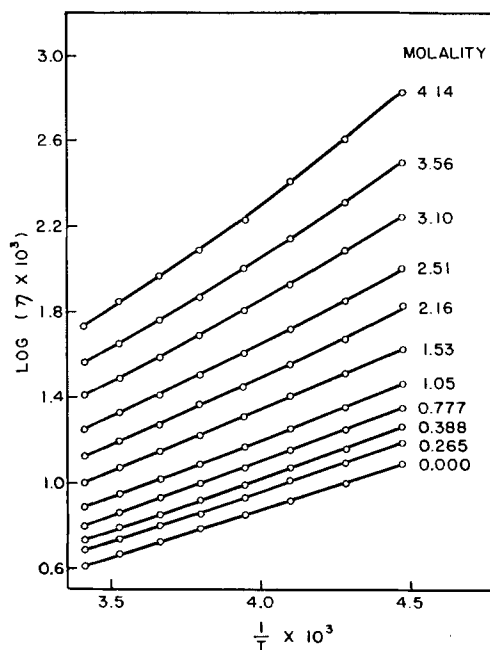


FIG. 4. Temperature dependence of the logarithm of the viscosity of more concentrated solutions of lithium bromide in 50-50 methanol-acetone.

the slopes and intercepts of such plots are listed in Table II. If the value of B were zero, equation (I) would reduce to an expression of the constancy of the conductance-viscosity product which is identical with the Walden relationship for infinite dilution. It may be noted from the data in Table II

TABLE II. Slopes and intercepts of plots of equations (I) and (III) for solutions of lithium bromide in 50-50 methanol-acetone

Molality	Equation (I)		Equation (III)	
	Slope	Intercept	— (Slope)	— (Intercept)
0.000	18	0.613	0.970	0.258
0.265	21	0.239	0.955	0.583
0.388	28	0.192	0.946	0.590
0.777	30	0.123	0.958	0.686
1.05	20	0.142	0.967	0.721
1.53	25	0.105	0.963	0.730
2.16	49	0.001	0.916	0.679
2.51	53	0.010	0.925	0.668
3.10	80	-0.034	0.891	0.589
3.56	102	-0.078	0.869	0.546
4.14	145	-0.177	0.866	0.514

that B is never zero, but tends to increase with increasing concentration for the system under consideration.

In addition to the relationship between conductance and viscosity discussed above, it has been observed that the logarithm of the equivalent conductance is a linear function of the logarithm of the viscosity over the temperature range for each solution studied. This may be represented by a relationship between conductance and viscosity introduced by Johnston (5) which takes the following form:

$$\Lambda \eta^n = k \quad (\text{II})$$

where n and k are constants. Putting into logarithmic form and rearranging, equation (II) becomes

$$\log \Lambda = \log k - n \log \eta \quad (\text{III})$$

Hence a plot of $\log \Lambda$ against $\log \eta$ should be linear and should have a slope and an intercept of $(-n)$ and $(\log k)$, respectively. Values of $(-n)$ and $(\log k)$ taken from plots of equation (III) for various more concentrated solutions of lithium bromide in 50-50 methanol-acetone may be found in Table II.

If a value of unity for the slope in equation (III) is evidence of the complete dependence of conductance upon viscosity, the data pertinent to the slope (Table II) indicate that the dependence approaches completeness in dilute solutions.

Any discussion of this paper will appear in a Discussion Section to be published in the December 1955 JOURNAL.

REFERENCES

1. F. M. SACKS AND R. M. FUOSS, *J. Am. Chem. Soc.*, **75**, 5172 (1953).
2. P. G. SEARS, R. L. MCNEER, AND L. R. DAWSON, *This Journal*, **102**, 269 (1955).
3. P. G. SEARS, R. R. HOLMES, AND L. R. DAWSON, *This Journal*, **102**, 145 (1955).
4. T. SHEDLOVSKY, *J. Franklin Inst.*, **225**, 739 (1938).
5. J. JOHNSTON, *J. Am. Chem. Soc.*, **31**, 1010 (1909).

Mathematical Studies of Galvanic Corrosion

II. Coplanar Electrodes with One Electrode Infinitely Large and with Equal Polarization Parameters¹

JAMES T. WABER AND MARSHALL ROSENBLUTH

University of California, Los Alamos Scientific Laboratory, Los Alamos, New Mexico

ABSTRACT

The expressions for the potential and current density distribution have been derived for the two mathematically similar corrosion problems, (a) tiny anodes buried in infinite cathodes, and (b) tiny foreign cathodic inclusions in a metal. The implication of using equal polarization parameters has been discussed. When the critical dimension of the tiny electrode becomes smaller than the polarization parameter, corrosion attack and the interfacial potential become more uniform over the galvanic cell. Figures and perspective drawings made to scale are included to illustrate the effect of polarization on the distribution of potential in the corrodent and the diminishing variation of corrosion attack.

INTRODUCTION

In a previous paper (1), the effect of polarization on the behavior of a coplanar galvanic couple was considered negligible. The present paper extends the analysis to include the effect of polarization, and deals with the corrosion behavior of an active metal which is covered by a more noble metal or film. When such barriers are slightly porous, rapid attack occurs at the tiny anodes. This attack is limited by the anodic polarization of these micro-cells. Another situation occurring frequently in commercial practice and pertinent to this investigation is the dissolution of a metal containing tiny foreign inclusions; in this case, the dissolution rate is regulated by polarization characteristics of the cathodes. To be consistent with the previous paper, the case of infinitesimal anodes will be discussed in detail.

Specifically, an assumption has been made which is more nearly akin to mixed anodic-cathodic control, that is, the polarization parameter,² \mathfrak{L} , as defined by Wagner (2), is assumed to be equal for both the anode and cathode.

Wagner (3) has pointed out that in many cases the IR drop in the electrolyte is relatively unimportant and that the corrosion behavior of a metal containing foreign inclusions is dictated almost exclusively by such things as the hydrogen overvoltage of the inclusions. Frumkin and Levich (4), in the case of "infinitely small" inclusions, have

shown that, when it is necessary to take the ohmic potential drop into account, concentration changes within the corroding solution in the vicinity of the tiny inclusions must also be considered. That is, appreciable concentration gradients must exist in solution in order to continue the supply of hydrogen ions which are rapidly being discharged at the cathode. In the present limiting case, secular changes in electrolyte composition, as well as concentration gradients, have been ignored.

Although the case to be discussed is a finite anode buried in an infinite cathode, it will be shown below that the resulting equations are easily modified to discuss a finite cathode imbedded in an infinite anode. Wagner (5) pointed out that the latter is an important case to analyze, because of its frequent occurrence.

In accordance with Wagner's definition

$$\mathfrak{L}_i = \sigma \left| \frac{d\Delta E_i}{dJ_i} \right| \quad [1]$$

where σ is the specific conductivity of the corrodent, ΔE_i is the overvoltage of the i -th metal or electrode, and J_i is the appropriate current density. The vertical bars denote the absolute value of the derivatives.

In a given environment, irrespective of physical dimensions, a galvanic cell may behave as though it were "macroscopic" or "microscopic" depending upon whether the critical dimension is larger or smaller than the parameter, \mathfrak{L} . The critical dimension, λ , is that one which affects the distribution of current density most strongly. In certain practical cases, it may be the separation of the electrodes, and in others it is the smallest dimension of one electrode.

If the resistance of the corrosive medium is high

¹ Manuscript received November 27, 1953. This paper was prepared for delivery before the Cincinnati Meeting, May 1 to 5, 1955.

² Herein \mathfrak{L} has been used in place of Wagner's k to emphasize the fact that this parameter has the dimension of length and to avoid any possible confusion with conductivity for which k is frequently used.

or if ξ is small in comparison to λ , then the previous analysis (1) which assumed negligible polarization is applicable. When λ/ξ is large, such galvanic cells will behave as though they were macroscopic. On the contrary, under corrosive conditions that permit strong polarization of the electrodes (ξ is large), even macroscopic elements may behave as though they had microscopic dimensions. The microscopic galvanic cells are characterized by relatively uniform distributions of current density. Wagner's treatment (2) establishes these features.

In the case under consideration, the critical dimension is a , the half width of the anode. The dependence of the maximum and the minimum anodic current densities on the ratio a/ξ are discussed, and the qualitative results discussed above are confirmed.

MATHEMATICAL FEATURES OF THE ANALYSIS

The model to be discussed is shown in Fig. 1. A very long anode of width $2a$ is embedded in the plane of a cathode, $2c$ units wide. The authors then choose the origin to lie at the center of the anode and choose the x axis perpendicular to the long direction of the anode and the y axis perpendicular to the plane of the anode and cathode. As discussed in the previous paper (1), this arrangement has even symmetry. Without the loss of a significant amount of generality one can erect insulating walls at $x = \pm c$, that is, parallel to the length of the anode and parallel to the y axis. The insulator eliminates edge effects and permits one to concentrate on the effects occurring at the anode-cathode junction. Because of the symmetry which has been assumed, current flow parallel to the x axis does not occur in plane $x = 0$. Consequently, attention may be restricted to the first quadrant where x is positive. The electrolyte is poured in at the top and it will be assumed that it extends to $y = \infty$. Flow parallel to the Z axis is assumed to be negligibly small because of the great length of the anode as compared with its width. These features of the model permit attention to be restricted to potential and current distributions which occur in the first quadrant of the XY plane.

Thus far the model is not different from that discussed in the previous paper (1). For the present analysis, however, assume that c is infinitely larger than a . Therefore, boundary conditions must be revised. If $P(x, y)$ is potential, then

$$\lim_{y \rightarrow \infty} P(x, y) < M \tag{2}$$

$$\lim_{x \rightarrow \infty} P(x, y) < N \tag{3}$$

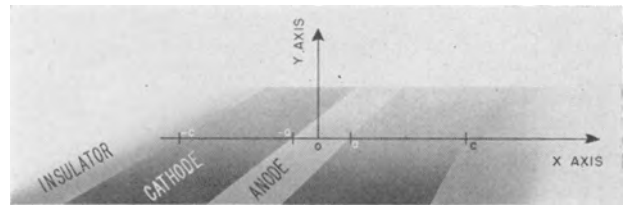


FIG. 1. Perspective sketch illustrating the geometric relation of the electrodes.

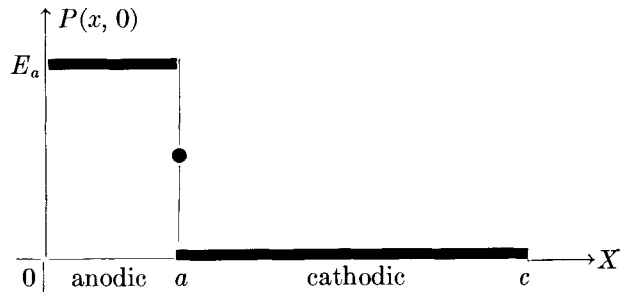


FIG. 2. Distribution of the unpolarized interfacial potential over the electrode.

where M and N are arbitrary large numbers. Since current flow at $x = 0$ and $x = c$ must not occur parallel to x axis, it is clear that

$$\frac{\partial P}{\partial x} \Big|_{x=0} = 0 \tag{4}$$

$$\lim_{c \rightarrow \infty} \frac{\partial P}{\partial x} \Big|_{x=c} = 0 \tag{5}$$

The anode induces a potential in the corrodent relative to the cathode. Define this difference as E_a such that

$$E_a = E_{a(0)} - E_{c(0)} \tag{6}$$

where $E_{a(0)}$ is the potential of the anode extrapolated to zero current density and $E_{c(0)}$ is the similar potential of the cathode; using the Lewis and Randall sign convention, E_a is positive.

In the absence of polarization, the potential on the anode-cathode plane is illustrated in Fig. 2 and is proportional to the step function, $S'_a(x)$.

A further boundary condition imposed by this choice of the galvanic cell is

$$P^*(x, 0) = E_a S'_a(x) + \xi \frac{\partial P^*}{\partial y} \Big|_{y=0} \tag{7}$$

where the infinite step function is

$$S'_a(x) = \begin{cases} 1 & \text{for } \begin{cases} 0 \leq x \leq a - 0 \\ a + 0 \leq x \leq \infty \end{cases} \\ 0 & \end{cases} \tag{7a}$$

and where it has been assumed that

$$\xi_a = \xi_c = \xi \tag{8}$$

Wagner (2) has discussed the use of the second term on the right hand side of equation [7] to take into account the effect of polarization.

In general, the values of ξ_a and ξ_c will not be equal because of different slopes of the anodic and the cathodic potential-current density curves. The special case ξ_a equals ξ_c , however, is amenable to a straightforward mathematical treatment, whereas a treatment of the more general case ξ_a is not equal to ξ_c requires rather cumbersome numerical methods. A mathematical analysis of the special case ξ_a equals ξ_c has been worked out, since disregard of polarization leads to inconsistencies. In particular, if polarization is ignored, the current densities at the boundary between local cathodes and anodes become infinite, and even average values of the cathodic or the anodic current density cannot be calculated as has been shown in Part I. Results for the special case ξ_a equals ξ_c show the general effect of polarization. These results may also be used for a qualitative discussion of the more general case ξ_a is not equal to ξ_c as is shown below.

Inasmuch as there are no sources or sinks for electrons or ions within the electrolyte and since there is no space charge, the potential satisfies Laplace's equation.

Consider first the case where $\xi = 0$, since the resulting integrals are useful for the further analysis of the more general nonzero case which will be discussed subsequently. The mathematical features of the derivation have been discussed elsewhere (6).

Negligible Polarization

It is clear that a potential of the form

$$P(x, y) = \int_0^\infty A(n) \cos(nx) \exp(-ny) \, dn \quad [9]$$

will satisfy the two dimensional form of Laplace's equation, and have even symmetry since

$$\begin{aligned} \int_0^\infty A(n) \cos(nx) \exp(-ny) \, dn \\ = \int_0^\infty A(n) \cos(-nx) \exp(-ny) \, dn \end{aligned} \quad [9a]$$

This function is bounded for all positive x and y values and both x -derivatives are zero as required by [4] and [5]. The quantity $A(n)$ is unspecified in definition [9] but is chosen so that condition [7] is satisfied. The procedure for evaluating $A(n)$ is equivalent to finding the unspecified coefficients of a Fourier series. When $\xi = 0$ in [7], then

$$P(x, +0) = \int_0^\infty A(n) \cos(nx) \, dn = S'_a(x)E_a \quad [10]$$

Multiplying both sides of [10] by $\cos(mx)$ and integrating with respect to x one obtains

$$\begin{aligned} \int_0^\infty dn A(n) \int_0^\infty \cos(mx) \cos(nx) \, dx \\ = E_a \int_0^\infty S'_a(x) \cos(mx) \, dx \end{aligned} \quad [11]$$

The inner integral is equal to the Dirac delta function $\delta(n - m)$. Using its definition, one sees that

$$\int_0^\infty A(n) \delta(n - m) \, dn = \frac{E_a}{m} \sin(am) \quad [12]$$

Thus

$$A(m) = \frac{2E_a}{\pi} \frac{\sin(am)}{m} \quad [13]$$

Consequently the value of the potential is

$$P(x, y) = \frac{2E_a}{\pi} \int_0^\infty \frac{\sin(an)}{n} \cos(xn) \exp(-yn) \, dn \quad [14]$$

By employing the pertinent trigonometric identity, one obtains

$$\begin{aligned} P(x, y) \\ = \frac{E_a}{\pi} \int_0^\infty \frac{1}{n} [\sin(a+x)n + \sin(a-x)n] \\ \cdot \exp(-yn) \, dn \end{aligned} \quad [15]$$

By noting that

$$\int_y^\infty \exp(-ku) \, du = \frac{1}{k} \exp(-ky) \quad [16]$$

the integrals in [15] may be simplified to

$$\begin{aligned} P(x, y) \\ = \frac{E_a}{\pi} \int_y^\infty du \int_0^\infty [\sin(a+x)n + \sin(a-x)n] \\ \cdot \exp(-un) \, dn \end{aligned} \quad [17]$$

Integrating the inner integral (in n) twice by parts and solving the resulting equation for the integral one can demonstrate that

$$\begin{aligned} P(x, y) \\ = \frac{E_a}{\pi} \int_y^\infty \left[\frac{(a+x)}{(a+x)^2 + u^2} + \frac{(a-x)}{(a-x)^2 + u^2} \right] du \end{aligned} \quad [18]$$

The latter integral may be evaluated as

$$\begin{aligned} P(x, y) \\ = \frac{E_a}{\pi} \left[\pi - \arctan\left(\frac{y}{a+x}\right) - \arctan\left(\frac{y}{a-x}\right) \right] \end{aligned} \quad [19]$$

or as

$$\begin{aligned} P(x, y) \\ = \frac{E_a}{\pi} \left[\arctan\left(\frac{a+x}{y}\right) + \arctan\left(\frac{a-x}{y}\right) \right] \end{aligned} \quad [20]$$

By simple algebra one may verify that, as y approaches zero, P converges to E_a for x less than a and to zero for x greater than a .

A further value of performing the integration with $\xi = 0$ is that the corrosion current may be derived from [20], whereas the integrals derived for the more general case are difficult to evaluate at $\xi = 0$. This subject will be discussed in a later section.

More General Case $\xi \neq 0$

The required procedure is strictly analogous to that discussed above. After differentiation of [9] with respect to y and substitution of the result into [7] it may be seen that

$$\int_0^\infty [A^*(n) + n\xi A^*(n)] \cos(xn) \, dn = E_a S'_a(x) \quad [21]$$

where $A^*(n)$ is written to distinguish it from the function $A(n)$. The asterisk is used throughout to denote the inclusion of polarization in the argument. Proceeding as in [11] and [12] it is clear that

$$A^*(m) = \left(\frac{2E_a}{\pi} \right) \frac{\sin(am)}{m(1 + \xi m)} \quad [22]$$

Upon substitution of [22] into [9] and use of the trigonometric identity it follows that

$$P^*(x, y) = \frac{E_a}{\pi} \left[\int_0^\infty \frac{\sin(a+x)n}{n(1 + \xi n)} \exp(-ny) \, dn + \int_0^\infty \frac{\sin(a-x)n}{n(1 + \xi n)} \exp(-yn) \, dn \right] \quad [23]$$

This can be integrated by decomposing the fraction into a sum of two simpler fractions, namely, by noting that

$$\frac{\sin(a+x)n}{n(1 + \xi n)} = \left(\frac{1}{n} - \frac{\xi}{1 + \xi n} \right) \sin(a+x)n \quad [24]$$

The potentials have been evaluated from the resulting integrals and are tabulated elsewhere (7).

Evaluation of Current Density

As was discussed in the previous paper (1), the anodic current density, J_a , is defined in terms of the normal gradient evaluated at the interface. That is

$$J_a^*(x) = -\sigma \left. \frac{\partial P^*}{\partial y} \right|_{y=0} \quad (0 \leq x \leq a - 0) \quad [25]$$

where σ is the specific conductivity. It is desirable to evaluate the current in a manner which is independent of the galvanic system under consideration. For convenience, introduce a dimensionless parameter to represent the current density. Thus

$$C_a^* = \left(\frac{-2a}{E_a} \right) \left. \frac{\partial P^*}{\partial y} \right|_{y=0} \quad [26]$$

This expression involves the potential difference of unpolarized electrodes, the critical dimension, and the normal gradient, which depends upon the geometry of the couple. Thus, C_a^* may be applied to any galvanic system, providing the polarization parameters are equal. Equations [20] and [23] are used most conveniently for calculating the normal derivative. Thus

$$-\left(\frac{2a}{E_a} \right) \frac{\partial P}{\partial y} = \frac{2a}{\pi} \left[\frac{a+x}{y^2 + (a+x)^2} + \frac{a-x}{y^2 + (a-x)^2} \right] \quad [27]$$

$$\left(\frac{-2a}{E_a} \right) \frac{\partial P^*}{\partial y} = \frac{2a}{\pi} \left[\int_0^\infty \frac{\sin(a+x)n}{(1 + \xi n)} \exp(-yn) \, dn + \int_0^\infty \frac{\sin(a-x)n}{(1 + \xi n)} \exp(-yn) \, dn \right] \quad [28]$$

Both of these expressions are simplified when $y = 0$. The integrals resulting from [28] may be evaluated by making the substitution,

$$s \equiv 1 + \xi n \quad [29]$$

by using [26], and the following definitions of λ and λ' .

$$\begin{aligned} \lambda &\equiv (a+x)/\xi \\ \lambda' &\equiv (a-x)/\xi \end{aligned} \quad [30]$$

Thus,

$$C_a^*(x) = \frac{2a}{\pi\xi} \cdot \left[\int_1^\infty \frac{\sin \lambda(s-1)}{s} \, ds + \int_1^\infty \frac{\sin \lambda'(s-1)}{s} \, ds \right] \quad [31]$$

Using the appropriate trigonometric identity one obtains

$$C_a^*(x) = \frac{2a}{\pi\xi} \cdot \left[\cos \lambda \int_1^\infty \frac{\sin \lambda s}{s} \, ds - \sin \lambda \int_1^\infty \frac{\cos \lambda s}{s} \, ds + \cos \lambda' \int_1^\infty \frac{\sin \lambda' s}{s} \, ds - \sin \lambda' \int_1^\infty \frac{\cos \lambda' s}{s} \, ds \right] \quad [32]$$

Values of the sine and cosine integrals in [32] are available (8). Using the following definitions of these integrals in their usual tabulated form

$$Si(\lambda) = \int_0^\lambda \left(\frac{\sin s}{s} \right) \, ds \quad [33]$$

$$Ci(\lambda) = \int_\infty^\lambda \left(\frac{\cos s}{s} \right) \, ds \quad [34]$$

$$-si(\lambda) = \frac{\pi}{2} - Si(\lambda) \quad [35]$$

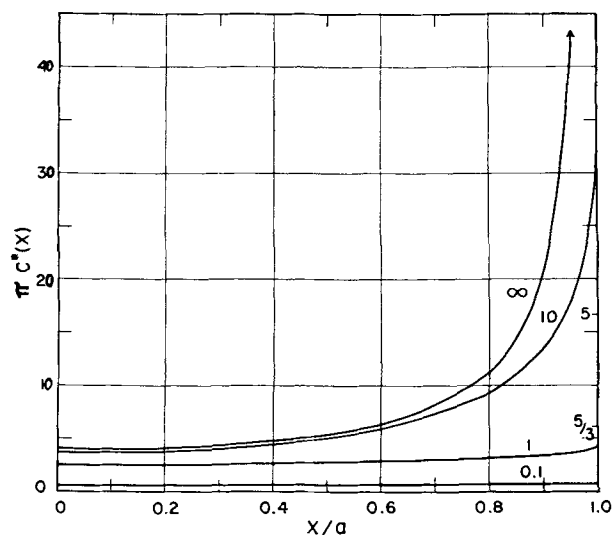


FIG. 3. Effect of polarization on the variation of anodic current density parameter. Curves are for different values of a/ξ .

TABLE I. Values of the current density parameter as a function of a/ξ

a/ξ	Max C_a^*	Min C_a^*	Max $C_a^*/$ Min C_a^*
0.001	0.002002	0.001998	1.0004
0.01	0.01944	0.01936	1.0045
0.1	0.1723	0.1644	1.049
1.0	1.2540	0.7913	1.585
$\frac{5}{3}$	1.9232	1.0262	1.874
5	5.3124	1.1976	4.436
10	10.317	1.2497	8.256
100	100.318	1.2707	78.95
1000	1000.32	1.2732	785.65
∞	∞	1.2732	∞

the anodic current may be written as

$$C_a^*(x) = \frac{2a}{\pi\xi} [Ci(\lambda) \sin \lambda - si(\lambda) \cos \lambda - \varepsilon i(\lambda') \cos \lambda' + Ci(\lambda') \sin \lambda'] \quad [36]$$

Expression [36] was used to evaluate the current density for several values of ξ and λ .

Since few tabulated values of Ci and Si are available (8) for λ greater than 20, it was necessary in some cases to employ the following complex variable relationship

$$Ci(\lambda) + i si(\lambda) = \frac{\exp(-i\lambda)}{i\lambda} H(i\lambda) \quad [37]$$

where the series $H(i\lambda)$ is defined as

$$H(v) \equiv \sum_{n=0}^{\infty} \frac{n!}{v^n} \quad [38]$$

This series is semiconvergent for modulus of v much greater than 1. It may be simply shown by separating real and imaginary parts that

$$Ci(\lambda) = \frac{i}{2\lambda} \quad [39]$$

$$\cdot [H(-i\lambda) \exp(-i\lambda) - H(i\lambda) \exp(i\lambda)]$$

$$si(\lambda) = \frac{-i}{2\lambda} \quad [40]$$

$$\cdot [H(-i\lambda) \exp(-i\lambda) + H(i\lambda) \exp(i\lambda)]$$

The maximum value of the current density parameter will occur at the anode-cathode junction and the minimum at the center of the total anode, i.e., at the origin. That is, the maximum and minimum values are

$$\text{Max } C_a^*(x) = C^*(a) \quad [41]$$

$$\text{Min } C_a^*(x) = C^*(0) \quad [42]$$

Employing a definition analogous to [26] for the case in which $\xi = 0$, i.e., for negligible polarization, the equivalent statements are

$$\text{Max } C_a(x) = C(a) = \infty \quad [43]$$

$$\text{Min } C_a(x) = C(0) = \frac{4}{\pi} \quad [44]$$

as can be seen from equation [27] which has been evaluated at $y = 0$. Equations [41] and [42] have been numerically evaluated for a large range of ξ values.

It may be shown, using l'Hopital's rule that

$$\lim_{\lambda' \rightarrow 0} Ci(\lambda') \sin \lambda' = 0 \quad [45]$$

and thus [36] may be evaluated at $x = a$.

Numerical Evaluation of the Current Density Parameter

Values of the current density parameter $C_a^*(x)$ have been evaluated for three ratios of a/ξ , namely 0.1, 1, and 10. In addition $C_a(x)$ has been computed. Equation [36] was employed to evaluate $C_a^*(x)$ and equation [27] was used to obtain $C(x)$ after substituting definition [26] and setting y equal to zero. These values have been plotted and presented in Fig. 3.

From Fig. 3 it is clear that the distribution of current density becomes more uniform as ξ increases for a fixed value of a . Or, expressed differently, the distribution approaches that characteristic of "microscopic" galvanic elements as a/ξ becomes "microscopically" small. The maximum values of $C^*(x)$ have been added to Fig. 3 for (a/ξ) equal to 5 and to $\frac{5}{3}$.

The results of a number of the evaluations of Max C_a^* and Min C_a^* as well as their ratio are presented in Table I. By looking at this ratio it is evident that corrosion attack is more uniform for

small values of a/ξ than for large; that is, it is more uniform when a is microscopic in comparison with the polarization parameter.

Evaluation of Relative Potentials

Space does not permit detailed reduction of equation [23] to a form involving only tabulated functions. Waber (7) has discussed this problem in detail and obtained numerical values for four values of the ratio of a/ξ .

Perspective drawings of the potential fields for various x , y , a , and ξ values have been prepared. In order to present such data in a form which is independent of the galvanic system under consideration, the reduced and dimensionless potential functions $P^*(x/2a, y/2a)/E_a$ as well as $P(x/2a, y/2a)/E_a$ have been plotted. These perspective views of the potential fields can be seen in Fig. 3, 4, 5, and 6.

In these drawings, the reduced potential function is plotted vertically and the reduced interfacial potential is plotted on the XY plane. The degree to which the interfacial potential has been reduced by polarization is indicated by the cross hatching. The unpolarized reduced potential is one in the anodic region and zero in the cathodic. However, polarization reduced the interfacial potential by a considerable amount. The authors have indicated the effect of polarization on the cathodic region by a different convention to indicate that this region is hidden from view by the curved potential surface. In Fig. 3, specifically, they have indicated the hidden portion of the interfacial potential by the same

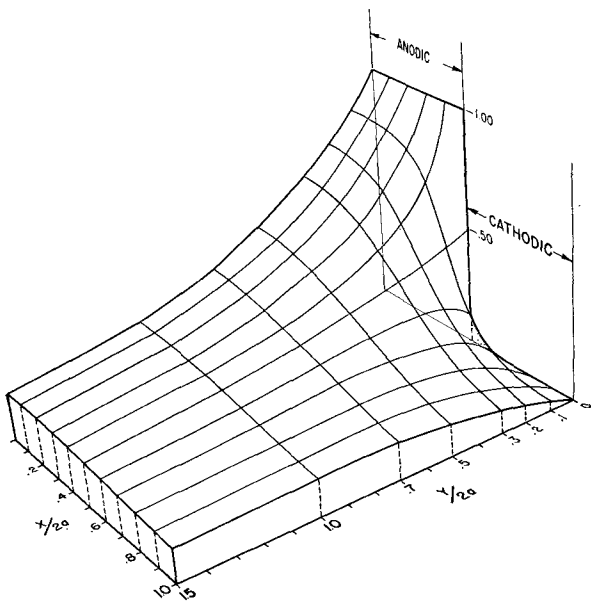


FIG. 4. Perspective scale drawing of the reduced potential function evaluated for a/ξ equal to infinity.

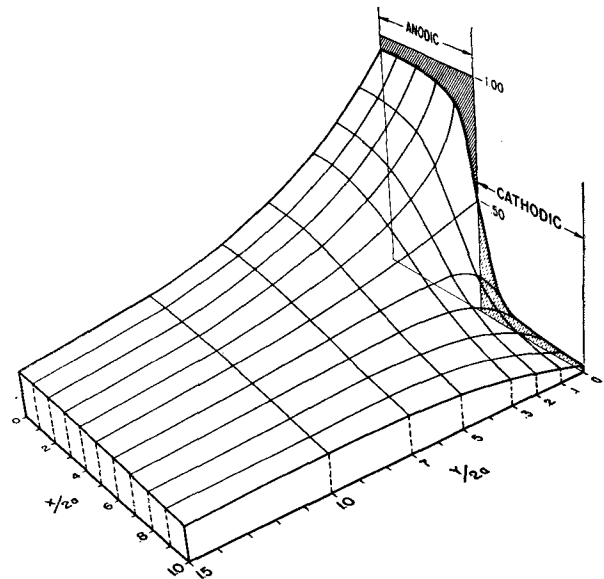


FIG. 5. Perspective scale drawing of the reduced potential function evaluated for a/ξ equal to 10.

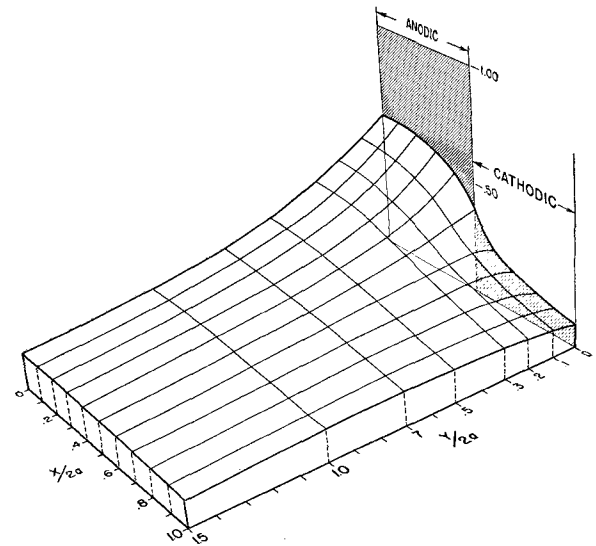


FIG. 6. Perspective scale drawing of the reduced potential function evaluated for a/ξ equal to 1.

convention. However, in this figure the polarization has been assumed to be negligible.

In Fig. 3, the reduced interfacial potential at the anode-cathode boundary, i.e., at $x/2a = 0.5$, is one-half. However, in the case of polarization, as shown by the other three figures, this potential value is less than one-half and approaches zero as ξ becomes very large.

Evaluation of the Interfacial Potential

Variation of the potential can be computed at the electrode-liquid interfaces from the relative current distribution. Equation [26] can be substituted back into [7] to give

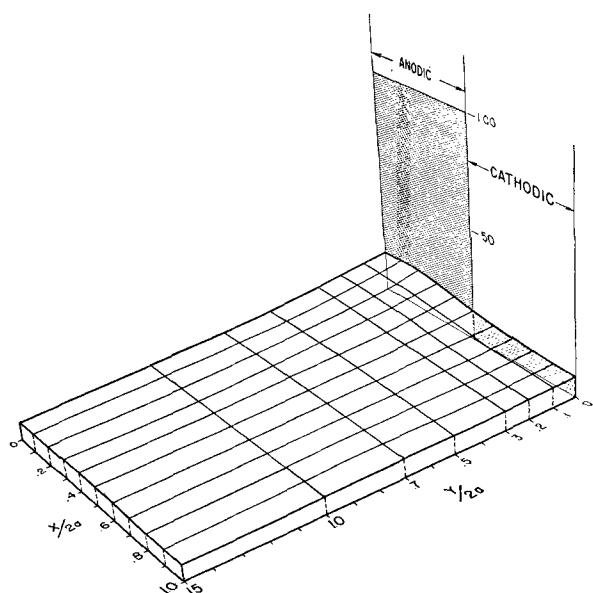


FIG. 7. Perspective scale drawing of the reduced potential function evaluated for a/ξ equal to 0.1.

$$P^*(x, 0) = E_a S'_a(x) - \xi E_a C_a^*(x)/2a \quad [46]$$

Thus, numerical values can be obtained from values of $C_a^*(x)$.

Since the cosine and sine integrals [33] and [34] are tabulated only for positive arguments (8), it is necessary to write the interfacial potential in a more general form which can be evaluated when x becomes larger than a or λ' becomes negative. Such an expression is

$$2P^*(x, 0) = E_a \left\{ 1 - \frac{2}{\pi} \sin \lambda Ci(\lambda) - \cos \lambda \left[1 - \frac{2}{\pi} Si(\lambda) \right] \right\} + E_a \nabla(x) \left\{ 1 - \frac{2}{\pi} \sin |\lambda'| Ci |\lambda'| \right. \\ \left. - \cos |\lambda'| \left[1 - \frac{2}{\pi} Si |\lambda'| \right] \right\} \quad [47]$$

where $\nabla(x)$ is defined by

$$\nabla(x) = 2S'_a(x) - 1 = \begin{cases} 1 & x < a \\ 0 & \text{for } x = a \\ -1 & x > a \end{cases} \quad [48]$$

The interfacial potential over the anode can be evaluated by means of either [46] or [47]. Certain features of the interfacial potential have already been discussed. Further discussion has been deferred to a later section.

Consideration of an Infinitely Small Cathode

The practical cases of tiny cathodes (arising from impurities) imbedded in a large anode warrant consideration. The only modification (6) required is a shift in the potential scale so that the extrapolated potential of the unpolarized anode is taken to be zero. The cathodic width is c , and the cathodic potential, E_c , can be obtained from boundary condition [6]. Thus

$$E_c = E_{c(0)} = -E_a \quad [49]$$

Boundary condition [7] may be written as

$$\frac{P^*(x, 0)}{E_a} = \frac{\xi}{E_a} \frac{\partial P^*}{\partial y} \Big|_{y=0} \quad [50]$$

for the new cathodic regions, namely

$$0 \leq x < c \quad [51]$$

The change of sign E_a in [49] also changes the sign of P . The sign of the derivative term in [50] is not changed because the direction of flow of ions remains correct. It is clear that

$$\frac{2c}{E_a} \frac{\partial P^*}{\partial y} \text{ is } \begin{cases} < 0 \\ > 0 \end{cases} \text{ for } \begin{cases} c < x \leq \infty \\ 0 \leq x \leq c - 0 \end{cases} \begin{matrix} \text{anodic} \\ \text{cathodic} \end{matrix} \quad [52]$$

Thus the problem of tiny imbedded cathodes leads to identical equations and results, except for a change in sign of the potential.

However, the proper value of $\nabla(x)$ must be used in [47] to obtain the cathodic current density function $C^*(x)$. It may be evaluated from the expression

$$C_c^*(x) = \frac{2a}{\pi \xi} \left[S'_a(x) - \frac{P^*(x, 0)}{E_a} \right] \quad [53]$$

with the condition that x is greater than a .

Some Experimental Values of Polarization Parameters

Numerical values of the polarization parameter ξ depend upon the electrolyte as well as on the anodic and cathodic metals involved. Wagner (2) has shown how ξ_c may be derived from Tafel's equation if hydrogen evolution and related phenomena are the predominant cathodic processes. Thus

$$\xi_c = \sigma \beta / J_c \quad [54]$$

where β is a coefficient in Tafel's equation for over-voltage, namely

$$\eta = \text{constant} + \beta \log_e J_c \quad [55]$$

One is forced in many cases to use this general expression since experimenters frequently do not

obtain polarization curves applicable to their experimental conditions.

Typical values have been calculated from the literature to indicate the order of magnitude of the polarization parameters. Using formula [54], Wagner (2) obtained an approximate value of ξ_c from Mantzell's data. Depending on the current density ξ_c lies in the range 0.025–0.083 cm. One may calculate from Copson's data (9) that ξ_c lies in the range 0.81–2.41 cm.

Anodic potentials have not been extensively studied. Piontelli and Poli have systematically studied the effect of current density on the anodic dissolution of lead, tin, antimony and bismuth, copper, cadmium, thallium, and silver in a wide variety of solutions (10). Certain of their data indicate that the potential curves for anodic dissolution at moderate current densities change from a logarithmic function of current density to a linear one as the temperature of the medium increases. Thus, one may use the slope of the linear curve to evaluate ξ_a . This has the advantage that ξ_a is not a function of J_a and, hence, more useful values can be obtained.

Using Piontelli's data for the anodic dissolution of lead in 0.5M lead perchlorate, ξ_a at 75°C was approximately 0.05 cm and increased to 0.14 cm at 50°C. The data for copper at 25°C dissolving in a 1M cupric perchlorate, 1M perchloric acid mixture gave ξ_a equal to 0.3 cm.

These data indicate that test specimen anodes larger than a few inches will probably behave "macroscopically" in a wide variety of conditions if strong electrolytes are used.

Previous Studies

No experimental investigations are known to the authors in which the distribution of corrosion attack was systematically studied on systems where one electrode was very large in comparison to the other. A number of authors have studied the effects of electrolyte composition on the rate of corrosion of relatively pure metals containing intentional (or unintentional) foreign inclusions in an effort to establish the importance of local cell action. Despite the general significance of such work, it does not seem germane to the present discussion.

The most pertinent experimental study was conducted by Thornhill and Evans (11) in 1938, who investigated the variation in current flowing between a scratch line made on iron wetted with sodium bicarbonate, the concentration of which was chosen to cause rusting along the scratch but not elsewhere. However, the experimental arrangement permitted them to investigate only the horizontal gradient of potential.

The studies of Jaenicke and Bonhoeffer (12) and Daniel-Bek (13) are not pertinent to the limiting case under discussion here since the anodes and cathodes were nearly equal in size. Their thorough experimental studies will be analyzed and compared in a subsequent report.

At approximately the same time, Wagner (3) as well as Frumkin and Levich (4) were carrying on important theoretical investigations. Specifically, these authors had addressed themselves to the significant problem of the acid dissolution of a metal containing foreign inclusions, and had described the conditions under which the *IR* drop in the electrolyte was unimportant.

Frumkin and Levich (4) showed that the ohmic potential drop (evaluated for zinc containing nickel inclusions dissolving in sulfuric acid) does not exceed 13 mv if the radius of the inclusions was approximately 1 μ . Guertler and Blumenthal (14) showed experimentally that the *IR* drop was very small in two rather similar cases. As these various authors have pointed out, the corrosion of metals containing foreign inclusions is regulated by the polarization characteristics of the inclusions.

DISCUSSION

It should be made clear that the present investigation is an idealized limiting case. The most serious limitation is that equal polarization parameters have been assumed. Not only may ξ_a and ξ_c be different in a given cell, but they may vary individually over the two electrodes.

As indicated above, the range of ξ values is relatively small in any of the studies made to date. The assumption that $\xi_a = \xi_c$ is not seriously in error if the ratio of a/ξ is either very small or very large, since in either range, fivefold changes, for instance, of this ratio do not significantly affect the interfacial potential or the current density.

The information gleaned from the two papers of Piontelli and Poli indicates that ξ_a may be relatively insensitive to the current density and thus remain constant over a given electrode element. The current density distribution does not change very much over a tiny cathode if a/ξ is smaller than one as shown in Table I. This in turn means that ξ_c does not change significantly over the tiny electrode as shown by equation [54].

The question of how ξ will vary over the infinite electrode, if it is dependent upon the current density, has not been fully investigated. One may use a qualitative argument. Since only a finite amount of cathodic current must flow which is equal in amount to the total anodic current, it is evident that J_c must decrease in size as x approaches infinity. This strongly indicates that ξ would not be

uniform if computed from equation [54], but would increase drastically as if it were computed from measurements farther and farther away from the anode-cathode junction. Fortunately, the current distribution becomes more uniform as a/ξ decreases; hence, this influence would tend to counterbalance any increase in ξ due to the forced decrease in J_c . At distances several times as large as ξ , the interfacial potential and, thus, current density on the infinite electrode side of the junction become relatively uniform. Take, for example, the most drastic case shown in this paper, namely $a/\xi = 10$, as shown in Fig. 5, the interfacial potential decreases rapidly near the boundary. At distances of, say, $3(\xi/a)$ beyond the boundary, i.e., at $x/2a = 0.65$, the interfacial potential becomes rather uniform. Clearly the same is true on the anodic side for $x/2a < 0.35$. The current densities have not been evaluated on the larger electrode; however, one can clearly see the equivalent trend in the anodic current density illustrated in Fig. 3. The quantity $C^*(x)$ is relatively uniform for distances $x/a < 0.7$ for the three finite values of a/ξ .

One may summarize this much of the discussion by saying that the interfacial potential is virtually the same for the anode and the cathode if both ξ_a and ξ_c are much greater than the width of the small electrode. In other words, the IR drop within the corroding electrolyte between anodic and cathodic areas will be relatively insignificant under these conditions, that is, when ξ is large in relation to a .

It is clear from inspecting the perspective drawings that the variation in potential in a direction parallel to the electrode surface is greatest at the interface between the electrode and the liquid. This variation in potential diminishes as one recedes from the interface and approaches a constant potential value at great distances. It has been shown (6) that this constant is equal to $E_a(a/c)$ for the condition $\xi_a = \xi_c$. This value has been called the potential of a composite electrode. It is evident that this potential, which is obtained with a remote reference electrode, is dependent not only on the potential difference E_a , but also on the relative proportions of anodic to cathodic material. In the present case, the composite electrode will have zero or negligible potential except in the immediate vicinity of the tiny electrode. This fact indicates the relative futility of attempting to locate individual anodic and cathodic areas by potential mapping of relatively homogeneous metal specimens. It is pertinent to the application of the rotogenerative technique as described by Francis (15) to practical problems.

Mathematically one can readily deduce these

results from the expressions for the potential function. It is evident that

$$P(x, \infty) = E_a \left(\frac{a}{c} \right) = 0 \quad [56]$$

from equation [20]. In equation [23], the integrands become zero as y approaches infinity and, thus, $P^*(x, \infty)$ becomes zero.

It is significant that the interfacial potential becomes $E_a(a/c)$ when ξ becomes infinitely large. This has been demonstrated in a companion study (7). It is evident from equation [23] that the integrands vanish for infinite ξ . Hence, P^* approaches the value for the composite electrode, namely, zero for infinite ξ .

The potential within the electrolyte is "squeezed" between the interfacial potential $P^*(x, 0)$ and the remote potential $P^*(x, \infty)$ and, as a/ξ becomes very small, any variation eventually vanishes. That is, any potential variation in the solution is smaller than that observed on the interface. Under conditions of strong polarization, variation of the latter becomes negligible.

The current density and the total anodic current remain finite for a given width of the anode. Consideration of tiny cathodes leads to equivalent results. This finite current density is different from calculations in which the effect of polarization is ignored. This fact justifies the present calculations in spite of the rather artificial condition of equal polarization parameters.

SUMMARY

The distribution of current density over the anode and the distribution of potential within the electrolyte have been obtained mathematically for the condition that one electrode is infinitely large in comparison with the other, and for the condition that the polarization parameter, as defined by Wagner, is equal for both electrodes. Values of the maximum and minimum values of the current density parameter have been obtained for nine values of the parameter (a/ξ) in the range from 0.001 to 1000. In addition, detailed values of the interfacial potential and anodic current densities were calculated for three values of (a/ξ) , namely, 0.1, 1, and 10. In agreement with the results of Wagner and others, the distribution of current density is more uniform for the smaller values of (a/ξ) .

ACKNOWLEDGMENTS

The authors are indebted to Max Goldstein, Jane Ingersoll, Chester Kazek, and John Ruth who assisted in evaluating the expressions and checking

the accuracy of the derivations. The friendly advice and inspiring suggestions of Carl Wagner are gratefully acknowledged.

Any discussion of this paper will appear in a Discussion Section to be published in the December 1955 JOURNAL.

REFERENCES

1. J. T. WABER, *This Journal*, **101**, 271 (1954).
2. C. WAGNER, *ibid.*, **98**, 116 (1951).
3. C. WAGNER, "Handbuch der Metallphysik," Vol. I, Part 2, p. 195, Akad. Verlagsgesellschaft Becker & Erler, K. G., Leipzig (1940).
4. A. FRUMKIN AND B. LEVICH, *Acta. Physicochim. U.R.S.S.* (in English), **18**, 325 (1943).
5. C. WAGNER, *This Journal*, **99**, 1 (1952).
6. J. T. WABER, "Mathematical Studies of Galvanic Corrosion, Part III. Effects of Polarization," AEC Document LA-1386, March 1952.
7. J. T. WABER, "Mathematical Analysis of Galvanic Corrosion, Part I. Potential Evaluations for Coplanar Electrodes with One Electrode Infinitely Large and with Equal Polarization Parameters," AEC Document LA-1651, June 1954.
8. ANON., "Tables of Sine, Cosine and Exponential Integrals," Vol. 2, Federal Works Agency, Works Project Administration for the City of New York (1940).
9. H. R. COPSON, *This Journal*, **84**, 71 (1943).
10. R. PIONTELLI AND G. POLI, *Gazz. chim. ital.*, for lead, **78**, 717 (1948); tin, **79**, 210 (1949); antimony and bismuth, **79**, 214 (1949); copper, **79**, 538 (1949); cadmium, **79**, 635 (1949); thallium, **79**, 642 (1949); silver, **80**, 107 (1950).
11. R. S. THORNHILL AND U. R. EVANS, *J. Chem. Soc. (London)*, **1938**, 614.
12. W. JAENICKE AND K-F. BONHOEFFER, *Z. physik. Chem.*, **193**, 301 (1944).
13. V. S. DANIEL-BEK, *Zhur. Fiz. Khim.*, **15**, 382 (1941); **18**, 247 (1944); **20**, 567 (1946).
14. W. GUERTLER AND B. BLUMENTHAL, *Z. physik. Chem.*, **152**, 197 (1931).
15. J. B. McANDREW, W. N. COLNER, AND H. T. FRANCIS, Nat. Advis. Council for Aeron., Tech. Note 2523 (November 1951) 12 pp.

Discussion Section



ELECTRONIC CONFIGURATION IN ELECTRODEPOSITION FROM AQUEOUS SOLUTION

I. The Effect of Ionic Structure

E. H. LYONS, JR. (pp. 363-375)

A. A. VLČEK¹: The rules which govern the relations of mechanism of electrode processes to structure of inorganic compounds are perhaps oversimplified in Lyons' paper. From the comparison of all experimental polarographic data on the behavior of inorganic compounds with their structure, especially their electronic configuration, it is possible to deduce the following rules.

1. It is most probable that irreversibility and over-voltage of an electrode process are not of an electrolytical, but of a chemical nature, due to a slow step in the whole electrode process, the primary electron transfer being rapid in comparison with other stages of the electrode process (in agreement with Heyrovský,² Libby,³ and Lyons⁴).

2. The electrode process (reduction or deposition of a metal) can follow one of three paths:

(a) Direct acceptance of an electron by a free stable orbital [this occurs especially with transition metal ions with free ($n - 1$) d orbitals]. If no change occurs in the structure of reacting particles after the acceptance of the electron, the electrode process is very rapid and reversible. (Only to this special case can Libby's symmetry rule and Lyons' definition of conditions for reversibility be applied.)

(b) Dissociation of one or more ligands resulting in loosening one or more *hybrid* orbitals by which the electron can be accepted (complexes of nontransition metal ions).

(c) Acceptance of the electron by a peripheral orbital (i.e., orbital higher than the orbitals occupied by electrons from ligands) with subsequent change of configuration of the particle. If this change is very slow, the particle is not reducible. This often holds for inner orbital complexes of transition metal ions which have the complete rare-gas structure, or for inert complexes of outer orbital type, especially for 6-coordinated complexes. This type of mechanism gives a specification of Lyons' rule according to which the metal is not deposited from inner orbital complexes. There are many examples of outer orbital complexes which are not reducible and of inner orbital complexes which are reducible,⁵ so that Lyons' rule is not generally valid.

This Discussion Section includes discussion of papers appearing in the JOURNAL of The Electrochemical Society, 101, No. 7-12 (July-December 1954). Discussion not available for this issue will appear in the Discussion Section of the December 1955 JOURNAL.

¹ Polarographic Institute of Czechoslovakia, Academy of Sciences, Prague, Czechoslovakia.

² J. HEYROVSKÝ, *Collection*, Suppl. II, 1954. In press.

³ W. F. LIBBY, *J. Phys. Chem.*, **56**, 39 (1952).

⁴ E. H. LYONS, JR., *This Journal*, **101**, 363 (1954).

⁵ A. A. VLČEK, *Collection*. In press.

In addition to the three above-mentioned mechanisms there is still another possibility. It is the acceptance of the electron by a free, but not stable, inner orbital as the first step of the electrode process, with subsequent rearrangement of electron shells and ligands.

These rules are only a primary rough description of possible mechanisms of electrode processes. A detailed study of this problem, especially the influence of the stereochemistry of complexes, of external conditions (temperature, solvent, composition of solution), and of potential of electrode is in progress in the discussor's laboratory.

Agreement of the theoretical and experimental slope on logarithmic analysis of polarographic curves is by no means a proof of reversibility of the electrode reaction concerned. A reversible process has to satisfy these three conditions: (a) equality of the half-wave potential of the cathodic and anodic waves of the supposed electrode reaction; (b) agreement of this half-wave potential (extrapolated to zero ionic strength) with the normal electrolytic potential; and (c) agreement of the theoretical and experimental slope on logarithmic analysis of the curve.

E. H. LYONS: A number of exceptions to the rule proposed were cited,⁴ and a thermodynamic basis for them was suggested. The most prominent are the six metals of the platinum group; mechanism 2c of Vlček appears to explain this deposition. Again, deposition of nickel from the inner orbital cyano complex at the dropping mercury electrode⁶ was ascribed to the properties of the amalgam; except for "flash" deposits, deposition at a solid cathode appears to be confined to solutions also containing hexacyanoferrate (II)⁷ or similar ions, a study of which is in progress in our laboratories.

Furthermore, it is not always easy to determine whether a complex ion is inner or outer orbital. According to Taube,⁸ covalent (as opposed to ionic) nature of the bonds is not a reliable criterion; neither color, magnetic susceptibility, nor structure appear to be entirely trustworthy. In some instances, the free energy of the inner orbital configuration is so close to that of the outer that mobile equilibrium is established and appreciable quantities of both states are present simultaneously. Deposition of copper from the salicylaldehydediimino ion and certain others⁹ may result from such a circumstance.

Besides ions characterized by rates of substitution and certain other data discussed by Taube, it is certain only that where no vacant inner orbitals exist prior to coordination, there can be no inner orbital complex. Thus, with metals such as zinc and cadmium, only outer orbital ions are formed. However, it is probable that certain structures

⁶ Y. P. HOKHSHEIN, *J. Gen. Chem. U. S. S. R.*, **7**, 2486 (1937).

⁷ L. E. STOUT AND J. CAROL, *Trans. Electrochem. Soc.*, **58**, 357 (1930).

⁸ H. TAUBE, *Chem. Rev.*, **50**, 69 (1952).

⁹ M. CALVIN AND R. H. BAILES, *J. Am. Chem. Soc.*, **68**, 949 (1946).

are not suitable for electrodeposition. For example, the phthalocyanine complex does not exchange zinc appreciably with the aquated ("free") ions,¹⁰ and it may be supposed that zinc will not be electrodeposited from similar complexes having substituted groups to confer solubility. Similar considerations should apply to porphyrins, porphyrazines, and other "fused-ring" structures.¹¹

Furthermore, the rule does not explain the failure of magnesium and aluminum to give deposits from aqueous solutions, although this failure would be expected from other considerations.

Nevertheless, the rule holds in so many instances as to be of general utility, particularly at solid cathodes. Thus, it led to the suggestion⁴ that certain copper (II) ions are outer orbital even though of square planar configuration, a view supported only by magnetic evidence¹² the interpretation of which was not entirely clear; quite recently infra-red absorption spectra¹³ have shown that the ions are almost certainly outer orbital, in accordance with the rule.

A. H. DU ROSE¹⁴: Mr. Lyons is to be commended for this presentation. More of this type of study will eventually lead to a much better understanding of electrochemical phenomena.

The statement was made that only an ultra-thin deposit of nickel could be obtained from a cyanide solution. I wonder if any nickel at all could be obtained from a very pure cyanide nickel solution. Our experience is that it cannot. If, however, a small amount of copper cyanide is added, a white deposit can be obtained, possibly because the resulting deposit is a solid solution of nickel and copper. How would the fact that nickel can be fairly easily deposited along with copper from a cyanide solution fit in with your theory?

E. H. LYONS, JR.: Our experience agrees with the remarks of Dr. Du Rose, but is not sufficiently extensive for a categorical statement that deposits cannot be obtained from pure baths. A number of such ultra-thin deposits which we have termed "flash" deposits, are doubtless alloy deposits with unrecognized impurities.

Deposition of iron, nickel, and copper as constituents of alloys from cyanide baths was reported some years ago.¹⁵ Alloy deposits of molybdenum¹⁶ and tungsten¹⁷ have also been obtained, although pure deposits of these metals are unknown from any baths. Apparently in alloys the free energy of the metal is low enough so that deposition is possible. Deposition may occur because the strength of the

coordinate bonds is altered by formation of heteronuclear complex ions. An investigation of this point is projected.

CORROSION OF ALUMINUM IN POTASSIUM CHLORIDE SOLUTIONS

I. Effects of Concentrations of KCl and Dissolved Oxygen

W. Beck, F. G. Keihn, and R. G. Gold (pp. 393-399)

M. E. STRAUMANIS¹⁸: It is a real satisfaction to learn that all the phenomena observed during your careful work can be explained by the action of local elements.

In your numerous experiments, the presence of hydrogen peroxide could not be proven. However, the presence of this peroxide, evidently formed during corrosion processes, has been found by some other authors. How do you explain this contradiction?

W. BECK: The authors could not detect H₂O₂ under the experimental conditions already described. This is not proof that H₂O₂ is not formed during the corrosion of other metals and Al alloys under different experimental conditions.

F. A. CHAMPION¹⁹: I have read with interest the paper by Beck, Keihn, and Gold. Their work adds most useful information on the subject, but it is unfortunate that some of their results have been analyzed on a false basis. They adopted the expression $w = at^n$ which Streicher observed for the dissolution of aluminum in sodium hydroxide solutions, and it is not surprising that they did not obtain a good fit with their results as indicated by the need for three slopes in their log/log plot. The asymptotic character of their w/t plots supports the expectation that the alumina film is playing a more important role in these chloride solutions. I suggest that the parameters of the exponential expression observed under such conditions²⁰ would provide a sounder basis for the analysis of the present results.

W. BECK: In the past many different mathematical expressions have been used to represent corrosion rates. The second part of this paper, which is concerned with the acceleration of the corrosion rate of Al by the addition of H₂O₂ to KCl solutions, will discuss this corrosion rate in greater detail. The authors appreciate Dr. Champion's suggestion which will be considered in a new analysis of the results.

ELECTROCHEMICAL POLARIZATION OF ZIRCONIUM IN SODIUM CHLORIDE SOLUTION

Norman Hackerman and Olin B. Cecil (pp. 419-425)

WALTER BECK²¹: The writer of this discussion was engaged in a study of the electrode potential and corrosion

¹⁸ School of Mines and Metallurgy, Department of Metallurgy, University of Missouri, Rolla, Mo.

¹⁹ Research Labs., The British Aluminium Co., Ltd., Chalfont Park, Gerrards Cross, Bucks., England.

²⁰ *Trans. Faraday Soc.*, **40**, 593 (1945); *Corrosion*, **5** (3), 92 (1949).

²¹ Department of Metallurgy, Syracuse University, Syracuse, N. Y.

¹⁰ D. C. ATKINS, JR., AND C. S. GARNER, *ibid.*, **74**, 3527 (1952).

¹¹ S. RUBEN, M. D. KAMEN, M. B. ALLEN, AND P. NACHINSKY, *ibid.*, **64**, 2297 (1942).

¹² P. RAY AND D. N. SEN, *J. Indian Chem. Soc.*, **25**, 473 (1948).

¹³ D. N. SEN, S. MIZUSHIMA, C. CURRAN, AND J. V. QUAGLIANO, *J. Am. Chem. Soc.*, **77**, 211 (1955).

¹⁴ Harshaw Chemical Co., Cleveland, Ohio.

¹⁵ L. E. STOUT, O. G. BUSCH, AND A. S. LANGSDORF, *Trans. Electrochem. Soc.*, **57**, 113 (1930); L. E. STOUT AND J. CAROL, *ibid.*, **58**, 357 (1930); L. E. STOUT AND C. L. FAUST, *ibid.*, **60**, 271 (1931), and **64**, 271 (1933); C. L. FAUST AND G. H. MONTILLON, *ibid.*, **65**, 361 (1934).

¹⁶ W. P. PRICE AND O. W. BROWN, *ibid.*, **70**, 425 (1936).

¹⁷ M. L. HOLT, *ibid.*, **66**, 453 (1934); *ibid.*, **71**, 301 (1937).

behavior of various borides of Zr and Mo, produced by powder metallurgy, by the American Electrometal Corporation in Yonkers, New York. He also made electrode potential measurements on pure Zr (Foote Mineral Company). Cylindrical specimens were immersed in a 0.1N KCl solution at 30°C under normal atmospheric conditions. In agreement with Dr. Hackerman's observations, it had been found that the potential of Zr increased very rapidly in cathodic direction during an initial period, which was short as compared with the total time of immersion of 200 hr. The potentials became stationary at -75 mv on the 1N Hg₂Cl₂ scale. The electrode potential behavior of intermetallic compounds between Zr and B was completely different from that revealed by the pure Zr and was strongly influenced by the number of B atoms present in the compound.

HYDROGEN OVERVOLTAGE ON BRIGHT PLATINUM

II. pH and Salt Effects in Acid, Neutral, and Alkaline Solutions

Sigmund Schuldiner (pp. 426-432)

MORRIS EISENBERG²²: If I recall correctly your H₂-overvoltage curves have shown a change to a larger slope (0.12) in alkaline solutions at current densities of about 10 ma/cm² and more. You have attempted to explain this by postulating another H₂-evolution reaction for the alkaline solutions. Wouldn't it be worthwhile to consider the effect of the concentration gradient which, for a given applied current density, would be larger in case of an alkaline solution than in case of an acidic solution. The resulting additional overpotential so-called concentration polarization can be expressed as

$$\Delta E_{\text{conc}} = \frac{RT}{nF} \ln \frac{(H^+)_i}{(H^+)_o} = \frac{RT}{nF} \ln \left(\frac{I_i - I}{I_i} \right)$$

where (H⁺)_i and (H⁺)_o are the H⁺-concentration at electrode surface and in bulk, *I_L*-limiting current density, *I*-applied current density.

You have compared curves for acids and alkalis within the same regions of applied current densities. Since in alkalis (H⁺)_o and, therefore, also *I_L* are low, then, for a given value of *I*, concentration polarization would become more significant and account for progressively higher total values, hence a larger slope.

While I do not exclude the possibility that other (e.g., catalytic) effects may also be involved, in this case I would like to submit for your consideration the above argument for a possible re-examination of your data for H₂-overvoltage in alkaline solutions.

S. SCHULDINER: Dr. Eisenberg's comments are largely covered in the discussion by Stern and the reply given below. In alkaline solutions, only one hydrogen producing mechanism was postulated (water reduction).

MILTON STERN²³: This paper is a most welcome contribution to our present growing knowledge of overvoltage

²² Stanford Research Institute, Stanford, Calif.

²³ Metals Research Labs., Electro Metallurgical Co., Niagara Falls, N. Y.

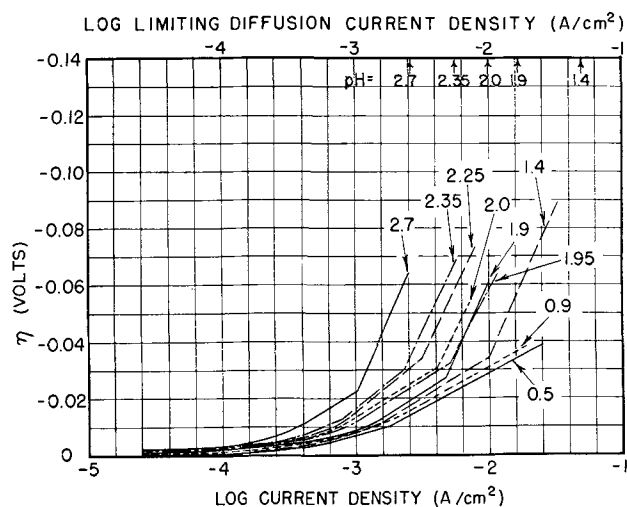


FIG. 3. Effect of pH on hydrogen overvoltage in acid solutions.

phenomena. Some comments are in order both to supplement the information presented and to discuss terminology and interpretation.

Since the experiments under consideration were conducted "in vigorously agitated solutions to minimize concentration overvoltage" one might assume that the use of η implies that only activation overvoltage (η_a) is involved in the reported polarization phenomena. This obviously need not be true at higher current densities, and one may estimate the current density where concentration overvoltage (η_c) will become a significant factor. For the experimental conditions used to obtain the data of Fig. 3, where the transference number of hydrogen ions may be neglected, one may use the following expression^{24, 25} which relates the limiting diffusion current for hydrogen ions to their activity.

$$i_L = \frac{\eta^F D}{\delta} \alpha_{H^+} \quad (I)$$

D is the diffusion coefficient for hydrogen ions estimated here as averaging 7 (10⁻⁵) cm²/sec, δ is the thickness of the diffusion layer which is approximately 0.005 cm in a vigorously stirred solution, and the other symbols have their usual meaning.

Limiting diffusion currents, so calculated for the pH values used, are superimposed on the original Fig. 3 and indicate that the measurements are in the range where concentration overvoltage (η_c) should be considered. The dependence of η_c on current density may be approximated^{24, 25} by the following equation:

$$\eta_c = 0.059 \log \frac{i_L - i}{i_L} \quad (II)$$

which indicates that concentration overvoltage starts to become significant when the current reaches the order of one-tenth the value of *i_L*.

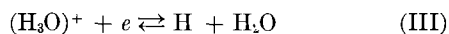
Concentration overvoltage, which is time dependent

²⁴ J. N. AGAR AND F. P. BOWDEN, *Proc. Roy. Soc.*, **169A**, 206 (1938).

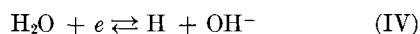
²⁵ C. W. TOBIAS, M. EISENBERG, AND C. R. WILKE, *This Journal*, **99**, 359C (1952).

upon initial application of current, can also account for the reported inconsistency of results in the pH range 2.7 to 7.1 where this effect would be pronounced at much lower current densities.

The hypothesis of two parallel hydrogen-producing reactions



and



appears to be quite sound. However, it is surprising to find a sharp, distinct change in mechanism which the author indicates takes place at the overvoltage (activation) where the Tafel slope changes abruptly from 0.029 to 0.12. Rather, one might expect deviation from Tafel behavior because of concentration overvoltage when depletion of hydrogen ions occurs. This behavior may be expressed by the relation

$$\eta = \eta_a + \eta_c = -\alpha - \beta \log i + 0.059 \log \frac{i_L - i}{i_L} \quad (\text{V})$$

Above the limiting diffusion current, Tafel behavior may again occur when reaction (IV) becomes controlling. Unfortunately, measurements presented on Fig. 3 at any given pH appear to have been stopped just short of the currents required to determine whether deviation from a slope of 0.029 truly results in another Tafel slope, or is actually that predicted when concentration polarization is considered. Placing of experimental points on Fig. 3 would be helpful in this direction. Why were the measurements not carried out to higher current densities?

Quantitative measurements²⁶ conducted at the Corrosion Laboratory, M.I.T., with iron and qualitative tests with smooth platinum show that deviation from Tafel behavior does occur at current densities which can be estimated from equations (I) and (II). The controlling Tafel regions for the two hydrogen-producing reactions discussed above are separated by a nonlinear region of concentration overvoltage resembling the limiting diffusion current behavior observed in polarography. Between pH values of 3 and 6, concentration overvoltage masks all signs of a Tafel region below the limiting diffusion current, and only one truly linear region exists.

S. SCHULDINER: Experimental results given in the above paper and in part I²⁷ indicate a sharp change from the first to second Tafel slopes with no substantial intermediary region. Experimental points are shown in part I. The same spread of points was observed in the above paper. Current densities given in these papers represent maximum values obtainable under the experimental conditions used. This was owing to either instrumental limitations or erratic results at higher current densities.

King²⁸ has plotted concentration overvoltage against log current density for various solutions. His curves show that a current density range in which a 0.12 slope could be

drawn would be much smaller than the actual current density ranges shown for this slope in these papers.

In the table below a typical set of data is applied to Stern's equation (II). Here the curve for pH 2.7 shown in the above figure (Fig. 3) was used in the calculation. The i_L , as calculated by Stern, for this case is 0.00263 amp/cm².

Current density, i (amp/cm ²)	η_c (v)	$\eta_{\text{expt.}}$ (v)	$\eta_a = \eta_{\text{expt.}} - \eta_c$ (v)
0.00100	-0.012	-0.022	-0.010
0.00159	-0.024	-0.042	-0.018
0.00200	-0.037	-0.052	-0.015
0.00229	-0.053	-0.060	-0.007
0.00251	-0.079	-0.062	+0.017

These results show that after reaching a peak, the activation overvoltage, η_a , declines with increasing current density and that the calculated concentration overvoltage actually exceeds the measured overvoltages when i_L is approached. This clearly shows that equation (II) does not apply for this system.

CRYSTAL STRUCTURE AND THERMODYNAMIC STUDIES ON THE ZIRCONIUM-HYDROGEN ALLOYS

Earl A. Gulbransen and Kenneth F. Andrew
(pp. 474-480)

JAMES C. WARF²⁹: You mentioned the use of a McLeod gauge in measuring dissociation pressures. Several authors refer to the influence of traces of mercury on the dissociation pressure of hydrides, suggesting that spurious and erratic behavior may result, possibly via poisoning of the surface.³⁰ Is there any evidence that mercury vapor from the McLeod affected the dissociation pressure of the zirconium hydride?

E. A. GULBRANSEN AND K. F. ANDREW: Mercury vapor could have a very important influence on the pickup of hydrogen by zirconium. In the apparatus used for this study, the McLeod gauge was separated from the specimen by a liquid nitrogen cold trap. The reversible character of the dissociation process is proof for the absence of any poisoning due to mercury vapor.

DETERMINATION OF BARRIER LAYER THICKNESS OF ANODIC OXIDE COATINGS

M. S. Hunter and P. Fowle (pp. 481-485)

C. J. L. BOOKER AND J. L. WOOD³¹: The September 1954 issue carries an account by M. S. Hunter and P. Fowle of a method for the determination of the barrier layer thickness of anodic oxide coatings. This is a problem in which we are particularly concerned, and a few comments may be of interest.

The method described depends on the assumption that

²⁹ Department of Chemistry, University of Southern California, Los Angeles, Calif.

³⁰ VIALARD, *Ann. Chim.*, **20**, 5 (1945); UBBELOHDE, *J. Chem. Soc.*, **1950**, 1943.

³¹ Sir John Cass College, Jewry St., Aldgate, England.

²⁶ M. STERN, Unpublished work, Corrosion Lab., Massachusetts Institute of Technology, Cambridge, Mass.

²⁷ S. SCHULDINER, *This Journal*, **99**, 488 (1952).

²⁸ C. V. KING, Private communication.

the current carrying characteristics of porous and barrier type coatings are comparable. Although on experimental grounds there is reason to believe that this is approximately true, two important limitations should be borne in mind. First, the effective area determining the current density flowing across a porous layer is that of the base of the pores—only a few per cent of the superficial area. Second, it is well known that the leakage current through barrier layers is highly dependent on the incorporation of impurities in the layer. In particular, the material around the bases of pores formed in acid electrolytes may differ considerably in both chemical and electrical properties from that of barrier layers prepared in neutral electrolytes.

In the course of research on the capacity of porous layers we have developed independently a number of methods providing information of the pore base dimensions. One that may be compared to that of Fowle and Hunter is as follows: the discharge current-voltage curves of a condenser with a porous aluminum oxide layer as dielectric are found to be similar to those obtained by Charlesby³² for barrier oxide layers. In particular, the current is given by

$$i = A_+ \exp(B_+F) + A_- \sinh(B_-F)$$

where the first term refers to the ion current and the second to the electron current, and F is the field across the dielectric. This relation may also be confirmed directly. These results indicate that pore bases are comparable in conducting properties with an equivalent area and thickness of barrier oxide.

The value of F directly gives the pore base thickness, while, in principle, the pore base cross section could be determined from A_- or A_+ . However, no reliable figures for these constants in the case of barrier layers are available for comparison.

As an example, for a porous layer formed by anodizing for 30 min in 17.5% v/v sulfuric acid at 17°C with a controlled current density of 40 ma/cm², the thickness of the pore bases is 85 Å. A_- is small, 0.0004 μ a/cm², consistent with the small cross-sectional area of the pore bases.

M. S. HUNTER AND P. FOWLE: The determination of barrier layer thickness from the discharge current-voltage curve of a condenser is an interesting method of establishing this dimension of anodic oxide coatings. Of particular interest is the conclusion from this work that pore bases and barrier oxide have comparable conducting properties.

We do not believe that our method of determining barrier layer thickness depends on the current carrying characteristics of the oxide, because voltage rather than current is measured, and because the effect of leakage is eliminated by first establishing the leakage current for the metal or alloy under consideration. It is true that the current carrying characteristics of the coating are important during formation of the coating when appreciable current flows but, in the case of our thickness measurement, current flow is so low as to be insignificant. Further, we do not believe that the relatively small cross-sectional area of the pores is of significance because practically no current is flowing during our measurement and, accord-

ingly, no current density effects are involved. Both current carrying characteristics and relative pore area would be significant in a method which involved measurement of current in determining barrier thickness.

THE pH IN CHLORINE-CAUSTIC ELECTROLYSIS BY THE MERCURY CELL PROCESS

Lars Barr (pp. 497-506)

PATRIZIO GALLONE³³: This paper gives a clear theoretical demonstration of the benefits to be found in feeding mercury cells with slightly acidic brine. This is, in fact, the procedure long since adopted in de Nora mercury cell plants. In addition to the advantages shown in the paper (smaller percentages of CO₂ and H₂ in cell gas, longer anode life, practically no chlorate formation), another important benefit given by an acidic pH is that it is possible to keep calcium at a concentration even higher than 1 g/l without any formation of "mercury butter."

Another point I would like to take up in this important paper is the method of calculating cathodic current loss. In equation [39] that is thus derived, this loss is expressed as a function of pH values in the bulk of the brine and at the alkaline cathode film, respectively. Therefore, the author makes the statement that the cathodic current loss "is independent of current density." It is now to be remarked that, although theoretically correct, this statement seems to contradict experimental evidence since usually the hydrogen per cent in cell gas, i.e., cathodic current loss, decreases when current density is increased. This is because the pH at the cathode film is itself a function of current density; in fact, if current density is increased, although other conditions are kept equal (cell temperature, pH in feed brine, mercury flow rate), the pH at the cathode film will decrease, so that the migration of OH⁻ ions from the cathode will also diminish and the current efficiency will be improved, according to equation [39]. That the pH value at the cathode film should decrease when increasing the current density can be immediately seen from equation [36]. In fact, in order to obtain an increase in the current density, the cathode potential e_k must be depressed, even though but slightly, so that the "affinity" will be increased for all reduction reactions occurring at the cathode and, therefore, the hydrogen discharge rate will become higher. However, the hydrogen overvoltage, i.e., function $f_3(i)$ in equation [36], rises so steeply with hydrogen current density that the second term on the right side must also increase, which involves a decrease in the pH value at the cathode film.

LARS BARR: The remarks from Patrizio Gallone provide an interesting discussion.

Demonstrating relationship between anolyte pH and current efficiency should be done by investigating the relation between pH (composition of solution) and various current density-voltage curves at the electrode concerned.

Unfortunately, the symbol " i " in my paper refers to different current densities, which has caused a defect in

³² CHARLESBY, *Proc. Phys. Soc. B*, **66**, 317, 533 (1953).

³³ Oronzio de Nora, Impianti Elettrochimici, Milan, Italy.

some equations. I am, therefore, anxious to make corrections here.

Equation [36] represents the current density (c.d.)-voltage curve of hydrogen discharge, and here i means the hydrogen c.d., which at constant total c.d. can be considered proportional to hydrogen pressure in cell gas or to $\{H_2(g)\}$ at the cathode film under equilibrium conditions. Differentiating equation [36] in order to obtain equation [37] should accordingly include differentiating $f_3(i) = a + b \ln i$. We arrive thus at equation [37] with another constant:

$$d \log \{H_2(g)\} = -(a \text{ positive constant}) d pH$$

In the same way there should be another positive constant than 4 in equations [24] and [25] concerning the anode.

However, the results of my calculations are not affected by these discrepancies.

Dr. Gallone's remark concerning equation [39] is correct. My remark under equation [39] was only intended to point out that the equation in question is independent of its i . Here i means total c.d.

It has been shown experimentally that cathodic current efficiency in a mercury cell increases when total c.d. is increased and approaches an asymptote near 100% efficiency.³⁴ This can be roughly explained by reaction [30] being reversible and reaction [32] polarized.

I think that pH at the cathode film should be a function both of loss c.d. and total c.d., loss c.d. governing the rate of feeding the film with OH^- ions, total c.d. governing the rate of emptying the film of OH^- ions. This function also contains room dimensions and concentration gradients.

Conditions at electrode films are complicated and likely to demand advanced scientific treatment.

I think, however, that Dr. Gallone has given here a good simple picture of this matter at the mercury cathode.

M. S. KIRCHER³⁵: This paper is of considerable interest to the writer since he made a similar study on the relationship between anolyte pH and current efficiency in the diaphragm type cell.³⁶ The derivation of the relationships between anolyte pH and log of the activity of H_3O^+ , ClO_3^- , $HClO$, ClO^- , Cl_2 , Cl_3^- , H_2CO_3 , CO_3^- , OH^- , HCO_3^- , and Cl^- and the plotting of these relationships in Fig. 1, 2, and 3 was elegantly done.

From Dr Barr's paper, one might conclude that good cell operation can be obtained by adjusting the brine pH to maintain an anolyte pH of 3, whereas it is our experience that, if cells are operated properly, a pH of approximately 3 will result. In other words, the performance of a cell depends on factors other than anolyte pH and the anolyte pH is an indication of the quality of performance.

The anolyte of either a mercury or diaphragm cell operating under steady-state conditions may be regarded as a reservoir into which OH^- ions are continuously being introduced and from which OH^- ions are continuously being discharged at the anode. Excepting to the extent

which the OH^- ions enter into chemical reactions such as the formation of ClO_3^- , the rate of OH^- ion discharge is equal to the rate of OH^- ion feed and the $O_2 + CO_2$ content of the chlorine gas is equivalent to the OH^- ion introduced into the anolyte. The pH of the anolyte depends primarily on the character of the anode (the anolyte pH would be different if, for instance, carbon or platinum anodes were used) and, secondarily, on the rate at which OH^- ion is passing through the anolyte reservoir.

The source of OH^- ions entering the anolyte reservoir may be (a) the brine feed, (b) back migration of OH^- ion through the diaphragm (diaphragm cell), (c) OH^- ion formed at the mercury cathode coincident to hydrogen formation (mercury cell).

With graphite anodes and with normal operation, the pH of the anolyte of either diaphragm or amalgam cells is approximately 3 (range of 2.5-4.5), and the pH of the anolyte is practically unaffected by a change in feed brine pH from 3 to 8. Only when the acid or alkali in the feed brine is equivalent to a substantial proportion of the total current efficiency (such as 1-2%) will an appreciable effect on anolyte pH be noted.

I believe these concepts are in agreement with Dr Barr's although presented somewhat differently. I should be interested in his comments.

LARS BARR: I have read Dr Kircher's discussion with great interest. His experiences are in accordance with my own.

The purpose of my calculations is only to demonstrate the relation between anolyte pH (concentration in anolyte of certain protolytes) and current efficiency. In chlorine-caustic electrolysis such a relation must exist theoretically. This relation ought to be open to laboratory studies where all other current efficiency determining variables, e.g., anode, temperature, current density, salt concentration, are kept constant.

If in practice current efficiency is low, for instance, because of an unsuitable anode material, we cannot of course obtain good cell performance by adjusting the brine pH . Also in this case, however, the result of my calculations should be valid, i.e., with this anode material the highest possible current efficiency will be obtained below an anolyte pH of 3. In adjusting feed brine composition this anolyte could be aimed at.

FACTORS AFFECTING THE FORMATION OF ANODIC OXIDE COATINGS

M. S. Hunter and P. Fowle (pp. 514-519)

ROBERT PINNER³⁷: The very interesting paper by M. S. Hunter and P. Fowle has recently come to my attention. One is indebted to these and other authors of the Research Laboratories of the Aluminum Company of America for much excellent work on the theory of anodic film growth on aluminum. Some comment, perhaps, is called for on their statements on p. 517 under the heading "Conditions Existing at Pore Bases." Here, the authors conclude that

³⁷ Electroplating and Metal Finishing, 85 Udney Park Rd., Teddington, Middx., England.

³⁴ R. TAUSSIG, *Trans. Faraday Soc.*, **5**, 258 (1909-10).

³⁵ Hooker Electrochemical Co., Niagara Falls, N. Y.

³⁶ R. L. MURRAY AND M. S. KIRCHER, *Trans. Electrochem. Soc.*, **86**, 83 (1944).

the dissolution rate, R , of the film at the pore base is proportional to current density, C , according to: $R = 310C$.

They base this on the assumption that dissolution rate at the barrier layer must balance film growth at this point because barrier thickness remains constant. From this the authors calculate that, in anodic oxidation of aluminum in 15% sulfuric acid, the acid concentration and temperature in the pore base must approximate 51% H_2SO_4 at bp of 128°C, in order to account for the high dissolution rate.

There is, in fact, no reason to assume a linear relation between current density and dissolution rate. Barrier thickness remains a more or less constant function of voltage, not because its growth is balanced by dissolution at the pore base, but because growth is balanced by break-through and conversion into porous type coatings.

The dissolution rate suggested by Hunter and Fowle as required to balance growth is, in fact, the dissolution rate not only of the barrier layer but also of the total coating (barrier plus porous coating) and even this only when the limiting total film thickness has been reacted. Of this total dissolution much the greater part will, of course, take place at or near the surface of the porous layer.

In view of the limited solubility of aluminum in 50% sulfuric acid and the necessarily very slow diffusion of Al ions from the pore base through the coating into the electrolyte, the very high rate of dissolution at the pore base could not be maintained at any rate, while, on the other hand, conditions for equilibrium between growth and rate of dissolution at the barrier layer only apply when no porous type of coating is formed as, e.g., in boric acid or ammonium tartrate electrolytes. It should be stated that this does not detract from the important part played by local rise in temperature inside the coating due to the dissipation of electric energy (with the heat of formation of aluminum oxide as a contributory factor). This temperature differential between electrolytes in the film and the bulk of the solution has been somewhat surprisingly ignored in many of the previous theories on anodic film growth.

M. S. HUNTER AND P. FOWLE: The linear relationship between solution rate and current density during the formation of the porous type of anodic oxide coatings may appear to be illogical because oxide formation, which is a function of current density, is an electrochemical process; whereas, solution of oxide is primarily a chemical process. Our measurements show, however, that the thickness of oxide between the pore base and the metal (barrier thickness) remains constant once current density has reached a steady value. Since the total thickness of oxide must equal barrier thickness plus the depth of the pores, and since barrier thickness is constant, the thickness of oxide formed in any period of time must equal the amount by which the depth of the pores is increased during this same period. Thus, the linear relationship between solution rate and current density is an established fact, unreasonable as it may seem.

We are not in agreement with the explanation that the constancy of barrier thickness is the result of a balance between growth and break-through, since our concept of the mechanism of the formation of porous type coatings is

based on the existence of a continuous layer of oxide in contact with the metal at all times. This has been discussed in previous papers.^{38, 39}

We are somewhat puzzled by Mr. Pinner's statement that equilibrium between growth and rate of solution only applies when no porous type of coating is formed, as is the case in boric acid or ammonium tartrate electrolytes. In the formation of nonporous or "barrier type" coatings such as those formed in the electrolytes cited, rate of solution is not involved, because the prime requisite for the formation of this type of coating is that the electrolyte shall have no solvent action on the oxide. If the electrolyte can dissolve the oxide, a porous type of coating will be formed.

DIFFUSION OF HYDROGEN AND DEUTERIUM IN HIGH PURITY ZIRCONIUM

Earl A. Gulbransen and Kenneth F. Andrew

(pp. 560-566)

MORRIS EISENBERG⁴⁰: I feel that this is indeed a very nice piece of work. I would like to comment with one question. You said at the outset that you assumed the diffusion coefficient to be independent of hydrogen concentration. Under such conditions obviously your values represent integral average diffusion coefficients. Now wouldn't it be possible to start with specimens of various initial hydrogen contents and, by experimenting within various concentration gradients, to obtain the dependence of D on the concentration of hydrogen or deuterium in zirconium metal?

E. A. GULBRANSEN AND K. F. ANDREW: The integral average diffusion coefficients are obtained in this study for hydrogen in the δ and ϵ hydride phases and not for the α -zirconium phase. It would be very difficult to determine these coefficients as a function of concentration.

The diffusion coefficient of hydrogen in the metallic phase can be studied as a function of concentration. Thus, if one considers the removal of hydrogen at temperatures above 400°C, where the solubility in α -zirconium is appreciable, it would be possible to determine the effect of concentration. This would be an interesting study.

HIGH TEMPERATURE CRYSTAL STRUCTURE OF THORIUM

P. Chiotti (pp. 567-570)

JAMES C. WARF⁴¹: Thorium metal ordinarily contains some oxide. What can you say about the constitution of this oxide in thorium at room temperature? Does the metal consist of two phases?

P. CHIOTTI: The thorium metal used in this investigation initially contained approximately 0.10 wt % oxygen.

³⁸ M. S. HUNTER AND P. FOWLE, *This Journal*, **101**, 481 (1954).

³⁹ F. KELLER, M. S. HUNTER, AND D. L. ROBINSON, *ibid.*, **100**, 411 (1953).

⁴⁰ Stanford Research Institute, Stanford, Calif.

⁴¹ Department of Chemistry, University of Southern California, Los Angeles, Calif.

At room temperature the oxygen is present as ThO_2 which appears as a gray phase in the microstructure. The oxide is face-centered cubic and its lattice constant corresponds very closely to that for pure ThO_2 , indicating no appreciable solubility of the metal in this compound. The solubility of the oxide in the metal is also considered to be very small or negligible at room temperature.

ANODIC BEHAVIOR OF COPPER IN HCl

Lee Stephenson and J. H. Bartlett (pp. 571-581)

N. IBL AND R. MULLER⁴²: We were particularly interested in this paper since we are engaged in an interferometric study of the diffusion layer at electrodes. In the course of this work some experiments were also made with Cu-anodes in 2N HCl which confirm the results of Stephenson and Bartlett. In the method⁴³ used by us a curve is obtained on the photograph which gives directly the function refractive index vs. distance from the electrode. Immediately after the electrolysis current starts to flow a refractive index continuously decreasing toward the electrode is observed, showing that a depleted layer of HCl is formed; after about 2 sec the curve of the refractive index is bent upward near the electrode surface and now exhibits a sharp minimum, indicating that a dissolution process is going on.

We would like to mention that we made quite similar observations with a Cu-anode in 2N H_2SO_4 (formation of a depleted layer in the first stages of the electrolysis; sharp minimum of the curve refractive index vs. distance from the electrode, when the electrolysis has been going on for more than about 2 sec). A Cu-anode in 0.6M CuSO_4 , however, showed a different behavior. In this case a layer more concentrated than the bulk of the solution is formed near the electrode surface right at the beginning of the electrolysis and this situation remains the same later on, unaffected by time. Current density in both cases was 200 ma/cm².

RALPH S. COOPER⁴⁴: In the article by Stephenson and Bartlett the total charge which has flowed during the first current plateau is expressed by a relation of the form $Q = a(i_0 - b)^{-c}$, where b is given the value 0.70. In graphs of this form b is determined by adjusting it to remove the curvature in a log Q vs. log i_0 plot. However, data presented in the article are too scattered to evaluate b with any degree of precision, and no distinct curvature can be observed on a log-log graph even with $b = 0$.

Recent work at this laboratory has considerably improved the reproducibility of the data with the following results: the correlation of Q with i_0 is found to be dependent on the external resistance R (Fig. 1), while log Q vs. log i_I (the current during the first plateau) yields a single curve for all R . This has the same form as the earlier relation, with $b = 0.54 \pm 0.02$ (Fig. 2).

⁴² Department of Physical Chemistry, Swiss Federal Institute of Technology, Zurich, Switzerland.

⁴³ See N. IBL, Y. BARRADA, AND G. TRÜMPLE, *Helv. Chim. Acta*, **37**, 583 (1954).

⁴⁴ Department of Physics, University of Illinois, Urbana, Ill.

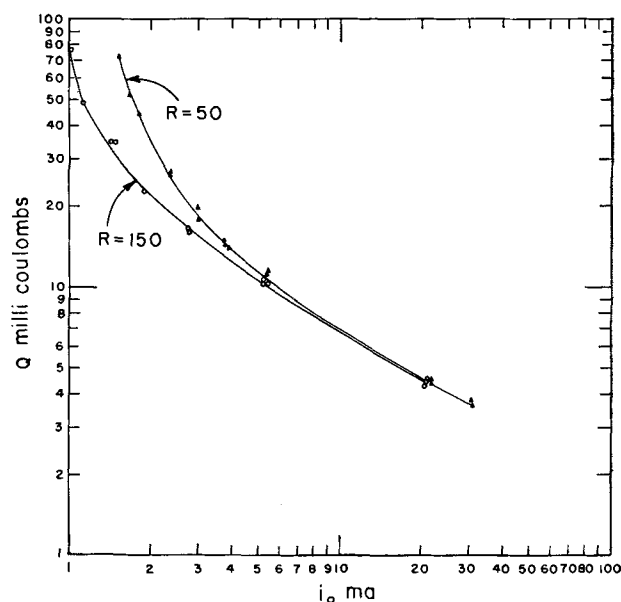


FIG. 1. Q as a function of i_0 , showing R dependence.

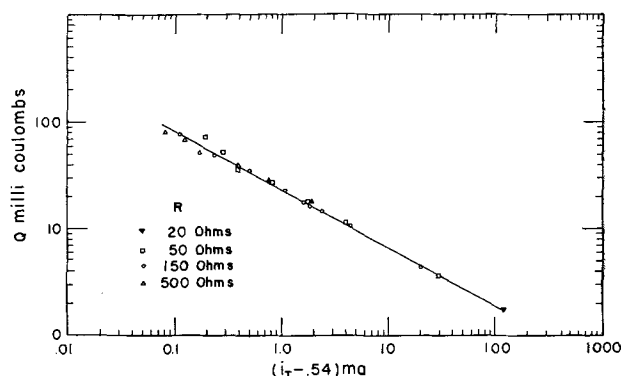


FIG. 2. Q as a function of i_I . $Q = 23(i_I - 0.54)^{-0.54}$.

In regard to the electrode reaction, theoretical calculations indicate that the reaction occurring during the first plateau is $\text{Cu} + 2\text{Cl}^- \rightarrow \text{CuCl}_2^- + e$. Details of this work will be published at a future date.

KILOGRAM SCALE REDUCTIONS OF VANADIUM PENTOXIDE TO VANADIUM METAL

Arthur P. Beard and Donald D. Crooks (pp. 597-600)

JOHN C. R. KELLY⁴⁵: In the powder metallurgy process, temperature at reaction centers in the reduction bomb can be computed by using Theoretical Flame Temperature methods. This calculation is verified by observing the proportion of fused beads to fine powder. This proportion varies with CaCl_2 content and, consequently, with the specific heat of the charge.

A. P. BEARD AND D. D. CROOKS: A further use of the calculations of the theoretical maximum temperatures shows that the temperature in the $\text{V}_2\text{O}_5 + \text{Ca}$ reaction should be much higher than the temperature in the $\text{V}_2\text{O}_3 + \text{Ca}$ reaction. Therefore, better agglomeration of the

⁴⁵ Westinghouse Electric Corp., Bloomfield, N. J.

vanadium into massive pieces may be expected in the V_2O_5 reduction, and powder in the V_2O_3 reduction.

M. D. BANUS⁴⁶: What is the estimated temperature inside the liners during the reaction?

Are the high pressures which cause the explosions that burst the bombs due to the vapor pressure of Ca metal or to a gas evolved by the reaction?

A. P. BEARD AND D. D. CROOKS: The temperature reached inside the bomb during a $V_2O_5 + Ca$ reaction is greater than the melting point of vanadium metal ($\sim 1900^\circ C$). Calculations indicate a maximum temperature of $\sim 3000^\circ C$. Estimated temperature inside the liners during the reaction is $\sim 2500^\circ C$.

Explosions that burst bombs may result from the reaction mass burning through the steel bomb, because of a cracked liner or high pressures of hydrogen or nitrogen from water and ammonium ion, which were not removed during the ignition of ammonium vanadate to V_2O_5 .

ROOM-TEMPERATURE DUCTILE CHROMIUM

H. Johansen and G. Asai (pp. 604-612)

MARVIN L. BROMBERG AND HUGH B. HIX⁴⁷: 1. Has any general relation been established between hardness and ductility?

2. Has there been found any significant difference in the properties of purified chromium prepared electrolyti-

⁴⁶ Metal Hydrides Inc., Beverly, Mass.

⁴⁷ Pigments Department, Chemical Division, E. I. du Pont de Nemours & Co., Newport, Del.

cally and chromium prepared by chemical reduction? If there is, has any explanation been forwarded?

3. Has any evidence of a high temperature phase transformation been found?

4. Is sigma phase formation a serious problem in all Cr-Fe alloys?

H. JOHANSEN AND G. ASAI: 1. If a larger tensile elongation value is to be considered as an indication of greater ductility, the softer material is more ductile. It has been shown that the ultimate tensile strength of chromium wires is increased by increased cold work. The tensile elongation has been found to decrease from 41% to 8% as the amount of cold work increases from 7% to 92%, respectively. Knoop hardness values increase from 122 to 230 for wires having no cold work and 92%, respectively.

2. No investigation of the properties of chromium produced by the magnesium reduction of chromous chloride ($CrCl_3$) has been undertaken recently and, therefore, no comparison can be made. However, there is no reason to expect any substantial differences from material prepared electrolytically.

3. No evidence of a high temperature phase transformation has been found.

4. Sigma phase formation in Cr-Fe alloys is not a serious problem here, but is certainly an item to be considered in Cr-Fe alloy work. Much work has been done here with Cr-base alloys varying in chromium content from 50 to 75%. Sigma phase formation at room temperature is very slow. Sigma phase formation during fabrication is evident but the formation is not of an extent to prevent successful working. Any sigma phase that is present in the final product is removed by heat treatment and quenching.

Dissolution of Metals in Aqueous Acid Solutions

I. Current-potential Relations for Iron and Mild Steel¹

A. C. MAKRIDES,² N. M. KOMODROMOS,³ AND NORMAN HACKERMAN

Department of Chemistry, University of Texas, Austin, Texas

ABSTRACT

The solution rate of iron in air-free hydrochloric acid solutions is a linear function of hydrochloric acid activity for activities between 1 and 10. The potential of dissolving iron is a logarithmic function of hydrochloric acid activity.

The potential of mild steel in acid solutions containing depolarizers is a linear function of the logarithm of the solution rate. It is suggested that the resulting potential-current curve (calculated from weight loss) constitutes an approximate polarization curve for the anodic reaction.

INTRODUCTION

An important step in elucidating the mechanism of wet corrosion of metals was the local-cell theory of corrosion (1). A more recent approach deals with corrosion and dissolution of metals in terms of two electrochemical reactions, an anodic and a cathodic one, rather than in terms of spatially separated local cells (2). The potential of an electrode placed in a solution containing an oxidation-reduction couple such that the electrode material takes part in the reaction is called the "mixed-potential." Measurements of potential of iron and mild steel electrodes in hydrochloric acid alone and in hydrochloric acid solutions containing depolarizers are reported in this paper and are discussed on the basis of the theory of mixed-potential.

EXPERIMENTAL

Iron coupons were mounted on a shaft driven by a $\frac{1}{4}$ hp motor through an arrangement of pulleys. Speeds up to 11,000 rpm could be obtained. The lower part of the shaft was covered with tygon tubing, and a rubber washer was used at the junction of the shaft with the coupon to prevent contact of the shaft with the solution. The coupons were tapped ($\frac{3}{8}$ in. thread hole along the axis) and attached to the shaft by screwing tightly on the lower part. Electrical contact was made through a mercury-filled recess drilled into the top of the shaft. The resistance of the junction was negligible.

Preparation of coupons.—Cylindrical coupons (2.5 cm x 1.9 cm) polished with 2 and 2/0 emery polishing

paper to a mirror-like finish were used. Emery and iron particles were removed, and the coupons were degreased with hot benzene. After weighing to the nearest 0.1 mg, the bottom and top parts as well as the edges were coated with paraffin. Coupons were stored in a desiccator until used. The projected exposed area was 10 cm².

Procedure.—A 600 cc beaker containing 400 cc of solution was fitted with a Lucite cover with holes for calomel cell, coupon, nitrogen inlet, and thermometer. For runs in air-free solutions, nitrogen was continuously bubbled through the solution via three fritted glass bubblers placed at the bottom of the beaker. The gas was purified by passing through a vanadyl sulfate train. After passing nitrogen for 30–45 min the beaker was placed under the coupon, which had been mounted on the shaft immediately before, and raised so as to immerse it. The motor was then started. A total of 5–7 sec elapsed between immersion and starting of the motor. The motor attained its full speed in 1 sec. The temperature was $30 \pm 1^\circ\text{C}$.

At the end of a run the coupon was rinsed with distilled water, then swabbed with a towel wetted with acetone. After washing in acetone, removing the paraffin with benzene, and drying, it was weighed at once or placed in a desiccator until weighed.

A student type Leeds and Northrup potentiometer and galvanometer were used. The open circuit potential, negative with respect to the saturated calomel cell, was recorded at one minute intervals. Contact with the solution was made through a 3% agar-saturated potassium chloride bridge.

Material.—Iron coupons were cut from an iron rod of 99.92–99.96% iron content supplied by the Swedish Iron and Steel Company, New York.

Steel coupons were cut from a cylindrical SAE 1020 steel rod. Spectrographic analysis showed negligible traces of copper.

¹ Manuscript received November 22, 1954. This paper was prepared for delivery before the Boston Meeting, October 3 to 7, 1954.

² Present address: Institute for the Study of Metals, University of Chicago, Chicago, Illinois.

³ Present address: E. I. du Pont de Nemours & Company, Flint, Michigan.

Hydrochloric acid solutions were prepared from C.P. concentrated acid.

Ferric chloride, potassium dichromate, and ceric sulfate were of C.P. grade. Concentrations of ferric chloride and ceric sulfate solutions were determined by titration.

Benzoquinone, tolu-*p*-quinone, sodium anthraquinone sulfonate, and hydroquinone were provided by Eastman Organic Chemicals and were of highest commercial purity available. They were recrystallized from ethyl alcohol.

RESULTS AND DISCUSSION

Solution Rates of Iron and Mild Steel in Hydrochloric Acid

Weight losses of iron and steel coupons in hydrochloric acid solutions were found to be linear functions of time. Accordingly, the weight loss in 15 min was generally obtained, and solution rates calculated on assumption of uniform dissolution during this interval.

Solution rates of stationary and rotating iron coupons in air-free and air-saturated solutions of hydrochloric acid are plotted in Fig. 1 and 2. The values given are averages of at least two runs, usually three or more. Mean deviations did not exceed 10% except at the lowest acid activity.

True surface area was calculated on assumption of a roughness factor of 4.0. The value obtained by gas adsorption using the BET method for iron coupons pickled in acid (other than the ones used in this work) was 3.6.

The weight loss is, within experimental error, a linear function of hydrochloric acid activity in air-free solutions. Hydrochloric acid activities were calculated from the data of Harned and Ehlers (3). Rotation decreases the rate of solution somewhat.

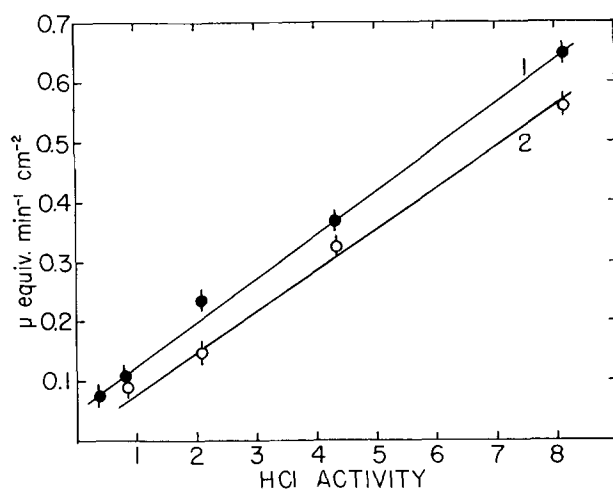


FIG. 1. Rate of solution of iron in air-free solutions as a function of HCl activity. Curve 1—Coupons stationary; curve 2—coupons rotated at 2180 rpm (12,700 cm/min).

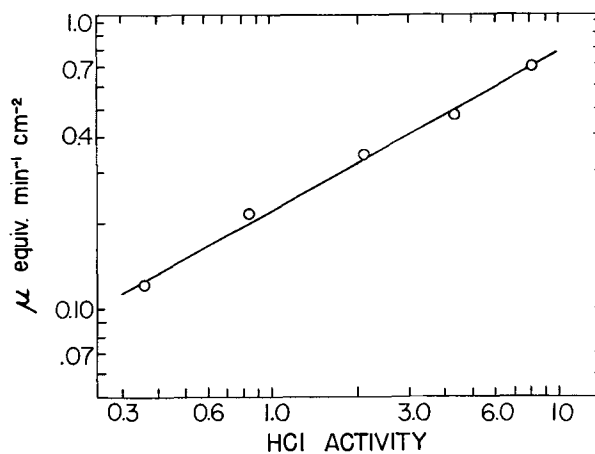


FIG. 2. Rate of solution of iron in air-saturated solutions as a function of the logarithm of HCl activity.

The slopes are 7.3×10^{-2} for stationary coupons and $6.9 \times 10^{-2} \mu \text{ equiv./min/cm}^2$ for rotating coupons. Fig. 2 shows that the solution rate in air-saturated solutions is a function of the 0.56 power of hydrochloric acid activity.

While the intercept of the solution rate vs. activity is zero in air-free solutions when the coupons are rotated at 2180 rpm, it is positive in solutions that either contain oxygen or are not agitated. The positive intercept in the presence of oxygen is understandable, since part of the reaction is to be accounted for by oxygen reduction. The reason for a positive intercept in air-free solutions that are not agitated is less clear; it may be connected with non-uniform conditions existing in the neighborhood of the surface and created probably by the solution process. This possibility is suggested by the fact that the intercept becomes zero on rotation of the coupons.

The solution rate in air-free 2*N* hydrochloric acid was independent of stirring speed. Rotation of coupons at 2180 rpm (12,700 cm/min) in air-saturated solutions increased the solution rate by a factor of about 1.6.

Similar results were obtained with mild steel coupons except that the weight loss was approximately 35% greater than with iron.

It is known that rate of solution in nonoxidizing acids is controlled by both the anodic and cathodic reaction rates (4) and is independent of ferrous ion concentration (5). When oxygen is present it is cathodically reduced and increases the solution rate; in its presence the solution rate is dependent on stirring speed (6), while in its absence it is independent of stirring speed (7, 8). Results reported above are in agreement with these observations.

In Fig. 3 the potential of dissolving iron vs. SCE is given as a function of time at various hydrochloric acid concentrations. The potential was reproducible

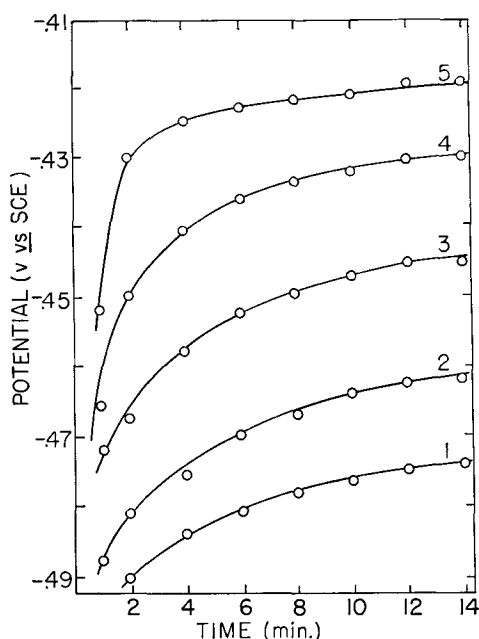


FIG. 3. Time-potential curves of iron in air-free solutions; coupons rotated at 2180 rpm. Curve 1—0.5N HCl; curve 2—1.0N HCl; curve 3—2.0N HCl; curve 4—3.0N HCl; curve 5—4.0N HCl.

to within ± 2 mv. The potential changes rapidly in the cathodic direction in the initial 3–4 min and more gradually from there on. It is obvious from Fig. 3 that the potential has not reached a steady-state value in 15 min, and it is known from other experiments that the drift continues for at least several hours. This drift may be caused by changes with time of the overpotential of either the anodic, the cathodic, or both reactions (9), or by changes of the electrode caused by solution of hydrogen in iron. It cannot be accounted for by changes in the solution, since ferrous ion had no effect on the potential, and since the decrease in acid activity was negligible.

Although a steady-state potential has not been achieved at the end of 15 min, the shape of the time-potential curves is the same at all hydrochloric acid concentrations; consequently the potential at the 14th minute can be used for purposes of comparison. A plot of this potential against the logarithm of acid activity is given in Fig. 4. The potential moves in the cathodic direction with increasing acid activity. The equation for air-free solutions is

$$E = \text{constant} + 0.047 \log \alpha_{\text{H}^+} \quad (\text{I})$$

For coupons rotated at 2180 rpm in air-free solutions the constant was -0.457 v.⁴

Current densities were calculated from the weight loss assuming a roughness factor of 4.0. Fig. 5 gives the potential at the 14th min vs. current density for

⁴ For a discussion of potentials of corroding or dissolving electrodes see reference (10).

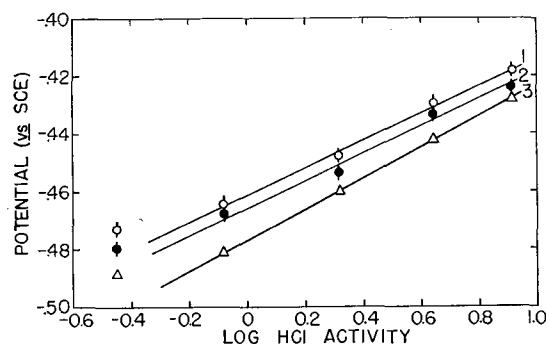


FIG. 4. Potential of iron (at 14th min) as a function of HCl activity. Curve 1—Air-free solutions; coupon revolving at 2180 rpm; curve 2—air-free solutions; coupon stationary; curve 3—air-saturated solutions; coupon stationary.

air-free solutions. It is sometimes maintained that such a plot involves the assumption that the so-called “total anodic area” does not change. Since in this case attack is uniform, and the whole of the surface undergoes dissolution at one time or another, the *total* surface area is the appropriate parameter. Thus, there is no ambiguity in the calculation of current densities.

On the assumption that a change in acid activity does not change the cathodic polarization curve but merely shifts it by an amount given by Nernst's equation, Fig. 5 can be considered to constitute an approximate polarization curve for the anodic process. This neglects any effects caused by changing the chloride ion concentration from 0.5 to 4.0N.

The equation obeyed for coupons rotated at 2180 rpm and at 30°C is

$$\text{Potential} = -0.415 + 0.054 \log i \quad (\text{II})$$

Here the potential is measured against a saturated calomel cell, and i is the current density in ma/cm^2 .

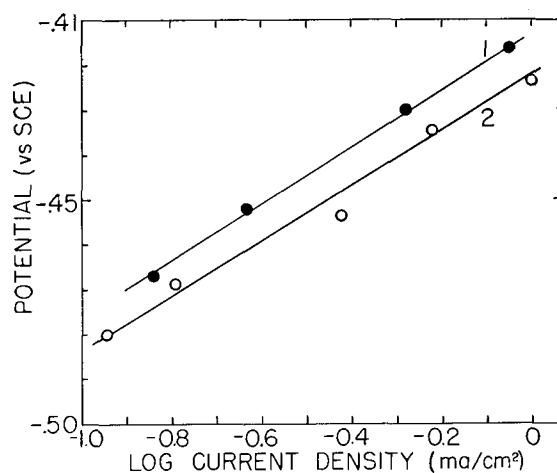


FIG. 5. Solution potential as a function of log current density (calculated from weight loss); air-free HCl solutions. Curve 1—Coupons rotated at 2180 rpm; curve 2—coupons stationary.

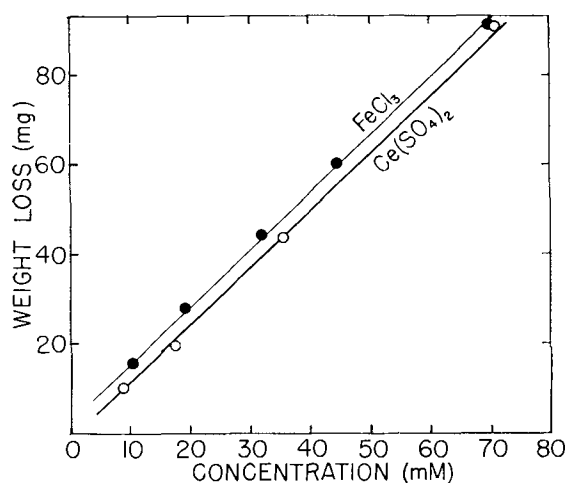


FIG. 6. Weight loss in 10 min as a function of depolarizer concentration at 2180 rpm.

Returning to solutions containing oxygen, the solution rate was partly controlled by diffusion and was dependent on stirring speed. The dissolution current density in air-saturated solutions is the sum of the limiting diffusion current for oxygen reduction and of the current for the hydrogen reaction. The relative contribution of the former (calculated from the difference between solution rates in air-saturated and air-free solutions) was about 50% at the lowest acid activity and decreased to about 10% at the highest acid activity. Its absolute contribution was approximately constant.

Since reduction of oxygen is believed to occur at a rate equal to its diffusion rate, and since its contribution to the over-all solution rate was constant, the cathode potential in solutions containing oxygen is determined by the hydrogen reaction; the polarization curve for hydrogen evolution is shifted on the

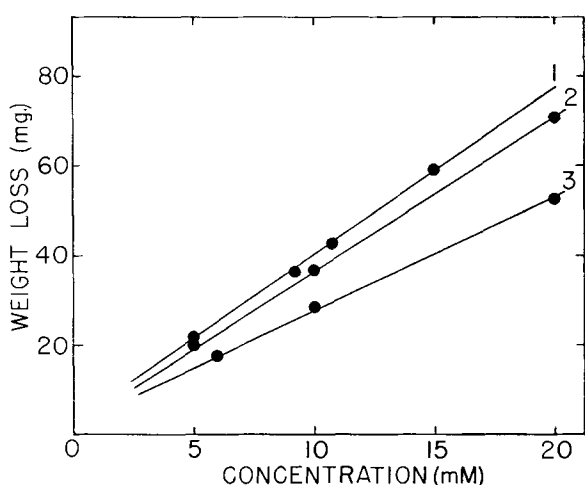


FIG. 7. Weight loss in 10 min as a function of depolarizer concentration at 2180 rpm. Curve 1—Benzoquinone; curve 2—tolu-*p*-quinone; curve 3—sodium anthraquinone sulfonate.

current axis by a constant amount. This is only an approximation, since it neglects any changes of the polarization characteristics of the hydrogen reaction caused by oxygen.

Depolarized Dissolution

In this series of experiments the volume, temperature, and exposed area were the same as before. Runs lasted 10 min and the solutions were 2*N* in hydrochloric acid and air-free throughout.

Fig. 6 to 8 show the weight loss as a function of depolarizer concentration at constant, 12,700 cm/min, linear speed. Points given are averages of two or more runs.

In the case of potassium dichromate the species in solution are $\text{Cr}_2\text{O}_7^{2-}$ and HCrO_4^- with an equilibrium constant $K = [\text{HCrO}_4^-]^2/[\text{Cr}_2\text{O}_7^{2-}] = 2.3 \times 10^{-2}$ (11). Writing the weight loss as

$$W = k_1[\text{Cr}_2\text{O}_7^{2-}] + k_2[\text{HCrO}_4^-] \quad (\text{III})$$

and solving the equations resulting upon substitution of experimental values, $k_1 = 6.1$ and $k_2 = 13.6$ mg/mM. In this calculation the change in the $[\text{HCrO}_4^-]$ to $[\text{Cr}_2\text{O}_7^{2-}]$ ratio with decrease in the total chromium concentration during the run is neglected.⁶ Agreement of observed and calculated values was within 5%.

Reduction products in the case of ceric sulfate and ferric chloride should have no effect on solution rate. Addition of hydroquinone, the reduction product of benzoquinone, changed neither solution rate nor potential. It is considered that this is also true for the other quinones. Any effect of the reduction product of $\text{Cr}_2\text{O}_7^{2-}$ and HCrO_4^- , viz., Cr^{+3} , is negligible.

Distribution of attack at small solution rates (up to 120 mg in 10 min) was uniform, or nearly so, in the absence as well as in the presence of depolarizers.

⁶ The problem can be solved exactly with

$$\frac{-d[\text{Cr}]}{dt} = k_1[\text{Cr}_2\text{O}_7^{2-}] + k_2[\text{HCrO}_4^-]$$

where $[\text{Cr}]$ is the total chromium concentration. Now $[\text{HCrO}_4^-]^2/[\text{Cr}_2\text{O}_7^{2-}] = K$ and

$$[\text{Cr}_2\text{O}_7^{2-}] = \frac{[\text{Cr}] - [\text{HCrO}_4^-]}{2}$$

substituting

$$\frac{-d[\text{Cr}]}{dt} = \frac{k_1[\text{Cr}] \frac{-K + K^2 + 8K[\text{Cr}]}{4}}{2} + \frac{k_2(-K + K^2 + 8K[\text{Cr}])}{4}$$

The differential equation is separable and can be integrated; the final expression is, however, too involved, the desired constants k_1 and k_2 being parts of logarithmic expression. Accordingly, values obtained from the simpler form were used.

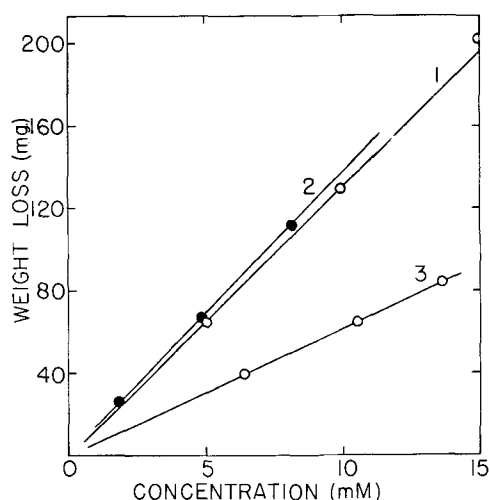


FIG. 8. Weight loss in 10 min as a function of depolarizer concentration at 2180 rpm. Curve 1— $K_2Cr_2O_7$; curve 2— $Cr_2O_7^{2-}$ (calculated); curve 3— $HCrO_4^-$ (calculated).

With depolarizers a uniform, thin, black film appeared on the coupon surface soon after immersion. The film was easily removed at the end of the run by scrubbing with a towel wetted in acetone. No attempt was made to determine the composition or structure of this film.

From results of other investigators (12-15), and from data to be given in a subsequent paper, it was concluded that the solution rate of mild steel in 2*N* hydrochloric acid containing the depolarizers used is controlled by the rate of diffusion of depolarizer to the metal surface. Evans (4) points out that the fact that dissolution in a particular medium, say ferric chloride solution, is diffusion-controlled, does not in itself afford evidence that the reaction is chemical rather than electrochemical; it is still legitimate to divide it into anodic and cathodic reactions. In the theory of "mixed-potential" the condition for diffusion control is clearly and unambiguously defined (2).

At 12,700 cm/min and in the presence of depolarizers, the acid reaction (displacement of hydrogen) was less than 5% of the total, except at very small depolarizer concentrations where it amounted to about 10-15%. At 20,000 cm/min these percentages were smaller.

Current-Potential Relations

The variation of potential with time in the presence of potassium dichromate and at 12,700 cm/min is shown in Fig. 9. This plot is typical of the depolarizers used.

A plot of the potential at the 9th min against the logarithm of solution current density is given in Fig. 10. Current density was calculated from weight loss, assuming a roughness factor of 4.0 and uniform so-

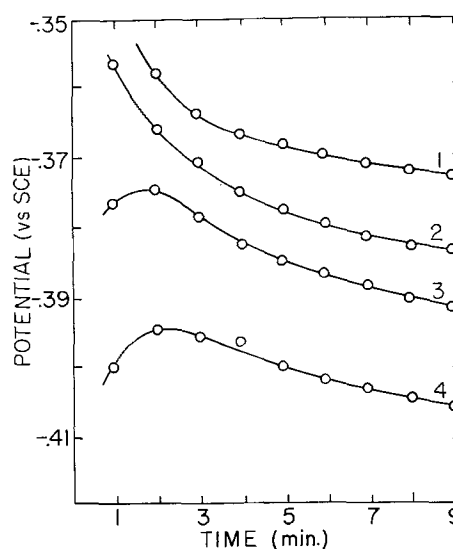


FIG. 9. Time-potential curves at 2180 rpm and at $K_2Cr_2O_7$ concentrations. Curve 1—5.0mM; curve 2—10.0mM; curve 3—15.0mM; curve 4—20.0mM.

lution rate over the 10 min interval. This is not strictly correct since the depolarizer concentration decreases with time, but at small solution rates the decrease in depolarizer concentration is small, and the approximation is justified.

It should be noted that in Fig. 10 points from all depolarizers at a given speed fall on the same straight line. Points with ceric sulfate did not fall on the curves and are not shown. In this case hydrochloric acid-sulfuric acid mixtures, 2*N* in total acidity, were used, and these results are therefore not directly comparable with the others.

A schematic representation of current-potential relations for dissolution in the presence of de-

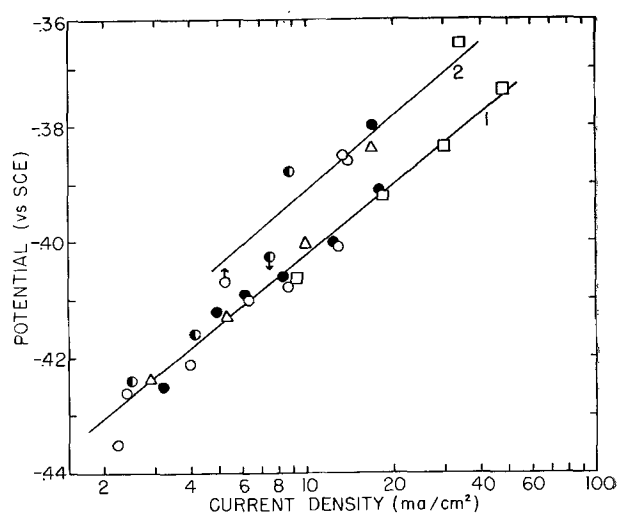


FIG. 10. Solution potential as a function of log current density (calculated from weight loss). \circ — $FeCl_3$; \bullet —benzoquinone; Δ —tolu-*p*-quinone; \ominus —sodium anthraquinone sulfonate; \square — $K_2Cr_2O_7$. 1—12,700 cm/min; 2—20,000 cm/min.

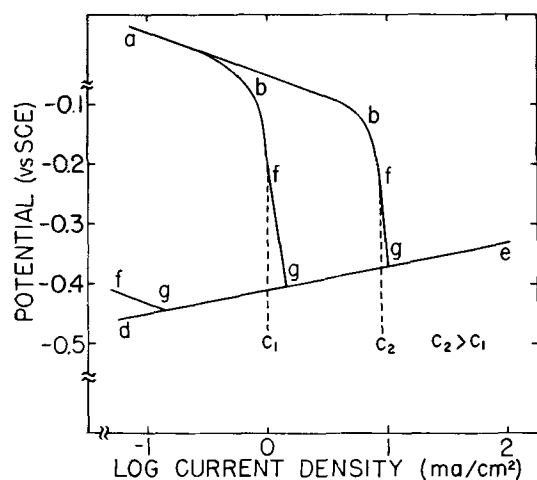


FIG. 11. Schematic representation of current-potential relations in air-free solutions.

polarizers is given in Fig. 11. Curve abc_1 is the cathodic polarization curve for reduction of depolarizer and de is the anodic polarization curve. The reaction is under diffusion control only if curve de intersects abc_1 at potentials more negative than that at point b . Curve fg is the polarization curve for hydrogen evolution. It is drawn with a slope of about 0.12.⁶ Since the current accounted for by hydrogen deposition is small compared to the total, the exact shape of the hydrogen evolution curve is of secondary importance.

An increase in depolarizer concentration shifts the curve as shown in Fig. 11. It can be seen that a plot of potentials determined at various depolarizer concentrations against current density would give approximately a polarization curve for the anodic reaction. Occurrence of the hydrogen reaction makes this interpretation somewhat uncertain at small current densities; however, its contribution becomes progressively smaller (in relation to the total) as the depolarizer concentration is increased.

Fig. 10 gives the relation between measured potential and the logarithm of the solution current density. The straight line obtained at 12,700 cm/min can be considered, from the above arguments, to be a polarization curve for the anodic reaction.

A straight line was also obtained at 20,000 cm/min. It has approximately the same slope as at 12,700 cm/min but is displaced by a constant amount in the cathodic direction. It is believed that this displacement is caused by a zeta potential drop. The potential of mild steel coupons in 2*N* hydrochloric acid alone is displaced in the cathodic direction with increasing rotational speed. This is shown in Fig. 12. Since the composition of the diffuse part of the electrical double layer is approximately the same in the absence and in the presence of depolarizers (in

⁶ The polarization curve for hydrogen deposition on iron was calculated from the data of Hickling and Salt (16).

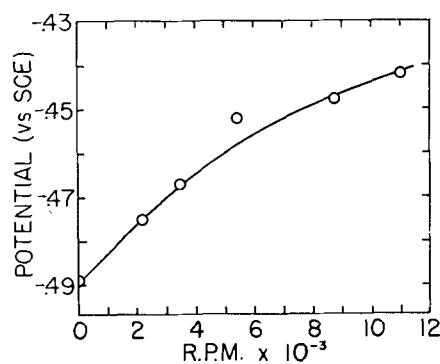


FIG. 12. Solution potential of mild steel in 2*N* HCl as a function of speed of rotation.

view of the large excess of hydrochloric acid) a similar potential shift on rotation in solutions containing depolarizers is to be expected.

The potential shift on rotation is of the right order of magnitude to be considered a zeta potential effect. It is unlikely that it is related to diffusion of ferrous or hydrogen ion since ferrous ion did not influence the potential and since the solution rate in hydrochloric acid alone was independent of stirring speed.

Returning to Fig. 10, the equation followed at 12,700 cm/min is

$$\text{Potential} = -0.44_2 + 0.04_0 \log i \quad (\text{IV})$$

where i is the current density in ma/cm². This equation is in reasonable agreement with the one obtained for iron in acid alone [see equation (II)].

Kuznesov and Iofa (17) and Kabanov, Burstein, and Frumkin (18) report a linear increase of potential with the logarithm of current density on anodic polarization of iron. The slope of the curve obtained by the former authors (17) was 0.07 in *N* hydrochloric acid. The slope obtained by Kabanov, Burstein, and Frumkin (18) in neutral or alkaline solutions containing chloride ions was approximately the same. The latter authors state that overvoltage values decreased with increasing chloride ion concentration. Our interpretation of the potential-solution rate curves appears therefore to lead to numerical values of the coefficient of the logarithmic term that are in reasonable agreement with direct measurement.

ACKNOWLEDGMENT

The authors gratefully acknowledge financial assistance from the Office of Ordnance Research under contract DA 23-072-ORD-216.

Any discussion of this paper will appear in a Discussion Section, to be published in the June 1956 JOURNAL.

REFERENCES

1. W. R. WHITNEY, *J. Am. Chem. Soc.*, **25**, 394 (1903).
2. C. WAGNER AND W. TRAUD, *Z. Elektrochem.*, **44**, 391 (1938); I. M. KOLTHOFF AND C. S. MILLER, *J. Am.*

- Chem. Soc.*, **62**, 2171 (1940); J. V. PETROCELLI, *This Journal*, **97**, 10 (1950).
3. H. S. HARNED AND R. W. EHLERS, *J. Am. Chem. Soc.*, **54**, 1350 (1932); **55**, 652, 2179 (1933).
 4. U. R. EVANS, "Metallic Corrosion, Passivity, and Protection," pp. 196-226, Edward Arnold Co., London (1937).
 5. S. RAM, *J. Soc. Chem. Ind.*, **54**, 107 (1935).
 6. C. H. WELLING, R. P. RUSSEL, AND W. C. WHITMAN, *Ind. Eng. Chem.*, **15**, 672 (1923).
 7. YA. V. DURDIN AND M. A. ORANSKAYA, *Zhur. Obschei Khim.*, **21**, 604 (1951).
 8. A. K. KRASIL'SHCHIKOV, *ibid.*, **14**, 261 (1944).
 9. J. O'M. BOCKRIS, *Chem. Rev.*, **3**, 525 (1948); see also reference (16).
 10. H. H. UHLIG, *Proc. Nat. Acad. Sci.*, **40**, 276 (1954).
 11. W. M. LATTIMER, "Oxidation States of the Elements and Their Potentials in Aqueous Solutions," p. 231, Prentice Hall, Inc., New York (1938).
 12. C. V. KING, "Pittsburgh International Conference on Surface Reactions," p. 5, Corrosion Publishing Co., Pittsburgh (1948).
 13. M. B. ABRAMSON AND C. V. KING, *J. Am. Chem. Soc.*, **61**, 2290 (1939).
 14. R. G. VAN NAME AND D. U. HILL, *Am. J. Sci.*, **42**, 301 (1916).
 15. M. HOCHBERG AND C. V. KING, *This Journal*, **97**, 191 (1950).
 16. A. HICKLING AND F. W. SALT, *Trans. Faraday Soc.*, **36**, 1226 (1940).
 17. V. A. KUZNESOV AND Z. A. IOFA, *J. Phys. Chem. (USSR)*, **21**, 201 (1947).
 18. B. KABANOV, R. BURSTEIN, AND A. FRUMKIN, *Disc. Faraday Soc.*, **1**, 259 (1947).

A Method for the Isolation of Surface Films from Aluminum Alloys and the Mechanism of the Reactions Involved¹

M. J. PRYOR AND D. S. KEIR

Kaiser Aluminum and Chemical Corporation, Spokane, Washington

ABSTRACT

Warm solutions of iodine in methanol were found satisfactory for isolating surface films from aluminum alloys not containing copper. Addition of sulfosalicylic acid to these solutions renders them satisfactory for isolation of films from aluminum-copper alloys. Attack is not selective at the film-metal interface, so all aluminum must be dissolved before uncontaminated films can be obtained. Hydrogen evolved during dissolution of the aluminum is believed due to the formation of aluminum methoxide. Iodide ions are also formed in these solutions. Aluminum methoxide is insoluble in dehydrated solutions but is decomposed by traces of water to soluble reaction products. A mechanism for the dissolution of aluminum in iodine-methanol solutions is suggested.

INTRODUCTION

Isolation of surface films from metals is a valuable tool for studying certain corrosion reactions. Although several techniques are available for isolating surface films from aluminum alloys, some are unsatisfactory because they yield contaminated films, and others because they involve highly toxic chemicals.

In the electrochemical method (1), specimens are subjected to anodic attack which dissolves the metal electrochemically from the surface film. This method is time-consuming and often leaves residual spots of metal. The saturated mercuric chloride (2, 3) and metallic mercury (4) methods depend on preferential corrosion of the film/metal interface by metallic mercury. Contamination limits the use of these methods since insoluble hydrated alumina is formed as a corrosion product. Dry hydrogen chloride at 300°–400°C (5) is effective for the rapid removal of aluminum from surface films. However, it is inconvenient to use, and the high temperature can result in transformation of films that are stable at low temperatures only. A solution of iodine in methanol was developed by Rooney and Stapleton (6), and has been successfully used for rapid and quantitative isolation of surface films from steel and stainless steel (7–9). The solution selectively attacks the film/steel interface, so that the film can be removed before the steel is completely dissolved. Under deaerated conditions this anhydrous solution prevents contamination of surface films with hydrated corrosion products. Use of iodine-methanol solutions on aluminum alloys demonstrated that all the aluminum must be dissolved before clean films

could be obtained (10). It was suggested that air need not be excluded during film isolation from aluminum, but it was not found possible to obtain uncontaminated films from aluminum alloys containing large additions of copper or silicon. The same authors (10) indicated that a solution of bromine in methanol containing 1% water resulted in a faster isolation of surface films from aluminum alloys.

Since excellent results were obtained previously on other metals using nonaqueous solutions containing either iodine or bromine, a suitable method of isolating surface films from aluminum alloys with similar solutions was investigated. Furthermore, since bromine is not as convenient for general use as iodine, this work was confined to iodine-methanol solutions, although satisfactory film isolation with methanol-bromine solutions has been reported (11). In addition, the mechanism by which aluminum dissolved in these solutions was investigated since there have been little published data on this subject.

METHOD OF ISOLATING SURFACE FILMS FROM ALUMINUM ALLOYS

All chemicals were of C.P. quality. The absolute methanol used had the following composition: acetone and aldehydes, 0.001% maximum; acidity (as formic acid), 0.002%; alkalinity (ammonia), 0.0003%; residue after evaporation, 0.001% maximum; water, 0.1% maximum.

The water content was typical of so-called "absolute" methanol and represents about the minimum concentration obtainable without additional drying.

High purity aluminum as cold-rolled, $\frac{3}{4}$ hard sheet, 0.16 cm thick had the following analysis: silicon, 0.0015%; iron, 0.001%; copper, 0.001%; balance, aluminum.

¹ Manuscript received November 10, 1954. This paper was prepared for delivery before the Boston Meeting, October 3 to 7, 1954.

TABLE I. Composition of the aluminum alloys whose rates of solution in iodine/methanol are shown in Fig. 2 and 3

Alloy	Temper	Wt %						
		Si	Fe	Cu	Mn	Mg	Cr	Zn
1100	H14	0.11	0.54	0.14	0.01	Tr	0.00	0.00
3003	H14	0.19	0.54	0.13	1.08	0.01	0.00	0.00
2024	T3	0.13	0.27	4.36	0.56	1.60	0.01	0.03
4043	H14	4.98	0.24	—	—	—	—	—
5050	H34	0.22	0.47	0.12	0.02	1.38	—	—
5052	H34	0.07	0.20	0.05	0.00	2.36	0.21	0.04
5056	H16	0.10	0.19	0.02	0.11	4.86	0.10	0.00
6061	T6	0.63	0.43	0.31	0.05	0.88	0.26	0.02
7075	0	0.11	0.26	1.63	0.01	2.60	0.25	5.69

Compositions of aluminum alloys used are shown in Table I.

Preliminary experiments were carried out at room temperature in Petri dishes using 1 cm² specimens of high purity aluminum. To observe better the progress of film isolation, specimens were anodized in sulfuric acid, dyed, and sealed. Scratch lines were ruled through the anodic coating in order to expose aluminum to the iodine-methanol solution (10 g iodine/100 ml absolute methanol). Although dissolution of the aluminum occurred slowly at room temperature, there was no preferential corrosion along the aluminum/film interface. After exposure periods of about 24 hr the aluminum was completely dissolved and the anodic film could be removed. The reaction products were completely soluble in the solution. The observation by previous workers that all the aluminum must be dissolved before the films could be obtained in the uncontaminated condition (10) was confirmed. Despite the fact that a wide variety of iodine contents and temperatures were investigated, no evidence of selective attack at the film/aluminum interface was observed. However, continuous evolution of gas always accompanied dissolution of the aluminum. Solutions from separate experiments together with any residue were carefully examined at a magnification of 500 diameters to determine whether any "spurious"² or secondary films were formed as a contaminant during the dissolution of the aluminum. In no case were these spurious films detected.

The experiments described above were next repeated at 50°C and in boiling iodine-methanol solutions. The dissolution rate of aluminum was greatly increased, and a brisk evolution of gas occurred at 50°C. In boiling solutions the aluminum was destroyed even more rapidly, but violent gas evolution

² If the specimens are first abraded with emery paper, thin surface films carry abrasion marks inherited from the underlying metal. Secondary or spurious films are invariably free from these abrasion marks and thus can easily be distinguished from the original film.

shattered the films. Consequently, boiling iodine-methanol solutions are unsatisfactory unless the films are supported by some means. However, even where relatively thick anodic films were supported with plastic films appreciable disintegration occurred in boiling solutions. Therefore, further work was confined to solutions at lower temperatures.

The action of iodine-methanol solutions was investigated at 50°C on aluminum alloys 1100, 3003, 2024, 4043, 5050, 5052, 5056, 6061, and 7075 (see Table I for chemical compositions), carrying surface films ranging from air-formed oxide films through films of increasing thickness formed in various passivating solutions to very thick anodic films. Excellent film isolation could be obtained from the alloys 1100, 3003, 5050, 5052, 5056, and 6061 of 0.16 cm thickness within a 4–8 hr period; Fig. 1 (a) shows a colored anodic film isolated from high purity aluminum. The copper-containing alloy, 2024, yielded films contaminated by metallic copper at 50°C and by cuprous iodide at 25°C, whereas the silicon-containing alloy 4043 yielded films contaminated by silicon. Silicon contamination was overcome by supporting the surface films with vinyl or formvar films and removing loosely adhering silicon by washing with methanol or by brushing gently with a soft bristle brush.

In order to eliminate contamination of surface

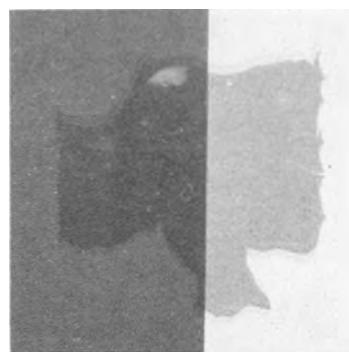


FIG. 1a. Surface films isolated from different aluminum alloys. Color anodized film from high purity aluminum.

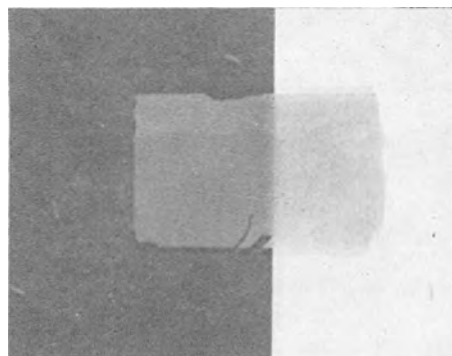


FIG. 1b. Anodic film from 2024 showing absence of copper and cuprous iodide.

films from aluminum-copper alloys, various additions were made to the original solution which would be expected to dissolve copper or cuprous compounds as soluble complexes. Additions of ethanolamine, triethanolamine, triethylamine, and ethylene diamine proved to be ineffective at keeping the copper completely in solution. Furthermore, they very greatly reduced the dissolution rate of aluminum-copper alloys. Dithizon (diphenyl thiocarbazon) was reasonably effective when added in concentrations of 0.05 g/100 ml solution in that it prevented precipitation of cuprous iodide for a period of about 30 min. However, sulfosalicylic acid ($C_7H_6O_6S \cdot 2H_2O$) proved to be by far the most effective of these additions in forming soluble complexes with the copper in aluminum-copper alloys. Sulfosalicylic acid is believed to form a 1:1 complex with copper in acidic solutions and a chelate containing double this proportion of sulfosalicylic acid in alkaline solutions (12) ($pH = 9.0$). It is also capable of forming a complex with zinc (13) and is thus very useful for film isolation from such alloys as 7075. It was determined that additions of sulfosalicylic acid should be used on aluminum alloys containing more than 1% copper. Fig. 1 (b) shows an anodic film that was isolated from 2024 by this method and emphasizes the lack of contamination. The presence of sulfosalicylic acid in a solution of 10 g iodine in 100 ml absolute methanol does not entirely prevent formation of cuprous iodide at 25°C or that of metallic copper at 50°C because the aluminum dissolves much faster than the copper. However, once all the aluminum is dissolved, the contaminant, either cuprous iodide or copper, will then dissolve, yielding uncontaminated films. Addition of 3 g sulfosalicylic acid/100 ml of the original iodine-methanol solution is recommended for this procedure.

However, to prevent contamination entirely, the action of the iodine-methanol solution on the aluminum must be reduced in rate. This can be achieved by using a solution containing 2.5 g iodine and 3.0 g sulfosalicylic acid/100 ml absolute methanol at 25°C. Although this solution attacked aluminum-copper alloys much more slowly, the dissolution rate of the aluminum did not exceed that of the copper. Consequently, no contamination was obtained at any stage during the dissolution of the alloy. This procedure, which is suitable for alloys of the 2024 and 7075 types, is best used when freedom from contamination is mandatory.

Subsequent experiments, described in the next section, indicated that:

1. The rate of attack of iodine-methanol solutions on high purity aluminum increases with increasing iodine concentration and with increasing temperature. A solution containing 10 g iodine/100 ml abso-

lute methanol is the optimum concentration for most film isolation.

2. If the solution is dried, or if access of moisture from the atmosphere is prevented, precipitation of bulky aluminum methoxide occurs and films are contaminated.

3. Addition of water to the iodine-methanol solution progressively reduces the rate of attack of the solution on the aluminum.

4. The dissolution rate of the aluminum is unaffected by the presence of dissolved oxygen.

Consequently, the best film isolation technique involves a solution containing 10 g iodine in 100 ml absolute methanol. 200 ml of solution should be used per gram of aluminum to be dissolved. The reaction should be carried out in contact with the atmosphere at about 50°C.

Film isolation can be performed most conveniently on foil specimens since the weight of metal to be dissolved is small. Thicker sections are best handled by grinding down one surface of the specimen. For very rapid film isolation the final thickness of the specimen should not exceed about 0.05 cm. The side of the specimen carrying the film can be cemented face downward with a vinyl chloride-vinyl acetate adhesive or with Formvar to a polyethylene holder. The holder was rigid in the case of foil, but polyethylene tissue was used for thicker specimens. The vinyl adhesives will withstand attack by the iodine-methanol solutions, but can be dissolved slowly by acetone or methyl-ethyl ketone. Specimens, cemented to polyethylene, can be exposed to the solution until all the aluminum is dissolved. This requires 1-2 hr for foil specimens and 4-8 hr for specimens prepared from the thicker sections. The polyethylene holders

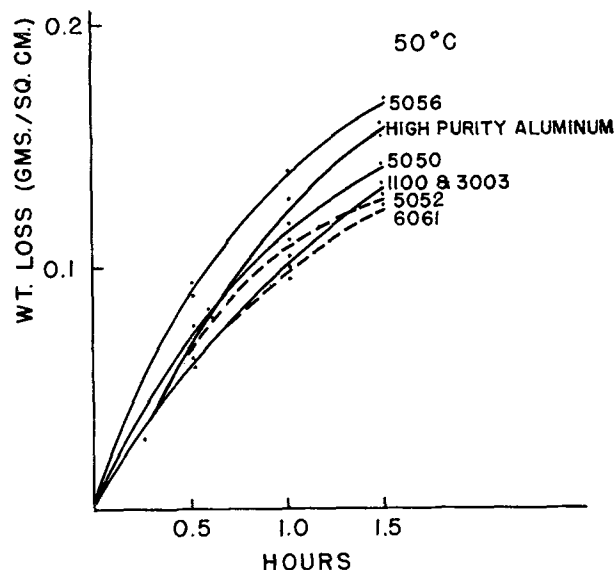


FIG. 2. Weight loss/time curves for aluminum alloys in a solution of 10 g iodine in 100 ml absolute methanol at 50°C.

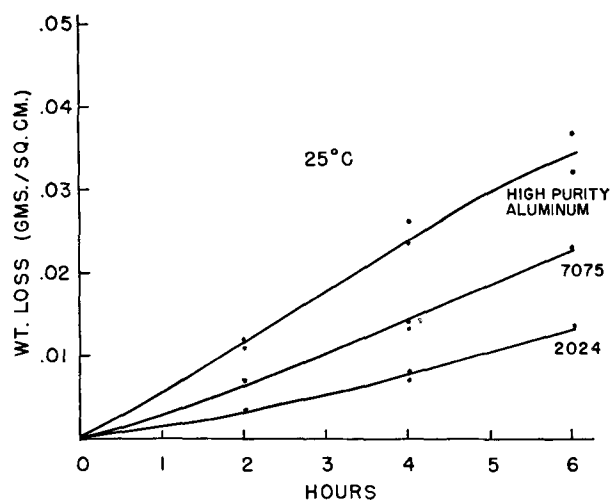


FIG. 3. Weight loss/time curves for high purity aluminum, 2024 and 7075 in a solution containing 2.5 g iodine and 3.0 g sulfosalicylic acid in 100 ml absolute methanol at 25°C.

and the films can be washed in methanol and the films subsequently removed by treatment with acetone or methyl-ethyl ketone.

The time taken for complete aluminum dissolution varies not only with the weight of metal but also with the alloy. Dissolution rates of aluminum alloys were determined at $50^\circ \pm 0.2^\circ\text{C}$ in a solution of 10 g iodine in 100 ml absolute methanol. 100 ml of solution per specimen ($1.5 \times 1.5 \times 0.16$ cm) was employed. Triplicate experiments were performed under reflux to prevent loss of solution. Results are shown in Fig. 2, which indicates that 5056 is most readily attacked (probably because of the ease of formation of magnesium methoxide) and 6061 least readily attacked by this solution. The rate of attack on other aluminum alloys is very similar to that on high purity aluminum. Fig. 3 shows weight loss/time curves for the dissolution of 2024, 7075, and high purity aluminum in a dilute iodine-methanol solution containing sulfosalicylic acid. Here it is evident that both 2024 and 7075 are somewhat less readily attacked than high purity aluminum. However, the dissolution rate is high enough to permit film isolation in a reasonable length of time from thin specimens. This method will easily isolate, from any aluminum alloy, all surface films that are not affected by this reagent.

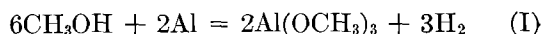
MECHANISM OF DISSOLUTION OF ALUMINUM IN IODINE-METHANOL SOLUTIONS

Experimental

Examination of gas evolved during dissolution of high purity aluminum.—It was noticed previously that dissolution of aluminum and aluminum alloys in iodine-methanol solutions was invariably accompanied by gas evolution. Furthermore, as the dissolu-

tion rate of aluminum increased the rate of gas evolution also appeared to increase. Gas evolution is not observed when similar solutions act upon steel, so it was felt that identification of this gas might throw considerable light on the mechanism of aluminum dissolution. Large volumes of the gas were collected by displacement over water from a refluxed reaction mixture containing 20 g iodine, 200 ml absolute methanol, and 1.8 g aluminum; air was expelled from the apparatus before any gas was collected. The gas could be ignited in air, and it did not contain detectable quantities of hydrogen iodide, saturated or unsaturated hydrocarbons, or carbon dioxide.

Gas analyses by ignition demonstrated that the gas was hydrogen. Tests on gas evolved from a similar reaction mixture that was not refluxed gave the same results. Consequently, it was believed that this hydrogen resulted largely from the interaction of aluminum and methanol catalyzed by the presence of iodine, possibly according to an equation such as:



Investigations of the formation of aluminum methoxide.—Since it appears possible that aluminum methoxide might be formed as a reaction product, an attempt was made to prepare this compound in an independent manner in order to study its properties. In general such alkoxides can be prepared by the interaction of the metal and boiling alcohol in the presence of a trace of iodine and mercuric chloride (14). Since alkoxides are believed to be sensitive to water, which may cause them to decompose into the alcohol and hydrated metal oxide, absolute methanol was first dried by refluxing for 1 hr with magnesium turnings and a trace of iodine. The dried methanol was then distilled into the reaction vessel without atmospheric contact.

The reaction vessel consisted of a three-necked flask fitted with a condenser and side arm (Fig. 4). The flask contained 2 mg dried iodine and 5 mg dried mercuric chloride. A weighed aluminum specimen ($1.5 \times 1.5 \times 0.16$ cm) was suspended in a glass cradle which could be lowered into the solution by rotating the glass windlass to which it was attached by a nylon thread (Fig. 5).

100 ml dried methanol was distilled into the reaction vessel. Two drying tubes containing calcium chloride were situated between the reaction vessel and the gas collection cylinder to prevent access of water vapor. The flask was disconnected from the distillation train, and partly immersed in a water bath maintained at $50^\circ \pm 0.2^\circ\text{C}$; after the solution had come to temperature, the specimen was lowered into it; gas evolution began almost immediately. The experiment lasted 2 hr and the total volume of gas

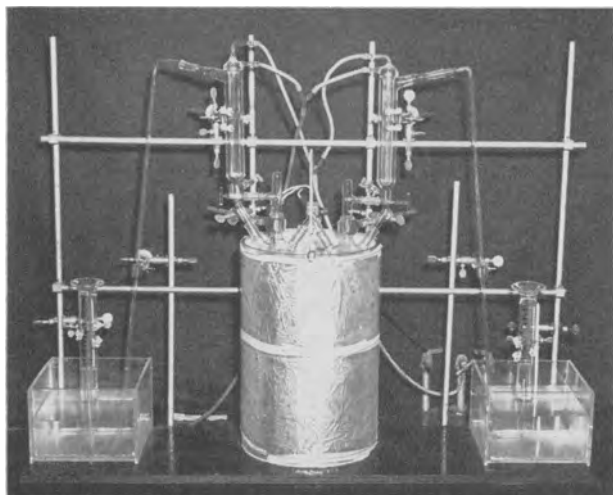


FIG. 4. Apparatus for determination of weight loss and volume of hydrogen.

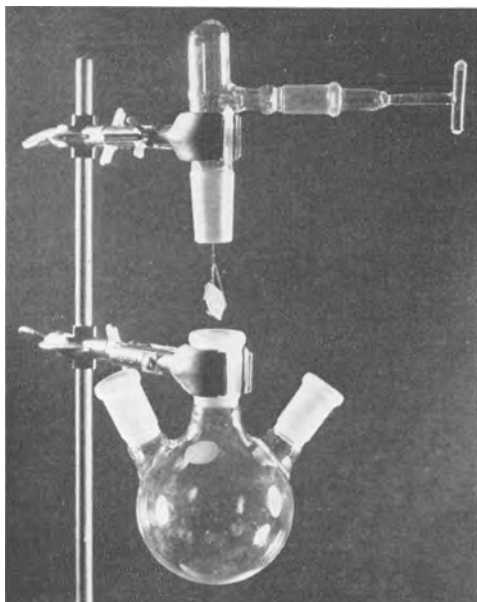


FIG. 5. Method of mounting and adjusting the specimen in the apparatus shown in Fig. 4.

evolved was determined at S.T.P. The specimen was cleaned in cold concentrated nitric acid and reweighed. Corrosion of the aluminum resulted in the formation of a voluminous white product which appeared to be insoluble in methanol. The gas was again found to be hydrogen, and calculation from the volume evolved indicated that, within the limits of experimental error, the aluminum had been corroded as aluminum methoxide.

The white product was filtered from solution and dried over calcium chloride in a desiccator. The methanol solution was then tested for soluble aluminum compounds; none was detected. The white product was insoluble in methanol and was not dis-

solved by a fresh solution of iodine in methanol. However, the white product could be dissolved in benzene as suggested by Hickinbottom (14). Since hydrated alumina is insoluble in benzene, it appears that the white product formed by the interaction of aluminum and methanol in the presence of traces of iodine and mercuric chloride is aluminum methoxide.

Samples of the reaction product which had been dried over calcium chloride for 6 hr were ignited and the weights of alumina, carbon dioxide, and water determined. The compound exploded when heated rapidly but, when heated more gradually, results were obtained that were consistent with aluminum methoxide contaminated with methanol. Samples of the compound that were dried for one week over calcium chloride contained about 40% aluminum methoxide and 60% alumina which presumably came from decomposition of the aluminum methoxide. These experiments confirm the suggestion that this corrosion product is aluminum methoxide and indicate that it is extremely easily decomposed by moist air and by heating. Attempts to determine a melting point on this compound were not successful as it decomposed when heated gently.

Action of absolute methanol on high purity aluminum.—To determine whether dried or absolute methanol alone had any action on aluminum, experiments similar to those described above were carried out except that iodine and mercuric chloride were not added. In no case was any detectable weight loss observed or any hydrogen evolved within a tempera-

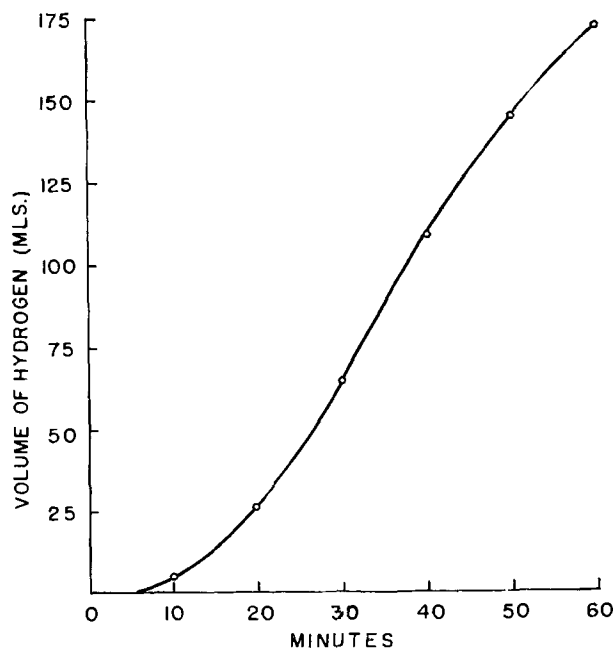


FIG. 6. Curve showing variation of volume of hydrogen with time on exposing high purity aluminum to an anhydrous solution of 5 g iodine in 100 ml dry methanol.

ture range of 25°–50°C. It was concluded that, within the temperature range studied, methanol in the absence of iodine had no action on aluminum.

Action of dried iodine-methanol solutions on high purity aluminum.—Since aluminum methoxide is insoluble in methanol, although soluble in benzene, the question arises as to whether this compound is formed in iodine-methanol solutions, since no insoluble reaction products were detected in solutions of iodine in absolute methanol which had reacted with aluminum in contact with the atmosphere. Since this absolute methanol contained around 0.1% water and undoubtedly picks up additional water from contact with the atmosphere, experiments under dehydrated conditions were next carried out.

The apparatus shown in Fig. 4 was used again. A weighed aluminum specimen was introduced into the reaction vessel together with 5 g dried iodine. Methanol was dried and introduced as described previously. The experiments were carried out at $50^{\circ} \pm 0.2^{\circ}\text{C}$. Fig. 6 shows the volume of hydrogen evolved as a function of time. A whitish coating quickly covered the specimen and flaked off intermittently. After 1 hr, 172 ml of hydrogen (S.T.P.) was evolved, which is equivalent to the calculated dissolution³ of 0.139 g aluminum via the formation of aluminum methoxide (or by any reaction in which the equivalent weight of aluminum is 9). The measured weight loss of the aluminum was 0.234 g, which indicates that aluminum was being destroyed by more than one reaction. This experiment was repeated several times, and the presence of an insoluble white compound formed under dehydrated conditions was confirmed.

Additional experiments were carried out in a solution of 5 g iodine in 100 ml absolute (undried) methanol with the access of moisture prevented, as before. Large quantities of an insoluble whitish compound, similar to that observed under more truly anhydrous conditions, were formed. It was found that the solution after reaction with an aluminum specimen for 1 hr gave a pH reading of 2.1 with a glass electrode and calomel half-cell. On the addition of several drops of water to a portion of the solution, the compound dissolved very rapidly and the pH of the solution increased to 3.5. Further small additions of water caused no precipitation of hydrated alumina or of iodine, but large additions of water resulted in the separation of hydrated alumina. Addition of even small volumes of water to a solution of iodine in methanol that had not reacted with aluminum resulted in almost immediate precipitation of iodine. This indicates that reaction of the solution with aluminum results in the formation of appreciable

³ Specimens were cleaned in cold concentrated nitric acid before weighing.

quantities of iodide ion, which stabilizes the iodine and prevents its immediate precipitation on the addition of water.

A further portion of the solution was filtered, and the white residue was washed with dried methanol and dissolved in benzene. Large quantities of aluminum ion were subsequently extracted from the benzene by dilute hydrochloric acid.

These tests indicate that the insoluble corrosion product formed in dried iodine-methanol solutions was aluminum methoxide. This was confirmed by chemical analysis which showed that, after drying over calcium chloride for one week, the sample contained about 40% aluminum methoxide and some hydrated aluminum, probably due to a partial decomposition of the methoxide. Storage of the dried product in a closed weighing bottle in contact with undried air again resulted in the formation of methanol droplets.

Action of iodine-absolute methanol solutions on high purity aluminum in contact with the atmosphere.—The experiments described above indicate that the reaction between aluminum and iodine-methanol solutions under dehydrated conditions leads to the formation of insoluble aluminum methoxide as one of the products of reaction. From the standpoint of film isolation, this is clearly undesirable since surface films isolated under these conditions will be contaminated unless a further operation such as treatment with water or with a dilute acid is carried out. However, it was observed previously that when no special precautions were taken to avoid traces of water or contact with the atmosphere, other than keeping the methanol in tightly stoppered bottles and using dry apparatus, the reaction products were completely soluble and excellent film isolation was obtained. Consequently, the rate of solution of high purity aluminum was determined in iodine-methanol solutions that were not specially dried or kept out of contact with the atmosphere. The following variables were investigated: surface pretreatment; volume of solution; temperature; iodine concentration; water additions; and dissolved oxygen.

In addition, experiments were performed to determine the nature of the reaction products with a view to advancing a tentative mechanism of reaction.

The effect of surface pretreatment on the form of the weight loss-time curves was first investigated. Weight losses on triplicate specimens were determined as a function of time in Erlenmeyer flasks fitted with reflux condensers. The flasks were placed in a water bath thermostatted at $25^{\circ} \pm 0.2^{\circ}\text{C}$; 50 ml of the solution of 10 g iodine in 100 ml absolute methanol was used for each specimen. The surface pretreatments investigated were: degreasing alone; etching in 20% sodium hydroxide; etching in 1/2%

TABLE II. Effect of surface pretreatment on weight losses at 25°C in a solution containing 10 g iodine/100 ml absolute methanol; 50 ml solution/specimen

Surface pretreatment	Wt loss (g/cm ²)											
	1 hr			2 hr			4 hr			6 hr		
Degreased in benzene.....	0.023,	0.025,	0.028	0.063,	0.065,	0.060	0.103,	0.099,	0.101	0.121,	0.120,	0.123
Etched in sodium hydroxide..	0.005,	0.004,	0.004	0.017,	0.016,	0.024	0.069,	0.058,	0.081	0.088,	0.103,	0.130
Etched in hydrofluoric acid..	0.018,	0.012,	0.012	0.035,	0.043,	0.048	0.093,	0.103,	0.092	0.129,	0.123,	0.117
Electropolished.....	0.001,	0.0005,	0.0005	0.004,	0.005,	0.011	0.040,	0.026,	0.042	0.042,	0.124,	0.087
Abraded under alcohol.....	0.030,	0.032,	0.032	0.062,	0.062,	0.062	0.104,	0.106,	0.100	0.132,	0.121,	0.120

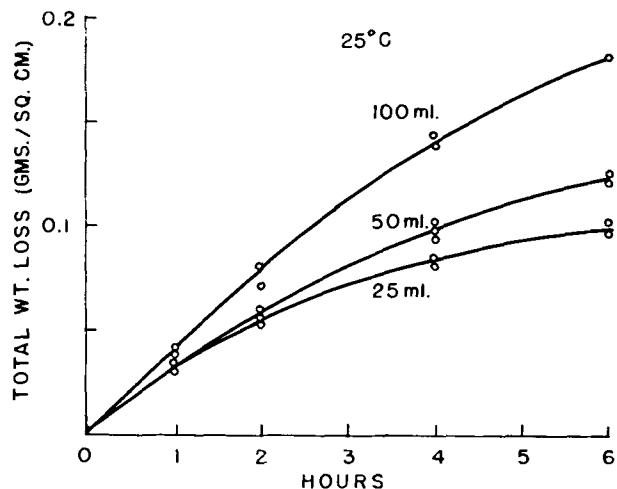


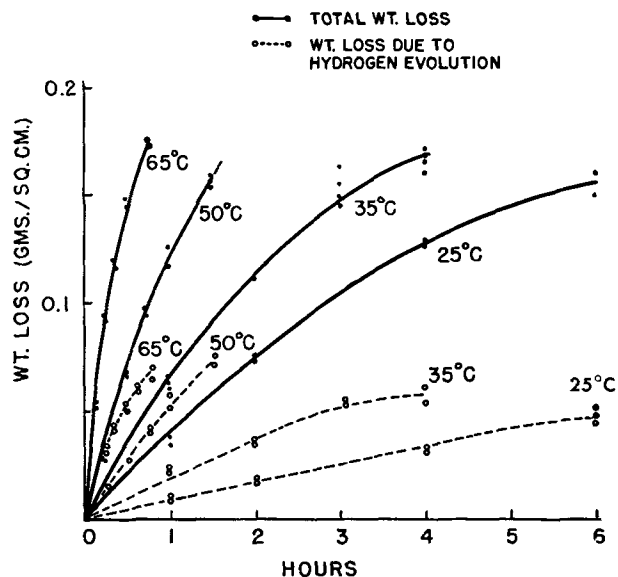
FIG. 7. Weight loss/time curves for high purity aluminum in different volumes of iodine methanol solution (10 g/100 ml) at 25°C.

hydrofluoric acid; electropolishing in 60% phosphoric acid with 40% sulfuric acid; and abrading with 320 grit emery paper under methanol.

In these experiments weight losses⁴ alone were determined. The results (Table II) show that the most reproducible weight losses and the smallest induction periods were obtained after abrasion under methanol. Consequently, this surface pretreatment was used in subsequent experiments described in this section.

Experiments were next performed to determine the effect of different volumes of solution on the dissolution rate of aluminum. These experiments were performed in triplicate at 25° ± 0.2°C using solutions containing 10 g iodine/100 ml absolute methanol. The volume of solution varied between 25 ml/specimen and 100 ml/specimen. The results (Fig. 7) show that the dissolution rate has less tendency to decrease with time in larger volumes of solution. This suggests that the dissolution rate of aluminum is largely controlled by the volume of the solution. Consequently,

⁴ Initially, specimens were cleaned in either cold concentrated nitric acid or warm chromic/phosphoric acid before weighing. Experiments indicated that, in the absence of insoluble reaction products, these cleaning operations were unnecessary.

FIG. 8. Relationship between time, total weight loss, and weight loss due to hydrogen evolution at different temperatures in a solution containing 10 g I₂/100 ml absolute methanol.

100 ml solution/specimen was used in subsequent experiments.

The effect of temperature within the range 25°–65°C was next investigated. In this case, weight losses and volumes of hydrogen evolved were determined using the apparatus shown in Fig. 4; drying tubes were not inserted between the reaction vessel and the gas collection cylinder. Temperatures were controlled at 25°, 35°, 50°, and 65°C ± 0.2°C by means of a thermostatted water bath. Solutions containing 10 g iodine in 100 ml absolute methanol were used. Each experiment required 100 ml of solution/specimen. The results (Fig. 8) show that the dissolution rate of aluminum and the rate of hydrogen evolution increased with increasing temperature.

Similar experiments were carried out to determine the effect of iodine concentration at temperatures of 25° and 50°C (±0.2°C) using 100 ml solution/specimen and iodine concentrations of 0, 2.5 g, 5.0 g, 7.5 g, and 10.0 g/100 ml methanol. The results (Fig. 9 and 10) confirm the previous observation that methanol alone has no detectable action on alu-

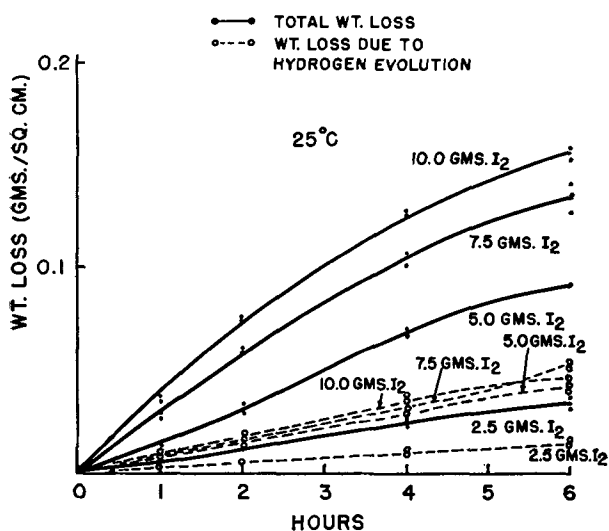


FIG. 9. Relationship between time, total weight loss, and weight loss due to hydrogen evolution at different iodine concentrations at 25°C.

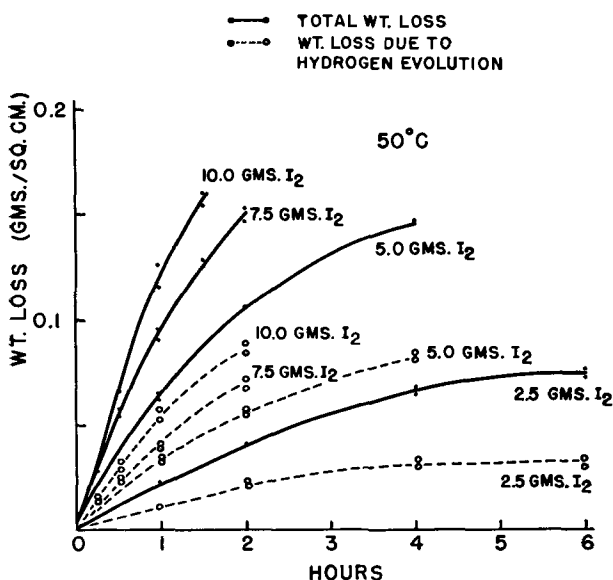


FIG. 10. Relationship between time, total weight loss, and weight loss due to hydrogen evolution at different iodine concentrations at 50°C.

minum. They also demonstrate that the dissolution rate of aluminum increases markedly with increasing iodine concentration. Calculations based on the initial slopes of these curves indicate that aluminum dissolution is first order with respect to iodine. Furthermore, the rate of hydrogen evolution increases with increasing iodine concentration, especially at 50°C.

Experiments were next carried out to determine the effect of water on the dissolution rate of aluminum. Variation of both weight loss and hydrogen evolution with time was first determined at 50°C in a solution containing 10 g iodine in 100 ml methanol containing 1% by volume of water. The results

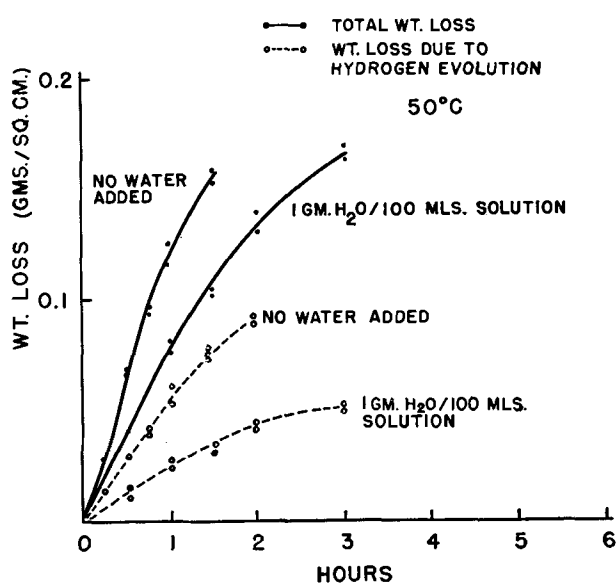


FIG. 11. The effect of 1% by volume of water on the weight loss/time curve and on the weight loss due to hydrogen evolution/time curve for high purity aluminum in a solution containing 10 g iodine in 100 ml absolute methanol at 50°C.

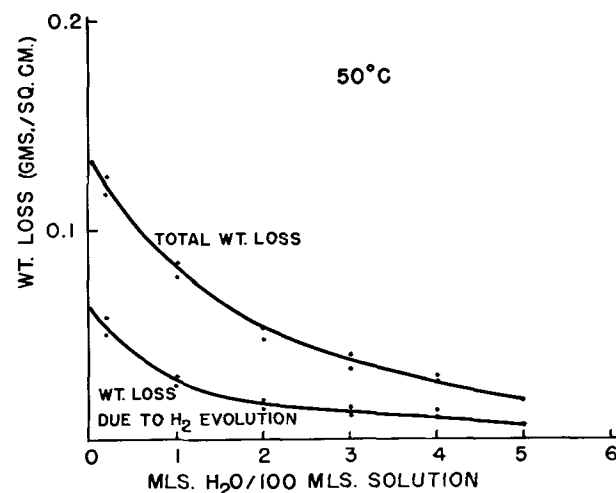


FIG. 12. The effect of water additions on the total dissolution and the weight loss due to hydrogen evolution of aluminum in a solution of 10 g I₂ in 100 ml absolute methanol at 50°C.

(Fig. 11) indicate that water additions reduced the weight losses of the specimens and the volumes of hydrogen evolved.

Additional experiments were carried out with water contents varying between 0 and 5% by volume. The temperature of these experiments was 50°C, the duration 1 hr, and the iodine concentration of the solution was 10 g/100 ml. At the end of each experiment, weight losses and volumes of hydrogen were measured and the free iodine contents of the solutions were determined. The results (Fig. 12) showed that increasing the water content of the

TABLE III. *Effect of oxygen on the attack of iodine/methanol solutions on high purity aluminum in 1 hr*

Concentration of solution	Temp, °C	Conditions of experiment	Wt loss g/cm ²
10 g I ₂ /100 ml CH ₃ OH	50°C	No bubbling	0.126
			0.117
			0.117
10 g I ₂ /100 ml CH ₃ OH	50°C	Nitrogen bubbled continuously	0.121
			0.116
			0.112
10 g I ₂ /100 ml CH ₃ OH	50°C	Oxygen bubbled continuously	0.117
			0.124
			0.122

solution decreased the dissolution rate of the aluminum and the rate of hydrogen evolution.

The effect of dissolved oxygen on the dissolution rate of aluminum in a solution of 10 g iodine in 100 ml absolute methanol (containing 0.1% of water) was next determined at 50°C. Experiments were carried out in which either tank oxygen or tank nitrogen was bubbled continuously through the solutions; weight loss determinations alone were made. The results (Table III) indicate that the rate of reaction at 50°C was unaffected by the bubbling of either oxygen or nitrogen.

The pH values of many of the solutions were determined after they had reacted with aluminum for different lengths of time. The reaction mixtures in all cases exhibited an acidic reaction to the glass electrode and were within the apparent pH range of 1.5–2.5. Although it is quite doubtful that these measurements of pH in organic solutions truly represent the actual hydrogen ion activities of the solutions, they do indicate that the solutions are acidic rather than alkaline in character. As a result of titration with sodium hydroxide it was calculated that the pH values of the solutions were within the range 3.0–3.5. In no case was it possible to boil off any acidic gas from these solutions.

Volumetric determinations of free iodine (using sodium thiosulfate) and of iodide (using cupric sulfate and sodium thiosulfate) in these reaction mixtures gave checks to within 1% with the total weights of iodine present initially in the solutions. However, when the weight of aluminum associated with the iodide was calculated and added to the weight of aluminum associated with the hydrogen evolved, the total weight appreciably exceeded the weight loss of the specimen sometimes by as much as 15%. This indicates that, in the presence of small amounts of water, either hydrogen may evolve from reactions other than the formation of aluminum methoxide or initially one aluminum ion is associated with less than three iodide ions. However, in dried solutions the order of agreement between these calculated and measured quantities is much closer. For example, an

aluminum specimen exposed to a solution of 5 g iodine in 100 ml dried methanol at 50°C for 1 hr showed a weight loss of 0.234 g. The aluminum associated with the iodide in solution (assuming that one aluminum ion is associated with three iodide ions) was 0.092 g, and that associated with the hydrogen evolved was 0.139 g, making a total of 0.231 g which is approximately 1.5% less than the total weight loss. This agreement is within the limits of experimental error of the weight loss determinations.

It has previously been suggested (15, 16) that the interaction of boiling methanol, aluminum, and iodine results in the formation of methyl iodide. Consequently, methyl iodide must be considered as a possible component of the reaction mixture. Its presence had not been detected in previous experiments since the water-cooled condensers which were used would prevent the escape of any methyl iodide from the reaction vessel.

Methyl iodide gives a precipitate of silver iodide with alcoholic silver nitrate (17) and forms a constant boiling mixture (39°C) with methanol containing 74.4 mole % methyl iodide (18). Therefore, a solution containing 10 g iodine in 100 ml absolute (undried) methanol that had been in contact with 0.9 g aluminum for 1 hr was distilled and the vapors passed into fresh alcoholic silver nitrate. It was found that a component of the solution distilled over at 39°C and gave a heavy precipitation of silver iodide when passed into the alcoholic silver nitrate. This indicates that methyl iodide is formed in this reaction mixture during its action on the aluminum. A similar solution was boiled vigorously and the gases passed into water. There was no decrease in pH of the water, which indicates that hydrogen iodide could not be boiled out of the reaction mixture in detectable quantities.

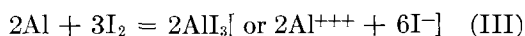
Similar experiments were carried out on solutions resulting from the interaction of aluminum, iodine, and dried methanol. Under these conditions it was not found possible to detect the presence of methyl iodide in the reaction mixtures. This indicated that methyl iodide was formed in detectable amounts only in solutions containing traces of water.

The presence of methyl iodide in reaction mixtures containing traces of water implies that formation of aluminum Grignard compounds such as CH₃AlI₂ is possible. However, such compounds would be expected to hydrolyze in the presence of water giving methanol (19), to combine with methanol to give methane (20), and to react with methyl iodide giving ethane (21). The fact that these saturated hydrocarbons were not detected in the gas evolved indicated that the formation of aluminum Grignard compounds is unlikely under these conditions.

DISCUSSION

Isolation of surface films from steel by means of the iodine-methanol solution occurs by a selective attack on the film-metal interface. Although a mechanism for this reaction has not been advanced, the steel is probably dissolved as a soluble iodide. There is no detectable gas evolution during film isolation from steel. The attack of similar solutions on film-covered aluminum results in the brisk evolution of hydrogen which, in dehydrated solutions, is accompanied by the formation of aluminum methoxide. Because the volume of hydrogen evolved is insufficient to account for the entire weight loss of the specimen, this suggests that a portion of the aluminum is being dissolved as a soluble iodide. Subsequent analyses of the solutions for iodide confirmed this suggestion. Since the major difference between the action of the same solution on the two different metals is the formation of the aluminum methoxide and hydrogen, it is considered that this reaction is mainly the cause of the general dissolution of aluminum rather than a selective dissolution at the aluminum/film interface.

In dried iodine-methanol solutions, the calculated weight of aluminum equivalent to the hydrogen evolved plus the weight of aluminum equivalent to the measured iodide in solution (assuming one aluminum ion is associated with three iodide ions) checks to within 1.5% with the actual weight loss of the specimen. In no case, in dried solutions, was the presence of hydrogen iodide, methyl iodide, methane, or ethane detected. Consequently, the two reactions taking place under dehydrated conditions may be represented as follows:



The reaction mixture is distinctly acidic to a glass electrode. This might conceivably be due to reaction of the methoxide with the alcohol (Meerwein reaction) to form an alkoxyacid which is believed to resemble sulfuric, phosphoric, and perchloric acids in its electronic configuration (22).



This is considered to be unlikely in view of the insolubility of aluminum methoxide in methanol. Instead, any acidity in these solutions is more likely to be the result of a very slow reaction between hydrogen and iodine to form minute traces of hydrogen iodide which could not be detected chemically in the vapor from the solutions.

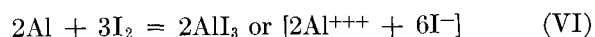
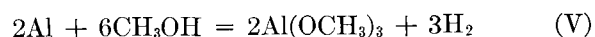
In the presence of water the reaction mechanism suggested above becomes greatly complicated; although the presence of several different reaction

products has been established, the mechanism advanced must be regarded as speculative. When solutions of absolute methanol (containing 0.1% water) were used in contact with the atmosphere no insoluble corrosion products were obtained. However, hydrogen was still evolved briskly, although in smaller quantities than in dried solutions. Furthermore, the rate of hydrogen evolution increased with increasing iodine concentration at 50°C (Fig. 10) but was almost independent of the iodine concentration at 25°C (Fig. 9). This may indicate that, at the higher temperature, hydrogen is formed by other reactions in addition to the interaction of aluminum and methyl alcohol which might be expected to be independent of the iodine concentration.⁵ Additional hydrogen could be generated by the interaction of aluminum with hydrogen iodide which might form as a product of hydrolysis of aluminum iodide. This belief was supported by the detection of methyl iodide in the solutions which must result from the interaction of hydrogen iodide and methanol.

Addition of a trace of water significantly reduces the rate of attack of the iodine-methanol solution on aluminum. The reason for this is not altogether clear, although cases have been recorded in which the corrosion of aluminum by an organic compound was greatly reduced by the presence of traces of water (23). This type of behavior has been believed to be associated with the formation of protective films of oxide or hydrated oxide by the traces of water (23, 24). However, this behavior in solutions of iodine in absolute methanol would be expected to be accompanied by the formation of spurious or secondary films which were never observed. Evidently further work will be necessary to clarify this point.⁶

It is believed that the reactions occurring in iodine-methanol solutions containing traces of water may reasonably be represented by the series of reactions shown below:

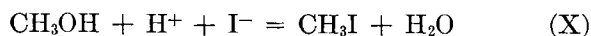
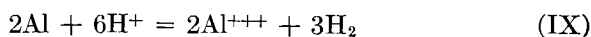
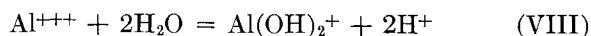
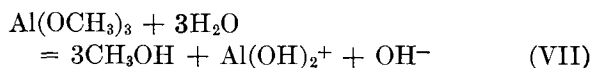
Primary



⁵ This effect may be due also to one aluminum ion in solution being initially associated with fewer than three iodide ions. However, the alternative suggested above is considered to be slightly more probable.

⁶ It has been suggested that the interaction of aluminum and iodine/methanol solutions could proceed by a free radical mechanism (28) as has been proposed for the interaction of aluminum and carbon tetrachloride (29). Since the presence of water will reduce the occurrence of free radicals, this type of mechanism would explain the effect of water on the dissolution rate of the aluminum.

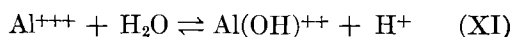
Secondary Reactions



Dissolved oxygen has been shown to have no effect on the reactions taking place in solution (Table III). Reactions (V) and (VI) are identical to those reactions taking place in the dried solutions. However, the different course subsequently taken by the reaction is believed to be due to the action of traces of water on the primary products of reaction.

Aluminum methoxide is believed to be hydrolyzed to soluble aluminum ions of the type shown in reaction (VII). Equally well, the hydrolysis of the aluminum methoxide might give ions of the type $\text{Al}(\text{OH})^{++}$ (25). Under the experimental conditions, hydrolysis to hydrated alumina did not occur presumably owing to the acidity developed by other hydrolysis and side reactions. However, hydrolysis of the aluminum methoxide to a soluble ion will result in the formation of hydroxyl ions.

Hydrolysis of aluminum ions (or aluminum iodide) is believed to result in the formation of such ions as $\text{Al}(\text{OH})^{++}$, $\text{Al}(\text{OH})_2^+$, and hydrogen ions (25). Such ions are stable in slightly acidic solutions, although they may be present in small quantities. They are considered as the first steps in the hydrolysis of aluminum ions to hydrated alumina. The dissociation constant of the reaction



has been given as 1.4×10^{-5} (25). The problem of determining hydrogen ion activity in equilibrium with aluminum ions and water is complicated by the formation of appreciable concentrations of $\text{Al}(\text{OH})_2^+$ from the second step of the hydrolysis (27). Nevertheless, it is undoubtedly true that a rather small concentration of hydrogen ions will be formed under equilibrium conditions in a slightly acid solution. However, hydroxyl ions formed by hydrolysis of aluminum methoxide [reaction (VII)], together with reactions (IX) and (X), will consume hydrogen ions and will throw reactions (VIII) or (XI) over to the right. Consequently, hydrolysis of aluminum ions by water can provide a reservoir of hydrogen ions that can combine with hydroxyl ions formed in reaction (VII) and that can take part in reactions (IX) and (X). Examination of the weight loss and hydrogen evolution data contained in Fig. 8-10 shows that this reservoir of hydrogen ions is sufficiently large to result in the over-all formation of slight acidity in solutions containing traces of water. In addition, it is

possible that some small quantities of hydrogen ions are formed by the interaction of the hydrogen evolved in reaction (V) and the iodine in solution, such as was suspected under dehydrated conditions.

It was observed that, in solutions containing traces of water, the sum of the aluminum equivalent to the combined iodine and that equivalent to the evolved hydrogen exceeded the total weight loss of the specimen. The over-all concentration of iodide formed in reaction (VI) will be unaffected by the hydrolysis of these products of reaction as suggested in reactions (VIII), (IX), and (X) since methyl iodide will give a quantitative test in aqueous solutions for iodide (17). However, reaction (IX), the interaction of hydrogen ions with aluminum, is a source of extra hydrogen gas; consequently it is believed that the difference between the actual and "calculated" weight loss may be due at least partly to this extra evolution of hydrogen resulting from reaction (IX).

The series of reactions believed to occur in solutions containing traces of water result in the over-all consumption of water, despite the fact that reaction (X) and a combination of reactions (VII) and (VIII) regenerate a portion of the water consumed. Thus, it would be expected that if the access of water to the solution were prevented, the water initially present might become exhausted, and insoluble aluminum methoxide might be precipitated. This actually occurred, as described earlier, in solutions of iodine in absolute methanol where the access of water vapor from the atmosphere was prevented by drying tubes. Consequently, this emphasizes the desirability of performing film isolation in contact with the atmosphere where the water that is consumed during reaction with the aluminum can be replenished by water vapor from the atmosphere.

ACKNOWLEDGMENTS

The authors wish to express their appreciation to Mr. R. V. Paulson for his original contributions to the theory and to Dr. B. de B. Darwent, Professor H. H. Uhlig, Dr. J. F. Murphy, Dr. F. J. Bowen, Dr. T. R. Pritchett, and Mr. F. L. Howard for their helpful discussions and suggestions.

Any discussion of this paper will appear in a Discussion Section, to be published in the June 1956 JOURNAL.

REFERENCES

1. U. R. EVANS, *J. Chem. Soc.*, **1927**, 1020.
2. S. WERNICK, *J. Electrodepositors' Tech. Soc.*, **9**, 163 (1933-34).
3. H. FISCHER AND F. KURTZ, *Korrosion u. Metallschutz*, **18**, 42 (1952).
4. G. TAMMANN AND F. ARNTZ, *Z. anorg. allgem. Chem.*, **192**, 45 (1930).
5. W. H. WITHEY AND H. E. MILLAR, *J. Soc. Chem. Ind. (London)*, **45**, 173T (1926).

6. T. E. ROONEY AND A. G. STAPLETON, *J. Iron Steel Inst.*, **131**, 249 (1935).
7. W. H. J. VERNON, F. WORMWELL, AND T. J. NURSE, *J. Chem. Soc.*, **1939**, 621.
8. J. E. O. MAYNE AND M. J. PRYOR, *ibid.*, **1949**, 1831.
9. M. J. PRYOR, *This Journal*, **101**, 141 (1954).
10. T. J. NURSE AND F. WORMWELL, *J. Appl. Chem. (London)*, **2**, 550 (1952).
11. E. C. PEARSON, H. J. HUFF, AND R. H. HAY, *Can. J. Technol.*, **30**, 311 (1952).
12. S. E. TURNER AND R. C. ANDERSON, *J. Am. Chem. Soc.*, **71**, 913 (1949).
13. C. V. KING AND E. HILLNER, *This Journal*, **101**, 79 (1954).
14. W. J. HICKINBOTTOM, "Reactions of Organic Compounds," p. 90, Longmans Green & Co., New York (1948).
15. M. T. DANGYAN, *J. Gen. Chem. (U.S.S.R.)*, **11**, 1215 (1941).
16. M. T. DANGYAN, *Bull. Armenian Branch Acad. Sci. U.S.S.R.*, **63**, No. 3/4 (1942).
17. M. KOHN, *Anal. Chim. Acta*, **9**, 249 (1953).
18. F. C. WHITMORE, "Organic Chemistry," p. 103, Van Nostrand & Co., New York (1946).
19. H. GILMAN, "Organic Chemistry," Vol. I, p. 497, John Wiley & Sons, Inc., New York (1948).
20. H. GILMAN, *op. cit.*, 499.
21. W. J. HICKINBOTTOM, *op. cit.*, 409.
22. F. C. WHITMORE, *op. cit.*, 112.
23. R. SELIGMAN AND P. WILLIAMS, *J. Soc. Chem. Ind. (London)*, **35**, 88 (1916).
24. J. M. BRYAN, "Aluminum and Aluminum Alloys in the Food Industry," Dept. of Scientific and Industrial Research Special Report #50, p. 22 (1948).
25. C. BROSSETT, *Acta Chem. Scand.*, **6**, 910 (1952).
26. N. BJERRUM, *Z. physik. Chem.*, **59**, 350 (1907).
27. W. M. LATIMER, "The Oxidation States of the Elements and their Potentials in Aqueous Solutions," p. 264, Prentice Hall, New York (1938).
28. H. H. UHLIG, Private communication.
29. M. STERN AND H. H. UHLIG, *This Journal*, **100**, 543 (1953).

The Rate and Mechanism of Dissolution of Purest Aluminum in Hydrofluoric Acid¹

M. E. STRAUMANIS AND Y. N. WANG

University of Missouri School of Mines and Metallurgy, Department of Metallurgy, Rolla, Missouri

ABSTRACT

Pure aluminum (99.99%) dissolves in hydrofluoric acid with a rate comparable to that of titanium in the same acid. The rate of dissolution, V (mm^2/cm^2 min of hydrogen), in 0.1–6*N* hydrofluoric acid is in agreement with the empirical equation $V = 28 + 275N$, and for 6–10*N* with $V = 20.44N^{2.35}$. Recrystallized aluminum showed the same rates within the error limits ($\pm 14\%$). Of the noble metal salts added to the acid, only nickel and gold increased the dissolution rate; deposits obtained from other salt solutions did not adhere to the surface of the dissolving aluminum. Ammonium fluoride and ammonium chloride additions to the acid decreased the dissolution rate (passivation) because a salt film was formed on the aluminum surface. The potential of aluminum in 2*N* hydrofluoric acid was -1.22 v, indicating that the extent or thickness of protective surface films was negligible. The dissolution rate of aluminum in sulfuric acid, phosphoric acid, and other acids can be increased considerably by addition of water-soluble fluorides. The behavior of aluminum in hydrofluoric acid, as well as in hydrochloric acid, could be explained qualitatively using the concept of local currents in a manner similar to that proposed earlier.

INTRODUCTION

Corrosion resistance of pure aluminum to atmospheric attack, as well as to the action of many acids, is explained by the presence of a thin but adherent and highly protective surface oxide film. If the oxide film is destroyed, e.g., by mercury or strong bases (1), the metal underneath quickly corrodes. Hydrofluoric acid attacks surface oxide layers also, e.g., on titanium, then dissolves the metal (2). So it was of importance to know whether the same is true in the case of aluminum (although aluminum fluoride formed during the reaction is difficultly soluble in the acid) and to elucidate the dissolution mechanism.

There is very little information in the literature about this dissolution process. Spacht has compiled all the available data (3), and Holmberg and Prange state that a film protects aluminum for a short time from attack by hydrofluoric acid (4).

MATERIALS USED

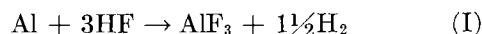
Samples in the form of squares (1 cm^2) were cut from a 1 mm thick, cold rolled, aluminum sheet supplied by the Aluminum Company of America. It was designated 99.99% pure, and contained as impurities: Si—0.0015, Fe—0.0007, Cu—0.0004, and Mg—0.0007%. To compare the corrosion properties of this metal with those of a 99.998% aluminum (5),² rate measurements in hydrochloric acid (6) were repeated using the 99.99% Alcoa aluminum. Plates made of this metal were relieved from internal

stresses due to cold working by annealing them at 470°C for 1 hr. Specimens exactly 1 cm^2 were ground, polished, and mounted in Bakelite (2). From the rate of hydrogen evolution in 2*N* hydrochloric acid (reagent grade), the average dissolution rate of this aluminum during the 44 hr duration of the experiment was $18.6 \text{ mm}^2/\text{cm}^2\text{min}$ in hydrogen units, while the French 99.998% aluminum developed a rate of only 0.56. Thus, the French metal was much purer, as was also indicated by its analysis of impurities: Si—0.0009, Fe—0.0002, and Cu—0.0003%.

All chemicals used were of reagent or of C.P. grade, and all experiments described below were performed with the 99.99% American aluminum.

EXPERIMENTAL RESULTS

Rate of dissolution in pure hydrofluoric acid.—The rate was determined by collecting hydrogen developed according to the reaction



as described previously (2). Glass parts of the apparatus were protected from attack by the acid by a brown wax.³ The volume of acid in each experiment was 200 cc, the temperature was $25^\circ \pm 0.1^\circ\text{C}$, and the aluminum sample was mounted on the foot of stirrers rotating at 200 rpm. Glass joints were used wherever possible, in order to reduce the loss of hydrogen by diffusion through rubber connections.

Experiments were made in 0.1, 0.5, 1, 2, 4, 6, 8, and 10*N* hydrofluoric acid solutions, the normality of

¹ Manuscript received December 15, 1954.

² From Alais, Froges, et Camargue, France.

³ Sunoco 1290, Sun Oil Company, Philadelphia, Pa.

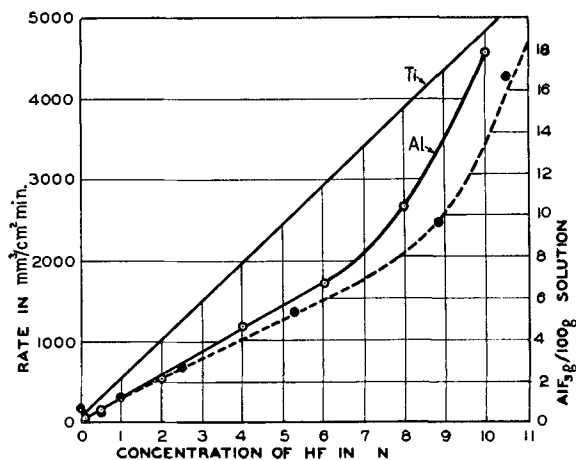


FIG. 1. Rate of dissolution of Al in different concentrations, N , of HF at 25°C. Each point represents an average of two runs. The volume of H_2 was reduced to normal conditions. 1 mm³ of H_2 corresponds to 0.000803 mg of Al metal. A similar curve for Ti is drawn for comparison (1 mm³ = 0.001424 mg Ti). Dashed line: solubility of AlF_3 in HF (in g/100 cm³ of solution) according to Seidell (7).

each being checked by titration. Reaction (I) started with an induction period of 30–50 min, then followed a flat maximum (about 120 min in diluted and 30 min in more concentrated acids), and finally declined gradually. In Fig. 1 the average maximum rate, a mean of two runs, is plotted against the acid concentration. For acids of lower concentrations (0.1 to 6N) the velocity of dissolution V conforms with the empirical equation

$$V = 28 + 275N \quad (II)$$

and at higher concentrations (6–10N) with the equation

$$V = 20.44N^{2.35} \text{ mm}^3/\text{cm}^2\text{min} \quad (III)$$

Deviation of observed from calculated rates [equations (II) and (III)] is within -7.2 and $+5.8\%$. However, the difference between the average maximum rates of duplicated runs was within 0.3 and 16.6%. These deviations may be due to irregular distribution of small amounts of impurities in the aluminum. Other reasons, such as heterogenous stress distribution set up from cold work, are of minor importance, as is shown below.

The metal surfaces after dissolution were glossy, clearly showing the cold work fibers. The surfaces were partially covered with a loose white precipitate of aluminum fluoride, especially at the edges and corners of the sample, resulting from reaction (I). However, the sample was evenly attacked, indicating that the dissolution reaction was not retarded appreciably by the presence of aluminum fluoride on the surface of the dissolving metal. Solubility of the fluoride is limited to 0.55 g ($AlF_3 \cdot H_2O$) in 100 g water and decreases in low acid concentrations (7). Hence,

if the solubility product is exceeded, the loose, white precipitate appears on the sample, and is also finally dispersed throughout the acid.

Experiments with aluminum samples recrystallized at temperatures of 400° and 575°C showed no appreciable difference in dissolution rates from those of cold worked metal (5). Differences of -7.5 to $+14.3\%$ were observed, but they are too small (and deviate to both sides) to state definite conclusions concerning the influence of cold work on the dissolution rate of aluminum.

Effect of additional reagents on the dissolution rate.—A series of qualitative tests were made to determine whether the dissolution rate of aluminum in sulfuric, nitric, phosphoric, acetic, and formic acids was increased by the presence of hydrofluoric acid. Pure aluminum reacts very slowly with 2N sulfuric acid. After addition of a small amount of ammonium fluoride to the acid, the sample was attacked immediately because of displacement of the free hydrofluoric acid; as was the case with titanium (8). Concentrated nitric, phosphoric, acetic, and formic acids did not react with the aluminum, even in the presence of ammonium fluoride, but there was a very slight reaction with phosphoric acid. However, when the fluoride was added to the diluted acids (1:1 and more), an immediate, rapid reaction went on for a considerable time. In the case of acetic acid the reaction was moderate.

To study the influence of salt additions on the dissolution rate of aluminum in hydrofluoric acid, ammonium fluoride and ammonium chloride were chosen. The results are shown in Fig. 2. This series of experiments began with aluminum dissolution in pure 1N hydrofluoric acid, and a rate of 344 mm³/cm²min was obtained instead of 303 (Fig. 1). The difference of 13.5% is still well within the error limits of the reproducibility of corrosion rate determinations, which is around 30%. While the reasons for

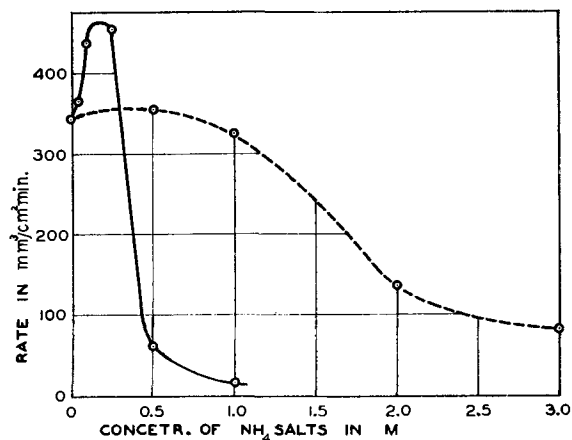


FIG. 2. Rate of dissolution of aluminum in 1N HF vs. concentration of ammonium salts added: NH_4F —solid curve, NH_4Cl —dashed curve.

increased rate of dissolution at small concentrations of the ammonium salts are not quite clear, the rate decrease at still higher salt concentrations can be explained satisfactorily. White salt films, porous, but adherent, were on the aluminum surface after such experiments, reducing the exposed metal surface. Evidently, at augmented concentrations of ammonium salts in the acid, the aluminum fluoride solubility was reduced, and a salt film, spreading in all directions with increasing ammonium salt concentrations, was formed on the surface and passivated the metal as was the case with titanium (8). The films were never thick enough to be collected for a complete chemical identification, but the presence of an ammonium radical could be proved in both kinds of films.

If a dissolution process is electrochemical in nature, metallic impurities present in the dissolving metal, or in the acid, in the form of noble metal salts should increase the reaction rate. Six salt solutions, CuSO_4 , HAuCl_4 , NiCl_2 , $\text{Pb}(\text{NO}_3)_2$, AgNO_3 , and PtCl_4 were added separately to the hydrofluoric acid in quantities of 2 cc of 0.1M aqueous solutions, in a manner, as previously described (2), so as not to dilute the acid. The runs with PtCl_4 were made in pure nitrogen to avoid any possible catalytic reaction in the formation of water from the liberated hydrogen and oxygen from the air. Results are shown in Table I.

The salt solutions of Table I were added to the acid when the dissolution rate of aluminum had reached its maximum. Only the nickel and gold solutions increased the rate, while the other solutions decreased it. Examination of aluminum samples after the runs showed that those in the nickel solution had a bright surface coating. Under the microscope the coating appeared tightly adherent to the aluminum surface, but had a porous appearance. This nickel film evidently acted as a local cathode accelerating the dissolution rate of aluminum. In the other instances no metal was observed on the sample surface, except in traces mixed up with the white salt deposit in the cases of gold, lead, and silver. Complete reduction occurred as evidenced by a dark metallic sediment on the bottom of the flask. Thus,

TABLE I. The effect of salt solutions, added to the 1N HF, on the dissolution rate of Al

Ions of the salts added	Change in rate in %
Cu^{2+}	-14.8
Au^{3+}	+25.1
Ni^{2+}	+118.0
Ag^+	-28.7
Pt^{4+}	-37.7
Pb^{2+}	-72.0

* PbF_2 partly precipitated from the solution; but there was sufficient Pb^{2+} to plate out on the Al.

the inefficiency of the salts mentioned is understandable, although not the severe drop in the dissolution rate after addition of the salts to the acid. Attempts were made to find the answer to this by measuring the potential of the dissolving aluminum under various conditions.

Potential measurements of the dissolving aluminum.—Potentials were measured against a 1N calomel electrode, and were converted to the standard hydrogen electrode scale (9, 10). Very few such measurements of the aluminum potential in hydrofluoric acid have been made (11). Just after immersion of the electrode in the hydrofluoric acid the potential dropped suddenly, then slowly became less negative. In most cases, there was a steady potential at the end of the experimental period. The potential is very negative and decreases with the acid concentration, approaching a limiting value (11).

Using an electrode freshly etched with hydrofluoric acid, slowly rising curves were obtained starting with the first minute (Fig. 3). If salt solutions were added to the acid of the etched electrode, changes in the electrode potential occurred immediately. Measurements were made in 100 cc 0.5N hydrofluoric acid; 1 cc of the 0.1M addition agent (NiCl_2 , PtCl_4 , HAuCl_4 , CuSO_4) together with 1 cc of the 1N acid, in order not to dilute the electrolyte, were added to it. Results are summarized in Fig. 3. In all four cases the potential of the dissolving aluminum increased considerably after addition of the noble metal salts, especially when gold and copper salts were added, raising the potential by 0.52–0.54 v. However, a good deposit on the surface of the dissolving aluminum was observed only in the case of

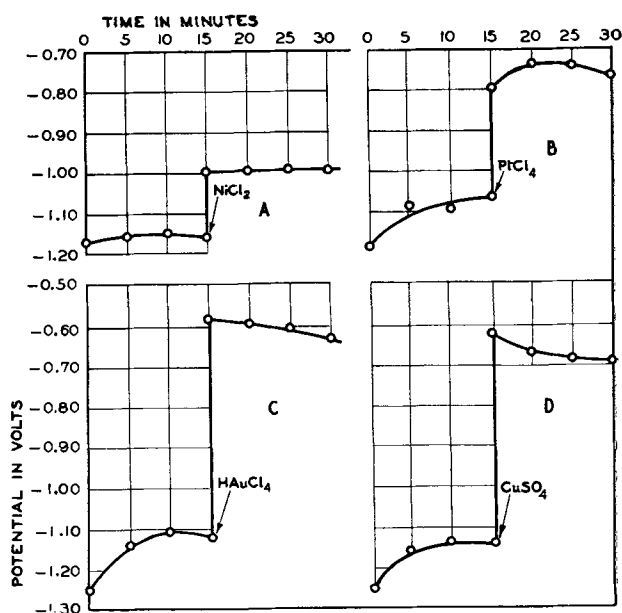


FIG. 3. Effect of additional agents on the aluminum electrode potential in 0.5N HF. Hydrogen scale.

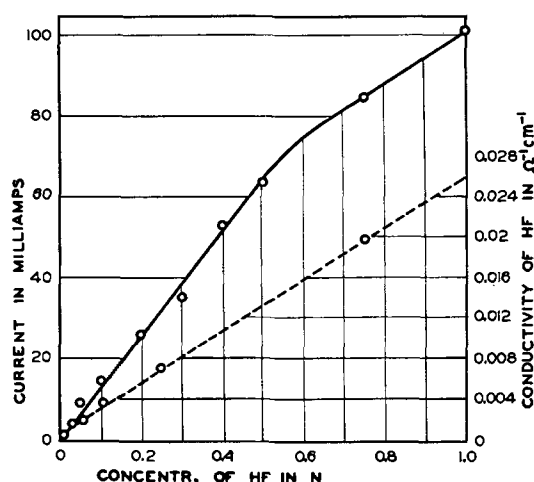


FIG. 4. Current produced by a cell Al-HF-Pt (platinized) vs. concentration of HF. Exposed electrode surfaces: 2 x 2 cm. Distance between the electrodes: 1 cm. Dashed curve: conductivity of the acid vs. concentration.

nickel chloride, and the presence of this metal was proved by qualitative tests. Other metals (Fig. 3 B, C, D) were reduced, but did not adhere to the electrode. A decrease in the rate of hydrogen evolution was observed after addition of the three salt solutions.

That aluminum, if in contact with particles of a noble metal, is capable of quickly going into solution in a bath of hydrofluoric acid, was proved by the behavior of the cell Al-HF-Pt (platinized). As soon as such a cell was closed through a milliammeter (9), current flowed. In dilute acids, the current was larger at first, dropped, then rose to a fairly steady value. At 0.75*N* and up no drop was observable, only an increase of current with time. The average current produced by the cell after 20 min of operation (usually between 20 and 50 min) is shown in Fig. 4, as a function of acid concentration.

Thus, local cathodes of low hydrogen overvoltage, being in contact with aluminum metal immersed in hydrofluoric acid, should accelerate the dissolution rate of the base metal.

DISCUSSION

Dissolution rates of pure aluminum in 2*N* hydrochloric acid and in hydrofluoric acid were 18.6 and 546 mm³/cm²min. This behavior is easily explained by the potential and difference effect measurements of the dissolving metal. The potential in 1*N* hydrochloric acid is around -0.6 v (12), and that in 2*N* hydrofluoric acid is -1.22 v (11). The consequence is that metallic impurities still present in the metal develop an emf about twice as large in the hydrofluoric acid. As aluminum dissolving in hydrochloric acid shows a negative difference effect, it is evident that the reacting surface of the metal is covered by a

protective film (11). Consequently, dissolution occurs only through the pores, with part of them acting as anodes and those filled with metallic residues as cathodes (13, 14). The high anodic polarization of aluminum in the pores shows up in the less active potential of -0.6 v of the metal. On the other hand, aluminum dissolving in hydrofluoric acid exhibits a positive difference effect (11), so no appreciable protective films are on the metal. Therefore, anodic polarization is low, the aluminum shows a very negative potential of -1.22 v, and action of local currents on the metal surface is not limited by the film. Thus, a comparatively high dissolution rate is developed in hydrofluoric acid, in spite of the low solubility of aluminum fluoride formed in the acid. Furthermore, the concept of dissolution because of local element action is confirmed by the augmentation of the current produced by the cell Al-HF-Pt along a straight line (Fig. 4), a fact which can be explained by the increase in conductivity of the hydrofluoric acid with concentration (15). Deviations occur at higher current densities because of increased polarization of the cell.

It was expected that the aluminum dissolution rate should increase linearly with hydrofluoric acid concentration, as does that of titanium (Fig. 1). However, deviation from the straight line relationship above 6*N* can be explained by increased solubility of aluminum fluoride with hydrofluoric acid concentration (7), as shown by the dashed curve (Fig. 1). Then aluminum fluoride formed at low acid concentrations to a certain degree hampered the dissolution rate; indeed the addition of salts (NH₄F, NH₄Cl) decreased the rate (Fig. 2) because of formation of the salt film which covered part of the local cathodes. The appearance of the difference effect, which is explained on the basis of the local element theory (11), also testifies to such an electrochemical mechanism of dissolution.

The hydrogen overpotential on aluminum, as with titanium (16), should be very negative, at least more negative than the potential of aluminum in hydrofluoric acid (11). This negative potential, required for hydrogen development on aluminum, is the reason for the low dissolution rate of the purest aluminum. The appearance of local cathodes of a nobler metal with a less negative overpotential should, therefore, greatly increase the dissolution rate of the base metal. However, this was true only in the case of nickel and gold (Table I), while the other metals proved to be inefficient and even decreased the rate. One reason for this behavior has been mentioned already: the precipitates, except nickel, did not adhere to the dissolving surface, so no efficient local currents could be formed. The other reason is the shifting of the potential of aluminum

toward noble values after addition of the salt solution (Fig. 3). Of course, this shift decreased the emf of the local currents, with the effect of decreasing hydrogen evolution also. There is still a question as to why these shifts occurred, as particles of the displaced noble metal quickly dropped from the dissolving aluminum surface. There is still no answer to this question, but it is believed that the phenomenon is the same as noticed by Schlain and Smatko (17) upon immersion of a titanium electrode in a solution of hydrochloric acid containing small amounts of noble metal salts. The electrode became passive without showing the presence of the displaced metals on its surface (17).

It can be concluded that the dissolution of aluminum in hydrofluoric acid is an electrochemical process and that it can be satisfactorily described qualitatively, if not quantitatively.

ACKNOWLEDGMENT

The authors are grateful to Dr. C. B. Gill for correcting the English of this manuscript.

Any discussion of this paper will appear in a Discussion Section to be published in the June 1956 JOURNAL.

REFERENCES

1. M. E. STRAUMANIS AND N. BRAKŠS, *This Journal*, **95**, 98 (1949); **96**, 21, 310 (1949); *Metall*, **3**, 41 (1949).
2. M. E. STRAUMANIS AND P. C. CHEN, *This Journal*, **98**, 234 (1951).
3. R. B. SPACHT, *J. Chem. Educ.*, **23**, 253 (1946).
4. M. E. HOLMBERG AND F. A. PRANGE, *Ind. Eng. Chem.*, **37**, 1030 (1945).
5. B. ROALD AND M. A. STREICHER, *This Journal*, **97**, 283 (1950).
6. M. STRAUMANIS, *Korrosion u. Metallschutz*, **14**, 1 (1938).
7. A. SEIDEL, "Solubilities of Inorganic and Metal Organic Compounds," 3rd ed., D. Van Nostrand and Co., Inc., New York (1940).
8. M. E. STRAUMANIS AND C. B. GILL, *This Journal*, **101**, 11 (1954).
9. M. E. STRAUMANIS AND P. C. CHEN, *Corrosion*, **7**, 229, 234 (1951).
10. A. J. DEBÉTHUNE, *Corrosion*, **9**, 336 (1953).
11. M. E. STRAUMANIS AND Y. N. WANG, *This Journal*, **102**, 304 (1955).
12. C. J. DE GRUYTER, *Rec. trav. chim.*, **44**, 960 (1925).
13. M. E. STRAUMANIS, *Korrosion u. Metallschutz*, **14**, 81, 82 (1938).
14. U. R. EVANS, "Metallic Corrosion, Passivity and Protection," p. 204, Longmans, Green and Co., New York (1948).
15. LANDOLT-BÖRNSTEIN (Roth-Scheel), "Physikalisch-chemische Tabellen," 5, Auflage II, pp. 1076-1077, Verl. J. Springer, Berlin (1923).
16. M. E. STRAUMANIS, S. T. SHIH, AND A. W. SCHLECHTEN, *J. Phys. Chem.*, **59**, 317 (1955).
17. D. SCHLAIN AND J. S. SMATKO, *This Journal*, **99**, 417 (1952).

Brightening Agents for the Tin-II Sulfate-Sulfuric Acid Electrolyte¹

C. A. DISCHER² AND F. C. MATHERS

Indiana University, Bloomington, Indiana

ABSTRACT

Addition agents capable of producing specular deposits directly from the acid tin plating bath are described. Concentration ranges of electrolyte and operating conditions are discussed. Properties of the electrodeposit are described. The role played by each of the addition agents is discussed.

INTRODUCTION

In an intensive study of the literature of addition agents for the tin-II sulfate-sulfuric acid electrolyte, it was found that the reported addition agents tend to fall into certain well-defined classes of substances. In the claims for good deposits, two of these classes of addition agents were of special interest: the phenols, and the surface active agents.

The simple phenols, i.e., phenol and β -naphthol, are named too frequently to be listed, especially since the crude phenols, i.e., cresol and various mixtures containing phenols as constituents, are of greater interest. Cooper and Light (1) have patented the use of tar acids such as cresylic acid, and/or pyroligneous acids. Schlötter (2, 3) has patented the system using two or more substances from the groups glue, gelatine, and agar-agar on one hand and sulfonated oils, resins, bitumen, wood tar on the other. Felger and Mathers (4) have reported the crude products of the fractional distillation of coal tar as exceptional addition agents.

Surface active agents appear frequently, especially in the newer literature. Sulfonates are often mentioned (2-4). Nachtman (5) has patented a mixture containing a colloid, sulfonated cresols or naphthols, and a wetting agent consisting of the sodium salt of the sulfate ester of organic alcohols having 8-12 carbon atoms.

After preliminary study of the older work it was decided to investigate thoroughly these two classes of substances as brightening agents for acid tin electrolyte.

¹ Manuscript received November 22, 1954. This paper was prepared for delivery before the Boston Meeting, October 3 to 7, 1954, and is taken from a thesis submitted by C. A. Discher to the Graduate College of Indiana University in partial fulfillment of the requirements for the Ph.D. degree.

² Present address: Rutgers University College of Pharmacy, 1 Lincoln Ave., Newark 4, New Jersey.

EXPERIMENTAL

Test solutions contained 100 g/l tin-II sulfate (commercial quality) and 100 g/l concentrated sulfuric acid. One hundred milliliter portions of this solution were used for each addition agent or combination of addition agents tested. Cathodes were 2.5 cm x 2.5 cm steel sheet. Pure tin anodes giving a cathode:anode ratio of approximately 2:5 were used. Each anode was sheathed in an envelope of filter paper to prevent anode sludges from contaminating the bath. The electrodes were placed opposite each other and pressed tightly against the sides of a 150 ml beaker.

Current density was maintained at 1.55 amp/dm², except for tests made to determine maximum current density without gassing. Agitation, unless otherwise noted, was provided by a 7 mm glass rod, flattened at its end and rotated at about 100 rpm.

RESULTS

It was found after many trials that the best brightening activity was obtained from the tars produced by the destructive distillation of saccharides: glucose, sucrose, starch, cellulose (cotton and filter paper), wood (pine and red wood), and the dried waste sulfite liquor of the paper industry. While the aqueous portions of the distillates possessed slight activity, it was shown that this was because they were saturated with respect to the tars. In order to eliminate much time-consuming work a commercial source of these tars was obtained.³ All subsequent work reported in this paper was done with this wood tar. PT will be used as its symbol.

The work now centered about solubilizing the PT. Sulfonated *p*-cymene, *p*-ethyl benzene sulfonic

³ Settled tar from destructive distillation of hardwood. Crossett Chemical Company, Crossett, Arkansas. Pyroligneous acid, methanol column slops, stripping oil, acetic acid still residue, and other by-products were also furnished, but were ineffective.

acid, sulfocarbolic acid, *p*-toluene sulfonic acid, sulfolane and dimethylsulfolane,⁴ alkane sulfonic acid,⁵ various sodium salts of aliphatic alcohol sulfates (i.e., Duponols, Tergitols), carbowaxes, celluloses, and carbital were tested. In most cases there was some improvement in the solubility of the PT and its effectiveness as an addition agent, but in no case could a bright deposit be obtained. Sodium aliphatic alcohol sulfate esters were more effective than the others. To see if further improvement of the deposit could be obtained it was decided to prepare and test the unneutralized sulfate esters.

The required quantity of concentrated sulfuric acid (to give 100 g/l in the finished electrolyte) was measured and the proper quantity of *n*-aliphatic alcohol added to it in 3–5 portions or rapidly dropwise good mixing. After standing 2–3 min the reaction mixture, which became warm, was added to water containing the tin-II sulfate. PT was added and the resulting electrolyte was filtered to remove any undissolved tin compounds and a small quantity of insoluble black sludge remaining from the tar.

Normal aliphatic alcohols having 2–12 carbon atoms were tested. Maximum solubilizing action was found in the *n*-octyl preparation, this solution giving mirror-bright deposits. Attempts to further increase the solubility of the PT by also including other surface active agents previously named were unsuccessful.

Composition of the bright bath.—The following composition appears to be the most effective: 100 g/l SnSO₄, 100 g/l H₂SO₄, 10 g/l *n*-octyl alcohol (reacted with the sulfuric acid), and 8 g/l PT. However, bright deposits are obtained with tin-II sulfate concentrations from 50 g/l to saturated. Concentrations as low as 30 g/l were tested, but matte deposits were obtained. Free sulfuric acid is essential. Bright deposits are obtained using 50–120 g/l. Lower concentrations cause excessive sludge; higher concentrations produce hard, rough deposits; very high concentrations (250 g/l) result in gassing.

The quantity of *n*-octyl alcohol used to prepare the acid sulfate ester may be varied from 5 to 15 g/l. Concentrations below the lower limit did not dissolve sufficient PT to give bright deposits; concentrations above 20 g/l give hard, gray, striated deposits. Nothing is gained by increasing the quantity of *n*-octyl alcohol above 10 g/l since the solubility of the PT does not improve beyond this level.

Concentration of the PT cannot be increased beyond 8 g/l. Baths prepared with higher concentrations of this substance separate into two phases, an oily upper layer and an aqueous layer. Neither

layer is effective in producing bright deposits. As the PT level is allowed to drop below 8 g/l the deposit becomes progressively less bright, passing into white matte and, finally, at very low concentrations, giving a visibly grainy crystalline appearance. *Control of concentrations.*—The usual analytical methods may be used for the tin-II and acid (6). PT acts as its own indicator. Solutions capable of giving mirror-bright deposits are dark brown, while matte deposits are obtained from solutions of a straw color. The bath may be regenerated as frequently as necessary by addition of PT to give the solution the depth of color necessary for the desired deposit. The *n*-octyl sulfate concentration may be controlled by making use of its foaming quality. As the electrolyte becomes depleted in this substance its foaming power decreases and its ability to dissolve PT decreases.

Operating conditions.—The bath has been operated successfully at temperatures as low as 5°C (some tin-II sulfate separates from the standard bath at this temperature) and as high as 65°C. The bath has been operated at current densities as high as 12 amp/dm². At this current density, with the stirring conditions used, gassing took place. With a higher stirring rate, higher current densities should be possible. Best brightening activity is obtained when the current density is maintained at a level just below that at which gassing begins.

Bath characteristics.—The cathode efficiency, for a series of 25 determinations, was found to be 98%. The anode efficiency is of the same order. Anode corrosion is very smooth and even. There is no intercrystalline corrosion.

The throwing power of *n*-octyl sulfate-PT bath is very good. A thick cathode was prepared by keeping it tightly against the side of the beaker. When cut in cross section the back side had $\frac{2}{3}$ the thickness of the front side. Irregular objects plate easily, even in deep crevices.

The life of the electrolyte is very good. One hundred milliliter baths were operated continuously for 4–5 month periods. Additions of various constituents were made as needed. The plate obtained at the end of this time was in every way comparable to that obtained initially.

Character of deposits.—Bright deposits have been produced on steel, copper, bronze, brass, and cast iron. Brightness on cast iron requires thicker deposits. On copper, at a current density of 5 amp/dm² bright plates are obtained at 0.00013 cm thickness, mirror bright at 0.00025 cm. Similar results were obtained on steel.

White matte deposits (obtained by using lower concentrations of PT) were flowed successfully in cottonseed oil (1% stearic acid) and by direct gas

⁴ Shell Development Corporation, Emeryville, California.

⁵ Standard Oil Company (Indiana), Chicago, Illinois.

heat (0.00007–0.0002 cm thickness at 1.5 amp/dm² and 0.0002–0.001 cm at 9.0 amp/dm²).

Deposits are soft and easily scratched. There is some increased hardness with brightness. Adhesion is excellent. Good adherent solder joints could be obtained with all plates.

The ferroxyl test gave results for this plate which were equal to or better than corresponding thicknesses of commercial plate.

Depletion of addition agents.—Study of baths in continuous operation for 3–5-month periods indicated that the octyl sulfate ester depletion can be accounted for entirely by dragout. This lends support to the theory that this substance serves solely as a solubilizing agent for the PT. On the other hand, the disappearance of PT is much greater than can be accounted for in the same way. Since no precipitates form during operation, it must be concluded that this substance is in some manner codeposited in the tin plate. Over a three-month period of continuous operation the following information was obtained. One hundred milliliters of electrolyte produced 630 g tin metal, consuming at the same time 0.5 g of *n*-octyl alcohol and 3.8 g of PT.

Nature of brightening agent.—A series of experiments were run in order to elucidate the chemical nature of the brightening agent. Fractional distillation of the PT established that the brightening activity is strongest in the highest boiling fractions and the still pot residue. This indicates a high boiling, high molecular weight substance.

Treatment of the solution of the PT in diethyl ether (a small amount of insoluble black solid forms which has no brightening action) with sodium hydroxide, potassium hydroxide, sodium carbonate, sodium bicarbonate (aqueous solution or solid) until basic gives two fractions, an ether-soluble portion and a water-soluble portion. The brightening activity is found to reside in the ether layer. This shows that the brightening agent is not an acid or phenol. (The phenols may be recovered from the water solubles.

While they are of no value for the bath under discussion, with glue these phenols give white matte deposits.)

Use with other metals.—PT is an effective addition agent for lead electrodeposition. Obviously sulfuric acid with the sulfate esters is not applicable. However, using the fluorosilicate bath with carbowax-1500 to increase the solubility of the PT, excellent matte deposits of lead may be obtained over long periods of time. PT was added to the bath as needed.

A copper bath analogous to the tin electrolyte is capable of giving bright flash deposits. However, thick deposits were not obtainable.

Attempts to adapt the brightener to iron (iron-II sulfate), zinc (zinc sulfate), and zirconium (zirconium sulfate) were unsuccessful.

CONCLUSIONS

A tin-II sulfate-sulfuric acid bath using *n*-octyl sulfate in the form of the free acid as a solubilizing agent and pyroligneous tars from the destructive distillation of saccharides as brightening agents is capable of producing tin deposits possessing specular reflection. The brightening agent is a high boiling, nonacidic, probably neutral substance.

The composition of the solution is readily controlled to maintain it in a condition to give matte to mirror-bright deposits of tin. These deposits are adherent, soft, and malleable.

Any discussion of this paper will appear in a Discussion Section to be published in the June 1956 JOURNAL.

REFERENCES

1. J. P. COOPER AND D. W. LIGHT, U.S. Pat. 2,156,427, May 2, 1939.
2. M. SCHLÖTTER, French Pat. 790,884, Nov. 28, 1935.
3. M. SCHLÖTTER, British Pat. 443,429, Feb. 27, 1936.
4. M. M. FELGER AND F. C. MATHERS, *Trans. Electrochem. Soc.*, **90**, 81 (1946).
5. J. S. NACHTMAN, British Pat. 528,240, Oct. 25, 1940.
6. P. R. PINE, *Trans. Electrochem. Soc.*, **80**, 640 (1941).

Antimony Oxide Phosphor with Red Emission¹

YOSHIHIDE KOTERA AND TADAO SEKINE

Fifth Division, Government Chemical Industrial Research Institute, Tokyo, Japan

ABSTRACT

A phosphor consisting of antimony oxide, boric oxide, and manganese activator is fairly efficiently excited by ultraviolet radiation. It emits a band spectrum with a peak at 6400 Å. The function of the boric oxide is to enhance fluorescent intensity, optimum composition being about 1 mole antimony oxide, 0.1 mole boric acid, and 0.002 mole manganese. Firing times, temperatures, and atmospheres (except hydrogen) are not critical. The structure of the phosphors is discussed on the basis of x-ray diffraction patterns.

INTRODUCTION

This is an account of a new phosphor which is capable of emitting red fluorescent light fairly efficiently when excited with ultraviolet radiation. It may, therefore, be used in fluorescent lamp applications. Heretofore, antimony oxide has been used rarely as a base material for phosphors. However, the present work shows that such phosphors do exist. While the manganese activator is responsible for the fluorescent emission, boric oxide serves mainly to enhance its intensity. Titanium may also be used as an activator, but its effect has not been investigated thoroughly as yet.

PREPARATION

In the preparation of phosphors, commercially available chemically pure grades of antimony trichloride, boric acid, and manganese sulfate were used as starting materials. Antimony chloride was dissolved in dilute HCl. After filtration, the solution was poured into about 10 times its volume of water. The precipitate formed was washed several times by decantation with water, then with dilute HCl and with ammonia, filtered, and dried at 110°C. Its purity was established spectrographically. After heating for 2 hr at 750°C the product became insoluble in solutions of acids and alkalis. It was found to be a mixture of Sb_2O_4 and Sb_2O_3 as determined by the method described below. Boric acid was purified by means of double recrystallization. Manganese sulfate was not further purified.

From preliminary work the optimum composition for the phosphor was found to be: antimony oxide—25.0 g; boric acid—0.50 g; manganese sulfate (anhyd.)—0.024 g.

These ingredients were thoroughly mixed in the dry state and then fired at 1100°C in air for 6 hr.

Experiments were also carried out with different experimental conditions. First, deviations from the above composition were tried, keeping the amount

of antimony oxide constant and varying singly each of the other two components. These were increased in steps, from zero up to 10 or 25 times their quantities in the base formula above. Next, the firing temperatures were varied from 1000° to 1200°C, and the time of firing from 2 to 12 hr.

Possible losses of boric acid in firing were determined by chemical analysis of the phosphors. In most cases the losses were negligible, but in some samples they amounted to about one-half of the amounts added without, however, producing characteristic differences.

Phosphor samples were excited with a low pressure quartz mercury lamp and their relative brightness was measured with a Pulfrich photometer equipped with a red filter transmitting between 5500 and 7000 Å. Experimental data were taken several times by two observers for each sample. Average brightness values obtained are given in Table I.

The table shows that changes in boric acid concentration are not highly critical, that changes of manganese concentration are somewhat more characteristic, that manganese, in fact, is essential for the fluorescence of the phosphors to develop, and that a second brightness maximum is found at higher manganese concentrations. It is also evident that the base formula given above is close to the optimum composition. Firing times and temperatures are likewise not very critical, except that the material becomes too volatile at higher temperatures. Thus, most of the batch was volatilized after 1 hr firing at 1200°C, hence the firing temperature should be kept below 1200°C. At 1100°C, a 10-hr firing schedule of the base formula mix was nearly equal to 6-hr firing, such that 6 hr of firing is adequate for practical purposes. Under these conditions the loss of weight amounted to some 10–20%.

Samples of base formula composition were also fired in atmospheres of hydrogen, oxygen, nitrogen, water vapor, and some mixtures of these gases. Hydrogen is not suitable, as the material is completely volatilized following reduction to the ele-

¹ Manuscript received February 11, 1952.

TABLE I. Factors affecting relative brightness

Changes of boric acid concentration in % of amount in base formula		Rel. brightness
0		53
50		52
80		73
100		100
200		97
500		75
1000		74
Changes in MnSO ₄ concentration in % of amount in base formula		
0		15
40		54
100		100
200		56
250		56
300		52
400		64
750		75
2500		64
Changes in firing schedule		
°C	hr	
1000	2	46
1000	4	39
1000	6	34
1000	8	87
1100	2	25
1100	4	71
1100	6	100
1100	8	96
1100	10	76
1100	12	65

mental state. The other gases showed some difference compared with air, as discussed later for oxygen and nitrogen.

The phosphor as prepared above was not attacked by acids. For example, the intensity of its fluorescence was fully retained after treating it with 2*N* HCl for $\frac{1}{2}$ hr and then drying it. However, when treated with 2*N* NH₃, phosphor brightness decreased to 85%, although no change of color or of the state of aggregation was observed.

A number of phosphor preparations were made in which other compounds were substituted for boric acid and other elements for manganese and for part of the antimony. Also, double activation with manganese and other secondary activators was tried. All these phosphors were fired at 1100°C in air. Following is a survey of the substitutions (on molar basis) and of the other activators which were introduced in amounts of 0.001 mole for 1 mole of antimony oxide:

1. As₂O₃, SnO₂, P₂O₅ for $\frac{1}{3}$ of the antimony oxide;
2. LiCl, MgCl₂, CaCl₂, MgF₂, CaF₂, KBr, NaNO₃, Na₂HPO₄, KH₂PO₄, Na₂B₄O₇·10H₂O, Al₂O₃, SiO₂, TiO₂, V₂O₅, As₂O₅, for H₃BO₃;
3. Cu, Ag, Sn, Pb, Co, Ni, Cr, Th, Bi, Fe, Mo, Ti, W, V, Ce for Mn;
4. Ce, Sn, Pb as second activators with Mn.

None of the substituents and second activators listed above produced a good phosphor, with the exception of titanium which gave a yellow fluorescence when excited with 2537 Å radiation. Details will be reported in the future.

PROPERTIES AND STRUCTURE

The phosphors are friable, free flowing powders which do not contain hard sintered particles when prepared as described. Fluorescence is weak to medium bright when excited by cathode rays and long ultraviolet of 3650 Å, respectively. It is fairly strong when excited with 2537 Å radiation. Under 3650 Å excitation with a high pressure mercury lamp and a Corning 5840 filter, the brightness as measured with a selenium photocell compares with that of manganese-activated strontium or magnesium aluminate phosphors. Under 2537 Å excitation the brightness is about one-half that of commercial magnesium arsenate phosphor.

The emission spectrum of a phosphor of base formula composition is shown in Fig. 1. The energy peak is at about 6400 Å and the wave lengths at which the energy is one-half of the peak value are 5830 and 6920 Å. No evidence of a spectral line structure was found. The emission curve is symmetrical with respect to frequency and has the general shape of the probability curve. The phosphor has a rather fast, probably exponential, decay. Other forms of excitation produce the same emission curve.

Considerable work was done in an effort to determine the exact composition and structure of the phosphors, by means of both chemical and x-ray diffraction analysis. The patterns were obtained by the Debye-Scherrer method using copper radiation and exposures of 3–5 hr. The x-ray tube was operated

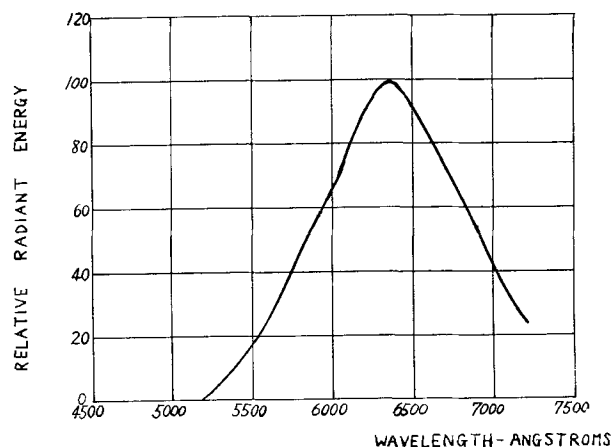


FIG. 1. Emission of manganese-activated antimony oxide phosphor with 2537 Å excitation.

TABLE II. X-ray diffraction pattern of Sb_2O_4Mn phosphor

d	Intensity	d	Intensity	d	Intensity	d	Intensity
3.19	m	1.498	m	1.110	s	0.937	w
3.03	w	1.479	v.w.	1.092	w	0.924	s
2.91	w	1.464	m	1.077	w	0.911	v.w.
2.86	m	1.430	w	1.066	m	0.907	v.w.
2.62	v.w.	1.394	m	1.062	m	0.899	s
2.41	w	1.316	v.w.	1.055	m	0.895	m
2.18	v.w.	1.293	v.w.	1.028	v.w.	0.885	s
1.98	v.w.	1.239	s	1.010	v.w.	0.881	m
1.82	m	1.214	v.w.	1.007	v.w.	0.875	v.w.
1.81	m	1.201	m	0.997	w	0.870	m
1.78	m	1.189	v.w.	0.988	m	0.858	m
1.71	v.w.	1.172	w	0.977	w	0.851	s
1.67	w	1.152	m	0.971	w	0.843	m
1.61	s	1.142	v.w.	0.968	w		
1.58	v.w.	1.127	v.w.	0.948	m		

TABLE III. Antimony content of antimony oxides

Sample	% Sb
b-0	83.13
b-2	79.65
b-4	80.88
Sb_2O_3 (theor.)	83.34
Sb_2O_4 (theor.)	79.19

at 35 kv and 10 ma. In addition to the phosphor samples, the following materials were prepared:

(a) The product of hydrolysis of antimony chloride was treated with dilute hydrochloric acid and ammonia, and dried at 110°C;

(b-0) Sample (a) was boiled with sodium carbonate solution and dried at 110°C;

(b-1) Sample (b-0) was heated at 300°C for 5 hr;

(b-2) Sample (b-0) was heated at 500°C for 5 hr;

(b-3) Sample (b-0) was heated at 600°C for 12 hr in an atmosphere of nitrogen;

(b-4) Sample (b-0) was treated with nitric acid and then heated at 750°C for 2 hr;

(b-5) Sample (b-4) was heated at 1100°C for 2 hr.

Results are shown in Tables II and III and Fig. 2. Data for cubic antimony trioxide and cubic antimony tetroxide in Fig. 2 were taken from Hanawalt and coworkers, from Dehlinger, and from Natta and coworkers (1). Conclusions drawn for these unactivated materials follow.

Sample (b-0) is a mixture of cubic antimony trioxide and hydrated antimony oxide. The latter also becomes cubic trioxide when heated to 300°C (b-1). Between 300° and 500°C the material (b-0) is converted into cubic antimony tetroxide, while some of the cubic trioxide is converted into orthorhombic trioxide [sample (b-2)]. This finding is supported by the results of chemical analysis. Gain in weight was not as high as would be expected on the

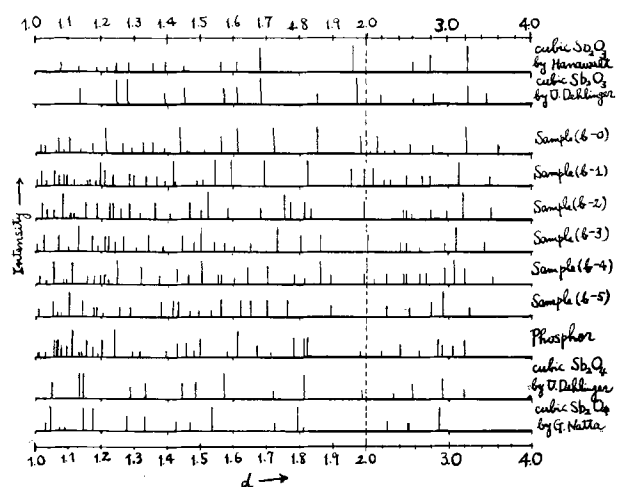


FIG. 2. X-ray diffraction patterns of various antimony oxide compositions.

basis of complete oxidation of trioxide to tetroxide. The sample gained only 4.48% compared with the theoretical value of 5.50% for complete oxidation. Fig. 3 shows that a final steady state was actually reached.

Diffraction lines of sample (b-2) were compared with the pattern for orthorhombic antimony trioxide as reported by Buerger (2) (not shown in Fig. 2). The latter material had been prepared by sublimation in a nitrogen atmosphere. Sample (b-3) is a comparable material. Sample (b-4), which was used for the preparation of phosphors, contains both antimony tetroxide and trioxide. The situation is similar in sample (b-5) and in the actual phosphor sample. Unfortunately, the structure of the phosphors themselves could not be determined satisfactorily. This is because of the lattice distortions brought about by additions of boric oxide and manganese. X-ray patterns of phosphors with low and with high manganese concentrations were taken of materials fired in air, oxygen, and nitrogen atmospheres, but they did not permit a clarification of the structure picture. Neither did the x-ray

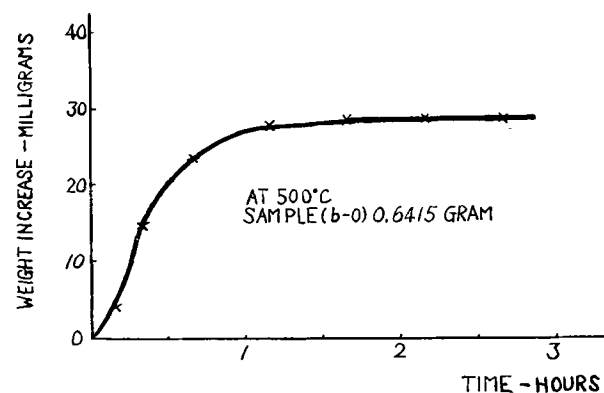


FIG. 3. Gain in weight of antimony oxide heated in air at 500°C.

TABLE IV. *Effect of firing atmosphere on brightness*

MnSO ₄ in % of amount in base formula	Rel. brightness after firing in		
	Oxygen	Nitrogen	Air (from Table I)
40	36	54	54
100	40	65	100
200	38	49	56
300	33	26	52
500	43	39	75*
750	39	37	75
1000	30	20	72*
2500	33	29	64

* Data obtained by repeat tests.

patterns of materials prepared with boric acid or with manganese alone, in the absence of antimony oxide. Examination under a petrographic microscope showed the phosphors to contain noncubic portions. At present, the phosphors are believed to be a mixture of cubic antimony tetroxide and some orthorhombic trioxide in close association with the former.²

This view is supported by the dependency of phosphor brightness upon manganese concentration. As shown in Table I, there are two brightness maxima. Although this seems to be an unusual result, it has been confirmed by repeat experiments which were carried out in oxygen and nitrogen, as well as in air. Data are shown in Table IV. Compared with normal firing in air, brightness is decreased in oxygen as well as in nitrogen. In oxygen, both peak values are decreased, but the first maximum is decreased more strongly. In nitrogen, the decrease of the first maximum is not as strong.

² Footnote added in print.

Patterns made of materials prepared without boric acid and manganese (a), with manganese alone (no H₃BO₃, b) and with boric acid alone (no Mn, c) were compared with that of phosphor (d) by means of a Norelco x-ray spectrograph. Patterns of antimony oxide fired alone or mixed with manganese sulfate and/or boric acid at 1100°C for 4 hr were also compared. The x-ray tube was operated at 35 kv and 15 ma and copper radiation was used.

The results confirmed the fact that addition of boric acid simplified the patterns, perhaps because boric acid acts as a flux and regularizes the crystal structure of antimony oxide. They also showed that by the addition of manganese the lattice of antimony oxide was expanded (a and b), while that of antimony oxide prepared with boric acid (c) was contracted. The presence of free boric acid or of a possible borate was not evident.

A tentative explanation for this follows. The incorporation of manganese in the lattice may take place in two forms, namely, in the tetroxide and in the trioxide phase, each giving rise to an emission at nearly the same wave length. However, these two phases are not necessarily mechanically separated, nor are they a solid solution of one in the other. Rather, they are assumed to be substantially a tetroxide material in which some of the oxygen positions are left vacant, giving rise to "trioxidic" and to "tetroxidic" surroundings for the manganese activator. It is the relative proportion of these surroundings in the crystal which determines the brightness at low and high concentrations of manganese, the latter apparently having an effect upon these proportions.

Assuming that manganese enters preferentially in "trioxidic" surroundings, increasing amounts of manganese first serve to intensify the first maximum, while larger amounts intensify the second maximum in "tetroxidic" surroundings. The change of the relative height of the brightness peaks with the nature of the firing atmosphere favors this assumption. In an oxygen atmosphere the trioxide content is reduced which should lead to a relative increase of the second maximum, and vice versa.

The reason manganese preferentially enters "trioxidic" surroundings is not clear. It might be explained with the stability and distribution of manganese ions in different lattice structures. Further work on this phosphor system is under way.

ACKNOWLEDGMENTS

The authors wish to express their thanks to M. Yamada and K. Mitsuhashi for the measurements of the spectral distribution, to E. Asada for the x-ray diffraction patterns, and to K. Nishida, N. Adachi, and S. Makishima for general discussions on the subject and some of their experimental work.

Any discussion of this paper will appear in a Discussion Section to be published in the June 1956 issue of the JOURNAL.

REFERENCES

1. J. D. HANAWALT, H. W. RINN, AND L. K. FREVEL, *Ind. Eng. Chem. Anal. Ed.*, **10**, 457 (1938); U. DEHLINGER, *Z. Krist.*, **66**, 108 (1927); G. NATTA AND M. BACCAREDDA, *Z. Krist.*, **85**, 271 (1933).
2. M. J. BUEGER, *Am. Mineral.*, **21**, 206 (1936).

Bomb Reduction of Molybdenum Trioxide by Calcium Metal

H. L. GILBERT² AND F. E. BLOCK

Northwest Electrodevelopment Experiment Station, U. S. Bureau of Mines, Albany, Oregon

ABSTRACT

Molybdenum trioxide has been reduced by calcium in a sealed bomb to produce massive reguli of molybdenum metal. A full description of the production of 25 lb reguli is given. Reguli are joined and employed as a consumable electrode in arc melting to produce ingot. Metal may be hot forged and rolled to desired form.

INTRODUCTION

Although the reduction of metallic compounds by carbonaceous materials may be dated in terms of the first use of bronze and iron by man, the use of more active metals as reducing agents perhaps was described first by Berzelius in 1825 in his salt bath reduction of zirconium fluoride by sodium metal (1). In 1898 Goldschmidt described his aluminothermic process for reducing oxides of metals, including molybdenum trioxide (2). These methods were re-examined by several workers, including Lely and Hamburger, who in 1914 developed the closed reactor or "bomb" for use in reducing various metal chlorides by sodium (3). Marden and Rich in 1926 applied this process to metal oxides in their work on the reduction of vanadium oxide by calcium metal in a bomb (4).

Many materials have been reduced on various scales under the supervision of Spedding (5). Gray (6) has described the production of certain rare earth metals, and the recent work of McKechnie and Seybolt (7) in the production of ductile vanadium answered questions remaining from the work of Marden (4) and Kroll (8).

The metal prepared by the early experimenters with bomb reductions was generally powder rather than massive metal. A powder product was frequently the result of a lack of thermal efficiency, but on occasion powder was desired in order to use powder metallurgy consolidation techniques. Also, most of the metal reduced in earlier work had a melting point considerably below that of molybdenum, hence experimental conditions did not require production of very high temperatures with the concurrent dangers involved as in the case of the reduction of molybdenum into a massive regulus. In the experiments about to be described, the objective was the production of massive metal rather than powder.

EXPERIMENTAL PROCEDURE

As a part of a larger research effort on new techniques for production of molybdenum metal, the bomb reduction of molybdenum oxide was first examined in a general manner. Successful bomb reduction requires the formation of massive metal if a high recovery is expected and, because the melting point of molybdenum is about 2600°C, one would perhaps not expect a massive regulus of molybdenum to be formed. Initial tests with molybdenum dioxide and calcium bore out expectations that only powder would be formed, while a rather rudimentary test with molybdenum trioxide, surprisingly enough, produced small metallic particles.

The reaction involved 525 g of molybdenum trioxide and 444 g of 1/4-in. mesh calcium metal. The mixture was placed in a freshly burned calcium oxide-lined steel bomb and the bomb closed and heated to 725°C to fire the charge. The metallic particles shown in Fig. 1 were obtained.

Repeated tests on a 1-lb (MoO₃)-size bomb showed that the method of ignition of the bomb left much to be desired since the external heating weakened the wall of the bomb and caused some burnouts. It was also felt that the random efficiencies encountered indicated that the reaction could be initiated at different points within the charge with different end results. To check this, and at the same time permit reaction within a cold wall bomb, a resistance igniter, consisting of a standard automotive sparkplug with an 18-gauge molybdenum wire connected across the points, was developed. This igniter was the key that permitted expansion of the process to the scale herein described.

An increase in the scale of the operation, using a 5-lb charge, showed that the calcium oxide refractory employed to line and protect the steel bomb was fused down into the slag during the reaction, leaving the wall unprotected. Replacement of the calcium oxide refractory by electrofused magnesia solved this problem. It was shown on the larger scale that the erratic results obtained previously could be attributed to accidental location of the initiation of

¹ Manuscript received September 29, 1954. This paper was prepared for delivery before the Cincinnati Meeting, May 1 to 5, 1955.

² Present address: Harvey Aluminum, Torrance, Calif.

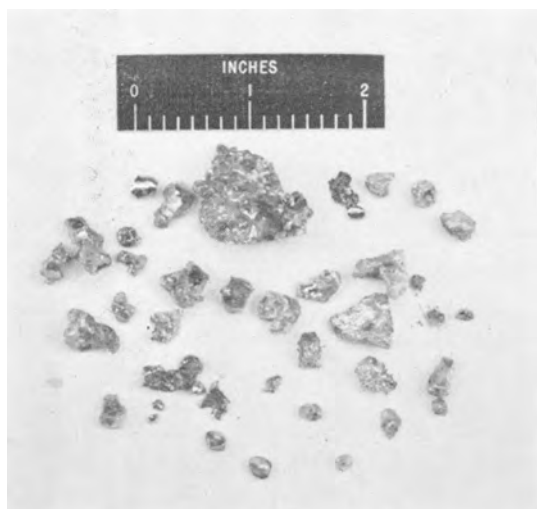


FIG. 1. Pellets of molybdenum formed in reduction of MoO_3 by calcium in exploratory test.

reaction. Metal recovery effected when the charge was ignited at the bottom, middle, and top of the bomb was 47, 68, and 84 %, respectively. This would indicate that the fall of molten metal progressively downward either accelerates the reaction or tends to collect the metal, or perhaps both. A concurrent study of bomb shape showed that, for optimum results, a bomb should have a height-diameter ratio of about 5:1.

Variations in the ratio of calcium to MoO_3 showed that the use of 50 % excess calcium over the stoichiometric requirement substantially reduced the molybdenum yield but improved the quality of that metal produced. Use of 10 % excess calcium gave the best yield of metal, but troublesome amounts of oxygen remained in the metal. A 20 % excess of calcium appeared to be a good compromise and this was used in the majority of the tests.

As indicated by McKechnie and Seybolt (7), use of iodine to boost the thermal energy of the charge is of definite assistance, but since iodine is a rather expensive reagent, an effort was made to minimize the amount employed. Small-scale (1 lb MoO_3) reactions required 80 g of iodine per pound of MoO_3 , while in larger (50 lb MoO_3) reactions this was reduced to 50 g of iodine per pound of MoO_3 . Theoretical calculations show that somewhere in the charge range of 75–100 lb of MoO_3 iodine would no longer be required, except for a few grams in the immediate vicinity of the igniter.

Although a variety of techniques was developed during the course of this work, much of the exploratory effort may be summarized by describing in some detail the technique finally employed. The bomb was made from 11-in. ID $1\frac{1}{16}$ -in. wall seamless-steel pipe with welded flanges at the ends. End plates were

held in place by twelve $1\frac{1}{4}$ -in. diameter alloy steel bolts. A high-pressure closure employing a round copper gasket sealed the bomb against leakage. The bomb was assembled with a paper-wrapped wooden mandrel located where the charge was desired. Electrofused magnesia, ground and mixed in an aggregate, 70 % of which would pass 200-mesh size, was tamped into the space between the mandrel and the bomb wall to form a liner. An alternate method was the use of sodium silicate (waterglass) to bond the magnesia. The amount used contributed 0.37 % silicon to the liner. After placement of the liner by either the wet or the dry method, firing was necessary to give the liner enough strength to withstand the loading operation. Firing was accomplished by means of a split graphite resistor placed inside the bomb and electrical strip-heaters clamped to the outside of the bomb. The graphite resistor was operated at 1500°–2000°C for 6 hr with an input of 1000 amp at 24 v a.c., at the conclusion of which time the liner had a moderately hard inner surface.

Molybdenum trioxide purchased on the open market was found to be pure and dry enough to use in making up bomb charges without further treatment. Commercial calcium metal is invariably contaminated with calcium oxide and nitride. The oxide, if not excessive, is of little consequence since the reaction involves an oxide, but nitrogen is very detrimental. Crude calcium metal was vacuum-sublimed to reduce the nitrogen level from the initial figure, 1700 ppm, to about 60 ppm. Sublimation had the further effect of creating a coarsely crystalline metal which was readily cut to pass $1/4$ -in. mesh in a

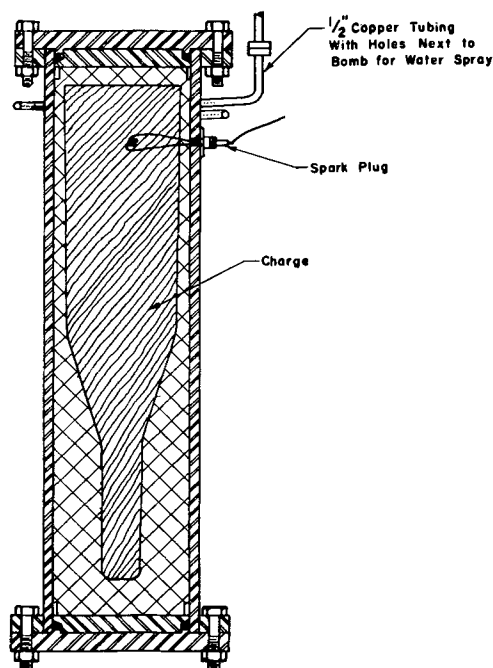


FIG. 2. Loaded bomb before firing

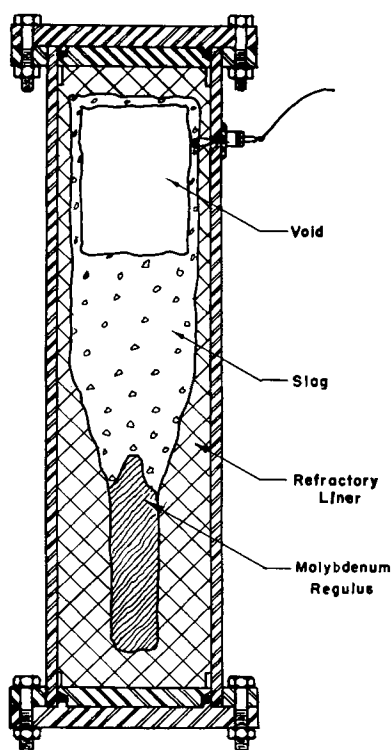


FIG. 3. Bomb after firing

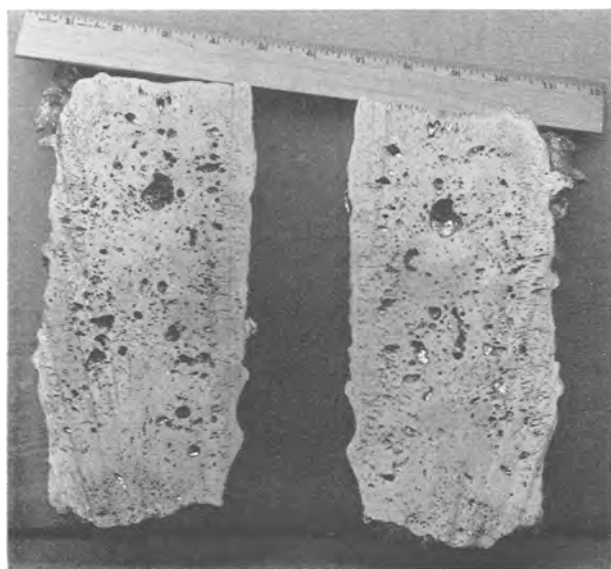


FIG. 4. Sectioned regulus showing typical porosity

Mitts & Merrill hog machine. No commercial source of such metal was found at the time of the tests.

As a safety feature the charge was prepared in about 50 increments, each consisting of 1 lb of MoO_3 , 1 lb of calcium, and 50 g of iodine.

The incremental charges were placed in the bomb, the igniter was inserted at the proper level, and a layer of magnesia was put in place to protect the lid of the bomb as shown in Fig. 2. The top seal was carefully placed in position since, if any leakage at all

occurred due to a dirty closure or gasket, the bomb was destroyed in the ensuing explosion.

The bomb was moved to a remote location for firing, and personnel and equipment were protected by concrete revetments. Before firing a heavy spray of cooling water was fixed to play on the bomb.

The reaction was initiated by applying a source of a-c power to the igniter. No sound accompanied a successful firing. Twelve hours later the bomb was opened to show the result pictured in Fig. 3. The regulus of metal and the slag were separated from the liner material, which was saved for reuse. The regulus was easily recovered, but averaged only 80% of the theoretical density owing to inner porosity, as shown in Fig. 4. An average molybdenum recovery of 97% of the charge was obtained as a single mass of metal.

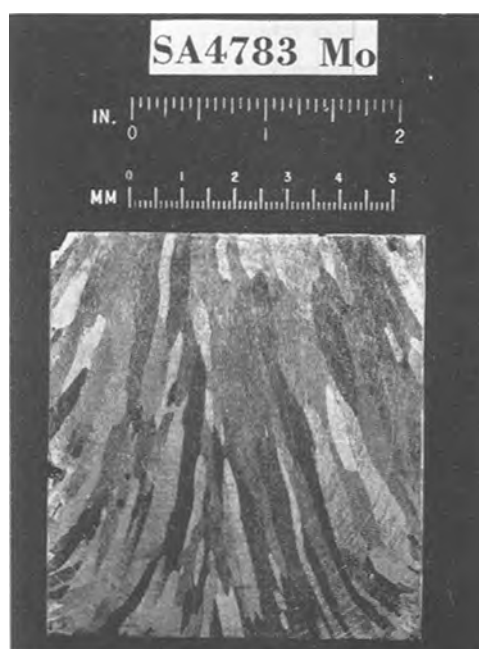


FIG. 5. Macro-etched test ingot showing typical large columnar grain structure.



FIG. 6. Microstructure of arc-melted calcium-reduced molybdenum. Etchant, $\text{NH}_4\text{OH}\text{-H}_2\text{O}_2$. 500 \times before reduction for publication.

Character of the Metal Produced

The quality of the reguli was studied by consumable-electrode arc melting them in a water-cooled copper mold and examining this ingot both metallographically and in forging tests. In the case illustrated, the 3½-in. diameter reguli were welded together and remelted into an 8-in. diameter ingot by a power input of 4500 amp at 32 v. A furnace atmosphere of 10% argon and 90% helium at atmospheric pressure was employed.

Ingot metal was sound and relatively clean. Macro- and microstructure of the metal is shown in Fig. 5 and 6. This material was not readily forgeable due to traces of residual oxygen, which, while present in only minute quantity, appeared to exert great influence through its location as thin planar crystals of molybdenum dioxide between the massive crystals of metal. Chemical analyses of typical reguli were as follows:

Chemical analyses of arc-melted molybdenum reguli

Sample No.	Assay, ppm		
	C	O ₂	N ₂
MoR62	380	55	190
MoR63	300	30	180
MoR65	190	70	110
MoR66	140	110	150
MoR68	300	150	70

To overcome the effect of the residual oxygen several materials capable of agglomerating the intergranular material were added to the bomb charge in small amounts.

Although this study is incomplete and no definite correlation can be made, additions of aluminum, thorium, or carbon in amounts ranging up to 2% of the weight of the molybdenum in the charge appear definitely to improve the ductility of the metal produced. It is believed that these materials influence



FIG. 7. Microstructure of arc-melted molybdenum, calcium-reduced in the presence of 3% aluminum. Etchant, NH₄OH-H₂O₂. 75X before reduction for publication.

the form of the oxygen in the final metal rather than actually removing it. The most ductile metal to date was produced by collecting the reduced molybdenum regulus in a graphite crucible embedded in the magnesia refractory inside the bomb.

The microstructure of aluminum-treated material is shown in Fig. 7. Such treated material could be hot forged and rolled to sheet.

In an effort to lower the cost for producing molybdenum by this method attempts were made to substitute magnesium for the more expensive calcium as a reductant. By this means, a smaller quantity of less costly reductant was necessary, with the result that a greater portion of the bomb charge could be utilized for molybdenum trioxide. Although the yield of molybdenum metal did not suffer in a magnesium reduction, the fused reguli showed increased porosity and more oxide appeared to be occluded in the grains and grain boundaries. Major complications arose when magnesium reductions were performed in the larger bombs. Because magnesium has a substantially higher vapor pressure than calcium, greatly increased pressures were developed inside the bombs with the result that the bomb wall failed in several tests. For this reason, magnesium reductions were discontinued.

Bomb conditions were studied by physical and theoretical means. The thermodynamics of the reaction of molybdenum oxide with various metals has been studied by Ward and coworkers (9). From this information and various collected values, a temperature of 3000°C has been calculated as possible in the reaction of molybdenum trioxide and calcium under adiabatic conditions. Although conditions within the bomb are not adiabatic, the reaction apparently does reach its peak in a matter of some 35 sec. Molybdenum trioxide may be considered to be a peroxide type material which sublimates below its melting point of 795°C at atmospheric pressure. As calcium has a boiling point of 1690°C and the two reaction products, calcium oxide and molybdenum, have essentially no vapor pressure even at elevated temperature, it is likely that the reaction is essentially one between calcium vapor and molybdenum trioxide vapor, which form and then condense instantly on contact or between liquid MoO₃ and calcium vapor. The average pressure peak of 1200 psi, as determined by a variety of strain-gauge tests, occurs about 35 sec after ignition.

CONCLUSIONS

The method described here has permitted the production in a bomb of massive reguli of molybdenum with 97% efficiency through reduction of molybdenum trioxide by calcium metal in the presence of iodine. Addition of thorium, aluminum,

or carbon to the bomb charge improved the forgeability of the metal produced. The 20-lb reguli produced were not satisfactory for use until consumable-electrode arc melted. The principal problem at present is in placing the refractory lining in the bomb shell. The safety of personnel during the mixing of the reactants and bomb loading is subject to question. Further improvement in metal quality would be of interest.

ACKNOWLEDGMENTS

Gratitude is expressed to John S. Nachtman of the Navy Bureau of Ordnance, under which this project was carried out, for permission to publish this article.

Bomb work was carried out by J. K. Hoy, M. M. Barr, and Gene Asai, supervised by H. A. Johansen, T. T. Campbell, and C. Q. Morrison. Arc melting was under the supervision of R. A. Beall, while

metallographic work was performed through the courtesy of E. T. Hayes.

Any discussion of this paper will appear in a Discussion Section to be published in the June 1956 JOURNAL.

REFERENCES

1. J. BERZELIUS, *Pogg. Ann.*, **4**, 121 (1825).
2. H. GOLDSCHMIDT, *Lieb. Ann.*, **301**, 19 (1898).
3. D. LELY AND L. HAMBURGER, *Z. anorg. u. allgem. Chem.*, **87**, 209 (1914).
4. J. W. MARDEN AND M. N. RICH, *Ind. Eng. Chem.*, **19**, 786 (1927).
5. F. H. SPEDDING, H. A. WILHELM, W. H. KELLER, D. H. AHMANN, A. H. DOANE, C. C. HACH, AND R. P. ERICSON, *ibid.*, **44**, 553 (1952).
6. P. M. J. GRAY, *Metal Ind., London*, **80**, 43 (1952).
7. R. K. McKECHNIE AND A. U. SEYBOLT, *This Journal*, **97**, 311 (1950).
8. W. J. KROLL, *Z. Metallkunde*, **28**, 30 (1936).
9. J. J. WARD, J. P. RAY, AND S. A. HERRES, Project Rand Report R-108, Battelle Memorial Institute, Columbus, Ohio, July 19, 1948.

The Thermodynamic Stability of Refractory Borides¹

LEO BREWER

Department of Chemistry and Chemical Engineering, University of California, Berkeley, California

AND

HAAKSON HARALDSEN

Universitetes Kjemiske Institutt, Blindern, Oslo, Norway

ABSTRACT

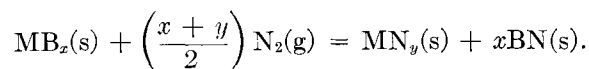
Reactions between nitrogen gas and metal borides and between graphite and metal borides have been studied to obtain qualitative information on the relative stabilities of the metal boride phases. At high temperatures many borides are inert toward carbon or nitrogen. The most stable borides are found to be those of Ti, Zr, Nb, and Ta of the fourth and fifth groups of the periodic table. Data are summarized in terms of limits to the heats of formation.

INTRODUCTION

The determination of the thermodynamic properties of refractory borides such as the borides of the transition metals of the fourth to sixth groups of the periodic system is an especially difficult problem. These borides are very inert and are not easily dissolved in any solvents. Thus, conventional calorimetric methods cannot be used to determine their heats of formation. Combustion calorimeters are not readily applicable to these compounds because of the difficulty of obtaining complete combustion and definite final products. A method that appears to be generally applicable is the determination of high temperature equilibria conditions in systems containing these compounds. One promising type of experiment would be the determination of the boron decomposition pressure in equilibrium with the boride phase as a function of temperature. This method can be expected to give accurate results, but high temperatures are required. Equilibration of two metals with boron and determinations of the boride phases formed can also give information about the thermodynamic stability of the borides. Other experiments that could give useful thermodynamic data would be the determination of the equilibrium between nitrogen gas and the boride and nitride phases or the determination of the equilibrium between graphite and the boride and carbide phases. This paper will describe the results of experiments of the last three types that were carried out in an endeavor to obtain even qualitative information about the relative stability of boride phases.

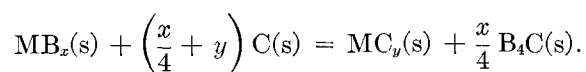
Nitrogen systems.—The equilibria involving nitro-

gen gas can be expressed by the general equation:



Knowing the free energies of formation of the nitride phases, the determination of the equilibrium constant for this reaction gives one the free energy of formation of the boride phase. For this result to apply to the pure boride phase, there must be little solubility of the solid phases in one another and no ternary phases must be formed. Evidence of such behavior can often be found by x-ray analysis. After these studies were under way, a paper by Kiessling and Liu (1) appeared in which they had carried out similar studies at much lower temperatures. Their experiments indicated that ammonia at atmospheric pressure always destroyed the metal boride phase yielding the metal nitride and boron nitride. The authors' experiments at higher temperatures had shown that the boride phases were stable in the presence of nitrogen. Thermodynamic calculations reconcile the two sets of results since the calculations show that increasing the temperature favors the borides over the nitrides. The authors' results obtained with the nitrogen system are tabulated in Table I. In the following discussion, these results will be combined with Kiessling's results and used in an attempt to evaluate thermodynamic data for the boride phases.

Carbon systems.—The equilibria in the carbon systems can be expressed by the general equation:



This system was studied by heating various borides with graphite and determining by x-ray analysis the phases at equilibrium with one another. After this

¹ Manuscript received November 1, 1954. This paper was prepared for delivery before the Wrightsville Beach Meeting, September 13 to 16, 1953.

TABLE I. *Heatings in 0.5 atm N₂ using molybdenum crucibles*

Starting phases	Temp., °K	Final phases
Ti + B + BN + N ₂ (g)	2270	$\frac{\text{TiB}_2}{s.} + \frac{\text{TiN}}{s.} + \text{BN}_w$
Ti + 3B + N ₂ (g)	1820	$\frac{\text{TiN}}{v.s.} + \frac{\text{TiB}_2}{w.} + \text{BN}?$
Zr + 3B + N ₂ (g) Zr + 3B + $\frac{1}{4}$ BN + N ₂ (g)	1820	$\frac{\text{ZrB}_2}{v.s.} + \frac{\text{ZrN}}{w.} + \text{BN}_{v.w.}$
Zr + B + BN + N ₂ (g)	2270	$\frac{\text{ZrN}}{v.s.} + \frac{\text{ZrB}_2}{s.}$
W + 3B + $\frac{1}{4}$ BN + N ₂ (g)	1820	$\frac{\text{W}_2\text{B}_5}{s.} + \text{WB}_m + ?_w$
W + 3B + N ₂ (g)	1820	$\frac{\text{WB}}{s.} + \frac{\text{W}_2\text{B}}{m.s.} + \text{W}_2\text{B}_5?_{v.w.}$
Cr + 3B + N ₂ (g)	1820	$\frac{\text{Cr}_2\text{N}}{m.s.} + ?$
Cr + 3B + $\frac{1}{4}$ BN + N ₂ (g)	1820	$\frac{\text{Cr}_2\text{N}}{m.s.} + \frac{\text{CrB}_2}{m.} + \text{BN}?$

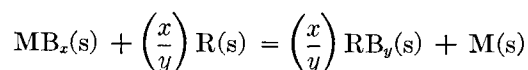
s. = strong, m. = medium, w. = weak, v. = very.

TABLE II. *Heating in 0.5 atm argon at 2050°K*

Starting phases	Final phases
Ce + 4B + C	$\frac{\text{CeB}_4}{m.} + \frac{\text{CeB}_6}{m.w.}$
Ce + 6B + $\frac{1}{2}$ C	$\frac{\text{CeB}_6}{s.} + \frac{\text{CeB}_4}{m.s.}$
Zr + 2B + C	$\frac{\text{ZrB}_2}{s.} + \frac{\text{ZrC}}{s.} + ?$
Nb + B + $\frac{1}{2}$ C	$\frac{\text{NbB}_2}{s.} + \text{NbC}_m$
Nb + 2B + C	$\frac{\text{NbB}_2}{s.} + \frac{\text{NbC}}{s.}$
2Mo + B + $\frac{1}{2}$ C	$\frac{\text{Mo}_2\text{B}}{m.} + \frac{\alpha\text{-MoB}}{m.}$
Mo + B + C	$\frac{\alpha\text{-MoB}}{s.} + \frac{\beta\text{-MoB}}{w.}?$
2Mo + 5B + C	$\frac{\text{MoB}_2}{s.} + \frac{\alpha\text{-MoB}}{m.}$

work had been completed, a paper by Glaser (2) appeared which presented similar experiments largely at higher temperatures. The authors' results are presented in Table II. In the following discussion all available data are used to attempt to fix the relative stabilities of the boride phases.

Metal exchange experiments.—The equation,



represents the equilibria obtained by heating two different metals together with boron such that there is insufficient boron for both metals. These experiments are more straightforward in principle than the experiments described above but are more complicated in practice due to more extensive solid solubilities among the boride phases than among the boride and nitride or boride and carbide phases. The results of these experiments are given in the following text.

EXPERIMENTAL PROCEDURE

All experiments were done in the same equipment and in the same manner as the experiments described by Brewer, Sawyer, Templeton, and Dauben (3). Molybdenum crucibles were used as containers. The heatings were done in 0.5 atm nitrogen gases when equilibria involving nitrides were studied and in 0.5 atm argon for the other experiments. Each experiment was held for about 50 min within 100° of the temperature given in the tables. The boron used was obtained from the Fairmount Chemical Company, Newark, New Jersey, and was 99.5% pure. The main impurities were several tenths of a per cent of Ni, and less than 0.1% of Al and Mg. The metal powders were 99.9% pure except for Ti and Zr which contained oxide and nitride impurities.

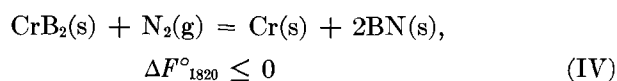
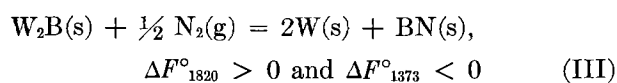
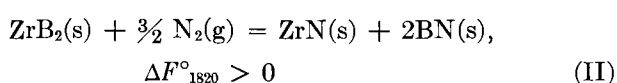
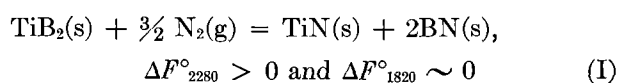
DISCUSSION OF EXPERIMENTS

Nitride equilibria.—The experiments described in Table I were carried out by mixing metal powder, boron powder, and boron nitride powder and heating in nitrogen gas or by just heating the mixture of metal and boron powders in nitrogen gas. The resulting phases are listed in order of importance with the main phases underlined. The intensities of the x-ray powder patterns are indicated, although it is understood that these do not indicate the actual abundances, as phases with simple patterns will give strong patterns even when not abundant. The question mark after BN indicates that only the strongest line of the pattern was observed. A question mark alone indicates the pattern of an unidentified phase. In addition to the experiments described in Table I, mixtures with sufficient metal to result in both boride and nitride phases were heated to determine if ternary compounds or solid solution formation could be expected. No ternary phases were observed and within the experimental uncertainty of $\pm 0.003 \text{ \AA}$, no evidence could be obtained for sufficient solid solution formation in the quenched products to cause variation of lattice constants.

Table I shows that strong x-ray patterns of TiN and ZrN, or solid solutions of these compounds with TiB and ZrB, are observed when the boron-to-metal ratio does not exceed two. This is due to the

nitride impurity in the metals as well as to some boron loss to the crucible. With higher boron-to-metal ratios the nitride diffraction patterns appear only weakly. As patterns of cubic phases appear very sensitively, the amount of the nitride phases must be very small and their occurrence is undoubtedly due to formation during cooling. Thus, the results of Table I indicate that ZrB_2 , WB , W_2B , and W_2B_5 are stable in the presence of N_2 at $1820^\circ K$. TiB_2 is largely converted to TiN at $1820^\circ K$ but it is quite stable at $2270^\circ K$. At $1820^\circ K$ borides of Cr are also largely converted to Cr metal which is converted to Cr_2N on cooling. Since the reaction of nitrogen with these borides can be shown to be exothermic with a large entropy decrease, the borides will be stable at high temperatures but become less stable with respect to nitrides as the temperature is lowered, and virtually all borides can be expected to react with nitrogen at lower temperatures. This explains why Kiessling and Liu (1) found tungsten borides to be converted to the metal or nitride at temperatures below $1370^\circ K$ while the authors find the tungsten borides stable at $1820^\circ K$. Also Kiessling and Liu's use of ammonia tends to give the nitriding reaction a greater driving force as is indicated by the formation of metastable nitrides such as the iron nitrides in the ammonia stream, but at $1370^\circ K$ the effect should not be large.

The experimental data can be expressed in thermodynamic quantities as indicated by the following equations.



To obtain limits to the heats of formation of the borides, the following thermodynamic data were used. Data for the elements were obtained from Brewer (4). For BN at $1820^\circ K$, $\Delta F^\circ = -15.7$ kcal was calculated from data given by Dworkin, Sasmor, and van Artsdalen (5) and Kelley (6). For TiN at $1820^\circ K$, $\Delta F^\circ = -40.0$ kcal was obtained from data given by Humphrey (7) and Kelley (6).

Thus for TiB_2 , $\Delta F^\circ_{1820} \sim -71.4$ kcal and $\Delta H^\circ_{298} \sim -71$ kcal since ΔS° and ΔC°_p will be close to zero.

For ZrN , $\Delta H^\circ_{298} = -87.3$ kcal (8), $\Delta S^\circ_{298} = -22.9$ e.u. (6), and $\Delta C^\circ_p = 0$ were used to obtain for $ZrB_2(s)$, $\Delta H^\circ_{298} < -77$ kcal.

In a similar manner one obtains for CrB_2 , $\Delta H^\circ_{298} \geq -31$ kcal and for W_2B , $\Delta H^\circ_{298} < -16$ kcal. From Kiessling and Liu's ammonia results, one can also give for W_2B , $\Delta H^\circ_{298} > -28$ kcal and for WB , $\Delta H^\circ_{298} > -22$ kcal.

In addition to the metals listed in Table I, cerium metal was also heated with boron and boron nitride in nitrogen gas at $2280^\circ K$. CeO_2 , Ce , and CeN x-ray diffraction patterns were obtained, but the main phases present after heating could not be identified from the diffraction patterns. Also the molybdenum crucible reacted with the sample to a considerable extent. CeB_4 and CeB_6 definitely were not present. It would seem that cerium borides are less stable than nitride or ternary phases at this temperature. This would fix ΔH°_{298} for CeB_4 as > -84 kcal using $\Delta H = -78.0$ kcal for CeN from Brewer (9).

Carbide equilibria.—The experiments presented in Table II were carried out by heating a mixture of metal powder with boron and graphite powders. From the results of Table II, one would conclude that CeB_6 , ZrB_2 , NbB_2 , Mo_2B , MoB , and MoB_2 are stable in the presence of graphite. Due to the low atomic weight of carbon, the graphite phase is difficult to demonstrate. ZrC and NbC patterns can be detected due to some boron loss to the crucible which leaves metal free to react with the graphite. No evidence was found for changes in lattice constant at room temperature due to solid solution formation. The combination of molybdenum with boron and graphite did not always give clear-cut results. Unidentified lines found in some of the samples are apparently due to high temperature modifications. Hexagonal MoB_2 was definitely identified and by comparison with the NbB x-ray pattern, some of the lines can be taken as a probable indication of the presence of MoB with the CrB structure. Two samples of the composition $2Mo + B + C$ did not give any identifiable phases after heating between 2170° and $2240^\circ K$. Although Glaser (2) reports Mo_2B stable in the presence of C and the authors find Mo_2B in a $2Mo + B + \frac{1}{2} C$ mixture, a reaction $2Mo_2B + C \rightarrow Mo_2B + MoB + MoCB_x$ could account for the authors' results if x is small. In a similar way the high CeB_6 content found for the $Ce + 4B + C$ composition indicates a reaction. This has been recently confirmed by Engelke (19) who finds evidence for a ternary $Ce-B-C$ compound.

The above results together with those reported by Brewer, Sawyer, Templeton, and Dauben (3), Glaser (2), Steinitz (10), and Nelson, Willmore, and Womeldorph (11) allow the borides to be divided into the two groups shown in Table III.

Where different investigators have carried out similar experiments, all of them agree except for W_2B . Glaser (2) and Schwarzkopf and Glaser (12)

TABLE III

Borides stable in presence of graphite	Borides unstable in presence of graphite
CeB ₆	CeB ₄
TiB ₂	Ti ₂ B, TiB, Ti ₂ B ₅
ZrB ₂	ZrB, ZrB ₁₂
ThB ₆	ThB ₄
NbB ₂	Nb ₂ B, NbB, Nb ₃ B ₄ , NbB _m
TaB ₂	Ta ₂ B, TaB, Ta ₃ B ₄ , TaB _m
Cr ₂ B, Cr ₃ B ₃ , CrB, Cr ₃ B ₄ , CrB ₂	Cr ₄ B?, Cr ₂ B ₅ ?
Mo ₂ B?, Mo ₃ B ₃ , α-MoB, β-MoB, MoB ₂ , Mo ₂ B ₃	Mo ₂ B?
WB, W ₂ B ₃	W ₂ B
Fe ₂ B, FeB	
Co ₂ B, CoB	
Ni ₂ B	

report preparation of W₂B in a graphite crucible and conclude that W₂B is stable in graphite. However Brewer, Sawyer, Templeton, and Dauben found a definite reaction between W₂B and C, when intimately mixed, to form WB and WC. Thus Glaser's result would seem to be due to poor contact. Krikorian (13) has recently rechecked this and has confirmed the reaction of W₂B and C to yield WC and WB. He has also shown that W₂C, WC, and W₂B exist together without reaction. Nelson, Willmore, and Womeldorf (11) report Cr borides stable in the presence of graphite without indicating which ones. Glaser reports that five chromium boride phases are stable, but gives no information for Cr₄B or Cr₂B₅ which probably react with carbon.

From the results given in Table III, one can write equations for the reactions of the borides with graphite for which one can indicate ΔF° as greater than or less than zero. The temperature is not of great importance for the carbide equilibria in contrast to the nitrogen systems, as ΔS° and ΔC_p° for the reactions of borides with graphite will be close to zero and ΔF° will change little with temperature. Also ΔH°_{298} can be used in place of ΔF°_T at any temperature for these approximate considerations. The following heats of formation limits can be derived on this basis.

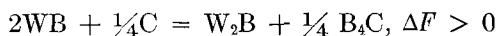
TiB ₂	ΔH°	< -51	TaB ₂	ΔH°	< -45
ZrB ₂		< -51	NbB ₂		< -37
ThB ₄		< -54	W ₂ B		< -22
ThB ₆		< -66	WB		< -13 kcal

In deriving these values, $\Delta H^\circ_{298} = -43.85$ kcal was used for TiC (7), $\Delta H^\circ_{298} = -44.4$ kcal was used for ZrC (8), $\Delta H^\circ_{298} = -8.41$ kcal was used for WC (14), $\Delta H^\circ_{298} = -38.5$ kcal was used for TaC (8), and $\Delta H^\circ_{298} = -46$ kcal for ThC₂ (9), and $\Delta H^\circ_{298} = -13.8 \pm 2.7$ kcal was used for B₄C (15). The entropies of formation were obtained from Brewer, Bromley, Gilles, and Lofgren (9). $\Delta H^\circ_{298} = -30$

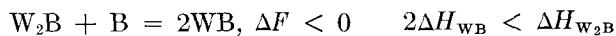
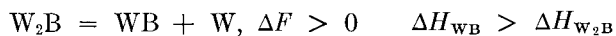
kcal was estimated for NbC. Where values are given for different boride phases of the same metal, disproportionation reactions were also considered. The types of equations used will be illustrated for the tungsten system.



$$\Delta H_{WB} < \Delta H_{W_2B} + 8.4 \text{ kcal}$$



$$\Delta H_{WB} < \frac{1}{2} \Delta H_{W_2B} - 1.8 \text{ kcal}$$



$$\Delta H_{WB} < -11.9$$

All of these equations can be satisfied by $\Delta H < -12$ kcal for WB and $\Delta H < -20$ kcal for W₂B, and the two ΔH values should not differ by more than 8 kcal.

Metal Exchange

Ce and B were heated at 1775°K with Mo, W, Nb, and Ta, respectively. The resultant samples were powdered and x-ray powder diffraction patterns of CeO₂ or Ce but no other Ce phases were obtained. Borides of the other metal were found in every instance. These experiments demonstrate that the cerium borides are less stable than Mo₂B, MoB, W₂B, NbB, and TaB. By similar experiments, Brewer, Sawyer, Templeton, and Dauben (3) have shown that Ta, Ti, and Zr can reduce the Mo and W borides. This fixes the ΔH limit given in Table IV for the Ta borides. Thus, the Mo and W borides are less stable than those of Ta, Ti, and Zr. They have also shown that the Mo and W borides are of similar stability. At most they could differ only by 10 kcal

TABLE IV. Summary of ΔH of formation in kcal per gram atom boron

	ΔH		ΔH
$\frac{1}{4}$ CeB ₄	> -21	$\frac{1}{x}$ CrB _x	< -15
		$\frac{1}{2}$ CrB ₂	< -15
$\frac{1}{x}$ TiB _x	~ -36	Mo ₂ B	-25.5
$\frac{1}{2}$ TiB ₂	~ -36	$\frac{1}{2}$ Mo ₃ B ₂	-21
$\frac{1}{5}$ Ti ₂ B ₅	< -21	MoB	
ZrB	< -39		-16.3
$\frac{1}{2}$ ZrB ₂	< -39	$\frac{1}{2}$ MoB ₂	-11.5
$\frac{1}{12}$ ZrB ₁₂	< -10	$\frac{1}{5}$ Mo ₂ B ₅	-10
$\frac{1}{4}$ ThB ₄	< -13	W ₂ B	-28 to -20
$\frac{1}{6}$ ThB ₆	< -11	WB	-22 to -12
$\frac{1}{x}$ NbB _x	< -18	$\frac{1}{5}$ W ₂ B ₅	-9 to -5
$\frac{1}{2}$ NbB ₂	< -18	1/x MB _x refers to all phases lower in boron composition than MB ₂	
$\frac{1}{x}$ TaB _x	< -26		
$\frac{1}{2}$ TaB ₂	< -26		

per gram atom of boron. In Table IV, the authors' results for the W borides are compared with those determined for the Mo borides by Gilles and Pollock (16). Within our uncertainty, one cannot distinguish any difference in stability between tungsten and molybdenum borides.

SUMMARY

By consideration of all available chemical data including information concerning disproportionation reactions, one can finally summarize all the data in terms of the composition triangles of the ternary phase diagrams as given in Fig. 1-11 or in terms of the thermodynamic values given in Table IV.

The phase diagrams show at a glance the reactions that can take place, as only phases with a common composition triangle can be at equilibrium with each other. Where some phases have only a limited temperature range of stability, the tempera-

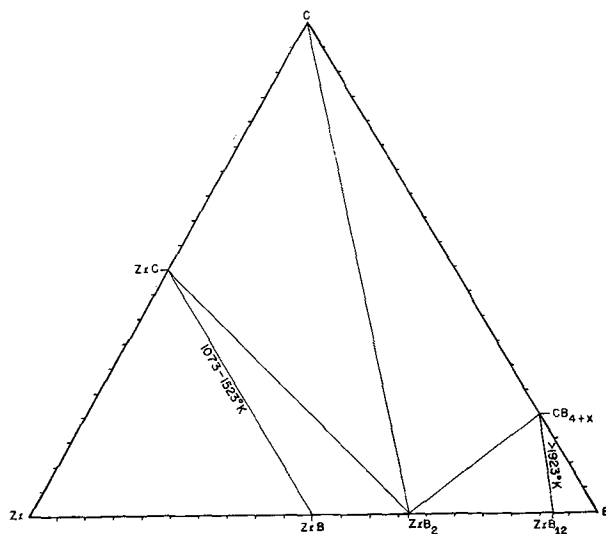


FIG. 3. Zr-B-C system

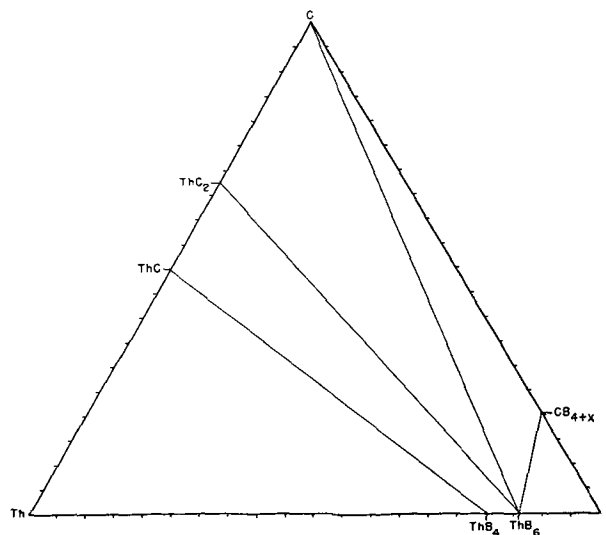


FIG. 4. Th-B-C system

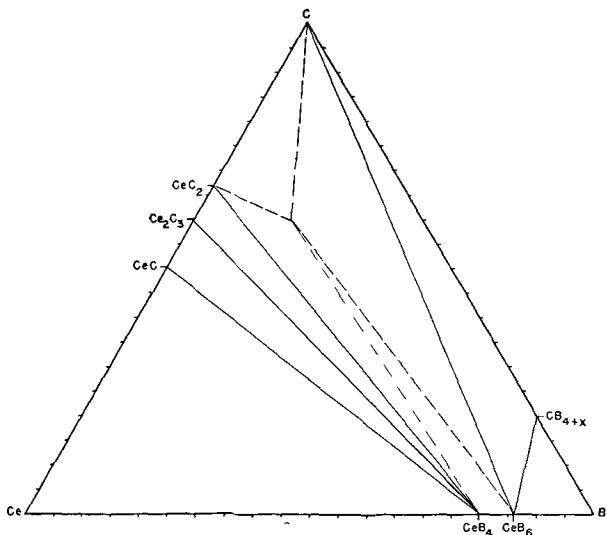


FIG. 1. Ce-B-C system

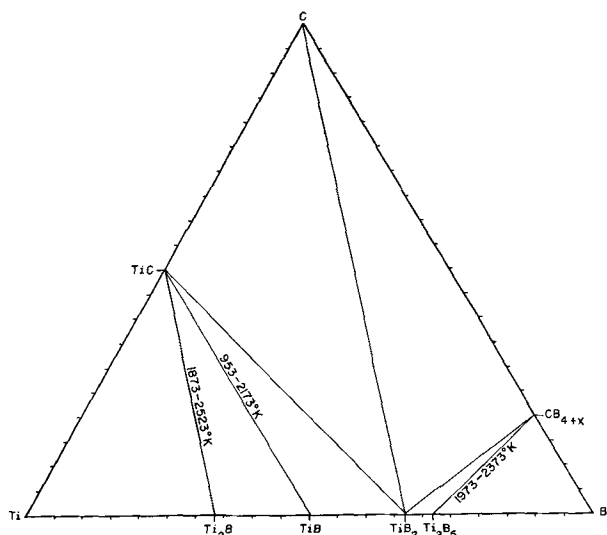


FIG. 2. Ti-B-C system

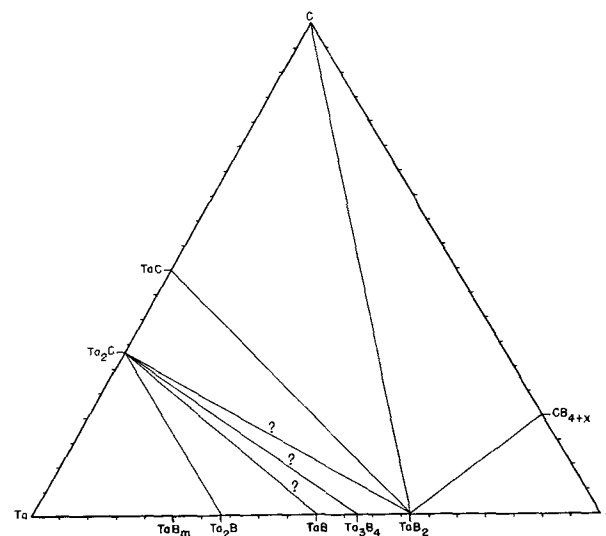


FIG. 5. Ta-B-C system

ture range is indicated on the joins when known. Thus in Fig. 3, the ZrC-ZrB join is to be considered only in the temperature range 1073°–1523°K which is the approximate stability range of ZrB as given by Schwarzkopf and Glaser. The last four diagrams that contain gaseous nitrogen as a component change considerably with temperature because of the large entropy change of reactions involving gaseous N_2 . Thus in Fig. 8, the TiN-BN join exists only below 1900°K. Above 1900°K TiN and BN will react to produce TiB_2 and N_2 which can coexist above 1900°K. The joins that are important only at low temperatures are dotted and the temperature limits are indicated.

The Nb-B-C diagram is not given, as the ternary diagram features are the same as shown for Ta-B-C. The Nb-B- N_2 , Ta-B- N_2 , and Mo-B- N_2 diagrams can be expected to be very similar to the W-B- N_2 diagram. No attempt is made to indicate the homogeneity

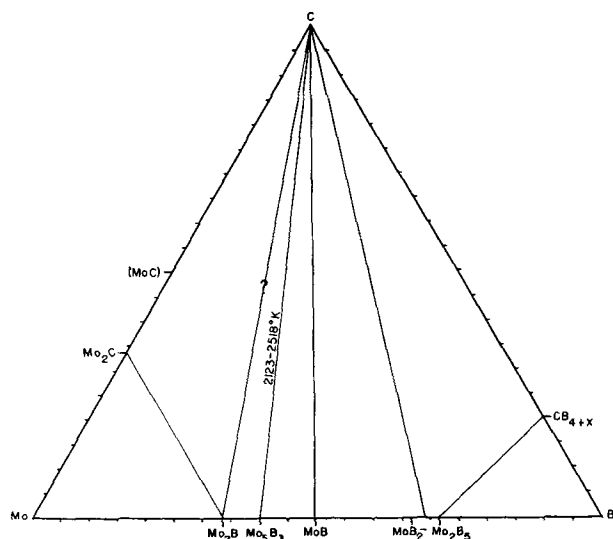


FIG. 6. Mo-B-C system

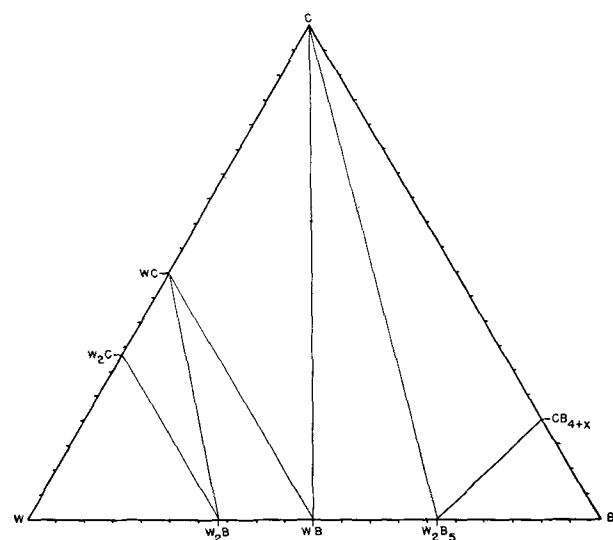
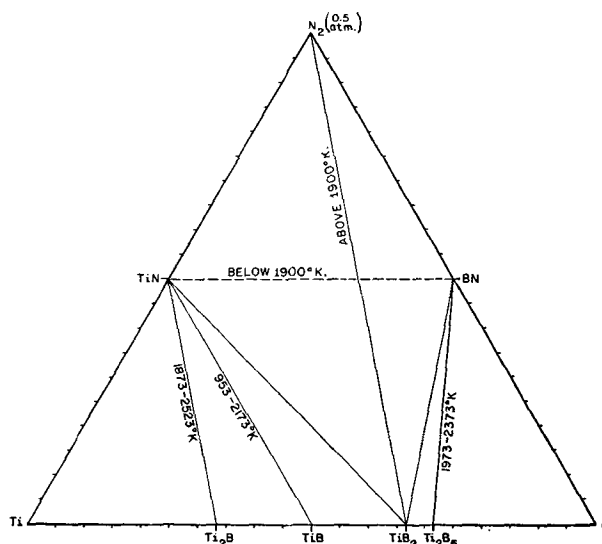
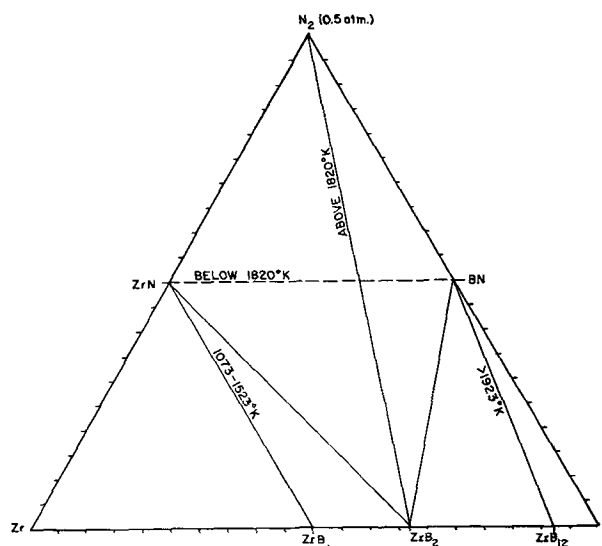
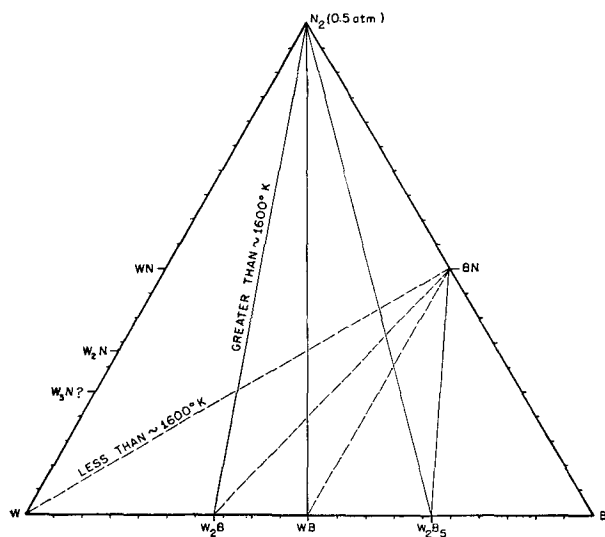
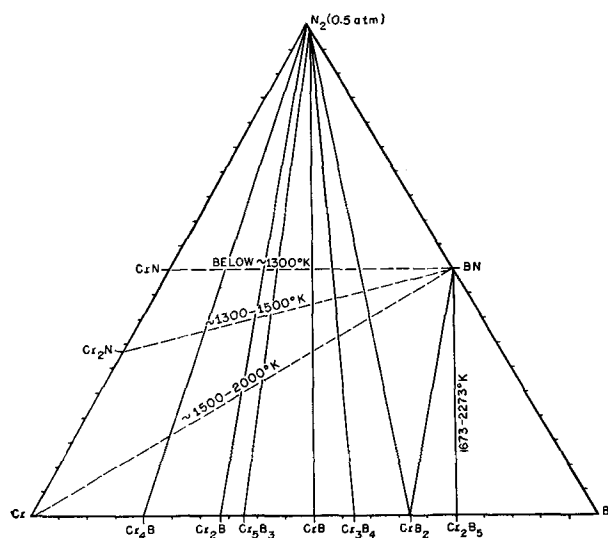


FIG. 7. W-B-C system

FIG. 8. Ti-B- N_2 systemFIG. 9. Zr-B- N_2 system

ranges of the phases other than to recognize the B_4C -B range by use of the term CB_{4+x} . The designation MoB_2 - Mo_2B_5 represents the two allotropic phases with homogeneity ranges in this composition region.

Kiessling (17) has noted that the stability of borides decreases in the order Mn, Fe, Co, Ni, Cu, and has pointed out that this behavior is similar to that for the nitrides and carbides in that the stability decreases as one moves to the right in the periodic table through the transition metals. In this work it is found that the most stable borides of the sixth group elements Mo and W are less stable than those of the fourth and fifth group elements Ti, Zr, and Ta. However, there is a maximum stability in the fourth groups and a decrease in stability is found if one moves to the left to the third group. Thus, as one compares compounds of F, O, N, C, and B, one finds that the region of maximum sta-

FIG. 10. W-B-N₂ systemFIG. 11. Cr-B-N₂ system

bility in the periodic table is decidedly shifted to the right as one goes from F to B. Except for the indication by the nitride studies that ZrB₂ is more stable than TiB₂, it is not known how stability varies with atomic weight within a group. It might be noted that ZrC is more stable than TiC and the tungsten carbides are more stable than those of molybdenum.

It is of interest to speculate as to the reason for the shift of the region of maximum stability toward the fourth and fifth groups of the periodic tables for the nitrides, carbides, and borides. One may note that the most stable metal lattices are found near this same region of the periodic table where a large number of *d*-electrons and orbitals are available for bonding. It would appear that the *d*-electrons of the metals play an important part in the bonding in the nitride, carbide, and boride lattices. The metal-like properties of these phases also indicate a common

type of bonding. Magnetic susceptibility measurements will be of special interest for possible insight into the type of bonding.

The data in Table IV may now be combined with the heat of sublimation of boron at 298°K of 141 kcal, recently determined by Searcy and Myers (18), to obtain qualitative information about the vaporization behavior of the borides. For borides decomposing to the solid metal and boron vapor at 2500°K, those with heats of formation as negative as -50 kcal per gram atom boron will have boron vapor pressures around 10⁻⁹ atm. Those with heats of formation as negative as -30 kcal per gram atom boron will have boron vapor pressures around 10⁻⁷ atm. Those with heats of formation near -10 kcal per gram atom boron will have boron vapor pressures around 10^{-5.5} atm. Thus it should be quite practical to obtain accurate thermodynamic data for the refractory boride phases by study of the boron vapor pressure in the range of 2000-2500°K.

Since the borides of the fourth and fifth groups appear to have the most negative heats of formation of any borides, these borides should be resistant against reduction by other metals. They should especially be resistant against attack by the alkali and alkaline earth metals on one hand and the low melting metals like Bi, Sn, Zn, Pb, etc., on the other hand if phases not too high in either boron or metal are used.

ACKNOWLEDGMENTS

The x-ray diffraction photographs were taken by Mrs. Helena Ruben and the x-ray diffraction patterns were interpreted by Mrs. Carol Dauben. The authors wish to express their thanks for their help, which was essential to this research. This work was made possible by Smith-Mundt and Fulbright grants for travel to Berkeley, California, in 1952, which are gratefully acknowledged.

Any discussion of this paper will appear in a Discussion Section to be published in the June 1956 JOURNAL.

REFERENCES

1. R. KISSLING AND Y. H. LIU, *J. Metals*, **3**, 639 (1951).
2. F. W. GLASER, *ibid.*, **4**, 391 (1952).
3. L. BREWER, D. SAWYER, D. H. TEMPLETON, AND C. DAUBEN, *J. Am. Ceramic Soc.*, **34**, 173 (1951).
4. L. BREWER, National Nuclear Energy Series, Vol. 19B, Paper 3 (1950).
5. A. S. DWORIN, D. J. SASMOR, AND E. R. VAN ARTSDALEN, *J. Chem. Phys.*, **22**, 837 (1954).
6. K. K. KELLEY, U. S. Bur. of Mines Bulls. 476 (1949) and 477 (1950).
7. G. L. HUMPHREY, *J. Am. Chem. Soc.*, **73**, 2261 (1951).
8. K. K. KELLEY, Private communication.
9. L. BREWER, L. A. BROMLEY, N. L. LOFGREN, AND P. W. GILLES, National Nuclear Energy Series, Vol. 19B, Paper 4 (1950).

10. R. STEINITZ, *Powder Met. Bull.*, **6**, 54 (1951).
11. J. A. NELSON, T. A. MILLMORE, AND R. C. WOMEL-DORPH, *This Journal*, **98**, 465 (1951).
12. P. SCHWARZKOPF AND F. W. GLASER, "Structural and Chemical Characteristics of the Borides of the Transition Metals of the Fourth, Fifth and Sixth Group," presented at the III^e Congrès International D'Électrothermie, and at Wrightsville Beach Meeting, ECS, September 1953.
13. O. KRİKORIAN, Unpublished work, University of California, Berkeley.
14. G. HUFF, E. SQUITIERI, AND P. SNYDER, *J. Am. Chem. Soc.*, **70**, 3380 (1948).
15. E. R. VAN ARTSDALEN, Private communication.
16. P. GILLES AND D. POLLOCK, *Trans. Am. Inst. Mining Met. Engrs.*, **197**, 1537 (1953); and unpublished work.
17. R. KIESSLING, *This Journal*, **98**, 417 (1951).
18. A. W. SEARCY AND C. E. MYERS, Unpublished work.
19. J. ENGELKE, Unpublished work.

High Temperature Oxidation of Two Zirconium-Tin Alloys¹

M. W. MALLETT AND W. M. ALBRECHT

Battelle Memorial Institute, Columbus, Ohio

ABSTRACT

The rate of oxidation of a zirconium-1.5 wt % tin alloy followed a cubic law in the temperature range 600°–900°C at 1 atm pressure. However, two different energies of activation were obtained. In the range 600°–800°C the activation energy was calculated to be $38,400 \pm 1100$ cal/mole and the cubic rate constant in $(\text{ml}/\text{cm}^2)^3/\text{sec}$ can be expressed as $k = 5.34 \times 10^4 \exp(-38,400/RT)$. An activation energy of $22,600 \pm 1400$ cal/mole was obtained in the range 825°–900°C and the cubic rate constant is $k = 87.2 \exp(-22,600/RT)$.

For a zirconium-2.5 wt % tin alloy, the rate of oxidation followed a parabolic law in the range 550°–900°C. The parabolic rate constant in $(\text{ml}/\text{cm}^2)^2/\text{sec}$ was calculated to be $k = 2.63 \times 10^3 \exp(-32,400/RT)$, where $32,400 \pm 1000$ cal/mole is the activation energy.

Adherent gray-black oxidation films were found to be *N*-type semiconductors and from this a mechanism for the oxidation of zirconium is proposed. The effect of tin in the zirconium is to increase the porosity of films and decrease the time before breakdown of the protective properties of the films.

INTRODUCTION

A previous study was made on the high temperature oxidation of zirconium (1). This study has been expanded to include the high temperature oxidation of two zirconium-tin alloys containing 1.5 and 2.5 wt % tin. In the zirconium study (1) the initial oxidation followed the cubic rate law for long times in the range 575°–950°C. This was one of the very few times that the cubic rate law was observed over a wide temperature range. Other investigators to report cubic oxidation were Tylecote (2), who studied the oxidation of copper, and Waber (3), who cited data on the oxidation of titanium and tantalum. Cabrera and Mott (4) have developed a theory for cubic oxidation for the growth of thin films containing excess anions and space charges. Besides studying the kinetics of the oxidation of the zirconium-tin alloys it was planned to carry out additional experimental work to determine some of the processes that occur during the cubic oxidation of zirconium and to determine what effect tin may have on these processes.

EXPERIMENTAL

Method.—Rates of reaction of oxygen with the zirconium-tin alloys were determined by measuring rates of consumption of the gas by the alloys in a modified Sieverts apparatus (1, 5).

The zirconium-tin alloy specimens were machined cylinders, 4 cm long by 0.7 cm in diameter. All

specimens were abraded with kerosene-soaked 240-, 400-, and 600-grit silicon carbide papers and washed in successive baths of naphtha, ether, and acetone.

Rate data were obtained as follows. A specimen was placed in the reaction tube of the apparatus and degassed in a vacuum for one hour at a temperature 50°C above the temperature of the run in the range 550°C–750°C and at temperature in the range 800°–950°C. All temperatures were maintained to $\pm 5^\circ\text{C}$. Measured amounts of oxygen were added to the reaction tube to atmospheric pressure. Pressure measurements were made every two minutes at the start of the reaction and at longer time intervals as the reaction rate decreased. Amounts of oxygen remaining in the apparatus as a gas phase were determined from pressure measurements on an open-end mercury manometer and the calibrated dead space of the reaction tube. The difference (to ± 0.04 ml STP) between the quantity of oxygen added and that remaining in the gas phase was the quantity reacted with the specimen. Original geometrical dimensions of the specimens were used to compute the quantity of gas reacted per unit surface area.

Materials.—Two zirconium-tin alloys, containing 1.5 and 2.5 wt % tin, were fabricated into $\frac{3}{8}$ -in. diameter rods. Test specimens were machined from these rods. Analyses of the alloys were obtained by spectrographic, chemical, and vacuum-fusion techniques. Results are given in Table I.

Oxygen was prepared from degassed potassium permanganate by the method described by Hoge (6). It was dried by passing through a dry ice-acetone cold trap.

¹ Manuscript received October 9, 1954. This paper was prepared for delivery before the Cincinnati Meeting, May 1 to 5, 1955. Work performed under AEC Contract W-7405-eng-92.

TABLE I. Analyses of zirconium-tin alloys

Element	Amount present, wt %	
	Zr-1.5 wt % Sn	Zr-2.5 wt % Sn
Fe	0.20	0.03
Cr	0.05	NF*
Ni	0.03	0.001
Si	0.007	0.002
Al	0.006	0.001
Mn	0.002	NF
Mg	0.002	NF
Pb	0.002	NF
O ₂	0.09	0.06
N ₂	0.003	0.002
H ₂	0.002†	0.004†

* NF—not found.

† Analysis before degassing.

Results

Zirconium-1.5 wt % tin.—Rates of consumption of oxygen at 1 atm pressure by zirconium-1.5 wt % tin alloy were measured from 600° to 900°C. Below 600°C the reaction was too slow and above 900°C the rapidity of the reaction made it difficult to control. It was found that the data could be fitted to the cubic law, $w^3 = kt$, where w is the ml STP of oxygen consumed per square centimeter of surface, t is time, and k is the cubic rate constant. Fig. 1 and 2 are plots of w^3 vs. t for a number of runs and it is seen that the data fall on straight lines. For cubic oxidation, a plot of $\log w$ vs. $\log t$ should be a straight line with a slope equal to 0.33. Values of rate constants, calculated from the various plots, and slopes of log-

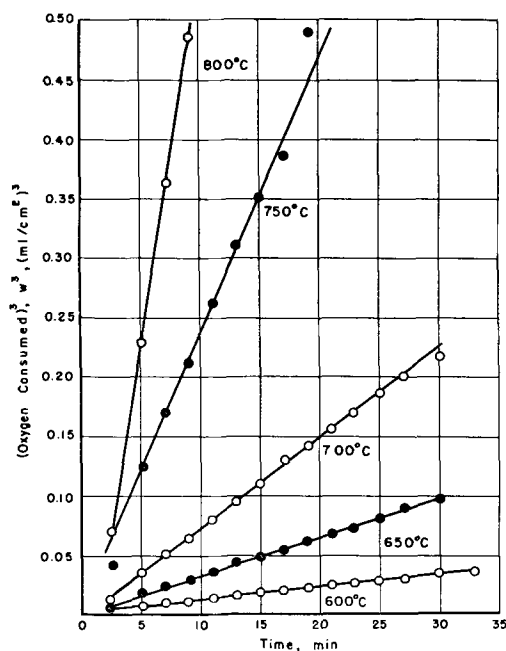


FIG. 1. Cubic plot of oxidation of zirconium-1.5 wt % tin alloy at 600°-800°C.

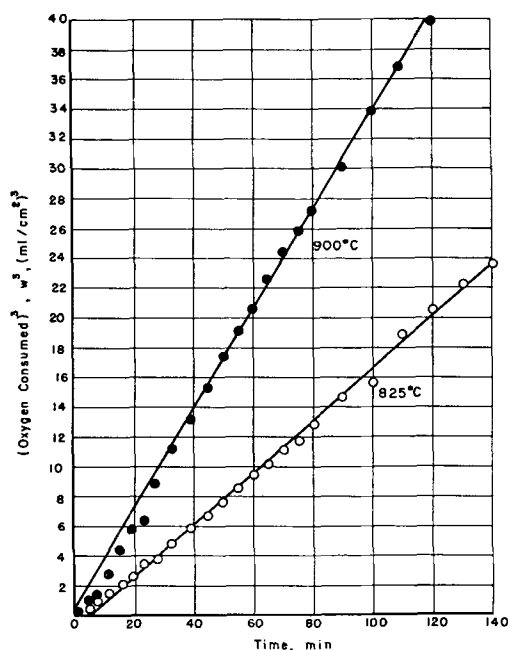


FIG. 2. Cubic plot of oxidation of zirconium-1.5 wt % tin alloy at 825° and 900°C.

log plots are given in Table II. Rate constants range from 1.5×10^{-5} (ml/cm²)³/sec at 600°C to 5.5×10^{-3} (ml/cm²)³/sec at 900°C.

Temperature dependence of the cubic rates of oxidation can be seen in Fig. 3. Two different straight lines were obtained, one in the range 600°-800°C, the other for 825°-900°C. Equations for the best straight lines through the two sets of points were determined by the method of least squares. Using the Arrhenius-type equation, $k = A \exp(-Q/RT)$, energies of activation and frequency factors were calculated. At 600°-800°C, the rate constant in (ml/cm²)³/sec is $k = 5.34 \times 10^4 \exp(-38,400/RT)$ where $38,400 \pm 1100$ cal/mole is the activation

TABLE II. Rate constants for the reaction of zirconium-1.5 wt % tin alloy with oxygen

Temp, °C	Rate constant (k), (ml/cm ²) ³ sec	Slope of log-log plot
600	1.5×10^{-5}	0.30
650	5.4×10^{-5}	0.33
650	3.0×10^{-5}	0.39
700	1.3×10^{-4}	0.34
750	3.9×10^{-4}	0.32
750	2.7×10^{-4}	0.34
800	7.3×10^{-4}	0.37
800	1.0×10^{-3}	0.35
825	3.0×10^{-3}	0.35
825	2.7×10^{-3}	0.34
850	3.5×10^{-3}	0.35
850	3.2×10^{-3}	0.32
900	5.4×10^{-3}	0.33
900	5.5×10^{-3}	0.32

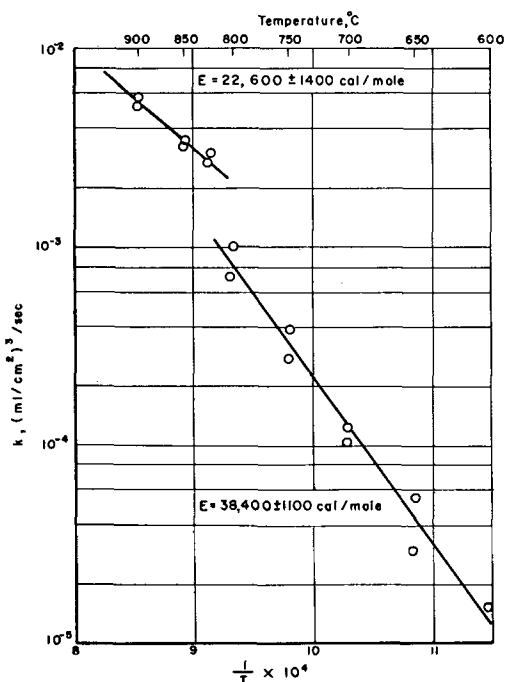


FIG. 3. Temperature dependence of cubic rate constant for zirconium-1.5 wt % tin alloy.

energy and the probable error² in a calculated k is approximately 16%. For 825°–900°C $k = 87.2 \exp(-22,600/RT)$ where $22,600 \pm 1400$ cal/mole is the activation energy and 4.3% is the probable error in a calculated k .

Zirconium-2.5 wt % tin.—Rates of oxidation at 1 atm pressure for the zirconium-2.5 wt % tin alloy were measured from 550° to 900°C. The data were found to follow a parabolic law, $w^2 = kt$, where k is the parabolic rate constant. In Fig. 4, the square of w is plotted as a function of t for a number of runs, and it is seen that the data fall on straight lines. For the parabolic law, a plot of $\log w$ vs. $\log t$ is a straight line with a slope of 0.50. Values of rate constant and slopes of log-log plots are given in Table III. Rate constants range from 3.8×10^{-6} (ml/cm²)²/sec at 550°C to 2.5×10^{-3} (ml/cm²)²/sec at 900°C.

Temperature dependence for the parabolic oxidation is given in Fig. 5. Between 550° and 900°C, the rate constant is $k = 2.63 \times 10^3 \exp(-32,400/RT)$ (ml/cm²)²/sec, where $32,400 \pm 1000$ cal/mole is the

² From the least square calculation, the probable error in k can be calculated by the equation $k = A \exp(-Q/RT) \exp \pm PE_k$. The probable error in $\log k$ is $PE_k = 0.6745 \sqrt{\sum d^2/n - 2}$, where $\sum d^2$ is the summation of the squares of the differences between the least square calculated values of $\log k$ and the experimental values of $\log k$, and n is the number of experimental values of $\log k$ used. For this work the approximation is used that $\exp \pm PE_k \approx 1 \pm PE_k$.

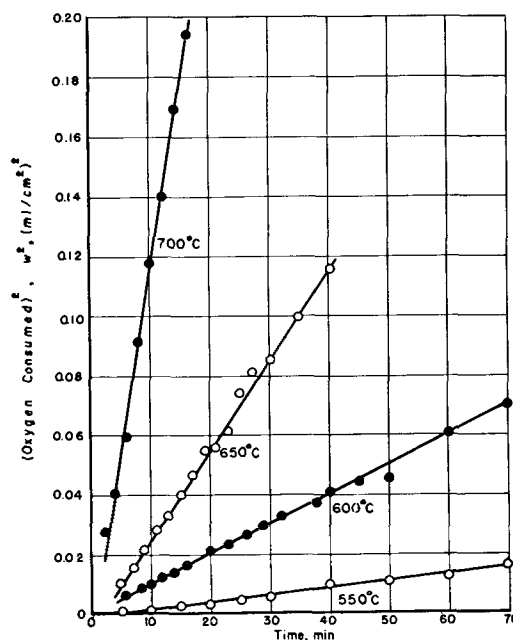


FIG. 4. Parabolic plot of oxidation of zirconium-2.5 wt % tin alloy at 550°–700°C.

activation energy and the probable error in a calculated k is 18%.

FILMS

At the end of reaction-rate runs, specimens were cooled to room temperature in a vacuum and examined. In all cases throughout the temperature ranges investigated, reacted specimens were covered with a gray-black film which adhered very strongly to the metal. Growth of this film is associated with the forementioned rate laws for the tin alloys. Where breakdown of these laws occurred and the rate increased toward linear behavior, a tan to white film started forming on the specimens. After a time, these light-colored films tended to flake off the specimens.

TABLE III. Rate constants for the reaction of zirconium-2.5 wt % tin alloy with oxygen

Temp, °C	Rate constant (k), (ml/cm ²) ² /sec	Slope of log-log plot
550	3.8×10^{-6}	0.56
600	1.7×10^{-5}	0.51
600	3.1×10^{-5}	0.44
650	5.1×10^{-5}	0.54
650	6.4×10^{-5}	0.46
700	1.2×10^{-4}	0.56
700	2.1×10^{-4}	0.53
750	3.1×10^{-4}	0.59
750	3.2×10^{-4}	0.48
800	5.5×10^{-4}	0.48
800	5.6×10^{-4}	0.40
850	9.8×10^{-4}	0.44
900	2.5×10^{-3}	0.45

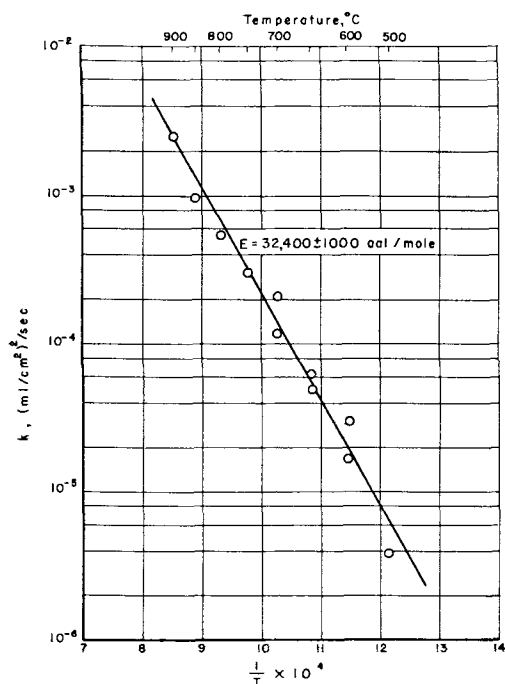


FIG. 5. Temperature dependence of parabolic rate constant for zirconium-2.5 wt % tin alloy.

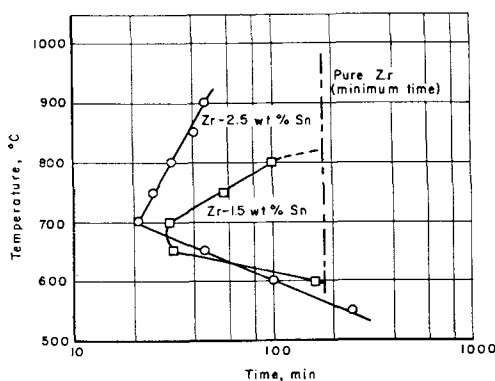


FIG. 6. Variation of breakdown time of gray-black film with temperature.



FIG. 7. Zirconium-1.5 wt % tin alloy reacted with oxygen at 825°C for 180 min. Surface layer is a gray-black film about 0.0025 cm thick. Aqua regia-HF etch. 500X before reduction for publication.

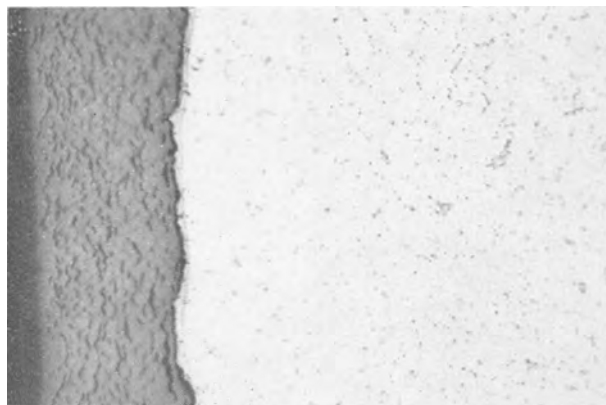


FIG. 8. Zirconium-1.5 wt % tin alloy reacted with oxygen at 700°C for 240 min. Surface layer is a light-colored film about 0.0050 cm thick. Aqua regia-HF etch. 500X before reduction for publication.

The time before occurrence of the breakdown of the gray-black film depended on temperature and tin content (see Fig. 6). During oxidation of the pure zirconium (1) the gray-black film persisted for times greater than 180 min in the entire range 575°–950°C. However, for the tin alloys in general the breakdown time of the dark film decreases with increasing tin content, and the minimum breakdown time comes at about 700°C (Fig. 6): No breakdown occurred for 180 min during the oxidation of the 1.5 wt % tin alloy in the range 825°–900°C.

Metallographic examination of the gray-black films of both tin alloys showed them to be a dense phase containing pores and a darker second phase (Fig. 7 and 9). Generally, it was found that films of the zirconium-2.5 wt % tin alloy contained more of the pores and second phase than the zirconium-1.5 wt % tin alloy. Maximum thicknesses of the gray-black films were of the order of 2 to 4×10^{-3} cm for the 1.5 wt % tin alloy and 0.6 to 2×10^{-3} cm

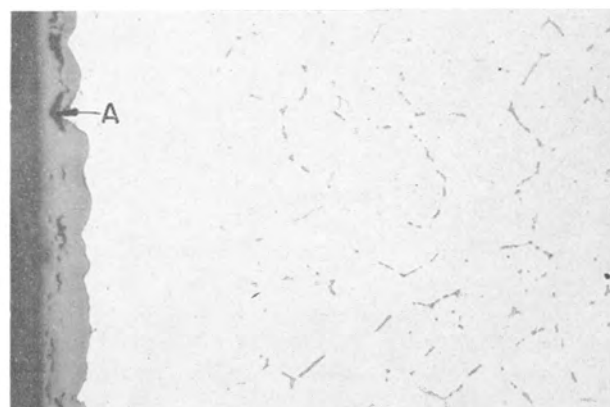


FIG. 9. Zirconium-2.5 wt % tin alloy reacted with oxygen at 800°C for 60 min. Surface layer is a gray-black film about 0.0012–0.0020 cm thick. Aqua regia-HF etch. 500X before reduction for publication.

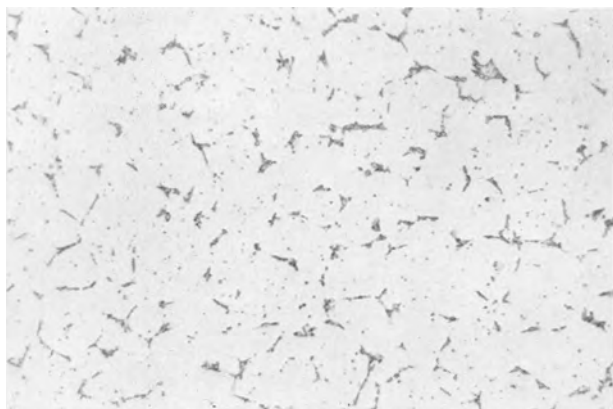


FIG. 10. Zirconium-1.5 wt % tin alloy vacuum annealed at 825°C for 1 hr. Aqua regia-HF etch. 500× before reduction for publication.



FIG. 12. Zirconium-2.5 wt % tin alloy vacuum annealed at 800°C for 1 hr. Aqua regia-HF etch. 500× before reduction for publication.

for the 2.5 wt % tin alloy. X-ray patterns taken at room temperature indicated that these films were preferentially oriented monoclinic ZrO_2 . The tan to white films that formed after longer times were found to be randomly oriented monoclinic ZrO_2 (Fig. 8). No identification could be readily made of the second phase (particles marked A in Fig. 9) in the dark films. However, this phase was also present in the bulky light-colored films and could be mechanically separated in the cases of the zirconium-2.5 wt % tin alloy. X-ray analysis gave patterns of metallic zirconium and of ZrO_2 . Apparently these particles are portions of the base metal which oxidize more slowly than the bulk of the metal. This phase was not noted in the oxidation films of pure zirconium (1).

Microstructures of the base alloys at the end of oxidation-rate experiments can be seen in Fig. 7, 8, and 9. Microstructures of the unoxidized alloys after a vacuum anneal of one hour appearing in Fig. 10, 11, and 12 show the condition of the specimens at the start of oxidation. A fine, random precipitate is

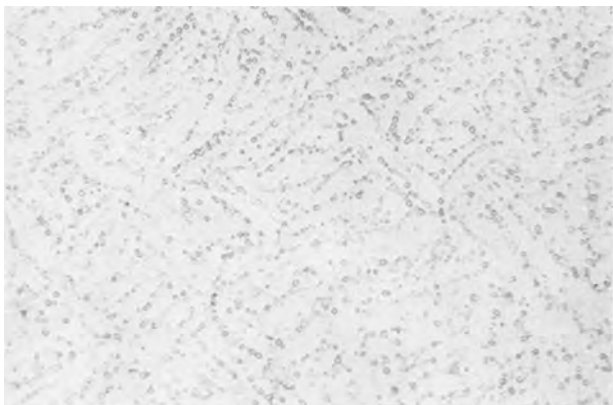


FIG. 11. Zirconium-1.5 wt % tin alloy vacuum annealed at 700°C for 1 hr. Aqua regia-HF etch. 500× before reduction for publication.

noted in alpha zirconium-1.5 wt % Sn alloy at 700°C (see Fig. 8 and 11). This precipitate is caused by the chromium, iron, and nickel contents of the alloy. At 825°C for the zirconium-1.5 wt % tin alloy, the transformed-beta structure is evident at the alpha grain boundaries (Fig. 7 and 10). Adjacent to the oxidation film (Fig. 7) is an area devoid of the transformed-beta structure. This was caused by diffused oxygen which stabilized the alpha phase. From these considerations it appears that there is a eutectoid temperature around 800°C that may be related to the change in the activation energy occurring between 800° and 825°C. In the case of the zirconium-2.5 wt % tin alloy where alloying constituents other than tin were very low, the alpha structure was stable over the entire temperature range investigated. However, the 800°C specimen in Fig. 9 and 12 shows some precipitation of intermetallic (not tin) compounds at the grain boundaries.

Semiquantitative spectrographic analyses for the presence of tin were obtained on the oxidation films of both alloys. About 2 wt % tin was found in each film. Calculations based on these crude analyses indicate that there was very little diffusion of the tin at the metal-film interface.

MECHANISMS

Formation of thick protective oxidation films is predominantly a diffusion-controlled process. The films are semiconductors and, according to Wagner (7), they are not of exactly stoichiometric composition, but are stable with an excess of either cation or anion. Various means have been devised to distinguish the diffusion mechanisms in semiconductors. A number of such tests were applied to the experimental oxidation films.

Marker experiments were made on the zirconium-tin alloys, pure zirconium, and a copper control. The marker was a thin layer of Cr_2O_3 powder (in

water) painted on the specimens. Specimens were then reacted with one atmosphere of oxygen at 800°C for 6 hr. In the case of copper, it was determined by various investigations that the cuprous ion is the diffusion specie. This work was reviewed by Kubaschewski and Hopkins (8). Accordingly, the marker was found at the metal-film interface after oxidation of copper. However, for pure zirconium and zirconium-tin alloys, the Cr₂O₃ marker remained entirely at the film-gas interface indicating that the oxygen ion is diffusing through the film and the reaction is occurring at the metal-film interface. From experiments of Weininger and Zemany (9) with a Nernst glower (85 mole % ZrO₂ and 15 mole % Y₂O₃), one would expect the oxygen ions to be the diffusing specie.

Theoretically, diffusion of the oxygen ion (anion) can occur by two mechanisms, either by anion holes (defects) in the zirconia lattice, or by interstitial anion diffusion through the lattice. Consideration of the ionic radii of Zr⁴⁺ (0.90 Å) and O²⁻ (1.36 Å) gives a ratio for R₊/R₋ of 0.66 for ZrO₂. Therefore, in the zirconia lattice, oxygen ions are in contact and zirconium ions fit in positions between the oxygen ions. Because of the size of oxygen ions, they could not occupy interstitial positions in the zirconia lattice. In view of these considerations, it is concluded that the mechanism of the anion diffusion is by lattice defects or holes.

Thermoelectric power measurements were made on the gray-black films to determine the type of electronic conduction. Negative thermoelectric power indicates that excess electrons are responsible for the conductivity, while a positive thermoelectric power indicates electron defects are responsible. Measurements made on films of pure zirconium and zirconium-tin alloys, using a hot (700°C) tungsten probe, gave negative thermoelectric powers. Therefore, electronic conduction in the films is through

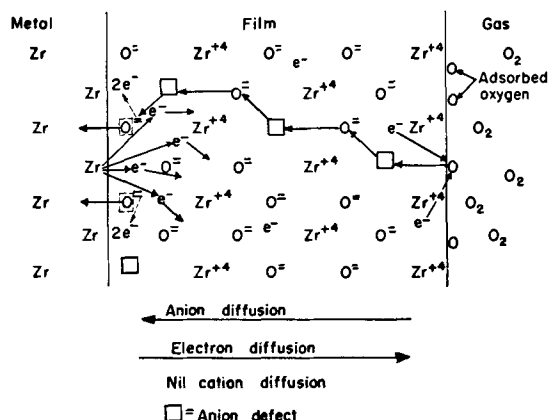
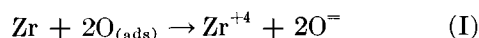


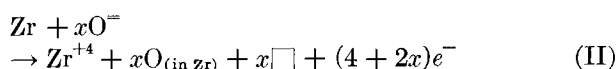
FIG. 13. Proposed mechanism for the oxidation of zirconium.

excess electrons. Since diffusion in the films is through anion holes and electronic conduction is by excess electrons, it was concluded that the dark oxidation films in the pure zirconium and zirconium-tin alloys are anion-deficit semiconductors (*N*-type).

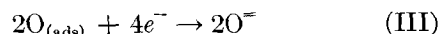
From the results of this work, a mechanism for the surface reaction of oxygen is proposed as follows. Starting with a clean metal surface, the initial reaction of the zirconium with oxygen is the formation of an adsorbed layer of oxygen with subsequent solution of oxygen into the metal. This is followed by the reaction



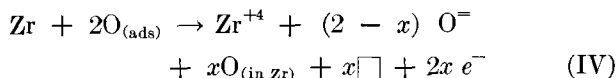
to form oxide. As soon as a finite layer has formed, anion holes are produced by solution of some of the anions into the metal, that is



which is the reaction occurring at the metal-film interface. Thus, anion holes are supplied to the oxide lattice and the gray-black film of substoichiometric ZrO₂ is produced. The reaction at the film-gas interface is



The summation of (II) and (III) is the equation for the over-all reaction.



The proposed mechanism for the formation of the gray-black film is shown in Fig. 13. At the metal-film boundary where the reaction to form oxide is occurring, zirconium atoms at the metal surface are ionized to tetravalent cations. The freed electrons

TABLE IV. Oxygen consumed at various temperatures by zirconium and zirconium-tin alloys

Temp, °C	Reaction time, min	Oxygen consumed, ml STP per cm ² of surface		
		Zr	Zr-1.5 wt % Sn	Zr-2.5 wt % Sn
600	10	0.19	0.24	0.10
	20	0.21	0.29	0.14
	100	0.35	0.46	0.34
700	10	0.38	0.42	0.38
	20	0.43	0.53	0.49
	30	0.51	0.60	—
800	10	1.0	0.82	0.59
	30	1.3	1.2	1.0
	100	2.1	1.8	—
900	10	1.9	1.3	1.4
	30	2.4	2.2	2.2
	100	3.6	3.2	—

enter the conduction bands of the zirconia lattice and start diffusing toward the film-gas boundary. About the newly formed cation, anion holes are produced by solution of the anions into the metal, and anions moving toward the metal surface fill these holes leaving anion holes behind. The greatest concentration of the holes is near the metal-film boundary and the smallest concentration is near the film-gas boundary. The reaction proceeds by a countercurrent of anion diffusion inward and anion holes diffusing outward through the film. The metal-film boundary is continually moving into the metal. Meanwhile, anions are formed at the film-gas boundary as adsorbed oxygen atoms pick up two electrons from the conduction bands of the film. To keep the film electrically neutral, there are two electrons in the conduction bands of the lattice for each anion hole.

Consideration is now given to the role of tin in the proposed mechanism. In Table IV are listed the amounts of oxygen consumed per square centimeter surface of pure zirconium and zirconium-tin alloys for various temperatures and reaction times. It is seen that, for equal times at any one temperature, the amount of oxygen consumed varied little with the tin content of the zirconium. However, as would be expected in view of the differences in oxidation rates and rate types, the relative positions of the materials in respect to amount of oxygen consumed changed as time progressed. At 600°C the zirconium-1.5 wt % tin alloy consumed the greatest quantity of oxygen, while at 900°C the pure zirconium consumed the most oxygen after equal times.

Room temperature specific resistivity measurements were made on the oxidation films to determine whether the tin has an effect on their electrical properties. Gray-black films of equal thickness (0.001 cm) were prepared at 800°C on pure zirconium and on the zirconium-tin alloys. Resistivities were determined by measuring the current flow from a small area of deposited silver (silver paste) through the oxide film to the base zirconium using a field strength of 3.7×10^4 v/cm. The values obtained were of the order of 6×10^{13} ohm-cm for pure zirconium and about 1×10^{14} ohm-cm for the two zirconium-tin alloys. These are only approximate values and it is believed that there is very little if any effect of tin on the electrical properties of the films.

DISCUSSION

The over-all oxidation mechanism of pure zirconium and zirconium-tin alloys is a complex process and changes with tin content. The kinetics of high temperature oxidation of zirconium, reported

in an earlier paper (1), followed a cubic rate law. In the present study, the zirconium-1.5 wt % tin alloy also oxidized according to the cubic law; however, oxidation of the zirconium-2.5 wt % tin alloy followed the parabolic law. These rate laws are associated with the formation of an adherent gray-black film of preferentially oriented monoclinic ZrO_2 (oxygen deficit) on the metal.

The natural volume ratio of monoclinic ZrO_2 to Zr is about 1.5. Therefore, for the gray-black film to be adherent to the metal, it must grow under highly compressive stresses. When the continuity of this film is disrupted, part of the oxide is no longer a part of the restrained coherent film. Consequently, it oxidizes to stoichiometric composition forming the light-colored randomly-oriented monoclinic ZrO_2 . Metallographic examination indicates that films on the 2.5 wt % tin alloy are more porous than films on zirconium and the 1.5 wt % tin alloy. This increased porosity could result in the parabolic behavior. Tylecote (2) found that the oxidation of annealed copper in moist air initially followed the cubic law at 210°C and in the range 520°–750°C. Between 210° and 520°C, the oxidation approached parabolic behavior. This was explained on the basis of porosity (blistering) of the films. However, in the range 520°–700°C, where the films were compact and nonporous, the cubic law was obeyed.

As in the present study, the film thicknesses (1 to 3×10^{-3} cm) obtained by Tylecote were greater than the limiting thickness (2×10^{-4} cm) permitted by the cubic growth mechanism proposed by Cabrera and Mott (4) for films containing excess anions (*P*-type semiconductor). Moreover, the present data show the formation of relatively thick films on zirconium and zirconium-1.5 wt % tin alloy during cubic-rate oxidation to form an anion-deficit semiconductor film (*N*-type semiconductor). Therefore, the theory of Cabrera and Mott cannot be applied to the cubic oxidation of zirconium and the zirconium-1.5 wt % tin alloy.

In comparing energies of activation for the cubic oxidation of zirconium and zirconium-tin alloy, the energy of activation decreases with increasing tin content of the zirconium. For zirconium, the energy of activation is 47,200 cal/mole (1), and for zirconium-1.5 wt % tin, 38,300 cal/mole. A still lower energy of activation of 22,500 cal/mole was found for the 1.5 wt % alloy (cubic reaction) in the high temperature range (825°–900°C). It was found that there is a eutectoid temperature at about 800°C for the zirconium-1.5 wt % tin alloy which could cause the change in the activation energy. The eutectoid temperature apparently results from the alloying constituents chromium, iron, and nickel.

For the parabolic oxidation of the zirconium-2.5 wt % tin alloy the energy of activation is 32,500 cal/mole. This value cannot be compared with those obtained for the cubic reactions.

ACKNOWLEDGMENTS

The authors gratefully acknowledge the assistance of Mr. B. G. Koehl in making the experimental reaction rate runs and of Mr. R. K. Willardson who did the thermoelectric power and resistivity measurements on the oxide films.

Any discussion of this paper will appear in a Discussion Section to be published in the June 1956 JOURNAL.

REFERENCES

1. J. BELLE AND M. W. MALLETT, *This Journal*, **101**, 339 (1954).
2. R. F. TYLECOTE, *J. Inst. Metals*, **81**, 681 (1952-53).
3. J. T. WABER, *J. Chem. Phys.*, **20**, 734 (1952).
4. N. CABRERA AND N. F. MOTT, *Repts. Progr. Phys.*, **12**, 163 (1949).
5. M. W. MALLETT, J. BELLE, AND B. B. CLELAND, *This Journal*, **100**, 1 (1954).
6. H. J. HOGE, *J. Research Natl. Bur. Standards*, **44**, 321 (1950).
7. C. WAGNER, *Z. Phys. Chem.*, **B 22**, 181 (1933).
8. O. KUBASCHEWSKI AND B. E. HOPKINS, "Oxidation of Metals and Alloys," p. 30, Academic Press, Inc., New York (1953).
9. J. L. WEININGER AND P. D. ZEMANY, *J. Chem. Phys.*, **22**, 1469 (1954).

Application of Backside Luggin Capillaries in the Measurement of Nonuniform Polarization¹

M. EISENBERG,² C. W. TOBIAS, AND C. R. WILKE

Department of Chemistry and Chemical Engineering, University of California, Berkeley, California

ABSTRACT

The backside capillary is demonstrated to be a suitable tool in the measurement of local values of polarization, particularly when interference with hydrodynamic conditions at the solution electrolyte interface needs to be avoided. The design and performance of several capillaries are described. A simple capillary machined of Teflon plastic is shown to yield satisfactory accuracy in polarization measurements. When the current distribution is nonuniform due to geometry or convection, cathodic polarization is shown to depend on the position of the capillary opening in the cathode.

INTRODUCTION

In the measurement of polarization, electrical contact on the solution side between the working electrode and reference electrode is established by means of a column of a suitable electrolyte, enclosed in a plastic or glass tube, which has a small (capillary) opening in the working cell (Fig. 1). The capillary serves to prevent flow of electrolyte between the reference half-cell and the main body of electrolyte, and also permits the assignment of a more or less exact location of the junction within the electric field of the working cell.

The capillary tube, if placed close to the electrode surface, shields the current from it (1), and the measured polarization values are lower than the "true" polarization corresponding to the average current density over the electrode. If the measurement of polarization is effected while the current is flowing across the cell (direct method), the emf measured between the electrode and the reference half-cell includes besides the half-cell potentials the *ohmic potential drop* between the working electrode and the end of the capillary tube. Recognition of the proper significance of these factors is due to Piontelli and co-workers (2, 3), who estimated the errors incurred in polarization measurements by various capillary designs and locations on the basis of studies conducted with scaled up models. Barnartt (4) extended these observations by the electric trough method, using models of somewhat improved accuracy. The conclusions of these researches indicate that the shielding effect may be eliminated for all practical purposes by locating the capillary end at a distance larger than four times the external radius of the capillary from

the surface [Fig. 1(a)]. The ohmic potential drop on the basis of Barnartt's model studies can be computed if the conductivity of the electrolyte, average current density, and exact dimensions and location of the capillary are known. Piontelli (3) recommended the use of a small diameter glass tube, closed at the end by a thin glass membrane, placing it tightly against the electrode surface, with its axis normal to the surface [Fig. 1(b)]. In this arrangement the area covered by the membrane is completely shielded. However, the electric field remains unaffected if the lines of flow in the field of the cell are parallel to the axis of the tube. The liquid junction between the solution in the cell and in the tube is established by a circular corona-shaped opening in the glass wall, 10–40 μ from the electrode surface. The ohmic drop in this arrangement is negligibly small. This junction has the added advantage of eliminating the error incurred when the ohmic drop between the capillary tip and surface is computed by assuming that the conductivity of the electrolyte adjacent to the working electrode is identical to the bulk value.

Both the above arrangements can be assumed to function satisfactorily as long as the geometry of the working cell and the hydrodynamic conditions are such that the current distribution over the electrodes is uniform. Parallel plane electrodes, connected by insulating planes normal to the electrodes, or concentric circular cylindrical electrodes terminated by insulator planes normal to the axis provide uniform primary distribution (5). (The concentric spherical arrangement is not practical.)

Secondary distribution, however, is affected by convection in the vicinity of the electrodes. In the absence of stirring this can cause a significant departure from the uniform primary current distribution.³ It has been shown that current density may

³ Convection is suppressed in the vicinity of an electrode if the concentration changes established by the current

¹ Manuscript received July 19, 1954. This paper was prepared for delivery before the Philadelphia Meeting, May 4 to 8, 1952.

² Present address: Stanford Research Institute, Stanford, California.

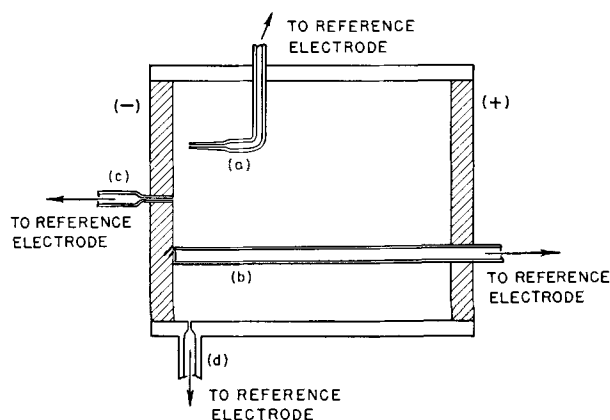


FIG. 1. Methods for coupling reference electrodes with working electrode surfaces.

vary as much as 100% over relatively short vertical distances (in the order of 10 cm) due to differences in ionic mass transfer rates (6, 7). Therefore, in polarization studies, effective stirring is of great importance. Establishment of a condition of uniform turbulence along the electrode surface cannot be achieved in the presence of an obstruction (such as the frontal capillary tube) in the hydrodynamic boundary layer. As a result, current density distribution may vary in the vicinity of the capillary tip, whether or not the latter is in contact with the surface.

When the effect of convection on current distribution is studied, introduction of a frontal capillary tube causes a more or less significant departure from the hydrodynamic conditions prevailing in the absence of such a disturbance. Since the quantitative prediction of these effects is extremely cumbersome, if not impossible, the *backside capillary* arrangement [Fig. 1(c)] possesses definite advantages over a frontal tube.

This junction was first suggested and used by Piontelli (8, 9) and Poli (8) and since subjected to thorough investigation with regard to errors resulting from the introduction of a discontinuity in the electrode surface. A small ohmic potential drop is included between the inside of the capillary hole and the electrode surface. In Barnartt's model experiments (4) this drop was found to be equal to the potential drop across an electrolyte layer of thickness $0.559 r$ (r = external radius of capillary) in a direction normal to the electrode. (Wall thickness was $\frac{1}{3} r$.) It is evident from these data that, if one uses small capillary openings and electrolytes of high conductivity, the error incurred up to moderately high current densities (0.01–0.1 amp/cm²) will not exceed a few millivolts.

are such that only vertical density gradients result, with the density decreasing with increasing elevation. The deposition of a metal on a horizontal top end plate of a vertical cell is a model where convection is negligible (10).

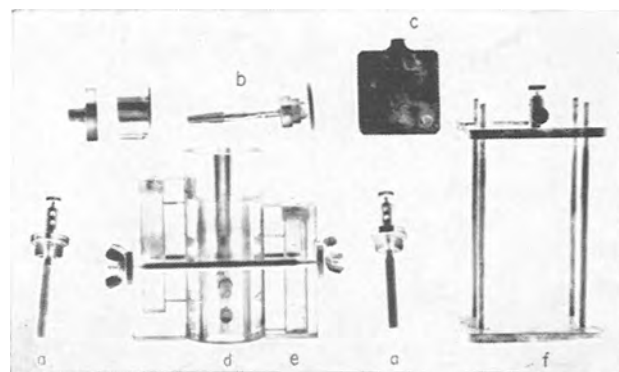


FIG. 2. Parts of cell for measurement of total polarization by the sidewall and backside capillaries. (a) Cu reference electrode; (b) Cu cathode disk with backside capillary; (c) Cu anode plate; (d) Lucite tube (for electrolysis); (e) side compartments, for reference electrodes; (f) clamp for holding anode and cathode in place.

WORKING TEST OF BACKSIDE CAPILLARY MODELS

In the following the development and testing of a backside capillary (designated by BSC) suitable for the measurement of local polarization is described.

A 1-in. ID, 5-in. long circular cylindrical Lucite tube was closed off at both ends by $\frac{1}{4}$ -in. thick copper plates, held in place by a clamping structure (Fig. 2). The BSC to be tested was mounted in the center of one of the electrodes and was connected by a glass or plastic tube to the reference half-cell, containing copper reference electrodes. In addition, two $\frac{1}{64}$ -in. holes were drilled through the Lucite wall, normal to the axis of the tube, at 0.1- and 1.0-in. distances, respectively, from the electrode containing the BSC. Each hole served to connect the cell to separate side compartments containing a copper reference electrode and filled with electrolyte of the same composition as in the working cell. When external potential is applied across the two end-plate electrodes, the ohmic potential drop in the column between them is proportional to the distance along the axis of the tube (10), provided the composition of the electrolyte remains uniform during the passage of the current. Knowing the conductivity of the electrolyte and the distance of a sidewall capillary (SWC) [Fig. 1(d)] from the electrode under investigation, the ohmic potential drop between the working electrode and either of the holes can be evaluated⁴ for any given current.

EXPERIMENTAL PROCEDURE

The cylinder equipped with sidewall capillaries (SWC) provided a convenient means for the investigation of the performance of several BSC de-

⁴ Uniform conductivity can be maintained approximately by effective stirring (electrolyte circulation) and the use of excess "supporting electrolyte" (10).

signs. The electrolyte was either 0.5M or 0.6M CuSO_4 in 1.45M H_2SO_4 . Both the cathode and the reference electrodes ($\frac{1}{4}$ -in. diameter, 2-in. long copper rods) were carefully preplated from a similar solution prior to each experimental series. After the cell, capillary connections, and reference half-cell compartments have been filled with the electrolyte, the desired current was applied across the cell, and after 5–15 min the potential between each reference electrode and the cathode was simultaneously measured.⁵ The potential difference between the two side compartment reference electrodes was also recorded [Fig. 2(a)] in order to establish the ohmic drop between the planes of the sidewall capillary openings.

Polarization values were obtained in the unsteady state. They included both chemical and concentration polarization. These measurements were intended only to clarify how closely a particular BSC yields the same polarization value as those obtained simultaneously by the sidewall capillaries.

The ohmic component was subtracted from the values measured by the sidewall capillaries, and then the polarization values obtained by the SWC and the BSC were plotted. (In all calculations the potential difference between the reference electrodes was taken into account.)

In the design of the BS capillaries the authors considered the following:

1. The diameter of the capillary should be as small as possible since both the ohmic potential drop and the current density at the edge of the hole in the metal increase with hole size (4).

2. The inside of the capillary hole must be effectively insulated from the metal surface inside the hole, and from the back side of the electrode, otherwise the polarization values measured will be smaller than the value corresponding to the uniform current density on the surface.

3. The outer end of the capillary must be smooth and flush with the working electrode surface (10).

Fig. 3 shows some of the capillaries tested by the above described method. Glass capillaries were found to be too fragile. Sealing the gap between the metal and the glass capillary and fitting the outer end of the capillary exactly in the plane of the electrode is a tedious operation. In type (a) (Fig. 3) a thin wire was inserted in the hole drilled through the electrode, and a resin lacquer⁶ was applied. After hardening, the wire was pulled out, leaving a well-defined capillary hole behind. In model (b), the ruby was a standard watchmaker's stone, inserted in the predrilled hole by a special tool. Model (b) gave very well-defined

⁵ Instruments: (a) Leeds and Northrup potentiometer Type K2; (b) Potentiometer-Recorder, G.E. Model 8 CESM19A.

⁶ G.E. Glyptal.

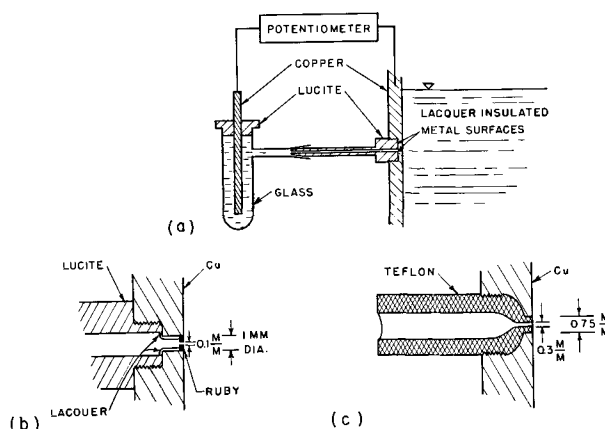


FIG. 3. Backside capillaries

hole geometry on the solution side, but still required lacquer insulation inside the hole. Capillaries (a) and (b) showed similar behavior in the authors' tests in the cylindrical cell (Fig. 2). Polarization values were consistently lower than the ones measured by the SWC, differences increased with increasing current density and hole diameter. This indicates that the lacquer layers were imperfect and the solution came into contact with the electrode inside the hole. Fig. 4 and 5 give typical sets of results for types (a) and (b).

The Teflon capillary (model c) was the easiest to manufacture, and yielded by far the most satisfactory results (Fig. 6). Fig. 7 shows the increase of total polarization of the cathode with time, at constant current in a horizontal position on the top of the cell. Again satisfactory agreement can be observed between values obtained by the two capillaries.

The Teflon need not be machined accurately to the dimensions of the hole in the electrode, because under pressure (provided by the thread) it can be forced

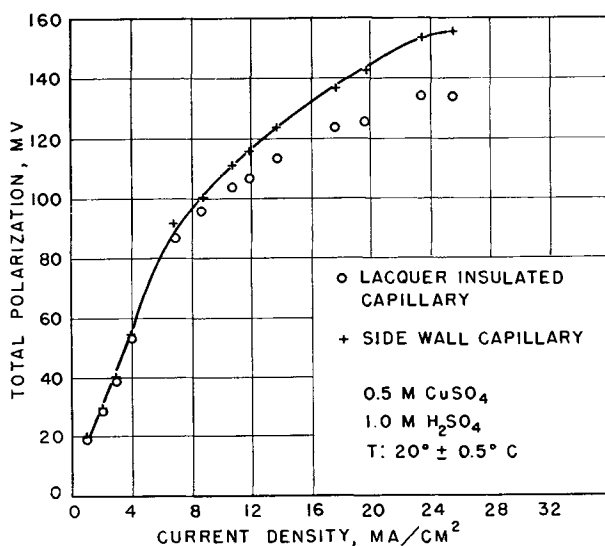


FIG. 4. Total cathode polarization as a function of current density.

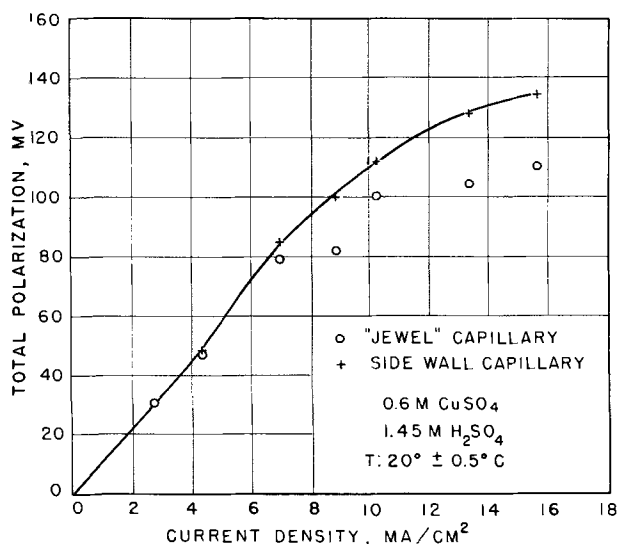


FIG. 5. Total cathode polarization as a function of current density.

through the capillary opening. The hole in the Teflon can be drilled after it has been fitted into the electrode. The solution side of the capillary was machined to eliminate any protrusions. This Teflon piece was attached to the reference half-cell by a piece of plastic tubing or by fitting it directly into a glass joint.

The Teflon capillary yielded consistently close agreement with values measured by the sidewall capillaries. (None of the values in Fig. 4, 5, 6, and 7 were corrected for the small *IR* drop that existed between the surface and the inside of the BSC.)

MEASUREMENT OF POLARIZATION VARIATION ALONG ELECTRODE SURFACES

The copper end plate of a rectangular Lucite cell of square cross section (Fig. 8) was equipped with three identical Teflon capillaries located on a line parallel to the bottom of the cell. The three capillaries connected to separate half-cell compartments, each provided with identical copper reference electrodes. Each reference electrode was connected to the

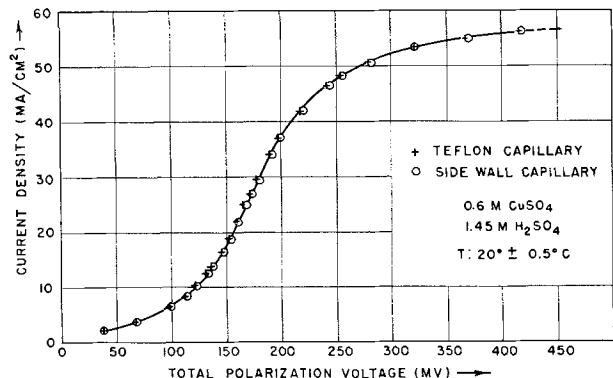


FIG. 6. Total cathode polarization as a function of current density.

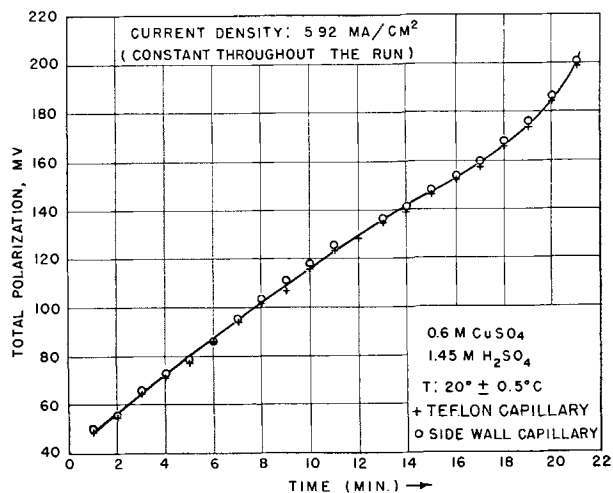


FIG. 7. Growth of the polarization of a "top" cathode with time, followed up simultaneously with the sidewall (o) and Teflon (+) capillary methods.

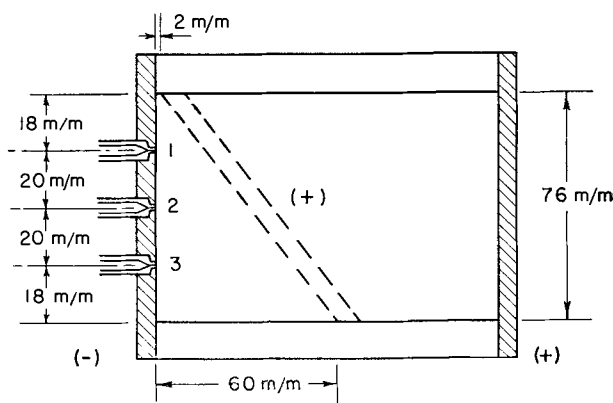
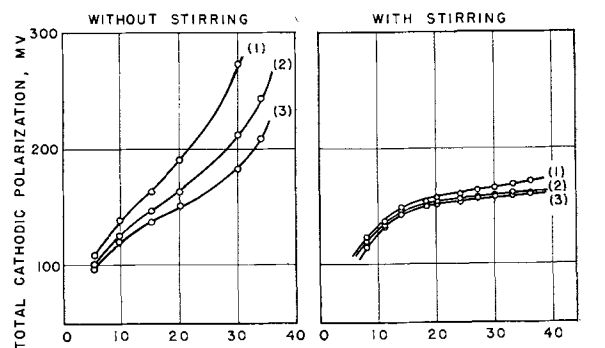


FIG. 8. Cell for measurement of nonuniform polarization; dashed lines indicate position of inclined anode.



$$\text{AVERAGE CURRENT DENSITY} = \frac{\text{TOTAL CURRENT}}{\text{TOTAL AREA}} = \frac{\text{MA}}{\text{CM}^2}$$

FIG. 9. Total cathode polarization along a horizontal line; inclined anode.

end plate through a potentiometer, and polarization was measured simultaneously for all three locations.

(a) *Line of capillaries in horizontal position.* Since the mass transfer boundary layer thickness along a horizontal line is the same (7) it is expected that all three locations yield the same polarization value. As shown in Fig. 9, indeed the values measured were identical within experimental accuracy (± 2 mv).

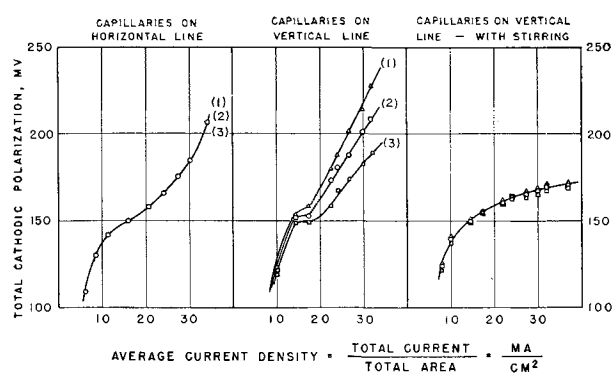


FIG. 10. Total cathode polarization vs. current density on a vertical Cu-cathode; uniform primary current distribution.

(b) *Line of capillaries in vertical position.* The end plate was turned by 90° , so that the lowest opening, 3, was 18 mm from the bottom. Due to natural convection the lower part of the electrode received a better supply of copper ions than the upper region. As a result, concentration polarization is higher at the top of the electrode than at the bottom (7). This fact is well illustrated by the appreciable difference between polarization values measured by the three capillaries, as illustrated in Fig. 10.

Stirring in the center of the cell by a small propeller at 1500 rpm almost completely eliminated the difference between locations.

(c) *Line of capillaries in horizontal position, anode in an inclined position.* The primary distribution of current is nonuniform, decreases with location 1 to 3. Without stirring, differences in polarization are quite pronounced, due to concentration polarization. With stirring, chemical polarization dominates, and polarization values fall close together (Fig. 9).

REMARKS

The backside capillary does not yield completely correct polarization values because of the ohmic drop included between the inside of the capillary and the electrode surface, and also because the current density, hence the polarization, is higher around the capillary wall than it would be on the electrode at the location where the hole was drilled in the metal in the absence of the hole. The ohmic correction is small unless the conductivity of the electrolyte is low and can be calculated approximately on the basis of Barnartt's recommendations (4). The error incurred due to higher polarization around the edge of the hole is negligible, provided the hole diameter is small and the conductivity is high.

Series of BS capillaries can be conveniently built into large electrode surfaces. In this laboratory one of the cells built for the study of the effect of forced convection (laminar and turbulent flow past flat plates) on ionic mass transfer and current distribution (10) was equipped with BS capillaries (Fig. 11). Any frontal tube or capillary would seriously af-

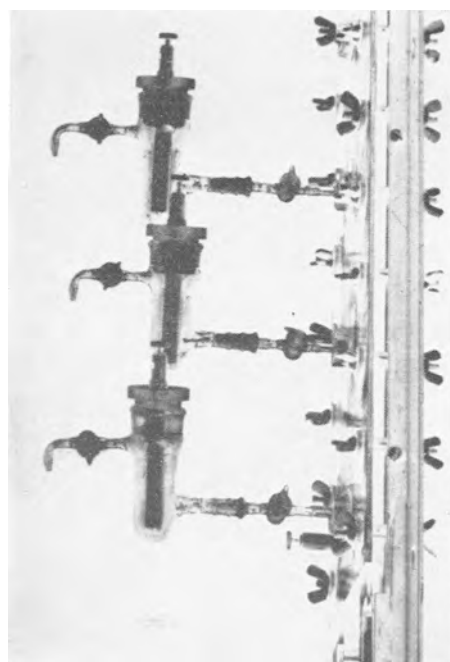


FIG. 11. Detail of cell for study of effect of laminar and turbulent flow past flat plate electrodes with reference half-cells connected to the cathode by backside capillaries.

fect the nature of the hydrodynamic boundary layer in such a model.

CONCLUSION

1. Due to relatively low interference with the flow of electricity and hydrodynamic conditions, the backside capillary was found to be a suitable means for establishing junction between working electrode surfaces and reference electrodes.

2. Properly designed capillary junctions lead to potential values which are in excellent agreement with those obtained simultaneously by independent methods of established accuracy.

3. Such backside Luggin capillaries permit the measurement of local (point) values of polarization and can serve as a valuable tool in obtaining data for mass transfer and overvoltage studies.

Any discussion of this paper will appear in a Discussion Section to be published in the June 1956 JOURNAL.

REFERENCES

1. A. E. MATTSON, *Svensk Kem. Tidskr.*, **62**, 83 (1950).
2. R. PIONTELLI, G. BIANCHI, AND R. ALETTI, *Z. Elektrochem.*, **56**, 86 (1952).
3. R. PIONTELLI AND G. BIANCHI, *This Journal*, **100**, 295 (1953).
4. S. BARNARTT, *ibid.*, **99**, 549 (1952).
5. C. KASPER, *Trans. Electrochem. Soc.*, **77**, 353 (1940).
6. C. WAGNER, *This Journal*, **95**, 161 (1949).
7. C. R. WILKE, M. EISENBERG, AND C. W. TOBIAS, *ibid.*, **100**, 513 (1953).
8. R. PIONTELLI AND G. POLI, *Gazz. Chim. Ital.*, **78**, 717 (1948).
9. R. PIONTELLI, *Z. Elektrochem.*, **55**, 128 (1951).
10. M. EISENBERG, M.S. thesis, University of California, Berkeley (1951).

Mathematical Studies of Galvanic Corrosion

III. Semi-infinite Coplanar Electrodes with Equal Constant Polarization Parameters¹

JAMES T. WABER

Los Alamos Scientific Laboratory of the University of California, Los Alamos, New Mexico

ABSTRACT

Mathematical analysis of a coplanar alternating array of long narrow electrodes was conducted subject to the limitation that polarization parameters for the anodes and cathodes are constant and equal. Interfacial potential and corrosion current parameters were computed for 18 values of a/ξ and for a/c equal to $1/2$ and $1/4$. Four perspective drawings of the distribution of potential throughout the corrodent were made to scale to illustrate the influence of polarization. Two experimental studies were found to be in reasonably good agreement with the present theoretical analysis.

INTRODUCTION

Two important limiting cases, namely that polarization was negligible and that one electrode was infinitely larger than the other have been discussed elsewhere (1, 2). It is difficult to find experimental studies of potential distribution or of variation of corrosion attack which correspond to these limiting cases. However, several studies (3-6) have been undertaken to demonstrate such distribution of corrosion and potential in the corrodent, and, in these, finite anode-cathode ratios were employed. Thus the distribution of corrosion attack using models similar in detail to these experimental conditions has been computed.

The most serious limitation imposed on this investigation, largely by convenience, is the assumption that the anode and cathode polarization parameters are equal. This parameter, ξ as defined by Wagner (7), has the dimensions of length and, as discussed previously (1, 2, 7), is extremely important in characterizing the behavior of a given galvanic cell. The use of equal parameters renders the case amenable to straightforward mathematical treatment, whereas, if the assumption were made that they are not equal, one would have to use cumbersome methods for solution of integral equations. Solutions require, in general, iterative or trial-and-error methods.

Previously (2) the magnitude of this parameter was calculated from various experimental data; it was found to lie in the range $1/4$ -25 mm. This indicates that in many cases, and particularly those cases in which extensive experimental work was done, the assumption of equal polarization param-

eters would be a reasonable approximation.² This special case of equality illustrates the effect of polarization and is useful for a qualitative discussion of the more accurate and general case of unequal parameters.

This investigation was undertaken to provide numerical data which could be compared with the experimental data of Copson (3) and Daniel-Bek (4). In a separate study (8) values of the potential were tabulated for nine widely different values of the ratio of the anode width to the polarization parameter and for each of these at over a hundred locations within the electrolyte. Detailed comparison of these potential values with the experimental results have not been made here.

A comparison of the variation of the current density can be made. These data indicate that there is good agreement between the mathematical and experimental results.

Important Limiting Cases

There are four pertinent lengths needed to characterize an alternating array of long, narrow, coplanar, galvanic cells, namely, the anode width, cathode width, and anodic and cathodic polarization parameters. In agreement with the notation of the previous papers these are identified as $2a$, $2(c - a)$, ξ_a and ξ_c , respectively. The behavior of a given galvanic system can be characterized by three dimensionless groups, (a/ξ_a) , $(c - a/\xi_c)$, and a/c . If even five values of each of these groups are used to illustrate the behavior of galvanic systems, 125 curves would have to be presented. The alternative is to

² That is, the electrodes employed by others range from 10 to 160 cm in width and are, therefore, macroscopically large in comparison with ξ_c . Even several fold variations between ξ_a or ξ_c will have a small influence on the corrosion current over much of these "large" electrodes.

¹ Manuscript received October 25, 1954. This paper was prepared for delivery before the Cincinnati Meeting, May 1 to 5, 1955.

discuss only limiting values of each ratio, and this procedure has been adopted in the present series of reports. One may distinguish four limiting conditions:

[1] *Negligible polarization* $a \gg \xi_a (c - a) \gg \xi_c$. This was considered earlier (1) with the further condition that $\xi_a = \xi_c$.

[2] *Strong polarization and high conductivity* $a \ll \xi_a (c - a) \ll \xi_c$. In this case as Wagner pointed out, IR drops within the solution represent a minor correction which can be disregarded. One may therefore use the usual diagram of electrode potential vs. current density in order to derive the corrosion potential and the operating current density.

[3] *Cathodic control and protection* $a \gg \xi_a (c - a) \ll \xi_c$. The case of cathodic control on dissolution of an almost pure metal has been discussed by Wagner (9). He also adopted this assumption in his contribution to cathodic protection (10). The special condition that $\xi_a = \xi_c$ has already been discussed briefly (2).

[4] *Anodic control* $a \ll \xi_a (c - a) \gg \xi_c$. This case has not been treated in general; however an analysis of the special condition that $\xi_a = \xi_c$ has been made (2).

In a preceding paper ξ was assumed to be zero, and several values of the anode-cathode ratio a/c were investigated (1). Later, ξ was permitted to vary over a wide range, but it was assumed that one electrode was infinitely larger than the other (2). In the present paper both these restrictions are removed, but ξ_a still equals ξ_c .

Important Experimental Studies

Electrostatic potentials have been known to exist in solution for many years, and many electrochemical problems and phenomena have been explained in terms of them. However, it was apparently not until 1938 that they were shown to exist in the vicinity of corroding specimens (10). About this time a number of independent investigations were started in Europe. The most significant contributions were made by Jaenicke and Bonhoeffer (6) and by Daniel-Bek (4). World War II interrupted similar work at Cambridge, and Copson (3) undertook to complete the work of Agar (12) here in the United States.

Jaenicke and Bonhoeffer (6) showed that, in a given medium, the absolute cathode size has a definite effect on potentials measured in the vicinity of the electrode surface. The ratio $(c - a/\xi_c)$ has important physical significance and thus should be applied in the discussion of galvanic systems in general.

Daniel-Bek (4) measured variation in corrosion attack near the anode-cathode junction by measur-

ing potentiometrically the approximate variation in normal potential gradient. Copson (3) obtained the variation in corrosion attack, as indicated by changes in thickness, by measuring with a micrometer the penetration into the metal.

MATHEMATICAL ANALYSIS AND EVALUATION

The techniques used have been well illustrated earlier (1, 2).

Boundary Conditions

Inasmuch as corrosion currents enter and leave a solution only at the electrodes, it is necessary to have the flow lines begin and end on the electrode surfaces. In order to eliminate edge effects at the boundary line of the electrode, an infinite repetition of the electrode arrangement with even symmetry has been assumed. This assumption restricts attention to what is happening at the anode-cathode boundary. Such an arrangement can be studied mathematically by using an even periodic function such as a Fourier cosine series which alternately takes on the potential of the anode and the cathode as a boundary condition, and which will give the potential within the corrodent. Consideration can thus be restricted to one period.

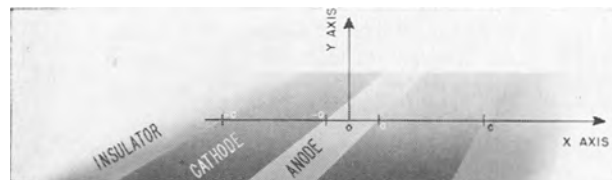


FIG. 1. Geometric relation and orientation of the electrodes.

The model galvanic cell consists of two bimetallic coplanar, juxtaposed infinite strips as indicated in Fig. 1. Since current is assumed not to flow between the electrodes in different cells or periods, one can place insulators at the remote electrode boundaries as shown in Fig. 1.

The unpolarized potential difference between the anode and cathode when immersed in the corrosive medium is designated as E_a . Conditions appropriate to the use of the slope of the polarization curve as though it were a linear polarization law have been discussed by Wagner (7). This reduces the problem to the solution of a simple Sturm-Liouville problem. As in the other papers of this series, both E_a and the potential $P(x, y)$ within the solution have been measured with respect to the cathode. Clearly P is bounded in the region under consideration.

Interfacial conditions for the solution of this

problem are:

$$P^*(x, 0) - \varrho \left. \frac{\partial P^*}{\partial y} \right|_{y=0} = E_a S_a(x) \quad (\text{I})$$

$$\left. \frac{\partial P^*}{\partial x} \right|_{x=c} = \left. \frac{\partial P^*}{\partial x} \right|_{x=0} = 0 \quad (\text{II})$$

where the step function S_a is defined as

$$S_a(x) = \begin{cases} 1 & \text{for } \begin{cases} 0 \leq x \leq a - 0 \\ a + 0 \leq x \leq c \end{cases} \\ 0 & \text{for } \begin{cases} 0 \leq x \leq a - 0 \\ a + 0 \leq x \leq c \end{cases} \end{cases} \quad (\text{III})$$

and in which $2c$ is the period of repetition. The quantity a is half of the width of the anode. The potential at the solution interface is illustrated in Fig. 2.

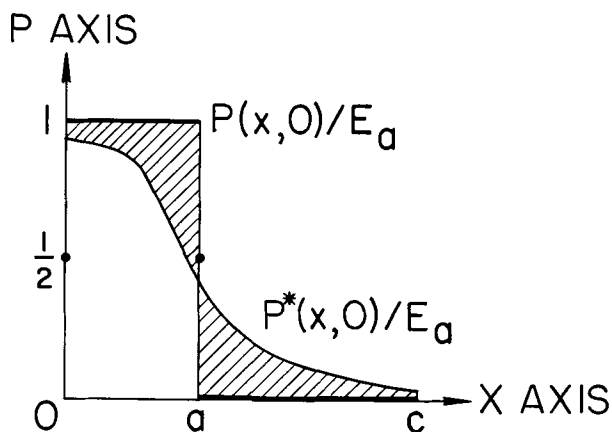


FIG. 2. Polarized interfacial potential. Variation is due to the changing current density in the two electrode regions.

Solution of the Problem

A Fourier Series which will satisfy the two boundary conditions, satisfy Laplace's equation, and converge for infinite nonnegative y is

$$P^*(x, y) = A_o^* + \sum_{n=1}^{\infty} A_n^* \exp\left(-\frac{n\pi y}{c}\right) \cdot \cos\left(\frac{n\pi x}{c}\right) \quad (\text{IV})$$

The starred coefficients may be determined by the boundary conditions (I) and (III). The asterisks indicate that polarization is being considered, in agreement with the convention adopted in earlier papers (2, 8). Substitution of this series into equation (I) leads to

$$A_o^* + \sum_{n=1}^{\infty} A_n^* \left(1 + \frac{n\pi\varrho}{c}\right)^{-1} \cdot \cos\left(\frac{n\pi x}{c}\right) = E_a S_a(x) \quad (\text{V})$$

The orthogonal properties of a cosine series can then be used to determine the coefficients. If this equation is multiplied by $\cos(m\pi x/c)$ and then integrated

TABLE I. Comparison of the coefficients obtained in the two reports

	$\varrho = 0$ Part I	$\varrho \neq 0$ Part III
A_o	$E_a(a/c)$	$E_a(a/c)$
A_m	$\frac{2E_a \sin\left(\frac{m\pi a}{c}\right)}{m\pi}$	$\frac{2E_a \sin\left(\frac{m\pi a}{c}\right)}{\pi m(1 + m\pi\varrho/c)}$

with respect to x , it is clear on using definition (III) that

$$\sum_{n=1}^{\infty} A_n^* \left(1 + \frac{n\pi\varrho}{c}\right)^{-1} \left(\frac{c}{2}\right) \delta_{mn} = \frac{cE_a}{\pi m} \sin\left(\frac{m\pi a}{c}\right) \quad (\text{VI})$$

where δ_{mn} is the Kronecker delta function. The left hand side of (VI) reduces to a single term of the series. The quantity A_o^* is determined in the usual way. The resulting coefficients A_m^* and A_o^* are presented in Table I, together with A_m and A_o which were derived earlier (1). The resulting equation for the potential is

$$P^*(x, y) = \frac{E_a a}{c} + \frac{2E_a}{\pi} \sum_{n=1}^{\infty} \frac{\exp\left(-\frac{n\pi y}{c}\right) \cos\left(\frac{n\pi x}{c}\right) \sin\left(\frac{n\pi a}{c}\right)}{n \left(1 + \frac{n\pi\varrho}{c}\right)} \quad (\text{VII})$$

It is clear that A_m^* reduces to A_m when ϱ is zero as would be expected.

As long as the electrodes polarize similarly, the remote reference potential of this composite electrode is equal to A_o or $E_a(a/c)$. This important result can be seen by setting y equal to infinity in equation (VII).

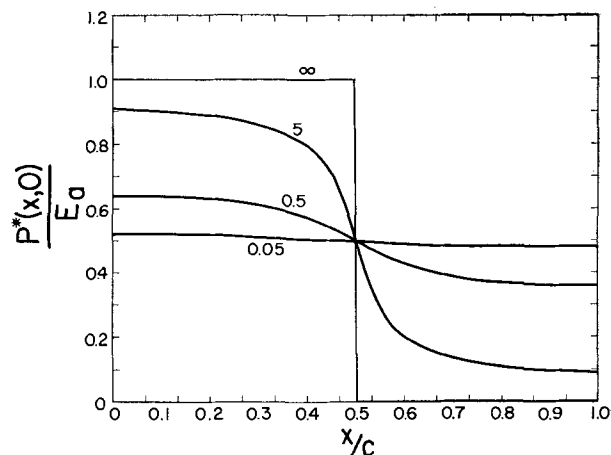


FIG. 3. Plot of the reduced interfacial potential, $P^*(x, 0)/E_a$, for four values of a/ϱ and with $2a = c$.

TABLE IV. Corrosion current parameter evaluated for $a/c = 1/2$ (Part 1)

a/ξ	x/c					
	0	0.1	0.2	0.3	0.4	0.499
0.01	0.009926	0.009928	0.009934	0.009946	0.009964	0.009999
0.05	0.04820	0.04825	0.04840	0.04867	0.04912	0.04998
0.1	0.09304	0.09323	0.09380	0.09484	0.09654	0.09992
0.5	0.3615	0.3647	0.3749	0.3940	0.4268	0.4979
1.0	0.5598	0.5687	0.5974	0.6523	0.7521	0.9920
5	0.9276	0.9649	1.0923	1.3730	2.0281	4.8454
10	0.9779	1.0241	1.1859	1.5671	2.5928	9.4673
50	1.0028	1.0542	1.2383	1.6999	3.1908	41.588
100	1.0141	1.0663	1.2532	1.7238	3.2671	74.236
∞	1.0000	1.0515	1.2361	1.7013	3.2360	318.47

TABLE IV. (Part 2)

a/ξ	x/c					
	0.501	0.6	0.7	0.8	0.9	1.0
0.01	-0.009999	-0.009964	-0.009946	-0.009934	-0.009928	-0.009926
0.05	-0.04998	-0.04912	-0.04867	-0.04840	-0.04825	-0.04820
0.1	-0.09992	-0.09654	-0.09484	-0.09380	-0.09323	-0.09304
0.5	-0.4979	-0.4268	-0.3940	-0.3749	-0.3647	-0.3615
1.0	-0.9920	-0.7521	-0.6523	-0.5974	-0.5687	-0.5598
5	-4.8454	-2.0281	-1.3730	-1.0923	-0.9649	-0.9276
10	-9.4673	-2.5928	-1.5671	-1.1859	-1.0241	-0.9779
50	-41.588	-3.1908	-1.6999	-1.2383	-1.0542	-1.0028
100	-74.236	-3.2671	-1.7238	-1.2532	-1.0663	-1.0141
∞	-318.47	-3.2360	-1.7013	-1.2361	-1.0515	-1.0000

Corrosion Current Density

More important than the interfacial potential is the distribution of corrosion attack over the anode and the cathodic current density over the other electrode. In agreement with the definition used elsewhere (1, 2), the corrosion current parameter

$$C^*(x) = \frac{-2a}{E_a} \left. \frac{\partial P^*}{\partial y} \right|_{y=0} \quad (\text{VIII})$$

It is clear that the normal gradient in (VIII) may be calculated by means of boundary condition (I) from the interfacial potential. Thus

$$C^*(x) = \frac{2a}{\xi} \left[S_a(x) - \frac{P^*(x, 0)}{E_a} \right] \quad (\text{IX})$$

An additional and important merit of calculating the interfacial potential is the facility with which current density can subsequently be calculated. It is apparent that this equation cannot be used if the polarization parameter is negligibly small, i.e., when ξ is zero. The current density distribution has been discussed for zero ξ elsewhere (1).

Values of this dimensionless parameter $C^*(x)$ which represents the corrosion current have been computed from (IX) and are presented in Tables IV and V. The dimensionless quantity employed to represent the current parameter (1) was $r(x)/E_a R_c h$ which is equal to $(c/4a)C(x)$.

Distribution of Potential in the Solution

Distribution of the potential can be obtained in the corrodent from equation (VII). Because the exponential factor is present in each term of the series, computation of the potential at a point in the solution is more rapid than equivalent computation of a value of the interfacial potential. That is, the series converges more rapidly in the former case.

As indicated above, the reduced and dimensionless polarization parameter $P^*(x, y)/E_a$ has been used to render the mathematical results applicable to the general problem. When this parameter is tabulated in terms of the reduced groups x/c , a/c , and a/ξ , which represent the physical dimensions of the galvanic cell, the results are independent of the actual quantities of any given galvanic cell, namely, E_a , a , c , σ , etc. By calculating the several pertinent ratios, a given problem can be solved.

Values of the reduced potential have been computed and presented elsewhere (8) for a variety of a/ξ and a/c values. The effect of ξ on the distribution of potential is best illustrated by the four perspective drawings of $P^*(x/c, y/c)$ which have been made to scale. In these drawings, the anodic material is assumed to be 50% of the total. Fig. 5 was constructed for the condition that $\xi = 0$. The cross hatching represents the portion of the interfacial potential which is hidden from view by the po-

TABLE V. Corrosion current parameter $C^*(x)$ evaluated for $a/c = 1/4$ (Part 1)

a/ξ	x/c					
	0	0.1	0.2	0.249	0.251	0.3
0.005	0.007460	0.007463	0.007472	0.007481	-0.002518	-0.002508
0.05	0.07123	0.07146	0.07229	0.07322	-0.02670	-0.02574
0.5	0.4192	0.5062	0.5629	0.6361	-0.3561	-0.2819
5	1.1316	1.3020	2.2561	4.9784	-4.4896	-1.7618
50	1.1887	1.4259	3.3617	37.368	-36.869	-2.8629
∞	1.207	1.4493	3.4693	159.26	-158.54	-2.9631

TABLE V. (Part 2)

a/ξ	x/c						
	0.4	0.5	0.6	0.7	0.8	0.9	1.0
0.005	-0.002497	-0.002491	-0.002486	-0.002483	-0.002481	-0.002479	-0.002479
0.05	-0.02473	-0.02410	-0.02367	-0.02337	-0.02317	-0.02306	-0.02302
0.5	-0.2160	-0.1808	-0.1589	-0.1449	-0.1361	-0.1312	-0.1296
5	-0.7588	-0.4637	-0.3333	-0.2657	-0.2288	-0.2100	-0.2042
50	-0.8731	-0.4923	-0.3428	-0.2690	-0.2298	-0.2101	-0.2042
∞	-0.8881	-0.5000	-0.3479	-0.2735	-0.2332	-0.2132	-0.2071

tential surface. Fig. 6, 7, and 8 were constructed for the conditions that a/ξ was 10, 1, and 0.1, respectively. In these figures the cross hatching represents the changes in the interfacial potential from the unpolarized values 1 and 0 caused by polarization.

Comparison between Theory and Experiments

Adequate comparison can be made only when values of ξ_a and ξ_c have been obtained under conditions comparable to the experimental conditions that were employed. In the studies made to

date, the author is not aware of any experimental study of current or potential distribution in which both ξ_a and ξ_c are available or can be computed. Any observed discrepancy revealed by comparing experiments with the present analysis will reveal mainly the degree to which ξ_a and ξ_c are dissimilar and will not reveal any fundamental error in the analysis.

There is a fairly large mass of experimental data available on the distribution of potential throughout the corroding medium (3-6, 11, 12). However, comparison is complicated by the difficulty of estimating the unpolarized potential difference E_a and the subject

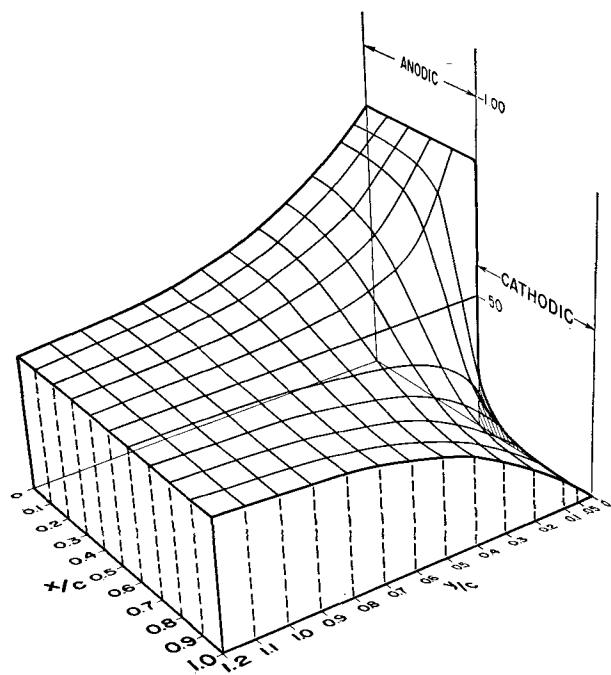


FIG. 5. Perspective scale drawing of the reduced potential function evaluated for $\xi = 0$.

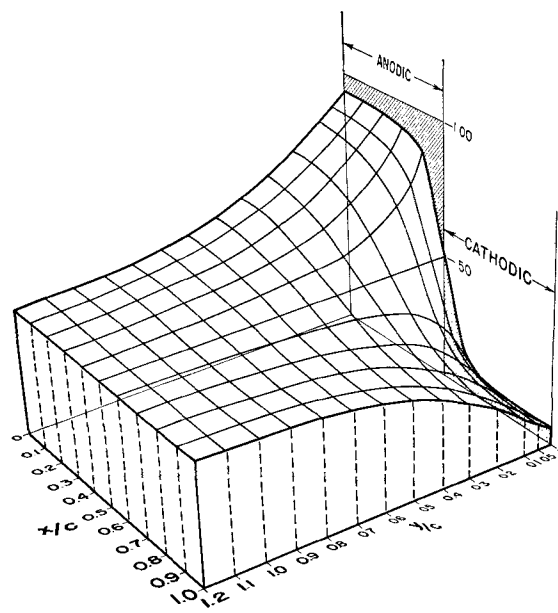


FIG. 6. Perspective scale drawing of the reduced potential function evaluated for $a/\xi = 10$.

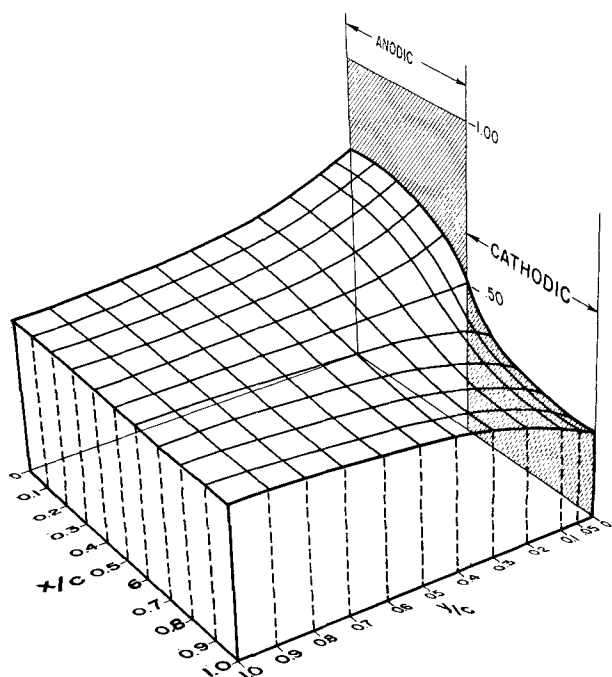


FIG. 7. Perspective scale drawing of the reduced potential function evaluated for $a/l = 1$.

is not as interesting, in the main, as the question of the distribution of the corrosion attack. Copson's (3) and Daniel-Bek's third paper (4) will be used for the comparison. Although only an experimental study designed for making this comparison can be adequate, these two investigations approximate the ideal conditions closely enough to merit consideration below.

Comparison with Daniel-Bek's Results

Daniel-Bek(4) employed an approximate form of equation (VIII) to calculate the distribution of cor-

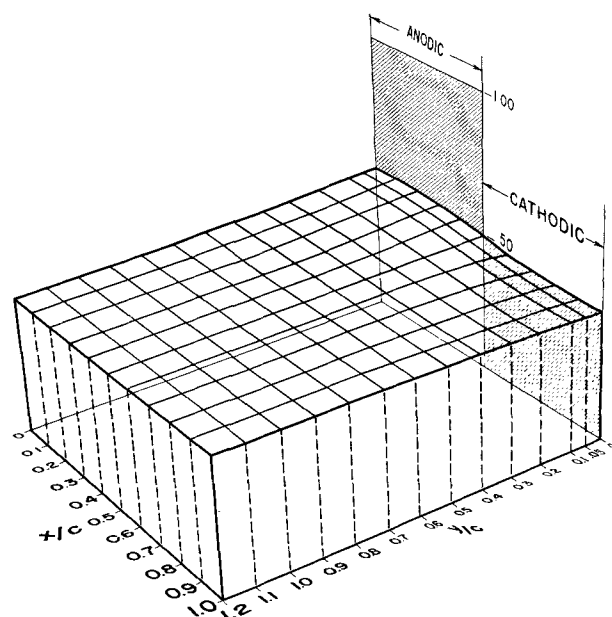


FIG. 8. Perspective scale drawing of the reduced potential function evaluated for $a/l = 0.1$.

rosion attack over the anode in the vicinity of the anode-cathode junction. He estimated $\partial P^*/\partial y|_y = 0$ by drilling tiny holes at several positions in the anode and fitting the capillary tip of a reference electrode into them. By measuring the potential difference between these electrodes and another held constant 0.55 mm in front of the metal surface, the normal potential gradient could be made roughly proportional to this potential difference. The assembly, consisting of one anode and one cathode, was 320 cm long, so that the ratio y/c appearing in the exponential term of the present series would be equal to 1.72×10^{-4} for his work. The difference form of the gradient $\Delta P/\Delta y$ was evaluated at approximately $y = 0$.

With this clever, approximate method he was able to show that there was a considerable variation in the amount of corrosion attack over the anode and in different strong electrolytes. Although conductivities of the solutions were high the anode width was equal to 160 cm, and thus l/a would be very small.

l can be estimated from the data which he gives since $a/c = 1/2$. In such a case it can be shown that³

$$J_a(a - s) = -J_c(a + s) \quad (\text{X})$$

Employing $s = 1/2$ cm, the largest J_c is 4.6 ma/cm² for 0.2N KClO₃, and the smallest J_c for $s = 8$ cm is 0.36 ma/cm² for 0.05N KCl. One may estimate the derivative of the overvoltage curve, $\partial \Delta E_c/\partial J_c$ from Tafel's equation

$$\Delta E_c = a + 0.050 \ln J_c \quad (\text{XI})$$

if hydrogen evolution is the principal cathodic process. On substitution into the definition of l ,

$$l_i = \left| \frac{\partial \Delta E_i}{\partial J_i} \right| \sigma \quad (\text{XII})$$

it is evident that

$$l_c = \frac{0.050\sigma}{J_c} \quad (\text{XIII})$$

The smallest value of the polarization parameter is 0.207 cm and the largest is 0.775 cm. These values are quite compatible with values estimated elsewhere (2). The largest value of l_a/c then would be 24×10^{-4} since in the theoretical analysis it has been assumed that $l_a = l_c$.

The corrosion current parameter was computed from equation (IX) for l/c , namely, 5×10^{-4} . When l is zero, equation [24] of reference (1) can be used to obtain the corrosion current parameter. Theoretical curves as well as experimental data for three electrolytes are presented in Fig. 9. Specifically,

³ Note that $J_a(x)$, the actual current density, is equal to $(\sigma E_a/2a)C_a^*(x)$.

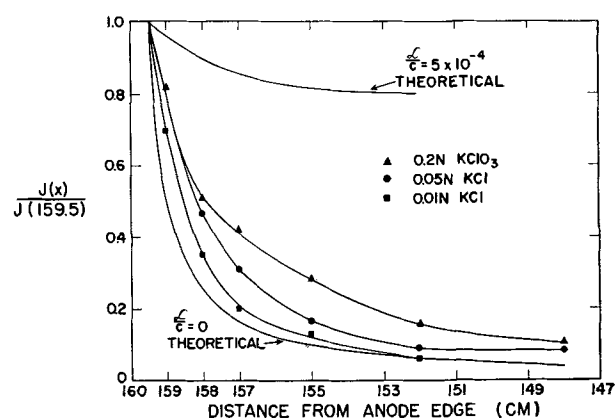


FIG. 9. Comparison of the theoretical current densities evaluated for $\xi/c = 5 \times 10^{-4}$ and 0 with Daniel-Bek's experimental results.

the ordinate is $J(160-s)/J(159.5)$ and the abscissa is $a - s$. The experimental data are well bracketed by $\xi = 0$ and $\xi = 1.6$ mm. Therefore, the agreement would appear to be quite satisfactory considering the idealizations which have been employed.

Comparison with Copson's Results

It is not practical to compare the potentials which Copson (3) measured in the corrodent, Bayonne tap water; however, the galvanic corrosion attack on the steel part of his steel-nickel couple can be compared with corrosion current parameter obtained in the theoretical analysis of this paper. He estimated the distribution of corrosion attack by graphically estimating the potential gradient from a map of the measured potentials. Fig. 7 of reference (3) shows the comparison between the actual change in thickness and the calculated attack. The graphical method is clearly inadequate near the steel-nickel junction as would be expected from the tables of the corrosion current parameter presented above. Near the junction the current increases very rapidly, and a linear average between two gradients is not very representative. In general, one would expect the average to be low because of the strong influence of the value taken more remotely from the junction. The estimated anodic current densities range from 0.138 ma/dm^2 or $1.38 \text{ } \mu\text{a/cm}^2$ at a point $\frac{1}{2}$ in. from the center of the anode ($x = \frac{1}{2}$) to $8.62 \text{ } \mu\text{a/cm}^2$ at 3.95 in. The cathodic current was estimated to vary from $4.32 \text{ } \mu\text{a/cm}^2$ at $x = 4.00$ to $1.45 \text{ } \mu\text{a/cm}^2$ at 7.80 in. In terms of the definitions employed herein, a is 4 in. and c is 16 in.

An estimate of the polarization parameter can be obtained from these data, using equation (XIII) for ξ_c . It would range from 0.81 cm to 2.42 cm. If an expression such as Tafel's equation could be used properly to represent the anodic polarization, the estimated values of ξ_a would lie in the range 0.41

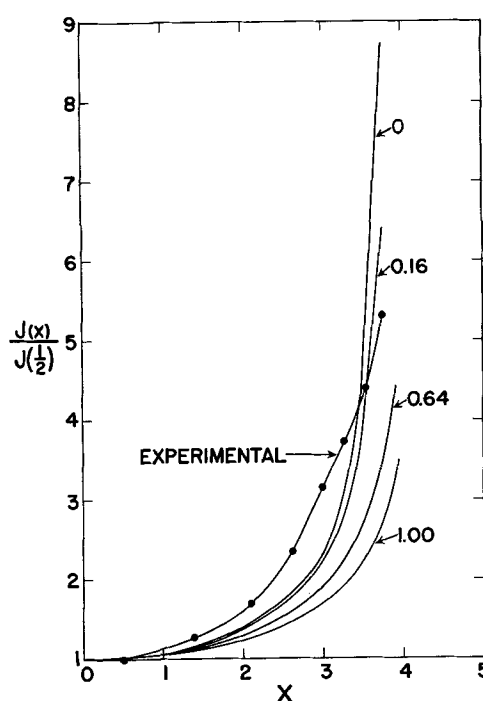


FIG. 10. Comparison between the distribution of Copson's experimental current densities and the theoretical variation evaluated for four ξ values.

to 2.54 cm. The justification for making this crude estimate of ξ_a is to indicate that ξ_a and ξ_c are approximately equal, and that the present idealized analysis is pertinent.

Values of the corrosion current parameter were computed using four values of ξ : 0.0, 0.16, 0.64, and 1.0 in. These data were plotted in Fig. 10 in the form of $C_a^*(x)/C_a^*(\frac{1}{2})$ which is equal to $J_a(x)/J_a(x = \frac{1}{2})$. Copson's experimental data are also plotted in Fig. 10 for comparison. Agreement is fairly good considering the idealizations involved in the theoretical analysis.

DISCUSSION

These numerical values of the polarized potential bear out the conclusions which have been deduced by others from experimental studies. The interfacial potential becomes more nearly the same for the anode and cathode as the parameter ξ increases.

This polarization parameter is very important in characterizing actual galvanic cells. In a given environment, irrespective of physical size, a galvanic cell may behave as though it were "macroscopic" or "microscopic" depending on whether the ratio of the critical dimension to ξ is large or small. This critical dimension cannot easily be defined in a precise manner, but it is that physical dimension which affects most strongly the distribution of current over the electrodes. Thus, it depends on the geometry of the cell.

If the critical dimension is small in comparison to ξ , that galvanic cell will behave as though it were microscopic. Since ξ is directly proportional to the conductivity of the solution, a particular system may appear to be either microscopic, or not, depending on whether the electrical resistance of the corroder is small or large, respectively. That is, more uniform potentials over the electrodes are observed in solutions which have good conductivity as shown by Jaenicke and Bonhoeffer (6), among others. The "microscopic" cells are characterized by nearly uniform current distributions, hence nearly uniform interfacial potentials.

It should be emphasized here again that the present investigation is an idealization since the restriction $\xi_a = \xi_c$ has been imposed. However, as indicated above, experimental values of ξ_c taken from a variety of studies range from a fraction of a millimeter to 3 cm. The assumption that ξ_a and ξ_c are equal is not seriously in error if either λ/ξ is very small or very large, since in either range fivefold changes, for instance, of this ratio do not significantly affect the interfacial potential or the current density.

Further, it is clear from the discussion that ξ is difficult to estimate from the current density and must be obtained properly from the polarization curve. For example, one chooses a value of ξ and then computes the current density. When these are taken to compute ξ_c one obtains a large range of values. This discrepancy becomes most serious when the ratio a/ξ is large, i.e., when there is small or negligible polarization.

Without going into it here, it is apparent from Wagner's analysis (7) of ξ that it is not a fixed quantity but depends upon the curvature of the polarization curve and, therefore, will in general vary over the electrodes in a macroscopic assemblage in the same way that the current density does. A further feature which may not be recognized at first is that $E_{a(c)}$ is not a fixed quantity and is not necessarily the difference between the two equilibrium single electrode potentials but is somewhat dependent upon the shape of the polarization curve [See Fig. 2, Ref. (7)]. Nevertheless, these simplifications in the treatment and accompanying increase in the tractability in mathematic analysis which is required, lead one to a more understandable picture of the influence of the various factors. The present analysis becomes increasingly accurate and pertinent if "microscopic" galvanic cells are considered.

The estimation of ξ_a depends upon a questionable technique if the anodic polarization curve is not obtained in any practical study. This is so because there is no recognized expression such as Tafel's equation for relating anodic polarization to current

density. A thorough analysis of the limited and scattered experimental data would be desirable.

It is clear from inspecting the perspective drawings that the variation in potential in a direction parallel to the electrode surface is greatest at the interface between the electrodes and the liquid. This variation in potential diminishes as one recedes from the interface and approaches a constant potential value at great distances. It has been shown (13) that this constant is equal to $E_a(a/c)$ for the condition $\xi_a = \xi_c$. This value has been called the potential of a composite electrode (1). Therefore, it is evident that this potential, which is obtained with a remote reference electrode, is dependent not only on the potential difference E_a but also on the relative proportions of anodic to cathodic material.

This qualitative effect of ξ is brought out in a previous paper (2). In the two experimental cases under consideration, the critical dimension was a , the half-width of the anode. Dependence of the maximum potential difference on a/ξ is clearly illustrated by the tables.

It is interesting to point out that

$$\lim_{\xi \rightarrow \infty} P^*(x, y) = E_a(a/c) \quad (\text{XIV})$$

since the coefficients A_m^* become zero. Thus, since the interfacial potential must converge to this value, it is clear that

$$\lim_{\xi \rightarrow \infty} P^*(x, 0) = P^*(x, \infty) = E_a(a/c) \quad (\text{XV})$$

As discussed above in connection with equation (VII), the right-hand side of this equation applies for all ξ . Thus the potential distribution within the solution must become more uniform as ξ increases, since these potentials are being squeezed between the limiting interfacial potential and the remote potential value of the galvanic cell. That is, any potential variation in the solution is smaller than that present on the interface. This feature has not been brought out clearly in any of the previous experimental studies.

Using the definition employed in a previous paper (2), that the anodic region in the electrolyte is that in which the potential exceeds $\frac{1}{2}E_a$, it is evident from the tables that shrinkage of the anodic region occurs as ξ increases and vanishes for sufficiently large ξ , if a/c is less than $\frac{1}{2}$. The use of $(a/c)E_a$ is not really more satisfactory since a study of Fig. 4 shows that for certain values of ξ/a , the liquid adjacent to the cathode is at potentials which lie between $\frac{1}{2}E_a$ and a/cE_a . No satisfactory definition has been suggested.

The current density and total anodic current remain finite for a given width of the anode. Consideration of tiny cathodes leads to equivalent re-

sults. This finite current density is different from calculations in which the effect of polarization is ignored. This fact justifies the present calculations in spite of the rather artificial condition of equal polarization parameters.

SUMMARY

A theoretical analysis of the influence of the percentage of anodic material and of the polarization parameter on corrosion attack has been made subject to the condition that anodic and cathodic polarization parameters are constant and equal. Two experimental studies of the distribution of corrosion attack were compared with the theoretical results and were found to be in reasonable agreement. Analysis shows that the potentials in the solution lie between the interfacial potential, as polarized, which is variable over the electrodes, and a constant value which is dependent upon the relative amounts of anodic and cathodic material. The variation in solution decreases with a/λ , that is, as the galvanic system approaches "microscopic" behavior.

ACKNOWLEDGMENTS

The author is deeply indebted to Professor Carl Wagner for his continuing interest, deep insight, and fruitful suggestions during this study. Many members of this laboratory have assisted in the preparation of this manuscript, and the author would like

to thank particularly Max Goldstein, Mark Wells, and Bertha Fagan for having obtained the numerical evaluations, and Elizabeth Scott for preparing the perspective drawings.

Any discussion of this paper will appear in a Discussion Section to be published in the June 1956 JOURNAL.

REFERENCES

1. J. T. WABER, *This Journal*, **101**, 271 (1954).
2. J. T. WABER AND MARSHALL ROSENBLUTH, *This Journal*, **102**, 344 (1955).
3. H. R. COPSON, *This Journal*, **84**, 71 (1943).
4. V. S. DANIEL-BEK, *Zhur. Fiz. Khim.*, **15**, 382 (1941); **18**, 247 (1944); **20**, 567 (1946).
5. G. V. AKIMOV AND A. I. GOLUBEV, *Zhur. Fiz. Khim.*, **20**, 303, 309 (1946).
6. W. JAENICKE AND K. F. BONHOEFFER, *Z. physik. Chem.*, **A191**, 193 (1942); **193**, 301 (1944).
7. C. WAGNER, *This Journal*, **98**, 116 (1951).
8. J. T. WABER, A. I. BENSON, AND M. GOLDSTEIN, Report No. LA-1651, Los Alamos Scientific Laboratory, April 1954.
9. C. WAGNER, "Handbuch der Metallphysik," (G. Masing, ed.) Vol. I, Part 2, pp. 195-200, Akademische Verlagsgesellschaft Becker and Erler K. G., Leipzig (1940).
10. C. WAGNER, *This Journal* **99**, 1 (1952).
11. R. S. THORNHILL AND U. R. EVANS, *J. Chem. Soc. (London)*, **1938**, 614.
12. J. N. AGAR, reported by U. R. EVANS, *J. Iron Steel Inst.*, **141**, 221 (1940).
13. J. T. WABER, Report No. LA-1386, Los Alamos Scientific Laboratory, March 1952.

Conductances of Some Moderately Concentrated Solutions of Metallic Perchlorates in the Mixed Solvent Methanol-Acetone at Low Temperatures¹

PAUL G. SEARS, WALTER W. WHARTON, AND LYLE R. DAWSON

Department of Chemistry, University of Kentucky, Lexington, Kentucky

ABSTRACT

Conductances and viscosities of solutions of lithium perchlorate in 50-50 wt % methanol-acetone at concentrations up to 4.75*M* have been measured over the temperature range -50° to 20°C . Similar measurements have been made on solutions of magnesium, zinc, and strontium perchlorates to concentrations slightly above 1.0*M*.

The maximum, which appears in the plot of conductivity as a function of concentration, shifts toward lower concentrations as the temperature is decreased. It has been shown that the four solutes studied exhibit very similar behavior and that the properties of solutions of the mixed solutes in this system depend primarily upon the total electrolyte concentration rather than the particular salts used.

Addition of water causes an increase in conductivity at room temperature; however, at low temperatures the presence of water markedly decreases the conductivity.

INTRODUCTION

This study was designed to investigate the conductance of some moderately concentrated solutions of metallic perchlorates in methanol-acetone mixtures at temperatures in the range -50° to 20°C . Magnesium, zinc, strontium, and lithium perchlorates were known to be rather remarkably soluble in both methanol and acetone (1, 2). An earlier investigation of conducting solutions of magnesium perchlorate in methanol and in acetone at 25°C had been reported by van Rysselberghe and Fristom (3). Their work was directed primarily toward the comparison of experimental and theoretically-predicted conductance behavior at low concentrations, whereas that reported in this paper has been concerned with a study of some factors affecting conductance at low temperatures.

EXPERIMENTAL

Materials.—Commercially available materials of good quality were used without further purification. Essentially anhydrous metallic perchlorates were obtained from the G. Frederick Smith Chemical Company. 'Baker Analyzed' reagent methanol and acetone had conductivities which amounted to less than 0.1% of that of the least conducting solution studied.

¹ Manuscript received December 2, 1954. This paper was prepared for delivery before the Cincinnati Meeting, May 1 to 5, 1955.

Based on research performed under a contract with the U. S. Army Signal Corps.

Procedure.—Solutions were prepared on a weight basis with all material transfers made in a dry box. A Jones bridge, manufactured by the Leeds and Northrup Company, was used to measure the resistance of the solutions by employing three conductance cells having constants of 31.99, 31.58, and 30.68 cm^{-1} . These constants were determined at 25°C through the intercomparison of resistances with cells having constants evaluated by the method of Jones and Bradshaw (4). Other aspects of the experimental procedure have been described adequately in a previous paper (5).

Measurements on each solution were completed within 48 hr after its preparation so that the results would not be altered appreciably because of instability effects which might appear.

DISCUSSION OF RESULTS

The conductance of lithium perchlorate in a 50-50 weight mixture of methanol and acetone was investigated rather extensively. The conductivity of this system, and of some solutions of magnesium perchlorate, at the various temperatures is shown in Fig. 1 as a function of the concentration expressed as gram-equivalent weights per 1000 g of solvent. It may be observed that the conductivity passes through a maximum at each temperature and that the concentration at which the maximum occurs decreases as the temperature is lowered. The corresponding viscosity data for these solutions have been incorporated into Fig. 2, where it may be seen that the viscosity of solutions of lithium perchlorate in

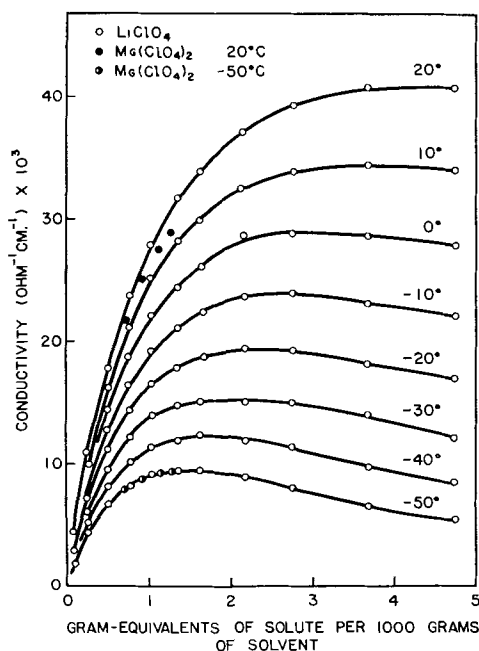


FIG. 1. Conductivities of lithium and magnesium perchlorates in 50-50 methanol-acetone as a function of the concentration.

50-50 methanol-acetone increases markedly with concentration at low temperatures. If the change of viscosity with concentration were relatively the same at each temperature, the concentration at which the maximum conductivity occurs should increase with decreasing temperature owing to increased dissociation of the solute resulting from the greater dielectric constant of the solvent. However, it appears that the more rapid increase of viscosity with concentration at lower temperatures has a counter-

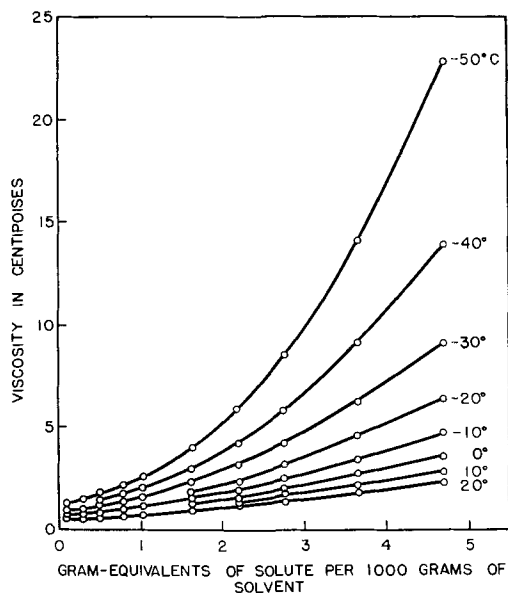


FIG. 2 Variation of the viscosity of lithium perchlorate solutions with concentration.

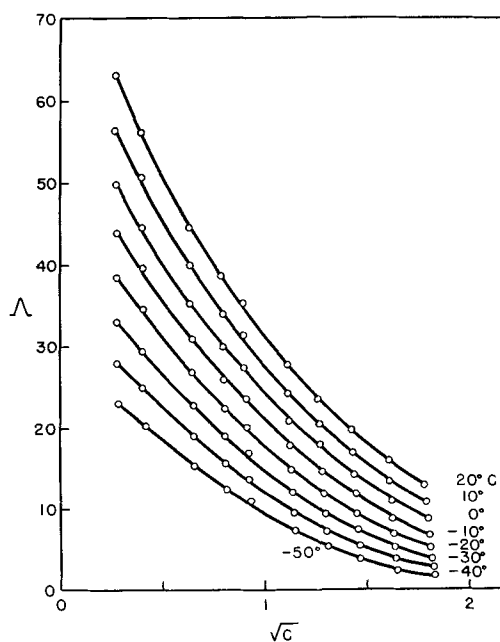


FIG. 3. Kohlrausch plots for some moderately concentrated solutions of lithium perchlorate in 50-50 methanol-acetone.

balancing effect great enough to shift the conductivity maximum toward a lesser rather than a greater concentration.

Kohlrausch plots for concentrated solutions of lithium perchlorate in 50-50 methanol-acetone are shown in Fig. 3. Graphs for the various temperatures are quite similar and are displaced at different magnitudes along the ordinate. No attempt has been

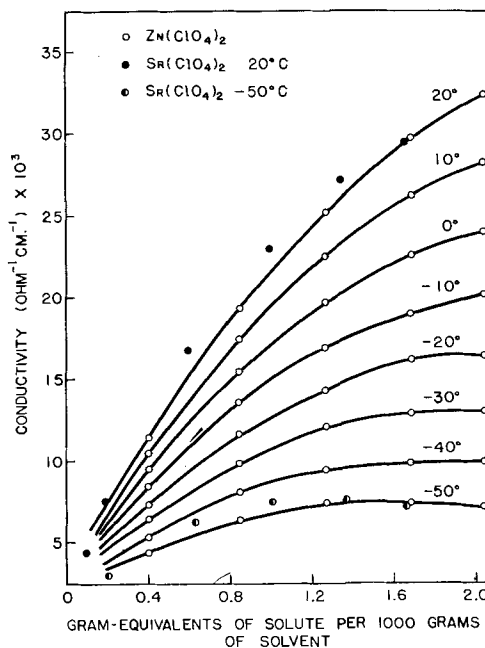


FIG. 4. Variation of the conductivities of zinc and strontium perchlorates with concentration.

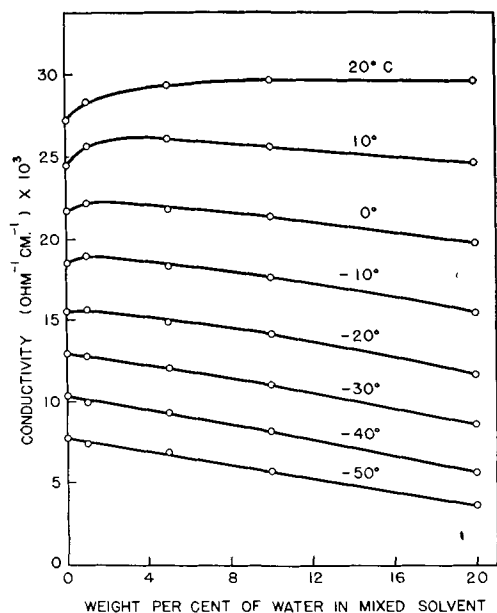


FIG. 5. Conductivities of 0.6M solutions of magnesium perchlorate in solvent mixtures of water and 50-50 methanol-acetone.

made to evaluate the limiting equivalent conductance from these data.

It may be observed from Fig. 1 that the conductivity of a magnesium perchlorate solution is approximately equal to that of a lithium perchlorate solution containing the same number of gram-equivalents of solute per 1000 g of solvent. Points representing conductance data for magnesium perchlorate solutions at intermediate temperatures have been omitted from this figure for purposes of clarity.

Fig. 4 shows conductivities of solutions of zinc perchlorate and strontium perchlorate in 50-50

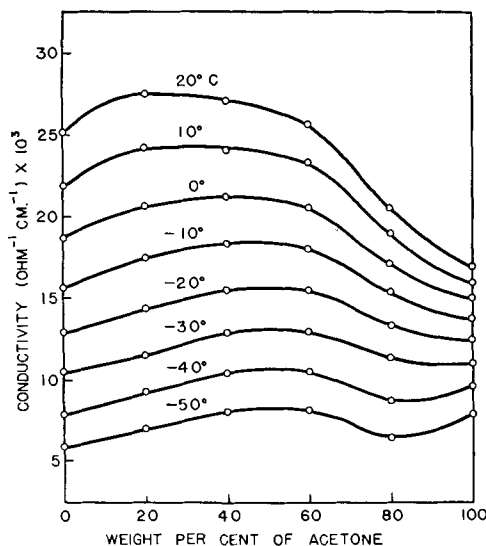


FIG. 6. Conductivities of 0.6M solutions of magnesium perchlorate in mixtures of methanol and acetone.

methanol-acetone as a function of the concentration. Conductances of these salts, which are almost equal, are approximately 15% less than that for the same concentration of magnesium perchlorate. It may be noted that the conductivity maxima for -50°C in Fig. 4 occur at a concentration of 1.2-1.4 gram-equivalents of solute per 1000 g of solvent which may be compared to about 1.4 on the same concentration basis for magnesium and lithium perchlorates as shown in Fig. 1.

Conductances of several solutions containing both magnesium and strontium perchlorates, magnesium and lithium perchlorates, or zinc and lithium perchlorates were measured at various temperatures; however, conductances of all of these perchlorate solutions of the same total electrolyte concentration were found to differ no more than a few per cent.

The effect of water in perchlorate solutions was studied by measuring the conductance of 0.6M solutions (i.e., 1.2 gram-equivalents of solute per 1000 g of solvent) of the magnesium salt in solvent mixtures of water and 50-50 methanol-acetone at temperatures within the range -50° to 20°C . Results are presented in Fig. 5. As may be observed from this figure, the presence of approximately 20% water at 20°C causes a 10% increase in the conductance; however, at -50°C 20% water in the solvent reduces the conductivity to approximately half that when water is absent.

Another study of the effect of solvent composition upon conductance was made by determining the conductance of 0.6M magnesium perchlorate solutions in solvent mixtures of methanol and acetone ranging from pure methanol to pure acetone. Results are shown in Fig. 6. For the particular concentration of magnesium perchlorate used, the most conducting solution at -50°C was in the 50-50 solvent and that at 20°C was in the 80-20 methanol-acetone mixture. Whether this is true for all concentrations of solute is unknown. In connection with this study, it is rather interesting that the conductivity of the 0.6M solution of the magnesium salt at 20°C divided by that at -50°C gives values of 4.26 and 2.13, respectively, for methanol and acetone. It seems to be merely fortuitous that the value for acetone is exactly half that for methanol.

In order to obtain some information regarding the stability of the solutions, the resistance of a 0.6M solution of magnesium perchlorate in 50-50 methanol-acetone was measured periodically over a period of nearly seven weeks. The resistance was found to increase steadily until after 47 days it was 8.5% greater than the initial value. Another solution 0.617 and 0.099M with respect to magnesium and strontium perchlorates was found to increase in

resistance 12% at 20°C and 23% at -50°C over a period of 82 days. The cause of the increase in resistance (or decrease in conductance) upon standing is unknown; however, it was observed that a very small amount of white flocculent precipitate usually appeared in most of the solutions after a few days.

Any discussion of this paper will appear in a Discussion Section to be published in the June 1956 JOURNAL.

REFERENCES

1. H. H. WILLARD AND G. F. SMITH, *J. Am. Chem. Soc.*, **45**, 286 (1923).
2. R. SALVADORI, *Gaz.*, **42**, i, 482 (1912).
3. P. VAN RYSSELBERGHE AND R. M. FRISTOM, *J. Am. Chem. Soc.*, **67**, 680 (1945).
4. G. JONES AND B. C. BRADSHAW, *ibid.*, **55**, 1780 (1933).
5. P. G. SEARS, R. R. HOLMES, AND L. R. DAWSON, *This Journal*, **102**, 145 (1955).

Kinetics of Nickel-Sulfur and Steel-Sulfur Reactions¹

ANDREW DRAVNIEKS

Engineering Research Department, Standard Oil Company (Indiana), Whiting, Indiana

ABSTRACT

The reaction of nickel with molten sulfur between 205° and 445°C follows the parabolic law. Up to 260°C the millerite form of NiS was the only sulfide detectable in the scale. At 340°C and higher, the high temperature B8 form of NiS was the only sulfide in the scale. The activation energy (Arrhenius) below approximately 300°C is in excess of 50 kcal; above this temperature, it is about 20 kcal. This compares with an activation energy of 41 kcal for the iron-sulfur reaction over the entire temperature range, where only one FeS form is known. Ni₃S₂, Ni₆S₅, two forms of NiS, and NiS₂, but not Ni₇S₆ and Ni₃S₄, were found to form upon exhaustive reaction of the corresponding mixtures of Ni and S. Formation of NiS₂ was several thousand times slower than the formation of NiS. NiS formed continuously. In the formation of FeS, definite evidence of scale failures and healings was found. A formal description of such a scale growth law is given and a term "microcataclysmic" is proposed to describe this form of kinetics.

INTRODUCTION

Nickel and some nickel alloys are known to be susceptible to attack by sulfur compounds. Relatively little is known, however, about the kinetics of nickel sulfide formation, especially in the moderately elevated temperature range. The present work was undertaken to obtain such kinetic data and to compare them with the kinetics of iron sulfide formation, investigated previously (1), together with some newer data. To avoid complications arising from the presence of foreign species, formation of sulfides was studied in a molten sulfur medium.

EXPERIMENTAL WORK AND RESULTS

The experiments were conducted by two methods.

In the first method, triplicate samples of A-nickel (45 × 8 × 0.62 mm) were immersed in molten sulfur at several temperatures for various periods of time. Nominal composition of this nickel was given as: 99.4% Ni, 0.1% Cu, 0.15% Fe, 0.2% Mn, 0.05% Si, and 0.10% C. The nickel content includes less than 1% cobalt. When specimens were removed from the sulfur, they were quenched in water. Weight loss was determined after mechanical removal of the sulfidic scale. A short pickling in 10% sulfuric acid was helpful in facilitating scale removal. Averages from the triplicate specimens were used for the reaction-time curves, drawn as the top portion of Fig. 1 on the basis of the parabolic law.

In the second method, the electrical conductivity of nickel strips immersed in molten sulfur was followed with time. Specimens were made of 0.025 mm (0.001 in.) A-nickel sheet. The technique and interpretation of the measurements have been described

elsewhere (1, 2). The electrical conductivity of nickel sulfides is quite high, so that, even after the total disappearance of the nickel metal by conversion to an initial form of sulfide, the specimen still has considerable conductivity. The sudden change in the slope of the plot of the relative conductivity vs. the square root of time, in the middle portion of Fig. 1, indicates the moment at which the metallic nickel phase disappears. This method indicated corrosion values somewhat higher than those indicated by weight loss measurements. However, since the samples of nickel used for the two techniques were of different thicknesses and origin, the discrepancy is readily explained.

At temperatures below 300°C corrosion becomes so slow that the weight loss method is no longer recommended because of the uncertainties involved in the removal of the sulfidic scale. The conductivity method gave an indication of the corrosion rate at a temperature as low as 210°C.

To determine whether any sulfur is dissolved by the metallic phase at lower temperatures, electrical conductivity-temperature curves were run on the nickel in the as-received condition, as well as on specimens which had been exposed to sulfur and the scale removed. The temperature coefficient was found to be unchanged after a 120-hr exposure to sulfur at 267°C. Thus, any appreciable solid solution of sulfur in nickel seems unlikely, at least at this temperature.

It was observed that, after the disappearance of the metallic nickel phase at about 445°C, additional, but slower, changes in the conductivity of the reaction product continued. To follow these changes, a small strip (10 × 2 × 0.025 mm) of A-nickel foil was fastened to the ends of four platinum wires and placed in boiling sulfur. Using the

¹ Manuscript received August 30, 1954. This paper was prepared for delivery before the Montreal Meeting, October 26 to 30, 1952.

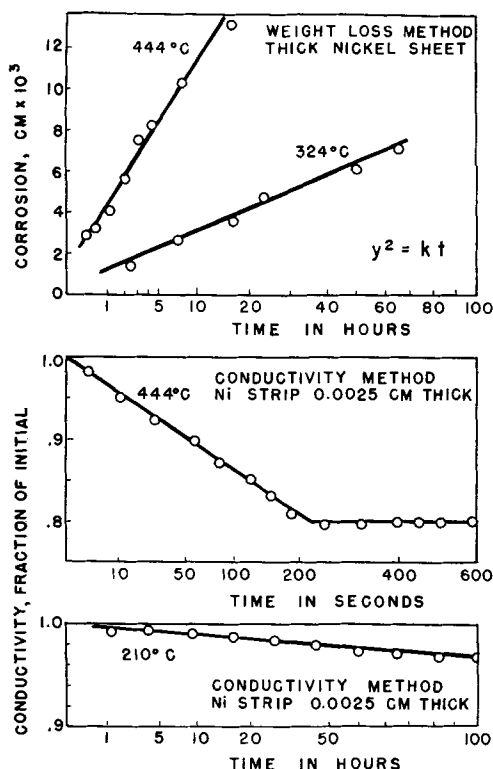
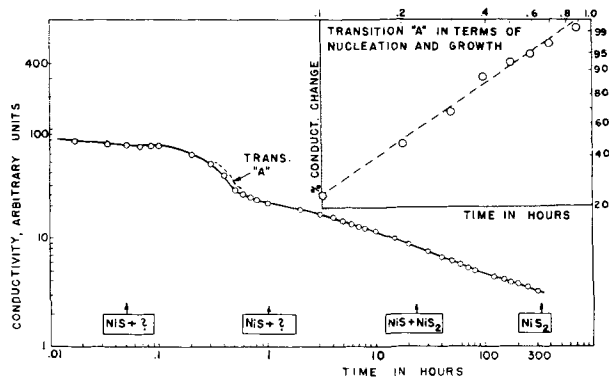


FIG. 1. Reaction of nickel with molten sulfur

FIG. 2. Changes in electrical conductivity during sulfuration of a nickel strip 0.0025 cm thick at 444°C .

platinum leads and an appropriate circuit, a record of the electrical resistance of the specimen was obtained. The record is replotted in log-log coordinates in Fig. 2. The conductivity of the specimen followed a complex curve as sulfuration proceeded. The temperature coefficient of the conductivity was of a metallic type for the early products of reaction. With advancing sulfuration, a semiconducting component with a negative temperature coefficient accumulated, offsetting the influence of the primary product; its effect was most important below approximately 360°C .

In order to make an x-ray study of the reaction products, strips of nickel were withdrawn from sulfur into a fast flowing stream of argon. Scaled

samples then were ground and were examined by powder x-ray methods. The patterns were compared with the Hanawalt-ASTM cards.

For metallographic examination, nickel strips 0.6 mm thick were reacted with sulfur kept at desired temperatures in thick Pyrex test tubes. After a completed exposure, the test tubes with specimens were rapidly cooled in a stream of air. Solid sulfur rods with the specimens embedded were cut and polished by the usual metallographic techniques. A 1-min etch in a mixture of freshly prepared 10% solutions of potassium cyanide and ammonium persulfate helped to differentiate the layers in the scale.

DISCUSSION

Kinetics of NiS Formation

From Fig. 1, the formation of nickel sulfides from nickel and molten sulfur follows the parabolic law between 210° and 444°C . Since a rate-limiting interface reaction seems unlikely in contact with molten sulfur, it appears safe to assume that the rate-limiting process is the diffusion through the sulfidic scale.

In the plot of $\log k$ vs. $1/T$ for the $\text{Ni} + \text{S}$ reaction (Fig. 3) there is a change in slope in the vicinity of 300°C . The high temperature activation energy (Arrhenius) above 325°C is approximately 20 kcal; below 300° it is higher and may be given tentatively as 53 kcal. This compares with 41 kcal for the $\text{Fe} + \text{S}$ reaction (1).

Farber and Ehrenberg (3) found parabolic kinetics in the sulfurization of nickel by 1% H_2S in CO or N_2 in the range 527° – 1003°C . However, in these mixtures the rate-limiting interface reaction apparently interfered, as indicated by the dependence of the rate on the nature of the gas (CO or N_2). Similar indications are found in the work of Hauffe and Pfeiffer (4, 5), who were concerned with the formation of NiS at 670°C at reduced pressure of

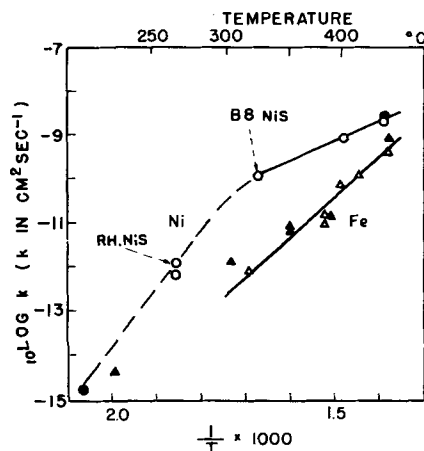


FIG. 3. Variation of $\text{Ni} + \text{S}$ and $\text{Fe} + \text{S}$ parabolic reaction rate constants with temperature. \circ \bullet Ni full: conductometric; \triangle \blacktriangle Fe open: gravimetric.

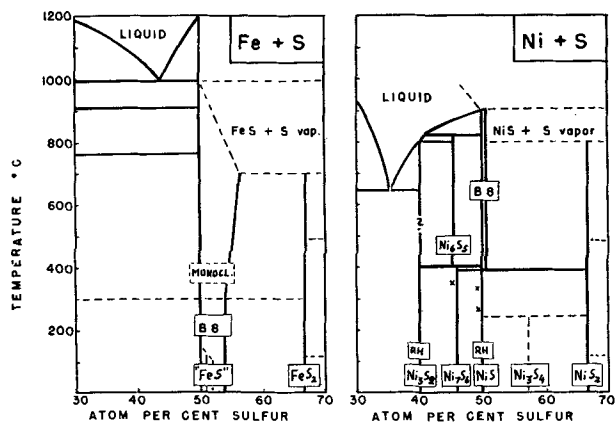


FIG. 4. Fe-S and Ni-S phase diagrams

sulfur vapor. On the other hand, Hauffe and Rahmel (5) found the parabolic law to hold for the formation of FeS at similar conditions in sulfur vapor. The activation energy for the latter case, as inferred from the plot in Hauffe's work, is not constant, however; its value approaches 23 kcal at 600°C, indicating that the reaction in sulfur vapor is not entirely diffusion controlled since in molten sulfur up to 445°C, where the surface reactions should be fast enough, E is 41 kcal.

It is best to discuss the kinetics on the basis of the nickel-sulfur and iron-sulfur phase diagrams, portions of which are reproduced in Fig. 4 [(6, 7), cf. also Ref. (18)]. As sulfurization proceeds, one should traverse the diagrams from left to right, with the final products being NiS₂ and FeS₂. As long as some metal is left, any or all intermediate sulfides may be present. The lowest sulfide would be next to the metal; the highest, however, not necessarily the NiS₂ and FeS₂, would be at the scale-sulfur interface. If interface reactions are disregarded, the thicknesses of individual sulfide layers would be proportional to diffusion rates in each sulfide (8, 9). If, in any of the sulfides, diffusion is very much slower than in others, this sulfide may be either missing or so disorganized as to escape detection in the x-ray or photomicrographic study. Furthermore, if surface reactions cannot be disregarded (4, 10), and the diffusion in one sulfide is sufficiently fast, the surface of such a sulfide, for example NiS, may be kept in such a condition by the rapid arrival of Ni ions that nucleation (11) of the next sulfide (NiS₂) may become impossible thermodynamically. Therefore, one does not necessarily expect to find in the scale all the sulfides listed in the phase diagrams if the metal-sulfur reaction is arrested while the metal is not fully consumed.

X-ray examination of the scale formed in the sulfurization of nickel showed the presence of the high temperature B8 form of NiS only from 340°C up. At 260°C, only the low temperature millerite form of

NiS was found in the scale. No other sulfides were detectable. A metallographic examination revealed, however, that the scales were composed of three irregular layerlike components in each case. The arrangement found at 260°C differed from that found at higher temperatures. It seems possible that all three layers were NiS, with differences in the texture and composition (within the solid solution range) alone. This sort of thing has been observed, for instance, in copper iodide formed on copper in iodine vapor (12). Of course, it also is possible that some of the components may be Ni₃S₂ or Ni₆S₅ or NiS₂ in amounts and forms not detectable in the x-ray patterns.

In the present work (cf. Fig. 2) formation of NiS₂ was shown to be very slow. Difficulties in preparing nickel by the reduction of Ni₃S₂ (13) point out that, similarly, diffusion in Ni₃S₂ should be relatively slow, at least in the Ni-rich region of the Ni₃S₂ phase field.

Regardless of these further details, the change in the nickel-sulfur reaction kinetics in the vicinity of 300°C seems to be explained adequately by the two forms of NiS. The B8 form has a somewhat wider solubility range (6) and, therefore, is "looser" in terms of the forms of lattice disorder (14).

This accounts for the lower activation energy for the reaction in the range of existence of the B8 form. It should be noted, that, under the existing dynamic conditions of scale growth, the B8 form is encountered in the sulfide formed at temperatures well below 400°C, although this generally is considered to be the transition temperature between B8 and millerite under equilibrium conditions.

In the iron-sulfur system, the corresponding transition is missing. Although the "monoclinic" phase reportedly has been found in minerals, it is questionable if it forms in laboratory conditions (15-18). Hence, the activation energy is essentially constant.

Formation of Sulfides Other than NiS

When a NiS strip prepared by exhaustive sulfurization of nickel was kept in molten sulfur at 445°C (Fig. 2) nickel disulfide, NiS₂, was formed, at a very slow rate, as the final reaction product. From the rate of formation, diffusion in NiS₂ is several thousand times slower than in NiS. In the iron-sulfur reaction, FeS₂ formed much slower than FeS, approximately by a factor of one thousand (1, 5).

It is interesting to note that the conversion from NiS to NiS₂ is preceded by an intermediate transition ("A," Fig. 2). While all nickel phase is consumed, with formation of NiS, within 2-3 min, the transition "A" begins only after 10 min. X-ray patterns of the product before and after the transition are identical. Formation of NiS₂ to any detectable amount begins

much later, after several hours. Thus, the nature of the phase formed in the transition "A" is not clear. It may be noted that this transition appears to proceed by a sequence of saturation, nucleation, and grain growth, as indicated by the insert in Fig. 2. In the coordinates used, the above type of kinetics would result in a straight line plot. It may be speculated that after the total consumption of Ni metal, at 3 min, saturation of the primary NiS with more sulfur proceeds for several minutes until some sort of recrystallization begins, accompanied by a decrease in the electrical conductivity.

By milling together proper proportions of vacuum-redistilled sulfur and hydrogen-reduced nickel powder in evacuated containers² at various temperatures, Ni₃S₂, (13, 19-24), Ni₆S₅, (13, 18), both forms of NiS, and NiS₂, (24, 25), all with characteristic x-ray patterns, were prepared without difficulty. The transition between the B8 form of NiS and millerite was placed between 360° and 430°C, in accordance with the data by Lundquist and Rosenqvist (6, 18).

Ni₇S₆, (6, 26), did not form. Instead, at 340°C (compare crossmark on Fig. 4) Ni₆S₅ formed. Ni₃S₄ also did not form, even on prolonged milling; in the corresponding mixture at 210°C only NiS₂ and millerite were found. After these unsuccessful attempts, corresponding mixtures were pressed into pellets with several hundred atmospheres pressure and kept in evacuated capsules at temperatures for several months. No new patterns appeared.

The failure to find Ni₃S₄ is in agreement with the results of De Jong and Willems and others (27, 18), who also were unable to prepare it synthetically; Ni₃S₄ has been reported only as a mineral (27, 28). Thus, it was concluded that either the earlier literature data on the existence of Ni₇S₆ and Ni₃S₄ are in error or, more probably at least for the Ni₃S₄, they form extremely slowly and play no part in the main nickel-sulfur reaction kinetics.

Continuity of Scale Growth

There was no indication that breaks, blisters, or failures of any other type would interrupt the smooth parabolic growth of nickel sulfide scale.

However, in the Fe + S reaction, thin films grew parabolically whereas, in thicker films, sudden accelerations occurred. Fig. 5 shows a replotted record for the reaction of steel with molten sulfur at 270°C, obtained on a small specimen continuously by using the electrical resistance method. The upper

² 500 ccm round bottom thick wall Pyrex centrifuge bottles, with a charge of ½ in. diameter porcelain balls. The milling crushes the scale on nickel or sulfide particles and accelerates the establishment of final equilibrium very considerably.

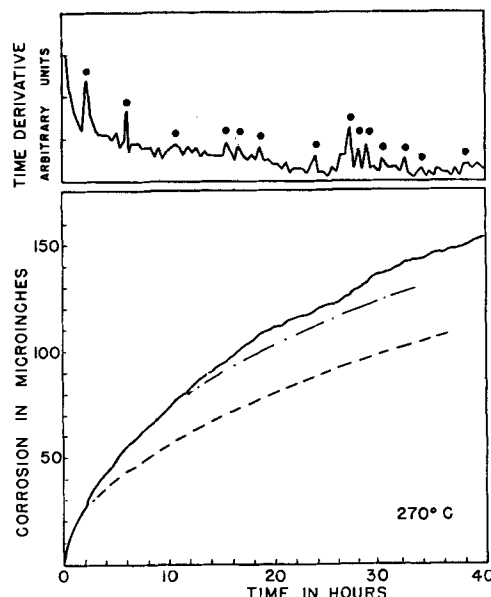


FIG. 5. Corrosion of steel in molten sulfur; microcataclysmic form of scale growth, $\bar{y} = kt^{n(t)}$.

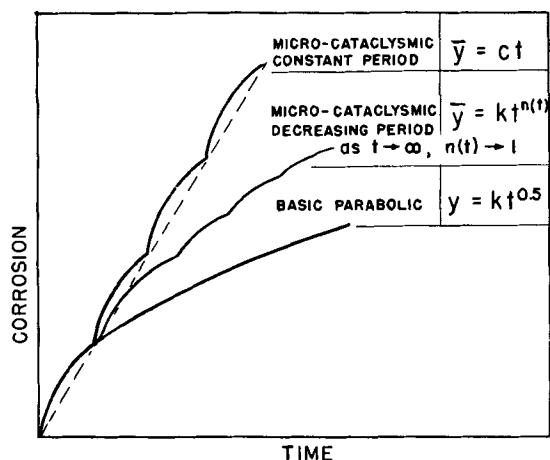


FIG. 6. Types of complex parabolic rate laws in scale growth.

plot represents differential rates of corrosion. The dots indicate periods of the fast accelerated growth where the acceleration was definitely larger than the resolution of measurements.

If the initial parabola were followed, as indicated by the broken curve, somewhat less reaction would have been expected. The experimental curve is never a parabola. The over-all shape is best described formally by the equation

$$\bar{y} = kt^{n(t)}$$

where \bar{y} is the average corrosion, disregarding small inflections and $n(t)$ is a time function. For the ideal parabolic law: $n(t) = \text{constant} = 0.5$. For the present case, $n(t)$ starts with 0.5 and keeps increasing.

At the same time, the empirical curve has a substructure of imperfect parabolas, each caused by a

localized failure in the scale such as cracking, peeling off, or open blistering followed by parabolic healing of the failure. The growth of an element of the scale is always basically parabolic, but is disturbed by ever-repeating microcataclysms. Related effects have been observed in the oxidation of metals (29, 30). It is proposed to denote such kinetics as the microcataclismic scale growth. Fig. 6 schematizes the types of curves.

Here two functional parameters describe the kinetics. One is the basic parabolic constant k . This is a fundamental property of the chemical system concerned, and depends on the diffusivity through the corrosion product. The other is an undefined long term function $n(t)$. This depends on volume change in reaction, adherence, and mechanical properties of the product. At the same time it is highly dependent on the operational factors such as curvature of the surface, vibration, temperature constancy, etc. In an extreme case $n(t) = 1$, and this simplification is frequently used in industrial corrosion considerations.

The primary cause of the continuously occurring failures in the FeS scale may be the change in volume of scale as the amount of sulfur increases. Alsen (31), and Hägg and Suckdorff (32) showed that FeS shrinks as it takes up more S. This would build up stresses in the sulfide scale and tend to initiate failures.

SUMMARY

Sulfurization of nickel by molten sulfur proceeds smoothly, without failures of the sulfidic scale. The reaction follows the parabolic law, but the activation energy changes in the vicinity of 300°C. The compound NiS was the only product found in the scale, and the change in the activation energy correlates with the change from the low temperature form of NiS to the high temperature form. In the sulfurization of iron the activation energy is constant, in agreement with absence of a phase transition. Higher sulfides such as NiS₂ and FeS₂ form much slower than the lower sulfides. It is doubtful if Ni₇S₆ and Ni₃S₄ exist. In the formation of FeS on steel in sulfur frequent sulfidic scale failures occur and the long-range kinetics are intermediate between the parabolic and linear. A term "microcataclismic" is proposed to describe such kinetics.

Any discussion of this paper will appear in a Discussion Section to be published in the June 1956 JOURNAL.

REFERENCES

1. A. DRAVNIKS, *Ind. Eng. Chem.*, **43**, 2897 (1951).
2. A. DRAVNIKS AND H. A. CATALDI, *Corrosion*, **10**, 224 (1954).
3. M. FARBER AND D. M. EHRENBERG, *This Journal*, **99**, 427 (1952).
4. K. HAUFFE AND H. PFEIFFER, *Z. Elektrochem.*, **56**, 390 (1952).
5. K. HAUFFE AND A. RAHMEL, *Z. physik. Chem.*, **199**, 152 (1951).
6. D. LUNDQUIST, *Arkiv Kemi, Mineral. Geol.*, **24A**, No. 21 (1947).
7. D. LUNDQUIST, *ibid.*, **24A**, No. 22 (1947).
8. W. JOST, "Diffusion u. Chem. Reaktion in festen Stoffen," p. 166, Verl. Steinkopff, Dresden (1937).
9. G. VALENSI, Pittsburgh International Conference on Surface Reactions, p. 156, Corrosion Publishing Co., Pittsburgh (1948).
10. W. J. MOORE, *This Journal*, **100**, 302 (1953).
11. A. DRAVNIKS, *J. Am. Chem. Soc.*, **72**, 3761 (1950).
12. A. DRAVNIKS AND H. J. McDONALD, *This Journal*, **94**, 139 (1948).
13. R. SCHENCK AND P. VON DER FORST, *Z. anorg. u. allgem. Chem.*, **241**, 145 (1939).
14. J. S. ANDERSON, *Proc. Roy. Soc. (London)*, **A185**, 69 (1946).
15. A. BYSTRÖM, *Arkiv Kemi, Mineral. Geol.*, **19B**, No. 8 (1945).
16. M. J. BUERGER, *Am. Mineralogist*, **32**, 411 (1947).
17. H. HARALDSEN, *Z. anorg. u. allgem. Chem.*, **231**, 78 (1937); *ibid.*, **246**, 169 (1941).
18. T. ROSENQVIST, *J. Iron Steel Inst.*, **176**, 37 (1954).
19. A. WESTGREN, *Z. anorg. u. allgem. Chem.*, **239**, 82 (1938).
20. V. A. VANYUKOV AND N. A. KISELEVA, *Yubil. Sbornik Nauch. Trudov. Inst. Tsvetnikh Met. i. Zolota*, **1939**, No. 7, 304.
21. A. N. VOL'SKI AND R. A. AGRACHEVA, *ibid.*, **1940**, No. 9, 5.
22. Y. I. GERASIMOV, N. I. PIRTKHALOV, AND V. U. STEPIN, *J. Gen. Chem. USSR*, **6**, 1736 (1936).
23. M. A. PEACOCK, *Univ. Toronto Studies, Geol. Ser. No. 51*, 59 (1946).
24. W. F. DE JONG AND H. W. V. WILLEMS, *Z. anorg. u. allgem. Chem.*, **160**, 185 (1927).
25. D. GHIRON, *Gazz. chim. ital.*, **68**, 559 (1938).
26. G. PEYRONEL AND E. PACILLI, *Atti reale accad. Italia, Rend. classe sci. fis. mat. e nat.*, **3**, 278 (1941).
27. W. F. DE JONG AND H. W. V. WILLEMS, *Z. anorg. u. allgem. Chem.*, **161**, 311 (1927).
28. G. NATTA AND L. PASSERINI, *Atti reale accad. Lincei*, **14**, 38 (1931).
29. B. W. DUNNINGTON, F. H. BECK, AND M. G. FONTANA, *Corrosion*, **8**, 2 (1952).
30. U. R. EVANS, *Trans. Electrochem. Soc.*, **91**, 547 (1947).
31. N. ALSÉN, *Geol. Fören. i. Förh.*, Stockholm **47**, 19 (1925).
32. G. HÄGG AND I. SUCKSDORFF, *Z. phys. Chem.*, **B22**, 444 (1933).

The Oxidation of Iron-Nickel Alloys¹

R. T. FOLEY

General Engineering Laboratory, General Electric Company, Schenectady, New York

AND

J. U. DRUCK AND R. E. FRYXELL

Transformer Laboratories Department, General Electric Company, Pittsfield, Massachusetts

ABSTRACT

The high temperature (600°–900°C) oxidation of an iron-nickel alloy containing 42% nickel has been studied with the objective of formulating the mechanism of reaction. The rate was determined gravimetrically. Reaction products were examined by means of metallographic and electron diffraction techniques, as well as chemical analyses after stripping.

The temperature dependence of the parabolic oxidation rate constant follows the Arrhenius equation with the parameters dependent on the method of surface preparation. The oxide film, upon cooling, possesses a two-phase structure consisting of a nickel ferrite (next to the alloy) and Fe₂O₃. Differences in activation energies and oxidation rates are explained on the basis of diffusion through ferrite structures of a varying percentage of nickel.

INTRODUCTION

Iron and nickel form a continuous series of substitutional solid solution alloys, with both components oxidizable. While the kinetics of oxidation for alloys up to 30% nickel has been studied (1), no systematic investigation of alloys of about equal percentage of nickel and iron has been made in the 600°–900°C temperature range. Alloys of this type are used in making glass-to-metal seals so that a clear understanding of the kinetics and mechanism of oxidation is important in the electrical and electronic industry.

The most extensive study of the oxidation of iron-nickel alloys was made by Bénard and Moreau (1) who investigated the behavior of alloys containing 5, 10, 20, 30% Ni. The films developed on the alloys after oxidation and cooling to room temperature consisted of Fe₂O₃, Fe₃O₄, and a mixed layer of FeO and Fe₃O₄ (proceeding inward to the metal from the atmosphere). Koh and Caugherty (2) used an x-ray fluorescent technique to study the oxide layer formed on an alloy of 50 Ni–50 Fe composition. A spinel of lattice parameter $a = 8.36 \text{ \AA}$ was identified along with weak lines for Fe₂O₃. Hickman and Gulbransen (3) followed the oxidation of 49 Fe, 49 Ni, 2 Mn alloy in purified O₂ at 1 mm pressure and from 300°–700°C by an electron diffraction method, the observation being made at temperature. A spinel with lattice parameter of 8.42–8.43 Å was observed. This was assigned to Fe₃O₄ rather than to NiFe₂O₄ because of the slightly higher observed value.

The purpose of the present work was to study the

kinetics of the oxidation of the iron-nickel alloy containing 42% Ni, and to formulate a mechanism of oxidation from the reaction rate and the nature of the surface layers. It was also desired to learn the influence of surface preparation on the kinetics and mechanism, with several "practical" surface preparations being included in the investigation.

EXPERIMENTAL

Metal preparation.—Strips of the iron-nickel alloy with an apparent surface area of 25.8 cm² were cut from a band which had been finally cold finished to a thickness of 0.051 cm. These strips were annealed and degassed in dry hydrogen (dew point = –50°F) for 2 hr at 1125°C, after which they were cooled in H₂ to about 75°C.

The chemical analysis of the alloy was: Fe = 57.4%; Ni = 41.8%; Si = 0.13%; Mn = 0.53%; C = 0.001%; Al = 0.05%; Co = 0.06%.

Various groups of samples received four different surface preparations before oxidation:

1. "As-rolled"—after annealing in hydrogen as described above, samples were swabbed with benzene and acetone, and dried before weighing. While these samples had a bright appearance, electron diffraction examination showed the presence, in faint but sharp pattern, of Fe₂O₃.

2. "Chemically cleaned"—the strip was pickled at 90°C for 2 min in an acid mixture made by dissolving one part by volume H₂SO₄ (95%), one part of HNO₃ (70%), and one part of HCl (37%) in nine parts of water. It was thoroughly rinsed, dipped in a mixture of two parts of H₂SO₄ and one of HNO₃, and again rinsed thoroughly. Samples were allowed

¹ Manuscript received December 7, 1954.

to stand for about 1 hr in sodium cyanide solution (5 g/100 ml of solution) to neutralize any residual acid and again rinsed thoroughly. Finally, samples were rinsed in acetone and allowed to stand in acetone until used. Electron diffraction examination of this surface showed only the pattern corresponding to the iron-nickel alloy.

3. "Sand-blasted"—the as-rolled and annealed strip was sand-blasted with a sand characterized by a particle size range (90%) from 0.3 to 0.6 mm (diameters). Electron diffraction examination revealed the patterns for Fe_2O_3 , and (possibly) Ni and Fe. These patterns were faint but sharp. No evidence of the sand remaining on the surface was seen in these patterns although analyses made after oxidation warranted the conclusion that the abrasive was embedded in the surface.

4. "Polished"—the annealed as-rolled strip was polished successively with Behr-Manning papers #240, #600, and #3/0, swabbed with benzene and acetone, and stored in acetone until used. Electron diffraction examination of a sample so polished and exposed to laboratory air gave the pattern of NiO. If the final polishing was carried out under kerosene, and if these two polishings were done with 3/0 and 4/0 paper successively, then only the Ni pattern was obtained.

It was apparent from the preliminary electron diffraction examination of the surface that the method of preparation affected not only the real surface area, but also the actual composition of the surface that would be presented to the oxidizing atmosphere.

Oxidation studies.—Oxidations were carried out in a resistance wire-wound furnace with a static air atmosphere. In most of the experiments, the small panels were placed directly on a nichrome hook which was attached to a pedestal in the hot zone. Thus, it was only required to bring the thin metal strip itself up to temperature. Oxidized samples were cooled in a desiccator before weighing. Hand polished samples blistered upon oxidation for times longer than a few minutes. These samples were weighed, oxidized, and transferred in crucibles.

Oxidation tests, with samples of the four surface preparations described above, were made at 600°, 700°, 800°, and 900°C for various time intervals up to 60 min. The temperature was controlled to $\pm 2^\circ\text{C}$. Duplicate determinations were made, and, if the precision was poor, further checks.

Chemical analyses.—Oxide layers developed on the alloy by the various treatments were stripped from the metal substrate. The method used involved preferential solution of the metal in a bromine-methyl acetate solvent. This solvent (6 ml bromine in 30 ml methyl acetate) has been used for the isolation of

inclusions in various ferrous alloys (4). Residues were filtered off, washed with methyl acetate, dried, and weighed. These were dissolved in 6*N* H_2SO_4 or 6*N* HCl.

The composition of the resultant solutions was determined spectrophotometrically, the nickel in the form of the dimethyl glyoxime complex and the iron as the orthophenanthroline complex. For each analysis the scale was removed and weighed, the iron and nickel separately determined, and the percentage of nickel of total metal analyzed calculated.

Electron diffraction examination of films.—Electron diffraction analyses by the reflection technique were made with a General Electric electron diffraction instrument. An accelerating voltage of 45kv and a filament current of 30–40 μa was used. The exposure varied, being of a duration of as high as 30 sec for certain samples. At least four patterns were obtained for each sample.

Metallographic examination of films.—Several representative oxidized metal strips were examined metallographically by standard techniques. For mounting several samples a resin (Selectron 5003, manufactured by the Pittsburgh Plate Glass Company) which polymerized at low temperature—about 45°C—was employed to preserve the fragile film. In addition, a few samples were studied by the taper section technique (5) which allows the interface to be magnified by a factor of 10X the normal magnification.

Treatment of data.—Examination of oxidation data indicated that the reaction could be represented mathematically by a parabolic equation as

$$(\Delta m)^2 = b + k_p t \quad (\text{I})$$

where, m = the gain in weight in g/cm² of a sample oxidized for t seconds; k_p is the parabolic rate constant expressed in g²cm⁻⁴sec⁻¹; b is a constant (g²cm⁻⁴).

The temperature dependence of the reaction was represented by the Arrhenius-type equation

$$k_p = A e^{-Q/RT} \quad (\text{II})$$

wherein A is a constant (sometimes called the action constant) and Q is another constant (called the activation energy). The activation energy and action constant were determined for each of the four surface preparations and compared with literature values for the oxidation of nickel and iron.

RESULTS

Kinetics of Reaction

Considering the fact that the plot of the data follows the well-known parabolic relation, it is not

TABLE I. Parameters of parabolic equation expressing kinetic data

Temp, °C	k_p ($g^2cm^{-4}sec^{-1}$) ($\times 10^{12}$)	b (g^2cm^{-4}) $\times 10^6$
"As-rolled" surface		
600	1.30	0.00
700	14.7	0.00
800	113	0.00
900	870	0.00
"Sand-blasted" surface		
600	20.7	0.0115
700	135	0.044
800	603	0.110
900	2430	0.040
"Polished" surface		
600	22.5	0.010
700	148	0.025
800	361	0.13
900	933	0.16
"Chemically-cleaned" surface		
600	0.95	0.00032
700	7.90	0.0038
800	45.3	0.030
900	367	0.00

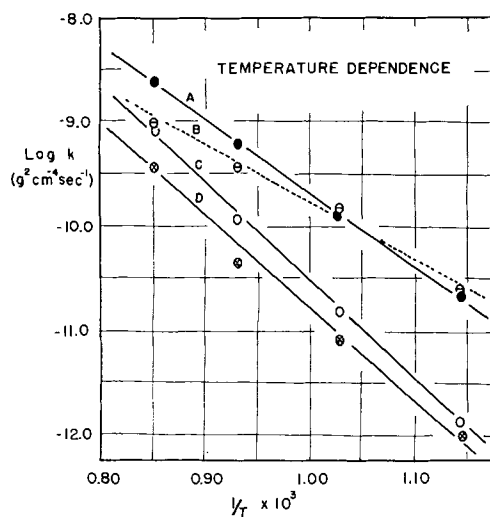


Fig. 1. Temperature dependence of the oxidation rate of the 42% nickel-iron alloy. A = sand-blasted surface; B = polished surface; C = as-rolled surface; D = chemically cleaned surface.

necessary to give these graphs. The equations may be constructed if the values of k_p and b are known. These are given in Table I.

The temperature dependence of the reaction may be concisely shown if $\log k_p$ is plotted against $1/T$. This plot is made in Fig. 1. From this the constants in equation (II) were calculated and are given in Table II.

The value of k_p may be taken as a quantitative measure of the oxidation rate. As evidenced in Table I, the oxidation rate of the iron-nickel alloy varies considerably in a manner difficult to explain by the expected surface area relationships. The "chemically cleaned" sample has the lowest rate. Ratios of the other rates to that of the rate of the "chemically cleaned" surface taken as unity are:

Chemically cleaned	As-rolled	Sand-blasted	Polished
1	2	7-22	2.5-24

The as-rolled surface oxidizes at a rate about double that of the chemically cleaned surface and this is fairly consistent varying from 1.4 to 2.5 over the temperature range investigated. However, from a surface area relationship, one would expect the opposite to hold because it is known that an etched surface has a much greater surface area than a rolled surface. Electron diffraction examination revealed that the as-rolled, bright, annealed surface, after exposure to laboratory air, was oxidized, yielding Fe_2O_3 as a reaction product. There was also a small amount of Fe in the surface which may, in itself, account for the greater rate. The sand-blasted surface oxidized at a much greater rate than the chemically cleaned surface, but the ratios between the two rates varied with temperature. At 600°C the ratio of rates was 22 to 1, while at 900°C it was 7 to 1. The increase in surface area may only account for part of this increase, for on this basis, one would expect the factor to remain about the same over the whole temperature range. Some of the sand used in abrading the steel, while not found by the electron diffraction examination of the surface prior to oxidation, was found in the oxide films by chemical analysis. It appears likely that the reason that the factor dropped with temperature may well be explained by the final disposition of the abrasive material. Oxidation measurements made with polished surfaces lacked precision. At 600° and 700° the rates were similar to those obtained with the sand-blasted surface, but at 800° and 900° the rates are considerably lower.

Because of the erratic nature of the results obtained with polished surfaces, the A and Q values in

TABLE II. Temperature dependence of reaction

Surface	A (action constant) ($g^2cm^{-4}sec^{-1}$)	Q (activation energy) (cal/gmole)
"As-rolled".....	0.129	44,200
"Sand-blasted".....	0.00276	32,600
"Polished".....	$7.0 \times 10^{-5}(?)$	25,300(?)
"Chemically cleaned".....	0.0124	40,800
Iron.....	0.37	33,000 (6)
Nickel.....	0.013-0.151	41,200-46,500(7, 8)

the temperature dependence equation for the reaction are reported as questionable in Table II.

From these results, it is very clear that not only time and temperature but also surface preparation must be exactly prescribed if one is to get a reproducible oxide layer.

Chemical Analyses

Representative results of chemical analyses made on oxide films stripped from samples which were oxidized after chemical cleaning are given as follows.

Oxidation temp., °C	Time, min	Weight gain, mg/cm ²	% Ni
600	5.0	0.0465	31.2
800	1.0	0.112	31.8
800	10.0	0.392	17.1

The per cent Ni reported is from a total weight of iron plus nickel found in the film. It is apparent that the first formed film is rich in nickel.

Further stripping and analyses were made with samples that had been sand-blasted before oxidation.

Oxidation temp., °C	Time, min	Weight gain, mg/cm ²	% Ni
800	0.5	0.209	13.3
700	10	0.392	6.3
800	30	1.05	5.6

These three tests were taken as representative of 15 analyses. Here, too, there is a greater percentage of nickel in the thin films. The nickel content decreases as the film grows and reaches a fairly constant value of 5-6% of the metal content in the film. However, the gradation is considerably less marked than in the films developed on chemically cleaned alloys. Considering that the 5-6% represents an average value for the film which is high in nickel near the metal-oxide interface, it is evident that nickel is either present in low concentration or absent from these layers removed from the interface. Strippings were carried out in a quantitative manner and it was observed that there was present a fair amount of acid-insoluble material, identified as the sand (quartz) with which the samples had been abraded. This sand has been embedded in the metal, but was so located beneath the surface that it had not been observed in the preliminary electron diffraction examination of these sand-blasted samples.

Electron Diffraction Analyses

In considering the results of the electron diffraction experiments, certain observations should be borne in mind. The formation of nickel ferrite (NiFe₂O₄) or iron ferrite (Fe₃O₄) seems possible. These ferrites crystallize in the spinel (face-centered cubic) form and have similar lattice constants, i.e., NiFe₂O₄ has an $a = 8.34$ and Fe₃O₄ an $a = 8.37$. The electron

TABLE III. Electron diffraction analyses of oxide films, surfaces chemically cleaned before oxidation

Temperature oxidized, °C	Time oxidized, min	Weight gained during oxidation, mg/cm ²	Patterns found
600	3	0.0078	Fe ₂ O ₃ , ferrite
600	5	0.0194	Fe ₂ O ₃ , ferrite
600	40	0.284	Fe ₂ O ₃ , ferrite, Ni(?)
700	7	0.0621	Fe ₂ O ₃ , NiO, Ni
700	30	0.135	Fe ₂ O ₃ , ferrite, Ni
700	1	0.0078	Fe ₂ O ₃ , ferrite
800	0.5	0.0155	Fe ₂ O ₃ , ferrite
800	3	0.135	Fe ₂ O ₃ , ferrite, Ni

TABLE IV. Electron diffraction analyses of oxide films, surfaces sand blasted before oxidation

Temperature oxidized, °C	Time oxidized, min	Weight gained during oxidation, mg/cm ²	Patterns found
600	20	0.213	Fe ₂ O ₃ , Fe, NiO
700	2.5	0.209	Fe ₂ O ₃ , ferrite
700	10.0	0.392	Fe ₂ O ₃ , ferrite, Fe, Ni
700	60	0.695	Fe ₂ O ₃ , ferrite, quartz
800	0.5	0.213	Fe ₂ O ₃ , ferrite, quartz
800	20	0.913	Fe ₂ O ₃ , ferrite, quartz
800	30	1.19	Fe ₂ O ₃ , ferrite, quartz
900	40	2.49	Fe ₂ O ₃ , ferrite, quartz

diffraction reflection method of determining lattice constants is not sufficiently accurate to differentiate between these two structures although, as discussed below, one may speculate on the existence of one structure or the other if several lines of evidence are available. Below, the term "ferrite" includes both structures.

In the following descriptions the constituent reported first was present with certainty. Other constituents for which there was evidence are also reported. The depth of penetration of the electron beam (200-300 Å) is such that, in a thick oxide layer of duplex structure, the outer layer would give the most pronounced pattern even though it might well be present in lesser amount. The first series analyzed reported in Table III had been chemically cleaned before oxidation. A second series was run with samples that had been sand-blasted prior to oxidation. The observations are reported in Table IV.

The main products of oxidation, viewed after the samples cooled to room temperature, were Fe₂O₃ and ferrite. In the thin films on the chemically cleaned samples these were the only compounds found. However, Ni was found when the films had increased in thickness. The sand-blasting technique used in preparing the second series of samples allowed quartz to be found in the films. Generally speaking, the products were Fe₂O₃ and ferrite.

A further sample was taken as-rolled and oxidized:

Oxidation temp, °C	Oxidation time, min	Weight gained, mg/cm ²	Patterns
700	40	0.194	Ferrite, Fe ₂ O ₃ (both distorted)

From the electron diffraction study, it may be concluded that alpha-Fe₂O₃ and a ferrite are consistently obtained upon oxidation of this alloy.

Metallographic examination of films.—The microscopic examination of the oxidized alloy strips (Fig. 2 and 3) demonstrate that two phases are present in stratified layers. The layer closest to the alloy is identified as the ferrite, while the lighter phase further removed from the alloy is alpha-Fe₂O₃. The taper section mount made of an oxidized sand-blasted surface accentuates the two-phase character of the film. This high magnification gives ample evidence of the high probability of entrapping metal in stripping the oxide film.

Some internal oxidation was seen in all of the metallographic sections at high magnification. However, the amount was not believed to be an important factor in the kinetics. The photomicrographs exhibited are of sand-blasted surfaces. The other surfaces appeared to oxidize in a manner that gave slightly more uniform layers but there was no qualitative difference in the oxide layers formed. In the very thin films the major portion of the oxide was ferrite. When cracking occurred within the film,



FIG. 2. Oxide film on iron-nickel alloy prepared by sand blasting. Oxidized for 60 min at 700°C. 2000× before reduction for publication.



FIG. 3. Oxide film on iron-nickel alloy prepared by sand blasting. Oxidized for 60 min at 700°C. Magnification in vertical direction, 15,000×, in horizontal direction, 1500×, before reduction for publication.

it did so in the ferrite phase indicating that that phase was in a stressed condition.

DISCUSSION

Electron diffraction analyses of these films made after cooling from the reaction temperature yielded evidence for both a ferrite and Fe₂O₃. Thermodynamically, Fe₂O₃ is stable at these temperatures (9). Gulbransen and Hickman (10) found that, as the oxide film which was grown on iron increased in thickness, the compound alpha-Fe₂O₃ was stable at higher and higher temperatures.

It is postulated that the ferrite is NiFe₂O₄ rather than Fe₃O₄. Ni in high concentration was found by chemical analyses of the stripped film. Also, calculation from many samples indicates a lattice constant $a = 8.33 \text{ \AA}$. Although literature values for NiFe₂O₄ are 8.34 Å and for Fe₃O₄, 8.37–8.40 Å, Hickman and Gulbransen (3) report 8.42–8.43 Å for Fe₃O₄ when this compound is grown on an iron surface during oxidation. The a value from the authors' experiments agrees well with that reported by Koh and Caugherty (8.36 Å) but not with that of Hickman and Gulbransen (8.43 Å). There is no obvious explanation for these different structures other than the limited accuracy of the experimental technique.

The rate-controlling factor in this reaction is diffusion through this nickel ferrite layer. In cases where the reaction rate is low, a high concentration of nickel was found in the film next to the basis metal. Diffusion rates in spinels have been observed to be lower than in the parent oxide (11). Also, Quarrell has indicated that spinels stabilized with Ni or Cr are more protective than Fe₃O₄ (12). The existence of a continuous series of spinels with gradations of nickel content is in accord with what is known of the chemical composition of these compounds as Ni⁺⁺ or Fe⁺⁺ can exist in substitutional solid solution in a spinel whose nominal formula is NiO·Fe₂O₃.

The sand-blasting preparation appears to hinder formation of a ferrite as rich in nickel as that formed on the chemically clean surface. The early nucleation of NiFe₂O₄ may be adversely influenced by the distorted structure, the presence of Fe₂O₃, or the presence of the quartz.

Results with a polished surface were lacking in precision. The calculated activation energy is not believed to be significant, insofar as a particular mechanism is concerned. Rather, it appears that at low temperatures a mechanism similar to that of the sand-blasted surface appears to be followed while at higher temperature that of the as-rolled surface.

Thus, it may be concluded that the method of surface preparation influences the composition of

the oxide formed and consequently has a major bearing on the rate of oxidation. Quarrell observed that either Fe_2O_3 or Fe_3O_4 could be formed by heating iron at 400°C depending on the type of abrasive (13). The favoring of the nucleation and growth of one oxide over another appears to be parallel with the case described here.

ACKNOWLEDGMENTS

The authors are pleased to acknowledge the preparation of the photomicrographs by Mr. W. L. Chu and Miss M. A. McGregor.

Any discussion of this paper will appear in a Discussion Section to be published in the June 1956 JOURNAL.

REFERENCES

1. J. BÉNARD AND J. MOREAU, *Rev. mét.*, **47**, 317 (1950).
2. P. K. KOH AND B. CAUGHERTY, *J. Appl. Phys.*, **23**, 427 (1952).
3. J. W. HICKMAN AND E. H. GULBRANSEN, *Trans. Am. Inst. Mining Met. Engrs.*, **171**, 344 (1947).
4. H. F. BEEGHLY, *Anal. Chem.*, **24**, 1095 (1952).
5. A. J. W. MOORE, *Metallurgia*, **38**, 71 (1948).
6. J. K. STANLEY, J. VON HOENE, AND R. T. HUNTOON, *Trans. Am. Soc. Metals*, **43**, 426 (1951).
7. O. KUBASCHEWSKI AND B. E. HOPKINS, "Oxidation of Metals and Alloys," p. 69, Academic Press, New York (1953).
8. E. A. GULBRANSEN AND K. F. ANDREW, *This Journal*, **101**, 128 (1954).
9. M. H. DAVIES, M. T. SIMNAD, AND C. E. BIRCHENALL, *J. Metals*, **3**, 889 (1951).
10. E. A. GULBRANSEN AND J. W. HICKMAN, *Trans. Am. Inst. Mining Met. Engrs.*, **171**, 306 (1947).
11. H. M. McCULLOUGH, M. G. FONTANA, AND F. H. BECK, *Trans. Am. Soc. Metals*, **43**, 404 (1951).
12. A. G. QUARRELL, discussion of paper by E. A. Gulbransen and J. W. Hickman, *Trans. Am. Inst. Mining Met. Engrs.*, **171**, 341 (1947).
13. R. JACKSON AND A. G. QUARRELL, *Iron Steel Inst., Spec. Rep. No. 24*, 65, (1939).

High Temperature Corrosion Rates of Several Metals with Nitric Oxide¹

MILTON FARBER,² ALFRED J. DARNELL,³ AND DONALD M. EHRENBERG

Jet Propulsion Laboratory, California Institute of Technology, Pasadena, California

ABSTRACT

An experimental study has been made of the high temperature corrosion rates of various metal filaments with nitric oxide. Corrosion rates have been determined for iron, tantalum, tungsten, molybdenum, nickel, copper, silver, and the alloys Inconel,⁴ and stainless steel. The temperature range included temperatures from 800° to 2000°K. The metals in order of decreasing corrosion resistance are Inconel, 25-20 stainless steel, molybdenum, nickel, tantalum, 18-8 stainless steel, tungsten, iron, and copper.

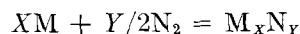
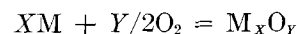
INTRODUCTION

Concerning reactions of metals with NO, some previous work of a qualitative nature has been reported. Adhikary (1) found that gold, silver, and iron were oxidized at temperatures above 650°K when NO and H₂ were passed over the heated metal. The NO was reduced to NH₃. Schröder and Tamman (2) studied the reactions of NO on various metals over a wide range of pressures and temperatures. They measured the thickness of the oxide coating on metal foils and found that the oxidation of copper with NO began at temperatures above 100°C. Also, they found that the corrosion rate was similar to that of Cu and O₂; however, upon increasing the pressure the reaction rate began to decrease. Reaction rates of iron in NO at temperatures of 600° to 700°K were observed by Schröder and Tamman to be similar to those of Fe and O₂. They found that, when Ni was subjected to NO at temperatures from 800°-1000°K, initially an impermeable film was formed which later became porous, and the reaction rate was accelerated. DeVoogd and Tadema (3) studied the resistance of different metals in flue gases containing NO.

Wise and Frech (4) made a study of the decomposition of NO in a quartz vessel over a wide temperature range. They obtained two expressions for the specific reaction-rate constant for this process. At temperatures above 1500°K a homogeneous mechanism prevails which has an activation energy of

78.2 kcal, whereas below 1000°K a heterogeneous mechanism applies which has an activation energy of 21.4 kcal. At temperatures between 1000° and 1500°K both heterogeneous and homogeneous mechanisms contribute to the decomposition rate of NO. It is interesting to note that, since the corrosion mechanism is heterogeneous, it would be expected that only the lower activation energy would be significant. This lower value is consistent with the observation that in all but one reaction (*see* Ta-NO under Results) the observed activation energies were less than 78 kcal/mole.

In studying the reaction of a metal with NO it is necessary to consider the surface of the metal and its temperature and to know whether the gas is reacting in its pure state or in a decomposed form. The gas-metal reaction involved is the formation of an oxide, nitride, or both.



Heat liberated upon the formation of the metal oxides from the elements varies from 7 kcal/mole for Ag₂O to 500 kcal/mole for Ta₂O₅. Thus, a consideration of the heat of formation of the metal oxide (or nitride) with thermal data for decomposition may aid in interpreting a particular mechanism.

EXPERIMENTAL PROCEDURE

The authors have previously employed this method for measuring the corrosion rates of various metals with H₂S and SO₂ (5) and only a brief description of the apparatus will be given here. Garner, Gray, and Stone (6) studied the reaction rate of copper with oxygen by measuring the increase in resistance of a copper film which was plated on the walls of a glass bulb. Wilson (7) and Hudson (8) studied corrosion rates by measuring the change in electrical conductivity of flat metal strips. The

¹ Manuscript received September 17, 1954. This paper presents the results of one phase of research carried out at the Jet Propulsion Laboratory under Contract No. DA-04-495-Ord 18, sponsored by the Department of the Army, Ordnance Corps.

² Present address: Aerojet-General Corporation, Azusa, California.

³ Present address: General Petroleum Corporation, Los Angeles, California.

⁴ Inconel is registered trade mark of the International Nickel Company.

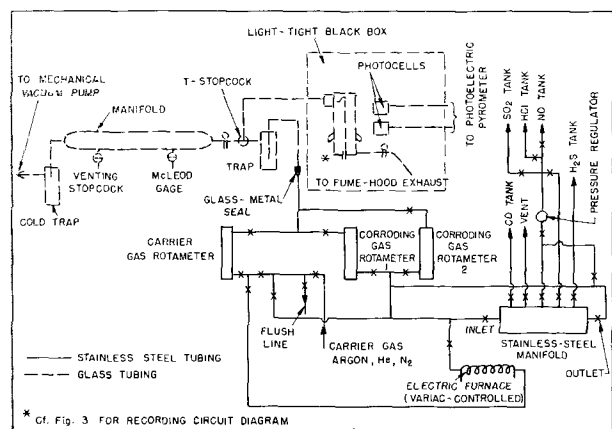


Figure 1. Flow diagram of corrosion apparatus

FIG. 1. Flow diagram of corrosion apparatus

method employed here and described in detail earlier (5) is concerned with the measurement of the change in resistance of a metal filament (hot wire) of 0.010 in. diameter in a corrosive medium. Since the corrosion rate is obtained directly from the resistance change, a recording mechanism is necessary to indicate the current and voltage across the filaments. Fig. 1 describes the arrangement of the equipment used to conduct corrosion rate experiments.

An exhaust manifold connected directly to a vacuum pump is used to evacuate the reaction bulb which is mounted in a light-tight box. The vacuum is measured by means of a McLeod gauge. The bulb is filled to atmospheric pressure with an inert carrier gas from the gas manifold, shown in Fig. 1, to which steady flow rates (as measured with rotameters) are maintained by use of a series of needle valves before and after the flowmeters. These rates are of the order of 100 cc/min of gas. The incoming inert gas (argon or N_2) is passed through an electrically heated tube filled with copper turnings to remove traces of oxygen impurities that may be present in the commercially purchased gas cylinders. After the bulb has been filled to atmospheric pressure, the filament is heated electrically to the desired temperature. The temperature is maintained by adjusting the resistance controls with the aid of either a photoelectric or an optical pyrometer, calibrated with the use of standard resistance data for tungsten filaments. The operation of the photoelectric pyrometer and the equations involved were given in detail earlier (5).

The corroding gas is metered through a separate rotameter into a manifold (from 1-10% of the total gas), together with the carrier, where mixing occurs for a period varying from 30 to 100 sec before the mixture enters the bulb. As the reaction takes place, the current and voltage are recorded simultaneously. Temperature is maintained by holding the response

ratio of the two photocells constant or by means of an optical pyrometer. The duration of most runs was 220 or 240 sec. All plots of A/A^0 vs. time (sec) were nearly linear (not shown), and the values of k in Table I are the slopes of these lines.

In order to obtain uniform corrosion of the wire, it is necessary to use filaments which have been accurately machine-drawn. Thus, hot spots can be eliminated, and consistent burnout times obtained, justifying the resistance method for measuring corrosion rates.

THEORY

The corrosion rate is directly proportional to the resistance change since resistance R is a function of the length and diameter of the filament

$$R = \rho l/A$$

where ρ = resistivity of wire, l = length of wire, and A = cross-sectional area of wire.

Since the specific resistivity ρ is a function of temperature only, for a constant length filament the rate of change of resistance with time at constant temperature is proportional to the rate of change of area. If R_0 is the initial resistance and R is the resistance after time t , then

$$R_0/R = A_0/A$$

or

$$\frac{R - R_0}{R} = \frac{A_0 - A}{A_0}$$

which leads to

$$\Delta R/R = -\Delta A/A_0$$

Three different rate laws have been proposed for corrosion processes: the parabolic rate law of Pilling and Bedworth (9) and the rectilinear and logarithmic rate laws (10, 11). For a cylindrical wire of initial cross-sectional area A_0 and radius r_0 , the thickness of the film dy for initial corrosion would be proportional to the decrease in radius r of the wire with time t , as shown in Fig. 2.

In order to obtain an expression for the parabolic rate law for cylindrical wires it is necessary to set up the rate law in differential form for the wire. For an initial radius of r_0 the parabolic rate law in differential form is

$$-dr/dt = k/(r_0 - r)$$

which integrates to

$$r^2 - 2r_0r + r_0^2 = 2kt$$

and in terms of the cross-sectional area becomes

$$A/A_0 = 1 - 2\sqrt{\frac{2\pi kt}{A_0}} + \frac{2\pi kt}{A_0}$$

(parabolic rate law)

TABLE I. Initial corrosion rates for several metals with nitric oxide

Gas mixture: 95% Argon and 5% NO			
Metal	T (°K)	k (% area loss/sec)	
Iron	970	0.0165	
	1040	0.0215	
	1100	0.0270	
	1154	0.0345	
	1167	0.0390	
	1176	0.0420	
	1187	0.0440	
	1204	0.0505	
	Tantalum	1468	0.0065
		1500	0.0125
1516		0.0110	
1532		0.0305	
1637		0.0485	
1730		0.0760	
Tungsten		1381	0.010
		1431	0.020
		1454	0.037
		1525	0.070
	1548	0.096	
	1602	0.085	
	1636	0.110	
	1676	0.100	
	1767	0.120	
	1825	0.170	
Molybdenum	1893	0.170	
	1429	0.0036	
	1445	0.0076	
	1455	0.0031	
	1467	0.0075	
	1493	0.0086	
	1571	0.0306	
	1584	0.0214	
	1637	0.0347	
	1699	0.0443	
1723	0.0461		
1774	0.0880		
1808	0.132		
1842	0.132		
Nickel	1093	0.00134	
	1104	0.00267	
	1123	0.00467	
	1154	0.00800	
	1189	0.0153	
	1212	0.0107	
	1239	0.0260	
	1255	0.0167	
	1288	0.0260	
	1297	0.0180	
	1308	0.0305	
	1333	0.0387	
	1355	0.0120	
	1383	0.0153	
	1415	0.0153	
	1464	0.0093	
	1474	0.0073	
	1520	0.0147	
1536	0.0067		
1593	0.0060		
1649	0.0053		
1651	0.0060		

TABLE I.—Continued

Metal	T (°K)	k (% area loss/sec.)
Copper	1113	0.0250
	1113	0.0255
	1160	0.0300
	1167	0.0280
	1208	0.0340
	1209	0.0370
	1247	0.0380
	1251	0.0400
Stainless steel 25-20	1271	0.0430
	1538	0.001
	1558	0.002
Stainless steel 18-8	1453	0.016
	1503	0.023

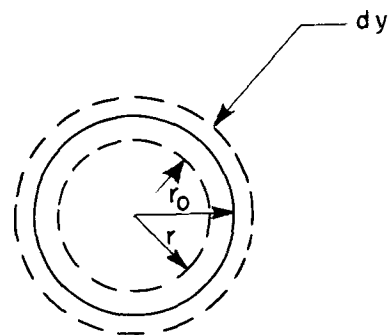


FIG. 2. Cross-sectional diagram of corrosion film on a wire.

Since the formation of oxide film is directly related to the loss in diameter of a cylindrical wire, the rectilinear rate law can be expressed in terms of diminishing radius as

$$-dr/dt = k$$

which integrates to

$$r_0 - r = kt$$

and in terms of cross-sectional area becomes

$$A/A_0 = 1 - 2(\pi/A_0)^{1/2} kt + \pi/A_0 k^2 t^2$$

(rectilinear rate law)

The equation for the logarithmic rate law can be expressed for cylindrical wires as

$$-dr/dt = ke^{-(r_0-r)}$$

which upon integrating and expressing in logarithmic form yields

$$(r_0 - r) = \ln(1 + kt)$$

This expression in terms of the cross-sectional area becomes

$$A/A_0 = 1 - 2(\pi/A_0)^{1/2} \ln(1 + kt) + \pi/A_0 \ln(1 + kt)^2$$

(logarithmic rate law)

The logarithmic rate law can be simplified for

initial thin coatings. The values for k are small (less than 0.01 in most cases) and for small values of t the third term can be neglected and the expression simplified to

$$A/A_o \cong 1 - 2(\pi/A_o)^{1/2} kt$$

(logarithmic rate law for thin coatings)

The results obtained for the metals studied (see Results) show that the initial rate of corrosion was nearly always linear with time as

$$-dA/A_o = k/100 dt$$

where k is expressed as per cent area change per second. This expression in integrated form is

$$A/A_o = 1 - k/100 t$$

(experimental rate law)

This expression is similar to the logarithmic rate law for thin coatings and also to rectilinear rate law for initial corrosion, wherein the third term is small compared to the second.

If the logarithm of the reaction rate is plotted against the reciprocal of the absolute temperature, an equation of the Arrhenius-type generally occurs, which when expressed in logarithmic form is

$$\ln \text{rate} = \ln a - E/RT$$

where E is the activation energy for the over-all process and a is the frequency factor. Both a and E are usually constant over a small temperature range. From this, it can be seen that a plot of $\ln \text{rate}$ vs. $1/T$ yields a straight line.

During the corrosion period a film is formed on the surface of the pure metal. The conductivity of the oxide coating is negligible compared with that of the pure metal. Veil (12) measured the resistivity of various oxides at high temperatures. He found for CuO at 1000°C a resistivity of 3×10^{-1} ohm cm which compares to the resistivity of Cu of 9×10^{-6} ohm cm at 1000°C. The resistivity of Fe₂O₃ at 1000°C was found to be 82 ohm cm as compared to 50×10^{-6} ohm cm. The resistivity of NiO at 1000°C is 144 ohm cm which compares to 62×10^{-6} ohm cm at 1000°C for pure Ni. The above examples show that conductivities of metal oxides are negligible to those of the pure metals.

The effect of the solubility of the gases on the resistance of the metal filaments investigated was negligible since there was no discernible change in their resistance at temperatures just below the point of corrosion. However, it was not possible to study the corrosion rates of metals such as zirconium or titanium because the solubility of oxygen and nitrogen changed their resistivities to such an extent that the change in resistance due to corrosion could not be measured.

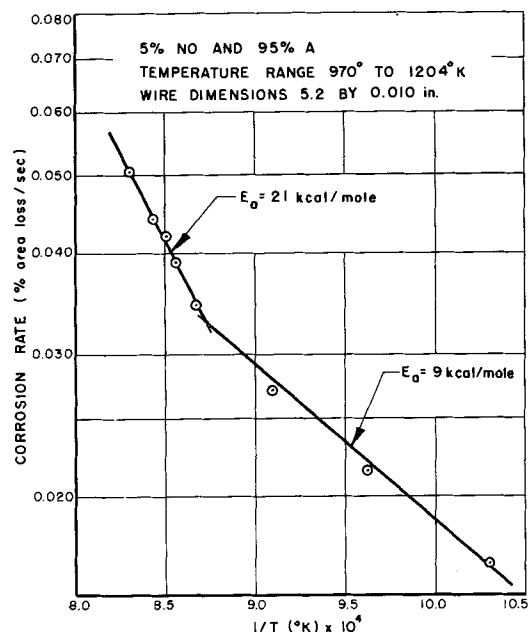


Fig. 3. Corrosion rate of Fe with NO as function of $1/T$.

RESULTS

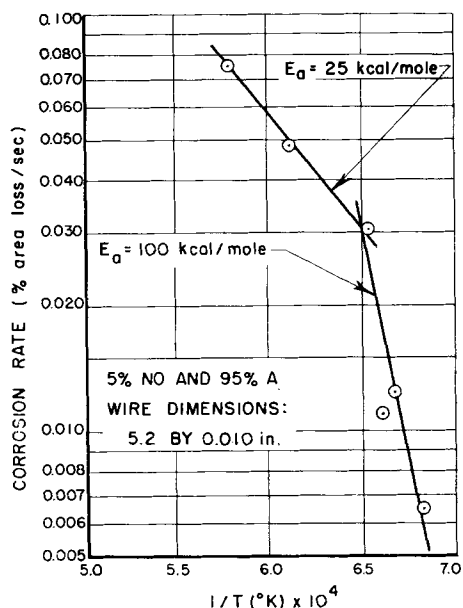
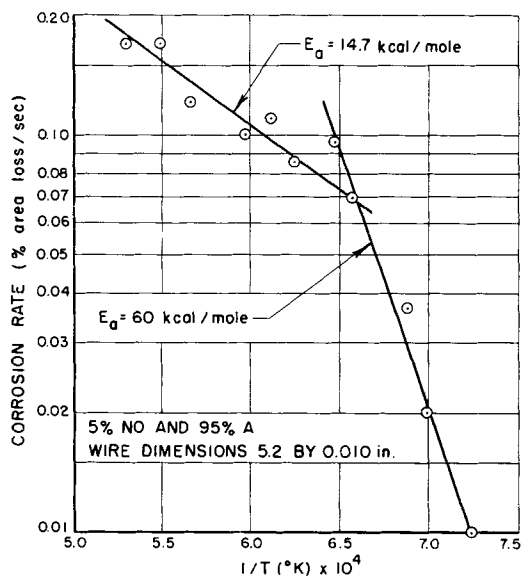
Corrosion rates of iron with NO.—Corrosion rates of iron in an atmosphere of NO (5%) and A (95%) and at a constant gas flow rate of 100 cc/min were studied over a temperature range of 970° to 1200°K. The iron employed was Armco⁵ iron of better than 99% purity.

Corrosion of iron in nitric oxide is quite rapid at all temperatures. Rate constants vary from 0.016 to 0.050 (% area loss/sec) over the range studied (cf. Table I). The temperature dependence of the rate tends to increase at temperatures over 1100°K. When the logarithm of the rate constant is plotted against the reciprocal of the absolute temperature, two activation energies are obtained over the temperature range studied, namely 9 kcal/mole from 970° to 1140°K and 21 kcal/mole from 1140° to 1200°K (cf. Fig. 3). The scale formed consisted entirely of various oxides of iron.

Corrosion rates of tantalum with NO.—Tantalum is much more resistant to corrosion with NO than is iron and shows very little corrosion in the low temperature range. The reaction rate at temperatures below 1400°K could not be detected. Therefore, it was necessary to obtain corrosion rate data in the range from 1450° to 1730°K. The increase in reaction rate with temperature was very rapid between 1470° and 1550°K.

Corrosion of tantalum with NO, together with that of several of the other metals including iron, gives two curves of apparent activation energy over

⁵ Armco is registered trade mark of American Rolling Mill Company.

FIG. 4. Corrosion rate of Ta with NO as function of $1/T$ FIG. 5. Corrosion rate of W with NO as function of $1/T$

the temperature range studied. In the lower temperature region (cf. Fig. 4) an activation energy of 100 kcal/mole is obtained, whereas the higher range gives an activation energy of 25 kcal/mole. Rate constants vary from 0.006 (% area loss/sec) at 1470°K to 0.076 at 1730°K (cf. Table I).

Corrosion rates of tungsten with NO.—The reaction rate of W with NO depends mainly on the availability of molecular or atomic oxygen from the decomposition of NO. In order to ascertain the dependence of oxygen concentration on the corrosion rates of W, an experimental study was made with both NO and O₂. In both cases the gas mixture contained 95% A as the inert gas and 5% of either O₂ or NO as the corroding gas.

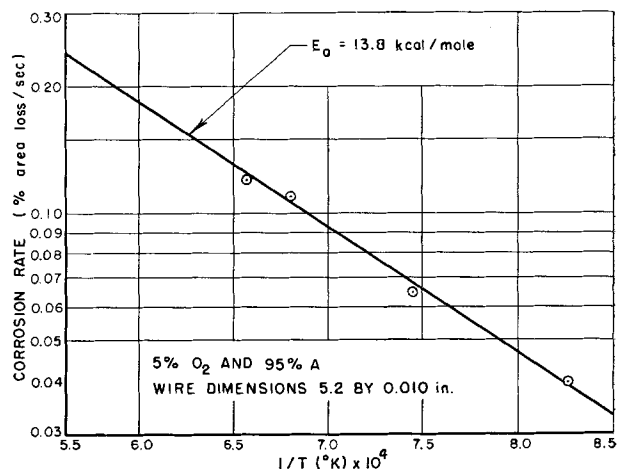
FIG. 6. Corrosion rate of W with O₂ as function of $1/T$

TABLE II. Initial corrosion rates of tungsten and molybdenum with oxygen

Gas mixture: 95% Argon and 5% oxygen

Metal	T (°K)	k (% area loss/sec)
Tungsten	1209	0.040
	1343	0.065
	1468	0.110
	1522	0.120
Molybdenum	1209	0.046
	1333	0.062
	1406	0.101
	1506	0.138
	1605	0.145

Corrosion rates of W with NO were taken over a temperature range of 1380° to 1890°K, and the rates with O₂ over the temperature range of 1200° to 1520°K. As can be seen from Fig. 5, the NO corrosion rates vary greatly with temperature in the region from 1300° to 1400°K, namely, from 0.01 to 0.07 (% area loss/sec). Corrosion rates increase rather slowly with temperature from 1400° to 1750°K, namely, from 0.07 to 0.18 (% area loss/sec).

A higher corrosion rate would be expected with O₂ since, as postulated, the rate of corrosion of W depends upon the dissociation of NO for availability of O₂. The corrosion rate of W with O₂ increases uniformly with temperature from 0.04 (% area loss/sec) at 1150°K to 0.12 at 1525°K.

The apparent activation energies as obtained from Fig. 6 are 13.8 kcal/mole for O₂ as compared to 14.7 kcal/mole for NO (cf. Fig. 5) at the higher temperatures. The fact that these energies are nearly equal indicates that the rate of dissociation of NO in this temperature range is not rate-determining in the corrosion process. In the low temperature range the apparent activation energy for NO is 55 kcal/mole. The rate constants for the reaction

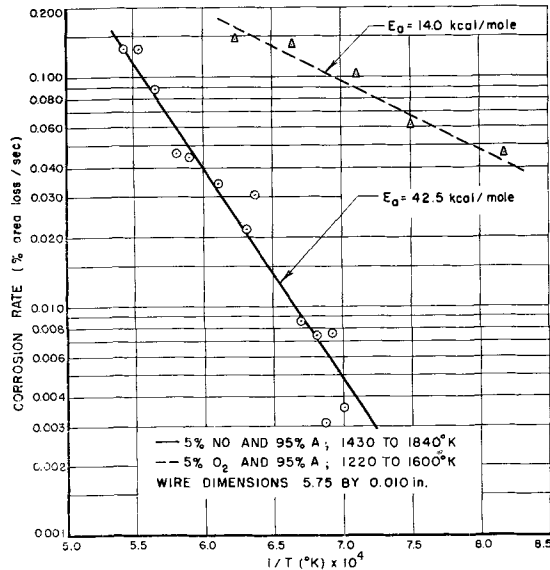


FIG. 7. Corrosion rate of Mo in NO and O₂ atmosphere as function of 1/T.

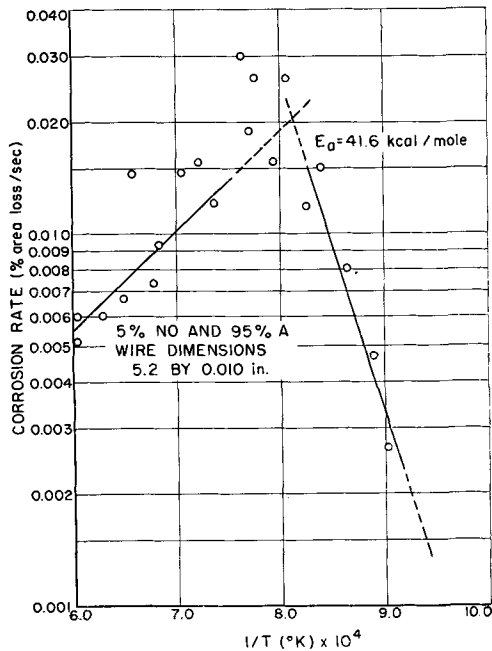


FIG. 8. Corrosion rate of Ni with NO as function of 1/T

rates of W and NO and O₂ are given in Tables I and II, respectively.

Corrosion rates of molybdenum with NO.—Molybdenum is quite resistant to corrosion in NO at temperatures below 1400°K but reacts quite readily at higher temperatures. Corrosion rates for Mo were obtained over a temperature range of 1400° to 1850°K. Rate constants (cf. Table I) vary from 0.0036 to 0.132 (% area loss/sec) over the temperature range studied, the activation energy being 43 kcal/mole as shown in Fig. 7. As in the case of tungsten, reaction rates of Mo were obtained with both O₂ and NO; corrosion of Mo with O₂ (95%

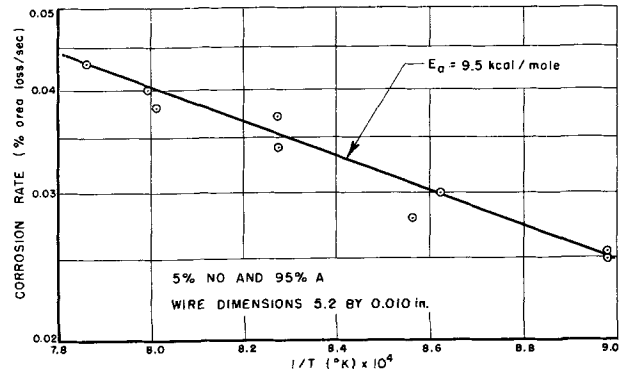


FIG. 9. Corrosion rate of Cu with NO as function of 1/T

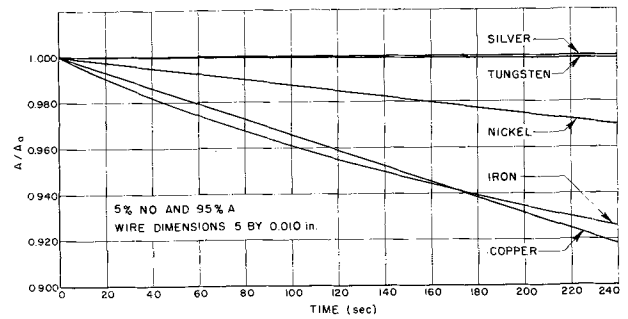


FIG. 10. Corrosion rates of several metals with NO at 1200°K.

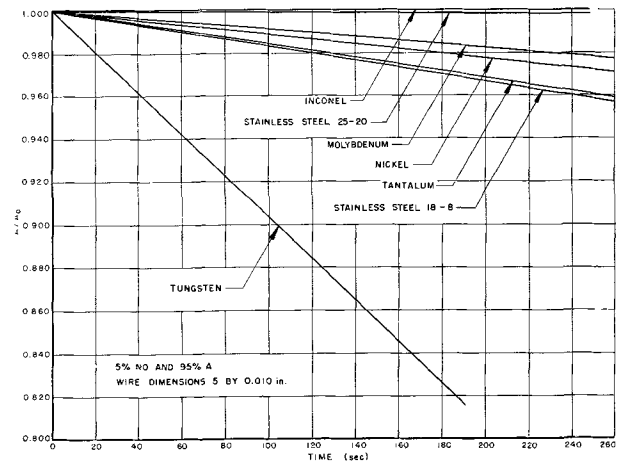


FIG. 11. Corrosion rates of several metals with NO at 1450°K.

A-5% O₂) was more rapid for a given temperature than was the rate with NO. An apparent activation energy shown in Fig. 7 gives a value of 14.0 kcal/mole for O₂ over the temperature range of 1220° to 1600°K. Gulbransen and Wysong (13) have obtained an activation energy of 36.5 kcal/mole for Mo in 7.6 cm of O₂ over a lower temperature range of 620° to 820°K.

Corrosion rates of nickel with NO.—Reaction rates of Ni with NO were studied over the temperature range of 1100° to 1650°K. Rates increase steadily until a temperature of 1200°K is attained. Above

1200°K the rate starts to decrease from a peak of 0.025 (% area loss/sec) to 0.005 at 1650°K. The rate-determining step is presumably the formation of NiO which forms a protective coating over the Ni. Upon plotting the logarithm of the rate vs. the reciprocal of the absolute temperature (cf. Fig. 8), a considerable amount of scatter was obtained in the region because of the oxide transition region. Experimental rate constants vary from 0.002 to 0.030 (% area loss/sec) and are listed as functions of temperature in Table I.

Two oxides of Ni are known to exist, namely, Ni₂O₃ and NiO. Since at high temperatures the Ni₂O₃ decomposes to the lower oxide, it was believed that the corrosion rate could probably be determined by the type of oxide formation. Consequently, x-ray diffraction patterns were taken in both the high and low temperature regions. Oxide samples at 1100° and 1570°K (at which temperatures the corrosion rates are the same) were analyzed for crystal structure and type of oxide. Both samples showed only one type of oxide, namely, NiO; however, the low temperature sample consisted of large crystals, whereas the high temperature sample had a small and compact crystalline structure.

Corrosion rates of copper with NO.—Reaction rates of Cu with NO were measured in an NO gas mixture (95% A-5% NO) over a temperature range from 1100° to 1275°K. A uniform rate increase was obtained, namely, 0.025 to 0.043 (% area loss/sec) over the temperature range studied. An examination of the oxide formed showed it to be predominantly the red cuprous oxide Cu₂O. A plot (cf. Fig. 9) of the logarithm of rate against the reciprocal of the temperature gave an apparent activation energy of 9.5 kcal/mole. In the temperature range studied, only one activation energy and one form of the oxide were obtained. Rate constants are given in Table I.

Corrosion rates of silver with NO.—Since the oxide of silver is unstable at temperatures over 500°K, no corrosion of silver was expected in the temperature range studied, 900°-1100°K. This fact was verified experimentally.

Corrosion rates of Inconel and stainless steel with NO.—Because of the considerable application of various alloys at high temperatures, it was considered of interest to obtain the reaction rates of Inconel and both 18-8 and 25-20 stainless steel with NO.

At all temperatures below the melting point the corrosion rate of Inconel with NO was negligible, and no temperature-time curves could be obtained. Stainless steel 25-20 (25% chromium-20% nickel) was nearly as resistant as Inconel, corroding only slightly at 1550°K and above. The rate constant

(cf. Table I) at 1538°K was 0.001 (% area loss/sec) and at 1558°K had doubled to 0.002. Stainless steel (18% chromium-8% nickel) corroded more readily at these temperatures, the rate constant being 0.016 (% area loss/sec) at 1450°K and 0.023 at 1500°K.

Corrosion rates of several metals with NO at 1200° and 1450°K.—A comparison of the corrosion rates of the several metals was made at two temperatures by obtaining the temperature-time curves. Fig. 10 shows the corrosion rate with NO for silver, tungsten, nickel, iron, and copper at 1200°K. As can be seen in the figure, silver and tungsten are very resistant at this low temperature. Both iron and copper are quite readily corroded. At 1450°K (cf. Fig. 11),

TABLE III. Initial corrosion rates of several metals with NO at 1200° and 1450°K

At 1200°K		At 1450°K	
Metal	(% area loss/sec)	Metal	(% area loss/sec)
Silver	Negligible	Inconel	Negligible
Tungsten	0.0005	Stainless steel 25-20	0.001
Nickel	0.013	Molybdenum	0.009
Iron	0.034	Nickel	0.011
Copper	0.039	Tantalum	0.015
		Stainless steel 18-8	0.017
		Tungsten	0.097

TABLE IV. Activation energies for the reaction of several metals with O₂ and NO^a
Gas (pressure = 1 atm)

Metal	5% O ₂ -95% A		5% NO-95% A	
	E (kcal/mole)	a	E (kcal/mole)	a
Fe	—	—	9.0 (950°-1150°K)	1.79
	—	—	21.0 (1150°-1225°K)	3.40×10^2
	—	—	—	—
Ni	—	—	41.6 (1090°-1220°K)	5.04×10^5
	—	—	—	—
Cu	—	—	9.5 (1100°-1270°K)	1.84
	—	—	—	—
W	13.8 (1200°-1550°K)	12.1	60 (1390°-1510°K)	2.95×10^7
	—	—	14.7 (1510°-1900°K)	8.85
	—	—	—	—
Mo	14.0 (1220°-1600°K)	13.3	42.5 (1430°-1840°K)	1.5×10^4
	—	—	—	—
Ta	—	—	100 (1470°-1540°K)	4.81×10^{12}
	—	—	25 (1540°-1740°K)	1.09×10^2
	—	—	—	—

^a E = activation energy; a = exponential constant; $k = ae^{-E/RT}$

however, tungsten is corroded quite readily, whereas the 25-20 stainless steel and Inconel are the most resistant to corrosion.

As is shown in Fig. 10 and 11, the metals in order of decreasing corrosion resistance are Inconel, 25-20 stainless steel, molybdenum, nickel, tantalum, 18-8 stainless steel, tungsten, iron, and copper. Corrosion-rate constants are listed in Table III. The apparent activation energies for the several metals and NO are listed in Table IV.

Any discussion of this paper will appear in a Discussion Section to be published in the June 1956 JOURNAL.

REFERENCES

1. B. B. ADHIKARY, *Chem. News*, **112**, 163 (1915).
2. E. SCHRÖDER AND G. TAMMAN, *Z. anorg. u. allgem. Chem.*, **128**, 179 (1923).
3. J. G. DEVOOGD AND H. J. TADEMA, *Het Gas*, **61**, 3 (1941).
4. H. WISE AND M. F. FRECH, *J. Chem. Phys.*, **20**, 1724 (1952).
5. M. FARBER AND D. M. EHRENBERG, *This Journal*, **99**, 427 (1952).
6. W. E. GARNER, T. J. GRAY, AND F. S. STONE, *Proc. Roy. Soc. (London)*, **A197**, 294 (1949).
7. E. WILSON, *Proc. Phys. Soc. (London)*, **39**, 15 (1926).
8. J. C. HUDSON, *ibid.*, **40**, 107 (1928).
9. N. B. PILLING AND R. E. BEDWORTH, *J. Inst. Metals and Metallurgical Abs.*, **1**, 528 (1923).
10. U. R. EVANS, Pittsburgh International Conference on Surface Reactions, p. 71, Corrosion Publishing Co., Pittsburgh (1948).
11. U. R. EVANS, "Metallic Corrosion Passivity and Protection," Longmans, Green and Co., New York (1948).
12. S. VEIL, Thesis, Paris (1920); International Critical Tables, **4**, p. 153.
13. E. A. GULBRANSEN AND W. S. WYSONG, *Trans. Am. Inst. Mining Met. Engrs.*, **14**, No. 6, 1 (1947).

Organic Peroxides as Source of Cations¹

ANDREW GEMANT

Engineering Laboratory and Research Department, The Detroit Edison Company, Detroit, Michigan

ABSTRACT

This is a continuation of a study on the problem of oxidation in service of electrical insulating liquids. Oxidation of such liquids, hydrocarbons by their constitution, is accompanied by increased electrical conductivity. In the present study, ozone was used as an agent for accelerated oxidation. It was found that aromatic hydrocarbons in the presence of small amounts of aliphatic acids on ozonization produce very high conductivities. This finding is significant because both aromatics and aliphatic acids may be present in small concentrations in insulating oils. By a detailed study of the effect observed, using ultraviolet absorption spectroscopy and measurement of paramagnetic susceptibility, among others, an attempt was made to establish the chemical nature of the ions that cause the high electrical conductivity.

PURPOSE OF STUDY

The following observations on oxidation-ions in electrical insulating hydrocarbon liquids have been made (1). Oxidation of aromatic orthodiols produces ions that are probably semiquinone type compounds. Reduction of these ions causes reversion to their original nonionic species. Ultraviolet irradiation of ortho-alkylated aromatics also produces ions. The positive ions are probably oxonium-ions of the aldehydes formed. These ions are also partially reducible to nonionic molecules.

This paper describes observations of high electrical conductivities, hence ion-concentrations, which exceed those reported previously by about three orders of magnitude. The chief source of these ions appears to be aromatic hydrocarbons. Ozone was used as the oxidizing agent since the amount acting on the substrate can be controlled easily.

When ozone oxidizes an aromatic hydrocarbon, the increase in electrical conductivity is negligibly small. The novel observation made in this study was that addition of a small concentration of aliphatic acid prior to oxidation with ozone produces high electrical conductivities of 10^{-9} mho/cm or more.

Whereas the chemical nature of the ions produced cannot be stated with certainty, it is possible on the basis of the various observations to describe their structure in a tentative manner.

BASIC OBSERVATIONS

Ozonization was carried out by bubbling ozone through the solution in a glass container without a catalyst. Ozone was produced in a glass-lined corona ozonizer, through which oxygen was passed. The field in the ozonizer could be varied, thus changing the ozone concentration in the stream. In

the majority of experiments the field was about $27 \text{ kv}_{\text{max}}/\text{cm}$ which corresponds to a corona current of about 0.15 ma. The rate of flow of oxygen was 200 cc/min, and the ozone concentration in it was 0.25%.

Of the various hydrocarbons, toluene was found most effective in increasing the conductivity, and it was used in most of the experiments. Myristic acid, generally at 20 mM/l, was used in the majority of experiments. All tests were carried out at room temperature.

Some of the crystalline compounds used in this and in previous studies were recrystallized from best Eastman products. Usually, no noticeable difference in conductivity increases was found between the original and purified compounds.

Fig. 1 shows a typical conductivity effect. After an hour the conductivity, σ , reached a level of about 5×10^{-10} mho/cm. The solution remained clear and had a faint yellow color.

Fig. 2 shows the increase of conductivity with increasing ozonizer field, i.e., ozone concentration.

These high ion concentrations are not permanent, indicating that the ions are probably intermediate oxidation products. Fig. 3 shows the time behavior of conductivity after oxidation. As a rule σ stays on a high level for about two days (a frequent initial increase in the first few hours is not shown), after which it drops rather rapidly. In about six days it reaches either a moderately high, constant level of about 3×10^{-12} (curve 1), or drops even lower (curve 3). In a mixture of toluene and transformer oil (curve 2) a moderately high level was obtained. This may be due to unsaturated compounds in the oil competing with toluene for the ozone.

The instability of σ is an indication that the high conductivity is not caused by a strongly polar decomposition product, for instance, benzaldehyde. Moreover, in such a case the dielectric constant

¹ Manuscript received November 1, 1954. This paper was prepared for delivery before the Cincinnati Meeting, May 1 to 5, 1955.

should show a marked increase which, however, is not observed. Water, as a possible oxidation product, cannot be the cause of the increased conductivity, since even saturation with water produces only small changes in conductivity. Carbon dioxide, a possible cleavage product of the peroxides, cannot increase the conductivity; in fact, it is sometimes used as a pressure medium in oil-impregnated high voltage cables.

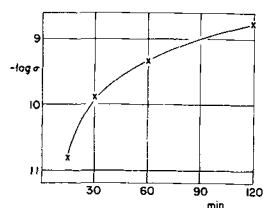


FIG. 1

FIG. 1. Electrical conductivity σ (mho/cm) vs. time of oxidation. Myristic acid (20 mM/l) in toluene. Ozonizer field 27.3 kv/cm.

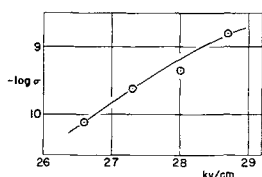


FIG. 2

FIG. 2. Conductivity vs. ozonizer field. 0.020*N* myristic acid in toluene. Oxidation time 60 min.

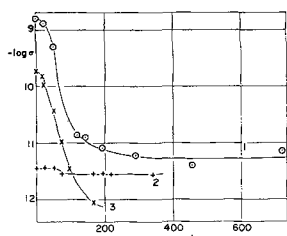


FIG. 3. Conductivity vs. time passed after oxidation. 0.02*N* myristic acid in toluene (curve 1); toluene-transformer oil 1:1 (curve 2); toluene-paraffin oil 1:1 (curve 3).

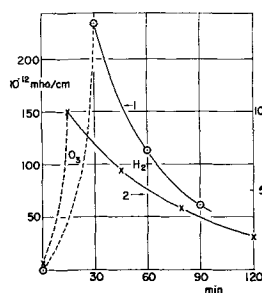


FIG. 4

FIG. 4. Decrease in conductivity on reduction in H_2 stream. 0.01*N* myristic acid in toluene. Oxidation time: 30 min for curve 1 (left-hand side ordinates), 15 min for curve 2 (right-hand side ordinates).

FIG. 5. Conductivity vs. dilution. 0.02*N* myristic acid in toluene. Oxidation time: 60 min.

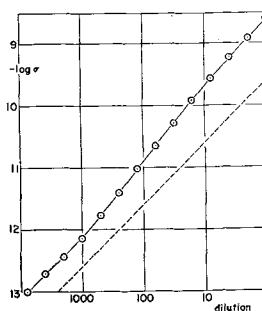


FIG. 5

Reduction in hydrogen stream (atmospheric pressure, room temperature, platinum-black catalyst) produced a drop in conductivity, as seen in Fig. 4. Hence, it appears that the oxidized ionic species can be, at least partly, converted into re-

duced, nonionic molecules. Reduction in conductivity was in a ratio of about 1:4 in 60 min, independently of the initial level, which was high for curve 1, moderately high for curve 2.

It was pointed out in earlier papers (1) that the slope of the curve conductivity vs. dilution permits differentiation between electrolytic and oxidation-ions. In the log-log plot the former approaches theoretically a slope of 22.5 degrees, the latter 45 degrees. Fig. 5 gives a dilution curve over a range of four orders of magnitude, the dotted line being a 45 degree slope. Although the experimental curve has not exactly a 45 degree slope, the deviation is not excessive, indicating that the ions in this system are not the result of electrolytic dissociation of a single parent compound.

AROMATIC HYDROCARBON

The question arises as to what aromatic hydrocarbons produced the effect observed. Table I gives the results, relating to several aromatics. An increase in conductivity is observable in all cases, it being the most pronounced in toluene. In order to obtain a measurable increase in σ in benzene and xylenes, it was necessary to increase both the ozonizer field and the time. For this reason the figures in the last column offer only qualitative comparison.

At the present stage of the study, and with the mechanism of ion formation as suggested (see later), differences between the various hydrocarbons cannot be explained. Such specific influences of side-chains are, of course, common in many reactions. Methyl-naphthalenes, as will be shown in another paper, also produce high conductivities, and so the observations are valid also for condensed aromatic compounds.

Table II presents comparative results on mono-alkyl benzene derivatives, indicating decreasing conductivity with increasing complexity of the side chain.

TABLE I. Comparison of various aromatic hydrocarbons; 0.02*N* myristic acid; initial conductivity about 10^{-13} mho/cm

Hydrocarbon	Ozonizer field kv/cm	Oxidation time, min	Conductivity, 10^{-12} mho/cm
Benzene.....	27.3	60	3.8
Benzene.....	28.0	60	7.5
Toluene.....	27.3	60	404
Ethylbenzene.....	27.3	150	91.0
<i>o</i> -Xylene.....	28.0	120	26.0
<i>o</i> -Xylene.....	28.3	160	132
<i>m</i> -Xylene.....	28.0	120	12.0
<i>p</i> -Xylene.....	28.0	120	12.0
<i>p</i> -Xylene.....	29.1	250	25.0
Mesitylene.....	28.7	220	17.6

TABLE II. Comparison of mono-alkyl benzenes, in solutions of 25% by volume in *n*-decane; 0.02*N* myristic acid; ozonizer current 0.15 ma; oxidation time 60 min

Hydrocarbon	Conductivity, 10^{-12} mho/cm
Toluene.....	2540
Ethylbenzene.....	218
<i>n</i> -Propylbenzene.....	528
<i>n</i> -Butylbenzene.....	191
<i>sec</i> -Butylbenzene.....	107
<i>tert</i> -Butylbenzene.....	76

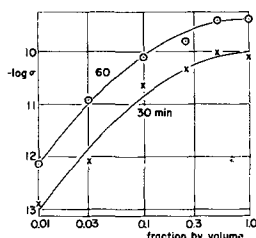


FIG. 6. Conductivity vs. fraction by volume of toluene in a mixture of toluene-*n*-octane. 0.02*N* myristic acid. Oxidation time: 30 and 60 min.

Since the aromatic hydrocarbon is the main source of ions, it was of interest to ascertain the concentration necessary for a positive effect. It was established that aliphatic hydrocarbons as well as saturated rings are ineffective, hence they can be used as diluents (Fig. 6). The relatively small increase in σ with low concentrations of toluene in this instance is caused by its partial evaporation during oxidation. In a solvent of lower boiling point small concentrations are very effective, as will be shown in another paper. Values shown in Fig. 6 are not directly transferable to a mixture of an aromatic with a viscous hydrocarbon oil.

ALIPHATIC ACID

Some experiments were carried out to determine whether all aliphatic acids would produce ions to the same extent. A number of aliphatic acids of varying chain length were tested (Fig. 7). From valeric to stearic acid the curve passes through a flat maximum at about 12 carbon atoms (lauric acid). However, for acids having fewer than five carbon atoms (valeric acid) the conductivities drop to quite low values.

Fig. 8 shows that about 10 mM/l of acid are needed; above that value, no further increase in σ occurs; below that value, the increase in σ drops sharply. From this it can be seen that about 10 mM/l are involved in the reaction. If the same amount of toluene is involved in the process, it would mean that about 1×10^{-3} mole fraction of toluene undergoes oxidation under the conditions of the experiment.

The bottom curve in Fig. 8 refers to a sample of

toluene oxidized without the addition of acid. There is no significant increase in conductivity, and, if the acid is added *after* the oxidation, no significant increase of σ occurs. Thus, the acid does not react with an oxidation product in a manner as it does with amines; it reacts *during* oxidation with some of the intermediates. This latter statement is offered as a hypothesis; it is substantiated, among others (see later), by the following observation. The peroxide of the aromatic compound usually precipitates out because of its limited solubility. If an acid is

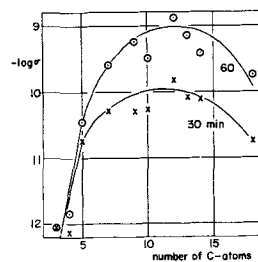


FIG. 7

FIG. 7. Conductivity vs. number of C-atoms of aliphatic acid (0.02*N*) in toluene.

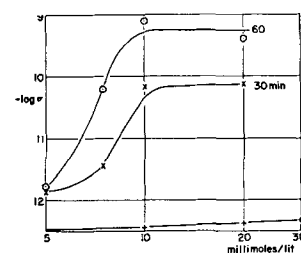


FIG. 8

FIG. 8. Conductivity vs. concentration of myristic acid in toluene. Bottom curve: addition of acid after oxidation without acid.

TABLE III. Additions other than saturated aliphatic acids to toluene, in 0.02*N* concentration; initial conductivity about 10^{-13} mho/cm

Compound	Oxidation time, min	Conductivity, 10^{-12} mho/cm
Oleic acid.....	30	1.0
Benzoic acid.....	60	1.0
Octadecyl acetate.....	60	0.05
Tripropionin.....	30	2.9
Heptaldehyde.....	60	0.3
Hexyl alcohol.....	60	1.7
Cetyl alcohol.....	30	0.1
Cholesterol.....	60	4050

present during oxidation, precipitation is either completely absent or markedly reduced. This is explainable if it is assumed that the aliphatic acid takes part in the reaction.

In this connection a number of other acids and related substances were tested, the result being shown in Table III. An unsaturated aliphatic acid, oleic acid, is ineffective, as is an aromatic acid, benzoic acid. The ineffectiveness of oleic acid may be explained by its double bond competing with the aromatic for the ozone. Esters, an aldehyde, and alcohols are seen to be equally ineffective. A large conductivity effect was found with cholesterol.

ULTRAVIOLET ABSORPTION SPECTRA

In order to ascertain the possible reaction mechanism and to find the probable chemical structure of

the ions, absorption spectroscopy was used. By this means some helpful indication, even if no direct evidence, is provided.

Fig. 9 presents the ultraviolet absorption spectra of toluene oxidized by ozone without (curve 1) and with (curve 2) the addition of 0.01*N* myristic acid. In order to eliminate the toluene spectrum, the water extracts of the organic solutions were used for absorption measurements. From the absorption measured in a Beckman spectrophotometer the average product $\overline{\epsilon c}$ was calculated (ϵ = extinction coefficient, c = concentration of compound). Since the concentration of the compounds responsible for absorption was not known, $\overline{\epsilon c}$, i.e., its logarithm, was plotted vs. the wave length λ in millimicrons. This product was calculated from the measured optical density, which is equal to ϵcl (l = optical path length). In curve 1 two characteristic peaks appear at 275 and 215 $m\mu$. In curve 2, referring to the sample with acid, additional peaks appear at 335 and 255 $m\mu$.

The basic process on oxidizing aromatics by means of ozone, according to the studies of Harries (2), is ozonide formation. The ozonides undergo cleavage and form diones (3, 4). If diones are formed, their spectrum must be present in the absorption spectrum of the water extract. Glyoxal and methylglyoxal are produced from toluene. As a comparison, an aqueous solution of 2, 3 butanedione was analyzed, the spectrum being given in curve 1 of Fig. 10. With its two peaks at 280 and 205 $m\mu$ (the latter to be interpreted with caution because of possible instrument anomalies), it resembles curve 1 of Fig. 9, which is in all probability due to the diones formed from ozonides.

The next point was to determine the kind of compound causing the additional peaks in curve 2, Fig. 9. This point is of particular interest since addition of the aliphatic acid leads to the high concentration of ions. The aliphatic acid itself possesses only one absorption peak near 200 $m\mu$; it does not

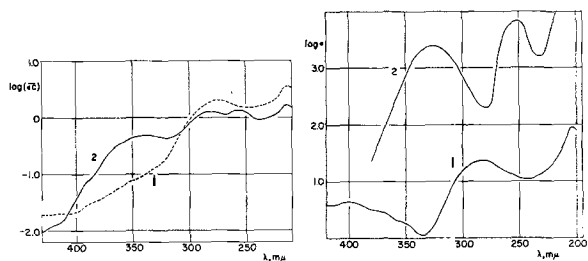


FIG. 9

FIG. 9. Extinction coefficient vs. wave length λ in millimicrons. Curve 1, toluene, oxidized by O_3 for 8 min; Curve 2, 0.01*N* myristic acid in toluene, oxidized by O_3 for 8 min.

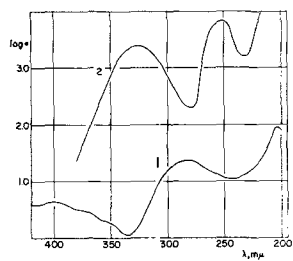


FIG. 10

FIG. 10. Extinction coefficient vs. wave length. Curve 1, 2-3 butanedione in water; curve 2, salicylaldehyde in alcohol (Kiss and Nyiri).

contribute essentially to the spectrum. Its presence, however, prevents the precipitation of peroxide; the solution remains clear, with a faint yellow color. The acid probably forms a soluble addition compound with the ozonide, the carboxyl group becoming attached to the peroxide group which links two neighboring carbon atoms of the ring. If this conclusion is correct, an aromatic ring with adjacent carbonyl and hydroxyl groups attached ought to be present. A compound approximating such a structure is salicylaldehyde which has a carbonyl and a hydroxyl in ortho position. The spectrum of the latter (5) is shown as curve 2 in Fig. 10; it has peaks at 325 and 255 $m\mu$. The location of these peaks agrees fairly well with the two additional peaks found in curve 2, Fig. 9. Thus, the absorption spectra are in agreement with the assumption of an addition compound formed by the aromatic hydrocarbon and the aliphatic acid. This compound is thought of as an intermediate product which oxidizes further in the course of the reaction. A fraction of it might dissociate into an aliphatic anion and an oxonium cation such as postulated in the previous studies. These ions, being relatively stable, might persist for some time, as was observed. The role of the acid, as here assumed, is verified by further experiments discussed in the following section.

TITRATION AND PRECIPITATION OF ACID

In order to clarify further the role of the aliphatic acid, total acidity was measured by titration.

The role of the aliphatic acid is of considerable interest from the standpoint of electrical insulation inasmuch as its connection with deterioration of oils is known (6). In this particular instance the acid is clearly the cause of high electrical conductivity due to the formation of oxidation ions.

Aliphatic acids are generally resistant to oxidation and it was therefore not expected that in the course of the reaction studied they should form low molecular, water-soluble acids. In order to check this, titration of toluene-myristic acid samples was carried out; the result is presented in Table IV. The titration was carried out in alcoholic system, with

TABLE IV. Titration results in ozone oxidation

Hydrocarbon	Myristic acid	Oxidation time, min	Normality of total acid		
			Original solution	Oxidized solution	Water extract of latter
<i>n</i> -Octane.....	+	30	0.019	0.020	0.001
Cyclohexane.....	+	30	0.019	0.020	0.000
Toluene.....	-	15	0.000	0.010	0.006
Toluene.....	+	15	0.019	0.027	0.005
Toluene.....	-	30	0.000	0.031	0.026
Toluene.....	+	30	0.020	0.058	0.024

alcoholic *N*/50 KOH as titrating agent and alkali blue as indicator. The first two samples, containing indifferent solvents with acid, show that the latter does not produce additional acidity and, in particular, no water-soluble acids are formed. The third sample, toluene, yields 10 mM/l of acid as secondary product, a large part of which is water soluble. If myristic acid is added prior to oxidation, the amount of excess (8 mM/l) and its water-soluble fraction are about the same as in the case without acid, showing that the latter does not affect the reaction as far as production of new acid is concerned. The last two samples with excess acid concentrations of 31 and 28 mM/l confirm the result.

The assumption of an addition compound formed by the aromatic and the acid as a precursor of ions, indicated by the absorption spectra, is strengthened by two further experiments.

If the acid forms an addition compound at the carboxyl group, then binding the latter prior to oxidation should reduce the ionic effect. Amines, by forming soluble salts, bind the carboxyl group of aliphatic acids. Fig. 11 shows the result of this test. The lower curves show that conductivity markedly decreases upon the simultaneous addition of tributylamine. There are no significant changes in σ on adding amine after oxidation since the main action of the acid takes place during oxidation.

If the conclusion that the acid forms an addition compound with an aromatic intermediate is correct, it should be more difficult to form salts of the aliphatic acid after oxidation than before. A visible criterion of salt formation is the precipitation of a white crystalline powder after addition of an equivalent amount of KOH in alcoholic solution. Prior to oxidation such visible precipitates were found to form. After oxidation, either no precipitate or only traces of crystals were formed; sometimes after an hour more precipitate was observed. As a control of such tests additional acid was dissolved in the samples after oxidation, leading to prompt precipitation with KOH. These data are summarized in Table V, and indicate that the acid, as a result of the reaction, was not in an entirely free state. While

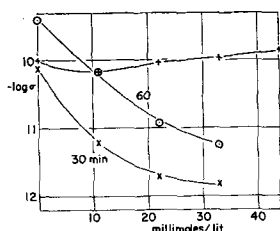


FIG. 11. Conductivity vs. concentration of tributylamine during oxidation. Top curve: addition of amine after oxidation.

TABLE V. Precipitation by KOH of the potassium salt of aliphatic acid

Acid	Normality	Oxidation time, min	% alcohol during precipitation	Precipitate of potassium salt	
				Without further addition of acid	With further addition of acid
Tridecanoic.....	0.02	15	25	—	+
Myristic.....	0.02	10	25	—	+
Palmitic.....	0.01	10	10	—	+
Stearic.....	0.01	15	10	—	+

the acid remained in a state to be titrated, precipitation of the potassium salt was delayed markedly. This might be explained on the basis of an acid-peroxide addition compound, held together by a loose electron pair. In analogy to the case of acid-amine compounds previously studied (7), dissociation to a small extent into ions (negative aliphatic and positive oxonium ions) is a possible result of such compound formation.

PARAMAGNETIC SUSCEPTIBILITY OF RADICALS

Oxidation-ion formation may be preceded by the occurrence of free radicals as was indicated in the case of orthodiols. Quite generally, radicals are assumed as intermediates in the cleavage of the —O—O— group (8). McLean (9) explains the action of inhibitors by their capture of radicals that occur under the action of the electrical discharge in dielectrics. In the present instance it is possible that the peroxide group in the ozonide cleaves by forming two unshared electrons in the aromatic molecule, the process being followed by addition of the aliphatic acid. While the majority of organic radicals is short-lived, there are others which are more or less stable and accessible to paramagnetic measurements (10). In fact, the paramagnetic technique (11), besides other methods, has been used extensively in the study of free radicals in usual organic solvents. Since the concentration of radicals or biradicals, if present, must be relatively large, it was attempted to detect and measure them by means of their paramagnetic susceptibility. This was done by the magnetostatic method, as devised by Quincke and Gouy (12). This method gives the algebraic sum of all the para- and diamagnetic moments present, and, as pointed out by Hutchison (13), is subject to error on this account. The paramagnetic resonance method as used by that author, among others, is free of this drawback. Since the total diamagnetic susceptibility might increase in the course of a reaction, the paramagnetic susceptibility as calculated from the static method is the lower

limit of a range and may be subject to a correction upward.

The method is based on the principle that a solution is attracted or repelled by a static magnetic field according to the sign of its susceptibility. All organic molecules are diamagnetic, except free radicals, the paramagnetic molar susceptibility χ_m of which for one unshared electron is 1300×10^{-6} cgs units. If radicals are produced in the course of oxidation, the oxidized sample should show a lesser repulsion than the original solution, the difference being a measure of the amount of radicals.

The solution of susceptibility κ and density ρ was contained in a U-tube having a narrow and a wide leg, the narrow leg being between the poles of an electromagnet. In switching on the field H (in Gauss), the meniscus level, observed by a microscope, was lowered by h cm in accordance with the relation

$$h\rho g = 0.5 \kappa H^2$$

In this simplified equation g = gravitational constant. Since κ for toluene is 0.63×10^{-6} and H was approximately 15,000 Gauss, by computation h is 86×10^{-3} cm; this value was confirmed by experiment. After oxidation the change in level was found to be somewhat less; the difference between the two being Δh .

If the molar fraction of radicals in toluene is denoted by r ($r \ll 1$), then the corresponding susceptibility is $1300 \times 10^{-6} r$. The molar susceptibility of toluene (molecular weight = 92, density = 0.87 g/cc) is $92 \times 0.63 \times 10^{-6}/0.87 = 66 \times 10^{-6}$, and the relative change due to radicals is $1300 \times 10^{-6} r/66 \times 10^{-6} = 20 r$. From the equation above the approximate relation $\Delta h/h = 20 r$ can be deduced, hence

$$r = 0.05 \Delta h/h$$

Fig. 12 shows the test results as a plot of $\Delta h/h$ vs. oxidation time. The precision of these measurements is moderate, but the order of magnitude of the difference observed was consistent. The crosses refer to control measurements made under the same

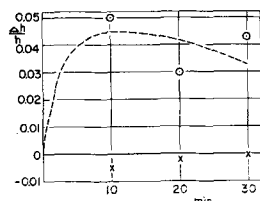
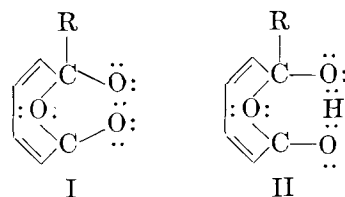


FIG. 12. Relative change in level in paramagnetic measurements vs. oxidation time. O toluene, 0.02*N* myristic acid, \times *n*-octane.

conditions with the exception that the indifferent solvent *n*-octane was used instead of toluene. As can be seen, $\Delta h/h$ was about 0.04 for toluene, and zero for *n*-octane. From the equation above, a value of $r = 2 \times 10^{-3}$ follows, i.e., about 0.2% toluene was present in the form of radicals immediately after oxidation. If biradicals are assumed to exist, this value would be about 0.1%. This order of magnitude is comparable with the 0.1%, previously arrived at, as the percentage of toluene involved in the reaction.

As for the cations formed on dissociation of the toluene-acid complex, it can be assumed that they are of the oxonium type. Structure I indicates the ozonide formed from a mono-alkyl benzene, and structure II indicates an oxonium cation upon addition of a proton. The formula is written for a monomer; actually the ion might be a dimer, tetramer, or the like. The ionic structure has additional stability due to the six-membered ring containing the proton. Either of the two oxygen atoms to the right could take up the additional pair of electrons, and this possibility of resonance stabilizes the ionic structure.



Structure II has a similarity with the semiquinone type of cation postulated previously as a result of the oxidation of catechol. These ionic structures need, of course, further verification.

The concept of ion pairs of the kind considered is perhaps unusual. The existence of aliphatic acid anions in hydrocarbons in the presence of amines was shown by the writer in a quantitative manner, by means of a radioactive tracer technique (14). The existence of oxonium cations as reaction intermediates from peroxides as well as other compounds is frequently assumed (15). The observations in this study are interpreted as an instance in which the presence of such ions is demonstrated owing to their electrical conductivity.

Any discussion of this paper will appear in a Discussion Section to be published in the June 1956 JOURNAL.

REFERENCES

1. A. GEMANT, *This Journal*, **100**, 320 (1953); **101**, 281 (1954); *J. Chem. Phys.*, **22**, 1705 (1954).
2. W. A. WATERS, in H. Gilman's, "Organic Chemistry," Vol. 4, p. 1174, J. Wiley & Sons, New York (1953).
3. A. A. LEVINE AND A. G. COLE, *J. Am. Chem. Soc.*, **54**, 338 (1932)

4. J. P. WIBAUT AND P. W. HAAYMAN, *Rec. trav. chim.*, **60**, 842 (1941).
5. A. v. KISS AND G. NYIRI, *Z. anorg. Chem.*, **249**, 340 (1942).
6. R. G. CALL, F. M. CLARK, AND T. A. MCCONNELL, *A.S.T.M. Spec. Tech. Pub. No. 135* (1952).
7. A. GEMANT, *This Journal*, **94**, 160 (1948).
8. E. R. BELL, F. F. RUST, AND W. E. VAUGHAN, *J. Am. Chem. Soc.*, **72**, 337 (1950).
9. D. A. MCLEAN, "Stabilization of Dielectrics," paper presented at the Chicago Meeting of The Electrochemical Society (1954).
10. E. MÜLLER, *Fortschr. chem. Forsch.*, **1**, 326 (1949).
11. M. F. ROY AND C. S. MARVEL, *J. Am. Chem. Soc.*, **59**, 2622 (1937).
12. S. GLASSTONE, "Textbook of Physical Chemistry," p. 611, D. van Nostrand Co., New York (1947).
13. C. A. HUTCHISON, JR., A. KOWALSKY, R. C. PASTOR, AND G. W. WHELAND, *J. Chem. Phys.*, **20**, 1485 (1952).
14. A. GEMANT, *This Journal*, **99**, 279 (1952).
15. A. V. TOBOLSKY AND R. B. MESROBIAN, "Organic Peroxides," p. 108, Interscience Publishers, New York (1954).

Electrodeposition of Molybdenum Alloys from Aqueous Solutions¹

D. W. ERNST, R. F. AMLIE, AND M. L. HOLT

Chemistry Department, University of Wisconsin, Madison, Wisconsin

ABSTRACT

Nickel-molybdenum, cobalt-molybdenum, and iron-molybdenum alloys have been electrodeposited from aqueous solutions containing sodium molybdate, the sulfate of the codeposited metal, sodium citrate, and ammonium hydroxide. Typical baths were made up with 0.3 M/l of the codepositing metal sulfate, 0.3 M/l of sodium citrate, varying amounts of sodium molybdate, and ammonium hydroxide to pH about 10.5. The maximum amount of molybdenum in the electrodeposited alloys depends on the alloying metal. When a typical bath was used, nickel alloys were found to contain up to 20% molybdenum, cobalt alloys contained up to 40% molybdenum, and iron alloys contained about 50% molybdenum. The cathode current efficiency in the above cases ranged from 75-85% for the nickel-molybdenum bath, 50-60% for cobalt-molybdenum, and 10-20% for iron-molybdenum. The effects of pH, concentration, temperature, and cathode current density on cathode current efficiency and alloy composition were studied.

These electrodeposited molybdenum alloys were metallic and either bright or light gray in appearance, with a large number of cracks in the bright deposits. Adherence of the deposit to well-cleaned flat cathodes seemed to be good, but adherence to tubing or rods was poor; usually these deposits could be brushed off in flake or powder form.

INTRODUCTION

The electrodeposition of molybdenum alloys containing iron, cobalt, or nickel has been reported previously from this laboratory (1) and a patent has been issued (2). Yntema and Ksycki (3, 4) described the use of solutions containing either aliphatic acids or their salts, or various fluorides to electrodeposit molybdenum alloys. Brenner and Burkhead (5) electrodeposited cobalt-molybdenum alloys from strongly alkaline solutions containing potassium carbonate, cobalt chloride, and sodium molybdate. Ma (6) described the electrodeposition of chromium-molybdenum alloys from a regular chromium plating bath containing molybdenum-(VI) oxide. A ternary alloy consisting of molybdenum, tungsten, and cobalt has been electrodeposited from aqueous citrate solutions by McElwee and Holt (7). The electrodeposition of nickel-molybdenum alloys from tartrate and citrate baths has been reported recently (8).

Seim and Holt (1) prepared their plating solutions using sodium molybdate, the sulfate of the codepositing metal, citric acid, and ammonium hydroxide. In this work sodium citrate was used in place of citric acid, being chosen after studying several different complexing agents. An attempt was also made to find another reagent for adjusting the pH

¹ Manuscript received September 4, 1953. This paper was prepared for delivery before the Wrightsville Beach Meeting, September 13 to 16, 1953.

of the plating solutions because of the volatility of ammonia.

EXPERIMENTAL METHODS AND RESULTS

The methods used were similar to those described previously (1) except that in some cases $\text{Na}_2\text{MoO}_4 \cdot 2\text{H}_2\text{O}$ was used instead of anhydrous Na_2MoO_4 . The volume of plating solution used for each electrolysis was 250 ml.

In analyzing cobalt-molybdenum and nickel-molybdenum deposits, the codeposited metal was always determined and molybdenum was usually found by difference. Occasionally molybdenum was determined by the lead molybdate method (9). When both metals were determined the analysis usually totaled 98% or more. Several of the nickel-molybdenum deposits were heated in hydrogen to about 850°C and showed a loss in weight of only 0.5%. Very few of the deposits obtained from the Fe-Mo bath were completely metallic, being covered in the center with a dark black material believed to be a molybdenum oxide; because of this, both components of these alloys were determined, and the total percentage varied from 80-95%, depending on the molybdenum content of the deposit. When several of the iron-molybdenum alloys were heated in hydrogen at about 850°C, the resulting loss in weight was 8 to 9% and the total analysis was then close to 100% (8.2% loss in weight, 40.0% Fe, 51.6% Mo).

Cathode current efficiencies were calculated using

the analysis and the equivalent weights based on the oxidation states Mo(VI), Ni(II), Co(II), and Fe(II). Calculations of C.C.E. based on Fe(III) and Co(III) were made and generally found to be 10–20% higher than those based on the bivalent state, and some efficiencies for the Co-Mo plating solutions were over 100%.

The pH of the plating solutions was determined using a Beckman model G pH meter and a glass electrode. No attempt was made to correct for salt effects.

Hull Cell Studies

The Hull cell described previously (1) was used to compare the nickel-molybdenum plating baths which contained different complexing agents. Cathode plates were obtained by electrolysis at 3 amp for 2 min and compared as to gain in weight and deposit appearance over the current density range of approximately 1–20 amp/dm². Plating solutions used for this investigation had the composition: 0.3 M/l of nickel sulfate; 0.3 M/l of the complexing agent; variable amounts of sodium molybdate; and a pH of about 10.5 with ammonium hydroxide. The concentration of 0.3 M/l was selected after numerous preliminary experiments as being the most suitable for the objectives in mind.

As a result of the Hull cell studies the complexing agents were classified as either poor or good for the electrodeposition of nickel-molybdenum alloys. Some of the complexing agents found to be good were: sodium citrate, sodium-potassium citrate, Rochelle salts, and sodium tartrate. For plating cobalt-molybdenum alloys the good complexing agents were: sodium citrate, malic acid, sodium malate, glycolic acid, and citric acid. Other complexing agents used were gluconic acid, dextrose, malonic acid, versene, oxalic acid, and the sodium and ammonium salts of some of these acids.

A schematic representation of Hull cell cathodes from a series of sodium citrate solutions classified "good" is given in Fig. 1 and in a similar manner those from a "citric acid" bath² classified "poor" is given in Fig. 2. Differences in the weights of the deposits as given in Fig. 1 and 2 should be noted particularly as an indication of changes in approximate current efficiencies.³

² Citric acid is used as the source of citrate ion and is neutralized by the ammonium hydroxide when the bath is prepared.

³ Work in this laboratory indicates that the deposit weight on the Hull cell cathode is reproducible if all conditions of the deposition process are kept constant (i.e., constant amperage, time interval, temperature, etc.). Individually made up Watts' baths used in a Hull cell (3 amp, 110 sec, 43°C, pH 1.8) gave the following deposit weights: 90.6, 90.9, and 91.5 mg.

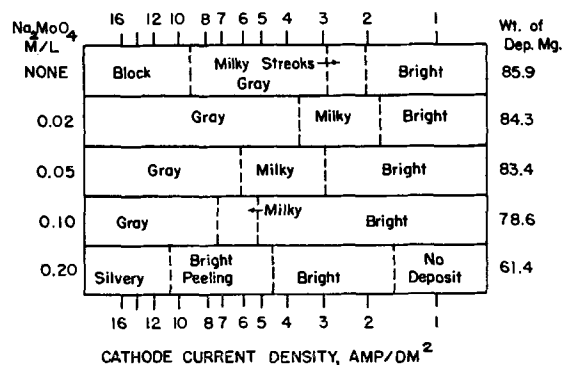


FIG. 1. Appearance of Hull cell cathodes, showing the plating range of sodium citrate nickel-molybdenum solutions containing varying amounts of sodium molybdate (3 amp for 2 min at room temperature; pH 10.5).

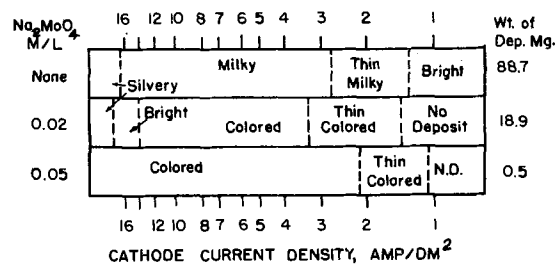


FIG. 2. Appearance of Hull cell cathodes, showing the plating range of "citric acid" nickel-molybdenum solutions containing varying amounts of sodium molybdate (3 amp for 2 min at room temperature; pH 10.5).

Regular Plating Procedures

Regular plating procedures were used to obtain more quantitative information about C.C.E. and alloy compositions from various citrate Ni-Mo baths. Results are given in Table I.

Table I shows that, for the Ni-Mo bath, the presence of NH₄⁺ or K⁺ appears to limit the amount of Na₂MoO₄ which can be added before the C.C.E. drops off appreciably. However, for a given concentration of Na₂MoO₄, a larger percentage of molyb-

A series of Hull cell runs made on 250 ml aliquots of a citric acid nickel bath at various pH values showed the following

Bath No.	Bath pH	Wt of deposit, mg Run 1	Wt of deposit, mg Run 2
1	1.3	9.0	9.7
2	6.5	54.5	55.6
3	9.5	81.9	81.4

If the above baths were judged only by deposit appearance, then baths 2 and 3 compare favorably with each other and there would be no basis for using one instead of the other; whereas, if the deposit weights are available, bath 3 can be chosen because it has good appearance and a higher C.C.E. Thus as an additional aid in determining the suitability of various complexing agents, the weight of the deposit should be considered. Baths could be regarded as having the same C.C.E. if the deposit weights agreed to within 1 or 2 mg.

TABLE I. Comparison of nickel-molybdenum citrate plating solutions containing increasing amounts of sodium molybdate

(0.3 M/l NiSO₄; 0.3 M/l citrate; NH₄OH to pH 10.5; 25°C; 10 amp/dm² for 10 min)

Bath				
Na ₂ MoO ₄	Na ₂ citrate	(NaK) ₂ citrate*	K ₂ citrate	(NH ₄) ₂ H citrate
M/l	C.C.E. %	C.C.E. %	C.C.E. %	C.C.E. %
None	82	80	85	82
0.02	82	79	82	10
0.05	81	80	51	3
0.1	80	78	Nil	Nil
0.2	78	81	Nil	Nil
	Ni in alloy	Ni in alloy	Ni in alloy	Ni in alloy
	per cent	per cent	per cent	per cent
None	100.0	100.0	100.0	100.0
0.02	98.3	95.6	95.6	89.5
0.05	95.9	91.7	83.4	77.0
0.1	92.6	84.3	—	—
0.2	86.7	79.4	—	—

* 0.15 M/l Na₂ citrate + 0.15 M/l K₂ citrate.

TABLE II. Effect of increasing amounts of ammonium citrate (and corresponding decrease of sodium citrate) on the nickel-molybdenum plating solution

Electrolysis for 10 min at 10 amp/dm²; pH about 10.5; room temperature

Citrate-0.3 M/l		Cathode deposit	Approx. C.C.E.	Nickel in deposit
Na ₂ Cit	(NH ₄) ₂ HCit			
		g	%	%
0.3 M/l	0.0 M/l	0.2383	82	86.1
0.25 M/l	0.05 M/l	0.1682	58	79.6
0.20 M/l	0.1 M/l	0.0208	8	69.2
0.15 M/l	0.15 M/l	0.0088	—	—
0.10 M/l	0.20 M/l	0.0057	—	—
0.0 M/l	0.3 M/l	0.0045	—	—

denum is obtained in the alloy deposit from baths containing these same two ions.

The observation that Ni-Mo plating solutions prepared from citric acid and ammonium hydroxide to pH 10.5 gave much lower C.C.E. than similar solutions prepared from sodium citrate suggested that it was the excess ammonium salts present in the former solutions which caused the lower C.C.E. The effect of ammonium ion was studied by using plating solutions with the standard concentration but with the 0.3 M/l of citrate ion supplied by varying amounts of sodium citrate, Na₂Cit, and ammonium citrate, (NH₄)₂HCit. The results, in Table II, show that increasing the ammonium ion concentration decreases both the C.C.E. and the nickel content of the alloy deposit. The same effect was noted for the cobalt-molybdenum citrate bath.

Sodium Citrate Bath

The early work on Ni-Mo plating solutions did not indicate that the sodium citrate bath was

better than, for example, a Rochelle salt bath, although the tartrate solutions had the disadvantage of forming a precipitate over the approximate pH range of 3.0–9.0. There is, however, no question about the superiority of sodium citrate as the complexing agent over citric acid or ammonium citrate for the deposition of molybdenum alloys. Extensive work had been done with the Ni-Mo citrate bath at the time that the study on the Co-Mo plating baths was started, and when sodium citrate was also found to be a "good" complexing agent, it was decided that a comparison of the electrodeposition of three alloys, iron-molybdenum, cobalt-molybdenum, and nickel-molybdenum from sodium citrate solutions, should be made.

Bath.—The alloy deposits compared were electrodeposited using the following bath concentrations and conditions unless otherwise stated:

Sulfate of codepositing metal	0.3 M/l
Sodium citrate	0.3 M/l
Sodium molybdate	0.2 M/l
Ammonium hydroxide	to pH 10.5
Current density	10 amp/dm ²
Time of electrolysis	10 min for nickel and cobalt alloys and 20 min for iron alloys
Temperature	25°C
Volume of solution	250 ml

These conditions were used for the Co-Mo and Fe-Mo baths even though they are probably not the best conditions for this purpose. No difficulty was encountered in the preparation of the plating solutions; however, the Fe-Mo solution was allowed to stand for several hours before use to help obtain consistent results. Some of the Fe-Mo baths had solid material settling out upon long standing.

Bath temperature.—A heating coil was used to maintain the bath at elevated temperatures during electrolysis. Measurements of pH were made at the operating temperature of the bath using a high temperature glass electrode. The results of electrolysis at three temperatures are given in Table III.

This table shows that increasing the bath temperature decreases the percentage of iron and nickel in the alloys, but increases the amount of cobalt. The molybdenum content of the iron-molybdenum alloys remained nearly constant. The fact that the iron and nickel content of the deposit decreases (the opposite would be expected) may be accounted for by the pH change of the bath. The pH of the Fe-Mo and Ni-Mo baths at 70°C is approximately a whole unit lower than at 30°C and Fig. 9 shows the percentages of codepositing metals to be approximately 32% iron and 71% nickel at the lower pH values. Thus, the percentage of iron and nickel is increased (36.8%; 78.8%) due to an increase in temperature,

TABLE III. Effect of bath temperature on the sodium citrate molybdenum alloy bath

Bath temp °C	Approximate bath pH	Bath C.C.E. %			% Codeposited metal		
		Fe-Mo	Co-Mo	Ni-Mo	Fe	Co	Ni
30	10.5	16	51	84	39.6	55.9	83.4
55	10.3-9.9	11	79	86	37.1	75.3	79.7
70	10.0-9.5	6	86	85	36.8	74.5	78.8

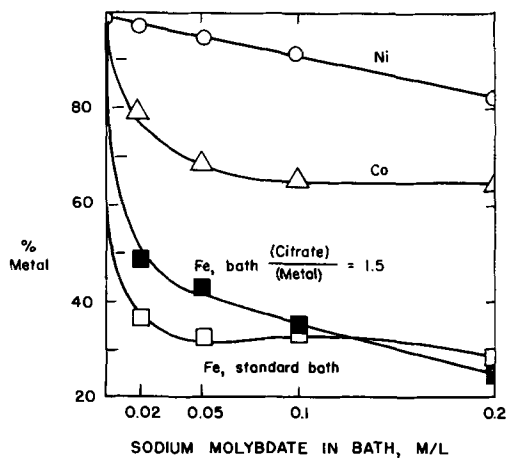


FIG. 3. Effect of sodium molybdate bath concentration on the composition of molybdenum alloys from sodium citrate molybdenum alloy baths.

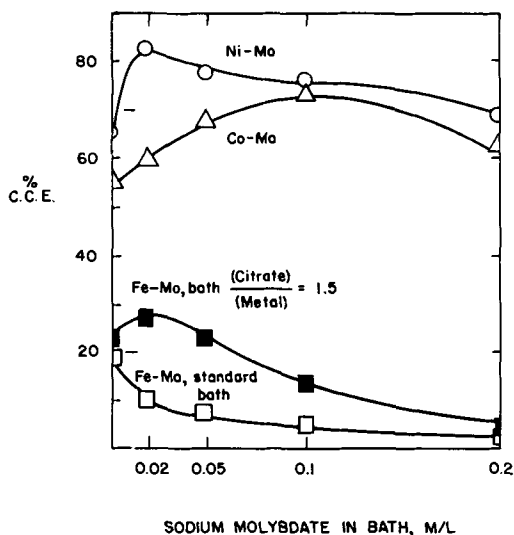
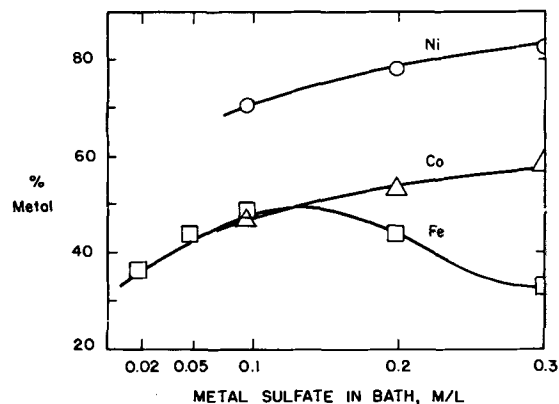


FIG. 4. Effect of sodium molybdate bath concentration on the cathode current efficiency of sodium citrate molybdenum alloy baths.

when the correction for pH is applied. It can be seen that at the higher temperature the C.C.E. of the Fe-Mo bath decreased, the efficiency of the Co-Mo bath increased, and there was slight effect upon the Ni-Mo bath.

Concentration of sodium molybdate.—Fig. 3 and 4 show the effect that the concentration of sodium molybdate has on the three sodium citrate solutions.

FIG. 5. Effect of concentration of metal sulfate on composition of molybdenum alloys from the sodium citrate molybdenum alloy baths (Fe-Mo bath, 20 amp/dm², 0.1 M/l Na₂MoO₄·2H₂O).

An increase of molybdate has the expected result of decreasing the percentage of iron, cobalt, or nickel in the alloy (Fig. 3) and increasing the molybdenum content. The percentage of molybdenum in the alloy deposit when small amounts of molybdate (0.02 to 0.05 M/l) are added to a bath is found to increase most rapidly in the iron-molybdenum alloy and least rapidly in the nickel-molybdenum alloy (Fig. 3). Fig. 4 shows that the C.C.E. increases and then decreases for the Co-Mo and Ni-Mo baths as the sodium molybdate concentration is increased. The efficiency for the Fe-Mo bath decreases from the start; however, if the citrate ion concentration is 1.5 times the iron concentration, there is an increase in the efficiency and then a decrease, similar to the Ni-Mo bath.

Concentration of codepositing metal sulfate.—The results of the electrolysis of a series of sodium citrate baths containing increasing amounts of metal sulfate are given in Fig. 5 and 6. Fig. 5 shows that the percentage of cobalt and nickel increases as their bath concentration increases, while the iron content of the alloy increases and then decreases as the iron sulfate concentration in the bath increases. The molybdenum content of the alloy decreases as the codepositing metal concentration increases; however, in the iron bath the molybdenum content increases at higher metal concentration. It is shown in Fig. 6 that the C.C.E. increases as the metal concentration is increased, and again the Fe-Mo bath has a lower C.C.E. when the iron sulfate concentration is high. It may be significant to note that an Fe-Mo bath, having a molar ratio of citrate to iron of 1.5, acts much like the Co-Mo and Ni-Mo baths. Note especially in Fig. 4 the effect that the concentration of sodium molybdate has on the C.C.E. of the Fe-Mo bath where the citrate concentration was 1.5 times the iron sulfate concentration.

Concentration of sodium citrate.—The results of the

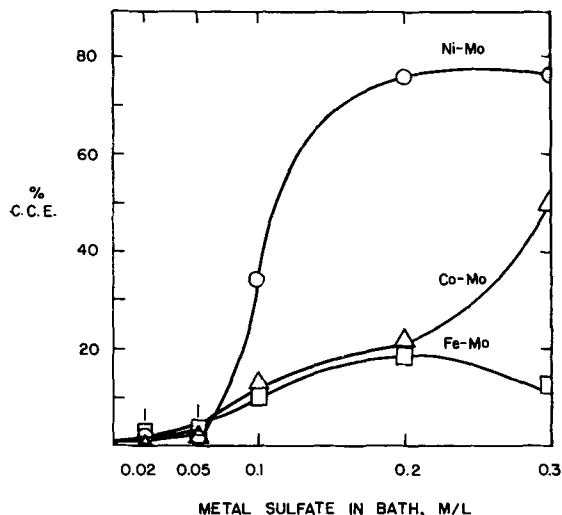


FIG. 6. Effect of concentration of metal sulfate on cathode current efficiency of sodium citrate molybdenum alloy baths (Fe-Mo bath, 20 amp/dm², 0.1 M/l Na₂MoO₄·2H₂O).

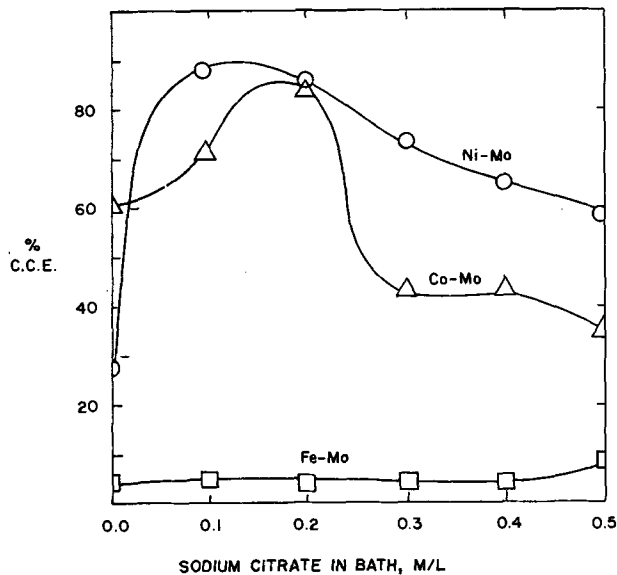


FIG. 8. Effect of concentration of sodium citrate on cathode current efficiency of sodium citrate molybdenum alloy baths.

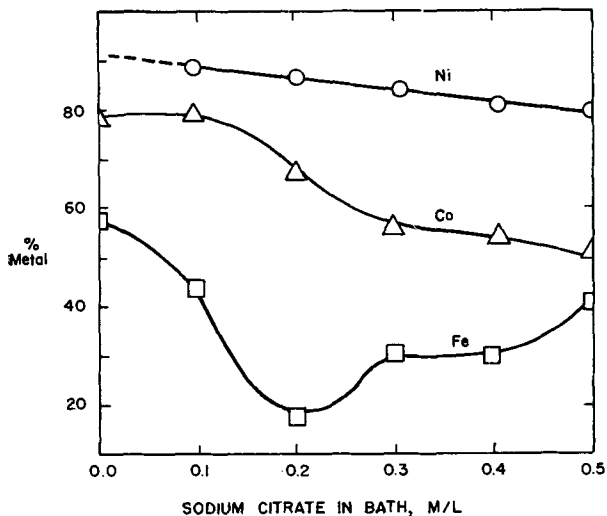


FIG. 7. Effect of concentration of sodium citrate on composition of molybdenum alloys from sodium citrate molybdenum alloy baths.

electrolysis of a series of plating solutions containing increasing amounts of sodium citrate are given in Fig. 7 and 8. It can be seen in Fig. 7 that the percentage of cobalt and of nickel in the alloys decreases and the percentage of iron decreases and then increases as the citrate concentration is increased. Other work with the Fe-Mo bath indicates that the iron content of the alloy steadily increases and that the molybdenum content increases and then decreases as the citrate content of the bath increases. The C.C.E. (Fig. 8) for the Ni-Mo and Co-Mo baths increases and then decreases while in the Fe-Mo bath it is nearly constant at mole ratios of citrate to iron below 1.5 (<0.5 M/l Na₃ citrate).

Bath pH.—All three plating solutions were studied

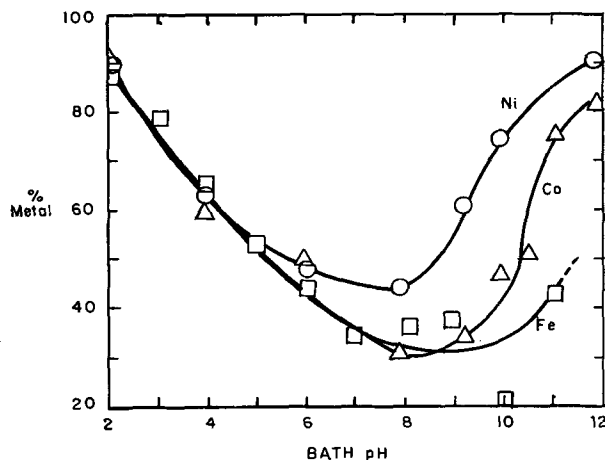


FIG. 9. Effect of bath pH on composition of molybdenum alloys from sodium citrate molybdenum alloy baths.

over the pH range 2.0 to about 12.0. The pH was adjusted downward with dilute H₂SO₄ and upward with NH₄OH. The pH in each case is the value given by the glass electrode (uncorrected). The results of the electrolysis of solutions at the various pH values are given in Fig. 9 and 10. In general it can be said that the iron, cobalt, and nickel content of the alloys decreased and then increased as the pH is increased (Fig. 9). The percentage of iron, cobalt, and nickel in the alloys from baths below pH 7.0 is nearly the same, while at higher pH values the three metals are present in widely different percentages; this effect of pH at the higher pH values may be due to the complexing action of NH₃ and not to the OH⁻ concentration. The lowest amount of codeposited metal in nickel-molybdenum and cobalt-molybdenum alloys occurs at approximately pH 8.0 while it

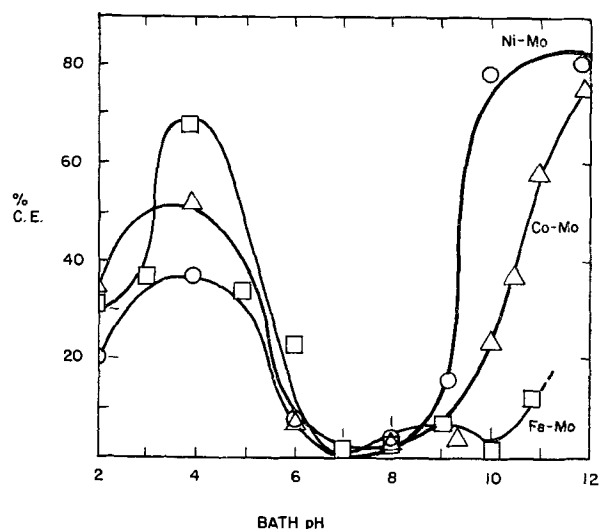


Fig. 10. Effect of bath pH on cathode current efficiency of sodium citrate molybdenum alloy baths.

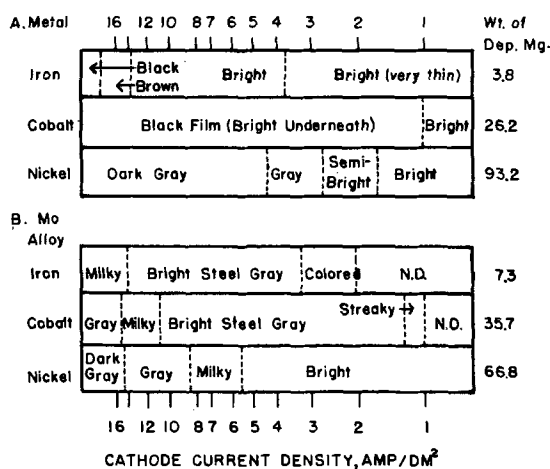


Fig. 11. Appearance of Hull cell cathodes comparing the plating range of a plain sodium citrate metal bath, (A), and of a sodium citrate alloy bath containing 0.1 M/l sodium molybdate, (B) (3 amp for 2 min; pH 10.5; room temp).

is lowest at pH 9.0 in the iron-molybdenum alloys. The percentage of molybdenum is highest at approximately the same pH values. Fig. 10 shows that at a pH of 7 to 8 a minimum in C.C.E. is obtained, while at pH 4 and pH 10-10.5 a maximum is obtained. At the higher pH the Ni-Mo bath operates with the highest C.C.E. followed by the Co-Mo and Fe-Mo baths, while at the lower pH the order is reversed with the Fe-Mo bath operating with the highest C.C.E.

Cathode current density.—The over-all effect of current density is best observed by means of the Hull cell. Fig. 11 shows Hull cell cathodes obtained from some of the baths studied.

More quantitative information was desired and regular plating procedures at several cathode current densities were tried with the results given in Table IV.

TABLE IV. The effect of cathode current density (C.C.D.) on cathode current efficiency (C.C.E.) and alloy composition using the sodium citrate bath

Bath	C.C.D.	Time	Wt. of deposit,	Approx. C.C.E.	% Codeposited metal in deposit
	amp/dm ²	min	g	%	
Fe-Mo	10	20	0.0242	2.5	28.5
Fe-Mo	20	20	0.0436	4.0	32.1
Co-Mo	1	100	0.0016	0.4	—
Co-Mo	5	20	0.0616	26	50.8
Co-Mo	10	10	0.0766	30	54.8
Co-Mo	20	5	0.1175	47	66.8
Ni-Mo	1	100	0.0852	34	71.8
Ni-Mo	5	20	0.1904	70	80.0
Ni-Mo	10	10	0.2299	82	83.2
Ni-Mo	20	5	0.2210	76	86.4

It is to be noted that the percentage of codepositing metal in the alloy increases somewhat as the current density increases. The C.C.E. increases with increasing current density for the Fe-Mo and Co-Mo baths and after increasing decreases for the Ni-Mo bath.

Substitutes for Ammonium Hydroxide

Since NH_4OH is a volatile base, its use in a plating bath should be avoided, particularly if an excess appears to be needed; thus numerous substitutes for raising the bath pH were tried. The standard sodium citrate bath without ammonium hydroxide was used with the possible substitutes. Small amounts of NaOH were added to portions of this bath to give solutions with pH values in the range 7-11.0. Electrolysis of these solutions resulted in only small cathode deposits with C.C.E. less than 1%. Various combinations of NaOH and NH_4OH gave plating solutions that showed good C.C.E. only with a large excess of NH_4OH . The following other substitutes were tried: ethyl amine, ethanol amine, diethanol amine, triethanol amine, ethylenediamine, pyridine, and hydrazine. In no case was a suitable plating bath obtained. Later, the above experiments were conducted on the Co-Mo plating bath and the results obtained for the Ni-Mo bath confirmed.

Anodes

Insoluble platinum anodes were used in all electrolyses reported in this article, but soluble anodes are likely to be required for proper maintenance of the plating solutions. Exploratory work on the Ni-Mo bath with soluble anodes indicates that, whereas Mo anodes dissolve readily, changes in bath composition are required before Ni anodes will dissolve sufficiently to maintain the nickel concentration of the bath. Ni anodes used in the sodium citrate bath, pH about 10.5, dissolve only slightly with anode

efficiencies less than 1%. As would be expected the addition of chloride ion, as NaCl, MgCl₂, or NiCl₂ increases the rate of anode dissolution. An increase in the anode current density was also found to increase the anode current efficiency in solutions containing chloride ions. Molybdenum anodes were found to dissolve with an efficiency of 95 to 100%.

Examination of Deposits

All the deposits which were examined were metallic in appearance. Some of the iron-molybdenum deposits were nonmetallic, but the properties of such deposits are not included in this paper. The nickel-molybdenum alloys were either silvery or gray in appearance and were bright when plated on polished cathodes. The cobalt-molybdenum alloys were either gray, silvery, or bright; in some cases the alloy was bright even though the basis metal was not polished. The iron-molybdenum alloys had the appearance of gray cast iron and no bright deposits were obtained. The alloy deposits examined usually ranged up to 0.0004 in. in thickness, but somewhat thicker deposits can be obtained. Alloys were readily soluble in 4*N* nitric acid which was used to dissolve the deposits for making analyses.

All of the deposits contained cracks (see Fig. 12), the brighter the deposit the more and finer the cracks (the surface has a spider web appearance). Iron-molybdenum deposits contained the fewest cracks, while the bright cobalt-molybdenum deposits had the most.

Adhesion of the deposits to flat cathode surfaces was good, but occasionally the deposit peeled in

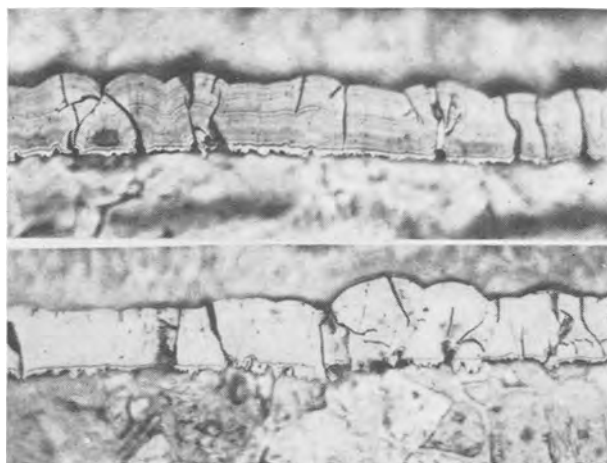


FIG. 12. Micrographs (500 ×) of typical nickel-molybdenum alloy deposits as plated on a copper tube, and then covered with copper electrodeposited from a cyanide bath. Etch: 2-min immersion in a H₂SO₄-H₂O₂ solution (2 ml 98% H₂SO₄, 10 ml 30% H₂O₂; 100 ml H₂O) at 30°C. The deposit is nodular, contains many cracks, and has a banded structure. Preferential etching of copper causes copper portions of micrograph to be out of focus.

spots and careful handling of the cathode after cleaning was necessary. In most cases adhesion was not good when the alloys were deposited on steel rods, or on copper or brass tubing. Such deposits were easily rubbed off in a flake or powder form, but in a number of cases a very thin layer (see Fig. 12) adhered strongly to the basis metal with the bulk of the deposit separating from this thin coating and not from the basis metal. Removal of the copper tube from some of the better nickel-molybdenum deposits by chemical means left a fragile shell which was porous and easily crumbled. Deposits plated on stainless steel cathodes were shriveled in appearance and could be brushed off in flake or powder form.

The alloy deposits on copper, when bent once 90° or 180°, cracked, usually along the initial crack lines showing the copper basis metal. The amount of copper exposed depended upon the size and distribution of the initial cracks, the many smaller spaced cracks showed less basis metal than the fewer larger spaced cracks. The adhesion of the nickel-molybdenum alloys to the basis metal during repeated bending was good and the alloy did not flake off until the cathode metal was nearly broken. The iron-molybdenum alloys after several bends began to flake off in areas around the bend. The cobalt alloys withstood the bending test better than the iron-molybdenum alloys but not as well as the nickel-molybdenum alloys.

The poor character of most of the deposits may be due to the hydrogen which was deposited on the cathode. Very little hydrogen is evolved from the cathode during plating but when the deposits (especially the iron-molybdenum and cobalt-molybdenum deposits) were washed, large amounts of gas were evolved. This absorbed hydrogen perhaps caused stresses in the alloy deposits and caused the shriveled appearance of the deposits when plated on the flat stainless steel and on the tubing.

DISCUSSION

The results presented make it reasonable to conclude that a practical aqueous plating bath for the electrodeposition of molybdenum alloys containing iron, cobalt, or nickel could be worked out. However, the development of such a plating bath was not the immediate objective of this work.

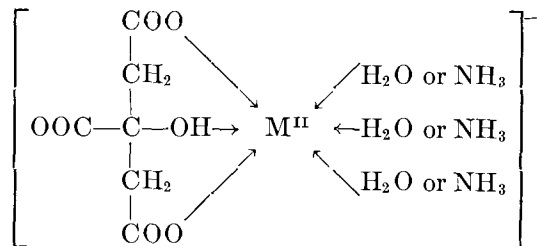
It was found that the Ni-Mo citrate bath operates much more efficiently (C.C.E. 75–85%) than either the Co-Mo (C.C.E. 50–60%) or the Fe-Mo (C.C.E. 10–20%) citrate baths, while a higher molybdenum content was found in the Fe-Mo (50% Mo) deposits than in either the Co-Mo (40% Mo) or the Ni-Mo (20% Mo) deposits. The sodium citrate bath is an improvement over that proposed earlier (1) in that higher current efficiencies are obtained.

The results obtained can be explained by assuming

a series of reactions involving citrate and ammine complexes of the codepositing metals, and molybdate ions. Bobtelsky and Jordan (10) suggest the following structures for the citrate complexes of bivalent and trivalent metals:

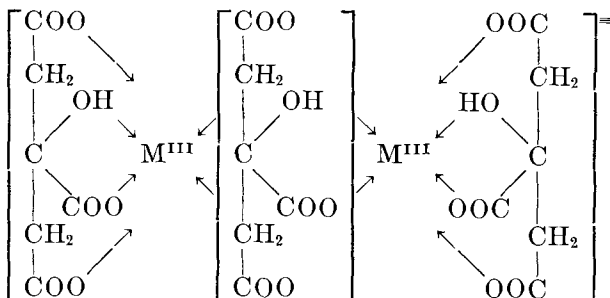
(Structure I)

Bivalent metal citrate complex where molar ratio of citrate to metal ion is 1.0



(Structure II)

Trivalent metal citrate complex where molar ratio of citrate to metal ion is 1.5



Since nickel has the stable oxidation state of plus two, its complex would have structure I. Iron and cobalt, however, can have either plus two or plus three oxidation states and, therefore, an equilibrium mixture of structures I and II could be present.

By referring to Fig. 6 and 8, the following observations about the C.C.E. of the Co-Mo bath may be noted. In Fig. 6, as the molar ratio of citrate to metal ion decreases and approaches 1.0 (0.3 M/l metal sulfate) the C.C.E. of the bath increases, whereas at higher molar ratios (0.1 and 0.2 M/l metal sulfate), the C.C.E. curve is similar to the C.C.E. curve for the Fe-Mo bath. In Fig. 8, the C.C.E. of the Co-Mo bath decreases when the molar ratio of citrate ion to metal ion is between 0.6 and 1.0 (0.2 and 0.3 M/l Na_3Cit) and levels off when the molar ratio is greater than 1.0 (above 0.3 M/l Na_3Cit). It is possible that, at a molar ratio of citrate ion to cobalt ion of one, the citrate ion is capable of complexing $\text{Co}(\text{II})$ tightly enough to prevent the $\text{Co}(\text{III})$ ammine complex from forming when the solution is made ammoniacal. These observations could indicate that at the concentrations used the cobalt complex present in greatest amount has structure I. The fact that the C.C.E. for some Co-Mo baths is as high as the C.C.E. for some Ni-

Mo baths is then to be expected since cobalt and nickel form the same type of bivalent metal citrate complex. If the trivalent metal complex were present to a larger extent, one would then expect the Co-Mo bath to behave more like the Fe-Mo bath. The following observations are made about the Fe-Mo bath from Figs. 6 and 8. In Fig. 6 the C.C.E. curve for the Fe-Mo bath starts to decrease when the mole ratio of citrate ion to metal ion is less than 1.5 (>0.2 M/l $\text{FeSO}_4 \cdot 7\text{H}_2\text{O}$) which may indicate that the structure I type of complex is being formed. In Fig. 8 the C.C.E. is constant up to a molar ratio of citrate ion to metal ion of 1.3 (0.4 M/l Na_3Cit) and when the molar ratio is 1.6 (0.5 M/l Na_3Cit) the C.C.E. curve starts to increase. These observations could indicate that a structure II complex for iron is involved. The fact that deposition occurs from highly ammoniacal solutions would make the bivalent complexes contain ammonia instead of water.

Assuming the above complex structures to be essentially correct, then for the deposition of the single metals (iron, cobalt or nickel) the following reactions may occur:

Metal citrate ammine ion \rightleftharpoons Metal ammine ion



Metal ammine ion \rightarrow Metal ammine-metal bridge



Metal ammine-metal bridge $\xrightarrow[\text{exchange}]{\text{electron}}$ metal



All three metals are capable of forming the metal ammine complex; nickel and cobalt form stable amines while the iron (II) ammine is rather unstable. It is assumed that for the iron and cobalt complexes there is an equilibrium between the two structures and that structure I can be formed from structure II by a dissociation mechanism and then structure I dissociates according to reaction (I). The metal ammine complex then migrates to the cathode and with the formation of a bridge complex, as postulated by Lyons (11), binds itself to the cathode and splits off ammonia. Deposition from the metal ammine ion can account for the C.C.E. observed. The nickel citrate ammine could easily split as in reaction (I) and would allow deposition to proceed at a greater rate than in the case of iron where the dissociation of the complex would be less, leaving little metal ammine ion from which deposition occurs. Therefore, the iron bath would be expected to operate at a lower C.C.E.

The fact that the percentages of nickel and cobalt in the deposit decrease when a series of deposits are made from the same bath without replenishing the metal ion concentration could indicate that reaction (I) is forced to the left due to common ion effect. The

main function of the citrate ion would be to keep the metal ion concentration low.

When molybdate is added, it does not necessarily have to be involved with the metal citrate ammine complex, but can retain its own identity as MoO_4^{2-} (the species most likely in an alkaline solution). Since the presence of iron, cobalt, or nickel is necessary to accomplish the reduction of molybdate to molybdenum [this would be reaction (IV)], these metals may be considered to be catalysts. Deposition of iron, cobalt, or nickel occurs as mentioned from the ammine complex, the MoO_4^{2-} may then be assumed capable of forming another bridge complex⁴ with the cathode and be reduced. The actual reduction of the molybdate at the cathode may be accomplished by hydrogen. The black oxide that is present on some deposits may be due to partial reduction of the molybdate bridge complex.

The rate at which the molybdenum content increases in the three alloys may be explained as follows. If the competing reactions for the deposition process are considered to be reactions (II) and (IV), then reaction (II) depends upon the dissociation of the metal citrate ammine complex [reaction (I)]. There would be a greater concentration of nickel ammine than iron ammine and therefore a small amount of MoO_4^{2-} in the Fe-Mo bath will give a larger percentage of molybdenum than the same amount in the Ni-Mo bath simply because the molybdate ion has a better chance to come in contact with the cathode.

The fact that high concentrations of sodium molybdate decrease the C.C.E. of the bath can perhaps be explained in the following way. The MoO_4^{2-} can be considered to reach the cathode by diffusion, as postulated for the tungstate ion by Clark and Lietzke (12). When the MoO_4^{2-} concentration is high the cathode becomes covered with a thin insoluble film containing molybdenum in some oxidation state or states intermediate between the free metal and Mo(VI). This cathode film may prevent the metal ammine from which deposition of the catalytic metal occurs from reaching the cathode.

The detrimental effect of ammonium ion could be due to the instantaneous discharge of ammonium

⁴ MoO_4^{2-} may be assumed capable of forming this bridge complex since it may have bonding orbits available in the 4d and 5s, p levels.

ion to ammonia and hydrogen in preference to the other cathode reactions.

Since the percentage of the codeposited metal in the alloy is increased with an increase in the bath temperature, it may be assumed that this is due to an increase in the dissociation of the metal citrate complex.

It is realized that the proof for this postulated mechanism is very scanty, but future work in this laboratory will be directed toward the investigation of the mechanism. It is quite probable that the process for the electrodeposition of tungsten alloys (13) from similar solution is much the same as the process involved in the electrodeposition of these molybdenum alloys.

ACKNOWLEDGMENT

This work was supported in part by the Office of Ordnance Research under contract DA 11-022-ORD-656 and also by the Research Committee of the Graduate School from funds supplied by the Wisconsin Alumni Research Foundation.

Any discussion of this paper will appear in a Discussion Section to be published in the June 1956 JOURNAL.

REFERENCES

1. H. J. SEIM AND M. L. HOLT, *This Journal*, **96**, 205 (1949).
2. M. L. HOLT AND H. J. SEIM, U. S. Pat. 2,599,178, June 3, 1952.
3. L. F. YNTEMA AND M. J. KSYCKI, U. S. Pat. 2,499,807, March 7, 1950.
4. L. F. YNTEMA AND M. J. KSYCKI, U. S. Pat. 2,499,808, March 7, 1950.
5. A. BRENNER AND P. S. BURKHEAD, U. S. Pat. 2,653,127, Sept. 22, 1953.
6. C. C. MA, U. S. Pat. 2,516,227, July 25, 1950.
7. R. F. McELWEE AND M. L. HOLT, *This Journal*, **99**, 48 (1952).
8. I. N. FRANTSEVICH, T. F. FRANTSEVICH-ZABLUDOVSKAYA, AND E. F. ZHELVIS, *J. Appl. Chem. U.S.S.R.*, **25**, 387 (1952) (English translation); *Zhur. Priklad. Khim.*, **25**, 350 (1952); *C. A.*, **48**, 8679b (1954).
9. "Scott's Standard Methods of Chemical Analysis," 5th ed., p. 589, D. Van Nostrand Co., Inc., New York (1952).
10. M. BOBTELSKY AND J. JORDAN, *J. Am. Chem. Soc.*, **67**, 1824 (1945); **69**, 2286 (1947).
11. E. LYONS, *This Journal*, **101**, 376 (1954).
12. W. E. CLARK AND M. H. LIETZKE, *ibid.*, **99**, 245 (1952).
13. L. E. VAALER AND M. L. HOLT, *Trans. Electrochem. Soc.*, **90**, 43 (1946); W. E. CLARK AND M. L. HOLT, *J. (and Trans.) Electrochem. Soc.*, **94**, 244 (1948); M. H. LIETZKE AND M. L. HOLT, *ibid.*, **94**, 252 (1948).

Periodic Current Reversal in Plating Copper-Lead Alloys¹

NELSON W. HOVEY, JOHN L. GRIFFIN,² AND ALBERTINE KROHN

Chemistry Department, University of Toledo, Toledo, Ohio

ABSTRACT

Apparatus based on the commutator principle was designed and constructed to convert direct current to square-wave alternating current, and was applied in electrodepositing copper-lead alloys from a cyanide-tartrate solution. The procedure was successful in eliminating the nodules which occurred in alloy deposits obtained in previous studies using this type of bath.

INTRODUCTION

Previous studies of various methods of electroplating alloys of copper and lead reported that the most promising bath for this purpose was a cyanide-tartrate solution having the following composition (1, 2): NaOH—40.0 g/l; NaCN—147.0 g/l; NaKC₄H₄O₆·4H₂O—211.7 g/l; CuCN—150.6 g/l; Pb-(C₂H₃O₂)₂·3H₂O—75.9 g/l. Using the operating conditions given in the experimental part of the earlier paper (but without current reversal), the alloy deposited from the freshly prepared solution contained approximately 70% copper. However, the deposits tended to be highly strained, brittle, and nodular. The work of Jernstedt (3) suggested the possibility of preventing the growth of nodules on deposits from this bath by the use of periodically reversed current.

The principal purpose of the research reported in this paper was to design and construct a simple, inexpensive device for converting direct current to square-wave alternating current of readily variable frequency and wave form. The limited work on copper-lead alloy plating using the apparatus described was done mainly to demonstrate that this method of producing periodic reversed current is practical. Data obtained were sufficient to show that nodule formation on deposits from this bath is inhibited by periodic current reversal.

No attempt was made to produce any particular alloy composition. The deposits obtained using periodic reversed current were higher in copper content than those produced with direct current under comparable conditions. Copper content increased as the percentage of anodic current was increased. Previous work (1) indicated that alloy composition

may be varied within wide limits when direct current is used. It should be possible to compensate for the relatively faster dissolution of lead during the period that the deposit functions as the anode and produce deposits of any desired composition. That smooth bright deposits are obtainable over a wide composition range has not yet been proved.

The commutator principle appeared to furnish the method most likely to give an apparatus which was flexible but economical to build. Equipment characteristics thought desirable for this investigation include: (a) low-frequency limit of 10 cps; (b) the frequency variable over a range of five to ten times the lower limit; and (c) a means for varying the alternating current wave form to give variable ratios of plating to polishing current. Preliminary studies showed that nodule formation began early in the plating process. Nodules were discerned on several samples obtained after 30-sec plating time. To facilitate the action of the polishing fraction of the cycle in preventing or removing nodules, a minimum frequency of about 10 cps was chosen so that the polishing could start very early in the process.

CONSTRUCTION OF THE COMMUTATOR

Two 60-bar commutators from standard 24 volt generators were utilized. Fig. 1 shows the machined output commutator. Two series of 19 bars each were connected by soldering a heavy copper strap to the bars on the outer shoulder of each. The two resulting segments were separated by two series of 11 free bars each. Holes were drilled between each of the 22 free bars and between the last free bar and the end bar of the large segment. These holes were tapped for small machine screws. This arrangement was designed to permit the use of the machine screws as shorting plugs to permit the adjustment of the wave form by varying the connections between the free bars and the large segments.

The commutator produces two complete plating-polishing cycles per revolution. Since two cycles involve 60 bars, one bar is equivalent to $\frac{1}{30}$ or $3\frac{1}{3}\%$

¹ Manuscript received January 4, 1954. This paper was prepared for delivery before the Wrightsville Beach Meeting, September 13 to 16, 1953, and was abstracted from a thesis presented by John L. Griffin to the University of Toledo in partial fulfillment of the requirements of the degree of Master of Science.

² Present address: Chemistry Department, University of Michigan, Ann Arbor, Michigan.

of a cycle. Thus, the ratio of effective plating current is variable from 93 1/3 % to 20 % of one cycle in steps of 6 2/3 %.

For example, suppose it is desired to have the plating current flow for 1/20 sec and the polishing current for 1/100 sec. The ratio of polishing current time to total cycle time is 1:6 or 16 2/3 %. The number of bars to be connected in the polishing current segment is then 16 2/3 divided by 3 1/3 or 5 bars.

To accomplish the required connection, the index bar in the polishing current section is connected to the following four free bars by inserting four of the brass screws. The hole between the fourth and fifth free bars is left open to isolate the polishing current segment from the plating current segment. The rest of the free bars are connected to the next large segment by inserting the rest of the screws. This procedure is repeated for the other side of the output commutator.

Fig. 2 shows the complete commutator and shaft assembly. The input commutator bars were connected by soldering a heavy copper strap to the outer end of each bar to form two segments of 30 bars each.

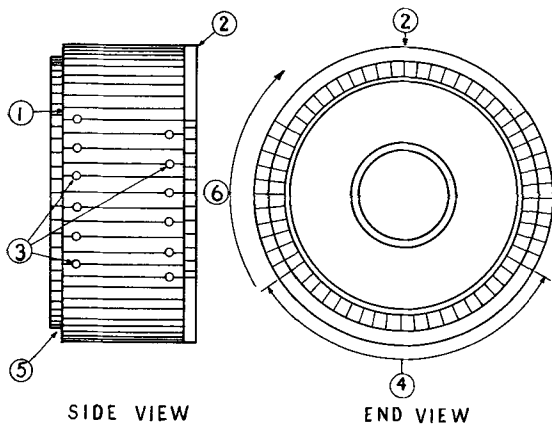


FIG. 1. Machined output commutator. 1—Index bar; 2—shorting strap; 3—holes tapped for machine screws; 4—large segment; 5—shoulder turned for connecting straps; 6—direction of rotation.

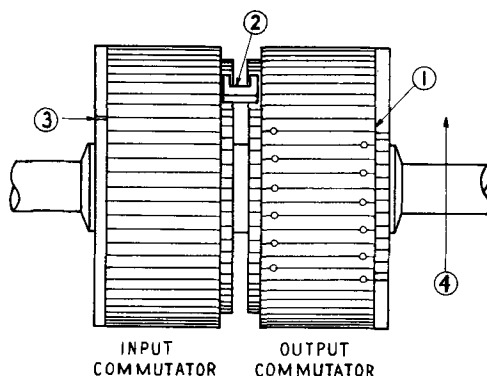


FIG. 2. Commutator and shaft assembly. 1—Index bar; 2—connecting strap; 3—segment separation point; 4—direction of rotation.

The separation points of these segments were positioned one bar ahead of the corresponding separation points on the output commutator. This resulted in a minimum polishing current fraction of 3 1/3 of a cycle. Each input segment was then connected to the large output segment nearest it with heavy copper strap. No adjustment of the input commutator was needed since its connections were fixed.

A diagram of the brush holder assembly is shown in Fig. 3. The holder was constructed to present two

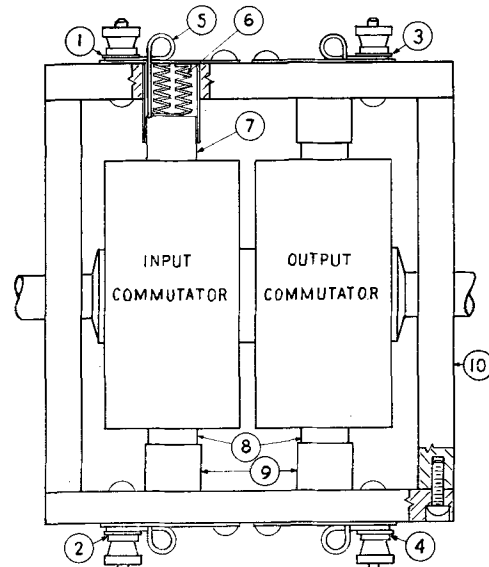


FIG. 3. Brush holder assembly. 1—D.C. plus input; 2—d.c. minus input; 3—a.c. to anode; 4—a.c. to cathode; 5—flexible lead to brush; 6—spring; 7—brush; 8—brushes; 9—holders; 10—Bakelite frame.

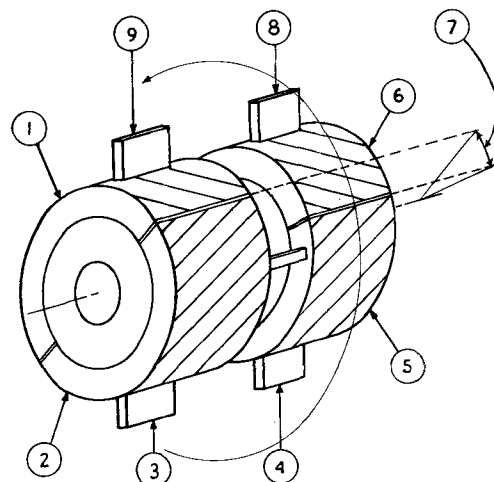


FIG. 4. Schematic representation of the principle of the commutator. 1—Input commutator segment, first half; 2—input commutator segment, second half; 3—input brush, d.c., negative; 4—output brush, a.c., to cathode; 5—output commutator segment, second half; 6—output commutator segment, first half; 7—angular separation of positions of polarity change in input and output commutators; 8—output brush, a.c., to anode; 9—input brush, d.c., positive.

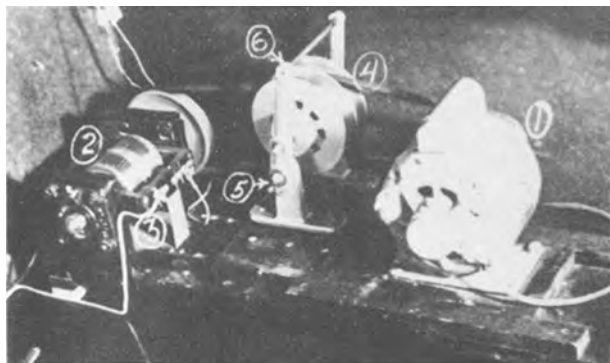


FIG. 5. Complete commutator assembly. 1— $\frac{1}{3}$ hp electric motor; 2—commutators; 3—brush holder; 4—speed changer; 5—pivot bolt; 6—control handle.

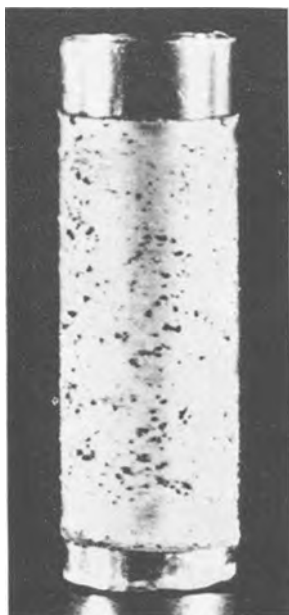


FIG. 6. Typical deposit using direct current

fixed brushes to each commutator, normal to the surface, 180° apart, and under moderate spring pressure.

The principle of the commutator, the construction of which is shown in Fig. 1–3, is schematically represented in Fig. 4. The device is equivalent to two metal disks on a single shaft, each disk consisting of two semicircular halves insulated from each other. A single electrical connection extends from each semicircle of one disk to a corresponding semicircle of the other disk. If the sectors of one disk, instead of paralleling the sectors of the other disk, are rotated, then the geometrical arrangement is equivalent to that accomplished by changing the positions of the screws.

The commutator and shaft assembly was mounted in ball bearings which were attached to a base containing the brush holder, motor, and speed changer.

The motor and speed changer drove the commutator shaft by means of V-pulleys and V-belts as shown in Fig. 5.

The frequency of alternation is changed by shifting the cone position of the speed changer. The control handle is moved toward the motor to decrease frequency and toward the commutator to increase

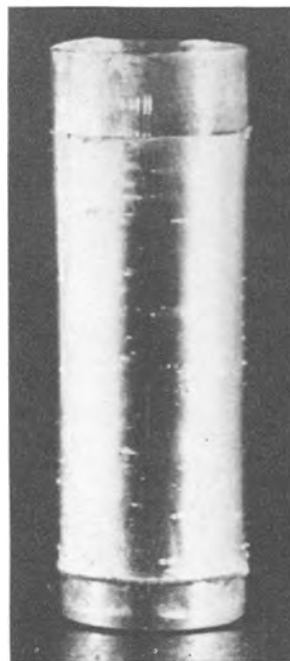


FIG. 7. Typical deposit with 10% anodic current.

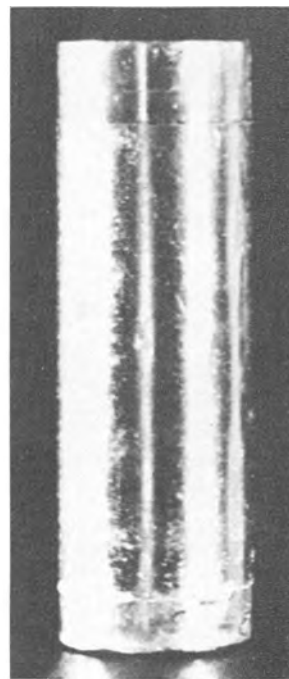


FIG. 8. Typical deposit with 20% anodic current.

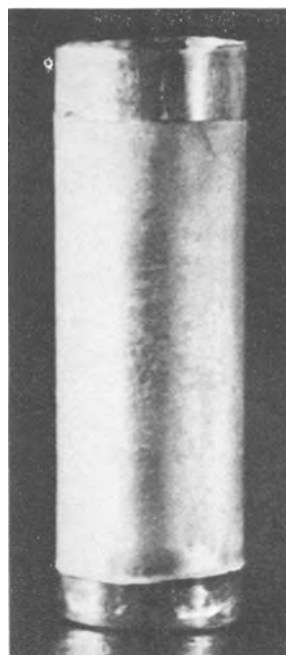


FIG. 9. Typical deposit with 30% anodic current.

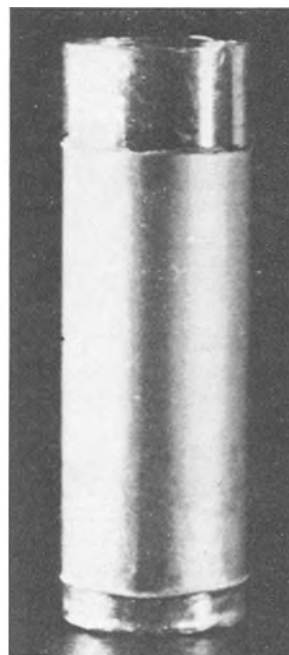


FIG. 10. Typical deposit with 40% anodic current.

frequency. Once set, the handle is locked in place by tightening the wing nuts on the pivot bolts.

EXPERIMENTAL

Except for plating time, procedures and conditions used were the same as those found best in the earlier studies (1, 2). These were: temperature, 40°C; current density, 3.3 amp/dm² (30 amp/ft²); and cathode rotation of 1750 rpm. To compensate for the reduced effective plating time resulting from the use of alternating current, the total time was extended to equal 25 min of actual plating time for each run.

RESULTS

The photographs of Fig. 6–10 show a typical series of deposits. The first (Fig. 6) is the extremely rough surface typical of a deposit using direct current. The nodules are dark gray, the background a dull, uneven copper color. This deposit was 57.6% copper.

The next series shows deposits made at a frequency of 30 cps with variations in the percentage of reverse current. Fig. 7 shows the deposit with 10% anodic current. The size and number of nodules have been reduced and the background is smooth. The deposit contained 60.3% copper.

The deposit when the current was 20% anodic is shown in Fig. 8. There are only a few rough spots; the rest is of high luster. Analysis showed 77.5% copper in the alloy.

With 30% anodic current, the deposit contained 93.6% copper and was free of nodules, but had only medium luster (Fig. 9).

Fig. 10, the deposit with 40% anodic current, is very smooth, of medium luster, and contains 98.8% copper.

Other runs made at 90 cps were similar in appearance and composition. Alloys deposited with anodic current values between 20–30% usually exhibited normal copper content and the most lustrous surfaces, while those deposited at high anodic current values showed a high copper content and smooth surfaces of medium luster.

Potential measurements indicated that polarization decreased with increasing percentages of anodic current, but no detailed study was made of this.

CONCLUSIONS

Very satisfactory apparatus for experimental work in electrodeposition using square-wave alternating current may be constructed at little cost.

Current reversal definitely reduces nodule formation on copper-lead alloy deposits from cyanide-tartrate solutions and makes it possible to obtain brighter deposits.

The deposits increase in copper content as the percentage of anodic current is increased. This indicates that lead is more active anodically than is copper in the cyanide-tartrate solution used. In order to compensate for this effect, either the solution must be modified or the plating conditions changed, or both, if relatively high lead content deposits are to be produced.

Any discussion of this paper will appear in a Discussion Section to be published in the June 1956 JOURNAL.

REFERENCES

1. A. L. FERGUSON AND N. W. HOVEY, *This Journal*, **98**, 146 (1951).
2. N. W. HOVEY, A. KROHN, AND A. L. FERGUSON, *ibid.*, **98**, 155 (1951).
3. G. W. JERNSTEDT, *Metal Finishing*, **45**, 68 (1947).

Graphite Anodes in Brine Electrolysis

III. Effect of Anode and Operating Variables on Caustic Color¹

M. JANES,² N. J. JOHNSON, AND E. B. PILCHER

Process Engineering Laboratory, National Carbon Company, A Division of Union Carbide and Carbon Corporation, Niagara Falls, New York

ABSTRACT

Caustic color data which have been obtained with a laboratory diaphragm chlor-alkali cell are summarized briefly. Effects of such cell operating variables as brine flow rate, brine concentration, and current density have been investigated. Measurements generally were made on the unevaporated catholyte effluent after addition of a reducing agent. The absorption spectrum appears identical with that of the compound isolated and identified by Heller. Light absorption by this pyromellitic acid chlor-quinol obeys Beer's law, so that degree of cell effluent coloration can be expressed in terms of the concentration of this compound. Chemical oxidation of graphite, as by hypochlorous acid, is believed to be an important factor in formation of the color-producing compound. As is known, caustic color is much less with treated graphite, consistent with the protection thus obtained against internal attack.

INTRODUCTION

The appearance of a blue or purple color in 50 % caustic produced by evaporating the cell effluent from diaphragm chlor-alkali cells equipped with graphite anodes has long been familiar (1). Heller's work (2) demonstrated that the color was due to an organic compound derived from oxidation of the graphite anodes. By extraction of used graphite stubs with water and subsequent purification of the extract a yellow crystalline compound was isolated which, when dissolved in caustic solution, would reproduce all the usual colors met in plant operation. Analytical and physicochemical studies of this compound led Heller to suggest a pyromellitic acid chlor-quinol structure.

As Heller noted (2), Cushing studied the caustic colors spectrophotometrically and found that a blue caustic solution prepared from the yellow compound isolated by Heller has the same spectral transmission curve as plant liquor.

Measurements of the degree of coloration as affected by variations in graphite or such cell operating conditions as temperature, brine concentration, etc., have been carried out in this laboratory during the past 13 years, employing a laboratory diaphragm cell. These measurements are fully in accord with Heller's conclusions and show the variation of concentration of colored compound with cell operating conditions and type of anode material.

¹ Manuscript received September 13, 1954. This paper was prepared for delivery before the Montreal Meeting, October 26 to 30, 1952.

² Present address: National Carbon Research Laboratories, Cleveland, Ohio.

EXPERIMENTAL

The laboratory diaphragm chlor-alkali cell in which these studies were made has been described (3). Unless otherwise stated, data presented here are for laboratory cell operation at 11 amp (approx. 0.5 amp/in.² anode current density), feed rate of 200 ml/hr saturated NaCl solution, and 80°C.

Color measurements were made directly on the cell effluent, with a reducing agent added to bring the light absorption by the color compound into the visual spectrum. Heller noted that a red or pink color develops if hot, unconcentrated cell effluent is treated with reducing agents such as dextrose, etc., and that the intensity of the red color seems to be an indication of the quantity of the coloring matter present. Sodium dithionite (hydrosulfite) at room temperature was used here.³ In the earliest work, the intensity of color developed was estimated visually in Nessler tubes, later with a photoelectric colorimeter, and recently with a Beckman Model "B" spectrophotometer. Fig. 1 shows the transmission curve of effluent from an operating laboratory diaphragm cell compared to a solution of the compound isolated by Heller⁴ in a synthetic medium of essentially the same composition as that of cell effluent (81 g/l NaOH, 223 g/l NaCl). Values of log A_s are plotted against wave length of light from 380 to 620 μ .⁵ The close correspondence of the two

³ Suggested by Howard Wells of Niagara Alkali Company.

⁴ Samples of this compound were kindly supplied to the authors by Heller.

⁵ The terminology and symbols for absorbancy (frequently called optical density) follow the recommendations of Mellon (4). The advantages of a log A_s plot are described by Stearns (5).

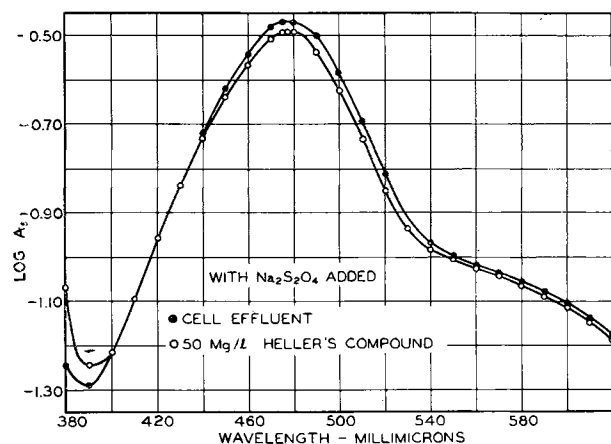


FIG. 1. Comparison of the absorption curve of laboratory cell catholyte with that of Heller's compound in alkaline chloride medium (with dithionite added).

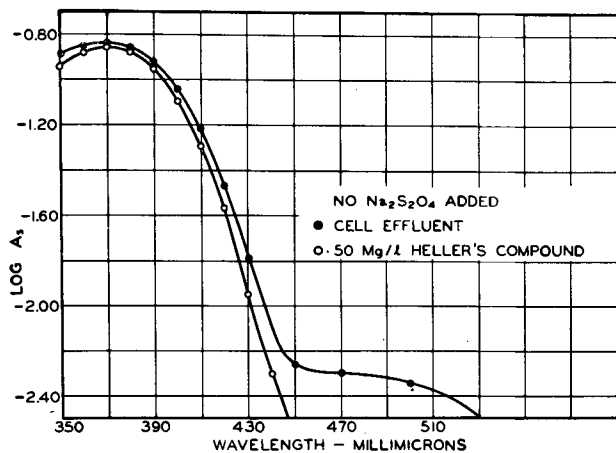


FIG. 2. Comparison of the absorption curve of laboratory cell catholyte with that of Heller's compound in alkaline chloride medium (no reducing agent added).

curves is strong evidence that the compound isolated by Heller is responsible for the color thus developed in cell effluent. There is a maximum absorption at 480 m μ ; but it is interesting that on adding $\text{Na}_2\text{S}_2\text{O}_4$ and gently agitating, a cherry red color appears initially which quickly changes to a reddish-brown. This change in color is so rapid that it has not been possible to obtain a transmission curve of the transient reduction product. The difference in absorption below 400 m μ indicated in Fig. 1 is no doubt due to slight differences in $\text{Na}_2\text{S}_2\text{O}_4$ concentration, which absorbs below this wave length.

In Fig. 2, the same cell effluent is compared with the same synthetic solution without addition of reducing agent. Again the curves correspond quite closely, with a maximum (in the spectral region shown) at about 372.5 m μ , possibly corresponding to the maximum observed by Heller for the compound in absolute alcohol solution at 350 m μ .

Fig. 3 shows that the absorption of Heller's com-

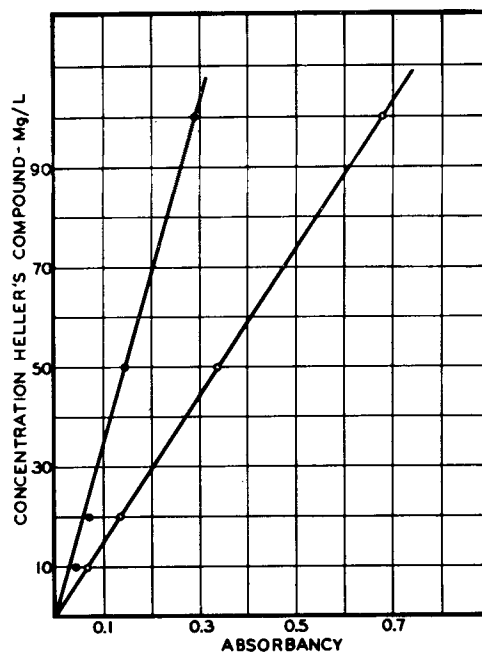


FIG. 3. Concentration of Heller's compound vs. absorbancy. \circ At 480 m μ with dithionite added; \bullet at 372.5 m μ without dithionite.

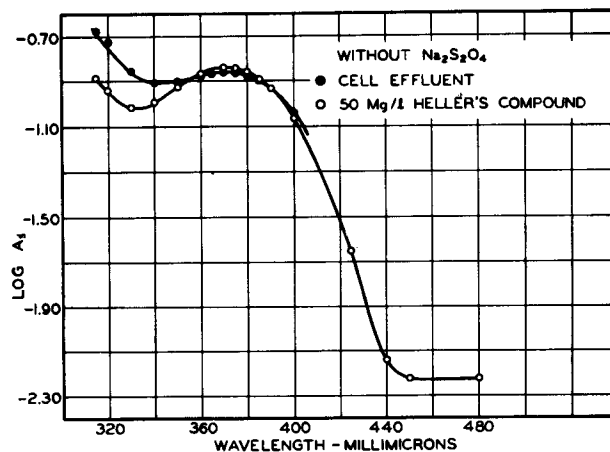


FIG. 4. Comparison of absorption of laboratory cell catholyte with that of Heller's compound in alkaline chloride medium at shorter wave lengths (no dithionite added).

pound at 480 m μ (after treatment with $\text{Na}_2\text{S}_2\text{O}_4$) follows Beer's law quite closely, i.e., the absorbancy is linear with respect to concentration. This relation has been used to convert the authors' absorption measurements to concentration of color compound.

The upper curve of Fig. 3 indicates that the absorption maximum at 372.5 m μ without treatment with a reducing agent does not follow Beer's law as well, and the measurement is less sensitive.

With an ultraviolet spectrophotometer, it is quite probable that equal sensitivity could be achieved without adding the reducing agent. As shown in Fig.

4, both the cell effluent and Heller's compound in an alkaline medium show increasing absorption below 330 $m\mu$. Measurements down to 315 $m\mu$ are shown, but these are not too reliable with the Model "B"

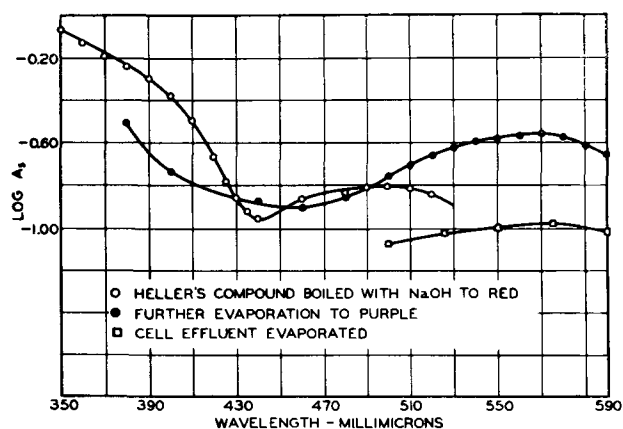


FIG. 5. Changes in absorption as a result of heating in the presence of NaOH.

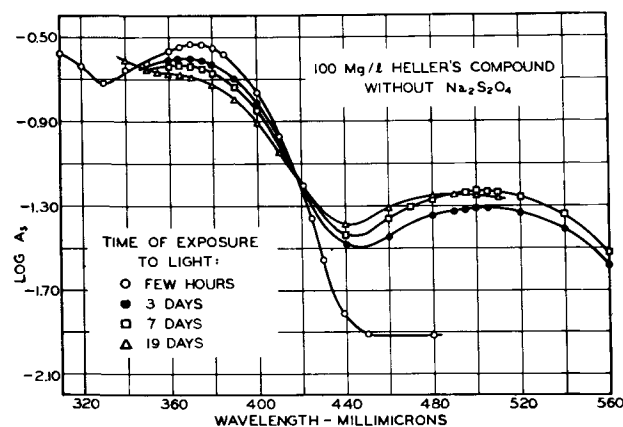


FIG. 6. Effect of exposure to light on absorption curve of Heller's compound in alkaline solution (no reducing agent added).

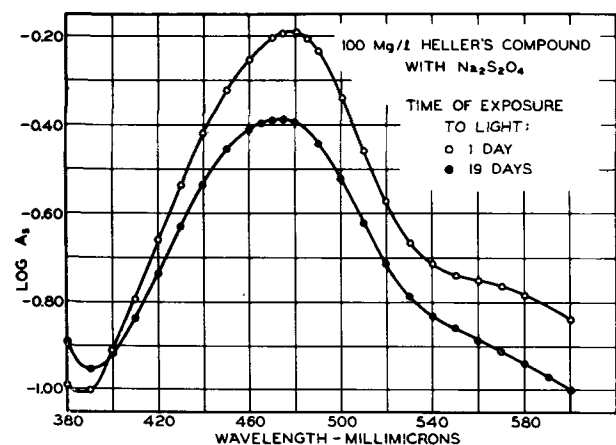


FIG. 7. Effect of exposure to light on absorption curve of Heller's compound in alkaline solution. Dithionite was added just prior to each series of measurements.

spectrophotometer (glass prism), requiring a very wide slit opening. Studies with an ultraviolet spectrophotometer might reveal the presence of other compounds similar to that isolated by Heller, but without the chromophoric quinone structure.

With the ultraviolet spectrophotometer not available, use of dithionite as a reducing agent and absorbancy measurements in the visual range was most convenient. Measurements should be made within 20 to 30 min after adding dithionite, since significant decreases in absorption have been observed after 2 or more hours. The cell effluent should be protected from light prior to addition of the reducing agent and performing the measurements.

Heller reported that the compound he isolated, when boiled with NaOH, behaves just as does cell effluent, developing a blue or purple color believed to be associated with the replacement of the chlorine atom by a hydroxyl group. Fig. 5 illustrates the changes in absorption. The effect of moderate heating appears to be the development of a flat absorption band at about 500 $m\mu$ (red); with further evaporation an absorption band at about 575 $m\mu$ is evident. Even moderate heating eliminates the peak at about 370 $m\mu$.

Samples of cell effluent and of a synthetic solution of Heller's compound in NaOH-NaCl medium turn red on exposure to sunlight. This phenomenon was noted previously by Heller (2). Changes in the absorption spectrum for various times of exposure (without addition of dithionite) are illustrated in Fig. 6. A broad absorption band was observed with a flat maximum at about 500 $m\mu$ accompanied by a decrease in absorption at 370 $m\mu$. The maximum at this latter wave length shifts slightly to shorter wave lengths and, after 19 days, the valley below 360 $m\mu$ has essentially disappeared. The changes produced in the absorption spectrum by exposure to light appear similar to those produced by mild heating.

The effect of exposure to light on the absorption spectrum with reducing agent added is illustrated in Fig. 7. The general form is little changed, but the absorption peak is considerably reduced and shifted slightly (to about 475 $m\mu$). If absorption at 480 $m\mu$ is characteristic of one form of the color compound,

TABLE I. Effect of standing exposed to light of a solution of 100 mg/l of the color compound in alkaline medium

Time in days	Na ₂ S ₂ O ₄ added	
	A _s at 480	mg/l
0	0.680	100
1	0.642	95
3	0.573	84.5
7	0.524	77.5
19	0.411	61

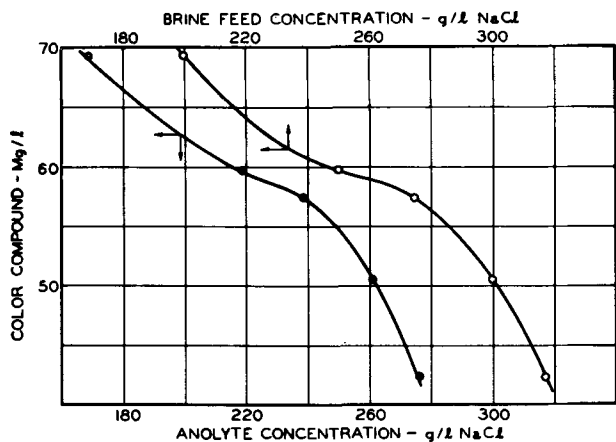


FIG. 8. Effect of anolyte chloride concentration on intensity of caustic color.

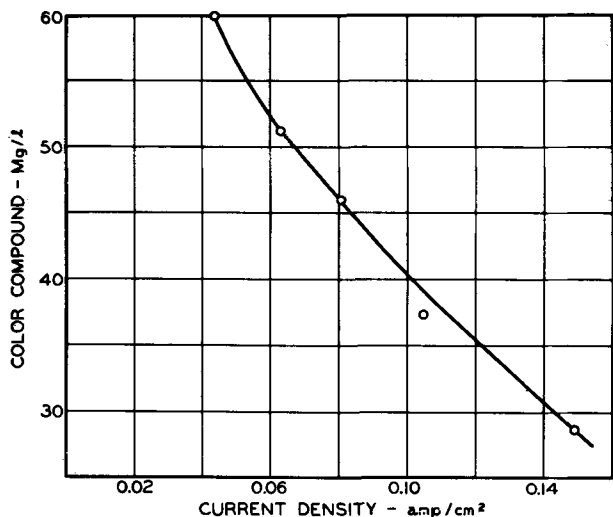


FIG. 9. Effect of anode current density on intensity of caustic color.

the decrease in concentration with time can be established (see Table I).

It is presumed that the apparent decrease in concentration represents not destruction, but transformation to another form which does not absorb at 480 m μ .

From Fig. 3, absorption can be expressed in terms of concentration of color compound. This same procedure was employed for certain of the older determinations made with a less selective photoelectric colorimeter, employing a plot of per cent transmission against concentration of the color compound in NaOH-NaCl medium. With the older instrument, Beer's law was not followed, because of the broad band of wave lengths of light used.

DISCUSSION

Laboratory diaphragm cell studies have confirmed Heller's conclusion that the color compound is pro-

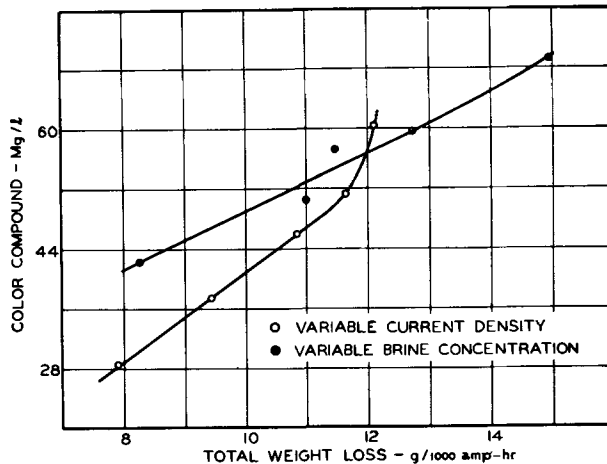


FIG. 10. Relation of intensity of caustic color to rate of anode attack.

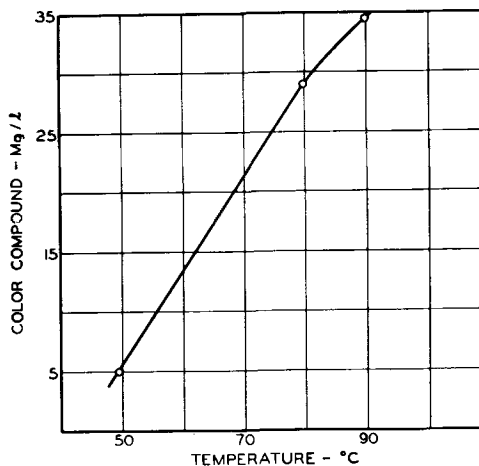


FIG. 11. Effect of anolyte temperature on intensity of caustic color.

TABLE II. Comparison of anodes processed from various raw materials

	Total weight loss G/KAH	Color compound mg/l
Standard graphite-high density..	6.41	25
Pregraphitized coal.....	7.88	36
Lignin.....	6.80	40
Lampblack.....	9.90	47
Charcoal.....	8.94	50

duced by oxidation of the graphite as indicated by the following observations.

1. With a nongraphitic anode such as platinum, no color is produced. This eliminates other cell materials as a possible source of color.

2. Spectroscopic purification of graphite does not decrease the amount of color compound produced, indicating that impurities in the graphite are not responsible.

3. Color intensity has been found in general to increase with increased rate of attack on the graphite.

Fig. 8 illustrates the increase in color concentration with decreasing brine feed concentration, with feed rate held constant at 200 ml/hr, current at 11 amp, and temperature at 80°C. The curve for color compound concentration against anolyte NaCl concentration has essentially the same form.

Fig. 9 shows the increase in color concentration with decreasing current density.⁶ Here the current was held constant at 11 amp, but the size of the anodes was varied from $\frac{5}{8} \times \frac{5}{8} \times 1\frac{1}{2}$ in. to $\frac{7}{8} \times \frac{7}{8} \times 4$ in. Feed rate was constant at 200 ml/hr of concentrated brine and temperature at 80°C.

Color concentration in the cell effluent for these two series is plotted against the total weight loss of graphite in Fig. 10. The general trend in both series for an increase in color concentration with increased rate of graphite attack is clearly evident. Cell temperature has quite a marked effect on color concentration, corresponding to an equally marked effect on rate of anode attack (see Fig. 11).

There is considerable evidence that chemical oxidation may be an important factor in the production of the color compound. Thus, the compound has

⁶ These data show the effect of current density on the concentration of color compound in the catholyte effluent with composition of the anolyte and catholyte (with respect to NaOH and NaCl concentration) held constant. From the definition of current density (amperes per unit area) a decrease in current density means an increase in graphite area exposed to the anolyte per unit of current. If the alternative procedure of maintaining constant area of graphite and varying the current is employed, it is necessary that the feed rate be varied in direct proportion to the change in current, in order to maintain a constant composition of anolyte and catholyte. If current is increased, with less than a proportional increase in flow rate, the NaCl concentration of the anolyte will be decreased and more migration and diffusion of hydroxyl ions from catholyte to anolyte will occur. The effect of such changes in the anolyte on the production of color compound could readily mask the effect of a decreased area of graphite per unit of current.

been produced by oxidation of graphite particles with a hypochlorite solution without current, the reddish-brown color developing on addition of alkali and dithionite to the supernatant solution.

The increased graphite attack with decreasing current density is believed to be associated with an increased amount of chemical oxidation as discussed previously (6). However, the evidence is certainly not sufficient to permit the statement that chemical oxidation is solely responsible, and a similar colored compound has been found to be formed when graphite is employed as anode in a sodium carbonate electrolyte. It would be difficult to explain the color formation in such an electrolyte by chemical oxidation alone.

With treated graphite, color concentration in the cell effluent is markedly lower, of the order of 5 mg/l as compared to 40 mg/l for untreated stock. This is believed largely a result of the protection afforded by the treatment against internal attack (chemical oxidation).

Table II shows that the use of less graphitic raw materials for the anode, such as lampblack or charcoal, gives increased color concentration in the cell effluent. It can be speculated that the smaller crystallite size results in a greater exposure of surface for the specialized mode of oxidation which leads to the formation of the color compound.

Any discussion of this paper will appear in a Discussion Section to be published in the June 1956 JOURNAL.

REFERENCES

1. *Trans. Electrochem. Soc.*, **86**, 35 (1944).
2. H. H. HELLER, *ibid.*, **87**, 501 (1945).
3. N. J. JOHNSON, *ibid.*, **86**, 127 (1944).
4. M. G. MELLON, Editor, "Analytical Absorption Spectroscopy," John Wiley and Sons, Inc., New York (1950).
5. E. I. STEARNS, Ref. (4), pp. 307 ff.
6. M. JANES, *Trans. Electrochem. Soc.*, **92**, 23 (1947).

The Influence of a Surface Active Agent on the Electropolishing of Copper¹

K. F. LORKING

Corrosion Group, Aeronautical Research Laboratories, Department of Supply, Melbourne, Australia

ABSTRACT

Previous work has shown that surface active agents can improve the finish obtained on copper electropolished in orthophosphoric acid solutions, and this beneficial action is examined in greater detail. The evidence indicates that the cationic surface active agent cetyl trimethyl ammonium bromide is adsorbed at both the anode surface and on the walls of oxygen bubbles. These factors are shown to account for the improvement in the micropolishing characteristics of the bath and in the reduction in the size of the pits formed on the anode during slow oxygen evolution.

INTRODUCTION

Research on the use of surface active agents in electropolishing baths was reported by Sparks (1) who showed that the presence of such agents could increase the "throwing power" of the bath. This work was confirmed by Tajuna and Mori (2) during experiments on the electropolishing of nickel. More recent work (3) has shown that the addition of the correct concentration of certain surface active agents improves the finish of the region of medium current density polishing produced on copper anodes in orthophosphoric acid solutions. The main effects are:

(A) The "throwing power" of the bath, i.e., the ability to produce continuous polishing over an anode placed at an acute angle to the cathode, is increased.

(B) The reflectivity of the polished surface is increased.

(C) The size of the surface mounds, produced as slow oxygen evolution commences, is greatly decreased.

These factors produce a general improvement in the electropolished surface, and the present paper describes work undertaken to determine the mechanism by which this occurs. Experiments were carried out on copper in orthophosphoric acid solutions, and the surface active agent chosen for examination was cetyl trimethyl ammonium bromide (subsequently referred to as C.T.A.B.) which was available in purified form, and which was known to improve the finish obtained on copper anodes (3).

EXPERIMENTAL METHOD

It is known (4, 5, 8, 9) that the anodic surface finish obtained in an electropolishing bath depends on the characteristics of the anode layer and the

anode surface film. Hence, the first step in determining the mechanism of the improvement produced in electropolishing by surface active agents was to determine whether such agents were adsorbed on the anode surface. This was investigated by the following three methods: (a) by observing the influence of increasing concentration of surface active agent on the finishes obtained on plates from Hull cell tests; (b) by measuring and comparing anode potential-current density relationships in solutions of gradually increasing concentration of surface active agent; and (c) by measuring the contact angles between the anode and a series of freshly blown bubbles pressed onto the surface. Such measurements were made for a number of values of the cell current between zero and that causing rapid oxygen evolution.

An important influence of suitable surface active agents in electropolishing solutions is to decrease the size of the mounds produced on the anode surface during oxygen evolution. These mounds have been shown (6) to be due to oxygen bubbles remaining for a significant period on the anode surface. Direct experimental investigation of the effect of surface active agents on the behavior of bubbles formed on the anode surface is difficult, so the following indirect methods were used.

(A) The effect of concentration of surface active agent on the surface tension of orthophosphoric acid was determined in an attempt to indicate the concentration of surface active agent at which significant adsorption occurred on oxygen bubbles.

(B) The effect of ageing a bubble in the solution on the contact angle between bubble and anode surface was determined.

(C) The effect of concentration of surface active agent on the size and speed of release of oxygen bubbles formed on the anode surface was determined qualitatively.

The solutions used in this work consisted of ortho-

¹ Manuscript received July 16, 1954.

phosphoric acid containing gradually increasing concentrations of C.T.A.B., prepared in the following way. A large quantity of orthophosphoric acid solution containing 581.9 g/l orthophosphoric acid was made up from May and Baker's orthophosphoric acid (sp gr 1.75) and distilled water, using a Griffin and Tatlock hydrometer to determine when the required specific gravity of 1.293 had been reached. A solution was then prepared containing 10 g/l C.T.A.B. (produced from cetyl alcohol purified by fractional distillation) in orthophosphoric acid. Solutions of orthophosphoric acid containing the required amounts of the surface active agent could then be prepared.

EXPERIMENTAL RESULTS

Adsorption of Surface Active Agents at Anode

(a) *Hull cell experiments.*—Experimental verification was first made of the fact that C.T.A.B. produces a beneficial effect on the electropolishing of copper in orthophosphoric acid solution. Hull cell experiments showed that the electropolished surface was improved, and the "throwing power" of the bath was increased, by the addition of surface active agent over the range of concentration 0.002–0.005 g/l. At concentrations smaller than 0.002 g/l, mounds were produced at the commencement of slow oxygen evolution, and this effect reappeared and became more pronounced in the concentration range 0.005–0.1 g/l of surface active agent. Higher current densities at the latter concentrations resulting in rapid oxygen evolution caused the formation of furrows in the specimen surface. These effects are shown diagrammatically in Fig. 1 and 6. The diagrams show the appearance of the immersed sections of "Hull" cell plates after being used as anodes in the phosphoric acid solutions.

(b) *Measurement of anode potential-current density relationships.*—The apparatus used consisted of two copper electrodes in a cubic glass cell 1½ in. high. The 1 in. x 1 in. anode rested on the bottom of the

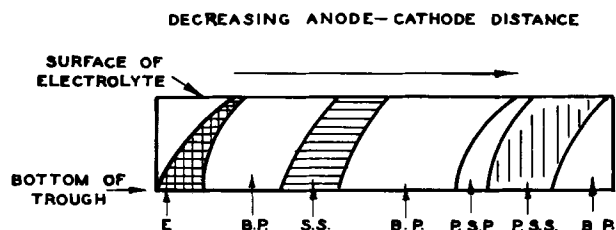


FIG. 1. Sequence of finishes produced on vertical copper anode placed at acute angle to cathode in Hull cell, using orthophosphoric acid electrolyte. The voltage across the cell was 6 v, the current 3 amp, and the average current density 1.5 amp/in.². E—electroetched surface; B.P.—bright polish; S.S.—smooth surface; P.S.P.—polished surface, pitted by slow oxygen bubble evolution; P.S.S.—polished surface, streaked by bubbles; P.S.H.S.—polished surface, heavily streaked.

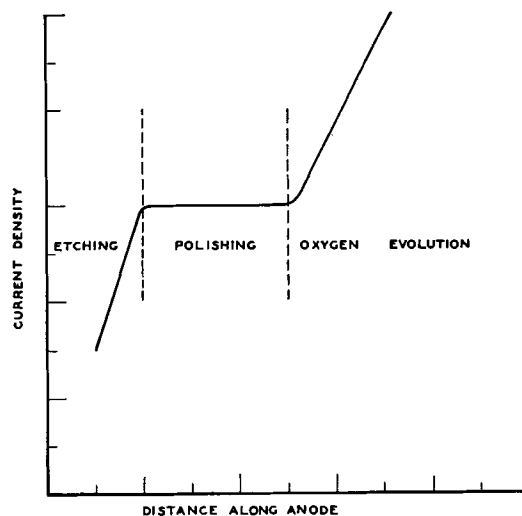


FIG. 2. Diagram showing current density distribution along Hull cell. The form of this graph was calculated by measuring the anode potentials corresponding to the various finishes while the cell was working, and determining the current densities corresponding to these potentials from current density-anode potential relationships determined for copper in an identical electrolyte.

cell and the 1⅜ in. x 1⅜ in. cathode was fixed horizontally at a distance of ¾ in. from the anode. Copper wire leads were welded to the electrodes and covered with several coats of lacquer. Current was supplied to the cell from a 6 v accumulator and regulated by suitable controls. The tubulus of the reference electrode projected through a hole in the center of the cathode so that the open end was within ⅛ in. of the anode surface.

The anode was subjected to an anodic current of 1 amp/in.² in orthophosphoric acid before each experiment. This standard treatment was necessary, as it was found that the anode potential-current density

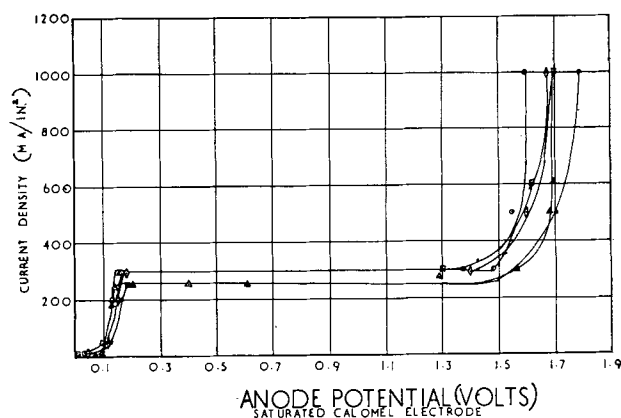


FIG. 3. Current density anode potential characteristics of copper in orthophosphoric acid solutions containing various C.T.A.B. concentrations. ●—581.9 g/l orthophosphoric acid; △—581.9 g/l orthophosphoric acid with 0.001 g/l C.T.A.B.; □—581.9 g/l orthophosphoric acid with 0.005 g/l C.T.A.B.; ◇—581.9 g/l orthophosphoric acid with 0.01 g/l C.T.A.B.; ○—581.9 g/l orthophosphoric acid with 0.1 g/l C.T.A.B.

relationship over the entire range of potentials was dependent on the initial state of the surface. The effect of surface active agent on the anode potential-current density relationship is shown in Fig. 3. The addition of as little as 0.001 g/l of C.T.A.B. decreased the potential corresponding to oxygen evolution. This effect tended to become more marked as the concentration of surface active agent was increased, indicating that the oxygen overvoltage on copper in orthophosphoric acid is decreased by the presence of surface active agent.

(c) *Measurements of contact angles of bubbles on anode surfaces.*—These experiments were made in an apparatus based on that devised by Taggart, Taylor, and Ince (7) for the measurement of contact angles on mineral surfaces for flotation studies. The electrolytic cell was the same as that described in the previous section except that a hole was drilled through the cathode so that a glass capillary, through which air could be bubbled, could be brought near the anode. The cell rested on an adjustable platform attached to a vertical stand immediately to the left of the camera, and the magnified image of the anode surface, air bubble, and the end of the capillary could be focussed on the ground glass screen at the rear of the camera (see Fig. 4). The contact angle between the bubble and the anode surface was measured from this image, using a transparent protractor, after tapping the cell to insure that the equilibrium angle was obtained.

The results are given in Table I. It is necessary to emphasize that it is impossible to measure accurately contact angles of less than 10° , and such angles could only be reported as "small."

At cell voltages below 1.5 v, etching took place; at higher voltages polishing occurred.

It was found that, as the concentration of surface active agent was increased, it was often impossible to make contact using bubbles which had "aged" in

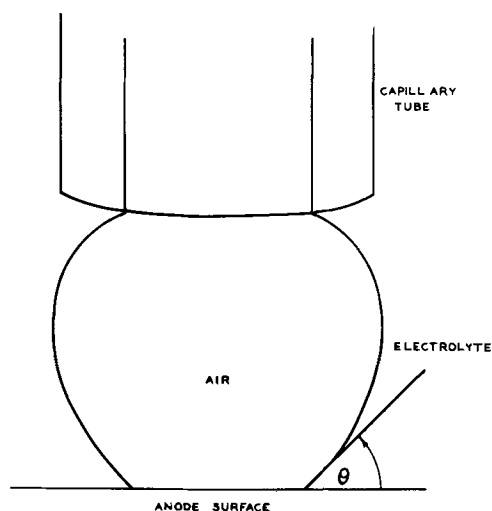


FIG. 4. Contact between air and anode surface

TABLE I. Effect of C.T.A.B. concentration on contact angle

Concentration of C.T.A.B. (g/l)	Current density (ma/in. ²)	Cell voltage (v)	Contact angle
0	200	1.3	0 } No tendency for bubbles to adhere to anode surface
	232	1.2	
	266	2.0	
	286	2.5	
	294	2.5	
0.001	0	0	20°
	200	1.4-1.7	0
	200	2.4	0
	200	2.6	0
0.002	0	0	50°
	135	1.3	25°
	150	1.4	10°
	160	2.6	Small
0.0025	0	0	65°
	150	1.5	10°
	200	2.0-2.3	Small
	200	2.6	Small
0.003	0	0	10°
	200	1.2	Small
	225	1.2	Small
	300	1.6	Small
	330	2.2-2.5	10°

solution for short periods, viz., 30 sec, so that it was necessary to blow the bubble directly onto the anode surface.

The results given in Table I indicated that surface active agent was adsorbed onto the copper surface and remained adsorbed up to quite high anode potentials. Further experiments showed that the surface active agent could remain adsorbed on the anode surface while polishing was proceeding, i.e., at cell voltage above 1.5 v (see Table II), but was gradually desorbed. It is possible that the positively charged C.T.A.B. ions were repelled from the anode surface, also that the cupric ions formed complex ions with the C.T.A.B. ions, which are substituted ammonium ions. Renewal of the solution or agitating the anode caused further adsorption of surface active agent.

Effect of a Surface Active Agent on Bubble Formation and Release

Surface tension measurements.—A determination was made of the effect of C.T.A.B. on the surface tension of orthophosphoric acid. The measurements were made by means of a Du Noüy tensiometer with a platinum ring. All glassware and the ring were cleaned with hot chromic acid and thoroughly washed with distilled water before making measurements. It was found that the surface tension values for the C.T.A.B. solutions decreased slowly, indi-

TABLE II. *Change of contact angle with time*
Current density was 300 ma/in.² and the solution contained 0.01 g/l C.T.A.B.

Time (sec)	Voltage (v)	Contact angle
30	1.3	40
90	1.5	40
150	1.6	40
210	—	Small
270	2.5	50
330	2.5	Small
390	2.5	Small

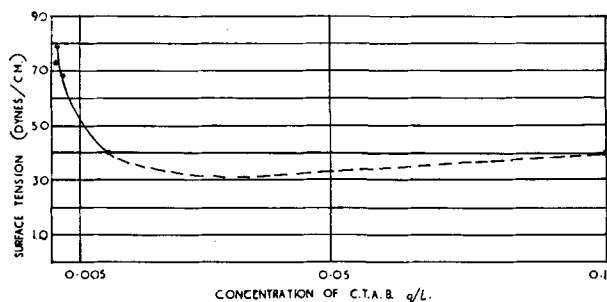


FIG. 5. Effect of C.T.A.B. concentration on the surface tension of orthophosphoric acid solution.

ating a slow increase of adsorption of C.T.A.B. at the interface. For example, when the C.T.A.B. concentration was 0.002 g/l the surface tension decreased from 70 to 62 dynes/cm in 10 min. Readings were therefore taken over a period of 10 min at 2-min intervals, and the mean result taken. With higher C.T.A.B. concentrations this effect was much less pronounced. This increasing adsorption of C.T.A.B. at the air-water interface was also noted during the contact angle measurements. Results are presented in Fig. 5 and show that the critical concentration (i.e., that corresponding to micelle formation) of C.T.A.B. in orthophosphoric acid is 0.01 g/l.

Influence of bubble "age" and concentration of surface active agent on the contact angle formed by a bubble pressed on the anode surface.—If a bubble was kept "ageing" in the solution for a period before being pressed against the anode surface, or if the concentration of C.T.A.B. in the solution was increased, then the amount of adsorption of surface active agent on the bubble wall was increased, and it became more difficult to make contact between the bubble and the anode surface. When the concentration of C.T.A.B. reached 0.003 g/l the rate of adsorption on the bubble was rapid, and it became more difficult to make bubble to anode contact.

Influence of surface active agent on bubble release.—It was noted that only very small oxygen bubbles were present on the anode surface with

0.001–0.005 g/l C.T.A.B. in the electrolyte, and these were rising freely from the anode surface.

Further Hull cell experiments.—A series of tests carried out with a surface active agent containing two ammine groups² showed that the effects of alterations in the concentration of this addition agent were very similar to those noted with C.T.A.B. Optimum electropolishing was obtained at the critical concentration (0.01 g/l) in the orthophosphoric acid bath.

When amyl xanthate was studied, it was found that at relatively high concentrations (≥ 0.05 g/l) xanthate was adsorbed on the anode surface and subsequently oxidized to form a yellow film (probably consisting of dixanthogene) which partially passivated the electrode surface. Unfilmed areas were electropolished. Using 0.0025 g/l of xanthate the same sequence of finishes was obtained as in the absence of the xanthate, but the quality of the electropolishing was significantly improved.

DISCUSSION

The experiments described in this paper show that addition of the correct quantity of C.T.A.B. to orthophosphoric acid solutions used as electrolytes for electropolishing copper has two main effects on the anodic finish obtained. First, a brighter polish was obtained, and second, the size of the mounds produced on the anode surface during slow oxygen evolution were reduced in size and number, giving an effective increase to the throwing power of the bath when using medium current density polishing.

The results of contact angle measurements showed that surface active agent was adsorbed on the copper surfaces before current was passed across the cell, and that significant quantities of the surface active agent remained adsorbed on the surface for a significant period while current was passing across the surface.

Results of other work indicate that as oxygen bubbles were formed on the anode surfaces, adsorption of surface active material occurred on the bubble walls. It is now necessary to consider how adsorption of C.T.A.B. on the anode surface and adsorption of the surface active agent on bubble walls could produce better anodic finishes.

It is considered (4, 5, 8, 9) that, in the electropolishing process, the polishing action is set up by an anode layer and an anodic film.

The anode layer is a layer of electrolyte, whose thickness is considerably greater than the wave length of the electrode profile for successful electropolishing to take place (10). The anode film is a thin layer of solid material or adsorbed atoms or

² Duomeen S, Armour & Co., Chicago, Illinois.

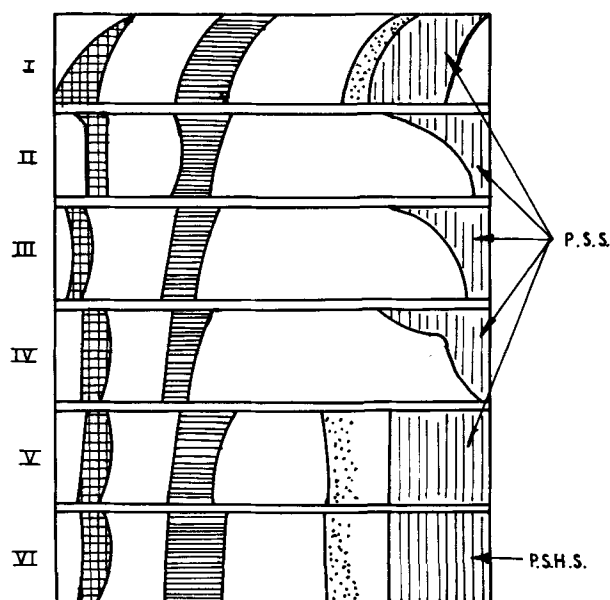


FIG. 6. Effect of C.T.A.B. on finishes produced on copper anodes, as shown by plates from Hull cell tests. I—581.9 g/l orthophosphoric acid; II—same as I with 0.001 g/l C.T.A.B.; III—same as I with 0.002 g/l C.T.A.B.; IV—same as I with 0.005 g/l C.T.A.B.; V—same as I with 0.01 g/l C.T.A.B.; VI—same as I with 0.1 g/l C.T.A.B.

molecules (4, 5). The polishing action is considered (8–11) to be due to a diffusion-controlled anodic solution process being set up through the anode layer and film.

It is thought probable that adsorption of surface active agent on and close to the anode surface could help to control ion diffusion processes in two ways: by mechanical blocking, and by replacement of water molecules in this region. The latter process may affect the dielectric constant of the medium and lower the number of water molecules available for solvating cations, hence lower the rate of diffusion of cations away from the anode surface.

The next question to be discussed is the influence of adsorption of C.T.A.B. on bubbles formed on anode surfaces during electropolishing. It has been found (6) that the protuberances surrounded by depressions which form on the anode surface are due to oxygen remaining on the surface for a period, there influencing the rate of anodic solution. The present work shows that adsorption of C.T.A.B. takes place on the bubble walls and this would be expected to accelerate the removal, by its buoyancy, of the bubble, due to the lowering of the surface tension at the air water interface by C.T.A.B. adsorption. [The force necessary to remove a bubble from contact with a solid surface is (12) $T(1 - \cos \theta)$, where T is the surface tension of the liquid, and θ is the equilibrium contact angle.]

The effect of high C.T.A.B. concentrations is to increase adhesion of oxygen bubbles to the surface,

as indicated by results shown in Fig. 6. When the C.T.A.B. concentration is increased to 0.01 g/l, bubbles formed as slow oxygen evolution commences adhere sufficiently long to cause pitting; if the concentration is increased to 0.1 g/l, the pitting is more evident, and the bubbles cling to vertical bubble-paths and produce deep grooves by preventing adequate anode layer formation.

Therefore, when the concentration of surface active agent becomes high enough, i.e., ≥ 0.01 g/l, for a significant quantity to remain on the anode surface at anode potentials positive enough to cause oxygen evolution, then the adhesion of the bubbles to the anode surface will become greater than in the absence of surface active agent. This change is due to the contact angle of the bubble formed on the anode surface increasing as the surface becomes more paraffinic in nature. Such a change is not indicated by contact angle measurements as the test bubble armored too rapidly for ready contact.

Finally, it is necessary to discuss the choice of the correct type of surface active agent to add to a polishing bath for a particular metal. In order to improve the surface finish obtained in aqueous electropolishing baths, there are two main objectives, as set out in the following paragraphs.

To reduce the size and number of mounds formed during oxygen evolution, it is considered that the addition of the critical concentration of the majority of long chain surface active agents will achieve this effect by causing the early release of oxygen bubbles from the anode surface.

To decrease the micro-irregularities and increase the brilliance of the finish, it is considered that it is necessary to achieve uniform formation and diffusion of cations from the anode surface, on a micro-scale. It is probable that addition of the critical concentration of the correct type of surface active agent contributes to this control, at least for the system copper in phosphoric acid. It is difficult to indicate which surface active agent will give satisfactory results. A surface active sulfate (3), ammine, and diammine, also potassium amyl xanthate have been shown to improve the electropolished surface obtained on copper in orthophosphoric acid.

The results obtained using xanthate also indicate that this agent was adsorbed on the anode surface, and substantiate the theory that adsorption of organic ions on or at the anode surface during electropolishing can take place.

CONCLUSIONS

It is believed that the addition of C.T.A.B. has two beneficial influences on the electropolishing of copper in orthophosphoric acid solutions. First,

the C.T.A.B. is adsorbed on the anode surface and supplements the action of the normal anodic film in improving the micropolishing action of the bath. Second, the C.T.A.B. is adsorbed on the surfaces of oxygen bubbles and accelerates their release from the anode surface, which markedly decreases the size of the pits formed.

ACKNOWLEDGMENTS

Thanks are due to Dr. Sutherland and the officers of the Physical Chemistry Section, Division of Industrial Chemistry, C.S.I.R.O., for helpful discussions and supplies of purified cetyl trimethyl ammonium bromide.

The author also wishes to thank the Chief Scientist, Department of Supply, for permission to publish this work.

Any discussion of this paper will appear in a Discussion Section to be published in the June 1956 JOURNAL.

REFERENCES

1. W. A. SPARKS, *J. Electrodepositors' Tech. Soc.*, **21**, 245 (1946).
2. S. TAJUNA AND T. MORI, *Compt. rend.*, **233**, 160 (1949).
3. K. F. LORRING, *Trans. Aust. Inst. Met.*, **5**, 109 (1952).
4. T. P. HOAR AND J. A. S. MOWAT, *Nature*, **165**, 64 (1950).
5. P. A. JACQUET, *Metal Finishing*, **48**, 53 (1950).
6. A. W. HOTHERSALL AND R. A. F. HAMMOND, *J. Electrodepositors' Tech. Soc.*, **16**, 91 (1940).
7. A. F. TAGGART, T. C. TAYLOR, AND C. R. INCE, *Trans. Am. Inst. Mining Met. Engrs.*, **87**, 285 (1930).
8. H. F. WALTON, *This Journal*, **97**, 219 (1950).
9. W. C. ELMORE, *J. Appl. Phys.*, **10**, 724 (1939); *ibid.*, **11**, 797 (1940).
10. C. WAGNER, *This Journal*, **101**, 225 (1954).
11. J. EDWARDS, *ibid.*, **100**, 189C (1953).
12. I. W. WARK, "Principles of Flotation", *Aust. Inst. Min. Met.*, pp. 78, 51 (1938).

Mechanisms of Hydrogen Producing Reactions on Palladium¹

JAMES P. HOARE AND SIGMUND SCHULDINER

Naval Research Laboratory, Washington, D. C.

ABSTRACT

The hydrogen overvoltage on palladium in H_2SO_4 and $\text{H}_2\text{SO}_4 + \text{Na}_2\text{SO}_4$ solutions was determined. Data showed that the overvoltage curves could be divided into three consecutive regions: (A) η was linearly dependent on i ; (B) there was a Tafel relationship between η and i in which the b slope, depending on the pH of the solution, was equal to 0.030 to 0.042; (C) depending on the pH of the solution, there was either a Tafel relationship between η and i with a b slope of 0.12, or η was virtually independent of i .

Hydrogen overvoltage mechanisms were postulated for each of these regions.

INTRODUCTION

The study of hydrogen overvoltage on palladium is complicated by the high solubility of hydrogen in this metal. Compared to the platinum cathode, $\text{Pt}(\text{H}_2)/\text{H}^+$, the palladium cathode may be represented by $\text{PdH}_x(\text{H}_2)/\text{H}^+$. The palladium-hydrogen system can exist in two distinct crystallographic phases (1) which are referred to as the α and β phases.

In this investigation the palladium cathode was initially saturated with hydrogen by cathodizing at a high current density. This converted the cathode to a β -palladium-hydrogen system. The hydrogen overvoltage was then measured over a current density range in which this electrode system was maintained.

EXPERIMENTAL METHOD

The experimental method was essentially the same as in reference (2) except that palladium (99.7+ % pure) was substituted for the platinum cathode. For data reported here the temperature was maintained at $39 \pm 1^\circ \text{C}$. In addition, preliminary data were also obtained at $25 \pm 1^\circ$; this work was not completed, but the results did agree satisfactorily with those of the higher temperature work. The temperature coefficient was too small to determine the activation energy.

The palladium cathode was activated differently from the platinum one. For solutions containing sodium sulfate, the palladium electrode was anodized at 10 ma for 30 min; for the more acid solutions it was anodized at 5 ma for 15 min. In all cases the electrode was then cathodized at 50 ma for at least 30 min before the run was started. At the start of the run the current was lowered to about 5 ma and was kept at this value until a steady-state reading was obtained. The current was then lowered by convenient increments, and overvoltage measure-

ments were taken. After the minimum current was applied the current was increased stepwise to the highest value at which reliable results could be obtained. Measurements for at least three such cycles were recorded. All recorded overvoltage measurements were corrected for solution IR drop, and concentration polarization was kept at a minimum by vigorous stirring with a stream of hydrogen.

According to Smith (1), the solid binary alloy, palladium-hydrogen, is produced by the diffusion of hydrogen into the already crystalline metal. The solid phases are a result of the expansion of the face-centered cubic lattice of palladium. The α -phase is formed by an expansion from the lattice-constant value for pure palladium of 3.883 Å to an only slightly higher value of about 3.894 Å. At room temperature, after absorption of some 30 relative volumes of hydrogen, the lattice becomes unstable and some of the crystal grains expand to a new, stable β -phase whose lattice-constant is about 4.02 Å. When the ratio of hydrogen to palladium is equal to about 0.6, all of the palladium is in the β -phase.

In this investigation, the palladium electrode was cathodized at a high current density so that it would be completely converted to the β -phase. During the lowering of current, care was taken not to reach a current density so low that there would be an appreciable reversion to the α -phase.² The $\beta \rightarrow \alpha$ transition was evident by a gradual lowering of potential with time. Once the transition current was reached and the α and β phases were simultaneously present, the potential was time dependent and would become more positive as the ratio α/β increased, until a potential 50 mv positive to the

² Hanawalt (3) cathodically charged palladium in weak sulfuric acid solution at 0.0001 amp/cm² (20°) and found that the lattice-constant of the resulting palladium-hydrogen alloy was equal to 4.017 Å. This corresponded to the β -phase. The minimum current density used in obtaining overvoltage data was about 0.001 amp/cm².

¹ Manuscript received October 25, 1954.

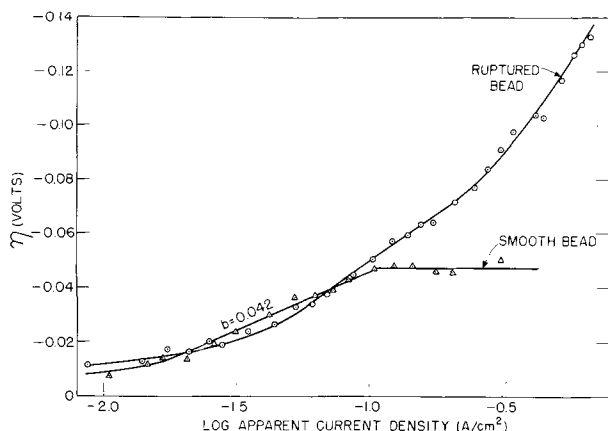


Fig. 1. Anomalous hydrogen overvoltage measurements owing to ruptured palladium cathode (in $2N$ H_2SO_4).

reversible hydrogen electrode in the same solution was reached. This was shown by Stout³ (4) who found that when the hydrogen-palladium atomic ratio is less than 0.35, the palladium potential was positive to the reversible hydrogen electrode. This transition was slow, but usually took place overnight. If a clean palladium electrode which had not been cathodized previously was placed in an acid solution which was saturated with hydrogen, its potential was also 50 mv positive to a hydrogen electrode in the same solution. Similar results were obtained by Stout (4), and Hitzler and Knorr (6). It is believed that this potential represents palladium in the α -phase. When such an electrode was polarized at low current densities, the polarization potentials were lower than the potentials for β -palladium.

The palladium electrode was prepared by melting the end of a palladium wire with an oxy-gas flame. The apparent area of the beads ranged from 0.03–0.05 cm^2 . It would have been very difficult to determine the true area of these electrodes, as was done for platinum (7), because of the area changes which took place during polarization. In most cases a newly prepared palladium bead was used for each overvoltage determination. These beads were initially bright and smooth; at the end of a run they were somewhat roughened and grayish in color. For a normal run there was no evidence of cracking or deep pitting of the cathode. However, with extensive cathodic polarization, deep pits, cracks, and blisters were evident. Electrodes which underwent such treatment gave abnormal results. A typical plot of

³ Several investigators (5) have shown that β -palladium is stable with respect to α -palladium at room temperature and a hydrogen partial pressure of one atmosphere. This work was all done in the absence of solution. In the presence of an aqueous solution of hydrogen ions, as was the case in this investigation, the stability of the beta phase with respect to the alpha phase was evidently altered.

such an electrode, compared with that of a normal run, is shown in Fig. 1. These anomalous results were interpreted as concentration polarization effects which took place in the ruptured areas. For high pH solutions cracking and pitting occurred so slowly that the same bead could be used for several runs, but for low pH solutions the effects were more serious, and a new bead was prepared for each run.

The initial cathodic treatment at 50 ma roughened the surface to such an extent that for the η vs. $\log i$ relationship there was an insignificant area change during a single run. The surface cleanliness of the palladium bead was determined both by pseudo-capacitance measurements (7) and by the tests listed in reference (2).

RESULTS

Fig. 2 shows curves for the palladium-hydrogen overvoltage, η , vs. \log of apparent current density, i , in the indicated solutions. The points given are average readings for the given current density. The actual maximum spread for each point is ± 2.5 mv.

In Fig. 2a are shown curves representing the pH range, 0.84–1.8 (same palladium bead used for all curves). These curves are divided into three regions. The first region, at the lowest current densities, shows a linear relationship between current density and overvoltage. The middle region shows a linear relationship between η and $\log i$ with Tafel b slopes progressing from 0.030 at pH 1.8 to 0.042 at pH 0.84. The third region, at the highest current densities, also shows a linear relationship between η and $\log i$, but with a b slope of about 0.12. The more acid solutions shown in Fig. 2b and Fig. 3 also indicate three ranges, the first two sections being essentially the same as for the pH 0.84 curve in Fig. 2a. However, the third section, at the highest current densities, flattens out and in this range η is virtually independent of current density. This corroborates the results of Clamroth and Knorr (8) who, in a study of hydrogen overvoltage on palla-

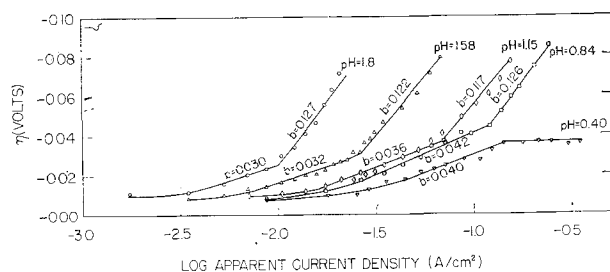


Fig. 2a. Hydrogen overvoltage on palladium. \odot —0.065N H_2SO_4 + 1N Na_2SO_4 , pH 1.8; \triangle —0.202N H_2SO_4 + 1N Na_2SO_4 , pH 1.58; \diamond —0.376N H_2SO_4 + 0.7N Na_2SO_4 , pH 1.15; \square —0.514N H_2SO_4 + 0.5N Na_2SO_4 , pH 0.84; ∇ —1.05N H_2SO_4 , pH 0.40.

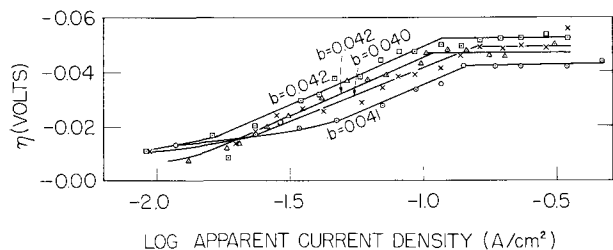


FIG. 2b. Hydrogen overvoltage on palladium. □—3.45N H₂SO₄; △—2.40N H₂SO₄; ×—5.10N H₂SO₄; ○—1.05N H₂SO₄.

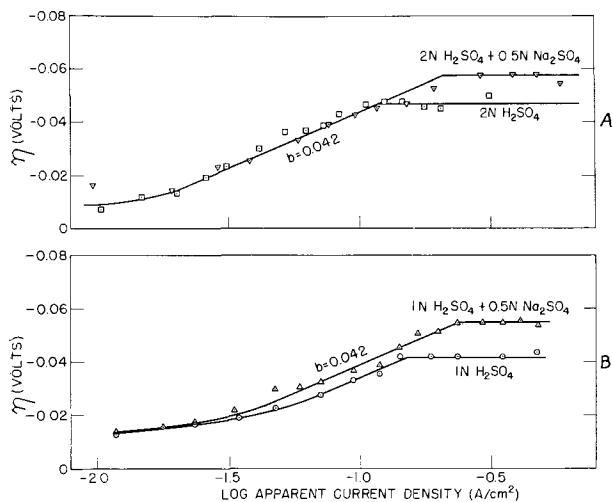


FIG. 3. Salt effect on hydrogen overvoltage

dium in 2N sulfuric acid solution, found that overvoltage was independent of current density after a similar limiting overvoltage was reached. They claimed that this limiting value of overvoltage remained constant to current densities as high as 50 amp/cm².

Fig. 3 shows the effects of adding 0.5N sodium sulfate to 1 and 2N sulfuric acid solutions. For the 1N sulfuric acid solution a weighed amount of sodium sulfate was added to the cell after the overvoltage curve for the pure acid was obtained.

DISCUSSION

By the use of the interrupter technique (7) the current could be cut off in an interval of 5×10^{-8} sec. The potential-time trace observed on the oscilloscope showed a rectangular pulse without rounding off and with a flat top [as in reference (7), Fig. 1a]; however, there was a small ringing effect on the leading edge. This was the result of a small a-c voltage component which was caused by the hydrogen bubble formation at the electrode surface. The rectangular pulse showed that there was initially a very rapid (faster than 5×10^{-8} sec) potential decay which was due to the IR drop from the reference electrode to the double layer at the cathode interface. This interpretation is supported

by the existence of a linear (ohmic) relationship between this potential decay and current.

The absence of a measurable polarization decay during an interruption interval of about 1000 μsec showed a pseudocapacitance effect which is normal for such a reversible-electrode system.

These results contradict the contention of Frumkin and Aladjalova (9) and Knorr and coworkers (6, 8) that the overvoltage on palladium can be divided into a rapidly decaying component which they call η_1 and a slowly decaying component, η_2 . The initial rapid drop in potential (their η_1) is merely an ohmic IR drop, the slow potential decay (their η_2) is the total hydrogen overvoltage η . In fact, Knorr [reference (10), Fig. 2] found a linear relationship between η_1 and current density; however, he did not interpret this as a purely ohmic drop.

Since the overvoltage curves for palladium can be divided into three regions, each of these are discussed separately.

Region in which $\eta = a - i/k$.—In this zone there is an appreciable reverse reaction taking place. Fig. 4 shows a plot of overvoltage as a function of current density at low current densities. The data are taken from a smooth curve drawn through the points shown in Fig. 2a. The relationship between the rate constant, $k = di/d\eta$, and pH is shown in Fig. 5. This relationship can be expressed as:

$$-(di/d\eta)_{pH\ 0.4-1.8} = 4.07 - 1.96\ pH \quad (I)$$

Similarly, for a platinum cathode (2):

$$-(di/d\eta)_{pH\ 0.5-2.7} = 0.165 - 0.052\ pH \quad (II)$$

A comparison of these relationships shows that the rate of change of the rate constant k with pH (dk/dpH) for the reversible hydrogen reaction near equilibrium is greater by a factor of about 38 on β -palladium than on platinum. This is a qualitative

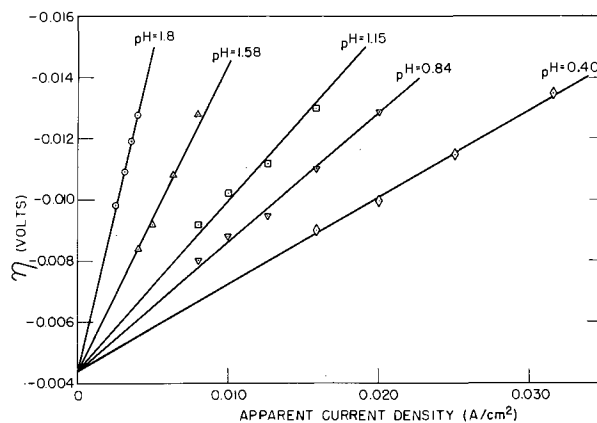
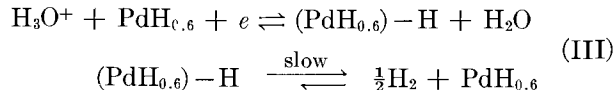


FIG. 4. Hydrogen overvoltage in the range in which η is linearly dependent on current density. (See Fig. 2a for solution composition for given pH values.)

comparison only since the current density on the platinum electrode was corrected for the true area, whereas this was not done for palladium.

The zero intercept, a , shown in Fig. 4 is 0.0044 v. This is presumably the extrapolated open circuit potential of the β -palladium electrode vs. the hydrogen electrode in the same solution. The β -palladium electrode is a reversible hydrogen electrode but is not equivalent to the reversible hydrogen electrode on platinum. It is suggested that this is because the hydrogen solubility in β -palladium gives, in effect, a hydrogen partial pressure slightly higher than atmospheric. Since the minimum ratio of hydrogen to palladium for the β -phase is about 0.6, the β -palladium hydrogen alloy can be represented by $\text{PdH}_{0.6}$. This formula does not necessarily represent a hydride formation; however, it has been shown both theoretically and experimentally (1, 4, 11) that one hydrogen solution process ceases at about $\text{H}/\text{Pd} = 0.6$. Above this ratio the dissolution of hydrogen becomes more difficult, but a hydrogen-palladium ratio of approximately 1 can be reached.

Region in which $\eta = a - (0.030 \text{ to } 0.042) \log i$.—Fig. 2 shows a transition from a Tafel b slope of 0.030 at $p\text{H}$ 1.8 to 0.042 in strong sulfuric acid solutions. The 0.030 slope indicated that the reaction mechanism is:

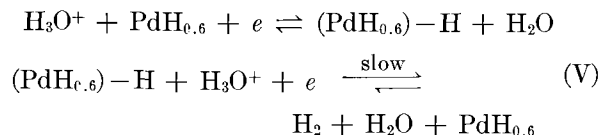


Such a mechanism in which the rate-controlling step is the combination of hydrogen atoms gives the Tafel equation:

$$\eta = a - 2.3(RT/\alpha F) \log i \quad (\text{IV})$$

where $\alpha = 2$ (the other symbols have their usual meaning). At 39°C , $2.3(RT/2F) = b = 0.0309$. This is the slope which was obtained experimentally in the $p\text{H}$ region 1.58–1.8.

The 0.040–0.042 slope for $p\text{H}$ values ≤ 0.84 indicates that the reaction mechanism is:



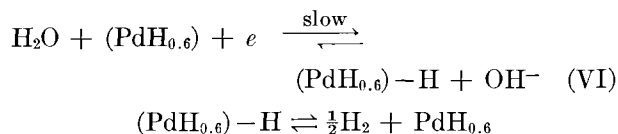
For such a mechanism in which the rate-controlling step is the electrochemical discharge, and the polarization is not far displaced from the equilibrium potential, α in the Tafel equation equals $3/2$ (12). At 39°C , $b = 0.0412$.

These results clearly indicate that both mechanisms (III) and (V) are occurring on the palladium cathode at all $p\text{H}$ values. However, at high $p\text{H}$ values the hydrogen ion concentration in the double

layer is relatively low, so most of the current goes into mechanism (III). At low $p\text{H}$ the hydrogen ion concentration is high enough that mechanism (V) is predominant.

In the intermediate range (about $p\text{H}$ 1.15) both mechanisms can be assumed to occur at about the same rate. This results in a slope such that b is between 0.03 and 0.04.

Region in which $\eta = a - 0.12 \log i$ or η is nearly independent of i .—Fig. 2 shows that from $p\text{H}$ 0.84–1.8 the b slope is equal to about 0.12. This indicates that the rate-controlling reaction mechanism is:



The reason water is assumed to be the primary reactant rather than hydronium ion has been discussed in detail earlier (2, 7). The α for mechanism (VI) is equal to $1/2$ which results in $b = 0.1235$ at 39°C .

At $p\text{H}$ values lower than about 0.8 and at over-voltages of about 50 mV, η is virtually independent of current density; this is true whether or not sodium ion is present (Fig. 2 and 3). A possible explanation is that for these higher acid concentrations there is saturation of the β -palladium with atomic hydrogen at the levelling off point. Under these conditions (1), the hydrogen-palladium ratio is approximately 1, and the lattice-constant is at

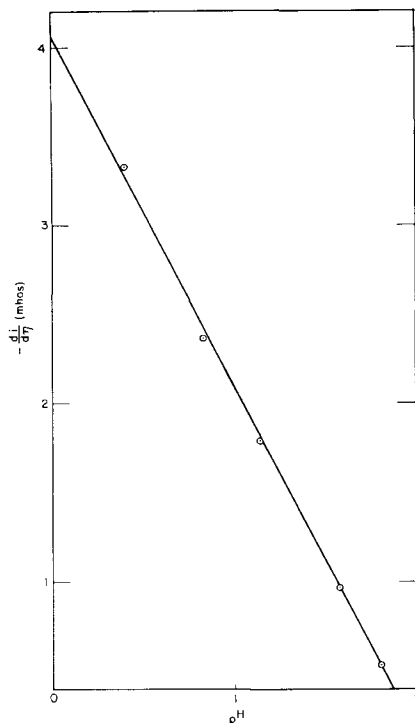
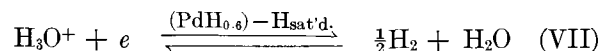


FIG. 5. Effect of $p\text{H}$ on the rate of the over-all hydrogen producing reaction in the range in which η is linearly dependent on current density.

its maximum (about 4.06 Å). At current densities above this limiting value, the mechanism for hydrogen production may be represented by:



The cathode material is now completely saturated with atomic hydrogen and is in effect a new electrode system at equilibrium. For such a reversible system near equilibrium there is a linear relationship between η and i :

$$i = (0.050 - \eta)k$$

where k is a rate constant equal to $-di/d\eta$. Since the data show that η is independent of i , the rate constant k must then be so large that the experimental technique used cannot detect changes in overvoltage with i for the current range covered.

The effect of added sodium ion (Fig. 3) was to raise the overvoltage at which the levelling off took place. This results because some of the hydrogen ions in the double layer were replaced by sodium ions which in effect reduced the hydrogen ion activity.

ACKNOWLEDGMENT

The authors are indebted to Dr. J. C. White for his valuable suggestions and comments.

Any discussion of this paper will appear in a Discussion Section to be published in the June 1956 JOURNAL.

REFERENCES

1. D. P. SMITH, "Hydrogen in Metals," pp. 84-119, Univ. of Chicago Press, Chicago (1948).
2. S. SCHULDINER, *This Journal*, **101**, 426 (1954).
3. J. D. HANAWALT, *Phys. Rev.*, **33**, 444 (1929).
4. N. F. MOTT AND H. JONES, "Properties of Metals and Alloys," pp. 190-200, Oxford University Press, London (1936); J. R. LACHER, *Proc. Roy. Soc.*, **A161**, 525 (1937); H. P. STOUT, *Disc. Faraday Soc.*, **1**, 107 (1947).
5. L. J. GILLESPIE AND F. P. HALL, *J. Am. Chem. Soc.*, **48**, 1207 (1926); H. BRÜNING AND A. SIEVERTS, *Z. physik. Chem.*, **A163**, 409 (1932); L. J. GILLESPIE AND L. S. GALSTAUN, *J. Am. Chem. Soc.*, **58**, 2565 (1936); E. A. OWEN AND I. J. JONES, *Proc. Phys. Soc.*, **49**, 587, 603 (1937).
6. M. HITZLER, C. A. KNORR, AND F. R. MERTENS, *Z. Elektrochem.*, **53**, 228 (1949); M. HITZLER AND C. A. KNORR, *ibid.*, 233 (1949).
7. S. SCHULDINER, *This Journal*, **99**, 488 (1952).
8. R. CLAMROTH AND C. A. KNORR, *Z. Elektrochem.*, **57**, 399 (1953).
9. A. FRUMKIN AND N. ALADJALOVA, *Acta Physicochim. U.R.S.S.*, **14**, 1 (1944).
10. C. A. KNORR, *Z. Elektrochem.*, **57**, 599 (1953).
11. B. SVENSSON, *Ann. Physik.*, **18**, 299 (1933); C. WAGNER, *Z. physik. Chem.*, **193**, 407 (1944); Z. L. VERT AND I. P. TVERDOVSKI, *Zhur. fiz. Khim.*, **28**, 317 (1954).
12. R. PARSONS, *Trans. Faraday Soc.*, **47**, 1332 (1951).

High Pressure Oxidation of Metals

Oxidation of Metals Under Conditions of a Linear Temperature Increase¹

JOHN P. BAUR, DONALD W. BRIDGES, AND W. MARTIN FASSELL, JR.

Department of Metallurgy, University of Utah, Salt Lake City, Utah

ABSTRACT

The oxidation behavior of metals was studied by subjecting the metal sample to a linear temperature increase at constant oxygen pressure. The advantages of this method over previous isothermal methods are that (a) a rapid preliminary examination of the oxidation behavior of any metal or alloy over a desired temperature and pressure range can be made quickly, (b) the region of pressure dependence usually can be found in a single experiment, (c) the number of samples needed is greatly reduced, and (d) the method serves as a guide for isothermal measurements at constant pressure.

The linear temperature increase method was applied to Ta, Nb, Mo, Cu, Zr, Mg, Ti, and W. Results are in good agreement with those of previous investigations made in this laboratory.

Theoretical considerations show that the results could be explained by imposing the conditions of a linear temperature increase on a general type rate equation.

INTRODUCTION

Prior to this time, the oxidation behavior of metals at high pressures has been determined by measuring oxidation rates at a series of constant temperatures and oxygen pressures. This method, although entirely satisfactory, is time consuming in that a separate sample must be used for each determination. This is particularly true in the preliminary search to ascertain the region wherein the pressure effect is most pronounced for a metal whose oxidation characteristics at high pressures are completely unknown. It would be desirable, therefore, to have a method whereby oxidation behavior could be surveyed quickly and the pressure sensitive region found. Such a method has been developed here.

The method consists of measuring the gain in weight of a metal at constant oxygen pressure while, at the same time, the metal temperature is increased in a linear manner. Similar methods have had wide application in the field of differential thermal analysis, and Olmer (1) has recently applied this technique to the reduction of iron oxides by hydrogen at atmospheric pressure.

EXPERIMENTAL TECHNIQUE

A linear temperature increase of approximately 5°C/min was obtained in one of the standard high-pressure furnaces (2) by modifying a standard Leeds & Northrup Micromax Controller. This was accomplished by connecting a small synchronous

motor-driven worm and worm gear drive unit to the controller set point. The controller then follows this linear increase in the set point, thereby raising the temperature of the furnace at a linear rate. The temperature of the guard windings must be manually increased to keep pace with the center winding. The rate of temperature increase varies slightly over the range of temperature covered, i.e., 400°–1000°C, because of the large thermal inertia of the furnace used and the absence of automatic controls on the guard ring windings. This thermal inertia also prevents the furnace from cooling quickly, requiring several hours to cool to starting temperature.

The operating procedure is as follows. The sample is introduced in the usual fashion (2, 3), and the furnace flushed several times with oxygen and pressurized to the desired oxygen pressure. A starting temperature is selected and the furnace allowed to reach equilibrium at this temperature. Simultaneously the sample is raised into the hot zone and the motor drive on the recorder is energized. The sample is allowed to remain in the hot zone a sufficient time to form a film 10^{-2} to 10^{-3} cm thick (calculated from mass gain data). This thickness is necessary in order to rule out such considerations as logarithmic and cubic oxidation laws and other electrostatic and nonequilibrium effects. At regular time intervals, the temperature is read on a Leeds & Northrup type (8662) potentiometer, and the gain in weight of the sample is determined by measuring the elongation of a helical quartz spring on which the sample is suspended. Data are recorded in the form of curves showing weight gained per unit of surface area as a function of temperature.

¹ Manuscript received November 1, 1954. This paper was prepared for delivery before the Cincinnati Meeting, May 1 to 5, 1955.

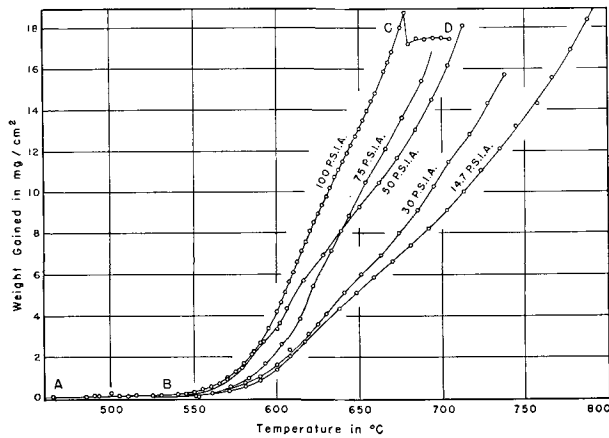


FIG. 1. Oxidation of tantalum under conditions of a linear temperature increase of 5°C/min.

INVESTIGATION OF THE OXIDATION OF TANTALUM IN OXYGEN WITH LINEAR TEMPERATURE INCREASE

In order to test the method it was decided to investigate the behavior of tantalum in oxygen because this metal had been thoroughly investigated previously (3) and all energy values were known. Fig. 1 shows the plot of weight gained per unit surface area as a function of temperature for five oxygen pressures: 14.7, 30, 50, 75, and 100 psia. From these curves, three temperature regions are apparent: A-B, a lower horizontal region, in which the oxidation rate is either too low to be recorded by the weighing system or is insensitive to pressure; B-C, a curved "knee" portion over which the metal is pressure sensitive, i.e., the slope of the curve (a function of the oxidation rate, dm/dt) changes with temperature and pressure; and C-D, upper horizontal portion indicating that the metal has been completely oxidized.

It has been found that the region B-C is in agreement with oxidation rate curves for tantalum at various pressures [Fig. 6 of reference (3)] which shows an increase in rate in the region 550°–650°C and a decrease in the region 650°–750°C].

THEORETICAL CONSIDERATIONS

Work in this laboratory has shown a general type of rate equation for pressure sensitive oxidation of the form:

$$\begin{aligned} \frac{dm}{dt} &= k_o f(\theta) \frac{kT}{h} \exp \left[\frac{-\Delta F^\ddagger}{RT} \right] \\ &= k_o f(\theta) \frac{kT}{h} \exp \left[\frac{-\Delta H^\ddagger}{RT} \right] \exp \left[\frac{\Delta S^\ddagger}{R} \right] \end{aligned} \quad (\text{I})$$

$$\begin{aligned} m \frac{dm}{dt} &= C_o f(\theta) \frac{kT}{h} \exp \left[\frac{-\Delta F^\ddagger}{RT} \right] \\ &= C_o f(\theta) \frac{kT}{h} \exp \left[\frac{-\Delta H^\ddagger}{RT} \right] \exp \left[\frac{\Delta S^\ddagger}{R} \right] \end{aligned} \quad (\text{II})$$

where m is the mass increase per unit of surface area; k_o is a proportionality constant with the dimensions of ML^{-2} and includes the correction factor for the true surface area (surface roughness and number of active sites per surface area) involved in the oxidation reaction; C_o is a constant for the parabolic case discussed in detail in Appendix II; and θ is the fraction of surface sites covered. The other terms retain their customary significance as in the Eyring theory (4, 5) with the transmission coefficient equal to unity. Equation (I) is applicable to linear oxidation, while equation (II) is the corresponding expression for parabolic oxidation, in a region where the oxidation rate is pressure sensitive (i.e., in a region where the oxidation rate is a function of the external concentration of oxygen).²

Experimental restrictions of an imposed linear temperature increase result in a possible variable substitution:

$$T = b \cdot t + c \quad (\text{III})$$

or

$$dT = b \cdot dt \quad (\text{IV})$$

where T is the absolute temperature; t is the time; b is the rate of increase of temperature per unit time; and c , the starting temperature in degrees Kelvin.

Incorporation of equation (IV) in equation (I) results in an expression for the mass increase per unit of surface area, under the conditions of linear temperature increase as given in equation (V)

$$\Delta m = \int_0^m dm = \frac{k'_o k}{bh} \int_{T_o}^T f(\theta) T \exp \left[\frac{-\Delta H^\ddagger}{RT} \right] dT \quad (\text{V})$$

where $k'_o = k_o \cdot e^{\Delta S^\ddagger/R}$ because the term $e^{\Delta S^\ddagger/R}$ is here assumed to be temperature independent over the range of temperatures used. Knowledge of the concentration term, $f(\theta)$, as a function of temperature would allow evaluation of the integral—by graphical means if no other method of solution were feasible.

Judicious choice of experimental conditions results in two limiting cases of equations (I) and (II) which are resolvable into standard functions and a tabled definite integral, the exponential integral. The concentration term, $f(\theta)$, is here assumed, as in reference (3), to be

$$f(\theta) = \theta = \frac{K_1 \cdot [O_2]}{1 + K_1 \cdot [O_2]} \quad (\text{VI})$$

where K_1 , the equilibrium constant for the adsorption process, is represented as a function of temperature by

$$K_1 = e^{-(\Delta F/RT)} = e^{-(\Delta H/RT)} \cdot e^{\Delta S/R} \quad (\text{VII})$$

² See Appendix II for a discussion of this point.

and the effective surface concentration of the oxygen in terms of the external gas concentration $[O_2]$ is given by:

$$[O_2] = \frac{n}{V} = \frac{P}{RT} \quad (\text{VIII})$$

This is in accordance with reference (3) on tantalum. The function, $f(\theta)$, could possibly be much more complex.

Substituting equation (VI) into equation (V) one obtains:

$$\begin{aligned} \Delta m &= \frac{k'_o k}{bh} \int_{\tau_o}^T \theta T \exp \left[-\frac{\Delta H^\ddagger}{RT} \right] \cdot dT \\ &= \frac{k'_o k}{bh} \int_{\tau_o}^T T \exp \left[-\frac{\Delta H^\ddagger}{RT} \right] \cdot \frac{K_1 [O_2]}{1 + K_1 [O_2]} dT \end{aligned} \quad (\text{IX})$$

Substitution of equations (VII) and (VIII) into equation (IX) yields the following expression for the mass increase:

$$\begin{aligned} \Delta m &= \frac{k'_o k}{bh} \int_{\tau_o}^T T \cdot \exp \left[-\frac{\Delta H^\ddagger}{RT} \right] \\ &\cdot \left\{ \frac{P/RT \cdot \exp(\Delta S/R) \exp(-\Delta H/RT)}{1 + P/RT \cdot \exp(\Delta S/R) \exp(-\Delta H/RT)} \right\} dT \end{aligned} \quad (\text{X})$$

If $\theta \ll 1$, $P/RT \cdot \exp(\Delta S/R) \cdot \exp(-\Delta H/RT)$ can be neglected in the denominator of equation (IX) resulting in the first approximate solution of equation (X), i.e., the limiting case for small surface coverage:

$$\begin{aligned} \Delta m &= -\frac{P}{R} \exp \left[\frac{\Delta S}{R} \right] \frac{k'_o k}{bh} \\ &\int \frac{1}{x^2} \exp \left[-\frac{(\Delta H^\ddagger + \Delta H)}{R} x \right] dx \end{aligned} \quad (\text{XI})$$

where $x = 1/T$ and $dT = -dx/x^2$.

Integration³ of equation (XI) yields:

$$\begin{aligned} \Delta m &= \frac{k'_o k P}{bh R} \exp \left[\frac{\Delta S}{R} \right] \left\{ T \exp \left[-\frac{(\Delta H^\ddagger + \Delta H)}{RT} \right] \right. \\ &\left. - \left[\frac{(\Delta H^\ddagger + \Delta H)}{R} \right] \cdot \left[-Ei \left(-\frac{(\Delta H^\ddagger + \Delta H)}{RT} \right) \right] \right\} \end{aligned} \quad (\text{XII})$$

where

$$-Ei(-x) = \int_x^\infty \frac{e^{-u}}{u} \cdot du; \quad x > 0$$

is called the exponential integral. This function is tabled (6, 7).

For the limiting case of complete surface coverage, i.e., $\theta = 1$, a pressure independent equation results from equation (IX) by a change in variable as in equation (XI).

$$\Delta m = -\frac{k'_o k}{bh} \int \frac{1}{x^3} \exp \left[-\frac{\Delta H^\ddagger}{R} x \right] dx \quad (\text{XIII})$$

³ Integral 302, p. 262, "Handbook of Chemistry and Physics," 31st ed., Chemical Rubber Publishing Co., Cleveland (1949).

Integration yields

$$\begin{aligned} \Delta m &= \frac{k'_o k}{bh} \left\{ \frac{1}{2} \left[-T^2 \exp \left(-\frac{\Delta H^\ddagger}{RT} \right) \right. \right. \\ &\quad \left. \left. + \frac{\Delta H^\ddagger}{R} T \exp \left(-\frac{\Delta H^\ddagger}{RT} \right) \right] \right. \\ &\quad \left. + \left(\frac{\Delta H^\ddagger}{R} \right)^2 \left[-Ei \left(-\frac{\Delta H^\ddagger}{RT} \right) \right] \right\} \end{aligned} \quad (\text{XIV})$$

Equations (XII) and (XIV) point the way to a possible method of obtaining energy values for the heat of activation and the heat of adsorption.

Graphical integration of equation (X) was chosen to fit the data for tantalum over the entire temperature range at any one pressure because either of the limiting case equations (XI) and (XIII) fails when applied to the entire range of surface coverage, i.e., $0 \leq \theta \leq 1$.⁴

In the case of tantalum, the data of Peterson and coworkers (3) provides a test for equation (V) and further substantiates the postulated mechanism of oxidation of tantalum. For tantalum, equation (X) is applicable. The following values of involved energies are available: $\Delta H = -27,350$ cal/mole; $\Delta H^\ddagger = 29,500$ cal/mole (600°–800°C); $\Delta S = 22.58$ entropy units. Equation (X) becomes for graphical integration:

$$\begin{aligned} \Delta m &= \left\{ 1.509 \times 10^{-6} \frac{k'_o k}{bh} \right\} \\ &\int_{873}^T \frac{T \cdot \exp(-1075/T)}{T/P + 1.509 \times 10^{-6} \exp(13,675/T)} dT \end{aligned} \quad (\text{XV})$$

where P is in atmospheres.

The test of the method can then be made by applying equation (XV) to the data on tantalum and using graphical integration to evaluate the integral. Equation (XV) can be rewritten as:

$$\begin{aligned} &\{ \Delta m_T - \Delta m_{\tau_o} \} \\ &\left\{ \int_{873}^T \frac{T \cdot \exp(-1075/T)}{T/P + 1.509 \times 10^{-6} \exp(13,675/T)} dT \right\}^{-1} \\ &= \text{const.} \quad (\text{XVI}) \end{aligned}$$

or

$$\frac{\Delta m_T - \Delta m_{\tau_o}}{\Sigma} = \text{constant} = C \quad (\text{XVII})$$

where Σ is the value of the definite integral. Table I shows the application of equation (XVI) to the data used to obtain Fig. 1. The agreement of the constants of Table I for each pressure is striking, but it will be noted that those for the pressures 14.7 and 100 psia are not in as good agreement with the other pressures as might be desired. These anomalies can be explained by considering the fol-

⁴ See Appendix I for a discussion of this point.

TABLE I. Application of equation (XVI) to the data of tantalum oxidized under conditions of a linear increase in temperature

14.7 psi				30 psi				50 psi				75 psi				100 psi			
°C	Σ	$\frac{\Delta m}{-\Delta m_{T_0}}$	C	°C	Σ	$\frac{\Delta m}{-\Delta m_{T_0}}$	C	°C	Σ	$\frac{\Delta m}{-\Delta m_{T_0}}$	C	°C	Σ	$\frac{\Delta m}{-\Delta m_{T_0}}$	C	°C	Σ	$\frac{\Delta m}{-\Delta m_{T_0}}$	C
608	2.327	0.657	0.282	608	4.694	0.741	0.159	606	7.688	1.303	0.170	614	15.809	1.263	0.080	610	18.712	1.991	0.106
617	4.971	1.396	0.281	619	11.232	1.540	0.137	616	17.448	2.649	0.152	622	27.528	2.842	0.103	619	35.919	3.810	0.106
625	7.345	2.238	0.305	630	17.886	2.514	0.141	628	29.393	3.912	0.133	633	43.935	4.541	0.103	630	57.409	5.517	0.096
638	11.272	2.990	0.265	641	24.662	3.545	0.144	639	40.550	5.072	0.125	644	60.659	6.248	0.103	641	79.414	7.131	0.090
648	14.352	3.753	0.262	651	30.919	4.424	0.143	650	51.932	6.242	0.120	654	76.177	7.849	0.103	651	109.798	8.838	0.080
659	17.790	4.499	0.253	663	38.568	5.344	0.139	662	64.609	7.392	0.114	666	95.158	9.477	0.100	661	130.625	10.740	0.082
670	21.286	5.248	0.247	674	45.722	6.415	0.140	673	76.436	8.622	0.113	676	111.245	10.993	0.099	670	149.683	12.840	0.086
681	24.830	6.023	0.243	685	52.965	7.522	0.142	684	88.439	10.001	0.113	688	130.870	12.794	0.098				
692	28.419	6.842	0.241	695	59.614	8.682	0.143	694	99.504	11.457	0.115	696	144.151	14.831	0.103				
703	32.045	7.727	0.241	704	65.671	9.870	0.150	704	110.702	13.132	0.119								
713	35.379	8.635	0.236	711	74.541	11.222	0.151	713	120.879	15.034	0.124								
724	39.102	9.683	0.248	728	82.128	12.713	0.155												
735	42.848	10.731	0.250	738	89.108	14.133	0.159												

lowing. In the case of 14.7 psia it can be seen by examination of equation (XVI) that this equation is extremely sensitive in the region about $P = 1$ atm or 14.7 psia. A slight increase in the absolute pressure yields a value for the constant more consistent with those obtained at the other pressures. For example, if the pressure were actually 16 psia (which is entirely possible because of the difficulty of setting the oxygen at 1 atm using the high pressure gauges, and the pressure increase due to the increase in temperature from 400° to 800°C), the value of the constant would be changed by 8%. In the case of the 100 psia run, the difference can possibly be explained by considering the high oxidation rate and the difficulty of following this rapid weight increase with the cathetometer telescope. Equation (XVI) is far less sensitive at 100 psia than at 14.7 psia. A slight increase in the value of $\Delta m_T - \Delta m_{T_0}$ would result in a more consistent value of the constant.

INVESTIGATION OF THE OXIDATION OF COPPER

Previous work in this laboratory on copper (8) has shown the oxidation rate to be independent of oxygen pressure between 1 atm and 20.4 atm. Evaluation of more recent data results in an energy of activation of 31,605 cal/mole (100–300 psia) and 31,437 cal/mole (1 atm) for the temperature range 700°–1000°C (9). Using equation (VI) of Appendix II, the general type of rate equation for parabolic oxidation can be integrated to yield an expression similar to equation (XIV) as follows:

$$\Delta m^2 = \frac{C'_0 k}{bh} \left\{ \frac{\Delta H^\ddagger}{R} T \exp \left[-\frac{\Delta H^\ddagger}{RT} \right] + \left(\frac{\Delta H^\ddagger}{R} \right)^2 \left[-Ei \left(-\frac{\Delta H^\ddagger}{RT} \right) \right] - T^2 \exp \left[-\frac{\Delta H^\ddagger}{RT} \right] \right\} \quad \text{(XVIII)}$$

where: $C'_0 = C_0 e^{\Delta S^\ddagger/R}$.

TABLE II. Application of equation (XVIII) to data of high purity OFHC copper oxidized under conditions of a linear increase of temperature

14.7 psia				100 psia			
°C	$\frac{\Delta m_T^2 - \Delta m_{T_0}^2}{\Sigma T - \Sigma T_0}$	$\Sigma T - \Sigma T_0$	C	°C	$\frac{\Delta m_T^2 - \Delta m_{T_0}^2}{\Sigma T - \Sigma T_0}$	$\Sigma T - \Sigma T_0$	C
715	0.473	0.620	0.763	714	0.273	0.475	0.575
726	0.909	1.368	0.664	726	0.879	1.198	0.733
738	1.508	2.277	0.662	737	1.341	1.981	0.677
750	2.404	3.374	0.713	748	2.156	2.918	0.739
762	3.290	4.466	0.736	759	2.891	4.041	0.715
773	4.297	6.120	0.702	771	3.839	5.389	0.713
783	5.374	7.579	0.709	780	4.743	6.596	0.719
796	6.827	9.928	0.688	791	6.080	8.330	0.730
805	8.391	11.679	0.718	802	6.887	10.249	0.672
817	10.143	14.392	0.705	812	8.750	12.336	0.709
829	11.974	17.622	0.680	823	10.545	14.768	0.714
839	14.641	20.430	0.717	834	12.801	17.589	0.728
852	17.766	25.080	0.708	844	15.370	20.611	0.746
862	21.245	28.898	0.735	854	18.227	24.083	0.757
872	25.158	33.239	0.757	865	21.871	28.083	0.779
883	29.727	38.624	0.770	875	26.662	32.298	0.826
895	35.432	45.484	0.779	887	30.824	38.379	0.749

For the temperature range 700°–1000°C the test of equation (XVII) can be made by illustrating that:

$$\frac{\Delta m_T^2 - \Delta m_{700^\circ\text{C}}^2}{\Sigma T - \Sigma_{700^\circ\text{C}}} = \text{constant} = C \quad \text{(XIX)}$$

where $\Sigma T - \Sigma_{T_0}$ is the value of the definite integral between $T = T$ and $T = 700^\circ\text{C}$. Table II shows the results of this evaluation applied to the data on high purity OFHC copper subjected to oxidation under a linear temperature increase of 5°C/min.

Agreement between the values of the constants of Table II is excellent and shows that the oxidation behavior of copper can be explained by application of equation (II).

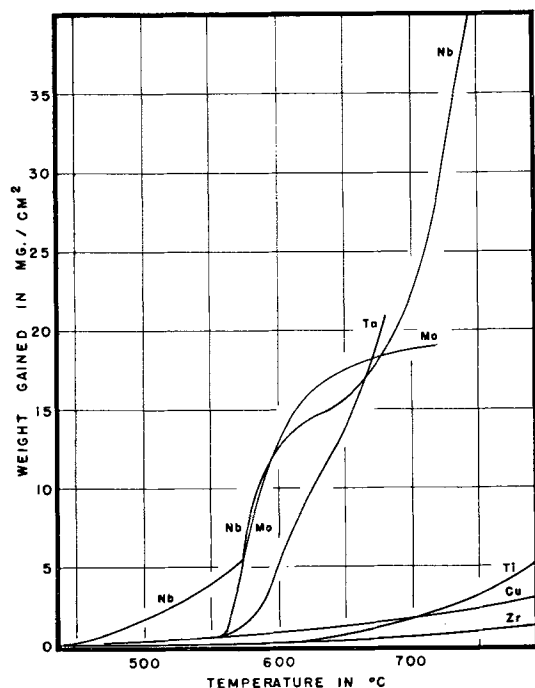


FIG. 2. Oxidation curves for various metals under conditions of a linear temperature increase of $5^{\circ}\text{C}/\text{min}$ and constant oxygen pressure of 100 psia.

OTHER METALS INVESTIGATED

As a preliminary survey, the oxidation behavior of a number of other metals, Nb, Zr, Ti, W, Mg, Mo, in addition to Ta and Cu, were also investigated under conditions of a linear temperature increase. Fig. 2 shows the oxidation curves for Nb, Zr, Mo, Cu, Ta, and Ti over the temperature range 450° – 790°C and oxygen pressure of 100 psia. Tungsten was not included on this graph because the pressure sensitive region occurs above 750°C , and the oxidation rates below this temperature are too low to be recorded. The curves clearly show the difference in oxidation behavior between those metals which oxidize according to the linear law (Ta, Nb, and Mo) and those (Cu, Ti, and Zr) which oxidize according to the parabolic law, i.e., in which a protective oxide film is formed.

The oxidation behavior of high purity magnesium is worthy of special mention at this point. Over the temperature range 417° – 584°C , the sample gained very little weight ($0.064\text{ mg}/\text{cm}^2$) until ignition occurred at 591°C .

An interesting comparison can be made between the oxidation behavior of molybdenum and that of tantalum and niobium. The curve of molybdenum shows a pressure sensitive region from 550° – 650°C after which the weight gained approaches a limiting value over the temperature range 650° – 700°C , as though the metal were forming a protective film. Samples ignited at 725°C . These findings are in excellent agreement with earlier work (10) which

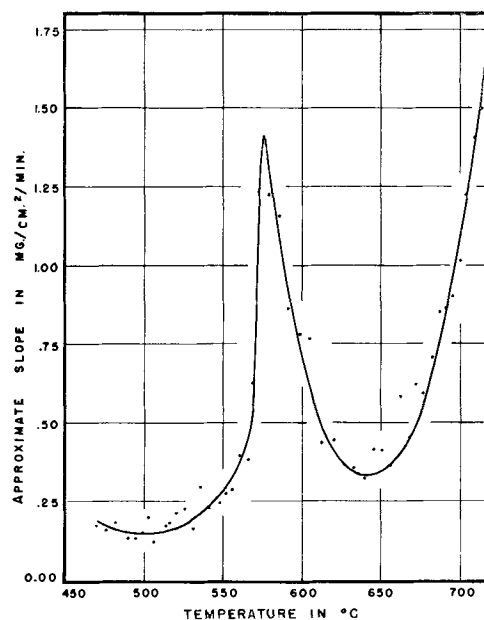


FIG. 3. Curve showing approximate oxidation rate for niobium calculated from the curve of Fig. 2.

gave the following regions for molybdenum: (A) no pressure dependence of oxidation rate was found from 500° to 525°C ; (B) from 550° to 700°C the oxidation rate was sensitive to pressure; and (C) a peculiar pressure sensitive transition region 650° – 700°C was observed. The curve for tantalum, included here for comparison, was described above.

Niobium oxidizes in a manner similar to that of tantalum but with a more pronounced pressure effect over the temperature region 530° – 700°C . The pressure sensitive region is strikingly shown in Fig. 3 in which the slope, determined from the niobium curve of Fig. 2, is plotted against the temperature. This cusped shaped curve is characteristic of metals which oxidize according to equation (I) and is in good agreement with the findings of this laboratory in the investigation of the oxidation of niobium recently completed (11). In regard to Fig. 3, it should be noted that the values of the rate constant are, at best, approximations within the limits of experimental techniques, and should not be used as absolute rate values.

CONCLUSIONS

A method of studying the oxidation behavior of metals in oxygen has been developed in which a metal sample is subjected to a linear increase in temperature at a constant oxygen pressure. The method was found to have the following advantages.

1. It yields a rapid cursory examination of the oxidation behavior of a metal over any desired temperature range.
2. It determines the temperature range over which the oxidation rate is pressure dependent.

3. It consumes a minimum number of samples, using one sample per run.

4. It gives approximate values of the rate constant over the temperature range, and can be used to evaluate values of the activation energy of the reaction and the enthalpy and entropy of adsorption by the solution of equations (XII) and (XIV).⁵

The method was applied to Ta, Nb, Mo, Cu, Zr, Mg, Ti, and W, and experimental results obtained are in good agreement with results of previous investigations of these metals made in this laboratory. It was shown by theoretical considerations that experimental results obtained on tantalum and copper could be explained by imposing the conditions of a linear temperature gradient on a general type of rate equation (developed in this laboratory) for pressure sensitive metals. It is believed that this method shows much promise and will prove to be of considerable value in future investigations of the oxidation behavior of metals and alloys, particularly those about which little or nothing is known.

ACKNOWLEDGMENT

The authors wish to express their appreciation to the Office of Ordnance Research, U. S. Army, for the funds that made this work possible and to Dr. John R. Lewis, Head, Department of Metallurgy, for his support and interest in this project.

Any discussion of this paper will appear in a Discussion Section to be published in the June 1956 JOURNAL.

REFERENCES

1. F. OLMER, *J. Chem. Phys.*, **47**, 313 (1943).
2. W. M. FASSELL, JR., AND R. C. PETERSON, *Technical Report No. IV*, Army Ordnance Contract DA-04-495-ORD-237, Aug. 10, 1953.
3. R. C. PETERSON, W. M. FASSELL, JR., AND M. E. WADSWORTH, *J. Metals*, **6**, 1038 (1954).
4. S. GLASSSTONE, K. LAIDLER, AND H. EYRING, "The Theory of Rate Processes," McGraw-Hill Book Co., New York (1950).
5. K. LAIDLER, "Chemical Kinetics," McGraw-Hill Book Co., New York (1950).
6. Tables of Sine, Cosine and Exponential Integrals, Vol. 1 and 2, Federal Works Agency, Work Projects Administration for the City of New York (1940).
7. E. JAHNKE AND F. EMDE, "Funktionentabellen," Teubner, Leipzig (1938).
8. W. MCKEWAN AND W. M. FASSELL, JR., *J. Metals*, **5**, 1127 (1953).
9. Unpublished data in Progress Report XI Army Ordnance Contract DA-04-495-ORD-237.
10. R. C. PETERSON AND W. M. FASSELL, JR., *Technical Report VI*, Army Ordnance Contract DA-04-495-ORD-237, September 1, 1954.
11. To be published as *Technical Report VIII* Army Ordnance Contract DA-04-495-ORD-237.
12. P. H. EMMETT, Editor, "Catalysis," Vol. II, Chap. V, p. 306, Rheinhold Publishing Co., New York.

⁵ Similar conclusions have been reached by H. Eyring and coworkers (12).

APPENDIX I

The range of convergence of the limiting case solutions of equation (X) can best be illustrated by rewriting equation (IX):

$$\Delta m = \int dm = \frac{k'_0 k}{bh} \int T \exp \left[-\frac{\Delta H^\ddagger}{RT} \right] \frac{K_1 \cdot [O_2]}{1 + K_1 \cdot [O_2]} \cdot dT \quad (\text{IXa})$$

Case I.— $K_1 \cdot [O_2] < 1$, i.e., $\theta < \frac{1}{2}$, using the variable substitution as above, equation (IXa) can be rewritten as follows:

$$\Delta m = -\frac{k'_0 k}{bh} \int \left\{ \frac{P}{R x^2} \exp \left[-\frac{(\Delta H^\ddagger + \Delta H)}{R} x \right] \exp \left[\frac{\Delta S}{R} \right] \right\} \sum_0^{\infty} (-1)^n \{K_1 [O_2]\}^n dx \quad (\text{IXb})$$

Upon expansion of the infinite series one obtains:

$$\Delta m = -\frac{k'_0 k}{bh} \int \frac{P}{R x^2} \exp \left[-\frac{(\Delta H^\ddagger + \Delta H)}{R} x \right] \exp \left[\frac{\Delta S}{R} \right] \{1 - K_1 [O_2] + K_1^2 [O_2]^2 - \dots\} dx \quad (\text{IXc})$$

It is obvious that this series converges for all values of $|K_1 [O_2]| < 1$ corresponding to $\theta < \frac{1}{2}$. It will also be noted that equation (XI) can be obtained from equation (IXc) by retaining only the first term.

Case II.— $K_1 [O_2] > 1$, i.e., $\theta > \frac{1}{2}$.

By multiplying numerator and denominator of equation (IXa) by $1/K_1 [O_2]$ one obtains:

$$\Delta m = \int dm = -\frac{k'_0 k}{bh} \int T \exp \left[-\frac{\Delta H^\ddagger}{RT} \right] \frac{1}{1 + K_1^{-1} [O_2]^{-1}} dT \quad (\text{IXd})$$

which, when expanded as in equation (IXb), yields

$$\Delta m = \int dm = -\frac{k'_0 k}{bh} \int \frac{1}{x^3} \exp \left[-\frac{\Delta H^\ddagger}{R} x \right] \sum_0^{\infty} (-1)^n K_1^{-n} [O_2]^{-n} dx \quad (\text{IXe})$$

Upon expansion as in equation (IXc) one obtains:

$$\Delta m = \int dm = -\frac{k'_0 k}{bh} \int \frac{1}{x^3} \exp \left[-\frac{\Delta H^\ddagger}{R} x \right] \left\{ 1 - \frac{1}{K_1 [O_2]} + \frac{1}{K_1^2 [O_2]^2} - \dots \right\} dx \quad (\text{IXf})$$

This series converges for all values of $|K_1 \cdot [O_2]| > 1$ corresponding to $\theta > \frac{1}{2}$ and equation (XIII) can be obtained by retaining only the first term of equation (IXf).

APPENDIX II

Clarification of the term pressure sensitive parabolic oxidation seems in order. Pressure sensitivity means that the oxidation rate is effected by the external concentration of the oxygen or, perhaps more realistically, by the concentration of the oxygen chemisorbed on the reaction surface. The effect of surface coverage upon the linear rate of oxidation has been noted above (see page 491 of text), and pressure effects have been observed in the case of parabolic oxidation (1). It should be kept in mind that pressure is not the desired variable but the concentration of the surface oxygen phase. The pressure of the gas is only directly proportional to the concentration of the gaseous phase for constant temperature. For variable temperature

(or in the comparison of one isothermal set of rates with another), the more complete expression, $[O_2] = n/V = P/RT$, should be used. This expression assumes the ideal gas law to hold and that the surface activity of oxygen is directly proportional to the bulk gas phase activity.

As first derived by Tammann (2), the rate of growth of an oxide layer is controlled by the concentration gradient of diffusing atoms; the thickness X of the oxide layer varies with time, t , as:

$$dX/dt = A/X \quad (\text{Ia})$$

or,

$$X^2 = 2At + \text{constant} \quad (\text{Ib})$$

Mott and Gurney (3) derive the expression for the constant A for a semiconductor to be:

$$A = \Omega D[n_1 - n_2] \quad (\text{II})$$

where Ω is the volume of oxide per metal ion, D is the diffusion coefficient, and the bracketed quantity is the concentration gradient of the interstitial migrating cations for excess metal oxides or, for a metal deficit oxide, the concentration of lattice vacancies. This quantity permits three types of concentration gradients, with n_2 and n_1 equal to: (a) concentrations of electrons at the respective interfaces when the conductivity of the electron is small compared to that of the ion species; (b) twice the concentrations of the metal ions at the respective interfaces when the oxide is a metal excess type semiconductor; and (c) twice the concentrations of the oxygen atoms at the respective interfaces when the oxide is a metal deficit type semiconductor, the mobility of metal ions through lattice vacancies in this case is directly proportional to the concentration of the oxygen.

For systems involving an oxygen/oxide interface of type (a) or (b), pressure sensitivity would not be expected excluding low pressure "oxygen starvation" effects or film growth involving electrostatic potential barriers. Type (c) oxide layers in contact with external oxygen would exhibit pressure sensitivity according to the degree of relative surface coverage.

For oxygen excess oxides Mott and Gurney state the following: "Now it was shown that cuprous oxide is a conductor only if it contains an excess of oxygen, and that its conductivity increases with increasing pressure of oxygen in contact with the crystal. On the other hand cuprous oxide in contact with copper is practically of stoichiometric composition. Thus in tarnishing reactions $n_1 \ll n_2$ and the rate of reaction is determined by n_2 , the concentration of excess oxygen at the free surface. . . ." (p. 257, *op. cit.*) Hence equation (II) becomes for an oxygen excess semiconductor oxide

$$A \approx -2\Omega Dn_2 = -2\Omega f(\theta) \cdot D \quad (\text{III})$$

where $f(\theta) = n_2$, and θ is the fraction of surface covered with chemisorbed oxygen.

According to Eyring (4) the diffusion coefficient, D , should be:

$$D = \lambda^2 K kT/h \cdot \exp[-\Delta F^\ddagger/RT] \quad (\text{IV})$$

where λ is the jump distance between interstitial positions in the lattice for metal excess oxides or the corresponding vacancy jump distance for metal deficit oxides; K is the transmission coefficient (usually assumed unity); k is the Boltzmann constant; h is Planck's constant; ΔF^\ddagger is the activation free energy associated with the jump of cations; T is the absolute temperature; and R is the molar gas constant.

Thus equation (II) of text results:

$$\begin{aligned} m \cdot dm/dt &= k_o \cdot A = -2\Omega k_o \cdot f(\theta) \cdot D \\ &= C_o \cdot f(\theta) \cdot kT/h \cdot \exp[-\Delta H^\ddagger/RT + \Delta S^\ddagger/R] \quad (\text{V}) \end{aligned}$$

where $C_o = 2\lambda^2 \cdot (-\Omega) \cdot k_o$, and k_o is defined on page 491 of the text.

The validity of the factor kT/h in the Eyring derivation has been challenged by Zener and others (5, 6). They replace the factor with a frequency of vibration function. However, this is of more theoretical importance than of immediate consequence, as the effect of a linear temperature factor when multiplied by an exponential term containing the variable is but slight.

It should be noted that the above derivation is essentially as that set forth by Gulbransen (7). However, Gulbransen does not distinguish the rate-determining ionic gradient species for the two known types of semiconductors, i.e., metal deficit and metal excess.

Equation (V) does not hold for metal excess semiconductors such as ZnO or Fe₂O₃ where n_2 would be the concentration of metal ions at the free surface. This concentration would be expected to be nearly constant, although recent work (8-10) shows pressure effects for this case.

Where the surface coverage is unity in the case of rate-controlling diffusion through an oxygen excess semiconductor [$f(\theta) = 1$] or where the semiconductor is a metal ion excess oxide [with no dependence on $f(\theta)$], the equation for parabolic growth reduced to

$$m \cdot dm/dt = C_o \cdot kT/h \cdot \exp[-\Delta F^\ddagger/RT] \quad (\text{VI})$$

The entire temperature dependence now rests with the temperature variation of the diffusion coefficient.

Application of the foregoing arguments is attempted in the text proper for the metal copper in region where two oxides are known to exist in equilibrium with the metal. The semiconductor properties of Cu₂O have been well established (1) but those of the other oxide of copper, CuO, are not well known (9, 11). Thus as the oxygen/oxide interface is probably O₂/CuO in the temperature-pressure range investigated it is impossible to state whether the observed pressure insensitivity of the system is due to complete surface coverage or to the fact that CuO is a type (a) or (b) semiconductor.

APPENDIX REFERENCES

1. C. WAGNER AND K. GRUNEWALD, *Z. physik. Chem. (B)*, **40**, 455 (1938).
2. G. TAMMANN, *Z. anorg. Chem.*, **111**, 78 (1920).
3. N. F. MOTT AND R. W. GURNEY, "Electronic Processes in Ionic Crystals," 2nd ed., p. 255 Oxford Press, New York (1948).
4. S. GLASSTONE, K. LAIDLER, AND H. EYRING, "The Theory of Rate Processes," McGraw Hill Book Co., New York (1950).
5. C. WERT AND C. ZENER, *Phys. Rev.*, **76**, 1171 (1949).
6. B. CHALMERS, Editor, "Progress in Metal Physics," Vol. 4, Chap. 6, pp. 265-332, Interscience Publishers, Inc., New York (1953).
7. E. A. GULBRANSEN, *Trans. Electrochem. Soc.*, **83**, 301 (1943).
8. W. J. MOORE AND J. K. LEE, *Trans. Faraday Soc.*, **34**, 485 (1938).
9. B. CHALMERS, Editor, "Progress in Metal Physics," Vol. 4, Chap. 2, pp. 71-102, Interscience Publishers, Inc., New York (1953).
10. H. H. VON BAUMBACH AND C. WAGNER, *Z. physik. Chem.*, **B22**, 199 (1933).
11. K. HAUFFE AND H. GRUNEWALD, *Z. physik. Chem.*, **198** 248 (1951).

Electrolytic Oxidation of Zinc in Alkaline Solutions¹

THEDFORD P. DIRKSE

Calvin College, Grand Rapids, Michigan

ABSTRACT

A study has been made of the mechanism of the reaction taking place when zinc is anodically treated in potassium hydroxide solutions. The zinc-containing ion present in solution as a result of the anodic treatment is $\text{Zn}(\text{OH})_4^-$. However, zinc oxide or hydroxide is an intermediate leading to the formation of $\text{Zn}(\text{OH})_4^-$. This latter ion then decomposes slowly to form zinc oxide.

INTRODUCTION

Although the electrolytic oxidation of zinc in aqueous alkaline solutions is an industrial reaction of some importance, comparatively little has been written or reported on the mechanism of this reaction which occurs during the discharge of alkaline batteries having zinc negative plates. It may also be the anodic reaction in alkaline zinc plating baths.

RESULTS AND DISCUSSION

When zinc is anodically treated in potassium hydroxide solutions, a white turbidity eventually appears in the electrolyte. This has been observed at temperatures of 0°–45°C, and in solutions of 10–40% potassium hydroxide. Many samples of this white substance have been collected and analyzed. Results indicate that it is zinc oxide. It has also been observed that, during the anodic oxidation of zinc in alkaline media, zinc gradually becomes covered with a dark colored substance. In some instances this material could be scraped off the electrode. Chemical analysis showed it to be zinc oxide. In other cases where this covering could not be scraped off, it was subjected to x-ray analysis and again found to be practically pure zinc oxide. It is possible that small amounts of finely divided zinc were also present. Thus it appears that the end product of this electrode reaction is zinc oxide which may be produced as a white substance eventually precipitating from the electrolyte, or as a dark colored substance adhering to the electrode.

Although on anodic oxidation of zinc in alkaline solutions zinc oxide ultimately precipitates from the solution, the appearance of this zinc oxide is not a simple solubility or supersaturation phenomenon. This was shown by using solutions of potassium hydroxide saturated with zinc oxide and then filtered. This clear filtrate was used as the medium for the anodic oxidation of zinc. In some cases the solu-

tion remained clear during several days of anodic oxidation of zinc. Yet analysis showed that the zinc content of the solution was gradually increasing (see Fig. 1). Eventually a white precipitate did appear and, when such solutions were allowed to stand, zinc oxide gradually precipitated out and the composition of the solution approached that of a potassium hydroxide solution saturated with zinc oxide. In some instances, over a year was necessary at room temperature for the solution to approach this composition. It appears then that at least two reactions are involved: (a) a reaction whereby zinc is introduced into solution; and (b) a reaction whereby this dissolved zinc species decomposes to zinc oxide.

There is other evidence for such an interpretation. Cells containing zinc negative plates, nickel oxide positives, and potassium hydroxide solutions as electrolyte were discharged at a low rate. A magnetic stirring device was used to agitate the electrolyte and provision was made for inserting a dip type conductivity cell into the electrolyte. The resistance, or conductance, of the electrolyte was followed during the course of the discharge. The specific conductance of the electrolyte decreased as the discharge proceeded until the turbidity appeared in the solution. After this, as the zinc oxide continued to precipitate out, the conductance increased slowly (Fig. 2). The rate at which the conductance recovers depends on the discharge current, which governs the dissolution rate of the zinc, and the rate at which the zinc oxide precipitates out. The fact that the conductance varies with time up to the appearance of a precipitate indicates that excess zinc is dissolved in the electrolyte and is not present in a colloidal form. Other physical properties such as density and viscosity also vary with excess zinc concentration.

To study this mechanism further it is obvious that some information is needed with respect to the zinc-containing species in solution. This is the substance that decomposes to form the zinc oxide and it is also the substance produced by the electrode reaction. The composition of this zinc-containing ion was

¹ Manuscript received January 3, 1955. This paper was prepared for presentation before the Boston Meeting, October 3 to 7, 1954.

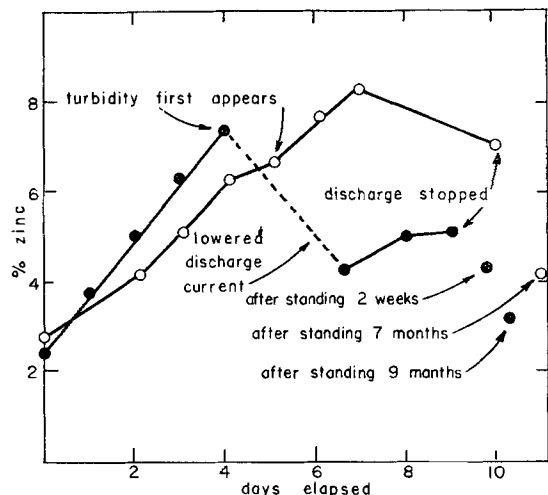


Fig. 1. Zinc content of electrolyte during discharge: ○—47% KOH saturated with ZnO; ●—25% KOH saturated with ZnO; current density, 0.005 amp/in.².

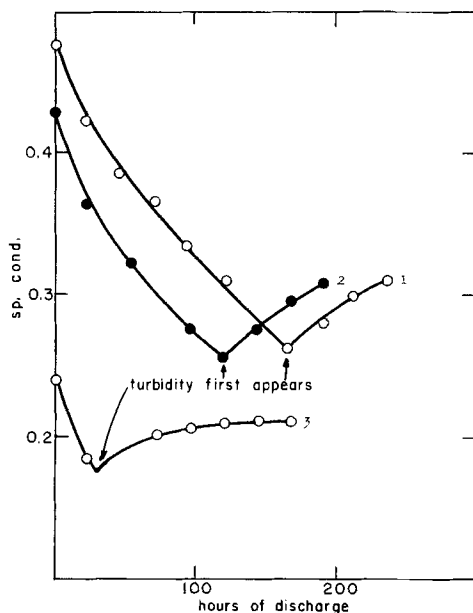
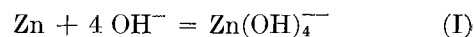


Fig. 2. Specific conductance of electrolyte during discharge: curve 1, 15% KOH; curve 2, 12% KOH; curve 3, 8% KOH; current density, 0.015 amp/in.².

determined by using galvanic cells (1). Certain potassium hydroxide solutions were used as the electrolyte in cells containing zinc negative and nickel oxide positive plates. As the cell was discharged, samples of the electrolyte were withdrawn at intervals. The potential of a zinc electrode in such a solution was then determined immediately and the solution was later analyzed for its zinc content.

Using the method previously described (1), a plot was made of $(E_{Zn} - 0.118 \log a_{H_2O})$ vs. $\log a_{OH^-}$. A straight line having a slope of 0.120 was obtained, showing that $Zn(OH)_4^{--}$ is the zinc-containing ion produced in solution by the anodic oxidation of zinc under such conditions.

From this it may tentatively be concluded that the mechanism of the reaction taking place is



followed by



Reaction (II) is obviously a slow reaction. These two reactions will now be considered separately.

Reaction (I).—It has been suggested by others (2, 3) that the electrode reaction produces a zinc oxide or hydroxide. This substance is then dissolved by the electrolyte. When the solvent action of the electrolyte is reduced to such an extent that the oxide layer can be built up on the electrode surface, then the electrode becomes passive. An intensive study was made of the electrode reaction and the evidence obtained is consistent with this interpretation.

Using the method described by Huber (2), the limiting current density at which the zinc electrode becomes passive was determined under a variety of conditions. Zinc electrodes were coated with polystyrene, leaving an exposed area of definite dimensions. These were used as anodes, while larger zinc electrodes served as cathodes. The electrolyte was aqueous potassium hydroxide. As the current applied to the cell was increased the potential between the anode and an auxiliary zinc electrode was measured. Curves of the type given by Huber (2) were obtained. The limiting current density varied with the time required for making the measurements. Consequently, values obtained are relative, not absolute. However, several runs were made under each set of conditions and results given here represent the average of all such runs.

Several factors affect the ability of potassium hydroxide solutions to dissolve the zinc oxide or hydroxide produced on the electrode surface. Some of these factors are: amount of electrolyte, rate of stirring, concentration of electrolyte, and temperature. In the first set of experiments the amount of electrolyte and rate of stirring were held constant. The effects of varying the temperature and electrolyte concentration are shown on Fig. 3 and 4. The variation with temperature is what would be expected. As the temperature increases the zinc oxide or hydroxide becomes more soluble in the electrolyte. As a result, with increasing temperature a higher limiting current density is obtained since the film formed on the electrode is removed more readily.

The variation of limiting current density with electrolyte concentration (Fig. 4) shows a maximum at about 20–30% potassium hydroxide, the exact value depending on the temperature. The decrease in the limiting current density at the higher concentrations is undoubtedly related to the high viscosity of such solutions. This decreases the mobility

of the ions and, thus, hydroxyl ions are not able to reach the electrode surface as readily. The hydroxyl ions used in the electrode process to produce the zinc oxide are not replaced rapidly enough by other hydroxyl ions which are necessary to dissolve the film that was formed.

In another set of experiments the zinc anode was allowed to operate at a given current density for five minutes before the current density was changed. The current density was increased by definite increments until the electrode became passive. In these runs the speed of stirring was changed, as was the amount of electrolyte. However, no great changes were noted by either of these variables. At the higher concentrations of electrolyte, increasing the speed of mechanical stirring did bring about a slight, but definite, increase in limiting current density. Apparently the increased stirring rate aided the mobility of the ions in solution. The fact, however, that this effect was slight, indicates that the mobility of the ions in solution is determined primarily by the potential gradient in the solution and the physical characteristics of the electrolyte.

In all these experiments relatively large amounts of electrolyte were used compared to the electrode surface area exposed. This ratio of electrolyte to surface area was much larger than used in batteries. Consequently, increasing the amount of electrolyte had no effect on the limiting current density since the limitation was due to the mobility of the ions, not to a lack of them.

There is still another factor that may have a bearing on the limiting current density, and that is the presence of dissolved zinc in the electrolyte. If, as the anodic process continues, the film produced is dissolved by the electrolyte, the concentration of zinc in the electrolyte increases. As this increases, the electrolyte becomes less able to dissolve more zinc oxide, and the limiting current density should be less. This effect was observed as shown in Fig. 5. At low concentrations of potassium hydroxide, addition of zinc oxide to the electrolyte had no effect on the limiting current density because such solutions do not contain much zinc. However, as the concentration of potassium hydroxide is increased, more zinc oxide can be dissolved. Thus, higher concentrations of potassium hydroxide, when saturated with zinc oxide, show increasingly lowered values of limiting current density.

These results are consistent with the idea that the electrode product is a very soluble form of zinc oxide or hydroxide which is removed by further reaction with the electrolyte.

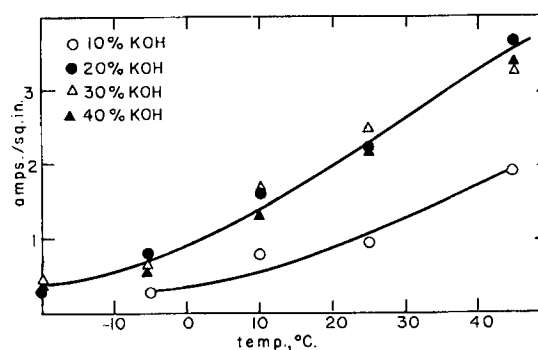
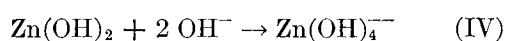
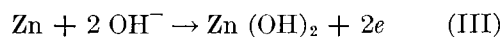


FIG. 3. Limiting current density as a function of temperature.

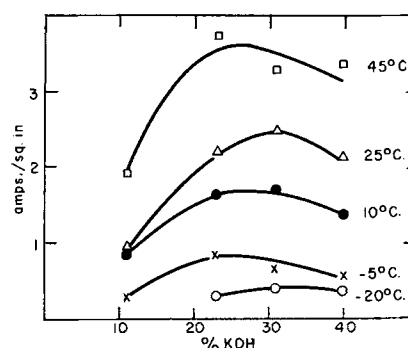


FIG. 4. Limiting current density as a function of electrolyte concentration.

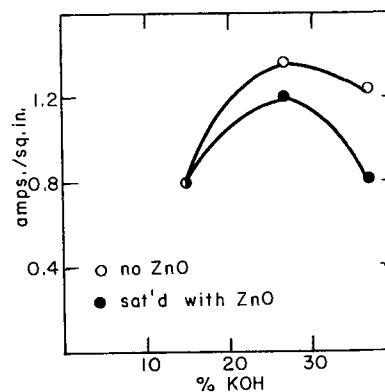


FIG. 5. Effect of dissolved zinc on limiting current density.

There is other evidence that supports this contention. It was observed in studying the conductance of cell electrolytes on discharge that the conductance of such electrolytes decreased even when the current was interrupted. An illustration of this is shown on Fig. 6. A likely interpretation of this phenomenon is that the anodic oxidation of zinc results in the formation of zinc oxide or hydroxide. A part of this, at least, is then dissolved slowly by the alkali. Thus, the zinc content, and, hence, the resistance of the electrolyte, increases when the discharge is discontinued.

Furthermore, it was also observed in studying the limiting current density at which the zinc electrode becomes passive that, after an electrode had become

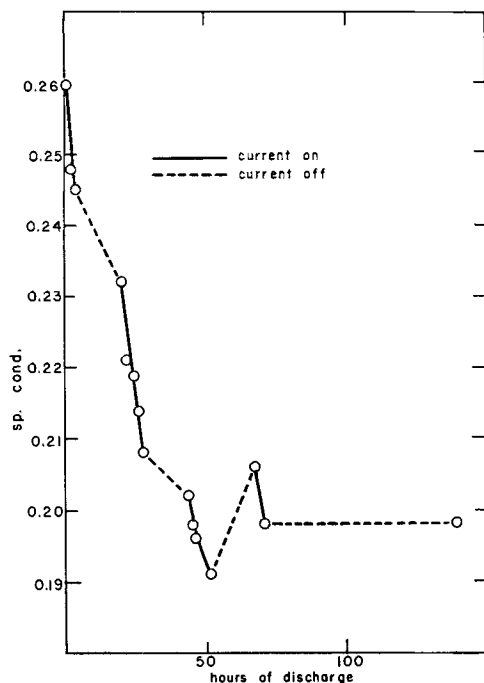


Fig. 6. Specific conductance of electrolyte during interrupted discharge.

passive, it would again become active if it remained in contact with the electrolyte with no current flowing. In some cases, standing only a minute was sufficient to allow the electrode to carry current again. At times the electrode could be made active again merely by reducing the current density. Apparently in such cases the rate of production of the zinc oxide film was then slowed down sufficiently so that it was again dissolved at least as fast as it was formed.

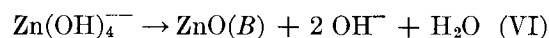
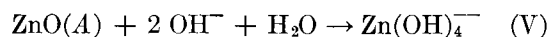
No attempt was made to identify further the nature of the film produced by the electrode reaction. However, it was observed that in all cases when an electrode was examined immediately after it had become passive that it was covered with a silver-like film. This film had a bright luster and may be that produced by electropolishing of zinc. In those cases where an electrode was allowed to remain in the electrolyte for some time after it had become passive, the exposed electrode area had a grayish cast, quite unlike the film on a passive surface. It was remarked earlier that the zinc electrode frequently became covered with a black or dark-colored film which is zinc oxide. This black film, while common, was not found on any passive surface. Hence, it is not responsible for the passivation of the electrode. When electrodes were oxidized at a low current density, the zinc electrode became covered with this black film soon after oxidation had begun. This film remained on the electrode until oxidation was complete, i.e., until the exposed zinc had been completely eaten away.

Reaction (II).—Since it has been shown that the main zinc-containing ion in solution is $\text{Zn}(\text{OH})_4^{--}$, concentration of free hydroxyl ions in solution can be determined by analysis. A given solution can be treated with a known excess of acid and back titrated with a base. From the total alkalinity so determined the number of hydroxyl ions bound up in the zinc complex ion can be subtracted. This difference then gives the concentration of the free hydroxyl ions.

Three different electrolytes, 10, 20, and 30% potassium hydroxide, were used in cells containing nickel oxide positive and zinc negative plates. These cells were discharged until the electrolyte became turbid. The electrolyte was then withdrawn, filtered, kept at 25°C, and stirred magnetically from time to time. Samples were withdrawn from this electrolyte, filtered, and analyzed over a period of up to a week. The ratio of increase of free hydroxyl ion to decrease of zinc in solution was thus determined. Ratios obtained ranged from 1.4 to 2.6. Considering the limitations of the method, it seems reasonable to assume that this ratio is two, in agreement with equation (II). Using these same data and plotting $\log M_{\text{Zn}}$ vs. time, a straight line is obtained, confirming the assumption that the reaction is a first order one with respect to zinc ion.

CONCLUSIONS

The fact that, during the electrolytic oxidation of zinc in alkaline solutions, two reactions [equations (I) and (II)] occur is not as unlikely as it may at first appear. A similar phenomenon has been noted with zinc oxide in potassium hydroxide solutions. Solutions of potassium hydroxide ranging from 15% to 32% were kept at 25°C. Then an excess of zinc oxide was added and the solutions were stirred thoroughly. Samples were taken at intervals, filtered, and analyzed. In each case the zinc content of the solution increased and reached a constant value in about three hours. After two weeks samples were again taken and in each case the zinc content was found to have decreased beyond experimental error. The extent of decrease was greater in more concentrated potassium hydroxide solutions. This, too, can be accounted for by a two-step process, the first being rapid and the second slow. The fact that in this case



the solutions reached equilibrium sooner than do cell electrolytes is probably due to the difference in the kind of zinc oxide which first dissolved in the potassium hydroxide solutions. If equations (V) and (VI) represent reactions taking place in the solution, then

it is likely that the zinc oxide referred to in each equation is physically different from the other, i.e., has a different free energy content.

Samples of hyperfine zinc oxide produced by Merck and Company were made available and, when this oxide was used in such solubility experiments, the decrease of zinc content in the solution on standing was still greater. The hyperfine zinc oxide is undoubtedly more soluble than the ordinarily available zinc oxide, due to its particle size. Because of this greater solubility, reaction (V) can proceed to a greater extent before reaction (VI) becomes of significance. Consequently, the zinc content of the solution can exceed the normal equilibrium value by a greater amount. On standing, then, the decrease of zinc content in solution will be greater.

It appears that the zinc oxide which precipitates from, and is in equilibrium with, potassium hydroxide solutions has a particular physical structure, different from other forms of zinc oxide which are available. For that reason a long time is necessary to establish equilibrium in potassium hydroxide solutions saturated with zinc oxide. For that reason, too, values reported for the zinc content of such solutions have varied (4). In many cases equilibrium had not been reached before the analyses were made.

It is very likely that the type of zinc oxide or hydroxide which is produced by the anodic treatment of zinc in alkaline solutions is a very soluble form. For this reason, and the fact that reaction (VI) is slow, the electrolyte in alkaline cells having zinc negative plates may be clear and yet have a zinc content higher than that of a saturated solution.

ACKNOWLEDGMENT

Thanks are due to Merck and Company, and the New Jersey Zinc Sales Company for supplying some of the materials used in this project. It is a pleasure to express thanks also to the Office of Naval Research under whose sponsorship this work was carried out.

Any discussion of this paper will appear in a Discussion Section to be published in the June 1956 JOURNAL.

REFERENCES

1. T. P. DIRKSE, *This Journal*, **101**, 328, 638 (1954).
2. K. HUBER, *Z. Elektrochem.*, **48**, 26 (1942); *Helv. Chim. Acta*, **26**, 1037 (1943); *This Journal*, **100**, 376 (1953).
3. Z. A. IOFA, S. YA. MIRLINA, AND N. B. MOISEEVA, *Zhur. Priklad. Khim.*, **22**, 983 (1949).
4. G. F. HÜTTIG AND B. STEINER, *Z. anorg. u. allgem. Chem.*, **199**, 149 (1931).

Anodic Polarization of Zirconium at Low Potentials

Formation Rates, Formation Field, Electrolytic Parameters, and Film Thicknesses of Very Thin Oxide Films¹

GEORGE B. ADAMS, JR., AND PIERRE VAN RYSELBERGHE

Department of Chemistry, University of Oregon, Eugene, Oregon

AND

MARIO MARAGHINI

Institute of Applied Chemistry, University of Rome, Rome, Italy

ABSTRACT

Methods are described for making quantitative studies on the growth of very thin oxide films on zirconium, and for estimating the film thickness as this growth progresses. These methods have been shown to be internally consistent and have been correlated with Mott's theory of metal oxidation. Experimental results so obtained are in agreement with previous work.

These methods should be readily adaptable to studies on the effect of temperature, ultraviolet radiation, electrolyte, and metal composition and physical properties, on the ionic current causing oxide film growth.

INTRODUCTION

A recent publication (1)² described the potential-time curve obtained when zirconium was anodized at constant current strength in certain aqueous electrolytes. This curve can be divided into three branches (Fig. 1). With a freshly abraded specimen there is initially a rapid rise in potential with a rate of change which decreases until a constant value is reached (branch AB).³ This constant rate is maintained until the potential has risen sufficiently for oxygen evolution to occur. Then the rate drops abruptly to a very low value, which gradually increases over a long time interval (branch BC). During this period, visible localized gas evolution takes place. Finally, after a time interval dependent on the current being passed, the potential rises at an accelerated rate which quickly attains a constant value, lower than that of branch AB; this rate is maintained as the potential climbs steadily to 100 v or more (branch CD). The maximum voltage then attainable is limited only by the breakdown potential of the film.

¹ Manuscript received December 27, 1954. This paper was prepared for delivery before the Pittsburgh Meeting, October 9 to 13, 1955.

² The caption of Fig. 8, in "Studies on the Anodic Polarization of Zirconium and Zirconium Alloys," by M. Maraghini, G. B. Adams, Jr., and P. Van Rysselberghe [*This Journal*, **101**, 404 (1954)] should read: "Logarithm of the rate of increase of potential vs. potential in aerated 1.5M HCl."

³ The initial curvature in branch AB is apparent only at current densities of about 10 $\mu\text{a}/\text{cm}^2$ or less. Its significance has been explained previously (1).

With varying current density the potential-time curves change as shown in Fig. 1; with very high current densities the flat branch is undetectable by instruments used in this study, and with very low current densities the upper branch is not reached. The length of the branch BC and the slope of the branch CD are both highly dependent on oxygen concentration in the solution. Increasing concentrations of oxygen in the electrolyte shorten the flat branch and increase the slope of the upper branch, but do not affect the slope of the lower branch. A change in electrolyte does not affect the qualitative pattern of the curves, but may change certain parameters which can be derived quantitatively from them. An important exception is that of electrolytes containing halide ions in concentration of 0.001M or greater; in this case a stable horizontal branch occurs at a potential below that of the branch BC.

Properties of the oxide film formed along this second steep branch of the curve have been studied most recently by Charlesby (2) who showed that the anodic film growth follows the empirical law

$$I_+^0 = A_+ \exp(B_+ F) \quad (\text{I})$$

between the true ionic current density I_+ and the electrostatic field F across the film. He re-evaluated the electrolytic parameters A_+ and B_+ , and the field F , using a better value for the dielectric constant of the oxide than that employed by Güntherschulze and Betz (3).

Mott (4) also obtained an equation of the form of (I). He assumes that at high fields equilibrium is not

established for the movement of metal ions across the barrier, and the derivation is carried out on the premise that the oxide film is so thin that the effect of any space charge built up by metal ions dissolving in the film in the course of its formation is negligible, with the consequence that the movements of ions and of electrons can be considered independently. On this basis, parameters A_+ and B_+ can be evaluated in terms of the barrier height, the barrier half-width, and certain physical properties of the metal. This film-building mechanism should be valid for the growth of thin oxide films formed by anodization as well as for the growth of oxide films on metals in air, caused by the electrostatic field set up across the oxide film when a contact potential difference is established between metal and adsorbed oxygen. Below a certain critical temperature, oxidation of metal in air or in aqueous electrolyte solution, due to this intrinsic field, will proceed only until a limiting oxide film thickness, generally of less than 100 Å, has been built up; it will stop effectively when this field has been decreased sufficiently by the growth of oxide film to reduce greatly further passage of metal ions across the metal-oxide interface.

It would thus seem that, in order to evaluate properly the electrolytic parameters A_+ and B_+ and their variation with temperature in studying the early stages of the oxidation process, it would be preferable to work with oxide films less than 100 Å in thickness, since the Mott equation was derived for oxide films so thin that the effect of space charge on the formation field is negligible.⁴ Indeed, as Cabrera and Mott (7) point out, recent experimental work would indicate that, at sufficiently low temperatures, it is probable that the initial stages of the growth of oxide films on all readily oxidizable metals is governed by this same barrier mechanism. Oxidation of aluminum, chromium, titanium, tungsten, zinc, zirconium, and many other metals follows this type of law at room temperature; barium, copper, iron, and other metals show the same behavior at liquid air temperatures. Oxidation is very rapid at first, then drops to low or negligible values with the formation of a stable oxide film 20–100 Å thick.

Films thicker than 200 Å can be studied accu-

⁴ Since this paper was submitted for publication, DeWald (5) has interpreted some of Vermilyea's results on the anodic oxidation of Ta (6) in terms of a theory which takes into account the action of space charge formation on the average formation field in the oxide film. He thus explains the observed temperature independence of the Tafel slope for films some thousands of Angströms in thickness, whereas the Mott theory for thin films requires a Tafel slope proportional to the absolute temperature.

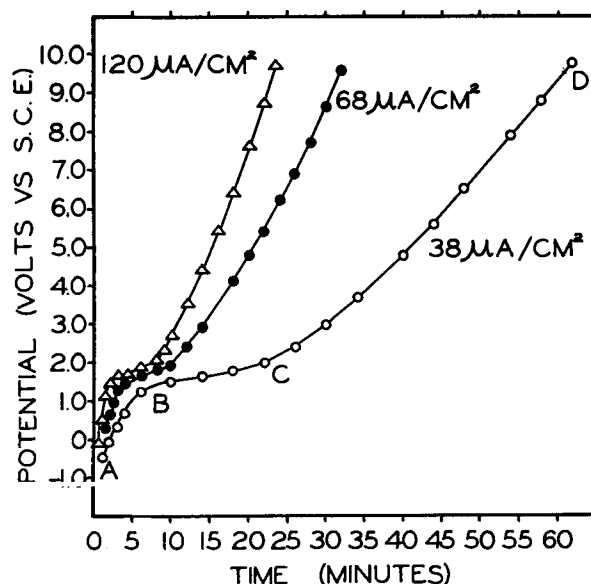


FIG. 1. Potential time curves for zirconium in air-saturated ammonium borate solution at 20.0°C.

rately by capacitance measurements, but for the thin films produced in the narrow range of potentials along the branch AB of the potential-time curve this method cannot be employed with certainty (8). These very thin films can be studied easily by following the change in the potential of the electrode surface with time, and the aim of the present research was to study the growth of these thin films over a potential range in which they exist, i.e., in the lower branch of the potential-time curve. Interpretation of results is greatly simplified by the fact that, for zirconium, the current efficiency of the film-building process is unity below oxygen evolution potentials. The principal uncertainty in quantitative interpretation along the lines of the Mott theory lies in the assumption that the density of these very thin films is that of the oxide in bulk.

In what follows, methods which have been used in the high potential range are adapted and extended for use in obtaining the parameters A_+ and B_+ from potential-time measurements taken in the low-potential range. Two equations are derived from (I) and two sets of experiments were carried out to test their validity. A third relationship derivable from (I) is shown to hold experimentally in the low potential range.

RATE OF CHANGE OF POTENTIAL AT CONSTANT CURRENT

Introducing the apparent ionic current density, calculated from the projected area of the electrode, $I_+ = \sigma I_+^0$ ($\mu\text{a}/\text{cm}^2$) where σ is the roughness factor for the electrode surface, and identifying the ionic

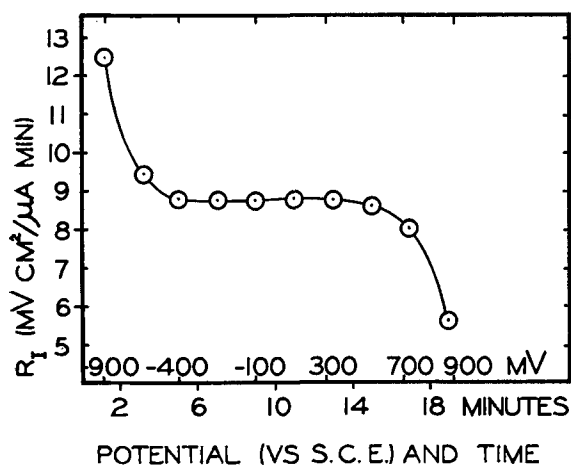


FIG. 2. Formation rate vs. potential and time for a single run at $12 \mu\text{a}/\text{cm}^2$, $1.0\text{M Na}_2\text{CO}_3$, air saturated, at 25.0°C .

current with the total anodic current I (in the absence of electron current), (I) becomes:

$$I = \sigma A_+ \exp(B_+ F) \quad (\text{II})$$

If X_0 is the oxide film thickness on the electrode before anodization is begun; r , the volume of oxide formed/ $\mu\text{a min}$ ($3.36 \times 10^{-9} \text{ cc}/\mu\text{a min}$), assuming, with Charlesby (2), that the oxide formed has a density of 5.7; X , the film thickness at time t built up by anodization, with $X = X_0 + r \int_0^t I/\sigma dt$; and E , the potential drop across the film at time t (mv), then

$$F = E/X = (1/B_+) \ln (I/\sigma A_+) \quad (\text{III})$$

When an external anodic current flows in the polarizing circuit between the zirconium anode and an auxiliary cathode, the potential measured in the potentiometric cell, zirconium-saturated calomel electrode (S.C.E.), will be

$$E' = E + K$$

where K is the constant sum of all potential differences in the chain other than that across the oxide film.

Substituting in (III),

$$E' = (r/B_+) \left[\int_0^t (I/\sigma) dt \right] \ln (I/\sigma A_+) + (X_0/B_+) \ln (I/\sigma A_+) + K \quad (\text{IV})$$

For I and σ constant in time,

$$\left(\frac{\partial E'}{\partial t} \right)_{I,\sigma} = \left(\frac{\partial E}{\partial t} \right)_{I,\sigma} = (rI/\sigma B_+) \ln (I/\sigma A_+) \quad (\text{V})$$

Designating the formation rate at apparent current density I , by R_I , where

$$R_I = 1/I \left(\frac{\partial E}{\partial t} \right)_{I,\sigma}$$

then

$$R_I = (r/\sigma B_+) \ln I + (r/\sigma B_+) \ln (1/\sigma A_+) = rF/\sigma \quad (\text{VI})$$

Potential-time measurements can be obtained for the film-building process at constant polarizing current after the local anodic current has decayed to a negligible value, i.e., along the linear portion of branch AB , Fig. 1. If $(\partial E/\partial t)_{I,\sigma}$ remains constant in time, it can be assumed that σ is also constant in time. If this is true, if equation (I) is valid for thin films, and if σ is independent of I , a plot of the formation rate vs. $\ln I$ should give a straight line. From the slope S of this line ($\text{mv cm}^2/\mu\text{a min}$), and its intercept H ($\text{mv cm}^2/\mu\text{a min}$),

$$B_+ = r/S\sigma \quad (\text{VII})$$

$$\ln (1/\sigma A_+) = H/S \quad (\text{VIII})$$

EXPERIMENTS AT CONSTANT CURRENT

Equation (VI) has been tested experimentally for zirconium in ammonium borate and sodium carbonate solutions, and it was found that $(\partial E/\partial t)_I$ becomes constant with time and that R_I is linear with $\ln I$.

In Fig. 2 a sample run is shown, where a plot of R_I vs. time and vs. potential indicates the constancy of the formation rate after the local anodic current has become negligible.⁵ In Fig. 3 the linearity of the plots of R_I vs. $\ln I$ is evident. Each point is the mean value of five determinations, and vertical bars mark off the probable errors. The lines were drawn on the basis of the method of least squares. The mean values of the constant rates for a given current density for borate and carbonate solutions are reported in Table I, together with the values of σA_+ , σB_+ , and F/σ derived therefrom.

Comparison with Previous Work

Results obtained in borate solution at 20.0°C may be compared directly with those of Charlesby (2), which were obtained from measurements taken on much thicker films over a potential range of 10–100 v and higher. His work was done at 18°C .

Line (A) of Fig. 3 has a slope of 1.69 and an intercept of 7.68.

⁵ The first descending branch of the curve in Fig. 2 indicates that, in addition to the effect of the constant external anodic current, there is additional oxide film building due to the direct chemical action of the freshly abraded Zr surface with the solution. This action can be expressed in terms of a local anodic current (I) which decays with increasing film thickness. When the local current has become negligible compared to the constant value of the impressed anodic current, the formation rate becomes constant for a given value of the impressed current.

TABLE I. Variation of formation rate with apparent current density

Solution	I $\mu\text{a}/\text{cm}^2$	$\text{Log } (I/1 \mu\text{a cm}^{-2})$	R_I $\frac{\text{mv cm}^2}{\mu\text{a min}}$	σB_+ cm/mv	σA_+ $\mu\text{a}/\text{cm}^2$	F/σ $\frac{\text{mv}/\text{cm}}{\text{at } 100 \mu\text{a}/\text{cm}^2}$
Ammonium borate, 20.0°C	1.22	0.085	7.84 ± 0.09	4.6×10^{-9}	2.9×10^{-5}	3.3×10^9
	3.85	0.585	8.63 ± 0.03			
	12.2	1.085	9.52 ± 0.04			
	38.5	1.585	10.4 ± 0.10			
	122.0	2.085	11.2 ± 0.06			
Sodium carbonate, 25.0°C	1.22	0.085	7.43 ± 0.08	6.0×10^{-9}	0.20×10^{-5}	2.9×10^9
	3.85	0.585	7.99 ± 0.02			
	12.0	1.078	8.70 ± 0.04			
	37.5	1.575	9.33 ± 0.07			
	118.0	2.074	9.94 ± 0.10			

From (III), (VII), and (VIII):

$$\begin{aligned}\sigma B_+ &= 4.6 \times 10^{-9} \text{ cm}/\text{mv} \\ \sigma A_+ &= 2.9 \times 10^{-5} \mu\text{a}/\text{cm}^2 \\ F/\sigma &= 3.29 \times 10^9 \text{ mv}/\text{cm at } 100 \mu\text{a}/\text{cm}^2\end{aligned}$$

Charlesby reports a B_+ value of 3.4×10^{-9} , an A_+ value of 1.6×10^{-5} , and an average value for F of 4.5×10^9 at $100 \mu\text{a}/\text{cm}^2$. These values include a roughness factor, which Charlesby takes as essentially unity.

If this evaluation is correct, then designating Charlesby's values by the subscript Ch:

$$\frac{\sigma B_+}{(B_+)_{\text{Ch}}} = 4.6/3.4 = 1.35; \quad \frac{\sigma A_+}{(A_+)_{\text{Ch}}} = 2.9/1.6 = 1.8;$$

$$\frac{F_{\text{Ch}}}{F/\sigma} = 4.5/3.3 = 1.35,$$

and, for agreement a roughness factor of about 1.4 must be assumed for the surface of the abraded specimens after the formation rate has decreased to its limiting value. The third ratio is independent of the other two because F_{Ch} was determined from capacitance measurements, which were not directly related to A_+ and B_+ . The second check does not carry the same weight as the others because of the large uncertainty involved in evaluating A_+ , due to its exponential relationship to the field.

The value of 1.4 thus deduced for the roughness factor of the surfaces of the abraded specimens after anodization to negligible local current has been substantiated further. The roughness factor for the freshly abraded specimens, prior to immersion, was found to be 2.1 ± 0.2 , using a small-volume gas adsorption apparatus with krypton gas as adsorbate.⁶ This value of the roughness factor must be considered as an upper limit. The actual electro-

⁶ Determinations of roughness factors were made for the authors by Ralph J. Brodd through the courtesy of Professor Norman Hackerman, University of Texas, Austin, Texas.

chemical roughness factor should lie between this value and unity. This has been shown by comparing formation rates for highly polished electrode surfaces with those for abraded surfaces. The average formation rate for a highly polished zirconium electrode surface is approximately 40% higher than the formation rate for an abraded surface, which again would indicate that, if the roughness factor for the polished electrode surfaces were very nearly unity, as Young claims for Ta (6), the roughness factor for the abraded surfaces after anodization to a constant rate would then be about 1.4.

A final check with Charlesby's results can be made independently of an assumed roughness factor. The product B_+F is dimensionless. For a current density of $100 \mu\text{a}/\text{cm}^2$ this product is $4.6/\sigma \times 3.3 \sigma = 15$, from the present measurements. If F is extrapolated to $1000 \mu\text{a}/\text{cm}^2$, using (II), this product becomes 17.6. Charlesby gives a value of 17 for this product, but does not state the corresponding current density. Much of his work, however, was done at current densities in the range 500–1000

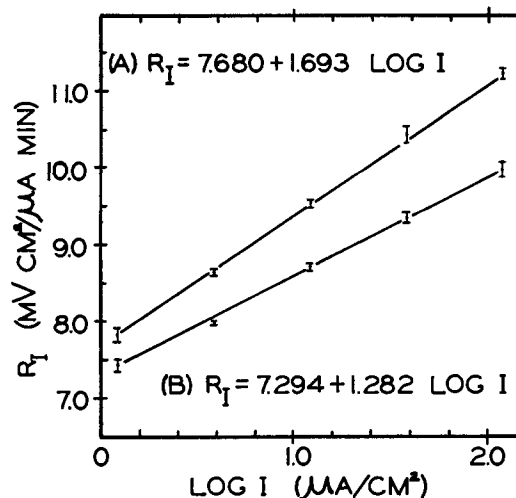


Fig. 3. Formation rate vs. log apparent current density for air-saturated solutions; (A) ammonium borate, 20.0°C; (B) sodium carbonate, 25.0°C.

TABLE II. Comparison of formation rates as calculated from equation (VI) or from equation (IX). Ammonium borate, 20.0°C

$I \mu\text{a}/\text{cm}^2$	$1/I \left(\frac{\partial E}{\partial t}\right)_I \frac{\text{mv cm}^2}{\mu\text{a min}}$	$1/I \left(\frac{\partial E}{\partial t}\right)_I \frac{\text{mv cm}^2}{\mu\text{a min}}$	% Difference
	Equation (VI)	Equation (IX)	
0.1	5.99*	6.64*	10.8
1	7.68	7.76	1.04
10	9.37	9.30	0.74
50	10.6	10.5	0.94
100	11.1	11.1	0.00
1000	15.7*	13.3*	15.3

* By extrapolation. Equation (VI) assumed valid.

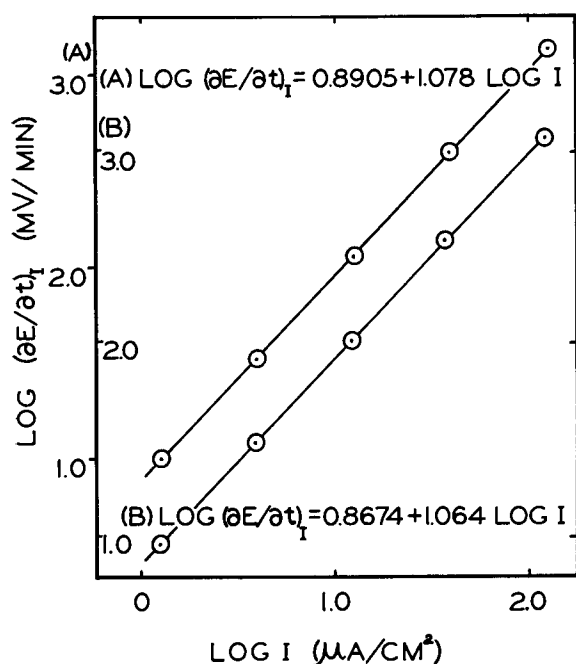


FIG. 4. Log rate vs. log apparent current density for air-saturated solutions: (A) ammonium borate, 20.0°C; (B) sodium carbonate, 25.0°C.

$\mu\text{a}/\text{cm}^2$. The agreement seems satisfactory, inasmuch as the comparison was made between zirconium specimens which differed somewhat in chemical composition.

Correlation with Previous Work

The empirical relation between rate of change of potential and current reported previously, namely,

$$\left(\frac{\partial E}{\partial t}\right)_I = AI^B \quad (\text{IX})$$

is a good approximation to equation (VI) over the range of current densities employed. This is shown in Table II. In Fig. 4, data used in constructing Fig. 3 are shown as log-log plots of the variables in (IX). The straight lines were drawn on the basis of the method of least squares. From these lines the empirical constants A and B have been evaluated.

A values of 7.77 and 7.37 mv/min and B values of 1.08 and 1.06 are obtained for ammonium borate and sodium carbonate solutions, respectively.

Equation (IX) is of a form which is directly applicable to the estimation of local currents from potential-time measurements in the manner outlined previously (1).

CHANGE IN POTENTIAL WITH CHANGE IN CURRENT AT CONSTANT FILM THICKNESS

Validity of the relationship expressed in (I) can be tested by another approach. Equation (III) may be written:

$$E' = X/B_+ \ln I + (X/B_+) \ln (1/\sigma A_+) + K \quad (\text{X})$$

For an experiment carried out at constant film thickness, a plot of the measured potential vs. the logarithm of the apparent current density should give a straight line. This experimental work was done, and the linearity of the plot of these variables is indicated by the straight lines of Fig. 5. Points such as those shown were obtained as follows.

After the freshly abraded zirconium electrode had been polarized at constant current density I_1 to give a value of $(\partial E/\partial t)_I$ which was constant with time, the current density was increased abruptly to another value I_2 by short circuiting a resistor in the polarizing circuit. The potential rose rapidly and passed through a maximum then a minimum value before settling down to another fixed rate of change with time. This behavior is shown in Fig. 6, where E'_1 is the value of the potential at time t_0 when the current density I_1 is suddenly increased to a value I_2 . E'_2 is the value of the potential as it passes through its minimum before attaining a new steady

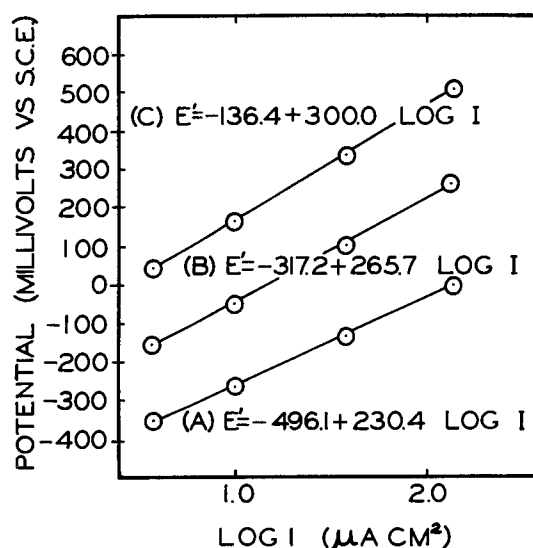


FIG. 5. Potential vs. log apparent current density at constant film thickness. Air-saturated ammonium borate solution, 20.0°C. (A) $\sigma X_a = 46 \text{ \AA}$; (B) $\sigma X_b = 53 \text{ \AA}$; (C) $\sigma X_c = 59 \text{ \AA}$.

rate. (If I_2 is large enough, the maximum and minimum merge to give only a momentary stop before the rate reaches its new value.) E'_1 corresponds to the potential drop across the film of thickness X_1 at current I_1 , and E'_2 corresponds to the potential drop across the same film of thickness X_1 at current I_2 (neglecting the small increase in film thickness occurring between the change in current and the new potential readings). Another run was begun with a freshly abraded electrode surface at a constant polarizing current density of value I_2 , and the potential was followed until it reached the value E'_2 . At that time the film again had reached the thickness X_1 ; the current density was increased abruptly to a new value I_3 with a potential value E'_3 which corresponded to the potential drop across the film necessary to pass current I_3 through the thickness X_1 . Again, starting with current density I_3 , and E'_3 being reached, the current was increased to I_4 and a value of E'_4 was determined, etc. When the above values of E'_1 , E'_2 ... are plotted against those of $\ln I_1$, $\ln I_2$..., a straight line should be obtained if (II) is correct.

This method has been tested experimentally in ammonium borate at 20.0°C and the results are shown in Fig. 5. Table III contains the data from which lines (A), (B), and (C), respectively, were constructed. Duplicate runs were generally found to be sufficient because of the good reproducibility.

The linearity indicated in (X) is thus experimentally established, giving further evidence for the validity of (I). Since the linearity indicated in (I) has already been verified by experiment, the linearity of the curves in Fig. 5 can be considered as a check on the experimental procedure just outlined, and it may be concluded that this procedure does, in fact, give potential increments corresponding to current increments at constant film thickness.

The most important conclusion from (X) is that the oxide film thickness should be given by

$$X = L(B_+) \quad (\text{XI})$$

where L is the slope of the line. From Fig. 5a an apparent film thickness σX_a of 45.7 Å is obtained. Referring to Table III, it is seen that this apparent oxide film thickness is that formed on a freshly abraded electrode anodized at 3.85 $\mu\text{a}/\text{cm}^2$ to a potential of -358 mv vs. the saturated calomel electrode. Similarly, from the slope of line (B) an apparent oxide film thickness of 52.7 Å is obtained, and it is seen that this apparent thickness is attained by anodizing a freshly abraded electrode to a potential of -159 mv at 3.85 $\mu\text{a}/\text{cm}^2$. The slope of line (C) gives an apparent thickness of 59.5 Å obtained by anodizing a freshly abraded electrode at 3.85 $\mu\text{a}/\text{cm}^2$ to a potential of 41 mv.

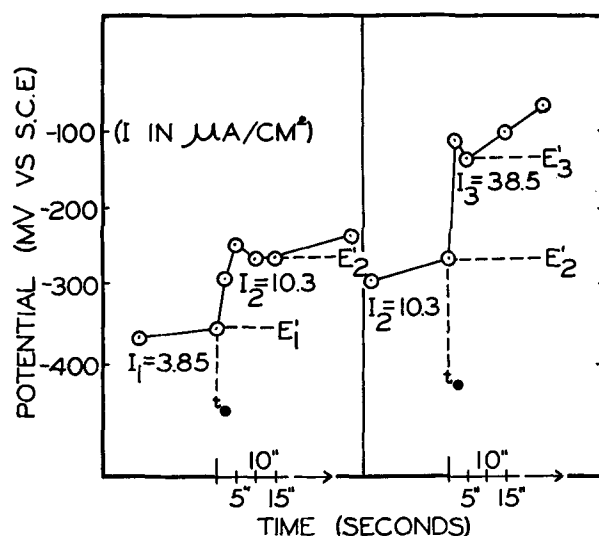


FIG. 6. Change in potential with change in current at constant film thickness. Air-saturated ammonium borate solution, 20.0°C.

TABLE III. Variation of potential with apparent current density at constant film thickness. Ammonium borate, 20.0°C

$\sigma X_a = 46 \text{ \AA}$		$\sigma X_b = 53 \text{ \AA}$		$\sigma X_c = 59 \text{ \AA}$	
Log $I / \mu\text{a}/\text{cm}^2$	E' mv vs. S.C.E.	Log $I / \mu\text{a}/\text{cm}^2$	E' mv vs. S.C.E.	Log $I / \mu\text{a}/\text{cm}^2$	E' mv vs. S.C.E.
0.585	-358	0.585	-159	0.585	41.0
1.015	-265	1.002	-52.5	1.002	164.0
1.585	-135	1.585	99	1.585	334.5
2.139	0	2.129	252	2.129	505.5

Thus, an increment in potential of 200 mv at 3.85 $\mu\text{a}/\text{cm}^2$ represents an increase of about 7 Å in apparent film thickness.

This increase in apparent thickness can be checked quantitatively. At 3.85 $\mu\text{a}/\text{cm}^2$ the unitary rate is 8.63 mv $\text{cm}^2/\mu\text{a min}$ (Table I); the time required for the potential to increase by 200 mv at this current density is $200/(3.85 \times 8.63) = 6.02$ min, or 23.2 $\mu\text{a min}$. This is equivalent to $23.2 \times 3.36 \times 10^{-9}$ cm or 7.7 Å in apparent thickness. This check is independent of the actual value of the roughness factor; the actual thickness is given by the ratio of the apparent thickness to the roughness factor.

It should be pointed out that each of the lines (A), (B), (C) of Fig. 5 is actually an anodic polarization curve at constant oxide film thickness. It is evident that the lines become steeper with increased film growth.

It is interesting to note that the ratio of the formation rates at two different current densities, I_1 and I_2 , is, from (I):

$$R_2/R_1 = \frac{r/\sigma B_+ \ln(I_2/\sigma A_+)}{r/\sigma B_+ \ln(I_1/\sigma A_+)} = \frac{\ln(I_2/\sigma A_+)}{\ln(I_1/\sigma A_+)}$$

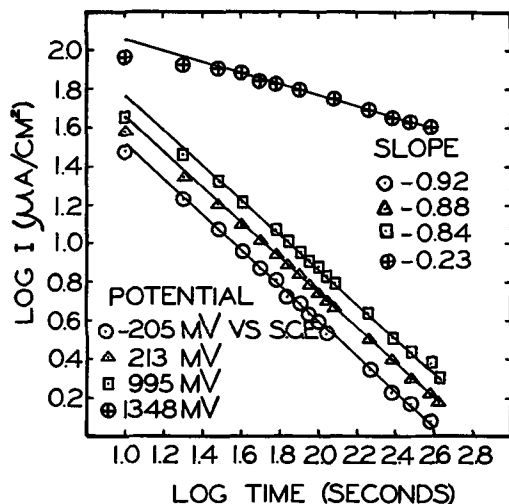


Fig. 7. Current decay at constant formation potential. Air-saturated ammonium borate solution, 20.0°C.

TABLE IV. Current decay at constant formation potential: slopes of the decay curves

E' mv vs. S.C.E.	$-d \log I/d \log t$	E' mv vs. S.C.E.	$-d \log I/d \log t$
-367	0.93	35	0.83
-320	0.86	120	0.87
-277	0.89	176	0.89
-264	0.92	213	0.88
-220	0.89	251	0.84
-220	0.83	313	0.89
-205	0.92	380	0.86
-204	0.89		
-172	0.90		
-20	0.90		

The ratio of the ordinates of lines (B) and (A) in Fig. 5 at the same current densities I_1 and I_2 is:

$$\frac{E_2' - E_2^a}{E_1' - E_1^a} = \frac{X_b - X_a}{X_b - X_a} \frac{1/B_+ \ln(I_2/\sigma A_+)}{1/B_+ \ln(I_1/\sigma A_+)} = \frac{\ln(I_2/\sigma A_+)}{\ln(I_1/\sigma A_+)} = R_2/R_1$$

Thus, an experimental verification of the equality of the first and last ratios should provide a check on the internal consistency of the two methods.

From line (A), Fig. 5

$$\frac{R_{\log t=0.5}}{R_{\log t=1.5}} = 0.834; \quad \frac{R_{\log t=1.0}}{R_{\log t=1.5}} = 0.916; \quad \frac{R_{\log t=2.0}}{R_{\log t=2.5}} = 1.083$$

and from the three lines in Fig. 5, taking the average value of the vertical distance between lines, (since $X_b - X_a \cong X_c - X_b$)

$$\frac{\Delta(E')_{\log t=0.5}}{\Delta(E')_{\log t=1.5}} = 0.834; \quad \frac{\Delta(E')_{\log t=1.0}}{\Delta(E')_{\log t=1.5}} = 0.925;$$

$$\frac{\Delta(E')_{\log t=2.0}}{\Delta(E')_{\log t=1.5}} = 1.075$$

The difference is within 1-2% error in the determination of formation rates.

This agreement serves as a check on the validity of the experimental procedure used in constructing Fig. 5, especially in the selection of the minimal values of the increased potential resulting from abrupt increases in polarizing current (E_2' , E_3' as sketched in Fig. 6).

CURRENT DECAY AT CONSTANT FORMATION POTENTIAL

A third test of equation (I) can be obtained from current decay measurements at constant formation potential in the low potential range.

Charlesby (2) has shown that, for an ion current decaying through a growing oxide film at constant formation potential according to the Mott relationship, (I), a plot of the logarithm of the current density vs. the logarithm of the time should be linear, with a slope determined by the value of the B_+F product for the film formation process. He gives values of -0.87 and -0.90 for this theoretical slope for B_+F ranges of 10-15, and 15-20, respectively.

A B_+F value of 15 was obtained for abraded zirconium specimens in the low potential range from the work reported above on formation rates at constant current. This value is for an apparent current density of 100 $\mu\text{a}/\text{cm}^2$ in dilute ammonium borate solution at 20.0°C.

In Fig. 7 typical curves of current decay at constant formation potential are shown. These were obtained using abraded zirconium in dilute ammonium borate solution at 20.0°C. The curves shown are for a single specimen electrode for which four consecutive current decay experiments were carried out at constant formation potentials. These formation potentials became progressively more positive from one run to another as the oxide film thickness increased.

It was noted that for each series of runs like that shown in Fig. 7 a definite trend of decreasing slope with increasing formation potential usually occurred. In Table IV the values of the slope obtained from 17 individual curves are tabulated with the value of the corresponding formation potential. Only runs with formation potentials definitely below that for oxygen evolution (600 mv vs. S.C.E.) have been included. The mean value of the slopes obtained for all 17 runs over the formation potential range -367 to 380 mv vs. S.C.E. is -0.88 ± 0.01 . For proper comparison with the B_+F value obtained from formation rates at constant current, only those slopes obtained from runs with formation potentials near -200 mv vs. S.C.E. should be taken, since all

formation rates were tabulated at this potential. The mean value of the slopes for the 7 runs over the formation potential range -277 to -172 mv vs. S.C.E. is -0.89 ± 0.01 . This value of $d \log I/d \log t$ corresponds to a theoretical B_+F value of 15. This checks with the value of 15 determined from the formation rate experiments at constant current, and again confirms the validity of equation (I) in the low potential range.

CURRENT EFFICIENCY OF OXIDE FORMATION IN THE LOW POTENTIAL RANGE

The agreement with Charlesby's work is based entirely on the assumption of unit current efficiency for oxide formation below the potentials for oxygen evolution. The fact that agreement was obtained is a point in favor of this assumption; another is the fact that the only reaction thermodynamically possible below the reversible potential for oxygen evolution is the oxidation of zirconium. Also, when the potential-time measurements are being taken, the constant rate drops abruptly soon after the reversible potential for oxygen evolution is reached, indicating that a second reaction is then starting (Fig. 2). Further evidence for unit efficiency in the low potential range accrues from formation rate measurements which have been obtained for the steep branch of the potential-time curve above 2 v, where oxide film formation and oxygen evolution occur simultaneously. It has been found that the concentration of oxygen in the solution affects the formation rate very noticeably. Thus, in borate solution at 20.0°C , increasing the oxygen concentration from its value in a nitrogen-saturated solution to that in an oxygen-saturated solution causes an increase in the formation rate of some 20%. This is in the direction to be expected for an oxygen electrode. However, when the same experiment was repeated in the low potential range, no difference in rate was observed between a nitrogen-saturated and an oxygen-saturated solution. This result would be expected if the current efficiency for oxide formation were, in fact, unity in the low potential range.

The agreement obtained in the work on current decay at constant formation potential reported above provides strong support for the assumption of unit current efficiency in the low potential range. An electron current which decayed at the same rate as the ion current would not manifest itself in a decreased value of $d \log I/d \log t$, but it is evident from Fig. 7 that the electron current involved in the oxygen evolution process decays much more slowly than the ion current. Thus, the assumption of unit

current efficiency in the region of -200 mv vs. S.C.E. would seem to be fully substantiated.

DISCUSSION

From Fig. 1 and Table I it is evident that the values of A_+ , B_+ , and F for ammonium borate are significantly different from the corresponding values for sodium carbonate solution. The inequality is larger than can be accounted for by the five degree temperature difference between the two sets of measurements. This inequality must be due mainly to specific effects of the electrolytes themselves. Any such effect should manifest itself at the oxide-solution interphase.

A tentative explanation might lie in the ability of small pores, located in the thin oxide film, to reduce the effective electrostatic field across the film. It is known that the concentration and size of such pores depend on the type of electrolyte in which the oxide film is formed (9).

Alteration of the field in this way would result in different values of A_+ and B_+ . Since A_+ is related exponentially to the field, a small change in F would cause an order-of-magnitude change in A_+ .

It should be mentioned that this experimental work has been interpreted on the assumption that the increase in potential of the electrode from initial immersion to the oxygen evolution potential results from the growth of a true oxide film. The agreement obtained with the work on visible oxide films, carried out in the high potential range, would support this view.

EXPERIMENTAL

Polarizing circuit and cell.—This apparatus has been described previously (1).

Preparation of metal electrodes.—Coupons were cut from 0.070-in. zirconium sheet in the shape of square electrodes with extensions for electrical connections. These were completely covered with an impervious baked coating of enamel. The enamel was then ground away from one face of the electrode to leave a projected area of 2.6 cm^2 . Prior to each run the exposed face of the electrode was abraded with 0, 2/0, and 3/0 emery cloth, using a standardized procedure.

Analysis of electrode specimens.—This work was done on a sample of hafnium-free zirconium prepared by the Kroll process, designated by the code number WA-3983. It was 10–20% cold worked with a Rockwell B hardness of 68–81. It had the following analysis (in ppm):⁷

⁷ The authors appreciate the cooperation of Dr. Earl T. Hayes, Chief, Physical Metallurgy Branch, Bureau of Mines, Albany, Oregon, in supplying them with this analysis.

Al	20	Cu	50	Ni	20	V	50
B	0.3	Fe	600*	O ₂	1650*	Zn	< 50
C	370*	Mg	10	Pb	30	Hf (esti- mated)	< 300
Cd	0.5	Mn	10	Si	100		
Co	< 10	Mo	10	Sn	500*		
Cr	< 5	N ₂	70*	Ti	50		

* Values marked with an asterisk were determined chemically; the others were determined spectroscopically.

Solutions.—All solutions were made up from A.R. salts and distilled water. The ammonium borate solution was prepared by saturating distilled water with boric acid at 20.0°C. Ammonia gas was bubbled through the solution until the pH reached a value of 8.0.

All results reported here were obtained with air-saturated solutions, unless otherwise stated.

Potential-time measurements at constant current.—Runs always were begun within 3 min after completion of the abrasion operation. All potentials were measured against the saturated calomel electrode. Polarizing current was maintained constant by manual control. Measurements of current, potential, and time, as well as current control, were all carried out with an accuracy of 1% or better. The range of current densities employed was from 1 to 100 $\mu\text{a}/\text{cm}^2$, and the potential ranged from -1200 to $+600$ mv.

During anodization, potentials were recorded at given time intervals and the formation rates calculated. Results for a single run are shown in Fig. 2, where it is seen that, after a period of decreasing rate corresponding to the decreasing local current, there is a constant rate period which terminates when potentials are reached for which a second reaction, the oxidation of hydroxide ion, is possible. The rate then decreases because the current efficiency for the film-building process is no longer unity. In order to avoid including portions of the first and last branch of this curve in the constant rate, the two values nearest -200 mv were averaged to give the formation rate to be used in equation (VI). The scatter in the five individual runs taken at each current density is higher than would be expected from the accuracy in the basic measurements. This scatter is probably due to differences which exist in the abraded electrode surfaces in one run compared to another.⁸ However, with five individual runs taken per point the probable error is reduced to a value of 1–2%.

⁸ Recent experiments have been carried out which indicate that increased precision can be obtained by pre-anodizing specimen electrodes at a current density of $0.1 \mu\text{a}/\text{cm}^2$ for about 12 hr, until each specimen has attained the same starting potential before a run is begun.

Potential Measurements at Constant Film Thickness

The general procedure has been discussed above. It should be added, however, that large current increments at constant film thickness give potentials which fall low, compared to those obtained with smaller increments. Thus, it was found that, for a current range of 10–316 μa , steps of 10–31.6, 31.6–100, and 100–316 μa gave points which fell on the same straight line. When this current range was divided into four, five, or six increments, the resulting points all fell on the same straight line as that obtained with three increments. However, if this range was divided into one or only two steps, the resulting points fell low. A safe change of current density was found to be one for which $\Delta \log I \cong 0.5$.

Current Decay Measurements at Constant Formation Potential

Zirconium electrode specimens were freshly abraded, and the 2.6 cm^2 exposed surface was masked down to a circular area of 1.0 cm^2 by partially covering the surface with a beeswax-rosin mixture.

Direct current was obtained from a battery-operated, low-power voltage regulator. Formation potentials were maintained constant to within ± 10 mv by the voltage regulator as the anodic current decayed from 100 through 1 μa . By manually controlling the grid potential of the voltage regulating tube, these formation potentials were maintained constant to within ± 3 mv.

Current was measured with a Weston milliammeter Model 622, over a range of 1–100 μa . The potential was measured vs. S.C.E. with a Beckman Model M pH meter in series with a student potentiometer. The temperature of the electrolyte was maintained constant at $20.0^\circ \pm 0.1^\circ\text{C}$ with a constant temperature bath.

Current decay runs were made by immersing the freshly abraded and masked electrode specimen in the dilute ammonium borate solution contained in the polarization cell. The polarization circuit was then closed, and the potential was increased until a current somewhat larger than 100 μa registered on the milliammeter. The potential was maintained constant by one operator while a second observer recorded the current. Zero time was taken as the instant the current decayed through 100 μa . After the current had decayed through 1 μa , a second run was begun by again increasing the potential until a current somewhat larger than 100 μa was obtained; the formation potential was then maintained constant at the new value as the second set of current decay measurements was taken.

SUMMARY

On the assumption that the time-linear potential increase observed when an abraded zirconium electrode is anodically polarized to oxygen evolution results from the growth of an oxide film, it is shown experimentally that in the range of low formation potentials ion current through the film varies exponentially with the formation field, $I_+ = A_+ \exp(B_+F)$. This well-established relationship for describing growth of anodic oxide films in the range of high formation potentials has now been extended to the low formation potential range.

From anodic potential-time measurements, taken below oxygen evolution potentials, formation rates at constant current, formation field, electrolytic parameters, A_+ and B_+ , and thicknesses of very thin anodic oxide films have been evaluated.

Results so obtained are compared with those of other work for thicker oxide films formed in the high potential range and are found to be in agreement. Correlation is established between these results and previously reported work on estimation of local currents from anodic polarization measurements.

Experimental verification of the relationship between ion current and formation field in the potential range below oxygen evolution was carried out along three lines: (a) evaluation of formation rates from potential-time measurements at constant current; (b) measurement of the change of formation potential with change of current at constant film

thickness; (c) measurement of the decay of ion current at constant formation potential.

Results obtained in these experiments were shown to be internally consistent.

Evidence is presented to substantiate the working assumption of unit current efficiency for the oxide-film-building process below oxygen evolution potentials.

ACKNOWLEDGMENT

The work reported in the present paper is part of a research program carried out at the University of Oregon under a contract with the U. S. Atomic Energy Commission.

Any discussion of this paper will appear in a Discussion Section to be published in the June 1956 JOURNAL.

REFERENCES

1. M. MARAGHINI, G. B. ADAMS, JR., AND P. VAN RYSSELBERGHE, *This Journal*, **101**, 400 (1954); Technical Report to the U. S. Atomic Energy Commission AECU-2797, September, 1953.
2. A. CHARLESBY, *Acta Met.*, **1**, 340 (1953); Atomic Energy Research Establishment, Harwell, Report M/R-1014, September, 1952.
3. A. GÜNTHERSCHULZE AND H. BETZ, *Z. Elektrochem.*, **37**, 726 (1931).
4. N. F. MOTT, *Trans. Faraday Soc.*, **43**, 429 (1947).
5. J. F. DEWALD, *This Journal*, **102**, 1 (1955).
6. D. A. VERMLYEA, *Acta Met.*, **1**, 282 (1952).
7. N. CABBERA AND N. F. MOTT, *Repts. Prog. Phys.*, **12**, 163 (1948-49).
8. L. YOUNG, *Trans. Faraday Soc.*, **50**, 153 (1954).
9. F. KELLER, M. S. HUNTER, AND D. L. ROBINSON, *This Journal*, **100**, 411 (1953).

Two Photoelectric Colorimeters for Television Picture Tubes^{1, 2}

RICHARD S. HUNTER

Hunter Associates Laboratory, Falls Church, Virginia

ABSTRACT

Two photoelectric tristimulus instruments for the colors of television picture tubes, fluorescent lamps, and the phosphors used in them are described. One uses a single photocell and three filters on a disk. The photocell currents corresponding to each of the three filters are converted by equations or nomographs to values of color. The second makes use of three photocells, each with different filters. The currents from these photocells are measured with a special current-balancing bridge which gives direct readings of luminance and chromaticity. A new reversed-signal circuit has been devised for improved sensitivity and precision.

INTRODUCTION

Television picture tubes fall in the category of extended-area light sources, the colors of which are specified by luminance and chromaticity. Luminance is luminous (visual) intensity, or projected light flux per unit of projected area; for television picture tubes it is commonly expressed in footlamberts. Chromaticity is a two-dimensional measure of the nonintensity attributes of color. Its customary dimensions, x and y , are the respective fractions of two of the tristimulus values in the total of three X , Y , and Z , which may be derived by integration from the spectral distribution of any specimen (1).

Fig. 1 is an x, y diagram on which the chromaticities of all colors may be located within the roughly triangular locus of spectrum colors. As is well known, near whites plot in the central area of this diagram, while saturated colors plot near the spectrum locus, each in a direction from the center corresponding to that of the wave length which it most resembles.

The instruments described are intended primarily for monochrome picture tubes. However, there appears to be no reason why they cannot also be used to measure the colors of color-television picture tubes and the phosphors used in them. A color-standard box with incandescent lamp, diffusing screen, and slot for color filters has been built to facilitate color measurements. This box is shown in Fig. 2.

Fig. 3 and 4 are diagrams of the two colorimeters.

¹ Manuscript received December 18, 1954. This paper was prepared for delivery before the Chicago Meeting, May 2 to 6, 1954.

² These instruments were developed at the suggestion of the Joint Electron Tube Engineering Council Subcommittee 6.3.

Fig. 5 is a photograph of the instrument diagrammed in Fig. 4. The exposure unit which receives the signal consists in each case of a stand supporting photocell or cells and filters and an aluminum housing 10 x 10 x 15 in. long. In the front of this box is a 12 cm round window where the television tube or other specimen is presented for measurement. Dotted lines in Fig. 4 show the positions of reflecting or transmitting specimens and the sealed-beam, reflector-type lamps which may be used to illuminate them. Also shown in dotted lines is the position of a daylight filter, D , which may be used to convert the incandescent-illuminant colors of objects to their daylight colors.

PHOTOELECTRIC TRISTIMULUS COLORIMETRY

The use of filters with barrier-layer photocells for photoelectric tristimulus measurements of color has been developed by Barnes (2), Hunter (3), and others. Filters are designed for barrier-layer photocells that will give these cells spectral relative responses nearly duplicating those of the CIE standard observer for colorimetry (1). The four tristimulus filters used in the present instruments are like those described by Barnes (2) and were designed by the Corning Glass Works.

In Fig. 6, the CIE \bar{x} , \bar{y} , and \bar{z} distribution functions are compared with spectral responses of the filter-photocell combinations used in the present apparatus. The filter-photocell curves have been adjusted so that the areas under them are the same as those under the corresponding CIE functions. The \bar{z} -blue filter consists of three components: the usual blue and Noviol components, and a third blue-green element to absorb the far red. The other three filters consist of two components each, one absorbing the short-wave side, and one the long-wave side of the

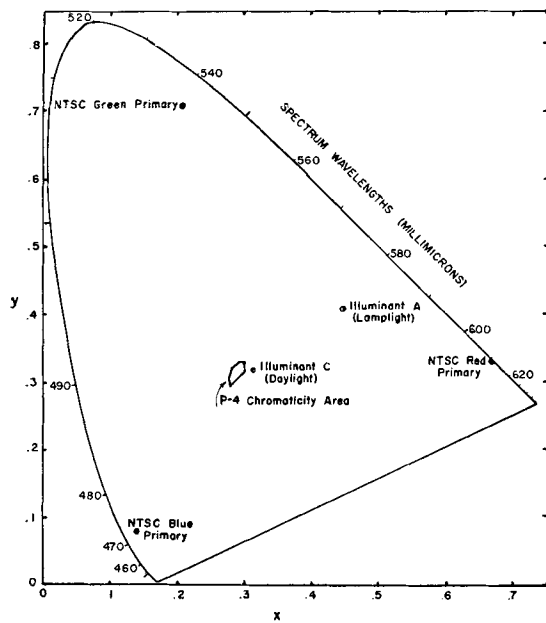


FIG. 1. CIE x, y chromaticity diagram with boundary of spectrum colors, standard illuminants C (daylight) and A (lamp light), area recommended by JETEC for P4 television picture tubes, and the NTSC red, green, and blue primaries.

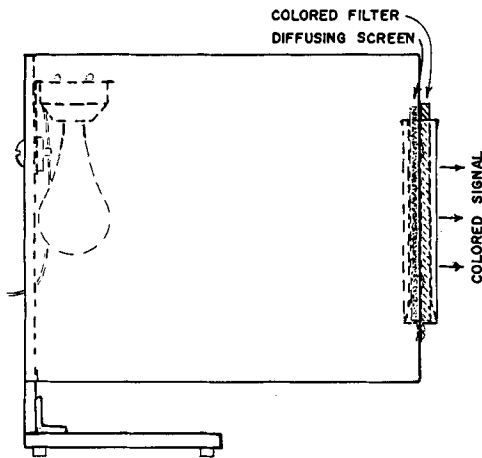


FIG. 2. Diagram of color-standard box with incandescent lamp, diffusing screen, and colored filter in slot.

spectral band passed by the filter. As will be shown below, the fourth \bar{x} -blue filter is used for only one of the two models of the new apparatus; thus there are two blue ends of the \bar{x} -filter-photocell function in Fig. 6, one for the four-filter set and the other for the three-filter set which used the \bar{z} -blue filter for the blue hump of the \bar{x} curve as well as for the \bar{z} curve.

Successful photoelectric tristimulus colorimetry requires standards similar to the specimens to be measured in both color and spectral distribution of energy. Hunter (3) showed that, on the average, a series of values of chromaticity measured by a

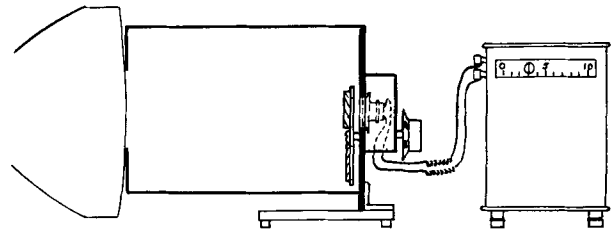


FIG. 3. Diagram of one-photocell, filter-disk colorimeter for television picture tubes.

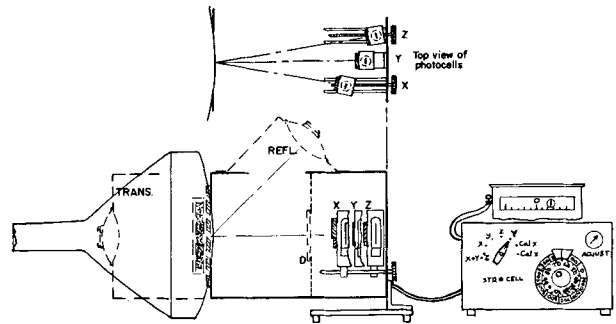


FIG. 4. Diagram of three-photocell, direct-reading colorimeter for television picture tubes, fluorescent lamps, and nonluminous objects. In dotted lines are shown the positions of reflecting and transmitting specimens, the sealed-beam lamps which may be used to illuminate them, and a daylight filter (D) which may be used to convert the incandescent-illuminant colors of objects to their daylight colors.

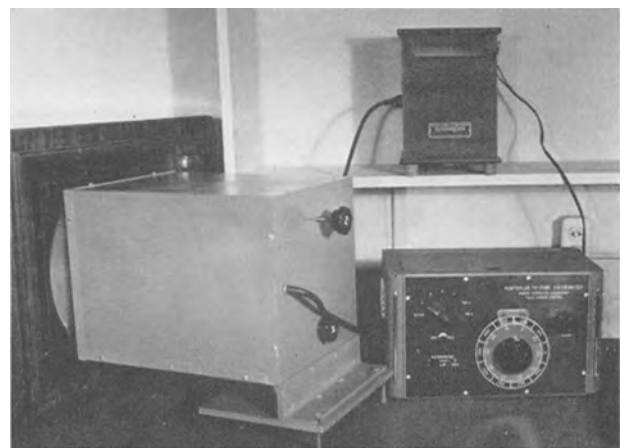


FIG. 5. Photograph of three-photocell, direct-reading colorimeter with exposure unit facing television tube at left, measurement unit at right, and galvanometer on shelf above.

photoelectric tristimulus instrument contains errors which are roughly 10% of the chromaticity differences between the specimens and the standard used. The source of this error is the failure of the source-filter-photocell combinations to duplicate spectrally the CIE functions (see Fig. 6). Fig. 7 shows examples of these errors by the present instru-

ment by illustrating the shifts from standard values (computed from spectrophotometric data) to values observed with the three-cell instrument. For color by reflection in daylight, the lamp (REFL.) and filter (D) shown in Fig. 4 were used.

Because these errors are spectral in origin, standards used for photoelectric tristimulus colorimetry must be similar in spectral distribution as well as in color to the specimens to be measured. In Fig. 8, the spectral distribution of a typical P4 phosphor is compared with that of the Illuminant C lamp and filter combination frequently used as standard. It was shown in Fig. 1 that these two are close in

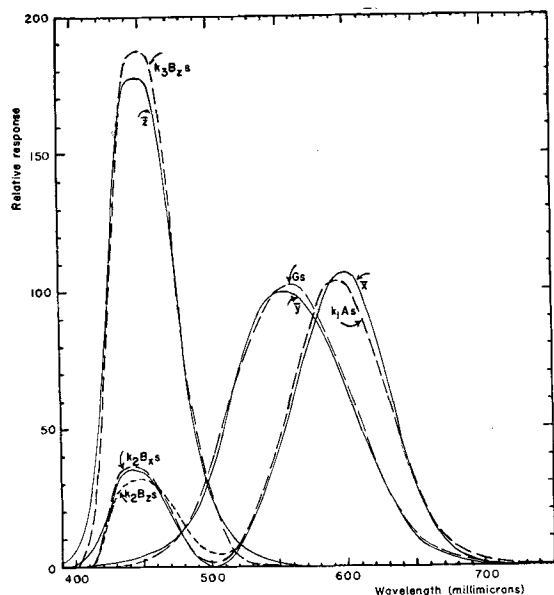


FIG. 6. Intercomparison of CIE \bar{x} , \bar{y} , and \bar{z} (solid lines) and the filter-photocell combinations designed to duplicate them (dashed lines). The dotted line, k_2B_{2s} shows the inferior duplication of the blue end of the \bar{x} curve obtained when the z -blue filter is used instead of the 4th x -blue filter.

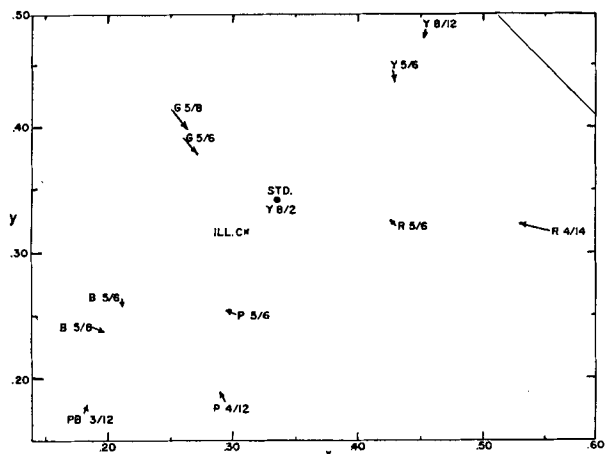


FIG. 7. Errors in measurements of Munsell colors for daylight. Munsell paper Y 8/2 was used as standard.

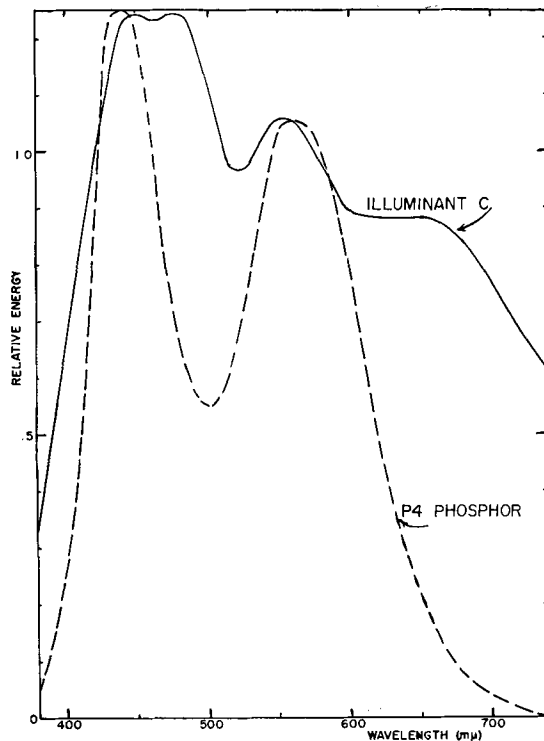


FIG. 8. Spectral distributions of CIE illuminant C and P4 phosphor which were shown in Fig. 1 to have nearly the same chromaticity.

chromaticity, but Fig. 8 shows them to be different spectrally. Because most monochrome phosphors differ spectrally from the standards regularly used for colorimetry, arrangements have been made for the calibration of monochrome television picture tubes as standards.³

FILTER-DISK MODEL

The simpler instrument shown in Fig. 3 is like one used by Martin, Noland, and Vogel (4), except that addition of the sheet-metal housing permits operation in a partially lighted room and readings of luminance as well as x and y . The hermetically sealed photocell (5), which has a sensitive area 2 in. in diameter, is behind a disk on which the filters are mounted. Signals from this photocell are measured by deflections of a spotlight galvanometer. There are four positions on the filter disk. One blocks all light from the photocell so that the galvanometer scale can be adjusted for zero deflection. The other three carry green, amber, and blue filters, respectively.

Measurements are made of a picture tube operating from a stabilized power supply at full-size raster with no picture information. The 12 cm window of

³ The Joint Electron Tube Engineering Council Cathode Ray Tube Committee (JTC-6) has arranged for this to be done by the RCA Industry Service Laboratories, Newark, N. J.

the photoelectric instrument is centered against the face of the picture tube. Its luminance is brought to at least 20 footlamberts as indicated by the green-filter deflection of the galvanometer.

After a suitable warm-up, deflections are read with each of the three filters. Luminance and chromaticity are derived by the use of four constants whose values are found by a calibrating procedure described in the following paragraphs. If G , A , and B are the deflections with the green, amber, and blue filters, respectively, then one may write:

$$\begin{aligned} \text{Luminance} &= k_L G \\ x &= \frac{k_1 A + k_2 B}{k_1 A + G + (k_2 + k_3) B} \\ y &= \frac{G}{k_1 A + G + (k_2 + k_3) B} \end{aligned}$$

The constants k_1 , k_2 , k_3 are required to adjust the filter-photocell responses A and B to the right magnitudes for combining with the response G in the computation of chromaticity. The adjusted X -response has the component $k_1 A$ corresponding to the long-wave-length portion of the \bar{x} curve in Fig. 6, and the component $k_2 B$ corresponding to the short wave-length portion. The Z -response is represented by $k_3 B$.

To calibrate a filter-disk instrument and find its values of k for a given type of specimen, one requires a standard spectrally similar to the specimens with known values of luminance (Y) and chromaticity (x, y, z). If, as before, G , A , and B are galvanometer deflections with the green, amber, and blue filters, respectively, this time for the standard, the k_1 for luminance and the k_3 constant to convert blue-filter signal are computed simply:

$$\begin{aligned} k_L &= \frac{\text{Lum}}{G} \\ k_3 &= \frac{G}{y} \cdot \frac{z}{B} \end{aligned}$$

The selection of constants for x is complicated by the fact that the \bar{x} function consists of blue and amber components, which are not reported as separate values in the calibration of the standard. Two methods are available for obtaining values of k_1 and k_2 for the amber and blue components, respectively. The simpler one makes use of the fact that the area under the blue hump of the \bar{x} curve in Fig. 1 is 0.167 of the area under the \bar{z} curve. From this fact, one may divide the x value of the standard into two parts:

$$\begin{aligned} x_b &= 0.167z \\ x_a &= x - 0.167z \end{aligned}$$

It is a simple matter to compute from the foregoing and the galvanometer deflections, G , A , and B of

the standard

$$\begin{aligned} k_1 &= \frac{G}{y} \cdot \frac{x_a}{A} \\ k_2 &= 0.167 k_3 \end{aligned}$$

The second method of computing these two constants requires two calibrated standards different in color to provide, in effect, simultaneous equations to solve for the two unknowns k_1 and k_2 .

$$\begin{aligned} k_1 &= \frac{x_1 f_1 B_2 - x_2 f_2 B_1}{A_1 B_2 - A_2 B_1} \\ k_2 &= \frac{x_2 f_2 A_1 - x_1 f_1 A_2}{A_1 B_2 - A_2 B_1} \end{aligned}$$

where f is the fraction G/y , and subscripts 1 and 2 refer to standard tubes 1 and 2, respectively.

The two methods of computing these two constants do not in general give the same values. Thus, in one experiment using two standardized P4 television picture tubes (Nos. 1 and 4), the two methods gave:

		k_1	k_2	k_3
By direct method	Std. 1	1.151	0.297	1.78
	Std. 4	1.191	0.307	1.83
Average		1.171	0.302	1.805
By simultaneous equations		1.009	0.433	—

Fig. 9 shows the effect of these differences on actual computed values of chromaticity. Even though tubes 1 and 4 were used as standards for the simultaneous-equation values of k_1 and k_2 , the observed values of chromaticity for these two tubes do not accord with those assigned because k_3 differed from one standard to the other and the average was used for k_3 .

Fig. 9 presents evidence of the accuracy of the filter-disk colorimeter used on television picture tubes. Assuming one of the standards had been used for the color measurement of the other, the chromaticity error would have been approximately the sum of the two distances between standard and measured values shown on the graph. This sum is roughly 0.007 for the separate-constants values and 0.005 for the equations-constants values. This suggests that the latter may be superior. The direct reading colorimeter gave an error of 0.005 when used to measure one of these standards after adjustment with the other.

Unfortunately, the filters used in these colorimeters when the foregoing values were obtained are not the best ones which are represented by filter-photocell curves in Fig. 6. The anticipated improvement in accuracy is less than a factor of two. Thus the better filters will not eliminate susceptibility of the instrument to appreciable errors when standards and specimens are spectrally different. Some further improvement may be possible by selecting photocells, but for substantial improvement in accuracy,

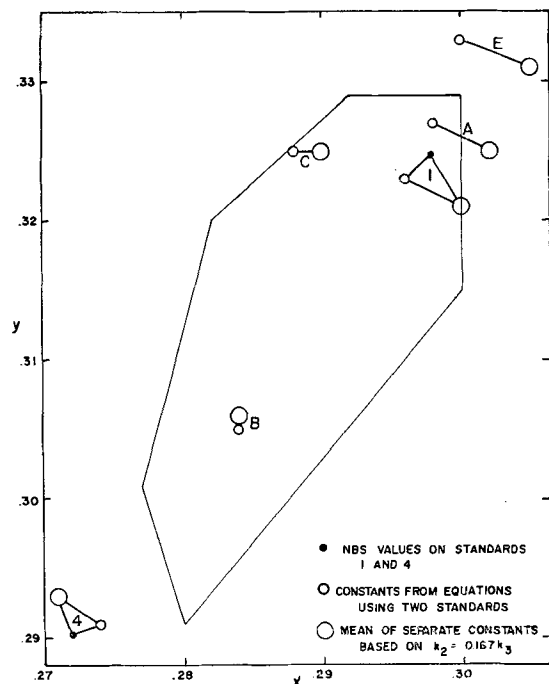


FIG. 9. Enlargement of the P4 area of the chromaticity diagram with values computed from readings with the filter-disk model using separate sets of the constants K_1 and K_2 .

additional or improved filter components will have to be developed.

THREE-CELL MODEL

The second instrument, shown by diagram in Fig. 4 and photograph in Fig. 5, is similar to the device described by Barnes (6). It uses a separate photocell for each of the three tristimulus functions. In the new device, the distances from the X and Z photocells to the viewing window are adjustable by screws through the back so that in calibrating the instrument these signals may be made proportional to the actual color values of the standard; thus, the k 's used with the first model are mechanically adjusted to unity in the second one. Color values for the specimens may then be read directly from the instrument scale. It should be noted that the filter over the X photocell has two parts, one blue and one amber. The areas of each are approximately proportional to the blue and amber components of the \bar{x} distribution function in Fig. 6.

As shown in Fig. 4 and 5, color values from this second instrument are read from the dial of a ten-turn potentiometer. This potentiometer adjusts the current from a 1.5-v No. 6 dry cell to that required to balance each photocell current subject to measurement. Condition of balance is indicated by zero deflection of a galvanometer or other suitable null indicator. The current-balancing circuit provides ideal "zero potential" conditions for operation of the

photocells, yet a sensitive high-resistance galvanometer or null indicator may be used.

In operating this instrument, all settings are made by placing the galvanometer spot at zero. At Y switch position, luminance (brightness) is read (standard cell maintains calibration); at $X + Y + Z$ switch position, the adjusting knob is turned for balance; then at x , y , and z switch positions, chromaticity is read directly from the dial.

The reversed-signal measuring circuit used to give values of chromaticity is more elaborate than the Barnes circuit previously used for the purpose. Instead of adjusting $X + Y + Z$ to 1.00 then measuring the separate X , Y , and Z currents one at a time, as with the Barnes circuit, the new instrument adjusts $X + Y + Z$ to 0.5 scale units, then for each component reverses the polarities of the other two components and reads the increment in scale units from the middle of the scale. Quantities actually measured by the new instrument are:

$$x = \frac{1}{2} \left[1 - \frac{-X + Y + Z}{X + Y + Z} \right]$$

$$y = \frac{1}{2} \left[1 - \frac{X - Y + Z}{X + Y + Z} \right]$$

$$z = \frac{1}{2} \left[1 - \frac{X + Y - Z}{X + Y + Z} \right]$$

Advantages of this reversed-current technique are:

1. The signal change obtained by reversing each component in the total signal is double that of the component itself; thus, sensitivity to interval differences is doubled.

2. Because differences between the chromaticity components are being measured, rather than the components themselves, fluctuations in total intensity to factors like voltage fluctuation in television tube power supply are minimized in the resultant observations.

The photocells are the hermetically sealed version of the very stable and widely used General Electric rectangular cell (5). Each filter is mounted on an aluminum coil can which is placed over the tubular glass photocell after a window of the proper size is cut in it. Because the three photocells lie in different directions from the specimen, it is important that light being measured be well diffused about the axis of the instrument, or nonuniform light distribution will be erroneously measured as color.

The problem of k_1 and k_2 constants is less serious with the three-cell model because it uses a separate blue filter designed specifically to fit the blue hump of the \bar{x} function. The relative magnitudes of these constants are in effect adjusted during assembly of the instrument by the setting of relative areas of amber and blue filters over the x photocell. Settings

on yellow and blue standards of known x value are used to make this adjustment.

Because all three signals are present during reversed-signal readings of x , y , and z , it is necessary to provide separate switch contacts for adjustments of the individual x , y , and z signals. The Cal X and Cal Z positions on the scale-selector switch shown in Fig. 4 are used only for calibration. At these positions, the X and Z signals are presented individually, and positions of the corresponding photocells are adjusted to standard, using screws that project through the back of the instrument. Where values of x and z alone are available for a standard, X and Z are computed:

$$\frac{X}{x} = \frac{Z}{z} = \frac{Y(\text{Lum})}{y}$$

SUMMARY

Compared with other instruments used for the same purpose, those described in the foregoing article have a number of advantages:

1. They are rapid and precise. During observation of seven picture tubes, the average difference between pairs of readings of chromaticity of the same tube was 0.001 with both models.

2. A separate meter is not required to read luminance.

3. A dark room is not required.

4. The instruments employ hermetically sealed photocells which are not subject to the changes in response with humidity that are characteristic of other barrier-layer photocells.

5. Both instruments may be used to measure the colors of reflecting surfaces and transmitting films and volumes as well as illuminant colors.

In addition to the foregoing advantages of both

instruments, several noteworthy features of the three-cell, reversed-signal model may be noted:

1. Values of chromaticity and luminance are read directly.

2. Errors from instability in television tube power supply are halved, the signal increment available for measurement is doubled by the reversed-signal technique.

3. The instrument uses a current-balancing circuit which gives high signal sensitivity, and, at the same time, the highly desirable condition of zero effective external resistance for the photocells.

4. With a frequency-insensitive electronic null indicator, the reversed-signal model may be operated in areas of severe vibration where conventional galvanometers will not work.

The major weakness of the new instruments is common to all photoelectric tristimulus colorimeters. Failure of the filter-photocell combinations spectrally to duplicate the functions of the CIE standard observer for colorimetry limits accurate color measurements to intercomparisons of samples and standards that are spectrally similar.

Any discussion of this paper will appear in a Discussion Section to be published in the June 1956 JOURNAL.

REFERENCES

1. Nat. Bur. Stds. Circular C 478, *Colorimetry* (1950); "The Science of Color," Optical Soc. of America, Crowell, New York (1953).
2. B. T. BARNES. *J. Opt. Soc. Amer.*, **29**, 440 (1939).
3. R. S. HUNTER. Nat. Bur. Stds. Circular C429 (1942); *J. Opt. Soc. Amer.*, **32**, 509 (1942).
4. A. E. MARTIN, J. A. NOLAND, AND R. Q. VOGEL, *ibid.*, **43**, 335 (1953).
5. General Electric Co. Catalog GEC-690, Photovoltaic Cell Types PV-1, PV-2, PV-10 (1950).
6. B. T. BARNES, *Rev. Sci. Instr.*, **16**, 337 (1945).

Oxidation States of Europium in the Alkaline Earth Oxide and Sulfide Phosphors¹

P. M. JAFFE² AND E. BANKS

Department of Chemistry, Polytechnic Institute of Brooklyn, Brooklyn, New York

ABSTRACT

Emission and absorption spectra of the alkaline earth sulfides activated with europium and fired in a neutral atmosphere have been re-investigated. The emission and absorption spectra of the alkaline earth oxides, also activated with Eu, and fired in a neutral or a reducing atmosphere have been obtained. The sulfides show both band emission and band absorption, as does SrO fired in hydrogen. The other hydrogen-fired oxides have band absorption, except for MgO, and give either mixed band and line emission or only line emission. The nitrogen-fired oxides, except MgO, give line emission and little, if any, selective absorption. MgO emits a broad line spectrum for both the nitrogen- and hydrogen-fired samples and shows no absorption peaks. Emission and absorption spectra have been correlated with the oxidation state of the activator in the several phosphors, the line emissions being associated with the presence of Eu⁺³ and the band emissions with Eu⁺².

INTRODUCTION

It is well known that alkaline earth sulfide phosphors containing europium as the activator show band emission (1-7). It is also known that europium-activated alkaline earth oxides show line emission (5, 6, 8, 9). This difference in emission character has been ascribed to a difference in the oxidation state of europium, which is divalent in the sulfides (10) and trivalent in the oxides. From a comparison of the energy required for inclusion of Eu⁺³ and the formation of lattice defects with the energy required for the reduction of Eu⁺³ to Eu⁺² and its substitution for the cation in an alkaline earth oxide or sulfide, Brauer (5) concluded that Eu must be divalent in the sulfides and trivalent in the oxides. He verified this by comparing the band spectra of europium-activated sulfides with the line spectra in the corresponding oxides. The present work is an attempt to verify Brauer's observations and to demonstrate that divalent europium may be introduced into certain oxides under chemically reducing conditions.

PREPARATION OF MATERIALS

Sulfides.—Magnesium sulfide was prepared from magnesium ammonium chloride, according to the method of Russo (11). Calcium, strontium, and barium sulfides were prepared by reduction of the respective sulfates by firing in hydrogen at 1050°C.

¹ Manuscript received March 15, 1954. This paper was prepared for delivery before the New York Meeting, April 12 to 16, 1953, and was submitted to the Polytechnic Institute of Brooklyn, Brooklyn, N. Y., in partial fulfillment of the requirements for the M.S. degree in Chemistry.

² Present address: Research Department, Westinghouse Electric Corporation, Bloomfield, N. J.

Sulfates were prepared according to the method of Ward (12, 13) except for barium sulfate, which was Mallinckrodt's Ultra-Pure grade.

Oxides.—Magnesium oxide was prepared from Mallinckrodt's Ultra-Pure magnesium carbonate by thermal decomposition at 1050°C. Calcium and strontium carbonates, which were prepared according to Ward (14), were similarly converted. Barium oxide was prepared from Mallinckrodt's S.L. barium carbonate by heating at 1050°C for 4 hr in vacuo.

Chlorides.—Magnesium chloride was prepared from magnesium ammonium chloride by heating at 600°C in an atmosphere of nitrogen and hydrogen chloride. Calcium, strontium, and barium chlorides were prepared by dissolving the respective carbonates in freshly prepared HCl and evaporating to dryness.

Fluxes.—Due to the nature of the base materials, the flux and the activator had to be added in the dry form. This was accomplished by incorporating the activator into the flux, which in all cases was the chloride of the metallic constituent of the matrix. The desired amount of activator was added to the matrix by weighing out the proper quantity of activated flux and then adding the necessary amount of unactivated flux to give a total flux concentration of 5 wt %.

Except in the case of magnesium oxide, activated mixtures were molded into cylindrical pellets $\frac{7}{8}$ in. in diameter and approximately 1 in. long in a stainless steel mold under 20,000 psi. After firing, the pellet was cleaved perpendicular to its cylindrical axis. This was done so that a fresh uncontaminated surface would be available for measurements. Although the mechanical stress involved in cleaving the

specimens may have reduced the luminescence efficiency, it was not expected to shift the emission or absorption bands since, to the authors' knowledge, no such effect has been observed in the alkaline earth sulfides. Magnesium oxide samples were prepared by pressing the powder into a cell built up on a microscope slide.

All firing was carried out in a silica tube 20 in. long and $1\frac{7}{8}$ in. ID, closed at one end. The open end was closed with a rubber stopper having a long silica tube as a gas inlet and a short tube for the outlet. All samples were fired for 1 hr at 1050°C .

METHOD OF MEASUREMENT

Emission spectra were obtained with the aid of a Schmidt-Haensch double Rutherford glass prism spectrograph. Eastman Kodak super-pan press plates, type C, which are sensitive in the range $3900\text{--}6700\text{ \AA}$, were used. The positions of the lines were obtained with a Gaertner comparator. Band spectra were recorded by taking a profile of the spectrograms with a recording densitometer. The profile was corrected for plate sensitivity by using a sensitivity curve supplied by the manufacturer. Absorption spectra were obtained with a Beckman Model DU spectrophotometer with a diffuse reflectance attachment. In order to show positive peaks for absorption bands, the measured per cent reflectance was subtracted from 100 and reported as "per cent absorption." The absorption below $400\text{ m}\mu$ was not investigated because of the lack of a suitable source at the time the work was done.

It should be noted that the use of the reflectance attachment (without filters) in the region where excitation may take place will lead to spurious results, particularly high apparent reflectance in these regions. It is, therefore, likely that the sharp dips in per cent absorption around $400\text{ m}\mu$ in Fig. 2, 4, 6, and 8 are incorrect. Since these dips are not essential to an argument based on the broad band character of these absorptions, no corrected absorption spectra were prepared. It is believed, however, that less pronounced dips than those shown are actually present for most of these phosphors, since they are not very efficient, and the emission is only a small fraction of the incident energy.

RESULTS

Sulfide phosphors containing 200 ppm europium and 5 wt % of the corresponding alkaline earth chloride as flux were prepared by firing in nitrogen. All the samples showed reflection colors: MgS—yellow orange, CaS—pink, SrS—orange, BaS—yellow. Emission spectra are given in Fig. 1. The position of the calcium sulfide peak is somewhat in doubt since it occurs near the region of plate cut-off. How-

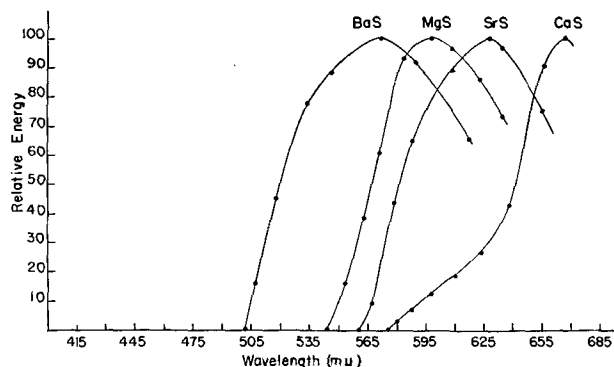


FIG. 1. Emission spectra of alkaline earth sulfides (MgCl_2 flux — Eu 220 ppm).

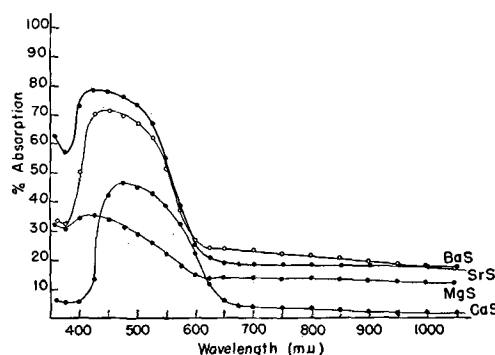


FIG. 2. Absorption spectra of europium-activated alkaline earth sulfides.

ever, it is in good agreement with previous work done in this laboratory (7). It will be noticed that the position of the peak depends on the matrix and shifts to shorter wave lengths on going from CaS to SrS to BaS. MgS is anomalous in that its emission falls between that of BaS and SrS. These findings agree with those of Brauer (6). Absorption bands are similar to each other and show a shift similar to, although not as great as, the shift in the emission spectra (Fig. 2).

Oxide Phosphors

Magnesium oxide.—Two samples containing 500 ppm Eu and 5 wt % MgCl_2 were prepared as powders, one in hydrogen, the other in nitrogen. Both samples were white. Excitation by 2537 \AA gave a red emission for both samples, while under 3650 \AA they were nonluminescent. Emission spectra appeared to consist of three overlapping broad lines. However, due to the poor resolution of the densitometer, the lines were not resolved. The apparent positions of these lines are given in Fig. 3.

Calcium oxide.—Two samples containing 150 ppm Eu and 5 wt % CaCl_2 were prepared as pellets, one in hydrogen, the other in nitrogen.

The nitrogen-fired samples were white under reflected light (Fig. 4). Excitation by 2537 \AA or 3650

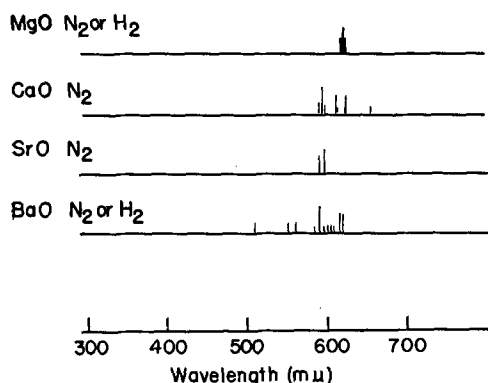


FIG. 3. Line emission spectra of europium-activated alkaline earth oxides.

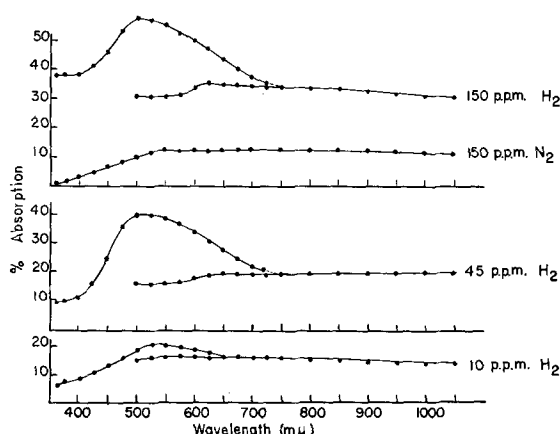


FIG. 4. Absorption spectra of CaO:Eu for various concentrations and firing atmospheres.

Å gave a pink emission which consisted of a series of lines (Fig. 3).

Hydrogen-fired samples appeared lavender. The absorption spectra of this sample and the next two samples discussed (Fig. 4) show two branches in the region of overlapping sensitivities of the two phototubes in the Beckman spectrophotometer. The reason for this effect is discussed below.

Excitation by 3650 Å gave a weak purple emission, while the emission under 2537 Å was much stronger. A spectrogram taken with the sample excited by 2537 Å showed a band in the blue, several lines, and a band in the red (Fig. 5). The positions of the lines are the same as those of the nitrogen-fired sample. To see what effect a low europium concentration would have, a sample containing 10 ppm Eu was prepared. This sample was light lavender and had a blue emission under both 2537 Å and 3650 Å. A spectrogram showed only a band in the blue and a very faint line (Fig. 5). After a 48-hr exposure to air, another spectrogram was taken. The line was just visible on the plate, whereas before it could be detected only by the densitometer. In order to see if the band in the red was due to trivalent Eu alone or to the presence of both Eu^{+2} and Eu^{+3} , a 45 ppm Eu

sample was prepared. A spectrogram showed the band in the blue and the lines and the band in the red (Fig. 5). Since neither the nitrogen-fired sample nor the hydrogen-fired 10 ppm sample showed the red band, it is suggested that the red band is due neither to Eu^{+2} nor to Eu^{+3} alone, but to the presence of both. The red band may originate from Eu^{+2} , as does the blue band, but may be shifted to longer wave lengths due to the presence of Eu^{+3} or associated cation vacancies. For example, the presence of a vacant cation site close to some of the Eu^{+2} ions might be responsible for a local distortion of the conduction band, with a consequent shift of the Eu^{+2} band to longer wave lengths. Such an interpretation would assume that europium emission is due to a transition from the conduction band to an Eu^{+2} center. This would be an untenable interpretation if photoconductivity were absent. Since no photoconductivity data are available, this suggestion cannot be very strongly supported. However, since europium-activated strontium sulfide and selenide do show photoconductivity under ultraviolet excitation (15), it seems plausible to suppose that it may also occur in europium-activated oxides.

In measuring the absorption of the "reduced" CaO (Fig. 4) and comparing readings of the blue-sensitive and the red-sensitive phototubes in the region of overlap (500–720 mμ) it was found they did not agree. This difference increased with increasing Eu and was larger at the long wave-length end. Apparently, excitation in the region of strong absorption gave rise to an emission in the red, which was not picked up by the blue-sensitive phototube. The "secondary" emission could be filtered out by insertion of a Corning No. 9780 filter in front of the phototube housing.

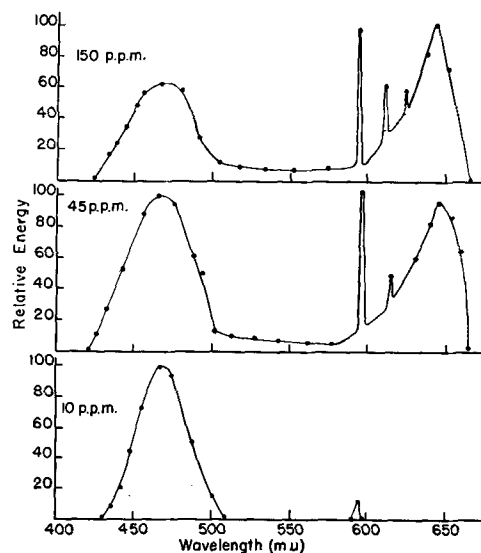


FIG. 5. Emission spectra of hydrogen-fired CaO:Eu

Attempts to photograph the secondary emission by excitation with either the Hg 436 $m\mu$ line or the Hg 546 $m\mu$ line were unsuccessful. Since the photographic plate cuts off at 6700 \AA , the emission seemed to be located beyond this limit. This is also suggested by the following facts: (a) the No. 9780 filter does not transmit in the region 680–1250 $m\mu$ so the emission must be in this range; and (b) no secondary emission is picked up by the blue-sensitive photocell. The latter is shown by the fact that the absorption measured by the red-sensitive phototube with the filter is the same as that measured with the blue-sensitive phototube. However, considering the uncertainty of locating the emission peaks by photographic methods, this secondary emission may actually be the red band shown in Fig. 5. If the true position of the peak is at longer wave lengths, the blue-sensitive photocell or the filter-photocell combination might not detect it. Failure to detect it photographically under excitation by 436 $m\mu$ and 546 $m\mu$ may be due to a low sensitivity to these wave lengths. Since the excitation spectra are not known, no estimate can be made of the significance of the nonappearance of the red band on the plate. Hence, the emission cannot be definitely attributed to the 6500 \AA band or to another band at longer wave lengths.

Strontium oxide.—Two pellets containing 100 ppm Eu and 5 wt % SrCl_2 were prepared, one in nitrogen, the other in hydrogen.

The nitrogen-fired sample was white (Fig. 6). The sample had a pink-orange emission under 2537 \AA . Spectroscopically, two lines were found as shown in Fig. 3.

The hydrogen-fired sample was lavender (Fig. 6). Excitation by 2537 \AA gave a weak red band emission, which was much stronger under 3650 \AA (Fig. 7). No secondary emission was found. After this sample was exposed to air for 24 hr, another spectrogram showed both line and band emission. The position of the lines was the same as that found with the nitrogen-fired sample.

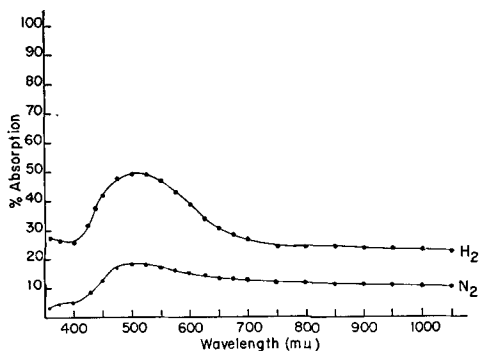


FIG. 6. Absorption spectra of SrO:Eu fired in H_2 and in N_2 .

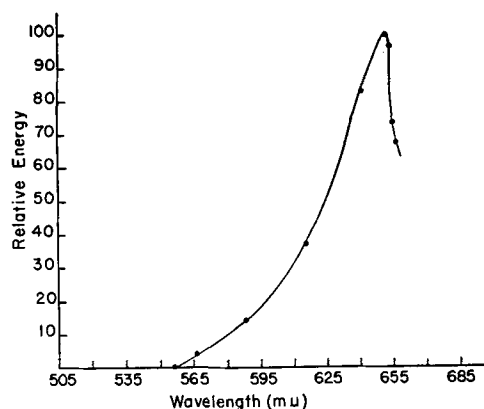


FIG. 7. Emission spectrum of H_2 -fired SrO:Eu

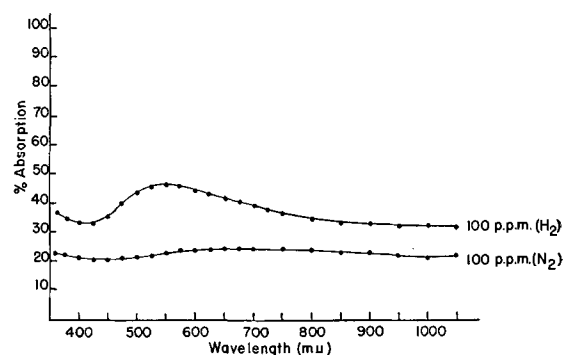


FIG. 8. Absorption spectra of BaO:Eu, fired in H_2 and in N_2 .

Barium oxide.—Two samples containing 100 ppm Eu and 5 wt % BaCl_2 were prepared, one in nitrogen, the other in hydrogen.

The nitrogen-fired sample was white (Fig. 8). Both 2537 \AA and 3650 \AA excited a pink-orange emission which was found to consist of a series of lines (Fig. 3).

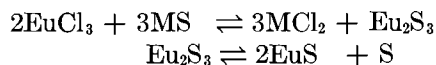
The hydrogen-fired sample was light lavender (Fig. 8). Refiring for one hour in hydrogen did not deepen the color. A 200 ppm sample was prepared which was slightly, if at all, darker than the one containing 100 ppm. Under 2537 \AA , a weak pink-orange emission was found. Emission under 3650 \AA was very weak. Even after a 50-hr exposure only line emission was found, as in the nitrogen-fired sample. If there is band emission, it is beyond the 6700 \AA plate cut-off and so could not be found.

DISCUSSION

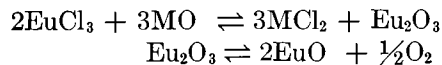
The most usual oxidation state of the rare earths is +3. Europium, however, can easily be reduced to the divalent condition by heating in a reducing atmosphere, while most of the other rare earths give the free metal (8, 16–19). All attempts to prepare EuO and Eu_2S_3 have been unsuccessful, and only Eu_2O_3 and EuS are known (17–19). On inclusion of

EuCl_3 into an alkaline earth oxide or sulfide, the following reactions may occur:

For the sulfide:



For the oxide:



where M is an alkaline-earth metal. That the conversion of Eu_2S_3 to EuS occurs has been shown by Prener (20) who heated coprecipitated SrSO_4 and EuSO_4 in hydrogen and obtained a phosphor very similar to one prepared by heating $\text{SrS} + \text{EuCl}_3$ in nitrogen. Heating the oxides in hydrogen reduces Eu^{+3} to Eu^{+2} and, unless Eu^{+2} can be stabilized, it will revert to Eu^{+3} as discussed below.

Samarium, which is one atomic number lower than europium, gives a line emission in both the alkaline earth oxide and sulfide phosphors (21, 22). Chemically, Sm is more difficult to reduce than Eu, so that it can be assumed Sm is in all cases trivalent. Eu^{+3} in pure europium(III) compounds has line emission similar to that of Eu incorporated into the "normal" oxide phosphors (6). Recently, it has been shown that divalent Eu salts have band emission (23, 24). Thus it appears that line emission is characteristic of Eu^{+3} and band emission of Eu^{+2} . The fact that oxides prepared in a reducing atmosphere show band spectra indicates that Eu in oxide phosphors can be present in two different oxidation states.

Consideration of the electronic configuration of Eu indicates the type of emission that should be exhibited by Eu^{+2} and Eu^{+3} . Line emission is associated with electronic transitions occurring within inner shielded electronic shells so that there is little, if any, influence by the surroundings. Band emission occurs when there are electronic interactions with the surrounding lattice. The ground state of Eu is, neglecting inner filled orbits, $4f^6 5s^2 5p^6 5d 6s^2$ (8, 25). Loss of the two 6s electrons to give Eu^{+2} leaves the 5d electron exposed and free to interact with the surroundings so that band emission is to be expected. Loss of the 6s² and 5d¹ electrons to give Eu^{+3} leaves, as the outer shell, the stable $5s^2 5p^6$ shells, so electronic transitions are now limited to the 4f shell. Since transitions are between discrete levels and not strongly influenced by the surroundings, line emission results. There is some influence by the surroundings, as shown by variation in the number and position of the lines of Eu^{+3} in different host lattices (Fig. 3).

If Eu is trivalent when dissolved in the oxides, as normally prepared, it would seem that heating in a

TABLE I

	Å		Å
Eu^{+2}	1.12	Ca^{+2}	0.98
Eu^{+3}	0.97	Sr^{+2}	1.15
Mg^{+2}	0.71	Ba^{+2}	1.31

hydrogen atmosphere produces divalent Eu. However, europium in MgO and BaO phosphors is not reduced, as evidenced by the presence of line emission only. Comparison of the absorption curves for the hydrogen-fired oxides of Mg, Ca, Sr, and Ba shows that the last three are similar, whereas absorption in hydrogen-fired MgO is very similar to that in nitrogen-fired oxide samples. Even though only line emission was found for the hydrogen-fired BaO , it is very possible that there is band emission located in the infrared. This seems plausible, since band emission in CaO and SrO containing divalent Eu is accompanied by band absorption, and the emission shifts from blue to red in going from "reduced" CaO to SrO and may be expected to shift in the same way on going from SrO to BaO . This shift is the reverse of the shift in the sulfides.

The presence of strong line emission in reduced CaO (10 ppm Eu) and the nonreduction of Eu in MgO can be partially explained by consideration of the size of the ions concerned. These are listed in Table I.

There is a 58% difference in size between Eu^{+2} and Mg^{+2} . As seen, EuO is not stable and so must be stabilized after formation by incorporation into a stabilizing crystal structure. Because of the large size difference between Eu^{+2} and Mg^{+2} , stabilization of EuO by incorporation into the MgO lattice is not possible. This concept of the stabilization of Eu^{+2} is supported by consideration of hydrogen-fired CaO . Reduced high activator CaO gives both line and band emission, whereas low activator CaO shows relatively strong band emission and faint line emission. This indicates that Eu^{+3} is being reduced, but only a limited amount of Eu^{+2} can be incorporated into the CaO lattice and so stabilized, while the excess reverts back to Eu^{+3} . The net result is the presence of both divalent and trivalent europium, each having its own emission spectra. It appears that a size difference of 14% between Ca^{+2} and Eu^{+2} allows only a limited solubility. Ba^{+2} differs from Eu^{+2} by 13%, which would, by comparison with Ca^{+2} , indicate that there should also be a limited solubility of Eu^{+2} in BaO . This must be the case since reduced BaO has an absorption spectrum similar to that of the other reduced oxides and also has line emission indicative of Eu^{+3} . Strontium oxide is the ideal case in that there is only a 3% difference in size between Sr^{+2} and Eu^{+2} , and there appears to be complete

solubility in concentrations up to 150 ppm, since no line emission is found.

Hydrogen-fired SrO showed the reappearance of line emission after long exposure to air. This indicates that some divalent Eu has been oxidized to the +3 condition and both oxidation states are emitting their characteristic type of spectrum. The spectrogram of 10 ppm CaO showed the presence of one extremely faint line whose intensity increased on standing in air. This indicates that initially there was a small amount of Eu^{+3} . Due to oxidation by oxygen or water vapor in the air, the concentration of Eu^{+3} has been increased, resulting in a more intense line spectrum.

CONCLUSION

Europium is divalent in the sulfides and trivalent in the oxides when they are prepared in inert atmospheres. Use of a reducing atmosphere in preparing oxide phosphors also gives divalent Eu, at least for CaO, SrO, and possibly BaO. As in the sulfides, the peak emission of the reduced oxides is dependent on the matrix, while the lines of the normal oxides show less dependence on the nature of the host crystal.

ACKNOWLEDGMENTS

The authors wish to thank Professor H. W. Schleuning, of the Polytechnic Institute of Brooklyn, for his advice and aid in obtaining the emission spectra, and Professor T. I. Taylor, of Columbia University, for the use of the recording densitometer.

Any discussion of this paper will appear in a Discussion Section to be published in the June 1956 JOURNAL.

REFERENCES

1. K. PRZIBRAM, *Nature*, **163**, 989 (1949).
2. F. URBACH, D. PEARLMAN, AND H. HEMMENDINGER, *J. Opt. Soc. Amer.*, **36**, 372 (1946).
3. P. BRAUER, *Z. Naturforsch.*, **1**, 70 (1946).
4. E. NICHOLS AND H. L. HOWE, *J. Opt. Soc. Amer.*, **13**, 573 (1926).
5. P. BRAUER, *Z. Naturforsch.*, **6A**, 255 (1951).
6. P. BRAUER, *ibid*, **6A**, 561 (1951).
7. Report on Preparation of Infrared Phosphors, p. 63, Contract No. OEMsr 982, Polytechnic Institute of Brooklyn, September 1, 1945.
8. W. HANLE AND A. SCHMILLEN in "FIAT Review of German Science," Part 3, Vol. 2, Wiesbaden, Germany (1948).
9. F. H. SPEDDING, *Trans. Faraday Soc.*, **35**, 67 (1939).
10. R. WARD in "Preparation and Characteristics of Solid Luminescent Materials," p. 299, Cornell Symposium of American Phys. Soc., John Wiley & Sons, Inc., New York (1948).
11. E. BANKS, V. J. RUSSO, AND R. WARD, *J. Am. Chem. Soc.*, **72**, 3173 (1950).
12. R. WARD, R. K. OSTERHELD, AND R. D. ROSENSTEIN in "Inorganic Synthesis," Vol. 3, p. 11, (L. F. Audrieth, Editor), McGraw-Hill Book Co., New York (1950).
13. R. WARD in "Preparation and Characteristics of Solid Luminescent Materials," Cornell Symposium of American Phys. Soc., Paper No. 2, p. 22, John Wiley & Sons, Inc., New York (1948).
14. W. PRIMAK, Dissertation, Polytechnic Institute of Brooklyn (1946).
15. J. J. DROPKIN, Thesis, Polytechnic Institute of Brooklyn (1947); Dissertation, Polytechnic Institute of Brooklyn (1948).
16. D. YOST, H. RUSSELL, AND C. GARNER, "The Rare-Earth Elements and Their Compounds," p. 10, John Wiley & Sons, Inc., New York (1947).
17. G. BECK AND W. NOWACKI, *Naturwiss.*, **26**, 495 (1938).
18. W. KLEMM AND H. SENFF, *Z. anorg. u. allgem. Chem.*, **241**, 259 (1939).
19. G. BECK AND W. NOWACKI, *Z. Krist.*, **99**, 339 (1938).
20. J. PRENER, Dissertation, Polytechnic Institute of Brooklyn (1949).
21. G. COHEN, Master's Thesis, Polytechnic Institute of Brooklyn (1947).
22. R. TOMASCHEK, *Physik Z.*, **33**, 878 (1932).
23. K. PRZIBRAM, *Z. Physik.*, **107**, 709 (1937).
24. S. FREED AND S. KATCOFF, U. S. Atomic Energy Commission Report, MDDC 1228 (1947).
25. H. EMELEUS AND J. ANDERSON, "Modern Aspects of Inorganic Chemistry," p. 11, Table 4, D. Van Nostrand Co., Inc., New York (1948).

Preliminary Studies of the Perovskite-Type Ternary Oxides as Luminophors¹

SALVADOR TEROL² AND ROLAND WARD

Department of Chemistry, University of Connecticut, Storrs, Connecticut

ABSTRACT

The properties of lanthanum aluminum oxide as a phosphor base material have been studied. The purest available lanthanum oxide samples gave products which were weakly cathodoluminescent because of the presence of praeodymium or samarium as impurities. The rare earth ions Pr^{+3} , Sm^{+3} , and Eu^{+3} were the only activators which were effective. Emission spectra of these phosphors are given. Other common activators were ineffective. The presence of rare earth impurities causes a pronounced body color to develop in the lanthanum aluminum oxide when the samples are ignited in air. This proves to be a more sensitive means of detection of impurities than spectrographic analysis.

INTRODUCTION

The perovskite structure is common among compounds of the type ABX_3 where A represents a large cation capable of 12-fold coordination with the anion X , B a smaller cation suitable for sixfold coordination with X , while X is nearly always the fluoride ion or the oxide ion. The ideal perovskite structure is cubic with the B cation at the corners of the unit cell, the A cation at the center, and the anion at the midpoint of the edges.

With a few notable exceptions, compounds of this type are stoichiometric. When X is the fluoride ion, the choice of cations represented by A and B is quite restricted, A usually being one of the larger alkali metal cations and B a divalent cation such as magnesium or zinc. It has been shown by Smith (1) that compounds such as KMgF_3 and KZnF_3 activated with manganese have an orange emission when excited by cathode rays. The divalent manganese would be expected to have sixfold coordination in these crystals. On the other hand, the cathodoluminescence of manganese-activated calcium fluoride, in which the manganese is presumably in eightfold coordination, is green.

With X representing the oxide ion, a greater variety of cations is possible since the sum of the positive valences is six. Many representatives of the types of $A^{\text{I}}B^{\text{V}}\text{O}_3$, $A^{\text{II}}B^{\text{IV}}\text{O}_3$, and $A^{\text{III}}B^{\text{III}}\text{O}_3$ are known. Moreover, it has been shown that the oxidation state of the B cation may be adjusted by valence compensation. The valence of manganese in the perovskite phase $(\text{La}_{1-x}\text{Sr}_x)(\text{Mn}_{1-x}^{\text{III}}\text{Mn}_x^{\text{IV}})\text{O}_3$, for example, is a function of the strontium content (2).

¹ Manuscript received December 27, 1954. This paper was prepared for delivery before the Cincinnati Meeting, May 1 to 5, 1955.

² Present address: Optical Institute and Naval Research Laboratory, Madrid, Spain.

It, therefore, occurred to the authors that a colorless ternary oxide of the perovskite type would offer very interesting possibilities as a base material for phosphors. A list of such compounds is given in Table I. There is but little information on the luminescent characteristics of these compounds. Kröger (3) reports some luminescence for BaZrO_3 , SrZrO_3 , CaSnO_3 , and CdSnO_3 . In seeking base materials for the activator titanium, Kröger also tried LaAlO_3 , but did not observe any luminescence.

The fact that $\text{Al}_2\text{O}_3:\text{Cr}$ has well-known luminescent characteristics was encouraging. In this luminophor, chromium is probably in sixfold coordination with oxide ions in the corundum lattice. The environment of chromium dissolved in the perovskite lattice of LaAlO_3 should be similar, and it was hoped to find a phosphor resembling artificial ruby. No such phosphor was obtained, but some luminescent materials were discovered which showed some interesting properties. This paper describes the preparation and properties of these phosphors.

EXPERIMENTAL

Purification of materials.—A solution of $\text{Al}(\text{NO}_3)_3 \cdot 9\text{H}_2\text{O}$ in distilled water was treated with H_2S at a pH near 6 and the mixture boiled and filtered. Aluminum nitrate, recrystallized from the filtrate, was treated by three different methods for the removal of iron: (a) by means of cupferron, (b) by acetylacetone, and (c) by boiling with excess potassium hydroxide and precipitating the alumina from the alkaline solution. Each of these procedures gave comparable products in which no trace of heavy metals was found by spectroanalysis.

Three samples of lanthanum oxide were used. A commercial sample (Fairmount Chemical Company) was dissolved as the nitrate, and recrystallized six times after treatment with hydrogen sulfide. The

TABLE I. Colorless compounds with perovskite structure*

Substance	a_0	Substance	a_0
BaZrO ₃	4.17	LaGaO ₃	3.89
SrZrO ₃	4.08	NaTaO ₃	3.88
CaZrO ₃	3.99	NaNbO ₃	3.88
KTaO ₃	3.98	CaTiO ₃	3.84
BaTiO ₃	3.97	CdSnO ₃	3.80
CaSnO ₃	3.92	LaAlO ₃	3.78
SrTiO ₃	3.89	YAlO ₃	3.67
PbTiO ₃	3.89		

* Wyckoff, Interscience Publishers Inc., New York (1948).

second sample, originating in Luigi Rolla's laboratory in Rome, Italy, had been purified by classical procedures. The third sample, obtained from the Atomic Energy Commission, had presumably been purified by use of ion exchange resins. The last two samples showed no trace of heavy metal impurities upon spectrographic examination.

Lanthanum aluminum oxide was prepared by heating stoichiometric mixtures of the two oxides at 1150°C for about 12 hr. The most convenient method of obtaining the oxide mixture was by coprecipitating the hydroxides from a solution of the nitrates using ammonium hydroxide. This procedure was especially useful when activators were being introduced. The products gave only the x-ray diffraction pattern of the cubic perovskite structure ($a_0 = 3.79$ Å). None of the lines of the reactants was discernible in the pattern. It was found, however, that a rather rapid hydrolysis of the lanthanum aluminum oxide occurred on exposure to moist air. The stronger lines of La(OH)₃ appeared in the pattern of the products which had been allowed to stand in the open for as short a period as two hours. It was necessary, therefore, to keep all samples in a good desiccator.

Solid solutions of lanthanum aluminum oxide with calcium titanium oxide and strontium titanium oxides were prepared over a wide range of composition. The composition-lattice constant relationship was found to obey Vegard's law within experimental error. With barium titanium oxide, on the contrary, no solid solution was detected by x-ray analysis.

Products which had been prepared by heating in a hydrogen atmosphere were invariably white, but those prepared by ignition in air showed a pronounced body color. The commercial sample of lanthanum oxide and the sample from the A.E.C. gave a pink colored product, while that from Rolla's laboratory gave a tan coloration. Use of different reaction vessels (zircon, alundum, silica, and platinum were tried) did not eliminate or change this body color. Hence, it was concluded that it must be due to the presence in the lanthanum oxide of an oxidizable impurity, presumably one of the lanthanide elements. Analysis using a 21-ft grating spectro-

graph did not reveal the presence of any rare earth impurity, in the lanthanum oxide from Fairmount or from the A.E.C., but a trace of samarium was found in Rolla's preparation. All samples of lanthanum oxide, however, remained white upon ignition in air.

Luminescent Properties

Although some of the samples were found to luminesce weakly under 2537 Å radiation, cathode ray excitation was apparently more efficient. Most of the authors' attention was given to the latter.

Cathodoluminescence was found for all samples prepared without the intentional addition of impurities. A fairly strong orange emission was obtained from the samples prepared with Rolla's lanthanum oxide, and a weak yellowish-green emission from the others.

The addition of several rare earth ions to lanthanum aluminum oxide gave the results listed in Table II. These samples were all prepared using the lanthanum oxide from the A.E.C. It was observed that the addition of praseodymium up to 10⁻³ gram atoms per mole of LaAlO₃ increased the in-

TABLE II. Lanthanides as activators in the cathodoluminescence of lanthanum aluminum oxide

Addition in atom/mole	Body-color firing in		Cathodoluminescence	
	Air	H ₂	Color	Intensity
10 ⁻⁴ Ce	PT	—	GY	4
10 ⁻⁴ Ce	—	W	G	4
10 ⁻³ Ce	FT	—	GY	4
10 ⁻³ Ce	—	W	G	4
10 ⁻² Ce	T	—	GY	5
10 ⁻² Ce	—	YW		
10 ⁻⁴ Pr	P	—	YG	2
10 ⁻⁴ Pr	—	W	GY	2
10 ⁻³ Pr	P	—	GY	1
10 ⁻³ Pr	—	W	GY	1
10 ⁻² Pr	P	—	GY	1
10 ⁻² Pr	—	W	GY	1
5.10 ⁻² Pr	PT	—	G	3
5.10 ⁻² Pr	—	W	G	3
10 ⁻³ Nd	FT	—	Y	4
10 ⁻³ Nd	—	W	YG	3
10 ⁻² Nd	T	—	Y	5
10 ⁻² Nd	—	W	GY	3
10 ⁻⁴ Sm	FT	—	Y	1
10 ⁻⁴ Sm	—	W	Y	1
10 ⁻³ Sm	FT	—	Y	1
10 ⁻³ Sm	—	W	Y	1
10 ⁻⁴ Eu	FT	—	RO	3
10 ⁻⁴ Eu	—	W	RO	3
10 ⁻³ Eu	T	—	RO	3
10 ⁻³ Eu	—	W	RO	3
10 ⁻³ Gd	W	—	YO	2
10 ⁻³ Gd	—	W	YO	2

KEY: T = tan colored, F = faint, P = pink, W = white, G = green, Y = yellow, R = red, O = orange. 1 = Very strong, 2 = strong, 3 = medium, 4 = weak, 5 = very weak.

tensity of yellowish green emission, while the addition of samarium caused a strong yellow emission. Addition of cerium and neodymium, on the other hand, did not increase the brightness of the emission and, in some cases, appeared to diminish the luminescence. Addition of europium and gadolinium gave materials with medium to strong cathodoluminescence. From these results it seemed most probable that the impurity which caused the orange cathodoluminescence in LaAlO_3 prepared from Rolla's lanthanum oxide was samarium, while that giving rise to the greenish-yellow luminescence was praeceodymium. Somewhat similar results have been reported with lanthanum oxychloride phosphors (4) prepared from lanthanum oxide from the Lindsay Light Chemical Company.

The emission spectra of some of the products are given in Fig. 1 to 5. With the exception of Fig. 2, all of these refer to preparations from lanthanum oxide obtained from the A.E.C. In Fig. 1 the emission curve for the "unactivated" phosphor is compared to a phosphor activated with 10^{-3} mole of praeceodymium. The major emission peaks at 510, 630, and 660–670 $m\mu$, obtained by this addition, are noticeable in the spectrum of the "unactivated" lanthanum aluminum oxide. A comparison is also given in Fig. 1 of the emission spectra of the phosphors prepared in oxidizing and reducing atmospheres. The lesser peaks at 490 and 550 $m\mu$ appear to be slightly increased while those at 630 and 670 $m\mu$ are somewhat diminished in the product prepared in hydrogen. The band width in these spectra was dependent on the slit width of the spectroradiometer used. Fig. 2 gives a comparison of the emission spectrum of $\text{LaAlO}_3:\text{Pr}$ obtained under 2537 Å excitation with the emission under cathode ray excitation. This

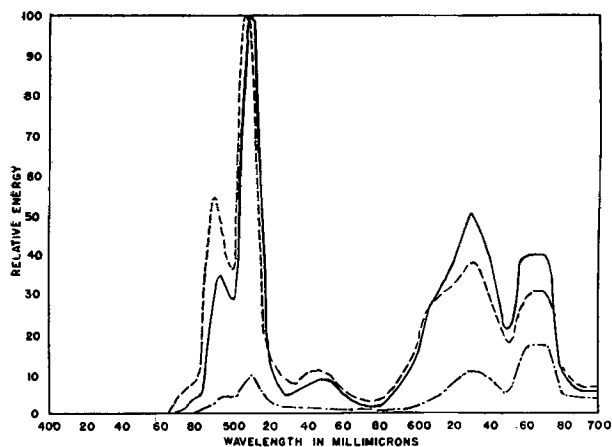


FIG. 1. Emission spectra under cathode ray excitation of lanthanum aluminum oxide prepared using lanthanum oxide from A.E.C. - - - - LaAlO_3 fired in air with no intentional addition of activator; — $\text{LaAlO}_3:10^{-3}\text{Pr}$ fired in air; - · - · $\text{LaAlO}_3:10^{-3}\text{Pr}$ fired in hydrogen.

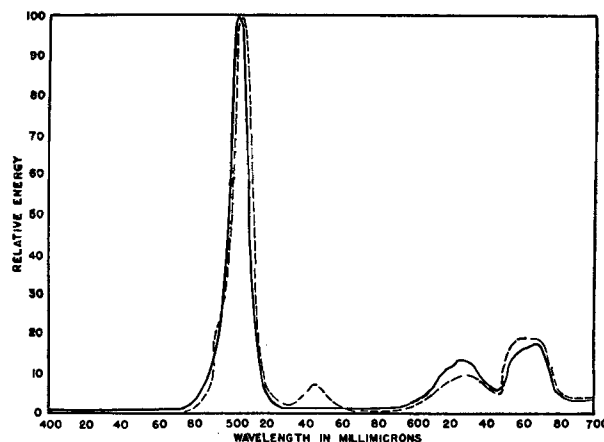


FIG. 2. Emission spectra of $\text{LaAlO}_3:10^{-3}\text{Pr}$ prepared using lanthanum oxide from The Fairmount Company. — excitation by 2537 Å radiation; - - - - excitation by cathode rays.

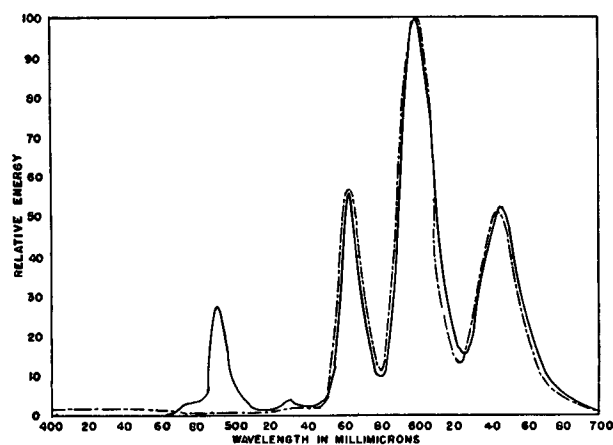


FIG. 3. Emission spectra under cathode ray excitation of LaAlO_3 containing samarium as activator. These samples were prepared using lanthanum oxide from the A.E.C. - - - - $\text{LaAlO}_3:10^{-4}\text{Sm}$; — $\text{LaAlO}_3:10^{-3}\text{Pr} + 10^{-4}\text{Sm}$.

phosphor was fired in a hydrogen atmosphere and was prepared from lanthanum oxide from the Fairmount Chemical Company. The spectra are essentially the same except for the absence of the minor peak at 490 $m\mu$ in the emission under ultraviolet excitation.

The addition of 10^{-4} mole of samarium gives a phosphor with three strong emission peaks at about 565, 600, and 645 $m\mu$ as shown in Fig. 3. When 10^{-3} mole of praeceodymium is added to this phosphor, the only praeceodymium band which appears in the spectrum is at 490 $m\mu$ while the samarium spectrum is substantially unaltered.

The emission curve for lanthanum aluminum oxide containing europium, shown in Fig. 4, consists of two sharp peaks at 590 and 620 $m\mu$. The same emission is obtained whether the phosphor is prepared in an oxidizing or a reducing atmosphere. The emission is

apparently due to trivalent europium, stabilized in this oxidation state in the lattice of the matrix.

With gadolinium, the same emission curve was obtained as with samarium. On account of the high sensitivity of samarium as an activator, this response is likely to be due to the presence of samarium as an impurity in the gadolinium.

Use of strontium or barium as charge compensators in the preparation of the praseodymium phosphor was apparently without effect. Substitution of one-third of the aluminum with gallium in preparations activated with samarium or praseodymium did not lead to any noticeable difference in the emission characteristics. Lanthanum oxide activated with praseodymium or with samarium gives essentially the same cathodoluminescence as is obtained with these activators in lanthanum aluminum oxide,

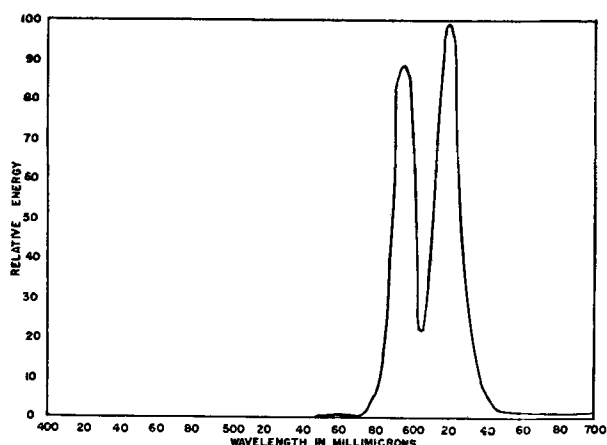


FIG. 4. Emission spectrum under cathode ray excitation of $\text{LaAlO}_3:10^{-3} \text{Eu}$. This sample was prepared using lanthanum oxide from the A.E.C.

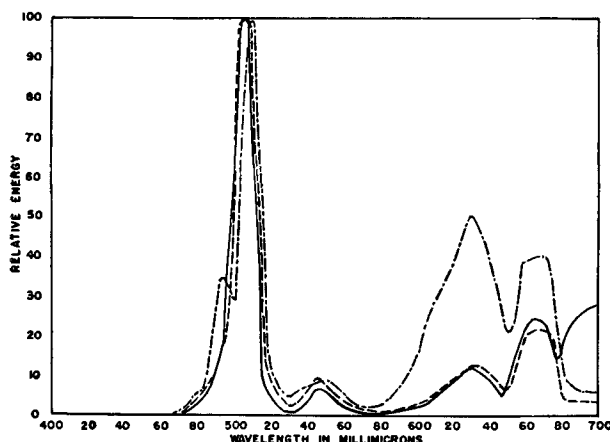


FIG. 5. Emission spectra under cathode ray excitation of $\text{LaAlO}_3:\text{Pr}$ containing additional activators. These samples were prepared using lanthanum oxide from the A.E.C. All samples were fired in hydrogen. - - - $\text{LaAlO}_3:10^{-3} \text{Pr}$; — $\text{LaAlO}_3:\text{Pr} + 2\% \text{V}_2\text{O}_5$; - · - $\text{LaAlO}_3:\text{Pr} + 4 \times 10^{-3} \text{Cr}$.

but the emission appears to be somewhat stronger with the latter as host crystal.

Several other elements which commonly act as activators were tested by themselves. Among these were chromium, vanadium, manganese, copper, bismuth, and antimony. No striking change in emission characteristics was noticed with any of them. Fig. 5 shows the emission curves obtained with the first two of these in comparison with the emission of the praseodymium phosphor. The effect of their presence is the suppression of the smaller praseodymium peaks at 490, 630, and 660–670 $m\mu$. A similar effect is obtained upon increasing the concentration of the praseodymium to 10^{-2} . A broad weak band in the neighborhood of 700 $m\mu$ is present in the vanadium-activated sample.

Addition of increasing quantities of manganese to $\text{LaAlO}_3:\text{Pr}$ causes progressive lowering of the intensity of emission. The body color of these samples fired in air becomes less marked with increasing manganese concentration and the samples containing $2 \times 10^{-3} \text{Mn}$ are white. No emission curves of these samples were obtained.

DISCUSSION OF RESULTS

The results of these experiments indicate that lanthanum aluminum oxide resembles lanthanum oxide as a host crystal rather than aluminum oxide.

The unavoidable presence of rare earth impurities in all of the products vitiates to some extent the original purpose of this investigation. There seems to be little reason to doubt that the transition metal activators which were used would enter the perovskite structure in the positions of sixfold coordination. The energy absorbed by the lattice, however, is not transferred to these impurities. Some of the energy is dissipated by emission from the rare earth impurity. It is possible that energy transfer to the transition metal impurity might occur in the complete absence of praseodymium or samarium. The emission curve of the vanadium-activated sample suggests this possibility.

Production of the distinctive body colors on ignition of the lanthanum aluminum oxide in air and the fact that cathodoluminescence is readily observed in the samples prepared without activation from the spectroscopically pure materials suggest that these phenomena might be useful in following the purification of lanthanum compounds.

ACKNOWLEDGMENTS

The authors are greatly indebted to Dr. Frank J. Studer of the General Electric Research Laboratories for his kindness in determining the emission curves,

to Dr. A. Camunas (Institute de Optica, Madrid) for his assistance to one of the authors in the use of the grating spectrograph, and to Dr. Edmond Botti for samples of pure rare earth oxides. They would also like to express their gratitude to the Consejo Superior Investigaciones Cientificas of Spain for sponsoring the stay of one of the authors in the U.S.A. during the period of this research.

Any discussion of this paper will appear in a Discussion Section to be published in the June 1956 JOURNAL.

REFERENCES

1. A. L. SMITH, *This Journal*, **101**, 189 (1954).
2. G. H. JONKER AND J. H. VAN SANTEN, *Physica*, **16**, 337 (1950).
3. F. A. KRÖGER, "Some Aspects of the Luminescence of Solids," Elsevier Press, Houston (1948).
4. F. E. SWINDELLS, *This Journal*, **101**, 415 (1954).

Infrared Quenching of Cadmium Sulfide¹

S. H. LIEBSON

United States Naval Research Laboratory, Washington, D.C.

ABSTRACT

Infrared quenching of CdS has been investigated as a function of applied voltage and both infrared and exciting light intensities. Infrared quenching of photoconductivity due to light of wave lengths shorter than that corresponding to the absorption edge increases as the voltage is increased. The quenching spectrum is found to shift with temperature in approximately the same amount as the corresponding shift of the absorption edge. An explanation of infrared quenching is offered based on infrared freed holes recombining with trapped electrons within the crystal.

INTRODUCTION

Luminescence and electrical properties of the hexagonal form of both cadmium and zinc sulfide crystals are affected by exposure to infrared radiation. As examples, infrared causes a decrease in the photoconductivity of CdS (1), a stimulation of phosphorescence in CdS-ZnS phosphors (2), an increase in the photovoltaic effect with CdS (3), stimulation of photocurrent in ZnCdS (4), and quenching of luminescence in a ZnS phosphor (5). Since these are closely related materials, it is reasonable to expect that, for those phenomena which respond to infrared peaking at 0.9 and 1.5 eV for CdS (6) and at about 0.95 and 1.8 eV for ZnS (7), absorption occurs in similar centers for both compounds. Different manifestations of response to infrared may be understood on the basis of double activation where, as an example, stimulation of phosphorescence originates with infrared absorption in one activation center and ends with emission in another (7).

Frerichs (8) has proposed a mechanism for quenching of photoconductivity wherein infrared empties electrons from traps located along conduction paths within the crystal, the emptied traps serving to inhibit the further passage of current. With the additional observation that an increase in current is observed prior to quenching action when infrared is first made incident on a photoconducting crystal, Rose (9) postulated that infrared frees holes which contribute to the current before combining with electrons from the conduction band. Taft and Hebb (10) favored this hypothesis and, based on the observed symmetrical quenching spectrum, suggested that infrared excited trapped holes to higher energy states which were then thermally freed to the valence band. From observations of a rectifying contact to

CdS, Liebson (3) has also proposed that holes were freed by infrared.

In the case of phosphors, Fonda (2) observed that the stimulation spectrum was independent of the activator for ZnS:Pb and ZnS:Mn and suggested stimulation to be related to a displacement of Zn atoms from their normal positions by the activator atoms. Pearlman, Nail, and Urbach (7) measured stimulation as a function of activator concentration and concluded that copper was responsible for infrared stimulation. Froelich (11), based on careful preparation of ZnS:Cu phosphors, also concluded that infrared stimulability was related to the presence of copper in the crystal. In this connection, Klasens (12) suggested that Cu produced hole traps which could be excited to the valence band. For the phosphor ZnS:Cu:In, as an example, Klasens proposed that under infrared stimulation holes were freed from Cu centers, migrating through the valence band to recombine with indium traps, giving the characteristic indium emission. Klasens also showed how this mechanism was capable of explaining some temperature effects in these phosphors.

This investigation was undertaken to supply additional information relating to infrared quenching of photoconductivity in CdS crystals.

DESCRIPTION OF CRYSTALS

Crystals of CdS were prepared by M. E. Bishop by a modification of Frerichs' method (13). Except where noted, crystals were chosen which showed no increased sensitivity at the indium electrodes, in an attempt to minimize the possibility of electrode barrier effects obscuring the measurements. The relative sensitivity of regions of the crystals was determined by scanning with a beam of blue light 0.001 in. in diameter, obtained by directing suitably filtered light through the eyepiece of a microscope and on to the crystal under the microscope objective. In general it was found that the photosensitive

¹ Manuscript received December 20, 1954. This paper was prepared for delivery before the Cincinnati Meeting, May 1 to 5, 1955.

region was also most affected by infrared. Crystals were examined for luminescence at the focus of a 100 watt mercury arc with an ultraviolet filter whose transmission centered around 3660 Å. Crystals were mounted with indium electrodes applied within a day of growth to insure ohmic contact. The first two digits of a crystal identifying number refers to a particular crystal batch.

Crystal 57-1 was a hexagonal needle about 0.1 in. long and about 0.03 in. wide after contacts were placed on it, and showed several sensitive regions under the light probe. It exhibited almost no ultraviolet luminescence. Its photoconductive spectrum peaked sharply at 5200 Å.

Crystal 57-4 was 0.1 in. long and about 0.02 in. wide, hexagonal in cross section, and exhibited a sensitive region as determined with the light probe, located 0.025 in. from one contact. This region showed both photoconductive and infrared quenching characteristics. The remainder of the crystal did not respond to photoconductive light to the limit of sensitivity of the apparatus, about two orders of magnitude less than the photoconductive peak reading. No observable photoconductive response was found at either electrode, making it likely that rectifying contacts did not affect current measurements, although the crystal did show internal rectification. The crystal was red luminescent under ultraviolet excitation.

Crystal 73-1 was about 0.002 in. thick and 0.16 in. long. No peaks were detected with the light probe, the crystal apparently having a sensitivity varying by less than two over its length. Reversal of polarity indicated little or no apparent polarization or rectification. This was the only crystal in several hundred examined that satisfied these conditions. The crystal was weakly red luminescent.

Crystal 73-2 was 0.3 in. long and 0.01 in. wide. Under probe by a beam of light, it showed a sensitive region internal to the crystal which determined its photoconductive behavior. This region seemed to be associated with a grain boundary when viewed under a microscope. This crystal exhibited a greater infrared sensitivity than any of the others tested, and was red luminescent.

Batches 57 and 73 were spectroscopically analyzed for metallic impurities. Both contained about 0.1% silicon with smaller amounts of magnesium, iron, silver, and copper. Batch 57 contained of the order of 0.0001% copper and batch 73 contained about 0.01% copper. Except for 57-1, as noted above, all crystals had a photoconductive spectrum peaking near 5150 Å, falling off sharply at longer wave lengths and more gradually toward shorter wave lengths.

EXPERIMENTAL

The infrared source consisted of a 100 watt tungsten lamp in conjunction with a Polaroid Company Type XR7X filter, having a short wave length cut-off at about 8000 Å. Infrared and visible light intensities were varied by means of gray filters whose transmissions were determined at 5000 Å and at 14,000 Å. A Gaertner quartz monochromator was used for all spectral determinations.

Crystals were mounted by means of their electrodes to terminals on glass insulators and inserted into a brass cylindrical container which was evacuated to about 10^{-6} mm Hg. The crystal could be heated or cooled by means of temperature baths mounted external to the container, thermal conductivity being obtained by means of a few microns pressure of helium which could be admitted to the container. The crystal was connected in series with a potentiometer across a battery supply. Light was admitted to the container through a quartz window.

The time constant for current equilibrium was of the order of $\frac{1}{2}$ hr for all crystals so that measurements, to insure reproducibility, were made after intervals of time approaching an hour. Measurements of current change due to infrared, at the higher values of photoconductive current, suffer from appreciable error due to the fact that the change in current due to infrared was of the order of magnitude of fluctuations in the crystal and current measuring system. This accounts in large measure for the relatively poor fit at larger photo-illumination readings in Fig. 1.

Voltage Dependence of Infrared Quenching

The voltage dependence of infrared quenching was determined for constant intensities of both photoconductive and quenching irradiation. Most crystals showed a behavior indicating polarization. This was evidenced for crystals whose current had come to equilibrium at a fixed voltage and photoconductive light intensity. Upon increasing the applied voltage, the current immediately increased approximately in proportion and then decreased slowly for several minutes, the final equilibrium values being those shown in Fig. 2 and 3. Fig. 2 shows the equilibrium current through crystal 57-4 as a function of applied voltage. These results are typical of those for all crystals at high voltages in that the proportional decrease in current due to infrared increased as the voltage was increased across the crystal. Crystal 73-1 was the only one in more than 100 tested which showed a comparative uniformity of response when scanned with a fine beam of light. This crystal was also the only one observed which had linear resistance characteristics with

photoconductive light, as shown in Fig. 3, and was the least sensitive in response to infrared, requiring approximately 300 times the infrared intensity used to obtain the data in Fig. 2. Crystal 73-1 was atypical in that infrared quenching decreased at high voltages for photo-excitation at 5200 Å, outside the absorption band.

The current through crystal 57-4 at low light intensities varied as the 0.7 power of the light intensity with 1 v across the crystal and as the 0.8 power of the intensity with 100 v across the crystal. Crystal 73-1 showed a linear variation of current vs. intensity at 10 v and 100 v. Crystal 57-1 current varied as 0.8

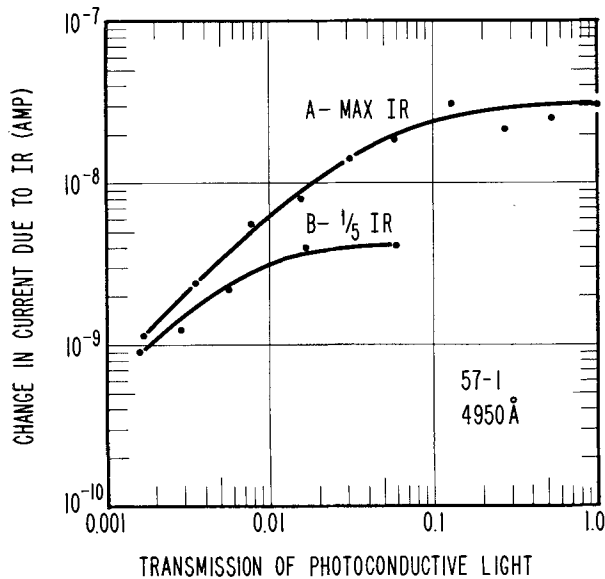


FIG. 1. Change in current due to infrared as a function of photoconductive light intensity.

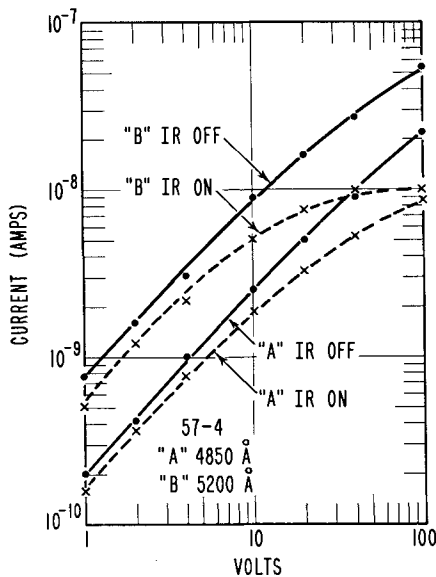


FIG. 2. Voltage dependence of infrared quenching for a typical CdS crystal.

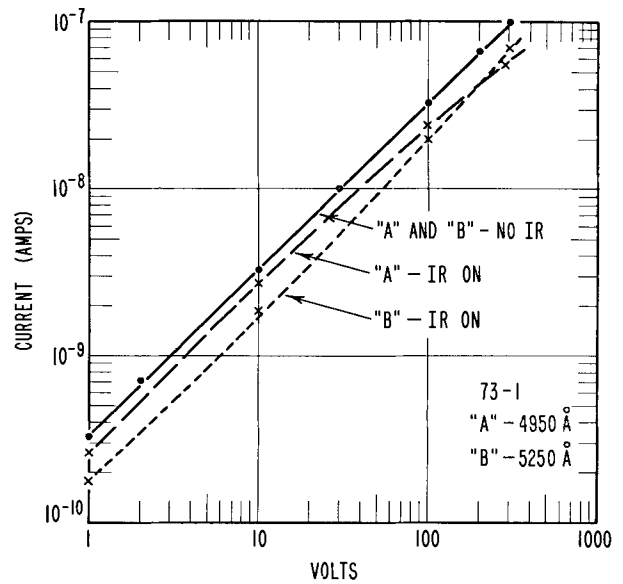


FIG. 3. Voltage dependence of infrared quenching for ohmic photoconducting crystal.

power of light intensity at 1 v and 0.95 power at 100 v.

For crystal 57-4 shown in Fig. 2 with the applied voltage in the low impedance direction, two sets of data are given, one with excitation at 4850 Å and the other at 5200 Å. The crystal exhibited a photoconductive peak at 5150 Å, the wave lengths used for the measurements in Fig. 2 lying on either side of both the photoconductive peak and the absorption edge. The effect of infrared was more pronounced at 5200 Å despite the fact that the current produced at this wave length was greater than that produced by the 4850 Å light.

Fig. 4 shows the proportional change in current with constant photoconductive and quenching light intensities as a function of voltage applied in the low and high impedance directions. In the high impedance direction the proportional quenching first decreased as the voltage was increased. The low impedance characteristic is typical of most crystals.

Quenching Linearity

Typical measurements of quenching action are shown in Fig. 1 for variable photoconductive light and in Fig. 5 for variable infrared intensity. The current change due to infrared, shown in Fig. 1, approached a constant value at high photoconductive light intensities. The scatter in experimental points is due to the fact that, as the photoconductive intensity is increased, the proportional change in current with infrared diminishes, making errors due to system fluctuations of increasing importance.

Curves A and B of Fig. 5 show the increased quenching action at higher voltages, tending to "saturate" sooner at lower values of infrared inten-

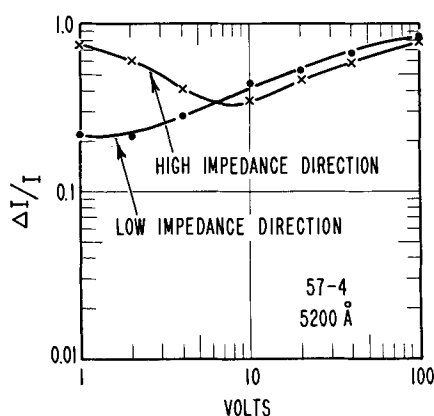


FIG. 4. Voltage dependence of proportional change in current due to infrared.

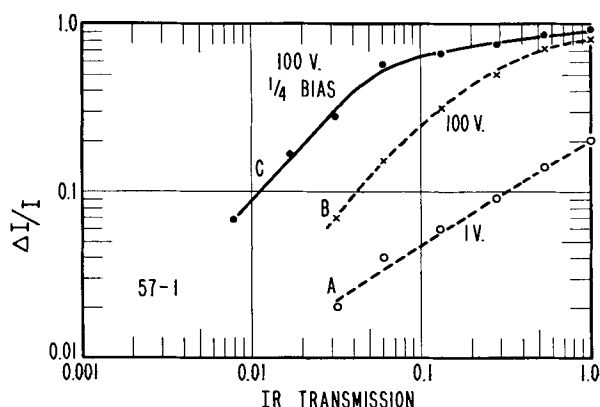


FIG. 5. Variation of proportional change in current with infrared intensity.

sity. In curve C, taken at reduced photoconductive light intensity, the quenching action for lower values of infrared intensity (at 100 v) increases to approximately the extent by which the photoconductive light is decreased.

Infrared Quenching Spectrum

The infrared quenching spectrum was first measured by Frerichs (8) and redetermined by Taft and Hebb (10) at room temperature and shown to consist of two broad bands peaking at 1.5 and 0.9 ev. For the purpose of measurement at low temperature a crystal (73-2) was chosen with a sensitive region approximately midway along the crystal. As observed by Taft and Hebb, there was a marked decrease in infrared quenching at low temperatures. For this crystal at -175°C a change in peak location was observed corresponding to an increase of approximately 0.13 ev of both peaks. This is approximately equal to the temperature shift measured by Kröger (14) of the absorption edge. The relative insensitivity of these crystals at low temperatures made it difficult to get a meaningful band shape.

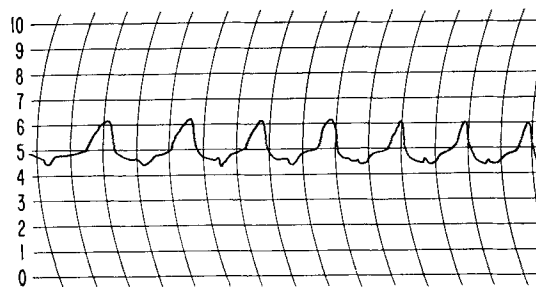


FIG. 6. Oscillations due to infrared incident on a rectifying contact.

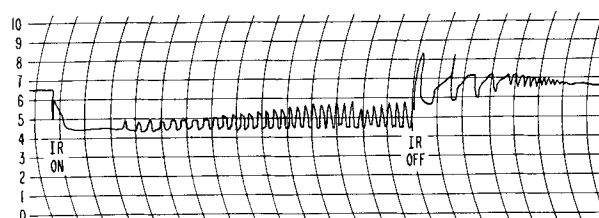


FIG. 7. Build up and decay of oscillations under infrared irradiation.

Oscillations

In the course of these investigations several crystals were prepared with rectifying contacts which exhibited variations in current of the nature of relaxation oscillations under conditions of simultaneous photoconductive and infrared irradiation. Fig. 6 shows a chart record of the current through such a crystal at chart speeds of one division per minute. Fig. 7 shows the manner in which these oscillations build up and diminish when infrared is turned on and off. The frequency of oscillations increases with voltage and is eliminated at either very high or very low infrared intensities, approaching a maximum amplitude somewhere in between. These oscillations have been observed only with crystals having rectifying contacts.

DISCUSSION

The increase of photovoltaic effects at contacts to CdS under irradiation by infrared has been previously attributed to the freeing of holes by infrared (3). This may be more easily seen by considering the potential of a planar barrier at the crystal contact, expressed in practical units

$$\phi = \frac{Me^2l^2}{2K} = \frac{\sigma el}{2K}$$

where ϕ is in volts, M is the density of positive centers within the barrier region of thickness l , K is the dielectric constant, and σ is the surface charge density. At a rectifying contact made with conducting electrodes, σ might be expected to show little change. As a consequence if M is reduced by the

action of infrared, l must increase, giving the new photovoltage as

$$\phi + \Delta\phi = \frac{\sigma e(l + \Delta l)}{2K}$$

The effect of infrared is to increase the generated photovoltage to $\phi + \Delta\phi$ and to increase the thickness of the barrier to $l + \Delta l$. The increase of barrier thickness may then result in a more effective utilization of the incident photoconductive light to provide an increase of generated current, in accord with observation. Oscillations shown in Fig. 6 and 7 are probably related to the ability of infrared to change the height of the barrier, although insufficient information is available to give a satisfactory explanation.

The curves presented in Fig. 1, 3, and 5 show a strong field dependence of infrared quenching. These crystals appeared to have internal regions of high impedance. In Fig. 2, for a crystal with no apparent internal barriers, comparatively little infrared quenching is observed. The results show that strong fields enhance infrared quenching. Klasens (15) has suggested that the increased field may increase the range of travel of holes to recombination regions resulting in greater quenching action. Another possible explanation is that the increased fields increase the internal space charge or polarization. For either case the following explanation is offered for infrared quenching. Referring to Fig. 8, infrared frees holes (step 1), perhaps with the aid of thermal ionization (10) (step 2), the holes are swept by the field to the potential barrier due to trapped electrons (step 3) when recombination takes place with the trapped electron (step 4). The empty trap is now available for removing electrons from the conduction band, resulting in quenching.

The decrease and subsequent increase in proportional infrared quenching in the high impedance direction shown in Fig. 3 for crystal 57-4 has two

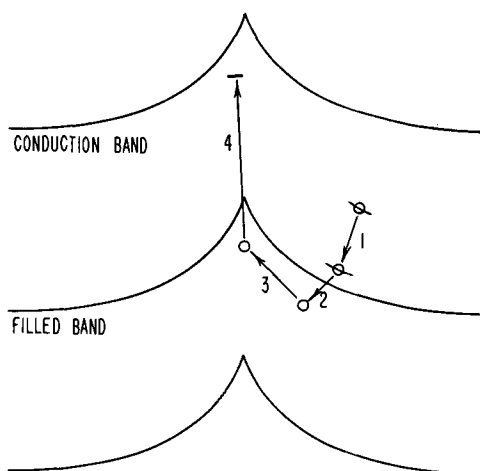


FIG. 8. Proposed recombination due to infrared

possible explanations. At low voltage, quenching may be determined by a residual internal barrier which is diminished by the applied potential and is supplanted at high voltages by other barriers, or, on the basis of Klasens' suggestion, the recombination region may change depending on the applied voltage.

The characteristics of Fig. 4 and 5 may be understood in terms of the relative amounts of infrared and photoconductive light. At high relative photocurrent, infrared may effect a fixed amount of recombination, resulting in a constant change in current independent of the total current through the crystal. At relatively low photocurrents the infrared is not effectively useful for quenching due to either an insufficient number of trapped holes or electrons, so that the diminution in current due to infrared increases as the photocurrent is increased.

The shift with temperature of the peaks of the infrared quenching spectrum of cadmium sulfide, of the same amount as the change in forbidden band width, implies that either the bottom of the conduction band or the top of the valence band moves with respect to the infrared absorption centers. If the nature of change in forbidden band width with temperature were known, it could help to decisively determine whether infrared frees electrons or holes.

ACKNOWLEDGMENTS

The author is indebted to Mr. M. E. Bishop who grew the crystals used, to Mr. S. Cress for the spectroscopic analysis, to Dr. R. E. Kagarise for calibration of the gray filters at 1.4, and to Dr. H. A. Klasens of the Philips Gloeilampenfabrieken, Eindhoven, for his helpful suggestions.

Any discussion of this paper will appear in a Discussion Section to be published in the June 1956 JOURNAL.

REFERENCES

1. A. E. HARDY, *Trans. Electrochem. Soc.*, **87**, 355 (1945).
2. G. R. FONDA, *J. Opt. Soc. Amer.*, **36**, 382 (1946).
3. S. H. LIEBSON, *This Journal*, **101**, 359 (1954).
4. H. KALLMAN, Prog. Rpt. 4, Fluorescence and Conduction Phenomena, NYU, May 1954.
5. N. T. MELAMED, *This Journal*, **97**, 33 (1950).
6. R. FRERICHS, *Phys. Rev.*, **76**, 1869 (1949).
7. D. PEARLMAN, N. R. NAIL, AND F. URBACH, "Preparation and Characteristics of Solid Luminescent Materials," John Wiley & Sons, Inc., New York (1948).
8. R. FRERICHS, *Phys. Rev.*, **72**, 594 (1947).
9. A. ROSE, *RCA Rev.*, **12**, 362 (1951).
10. E. A. TAFT AND M. H. HEBB, *J. Opt. Soc. Amer.*, **42**, 249 (1952).
11. H. C. FROELICH, *This Journal*, **100**, 280 (1953).
12. H. A. KLASENS, *ibid.*, **100**, 72 (1953).
13. M. E. BISHOP AND S. H. LIEBSON, *J. Appl. Phys.*, **24**, 660, 963 (1950).
14. F. A. KRÖGER, *Physica*, **7**, 1 (1940).
15. H. A. KLASENS, Private communication.

Studies on Alternating-Current Electrolysis

III. Effects of Concentration on Polarization Capacity and Polarization Resistance¹

A. EDWARD REMICK AND HERBERT W. McCORMICK

Department of Chemistry, Wayne University, Detroit, Michigan

ABSTRACT

The main purpose of this work was to study the influence of electrolytic concentration on the equivalent series capacitance (C_s) and resistance (R_s) of an a-c cell and to analyze these three variables into their components. The cell electrolytes were aqueous solutions containing equimolar concentrations of potassium ferrocyanide and ferricyanide together with potassium sulfate or sodium benzene sulfonate as supporting electrolytes. Platinum electrodes were used and the interelectrode distance was variable. A suitable cleaning method for platinum was discovered which gave reproducible electrodes.

Studies at low current densities resulted in the discovery of a component of the resistance which has its seat at the electrode surface and is frequency-independent. Adding this circuit element (R_L) to Grahame's equivalent circuit and using his mathematical theory of the faradaic admittance together with the authors' bridge data made it possible to calculate the equivalent series capacitance (C_s^*) and resistance (R_s^*) of the faradaic branch of the circuit. The variations of C_s^* , R_s^* , and R_L with depolarizer concentration, ionic strength, and frequency were studied. It was found that the variations of C_s^* and R_s^* with frequency and depolarizer concentration accorded well with the quantitative requirements of Grahame's theory only if the speed of electron transfer were considered to be much faster (i.e., Grahame's θ to be much smaller) than had hitherto been suspected. No satisfactory theory was found to account for the variations of C_s^* and R_s^* with the ionic strength.

INTRODUCTION

Contemporary research on a-c electrolytic cells has been directed largely toward the goal of describing the polarization process in terms of an "equivalent circuit" which will represent adequately the known electrical properties of the cell. Although certain complexities sometimes occur which seem to demand additional circuit elements, there seems to be general agreement at the present time on what might be called a basic equivalent circuit which is adequate in the absence of these complexities. This basic circuit is, in the authors' opinion, best represented by Grahame's (1) diagram, although it differs only in symbolism from those used by Rozental and Ershler (2), Randles (3), and Gerischer (4). Grahame's circuit is the same as that shown in Fig. 1 except that R_L has been added. In this figure, C_d is the double layer capacitance at a single electrode; θ is a pure resistance related to the activation energy of ionic discharge; W is the "Warburg impedance" brought into being by concentration polarization; R_T is the electrolytic resistance of the entire cell; i_T is the total current through the cell; i_C is the charging current; and i_F is the faradaic current.

¹ Manuscript received August 6, 1954. This paper was prepared for delivery before the Chicago Meeting, May 2 to 6, 1954.

Some additional related symbols which are used in this paper are as follows. R_s and C_s are, respectively, the equivalent series values of the resistance and capacitance of the whole cell. R_s^* and C_s^* are the corresponding values for the faradaic branch of the half-cell. It is customary to use the equation

$$R_s = R_T + \Delta R \quad [1]$$

to indicate that R_s may be broken down into two series components, one (R_T) independent of the frequency, the other (ΔR) dependent on it. It appears that ΔR increases as the electrolytic concentration decreases (2, 8-10). An exception to this generalization was found by Jones and Christian (8) who observed that ΔR decreased with decrease in concentration when platinum electrodes were used in potassium chloride solution. Grahame (11), using mercury electrodes in various salt solutions, found that ΔR is zero when no faradaic current flows.

The same investigators mentioned above in relation to the equivalent circuit [see (5)] have also succeeded in developing from basic principles a mathematical theory which extends the earlier theory as developed by Warburg (6) and Krüger (7). It explains the origin and describes the properties of the circuit elements, most of which are not the conventional circuit elements of physics.

Certain phases of the mathematical theory of the faradaic admittance have been tested experimentally. The theory demands that plots of R_s^* and X_s^* ($= 1/C_s^*\omega$) against $1/\sqrt{\omega}$ (where ω is the frequency in radians per second) be linear and parallel. Such linear relations have been found by Rozental and Ershler (2) using a mercury electrode in a solution of mercurous nitrate containing a large excess of perchloric acid, by Gerischer (12) using a mercury electrode in mercurous perchlorate containing a large excess of perchloric acid, by Randles (13) using both mercury and platinum electrodes with various redox systems including the ferrocyanide-ferricyanide system, and by Vetter (14) who used platinum electrodes with the iodide-iodine system in 1*N* sulfuric acid solution.

The mathematical theory also expresses R_s^* and C_s^* as functions of the concentration(s) of the depolarizer(s) (i.e., of the "potential-determining substances"). No one except Vetter (14) appears to have checked this phase of the theory experimentally. He found that the "complex diffusion resistance" (i.e., the "Warburg impedance" of Grahame) multiplied by $\sqrt{\omega}$ is a linear function of the reciprocal of the concentration of one component of his redox system when the concentration of the other is held constant. This relationship is required by the theory. He also demonstrated that the redox system in question gave the required relationship between concentration and exchange current. However, despite these demonstrations of accord between theory and experiment, diffusion constants calculated from the variation of the "complex diffusion resistance" with the concentration did not accord well with values given in the literature.

The effect of concentration on the double layer capacity has been formulated in terms of the thermodynamic theory of electrocapillarity by Grahame (15).

Much evidence is to be found in the chemical literature that poorly conducting layers are formed on solid electrodes during electrolysis by either direct or alternating currents and give rise to "resistance polarization" (19). Vetter (14) has remarked that an electrode-layer resistance should theoretically be accompanied by a capacitance, but that in practice this capacitance is found to be negligible. He argued that the electrode-layer resistance, when it occurs, must be added to the electrolytic resistance. In line with this suggestion the authors have added an electrode-layer resistance, R_L , to the basic equivalent circuit to give the circuit shown in Fig. 1.

It is hoped that this research will be of value in furnishing a test of the theoretically predicted relation between concentration and the faradaic admit-

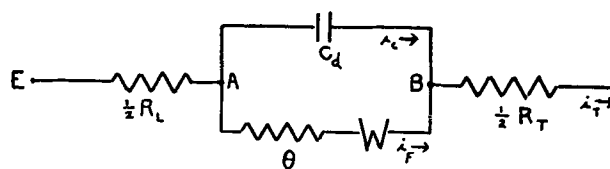


FIG. 1. Equivalent circuit for half-cell. Platinum electrode is placed at *E*.

tance by using a different redox system from that used by Vetter and carefully controlling conditions so that the two "components" of the concentration effect, viz., ionic strength and concentration of the depolarizer as such, can be studied separately. This has been done using conditions of especial interest to the authors' plans for future research, viz., solid electrodes (platinum), a reversible redox system (ferrocyanide plus ferricyanide), and alternating current without superimposed direct current. As far as they are aware, the authors' test of the theory in relation to the concentration of the depolarizer is the first one made at constant redox ratio (i.e., the ratio of the concentration of oxidant to that of reductant). A further objective is to determine whether or not an additional resistance occupying a place in the equivalent circuit indicated by R_L in Fig. 1 is present under the chosen experimental conditions and to study its dependence on ionic strength and depolarizer concentration in case it is found to exist.

EXPERIMENTAL METHOD

Measurements of the resistance and capacitance of the electrolytic cells were made by means of an impedance bridge constructed in the same general manner and using the same circuit elements as the bridge described by Shaw and Remick (16) except that: (a) shielded wire was used much more judiciously than before in order to improve frequency-independence, (b) both the source of alternating current and the oscillograph used as a null point detector were isolated from the bridge by shielded transformers (General Radio Co.'s type 578-B), (c) a Ballentine model 300 electronic voltmeter was used as a voltage amplifier in the detector circuit, (d) the power amplifier was shielded, and (e) a somewhat different type of electrolytic cell was used. As before, the cell was immersed in a constant temperature bath kept at $30^\circ \pm 0.1^\circ$, purified nitrogen was bubbled through it, and the platinum electrodes employed were made by sealing platinum disks in glass tubing so that the platinum surfaces were flush with the ends of the tubes. The new features of the cell were: (a) electrodes were mounted one above the other and the upper electrode was mounted in a threaded brass sleeve so that the interelectrode

distance could be varied and measured with a cathetometer, and (b) a piece of glass tubing, open at both ends, was slipped over the electrodes. Its inside diameter was just large enough to allow free motion of the upper electrode within it, and its upper end projected above the surface of the solution. Its purpose was to provide a conducting path of fixed diameter so that the interelectrode distance would be the only geometrical variable.

Resistances of the connecting wires and the mercury columns within the electrode tubes were measured and found to be utterly negligible.

R_T and ΔR were determined by a method introduced by Miller (17) and used effectively by Jones and Christian (8). This method is based on the equation

$$R_s = \frac{l}{a\kappa} + \Delta R \quad [2]$$

where l is the interelectrode distance in centimeters, κ is the specific conductance of the electrolyte, and a is the electrode area in square centimeters. It is evident from equation [2] that a plot of R_s against l will give a straight line with an R_s intercept equal to ΔR . Equation [1] can then be used to calculate R_T .

The potassium sulfate, potassium ferrocyanide, and potassium ferricyanide used were Baker's analyzed reagents. Sodium benzene sulfonate was prepared from a "practical" grade of benzene sulfonic acid and twice recrystallized.

Reproducibility of Electrodes

The difficulty of getting reproducible measurements with metallic electrodes under nonequilibrium conditions is well known. The most reproducible results were obtained by immersing the electrodes in the alkaline cyanide solution recommended by Shaw and Remick (16) and cleaning them anodically for 2 min and cathodically for 4 min using 3 v with an electrode separation of about 1.8 cm. This cycle of operations was performed three times. The electrode was very quickly washed with distilled water, then with a portion of the cell solution, and immediately immersed in the cell. Electrodes so prepared gave steady readings after approximately 30 min and never changed after that by more than 2% on standing for 24 hr. In order to establish the reproducibility of electrodes prepared by this method, the electrodes were immersed in the solution of ionic strength 0.2314 shown in Table I, and allowed to stand 20–40 min; bridge measurements were made at a frequency of 800 cps. The electrodes were then removed and cleaned again. This complete cycle was carried out nine times. The mean deviation was $1.5 \mu\text{F cm}^{-2}$ (0.78%) for C_s and 0.2 ohm (0.31%) for R_s . The corresponding maximum deviations from the mean were $4 \mu\text{F cm}^{-2}$ (2.1%) and 0.5 ohm (0.77%). As a further check on reproducibility, a completely independent check run was made on the dispersion of C_s and R_s at ionic strength 0.2314 (Table I). Resistance measurements checked to within a few tenths of an ohm and the capacitance measurements within $2 \mu\text{F}$

TABLE I. *Q*-dispersion as a function of ionic strength

Ferrocyanide = 0.005M; ferricyanide = 0.005M; supporting electrolyte = K_2SO_4 ; half-wave area = 0.685 microcoulomb/cm²; interelectrode distance = 1.80 cm; electrode area = 0.253 cm²; capacitance given in microfarads/cm², resistance in ohms/cm

Freq. (cps)	Ionic strength							
	0.2314		0.3821		0.5300		0.6805	
	C_s	R_s	C_s	R_s	C_s	R_s	C_s	R_s
200	343.5	52.37	359.2	33.33	369.9	24.31	397.6	19.73
400	252.1	51.61	258.1	31.65	267.5	23.58	278.1	19.18
600	200.9	51.31	202.5	31.52	215.2	23.28	215.1	18.95
800	174.8	51.15	176.3	31.37	185.3	23.12	192.2	18.80
1000	156.1	51.03	158.8	31.30	168.6	23.00	173.7	18.67
1500	122.8	50.85	127.1	31.09	134.6	22.82	138.8	18.47
2000	100.3	50.75	103.6	30.97	112.5	22.69	118.2	18.38
2500	86.9	50.73	88.6	30.92	97.7	22.64	101.4	18.34
3000	77.1	50.62	88.0	30.84	90.5	22.62	92.6	18.29
3500	69.9	50.57	73.4	30.79	82.8	22.52	84.9	18.24
4000	63.5	50.55	67.6	30.74	77.9	22.47	78.6	18.19
5000	53.4	50.45	57.9	30.64	67.8	22.44	69.9	18.14
	$R_T = 33.39$ $R_L = 16.64$		$R_T = 19.76$ $R_L = 10.35^*$		$R_T = 14.92$ $R_L = 7.03$		$R_T = 11.81$ $R_L = 5.99$	

* Plot of R_s against $1/\sqrt{\omega}$ was slightly curved.

cm⁻² except at 400 cps where the deviation was 4.4, and at 200 cps where it was 18 (or 5.2%).

A related difficulty occurs when electrodes are subjected to high current densities. When the current density gets high enough, a sort of "hysteresis" sets in. Bridge readings become unstable, drifting with time, and, if the current density is lowered, the resistance and capacitance show reluctance to return all the way to their former values. A similar hysteresis was observed by Slygin and Frumkin (18) in making direct-current charging curves for platinum in aqueous sulfuric acid.

RESULTS OF MEASUREMENTS

Most of the dispersion studies reported earlier (16) were made at constant current density, this fact being emphasized by designating them as "*I*-dispersion" studies. Dispersion measurements reported in this paper are of the "*Q*-dispersion" type (i.e., the number of coulombs per half-cycle—the "half-wave area"—being kept constant). All measurements reported in the present paper were made at low current densities corresponding to a half-wave area of 0.685 microcoulomb/cm². In all cases the electrodes were cleaned by the authors' improved technique. No distortion of the voltage or current waves was ever observed.

Electrode Layer Resistance

Q-dispersion plots of R_s against $1/\sqrt{\omega}$ were all linear, with the one exception noted in Table I. Extrapolated values of R_s at infinite frequency were higher than R_T as determined by extrapolation to zero interelectrode distance. Inasmuch as the latter method gave the same values of R_T as determined by the Kohlrausch method (i.e., using platinized electrodes), it was deemed reliable, and the higher values obtained by the frequency extrapolation interpreted to mean that there must be at the electrode surface a frequency-independent component of R_s . Reasons are given later for suspecting that this resistive component is not the resistance associated with surmounting an activation energy hump in the electron transfer step, symbolized as θ by Grahame (1), but rather a resistance associated with a poorly conducting layer on or at the electrode surface. Tentatively it will be called the "electrode layer resistance" (R_L) and put into the equivalent circuit as shown in Fig. 1. This means that ΔR has two components, one depending and one not depending on the frequency, and that equation [1] may be rewritten as follows:

$$R_s = R_T + R_L + R_\Delta \quad [3]$$

where R_Δ is the frequency-dependent component of ΔR .

In a series of preliminary experiments R_L varied from 2.3 to 10.3 ohms/cm² in a solution having the composition of the second one in Table I when the electrodes were cleaned by different methods. It is interesting to note that the improved method of cleaning electrodes makes a constant contribution to R_L as shown by a check run on the solution of ionic strength 0.2314 (Table I). The value of R_L obtained in this run was 16.37 ohms cm⁻² which compares favorably with the value of 16.64 given in the table.

Effect of Concentration

Tables I to IV give data on the effects of ionic strength, supporting electrolyte, and concentration of depolarizer on C_s , R_s , R_Δ and their dispersions. Values of R_T and R_L are also given. Ionic strength

TABLE II. *Q*-dispersion of C_s for supporting electrolyte

Supporting electrolyte = K₂SO₄; half-wave area = 0.685 microcoulomb/cm²; interelectrode distance = 1.80 cm; electrode area = 0.253 cm²; capacitance given in microfarads/cm².

Freq.	Ionic strength			
	0.2314 C_s	0.3821 C_s	0.5300 C_s	0.6805 C_s
200	8.94	9.12	9.11	9.10
400	8.78	8.82	8.88	8.93
600	8.63	8.66	8.82	8.85
800	8.48	8.55	8.73	8.78
1000	8.37	8.44	8.67	8.74
1500	8.08	8.23	8.53	8.64
2000	7.88	8.08	8.41	8.56
2500	7.70	7.93	8.31	8.45
3000	7.53	7.82	8.18	8.36
3500	7.32	7.71	8.10	8.29
4000	7.17	7.60	8.01	8.21
5000	6.96	7.34	7.84	8.08

TABLE III. *Q*-dispersion in sodium benzenesulfonate solution

Ferrocyanide = 0.005M; ferricyanide = 0.005M; supporting electrolyte = sodium benzene sulfonate; ionic strength = 0.2314; half-wave area = 0.685 microcoulomb/cm²; interelectrode distance = 1.80 cm; electrode area = 0.253 cm²; R_T = 35.93 ohms/cm²; R_L = 17.03 ohms/cm².

Freq.	C_s	R_s
200	350.7	54.87
400	249.6	54.16
600	203.3	53.79
800	172.5	53.69
1000	156.9	53.61
1500	125.2	53.43
2000	105.9	53.36
2500	91.2	53.28
3000	83.2	53.23
3500	75.2	53.18
4000	67.8	53.13
5000	60.5	53.05

TABLE IV. *Q*-dispersion as a function of concentration of depolarizer

Depolarizer = ferrocyanide and ferricyanide; redox ratio = unity; supporting electrolyte = K_2SO_4 ; half-wave area = 0.685 microcoulomb/cm²; ionic strength = 0.6805.

Freq.	m. of OX. and Red.							
	0.005M		0.010M		0.015M		0.0425M*	
	C_S	R_S	C_S	R_S	C_S	R_S	C_S	R_S
200	397.6	19.73	736.9	19.91	1096	20.49	2693	25.58
400	278.1	19.18	534.1	19.51	763.7	20.24	1998	25.53
600	215.1	18.95	430.7	19.45	638.4	20.16	1611	25.50
800	192.2	18.80	380.5	19.38	569.1	20.11	1466	25.48
1000	173.7	18.67	342.3	19.33	517.0	20.06	1311	25.45
1500	138.8	18.47	282.9	19.23	427.2	20.01	1137	25.43
2000	118.2	18.37	237.7	19.18	351.4	19.96	1069	25.40
2500	101.4	18.34	210.3	19.15	312.7	19.94	932	25.40
3000	92.6	18.29	194.5	19.13	294.3	19.93	785	25.37
3500	84.9	18.24	175.3	19.10	265.5	19.91	699	25.37
4000	78.6	18.19	162.7	19.08	245.8	19.88	681	25.35
5000	69.9	18.14	145.0	19.03	226.9	19.86	646	25.32
	$R_T = 11.81$ $R_L = 5.99$		$R_T = 12.27$ $R_L = 6.55$		$R_T = 12.82$ $R_L = 6.93$		$R_T = 16.95$ $R_L = 8.35$	

* Ferrocyanide and ferricyanide only (no supporting electrolyte).

values were calculated on a molarity basis. From this data, the following conclusions can be drawn.

1. At constant concentration of depolarizer, R_L decreases as the ionic strength increases. At constant ionic strength, R_L increases rather rapidly as the depolarizer concentration increases. The relative magnitudes of this decrease and increase were judged from the numerical values of the slopes of the respective curves.

2. At constant concentration of depolarizer, C_S increases moderately as the ionic strength increases. At constant ionic strength, C_S increases markedly as the depolarizer concentration increases. Fig. 2 shows clearly that in the presence of sufficient supporting electrolyte (i.e., all points except the one at 0.0425M) C_S is a linear function of the depolarizer concentration and that the rate of change of C_S with the concentration is greater at lower frequencies, the half-wave area being constant.

3. In view of the method used for the calculation of R_{Δ} , values cannot be expected to show good precision. The figures indicate that R_{Δ} is almost independent of ionic strength and decreases with an increase in depolarizer concentration.

It remains to be shown whether the above conclusions involve the ionic strength as such. In order to answer this question, sodium benzene sulfonate was used in place of potassium sulfate as supporting electrolyte at a total ionic strength of 0.2314 (Table III). Comparison of this data with the corresponding data of Table I shows that: (a) R_L is the same, within the limits of precision with which R_L can be reproduced by successive cleaning operations, in supporting electrolytes of two different charge types, at

the same total ionic strength and the same depolarizer concentration; (b) when C_S is plotted against $1/\sqrt{\omega}$, all points fall on the same straight line regardless of which supporting electrolyte was used; and (c) values of ΔR are rather accurately the same for the two experiments, but values of R_{Δ} range from 0.9 to 1.7 ohms less (or an average of 1.3 ohms less) for sodium benzene-sulfonate than for potassium sulfate. The discrepancy in the two sets of R_{Δ} values is clearly the result of the difficulty of reproducing

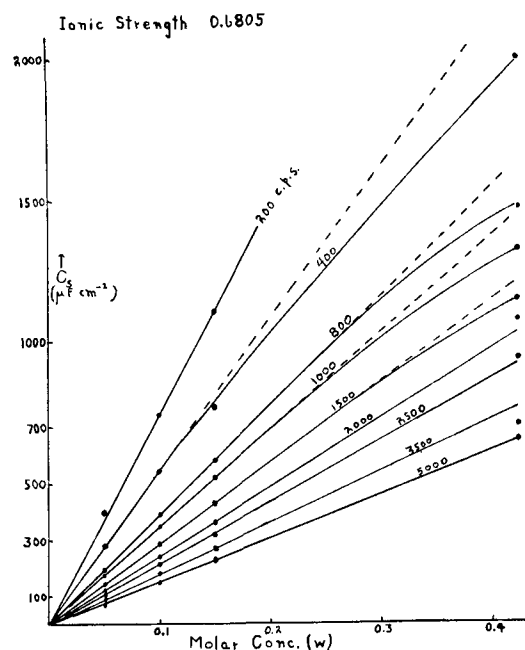


FIG. 2. Polarization capacitance (C_S) as a function of depolarizer concentration (data from Table IV).

exactly the same electrode surface each time, as shown by the fact that the difference in the two values of R_L is 1.5 ohms in the opposite direction (cf., equation [3]). Apparently, then, alteration of the kind of supporting electrolyte does not affect R_Δ .

In Fig. 2 all points correspond to the same ionic strength, but no supporting electrolyte was used in the most concentrated solution. The fact that, at each frequency, only the point corresponding to the most concentrated solution fails to be on a straight line going through the origin shows that part of the effect of the supporting electrolyte is something other than an ionic strength effect. It is presumably the elimination of electrical migration of the depolarizer ions.

Although it clearly would be desirable to have more data bearing on the subject, one can tentatively conclude from the above discussion plus the observations (a), (b), and (c) that conclusions 1, 2, and 3 are correctly stated in relation to "ionic strength."

Determination of the Double Layer Capacity

A satisfactory theoretical analysis of the data demands an accurate value for the double layer capacity. The method involving an extrapolation of C_s to a zero value of $1/\sqrt{\omega}$ is not to be recommended for Q -dispersion data when alternating current alone is used because the double layer capacity, C_d , is a function of E_{AB} (the potential drop from A to B of Fig. 1) and E_{AB} changes with the frequency because the Warburg impedance is frequency-dependent.

Therefore, C_d was determined by measurements on the supporting electrolyte alone as is commonly done in polarography. Results are given in Table II. Ionic strengths listed in Table II are not actual values but those which would obtain if enough depolarizer were added to each potassium sulfate solution to make the solution 0.005M in both ferrocyanide and ferricyanide. Thus, each value of C_s in Table II may be taken to be one-half of the C_d value corresponding to the same ionic strength and the same frequency in Table I (note that C_s refers to the whole cell and C_d to one electrode).

The slight dispersion observed in the capacitance values given in Table II probably is to be ascribed to a slight participation of some extraneous faradaic process. Assuming that this extraneous process persists in the presence of a ferrocyanide-ferricyanide mixture, the authors' method of correcting for the effect of the double layer capacity would correct incidentally for the extraneous impedance. In any event, the correction is a small one.

THEORETICAL INTERPRETATIONS

In seeking a theoretical interpretation of the authors' observations, first turn to Grahame's theory of the faradaic admittance (1). All of his equations are developed for the faradaic branch of the equivalent circuit. This means that C_s and R_s must be related mathematically to the corresponding quantities C_s^* and R_s^* for the faradaic branch alone. Proceeding by the conventional method of a-c circuit analysis up to the point where the horizontal and vertical components are separated, and introducing R_Δ from equation [3],

$$\frac{2R_\Delta}{R_\Delta^2 + X_s^2} = \frac{R_s^*}{(R_s^*)^2 + (X_s^*)^2} \quad [4]$$

$$\frac{2X_s}{R_\Delta^2 + X_s^2} - C_d\omega = \frac{X_s^*}{(R_s^*)^2 + (X_s^*)^2} \quad [5]$$

where X_s and X_s^* are the reactances corresponding respectively to C_s and C_s^* . These two equations may now be solved simultaneously to get:

$$R_s^* = \frac{M}{M^2 + N^2} \quad [6]$$

and

$$C_s^* = \frac{M^2 + N^2}{N\omega} \quad [7]$$

where

$$M = \frac{2R_\Delta}{R_\Delta^2 + X_s^2} \quad [8]$$

and

$$N = \frac{2X_s}{R_\Delta^2 + X_s^2} - C_d\omega \quad [9]$$

Grahame's theory leads to his equations [38] and [39]. Using the authors' symbols, they become

$$R_s^* = \theta + \eta/\sqrt{\omega} \quad [10]$$

$$C_s^* = 1/\eta\sqrt{\omega} \quad [11]$$

θ is expected to be zero for reversible systems and η is defined by the equation

$$\eta \equiv \sum_i \beta_i \nu_i / \sqrt{2\epsilon_i} \quad [12]$$

where

$$\beta_i \equiv \partial E / \partial w_i \quad [13]$$

Here w_i is the concentration, expressed in coulombs per cubic centimeter, of the i th kind of substance at a distance from the electrode "just exceeding that at which the effect of the double layer begins to be appreciable." When diffusion occurs in the aqueous phase and a supporting electrolyte is pres-

TABLE V. Calculated values of pseudocapacitance (C_s^*) and pseudoresistance (R_s^*)
(Resistance is in ohm/cm², capacitance in microfarad/cm²)

Ionic strength, Conc. of OX. & Red.	0.6805		0.6805		0.6805		0.6805		0.5300		0.3821		0.2314	
	0.005M		0.010M		0.015M		0.0425M		0.005M		0.005M		0.005M	
Freq. (cps)	R_s^*	C_s^*	R_s^*	C_s^*	R_s^*	C_s^*	R_s^*	C_s^*	R_s^*	C_s^*	R_s^*	C_s^*	R_s^*	C_s^*
200	1.00	794	0.56	1457	0.37	2192	0.14	5927	1.23	744	1.17	719	1.23	687
400	0.73	556	0.35	1066	0.24	1525	0.12	4004	0.86	540	0.82	518	0.84	505
600	0.62	429	0.33	863	0.21	1276	0.10	3230	0.71	435	0.77	410	0.69	402
800	0.54	384	0.29	765	0.18	1138	0.09	2946	0.64	376	0.69	359	0.61	350
1000	0.48	347	0.27	689	0.15	1080	0.08	2632	0.58	343	0.66	328	0.49	309
1500	0.37	275	0.22	570	0.13	855	0.07	2289	0.49	276	0.56	265	0.46	245
2000	0.32	233	0.19	478	0.10	699	0.05	2154	0.42	229	0.50	216	0.42	199
2500	0.31	200	0.18	425	0.09	622	0.05	1884	0.40	201	0.48	187	0.41	174
3000	0.29	182	0.16	395	0.09	590	0.04	1570	0.39	191	0.43	190	0.35	152
3500	0.26	166	0.15	355	0.08	528	0.04	1402	0.34	170	0.42	156	0.33	137
4000	0.23	152	0.14	328	0.07	486	0.02	1358	0.31	160	0.41	146	0.32	124
5000	0.21	134	0.12	290	0.05	447	0.01	1280	0.30	141	0.34	119	0.26	100

ent in a sufficiently high concentration to reduce the transference numbers of the depolarizer ions to zero, ν_i is the number of equivalents of an ion produced by chemical action when one faraday of electricity crosses the phase interface. According to Grahame's conventions, ν_i has a value of -1 for ferricyanide ions and $+1$ for ferrocyanide ions. Finally, ϵ_i is the diffusion coefficient of the substance W_i , and E is the potential across the entire double layer corrected for the IR drop.

Equations [10] and [11] give a simple method of comparing experiment and theory. They require that plots of both R_s^* and C_s^* against $1/\sqrt{\omega}$ be linear and that the same value of η be obtained from the slope of either curve. Both curves should pass through the origin (if θ is zero). Randles' approximate equations [16] and [17] also demand these same linear relations.

The necessary data for making these tests have been computed from the data given in Tables I, II, and IV and are assembled in Table V. C_s^* is Grahame's "pseudocapacitance" and R_s^* may reasonably be called "pseudoresistance" when θ is zero. They were calculated by use of equations [7] and [6], respectively. All plots of R_s^* against $1/\sqrt{\omega}$ are linear except the one at 0.0425M and, with the same exception, all curves at ionic strength 0.6805 pass through the origin within ± 0.02 ohm. (It should be recalled that the 0.0425M solution contained no supporting electrolyte.) With the same exception, the plots of C_s^* against $1/\sqrt{\omega}$ are linear for the solutions of ionic strength 0.6805, although for the 0.010M solution the points at 200 and 400 cps lie off the line just sufficiently to suggest slight curvature. These lines very nearly pass through the origin. With solutions of lower ionic strength, the lines are all curved at their low frequency ends, the curvature decreasing as the ionic strength increases, until at 0.5300

the line is almost linear and at 0.6805 completely linear.

The next phase of the test is to show that the values of η calculated respectively from the dispersion curves of R_s^* and C_s^* are the same. This may be done by eliminating η from equations [10] and [11] to get Grahame's equation [41], viz., $R_s^* C_s^* \omega = 1$ when $\theta = 0$. Values of this product are readily calculated from the data in Table V and are given in Table VI for the solutions of highest ionic strength. Agreement with theory is very good up to 2500 cps for the solution in which the excess of supporting electrolyte is the greatest.

The above tests furnish reasonably good verification for the equations developed by Grahame and by Randles insofar as they are concerned with the dispersion of C_s^* and R_s^* . This leads to examination of the concordance between theory and experiment achieved with relation to variations of the concentration of the depolarizer in the bulk of the solution, the ionic strength being maintained constant.

TABLE VI. Values of $R_s^* C_s^* \omega$ for solutions of ionic strength 0.6805

Freq.	Depolarizer conc.		
	0.005	0.010	0.015
200	1.00	1.02	1.02
400	1.02	0.94	0.92
600	1.00	1.07	1.01
800	1.05	1.11	1.03
1000	1.04	1.17	1.00
1500	0.97	1.18	1.05
2000	0.95	1.14	0.92
2500	0.98	1.20	0.93
3000	0.80	1.21	1.06
3500	0.95	1.20	0.79
4000	0.09	1.13	0.84
5000	0.88	1.07	0.76

Experimentally, plots of the bulk concentration of oxidant (or reductant) against the values of C_s^* at ionic strength 0.6805 (Table V) look like Fig. 2, i.e., the lines are linear up to 0.015M and nearly pass through the origin. It is not surprising that the points at 0.0425M fail to fall on the straight lines since no supporting electrolyte was used in this solution. Corresponding plots of R_s^* against the reciprocal of the depolarizer concentration are straight lines passing through the origin. No point lies more than 0.02 ohm off the line even though the points for the 0.0425M solution are included. Below 1000 cps the points lie on the lines within 0.01 ohm (the precision measure of R_s).

Evidence that these linear relationships are in accord with theory is supplied by the fact that they are demanded by Randles' equations [16] and [17]. However, if these equations are to be used for ferrocyanide-ferricyanide solutions, they involve the assumption that the diffusion coefficients of ferrocyanide and ferricyanide are the same. This assumption is not completely justified since Kolthoff and Lingane (20) give 0.74×10^{-5} and 0.89×10^{-5} cm² sec⁻¹, respectively, for the diffusion coefficients at infinite dilution.

Grahame's equations express concentrations in terms of w_i , not in terms of concentrations in the bulk of the solution, and are therefore difficult to apply rigorously to the authors' experimental data. An approximate solution of the problem may be achieved, however, on the basis of two reasonable assumptions: (a) equilibrium in the electron transfer reaction is continuously established between the electrode and the adjacent layer of electrolyte, and (b) using time-average values, $w_{ox} = C_{ox}$ and $w_{red} = C_{red}$, where C symbolizes molar concentrations in the bulk of the solution. The first assumption is surely justified at sufficiently low frequencies, the determination of the maximum valid frequency being an experimental matter. In regard to the second assumption, it must be recognized that bridge measurements give only average values of R_s and C_s and these are related to average values of w_{ox} and w_{red} . In the steady state (or, better, in the cyclic state), which is presumably achieved in the electrolytic cell when alternating current alone is used, it would seem that w_{ox} would vary cyclically above and below C_{ox} so that on the average the two would be equal for small currents. A similar statement applies to w_{red} and C_{red} .

The Nernst equation in terms of concentrations rather than activities is given by

$$E = E_o - (RT/nF) \ln (w_{ox}/w_{red}) \quad [14]$$

Partial differentiation of this equation with respect to concentration and combination with equation

[13] gives:

$$\beta_{ox} = \partial E / \partial w_{ox} = -RT/nFw_{ox} \quad [15]$$

$$\beta_{red} = \partial E / \partial w_{red} = RT/nFw_{red} \quad [16]$$

Combination of equations [12], [15], and [16], introduction of the numerical values for ν , and recognition that in the poised solutions $C_{ox} = C_{red} = w_{ox} = w_{red} = C$, yields the equation:

$$\eta = \frac{RT}{nFC} \left(\frac{\sqrt{2\epsilon_{red}} + \sqrt{2\epsilon_{ox}}}{2\sqrt{\epsilon_{ox}\epsilon_{red}}} \right) \quad [17]$$

Combination of equations [11] and [17] gives:

$$C_s^* = \frac{2nFC}{RT\sqrt{\omega}} \left(\frac{\sqrt{\epsilon_{ox}\epsilon_{red}}}{\sqrt{2\epsilon_{red}} + \sqrt{2\epsilon_{ox}}} \right) \quad [18]$$

If the temperature and frequency are held constant and assuming, as a first approximation, that in the presence of an appreciable excess of supporting electrolyte and at constant ionic strength the diffusion coefficients are independent of C , equation [18] becomes:

$$C_s^* = kC \quad [19]$$

where k is a constant. Similarly, equations [10] and [17] give:

$$R_s^* = \frac{k'}{C} + \theta \quad [20]$$

Remembering that $\theta = 0$ for reversible reactions, it is obvious that equations [19] and [20] are the desired equations showing that C_s^* and R_s^* are linear functions of C and $1/C$, respectively, and that both curves pass through the origin, as observed experimentally in the presence of a fairly large excess of supporting electrolyte. This same dependence of C_s^* and R_s^* on the concentration is demanded by equation [4] of Rozental and Ershler (2) although their constants are not the same as the authors'—indeed their equations were developed for a metal-metallic ion type of electrode.

The relationship between the constants in equations [19] and [20] is:

$$k = 1/k'\omega \quad [21]$$

This equation can be tested by determining the two constants, respectively, from the slopes of the plots

TABLE VII. Test of equation [21]

f	k	$1/k'\omega$	f	k	$1/k'\omega$
200	0.0378	0.0382	2000	0.0119	0.0130
400	0.0273	0.0286	2500	0.0105	0.0109
600	0.0216	0.0215	3000	0.0098	0.0098
800	0.0194	0.0183	3500	0.0089	0.0097
1000	0.0175	0.0175	4000	0.0081	0.0097
1500	0.0133	0.0141	5000	0.0073	0.0087

of C_s^* against C and of R_s^* against $1/C$. Table VII gives the calculated values of k and $1/k'\omega$. The comparison is very satisfactory, especially in view of the difficulty of getting precise values for R_s^* . It is apparent, incidentally, that the assumptions which went into equation [21] are good approximations to the truth at frequencies below 1000 cps.

CRITICAL CONSIDERATION OF ELECTRODE-LAYER RESISTANCE

The accord between theory and the experimental data was achieved on the basis of two debatable assumptions, viz.: (a) there is a resistance R_L , tentatively described as an electrode-layer resistance, entering the equivalent circuit as shown in Fig. 1; and (b) the resistance θ is essentially zero for the ferrocyanide-ferricyanide system under present experimental conditions.

These two assumptions are closely related and may be considered critically. Accepting the equivalent circuit of Fig. 1 with neither R_L nor θ equal to zero and using equation [11] and the definition of reactance, the reactance of the faradaic branch is given by:

$$X_s^* = 1/C_s^*\omega = \eta/\sqrt{\omega} \quad [22]$$

Combination of equations [4], [10], and [22] gives:

$$\frac{2R_\Delta}{R_\Delta^2 + X_s^2} = \frac{\theta + \eta/\sqrt{\omega}}{\theta^2 + 2\theta\eta/\sqrt{\omega} + 2\eta^2/\omega} \quad [23]$$

At infinite frequency this reduces to

$$(R_\Delta)_{\omega=\infty} = 2\theta \quad [24]$$

and substitution of 2θ for R_Δ in equation [3] gives

$$(R_s)_{\omega=\infty} = 2\theta + R_L + R_T \quad [25]$$

as the limiting value of R_s at $\omega = \infty$.

If neither θ nor R_L is zero, the extrapolation method used to get R_L gives, instead, $R_L + 2\theta$. From these data there appears no way in which R_L and θ can be evaluated separately, so the expedient of ascertaining whether the assumption of a zero value for θ or for R_L is in better accord with the experimental facts is used.

When θ is zero, theory demands that $R_s^*C_s^*\omega = 1$. The data were shown to be in rather good accord with this equation when R_L was taken into account. When θ is not zero, this relationship becomes

$$(R_s^* - \theta)C_s^*\omega = 1 \quad [26]$$

When R_L is taken as zero, θ being evaluated from equation [25] and R_s^* and C_s^* calculated from equations [6] and [7] using $R_\Delta = R_s - R_T$ for the evaluation of M and N , one finds that equation [26] is not at all in accord with the best data in Table I. There-

fore, the assumption of a zero value for θ is in much better accord with the data than the assumption of a zero value for R_L .

It is desirable to examine critically several paradoxical questions which arise in relation to this conclusion.

Experimentally, R_s is a linear function of $1/\sqrt{\omega}$. However, it is clear from Fig. 1 and equation [10] that this could not possibly be true unless C_d were negligible and hence considered as absent from the circuit. If this were true, $1/2 R_L$ and θ would appear as two series resistances in a purely series circuit and would be indistinguishable. Yet when the validity of equation [26] was compared with that of equation $R_s^*C_s^*\omega = 1$, it was found that it made a great deal of difference whether θ or R_L was assigned a value of zero. This could only be true if C_d had a very appreciable influence.

The answer to this paradox emerges clearly from the following considerations. It can readily be shown that the following equation comes from Grahame's equations, equations [10] and [11], and the authors' equivalent circuit:

$$R_\Delta = \frac{2(\theta + \eta/\sqrt{\omega})}{1 + \eta C_d \sqrt{\omega} + C_d^2 \omega^2 \left(\theta^2 + \frac{\theta\eta}{\sqrt{\omega}} + \frac{2\eta}{\omega} \right)} \quad [27]$$

The third term in the denominator is negligible so that, if C_d is to be negligible in the determination of R_Δ , it is necessary that

$$\eta C_d \sqrt{\omega} \ll 1 \quad [28]$$

Similarly, it may be shown that if C_d is to be negligible in the determination of the quantity $C_s^*R_s^*\omega$, it is necessary that

$$\eta C_d \sqrt{\omega} \ll \frac{X}{\theta^2 \omega + \eta^2 + X} \quad [29]$$

where $X = \theta\eta\sqrt{\omega} + \eta^2$. Over the frequency range employed, the term on the right hand side of the inequality [29] is much smaller than unity and, therefore, condition [29] is much more difficult to satisfy than condition [28]. This fact explains the paradox and emphasizes that the required relation, $R_s^*C_s^*\omega = 1$, should give a sensitive test by which to distinguish between resistances occupying, respectively, the positions of θ and R_L in Fig. 1.

Another question which deserves brief consideration is this: if R_L results from a poorly conducting surface layer, why is it not shunted by a capacitance in Fig. 1? Considering that Vetter (14), like the authors, found no evidence that such a capacitance is appreciable, it may be concluded tentatively that such may well be the case. This is not unreasonable since one may readily calculate from the equation for a parallel plate condenser that, if the dielectric

constant of the electrode layer is about 15, then the minimum thickness of the layer required to render its capacitance negligible within limits of error and within the range of R_L values would be from 15 to 80 Å at 200 cps and proportionately larger at higher frequencies. Such layers could easily escape visual detection on electrodes like those used whose surfaces are dull, not shiny.

It has been pointed out that the data in Table IV compel one to conclude that an increase in the depolarizer concentration at constant ionic strength and constant redox ratio results in an increase of R_L . This is the reverse of the effect to be expected for θ , as is clear from Grahame's equation [24]:

$$\frac{\partial i}{\partial E} = \frac{1}{\theta} = (w_1 k_1 \alpha n^2 F^2 / RT) \exp(\alpha n F E / RT) \\ + [w_2 k_2 (1 - \alpha) n^2 F^2 / RT] \exp[-(1 - \alpha) n F E / RT]$$

This is an additional reason for concluding that the extrapolated value $(R_s)_{\omega=\infty}$ is not 2θ .

Evidence unequivocally establishing the nature of R_L has not been presented, but it has been established that R_L : (a) is a resistance which is frequency-independent over the range 200 to 5000 cps, (b) has its seat at the electrode surface, (c) is of a magnitude dependent on the method employed in cleaning the electrodes, (d) increases with increase in depolarizer concentration at constant ionic strength and constant redox ratio, (e) decreases with increasing ionic strength at constant depolarizer concentration and constant redox ratio, and (f) fits best into the equivalent circuit as pictured in Fig. 1.

Points (a), (b), and (f) are in accord with the findings of Falk and Lange (19) in their studies on the resistance of thin electrode layers and with the experience of Vetter (14). Point (c) also suggests that R_L is an electrode layer resistance. Points (d) and (e) make it clear that part of the electrode layer is built up after the electrode is immersed in the solution and indeed this accords with observations that the impedance bridge readings became constant only after the electrodes had been immersed for about a half hour. Point (d) suggests that either the ferrocyanide or ferricyanide ions, or both, are adsorbed on the electrode and that the thicker or more complete layer which would form at higher concentrations impedes the electron transfer. Finally, point (e) might conceivably mean that the adsorbed layer is permeable to the supporting electrolyte. Beyond these suggestions the authors do not wish to venture at the present time.

EFFECT OF IONIC STRENGTH

Table V shows that an increase in ionic strength at constant depolarizer concentration and constant

frequency results in an increase of C_s^* , while R_s^* usually rises slightly to a maximum and then falls comparatively rapidly. The maximum may not be real.

There is no theory which is even in semiquantitative accord with these experimental results. One theory, based on the diminution of coulombic interactions between the electrode and the depolarizer ions caused by an increase in ionic strength, this diminution being reflected in a decrease in the rate constant (13), is not acceptable. This is so because the electron transfer is not rate controlling. The possibility that ionic strength affects the activity coefficients of the depolarizer ions, thereby resulting in a thermodynamic effect, has also been considered. To test this possibility, the Debye-Hückel limiting law was used in connection with equations [11] and [17] and showed that the change of C_s^* with the ionic strength thus predicted occurred in a direction opposite to that observed experimentally. Of course the limiting law would not be expected to hold accurately at the concentrations used, but it is probably safe to conclude that the observed effect of ionic strength on C_s^* is not to be ascribed primarily to this thermodynamic influence.

There remains the possibility that alterations in ionic strength affect C_s^* because electrical migration of the depolarizer ions is not completely eliminated in any of the solutions of Table I except the one of highest ionic strength. This possibility could be investigated, at least in principle, by using Grahame's theory of the faradaic admittance (1) and developing the equations which would follow from that theory if electrical migration were not assumed to be absent. If it could be done and combined with the "thermodynamic effect" to give equations in accord with experimental observations, it would give a means of determining the charge type of the participating species in electro-redox reactions. Such information would be very valuable to those engaged in the study of redox mechanisms.

ACKNOWLEDGMENT

The authors wish to acknowledge with gratitude the generous financial support given to this research project by The Office of Naval Research.

Any discussion of this paper will appear in a Discussion Section to be published in the June 1956 JOURNAL.

REFERENCES

1. D. C. GRAHAME, *This Journal*, **99**, 370C (1952).
2. K. ROZENTAL AND B. ERSHLER, *Zhur. Fiz. Khim.*, **22**, 1344 (1948).
3. J. E. B. RANGLES, *Disc. Faraday Soc.*, **1**, 11 (1947).
4. H. GERISCHER, *Z. physik. Chem.*, **193**, 286 (1951).
5. B. V. ERSHLER, *Zhur. Fiz. Khim.*, **22**, 683 (1948).
6. E. WARBURG, *Ann. Physik. u. Chem.*, **67**, 493 (1899).

7. F. KRÜGER, *Z. physik. Chem.*, **45**, 1 (1903).
8. G. JONES AND S. M. CHRISTIAN, *J. Am. Chem. Soc.*, **57**, 272 (1935).
9. M. WIEN, *Ann. Physik. u. Chem.*, **58**, 37 (1896).
10. S. BARNARTT, *This Journal*, **97**, 235 (1950).
11. D. C. GRAHAME, *J. Am. Chem. Soc.*, **68**, 301 (1946).
12. H. GERISCHER, *Z. Elektrochem.*, **55**, 98 (1951).
13. J. E. B. RANGLES, *Trans. Faraday Soc.*, **48**, 828, 937 (1952).
14. K. J. VETTER, *Z. phys. Chem.*, **199**, 285 (1952).
15. D. C. GRAHAME, *Chem. Revs.*, **41**, 441 (1947).
16. M. SHAW AND A. E. REMICK, *This Journal*, **97**, 324 (1950).
17. C. W. MILLER, *Phys. Rev.*, [2], **22**, 622 (1923).
18. A. SLYGIN AND A. FRUMKIN, *Acta Physicochim. U.R.S.S.*, **3**, 791 (1935).
19. G. FALK AND E. LANGE, *Z. Naturforsch.*, **1**, 388 (1946); *Z. Elektrochem.*, **54**, 132 (1950).
20. I. M. KOLTHOFF AND J. J. LINGANE, "Polarography," p. 52, Interscience Publishers, Inc., New York (1952).

Potentiometric Titrations in Liquid Ammonia

VIII. Mercury-Saturated Mercury(II) Chloride Working Reference Electrode^{1,2}

GEORGE W. WATT AND DONALD M. SOWARDS

Department of Chemistry, The University of Texas, Austin, Texas

ABSTRACT

The results of an investigation of the mercury-mercury(II) halide electrode in liquid ammonia are reported. Variation of electrode potential with mercury(II) ion concentration was determined by measurement in concentration cells. These data have been interpreted and the activity coefficients of mercury(II) iodide, alone and in potassium iodide solutions, are estimated. Harned's rule was found to be obeyed in the mixed-electrolyte solutions.

It is shown that the mercury-saturated mercury(II) chloride electrode is a reversible electrode that rapidly establishes and maintains the same potential within limits which permit its use as a working reference electrode in liquid ammonia. The potential of this electrode with respect to the standard mercury-mercury(II) iodide electrode was found to be -0.068 ± 0.004 v.

A direct derivation of Harned's rule in functional form is illustrated and discussed. Variation of the coefficient α_{12} in dilute solutions is verified by experimental results, which also suggest that these coefficients are independent of solvent and dielectric constant, and are a function of temperature at higher concentrations.

INTRODUCTION

Previous work (1) shows that the difference indicator electrode is a satisfactory reference electrode for potentiometric titrations in liquid ammonia. However, the potential of this electrode was not found to be reproducible, which prohibits an accurate comparison of titration curves based on its potential. The low emf-sensitivity of measurements made with this electrode does not permit its use in cases where small changes in potential must be measured.

Concurrent with the characterization of the difference indicator electrode, equipment and procedures suitable for the study of simple electrodes in liquid ammonia were developed. It was also shown that the physical parameters of the cell, at least within the present limits, do not effect the results obtained.

Cady and Groening (2) found that, in iodide, chloride, and nitrate solutions, the mercury-mercury(II) ion electrode has a low metal-deposition over-voltage. Laitinen and Shoemaker (3) conducted a polarographic investigation of this electrode (the mercury pool anode) and found that the current-voltage relationship indicates a reversible two-electron electrode process³ at -36°C . They also report that the electrode potential is a function of

the mercury(II) ion concentration and is not influenced by nitrate, chloride, iodide, and ammonium ions. They confirm reported values (4, 5) for the potential of this electrode with respect to the lead-lead(II) nitrate electrode. An accurate calculation of the relative potentials in an electrochemical series in liquid ammonia is not possible, in most cases, because the activity coefficients are not known. The activity coefficient of mercury(II) iodide in a 0.1*N* solution has been estimated (5) to be 0.05.

This paper reports the results of measurements with various mercury-mercury(II) halide electrodes, and especially the mercury-saturated mercury(II) chloride electrode which is shown to be a reversible electrode with a rapidly attained, constant, known potential.

EXPERIMENTAL

The essential features of the cell and electrodes are shown in Fig. 1. Potentials were measured by the null method using equipment described elsewhere (1). The potential-measuring current was about 10 millimicroamp. The surface area of the metallic electrode elements in the reference electrodes was about 3 cm²; that of the mercury pool, *c*, about 10 cm².

Reagent grade chemicals and triple-distilled mercury were used in this work. Ammonia and nitrogen were purified by scrubbing them through a solution of potassium in ammonia (1). All ammonia used in the cell was taken from cylinders where it was stored over sodium amide.

¹ Manuscript received December 15, 1954.

² For previous papers in this series, see reference (1).

³ The mercury(I) ion is unstable in liquid or gaseous ammonia; reference (3) gives many references pertaining to this subject.

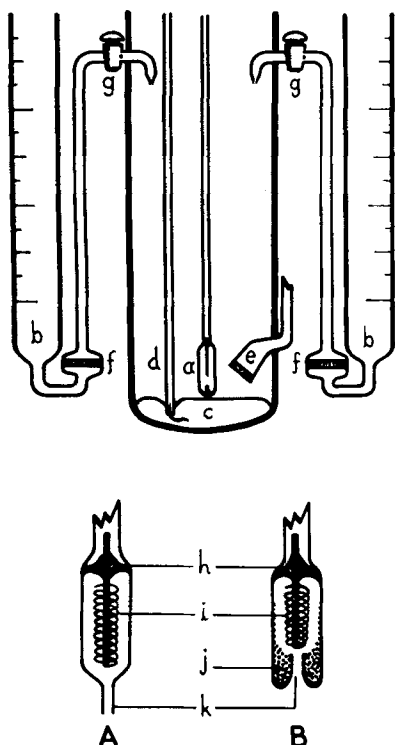


Fig. 1. Cell and electrodes. (a) Reference electrode assembly, A or B below; (b) burets; (c) mercury-pool electrode; (d) electrode lead; (e) fritted glass bubbler (stirrer); (f) fritted glass filter; (g) microstopcocks; (h) platinum lead sealed in Pyrex glass; (i) mercury electrode element supported on gold wire; (j) mercury(II) chloride; (k) capillary tube of about 0.6 mm OD.

The gas-scrubbing unit, burets, and cell were cleaned with aqua regia, rinsed with several portions of distilled water, rinsed with absolute ethanol, and dried. Potassium was placed in the scrubber, weighed quantities of electrolyte were put into the burets, mercury was put in the cell (at *c*), and the units were assembled. The entire system was evacuated to a pressure of 0.001 mm for several hours and then filled with gaseous ammonia at a reduced pressure. After ammoniation of the electrolyte was complete, the system was re-evacuated and filled with nitrogen. The nitrogen in the burets was replaced with a dilute solution of ammonia in nitrogen. Ammonia was next condensed in the gas-scrubbing unit until a 6–8 in. head of potassium solution obtained.

Standard solutions were prepared by condensing a measured volume of ammonia in the burets; the remaining gaseous ammonia was replaced with nitrogen. The transfer of solution from a buret to the cell was accomplished by regulating the nitrogen pressure above the solution in the buret. The pressure in the cell remained at about 5 mm above atmospheric pressure.

The temperature was -36.5°C , except where noted otherwise. It was determined with a toluene

thermometer which had been checked at room temperature, the freezing point of water, and the normal boiling point of ammonia. The error in temperature measurement was probably less than 0.2°C and the variation of temperature during a series of measurements was usually less than 0.5°C .

Uncertainties in concentration are considered to be the major source of experimental error, which is estimated to be about 1%. The error is probably greater in solutions more dilute than 4 mM.

Mercury(II) halides may ammonolyze or ammoniate depending on conditions of exposure to ammonia; thus, some precautions are necessary in preparing solutions of these salts in liquid ammonia. Mercury(II) chloride was used in the working reference electrode because it reacts with ammonia to produce a single, electrochemically active mercury(II) ion species which has a desirable solubility. Further, traces of mercury(I) ion⁴ react with ammonia to produce ultimately either this same mercury(II) ion species, $\text{HgCl}_2 \cdot 2\text{NH}_3$, or another, HgNH_2Cl , of considerably lower solubility (6).

Ammoniates of mercury(II) chloride and bromide are not sufficiently soluble to permit preparation of concentrated solutions of these salts. On the other hand, more care must be exercised with mercury(II) iodide if ammonolysis is to be prevented. When an evacuated system containing mercury(II) iodide is suddenly filled with gaseous ammonia at atmospheric pressure, the salt ammonolyzes irreversibly to produce a fused red material of relatively low solubility in liquid ammonia. Solutions of this compound undergo a gradual decomposition which is evident because of the simultaneous precipitation of a rust colored solid, probably Hg_2NI (7). Even though these solutions are stabilized by dilute ammonium iodide, they are not satisfactory for the type of work described below.

When mercury(II) iodide is exposed to ammonia either diluted with nitrogen or at a reduced pressure, the familiar $\text{HgI}_2 \cdot 2\text{NH}_3$ is produced slowly. It has a rather high decomposition pressure (7) and may be decomposed simply by reducing the pressure. At -35°C , this ammoniate, in the presence of gaseous ammonia, changes to a colorless solid which is probably $\text{HgI}_2 \cdot 4\text{NH}_3$ (7). Repeated ammoniation and deammoniation did not appear to influence the electrochemical activity of the species occurring in solutions of the ammoniated salt; thus, it was considered suitable for use in the present study.

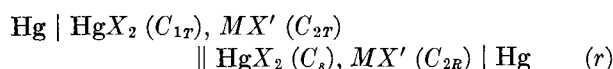
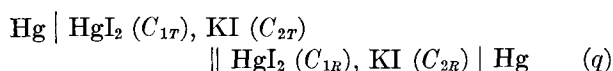
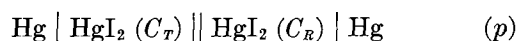
Solutions of mercury(II) acetate produce a much smaller change in potential with changing concen-

⁴ Mercury(II) ion reacts with the mercury at the electrode to produce mercury(I) ion unless the electrode is filled with ammonia. Therefore, it is desirable to store the electrode in an ammonia atmosphere.

tration than solutions of mercury(II) halides. Further, as potassium bromide or iodide solution is added to mercury(II) acetate solution, the change in potential indicates an initial increase in activity followed by a decrease as more halide solution is added. Also, it was observed that mercury(II) halide solutions containing traces of water were less active than anhydrous solutions, which is contrary to a previous report (3). It is evident that there is extensive and specific interaction of mercury(II) ion with the various species present in these solutions.

Solutions of dipotassium tetraiodomercurate(II) 2-hydrate were found to be similar in electrochemical activity to solutions of ammoniated mercury(II) iodide containing traces of water. Both of these, as well as solutions of di-(tetra-*n*-butylammonium) tetraiodomercurate, decomposed to produce ammoniated mercury(II) iodide and the other iodides when the liquid ammonia evaporated. The latter anhydrous compound is quite stable, while the corresponding potassium salt usually decomposes on dehydration. These observations, as well as the results of electrical measurements in the mixed-iodide solutions, suggest that the triiodomercurate and tetraiodomercurate ions are not present in solution.

The results in this work were obtained using three types of concentration cells with homoionic liquid junctions:



where *M* is Na or K ion, *X* and *X'* are halide ions which are not necessarily the same, *C* is molar concentration, subscripts *T* and *R* distinguish between the electrodes at *c* and *a*, respectively (Fig. 1), and 1 and 2 indicate the electrolyte in mixed-electrolyte solutions. Cells (*p*) and (*q*) involve the use of electrode *A* of Fig. 1, while cell (*r*) utilizes electrode *B* with *C_s* as the saturation concentration.

In a typical series of measurements, solution of composition *C_R* (or *C_{1R}* - *C_{2R}*) was prepared in the cell by appropriate additions from the burets. The reference electrode, which had previously been evacuated and filled with gaseous ammonia, was inserted in the solution. Gaseous ammonia condensed, thereby completely filling the electrode compartment with solution. Additions were then made to the cell to give a series of solutions of composition *C_T* (*C_{1T}* - *C_{2T}*). The solution was stirred with nitrogen at *e* in Fig. 1.

INTERPRETATION OF DATA AND RESULTS

Because the experimental error is relatively large, experimental data are not tabulated here; rather, the method of interpretation and the results of its application are given.

Mercury-saturated mercury(II) chloride electrode.—The reproducibility of the potential of this electrode (Fig. 1A) was determined by measuring its potential with respect to a series of Hg-HgX₂ (*C_{1T}*) electrodes, where *C_{1T}* had a sufficient number of values between 0.2 and 5.0 mmolar for the construction of the log *C_{1T}* vs. potential curve. These measurements were made at random times, with electrodes in general use, and under conditions of present use of reference electrodes in this laboratory, i.e., varying the supporting electrolyte and its concentration, and with minor variations in temperature. Since mixed mercury(II) halides are present in the electrode whenever it is reused, results are reported for both newly prepared (New) and previously used (Reused) electrodes. (In general, the reuse of this kind of electrode is not recommended; it is quite easy to clean and recharge.) The mercury(II) halide used at electrode *T* was also varied to determine whether any significant deviation dependent upon halide ion occurred.

The log *C_{1T}* vs. potential curves show a slight curvature, but they are sufficiently linear to permit a short range interpolation. Thus, the potential of the Hg-HgCl₂ (sat'd) electrode vs. a Hg-Hg²⁺ (0.001 m) electrode was found for a number of conditions. Results are shown in Table I. The slope of the curves from which these data were taken shows no unaccounted for deviation from the theoretical slope calculated for a two-electron electrode process; average deviation is 0.0005, maximum deviation is 0.0015. The emf-sensitivity of the measurements

TABLE I. *Reproducibility of the potential of the Hg-HgCl₂ working reference electrode*

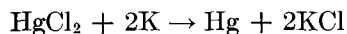
Reference electrode No.	<i>MX'</i>	<i>C_{2T}</i> mM	Reference potential vs. Hg-HgX ₂ (1 mM) electrode (v)	<i>X</i>	Temp °C
1 New	KBr	93	0.012	Br	-38
1 Reused	KI	94	0.020	I	-36
2 New	KCl	16 ^a (sat'd)	0.016	C ₂ H ₅ O ₂	-37
2 Reused	NaCl	98	0.013	I	-36
2 Reused	KBr	37	0.019	Br	-34
3 New	KBr	13	0.017	Br	-36
4 New	KBr	18	0.019	Br	-38
4 Reused	KI	79	0.014	I	-41

Avg: 0.016 ± 0.004 v.

^a See reference (12).

was about 0.05 mv and the potential was observed to remain constant to within 0.1 mv for 1-hr periods.

The concentration of a saturated solution of mercury(II) chloride was determined by potentiometric titration of a measured volume of saturated solution with standard potassium solution in liquid ammonia. The average of three determinations based on the reaction



was $C_s = 0.019 \pm 0.004$ moles/l at -37°C . Using the activity coefficient below (from Fig. 3), the potential of the mercury-saturated mercury(II) chloride electrode vs. the standard mercury-mercury(II) iodide electrode is -0.070 ± 0.001 v. This compares quite favorably with the value of -0.067 ± 0.004 v calculated from the data of Table I.

An electrode similar to that in Fig. 1B was constructed with a cadmium electrode element, i , and containing cadmium(II) chloride at j . This was used as the reference electrode for the determination of the $\log C_{1T}$ vs. potential curve for mercury(II) iodide in a cell of type (p) with no supporting electrolyte present. The solubility of CdCl_2 at 25°C is 0.001 moles/l (8) and is probably about one-tenth of this at -36°C . Using the limiting law activity coefficients (see below) for these concentrations, the potential of the standard Cd-CdCl₂ electrode with respect to the standard Hg-HgI₂ electrode is calculated to be -0.93 v. This compares favorably with the reported value (5) of -0.933 v at -50°C .

In the course of measurements with the Hg-sat'd HgCl₂ electrode, potentials with respect to the (Pt)H₂-NH₄Br, Pb-PbCl₂, and (Pt)K-KBr electrodes at -37°C were found to agree with the reported values (5) at -50°C . However, data for these comparisons were obtained in the course of other work and values within 0.05 v were considered to be in agreement.

The Hg-HgCl₂(sat'd) electrode attains a constant potential within 30 min after it is filled. The electrode recovered from the effects of short-circuiting and the application of 1 v for 15 sec within 1 min. For these and reasons mentioned below, this is considered to be a reversible electrode in so far as its use as a working reference electrode is concerned.

Activity of mercury(II) iodide in liquid ammonia solutions.—The relationship of potential E and electrolyte activity a for a concentration cell is

$$E = 2.303 \frac{RT}{nF} \log (a_T/a_R) \equiv 1/K \log (a_T/a_R) \quad (\text{I})$$

where R is the gas constant, T is the absolute temperature, n is the electron change in the electrode process, F is the faraday, the subscripts T and R

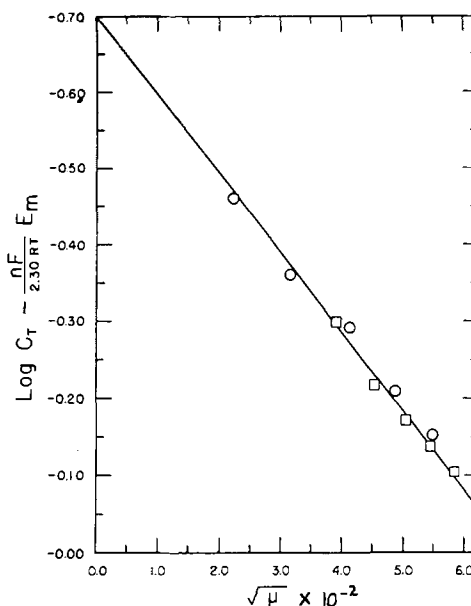


FIG. 2. Extrapolation curve according to equation (II). — extrapolation used, slope -9.70 . \square scale reading -3.284 ; \circ scale reading -5.290 .

distinguish between the electrodes in the cell, and K is as shown.

If the potential measured, E_m , differs by a constant factor, E_e , from the cell potential, E [with the usual assumptions concerning single ion activities and the distinction of the potentials in cells with transference (9a)] equation (I) gives

$$-\log f_T + (\log a_R - KE_e) = \log C_T - KE_m \equiv Y \quad (\text{II})$$

where f is the mean molar activity coefficient, C is the molar concentration, and Y is as shown.

The results of measurements in cell (p) are expressed as Y and shown as a function of the square root of the ionic strength, $\sqrt{\mu}$, in Fig. 2. The parenthetical term on the left side of equation (II) was evaluated by extrapolation in Fig. 2 and substituted with Y into equation (II) to find values of the activity coefficients. The activity coefficients were applied to the reference electrode solution and E_e was found. It is a function of the concentration of the electrolyte in the electrode compartment: C_R , mmolar, 0.16, 0.31, 0.36, 1.35; E_e , mvolts, 24.5, 7.5, 4.5, 2.5. This is the result which is expected if the major part of E_e is attributed to a resistance in the cell solution. It should be noted that in the present cell over nine-tenths of the electrolyte between the electrodes does not change during a series of measurements because it is confined to the electrode compartment and connecting tube. The tip of this tube was always within 1 mm of the surface of electrode c (Fig. 1); thus the connecting-solution resistance remains essentially constant. No account has been

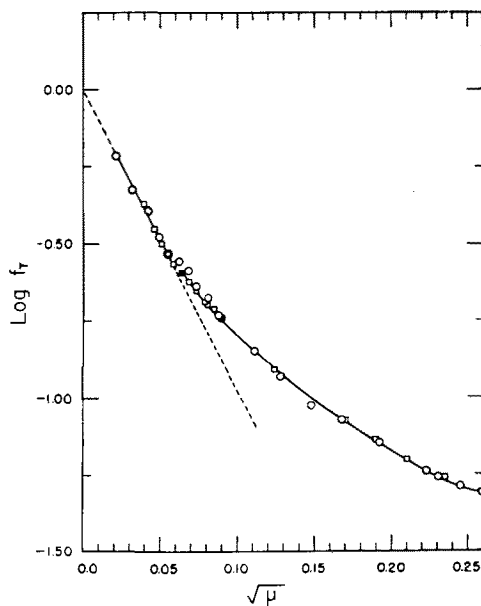


FIG. 3. Logarithm of the activity coefficient of mercury (II) iodide as a function of the square root of the ionic strength.

taken for the effects of the junction potential, except for its possible inclusion in E_e .

For measurements at higher concentrations, it is desirable to increase C_R in order to increase the electrical conductivity of the connecting solution, minimize the effects of large concentration gradients, and further lessen the chances of concentration polarization during measurement. Results at higher concentrations cannot be dealt with by means of the extrapolation procedure discussed above. In this case, the cell has been such that C_R is in the concentration range of Fig. 2. Thus, with $C_R = C_T$, the initial point in a series of measurements at high concentrations has been adjusted to data for dilute solutions. The parenthetical term on the left side of equation (II) was thus calculated and applied to the remaining data. The results of measurements over both concentration ranges are illustrated in Fig. 3. The adjusted values are represented by the solid points. The experimental curve continues in the suggested direction to $\sqrt{\mu} = 0.35$, the highest concentration measured. It is noted that $f_T = 0.05_5$ for 0.1N HgI_2 which is in almost exact agreement with Pleskov's (5) estimated value, 0.05.

Activity of mercury(II) iodide in potassium iodide solutions.—Previous work (1) as well as the results above indicate that for C_R greater than about 10 mM, $E_e \approx 0$. In this case equation (II) may be rearranged to give

$$\log C_{1R} - Y = \log f_{1T}/f_{1R} \quad (\text{III})$$

The results of measurements in cell (q) and at constant ionic strength, $\mu = \mu_{1T} + \mu_{2T}$, are seen in Fig.

4 to obey Harned's rule (10a)

$$\log f_{1T} = \log f_{(0)1} + \alpha_{12}\mu_{1T} = \log f_{1(0)} - \alpha_{12}\mu_{2T} \quad (\text{IV})$$

where $f_{(0)1}$ is the activity coefficient of mercury(II) iodide at infinite dilution in a solution of potassium iodide of ionic strength μ , $f_{1(0)}$ is the activity coefficient of mercury(II) iodide in a solution of ionic strength μ , α_{12} is a constant which is discussed below, μ_{1T} is the contribution of the mercury(II) iodide to the ionic strength of the solution, μ_{2T} is the contribution of the potassium iodide to the ionic strength of the solution, and f_{1T} is the activity coefficient of the mercury(II) iodide (in the mixed electrolyte solution).

It was found that a variation greater than 1% in the total ionic strength resulted in excessive distortion of the linear relationship shown in Fig. 4. The value of α_{12} may be found without specific knowledge of the activity coefficients on the basis of equation (III). This permits a calculation of the ratio of the limiting activity coefficients; thus, with the value of $f_{1(0)}$ or f_{1R} , all of the terms in equation (IV) may be evaluated.

Reversibility of the mercury-mercury(II) iodide electrode.—In all measurements with electrode A, there has been only one indication that the electrode was not behaving reversibly (9b); in most instances there was a potential of from 0.1 to 1 mv when identical solutions were at each electrode. This potential appeared to be reproducible and a function of the electrolyte concentration at concentrations less than about 5 mM. With total electrolyte concentrations above 0.1 m, the potential was zero for this condition. In the intermediate concentration range, the potential was small and unpredictable.

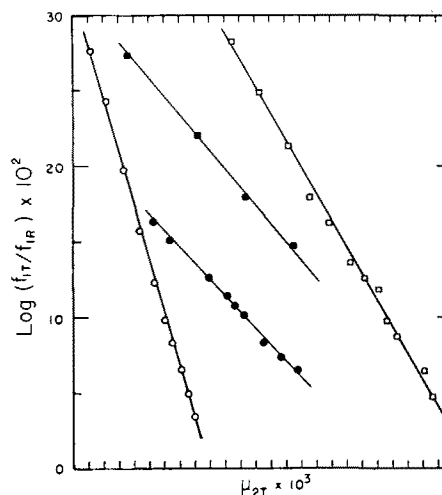


FIG. 4. Logarithm of the activity coefficient of mercury (II) iodide in solution with potassium iodide at constant total ionic strength as a function of the ionic strength of the mercury(II) iodide. Total ionic strength; \circ , 15.5 mmolar; \bullet , 50.6 mmolar; \blacksquare , 121 mmolar; \square , 322 mmolar.

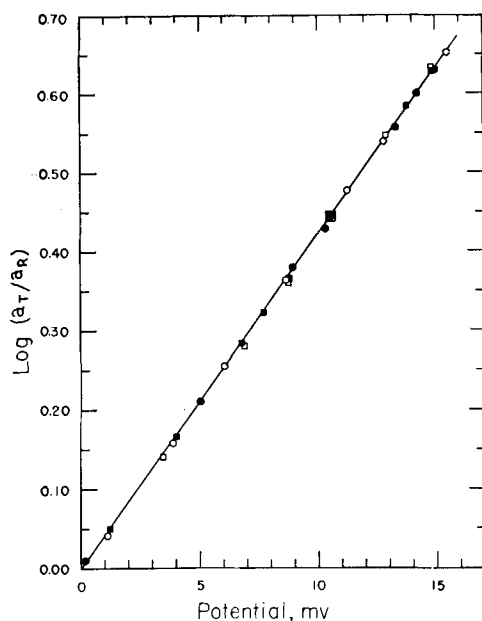


FIG. 5. The potential of the mercury-mercury(II) iodide electrode as a function of the logarithm of the activity of mercury(II) iodide. ●, No co-solute; with potassium iodide at a constant ionic strength of 15.5 mmolar ○, 50.6 mmolar ■, 322 mmolar □.

It is thought that the major part of the potential is attributable to the solution resistance, especially in the dilute solutions.

On the other hand there are many indications that the electrode was behaving reversibly. As with the previous electrode, within 20 min after the electrode was filled, the potential was constant; when the electrodes were short-circuited, they recovered within a few minutes. Vigorous stirring or stagnant conditions had no apparent effect on the measured potential. The equilibrium potential was attained within 2 or 3 min after the solution composition was changed. Equation (IV) substituted into equation (III), on rearrangement, gives

$$E_m = E = 1/K (\log f_{1(0)}/f_{1R} - \alpha_{12}\mu_{2T} + \log C_{1T}/C_{1R}) \quad (V)$$

which is the Nernst relation with the present notation. The activity coefficients taken from Fig. 3 and 4 have been used in equations (I) and (V); results are adjusted to a common scale by the addition of the required constants to the equations in order to show the results on a single plot (Fig. 5). It is seen that this criterion for reversible behavior is also satisfied. The electrode is, therefore, considered to be behaving reversibly.

DISCUSSION

While the purpose of this paper is to demonstrate the utility of the Hg-HgCl₂ (sat'd) working reference electrode and report its potential, several observa-

tions have been made during the course of this study that are of sufficient general interest to warrant further comment.

In spite of the relatively large experimental error and the possible oversimplification in interpretation of the data, the linear relationship shown in Fig. 2 strongly suggests that the Debye-Hückle limiting law is applicable to solutions of this electrolyte with concentrations as high as 1 mM. For a dielectric constant of 22 (11) and a temperature of -36.5°C , the limiting law for an electrolyte with cations of valence z_c and anions of valence $-z_a$ is

$$-\log f = 4.85 z_c z_a \sqrt{\mu} \quad (VI)$$

which results in a slope in exact agreement with that in Fig. 2. This degree of agreement is probably fortuitous.⁵

Results shown in Fig. 3 are suggestive of a high degree of ionic interaction which is not an unexpected result for solutions of electrolytes that produce small ionic species in media of low dielectric constant. The curve is not amenable to expression over any appreciable concentration range by the usual one or two parameter equations. Because of results obtained in solutions which also contained relatively high concentrations of potassium iodide, results in Fig. 3 are attributed to extensive interaction of mercury(II) ion with the solvent. This conclusion has been suggested for both silver(I) and mercury(II) ions in ammonia and was an important factor for the previous low estimate of the activity coefficient of mercury(II) iodide (5). However, as is shown below, there is specific interaction between ammoniated mercury(II) and iodide ions in these solutions.

Previous discussion (10b) of the thermodynamic theory of mixed electrolyte solutions is based on the assumed validity of Harned's rule. There appears to be little mention in the literature of the possible direct derivation of this rule and its connection with the thermodynamic theory of single electrolyte solutions, except for the implications of its application. Thus, it has been shown (10c) that α_{13} and α_{23} in

$$\log f_{13} = \log f_{(0)1} + \alpha_{13}\mu_{13} = \log f_{1(0)} - \alpha_{13}\mu_{23} \quad (VII)$$

$$\log f_{23} = \log f_{(0)2} + \alpha_{23}\mu_{23} = \log f_{2(0)} - \alpha_{23}\mu_{13} \quad (VIII)$$

are thermodynamically connected through the activity coefficients or osmotic coefficients of single electrolyte solutions. Here the notation is as in equation (IV) except for the subscripts 13 and 23 which

⁵ Sedlet and DeVries [*J. Am. Chem. Soc.*, **73**, 5808 (1951)] report a value of 23.8 for the dielectric constant of ammonia at -36°C , which results in a limiting law constant of 4.31. However, the specific electrical conductivity of the ammonia used in those measurements suggests that the solvent was contaminated [cf. reference (12)].

refer to the electrolyte in question on the basis of its being composed of cation 1 or 2 and anion 3 (which is common to both salts). It has also been shown *a posteriori* that the α 's are coefficients of ionic strength rather than concentration terms (13) and that they are essentially independent of concentration in the range between 0.5 and 5M (14). From studies in aqueous methanol it was suggested that the α 's are independent of the dielectric constant of the medium and dependent on the temperature (15).

Guggenheim (16) developed Brönsted's principle of specific interaction (17) to produce an expression that accounts for the individual characteristics of electrolytes and reduces naturally to the limiting law at high dilutions; thus for 1:1 electrolytes, for example, there results

$$\log f = \frac{A\sqrt{C}}{1 + \beta\sqrt{C}} + \beta_n C \quad (\text{IX})$$

Here, the first term on the right is the familiar Debye second approximation and β_n is a constant "interaction coefficient" which may take any value depending on the nature of the electrolyte and the value of β chosen. For the sake of simplicity, Guggenheim arbitrarily gave β the value 1 and made all of the specific properties of electrolytes appear in the β_n term. Equation (IX), when applied in this way, yields accurate activity coefficients for concentrations as high as 0.1M; further, this equation is applicable to mixed electrolyte solutions. Objections to this expression (10*d*) have been directed to the choice of standard electrolyte, i.e., setting β equal to unity. However, such a choice is not a necessity and β may be considered to be either an experimental or theoretical parameter with limited adjustability.

The working equation arrived at by Guggenheim (16*b*) considers only the interaction of cations R and anions X, and may be expressed as

$$G^{e1} = G^{sta} + (kT/V) \sum_{R,X} N_R N_X \nu_{R,X} \quad (\text{X})$$

where G^{e1} is the contribution of interionic potential to the (Gibbs') free energy of the electrolyte; G^{sta} is the contribution of the perfect Debye-Hückle electrolyte chosen as standard electrolyte to G^{e1} and has the property

$$(1/2.303 kT) \frac{\partial G^{sta}}{\partial N_i} = \frac{A\sqrt{\mu}}{1 + \beta\sqrt{\mu}} \equiv \log f^{sta} \quad (\text{XI})$$

with k , the Boltzman constant; T , the absolute temperature; V , the volume in liters; N_i , any ion; and $\nu_{R,X}$ is a coefficient based on the attractive forces between anions and cations, and which depends only on the temperature and the solvent. The original discussion of this equation should be consulted for further details.

An expression for the activity coefficients of the electrolytes in the mixed electrolyte solutions involved in the present studies may be found by taking the partial derivative of G^{e1} with respect to N_i in equation (X). In this case $2N_1 + N_2 = N_3$ and for the condition of constant ionic strength $3N_1 + N_2 = I = \text{a constant}$ which is a function of the ionic strength. Using the previous (16*b*) definition of the interaction coefficient: $\beta_{RX} = 1/2N \cdot 10^{-3} \nu_{R,X}$, where N is the Avogadro constant, there results at constant temperature⁶

$$\log f_{13} = \log f_{13}^{sta} + B(\beta_{13} - 4\beta_{23})\mu + 2B \left(\beta_{23} - \frac{\beta_{13}}{3} \mu_{13} \right) \quad (\text{XIIa})$$

$$= \log f_{13}^{sta} + B \left(\frac{\beta_{13}}{3} - 2\beta_{23} \right) \mu - 2B \left(\beta_{23} - \frac{\beta_{13}}{3} \right) \mu_{23} \quad (\text{XIIb})$$

$$\log f_{23} = \log f_{23}^{sta} + B \left(\frac{4}{3} \beta_{23} - \frac{\beta_{13}}{3} \right) \mu - 2B \left(\frac{\beta_{23}}{3} - \frac{\beta_{13}}{9} \right) \mu_{13} \quad (\text{XIIIa})$$

$$= \log f_{23}^{sta} + B \left(\frac{2}{3} \beta_{23} - \frac{\beta_{13}}{9} \right) \mu + 2B \left(\frac{\beta_{23}}{3} - \frac{\beta_{13}}{9} \right) \mu_{23} \quad (\text{XIIIb})$$

where $B = 2/2.303$. The other terms are defined above.

Comparison of equations (VII) and (VIII) with (XII) and (XIII) shows that they are identical in the functional relationship between $\log f_{13}$ and $\log f_{23}$, and μ_{13} and μ_{23} . According to equations (XII) and (XIII), the terms of equations (VII) and (VIII) are functions of the interaction coefficients, thus

$$\log f_{(0)1} = \log f_{13}^{sta} + 2/2.303 (\beta_{13} - 4\beta_{23})\mu \quad (\text{XIVa})$$

$$\log f_{1(0)} = \log f_{13}^{sta} + 2/2.303 \left(\frac{\beta_{13}}{3} - 2\beta_{23} \right) \mu \quad (\text{XIVb})$$

⁶ The present derived functional relationship results, in general, for mixed electrolyte solutions containing a single anion (cation) species and cations (anions) of different valence. For similar results with mixed electrolytes of the same valence, it is necessary to include in equation (X) terms accounting for solvent-ion, cation-cation, or anion-anion interaction. Harned [ref. (10), p. 466] has pointed out the implications inherent in neglecting the solvent-ion interaction term. Its importance has long been recognized. It first appeared in Hückle's [*Physik. Z.*, **26**, 93 (1925)] extension of the limiting law and has recently been discussed by Scatchard and Breckenridge [*J. Phys. Chem.*, **58**, 596 (1954)].

$$\log f_{(0)2} = \log f_{23}^{sta} + 2/2.303 \left(\frac{2}{3} \beta_{23} - \frac{\beta_{13}}{9} \right) \mu \quad (\text{XVa})$$

$$\log f_{2(0)} = \log f_{23}^{sta} + 2/2.303 \left(\frac{4}{3} \beta_{23} - \frac{\beta_{13}}{3} \right) \mu \quad (\text{XVb})$$

$$\alpha_{13} = 4/2.303 \left(\beta_{23} - \frac{\beta_{13}}{3} \right) \quad (\text{XIVc})$$

$$\alpha_{23} = 4/2.303 \left(\frac{\beta_{23}}{3} - \frac{\beta_{13}}{9} \right) \quad (\text{XVc})$$

Of course such term by term correspondence is no more than a necessary condition for the interpretation of Harned's rule in terms of interaction. The comparison may be carried further. Thus, Harned's recent generalization (18) is complied with

$$z_{c(1)} \alpha_{23} + \alpha_{13} = \text{constant} \neq \text{function of } \mu \quad (\text{XVI})$$

The α 's are explicitly coefficients of ionic strength rather than general concentration terms, if consistent values of α are to be calculable from (a) and (b) in equations (XII) and (XIII). The α 's also have no obvious dependence on ionic strength or concentration. While the cross-differentiation relations at constant molalities (19) cannot be found without further generalization or actual experimental values, the relationship

$$(\partial \log f_{13}/\partial N_2)_\mu = (\partial \log f_{23}/\partial N_1)_\mu$$

is satisfied, thus indicating that equations (XII) and (XIII) are self-consistent.

There is an explicit difference between $f_{(0)R}$ and $f_{R(0)}$ according to equations (XIV) and (XV), even if the f^{sta} 's are all considered to be the same. Also, the relationships

$$\log (f_{1(0)}/f_{(0)1}) = \alpha_{12}\mu \quad (\text{XVIIa})$$

$$\log (f_{2(0)}/f_{(0)2}) = \alpha_{23}\mu \quad (\text{XVIIb})$$

result from the accumulation of terms in either (a) and (b) of (XII) and (XIII), or (a), (b), and (c) of (XIV) and (XV), respectively.

On the basis of the above interpretation, the results in Fig. 4 suggest that there is specific cation-anion interaction in these solutions; this is not an unexpected result. The previous suggestion (10e) that the α 's vary at low total ionic strength is conclusively established for these solutions. In fact, from (XVIIa), the plot of $\log \alpha_{12}$ vs. $\log \mu$ should be a straight line with a slope of -1 if the term on the left side of the equation is constant. This is seen in Fig. 6 to be the result obtained using the data from

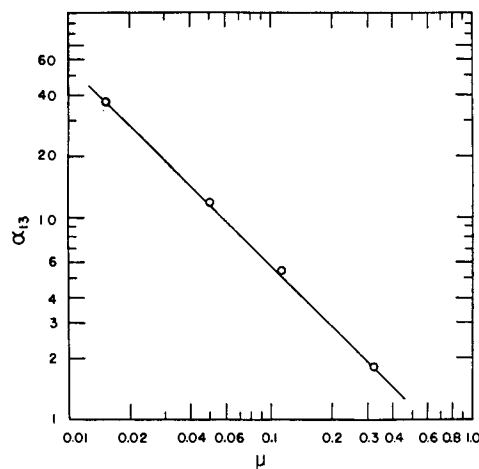


Fig. 6. Logarithm of α_{13} as a function of the logarithm of the total ionic strength in mixed-electrolyte solutions.

Fig. 4. This variation of α_{12} with ionic strength is in agreement with the conclusions of McKay and Perring (20), although, their complete expression is different from the above. Also, Glueckauf (21) suggests that Guggenheim's approach may be applied with the assumption that β_n of equation (IX) is a function of the concentration, the β_n 's being eliminated from the working equation derived. The ultimate expression is found to be applicable over a large concentration range for the cases used as illustrations.

A limited comparison of the present results with those general to aqueous solutions is possible. Harned (18) reports that $\alpha_{13} = 0.085$ for aqueous $\text{SrCl}_2\text{-HCl}$ solutions, $\mu = 3$ to 5. Using the temperature coefficient of α from results in the HCl-NaCl -aqueous methanol system (15), α_{13} in the present case should be about 0.12. Extrapolation of the curve in Fig. 6 yields a value of 0.15 for this μ range in the $\text{HgI}_2\text{-KI}$ -ammonia system. This is quite good agreement considering the nature of the comparison; it indicates that α_{13} is independent of the solvent as well as the dielectric constant of the medium. This conclusion was not entirely evident in previous work (15) since the aquated ions were present in all of the solutions.

Further application of the equations above is not possible at this time because of the limited amount of data; the present result is certainly sufficient in general applicability to conclude that Harned's rule is obeyed in these liquid ammonia solutions. The present interpretation of theory to obtain the parameters of this rule in terms of interaction coefficients is consistent with previous usage (10) and does not restrict the present applications of the rule. The conclusions offer a direction of attack and point out further the necessity for considering the interaction coefficients as variable parameters in dilute solutions, at least.

ACKNOWLEDGMENTS

This work was supported in part by the Atomic Energy Commission, Contract AT-(40-1)-1639. The liquid ammonia employed in these studies was generously supplied by the Polychemicals Department, E. I. du Pont de Nemours and Company, Wilmington, Delaware.

Any discussion of this paper will appear in a Discussion Section to be published in the June 1956 JOURNAL.

REFERENCES

1. G. W. WATT AND D. M. SOWARDS, *This Journal*, **102**, 46 (1955).
2. H. P. CADY AND A. A. GROENING, *J. Phys. Chem.*, **30**, 1597 (1926).
3. H. A. LAITINEN AND C. E. SHOEMAKER, *J. Am. Chem. Soc.*, **72**, 663 (1950).
4. F. M. G. JOHNSON AND N. T. M. WILSMORE, *Trans. Faraday Soc.*, **3**, 77 (1907).
5. V. A. PLESKOV AND A. M. MONOSSOHN, *Acta Physicochim. U.R.S.S.*, **1**, 871 (1935).
6. S. D. ARORA, W. N. LIPSCOMB, AND M. C. SNEED, *J. Am. Chem. Soc.*, **73**, 1017 (1951).
7. E. C. FRANKLIN, *ibid.*, **29**, 35 (1907).
8. C. S. GARNER, E. W. GREEN, AND D. M. YOST, *ibid.*, **57**, 2055 (1935).
9. G. KORTUM AND J. O'M. BOCKRIS, "Textbook of Electrochemistry," Elsevier Publishing Co., New York (1951), (a) p. 269, (b) p. 581.
10. H. S. HARNED AND B. B. OWEN, "The Physical Chemistry of Electrolytic Solutions," Reinhold Publishing Corp., New York (1943), (a) p. 459, (b) p. 461, (c) p. 462 ff, (d) p. 387, (e) p. 468.
11. C. P. SMYTH, "Dielectric Constant and Molecular Structure," Chemical Catalog Co., New York (1931).
12. C. A. KRAUS AND V. F. HNZIDA, *J. Am. Chem. Soc.*, **71**, 1565 (1949).
13. H. S. HARNED AND C. M. MASON, *ibid.*, **53**, 3377 (1931).
14. G. AKERLOF AND H. C. THOMAS, *ibid.*, **56**, 593 (1934).
15. G. AKERLOF, J. TEARE, AND H. TURCK, *ibid.*, **59**, 1916 (1937).
16. (a) E. A. GUGGENHEIM, *Phil. Mag.*, **19**, 588 (1935); (b) E. A. GUGGENHEIM AND R. H. FOWLER, "Statistical Thermodynamics," p. 416 ff, Cambridge University Press, New York (1952).
17. J. N. BRÖNSTED, *J. Am. Chem. Soc.*, **44**, 877 (1922).
18. H. S. HARNED, *J. Phys. Chem.*, **58**, 683 (1954).
19. E. GLUECKAUF, H. A. C. MCKAY, AND A. MATHIESON, *J. Chem. Soc.*, **1949**, S 299.
20. H. A. C. MCKAY AND J. K. PERRING, *Trans. Faraday Soc.*, **49**, 163 (1953).
21. E. GLUECKAUF, *Nature*, **163**, 414 (1949).

The Electrodeposition of Lead from Lead Phenol Sulfonate Solutions¹

HARRY C. GATOS² AND FRANK C. MATHERS

Indiana University, Bloomington, Indiana

INTRODUCTION

Organic lead sulfonates are suitable for lead electroplating because they are stable, easily prepared, sufficiently soluble in water, and their aqueous solutions exhibit satisfactory electrical conductivity. This suitability for electroplating was recognized long ago (1), but further investigation has been limited. This could be attributed to the fact that the quality of lead electrodeposits obtained from aqueous solutions of lead sulfonates in the absence of suitable addition agents is unsatisfactory (2). Successful results have been reported with aqueous solutions of lead ethylbenzenesulfonate (3) and lead toluolsulfonate (4) by employing various addition agents. Sulfonate baths have the distinct advantage of being far less hazardous in handling than the commonly used fluoborate or fluosilicate baths.

LEAD PHENOL SULFONATE BATHS AND EXPERIMENTAL TECHNIQUES

Solutions of lead phenol sulfonate were prepared by neutralizing phenol sulfuric acid with lead carbonate. Insoluble lead sulfate formed by the free sulfuric acid present in the phenol sulfuric acid was filtered, and the solution was diluted with water. From this solution the final electroplating bath was prepared containing 40 g/l of lead and 70 g/l of free sulfonic acid. About 100 ml of the solution was used in each experiment.

Lead anodes (5 x 3.5 x 1 cm) were cast in a graphite mold. The cathodes were 6.3 cm² sheets of mild steel. They were pickled with dilute hydrochloric acid, washed thoroughly with tap and distilled water, and dried before using. The anode and cathode were suspended by thin copper wire and were approximately 3 cm apart.

During electrolysis the baths were gently stirred. Slime formed from the anodes remained at the bottom of the beakers and was not disturbed by the stirring. All experiments were performed at room temperature and 2.8 amp/dm² (26 amp/ft²).

¹ Manuscript received October 26, 1954. This paper was prepared for delivery before the Boston Meeting, October 3 to 7, 1954.

² Present address: Engineering Research Laboratory, Engineering Department, E. I. du Pont de Nemours and Co., Inc., Wilmington, Delaware.

About 150 combinations of 40 different addition agents and 30 single addition agents were employed.

Addition agents were used in quantities sufficient to obtain maximum beneficial action. Usually this was accomplished with 0.1–0.2 g of solid and 1–5 ml of liquid addition agents per 100 ml of electrolyte. In some cases as much as 10 g/100 ml were employed, but to no considerable advantage. Relatively insoluble addition agents were added in sufficient quantities to insure saturation.

The time of continuous electrolysis was varied. If the electrodeposits appeared treelike, very crystalline, or nonadherent, electrolysis was interrupted within the first 24 hr, whereas in the case of adherent deposits it was carried on usually for 7–8 days.

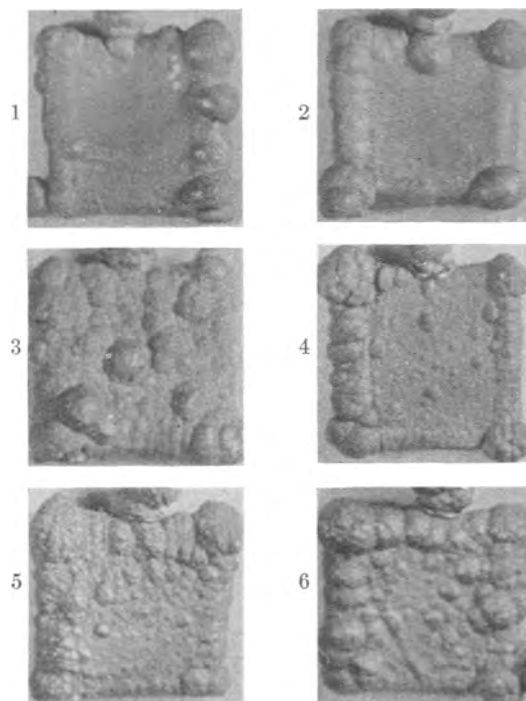


FIG. 1. Lead electrodeposits obtained from 100 ml lead phenol sulfonate electrolyte¹ at 26 amp/ft² (2.8 amp/dm²) in the presence of the following addition agents: 1—0.1 g aloes residue, 0.2 g furfural polymer, and 0.2 g goulac; 2—0.1 g aloes residue and 0.2 g furfural polymer; 3—0.1 g aloin residue, 2 cc *p*-cresol, and 0.2 g goulac; 4—0.2 g goulac and 2 cc eugenol; 5—5 cc *p*-cresol; 6—0.1 g aloes residue and 0.2 g pyrogallol.

TABLE I. *Effect of combinations of addition agents on lead electrodeposits*

No.	Addition agents	Type of electrodeposit
1	0.1 g aloes residue 2 cc <i>p</i> -cresol 0.2 g goulac	Smooth and adherent
2	0.1 g aloes residue 2 cc eugenol	Not very smooth surface
3	0.1 g aloes residue 0.2 g furfural polymer	*
4	0.1 g aloes residue 0.2 g furfural polymer 0.2 g goulac	*
5	0.1 g aloes residue 0.2 g goulac 0.1 g phenol	Similar to 1
6	0.1 g aloes residue 0.2 g pyrogallol	Not very smooth*
7	0.1 g aloes residue 0.2 g resorcinol	*
8	0.1 g aloes residue 0.2 g thymol	Similar to 1
9	0.1 g aloin residue 2 cc <i>p</i> -cresol	Rough surface
10	0.1 g aloin residue 2 cc <i>p</i> -cresol 1 cc furfural	*
11	0.1 g aloin residue 2 cc <i>p</i> -cresol 0.2 g goulac	*
12	0.1 g aloin residue 1 cc furfural 5 cc glycerol	Heavy corners
13	0.1 g aloin residue 1 cc furfural 0.2 g goulac	Knobby*
14	0.1 g aloin residue 1 cc furfural 0.1 g thymol	Similar to 1
15	0.1 g aloin residue 0.2 g furfural polymer†	Striated
16	0.1 g aloin residue 0.05 g glue 0.2 g goulac	Similar to 1
17	0.1 g aloin residue 0.2 g goulac 0.1 g phenol	Heavy corners
18	1 cc furfural 0.2 g goulac 0.2 g tannic acid	Similar to 1
19	1 cc furfural 0.2 g tannic acid	Rough surface
20	0.05 g glue 0.1 g β -naphthol	Similar to 1
21	0.2 g goulac 2 cc eugenol	*
22	0.2 g goulac 5 cc salicylaldehyde	Similar to 1

* These electrodeposits were the best obtained during this investigation. They were very adherent and dense even when approximately $\frac{1}{2}$ in. thick. They had metallic appearance and were considerably smooth. The rest of the deposits listed were also satisfactory, but to a somewhat lesser extent.

† This solid polymer was formed from common furfural after standing for about three years.

RESULTS

Electrodeposits obtained from the phenol sulfonate bath containing no addition agents were entirely unsatisfactory, having a spongelike texture. Individual addition agents improved the quality of the electrodeposits. In general, however, a single addition agent improved only one of the desirable characteristics of the electrodeposits, i.e., denseness, adherence, crystallinity, or smoothness. Among the addition agents employed individually, *p*-cresol yielded solid, adherent, and fairly smooth electrodeposits (Fig. 1, part 5). Deposits somewhat inferior to the latter, but fairly satisfactory, were obtained with glycerol, goulac, β -naphthol, phenol, resorcinol, and diphenyl sulfone.

In combining the various addition agents, an effort was made to intermix members which, when employed individually, exhibited beneficial effect on different properties of the electrodeposits. Thus, members which improved the denseness of the deposits, but did not repress the treelike formation (like pyrogallol), were combined with members which repressed the treelike formation, but not the density (like aloes residue). This approach led to very effective combinations in a number of cases. Thus, a combination of the individual addition agents mentioned above (aloes residue and pyrogallol) gave very good deposits (Fig. 1, part 6). In many cases, however, the effect of combinations of addition agents did not correspond to the sum of the individual effects.

The combinations of addition agents which gave satisfactory results are listed in Table I with a qualitative description of the nature of the electrodeposits. Some of the electrodeposits are shown in Fig. 1.

DISCUSSION

Addition agents, alone or in combinations, which favored the formation of adherent, dense, and smooth lead electrodeposits from the lead phenol sulfonate bath contained, with few exceptions, hydroxyl or carbonyl groups. These compounds have a marked tendency to form covalent, complex ions with metal cations. Upon formation of such complex ions, concentration of the free metal cations is controlled by the dissociation-equilibrium of the complex ions and is at all times maintained quite small at the cathode-electrolyte interface. This is usually a desirable condition for electrodeposition (5). To maintain equilibrium, the electrodeposited cations are replenished by dissociation of the complex. The addition agents themselves are not usually completely consumed and continue to serve as complexing agents so that relatively small amounts of addition agents may suffice for the electroposition of large amounts of metal.

High molecular weight colloidal substances like glue and goulac are effective addition agents very likely by adsorbing at the cathode and "interfering" with the crystal growth, allowing the formation of small crystallites, which in turn favor the formation of dense and adherent deposits (6).

Among the single addition agents tested, *p*-cresol proved the most efficient in electrodeposition of lead from the phenol sulfonate electrolyte. Rather simple combinations of furfural gave very satisfactory deposits. The various polymeric forms of furfural should perhaps be studied further as addition agents in sulfonate baths.

The best combination of rather easily available addition agents found for a current density of about 26 amp/ft² (2.8 amp/dm²) was 2 ml *p*-cresol, 0.2 g goulac, and 0.1 g aloin residue per 100 ml of electrolyte.

Any discussion of this paper will appear in a Discussion Section to be published in the June 1956 JOURNAL.

REFERENCES

1. W. BORCHERS, *Z. angew. Chem.*, **4**, 596 (1891).
2. A. G. BETTS, "Lead Refining by Electrolysis," p. 23, John Wiley & Sons, Inc., New York (1908).
3. F. C. MATHERS AND J. F. SUTTLE, *J. (and Trans.) Electrochem. Soc.*, **93**, 47 (1948).
4. F. C. MATHERS AND J. C. GRIESS, JR., *This Journal*, **94**, 46N (1948).
5. W. BLUM AND G. B. HOGABOOM, "Principles of Electroplating and Electroforming," 3rd ed., p. 70, McGraw-Hill Book Co., New York (1949); G. FUSEYA AND K. MURATA, *Trans. Electrochem. Soc.*, **50**, 235 (1926); G. FUSEYA AND M. NAGANO, *ibid.*, **52**, 249 (1927); F. C. MATHERS, *Proc. Am. Electroplaters' Soc.*, **27**, 134 (1939).
6. R. TAFT AND H. E. MESSMORE, *J. Phys. Chem.*, **35**, 2585 (1931); J. A. HENDRICKS, *Metal Finishing*, **41**, 134 (1943).

Formation of Manganese(II) Ion in the Discharge of the Manganese Dioxide Electrode

A. M. CHREITZBERG, JR., D. R. ALLENSON, AND W. C. VOSBURGH

Duke University, Durham, North Carolina

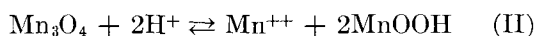
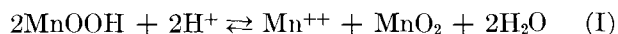
ABSTRACT

In the discharge of electrodeposited manganese dioxide electrodes in ammonium chloride electrolyte at pH 7, very little manganese(II) ion enters the solution during the first third of the discharge, but it appears at an increasing rate thereafter. The effects of current density, pH , ammonium chloride concentration, and interruption of the discharge were studied. A mechanism is suggested involving the assumptions that the electrode reaction takes place on the exterior surface of the manganese dioxide and that the primary product is a lower oxide, which reacts with the electrolyte to give the manganese(II) ion formed. Additional evidence is presented for the first assumption.

INTRODUCTION

It was shown (1, 2) that manganese(II) ion is a product of the discharge of the manganese dioxide electrode. With a large volume of electrolyte and low pH (less than 4) it may be the only manganese-containing product (1). When electrodes made by electrodeposition of manganese dioxide on graphite are discharged at pH 7, the ion is produced in considerable quantity, but the main product is an oxide (2). When the discharge is continued to a cut-off value of zero against the saturated calomel electrode, the oxide has a composition of about $MnO_{1.6}$.

Two different hypotheses may be made concerning the mechanism of manganese(II) ion formation: (A) the ion is the primary product of the electrode reaction, and it may take part in a secondary reaction with manganese dioxide, giving the oxyhydroxide, $MnOOH$ (1); (B) a lower oxide is the primary product, and this reacts with the electrolyte, giving manganese(II) ion and a higher oxide in accordance with one of the following equations:



Formation of manganese(II) ion was investigated further with results that are in better accord with the second hypothesis. Results can be correlated with the theory of the reaction mechanism previously proposed (3).

EXPERIMENTAL

Electrodes were prepared by electrodeposition of manganese dioxide on graphite rods of 0.48 cm

¹ Manuscript received October 18, 1954. This paper was prepared for delivery before the Boston Meeting, October 3 to 7, 1954.

diameter and 8 cm² surface area from an acid sulfate bath at 75°–90°C for 30 min with a current of 25 ma (3). This procedure gave a deposit with about 0.2 millimole of total manganese (2). The electrodes were washed thoroughly with water (2) and kept immersed in a solution of 2M ammonium chloride and 0.5M ammonia ($pH = 8.8$) for a week. They were then stored until used in the electrolyte to be used in the cells.

For discharge, an electrode was mounted in a central position in a glass vessel of 200-ml capacity with a cylindrical silver anode fitted around the inside wall. This had been coated with silver chloride in previous work. A Luggin capillary with its tip at a distance from the electrode approximately two to four times the tip diameter (4) allowed measurement against a saturated calomel reference electrode. Except as otherwise noted, the electrolyte was 190 ml of 2M ammonium chloride solution containing enough ammonia to give a pH of 7.3, about 0.01 mole/l.

For regulation of the temperature during discharge, the cells were placed in a test cabinet maintained at $25^\circ \pm 0.5^\circ C$. Purified nitrogen that had been washed with some of the electrolyte was passed through the cell electrolyte during discharge to provide an inert atmosphere and for stirring. Occasional checks of the pH showed that no appreciable changes occurred.

Electrodes were discharged by passage of an approximately constant current through the cells. Current was measured in terms of potential drop across a known resistance. Current and potential against the calomel electrode were measured and recorded continuously during a discharge by a L&N Speedomax, x_1 , x_2 recording potentiometer.

Samples of the electrolyte of 10 ml each were

taken at intervals during the discharge and replaced with equal volumes of fresh electrolyte to keep the total volume constant. Manganese was determined in each sample colorimetrically as permanganate after evaporation with sulfuric and nitric acids and oxidation with periodate. At the end of the discharge manganese was titrated potentiometrically in the entire electrolyte, after addition of pyrophosphate. The two methods agreed satisfactorily. In calculating the manganese(II) ion produced in the discharge, correction was made for the manganese content of the samples removed.

Some of the discharges were allowed to proceed continuously to the end, and some were interrupted at intervals. In the latter case, a sample was taken immediately after each interruption and another after the cell had stood on open circuit for 24 hr. The circuit was kept open for 24 hr after each interruption, then the discharge was continued. Some similar discharges, but without the manganese determinations, were made by Ferrell and Vosburgh (3) and the results are shown in their Fig. 6 and 7. The present data were quite similar.

RESULTS AND DISCUSSION

The amounts of manganese(II) ion formed in several discharges are shown in Fig. 1. The manganese ion found in the electrolyte, in hundredths of millimoles, is plotted against the amount of discharge in milliamperes-minutes. It can be seen that at pH 5 in the presence of zinc the formation of manganese(II) ion starts at the beginning of the discharge and continues at a slowly increasing rate throughout.

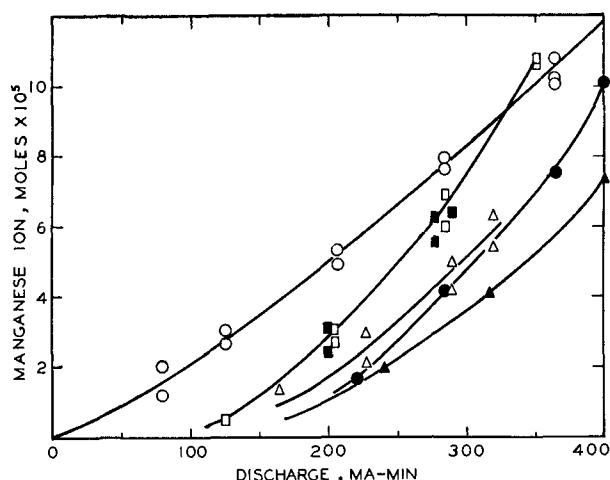


FIG. 1. Manganese(II) ion formed during the discharges of manganese dioxide electrodes. ○—Interrupted discharge with $ZnCl_2$ at pH 5, current density 0.1 ma/cm^2 ; □ and ■—two similar interrupted discharges at pH 7.3 showing reproducibility, 0.1 ma/cm^2 ; △—interrupted discharge at pH 7.3, 0.4 ma/cm^2 ; ●—continuous discharge at pH 7.5, 0.025 ma/cm^2 ; ▲—continuous discharge at pH 7.4, 0.05 ma/cm^2 .

TABLE I. Total manganese(II) ion produced in various discharges; pH 7

Current <i>ma/cm</i> ²	Capacity <i>ma-min</i>	Type of discharge	Manganese(II) ion	
			Observed <i>mmoles</i>	Calculated* <i>mmoles</i>
0.025	400	Continuous	0.100	0.125
0.05	400	Continuous	0.074	0.125
0.1	383	Continuous	0.055†	0.119
0.2	358	Continuous	0.039	0.112
0.4	346	Continuous	0.033	0.108
0.025	367	Interrupted	0.098	0.114
0.1	350	Interrupted	0.108	0.109
0.1	290	Interrupted	0.066	0.090
0.4	393	Interrupted	0.100	0.122
0.4	320	Interrupted	0.064	0.100

* Calculated from the capacity as if manganese(II) ion were the only product.

† Ammonium sulfate electrolyte.

At pH 7 without zinc, no measurable manganese(II) ion was found in the electrolyte until after 100 ma-min. Manganese(II) ion was formed at an increasing rate throughout the remainder of the discharge.

On the curves for interrupted discharges, two manganese ion values are usually given for each milliamperes-minute value, with the curve passing between them. The lower of the two manganese ion values is the amount found immediately after breaking the circuit, and the higher is the amount found 24 hr later, the circuit having been open and the nitrogen atmosphere maintained during the 24 hr. In interrupted discharges the manganese ion concentration nearly always increased during the period of open circuit, and a decrease was never observed.

Data of Fig. 1 are typical. Several other discharges agreed with those shown, but were omitted from Fig. 1 to avoid confusion. Total amounts of manganese in solution at the ends of the discharges, current densities, and capacities for the discharges at pH 7 are given in Table I.

In the last four lines of the table the reproducibility appears poor, but the lower amounts of manganese were obtained from electrodes giving abnormally low electrical capacities. Up to the points at which these latter electrodes became discharged, they agreed fairly well in manganese in solution with their duplicates. This is shown for the 0.1 ma/cm^2 discharges in Fig. 1.

The last column of Table I shows how closely the amount of manganese(II) ion formed approaches the amount calculated as if this were the only product. In one of the interrupted discharges practically the theoretical amount was formed. In the other discharges 30–86% of the theoretical amount was formed. Some discharges at pH 5 which were cut off at 125 ma-min gave an average of 0.040 ± 0.002 m mole of manganese(II) ion with no regular variation

with current density (theoretical amount, 0.039 moles).

Fig. 1 and Table I show that the more rapid continuous discharges gave less manganese in solution than the slower ones. Also, more manganese was formed in solution by the interrupted discharges than in all but the slowest continuous ones.

Absence of manganese(II) ion in the electrolyte in the first part of the discharge at *pH* 7 suggests that an oxide is the primary product of the discharge. The manganese(II) ion may be assumed to be formed by reaction of the oxide with the electrolyte when conditions are favorable.

Because of the importance of this conclusion an additional check in the early part of a discharge was made with more efficient stirring of the electrolyte. With stirring by a magnetic stirrer, no manganese(II) ion was detected after 20 ma-min of discharge, and a faint trace, about 2×10^{-6} M, was present after 40 ma-min.

Another check on the above theory is to inquire whether the lower manganese oxides, especially the oxyhydroxide and trimanganese tetroxide, do in fact react with an ammonium chloride solution of *pH* 7 or above. Samples of these two oxides prepared by precipitation (5) and having nearly the correct composition were available. These were washed repeatedly by stirring with water and decantation (as the analytical samples had been washed when the composition was determined) until excess manganese(II) salts were removed and a colorimetric test for manganese gave constant results with further washing. Then water in which the oxyhydroxide had been stirred for some time gave no trace of manganese in the test, while water stirred with trimanganese tetroxide for 2 hr gave a faint trace. On stirring with 1M ammonium sulfate (of *pH* 7.0) the oxyhydroxide gave a trace of manganese, about 7×10^{-6} M, and the trimanganese tetroxide gave 1.2×10^{-4} M after 2 hr stirring. The latter increased further with time. These experiments were carried out at about 30°C.

Reaction of trimanganese tetroxide with an ammonium sulfate solution seems to be slow. It may be assumed that the similar formation of manganese(II) ion from a reduced manganese dioxide surface is also slow. This suggests an explanation of some of the above observations. More manganese(II) ion is formed in a slow, continuous discharge than in a fast one because there is more time. The amount dissolved is not proportional to time because the closed-circuit electrode potential is higher in the slower discharges, corresponding to less reduction at the surface. More manganese(II) ion is dissolved in intermittent discharges than in continuous, because the dissolving process goes on during the period of

interruption, or at least during the first part of the period. On prolonged standing on open circuit the process should be reversed; equilibrium conditions require that at *pH* 7 the manganese(II) ion return to the electrode.



The theory of the discharge can now be made a little more detailed. In the early part of a discharge at *pH* 7, and in the absence of zinc ion, the primary reaction product is probably manganese(III) oxyhydroxide. It is probable that this is formed on the exterior surface of the manganese dioxide. Later in the discharge the oxyhydroxide is reduced further. Reduction of part of the manganese(III) ions at the surface to manganese(II) (with an accompanying decrease of oxide ion, or change to hydroxide) would give a surface resembling that of trimanganese tetroxide, subject to attack by the electrolyte.

When the circuit is broken in the latter part of the discharge, the electrode still has on its surface some manganese(II) ions which may disappear in two ways. (A) They may go into solution, accompanied by oxide or hydroxide ions. This would account for the increase in manganese(II) ion in the solution after the breaking of the circuit. (B) They may be oxidized to manganese(III) ions by the dioxide and may then diffuse into the interior of the oxide layer. In the early part of the discharge the diffusion process is the only one in operation on breaking the circuit.

At *pH* 5 an ammonium salt solution can react with manganese(III) oxyhydroxide or mixtures of this with dioxide to give manganese(II) ion in solution (5). The favorable effect of the higher hydrogen ion activity on this reaction is apparent from equation (I). Therefore, in a discharge at *pH* 5, manganese(II) ion appears in the solution soon after the beginning.

In addition to the discharges shown in Table I, three continuous discharges in 4M, 2M, and 1M ammonium chloride electrolytes, all of *pH* 7, gave totals of 0.054, 0.038, and 0.021 mmole of manganese(II) ion, respectively.

Ferrell and Vosburgh (3) assumed that the discharge reaction of electrodes of the type used in the present investigation takes place at the inner surface of the manganese dioxide, next to the graphite. Their theory is not dependent on this assumption, and it now seems much more probable that the reaction takes place on the outer surface, and the electrode potential is determined by the composition of the outer surface. The formation of manganese(II) ion is best understood if it is assumed that the reaction takes place at the surface exposed to the solution.

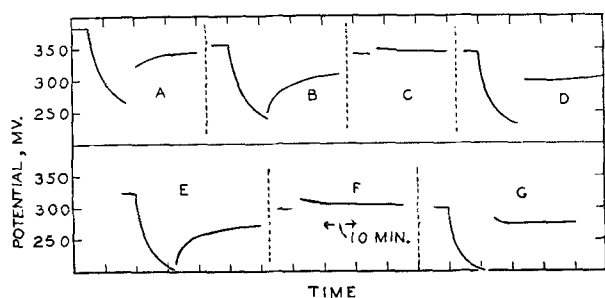


FIG. 2. Five successive 20 ma-min discharges followed by recovery periods, showing effect of pyrophosphate treatment immediately after discharge (A, D, and G) and on electrode at equilibrium (C and F); B and E are controls.

An experiment was undertaken to provide additional evidence on this point.

An electrode was discharged in 1M ammonium sulfate containing 0.01M ammonia, pH 7.0, against a lead anode in the usual way for about 20 ma-min at 1.6 ma. Then the circuit was broken, and the electrode was quickly transferred to a 1M ammonium sulfate solution containing sodium pyrophosphate at a concentration of 0.08M and having a pH of 7.0. It was kept in this solution 2 min while the solution was stirred mechanically at the same rate as during the discharge. After a quick washing with electrolyte, the electrode was replaced in the discharge vessel, and the record of its potential continued. The record of the discharge and recovery is shown in Fig. 2A. After complete recovery, a second discharge and recovery were carried out without the pyrophosphate treatment, as a control (Fig. 2B). It is evident from Fig. 2A and 2B that the pyrophosphate treatment after the first discharge accelerated the recovery from polarization. This behavior was probably the result of the extraction of some lower oxide from the electrode surface by the pyrophosphate. Following recovery from the second discharge, a pyrophosphate treatment similar to that following the first discharge was given (Fig. 2C). This delayed pyrophosphate treatment caused a small increase in potential followed by a decrease to a value slightly above the constant value preceding the treatment.

In two more 20 ma-min discharges on the same electrode the hastening of the recovery after a pyrophosphate treatment immediately following discharge was observed to an increasing extent (Fig. 2D and 2G). In the last discharge the potential immediately after pyrophosphate treatment was decreasing, followed later by an upturn in the recovery curve. The two treatments described above were separated by a 20 ma-min discharge followed by normal recovery and subsequent pyrophosphate treatment (Fig. 2E and 2F), the latter causing a somewhat larger temporary increase in potential than that of the previous delayed treatment.

The amount of manganese(II) and (III) ion that had dissolved in each of the pyrophosphate treatment solutions was determined and found to increase from the first to the third to the fifth solution, and to be present in much smaller and about equal amounts in the second and fourth solutions. A series of experiments similar to the above with a second electrode using ammonium chloride electrolyte gave comparable although less pronounced results, with practically no effect of the pyrophosphate treatment evident until the third in the series, comparable to Fig. 2D.

The use of pyrophosphate ion was based on its ability to form complex ions with manganese(II) and (III) ions. A brief treatment with pyrophosphate must extract lower oxide from the exterior surface. This causes an increase in electrode potential on an electrode which had previously been at equilibrium, when it contains sufficient lower oxide. When a freshly discharged electrode is treated with pyrophosphate, increase in potential and amount of manganese extracted is larger than for an electrode at equilibrium, indicating that there must be more lower oxide on the outside surface of the polarized electrode. The small decrease in potential following the last pyrophosphate treatment (Fig. 2G) is caused by the removal of sufficient lower oxide from the surface layer to make it richer in dioxide than the layer immediately beneath it, and diffusion of lower oxide at first takes place toward the outer layer.

A different experiment led to similar conclusions. An electrode was placed in 2M ammonium chloride electrolyte of pH 7.1 containing $10^{-3}N$ hydrogen peroxide. The solution was stirred, and the electrode potential was measured continuously. The potential dropped rapidly at first and then more slowly as in a normal discharge. After 37 min the electrode was quickly transferred to another vessel containing identical electrolyte but without hydrogen peroxide.

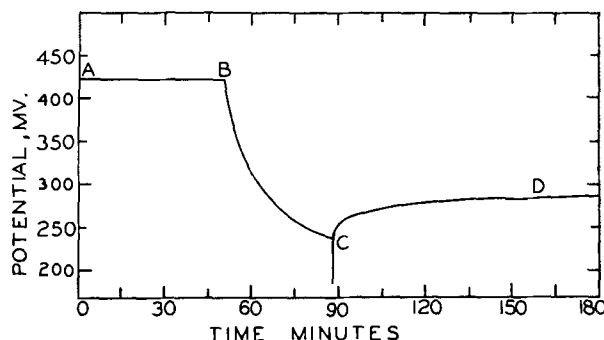


FIG. 3. A chemical discharge by the action of H_2O_2 in NH_4Cl electrolyte on MnO_2 electrode at $30^\circ C$. A-B, Electrode in 2M NH_4Cl , 0.01M NH_4OH , pH 7.11; B-C, electrode in 2M NH_4Cl , $10^{-3}N H_2O_2$, pH 7.12; C-D, electrode in 2M NH_4Cl , 0.01M NH_4OH , pH 7.12.

The potential started to rise and followed a curve resembling that of recovery from polarization, as shown in Fig. 3. Since hydrogen peroxide in ammonium chloride solution reduces manganese dioxide, this experiment is in agreement with conclusions that the discharge reaction takes place at the exterior surface and that the electrode potential is determined by the composition of the exterior surface.

ACKNOWLEDGMENTS

This work was carried out under Contract Nonr-1016(00) with the Office of Naval Research. The

authors are indebted to Mr. John S. Reiser for a number of preliminary experiments.

Any discussion of this paper will appear in a Discussion Section to be published in the June 1956 JOURNAL.

REFERENCES

1. N. C. CAHOON, *This Journal*, **99**, 343 (1952).
2. W. C. VOSBURGH, R. S. JOHNSON, J. S. REISER, AND D. R. ALLENSON, *ibid.*, **102**, 151 (1955).
3. D. T. FERRELL, JR., AND W. C. VOSBURGH, *ibid.*, **98**, 334 (1951).
4. S. BARNARTT, *ibid.*, **99**, 549 (1952).
5. R. F. STALZER, Ph.D. Thesis, Duke University (1951).

Nature of the Passive Film on Iron in Concentrated Nitric Acid¹

HERBERT H. UHLIG AND THOMAS L. O'CONNOR²

Corrosion Laboratory, Department of Metallurgy, Massachusetts Institute of Technology, Cambridge, Massachusetts

ABSTRACT

The film responsible for passivity when iron is immersed in concentrated nitric acid is shown to be ferric acid or a related higher valence iron compound. This was proved (a) by demonstrating formation of chromates when a 2.84% Cr-Fe alloy is passivated, (b) by showing complete suppression of the iron-nitric acid reaction when iron is previously immersed in potassium ferrate solution, and (c) by immersing passive iron in NaOH solution and observing higher valence iron compounds displaced from the surface by adsorbed OH⁻. The maximum of 2×10^{-8} mole ferric acid/cm² that was found is the same order of magnitude as moles chromate adsorbed on iron from chromate solutions as reported by other investigators. This amount of ferric acid, when it decomposes, is calculated to form a film of ferric oxide 40–125 Å thick, which thickness range agrees with that of residual oxide films on passive iron measured previously by others.

The higher valence iron compound forms at anodic areas of the iron surface during the iron-nitric acid reaction. When sufficient local concentration is achieved, the compound adsorbs (chemisorbs) on iron, satisfies metal surface affinities, and is itself stabilized against decomposition by adsorption. The metastable compound breaks down by cathodic reduction, mechanical shock, or presence of halide ions, the latter either displacing the adsorbed compound or hastening its decomposition. The roles of urea and hydrogen peroxide in nitric acid are discussed.

INTRODUCTION

In a previous paper (1), several experiments on passivation of evaporated iron films established that a certain amount of iron reacts rapidly with concentrated HNO₃ before the reaction is retarded. Pre-exposure of the iron films to oxygen, carbon monoxide, or dilute potassium dichromate solution appreciably reduced the initial amount of iron reacting. This was explained in terms of local action currents on the iron surface serving to polarize anodic areas. The above substances adsorbed on iron increase the effective cathodic area, thereby increasing the anodic current density. It was observed, correspondingly, that external anodic polarization of iron in nitric acid decreased the amount of iron reacting before passivation. Continued investigation along similar lines is reported herewith. These results, combined with important contributions to the subject by Bonhoeffer and co-workers (2), provide a clearer interpretation of the passivation mechanism by nitric acid than has been available heretofore. The process apparently is not so simple as the formation of a barrier film of ferric oxide.

¹ Manuscript received January 31, 1955. This paper was prepared for delivery before the Boston Meeting, October 3 to 7, 1954.

² Present address: American Cyanamid Company, Piney River, Virginia.

EXPERIMENTAL PROCEDURE

Experimental techniques were essentially the same as those employed by Gatos (1). Two types of iron surfaces were utilized; in one case by evaporation of iron onto glass, and in the other by employing Armco iron foil. Evaporated films were prepared by heating in vacuum either pure iron wires of 0.040-in. diameter, or by wrapping iron wire on electrically heated tungsten filaments of 0.025-in. diameter. The iron vapor was condensed on slowly rotating glass cylinders 35 mm long and 4 mm in diameter. The coated cylinders were then removed magnetically from the evaporation chamber and sealed off in glass tubes, or, when surface area determinations were made, the cylinders were transferred to another portion of the vacuum system through glass tube conduits without exposure to air.

Absolute surface area measurements were made on a number of such films by the B.E.T. method (3) in which ethane was adsorbed on the metal at liquid oxygen temperatures (−183°C). Use of ethane permitted surface area measurements on specimens having as little as 100 cm² of absolute surface. It was found that relatively smooth films, of roughness factor 1.7, were obtained from iron-wrapped tungsten wires, whereas films of greater absolute surface were formed by evaporation from iron filaments (roughness factor = 5–11). Apparently, the lower deposi-

TABLE I. *Effect of source of iron, N₂ and O₂ exposure, and absolute surface area on amount of iron reacting with HNO₃. Sp gr 1.43*Area of evaporated iron film on glass = approx. 4.2 cm²

Source of iron	No. of films tested	Original film thickness* Å	Exposure of film before reaction	Mg Fe reacted per cm ² geometric area
National Bureau of Standards.	10	1700-2680	Vacuum	0.092 ± 0.019
Westinghouse (Puron).....	13	2320-3400	Vacuum	0.095 ± 0.013
Mallinckrodt.....	5	2350-2400	Vacuum	0.090 ± 0.006
Westinghouse (Puron).....	5	1980-4330 (Roughness factor = 8.7-10.8)†	Vacuum	0.108 ± 0.012
Westinghouse (Puron).....	9	1940-2500	1 atm O ₂ , 30 min	0.040 ± 0.008
Westinghouse (Puron).....	8	Approx. 2000	1 atm O ₂ , 30 min subsequent evacuation	0.043 ± 0.011
Westinghouse (Puron).....	6	Approx. 2000	1 atm N ₂ for <1 min	0.091 ± 0.019

* Based on total amount of evaporated iron (density = 7.86), and geometric area.

† Roughness factor for other films listed in this table is approximately 1.7.

tion temperatures using iron filaments retarded sintering of the condensed film, resulting in an irregular array of crystals and perhaps a porous structure. These films of higher roughness factors were used only in comparison experiments, the majority of the data being obtained with the smoother films. Little difference in reacted iron was found on passivating the rough or smooth films (Table I).

The Armco foil specimens were generally 3 x 3 cm and 0.0075 cm thick. After preliminary degreasing in boiling benzene, they were pickled for 2 min in 15% HCl at 100°C (210°F), washed, and immersed successively in boiling acetone and boiling benzene. Specimens before use were aged in a desiccator overnight; reproducibility was thereby improved probably by allowing escape of interstitial hydrogen absorbed during the pickling operation.

It was necessary to bring the iron-coated glass cylinders into contact with concentrated nitric acid without contamination by exposure to the atmosphere. This was done by inscribing a circumferential scratch on the glass tube in which the iron-coated cylinder was contained, and placing the tube in an H-shaped glass holder of proper dimensions at the bottom of a beaker of concentrated nitric acid. Using a glass rod, sufficient pressure was applied to break the tube and bring the acid into rapid contact with the iron film. In some experiments, the evacuated specimen tube was broken inside a nitrogen-filled test box fitted with rubber gloves, and the specimen quickly immersed in nitric acid. Films exposed a short time to nitrogen behaved the same as those retained in vacuum.

Nitric acid was purified by distillation in an all-Pyrex still to remove small but annoying traces of iron. Immediately before use, the distilled acid was freed of dissolved oxides of nitrogen by bubbling through gaseous nitrogen for one or more hours. This operation was necessary because of the significant

effect of nitrogen oxides on the passivation reaction. The specific gravity of the distilled acid was 1.43 ± 0.005 at 15.6°C (60°F).

The amount of iron reacting with nitric acid previous to passivation³ was analyzed colorimetrically using the orthophenanthroline method. Nitric acid solutions were evaporated to dryness, the residues taken up in 1:1 HCl, and iron determined using an electrophotometer according to the method described by Sandell (4). This method was considered an improvement over the KSCN colorimetric method used by Gatos.

Chromium, in the hexavalent state, was determined colorimetrically using di-phenylcarbazide. The method was essentially that described by Sandell (5), except that nitric acid was used instead of sulfuric acid to provide the required acidity for development of a violet color. Total chromium was obtained by the same method after oxidation of Cr³⁺ to Cr⁶⁺ with hydrogen peroxide in dilute alkali. For both iron and chromium analyses, appropriate standards were prepared in solutions of the same kind as those common to the passivation experiments.

EFFECT OF OXYGEN PRE-EXPOSURE

Exposure of evaporated iron films to oxygen for 30 min or longer was found previously to reduce, by approximately one half, the amount of iron reacting with nitric acid before passivity was established. This was confirmed by the present series of experiments (Table I). The next step was to determine minimum partial pressure of oxygen at which the effect is observed. Evaporated films of iron on glass cylinders were allowed to remain in the glass evaporation system, and were then exposed to oxygen at various pressures for a total of ½ hr. Adjustment of

³ Time of immersion, 2 min, was not critical.

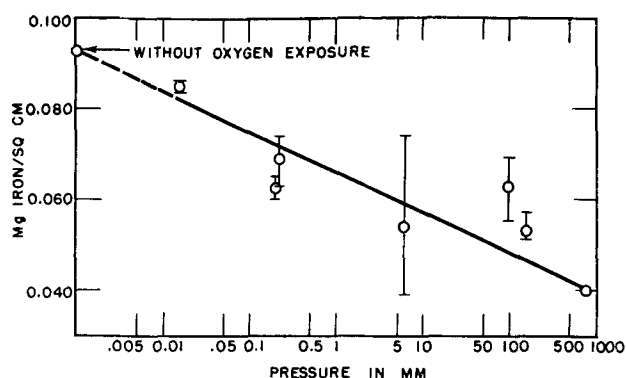


FIG. 1. Amount of iron reacting in nitric acid after exposure to oxygen at various pressures for $\frac{1}{2}$ hr.

pressure to the required value necessitated an additional preliminary time of 15–30 min. After exposure, specimens were sealed off in glass tubes and immersed directly in nitric acid by breaking the container under acid as described previously. Analyses for iron as a function of the oxygen pressure to which the films were exposed are plotted in Fig. 1. There is a gradual trend from the maximum amount of reacted iron for films retained in vacuum, to about one half this value for films exposed to 1 atm O_2 . The scatter of data is typical of passivation phenomena, and is not unexpected. No critical pressure of oxygen was found, but instead a trend toward lesser amounts of iron reacting as the pressure of oxygen was increased.

Further tests showed that the effect of oxygen at 1 atm can also be achieved at lower pressures if time of exposure is prolonged. Three films exposed to 2.7×10^{-4} mm oxygen for 24 hr and then reacted with nitric acid in the usual way gave values of 0.055, 0.054, and 0.067 (average 0.058) mg Fe/cm², which can be compared with the value of 0.040 mg Fe/cm² after exposure to 1 atm O_2 for 30 min. Two films sealed off after six hours' exposure at 4×10^{-3} mm O_2 pressure produced 0.047 and 0.059 (average 0.053) mg Fe/cm². Oxygen apparently chemisorbs on iron more rapidly the higher the external pressure. Hackerman and Antes (6) came to the same conclusion through Volta potential measurements of iron films exposed to oxygen at various pressures. It is also possible that rate of oxidation of iron to iron oxide increases with O_2 pressure. However, Tammann and Köster (7) reported that partial pressure of oxygen has no effect on oxidation rate of iron at 331°C where thin films are formed, and, hence, an effect of pressure instead on rate of chemisorption is favored.

EFFECT OF SUBSEQUENT EVACUATION

After exposure of several films to 1 atm of oxygen for $\frac{1}{2}$ hr, the system was evacuated to 10^{-6} mm pressure for periods ranging from 4 to 12 hr. These

films on immersion in nitric acid reacted to the same extent as did those not subject to evacuation after exposure to oxygen. In other words, effects of oxygen exposure were not removed by evacuation. Data for eight different films gave an average value of 0.043 ± 0.011 mg Fe/cm² (Table I), which compares with the average value for nine films, exposed similarly to oxygen but not evacuated, of 0.040 ± 0.008 mg Fe/cm². These measurements can be taken as evidence that effects of oxygen at 1 atm after 30-min contact with iron cannot be removed from the surface by subsequent lowering of the pressure.

Independent measurements of oxygen adsorption on iron films confirmed that the gas is irreversibly adsorbed. These measurements, to be reported in detail elsewhere, showed that adsorption of oxygen proceeds at a high rate initially, followed by a slow rate after a certain amount of oxygen covers the surface. Several iron films were exposed to oxygen at a final pressure of 1.8 to 7×10^{-3} mm Hg pressure for 1–5 hr, and were then evacuated at less than 10^{-6} mm Hg pressure for 5–12 hr. Oxygen was then allowed to adsorb on the surface again, but the observed rate of adsorption was always low and not characteristic of the high initial rate for a clean iron surface. Failure to regenerate the initial high rate of adsorption is proof that the original surface of iron is not regained by evacuation. A further check was made by adsorbing 17.4 cc-mm (9.4×10^{-7} mole) oxygen at a final pressure of 3.6×10^{-3} mm, and allowing the gas (17 ml) in contact with 167 cm² iron (absolute surface) to expand into a known volume (428 ml). The calculated final pressure (0.14×10^{-3} mm), assuming no release of previously adsorbed gas on iron, checked the observed pressure (0.13×10^{-3} mm). Armbruster and Austin (8) also reported that oxygen is irreversibly adsorbed on iron at room temperature.

The foregoing effects of evacuation on passivity differ from the previous observations by Gatos and Uhlig who reported that the effects of oxygen exposure were removable by pumping out the system. Detailed scrutiny and careful examination of all the facts revealed no certain reason for the discrepancy, but it is possible that the method they used to introduce oxygen-exposed specimens into the acid was at fault. This was done by heating one end of the glass tube and plunging it into acid, whereupon the tube fractured by thermal shock. If in so doing the iron films were heated unintentionally, the effect of oxygen would have been erased as Freundlich and co-workers showed (9), and with whose results present experiments are now in accord. Heating converts adsorbed oxygen to iron oxide (or, alternatively, the iron oxide film is sintered) which is not as effective a cathode as the adsorbed gas (or the initial oxide)

and, hence, larger amounts of iron dissolve subsequently in the passivation reaction.

Present results otherwise are in qualitative agreement with those reported earlier, including the indifferent effect of pre-exposure to nitrogen (Table I). Quantitatively, the amounts of iron reported per unit area for the present experiments are roughly one half those reported by Gatos and Uhlig. The differences were not found to be caused by variation of true surface area or source of iron, as summarized data of Table I show. The main factor appeared to be the present adoption of an improved method of analysis for small amounts of iron. This method required evaporation of numerous nitric acid solutions to dryness, hence was tedious and extremely corrosive to adjacent equipment. Nevertheless, the accuracy of results was much better than omitting evaporation, both because the concentrated acid no longer interfered with the color reaction, and because the possible size of sample for analysis was inherently larger. It is felt, therefore, that the present values for iron are more nearly correct.

Additions to Nitric Acid

Gatos (1) reported that exposure of iron films to oxygen-saturated 0.1% $K_2Cr_2O_7$ reduced the amount of iron reacting with concentrated nitric acid as time of exposure increased, with very little or no iron reacting for exposures greater than 30 min. This was confirmed by the present series of experiments using two evaporated iron films, three hydrogen-reduced Armco foil specimens, and four pickled Armco foil specimens. Each was pre-exposed 45 min to 0.1% $K_2Cr_2O_7$, and the excess solution drained off on filter paper before immediate immersion into nitric acid. For all specimens, the weight loss on passivation was 0.000 ± 0.001 mg/cm². In other words, pre-exposure of iron to dilute chromate solutions completely passivates it with respect to reaction with concentrated nitric acid.

Addition of potassium dichromate directly to nitric acid was found to accomplish the same thing, although the concentration required was higher than 0.1%. Armco foil specimens were used, previously pickled in 15% HCl at 100°C for 2 min, and allowed to age in a desiccator overnight. Data are plotted in Fig. 2. There is no effect on the reaction by dissolved chromate up to 0.1 g/50 ml acid (2 g $K_2Cr_2O_7$ /liter). The higher value for reacted iron using Armco foil (0.07 mg/cm²) than for evaporated films (0.04 mg/cm²) has an uncertain origin; it may be caused by interstitial hydrogen, impurities in the metal surface, or, more likely, edge effects and specimen shape, since convection currents and stirring, for example, are known to affect the passivation reaction. A rather sudden reduction in reaction rate occurs between 0.1

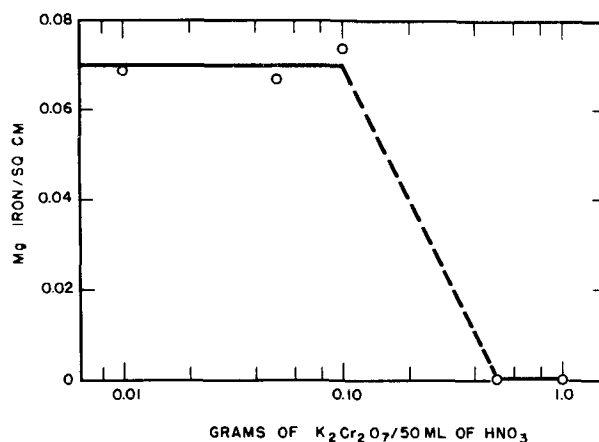


FIG. 2. Effect of addition of $K_2Cr_2O_7$ to nitric acid (sp gr 1.43) on amount of iron reacting.

and 0.5 g $K_2Cr_2O_7$ /50 ml nitric acid (2 to 10 g $K_2Cr_2O_7$ /liter), and the rate remains essentially zero for higher concentrations. The data indicate, therefore, that the passivating effect of chromates can be induced either by pre-exposure of iron to dilute solutions of chromates for a sufficient time, or by adding chromates directly to the nitric acid.

Similar experiments were carried out with addition of potassium nitrite to the acid (Fig. 3). Liberation of nitrous acid has an appreciable effect on the amount of iron reacting when the KNO_2 concentration is over 0.1 g/50 ml HNO_3 (2 g/l). Below this concentration, the effects are erratic, with either the usual amount of iron reacting, as when nitrites are absent, or almost none reacting as is uniformly true of concentrations over 0.1 g KNO_2 /50 ml acid. It is important to note, from the standpoint of mechanism discussed later, that the average amount of iron reacting in acid containing more than the critical amount of dichromate or nitrite was essentially 0.000 mg Fe/cm² for dichromate (5 determinations), but measurably higher for nitrite, namely 0.0013 mg Fe/cm² (8 determinations).

The obvious importance of nitrous acid or its de-

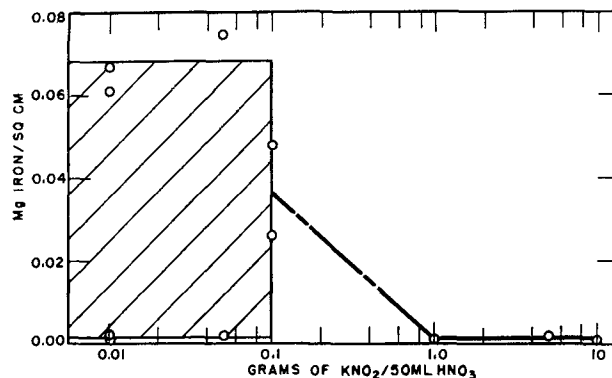


FIG. 3. Effect of addition of KNO_2 to nitric acid (sp gr 1.43) on amount of iron reacting.

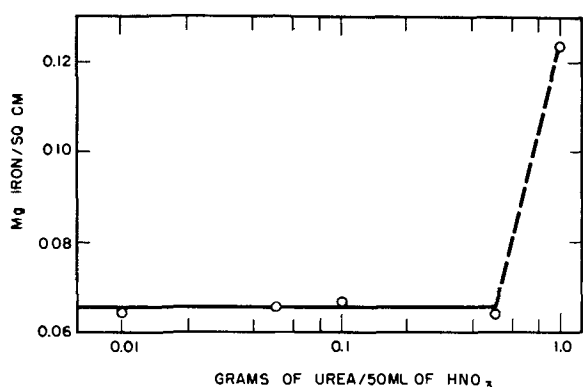
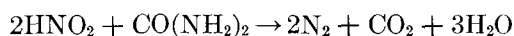


FIG. 4. Effect of addition of urea to nitric acid (sp gr 1.43) on amount of iron reacting.

composition products to the passivation reaction suggested adding substances capable of reaction with HNO_2 and which reduce its concentration. Urea is one such substance, which is stated (10) to react as follows:



The reaction products have also been stated to include cyanic acid, HCNO .

According to Vetter (11), an excess of urea reduces the ultimate concentration of nitrous acid in nitric acid to about 1×10^{-5} mole/liter. Fig. 4 shows that below 0.5 g urea/50 ml HNO_3 , iron was passivated with approximately the usual amount of iron reacting. Even with as little as 0.01 g urea, however, no color developed in the acid, and considerable gas was evolved, showing that urea was effective in removing the nitrous acid. At the highest concentration or 1.0 g urea/50 ml, HNO_3 , which approached the solubility of urea in the acid, approximately

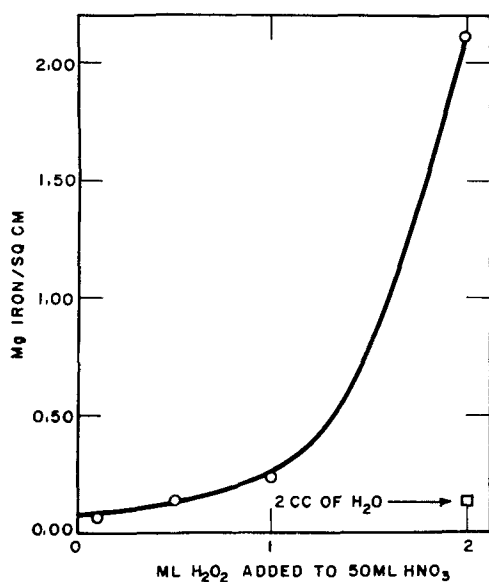


FIG. 5. Effect of addition of 30% hydrogen peroxide on the amount of Fe reacting in nitric acid (sp gr 1.43).

twice as much iron reacted as for smaller concentrations. In the latter solution, however, iron was passive only temporarily, with periods of passivity alternating with periods of activity. Naturally, more iron reacts under these conditions than when passivity is stable over the usual 2-min period of immersion in the acid.

Addition of hydrogen peroxide showed a more marked effect on the amount of iron reacting. Data are plotted in Fig. 5, each point representing an average of two determinations. As in the case of urea, the effect was accompanied by periodic breakdown and re-formation of the passive state, each cycle being attended by dissolution of iron. The higher the concentration of H_2O_2 , the more rapid was the frequency of breakdown. The effect observed is not one of dilution, because addition of water equivalent to that added with hydrogen peroxide showed only a small effect (Fig. 5).

FORMATION OF HIGHER VALENCE COMPOUND

The facts thus far provided evidence that $\text{K}_2\text{Cr}_2\text{O}_7$ either on the surface of iron or in nitric acid substantially reduces attack of iron during the passivation reaction. Potassium nitrite added to nitric acid also reduces the attack, with an effect slightly less than for dichromate. Further experiments showed that pre-exposure of iron to saturated nitrite solution for 1 hr followed by washing in water had no measurable effect on the amount of iron reacting with nitric acid, contrary to similar pre-exposure to dichromate. Potential measurements in distilled water of iron wires (0.040-in. diameter, sealed in lead glass) previously passivated either in concentrated HNO_3 or in 0.1% K_2FeO_4 and washed in water, were of the same order initially, namely 0.9–1.0 v on the normal hydrogen scale. It seemed reasonable, therefore, to hypothesize the formation of a compound during the iron-nitric acid reaction similar in structure and properties to ferric acid, H_2FeO_4 , as the key substance responsible for passivity. Any of the normal oxides of iron cannot account for the observed noble potential, as Bonhoeffer (2) showed. Although ferric acid is unstable when dissolved in acids, its decomposition rate is probably retarded when it is adsorbed on iron.

To check the role of ferric acid, potassium ferrate was prepared, in accord with a method described by Thompson, Ockerman, and Schreyer (12). Exposure of Armco iron specimens to freshly dissolved 0.1% solution⁴ for 45 min, draining of excess ferrate solution onto filter paper, and immersion of the specimen into nitric acid in the usual way showed indeed that iron was protected from reaction with nitric acid in

⁴ The solution decomposed slowly, but the purple color of ferrate was still visible at the end of 1 hr.

the same manner as was provided by pre-exposure to dichromate solutions. A small amount of iron was found in nitric acid after immersion (0.003 and 0.002 mg Fe/cm² in two experiments), which is accounted for by residual ferrate solution adhering to the iron surface. It was not possible, of course, to check the effect of ferrate added directly to nitric acid as was done with chromate because of the instability of the compound in acid solutions.

The next experiments were directed toward detection of hexavalent iron compounds possibly formed in the passivation reaction. The transient nature of such compounds and their obviously small concentration at any time during the reaction made the task difficult. However, since chromates are relatively stable, and conditions for their formation are reasonably parallel to those for hexavalent iron compounds, it was decided to use a small amount of alloyed chromium in iron as a tracer element. Accordingly, specimens of a laboratory-prepared melt of 2.84% Cr-Fe alloy were fabricated into sheet specimens each having a total geometric area of about 6 cm². This alloy, immersed in concentrated nitric acid for 2 min, lost 0.025 mg/cm², which is about one third the value, 0.07 mg/cm², for pure iron. (Higher chromium alloys corroded still less.)

Because iron interfered to some extent with analyses for chromium using the di-phenyl carbazide color reaction, the solution was made alkaline to pH 8, and the ferric hydroxide centrifuged off. A calibration curve was constructed using weighed amounts of K₂Cr₂O₇ in concentrated HNO₃. Total chromium, when required, was determined by first oxidizing Cr³⁺ to Cr⁶⁺ in dilute alkali using H₂O₂.

The first experiments involved successively passivating the 2.8% Cr-Fe alloy for a total of 100 times in 50 ml of concentrated HNO₃, activating the specimen each time in dilute HCl followed by thorough washing in distilled water. Large amounts of oxides of nitrogen were generated in the nitric acid, and the passivating reaction each time was characterized by a dark reddish-brown film creeping over the alloy surface. Careful analysis of the acid revealed complete absence of hexavalent chromium, with the analytical method estimated to be sensitive to about 50 μg of dichromate. The test was repeated using cathodic activation of the specimen in water so as to avoid possibility of contamination by chloride ion, but with the same result.

The next experiment was the anodic polarization of the alloy specimen (5.6 cm²) in 3% Na₂SO₄ for 1 hr at a current density of 40 ma/cm². Oxygen was evolved over all the surface of the anode indicating that the alloy was passive, and slight precipitation of ferric hydroxide within the solution revealed some metal dissolution in addition. The anodic corrosion

TABLE II. Analysis of corrosion products of passivated 2.8% Cr-Fe alloy

Passivation treatment	Total metal in solution		Cr ₂ O ₇ found	Current efficiency for Fe → Fe ³⁺ + 3e ⁻
	Cr	Fe		
	mg	mg	mg	%
1. HNO ₃ 100X, HCl activation.....	1.30	—	0.0	—
2. HNO ₃ 50X, cathodic activation.....	0.63	29.2	0.0	—
3. Anodic polarization 3% Na ₂ SO ₄ , 40 ma/cm ² , 1 hr...	0.046	1.6	0.095	1
4. Anodic polarization, HNO ₃ , 40 ma/cm ² , 1 hr...	2.4	98.7	0.0	63
5. Anodic polarization, HNO ₃ , 40 ma/cm ² , ½ hr, H cell.....	1.5	57.0	1.6	67
6. Same as 4, HNO ₃ saturated with urea, ½ hr:				
(a) Analysis for Cr ⁶⁺ immediately.....	1.21	53.0	0.36	63
(b) Analysis for Cr ⁶⁺ 2½ hr after electrolysis...	—	—	0.25	—
(c) Analysis for Cr ⁶⁺ 12 hr after electrolysis...	—	—	0.0	—
7. HNO ₃ saturated with urea, 50X, cathodic activation...	0.62	—	0.0	—

accounted for 1% of the total electricity passing through the cell. In this instance chromate was found, and, furthermore, all the chromium going into solution was hexavalent. Data for this and the following few experiments are summarized in Table II.

The fourth experiment consisted of anodically polarizing the alloy in concentrated nitric acid, again for 1 hr at 40 ma/cm². There was more anodic corrosion than before, about 63% of the current representing anodic dissolution compared with 1% for Na₂SO₄. However, no dichromate was detected.

The difference in results, depending on electrolyte, suggested that hexavalent chromium in nitric acid was probably being reduced by cathodic reduction products freely circulating throughout the volume of acid. In Na₂SO₄, the cathodic products are H₂ and NaOH, the hydrogen escaping from the solution, but in nitric acid, products such as nitrous acid remain in solution. It was found, in accord with this reasoning, that small quantities of potassium nitrite added to concentrated HNO₃ containing dissolved K₂Cr₂O₇ completely reduced the dichromate, as determined by analysis. In other words, dichromate rapidly oxidizes nitrous acid (Table III).

The fifth experiment, therefore, was to repeat the foregoing experiment, but with separation of anolyte and catholyte in an H-type cell with a fritted glass disk separating the two compartments. In addition, a stream of nitrogen was passed through

TABLE III. Reduction of $K_2Cr_2O_7$ in concentrated HNO_3 by additions of KNO_3

g KNO_3 added to 50 ml HNO_3 + 0.41 ppm $Cr_2O_7^{--}$	ppm $Cr_2O_7^{--}$ found by analysis
0.10	0.0
0.05	0.0
0.01	0.0
0.0	0.42
0.0	0.39

both compartments to remove any oxides of nitrogen from solution.

Using this arrangement with a current density of 40 ma/cm² for 30 min (area anode = 6.1 cm²), analysis of the anolyte now revealed positive presence of dichromates, with a current efficiency for anodic dissolution remaining at about 60–70%. In absence of reducing agents, therefore, hexavalent chromium is formed on anodic polarization of the 2.8% Cr-Fe alloy in nitric acid.

The sixth experiment involved the addition of urea to concentrated nitric acid which, as noted previously, reacts with nitrous acid and greatly reduces its concentration. Using the electrolytic cell without separation of anolyte and catholyte, dichromates this time were found. The amount of dichromate decreased with time after electrolysis was discontinued, as data of Table II show, probably because urea is oxidized slowly by dichromates. This, plus the fact that some nitrous acid is present, also explains the smaller quantity of Cr_2O_7 found compared with experiment 5. However, in absence of anodic polarization, and by merely dipping the specimen 50 times into the urea-nitric acid mixture, activating the specimen cathodically in water each time, no dichromate was found (experiment 7, Table II). Apparently, the dichromate under these conditions is reduced by HNO_2 , formed in close proximity to the anodes, more rapidly than urea can diffuse to the metal surface and react with HNO_2 . Vetter (11) has shown, for example, that it requires approximately 1 min for a 1% solution of urea in concentrated HNO_3 to reduce the nitrite concentration from 4×10^{-3} to 1×10^{-4} mole/liter.

DETECTION OF HEXAVALENT CHROMIUM COMPOUND

With definite formation of dichromates on anodic polarization of the Cr-Fe alloy in nitric acid, the next question concerned the analogous formation of a hexavalent iron compound and its similar properties as a passivator. This question previously had been answered in part by pre-exposing iron to dilute potassium ferrate or to potassium chromate, and observing in either instance the complete suppression of reaction with nitric acid.

Evidence from the potential behavior of iron in

various chromate solutions indicated that the Langmuir adsorption isotherm is obeyed (13), confirming that passivation by chromates is accompanied by their adsorption on iron, as had been suggested earlier (14). Radioactive tracer studies (15) on the amount of radioactive chromium on the surface of iron as a function of chromate concentration also showed that an approximate adsorption isotherm is followed. Evidence for adsorption accompanying passivation was also reported by Powers and Hackerman (16). They showed that chromates were adsorbed on iron below pH 11 and could not be washed off (chemisorption), whereas above pH 11 chromates were not adsorbed at all. These facts immediately suggested that hexavalent iron compounds analogously may adsorb on iron. Furthermore, if they are the cause of passivity in nitric acid, they should be released from the metal surface by immersing passive iron in strong alkalis, and, in the case of iron containing alloyed chromium as tracer, some chromates should be released simultaneously.

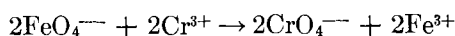
The next experiment, therefore, was to passivate the 2.84% Cr-Fe alloy (6.1 cm² area) in concentrated HNO_3 , wash in water, immerse in 2N NaOH, then in dilute HCl, and again wash in distilled H_2O , repeating this procedure successively 50 times. Analysis of the sodium hydroxide solution, carrying out this procedure, showed indeed the presence of 53 μ g of Na_2CrO_4 . Repetition of the same procedure using HCl instead of HNO_3 did not passivate iron and, correspondingly, produced no detectable amount of chromate. This experiment proved, therefore, that hexavalent chromium forms when the chromium-iron alloy is passivated in concentrated nitric acid, and furnishes strong evidence that the chromates so formed are in part chemisorbed.

FORMATION OF HEXAVALENT IRON COMPOUNDS IN NITRIC ACID

With the preceding evidence for hexavalent chromium, a cell was set up to demonstrate the possibility that hexavalent iron can form by the nitric acid-iron reaction. To one compartment of an H-type cell, 5N NaOH was added in contact with an Armco iron electrode (2 x 2 cm), and concentrated HNO_3 was added to the other compartment in contact with a platinum electrode of similar size. On electrically short circuiting the two electrodes, light purple reaction products, characteristic of sodium ferrate and exhibiting typical oxidation reactions, streamed off the iron, accompanied by oxygen evolution. A similar experiment was repeated using 0.1N NaOH instead of the more concentrated alkali with identical although less pronounced results. By employing 3% Na_2SO_4 instead of NaOH, however, no ferrate formed visibly, oxygen being the only ob-

servable anodic product. In a solution such as this, it is probable that if ferrate is formed, it is immediately adsorbed on the electrode surface with no tendency for its release, whereas in NaOH the hydroxyl ion adsorbs preferably and continuously displaces ferrate ions.

It remained to demonstrate that the compound formed on pure iron and displaced by hydroxyl ions has oxidizing properties typical of ferrates. Analysis of the suspected compound was based on a method described by Schreyer, Thompson, and Ockerman (17). To 20 ml saturated NaOH, 1 ml of chromic chloride solution (1.7 g CrCl₃/100 ml) and 5 ml H₂O were added. Any ferrate introduced into this solution reacts with Cr³⁺ to form chromate in accord with:



The corresponding chromate was analyzed by diluting the solution to 50 ml, taking a 10 ml aliquot, diluting this to 15 ml and carefully adding H₂SO₄ to pH 8 or 9. Ferric hydroxide was centrifuged off, and the solution then acidified with 2 ml of 5N H₂SO₄. On dilution to 40 ml, 2 ml of di-phenyl carbazide reagent were added, dilution carried to 50 ml, and the violet color as developed by dichromate was compared with suitable standards using the electro-photometer.

A coiled Armco iron specimen of 60 cm² area, suspended from a glass hook, was passivated in concentrated nitric acid, and carefully washed in one or more beakers of distilled water without destroying passivity. The coil was then plunged into the above-described NaOH solution containing Cr³⁺ and allowed to remain about 10 min, after which analysis of the alkaline solution was carried out for CrO₄⁻⁻. Blank determinations using the identical procedure were run with platinum sheet having the same area as iron. Chromates were found over and above small blank corrections, indicating that ferrate or an analogous compound is formed when iron reacts with concentrated nitric acid. A summary of results is given in Table IV. The data show that reproducibility, typical of most experiments in passivity, was not good, but nevertheless was adequate to prove the point. The amount of ferrate corresponding to the analyzed chromate appeared to be independent of whether one or three washes were employed, which may be taken as further evidence that the compound is chemisorbed on iron.

The variable amounts of ferrate may indicate partial decomposition taking place during washing and at the time of immersing the iron specimen into NaOH. Some specimens may have lost most of their passivity, judging by the amount of ferrate found and that produced by a specimen known to be

TABLE IV. Analyses of passive film on iron for ferrates and iron content

No. of washes in water	μg CrO ₄ ⁻⁻ formed on immersion in NaOH + Cr ³⁺ solution*	μg Fe in NaOH + Cr ³⁺ solution†	Equivalent micromoles/cm ²	
			FeO ₄ ⁻⁻	Fe
1	138	1750	0.020	0.52
1	31	1310	0.005	0.39
1	57	1230	0.008	0.37
1	82	1580	0.012	0.47
2	89	1100	0.013	0.33
2	125	780	0.018	0.23
3	34	360	0.005	0.11
3	109	490	0.016	0.15
3	20	—	0.003	—
3‡	10	80	0.001	0.02

* Corrected for blank equal to 24 μg CrO₄⁻⁻.

† Corrected for blank equal to 120 μg Fe.

‡ Passivity intentionally destroyed by striking specimen on side of beaker in second wash.

active. Any nitrate or nitrite carried over on the passive iron surface could not have oxidized Cr³⁺ to CrO₄⁻⁻, because a check run showed that 100 mg KNO₃ or KNO₂ added to the NaOH solution containing Cr³⁺ did not produce chromate in excess of the normal blank. Moles of iron far in excess of moles of ferrate originated probably through carry-over of ferric nitrate and by corrosion of the iron specimen by an adhering film of acid not easily removed by washing. Data of Table IV show that additional water washes removed more of the residual acid solution, and thereby also reduced the amount of iron in the NaOH wash. It is questionable whether all the adhering solution can be removed without destroying passivity. Because of these factors, a more precise analysis of the surface compound responsible for passivity was not attempted.

DISCUSSION

The experimental evidence can be interpreted, accordingly, in terms of a hexavalent iron compound, related to or identical with ferric acid, H₂FeO₄, which forms at the anode areas as a result of intense local action galvanic currents when iron reacts with concentrated nitric acid. The compound in part appears to be chemisorbed on the metal surface simultaneous with its formation. According to Bonhoeffer (2) and Vetter (18), local action currents increase with accumulation of nitric acid reduction products, in particular HNO₂, which act as cathodic depolarizers, the anodic current density eventually reaching the critical value for anodic passivation. Franck's (19) measurements of anodic passivation of iron in dilute H₂SO₄ showed that the critical value may be about 17 amp/cm². Anodic polarization of this magnitude suffices to produce ferrate or its analog either in situ, or in high concentrations at anodic

regions. The compound upon chemisorbing on iron is more stable chemically than in the free state. Chemical stabilization of the passive film by adsorption was suggested earlier by Bennett and Burnham (20) and by Bancroft and Porter (21) who considered that adsorbed metastable FeO_3 was responsible for passivity.

The chemisorbed compound, according to present authors' viewpoint, satisfies surface affinities of iron, and thereby reduces tendency of the metal surface to react, making it passive in the same sense as chromates are thought to cause passivity when chemisorbed on iron (13, 14, 22-24), or oxygen when chemisorbed on the stainless steels (13, 22-25).

In this connection, it may be significant that the maximum amount of ferrate released from passive iron is approximately 2×10^{-8} mole/cm² of geometric surface (Table IV). Geary (26) found a comparable amount of chromate to adsorb on oxide-free iron from 0.001M chromate solution, namely 5×10^{-8} mole/cm² geometric surface. Powers and Hackerman's (16) data for air-exposed iron correspond to 0.9×10^{-8} mole/cm², as do data of Brasher and Stove (15).

No iron reacts with nitric acid if iron is pre-exposed to ferrates or to chromates, because the surface is already covered with a passive film of the same kind as forms by reaction of acid with iron. At the same time, ferrate or its analog adsorbed on iron no longer has the same affinity for its external environment because of chemical attachment to the metal lattice underneath, and it is, therefore, relatively more stable with respect to acids, hydrogen peroxide, nitrous acid, and other reagents with which it normally reacts when in the free state.

High anodic local action current densities necessary for passivation are favored by adsorbed oxygen on iron, both because oxygen forms effective cathodic surfaces, and because local action currents are confined to smaller exposed anodic areas. Hence, less iron reacts with HNO_3 if the iron is pre-exposed to air. Pre-exposure to carbon monoxide similarly aids passivation through increased cathodic surface of adsorbed CO, similar to the behavior of adsorbed oxygen. At such time as the hexavalent iron compound forms an adsorbed layer or layers, the compound thereafter is continuously renewed at incipient small anode areas by continuing local action currents. The measured corrosion rate of passive iron in unstirred concentrated HNO_3 after several hours' immersion was found equal to about 20 mdd, which is equivalent to a total corrosion current ($\text{Fe} \rightarrow \text{Fe}^{+++} + 3e$) of $12 \mu\text{amp/cm}^2$. At exposed anodes, of course, the current density is much higher. If 17 amp/cm^2 is necessary to achieve passivity, as Franck indicated, the ratio of anode to cathode

area is $12 \times 10^{-6}/17$ or 7×10^{-7} . Vetter (11), using corrosion rates of iron in stirred concentrated HNO_3 containing 2% urea, similarly calculated the ratio to be 30×10^{-7} . Both values indicate that practically all the surface is cathode, a very small portion of which at any moment acts as anode.

Repair of the adsorbed film of compound occurs even in relatively dilute nitric acid. The lower conductivity and limited oxidizing properties of the dilute acid, together with a correspondingly large anodic area of iron when first immersed, are not sufficient to induce passivity. But when passivity is previously induced by immersion of iron into concentrated HNO_3 , corrosion currents in dilute acid are entirely adequate for maintaining passivity.

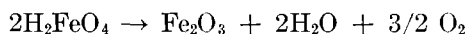
So long as the compound remains on the surface and is repaired by local action currents, the specimen remains passive. Of course, if the metastable compound is broken down over more than a small region by mechanical action or heat, ensuing galvanic action of the induced anode in contact with a large area of cathode differing in potential by as much as 0.9 v (the potential difference between passive and active iron in water) is sufficient to reduce cathodically the compound at adjoining areas of the surface. This action is observed by a rapidly moving front of nonpassive iron increasing in area as more and more of the surface is activated. Bonhoeffer (2, 27) and his co-workers (18, 19) have studied in detail the mechanism of propagation of active-passive fronts as a model for nerve impulse propagation, following the earlier studies of passivity in this relation by Heathcote (28) and by Lillie (29).

Admission of halogen ions quickly breaks down passivity, possibly because these ions compete with the passivating compound for sites on the iron surface. Chloride ions adsorbed on iron have very short life (small activation energy for the corrosion reaction), contact with the surface being followed by rapid hydration and solution of metal ions. Such areas become anodes with subsequent progressive breakdown of passivity by electrolytic action, as noted above. It is also possible that chloride ions hasten reduction of the surface iron compound by reaction to form chlorine, or by some other mechanism.

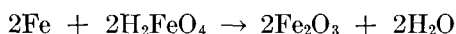
The present conclusion that ferric acid or a related compound is responsible for passivity agrees with the deductions of Bonhoeffer, who suggested that the "oxide film" on iron passivated in nitric acid must have a higher oxygen dissociation pressure than any known normal oxide (2, 30). Ferric acid certainly fits into this category. It also agrees with the previous proposal of Bennett and Burnham (20) and of Bancroft and Porter (21) that a higher oxide FeO_3 appears to be necessary to explain their

passivation experiments and potential measurements. The present work shows indeed that an unstable, higher oxide exists. This work does not support the proposal of Vetter (31) that a common oxide of iron unsatisfied in composition with respect to its environment covers the surface, since such an oxide would not account for hexavalent iron or a structure analogous to the chromates.

Some investigators have concluded that the passive film on iron is a physical barrier layer consisting of Fe_2O_3 (32, 33). Support for this assumption was obtained in part by isolating an oxide film of the composition Fe_2O_3 using the iodine reaction or anodic dissolution techniques. However, an isolated film of Fe_2O_3 , according to the present discussion, is merely an end product of the metastable hexavalent compound, and probably plays a small part, if any, in the passivation phenomenon. Ferric acid, for example, may decompose as follows:



or



On this basis, the maximum amount of ferrate found per apparent square centimeter of passive surface (2×10^{-8} mole/cm², Table IV) decomposes to a residual film of Fe_2O_3 ($d = 5.12$) 125 Å thick. The corresponding thickness, based on a reasonable roughness factor of 2 or 3, is 40–60 Å. These values agree approximately with optically determined values of 25–100 Å for the primary film reported by Tronstad and Borgmann (34), and with thicknesses for the decomposed primary film of 78 Å by microbalance weighings of Gulbransen (35), and with 80 Å by dissolution of oxide in acid as reported by Schwarz (36). The values are somewhat higher than 23 Å calculated by Vetter (37) from the amount of electricity required to reduce the passive film.

An explanation is still required for the function of urea and hydrogen peroxide in the passivation phenomena. In accord with the function of HNO_2 as depolarizer, enough iron must first react with nitric acid to produce a high concentration of nitrous acid near the metal sufficient for effective cathodic depolarization and corresponding achievement of the critical anodic current density for passivity. Consequently, if nitrous acid is added beforehand, as when potassium nitrite is added to nitric acid, iron becomes passive with much less than the normal amount of iron reacting. Urea destroys nitrous acid, but the reaction is not sufficiently rapid, as Vetter showed (11), to prevent build-up of nitrous acid at the metal surface by the iron-nitric acid reaction. Hence, approximately the normal amount of iron reacts with nitric acid plus urea to produce passivity,

as the foregoing experiments show. After passivation, urea apparently succeeds in reducing the prevailing HNO_2 concentration at the surface and reduces the corresponding local action currents, thereby preventing repair of the adsorbed film, and causing loss of passivity, but only momentarily, because when larger anode areas form, nitric acid is more rapidly reduced at adjacent cathodes, HNO_2 again forms in greater concentration, and local action currents increase, followed by recovery of passivity. This situation accounts for periodic active-passive phenomena when iron is immersed in HNO_3 -urea mixtures.

Hydrogen peroxide apparently reduces the concentration of nitrous acid by oxidizing it to nitric acid (38). It may also act to reduce ferric acid in the same manner it reduces chromates. Hence, periodic breakdown of passivity occurs, and more iron reacts during the 2-min immersion in concentrated HNO_3 containing H_2O_2 .

As mentioned before, the metastable compound after adsorption on passive iron is not as easily reduced as properties of ferrates otherwise suggest, in the same sense that chemisorbed oxygen on tungsten is not easily reduced by hydrogen at elevated temperatures (39). Through chemisorption, both the metal and the adsorbate are passive to their environment, until such time as localized breakdown occurs in some portion of the passive film.

ACKNOWLEDGMENT

This research was supported by the Office of Naval Research under Contract N5ori-07815 to whom the authors express their appreciation.

Any discussion of this paper will appear in a Discussion Section to be published in the June 1956 JOURNAL.

REFERENCES

1. H. C. GATOS AND H. H. UHLIG, *This Journal*, **99**, 250 (1952).
2. K. F. BONHOEFFER, *Z. Metallkunde*, **44**, 77 (1953). (This paper summarizes earlier papers.)
3. S. BRUNAUER, P. EMMETT, AND E. TELLER, *J. Am. Chem. Soc.*, **59**, 2682 (1937).
4. E. B. SANDELL, "Colorimetric Determination of Traces of Metals," p. 378, Interscience Publishing Co., New York (1950).
5. Ref. 4, p. 260, 265.
6. N. HACKERMAN AND L. ANTES, *Science*, **112**, 471 (1950).
7. G. TAMMAN AND W. KÖSTER, *Z. anorg. u. allgem. Chem.*, **123**, 196 (1922).
8. M. ARMBRUSTER AND J. AUSTIN, *J. Am. Chem. Soc.*, **68**, 1347 (1946).
9. H. FREUNDLICH, G. PATSCHEKE, AND H. ZOCHER, *Z. physik. Chem.*, **128**, 321 (1927).
10. F. EPHRAIM, "Inorganic Chemistry," Transl. by P. Thorne and A. Ward, p. 684, Gurney and Jackson, London (1939).
11. K. VETTER, *Z. Elektrochem.*, **55**, 274 (1951).

12. G. THOMPSON, L. OCKERMAN, AND J. SCHREYER, *J. Am. Chem. Soc.*, **73**, 1379 (1951).
13. H. H. UHLIG AND A. GEARY, *This Journal*, **101**, 215 (1954).
14. H. H. UHLIG, *Chem. Eng. News*, **24**, 3154 (1946).
15. D. BRASHER AND E. STOVE, *Chemistry & Industry*, **1952**, No. 8, 171.
16. R. POWERS AND N. HACKERMAN, *This Journal*, **100**, 314 (1953).
17. J. SCHREYER, G. THOMPSON, AND L. OCKERMAN, *Anal. Chem.*, **22**, 1426 (1950).
18. K. BONHOEFFER AND K. VETTER, *Z. physik. Chem.*, **193**, 127 (1950).
19. U. FRANCK, *Z. Naturforsch.*, **4a**, 383 (1949).
20. C. BENNETT AND W. BURNHAM, *Trans. Electrochem. Soc.*, **29**, 217 (1916).
21. W. BANCROFT AND J. PORTER, *J. Phys. Chem.*, **40**, 37 (1936).
22. H. H. UHLIG, *This Journal*, **97**, 215C (1950).
23. H. H. UHLIG, "Metal Surface Phenomena," chapter of "Metal Interfaces," pp. 312-35, American Society for Metals, Cleveland (1952).
24. H. H. UHLIG, *Ann. N. Y. Acad. Sci.*, **58**, 843 (1954).
25. G. TAMMANN, *Z. anorg. u. allgem. Chem.*, **107**, 104, 236 (1919).
26. Ref. 13, p. 221.
27. K. BONHOEFFER, *J. Gen. Physiol.*, **32**, No. 1, 69 (1948).
28. H. HEATHCOTE, *Z. physik. Chem.*, **37**, 368 (1902); *J. Soc. Chem. Ind.*, **26**, 899 (1907).
29. R. L. LILLIE, *Biol. Revs. Cambridge Phil. Soc.*, **11**, 181 (1936).
30. K. BONHOEFFER, *Z. Elektrochem.*, **47**, 147 (1941).
31. K. VETTER, *Z. physik. Chem.*, **202**, 1 (1953).
32. E. S. HEDGES, "Protective Films on Metals," p. 114, Chapman and Hall, London (1937).
33. U. R. EVANS, *Trans. Faraday Soc.*, **40**, 120 (1944).
34. L. TRONSTAD AND C. BORGMANN, *Trans. Faraday Soc.*, **30**, 349 (1934).
35. E. A. GULBRANSEN, *Trans. Electrochem. Soc.*, **82**, 375 (1942).
36. W. SCHWARZ, *Z. Elektrochem.*, **55**, 170 (1951).
37. K. J. VETTER, *ibid.*, **55**, 683 (1951).
38. Ref. 10, p. 685
39. I. Langmuir, *J. Am. Chem. Soc.*, **38**, 2221 (1916).

Effect of Fluorides and Other Addition Agents on the Cathodic Potential of Titanium in Hydrofluoric Acid¹

M. E. STRAUMANIS, S. T. SHIH, AND A. W. SCHLECHTEN

University of Missouri School of Mines and Metallurgy, Department of Metallurgy, Rolla, Missouri

ABSTRACT

The absolute hydrogen overvoltage values of titanium in hydrofluoric acid increase, or the cathodic potentials, η_{II} , decrease (become more negative) with addition of alkali fluorides to the acid. The η_{II} decreases with increasing concentration of the salt in the sequence $NH_4F \rightarrow KF \rightarrow NaF$, which is also the sequence of decreasing cationic radius. For example, at 50 ma/cm² η_{II} decreases from -0.8 v in pure 0.1N hydrofluoric acid to -1.68 v in the same acid if it is 1M with respect to sodium fluoride. If the titanium cathode dissolves in the acid, the η_{II} -current density relationship is linear; if the dissolution ceases (at higher concentrations of the added fluoride), Tafel's relationship is fulfilled. In between there is a mixed straight line and quasi logarithmic relationship, the latter occurring at higher current densities. Organic colloid solutions of agar-agar or arabic gum appreciably decrease η_{II} ; methylene blue solutions increase it slightly.

INTRODUCTION

In connection with the general problem of titanium deposition from aqueous solution, consideration was given to the means of making the cathodic potential of the hydrogen-developing electrode as negative as possible. In other words, what conditions would increase the absolute value² of hydrogen overvoltage, which actually is a cathodic potential, thus favoring metal deposition?

First, the cathodic behavior of titanium was studied in pure bases and in hydrofluoric, hydrochloric, hydrobromic, sulfuric, and acetic acids (1). There was a straight line potential-current density relationship (equation I) in cases when the titanium cathode dissolved with an appreciable rate in the acid, evolving hydrogen in addition to that developed by the current. However, Tafel's logarithmic relationship (equation II) appeared if the titanium cathode did not dissolve in the acid, or if the dissolution rate was appreciably decreased (1, 2).

In order to study the lowering of the titanium cathode potential by use of different electrolytes, with the addition of different agents, and to compare the results, it was necessary to make the measurements with the same reference electrode. The 1N calomel electrode was chosen for this purpose, but the resulting potential measurements were reduced to the potential as compared to the standard hydro-

gen electrode. The cathodic potentials measured in this way are designated by η_{II} . The subscript II means that the potentials were measured in all cases against the same reference electrode, while hydrogen overpotential measurements (designation η) were usually made against a reversible hydrogen reference electrode immersed in the same solution (3) as that used for the electrolyte around the cathode. So the values η_{II} and η of an electrode in the same solution differ only by the effect of hydrogen ion concentration on the potential of the hydrogen reference electrode.

The cathodic potential (as well as the hydrogen overvoltage) on a metal in a pure electrolyte usually changes upon the addition of an organic compound to the electrolyte. Salt additions (4) may cause a decrease of the a constant of Tafel's equation (e.g., on mercury cathodes), although the b constants may remain unaffected (5, 6). The cathodic potential on copper and platinum in hydrofluoric acid is strongly decreased when ammonium fluoride is added to the acid (2). Organic compounds with oxidizing properties usually decrease the absolute value of hydrogen overvoltage (7).

The strong influence of soluble fluorides on the hydrogen overvoltage on platinum and copper (2) suggested the study of the cathodic potential of titanium in presence of water soluble fluorides.

Some experiments were also made with the addition of organic colloids.

EXPERIMENTAL PROCEDURE AND MATERIALS USED

Of the two methods (8, 9) most commonly used for cathodic potential determinations, the "direct" method was chosen. This method is simpler, and,

¹ Manuscript received March 25, 1955. This paper was prepared for delivery before the Pittsburgh Meeting, October 9 to 13, 1955.

² For "absolute value" algebraic signs (of the potentials) are disregarded; "increase" means moving in a positive direction (more cathodic); "decrease" means moving in a negative direction (more anodic).

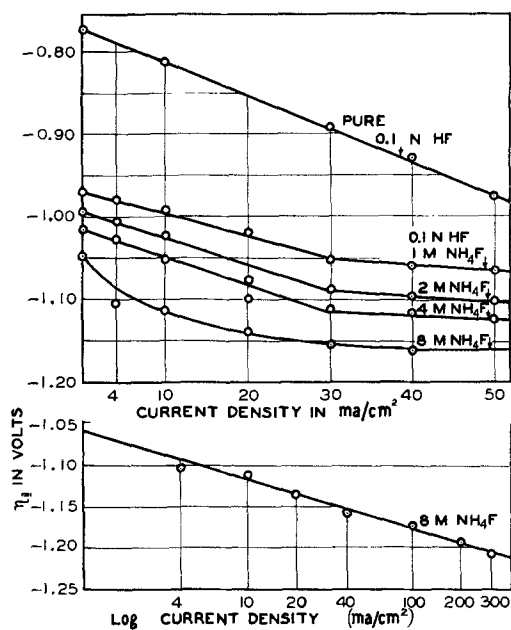
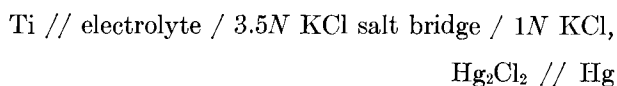


FIG. 1. Cathodic potential, η_{II} , of pure titanium in 0.1N HF with NH_4F added vs. current density and vs. log current density. Each experimental point is the average of two runs. Hydrogen scale.

according to authoritative views (8, 10), is as accurate and reliable as the "indirect" method, if applied correctly.

The electrolytic cell, made of a polyethylene beaker, contained the titanium cathode, a 2 x 2 cm platinum anode, and a stirrer making 375 rpm (11). The electrodes were mounted on a frame at a definite distance apart. The emf of the cell:



was measured with a potentiometer equipped with a sensitive external galvanometer, while a current of a certain strength passed through the platinum anode and titanium cathode. The latter was cut from an iodide titanium crystal bar and had an exposed surface area of 1.8 x 0.85 cm². The glass handle of the electrode, as well as parts of the metal not to be exposed, were covered with a layer of Pyseal Wax to protect these parts from attack by hydrofluoric acid. The exposed surface was polished before each experiment through No. 00 emery paper, then etched by immersing the electrode in 1N hydrofluoric acid for about 1 min, followed by quick rinsing in distilled water. The end of the Luggin capillary was pressed horizontally and laterally against the titanium surface, thus preventing shielding of the metal by the tip itself.

No corrections, except reduction to the potential as determined against the standard hydrogen electrode, were introduced in the potential values measured. Consequently, values obtained with ti-

tanium in 0.1N hydrofluoric acid in the presence of various additions in different amounts represented cathodic potentials η_{II} of hydrogen evolution at a certain current density (1). As fairly strong currents were applied, the influence of atmospheric oxygen on the potential was so small (1, 12) that it was disregarded, and the air was not removed from the cell.

All chemicals were of reagent grade. The 99.99% iodide titanium (13) was supplied by the Foote Mineral Company.

RESULTS

Effect of ammonium fluoride.—Solutions for the electrolysis were prepared so that the concentration of hydrofluoric acid was kept constant at 0.1N, and the concentration of the ammonium fluoride was varied to give 1, 2, 4, and 8M solutions. The cathodic potentials measured are plotted against current density in Fig. 1. Ammonium fluoride additions decrease the cathodic potential of titanium, reaching a value of about -1.21 v (300 ma/cm²) in 8M ammonium fluoride solutions. The straight line relationship

$$\eta_{II} = a' + b'i \quad (\text{I})$$

holds up to 4M solutions, although a break occurs at about 30 ma/cm². In this equation a' is the potential of titanium at a current density $i = 0$, and b' is the slope constant. Equation (I) changes to the logarithmic or Tafel's relationship (14):

$$\eta_{II} = a + b \log i \quad (\text{II})$$

as the concentration of ammonium fluoride approaches and surpasses 4M (see lower curve of Fig. 1). The constant a in equation (II) is the potential of the titanium cathode at a current density of $i = 1$ ma/cm², and b is the slope constant of the Tafel lines.

It was observed that in 8M electrolytes the dissolution of titanium ceased almost completely. This indicates that the straight line relationship is maintained if the titanium dissolves in the acid, while the Tafel relationship holds if the titanium ceases to dissolve because of ammonium fluoride additions (1, 2). At low concentrations of this salt, up to 2M, a dark grayish scale was noticeable on the titanium electrode, and the solution became milky in appearance because of high dispersion of the evolved hydrogen; no scale could be detected at higher concentrations of ammonium fluoride.

Effect of sodium and potassium fluoride.—Sodium fluoride concentrations used were 0.02, 0.1, 0.2, 0.3, 0.5, and 1M, while the strength of hydrofluoric acid was kept at 0.1N. Sodium fluoride concentration was limited to 1M because of the low solubility of this salt in the acid. A summary of the results is given in Fig. 2, which shows that the addition of sodium fluoride has a very marked effect on the

cathodic potential. The straight line relationship [equation (I)] holds only at low concentrations of the fluoride; the linear portion of the curves becomes shorter and shorter with increasing concentration of the fluoride, while the remaining parts of the curve, especially the curves obtained with 0.3 to 1M solutions, obey Tafel's relationship [equation (II)]. The change from the straight line to the logarithmic relationship is accompanied by almost complete cessation of the dissolution of the titanium cathode in the acid. A dark grayish to slightly purplish scale appeared on the cathode at concentrations higher than 0.2M of sodium fluoride. Spectral analysis of the scale showed titanium with practically no sodium lines.

Curves obtained in 0.1, 0.5, 1, 2, and 8M solutions of potassium fluoride in 0.1N hydrofluoric acid were very similar to those shown in Fig. 2. The cathodic potential decreased strongly with the salt concentration, and the change from the mixed straight line-logarithmic relationship to the pure logarithmic one occurred between 1 and 2M concentration of potassium fluoride. Dissolution of the cathode in the latter solution ceased almost completely within 20 min after immersion of the electrode in the acidic solution. Scale formation was observed, but it decreased substantially in stronger fluoride concentrations.

Effect of complex fluorides.—A complex sodium titanium fluoride solution was prepared by adding cautiously a sodium fluoride solution to a titanium (III) fluoride solution, until the formation of a violet precipitate, probably of the composition Na_2TiF_5 (15), just started. Then the pink solution was diluted with hydrofluoric acid so that it became 0.1N and approximately 0.1M with respect to the Na_2TiF_5 . A curve very similar to that obtained in 0.1M sodium fluoride (Fig. 2) could be drawn to represent the results from this solution. Hence, the presence of complex ions (pink color) did not change the curve from that obtained previously in sodium fluoride.

Effect of some colloids and organic substances.—The absolute value of the hydrogen overvoltage on metals is usually increased by the presence of organic colloids. This was also observed when a titanium cathode was used. The 0.1N hydrofluoric acid solution containing 0.1 wt % agar-agar (U.S.P. grade) was fairly viscous, but did not influence very much the cathodic potential of titanium. The current density-potential relationship could be described by equation (I) and the η_{II} values could be calculated in volts by equation (III)

$$\eta_{\text{II}} = -(0.83 + 0.0033i) \quad (\text{III})$$

up to $i = 30 \text{ ma/cm}^2$, beyond which the potential

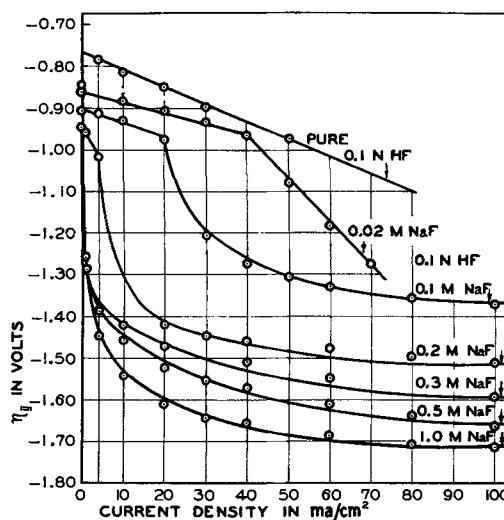


FIG. 2. Cathodic potential, η_{II} , of titanium in 0.1N HF with NaF added vs. current density. Each experimental point is the average of two runs. Hydrogen scale.

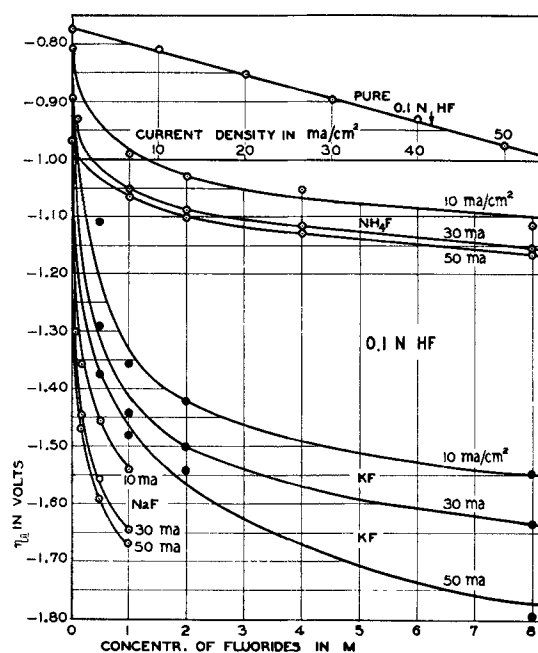


FIG. 3. Cathodic potential of Ti, η_{II} , in 0.1N HF vs. concentration of fluorides at constant current densities. Top inset: η_{II} vs. current density in pure 0.1N HF for comparison. Hydrogen scale.

readings fluctuated too much to obtain reliable readings.

A greater effect was observed with a 0.2% arabic gum solution (technical grade); the potential values conformed with equation (IV) up to $i = 50 \text{ ma/cm}^2$:

$$\eta_{\text{II}} = -(0.83 + 0.0077i) \quad (\text{IV})$$

The cathodic potentials obtained with titanium in pure 0.1N hydrofluoric acid (see Fig. 1 or 2) were more noble and corresponded to equation (V):

$$\eta_{\text{II}} = -(0.77 + 0.004i) \quad (\text{V})$$

Considering the small amounts of these colloids added to the acid, they are nearly as effective as the solutions containing sodium fluoride on the basis of weight per cent.

Methylene blue additions to the 0.1*N* hydrofluoric acid even in such small amounts as 0.005 and 0.02% by weight increased the cathodic potential, as represented by equations (VI) and (VII) up to $i = 100$ ma/cm²:

$$0.005\% \eta_{II} = -(0.72 + 0.0048i) \quad (\text{VI})$$

$$0.02\% \eta_{II} = -(0.58 + 0.0056i) \quad (\text{VII})$$

In all of these cases equation (I) is valid because the titanium dissolved in the acid with the evolution of hydrogen in addition to that developed by electrolysis.

Finally, a complex titanium citrate solution was used as an electrolyte in which the metal did not dissolve at all. In such a solution the Tafel relationship was obtained as expected. The clear solution contained 20 g titanium chloride, 260 g sodium citrate per liter, and some ammonium hydroxide so that the solution showed a $pH = 8.7$. The potential values agreed with equation (VIII) up to $i = 100$ ma/cm²:

$$\eta_{II} = -(0.93 + 0.045 \log i) \quad (\text{VIII})$$

As compared with the potential values in pure 0.1*N* hydrofluoric acid [equation (V)], the results are much more negative in the complex titanium citrate solution.

DISCUSSION AND CONCLUSION

Fig. 3 demonstrates the influence of fluoride additions on the cathodic potential, η_{II} , of titanium. Comparison of the potential values in solutions of varying molar concentrations of the fluorides reveals the strong influence of sodium fluoride, representing the salt effect (4).

There are several possible ways to explain the effect of alkali fluorides, but none of them is satisfactory. The negative potential of the titanium electrode [a' constant of equation (I)] may be caused by the very low concentration of Ti^{3+} as a result of complex ion formation with the fluorides added (2). However, if this is so, at equal concentrations of the three fluorides, nearly the same potential-current density curves should be expected; however, this is not the case as can be seen in Fig. 3. That there is a specific effect of the fluorides on the overvoltage, independent of the Ti^{3+} or Ti^{4+} concentration, is indicated by the fact that the absolute overvoltage values on copper and platinum also increased in the presence of ammonium fluoride (2). Another explanation of this salt effect is given by deBéthune (4).

Adsorption phenomena as well as formation of

some oxide and salt layers on the titanium cathode may be responsible for the increased overvoltage. This is possibly correct in the case of the addition of organic colloids to the hydrofluoric acid, as only weak currents of 50 ma/cm² maximum were obtained through the cathode without fluctuation. However, tests showed that such colloids, dissolved in 0.1*N* hydrofluoric acid, added to pure acid solutions through which a current is already flowing, decreased the current only a small amount.

If fluorides are added to the acid, the conductivity of the electrolyte increases and, under comparable conditions, currents up to 300 ma/cm² could be passed through the cathode. This certainly would not be possible if oxide or salt layers were present in any appreciable amount on the titanium surface. Visual examination of the electrodes showed that layers are not noticeable at higher concentrations of potassium and ammonium fluoride. Finally, it follows from Fig. 3 that the cathodic potential values decrease with decreasing cationic radius, $NH_4^+ \rightarrow K^+ \rightarrow Na^+$, of the fluoride added, the radius being obtained from x-ray data. The sizes of the hydrated ions were discussed by Bockris (16).

ACKNOWLEDGMENT

The authors are grateful to the Wright Air Development Center for support of this work under Contract AF 33(616)-75 and for permission to publish the results obtained.

Any discussion of this paper will appear in a Discussion Section to be published in the June 1956 JOURNAL.

REFERENCES

1. M. E. STRAUMANIS, S. T. SHIH, AND A. W. SCHLECHTEN, *J. Phys. Chem.*, **59**, 317 (1955).
2. M. E. STRAUMANIS AND C. B. GILL, *This Journal*, **101**, 10 (1954).
3. See, e.g., P. DELAHAY, "New Instrumental Methods in Electrochemistry," p. 38, Interscience Publishers, New York (1954).
4. A. J. DEBÉTHUNE, *J. Am. Chem. Soc.*, **71**, 1556 (1949).
5. S. LEVINA AND V. ZARINSKY, *Acta Physicochim. U.R.S.S.*, **7**, 485 (1937).
6. Z. A. JOFA, B. KABANOV, AND E. KUCHINSKI, *ibid.*, **10**, 317 (1939).
7. A. WETTERHOLM, *Trans. Faraday Soc.*, **45**, 861 (1949).
8. J. O'M. BOCKRIS, *Chem. Rev.*, **43**, 525 (1948).
9. M. E. STRAUMANIS, in G. M. Schwab's, "Handbuch der Katalyse," Vol. VI, pp. 132, 137-143, Springer-Verlag, Wien (1945).
10. A. L. FERGUSON, *Trans. Electrochem. Soc.*, **76**, 113 (1939).
11. C. V. KING, *This Journal*, **102**, 193 (1955).
12. N. HACKERMAN AND C. D. HALL, JR., *ibid.*, **101**, 321 (1954).
13. M. E. STRAUMANIS AND P. C. CHEN, *ibid.*, **98**, 234 (1951).
14. J. TAFEL, *Z. physik. Chem.*, **50**, 641 (1905).
15. A. PICCINI, *Atti accad. Linc.*, [4]1, 47 (1885).
16. J. O'M. BOCKRIS, "Modern Aspects of Electrochemistry," p. 62, Academic Press Inc., New York (1954).

Influence of Specimen Area on the Pitting Probability of Aluminum¹

P. M. AZIZ AND HUGH P. GODARD

Aluminium Laboratories Limited, Kingston, Ontario, Canada

ABSTRACT

The pitting probability of 2S aluminum was determined in Kingston tap water as a function of area, for areas ranging in size from 0.06 cm² to 243 cm². The pitting probability was found to vary uniformly with area, from 0.001 to 1 as the area increased from 0.06 cm² to 60 cm²; extrapolation indicated that the pitting probability becomes zero at an exposed area of about 0.055 cm². This work supports the contention that pitting sites in aluminum are not specific macrodefects in the metal surface, but rather arise in a random fashion through the interaction of myriads of anodic and cathodic elements on the metal surface.

INTRODUCTION

Previous publications (1, 2) have reported the development of a theory of the pitting corrosion of aluminum. In this work it has been shown that when a sheet of aluminum is immersed in a natural water that is aggressive, pitting-wise, the initial attack takes the form of general corrosion so that the surface is covered with myriads of local cells. As reaction proceeds, aluminum goes into solution at the local anodes, while alkali forms at the local cathodes through reduction of oxygen and hydrogen ions. As the anodic and cathodic reaction products intermingle, alumina is precipitated from solution, stifling the reaction and passivating the surface, through the formation of a protective film. If the precipitation of alumina does not completely stifle the local cells, then reaction can continue with a consequent continuing modification of the environment about the sites of the reactions. These environmental changes further stimulate local action so that the attack is autocatalytic in nature and those local cells that have survived consequently develop into pits. An autocatalytic mechanism of pitting corrosion very similar to the one here presented has been developed by Edeleanu and Evans (3) from electrochemical measurements carried out on two-compartment cells. If this picture is correct, local environmental differences must be established and maintained if a pit is to initiate and propagate. These environmental differences will be maintained by the local action currents and dissipated by convection and diffusion so that, for any given set of experimental conditions, it is to be expected that a minimum local action current will be required to initiate and maintain pitting. Support for this comes from the fact that a moderate movement of water over the surface

reduces the incidence of pitting and, at only 8 fpm, pitting is completely prevented in an otherwise aggressive medium (4).

As the corrosion of aluminum has been shown to be under cathodic control a reduction of the total area exposed will reduce the local current since it will reduce the available cathode area.

Thus, on this view of pitting corrosion the pitting probability should decrease as the sample area exposed is reduced and should become zero at some small value of the exposed area.

The influence of area on corrosion probability has been studied by Mears and Brown (5). Their work, however, did not cover a range of areas sufficient to test the authors' hypothesis that the pitting probability becomes zero at some small finite value of the area.

EXPERIMENTAL

Since this work was carried out to determine whether there is a minimum area required to sustain pitting, attention was confined to pits actively propagating in tap water at the end of a week.

Description of Material

2S aluminum of the composition shown in Table I was employed throughout this investigation. The metal, obtained in the form of full hard sheets 0.064 in. thick, was sheared into 8 in. x 6 in. panels and annealed for ½ hr at 400°C preparatory to use.

The corrosive medium employed throughout was Kingston tap water, the composition of which is given in Table II.

Procedure

The panels were etched in phosphoric acid at 70°C for 2 min, washed in running tap water for 20 min, and air-dried for 15 hr. The surface of an 18.1 x

¹ Manuscript received February 14, 1955.

TABLE I. % Composition of metal used

Cu	Fe	Si	Ti	Al (by difference)
0.02	0.55	0.13	0.015	99.29

TABLE II. Composition of Kingston tap water

	ppm
pH.....	8.0
Residue on evaporation.....	161
Total hardness.....	127
Bicarbonates as HCO ₃	113
Sulfates as SO ₄	22
Chlorides as Cl ₂	16
Calcium.....	37
Magnesium.....	8
Silica.....	4
Iron.....	0.05
Copper.....	0.015
Electrical conductivity.....	270 recip. megohms at 20°C

TABLE III. Square sizes studied

Size of square	Square area	Squares per panel
cm	cm ²	
0.25 x 0.25	0.06	3858
0.50 x 0.50	0.25	912
0.75 x 0.75	0.5	432
1.0 x 1.0	1.0	252
1.5 x 1.5	2.2	108
4.5 x 3.4	15	16
4.5 x 6.75	30	8
9 x 6.75	61	4
9 x 13.5	122	2
18 x 13.5	243	1

TABLE IV. Pitting probabilities and total number of pits measured

Total No. of squares	Size of square	Area of square	Pitting probability	Total No. of pits	Probability of obtaining one pit
	cm	cm ²			
14,432	0.25 x 0.25	0.06	0.001	46	0
3858	0.50 x 0.50	0.25	0.10	604	0.15
1728	0.75 x 0.75	0.56	0.25	724	0.38
1008	1.0 x 1.0	1.0	0.47	644	0.55
432	1.5 x 1.5	2.25	0.50	293	0.42
64	4.5 x 3.4	15.2	0.88	339	0.14
32	4.5 x 6.75	30.4	0.91	219	0.03
16	9 x 6.75	61	1	376	0
8	9 x 13.5	121	1	238	0
4	18 x 13.5	243	1	321	0

13.5 cm area of the panel was then divided into the requisite number of squares with wax solution (Xylol saturated with paraffin at 30°C) preparatory to exposing the samples. The various square sizes employed are given in Table III. Wax lines were

applied to the panels with 1, 2, 4, 8, and 16 squares with an ordinary ruling pen. The remaining panels were prepared by stamping a wax grid onto the surface with a rubber stamp (6). The wax was permitted to dry for 15 hr and then drops of tap water were placed in each of the squares formed by the grid. The panels were placed for seven days in a closed space over water as previously described (7), then removed, washed, and dried. The number of pits in each square was counted and the pitting probabilities computed. Four panels of each square size were exposed simultaneously.

RESULTS AND DISCUSSION

The probability of obtaining one or more pits per square, and the probability of obtaining only one pit per square were computed from the experimental data and are recorded in Table IV. In addition, the total number of pits developed at each level of subdivision is also presented.

These data are also presented graphically as a function of the logarithm of the surface area exposed at each square size in Fig. 1.

Examination of this figure shows that as the area exposed decreases from 243 cm² the pitting probability remains constant at a value of 1 until the area has decreased to a value of about 60 cm². Thereupon the probability decreases with decreasing area until it reaches a value of 0.001 at an area of 0.06 cm². If the curve of the total number of pits developed is extrapolated to zero, it will cut the axis at an area of about 0.055 cm²; thus, at and below this value the pitting probability is zero. Hence it may be concluded that an exposed area of at least 0.055 cm² is required for the initiation and propagation of a pit under the conditions of the experiment.

These results are considered good evidence in favor of the view that pitting is due to a mechanism of the type presented in the introduction to this

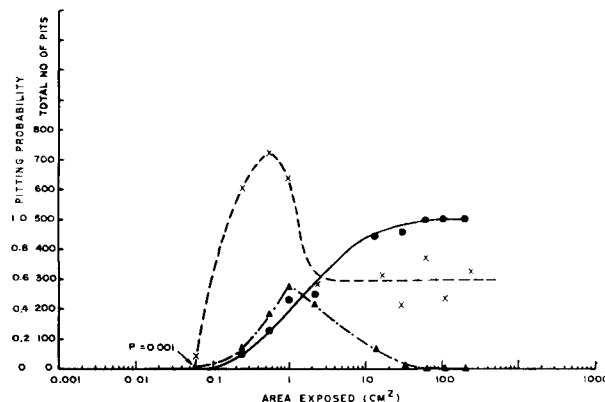


FIG. 1. Pitting probabilities and total number of pits developed as a function of area. \blacktriangle — \blacktriangle , Probability of one pit vs. area; \bullet — \bullet , pitting probability vs. area; \times — \times , total number pits vs. area.

paper in which pitting is considered to be due not to specific macrodefects in the surface of the sheet, but rather to the prevention of complete passivation of the metal surface because of environmental differences set up through the agency of local action currents flowing over the surface of the metal.

It is interesting to examine the dependence of the total number of pits developed on four panels on the degree of subdivision. This remains essentially constant with decreasing area until an area of about 5 cm² is reached, whereupon the number of pits starts to increase, goes through a maximum, and falls rapidly to zero.

These results can be explained as follows. The total number of pits on a fixed area remains constant as long as the linear dimensions of the individual squares are greater than the distances over which the pits interact with each other. When the dimensions of the waxed squares become less than these interaction distances, then the total number of pits increases because interaction and suppression of pits between areas that originally pitted and areas that did not pit is now prevented by the wax lines and hence originally unpitted areas can now pit. When these dimensions are decreased still further so that the size of the waxed-off areas approaches the minimum required to sustain pitting the total number of pits falls.

The maximum probability that a square will contain one pit occurs at a size of 1 cm². Since the pits were observed to be distributed randomly within the waxed-off squares, the maximum distance of influence of a pit is about $\sqrt{2}$ cm, in other words, it will draw current from a cathode area of about 1 cm in radius under the conditions studied.

It should be pointed out that the positions of the maxima and the shape of the curves will depend on the medium employed and especially on its conductivity, since changes in conductivity alter the extent of the cathode area from which the pit can draw current.

Furthermore, more aggressive solutions or those of greater conductivity than the one herein employed permit greater local action currents to flow during the initial stages of attack and hence environmental differences are more easily established so that a

smaller exposed area is necessary to sustain pitting than that found in this work. Similarly, smaller local action currents would flow in solutions less aggressive or of lower conductivity than the tap water here employed and under these conditions a larger area would be needed to sustain pitting.

The experimental results reported here substantiate the views developed in the introduction to this paper and are considered good evidence that pit sites are not due to specific local macrodefects in the surface of the metal, but rather arise in a random fashion through the interaction of myriads of anodic and cathodic elements on the metal surface between which local action currents flow on initial immersion of the sample in the corrosive environment. The net result of this interaction would be the production of an insoluble corrosion product which can be precipitated in one of the three following ways leading to the three types of behavior indicated:

(A) The corrosion product may be precipitated in contact with the metal surface completely passivating it and stifling reaction.

(B) The corrosion product may be precipitated in contact with the metal surface but incompletely passivating it, causing a localization of the attack and thus leading to pitting.

(C) The corrosion product may be precipitated out of contact with the metal surface leading to general corrosion.

If (B) occurs, the case in which we are here interested, it can be seen that pit sites will be distributed in a random fashion.

Any discussion of this paper will appear in a Discussion Section to be published in the June 1956 JOURNAL.

REFERENCES

1. P. M. AZIZ, *This Journal*, **101**, 120 (1954).
2. P. M. AZIZ, *Corrosion*, **9**, 88 (1953).
3. C. EDELEANU AND U. R. EVANS, *Trans. Faraday Soc.*, **47**, 1121 (1951).
4. T. E. WRIGHT AND H. P. GODARD, *Corrosion*, **10**, 195 (1954).
5. R. B. MEARS AND R. H. BROWN, *Ind. Eng. Chem.*, **29**, 1087 (1937).
6. J. P. CHILTON AND U. R. EVANS, *J. Iron Steel Inst. (London)*, In press.
7. P. M. AZIZ AND H. P. GODARD, *Ind. Eng. Chem.*, **44**, 1791 (1952).

Electron Microscope Studies on Copper Deposits from Sulfate and Cyanide Baths¹

SHINZŌ OKADA AND SABURŌ MAGARI

Engineering Research Institute, Kyoto University, Kyoto, Japan

ABSTRACT

Copper deposits from sulfate and cyanide baths, at low current densities, show lack of uniformity on various cathodes. The crystal structure of the base metal has a profound influence on the nonuniformity, which is characteristic for a given single crystal cathode, but differs markedly for the two different electrolytes. Planes parallel to (010) and (111) planes of the base crystal develop in a copper sulfate bath while, in a cyanide bath, planes develop parallel to the (130) plane of the base crystal.

INTRODUCTION

It has generally been considered that deposition of copper on a copper cathode tends to perpetuate the structure of the base metal. The relation between crystal growth and number of nuclei has been studied by Glazunov (1), while Takeyama has reported that, under favorable conditions, the copper deposited in the early stages of deposition consisted of a nearly perfect single crystal (2).

The present study was made to determine the orientation of the deposit relative to that of the base metal, by means of the electron microscope. This approach presented two problems. One was the reproducibility of replicas, the other was to locate the identical spot on the cathode under the electron microscope before and after electrolysis. Satisfactory experimental solutions to these problems have been discussed elsewhere (3) and need not be detailed here.

EXPERIMENTAL

The copper sulfate bath contained 150 g/l copper sulfate pentahydrate and 40 g/l sulfuric acid. The cyanide bath contained 22.5 g/l copper cyanide, 30.0 g/l sodium cyanide, and 10.0 g/l sodium carbonate. Electrolysis occurred, without agitation, at 30°C in all experiments. The anodes were 2 cm x 2 cm rolled copper plates, while the cathodes were copper plates, characteristics of which varied for different experiments. One side of each anode and cathode was coated with polyvinyl formal.

The negative replica method was used for electron microscopy. A benzol solution of polymethyl methacrylate was poured on the surface of the electrode before electrolysis and allowed to dry. The resin film was then carefully removed from the electrode, placed in a vacuum evaporator, first

coated with aluminum and then shadowed with chromium in the usual manner. After deposition, the electrode was successively rinsed with distilled water and ethanol, dried, and again treated with polymethyl methacrylate as outlined above. The technique outlined previously (3) was used to locate the identical spot on the electrode under the electron microscope before and after electrolysis.

RESULTS

Deposition from Copper Sulfate Electrolyte

On electropolished rolled copper.—Copper was deposited on the electropolished surface of a rolled copper plate, 2 cm x 2 cm in area and 0.5 mm thick, at current densities between 20 ma/cm² and 1.6 ma/cm². The deposit was almost uniform over the cathode, at higher, but not at lower, current densities. The lower the current density the more exaggerated was the nonuniformity. The electrolysis at higher current densities has been discussed earlier (4), and only the results for lower current densities are discussed here.

In Plate I (a) is shown the initial surface of a copper electrode that has been electropolished in 50% phosphoric acid solution, in preparation for electrolysis. The "pine needle" appearance was characteristic of all specimens prepared in this way.

Electrodeposition for 2 min at 1.6 ma/cm² gave the nonuniform deposit shown in Plate I (b), which, on further electrolysis for 22 min, gave the accentuated unevenness of Plate I (c). If it is assumed that the deposit is uniform over the surface, and that the current efficiency is 100%, the thickness of the deposit is about 1 μ .

The nonuniformity of the deposit is believed to be due to preferential discharge of copper ions at different rates at the most readily accessible points on differently oriented crystals of the base metal. Under an optical microscope, it appeared that uniform portions of the surface carried no deposit and

¹ Manuscript received August 30, 1954. This paper was prepared for delivery before the Pittsburgh Meeting, October 9 to 13, 1955.

that the uneven parts were due to "islands" of the deposit.



PLATE I(a). $\times 2600$

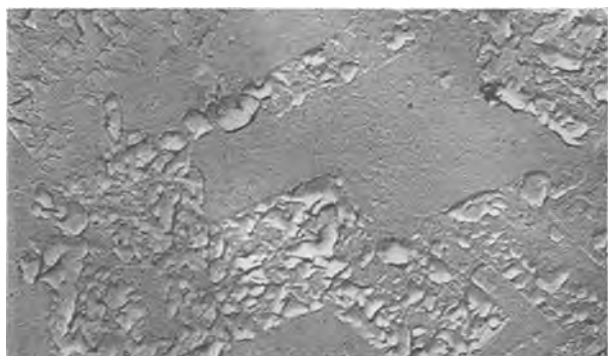


PLATE I(b). $\times 2600$

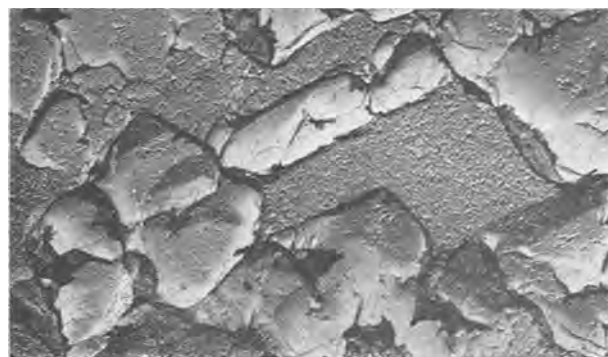


PLATE I(c). $\times 2600$



PLATE II. $\times 2600$

On chemically etched rolled copper.—Copper was deposited at current densities between 20 ma/cm² and 1.6 ma/cm² on a rolled copper cathode etched with 10% ammonium persulfate to reveal the (100) planes (5). The nonuniformity of the deposits was again observed at the lower current densities, as shown in Plate II.

On annealed copper.—With the rolled cathodes used in the previous experiments it was not possible to discern each crystal of the base metal clearly. It seemed possible that the rolling process had strained the metal in the cathodes, and the strains might have affected the deposits. A study was made, therefore, of the nature of deposits on rolled cathodes which had been annealed at 800°C for 5 hr to induce

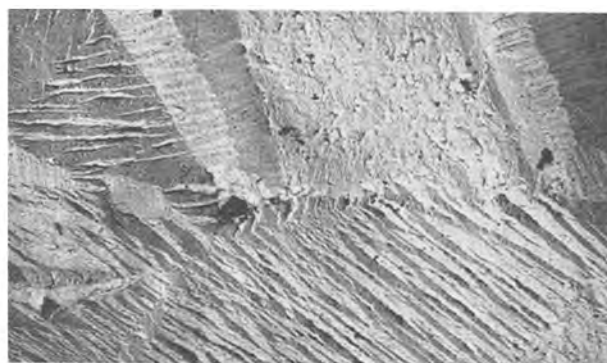


PLATE III(a). $\times 2600$

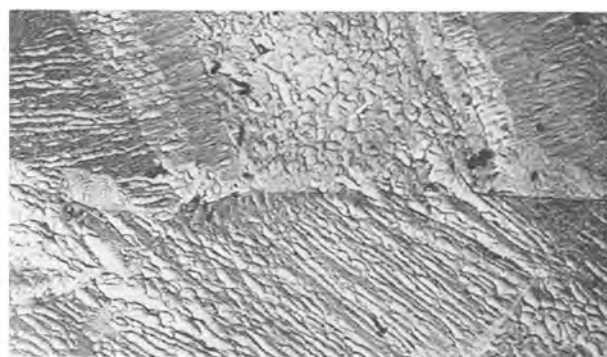


PLATE III(b). $\times 2600$

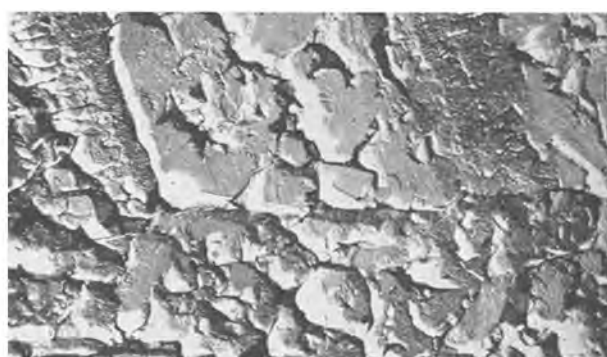
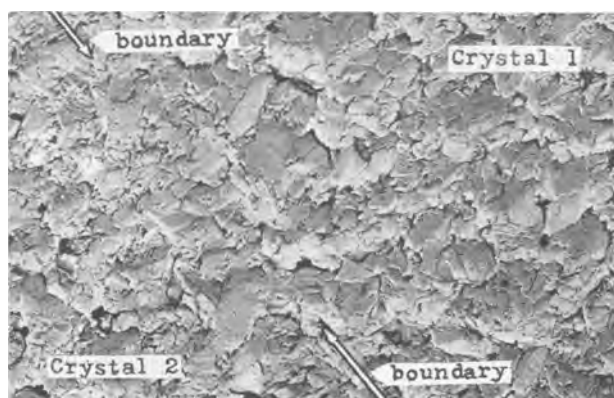
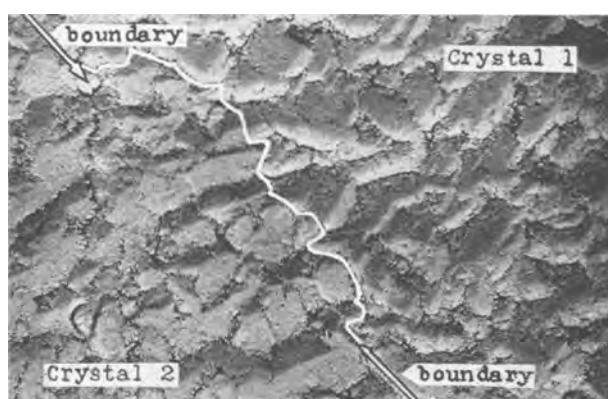


PLATE III(c). $\times 2600$

PLATE IV(a). $\times 3000$ PLATE IV(b). $\times 3000$

larger crystals and relieve working strains. The initial surface of these cathodes, after etching with 10% ammonium persulfate, is shown in Plate III (a). After electrolysis at 1 ma/cm² for 3 min, the surface depicted in Plate III (b) was obtained. Further electrolysis for 30 min gave the surface revealed in Plate III (c). The isolated patches of deposit, characteristic of Plate I, did not appear, and the surface of the deposit was of uniform appearance. It appears that strains present in the rolled cathodes were, indeed, responsible for the lack of uniformity in deposits on such cathodes, and that the nature of the deposit over a given crystal was determined by the underlying crystal.

On single crystal-copper.—To determine the relation between the orientation of the deposit and the crystal orientation of the base metal, copper was deposited on an electropolished cathode composed of two single crystals of known orientation. The cathode shows the pine needle design, with no crystal boundary evident, characteristic of the electropolished surface. After electrodeposition for 17 min at 1 ma/cm², the surface assumed the condition shown in Plate IV (a), where the crystal boundary is discernible. The boundary became accentuated after 53 min additional deposition, as shown in Plate IV (b); this is shown more clearly by the greater magnification of Plate V. The ability

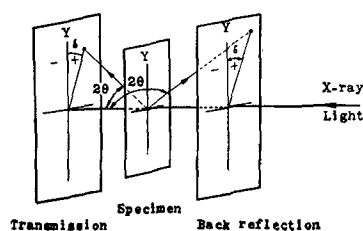


FIG. 1

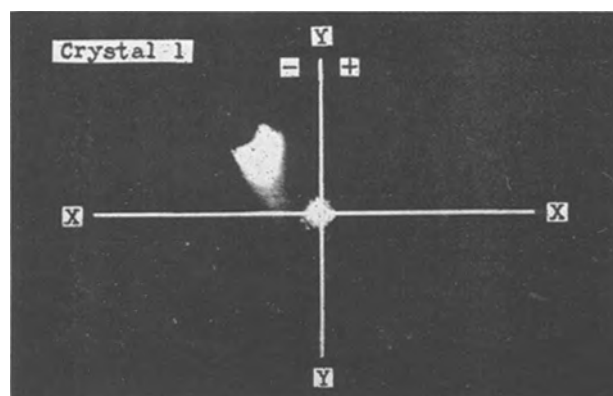


FIG. 2(a)

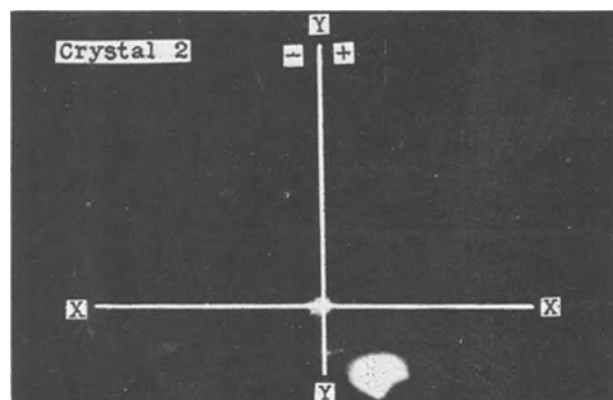


FIG. 2(b)

to distinguish the boundary after deposition shows that the deposits on the two crystals were different.

To determine the orientation of the mosaic blocks composing the two deposits, ordinary light reflected from the crystal facets of the electrodeposit was used as a means of establishing the position of the facets relative to a certain arbitrary set of axes (6). Then, with the crystal in the same position and using transmitted x-ray, the orientation of the original single crystal which was used as the base metal was determined. By comparison of the two sets of data it was learned which planes in the original base-metal crystal were approximately parallel to the facets of the electrodeposit. The x-ray study, however, does not yield information on the crystal orientation of the electrodeposit; such information can be obtained only by electron diffraction.

The two methods are illustrated schematically

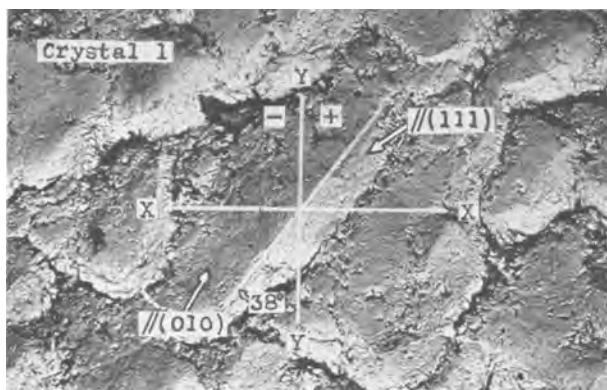


PLATE V(a). $\times 5900$

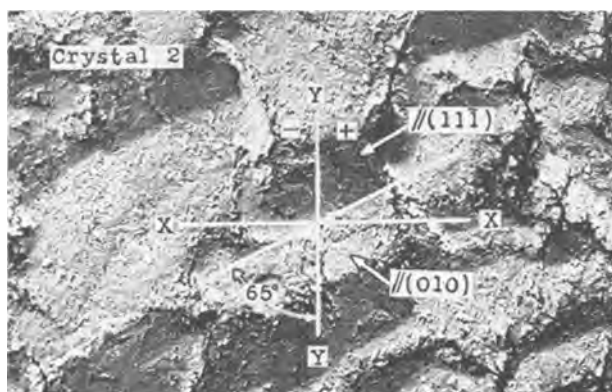


PLATE V(b). $\times 5900$

TABLE I (a)

		Crystal 1		Crystal 2		
		δ	θ	δ	θ	
Sulfate bath	Deposit on polished surface	Optical	-40° (P_1)	72°	145° (P_2)	73°
	Deposit on etched surface	Optical	-40° (E_1)	72°	142° (E_2)	73°
	Index of (010) of base crystal	X-ray	-40°	68°	145°	65°

TABLE I (b)

		Crystal 1		Crystal 2		
		δ	θ	δ	θ	
Sulfate bath	Deposit on polished surface	Optical	113° (P_1)	59°	-14° (P_2)	59°
	Index of (111), (11 $\bar{1}$) of base crystal	X-ray	114° (111)	56°	-9° $(11\bar{1})$	58°

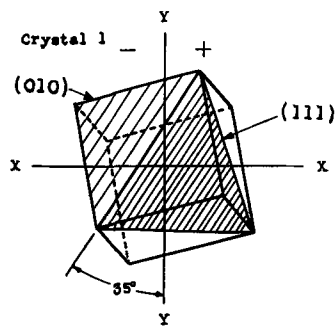


FIG. 3(a)

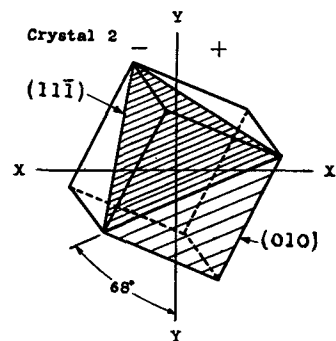


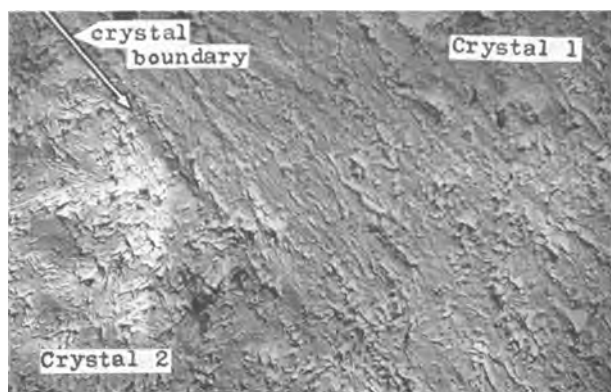
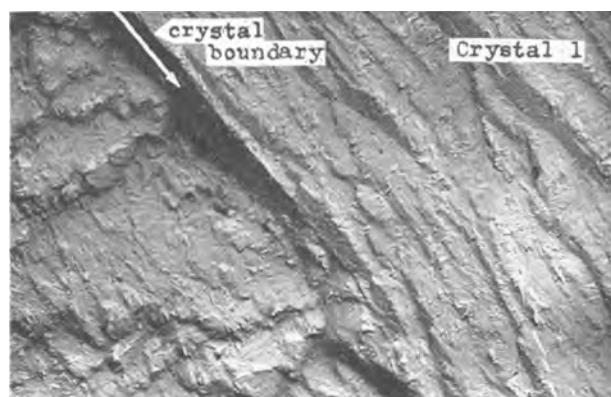
FIG. 3(b)

in Fig. 1. The specimen was not rotated for the optical examination, and the reflected light was received on a photographic plate rather than observed visually. Optical data were directly comparable with the transmission data; these are recorded in Table I (a) and (b). The patterns of the back reflection from the deposits on crystals 1 and 2 are shown in Fig. 2 (a) and (b), respectively. It will be noted that the reflection spread considerably, with the 0.5 mm aperture used, probably because of imperfect orientation of the facets of the deposit. In Fig. 3 (a) and (b) are shown the corresponding unit cells for crystals 1 and 2, as determined from x-ray patterns. In Table I, the δ and θ values for the base crystals, from the x-ray analysis, show only the index of the plane in the original crystal which most nearly corresponds to the plane of the reflecting facet of the deposit, as given by the reflection with ordinary light.

When the single crystal-cathode was etched with 10% ammonium persulfate, rather than electropolished, and electrodeposition continued for 2 hr at 1 ma/cm², the optical back reflection gave results comparable with those obtained on the electropolished crystals (Table I).

It might be noted that, although the results in Table I are for intermittent electrolysis, the same results were obtained by continuous electrolysis.

Deposition from Copper Cyanide Electrolyte
On electropolished and etched rolled copper.—Copper

PLATE VI(a). $\times 4000$ PLATE VI(b). $\times 4000$

was deposited from a cyanide bath on rolled copper cathodes at current densities between 10 ma/cm^2 and 1.6 ma/cm^2 . Regardless of whether the cathode had been electropolished or chemically etched, in the manner of the earlier experiments, no nonuniformity of the deposit was observed at any current density. All the deposits were very fine in crystal grain and smooth.

On single-crystal copper.—To determine whether the deposit from a cyanide electrolyte would show a characteristic plane on a single-crystal cathode, copper was deposited on the electropolished bicoystal cathode described previously, at 0.5 ma/cm^2 . The initial surface of the cathode again did not reveal the crystal boundary.

After electrolysis for 30 min, however, the boundary became evident [Plate VI (a)], and further electrolysis for more prolonged periods made it much more pronounced [Plate VI (b), electrolysis time of 150 min]. Plates VII (a) and (b), show the surface corresponding to Plate VI (b) under greater magnification. It is clear from the evidence presented that the deposit was influenced by the orientation of the base crystal. Data for the optical back reflection of the deposit and x-ray examinations of the base crystals respectively are given in Table II. As before, x-ray data show which plane in the base crystal has indices nearest to those of the facet of

TABLE II

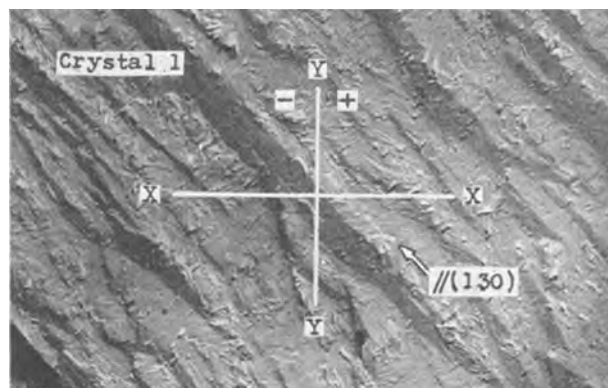
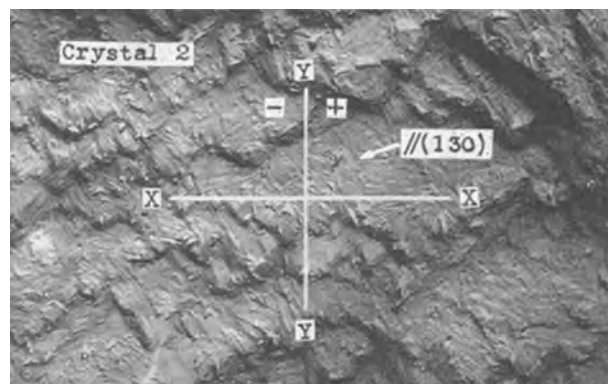
		Crystal 1		Crystal 2		
		δ	θ	δ	θ	
Cyanide bath	Deposit on polished surface	Optical	-105° (P_1)	78°	-165° (P_2)	78°
	Deposit on etched surface	Optical	-102° (E_1)	80°	-165° (E_2)	80°
	Index of (130) of base crystal	X-ray	-100°	80°	-170°	77°

the deposit that gave the back reflection. Again, data for intermittent electrolysis were the same as those for continuous electrolysis.

When the single-crystal cathode was chemically etched, electrolysis in the cyanide bath for 2 hr at 0.5 ma/cm^2 yielded a deposit for which the back reflection values are those shown in Table II.

DISCUSSION

Deposition from copper sulfate electrolyte.—The data of Table I are summarized stereographically in Fig. 4. P_1 and P_2 represent the normals to the

PLATE VII(a). $\times 3700$ PLATE VII(b). $\times 3700$

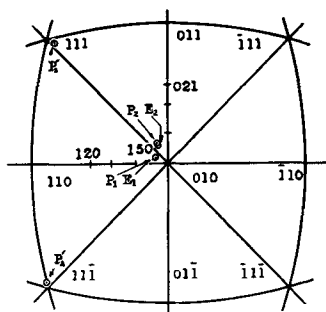


FIG. 4

optical reflecting facets for the deposit on the electropolished crystals 1 and 2, respectively. E_1 and E_2 represent the corresponding facets for the deposit on the etched crystals 1 and 2. While the four points conceivably represent the (171) plane, it is adequate to associate them with the simpler (010) index. The optical back reflecting facets of the deposit on crystal 1, with the normals P_1 and E_1 , are heavily shadowed planes of Plate V (a), and these are parallel to the (010) plane of the base crystal. From Table I (b), the lightly shadowed planes of Plate V (a) are considered to be parallel to the (111) planes of the base crystal. The back reflection facets of the deposit on crystal 2, with the normals P_2 and E_2 , are the lightly shadowed planes of Plate V (b), and these planes are parallel to the (010) planes of this base crystal. From Table I (b), heavily shadowed planes

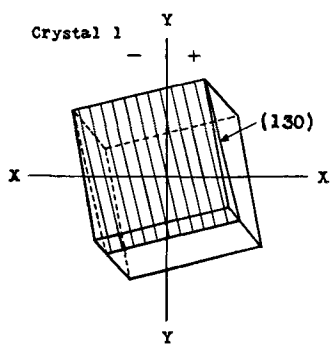


FIG. 5(a)

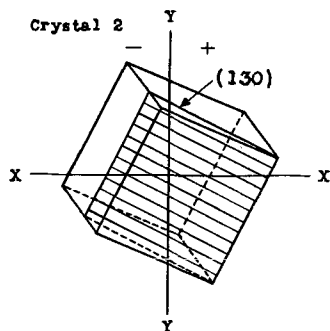


FIG. 5(b)

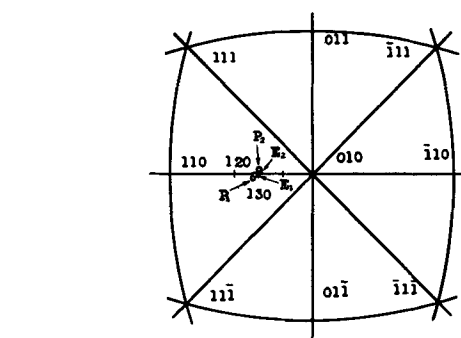


FIG. 6

are thought to be parallel to the $(11\bar{1})$ planes of the base crystal.

It is concluded that the deposition from a sulfate bath on a single crystal occurs with planes parallel to the (010) and (111) planes of the base crystal.

Deposition from copper cyanide electrolyte.—The data of Table II are summarized stereographically in Fig. 6. As before, P_1 and P_2 represent the normals to the optical back reflecting facets for the deposit on the electropolished crystals 1 and 2, respectively, and E_1 and E_2 the corresponding facets on the chemically etched crystals. The normals to these facets are near the normal to the (130) planes of the base crystal. Hence, the back reflecting facets are parallel to the (130) plane of the base crystal. Fig. 5 (a) and (b) shows a unit cell of the base crystals 1 and 2, corresponding to Plates VII (a) and (b). The lightly shadowed planes in Plates VII (a) and (b) are parallel to the (130) plane of the base crystal, shown by hatching in Fig. 5 (a) and (b).

It is concluded that the deposit from a cyanide bath on a single crystal shows planes parallel to the (130) plane of the base crystal.

ACKNOWLEDGMENTS

The authors are deeply indebted to Dr. J. Takamura, Faculty of Engineering, Kyoto University, for supplying the copper single crystals and for his valuable advice. The authors also are indebted to Dr. M. Kawane, Engineering Research Institute, Kyoto University, for his advice.

Any discussion of this paper will appear in a Discussion Section to be published in the June 1956 JOURNAL.

REFERENCES

1. V. GLAZUNOV, *Z. phys. Chem.*, **167**, 399 (1933).
2. S. TAKEYAMA, *Mem. Coll. Sci. Univ. Kyoto*, **13**, 363 (1930).
3. S. OKADA AND S. MAGARI, *Bull. Eng. Research Inst. Kyoto Univ.*, **3**, 59 (1953), (text in Japanese).
4. S. OKADA AND S. MAGARI, *ibid.*, **4**, 93 (1953), (text in Japanese).
5. S. OKADA AND S. MAGARI, *ibid.*, **5**, 83 (1954), (text in Japanese).
6. B. FUJITA, *Mem. Coll. Sci. Univ. Kyoto*, **12**, 160 (1929).

A Study of the Etching Rate of Single-Crystal Germanium¹

PAUL R. CAMP²

RCA Laboratories, Radio Corporation of America, Princeton, New Jersey

ABSTRACT

A study has been made of the rate at which single-crystal germanium is etched under various conditions. For simplicity, the principal etchants used were composed of only H₂O₂, HF, and water. Data are given for the rate as a function of temperature and composition of the etchant, and as a function of the orientation and impurity content of the crystal. An equation which assumes two reactions taking place in sequence on the surface fits the rate vs. temperature data within the limits of experimental error. In the range studied, the rate-controlling processes are sensitive to sample orientation. From etching data, a value was obtained for the thickness of the disturbed surface layer due to abrasive grinding. This was found to be in the range of 2–10 μ and to depend on sample orientation and abrasive particle size. Comparative data are given for two common etchants of a more complicated composition.

INTRODUCTION

For several years, the treatment of germanium by etching has played an important role in the production of germanium devices and in the preparation of samples for research purposes. In the last two years, such treatment has become an increasingly important tool for investigating the orientation and quality of germanium samples, different treatments revealing different properties of the material. But the treatments themselves have not been well understood. In the hope of progressing toward an understanding of these processes, a study has been made of the etching rate of germanium crystals under various conditions. For simplicity, most of the work has been confined to etchants containing only HF, H₂O₂, and water. In order to insure sample uniformity, all samples were cut from one large single crystal of As-doped, *n*-type germanium. Since the resistivity of the crystal varied slowly along its length, resistivities between 1 and 9 ohm-cm could be obtained by selecting samples from the proper region of the crystal. The samples were thin, usually of the order of 30 mils thickness, so that the ratio of face area to edge area was large. The error introduced by including the edge area as if it were of the same orientation as the face was less than 2%. The samples were held with polyethylene-coated tweezers and the area of contact was small enough to be neglected. Etching rates were obtained by measuring the loss of weight of a sample after a known etching time. Weights were measured to 0.2 mg and the weight differences were usually of

the order of 20 mg. Considerable attention was given to the freshness and composition of the etchants and to the surface preparation of the samples. In order that the circulation of the etching solution should not influence the results, all experiments were performed under conditions of agitation sufficiently violent that substantial changes in agitation made no difference in the etching rate.

GENERAL PRECAUTIONS

Since little was known about the effects of various parameters on the etching rate, much effort was devoted to insuring that only the parameter under investigation was influencing the results. This was done either by comparison of samples differing in only one respect, or by direct experiment to determine what parameters could be ignored safely.

Temperature.—The temperature was maintained constant by immersing the etching vessel in a constant temperature bath. The volume of etchant used, about 60 cc, was large compared to the volume of the samples. The temperature of the etchant was measured directly to $\pm 0.3^\circ\text{C}$ by means of a polyethylene-coated thermometer.

Resistivity.—The samples used were kept short so that the variation in resistivity along the length was less than $\pm 5\%$ from the mean except for the 1 ohm-cm sample. Insofar as possible, samples were compared which were cut from the same depth in the crystal. All samples were labeled to show from what part of the crystal they came. Thus, the notation 4(100)3-2 means that the sample was from the fourth resistivity region of the crystal, a (100) cut, and the third slab from the surface. This sample was then cut into smaller pieces, the -2 indicating the second such piece.

Etch composition.—Etches were made up fresh

¹ Manuscript received January 11, 1955. This paper was prepared for delivery before the Chicago Meeting, May 2 to 6, 1954.

² Present address: Polytechnic Institute of Brooklyn, Brooklyn, New York.

each day in batches large enough that the composition was measured with an accuracy greater than the assay of the reagents used. Most work was done with the simplest etch (1 HF, 1 H₂O₂, 4H₂O), called the No. 2 etch (see appendix for etch compositions). The variation in the concentration of the reagent H₂O₂ used (5 parts in 30) was sufficient to introduce a rate error of about $\pm 4\%$. However, in most experiments, the same reagent was used. Therefore, although the absolute values may have been affected, the accuracy of the comparisons was determined by other factors.

Faust (1) reported that the presence of polyethylene in contact with the HF-H₂O₂ etch increases the reaction rate. Both the reagent HF and H₂O₂ in the present study were stored, prior to use, in polyethylene bottles. To determine stability, a stock solution of No. 2 etchant was kept in a polyethylene bottle for an additional six weeks; the rate measured at the end of this period was the same as that measured at the start. This indicates that etching solutions may actually be made up in large quantities and used over a considerable period of time.

Weighing.—Etching rates were obtained by measuring the loss of weight of the sample during a measured time of etching. Weights were measured to ± 0.2 mg. Weight differences were usually of the order of 20 mg.

Agitation.—In order to make certain that the rate of agitation used did not influence the results, a set of measurements was made of the weight loss of a sample etched under different conditions of agitation. This experiment was done at 40°C, a temperature at which the rate of etching was known to be high. The curve is shown in Fig. 1. One agitation is a movement to and fro of 1 in. in a 60-cc beaker containing 40 cc of solution, and it is seen that one or two agitations per second are enough to stabilize the etching rate. All subsequent measure-

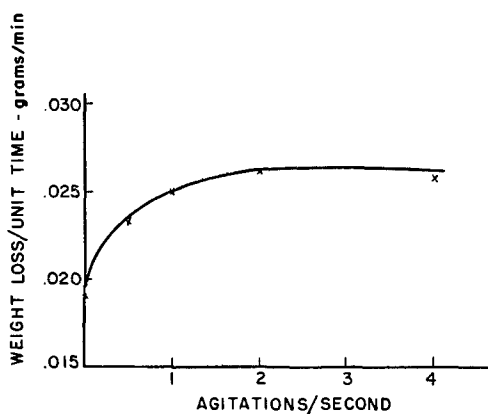


FIG. 1. Effect of agitation on the etching rate. (One agitation is a movement to and fro of 1 in.)

ments were made at a rate of 2-4 agitations per second, well above the critical region.

Surface preparation.—Most samples were fine-ground with American Optical Company No. 305 abrasive and all were pre-etched for 5-20 min in No. 2 etch at room temperature. As will be seen in the next section, this was apparently more than sufficient to remove the disordered surface layer.

RATE VS. TIME OF ETCHING

A number of thin samples was prepared by uniformly grinding their surfaces with No. 305 abrasive in water on a glass plate. They were weighed, etched for a short time in No. 2 etch at constant temperature, and weighed again. The average etching rate for this interval was then computed. The etching and weighing process was repeated until the rates became constant. Average rates were plotted at the mid points of their respective intervals and a rate-vs.-time curve obtained. A representative sample of the experimental results is shown in Fig. 2. The values shown are for three differently oriented samples cut from the same 9 ohm-cm crystal. A second set of data, obtained with 1-6 ohm-cm samples, resulted in similar curves, as did data for these samples ground with a coarser abrasive (No. 303½).

The following explanation can account for the shape of the experimental curves, the measured

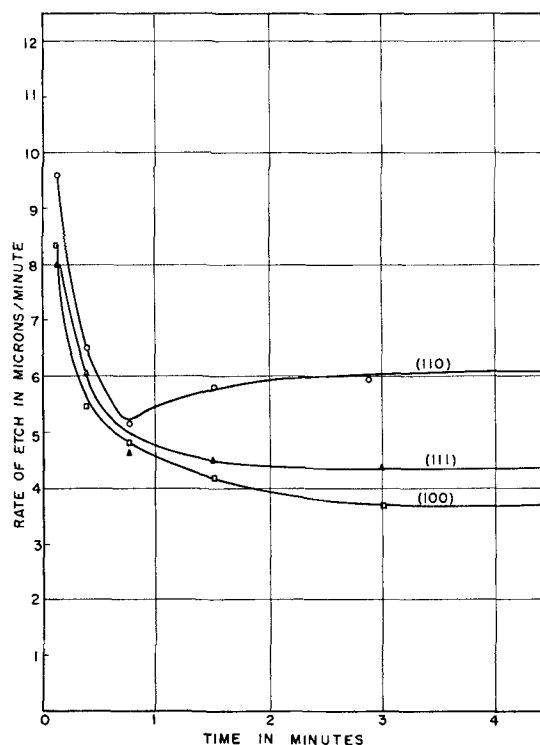


FIG. 2. Rate of etching as a function of time of etching and crystal orientation. Before etching was begun, the surface was finely ground with No. 305 abrasive.

TABLE I. Thickness of disordered layer vs. crystal orientation

Sample	Approximate thickness of disordered layer in microns, for surface indicated		
	(100)	(111)	(110)
Set 1. 9 ohm-cm No. 305 Abrasive	7	5	3
Set 2. 1-6 ohm-cm No. 305 Abrasive	5	4	3
Set 2. 1-6 ohm-cm No. 303½ Abrasive	10	10	5
Predicted relative values (see text)	10	0-12	5

thickness of the disordered layer, and its dependence on particle size and crystal orientation. Grinding produces pits whose basal area is of the order of magnitude of the cross-section area of the grinding particles. In the pits, there is a tendency for the cleavage planes (111) to be exposed. If the pits were simply formed by (111) planes, their depths would be in the order shown in the last line of Table I. (Only a range of values can be given for pits of this kind on the (111) surface because they may be truncated at any depth by the (111) plane parallel to the surface.) Pitting increases the etching rate by increasing the surface area. However, the rate will be modified by the particular faces present in the pits. As the crystal etches, the slow etching planes develop as pit faces in preference to the rapidly etching ones. For the (110) cut, the decrease in rate due to the development of slow etching faces in the pits ultimately dominates the increase due to area and results in the dip shown in Fig. 1. As etching progresses, the pits widen and grow shallower until their effect is negligible. The rate becomes a constant characteristic of the initial orientation of the sample and independent of previous surface history.

The thickness of the layer which must be removed before the etching rate becomes constant can be estimated from the curves of Fig. 2. Values of the range 2-10 μ are obtained. These are in the same range as the values for the thickness of the disordered layer reported by Faust (1) from life-time measurements and by Weissman (2) from x-ray line broadening studies. Clarke (3) has reported that the thickness of the disturbance which causes a change in the resistivity is an order of magnitude smaller (0.5 μ). This suggests that those properties of the lattice which affect lifetime and line width are disturbed to about the same depth as the surface is cracked and pitted. If this is true, the disturbed surface layer should be a function of crystal orientation and abrasive particle size. If the limit of the disturbance is arbitrarily defined as that depth at which the rate of etching has dropped to within 10% of its final value, the results are as shown in Table I.

RATE VS. TEMPERATURE FOR VARIOUS ORIENTATIONS

The temperature dependence of the etching rate was measured for three crystal orientations. Data are plotted in Fig. 3, and it is seen that they do not lie on a simple straight line corresponding to a single activation energy. The points with the dots in the center were taken initially, while those with the crosses in the center are supplementary data taken with the same samples at a later date. The data are fitted approximately by pairs of straight lines which intersect at a knee in the vicinity of room temperature; the mean square deviation from these lines is about 5½%. The slopes of the lines give the approximate activation energies above and below room temperature as shown in Table II.

There are three particularly interesting features of these data: the change in order as the temperature is reduced, the knee occurring in all three curves at about room temperature, and the parallelism of the (110) and (111) curves.

At temperatures above 25°C, the rate is greatest for the (110) orientation and least for the (111) orientation. This order is in agreement with the order predicted some time ago from the etching of small germanium spheres (4). To check the reversal of order of the rates for the (100) and (111) surfaces at low temperatures, two adjacent samples were cut so that the (110), (111), and (100) surfaces were exposed. They were then ground identically and

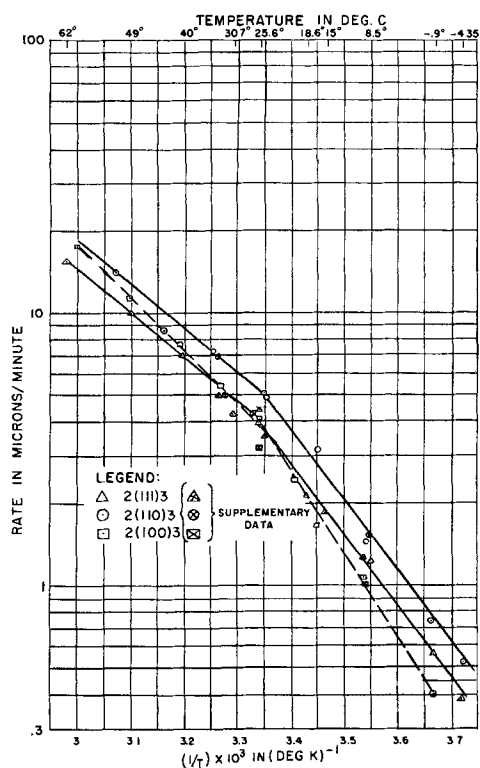


FIG. 3. Rate of etch vs. $1/T \times 10^3 (\text{deg K})^{-1}$ for 3 crystal orientations. (No. 2 etch, 1 ohm-cm *n*-type germanium.)

TABLE II. Activation energy in kilocal/mole

Face	Above room temp		Below room temp	
	From slope	Fitting by eq. (I) (see below)	From slope	Fitting by eq. (I)
(100)	8.6	7	13.6	17
(110)	7.4	6	12.0	15
(111)	7.4	6	12.0	15

etched to remove the same amount of material. One was etched at 36.5°C, the other at 0°C, and the pit shapes compared. Characteristic pits were different and, assuming that the slow etching faces predominate in the pits, their shapes tended to confirm the rate data.

The question arises as to whether or not, on a microscopic scale, more than one crystal face etches. It seems evident that at least two different faces must etch, for Fig. 3 shows at least two orientation-dependent activation energies. Furthermore, if only two faces do etch, the measured rate should be a linear combination of these two rates. If only two faces etch and these are included in the group measured, the crystal geometry indicates that the rate for the third must be strongly affected by both. Thus, the reversal of order of the (100) and (111) at low temperatures becomes difficult to interpret. Apparently, therefore, if only two faces do etch, they are not any pair of the three studied.

The general shape of the rate vs. temperature curves cannot be accounted for either as the product or as the sum of terms of the form $A \exp(-E/kT)$. However, if the process is analyzed as a sequence of operations taking place on a limited surface, an equation is obtained which fits the data to within the limits of experimental error. The fact that the surface plays an important role is clear from the dependence on orientation over the whole temperature range.

Consider n reactions taking place consecutively on a surface. The rate of each process will be controlled not only by the temperature and concentration of the particular reactant involved, but also by the fraction of the surface available to that reaction. Thus,

$$R_j = a_j c_j^{p_j} f_j \exp(-E_j/kT)$$

where a_j = constant associated with reaction j ; c_j = concentration of reactant involved in reaction j ; p_j = power to which c_j enters reaction j ; f_j = fraction of area available to reaction j ; E_j = activation energy associated with reaction j . For the steady-state case, $R_1 = R_2 = \dots = R_j = \dots = R_n = R$ and by definition $f_1 + f_2 + \dots + f_j + \dots + f_n = 1$. Applying these two conditions and solving for the

rate one obtains

$$R = 1 / \sum_1^n \frac{e^{E_j/kT}}{a_j c_j^{p_j}} \quad (I)$$

For a surface reaction in which there are only two important rate-controlling processes, this reduces to

$$R = \frac{1}{\frac{\exp(E_1/kT)}{a_1 c_1^{p_1}} + \frac{\exp(E_2/kT)}{a_2 c_2^{p_2}}} \quad (II)$$

Equation (II) correctly describes the observed rate temperature behavior over the range covered. For the (111) and (110) surfaces, this gives

$$\begin{array}{ll} E_1 \text{ 6 kcal/mole} & a_1 c_1^{p_1} \text{ 1.41} \times 10^5 \\ E_2 \text{ 15 kcal/mole} & a_2 c_2^{p_2} \text{ 8.48} \times 10^{11} \end{array}$$

and for the (100) surface it gives

$$\begin{array}{ll} E_1 \text{ 7 kcal/mole} & a_1 c_1^{p_1} \text{ 7.50} \times 10^5 \\ E_2 \text{ 17 kcal/mole} & a_2 c_2^{p_2} \text{ 2.37} \times 10^{13} \end{array}$$

RATE VS. COMPOSITION

Much of the published data on etching has stressed the importance of specific composition. A number of experiments were performed to learn how critical this dependence might be. From preliminary experiments, it had been supposed that the etching process proceeded by the oxidation of the germanium and the subsequent solution of the oxide. It was hoped that the composition experiments might also help in testing this interpretation.

If the etching process does proceed by oxidation and subsequent solution, it would be of interest to find out what one can about the oxidation process. If GeO is formed, then since this is insoluble, a second oxidation to GeO₂ very probably takes place. It can be seen from equation (I) that insight into these steps cannot be obtained from rate vs. concentration data taken at constant temperature. For if there are h successive reactions which involve the same reactant to the same power, then the form of the equation is identical to that in which these h reactions are replaced by only one. That is, the terms $1/a_1 c^p + 1/a_2 c^p \dots + 1/a_h c^p$ can be lumped together as $1/\text{const. } c^p$. (The exponential term is a constant at a fixed temperature and is included in the a 's.) Therefore, one cannot separate these h stages. Such a situation would arise if there were successive oxidations as proposed.

As the concentration of one reactant approaches zero, it is seen from equation (I) that

$$\lim_{c_j \rightarrow 0} \frac{\partial R}{\partial c_j} = \begin{cases} \infty & \text{if } p_j < 1 \\ a_j & \text{if } p_j = 1 \\ 0 & \text{if } p_j > 1 \end{cases}$$

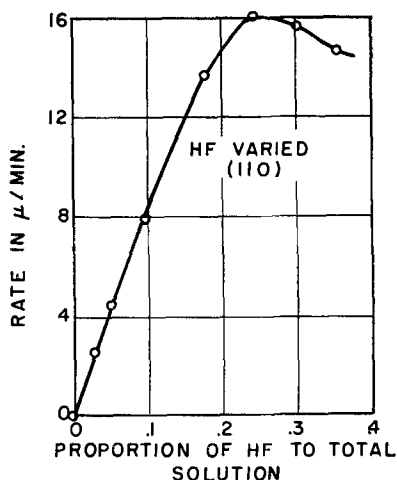


FIG. 4. Rate of etch vs. the ratio of the volume of reagent HF to total volume of solution.

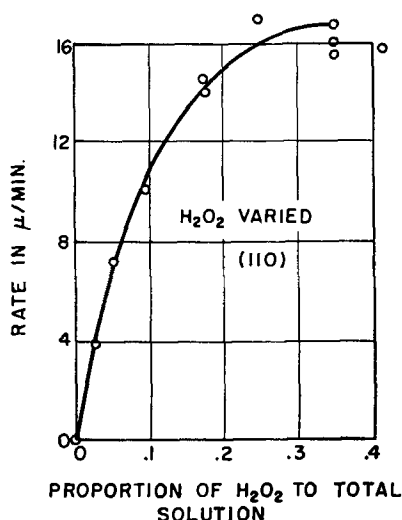


FIG. 5. Rate of etch vs. the ratio of the volume of reagent H₂O₂ to total volume of the solution.

Therefore, rate vs. concentration data should approach the origin asymptotically to the rate axis if $p_j < 1$, asymptotically to the concentration axis if $p_j > 1$, and with a finite slope if $p_j = 1$. From the measurements of rate vs. concentration for H₂O₂ and HF, Fig. 4 and 5, it appears that $p = 1$ for dilute solutions in each case. If the concentration of both the H₂O₂ and HF are varied simultaneously, as by simple dilution, the rate varies as shown in Fig. 6.

Fig. 7 shows the rate temperature behavior for several compositions. Curve (a) is for the standard composition, curve (b) for simple dilution, and curve (c) for a solution in which the concentration of the H₂O₂ has been reduced. The high temperature portions of all three curves have nearly the same slopes. The low temperature portions of (b) and (c) have the same slope, but this is different from that of (a). It is possible that when the rate is

reduced sufficiently by reduction in the concentration of one or both of the reactants, a third limiting process (e.g., diffusion) begins to appear. In the light of equation (I), Fig. 7 might be interpreted to mean that both rate-controlling processes are dependent only on the concentration of the oxidizing agent, for example, the formation of a monoxide and then a further oxidation to a dioxide. In this case, energies obtained from the curve would be for successive oxidations. However, comparison of the rate vs. dilution data, Fig. 6, and the measurements of the rate as a function of the concentration of H₂O₂ and HF (Fig. 4 and 5) show that both the H₂O₂ and HF play rate-controlling roles over a wide range of concentrations. If the measured concen-

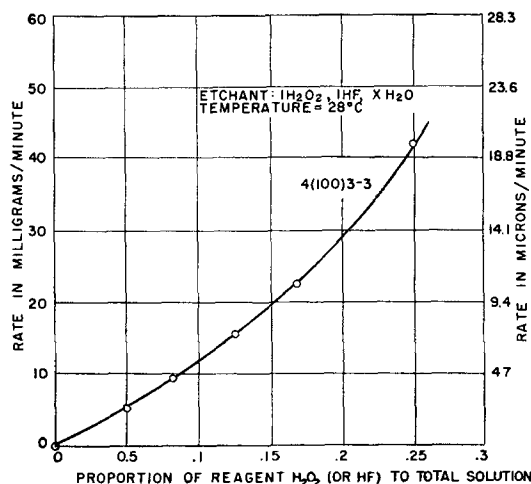


FIG. 6. Effect on etching rate of diluting etchant with water.

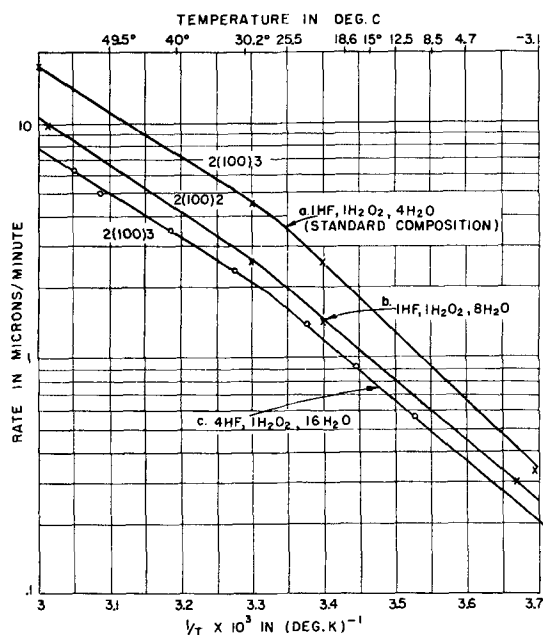


FIG. 7. Effect of etchant composition on rate vs. reciprocal temperature curves for samples in the (100) plane.

TABLE III. Ratio of etching rates for 4-1-16 and 1-1-4 compositions of HF-H₂O₂-H₂O etchant

10 ³ /T °K	Relative etching rate	
	Calculated	Measured
3.7	0.7	0.6
3.3	0.38	0.46
3.0	0.33	0.48

trations are substituted into equation (I) (only c_1 and c_2 are changed), one obtains a new curve which should coincide with the experimental curve for the new composition. Calculated and experimental ratios relating the rates for a 4-1-16 (HF, H₂O₂, H₂O) composition to that of the standard 1-1-4 composition are given in Table III.

The agreement is not particularly good, but allowance has been made neither for dissociation in computing the new concentrations, nor for a third limiting process.

Using equation (I) to solve for the fractions, f_1 , f_2 , etc., one finds that $f_j = R / \frac{a_j c_j^{P_j}}{\exp E_j/kT}$. It be-

comes clear that, by varying the conditions, the fraction of the surface area covered with any particular reaction product may be varied. In this connection, it is worth mentioning a film which has been observed to form under conditions of reduced concentration of H₂O₂ (about 1 part pure H₂O₂ to 20 parts of total solution). It did not form during the etching or in distilled wash water. However, it did form immediately upon exposure of the freshly etched surface to air. The film is not soluble in water or in a 15% solution of HF in water. It is quickly removed by washing in a dilute H₂O₂ solution. It seems quite possible that the Ge is nearly bare when washed but that, on exposure to air, a monoxide layer forms. This is then fairly stable until oxidized to a dioxide by the H₂O₂. The dioxide is slightly soluble in water.

RATE VS. IMPURITY

To determine to what extent these results could be generalized to apply to other crystals differing in impurity content, measurements were made of the effect of varying the concentration of arsenic, the effect of changing the type of impurity, and the effect of thermally quenching a sample.

Fig. 8 is a plot of the temperature dependence of the etching rate of a 9.4 ohm-cm sample, (111) surface. Plotted on the same graph are the points for a 1 ohm-cm sample, (111) surface orientation, as a function of temperature, and data for (100) and (110) surfaces at one temperature. The single

temperature points are the result of more than one observation. Close inspection of the results indicates that the 9 ohm-cm material etches slightly more rapidly than the 1 ohm-cm material. The difference is close to the estimated limit of experimental error, but appears to be reproducible. These samples were arsenic doped.

Further, more careful measurements have been made for all three orientations at room temperature. It was found that in each case the rate for 9 ohm-cm material was 7% greater than that for 1 ohm-cm material. Thus, somehow, four parts per hundred million of arsenic seem to inhibit the etching significantly. It is quite remarkable if one impurity atom on the surface masks 2.3 million germanium atoms or if the cross section for inhibition is 1.8×10^{-9} cm². It is significant also that somewhat incomplete data (Fig. 8) show this to be true over a wide range of temperatures. This offers a tempting subject for further study.

To find out if the rate of etching is strongly dependent on the type of impurity, samples containing vanadium (6 ohm-cm), antimony (2 ohm-cm), gallium and antimony balanced (0.7 ohm-cm), and indium (0.02 ohm-cm) were measured. All etched faster by about 10% than arsenic-doped material of 2 ohm-cm resistivity. However, control on the orientation was poor and these results are in doubt by perhaps 15%. At least no striking differences were

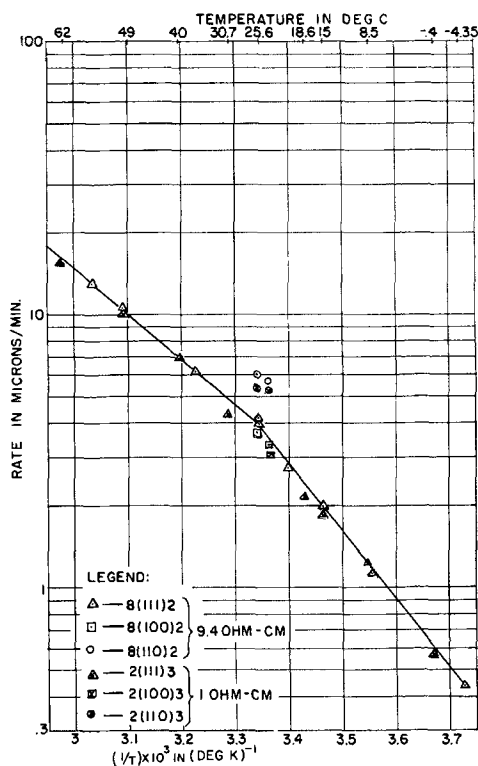


FIG. 8. Rate of etch vs. $1/T \times 10^3 (\text{°K})^{-1}$ for different resistivities (No. 2 etch).

observed. The best evidence to date that some impurities have a different effect on the etching rate than others came from the etching of small spheres. Spheres from crystals containing antimony and indium balanced (6 ohm-cm), phosphorus (0.1 ohm-cm), thallium (0.8 ohm-cm), and gallium (0.3 ohm-cm) were all etched to equilibrium form in the No. 2 etch. Of these, only the gallium-doped sample showed a marked difference from samples doped with arsenic. This difference was not great. For the gallium-doped sample alone, the equilibrium form was not a dodecahedron. This was an indication that the (110) plane was not the fastest etching plane. It appeared rather that a plane tilted very slightly away from the (110) toward the (100) etched most rapidly.

In order to find out quickly the effect of prior thermal treatment on the rate of etch, a simple experiment was tried. Two adjacent (100) slabs were cut from crystal T125N (*n*-type, 1 ohm-cm, arsenic doped). One of these was heated to a dull red heat in a gas-air flame for about a minute and then quenched by removal. This was repeated three times. The etching rate of the two samples was then compared at 21.8°C and found to be identical to better than the estimated error (2%).

COMPARISON OF ETCHANTS

Many different etchants are used in practice. Some of the most common are listed in the Appendix. The rate-vs.-temperature dependence of the No. 2, No. 3, and No. 4 etchants have been studied. Some results are plotted in Fig. 9. Data for the No. 3 etchant are very erratic and data for the No. 4 etchant are even worse, so that no curve can be drawn. Two of the points are completely off the graph. Some of the experiments performed in obtaining these data suggest that sometimes there is formed, on the surface of the germanium, a layer which acts to passivate or otherwise inhibit the reaction in these etchants. For example, a brief etch in No. 2 will make the sample almost immune for a time (a minute or more) to the action of the No. 3 etchant. No such inhibiting action has been observed in using the No. 2 alone. It follows that it may be desirable to use a concentrated version of the No. 2 etchant for the operations in which the No. 3 or No. 4 is normally used. An idea of the rates obtainable may be derived from the rate-vs.-dilution curve, Fig. 6. An undiluted mixture of reagent H₂O₂ and HF gives a rapid etch. If a dioxide forms ultimately in H₂O₂, then peroxide and pure water should etch germanium. An experiment to determine this was performed and it was found that a (111) surface is etched by 1 part 30% H₂O₂ in 5 parts

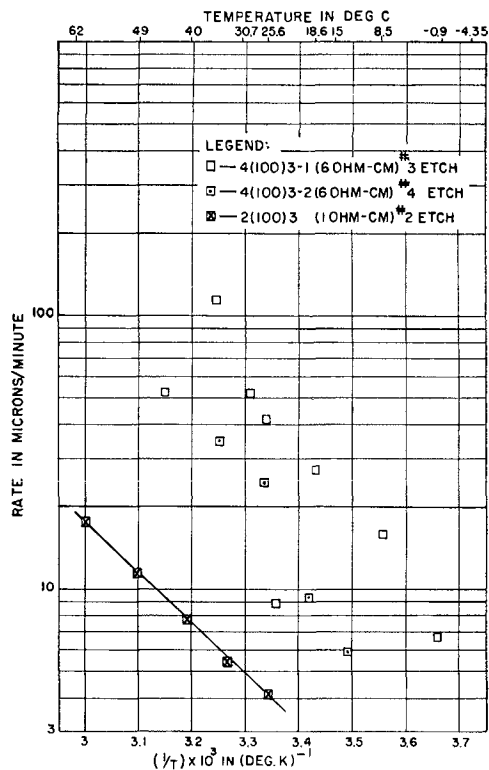


FIG. 9. Rate of etch vs. $1/T \times 10^3$ ($^{\circ}\text{K}$)⁻¹ for three different etchants. The erratic behavior of the No. 3 and No. 4 etchants makes it useless to draw curves through these data.

water at 26°C at a rate of 0.0275 μ /min. This may constitute a useful slow etchant.

CONCLUSIONS

It has been found that an aqueous solution of HF and H₂O₂ is a reliable etchant for germanium. It is stable for long periods of time when stored in polyethylene and yields readily reproducible results for a wide range of temperatures and compositions when used under conditions of vigorous stirring. By suitably adjusting conditions, rates as low as 0.03 μ /min or as high as 20 μ /min may be obtained at room temperature. The etching rate is dependent on crystal orientation, surface disorder, and crystal impurity content, the rate being fastest for the (110) surface and pure germanium. The increase with surface disorder is comparable to the increase in surface area. The etching attack is apparently limited by two distinctly separate processes which take place in sequence on the surface of the crystal. Over the temperature range 0–60°C the rate of etching is found to obey an equation of the form

$$R = 1 / \sum_{i=1}^n \frac{e^{E_i/kT}}{a_i c_j^{P_i}}$$

Any discussion of this paper will appear in a Discussion Section to be published in the June 1956 JOURNAL.

REFERENCES

1. J. W. FAUST AND J. P. MCKELVEY, Joint IRE-AIEE Conference on Transistor Research, Penn State College, July 6-8, 1953.
2. S. WEISSMAN, Private Communication.
3. E. N. CLARKE AND R. L. HOPKINS, Reported at Joint IRE-AIEE Conference on Transistor Research, Penn State College, July 6-8, 1953.
4. P. R. CAMP, MIT Conference on Physical Electronics, Cambridge, Mass., March 27-29, 1952.

APPENDIX

COMPOSITION OF COMMONLY USED

GERMANIUM ETCHANTS

H₂O₂ Technical Quality (Allied Chemical Co.) Assay
30-35%

HNO₃ Reagent Quality (Baker) Minimum Assay 69.2%
HF Reagent Quality (Allied Chemical Co.) Minimum
Assay 48%
CH₃COOH Reagent Quality (Merck) Minimum Assay
99.8%

No. 2

1 part HF
1 part H₂O₂
4 parts H₂O

No. 4

50 cc HNO₃
30 cc CH₃COOH
30 cc HF
0.6 cc Br

No. 3

56 cc HF
56 cc HNO₃
12.5 cc H₂O

Electrokinetic Potentials of Bulk Metals by Streaming Current Measurements

I. Method¹

RAY M. HURD AND NORMAN HACKERMAN

Defense Research Laboratory and Department of Chemistry, The University of Texas, Austin, Texas

ABSTRACT

A method for making a direct measurement of the streaming currents developed by fluid flow through metal capillaries is described, by means of which the electrokinetic (ζ) potentials of bulk metals can be determined. Experimental data proving the validity of the method are presented.

STREAMING POTENTIAL VS. STREAMING CURRENT

Although the electrokinetic phenomenon resulting from fluid flow through a capillary has been historically referred to by the expression "streaming potential," it is nevertheless a fact that the primary result of the fluid flow is a streaming *current*. The value of this current is given by the equation

$$I = \frac{\Delta P r^2 D \zeta}{4 \eta l} \quad (\text{I})$$

where ΔP is pressure drop across the capillary; r and l the capillary radius and length; D and η the dielectric constant and viscosity of the fluid; and ζ is the electrokinetic (or zeta) potential.

With but one exception, all previous measurements on this phenomenon have been made by placing measuring electrodes at the ends of the capillary and, by means of a potentiometer, applying just enough potential, E_s , to force an equal electrolytic current back through the center of the capillary (1). Since the electrolytic resistance R of the fluid inside the capillary is easily obtainable from the capillary dimensions and the conductivity k of the fluid, a direct relation between ζ and E_s is available, i.e.,

$$E_s = IR = \frac{\Delta P D \zeta}{4 \pi \eta k} \quad (\text{II})$$

The fact that investigations in this field have been restricted almost exclusively to measurements of the streaming potential is explained by the exceedingly low value of the streaming current, which is usually in the order of 10^{-10} to 10^{-11} amp. Instruments for measuring currents of this magnitude directly have not been available. On the other hand, the electrolytic resistance of the capillaries studied is often as high as 10^9 ohms, so that the values of

streaming potentials obtained run into the hundreds of millivolts, a value easily and accurately measurable with a potentiometer. Furthermore, as long as the return current necessary to balance the streaming current could be forced to take a path of *known* resistance, there was no necessity for actually measuring the streaming current, as it could be obtained simply from Ohm's law. This has been precisely the case in almost all previous studies on this phenomenon, i.e., the materials used to form the capillaries have been nonconductors, so that the only path available for the return current has been the known electrolytic resistance back through the center of the capillary. The only appreciable trouble with potential measurements has been in determining the value of "surface conductance," a correction to the calculated electrolytic conductance which is necessary because the concentration of ions near the wall of the capillary is somewhat higher than that in the bulk of the liquid.

If now the nonconducting capillary wall is replaced by an electronic conductor, e.g., platinum, then measurements of streaming potentials as usually made are likely to be meaningless, or at best very difficult of interpretation, since the value of R can no longer be determined unequivocally. In this case, the path for the return current is a parallel circuit of three separate resistances, which are: (a) electrolytic resistance, R_1 , which can be determined exactly; (b) resistance to conductivity along the surface, R_2 , usually much larger than R_1 , and which can be estimated with fair accuracy; and (c) resistance through the metal wall, R_3 , which is itself composed of three parts (see below), only one of which can be determined.

It can be stated with reasonable certainty, however, that in most cases the values of R_1 and R_2 will be so very much larger than R_3 that they may be neglected entirely. Thus, for the largest diameter

¹ Manuscript received February 9, 1955.

capillary used in these experiments, the electrolytic resistance (R_1) with distilled water is calculated to be 1.2×10^9 ohms. Surface conductivity (through R_2) may decrease the total electrolytic resistance some 10%, so that these two parallel paths yield a resistance of some 10^9 ohms. Now, as shown below, even with all possible precautions taken to increase the value of R_3 , it is still no larger than about 5×10^7 ohms. It remains, then, only to investigate the nature of R_3 . In order for the return current, I , to flow through the capillary wall, it must: (a) enter at one end by means of an electrode reaction requiring a potential drop, E_1 , (b) flow electronically through the metal wall causing an IR potential drop, and (c) return to the solution at the other end via another electrode reaction and an additional potential drop, E_2 . Because of the very small values of I and of the electronic resistance of the capillary wall, the second term may be disregarded, and the measured streaming potential is then composed of the terms E_1 and E_2 . Although there is very probably some relation between the streaming current and the potentials E_1 and E_2 , it would be exceedingly difficult to determine, and would change radically from one system to another.

In view of the difficulties described above, it is apparent that any attempt to determine ζ -potentials by making streaming potential measurements on metal capillaries is foredoomed to failure. This was recognized by Kruyt and Oosterman (2), who attempted to make streaming potential measurements on platinum capillaries with no success. They explained the failure of their experiments by pointing out the existence of the lower resistance path through the metal. An earlier investigation by Zakrzewski (3) on silvered glass capillaries also yielded results which showed only that some type of electrical phenomena did result when a liquid was forced through a metal-walled capillary.

BASIS OF THE STREAMING CURRENT METHOD

The solution to the problem of measuring the ζ -potential of bulk metals² lies in the use of an external measuring circuit with an electrical resistance so low that the bothersome shorting resistance of the capillary wall is itself shorted by a known resistance. Under these conditions, all the streaming current, except for a negligible fraction, must return through the external shunt. Preliminary investigations indicated that the value of the "apparent" resistance of the capillary is in the order of 10^6 to

10^7 ohms. An external measuring resistor of 10^4 ohms, then, should effectively shunt the capillary, so that measurements of the emf developed across the shunting resistor should give a true value for the streaming current. The applicability of this method was recognized earlier by Eversole and Boardman (4), in a study designed primarily to eliminate the effect of surface conductance. They pointed out, however, that use of this method should give true values of the streaming currents on metal capillaries, and reported results of measurements made on one platinum capillary. They were unable to short the capillary entirely, but used an extrapolation method to obtain the "true" value of the current. Use of the extrapolation method was necessary because instrumentation capable of measuring the low voltages developed by currents of 10^{-10} amp flowing through 10^4 ohm resistors (microvolts) had not at that time been perfected. The lowest value of external resistance they were able to use was 1.6×10^7 ohms, which is near the value of the capillary resistance itself. Recent advances in electronic circuitry have resulted in the development of extremely sensitive, yet stable, instruments for measuring voltages in the microvolt region. With these instruments it is possible to use the streaming method on metal capillaries, and thereby obtain a true value for the ζ -potential of bulk metals in contact with various liquids.

CIRCUIT ANALYSIS

The construction of the metal capillaries, pressure regulating system, and other experimental procedures, will be given in a subsequent paper, along with the results obtained on capillaries of three different metals (platinum, gold, and silver). The purpose of the present paper is simply to describe the method and demonstrate its validity.

Fig. 1 shows a line drawing of the electronic circuit and the fundamental parts of the fluid flow circuit. The streaming current was measured by recording the voltage drop across a ten thousand ohm resistor inserted into the external "shunting" circuit. This arrangement creates a closed circuit of two electrolysis cells in parallel, equivalent to the type shown in Fig. 2. Here A and B represent the measuring electrodes, C and D the ends of the capillary, and R the external resistor. The measuring electrodes are placed as near the capillary ends as possible so that electrolytic resistance through that part of the solution may be neglected. The solution contact through the capillary is not shown. The + and - signs indicate that ionic charge has been transferred through the capillary by fluid flow, and must now be returned by one or both of the two

² Potentials of metals have often been measured by using electrophoretic methods on metal sols. The validity of this method can also be questioned because of the conducting properties of the particles.

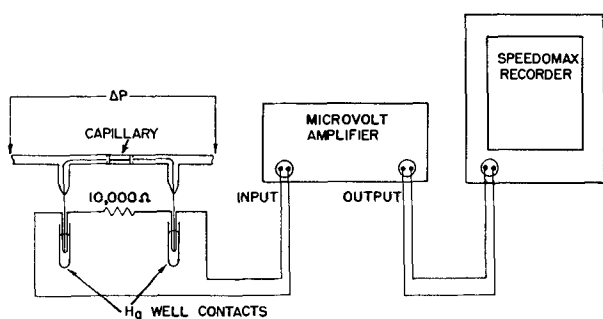


FIG. 1. Electronic circuit for streaming current measurements.

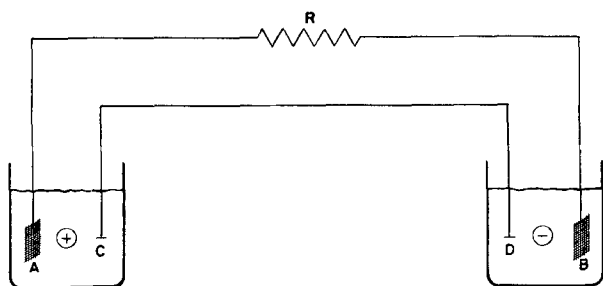


FIG. 2. Equivalent electrolysis cell. *A* and *B* are measuring electrodes, *C* and *D* are the capillary ends, *R* is the external resistor, + and - indicate transfer of charge by fluid flow.

circuits *A - B* or *C - D*.³ The potential drop through the measuring circuit is composed of three terms, viz.:

$$E_1 = E_A + I_1 R + E_B \quad (\text{III})$$

The potential drop through the capillary was shown earlier to be composed of two terms, which is written here as:

$$E_2 = E_C + E_D \quad (\text{IV})$$

Since the circuits are in parallel, $E_1 = E_2$, and

$$E_A + I_1 R + E_B = E_C + E_D \quad (\text{V})$$

At low current densities, each of these E 's may be replaced by a term kI/a (4), where a is the area of the electrode (or metal) exposed to the solution, I the current flowing into (or out of) the electrode, and k a "constant" of proportionality, so that equation (V) becomes

$$I_1 \left[\frac{k_A}{a_A} + \frac{k_B}{a_B} + R \right] = I_2 \left[\frac{k_C}{a_C} + \frac{k_D}{a_D} \right] \quad (\text{VI})$$

³ As pointed out previously, the ionic resistance through the capillary is so large that it may be neglected as a return path.

and since $a_A \cong a_B$ and $a_C \cong a_D$, then

$$\frac{I_1}{I_2} = \frac{\left[\frac{k_C + k_D}{a_{CD}} \right]}{\left[\frac{k_A + k_B}{a_{AB}} + R \right]} \quad (\text{VII})$$

Although the values of the k 's in this equation are not known, it is possible to show that the ratio I_1/I_2 can be made so large that the value of I_1 truly represents the streaming current.

If the value of R is much less than the quantity $[k_A + k_B]/a_{AB}$, equation (VII) reduces to:

$$\frac{I_1}{I_2} = \left[\frac{k_C + k_D}{k_A + k_B} \right] \left[\frac{a_{AB}}{a_{CD}} \right] \quad (\text{VIII})$$

which means that small changes in R (doubling, tripling, etc.) should not affect the measured quantity, I_1 . However, if R is much larger than $[k_A +$

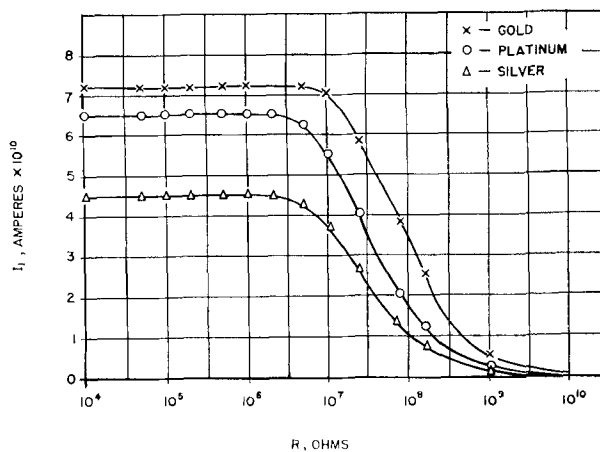


FIG. 3. Current in the external circuit as a function of the external resistance.

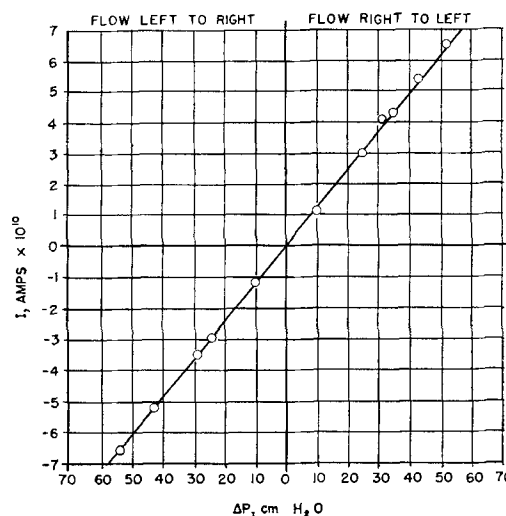


FIG. 4. Pressure-current curve for the 0.0138 x 1.724 cm gold capillary in distilled water.

k_B/a_{AB} , then equation (VII) becomes

$$\frac{I_1}{I_2} = \frac{k_C + k_D}{a_{CD}R} = \frac{k'}{R} \quad (\text{IX})$$

and small changes in R will be immediately reflected in I_1 . Furthermore, if equation (VIII) applies when $R = 10,000$ ohms, it is possible to increase the value of R until equation (IX) applies, at which point I_1 will begin to decrease, and with still larger values of R it will approach zero asymptotically. This experiment was carried out with distilled water (conductivity $< 2.0 \times 10^{-6}$) and capillaries of each of the three metals, and gave the results shown in Fig. 3. A similar curve was obtained when the measuring electrodes were removed further and further from the ends of the capillary, with no decrease in I_1 noted until the electrodes were some 10 cm removed. It is apparent from the figure that, for values of R less than 10^6 ohms, equation (VIII) applies, and that I_2 is negligibly small. For the platinum capillary, since the measuring electrodes are also platinum, $k_A + k_B$ is approximately equal to $k_C + k_D$, so that the currents will split according to the ratio of the areas a_{AB}/a_{CD} . The results shown in Fig. 3 indicate that this is also true for the gold and silver capillaries. For this reason, the capillaries were constructed so that as little metal as possible (a_{CD}) would be exposed to the solution. With a_{CD} small, increasing a_{AB} , as by platinizing, had no measurable effect on the current I_1 .

The potential drop across the 10,000 ohm resistor was amplified by means of a L&N Model 9825-B microvolt amplifier, and then fed into a

L&N Model "G" Speedomax recorder. This combination results in a recording millimicro-ammeter with an internal resistance of 10,000 ohms. Current readings were easily reproducible to within 1%, and held steady for long periods of time (> 5 min). The ζ -potential was calculated from the equation

$$\zeta = \left[\frac{4\eta}{D} \right] \left[\frac{l}{r^2} \right] \left[\frac{I}{\Delta P} \right] \quad (\text{X})$$

which was obtained upon rearranging equation (I). Measured values of I were plotted against the applied pressure, the slope of this line giving the quantity $[I/\Delta P]$. A typical plot is shown in Fig. 4. Measurements were made on platinum, gold, and silver capillaries in contact with distilled water and dilute aqueous electrolytes; results of these measurements will be presented in a second paper.

Any discussion of this paper will appear in a Discussion Section to be published in the June 1956 JOURNAL.

REFERENCES

1. J. A. V. BUTLER, "Electrokinetic Phenomena at Interfaces," Methuen and Co., Ltd., London (1951). A review of the theories and measurements of electrokinetic phenomena is given in Chapter 3, by J. M. Creeth.
2. H. KRUYT AND J. OOSTERMAN, *Kolloid Beihefte*, **48**, 377 (1938).
3. C. ZAKRZEWSKI, *Physik. Z.*, **2**, 146 (1900).
4. W. EVERSOLE AND W. BOARDMAN, *J. Phys. Chem.*, **46**, 914, (1942).
4. C. KORTUM AND J. O'M. BOCKRIS, "Textbook of Electrochemistry," pp. 452-553, Elsevier Publishing Co., New York (1951).

Impedance Measurements at Solid Electrodes in Molten Lithium Chloride-Potassium Chloride¹

H. A. LAITINEN AND R. A. OSTERYOUNG²

Department of Chemistry and Chemical Engineering, University of Illinois, Urbana, Illinois

ABSTRACT

Impedance measurements have been made at solid microelectrodes in molten potassium-lithium chloride eutectic, and in dilute solutions of platinum(II), nickel(II), and cobalt(II) in the eutectic as a solvent. Capacitance and resistance measurements are described for forward (cathodic) polarization of a platinum microelectrode and for reverse polarization of the plated microelectrode. The results are interpreted in the light of a theoretical interpretation of pseudocapacity.

INTRODUCTION

Impedance measurements at microelectrodes have been used to obtain information relating to the kinetics of electrode reactions occurring at the microelectrode surface. The theories involved have been developed by several authors, especially Randles (1), Grahame (2), Ershler (3), and Gerischer (4). Generally, these techniques have found most application to reactions in aqueous solutions using dropping mercury electrodes. Ershler (3) and Hillson (5) have developed the theory for a metal electrode in equilibrium with its ions.

The normal procedures used in obtaining the needed measurements are as follows. An a-c bridge is used to measure a gross series or parallel resistance-capacitance combination. The solution resistance is measured in the presence of the excess supporting electrolyte which must be used and before any reducible species are added. The double layer capacity is measured as a function of potential in a solution of the supporting electrolyte. Measurements of the gross resistive-capacitive components are then made with the reacting species present. For rate constant determinations, this is usually done at the null potential, generally by having equal concentrations of the reduced and oxidized form in solution, or, for metal deposition, using a mercury amalgam of the same concentrations as the reducible metal ion in solution. Where a solid metal electrode is used, as in the study of copper deposition by Hillson (5), the use of a large copper reference electrode and copper microelectrode places the system at its null potential. From these measurements, it is possible to separate vectorially the gross

measurements into the separate components (1, 6). The expressions for the pseudocapacity and polarization resistance as applied to a case of a solid electrode, where the diffusing oxidized species is reduced to the metal which deposits on the electrode, are (4, 5, 7):

$$R_r = \frac{RT}{n^2 F^2 AC} \left(\sqrt{\frac{1}{2\omega D}} + \frac{1}{k} \right) \quad (\text{I})$$

$$C_r = \frac{n^2 F^2 AC}{RT} \sqrt{\frac{2D}{\omega}} \quad (\text{II})$$

$$R_r - \frac{1}{\omega C_r} = \frac{RT}{n^2 F^2 AC} \frac{1}{k} \quad (\text{III})$$

Where R , T , n , and F have their usual significance, C is the concentration of the oxidized form in solution, A the area of the electrode, D the diffusion coefficient of the diffusing oxidized form, k the heterogeneous rate constant defining the rates of the opposing dissolution and deposition reactions at the equilibrium potential as kC moles per second per unit of area of electrode surface, and ω being 2π times the frequency of the small a-c bridge signal. Thus, according to the theory, if the polarization resistance and the impedance due to the pseudocapacity are plotted against the reciprocal of the square root of frequency, two parallel straight lines should be obtained and the separation between the two straight lines is related to the rate constant k by equation (III).

The more general technique of Grahame (2) consists of applying a d-c base potential, on which is impressed the small (10 mv or less) a-c bridge signal. In this manner, a plot of the resistive and capacitive component due to the electrode reaction against the applied d-c potential is obtained. For reversible reactions occurring at the dropping mercury electrode, Grahame has shown that the impedance reaches a minimum at the polarographic half-wave potential and that, as the rate of the

¹ Manuscript received January 24, 1955. This paper was prepared for delivery before the Cincinnati Meeting, May 1 to 5, 1955, and was abstracted from the Ph.D. thesis of R. A. Osteryoung, University of Illinois, 1954.

² Present address: Department of Chemistry, Rensselaer Polytechnic Institute, Troy, New York.

reaction decreases, that is, it becomes less reversible, the extent of the minimum in the impedance-d-c potential curve lessens and gradually shifts away from the reversible half-wave potential.

For the case of a single diffusing species, such as an infinitely rapid reversible metal-metal ion electrode, the impedance should be inversely proportional to the slope of the c.-v. curve (7), and should approach infinity with cathodic polarization as the diffusion-limited plateau is approached. With anodic polarization, no plateau is approached, and the impedance should approach zero.

In the present work, impedance measurement techniques were applied to dilute solutions of platinum(II), nickel(II), and cobalt(II) in a lithium chloride-potassium chloride eutectic melt at a temperature of $425^\circ \pm 10^\circ\text{C}$, using platinum electrodes.

EXPERIMENTAL

Fig. 1 is a diagram of the a-c bridge used in this work. The signal generator was a Heathkit Audio Generator, the output of which was fed into the bridge through the shielded audio transformer, T , which was a 4:1 stepdown transformer. The output of the signal generator was set at 40 mv; this coupled to the bridge through the transformer meant a 10 mv applied alternating signal. R_1 and R_p were Leeds & Northrup decade resistance boxes. C_p was a General Radio precision decade capacitor, which was wrapped in copper screening to reduce stray pickup. C_1 was a General Radio 1.0 μf precision mica capacitor. The potentiometer was a Leeds & Northrup student type. R_2 was a 0-0.5 megohm wire wound resistor, which led to the positive lead of the Sargent "Ampot." The amplifier was a Heathkit WA P-2 audio amplifier. The high voltage to the amplifier was supplied by a Heathkit variable Voltage Regulated Power Supply. The filament supply was a 6 v lead storage battery. A 304H du Mont Cathode Ray Oscilloscope was used.

The cell was a Pyrex glass tube, 13 in. long, 40 mm in diameter with a side arm of 9 mm tubing attached to a vacuum pump. The electrodes were inserted into holes in a No. 9 rubber stopper. The microelectrode was made of B. and S. gauge No. 26 platinum wire sealed into 6 or 8 mm tubing. The exposed length was approximately 1 mm. The two foil electrodes were hammer-welded to platinum wire. They had a surface area greater than 2 cm^2 .

The cell was filled with 100-120 g KCl-LiCl eutectic mixture, and a solid rubber stopper was placed in the opening. The mixture was fused under vacuum and allowed to remain under vacuum overnight. Air was then admitted, the solid stopper removed, and the stopper with the electrodes inserted. Small amounts of reducible material could

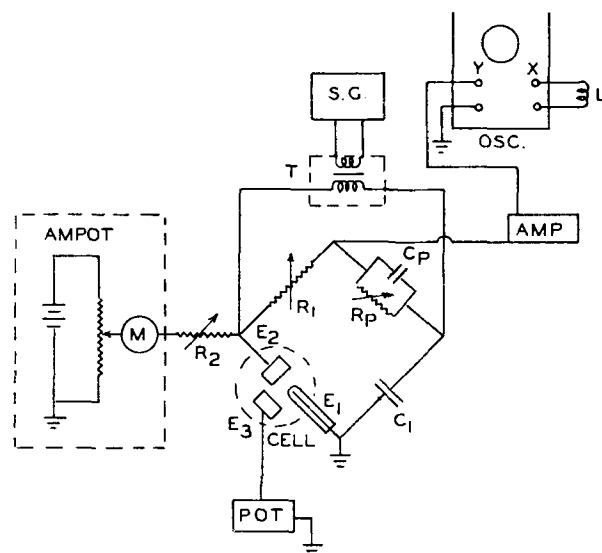


FIG. 1. Impedance bridge. S.G.—Heathkit audio generator; Pot.—student-type potentiometer; Ampot—E. H. Sargent and Co.; R_1 , R_p —0-11, 110 ohm variable decade resistors; C_p —0-1.110 μf variable capacitor; C_1 —1.00 microfarad capacitor; R_2 —500,000 ohm variable resistor; Amp—Heathkit WA-P2 audio amplifier; Osc—du Mont cathode ray oscillograph; T —4:1 stepdown shielded audio transformer; L —60 cycle pickup loop; E_1 —platinum microelectrode; E_2 —platinum foil working electrode; E_3 —platinum foil reference electrode.

be added by removing the electrodes and dropping the desired material down a large glass tube which served as a funnel.

To determine if the bridge was operating properly a decade resistor and capacitor were connected in series in place of the cell and measurements made at various frequencies.

By means of the Ampot, a d-c potential could be applied across the microelectrode, E_1 , and the working platinum foil, E_2 . The potential at E_1 was measured with respect to the platinum foil E_3 , using the potentiometer. R_2 served to prevent shorting the a-c signal. By having the balancing resistor, R_p , and capacitor, C_p , in parallel, the impedance of the cell appeared as a resistance and capacitance in series (8). The impedance measured is that associated with the microelectrode, since any impedance due to the large electrode would be in series with that of the microelectrode, and would be much smaller than that of the microelectrode. With R_1 adjusted to a suitable value, a potential was applied with the Ampot. The off balance a-c signal was fed through the amplifier to the Y plates of the oscilloscope. A loop of wire attached to the X plates of the oscilloscope served to pick up a 60-cycle signal. The result on the oscilloscope face was a pulsating Lissajou figure. By adjusting R_p and C_p , pulsations were brought to a minimum, which was

taken as the balance point. This type of balance was used because of considerable 60-cycle pickup introduced to the *Y* plates from the electrodes in the furnace.

Calculations of R_{zs} and C_{zs} , the gross series resistance and capacitance, were made by the following formulas (8):

$$C_{zs} = (R_p/R_1)C_1$$

$$R_{zs} = (C_p/C_1)R_1$$

The advantage of the parallel measuring circuit is apparent in that large values of capacity can be measured without the necessity of using a large standard capacitor. Rather, the measured capacity depends on the ratio of R_p to R_1 .

Curves were run by applying the fixed d-c potential, balancing the bridge at the desired frequency setting, then changing the d-c potential and again balancing.

As the d-c potential was increased, an electron current began to flow from ground to E_1 , through E_2 to the resistance R_2 , through the Ampot, where the meter, *M*, measured the current, then back to ground. Thus, a plot of the current behavior as the potential was changed could be obtained at the same time as the impedance. Residual current did not affect impedance measurements. Since the maximum potential output of the Ampot was only 3 v, it was necessary to lower the resistance of R_2 if currents greater than 4 μ a were to pass. The effect of lowering R_2 was to increase the potential across E_1 and E_2 .

The result of changing the d-c potential, with a reducible ion in the melt, was to deposit the metal on the platinum microelectrode. By then reversing the direction of polarization, the current-voltage curve was retraced, except that the curve crossed the zero current axis because of the oxidation of the metal deposited on the microelectrode. By changing the d-c potential, a larger and larger anodic current could be drawn. This current, of course, was not diffusion limited as was the reduction current. Thus, the combination of the ammeter, *M*, and the potentiometer gave a current-voltage curve and the bridge could be balanced at fixed microelectrode potentials and fixed anodic currents.

An equilibrium potential, that is, the potential of the metal plated microelectrode with respect to the reference platinum foil, could be measured by opening the direct current path through resistor R_2 and measuring the open circuit potential between E_1 and E_3 .

RESULTS

The results of the experiments are best presented in a series of graphs. The conditions under which

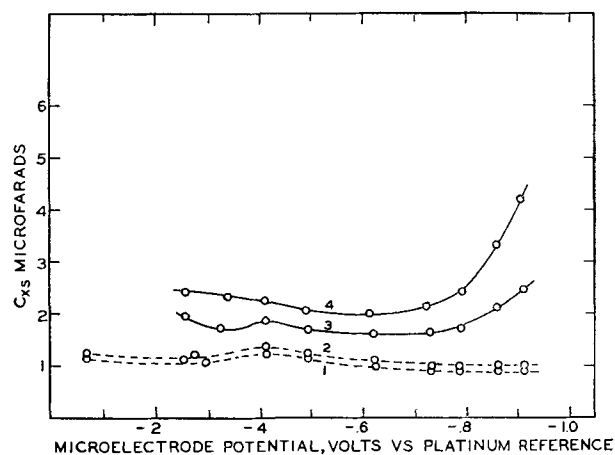


FIG. 2. Residual capacity, C_{zs} for KCl-LiCl. Curve 1, 2000 cps; curve 2, 1000 cps; curve 3, 100 cps; curve 4, 40 cps.

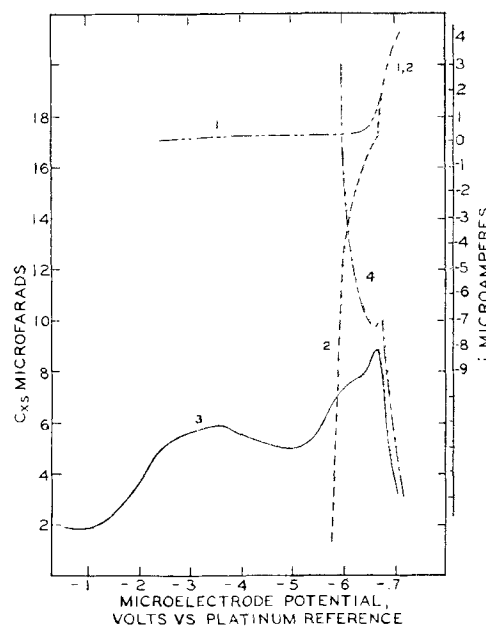


FIG. 3. C_{zs} and current for NiCl_2 (29 mg) in KCl-LiCl (113 g); $f = 1000$ cps. Curve 1, current, forward polarization; curve 2, current, reverse polarization; curve 3, C_{zs} , forward polarization; curve 4, C_{zs} , reverse polarization.

the experiments were run are presented on the graphs. Since the area of the solid microelectrodes was not known exactly, values of C_{zs} and R_{zs} are presented for the microelectrode used, rather than being expressed as microfarads per square centimeter or ohm cm^2 .

Fig. 2 shows the residual value for C_{zs} , that is, the value obtained for the capacity of the measured series circuit without any reducible ions added. At the more negative potentials, a small residual current, due to the reduction of hydrogen from traces of water or hydroxyl ion in the melt, was drawn.

The graphs for C_{zs} , R_{zs} , and i , the current at the microelectrode, are plotted against the potential

measured with respect to the platinum foil reference electrode for the forward polarization for melts containing nickel ions, Fig. 3, and cobalt ions, Fig. 4. It is observed that the maximum in the value for C_{xs} and minimum for R_{xs} occur at the measured equilibrium potential. For the reverse polarization, Fig. 3 and 5, it is seen that the curves retrace that for the forward polarization until the maximum or minimum is reached, then show a slight jog, after which C_{xs} continues to increase and R_{xs} to decrease as the current becomes more and more anodic. Note that the jog in the current-voltage curve corresponds to the jog in the C_{xs} and R_{xs} plots. Fig. 6 shows the effect of frequency variation on C_{xs} for nickel ions in the melt. The effect of concentration changes of the reducing species is shown in Fig. 7. It is observed

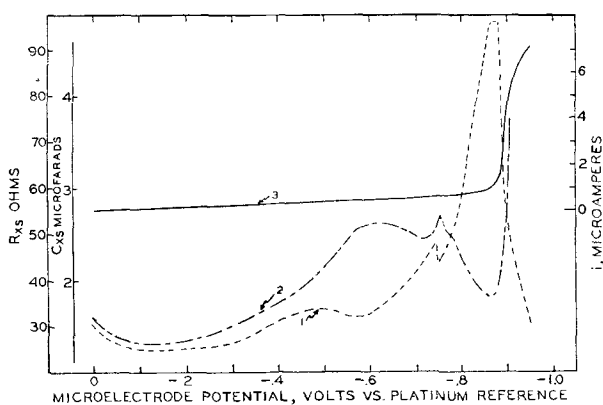


FIG. 4. C_{xs} , R_{xs} , and current for CoCl_2 (22 mg) in KCl-LiCl (106 g) forward polarization, null potential = -0.85 v.; $f = 1000$ cps. Curve 1, C_{xs} ; curve 2, R_{xs} ; curve 3, current.

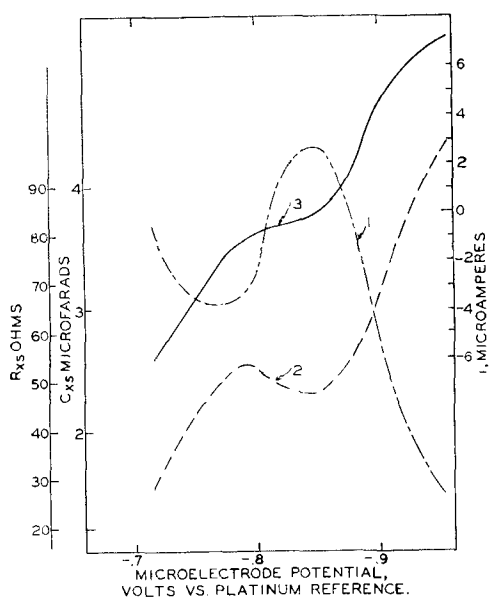


FIG. 5. C_{xs} , R_{xs} , and current for CoCl_2 (22 mg) in KCl-LiCl (106 g) reverse polarization, null potential = -0.85 v.; $f = 1000$ cps. Curve 1, C_{xs} ; curve 2, R_{xs} ; curve 3, current.

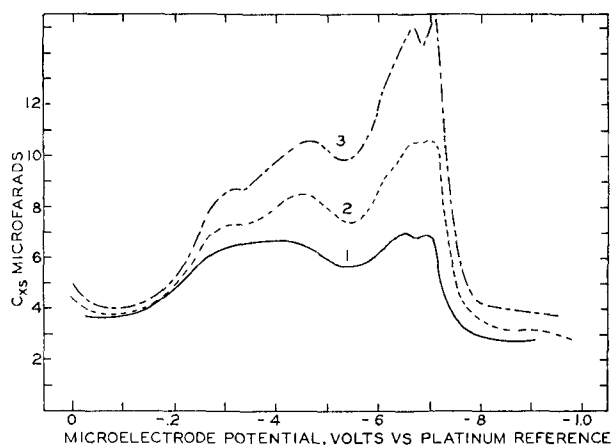


FIG. 6. C_{xs} for NiCl_2 (ca 30 mg) in KCl-LiCl (ca 100 g). Forward polarization, null potential = -0.68 v. Curve 1, 1000 cps; curve 2, 200 cps; curve 3, 100 cps.

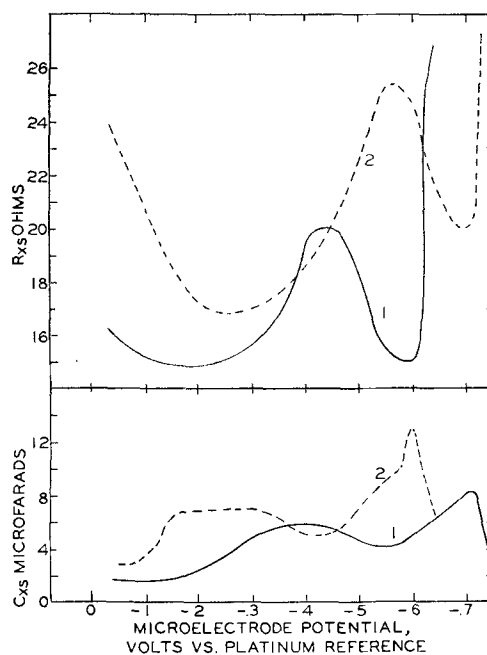


FIG. 7. C_{xs} and R_{xs} for NiCl_2 in KCl-LiCl ; $f = 1000$ cps. Curve 1, 29 mg; curve 2, 54 mg NiCl_2 in 112 g KCl-LiCl .

that the shift in the maximum in C_{xs} and minimum in R_{xs} corresponds to the shift in the equilibrium potential. The abnormally large shift in equilibrium potential is probably attributable to a drift in the potential of the reference electrode.

Fig. 8 shows a plot of C_{xs} , R_{xs} , and i against the microelectrode potential for the forward and reverse polarization with potassium tetrachloroplatinate(II) present in the melt. In this case, zero volts against the platinum reference corresponds to the equilibrium potential. In Fig. 9, values of C_{xs} are plotted against the reciprocal of the square root of the frequency for varying values of anodic current with the tetrachloroplatinate(II) present in the melt.

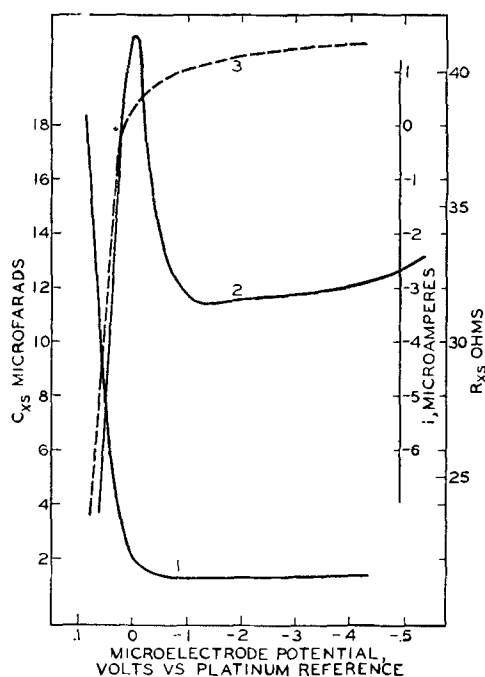


FIG. 8. C_{xs} , R_{xs} , and current for K_2PfCl_6 (27 mg) in $KCl-LiCl$ (113 g); $f = 1000$ cps. Curve 1, C_{xs} ; curve 2, R_{xs} ; curve 3, current.

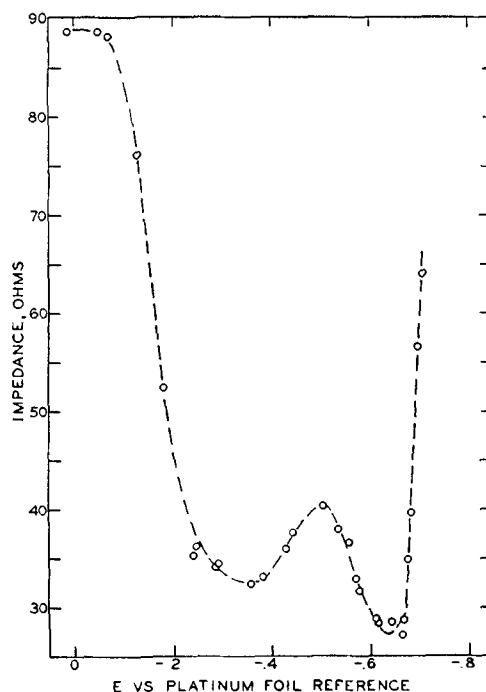


FIG. 10. Electrode impedance as function of potential, for $NiCl_2$ (29 mg) in $KCl-LiCl$ (113 g), $f = 1000$ cps.

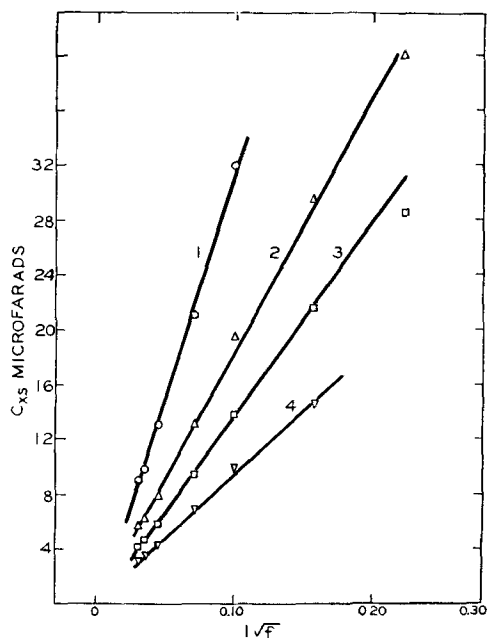


FIG. 9. C_{xs} as function of frequency, for K_2PfCl_6 (27 mg) in $KCl-LiCl$ (113 g) at various values of anodic current. Curve 1, $i = -4$; curve 2, $i = -1.5$; curve 3, $i = -0.5$; curve 4, $i = 0 \mu a$.

The total measured impedance,

$$Z = \sqrt{(1/\omega C_{xs})^2 + R_{xs}^2}$$

for the electrode in a melt containing nickel(II) ions, is shown in Fig. 10 for the forward polarization.

Note that the minimum in the impedance curve occurs at the equilibrium potential.

DISCUSSION

When impedance measurements are made in aqueous solutions using the dropping mercury electrode, the solution resistance and double layer capacity are measured and are found to be frequency independent. However, as indicated in Fig. 2, the "residual" capacity and resistance are not frequency independent. This has been attributed to the non-homogeneous character of the surface of a solid microelectrode (2, 9). Hillson (5) has suggested that a measurement of the double layer capacity at a solid electrode could be made by plotting C_{xs} against the reciprocal of frequency, and extrapolating to infinite frequency. The solution resistance might also be measured in a similar manner. However, the residual current in fused salt polarography, or in aqueous polarography employing solid electrodes, is a faradaic current, while the residual current obtained with a dropping mercury electrode is nonfaradaic, caused by the charging of the double layer at the continuously forming electrode-solution interface. The faradaic residual current would probably contribute some frequency dependent character to any resistance or capacity measurements, especially at lower frequencies. Thus, even if the values of C_{xs} and R_{xs} were extrapolated to a value at infinite frequency, the use of these values might lead to

serious error, since it would be used in a case where the frequency dependent component arises from the residual reaction plus that of the primary reaction being studied.

Attempts to calculate R_r and $1/\omega C_r$, equations (I) and (II), by subtracting vectorially the measured residual resistance and capacitance at a given frequency, were unsuccessful, leading to nonlinear and "inverted" plots against $1/\omega^{-1/2}$ in which the resistive component was less than the capacitive component of the impedance. A similar inversion was observed in plotting the uncorrected R_{zs} and $1/\omega C_{zs}$ values. Such an inverted behavior has been attributed to adsorption of the reacting species at the electrode surface (6). Unfortunately, there is no independent indication of adsorption in the present instance, although such a process is certainly possible. An adsorbed layer of reacting ions would lead to another (frequency independent) combination of resistance and capacitance across the double layer.

The resulting complexity of the impedance network, particularly in view of the abnormal frequency dependence of the double layer capacity and solution resistance, renders a quantitative interpretation impossible. Nevertheless, certain gross effects may be noted from the raw C_{zs} and R_{zs} plots.

For platinum(II), the current-voltage curve and C_{zs} conform closely to the expected behavior for a reversible couple. As shown in Fig. 9, the values of C_{zs} plotted against the reciprocal of the square root of frequency do fall reasonably well on a straight line, showing that the major portion of the impedance shows the proper frequency dependence. The pseudocapacity, C_r , is proportional to the slope of the current-voltage curve, di/dE , which in turn is proportional to the quantity $(i_a - i)$. In Fig. 9, the slopes of the curves, neglecting double layer capacity, should thus be proportional to $(i_a - i)$. Taking $i_a = 1.5 \mu\text{a}$, the calculated ratios of the slopes to the value of $(i_a - i)$ are respectively 2.5, 2.7, 2.7, and 2.2 for $i = 0, -0.5, -1.5,$ and $-4 \mu\text{a}$. It follows from these observations that the observed pseudocapacity at a given potential (not the equilibrium potential) for a *reversible* electrode should be independent of the bulk concentration of the metal ion, because the surface concentration is determined by the electrode potential and the pseudocapacity measurement is not affected by the passage of a direct current. An unexpected irregularity is the crease of R_{zs} with cathodic polarization (Fig. 8). It has already been pointed out that R_{zs} is abnormal, perhaps due to adsorption.

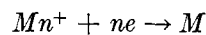
For nickel(II) (Fig. 3) and cobalt(II) (Fig. 5), the current-voltage curves show increasing deviation

from reversible behavior. As the reaction rate kC at the equilibrium potential decreases in relation to the diffusion flux, the current-voltage curve shows a region of diminished slope in the vicinity of the zero current point. Correspondingly, the value of C_{zs} does not increase smoothly in passing through the zero current point toward anodic polarization, as would be the case for a strictly reversible reaction. Actually, the jog is barely noticeable in the case of nickel(II), and the electrode reaction normally would be considered to be reversible by polarographic standards (10). By equilibrium potential methods, even the cobalt reaction probably would show reversible Nernst behavior, but its polarographic behavior is irreversible (11).

An unexpected but very striking observation was the increase in measured capacity C_{zs} which was observed on cathodic polarization of a platinum electrode in solutions of nickel(II) and cobalt(II) at potentials well before the equilibrium potential was reached. The strong frequency dependence of the capacity (Fig. 6) suggests that the diffusing metal ion is involved. The total impedance (Fig. 10) is considerably smaller in the potential region -0.2 to -0.6 v than in the absence of nickel(II) ion. Moreover, in blank experiments using the LiCl-KCl melt, a steady increase of total impedance with cathodic polarization was observed in this region, whereas two pronounced dips occurred in the presence of the nickel(II). No corresponding changes of slope in the current voltage curve were detected. This would appear to indicate that the peculiar impedance effects were not caused by residual electrode reactions in the blank melt.

The expected behavior would be to find only the double layer capacity at potentials more positive than the equilibrium potential of the plated metal. A pseudocapacity suddenly should appear at the reversible potential, and gradually decrease with increasing cathodic potential.

Since the pseudocapacity depends on the occurrence of the reaction



and since there should not be any metal deposited on the inert electrode before the equilibrium potential, the possibility of metal deposition before the equilibrium potential must be considered. Rogers has shown that, in very dilute aqueous solutions, a deposition of silver of less than a monolayer takes place at a potential more positive than that predicted by the Nernst equation (12-14). Although further proof would be needed to establish the existence of such a deposit in the fused salt melt, such behavior might explain why the pseudocapacity,

although reaching a maximum at the equilibrium potential on the forward polarization, does start to increase well before the equilibrium potential.

ACKNOWLEDGMENT

The authors wish to acknowledge the financial aid of the Department of Defense, Diamond Ordnance Fuze Laboratory, for the research assistantship held by one of the authors (R. O.).

Any discussion of this paper will appear in a Discussion Section to be published in the June 1956 JOURNAL.

REFERENCES

1. J. E. B. RANGLES, *Disc. Faraday Soc.*, **1**, 11 (1947).
2. D. GRAHAME, *This Journal*, **99**, 270C (1952).
3. B. ERSHLER, *Zhur. Fiz. Khim.*, **22**, 683, 344 (1948).
4. H. GERISCHER, *Z. physik. Chem.*, **198**, 286 (1951).
5. P. HILLSON, *Trans. Faraday Soc.*, **50**, 385 (1954).
6. H. A. LAITINEN AND J. E. B. RANGLES, *Trans. Faraday Soc.*, **51**, 54 (1955).
7. P. DELAHAY, "New Instrumental Methods in Electrochemistry," p. 170, Interscience Publishers, Inc., New York (1954).
8. H. C. ROBERTS, "Mechanical Measurements by Electrical Methods," p. 207, Instrument Publishing Co., Pittsburgh (1951).
9. P. DELAHAY, *loc. cit.*, p. 178.
10. E. D. BLACK AND T. DEVRIES, *Anal. Chem.*, **27**, 906 (1955).
11. R. A. OSTERYOUNG, Ph.D. Thesis, University of Illinois, Urbana, 1954.
12. L. ROGERS, D. KRAUSE, J. GUESS AND D. EHRLINGER, *J. (and Trans.) Electrochem. Soc.*, **95**, 33 (1949).
13. L. ROGERS, J. BYRNE, AND J. GUESS, *This Journal*, **98**, 447 (1951).
14. L. ROGERS AND J. BYRNE, *ibid.*, **98**, 457 (1951).



The Nature of Aluminum as a Cathode¹

M. J. PRYOR AND D. S. KEIR

Kaiser Aluminum & Chemical Corporation, Spokane, Washington

During the course of an investigation of galvanic corrosion, it was observed that aluminum, copper, and mild steel exhibited markedly different cathodic polarization curves in sodium chloride solution.

The results of this preliminary investigation are summarized in Fig. 1 which shows cathodic polarization curves for cold rolled aluminum² etched in 1/2% hydrofluoric acid, mild steel etched in 2% nital, and copper etched in 1:1 nitric acid. After etching, all specimens were stored in dry air for 24 hr to permit the growth of air-formed oxide films. The curves were determined in normal sodium chloride at 25° ± 0.1°C on specimens having an area of 100 cm² and probably represent continuations of the local-cell cathodic polarization³ curves.

In the absence of an applied current, corrosion of iron (1), copper (2), and aluminum (3) in sodium chloride solutions involves the consumption of dissolved oxygen. The reduction of dissolved oxygen at iron and copper cathodes results in the formation of water or hydroxyl ions (4). Hydrogen peroxide may be formed transiently as an intermediate product of reduction (5), but will be rapidly catalytically decomposed by these two metals (4). Whether detectable quantities of hydrogen peroxide are formed at aluminum cathodes has been the subject of much argument (4, 6, 7) over the years. However, if hydrogen peroxide were formed as the cathodic reaction product during the corrosion of aluminum, this alone would not explain the very high cathodic polarization shown in Fig. 1 since this polarization is observed not only at low currents where oxygen is reduced but also at higher currents where hydrogen is evolved.

Cathodic reactions on these metals presumably occurred by the migration of electrons through the surface oxide films and the subsequent interaction of these electrons with hydrogen ions and dissolved oxygen at the film/solution interfaces. In order for this reaction to occur over most of a specimen, oxide films should have a low electronic resistance. The

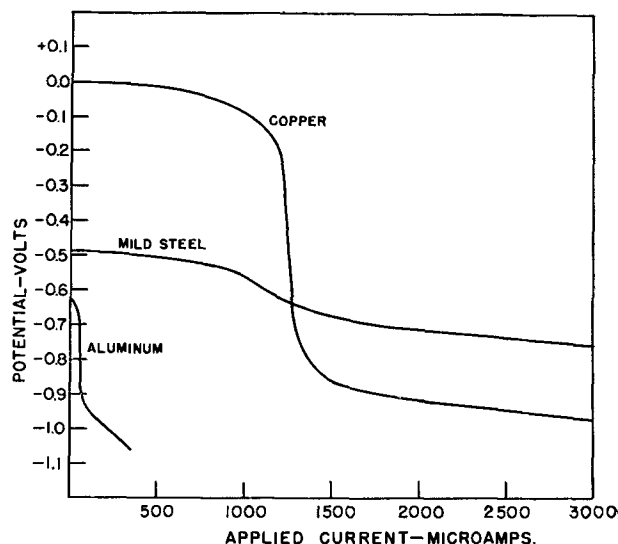


FIG. 1. Cathodic polarization curves for aluminum, mild steel, and copper in 1*N* sodium chloride solution at 25°C.

TABLE I. Chemical compositions of the metals used

Metal	Composition
Aluminum	Silicon 0.001%, iron 0.001%, copper 0.002%, balance aluminum.
Mild steel	Carbon 0.07%, silicon 0.02%, manganese 0.45%, phosphorus 0.010%, sulfur 0.030%, copper 0.06%, nickel 0.08%, molybdenum 0.005%, cobalt 0.03%, balance iron.
Iron	Carbon 0.005%, silicon 0.0075%, sulfur 0.013%, phosphorus 0.003%, manganese 0.007%, nickel 0.018%, chromium 0.02%, copper 0.003%, oxygen 0.12%, nitrogen 0.008%, hydrogen 0.00009%, balance iron.
Copper	Silicon 0.002%, iron 0.002%, magnesium <0.001%, silver <0.001%, oxygen 0.085%, balance copper.
Magnesium	Silicon 0.09%, iron 0.006%, manganese 1.69%, copper 0.004%, zinc 0.08%, balance magnesium.
Zinc	Silicon 0.08%, iron 0.001%, magnesium 0.008%, copper 0.009%, lead 0.002%, calcium 0.002%, balance zinc.
Tin	Silicon 0.06%, iron 0.005%, magnesium 0.02%, copper 0.005%, lead 0.002%, calcium 0.004%, balance tin.
Lead	Silicon 0.1%, iron 0.0005%, magnesium 0.03%, copper 0.03%, balance lead.

¹ Manuscript received February 21, 1955.

² See Table I for chemical compositions.

³ All potentials are expressed on the Standard Hydrogen Scale.

TABLE II. Results of tests for cathodic areas on metals

Metal	Phenolphthalein test for alkalinity	Cupric sulfate test for distribution of deposited copper	Sodium molybdate test for hydrogen peroxide
Iron	Development of alkalinity over whole specimen.	Uniform layer of copper deposited over entire specimen (Fig. 2a).	—
Copper	Development of alkalinity over whole specimen.	Uniform layer of copper deposited over entire specimen (Fig. 2a).	—
Magnesium	Development of alkalinity over whole specimen.	Loose deposit of copper formed over most of the surface; however, vigorous evolution of hydrogen continually detaches the copper.	—
Tin	Development of alkalinity over whole specimen.	Uniform layer of copper deposited over entire specimen.	—
Lead	Development of alkalinity over whole specimen.	Uniform layer of copper deposited over entire specimen.	—
Zinc	Only very slight pink color developed within the current range 0.5–2.5 microamp/cm ² . Above 2.5 microamp/cm ² alkalinity is developed over the whole surface.	Uniform layer of copper deposited over entire specimen.	Uniform reddish-brown coloration over most of the surface.
Aluminum	No alkalinity detected when the current is less than 20 microamp/cm ² ; at currents higher than 20 microamp/cm ² intense alkalinity is developed at some isolated areas, whereas the remainder of the specimen is faintly pink.	Small randomly distributed spots of copper are deposited on a cold rolled specimen (Fig. 2b). On an annealed specimen, spots of copper appear to be smaller, vary in number from grain to grain, and in many cases follow the grain boundaries (Fig. 2c).	Small isolated areas of reddish-brown coloration indicating localized formation of hydrogen peroxide.

resistance of air-formed oxide films on iron (8) and copper (9) is sufficiently low to permit uniform migration of electrons at low current densities. However, the electronic resistance of aluminum oxide (10) is several orders of magnitude higher than that of either ferric oxide or cupric oxide (11). Consequently, this fact might well lead to electrons migrating through thin air-formed aluminum oxide films at

local "weak" or thin points, as has been previously supposed by Evans (12).

In order to determine the distribution of effective cathodic areas, tests were carried out on cold-rolled and annealed aluminum (both etched in 1/2% hydrofluoric acid), iron and magnesium (etched in 2% nital), tin (etched in 5% nital), copper (etched in 1:1 nitric acid), lead (etched in concentrated

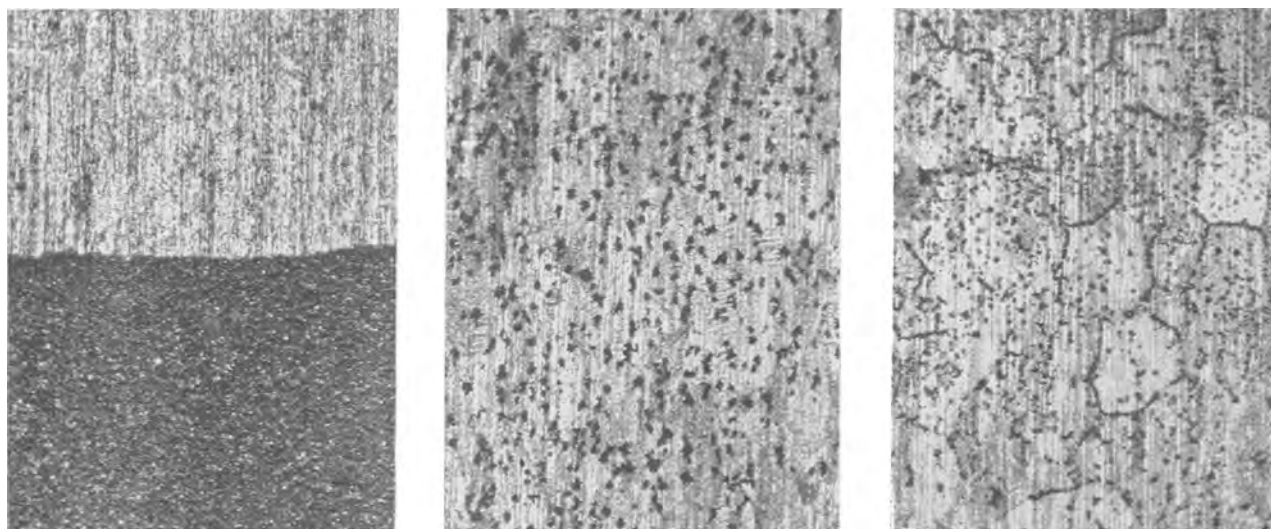


FIG. 2. Distribution of deposited copper on iron, cold rolled aluminum, and annealed aluminum after 2-min cathodic treatment in normal sodium chloride containing 0.1% cupric sulfate. From left to right—(a) uniform deposition on iron; (b) localized deposition on cold rolled aluminum; (c) localized and grain boundary deposition on annealed aluminum. (Magnification 50 \times before reduction for publication.)

nitric acid), and zinc (etched in 20% chromic acid plus 7.5% sodium sulfate). All specimens had an area of 10 cm² and were stored in dry air for 24 hr after etching in order to permit the formation of air-formed oxide films.

The tests used to investigate the initial distribution of cathodic areas were:

(A) Cathodic treatment of the specimen in normal sodium chloride containing one drop of phenolphthalein at a current of 1 microamp/cm² of specimen using a platinum anode. In some experiments the current was varied as shown in Table II. The distribution of the alkali formed during the cathodic reaction indicated the position of the cathodic areas.

(B) Cathodic treatment of the specimen for 2 min in normal sodium chloride containing 0.1% of cupric sulfate at a current of 1 microamp/cm² of specimen using a platinum anode. Deposited copper on the specimen also gave an indication of the distribution of the cathodic areas which could be readily photographed.

(C) Cathodic treatment in normal sodium chloride containing sodium molybdate at a current of 1 microamp/cm². The distribution of the reddish-brown permolybdate (13) indicates the distribution of hydrogen peroxide on zinc and aluminum cathodes.

In all tests the applied current flowed as soon as the specimen came in contact with the solution.

The results of these tests are shown in Table II. Tests [1] and [2] show that iron, copper, magnesium, zinc, tin, and lead, all carrying air-formed oxide films, act as effective cathodes over most of their surfaces (Fig. 2a). However, tests [2] and [3] show that aluminum, when covered with an air-formed oxide film, acts as an efficient cathode only at small isolated points. On cold-rolled aluminum these small cathodes appear to be randomly distributed over the surface of the specimens (Fig. 2b). Somewhat similar isolated deposition of copper (from coolant solutions containing cupramines) has been observed on aluminum previously (14). On annealed aluminum the average size of the spots of copper is smaller than on cold-rolled aluminum, but a distinct correlation between the grain boundaries and the copper deposition is apparent (Fig. 2c).

These results may be interpreted as meaning that the electronic resistance of the air-formed oxide film on aluminum, unlike those on the other metals studied, is so high that it prevents the migration of electrons to the film/solution interface except at small "weak" points of low electronic resistance. Thus, instead of the cathodic reaction taking place at low current density over most of the surface, as in the case of iron and copper, it takes place at a much higher current density over a small portion of the surface. This will lead to high polarization of the cathodic reaction as shown in Fig. 1. Whereas the "weak" points are randomly distributed on the distorted-cold rolled aluminum, they appear to follow the grain boundaries of annealed aluminum, possibly due to a high degree of lattice misfit in the underlying metal at these areas.

Although additional work remains to be carried out before general conclusions can be advanced, it is felt that these observations throw new light on the high resistance of aluminum to chloride solutions and on the limited sensitivity of the corrosion of this metal to the presence of oxygen.

Any discussion of this paper will appear in a Discussion Section to be published in the June 1956 JOURNAL.

REFERENCES

1. G. D. BENGOUGH, J. M. STUART, A. R. LEE, AND F. WORMWELL, *Proc. Roy. Soc. (London)*, **121**, 88 (1928).
2. G. D. BENGOUGH AND R. MAY, *J. Inst. Metals*, **32**, 139 (1924).
3. F. A. CHAMPION, *Trans. Faraday Soc.*, **41**, 593 (1945).
4. P. DELAHAY, *This Journal*, **97**, 205 (1950).
5. W. M. LATIMER, "Oxidation Potentials," p. 38, Prentice-Hall, Inc., New York (1950).
6. E. HERZOG AND G. CHAUDRON, *Compt. rend.*, **190**, 1189 (1930).
7. W. BECK, F. G. KEIHN, AND R. G. GOLD, *This Journal*, **101**, 393 (1954).
8. M. J. PRYOR AND U. R. EVANS, *J. Chem. Soc.*, **1950**, 1259.
9. H. A. MILEY, *J. Am. Chem. Soc.*, **59**, 2626 (1937).
10. H. ROGENER, *Z. Elektrochem.*, **46**, 25 (1948).
11. International Critical Tables, **6**, 153, McGraw-Hill Book Co., New York (1929).
12. U. R. EVANS, "Metallic Corrosion, Passivity and Protection," p. 364, Arnold, London (1937).
13. A. D. FUNCK, *Z. Anal. Chem.*, **63**, 283 (1926).
14. P. F. THOMPSON, *J. Council Sci. Ind. Res. (Australia)*, **19**, 157 (1946).

The Electrochemical Behavior, Including Hydrogen Overvoltage, of Iron in Acid Environments¹

MILTON STERN²

Corrosion Laboratory, Massachusetts Institute of Technology, Cambridge, Massachusetts

ABSTRACT

The corrosion rate of pure iron in deaerated acid media was studied as a function of *pH*. The rate was found to be essentially independent of *pH* over the range 1-4 in 4% sodium chloride. Potential and polarization measurements are used to explain this behavior. A method for calculation of corrosion rates from electrochemical measurements alone is described. Limitations and environmental conditions required for this method are discussed.

INTRODUCTION

The purpose of this investigation is to show the relations that exist between the electrochemical behavior of pure iron and its corrosion rate in oxygen-free, acid environments. Such information permits a better understanding of the fundamental factors which influence the corrosion rate and supplies a basis for predicting corrosion rates of iron and steel from independent data. Additional information concerning the effect of various alloy additions will be published later.

Recently, D'Ans and Breckheimer (1) reported potential measurements for carbonyl and electrolytic iron in a variety of air-free, acid media as a function of *pH*. They found for each system examined that a *pH* range exists within which the corrosion potential varies by approximately 0.059 volt for each unit *pH* change. The range over which this behavior holds varies, depending on the electrolyte and ferrous ion concentrations, but in general falls within *pH* values 1-5. Similar results have been reported by Bonhoeffer and Jena (2) and by Bodforss (3).

This means that over a given *pH* range, the steady-state corrosion potential of an iron electrode appears to behave in much the same manner as a reversible hydrogen electrode ($dE/dpH = 0.059$), with absolute value of the iron potential being more active than a hydrogen electrode in the same solution. A general summary of data up to 1938 is provided by Gatty and Spooner (4), and an explanation of the effect of *pH* is suggested by Uhlig (5) who showed, in accord with the electrochemical theory of corrosion, that the observed iron potential is a result of surface anode and cathode potentials polarized by local action currents.

¹ Manuscript received March 17, 1955. This paper was prepared for delivery at the Boston Meeting, October 3 to 7, 1954.

² Present address: Metals Research Laboratories, Electro Metallurgical Company, Niagara Falls, New York.

Since it is known that the potential of iron is determined by local polarization characteristics, an explanation of the above potential behavior resides in a determination of hydrogen overvoltage, anodic polarization, and corrosion rate.

APPARATUS AND PROCEDURES

It was desirable to determine the relations between corrosion rate, corrosion potential, hydrogen overvoltage, and anodic polarization; therefore, arrangements were made to measure all these properties in the same equipment under the same conditions. This was achieved in the cell illustrated in Fig. 1, holding about 2 liters of electrolyte.

Deaeration was accomplished by passing purified electrolytic hydrogen through the solution for a minimum of 6 hr. The gas was purified by passing over copper chips at 500°C, ruthenium catalyst at 300°C, and finally over palladium catalyst at room temperature. With momentary increase of hydrogen flow rate, the specimen was introduced into the cell, and deaeration continued for about 4 hr. The hydrogen was then by-passed over the top of the solution by turning appropriate stopcocks and a slight positive pressure maintained in the vessel. All tests were conducted in unstirred solutions except where otherwise indicated.

The amount of corroded iron was determined by periodically withdrawing and analyzing known quantities of solution, using the orthophenanthroline colorimetric method (6). Analyses were continued until a steady state was reached. The minimum test time was 75 hr, with the majority of measurements being taken over periods averaging 150 hr. Reported corrosion rates were determined from the slope of the linear portion of weight loss-time curves.

Corrosion potentials were measured using a platinized platinum reference electrode immersed directly in the same solution. This hydrogen electrode

was compared before and after each run with a glass electrode using a Beckman Model G meter.

After steady state was achieved, indicated by a constant corrosion potential and corrosion rate, two auxiliary iron electrodes were immersed in the solution along with a salt bridge probe which could be brought up to the surface of the corroding specimen by rotating two eccentric joints at the top of the cell. The salt bridge was filled with solution taken from the corrosion cell. Cathodic polarization measurements were conducted prior to similar anodic

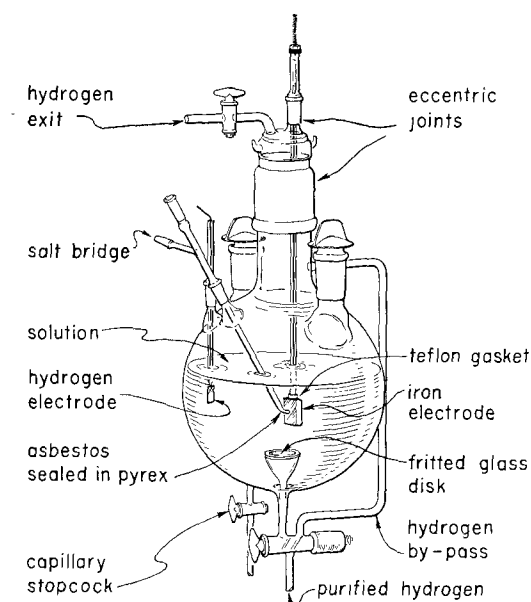


FIG. 1. Cell used for measuring corrosion potential, corrosion rate, and overvoltage phenomena.

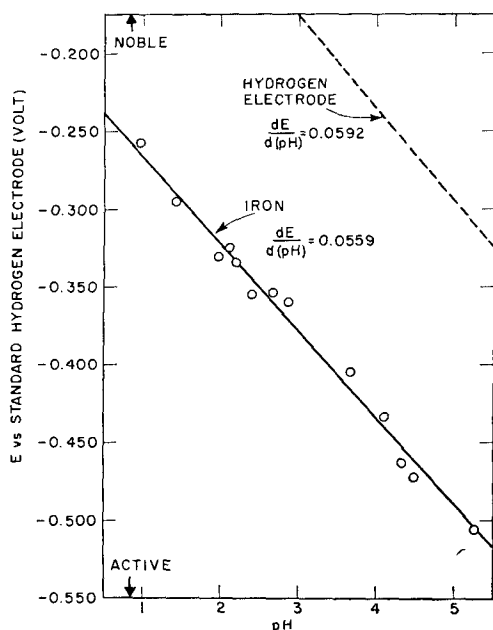


FIG. 2. Effect of pH on the corrosion potential of pure iron in deaerated 4% NaCl.

measurements. It was found that cathodic polarization did not affect appreciably the corrosion potential of an electrode after the applied current was stopped. Anodic measurements, however, caused a pronounced shift of corrosion potential in a manner which will be discussed later, and several hours were necessary thereafter for the sample to return to its original steady state.

During prolonged polarization, when chemical changes became greater, it was necessary to separate anodic and cathodic compartments. Therefore, the cell of Fig. 1 was modified into a three-compartment cell separated by fine glass fritted disks. The outer compartments, each approximately 200 ml in volume, and containing iron auxiliary electrodes, could be deaerated in the same manner as the larger center compartment.

Electrodes were cut from research-grade, high-purity iron originally made from carbonyl iron which was melted, purified, and cast under high vacuum. The analysis received from the supplier³ was 0.005% carbon, 0.023% oxygen, and 0.0002% nitrogen. No further analysis was obtained, but presumably the other impurities present were within the limits claimed by the supplier who indicated the iron content as 99.95–99.98%. Surfaces were filed and abraded smooth, pickled a number of times in concentrated nitric acid followed by concentrated hydrochloric acid to remove the cold-worked surface, rinsed thoroughly in distilled water, and immediately placed in the solution. It was found that this procedure allowed steady-state attainment in a minimum time. Electrical contact was achieved by silver soldering a $\frac{1}{16}$ -in. drill rod to a stem machined on the electrode, the drill rod and stem being isolated from the solution by a glass tube and a thick Teflon gasket (Fig. 1).

Solutions were prepared from distilled water and reagent-grade chemicals. The pH of sodium chloride solution was adjusted with hydrochloric acid. The latter solutions were pre-electrolyzed between platinum electrodes at a current density of $15 \mu\text{a}/\text{cm}^2$ for 24 hr. All measurements were conducted in a thermostated room maintained at $25^\circ\text{C} \pm 1^\circ\text{C}$.

RESULTS

Corrosion potential.—The variation of corrosion potential of pure iron in 4% sodium chloride as a function of pH is presented in Fig. 2. It is important to note that the variation of potential with pH is close to, but below, the value for a reversible hydrogen electrode. The slope $dE/dpH = 0.0559$ was determined by the method of least squares. Fig. 2 also illustrates that, over the pH range investigated, iron

³ Vacuum Metals Corporation.

is approximately 200 mv more active than a reversible hydrogen electrode in the same solution.

Corrosion rates.—Corrosion rate determinations for pure iron as a function of pH are shown in Table I. Duplicate runs at pH 0.96, conducted at different times with different specimens, illustrate the reproducibility attained. In all these tests pH of the solution was maintained essentially constant. In order to do this for the run at pH 4, where the difficulty was greatest, it was necessary to increase the volume of the solution to 5.5 l. It is evident that the corrosion rate does not vary significantly over the pH range 1–4 in deaerated solutions, the value ranging from 29 mdd at pH 1 to 25 mdd at pH 4. Gemmel (7) reports similar behavior for mild steel in the same environment. The effect in aerated solutions is very much larger (8).

It is no longer practical to measure corrosion rates by iron analysis in deaerated solutions of pH greater than about 4, because the volume of solution necessary to maintain a constant pH becomes extremely large, and insoluble corrosion products form on the surface.

Concentration polarization.—Cathodic polarization measurements were then conducted to determine the variation of hydrogen overvoltage with pH . Fig. 3 summarizes the results obtained. Instead of a complete linear relation between potential and the logarithm of current density in accord with the Tafel relations, only portions of the various curves exhibited this behavior. Sharp breaks, dependent on pH , were observed at critical values of current density measurements, after which the curves approached one common straight line. Various interpretations of such breaks have been offered recently (9) but their origin can be shown to result from concentration polarization.

This can be proved by the following sequence of reasoning and experiment. At a surface where hydrogen ions are being removed to form hydrogen gas, more ions reach the surface by three distinct mechanisms: (a) diffusion from the bulk of the solution, (b) migration under the influence of the existing electric field, and (c) convection caused by stirring which brings fresh solution to the metal surface. Of these three, only the first is of major significance, since the solution was not stirred, and the transference number of hydrogen ions in 4% sodium chloride is negligible. (The major current is carried by Na^+ and Cl^- .) Therefore, the limiting diffusion current for hydrogen ions can be calculated with the aid of the following equation derived from Ficks' First Law (10, 11):

$$i_L = \frac{nFD}{\delta} (10^{-3})a_{H^+} \quad (I)$$

TABLE I. Corrosion rate of pure iron in oxygen-free 4% NaCl as a function of pH at 25°C

pH	Corrosion rate (mdd)
0.96	29.7
0.96	27.6
2.0	28.2
2.91	29.3
3.96–4.03	25.0

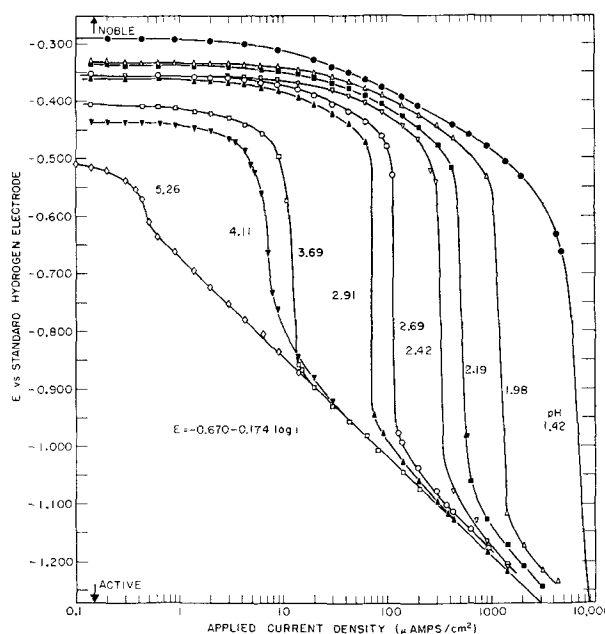


FIG. 3. Effect of pH on the cathodic polarization of pure iron in deaerated 4% NaCl.

where i_L = limiting diffusion current (amp/cm²), n = number of electrons taking part in the reaction, F = Faraday constant, δ = thickness of the diffusion layer (cm), a_{H^+} = activity of hydrogen ions (moles/liter), D = diffusion coefficient for H^+ (cm²/sec). With D equal to 7.39×10^{-5} cm²/sec (12) and δ equal to 0.05 cm (13),

$$i_L = 0.143 a_{H^+} \quad (II)$$

$$\log i_L = -0.845 - pH \quad (III)$$

Therefore, the logarithm of the limiting diffusion current is expected to vary in a linear manner with pH .

The calculated expression for this variation (equation III) is given in Fig. 4, together with the experimental determination of the limiting diffusion current found at various pH values. Deviation from a straight line relation at low pH values is expected because of the stirring effect of hydrogen gas liberated in greater quantities at the higher current densities. Stirring reduces the stagnant film thickness, δ , and introduces the factor of convection which has been neglected in the above derivation. A high trans-

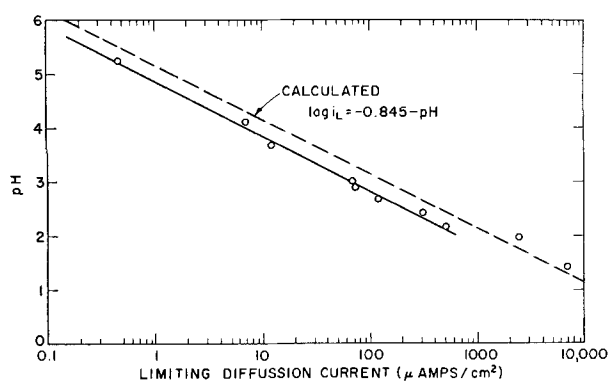


FIG. 4. Effect of pH on the limiting diffusion current for hydrogen ions in 4% NaCl.

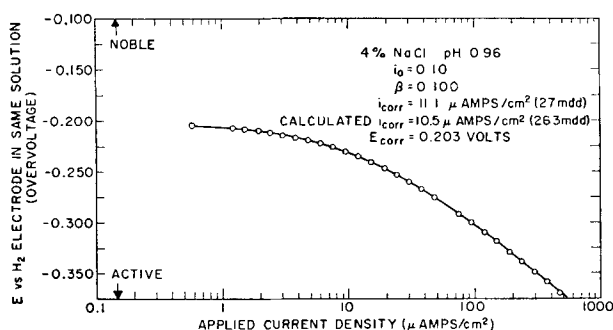


FIG. 5. Hydrogen overvoltage (activation) on pure iron in 4% NaCl at pH 0.96.

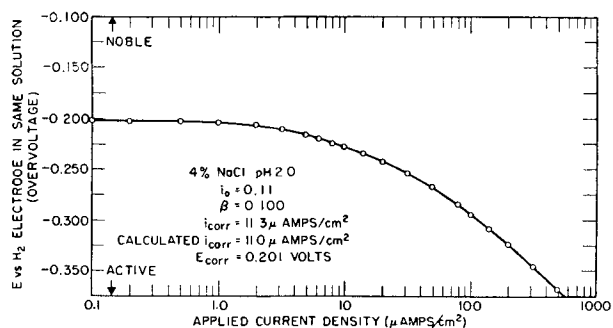


FIG. 6. Hydrogen overvoltage (activation) on pure iron in 4% NaCl at pH 2.0.

ference number for hydrogen ions at the lower pH values would also cause higher limiting diffusion currents. Agreement between equation (III) and the experimental values is convincing proof that deviations from the Tafel relation may be caused by concentration polarization of hydrogen ions. This important factor has sometimes been overlooked in interpretation of reported data on polarization and overvoltage; yet, the actual potential change introduced by concentration polarization can be greater than that from any other source. In addition, the indiscriminate use of surface roughness factors for calculating current densities is inconsistent with the concept of concentration polarization since δ would not be affected by very small surface irregularities.

Further simple experimental evidence that the breaks in the cathodic polarization measurements of Fig. 3 are caused by an increase in pH at the iron surface was obtained by introducing phenolphthalein into the solution, and observing a red color formation on the electrode surface at current densities corresponding to the rapid change of slope.

Behavior above the limiting diffusion current.—The above experiments clearly show that attempts at measurement of activation overvoltage in sodium chloride solutions above pH of about 2 are liable to include an appreciable contribution because of concentration polarization. The common linear overvoltage relation found for all the hydrogen ion concentrations above their respective limiting diffusion currents may be explained by assuming that the limiting pH produced at the surface is the same in all the solutions. The value of this limiting pH is not known precisely, but probably approaches values of 12–14 (14, 15). Above the limiting diffusion current the predominant reaction presumably changes from reduction of hydrogen ions to the direct reduction of water (14, 16), accompanied by a high pH at the electrode surface. This change in mechanism appears quite reasonable, since Delahay (14) has shown that dissociation of water is too low to account for the experimental current densities used in generation of hydrogen in neutral and alkaline media. Also the discharge of water has been established for copper in solutions of high pH by Bockris and Pentland (17).

Since the actual pH at the electrode surface is not known precisely, the linear relation found in Fig. 3 cannot be justifiably expressed in terms of overvoltage (potential vs. a hydrogen electrode in the same solution), and a reference electrode scale which is independent of pH must be used; therefore, using a modified expression of the Tafel relation

$$E_H = A - \beta \log i \quad (IV)$$

where E_H = potential on standard hydrogen scale, A and β are constants, and i = current density ($\mu A/cm^2$).

The experimental results for reduction of water on an iron surface follow the relation

$$E_H = -0.670 - 0.174 \log i \quad (V)$$

Activation overvoltage and corrosion rate calculation.—Cathodic polarization measurements at current densities low enough to avoid concentration polarization are shown for pure iron in 4% sodium chloride at pH 0.96 and 2.0 in Fig. 5 and 6. The curves are essentially horizontal at the low current densities and exhibit the Tafel relationship only at higher values of applied current. The relation be-

tween hydrogen overvoltage (activation polarization) and current density may be expressed (18):

$$\eta_a = -\beta \log \frac{i}{i_o} \quad (\text{VI})$$

where η_a = hydrogen (activation) overvoltage or potential measured against a hydrogen electrode in the same solution, β = constant (the slope of the Tafel region), i = total cathodic current density, and i_o = exchange current density or the current equal to the equilibrium rate of hydrogen reduction at the reversible hydrogen potential.

Equation (VI) may be applied both for an iron or a platinum electrode; however, iron, unlike platinum, does not function as a reversible hydrogen electrode when no external current is impressed. This is true primarily because iron corrodes (local action current flows) and one may consider the iron potential as that of a hydrogen electrode polarized cathodically in accord with equation (VI). When a cathodic current is impressed on a corroding metal it becomes evident that i , the total cathodic current density in equation (VI), should be replaced by the sum of two separate current density terms; i_x , the externally applied cathodic current and i_{ia} , the local action current. The two are obviously not independent since the principle of cathodic protection is based on the reduction of i_{ia} with an increase of i_x . From what has been described above, equation (VI) may be written in a more general form:

$$\eta_a = -\beta \log \frac{i_x + i_{ia}}{i_o} \quad (\text{VII})$$

Equation (VII) is consistent with the horizontal portion of the experimental curves, since it predicts that the potential will not change significantly until the external current approaches values of the same order of magnitude as the local action current. This is in accord with observations.

It is important to note that with no external applied current ($i_x = 0$), η_a equals the corrosion potential, E_{corr} , on the hydrogen overvoltage scale, and i_{ia} equals the corrosion current, i_{corr} ; hence,

$$E_{\text{corr}} = -\beta \log \frac{i_{\text{corr}}}{i_o} \quad (\text{VIII})$$

Equation (VIII) may be used to calculate the corrosion current if β , i_o , and the corrosion potential are known. The slope β is determined graphically from the Tafel region of a cathodic polarization measurement. The exchange current is determined by extrapolation of the Tafel region to the reversible hydrogen potential.

The rate determined by iron analysis and that calculated with equation (VIII) are tabulated in Fig. 5 for iron in 4% sodium chloride at pH 0.96 and in

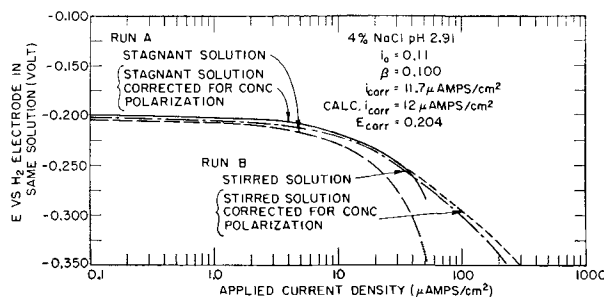


FIG. 7. Effect of stirring on concentration polarization of pure iron in 4% NaCl at pH 2.91.

Fig. 6 for a pH of 2.0. The two methods agree within experimental error.

The above-described electrochemical method cannot easily be applied at higher pH values because of the interference of concentration polarization on the determination of β and i_o ; however, Fig. 7 shows cathodic polarization measurements conducted at pH 2.91 with and without stirring. Stirring tends to eliminate concentration polarization in a manner already discussed. This figure shows that the limiting diffusion current with the stirring rate used is about ten times that in a stagnant solution. The dependence of concentration polarization on current density can be expressed as (10):

$$\eta_c = 0.059 \log \frac{i_L - i}{i_L} \quad (\text{IX})$$

where η_c = concentration polarization, and i_L = limiting diffusion current density.

Although equation (IX) has been shown to provide only approximate agreement with experiment when i approaches i_L (16), it can be used to correct the experimental data of Fig. 7. Such correction leads to a short linear portion of the activation overvoltage curve at pH 2.91. Values of the overvoltage constants and calculated and experimentally determined corrosion rates are tabulated in this figure.

It is of interest to compare the behavior of pure iron in sodium chloride solutions with that in other environments because of the influence of other anions, particularly as complexing agents for ferrous ions; therefore, measurements were conducted in 0.1M citric acid (pH 2.06) and 0.1M malic acid (pH 2.24). Fig. 8 shows overvoltage measurements in these media along with the calculated and measured corrosion currents. It is important to note that β values in these media are somewhat different from the value found for sodium chloride. In addition, there is an effect of environment on the exchange current, i_o , the values being $1 \times 10^{-1} \mu\text{a}/\text{cm}^2$ in 4% sodium chloride, $9.3 \times 10^{-2} \mu\text{a}/\text{cm}^2$ in 0.1M citric acid, and $1.5 \times 10^{-2} \mu\text{a}/\text{cm}^2$ in 0.1M malic acid.

Agreement between electrochemical calculation

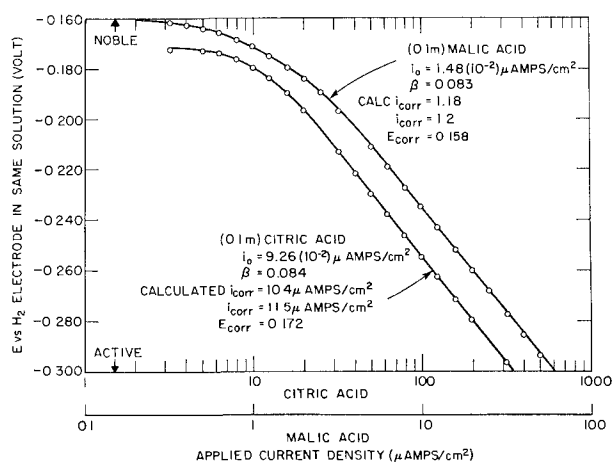


FIG. 8. Hydrogen overvoltage (activation) on pure iron in 0.1M citric acid and 0.1M malic acid.

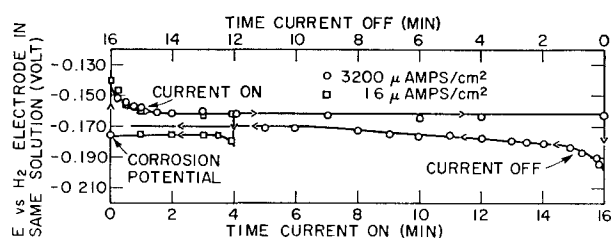


FIG. 9. Effect of time on the potential of pure iron in 0.1M citric acid after anodic currents of 16 and 3200 $\mu\text{A}/\text{cm}^2$ were applied, then stopped.

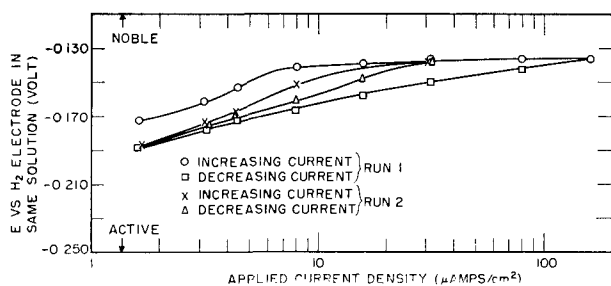


FIG. 10. Typical hysteresis phenomenon observed during anodic polarization of iron in acid media. Curves obtained in 0.1M citric acid by alternately increasing and decreasing the anodic current.

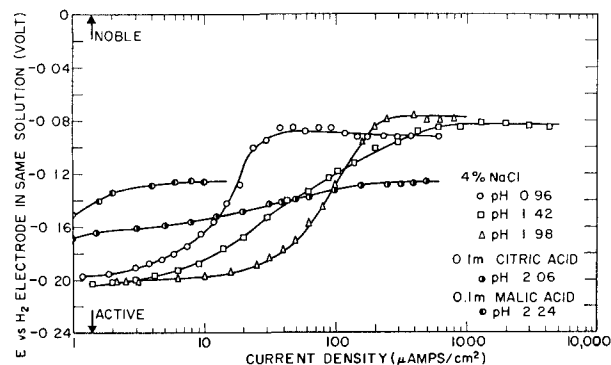


FIG. 11. Typical anodic polarization measurements for iron in various acid media.

and experimental determination of corrosion current is important because it indicates the existence of a very large cathode-to-anode area ratio. This is true since the constants used in the electrochemical calculation were determined in a current region where the specimen would be expected to function entirely as a cathode. The concept of a very large cathode-to-anode area ratio already has been expressed independently by Uhlig (5) and Hoar (19) for iron in acid environments.

Anodic polarization behavior.—Anodic polarization behavior is much more complex than cathodic behavior. Anodic measurements were not as reproducible, exhibiting marked hysteresis depending on whether current was increasing or decreasing. In addition, such measurements were dependent both on time at a given current density and on the arbitrary current density increments used. Time dependence is illustrated in Fig. 9 which shows how the potential of a pure iron electrode in 0.1M citric acid changes with time at anodic current densities of 16 $\mu\text{A}/\text{cm}^2$ and 3200 $\mu\text{A}/\text{cm}^2$. When anodic current is applied, the potential changes sharply to a more noble value, then drifts slowly in the active direction. When the current is shut off, the reverse situation occurs. The potential drops to a more active value, then slowly drifts in the noble direction. In addition, after anodic current shutoff, the potential of the iron specimen is more noble than its original steady-state value, and several hours are required before the potential assumes its original value.

The hysteresis phenomenon previously referred to is illustrated in Fig. 10 which shows anodic polarization measurements in 0.1M citric acid obtained by increasing and decreasing the applied current a number of times. It is evident that increasing anodic current yields an entirely different curve from decreasing current. Anodic polarization measurements were taken allowing 2–4 min between current increments.

Fig. 11 contains typical anodic polarization measurements conducted in a variety of media. It is apparent that iron does not polarize significantly at the higher anodic current densities. The anodic measurements illustrated should be considered as only typical of the general shape of the many curves actually obtained for reasons discussed later.

DISCUSSION

Cathodic polarization measurements on pure iron in 4% sodium chloride indicate that the activation overvoltage constants for reduction of hydrogen are essentially independent of pH, i_0 being approximately 0.1 $\mu\text{A}/\text{cm}^2$, and β having a value of 0.100.

From what has already been discussed, it becomes

obvious that the equation for local cathodic polarization in this medium may be expressed:

$$\eta_a + \eta_c = -\beta \log \frac{i}{i_o} + 2.3 \frac{RT}{nF} \log \frac{i_L - i}{i_L} \quad (\text{X})$$

for situations where i , the total cathodic current, is less than i_L .

This may be extended to give the more general equation:

$$\eta_a + \eta_c = -\beta \log \frac{i_x + i_{ia}}{i_o} + 2.3 \frac{RT}{nF} \log \frac{i_L - i_x - i_{ia}}{i_L} \quad (\text{XI})$$

or

$$E_H = -0.059pH - \beta \log \frac{i_x + i_{ia}}{i_o} + 2.3 \frac{RT}{nF} \log \frac{i_L - i_x - i_{ia}}{i_L} \quad (\text{XII})$$

When the total current appreciably exceeds i_L , equation (XII) becomes equation (V).

With a knowledge of the limiting diffusion current as a function of pH , β , and i_o , a family of local cathodic polarization curves may be drawn for iron in 4% sodium chloride as presented in Fig. 12. Combining this series of local cathodic polarization curves with the observed facts that the corrosion potential varies by 0.0559 v for each pH unit change and the corrosion current is essentially constant over the pH range 1-4, it is concluded that the local anodic polarization curve for iron at currents corresponding to the corrosion current is extremely steep. This is also consistent with the concept of a very large cathode-to-anode area ratio since even small currents would yield high current densities at a small area and, therefore, cause marked polarization.

The anodic behavior of iron can probably best be explained as follows. At high applied current densities, the major portion of the iron surface functions as anode, whereas only a small fraction is anode without external applied current. A sluggish shift in the anode-to-cathode area ratio (18), as anodic current is applied, is sufficient to explain both the time dependence and hysteresis phenomena observed. The difficulty in reproducing anodic curves and their marked dependence on experimental methods indicate that a more quantitative discussion of the measurements would at best lead to very uncertain conclusions. The necessity for more research to improve the present understanding of basic anodic polarization phenomena was amply demonstrated in this work.

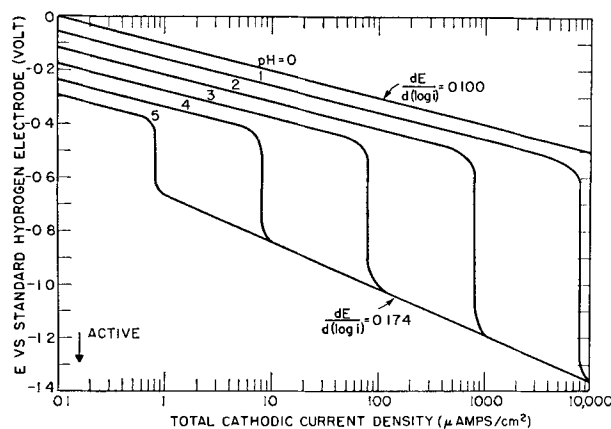


FIG. 12. Calculated local cathodic polarization curves for pure iron in deaerated 4% NaCl at various pH values.

Pure iron, in the acid environment discussed, corrodes uniformly in the sense that no pitting or intergranular attack occurs; however, there appears to be a marked effect of orientation. After a prolonged corrosion test, certain crystal faces are attacked more than others, the net result being that some faces appear to protrude from the surface. The electrochemical measurements presented here therefore must be considered as average values for random orientation. The marked effect of orientation indicates that there is a significant variation of the overvoltage constants for different crystal orientations.

The electrochemical calculation of corrosion rate is certainly not universally applicable because of its many limitations. The most important of these are the necessity for complete absence of any depolarizer, and the necessity for elimination of concentration polarization and resistance potential drops in the measurements. Although resistance polarization was not important in the cases discussed here because of the low currents and high conductivity used, an illustration of its interference will be demonstrated in a later publication which discusses application of the method to the testing of alloys. The resistance polarization became important because the corrosion current of one alloy was so high that considerable external current was required to polarize the material up to the Tafel region. [See equation (VII).] This gave some difficulty from the point of view of both resistance and concentration polarization behavior. As already indicated, concentration polarization alone is sufficient to interfere with the method above a pH value of about 3. Indeed, above about pH 5 the local action current alone appeared to be sufficient to bring the specimen into the concentration polarization region, causing a pH increase at the surface.

A further requirement of the method is that the environment be such that platinum functions as a

hydrogen electrode; in addition, the metal used must not exhibit passivity phenomena in the environment, nor should the metal have any insoluble surface films which are reduced by the cathodic current; finally, the surface should exhibit Tafel hydrogen over-voltage behavior.

The work of Wagner and Traud (20) and Bockris (21) is most important in the development of many of the concepts described here. Consideration of the ideas presented by these investigators will lead undoubtedly to marked advances in the understanding of corrosion mechanisms.

ACKNOWLEDGMENT

This program was supported by a Post-Doctoral Fellowship established by the Weirton Steel Company. The discussions and guidance of Professor H. H. Uhlig were invaluable throughout the course of the work.

Any discussion of this paper will appear in a Discussion Section to be published in the June 1956 JOURNAL.

REFERENCES

1. J. D'ANS AND W. BRECKHEIMER, *Z. Elektrochem.*, **56**, 585 (1952).
2. K. BONHOEFFER AND W. JENA, *ibid.*, **55**, 151 (1951).
3. S. BODFORSS, *Z. physik. Chem.*, **160**, 141 (1932).
4. O. GATTY AND E. SPOONER, "Electrode Potentials of Corroding Metals," p. 312, Oxford Press, New York (1938).
5. H. H. UHLIG, *Proc. Nat. Acad. Sci.*, **40**, 276 (1954).
6. E. B. SANDELL, "Colorimetric Determination of Traces of Metals," p. 374, Interscience Publishers, Inc., New York (1950).
7. G. D. GEMMEL, Masters Thesis, Massachusetts Institute of Technology (1953).
8. G. W. WHITMAN, R. P. RUSSELL, AND V. J. ALTIERI, *Ind. Eng. Chem.*, **16**, 665 (1924).
9. S. SCHULDINER, *This Journal*, **101**, 426 (1954).
10. J. N. AGAR AND F. P. BOWDEN, *Proc. Roy Soc.*, **169A**, 206 (1938).
11. C. W. TOBIAS, M. EISENBERG, AND C. R. WILKE, *This Journal*, **99**, 359C (1952).
12. L. J. BURRAGE AND A. J. ALLMAND, *J. Phys. Chem.*, **41**, 887 (1937).
13. S. GLASSTONE, "Introduction to Electrochemistry," p. 451, D. Van Nostrand Co., Inc., New York (1942).
14. P. DELAHAY, *J. Am. Chem. Soc.*, **74**, 3497 (1952).
15. J. O'M. BOCKRIS AND E. C. POTTER, *This Journal*, **99**, 176 (1952).
16. G. E. COATES, *J. Chem. Soc.*, **1945**, 484.
17. J. O'M. BOCKRIS AND N. PENTLAND, *Trans. Faraday Soc.*, **48**, 833 (1952).
18. J. O'M. BOCKRIS, "Electrochemical Constants," p. 243, National Bureau of Standards Circular 524 (1953).
19. T. P. HOAR AND R. D. HOLLIDAY, *J. Appl. Chem.*, **3**, 502 (1953).
20. C. WAGNER AND W. TRAUD, *Z. Elektrochem.*, **44**, 391 (1938).
21. J. O'M. BOCKRIS, "Modern Aspects of Electrochemistry," Academic Press, New York (1954).

Some Properties of Tin(II) Sulfate Solutions and Their Role in Electrodeposition of Tin

III. Solutions with Tin(II) Sulfate, Sulfuric Acid, and Addition Agents¹

C. A. DISCHER

Rutgers University, The State University of New Jersey, College of Pharmacy, Department of Chemistry, Newark, New Jersey

ABSTRACT

Density, refractive index, surface tension, viscosity, freezing point, conductivity, transference numbers, and electrode potentials were measured for tin(II) sulfate-sulfuric acid solutions containing addition agents. The addition agents were selected to give a range of deposit types.

Solutions were classified as to the deposits obtained from them. Specific properties of each solution were studied to determine the correlation between deposit type and the magnitude of a given property. Molar refraction, equivalent conductance, surface tension, and van't Hoff's i were found to have a well-defined relationship to deposit type. Transference and viscosity show some correlation to deposit. The other properties show no correlation.

Findings are critically analyzed in an attempt to reveal the nature of the cathode processes.

INTRODUCTION

Some physical properties of aqueous tin(II) sulfate and tin(II) sulfate-sulfuric acid solutions have been reported previously (1, 2). In the present paper the same properties are reported for a series of tin(II) sulfate-sulfuric acid solutions containing addition agents. The data have been critically analyzed in order to determine the role of each property in the deposition of tin at the cathode.

EXPERIMENTAL

The procedures and equipment used for this work have been described (1). However, because of the relatively large freezing point depressions of the solutions studied, a differential thermometer could not be used. A low temperature thermometer graduated in 0.1°C divisions was substituted. Nitrogen atmospheres were not used with those solutions which previous experience had shown to be relatively insensitive to air oxidation for the periods of time needed to conduct the measurements.

The solutions were prepared to give tin(II) sulfate and sulfuric acid concentrations of approximately 100 g/l each, the exact composition being determined analytically. This is a ratio of approximately one mole of tin(II) sulfate to slightly more than two moles of sulfuric acid, which was the ratio most thoroughly investigated before (2). This concentration also made it possible to draw upon previous

work with addition agents in tin(II) electrolytes of similar concentrations.

The addition agents were selected to give electrodeposits of widely different characteristics, ranging from bright deposits to uncontrolled masses of needles and trees. Some of the addition agents used, e.g., cresol, β -naphthol, and animal glue, are well known (3). Others, e.g., eugenol, 8-hydroxyquinoline, quinoline, *n*-octyl alcohol, *o*-toluidine, Carbowax-1500², Tergitol-7, were reported by Mathers and Discher (4). Still others, e.g., amylene (saturated), *n*-butyl alcohol (30 g/l), *n*-butylamine (1 g/l), butyl carbitol (10 g/l), benzyltrimethylammonium hydroxide (1 g/l), dimethylsulfolane (5 g/l), dithiobiuret (1 g/l), ethyl methyl ketone (80 g/l), mannitol (30 g/l), methyl cellulose (saturated), and sodium *p*-cymene sulfonate (1 g/l), were selected from unpublished experiments performed in Mathers' laboratory³ and in this laboratory. Addition agents used to give bright deposits, i.e., wood tars and *n*-aliphatic alcohol sulfates, have been reported (5). The substances listed were used singly or in combinations to give a total of 32 different electrolytes for study. Plating samples were prepared as previously described (1).

RESULTS

Deposit types.—Tin deposits obtained from the various solutions studied were classified into five

¹ Manuscript received June 28, 1954. This paper was prepared for delivery before the Chicago Meeting, May 2 to 6, 1954.

² Carbide and Carbon Chemicals Company, New York, N. Y.

³ Indiana University, Bloomington, Indiana.

TABLE I. Classification of deposits and the symbols used for each classification

Type	2-dimensional	3-dimensional	Description of deposit
I	Open circle	Light sphere	Bright
II	Blackened circle	Dark sphere	Matte
III	Dot in circle	Cube	Crystal growth well controlled, but surface rough or visibly grainy in appearance.
IV	Open triangle	Pyramid	Surface crystal growth controlled as in Type III, but poor control of crystal growth from the edges and corners.
V	Blackened triangle	Pyramid	No control of crystal growth from either edges, corners, or surface. Deposit a mass of needles or trees.

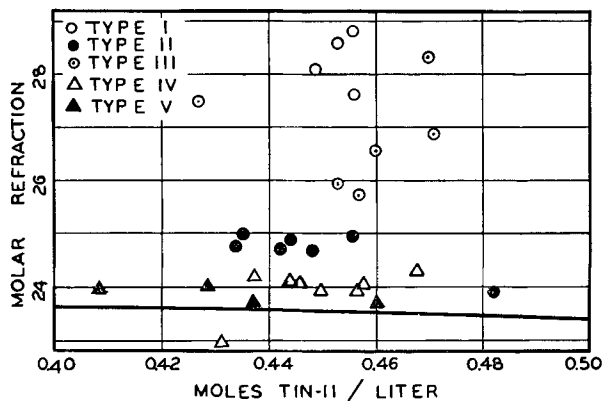


FIG. 1. Effect of molar refraction in grouping the electrolytes studied according to the type of deposit obtained. The molar refraction of corresponding solutions without addition agents is represented by the heavy line.

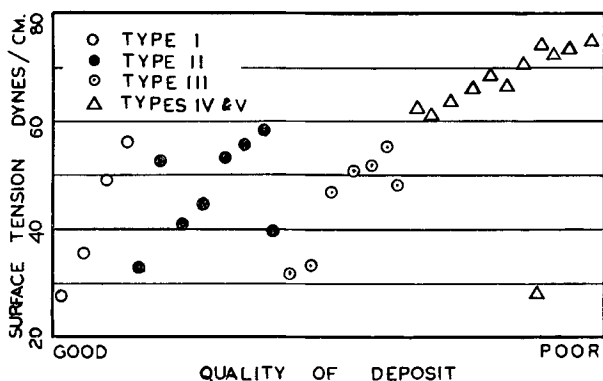


FIG. 2. Surface tension of each of the solutions studied arranged in the order of the deposit quality. The solution giving the brightest deposit is on the extreme left and the poorest on the extreme right.

types. The characteristics of each type together with the symbol used to represent it in the figures are presented in Table I. These classifications are based on visual examination. In some cases it was difficult

to judge to which of two classifications a given deposit belonged. It is interesting that in these cases the plotted points also fall in the borderline regions.

Essentially the five types may be further classified into only two groups, those deposits in which crystal growth from the edges and corners is restrained and controlled, Types I, II, and III, and those in which there is no control of crystal growth from the edges and corners, Types IV and V. It should be pointed out that in some of the plots presented, Type V deposits are not distinguished from Type IV.

Except for surface tension data the results obtained are not presented as raw experimental data. Since the concentration of tin(II) sulfate varied slightly among the different solutions, it was necessary to compensate for this variation by presenting the data on a molar or equivalent basis. For example, refractive index data is presented as molar refraction.

Refractive index.—The results are presented in Fig. 1 as a plot of molar refraction against concentration of tin(II) sulfate. The molar refraction is based upon the tin(II) present with appropriate corrections applied for the contributions to the refractivity by the sulfuric acid and the addition agent. It is clear from this plot that those solutions capable of producing bright deposits (Type I) have comparatively high molar refractions, while those which yield completely uncontrolled deposits (Type V) have molar refractions approximating those for similar tin(II) sulfate-sulfuric acid solutions without addition agents. Type IV deposits are obtained from solutions whose molar refraction varies only slightly from solutions without addition agents. Molar refractions for deposits of Types II and III fall in separate areas between Types I and IV.

It is also evident from this figure, as from subsequent figures, that variation of tin(II) concentration within the range 0.4–0.5M does not affect deposit type.

Surface tension.—Fig. 2 gives the surface tension of the solution in relation to quality of deposit. This property separates the solutions studied into two categories, (a) those which control edge crystal growth (Types I, II, and III), and (b) those which do not (Types IV and V). The limiting surface tension is apparently 60 dynes/cm, with controlled deposits being obtained from solutions having lower surface tensions. However, values of less than 60 for this property do not insure deposit control since one electrolyte had a surface tension of 29 dynes/cm but showed no control of edge crystal growth. On the other hand, no solution with a surface tension greater than 60 was found which could control crystal growth from the edges and corners of the cathode.

Conductance.—Equivalent conductances at in-

finite dilution are presented in Fig. 3 as a plot against the concentration of tin(II). The Onsager equation was used for the calculation, which is based on the total equivalents of electrolyte [tin(II) sulfate plus sulfuric acid] present in the solution. Calculations using equivalents of tin(II) give similar distributions of points when plotted, as do experimental equivalent conductances.

This property groups the solutions into three general regions in the graph. Those solutions giving Type IV and V deposits usually have equivalent conductances appreciably higher than corresponding solutions without addition agents, while those giving Type III deposits show appreciably lower values of this property. Solutions giving Type I and II deposits fall between and generally have equivalent conductances approximating those for corresponding solutions without addition agents.

Freezing point depression.—van't Hoff's i was calculated for each solution, and the following regularities were noted. All values of i fall between 1.6 and 2.0. Solutions giving Type III deposits are well grouped, with values between 1.6 and 1.8. Solutions giving Type IV and V deposits have i values between 1.8 and 1.9, approximating those for corresponding solutions without addition agents. Types I and II generally have i values greater than 1.9 but the picture is not as clear since in a few cases the i value falls within the range for Types IV and V.

Viscosity.—There is a tendency for the points representing each of the solutions to arrange themselves according to deposit. However, the boundaries between the areas are diffuse due to overlapping.

Transference numbers.—Experimental transference numbers for these solutions appeared confusing at first glance. Determinations were made for both the anode and cathode compartments in the hope that checks would be obtained. Those solutions which gave concordant results for both compartments were few indeed. Usually differences were much greater than experimental error. Continued study of the experimental data, however, showed several regularities. This would seem to indicate that the differences are real in solutions of the concentrations used in this study. Unless otherwise specified, average values for transference are used.

Solutions giving Type I or II deposits have transference numbers for tin(II) of either about 0.10 or 0. They range around zero for Type III deposits. Solutions giving Type IV or V deposits have tin(II) transference values in the range 0.04–0.07. The relative sign for the tin(II) transference numbers with respect to each compartment is extremely interesting. For the bright and matte deposits (Types I and II) the cathode transference numbers are usually smaller, i.e., more negative, than the anode transference numbers. For Type III the cathode

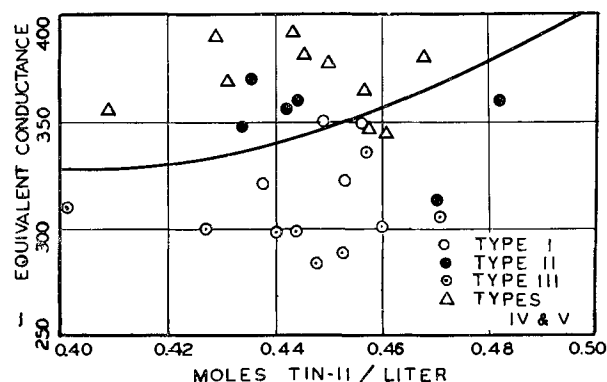


FIG. 3. Effect of equivalent conductance in grouping the electrolytes studied according to the type of deposit obtained. The equivalent conductance of corresponding solutions without addition agents is shown by the heavy curved line.

value was always positive with respect to the anode value. The Type IV and V values were about equally divided in this respect.

Values for hydrogen transference ranged from 0.80 to 1.05. With only five exceptions, cathode values were smaller than corresponding anode values. This seems to indicate some hydrogen deposition and occlusion despite the relatively low current used for these measurements (*ca.* 10 ma).

Another interesting regularity noted is the ratio of the transference by hydrogen (n_{H^+}) with respect to total transference by hydrogen and tin(II) ($n_{H^+} + n_{Sn^{++}}$). This fraction is 1.00 for the Type I and III deposits and 0.90 for the matte deposits. On the other hand, values for Type IV and V deposits ranged from 0.93 to 0.95, with the average value of 0.94.

Electrode potentials.—Experimental values obtained for the potentials of the hydrogen electrode and the tin electrode, respectively, vs. the n -calomel electrode fail to show any pattern with respect to the plating properties of the solutions studied; neither do activities or activity coefficients calculated on the basis of these experimental results. A variation by which activity and activity coefficients were plotted against ionic strength instead of concentration also failed to show any regularities.

The solutions were all of pH less than 1. This, together with the fact that reducible organic substances were present in most solutions, may account for failure of plating properties to correlate with hydrogen ion activity.

It is also possible that the organic compounds interfered with the process at the tin electrode. Roth and Leidheiser (6) showed that, in the case of nickel solutions, concentration of addition agent is a factor in the value of the electrode potential. This factor was not controlled in the work presented in this paper, the concentration of addition agent being

selected solely on the basis of the plating sample to be obtained from the electrolyte.

DISCUSSION

The following generalizations may be drawn directly from the work as presented to this point. First, those electrolytes whose properties (other than equivalent conductance) most closely approximate the properties of corresponding electrolytes without addition agents give poor deposits. (Electrode po-

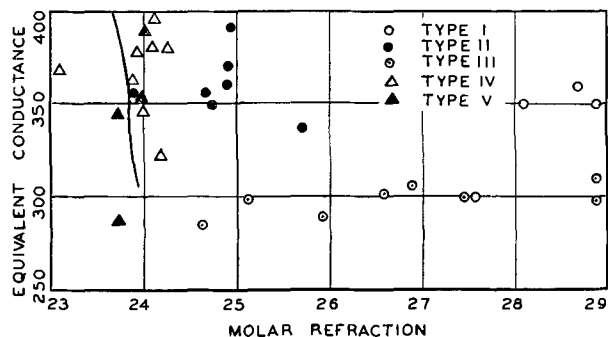


FIG. 4. Effect of both equivalent conductance and molar refraction in grouping the electrolytes studied according to the type of deposit obtained. Corresponding solutions without addition agents are represented by the curved line.

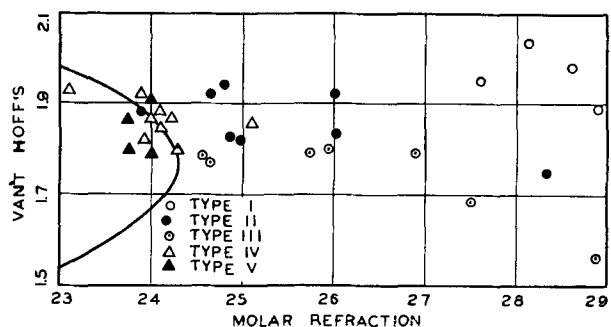


FIG. 5. Effect of both molar refraction and van't Hoff's i in grouping the electrolytes studied according to type of deposit obtained. The curved line represents these properties for solutions without addition agents.

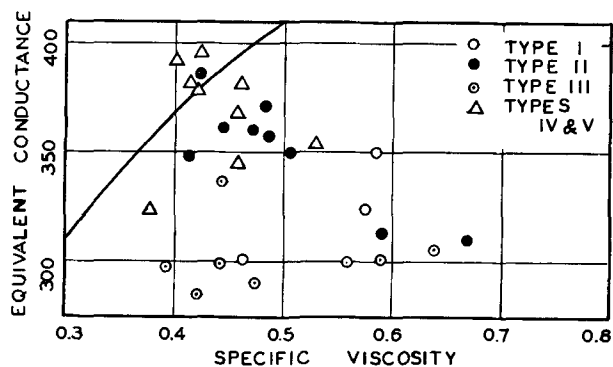


FIG. 6. Effect of equivalent conductance and specific viscosity in grouping the electrolytes studied according to the type of deposit obtained. Corresponding solutions without addition agents are represented by the curved line.

tentials must be omitted since no correlations were observed.) Second, in determining deposit type, failure to control crystal growth at the edges of the cathode was frequently more important than the nature of the surface growth. This is especially apparent in the case of surface tension.

When properties are plotted against molar concentration of tin(II), it is observed that there are points in each of the plots which apparently do not fit into the general pattern. Since tin(II) concentration is not important within the range of concentrations used, it was necessary to resort to other means to determine whether these points were significant variants or were merely the result of the use of a nondeterminant [tin(II)] as one of the axes. The data were therefore studied by means of a series of graphs in which all possible pairs of properties were used as variables. Fig. 4-6 are representative of this study; others could do equally well. Fig. 6 does not show good separation of points, but it is presented to show the role of viscosity. Specific viscosity, while important to some extent, does not separate the deposit types as effectively as some of the other properties, e.g., molar refraction. In Fig. 4 and 5 it is apparent that the number of points falling outside the area in which similar points are found have been greatly reduced, as compared to those figures in which tin(II) concentration was used as one of the axes.

Three dimensional plots were next attempted. Fig. 7 shows this type of plot using equivalent conductance, molar refraction, and van't Hoff's i as the variables. Each point falls into a volume occupied only by points representing similar deposits. There are no exceptions. Fig. 8 is based on Fig. 7. The planes approximate the boundaries between the volumes occupied by the points representing a given deposit type.

A similar plot, not shown, substituting Macleod's constant for van't Hoff's i gives similar results. Even the point for the solution having a surface tension of 29 dynes/cm, but giving a poor deposit, is within the volume occupied by points which represent solutions giving similar deposits.

From these studies it is evident that molar refraction, equivalent conductance, surface tension, and van't Hoff's i are definitely related to the type of deposit obtained from a given electrolyte. Transference data suggest the involvement of this property. Viscosity is a factor, but not as sharply defined in its effect. To obtain a given type of tin deposit each of these properties must have values within a limited range. For example, if a solution could be tailored to have a molar refraction of 28, a surface tension of 35, a van't Hoff's i of 3.95, and an equiv-

alent conductance of 340 (all in conventional units), it should give bright deposits of tin.

While all measurements made represent properties of the body of electrolyte they do throw some light on the electrode process involved in tin deposition. The following discussion indicates how the properties which were shown determinants of deposit type may modify the cathode environment or film.

Equivalent conductance.—Since there is no visible hydrogen evolution under the conditions used to prepare plating samples, it must be assumed that diffusion of tin(II) into the cathode reaction area is not a limiting factor for the deposition rate in these baths. It therefore follows that conductance is a measure of the rate at which the primary electrode process may proceed, since the rate at which electrons become available at the cathode is limited by conduction through the solution. Apparently the reduction rate is quite critical since the bright and matte deposits have equivalent conductivities intermediate between the Type III and the Type IV and V deposits. It may be said that values of equivalent conductivity between 325 and 375 represent conductivities which allow the optimum rate of transfer of electrons to the tin(II) ions. van't Hoff's i would also be expected to group the deposits, since it is a measure of the number of particles available to conduct the current in the solution.

Surface tension.—Substances which lower surface tension concentrate in the interfacial film. Since all effective addition agents for this bath lower the surface tension below 60 dynes/cm, it follows that the interfacial film at the cathode surface must be richer in addition agent than is the body of the electrolyte. Since a uniform electrical field is essential for a smooth deposit (6), it seems possible that effective addition agents concentrate sufficiently in the cathode film to insure or at least aid in establishment of a uniform field and thus prevent excessive crystal growth from the otherwise high current density areas at the edges and corners of the cathode.

Surface tension properties must also be involved in the modification of the cathode film in still another way. Electrolytes tend to increase surface tension and to concentrate in the body of the solution, leaving the interfacial film less concentrated in their respect. It has previously been shown that tin(II) sulfate and tin(II) sulfate-sulfuric acid solutions (without addition agents) have higher surface tensions than water (1, 2). This means that the cathode film is depleted in tin(II) not only because of the electrode reaction, but its concentration in tin(II) is normally lower than that determined for the body of the electrolyte because of this tendency for ionic substances to concentrate in the body of the solution. Due to these negative concentration gradients, the

complex sulfatostannite ion of the body of the solution must be degraded to a large extent into simpler particles, especially neutral molecules, since the existence of the complex is dependent on concentration.

Viscosity.—This property would modify the rate at which ions can approach the cathode, but on the basis of this work the property is not as important a determinant of deposit type as molar refraction, equivalent conductance, or surface tension.

Molar refraction.—The refractive index measurements were made relative to the D-line of sodium.

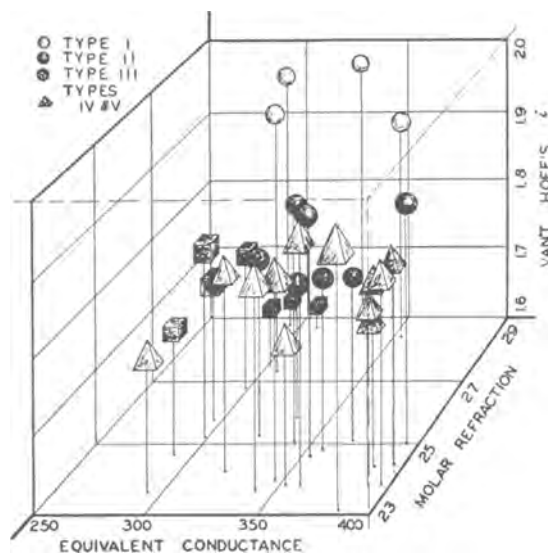


FIG. 7. Effect of equivalent conductance, molar refraction, and van't Hoff's i in grouping the electrolytes studied according to the type of deposit obtained.

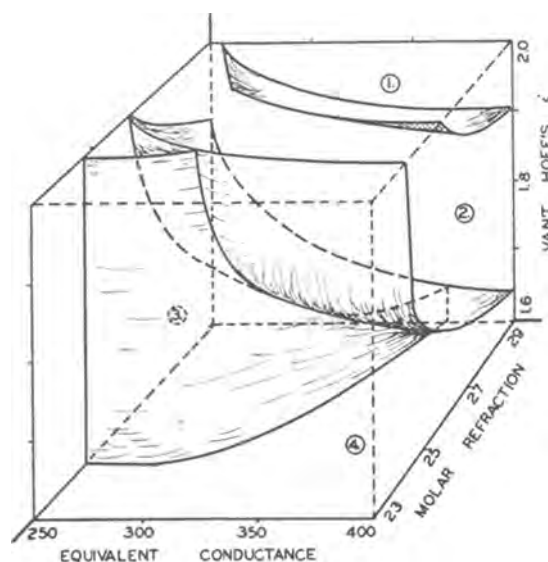


FIG. 8. Approximate volumes occupied by points representing the properties, equivalent conductance, molar refraction, and van't Hoff's i for the solutions studied. The numbers correspond to the deposit type except that the deposit types IV and V both fall in volume 4.

Therefore, it may be said that the molar refraction, as calculated, represents the distortion or deformability of the electron shell of the tin(II) (electron polarizability). The conclusion drawn is that increased polarizability of the tin(II), whatever its form in the cathode film, favors increased control of deposit, since molar refractions of all solutions which show controlled crystal growth are greater than those of solutions which do not. As the tin(II) unit moves into the field surrounding the cathode, increased polarizability would affect its behavior in the cathode film. On reaching the cathode surface the tin(II) unit must be oriented so as to present its positive pole to the negatively charged cathode; presumably the enhanced electrostatic attraction thus afforded facilitates the transfer of electrons from the cathode to the tin(II) unit.

Transference.—The fact that the hydrogen transference, as measured in the cathode compartment, is relatively more negative than that measured in the anode compartment would seem to indicate some reduction of hydrogen ion at the cathode. However, hydrogen gas was never observed at the cathode.

The constancy of the ratio between transference by hydrogen to total transference by hydrogen and tin(II) for given deposit types indicates that a definite ratio of hydrogen to tin(II) is essential. However, since tin(II) transference numbers are small, zero, or slightly negative, it seems probable that the net cathode process must be kinetic diffusion of tin(II) toward the cathode film. In light of the discussion under surface tension, the unit diffusing into the cathode film should be tin(II) sulfate molecules. This would be aided by the induced dipoles, indicated in the discussion of molar refraction.

Recently, Finch, Wilman, and Yang (7) summarized the factors influencing crystal growth at the cathode. Of these, (a) rate of arrival of metal ions, and (b) uniform concentration of the electrostatic field at the cathode surface, are substantiated for the tin(II) sulfate-sulfuric acid bath by this work. (Another point, atomic arrangement of the sub-

strate surface, was essentially a constant for the purposes of the present paper.) However, in the light of this new work it is necessary to include polarizability of the metal unit as a determining factor.

CONCLUSIONS

It was found that the cathode deposit obtained from tin(II) sulfate-sulfuric acid electrolytes is clearly related to the surface tension, molar refraction, van't Hoff's i , and equivalent conductance of the solution. Viscosity and the ratio of transference by hydrogen to total transference were also factors, but less clearly so.

In terms of the cathode process, the data indicate that increased polarization favors better deposits. There is a preferred rate of reduction at the cathode, which is a function of equivalent conductance. Surface tension must be below 60 dynes/cm for good deposits. Transference data indicate that for a good deposit, hydrogen is for practical purposes the sole carrier of the current in the electrolyte, and that the tin(II) migrates into the cathode film by diffusion rather than by conduction.

ACKNOWLEDGMENT

The author is grateful to the Rutgers University Research Council for funds for the employment of Mr. Abel Dominguez to aid in the conduct of the vast amount of routine laboratory work necessary for this paper.

Any discussion of this paper will appear in a Discussion Section to be published in the June 1956 JOURNAL.

REFERENCES

1. C. A. DISCHER, *This Journal*, **100**, 45 (1953).
2. C. A. DISCHER, *ibid.*, **100**, 480 (1953).
3. A. G. GRAY, Editor, "Modern Electroplating," John Wiley & Sons, Inc., New York (1953).
4. F. C. MATHERS AND C. A. DISCHER, *Proc. Indiana Acad. Sci.*, **56**, 141 (1946).
5. C. A. DISCHER AND F. C. MATHERS, *This Journal*, **102**, 387 (1955).
6. C. C. ROTH AND H. LEIDHEISER, JR., *ibid.*, **100**, 553 (1953).
7. G. I. FINCH, H. WILMAN, AND L. YANG, *Disc. Faraday Soc.*, **1**, 144 (1947).

Separations with a Mercury Electrode

Determination of Certain Metallic Impurities in Vanadium Salts¹

WILLIAM E. SCHMIDT² AND CLARK E. BRICKER

Princeton University, Princeton, New Jersey

ABSTRACT

By means of electrolysis with a mercury cathode, microgram quantities of copper, lead, cadmium, zinc, iron, cobalt, and nickel can be separated from at least 0.5M vanadium solutions. Quantitative recovery of all these traces of metals except cadmium from the mercury by distillation is satisfactory, and their subsequent estimation by either polarographic or spectrophotometric methods is adequate.

Electrolytic stripping of dilute amalgams at controlled potentials shows that the electrodeposited metals could not only be separated into the two major groups of passive (Fe, Co, and Ni) and nonpassive (Cu, Pb, Cd, and Cu) metals, but that separations within the nonpassive group are also possible.

INTRODUCTION

A mercury cathode has long been used to remove interfering metallic ions from solutions and to determine major constituents in mixtures of metals or metallic salts. However, it has only recently been used in conjunction with polarography to separate trace quantities of metals electrolytically before distillation of the Hg (1, 2).

In an effort to extend the electrolytic-polarographic method to the determination of trace metallic impurities in vanadium, some difficulties were encountered with regard to cadmium recovery after the distillation of mercury. Therefore, other methods of removing trace impurities were investigated.

Russell and co-workers (3, 4) determined the order of removal of 15 elements from amalgams by oxidizing agents and found that most common metals, except cobalt, nickel, and tungsten, could be removed without introducing large amounts of mercury ions. Liebhafsky (5, 6) reported that the oxidation rate of amalgams of copper, tin, thallium, lead, zinc, and cadmium by air in contact with acid, provided agitation is sufficiently violent, is virtually independent of the metal concentration and is limited mainly by the rate at which fresh amalgam is exposed. Therefore, since he concluded that the removal of these metals from mercury ought to become progressively easier as their concentration decreases, chemical oxidation might be used for

nonselective recovery of metals deposited in a mercury cathode. It was shown (7) that treatment of dilute amalgams by various reagents either gave incomplete removal of the metal or introduced sufficient mercury salts to make subsequent determination of the trace amount of metal difficult.

Because chemical methods of removing trace metals from amalgams did not look too promising, a method involving electrolytic stripping was studied. Later the electrolytic-polarographic method (1) was adapted for stripping amalgams and for selective and successive removal of trace metals from a mercury cathode.

Since completion of this work, several studies of electrolytic decomposition of dilute amalgams have been published (8-10).

APPARATUS, MATERIALS, AND METHODS

Standard sulfate solutions of nickel, cadmium, zinc, and copper were prepared from C.P. or reagent grade shot or turnings. Since lead sulfate is insoluble, lead shot was converted to lead acetate. Cobalt solutions were prepared from reagent grade cobaltous sulfate. Iron solutions were prepared from primary standard ferrous ethylenediamine sulfate tetrahydrate or from reagent grade ferrous ammonium sulfate.

Pure solutions of vanadic sulfate or vanadyl sulfate were prepared from C.P. ammonium vanadate in two ways. A pure solution of vanadic sulfate was obtained directly by electrolysis of a suspension of ammonium vanadate in dilute sulfuric acid with a mercury cathode. Or, a hot acid solution of ammonium vanadate was converted stepwise by sulfur dioxide water to vanadyl sulfate, then by electrolysis to vanadic sulfate; excess sulfur dioxide was boiled off. Pure solutions of vanadyl sulfate were

¹ Manuscript received August 6, 1954. This paper was prepared for delivery before the Boston Meeting, October 3 to 7, 1954, and is based on a thesis submitted by William E. Schmidt in partial fulfillment of the requirements for the Ph.D. degree at Princeton University.

² Present address: Chemistry Department, George Washington University, Washington, D.C.

obtained by oxidizing pure solutions of vanadic sulfate with a stream of air or oxygen. Ordinarily the initial ammonium vanadate solutions contained 10 g vanadium per liter (0.2M) and sufficient sulfuric acid to supply hydrogen ions for conversion of ammonium vanadate to vanadic acid and for reduction of vanadic acid to vanadium(III). Reagent grade formic acid was added frequently to the vanadium solution to adjust the acidity; if the solution had already been purified by electrolysis, the formic acid was distilled before addition; otherwise, it was added without distillation.

Mercury was purified by oxidation with an Oxifier and filtration with a Gold-Adhesion Filter.³ No significant amounts of metallic impurities were detected in this mercury.

The electrolysis cell has been described by Furman and co-workers (1). In some experiments an anode compartment, equipped with a fine sintered-glass disk, was mounted in the cell through a hole in the center of a Bakelite cover, and a tight fitting rubber crucible holder was used to adjust the depth of this compartment in the cell. If necessary, a cooling coil of 4 mm Pyrex tubing could be fitted beneath the anode compartment and connected to the faucet to cool the electrolyte. A suitable length of 15 gauge platinum wire alloyed with 10% iridium was used as the anode; a pool containing various amounts of mercury, usually 1.0–2.5 ml, served as the cathode. Power for the electrolysis was drawn through a rheostat from the laboratory d-c supply. A 12-in. split-tube furnace was employed for distillation.

The apparatus employed to regulate stripping was adapted from the diagram of a battery-operated electronic plating-cell control (11). Circuit changes to permit control of anodic potential instead of cathodic were made reversible. A more elaborate plating-cell control, which is a-c powered, could also be redesigned to permit stripping (12). Either circuit is entirely electronic in operation in contrast to those constant potential devices which utilize a number of mechanical parts. Simple all-electronic regulators pass the electrolysis current through vacuum tubes and thus possess limited current capacity. However, their current capacity is adequate for the stripping of dilute amalgams. References to other control devices have been listed elsewhere (13).

The stripping cell and its cover were made from the inner and outer parts of a 38/30 ground glass connection. The cell was 9 cm high and had a flat bottom which exposed the maximum stripping area of the mercury pool. The platinum-iridium contact to the pool just barely extended through the bottom. The cover was fitted with 7/25 ground glass joints in which a platinum cathode assembly and a probe from the salt bridge of a lead/lead sulfate reference

electrode could be mounted. Probes varied in diameter from 4 mm to less than 1 mm; the tips were fitted with sintered-glass plugs. Both the stripping cell and the reference electrode were held by clamps having Tygon tubing on the prongs to maintain a high resistance pathway to ground.

A resistance not exceeding 20 megohms must be inserted between the reference electrode and the electrode under control. This resistance may be furnished by the internal resistance of an ordinary vacuum tube voltmeter, which is used to set the stripping voltage at the desired operating value. If the voltmeter has a high input impedance, its input leads should be shunted by a suitable resistance. A L&N vibrator type pH indicator⁴ was used to measure all potentials, including pH.

Except for iron, which was estimated spectrophotometrically, metallic impurities were determined polarographically using a L&N Type E Electrochemograph. Both a Beckman Model DU and a Beckman Model B spectrophotometer were used for the spectrophotometric determination of iron.

EXPERIMENTAL

Electrolysis

In order to extend the electrolytic-polarographic method to the determination of trace impurities in vanadium, the separation of one metallic impurity from a vanadium solution was examined in the absence of all other metallic impurities except, of course, for the minute traces in the reagents. Since cadmium is not a usual impurity in most reagents, its recovery was studied first.

For these studies either 1.0 or 2.5 ml of purified mercury was introduced into the electrolysis cell followed by 100 ml of purified vanadium solution and an appropriate aliquot of the standard cadmium solution. The anode compartment, which was filled with 10 ml of 0.3N sulfuric acid, was lowered into the electrolyte through the Bakelite cover, and the depth was adjusted so that the anolyte level stood slightly above the catholyte level. The platinum-iridium anode was inserted to the bottom of the anode compartment, and a Gooch crucible was placed in the top of the compartment to prevent evaporation of the anolyte, which became quite hot during an electrolysis. Between 10 and 20 volts were applied to the cell, and the current was regulated to obtain the desired current density. At the end of the electrolysis, which was normally run overnight although some were run for shorter periods, the mercury cathode was removed from the cell and distilled, and the residue was analyzed polarographically.

The catholyte frequently acquired the purple color of vanadous ion within two or three hours. Usually the oxidation-reduction potential of the

³ Bethlehem Apparatus Company.

⁴ Catalogue No. 7664.

catholyte was measured at the completion of electrolysis, employing the mercury pool as the indicator electrode and a saturated calomel half-cell as the reference electrode.

In a series of 10 determinations of cadmium, ranging from 0.1 to 1 mg in weight, from 100 ml of 0.2M vanadium solution, the usual electrolytic-polarographic method gave recoveries of 39–93%. However, when lead or copper impurities were substituted for the cadmium, recovery of these metals was 95–103%. Since usually even traces of zinc could be determined quantitatively, it would appear that the potential of the vanadium redox buffer, which was obtained during the electrolysis, did not cause the low recoveries of cadmium. Thus, there seemed to be no need to obtain the most negative solution potential by separating anode and cathode compartments. When experiments were run without separating the anode from the cathode, recovery of impurities was equally good even though the vanadium solution did not acquire the dark purple color obtained when the electrodes were shielded from each other.

Many variables were considered in establishing optimum conditions for separating metal impurities at a mercury cathode, but most of them were found to have relatively minor or inconclusive effects on the recovery of lead, nickel, cadmium, and zinc. Current density, however, definitely improved reproducible recovery of zinc. Table I shows that a current density of not less than 0.45 amp/cm² should be used for consistent quantitative recoveries. Changes in current densities given in Table I were accomplished by increasing the current passing through the electrolysis cell and/or by decreasing the volume, and therefore area, of the mercury cathode.

Electrolyses of identical solutions were carried out for varying lengths of time, and the results of these experiments are shown in Table II.

Results of Tables I and II indicate that recovery of cadmium is about 5–10% below recovery of lead, nickel, and zinc. The poor recovery of cadmium was shown subsequently to be a result of the volatility of this element during distillation.

The conditions of electrolysis which were established for achieving essentially complete recoveries of the metallic impurities from vanadium were: volume of mercury, 1.0 ml; current strength 0.8–1.0 amp; current density, 0.45–0.9 amp/cm²; volume of electrolyte, 100 ml; maximum concentration of vanadium, 0.2M; separation of anolyte and catholyte, unnecessary; acids, sulfuric only, with no anode compartment; length of electrolysis, as short as 6 hr.

Distillation and Polarographic Analysis

After electrolysis the dilute amalgam electrode was drained into a silica boat without interrupting

TABLE I. Recoveries of zinc and other metals from 100 ml of approximately 0.2M vanadium solution

Current density amp/cm ²	Pb	Metal found, Ni	% Cd	Zn
0.03–0.06	—	—	—	24*
0.06–0.12	—	—	—	65*
0.20–0.25	95	87	—	100
0.20–0.25	105	97	—	96
0.10–0.15	83	89	75	95
0.10–0.15	87	92	77	81
0.45–0.9	99	96	84	97
0.45–0.9	100	95	92	96
0.45–0.9	101	95	81	96

* 0.5 mg of metal added; all other additions were 0.1 mg. All electrolyses proceeded for a minimum of 11 hr.

TABLE II. Recoveries from 100 ml of 0.2M vanadium solution by electrolysis at a current density of 0.6–0.9 amp/cm²

Electrolysis period, hr	Pb	Metal taken, mg			Metal found, %			
		Ni	Cd	Zn	Pb	Ni	Cd	Zn
1	0.101	0.096	0.102	0.101	41	10	49	28
3	0.101	0.096	0.102	0.101	71	30	57	31
6	0.101	0.096	0.102	0.101	104	96	87	105
9	0.101	0.096	0.102	0.101	102	93	91	96

the current. The last drop of amalgam was received on a dry filter paper to prevent contamination by a trace of electrolyte, then added to the boat. Usually a small globule of mercury still remained in the cell following this procedure. This was removed by running out a small amount of the electrolyte into a filter paper cone with the stopcock turned completely open for a brief moment; it was blotted dry and added to the boat. If a small amount of vanadium solution contaminated the amalgam during its removal, the nickel and zinc polarographic waves were obscured and quantitative measurements were impossible.

The boat temperature was observed during the distillation with a thermometer inserted through the cork stopper at the inlet of the combustion tube. The tube was swept by a stream of tank nitrogen, and the mercury vapor was condensed in a beaker of water. The temperature was elevated quickly and maintained at 350°–360°C until only the metal impurities remained. Generally, the power was cut off as soon as the last of the mercury had volatilized. When the boat returned nearly to room temperature, it was removed through a cylinder of paper, which prevented droplets of condensed mercury from adhering to the walls of the boat.

The boat was placed in a silica beaker and the residue was dissolved with 3 ml of aqua regia. After the boat was rinsed by a small stream of distilled water and removed from the beaker, the solution was evaporated to dryness. The residue was dissolved in 0.5 ml of hydrochloric acid plus an aliquot

TABLE III. *Typical recoveries of cadmium from an amalgam by distillation*

Volume of Hg, ml	Cd taken mg	Cd found mg	Cd found %
In a stream of nitrogen			
2.5	0.083*	0.080	96
2.5	0.092*	0.084	91
2.5	0.096*	0.089	93
2.5	0.101	0.091	90
2.5	0.479	0.390	82
1.0	1.243	1.056	85
In a stream of air			
1.0	0.0215	0.0215	100
1.0	0.0917	0.0879	96
1.0	0.1226	0.1192	97

* Lead, nickel, and zinc also present (0.1 mg of each).

of solution containing 25 mg of potassium chloride and the evaporation was repeated. Following addition of another 0.5 ml of hydrochloric acid together with a little water, the residue was evaporated a third time. Heating was stopped while the odor of hydrogen chloride was faint in the dry residue. The final residue was dissolved in 2.90 ml of water, to which was usually added a drop (0.05 ml) of 0.2% methyl cellulose as maximum suppressor. The solution was placed in a polarographic cell, deaerated for 5–10 min by a stream of tank nitrogen, then polarographed. Lead and cadmium were determined from their diffusion currents in this medium. The polarographic waves of copper, nickel, and zinc, as well as cadmium, are well separated in an alkaline background, and were determined in a pyridine-pyridinium chloride medium or in an ammonia-ammonium chloride medium. Since pyridine-pyridinium chloride is preferable when iron is present (14), this medium was used almost exclusively for the alkaline background. After the polarogram was recorded from acid solution, one drop of hydrochloric acid and five drops of pyridine (0.15 ml) were added to the polarographic solution. Ordinarily no difficulty was encountered in obtaining typical waves for each metal, although in a number of samples the zinc and pyridine waves were partially coalesced.

A strictly comparative polarographic method was employed. Using the same capillary and the same experimental conditions, heights of the characteristic waves obtained from unknown solutions were usually compared with heights obtained from identical, or nearly identical, standard solutions. Interpolation between the values for two different known concentrations was occasionally used to obtain a value for a third concentration.

With the optimum electrolysis conditions the re-

coveries of cadmium that could be expected from an amalgam by the distillation and polarographic method are shown in Table III. Since nearly all the recoveries of cadmium reported by Furman and co-workers (1) lie in the 95–100% range, some loss of cadmium by volatilization was suspected as being the most likely source of this discrepancy. This may be prevented by selective oxidation of cadmium vapors in the presence of mercury vapors. Several distillations of cadmium amalgams were made with an air stream passing slowly through the distillation tube. Although some mercury was oxidized, this did not interfere with polarographic analysis of the cadmium residues (Table III). As a further proof that cadmium was volatilized when a stream of pure nitrogen was used during the distillation operation, both the mercury distillate and the walls of the distillation tube were found to contain about 3% of a cadmium sample.

Electrolytic Stripping

Deposition of metallic ions at controlled potentials has long been used as a method to separate metals selectively. Recently the development of adequate instruments to control the cathode potential automatically has stimulated renewed interest in this method (15, 16). The reverse process, selective stripping of metals from an electrode into a solution at a controlled anode potential, has not been similarly exploited for analytical separations. However, Kozlovskii and co-workers (17) have recently reported amalgam methods of separation for macro quantities of nonferrous metals which utilize controlled anodic oxidation. Moreover, anodic dissolution has been used for many years to dissolve solid alloy samples, to measure the thickness of plated coatings, and to determine nonmetallic inclusions in metals (15).

If the anodic oxidation of metals from amalgams follows the same pattern as that reported (3, 4) for oxidizing solutions, base metals should strip very readily from amalgams at controlled potentials, whereas the removal of iron, cobalt, and nickel from amalgams without introduction of mercury ions may not be possible. Thus in composite amalgams, i.e., in amalgams containing several metals, it should be possible to separate zinc, cadmium, lead, and copper from iron, cobalt, and nickel even though the effect of large concentrations of the passive metals on the stripping of the nonpassive metals may introduce some unexpected difficulties.

The degree of separation attainable by electrolytic stripping of amalgams should be determined by the minimum concentration of metal required to maintain the potential of an amalgam. Erdey-Gruz (18) and others (19–22) showed that for amalgams with a concentration of 10^{-5} – 10^{-4} g-atom/l, the potential

is determined solely by the electrochemical distribution: equilibrium metal/metallic ion. Thus, the concentration effect follows the Nernst equation. In the concentration range 10^{-6} – 10^{-5} g-atom/l, the change of potential is greater than that demanded by the Nernst equation. If the concentration of the amalgam falls below 10^{-6} g-atom/l, the potential is the same as that of pure mercury. From these data the number of micrograms of a given metal which remain in a 1.0 ml amalgam electrode when the potential of the electrode is the same as that of pure mercury may be calculated. Results are: zinc, 0.06; cadmium, 0.1; lead, 0.2; and copper, 0.06 μ g. If the mercury electrode contained initially 10 μ g of each of these metals, the following percentages of metals would remain in the mercury after stripping: zinc, 0.6%; cadmium, 1%; lead, 2%; and copper, 0.6%. Thus, for samples containing about 10 or more μ g of a given metal, the unstripped fraction should be no larger than the uncertainty of the subsequent polarographic analysis.

Stripping of nonpassive metals.—The recovery of trace metals from an amalgam by electrolytic stripping was applied to many amalgams containing various amounts of one or more of the metals, copper, lead, cadmium, and zinc. Amalgams were prepared by electrolyzing known amounts of these metals in solutions from a 0.1*N* sulfuric acid or dilute acetic acid solution into a known weight of mercury. If the amalgam was not prepared directly in the stripping cell, it was drained into this cell in the manner described above. Otherwise, at the completion of electrolysis the electrolyte was siphoned without interrupting the current, and the vessel was rinsed with water until the conductance of the solution was negligible.

The stripping electrolyte generally consisted of 5 or 10 ml of 0.1–0.5*N* potassium sulfate or potassium chloride. Potassium sulfate was preferred, especially for stripping copper amalgams, because of the greater potential difference between mercury-mercurous sulfate and the amalgam as opposed to the potential difference between mercury-mercurous chloride and the amalgam. However, it was essential to use potassium chloride when the amalgam contained lead. Obviously, the number of metals which can be separated from mercury by the stripping process and the degree of selectivity of the separations among the metallic impurities will vary with the composition of the stripping electrolyte.

Copper amalgams, which formed a coating of cuprous oxide on the surface of the amalgam in a neutral electrolyte, were slightly acidified with a drop of acetic acid. If the electrolyte was initially neutral, it became basic during the stripping. Hydroxides of zinc, cadmium, and lead, which formed a readily

visible precipitate when the amalgam contained about 1 mg or more of one of these metals, did not appear to interfere in any way with the stripping process. Ordinarily the solution did not become sufficiently basic to establish the potential of the mercury-mercuric oxide couple, which is considerably more negative than the potentials of the mercury-mercurous salt couples.

A quiescent mercury pool strips fairly rapidly and smoothly. For example, the current-time data for the stripping of 124 μ g of cadmium from 5 and 15 g of amalgam are shown in Fig. 1, where the maximum stripping rate was used. This rate was attained by setting the electronic control so that the stripping would stop at a potential 0.5–0.1 v before the dissolution of mercury would begin. As can be seen from Fig. 1, the initial current during a stripping operation was almost a "surge current" but rapidly fell during the first minute to a value of several hundred microamperes. The stripping operation was considered to be complete when the current fell to about 0.1 μ a. The current was never observed to reach a zero value unless extremely long times were allowed for the amalgam to reach equilibrium.

Although rotating the amalgam or stirring the solution increased the rate of stripping, neither of these stirring procedures was employed. Passing oxygen or nitrogen through the solution appeared to have no effect other than that of stirring. This has

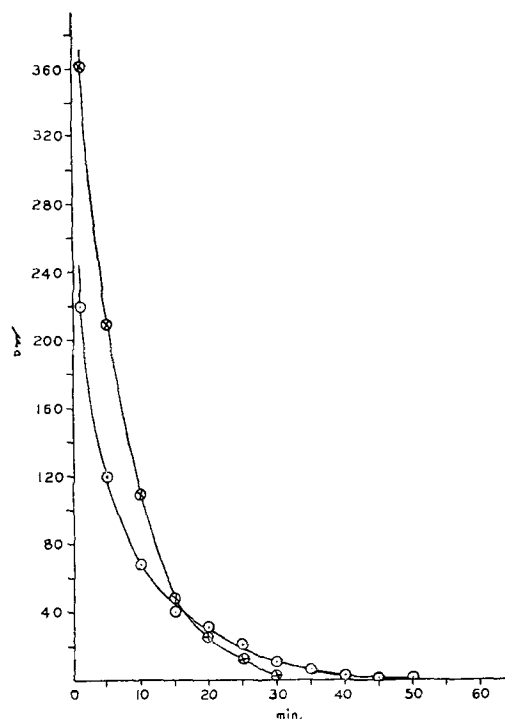


Fig. 1. Current-time curves for discharging dilute amalgams. \otimes = 5g; \odot = 15g.

TABLE IV. Typical recoveries from simple and composite amalgams by the stripping procedure

Wt of Hg, g	Metal taken, mg				Metal found, %			
	Cd	Cu	Pb	Zn	Cd	Cu	Pb	Zn
5.0	0.0101	—	—	—	95	—	—	—
34.0	0.0101	—	—	—	98	—	—	—
5.0	0.0248	—	—	—	99	—	—	—
5.6	0.1223	—	—	—	98	—	—	—
15.0	1.216	—	—	—	99	—	—	—
5.0	1.243	—	—	—	98	—	—	—
28.0	2.486	—	—	—	97	—	—	—
28.0	6.215	—	—	—	100	—	—	—
20.2	—	1.012	—	—	—	100	—	—
34.0	—	—	0.498	—	—	—	98	—
34.0	—	—	0.498	—	—	—	100	—
34.0	—	—	—	0.458	—	—	—	97
34.0	1.243	—	0.498	—	100	—	104	—
5.0	0.124	—	—	0.498	101	—	—	102
34.0	0.124	—	—	0.498	103	—	—	95
34.0	0.124	—	0.498	0.498	103	—	101	102

been reported previously by Bowden (23) and indirectly by Liebhfasky (5, 6).

In a number of cases dilute amalgams containing about 50 μg or less of zinc or cadmium in 1–2.5 ml of mercury did not give an amalgam potential when prepared for stripping. This behavior, which was more common with zinc amalgams than with cadmium amalgams, was traced to the spontaneous decomposition of the dilute amalgams. For example, an amalgam composed of 13.5 g (1 ml) of mercury and 44 μg of zinc, which was allowed to stand for 20 min in contact with 5.00 ml of ammonia-ammonium chloride solution, was completely decomposed as shown by the polarographic determination of zinc in the solution.

If desired, the amalgam potential could be regained by electrolyzing the stripping electrolyte with the mercury pool as the cathode for a minute or two at 0.1–0.2 amp. If potassium was deposited, it began to react with the solution as soon as the electrolysis current was broken. Thus, when the cell was prepared for stripping, the potential of potassium amalgam was obtained and persisted until all the potassium had reacted. The potential of zinc or cadmium amalgam was now obtained and the stripping could be followed in the usual manner. It was shown that zinc or cadmium ions could be removed quantitatively from solution by an internal electrolysis utilizing the reaction of a potassium amalgam alone on the solution to deposit the less active metals.

Solutions from the stripping operation were analyzed in one of two ways. If the stripping was performed in a known volume of electrolyte, the resulting solution was merely polarographed. Otherwise, the stripping solution was acidified with acetic acid, then evaporated to dryness. The residue was dissolved in a known volume of water or neutral electro-

lyte (potassium sulfate or potassium chloride) and polarographed as described previously.

Typical recoveries of metals from simple and composite amalgams are shown in Table IV, and clearly indicate that quantitative results were obtained in all cases.

Use of an internal electrolysis instead of electronically controlled electrolytic stripping to recover nonpassive metals from a mercury electrode was tested by discharging an amalgam containing nonpassive cadmium and passive nickel against a half-cell composed of a copper amalgam electrode and a solution of saturated copper sulfate slightly acidified with sulfuric acid. Each amalgam pool, together with its appropriate electrolyte, was contained in an open stripping cell which was connected to the opposing cell by a salt bridge of agar and saturated potassium sulfate. A resistor was included in the discharging circuit to limit the initial current to about 100 μa or less. Eventually, as the potential difference between the half-cells decreased, this external resistance was removed, and the half-cells were short-circuited until the current became negligible. A saturated calomel reference electrode was included to check the potential of both amalgam electrodes.

Recoveries of cadmium from amalgams containing cadmium and nickel using the internal electrolysis technique for cadmium removal were determined polarographically and averaged $101 \pm 1\%$. The amalgam remaining after the removal of cadmium was distilled, and nickel recovery was $99 \pm 2\%$. Therefore, the very simple internal electrolysis assembly can be used to separate passive from nonpassive metals from an amalgam without introducing mercuric ions into solution.

Stripping of passive metals.—Separation of cadmium from nickel by means of internal stripping and the work of Russell (3, 4) suggested that the passive metals, iron, cobalt, and nickel, would be removed from mercury, if at all, only after copper was removed. When the stripping of amalgams of nickel and iron was attempted, no detectable amount of either element could be found in the electrolyte unless mercury was also dissolved. However, small to substantial amounts of cobalt were stripped in a sulfate electrolyte at a potential close to the dissolution potential of mercury, but complete removal of the cobalt was never attained without resorting finally to distillation. In no case where stripping was performed so that no mercuric ions were introduced into solution was any trace of the nonpassive metals detected in the distillation residue.

Typical recoveries from a mercury electrode by stripping of one or more nonpassive metals in the presence of one or more passive metals, together with the recoveries of the passive metals by the dis-

TABLE V. Typical recoveries of nonpassive metals from a mercury electrode by the stripping procedure and of passive metals by the distillation procedure

Wt of Hg g	Nonpassive metal taken, μg				Passive metal taken, μg			Nonpassive metal found, %				Passive metal found, %		
	Cu	Pb	Cd	Zn	Fe	Co	Ni	Cu	Pb	Cd	Zn	Fe	Co	Ni
20.2	1012	—	—	—	—	—	56	97	—	—	—	—	—	97
5.0	1012	—	—	—	—	500	—	103	—	—	—	—	103	—
13.5	—	500	—	—	500	—	—	—	98	—	—	*	—	—
13.5	—	—	—	456	—	500	—	—	—	—	100	—	104	—
13.5	—	—	17	—	—	—	56	—	—	101	—	—	—	100
34.0	—	—	25	—	0.1g	—	—	—	—	103	—	*	—	—
13.5	—	—	110	—	—	—	56	—	—	102	—	—	—	101
13.5	—	—	110	—	—	—	565	—	—	100	—	—	—	97
20.2	—	—	110	—	—	—	565	—	—	103	—	—	—	*
20.2	—	—	125	—	—	—	565	—	—	98	—	—	—	100
34.0	—	—	125	—	500	—	—	—	—	101	—	105	—	—
5.0	—	—	1251	—	—	—	56	—	—	96	—	—	—	97
5.0	1012	—	876	—	—	500	—	103	—	98	—	—	103	—
20.2	—	—	876	—	—	500	565	—	—	99	—	—	102	96
5.0	—	1000	876	450	—	500	565	—	102	100	99	—	105	95
5.0	—	—	—	—	1000	—	—	—	—	—	—	100	—	—
13.5	—	—	—	—	—	—	56	—	—	—	—	—	—	96
13.5	—	—	—	—	—	500	565	—	—	—	—	—	105**	97
13.5	1012	—	—	—	—	500	—	99	—	—	—	—	105†	—
20.2	—	—	112	—	—	500	—	—	—	100	—	—	53‡	—

* Per cent found was not determined.

** 16% cobalt was found in stripping step.

† 7% cobalt was found in stripping step.

‡ 53% cobalt was found in stripping step; distillation was omitted.

Stripping of the passive metals was attempted in the bottom five samples.

TABLE VI. Typical recoveries from 0.2M vanadium solution using the stripping and distillation procedures

Wt of Hg g	Metal added μg						Metal found (stripping) %			Metal found (distillation) %		
	Cu	Pb	Cd	Fe	Co	Ni	Cu	Pb	Cd	Fe	Co	Ni
13.5	—	—	25	—	—	—	—	—	97	—	—	—
13.5	—	—	50	—	—	—	—	—	98	—	—	—
13.5	—	—	124	—	—	—	—	—	98	—	—	—
13.5	—	—	124	—	—	—	—	—	101	—	—	—
13.5	—	—	1243	—	—	—	—	—	98*	—	—	—
28.0	—	—	2486	—	—	—	—	—	97	—	—	—
20.2	—	—	876	10mg	—	—	—	—	96	†	—	—
20.2	—	—	876	—	500	565	—	—	99	—	102	96
13.5	—	—	1251	—	500	565	—	—	98	—	100	95
13.5	—	500	876	—	500	565	—	103	103	—	102	97
13.5	1012	—	876	500	500	565	99	—	97	†	96	100
20.2	2024	500	250	500	500	565	100‡	98	101	†	104	97

* The electrolyte was 0.5M in vanadium.

† Not determined.

‡ Separated by distillation instead of stripping.

tillation of the mercury, are shown in Table V. Iron was determined spectrophotometrically by the *o*-phenanthroline method (24). Special attention should be called to the sample in which 25 μg of cadmium were recovered from 34.0 g of mercury containing 0.1 g of iron. Presumably, deposition followed by stripping could be used as a general method for separating a small amount of a nonpassive metal from a large amount of a passive metal.

Application to vanadium salts.—Using the optimum

conditions for electrolysis of vanadium solutions, as given previously, the electrodeposited "impurities" were recovered and analyzed according to the procedures just given. The results of typical recoveries of trace amounts of six metals from 100 ml of 0.2M vanadium solution using this procedure are shown in Table VI. It is significant that all metals listed in Table VI (cf. Tables I and II) are obviously separated from vanadium by electrolysis and subsequently recovered from mercury by the procedure employed.

DISCUSSION

The accuracy of the polarographic analysis of a mixture depends on the ratio in which the various substances occur. The determination of a cation in a solution containing a group of metal ions for which the half-wave potentials differ by about 0.2 v or more is readily accomplished if the cations are present in similar concentrations in the range 10^{-3} – 10^{-5} M. When the cations are present in concentrations which vary widely, the determination is still readily accomplished if the concentration of each cation *increases* in the order of decreasing reducibility. If, however, the concentration of each ion *decreases* in the order of decreasing reducibility, the accuracy of the analysis progressively drops as the difference in the concentrations of the cations becomes greater. Thus separation of the nonpassive and passive metals by stripping and distillation procedures described here,

together with selective stripping among nonpassive metals, greatly simplifies polarographic analysis of a mixture of metals which has been electrodeposited with a mercury cathode.

Presumably, the nonpassive metals could be analyzed coulometrically while being selectively stripped at a controlled potential, unless there were sufficient spontaneous decomposition of the amalgam to invalidate the measurements. Either the quantity of electricity or the discharging time, which was recently studied by Juliard and Gierst (25), could be measured. The latter measurement is dependent on the weight and dimensions of the liquid pool.

An estimate of the agreement between the quantity of electricity put through a stripping cell by the control apparatus and the amount of metal stripped was made by stripping a 1.24 mg sample of cadmium while the cell current was held constant within 10% by manual control of the constant potential device. For example, the current was held initially to $500 \pm 50 \mu\text{a}$ for over 56 min, then it was held to $50 \pm 5 \mu\text{a}$, etc., until completion of the process. This crude technique accounted for 1.7 coulombs of the theoretical 2.1 coulombs required to strip 1.24 mg of cadmium, if no spontaneous reaction of the metal with the electrolyte occurred.

The results in Fig. 1 show clearly that the initial current in the smaller pool (area, approximately 1.3 cm²) was considerably greater than the initial current in the larger pool (area, approximately 3.5 cm²). Moreover, the smaller pool, having the smaller surface area, discharged at a faster rate, and eventually the two curves crossed. Thus, in a cadmium amalgam the cadmium must be distributed throughout the mercury rather than concentrated near the amalgam-electrolyte interface. Otherwise, the larger pool, having the larger surface area, would have discharged more rapidly. This conclusion regarding the homogeneity of cadmium amalgams should be checked for the various metal amalgams because the same results may not be obtained with all metals.

SUMMARY

By electrolysis, copper, lead, cadmium, and zinc present in quantities as small as 10 μg , may be removed essentially quantitatively from solutions as concentrated as 0.5M in vanadium. The small quantities of nonpassive metals (copper, lead, cadmium, and zinc) may then be recovered by back electrolysis at controlled potentials, and the passive metals (iron, cobalt, and nickel) may be recovered by the distillation of the mercury cathode following this stripping. All the metals may be recovered by distillation, but losses of cadmium are likely to occur unless the nitrogen stream is mixed with a sufficient amount of oxygen or air. Subsequent estimation of the metals may be made polarographically or by any other valid

method. Use of the stripping technique to separate the electrodeposited metals into two groups, as well as the possibility of selective and successive stripping within the nonpassive group, simplifies the polarographic analysis.

ACKNOWLEDGMENT

Support of this research by Contract AT(30-1)-937 Scope I of the U. S. Atomic Energy Commission to Princeton University is gratefully acknowledged.

Any discussion of this paper will appear in a Discussion Section to be published in the June 1956 JOURNAL.

REFERENCES

1. N. H. FURMAN, C. E. BRICKER, AND B. McDUFFIE, *J. Wash. Acad. Sci.*, **38**, 159 (1948); C. C. CASTO IN C. J. RODDEN, "Analytical Chemistry of the Manhattan Project," pp. 518-21, McGraw-Hill Book Co., New York (1950).
2. H. CORIOU, J. GUERON, H. HERING, AND P. LEVEQUE, *J. chim. phys.*, **48**, 55 (1951).
3. A. S. RUSSELL, D. C. EVANS, AND S. W. ROWELL, *J. Chem. Soc.*, **1926**, 1872.
4. A. S. RUSSELL, *ibid.*, **1929**, 2398.
5. H. A. LIEBHAFSKY, *J. Am. Chem. Soc.*, **59**, 452 (1937).
6. H. A. LIEBHAFSKY AND A. F. WINSLOW, *ibid.*, **63**, 3137 (1941).
7. C. E. BRICKER, Ph.D. Thesis, Princeton University (1944).
8. H. CORIOU, J. HURE, AND N. MEUNIER, *Anal. Chim. Acta*, **9**, 171 (1953).
9. J. T. PORTER AND W. D. COOKE, *J. Am. Chem. Soc.*, **77**, 1481 (1955).
10. A. HICKLING AND J. MAXWELL, *Trans. Faraday Soc.*, **51**, 44 (1955).
11. W. C. ELMORE AND M. SANDS, "Electronics: Experimental Techniques," pp. 401-405, McGraw-Hill Book Co., New York (1949).
12. J. W. HEYD, P. E. OHMART, AND C. E. HITES, Laboratory Report of Monsanto Chemical Co., 48-12-65, Dec. 20, 1948.
13. J. J. LINGANE, "Electroanalytical Chemistry," Chap. XI, Interscience Publishers, New York (1953).
14. J. J. LINGANE AND H. KERLINGER, *Ind. Eng. Chem., Anal. Ed.*, **13**, 77 (1941).
15. S. E. Q. ASHLEY, *Anal. Chem.*, **24**, 91 (1952).
16. D. D. DEFORD, *ibid.*, **26**, 135 (1954).
17. M. T. KOZLOVSKII, P. P. TSYB, AND E. F. SPERANSKAYA, *Trudy Komissii Anal. Khim. Akad. Nauk S. S. S. R. Otdel. Khim. Nauk*, **4** (7), 255 (1952); *Chem. Abstr.*, **48**, 1878 (1954).
18. T. ERDEY-GRUZ AND A. VAZSONYI-ZILAHY, *Z. physik. Chem.*, **A177**, 292 (1936).
19. G. A. HULETT AND R. E. DELURY, *J. Am. Chem. Soc.*, **30**, 1805 (1908).
20. J. L. CRENSHAW, *J. Phys. Chem.*, **14**, 158 (1910).
21. J. N. PEARCE AND J. F. EVERSOLE, *ibid.*, **32**, 209 (1928).
22. J. L. CRENSHAW, *ibid.*, **34**, 863 (1930).
23. F. P. BOWDEN, *Trans. Faraday Soc.*, **36**, 1226 (1927).
24. E. B. SANDELL, "Colorimetric Determination of Traces of Metals," 2nd ed., p. 375, Interscience Publishers, New York (1950).
25. A. JULIARD AND L. GIERST, *Comite intern. thermodynam. et cinet. electrochim. Compt. rend. reunion*, 279 (1950); *Chem. Abstr.*, **47**, 993 (1953).

Magnesium Fluorosilicate Phosphors¹

P. W. RANBY AND S. T. HENDERSON

Thorn Electrical Industries, Ltd., London, England

ABSTRACT

The preparation of phosphors with a matrix of magnesium, silicon, oxygen, and fluorine, and activated by titanium or titanium and manganese is described. X-ray data are given. The materials when excited by mercury resonance radiation have wide emission bands with a high proportion in the long wave-length region of the spectrum. They are useful fluorescent lamp phosphors. The mechanism of luminescence appears to be sensitization by titanium, although there are unusual features in the case.

INTRODUCTION

This paper describes a new phosphor which can be used in fluorescent lamps. It is a magnesium fluorosilicate activated by titanium; incorporation of manganese produces a change in the color of the emission so that a range of materials with fluorescence varying from greenish-yellow to orange-pink can be obtained. An outstanding feature of these materials, whether manganese is present or not, is the high proportion of red in the fluorescent emission. This fact, combined with their good maintenance characteristics, makes them of special interest in the manufacture of fluorescent lamps of good color rendering properties. Another advantage is that these phosphors are prepared from relatively inexpensive and plentiful raw materials and require no elaborate atmosphere control during their preparation.

Magnesium meta- and ortho-silicates activated by titanium have been known as luminescent materials for some time and a few of their properties have been briefly described (1). The proportion of titanium used in order to obtain maximum luminescence is high, e.g., 10 molar % of the matrix, and the color of the luminescence is blue. Manganese cannot be incorporated in these silicates as an additional activator, but magnesium silicate containing manganese alone is known to emit a red luminescence under cathode rays. Recently, Anderson and Wells (2) have described a wide range of magnesium silicates and titanosilicates prepared in the presence of magnesium fluoride; they fluoresce greenish-yellow when excited by short wave ultraviolet radiation. These latter materials resemble the previously known titanium-activated magnesium silicates in that the preferred concentration of titanium in the matrix is high, but differ in that if manganese is incorporated in addition to the titanium, then the color of the luminescence excited by cathode rays is moved toward the red.

For maximum brightness, the magnesium fluorosilicate phosphors described below (3) require a high proportion of magnesium fluoride, but only a low concentration of titanium dioxide during their preparation; also, the incorporation of manganese markedly alters the color of the luminescence excited by short ultraviolet radiation, and the materials therefore differ from those described by Anderson and Wells.

NATURE OF MATRIX

The term "fluosilicate" is normally used to describe a salt of fluosilicic acid H_2SiF_6 , and consequently an acid radical free from oxygen. In the present paper the term magnesium fluorosilicate is used to indicate a matrix in which silicon, oxygen, and fluorine are all combined together with magnesium.

If a mixture of magnesium oxide and silica in the metasilicate proportions is heated at about 1100°C with 2 moles of magnesium fluoride per mole of silica a product is obtained which x-ray analysis shows to be a new phase. X-ray diffraction lines for such a magnesium fluorosilicate are shown in column 1 of Table I. Columns 2, 3, and 4 list the characteristic x-ray diffraction lines of magnesium ortho- and meta-silicates and magnesium fluoride, respectively, as given by Hanawalt, Rinn, and Frevel (4), and column 5 the lines for norbergite from the A.S.T.M. index.

Materials having the structure of this magnesium fluorosilicate provide the matrix for the new phosphors. The x-ray pattern of a fluorosilicate containing titanium and manganese is virtually indistinguishable from that of the unactivated matrix. This shows considerable agreement with the pattern of norbergite apart from lines in the latter which appear to be due to magnesium orthosilicate. On the other hand, x-ray examination of materials prepared according to the examples given by Anderson and

¹ Manuscript received January 31, 1955. This paper was prepared for delivery before the Cincinnati Meeting, May 1 to 5, 1955.

TABLE I. X-ray powder diffraction lines of magnesium fluorosilicate, orthosilicate, metasilicate, and fluoride, and norbergite, $Mg_3SiO_4 \cdot (F,OH)_2$

Magnesium fluorosilicate		Magnesium orthosilicate		Magnesium metasilicate		Magnesium fluoride		Norbergite	
<i>d</i>	Intensity	<i>d</i>	Intensity	<i>d</i>	Intensity	<i>d</i>	Intensity	<i>d</i>	Intensity
5.10	medium	5.10	0.11	3.16	1.00	3.29	0.80	5.2	0.4
4.33	medium	3.89	0.40	2.91	0.33	3.14	0.05	4.8	0.4
4.07	medium	3.72	0.05	2.72	0.20	2.56	0.20	4.41	0.5
3.33	weak	3.49	0.20	2.55	0.27	2.24	1.00	3.37	0.6
3.22	weak	2.99	0.13	2.30	0.20	2.07	0.32	3.08	0.8
3.05	very strong	2.77	0.40	1.97	0.47	1.93	0.12	2.94	0.4
2.64	strong	2.51	0.32	1.71	0.10	1.72	1.00	2.77	0.4
2.46	weak	2.45	0.40	1.64	0.13	1.64	0.32	2.66	0.7
2.40	medium	2.26	0.40	1.490	0.40	1.53	0.20	2.52	0.6
2.34	medium	2.15	0.11	1.312	0.27	1.460	0.05	2.43	0.4
2.29	weak	2.02	0.02			1.437	0.01	2.35	0.4
2.26	medium	1.95	0.02			1.408	0.01	2.26	0.8
2.23	strong	1.88	0.03			1.378	0.60	2.03	0.2
2.03	very weak	1.81	0.03			1.340	0.01	1.94	0.6
1.94	weak	1.74	1.00			1.319	0.08	1.86	0.2
1.84	weak	1.67	0.10					1.81	0.2
1.73	strong	1.62	0.11					1.74	1.0
1.70	very weak	1.57	0.08					1.65	0.5
1.612	weak	1.490	0.32					1.60	
1.597	weak	1.395	0.20					1.54	0.2
1.578	weak	1.350	0.28					1.49	0.8
1.524	weak	1.315	0.10					1.47	0.4
1.476	medium							1.41	0.4
1.454	medium							1.35	0.6
1.401	very weak								
1.331	weak								

In all columns *d* represents the interplanar spacing in Ångström units. The terms in column 1 correspond approximately to the intensity values, as follows: very strong = 1.0-0.80; strong = 0.80-0.60; medium = 0.60-0.40; weak = 0.40-0.20; very weak = below 0.20.

Wells (2) shows that they have a crystal structure which is very similar to magnesium orthosilicate.

PREPARATION OF PHOSPHORS

A convenient method of preparation of the phosphor is to heat an intimate mixture of 1 mole magnesium oxide and 1 mole silica with 2 moles magnesium fluoride and about 0.015 mole titanium dioxide, but alternative starting materials can be used, such as ammonium fluoride with additional magnesium oxide in place of the magnesium fluoride in the initial mixture. Heating is carried out at 1100°-1200°C in air and, despite the high concentration of fluoride in the mixture, ordinary silica crucibles do not show excessive attack during the heating and can be used satisfactorily in the preparation. Some fluorine and silicon are lost during the firing, hence the value of the x-ray pattern for identification of the phosphors. Fairly wide variations in the ratios of the matrix-forming components can be used and these produce

relatively small differences in the intensity of the fluorescence of the product.

When manganese is incorporated in addition to titanium it may be added to the mixture before firing in the usual way as carbonate, nitrate, fluoride, etc.

GENERAL LUMINESCENCE CHARACTERISTICS

When excited by short wave-length ultraviolet, e.g., 2537 Å radiation, these phosphors emit a bright greenish-yellow fluorescence if activated by titanium alone. If manganese is present as well, the color of the fluorescence changes through yellow to pink with increasing concentration of manganese. Fig. 1 shows a selection of spectral energy distribution curves. The intensity of luminescence decreases only slowly with rise in temperature of the phosphor above room temperature, as shown in Fig. 2 for phosphors with and without manganese. Materials free from manganese are practically nonfluorescent under long wave-length ultraviolet, e.g., 3650 Å radiation, but they

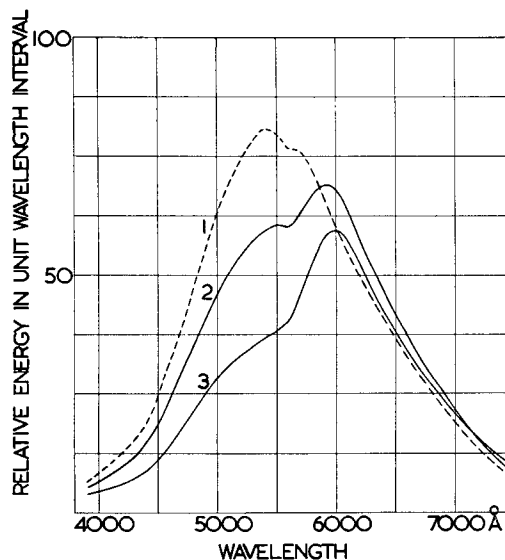


FIG. 1. Spectral energy distribution curves of fluorosilicate phosphors under 2537 Å, plotted on a wave-length basis. Curves 1-3 refer to phosphors with 0, 0.1, 0.2% Mn by weight, respectively.

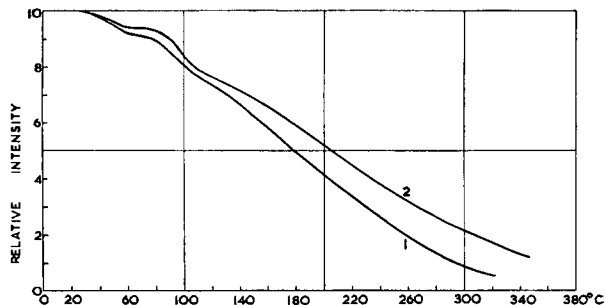


FIG. 2. Effect of temperature on fluorescent intensity under 2537 Å, measured through viscor filter. Curves normalized to 20°C. Curve 1, phosphor with Ti only; curve 2, phosphor with Ti and Mn.

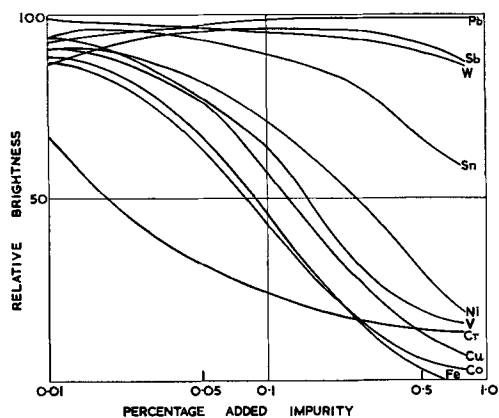


FIG. 3. Reduction of fluorosilicate brightness under 2537 Å by traces of impurities. Phosphor contains Ti but no Mn. Impurities in per cent by weight.

show a weak yellow-pink fluorescence if manganese is incorporated. The main region of the excitation spectrum of the material overlaps the low pressure mercury resonance line at 2537 Å (5).

The intensity of the fluorescence is greatly reduced by the presence of traces of certain impurities incorporated in the matrix during preparation. Especially harmful are traces of the transition elements which occur in the same periodic series as titanium and manganese, whereas much higher concentrations by weight of lead, antimony, tungsten, and to a slightly lesser extent tin, can be tolerated (see Fig. 3). The transition elements, though normally having colored ions in solution, do not appear to be causing loss of efficiency merely by discoloration of the phosphor matrix: for example, as much as 0.5% copper can be incorporated with only slight discoloration.

USE OF MAGNESIUM FLUROSILICATE PHOSPHORS IN LAMPS

Fluorescent lamps using the titanium-activated magnesium fluorosilicate give an initial efficiency of 58 lpw for the 48 T12 40W type, with indications that this will be improved after further experience. The very good lumen maintenance (e.g., 95% at 100 hr, 92% at 500 hr) is characteristic of the phosphor. Lower brightnesses are obtained from lamps made with materials containing manganese. Fig. 4 shows the chromaticity on the C.I.E. color triangle of 48T12 40W lamps made from phosphors containing increasing concentrations of manganese. Incorporation of manganese produces a drift in color across the black body locus but, owing to the mechanism by which the color change is produced, the initial efficiency of a lamp giving a color close to the black body line is only 39 lpw.

Since the material activated by titanium without manganese emits strongly in the red, this phosphor is of particular interest for incorporating in blends

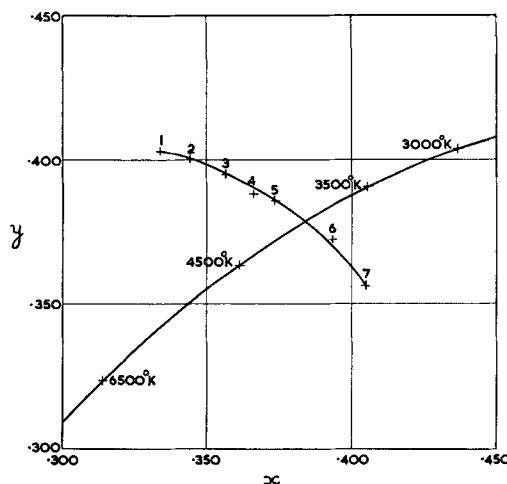


FIG. 4. Chromaticity plot of 48T12 40W lamps containing fluorosilicate phosphors. Phosphors 1-7 contain 0, 0.05, 0.14, 0.24, 0.28, 0.48, 0.75% Mn by weight, respectively.

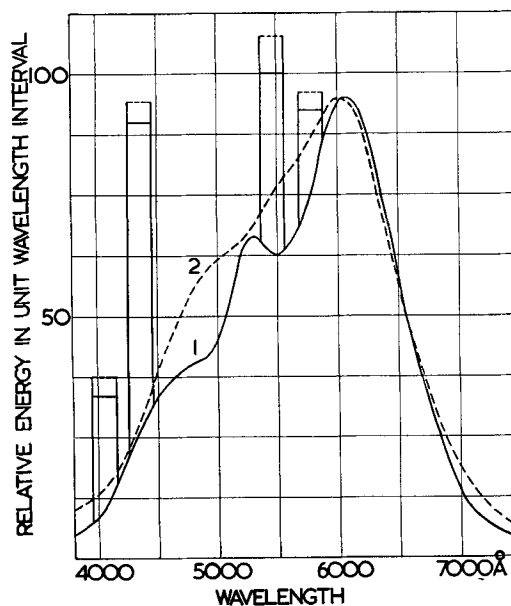


FIG. 5. Spectral energy distribution curves of lamps with (1) Cool White de Luxe phosphor and (2) fluorosilicate 4500°K blend.

with other phosphors of good maintenance in order to obtain fluorescent lamps with improved color rendering properties. A lamp of 4500°K color with good red emission is thus obtained from a mixture of approximately 50 parts magnesium fluorosilicate (Ti), 25 parts calcium silicate (Pb, Mn), and 25 parts barium titanium phosphate; the spectral energy distribution is shown in Fig. 5, compared with a conventional Cool White de Luxe lamp. Lamps using the fluorosilicate 4500°K blend have initial efficiencies of 51 lpw with good maintenance characteristics.

SPECTRAL ENERGY DISTRIBUTION OF FLUORESCENCE

Spectral energy distribution measurements on phosphors containing titanium but spectrochemically

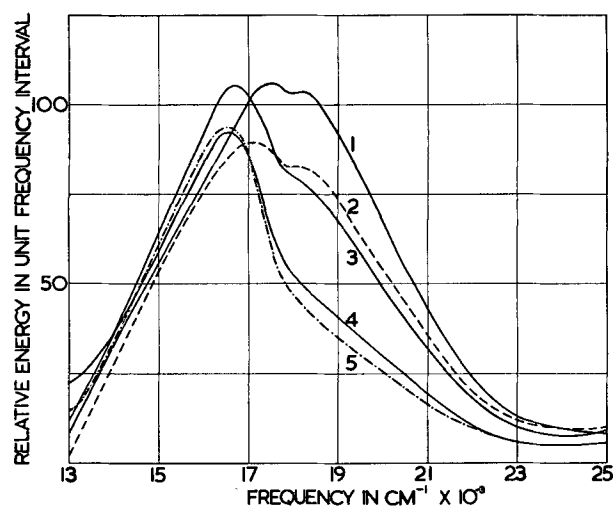


FIG. 6. Spectral energy distribution curves of fluorosilicate phosphors under 2537 Å, plotted on a frequency basis. Curves 1-5 refer to phosphors with 0, 0.05, 0.1, 0.2, 0.3% Mn by weight, respectively.

free from manganese show that the emission under 2537 Å radiation consists of a wide band with a peak at about 17700 cm^{-1} and a distribution close to Gaussian (curve 1, Fig. 6), with $a = 8.45 \times 10^{-8}\text{ cm}^2$ in $I = I_0 \exp \{-a(\nu - \nu_0)^2\}$. An unusual feature which has been established by repeated trials, both on fluorescent lamps made with the phosphor and also on the bulk power excited by an external source of radiation, is the splitting of the peak into two closely spaced maxima. These peaks appear to diverge and become distinct as increasing amounts of manganese are incorporated (curves 2-5, Fig. 6). When the manganese content is sufficient, analysis of the band structure is possible by the usual methods, as shown in Fig. 7. This shows the presence of the 17700 cm^{-1} band in moderate amount, and at least two bands of longer wave length which may be attributed to manganese presumably excited by a normal sensitization process. The separation of these bands, 1600 cm^{-1} , is similar to that found for manganese bands in the halophosphates (6) and pyrophosphates (7). The main band attributed to manganese is at 16400 cm^{-1} , and it seems likely that this will move to somewhat higher frequency when the manganese content decreases. This position is so close to the titanium band that it is difficult to disprove the possibility that it might be present to a small extent in the emission of materials containing no manganese (curve 1, Fig. 6); against this possibility are (a) the almost complete symmetry of the band in the absence of manganese, and (b) the acceptability of the sensitization theory to explain the general behavior of the materials. In other words, the small double peak seen when manganese is absent is not evidence of the presence of the "manganese" band, but it does suggest some

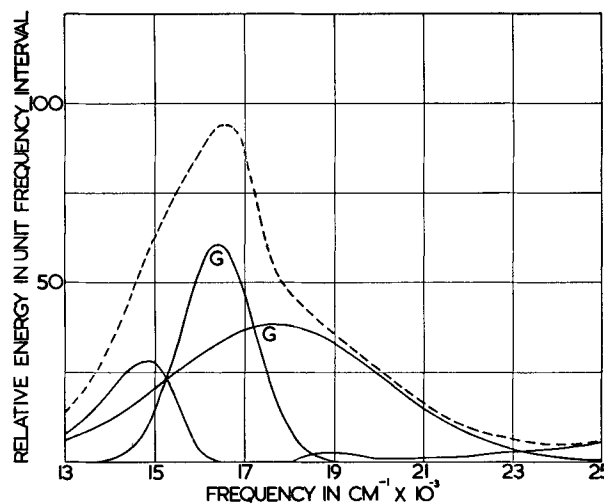


FIG. 7. Analysis into Gaussian bands (GG) of spectral energy distribution curve of fluorosilicate phosphor containing 0.3% Mn (as curve 5, Fig. 6).

kind of fine structure or double band in the titanium emission; compare the halophosphates, where the antimony band is double (6).

It should be noted that all the peaks mentioned are derived from curves of relative energy per unit frequency interval plotted against frequency. If the more usual curves of relative energy per unit wavelength interval against wave length are examined, the maxima are in somewhat different positions and the double peak becomes less evident (see Fig. 1). The original titanium band then has a peak at 5400 Å and the prominent manganese band moves from 5920 Å to 5990 Å . These values apply to both phosphors and lamps. The high red emission in the fluorosilicates is evidently due in large measure to the presence of emission bands of still longer wave length than the main one (see Fig. 7).

MECHANISM OF LUMINESCENCE

It is unusual to find that manganese can be incorporated in a titanium-activated phosphor (excited by ultraviolet); in most phosphors activated by titanium, manganese functions as an impurity quencher. For example, 0.1% by weight of manganese as manganese phosphate incorporated in barium titanium phosphate reduces the intensity of the fluorescence by about 50% without affecting the color of the emission (8). A similar effect is found with magnesium titanium borate (9). However, in former titanium-activated phosphors excited by ultraviolet radiation, the proportion of titanium is high, whereas in the present magnesium fluorosilicates the optimum proportion is about 0.015 at.%, and this difference may have a bearing on the difference in the function of manganese.

The known cases of sensitization in inorganic phosphors excited by ultraviolet radiation show a variable gap between the peak positions of the sensitizer and of the secondary activator. This difference is 13700 cm^{-1} for $\text{CaSiO}_3 \cdot \text{Pb}$, Mn; 13400 cm^{-1} for $\text{Ca}_3(\text{PO}_4)_2 \cdot \text{Ce}$, Mn; 8750 cm^{-1} for Ca halophosphate, Ag, Mn (10); about 7000 cm^{-1} for $\text{CaF}_2 \cdot \text{Ce}$, Mn (11); about 6000 cm^{-1} for $\text{CaSrP}_2\text{O}_7 \cdot \text{Sn}$, Mn (7); about 3700 cm^{-1} and 3000 cm^{-1} for chloro- and fluoro-phosphates, Sb, Mn, respectively (6). In the present phosphors the difference appears to be no more than 1300 cm^{-1} ; in fact the two bands largely overlap, and this tends to obscure the nature of the mechanism. For efficient energy conversion between sensitizer and activator there is an advantage in proximity of the bands; thus, calcium silicates are not very efficient phosphors, while halophosphates are much more efficient. In the latter case, the bands of Sb and Mn overlap to a small extent, and it is suggested that still greater overlap in the fluorosilicates fails to yield the energy conversion advantage to the full because some of the quanta available from the sensitizer centers, if they correspond to the wide range of quanta which would otherwise be emitted as light in the 17700 cm^{-1} band, are too small to excite some of the emitting states in the manganese ions. That is, if anti-Stokes emission does not occur, there will be a loss of efficiency in the sensitization process. There is likely to be an optimum spacing of the two bands in terms of energy output, and this may possibly have been reached in the halophosphates, where the positioning of the bands in the spectrum is also favorable in relation to the spectral sensitivity of the eye.

Computations have been made to estimate the efficiency of energy conversion from the titanium band to the manganese bands. Measured efficiencies and spectral distributions of lamps were used, together with the standard colorimetric data; no account was taken of the possible nonavailability of some "Ti quanta" due to band overlap, but allowance was made for the unconverted proportion of the titanium band. For the phosphor of Fig. 7, the energy conversion is found to be about 65%, or a quantum conversion of 71%. If this last figure had been 100%, that is, if all the "Ti quanta" which had disappeared had reappeared as "Mn quanta," the lamp would have had an efficiency of 48 lpw instead

of 39 lpw. A similar computation for experimental halophosphates containing fluorine but no chlorine, and alternatively antimony or antimony with manganese, gave higher values. The energy conversion appears to be about 100%, and the quantum conversion 110%. The latter cannot exceed 100%, and the figures therefore emphasize the approximate nature of the determination; but they also confirm that the halophosphate is, comparatively, a very efficient phosphor, in agreement with the suggestion made in connection with band positions.

CONCLUSION

In the past, titanium and manganese have appeared incompatible as activators (as distinct from titanium forming a component of the matrix) in phosphors excited by ultraviolet radiation to the order of efficiency required in fluorescent lamps. The magnesium fluorosilicate phosphors show that this is not always the case and seem to be the first example of joint activation by titanium and manganese.

ACKNOWLEDGMENTS

The authors are indebted to Mr. D. H. Mash for x-ray powder measurements, to Miss M. B. Halstead for spectrophotometric work, and to the Directors of Thorn Electrical Industries, Ltd., for permission to publish.

Any discussion of this paper will appear in a Discussion Section to be published in the June 1956 JOURNAL.

REFERENCES

1. F. A. KRÖGER, "Some Aspects of the Luminescence of Solids," Elsevier Publishing Co., Inc., New York (1948).
2. J. T. ANDERSON AND R. S. WELLS, British Pat. 714,057, Aug. 25, 1954.
3. P. W. RANBY, British Pat. Appln. No. 26659/53, Sept. 28, 1953.
4. J. D. HANAWALT, H. W. RINN, AND L. K. FREVEL, *Ind. Eng. Chem.*, **10**, 457 (1938).
5. K. H. BUTLER, Private communication, April 1954.
6. K. H. BUTLER AND C. W. JEROME, *This Journal*, **97**, 265 (1950).
7. P. W. RANBY, D. H. MASH, AND S. T. HENDERSON, *Brit. J. Appl. Phys.*, Supp. 4, 18 (1955).
8. S. T. HENDERSON AND P. W. RANBY, *This Journal*, **98**, 479 (1951).
9. P. W. RANBY, British Pat. Appln. No. 26194/52, October 18, 1952.
10. P. W. RANBY, *This Journal*, **98**, 299 (1951).
11. R. J. GINTHER, *ibid.*, **101**, 248 (1954).

Investigations of Surface Recombination Velocities on Germanium by the Photoelectromagnetic Method¹

T. M. BUCK AND W. H. BRATTAIN

Bell Telephone Laboratories, Inc., Murray Hill, New Jersey

ABSTRACT

The Photoelectromagnetic, or "Deathium Meter," method has been used to detect changes in surface recombination velocity on germanium produced by various chemical surface treatments and by heating to temperatures of 65°–100°C. The method consists of measuring the open circuit voltage due to the P.E.M. effect. Measurements may be made rapidly; small changes in specimen thickness caused by a surface treatment may be ignored; the method can be used to investigate surfaces covered by opaque protective coatings. While it was found that the open circuit voltage depended on surface recombination in a manner which agreed qualitatively with theory, the agreement was not good enough to permit calculation of quantitative values of recombination velocity.

INTRODUCTION

It is widely recognized that surface properties of semiconductor materials have a very important influence on the behavior of semiconductor devices, and the surface recombination velocity is one of these important surface properties. Surface recombination and volume recombination control the lifetime of minority carriers in germanium (1); high recombination rates cause short lifetimes. A long lifetime is usually desired since, for example, this favors low reverse saturation currents in *p-n* diodes and high alphas in transistors. Therefore, a low and constant surface recombination velocity is ordinarily preferred.

The concept of surface recombination velocity arises from the fact that, for small concentrations of excess minority carriers, the rate at which these excess carriers recombine per unit area of surface is proportional to their concentration just below the surface. The constant of proportionality has the dimensions of a velocity and is called the surface recombination velocity, S (cm/sec).

The photoelectromagnetic method of measuring S used in the present work was proposed by workers at the Telecommunications Research Establishment. They had observed the photoelectromagnetic effect in germanium and then developed a theory which predicted that the effect could be applied to this measurement. The theory, together with experimental results for two types of germanium surfaces, chemically polished and lapped, has been reported on by Moss, Pincherle, and Woodward (2).

Kikoin and Noskov (3) observed the effect in cuprous oxide in 1934, while Aigrain (4, 5) and Bulliard (4, 6) have recently investigated the effect in

germanium. These workers, however, did not apply it specifically to the measurement of surface recombination velocities in the manner of Moss, Pincherle, and Woodward.

The present work is concerned with the use of the method to detect changes in recombination velocity on germanium produced by various chemical surface treatments and by heating to temperatures of 65°–100°C. It is found that measurements may be made rapidly; small changes in specimen thickness caused by a surface treatment may be ignored; the method can be used to investigate surfaces covered by opaque protective coatings. It is felt that the method is quite useful for qualitative comparisons of surface treatments, as regards surface recombination. It should be emphasized, however, that the method is a qualitative rather than a quantitative measure of surface recombination velocity. This point is discussed later.

EXPERIMENTAL METHOD

The principle of the method is pictured in simplified form in Fig. 1 which represents a side view of a thin slab of germanium. The intense light shining on the front surface creates a high concentration of both holes and electrons at that surface; if S at this surface is not too large, most of them diffuse toward the dark side where they recombine at a rate determined by the recombination velocity there. Recombination in the interior is neglected since material of high body lifetime may be used and the thickness of the specimen kept less than a diffusion length. In the magnetic field the holes and electrons in the diffusion current tend to be deflected in opposite directions and this sets up a difference of potential, similar to a Hall voltage, which is the quantity measured.

This voltage, V_x , evidently depends on magnetic field strength and on diffusion current. Diffusion

¹ Manuscript received January 28, 1955. This paper was prepared for delivery before the Chicago Meeting, May 2 to 6, 1954.

current depends on the concentration gradient which, in turn, depends on the intensity of the light and on the recombination rates at the two surfaces. The Moss, Pincherle, Woodward theory predicts that, when recombination at the front surface is small, V_x should reach a saturation value at high light intensity and that under these conditions the equation

$$\frac{V_x}{l} = E_x = - \left(\frac{H}{C} \right) S$$

relates the voltage to the recombination velocity S at the back surface. H is the magnetic field strength (6400 gauss, in the present work); C is the velocity light; and l is the spacing between contacts.

In practice it is found that V_x does saturate at intensities approaching 10^{18} quanta/cm² sec. However, it now appears that the saturation effect may be due to heating of the specimen under the intense illumination. If readings are taken quickly enough so that no appreciable heating occurs, V_x continues to increase with intensity somewhat beyond 10^{18} quanta/cm² sec which is as high as the intensity dependence has been followed. Furthermore, as is seen later, the value of S for sand-blasted surfaces is not as high as previous estimates by other methods.

The determination of actual values of surface recombination velocity by this method must depend on a knowledge of the surface recombination mechanism. If one assumes that the process is governed by the mass action law, one would have

$$\text{Net rate of recombination} = C (np - n_0p_0)$$

where C is a constant determined by surface treatment, n and p are electron and hole concentrations, and the subscript zero denotes equilibrium values. The M.P.W. theory used the small signal approximation of this law, i.e., $np - n_0p_0 = (n_0 + p_0)\delta p$ for a situation where because of light intensity such an approximation does not hold. Unfortunately, if one assumes the mass action law without approximations, the theory becomes much more complicated and difficult to test experimentally.² In addition, the question of whether this law is the correct one arises. Furthermore, it should be pointed out that, if this law is correct, one would expect S for a given surface treatment to vary with hole and electron concentration (7), other things being constant. Thus, the values of S quoted in this paper apply only to material of the specified resistivity.

Nevertheless, while the absolute values of S are in some doubt, experiments show that V_x values do vary in the proper direction with recombination velocity, and that the method is useful for comparing surface treatments. For example, in Fig. 2 V_x is plotted against etching time. The downward curve

² The authors are indebted to W. van Roosbroeck, of this laboratory, for having investigated this.

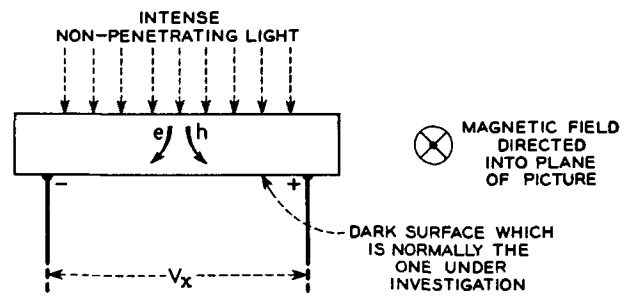


FIG. 1. Photoelectromagnetic method of measuring surface recombination velocity. Schematic diagram of principle of operation.

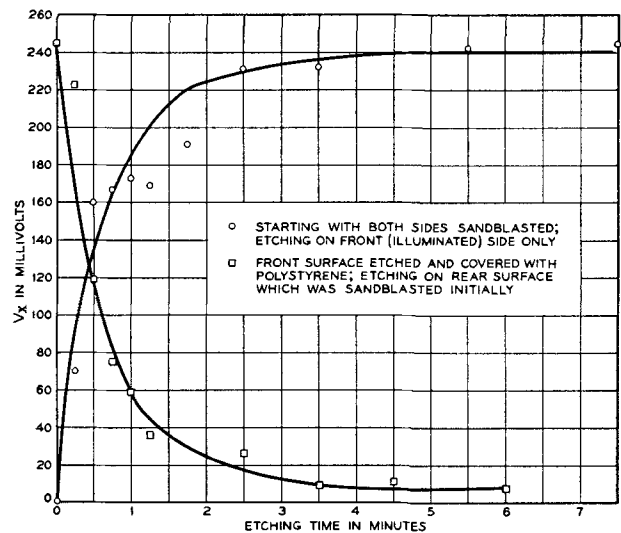


FIG. 2. Change of V_x as a function of etching time on a sandblasted surface. CP-4 etchant. Measurements in dry nitrogen atmosphere; p -type germanium specimen; 13 ohm-cm, 2000-3000 μ sec body lifetime.

shows the case where initially the illuminated surface was chemically etched and the dark side sand blasted, giving a value of 240 mv corresponding to about 2000 cm/sec by the M.P.W. theory. (Estimates of at least 10^4 cm/sec are usually made for such a surface.) A series of short chemical etching treatments on the back surface (10-15 sec each) brought V_x down progressively until it became substantially constant at about 15 mv, or 135 cm/sec.

In the upward curve of Fig. 2 both the front and back surfaces were sand blasted initially, leading to a V_x value of only a fraction of a millivolt since most of the carriers created by the light recombined at the front surface and there was little or no concentration gradient or diffusion current. The front surface, only, was then given several brief (10-15 sec) chemical etches; V_x increased with each treatment until a value of about 240 mv was reached, i.e., with each etching treatment recombination at the illuminated surface decreased and the diffusion current to the high recombination sink at the back surface in-

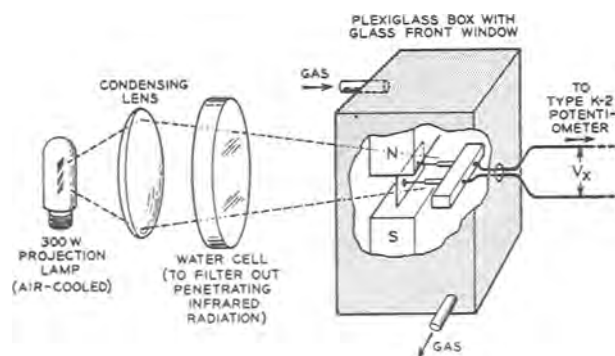


FIG. 3. Schematic diagram of apparatus for photoelectromagnetic measurement of surface recombination velocity.

creased. Most of the scattering of points about the curves was probably due to variation in etching rate. Hereafter in the discussion the dark surface is the one under investigation with the front surface assumed to stay constant at a fairly low value of S , except in the case of heating effects to be mentioned later.

Fig. 3 is a schematic diagram of the equipment used. Light from the 300-watt projection lamp passed through a condensing lens and then through a 1.5-cm water cell to remove the penetrating infrared radiation. The specimen was supported in the magnetic field (6400 gauss) by phosphor bronze wires soldered 1.75 cm apart on the back surface.

The germanium specimens used were 10–15 ohm-cm slabs about 2.5 x 0.8 x 0.05 cm in dimension, the thickness being considerably less than a diffusion length since body lifetime was 2000–3000 μsec .

RESULTS

Chemical treatments.—Table I shows results of comparisons among a few surface treatments which have been used by various workers at this laboratory. In some cases both surfaces received the treatment, while in others the chemically etched front surface was covered by a thin coat of polystyrene to protect it from the treatments. According to the M.P.W. theory, small changes at low values of S on the front surface should have a negligible effect on V_x ; rather V_x should be determined by the recombination velocity at the back surface which is under investigation. This seemed to be borne out in the experiments. However, it is preferable, if possible, to operate with the front surface sealed off by a transparent plastic coating. This is especially important when a surface treatment may be a very bad one because, as shown in Fig. 2, a very high recombination velocity on the front surface can cause a low response. That is, when both surfaces are exposed to an unknown treatment, a low reading may mean a good back surface or a very poor front surface.

The specimens were re-etched in CP-4 and washed

in distilled water to present a fresh surface for each new treatment. All of the treatments were followed by a distilled water rinse.

The HF dip produced, temporarily, a reading as high as for sand blasting, in accordance with the findings of Keyes and Maple (8). Values for the last three treatments in the table fell in the same order for all four specimens. Thus the method seemed capable of detecting small but reproducible differences among the treatments. Values for CP-4 seemed less stable and reproducible than those for the other treatments; the KOH electrolytic etch seemed especially good in this respect.

Fig. 4 shows how V_x changed as the two p -type specimens received the series of treatments.

Heat effect.—It has been mentioned that the method employs nonpenetrating light of high intensity. Heating of the specimen by the light causes some trouble in the measurements. V_x readings were taken on the type K-2 potentiometer a few minutes after illumination to allow the specimen to reach thermal equilibrium at about 35°C. During this waiting period V_x settled down to a fairly constant value several millivolts lower than would be obtained immediately after illumination. (Recently it has been found more satisfactory to take readings quickly enough, by trial and error, so that no appreciable heating occurs.)

Aside from this transient effect, heating to temperatures much higher than 35°C should be avoided. For example, if the water filter is removed the sample then heats to about 65°C and if the light is left on for a few minutes a rather large increase in V_x occurs,

TABLE I. Photoelectromagnetic measurements for various surface treatments on germanium

Treatment*	V_x (mv)	S (Recombination velocity at dark surface, cm/sec) calculated from M.P.W. theory
Sand-blasted (back surface, 180 mesh silicon carbide).....	240	2160
5 min HF dip after (8) thorough etching in CP-4.....	240	2160
KOH electrolytic etch ..	17.8	160
Antimony oxychloride —“Long Life” treatment.....	23.4	210
Nitric acid soak.....	26.7	240

} averages of eight treatments on four specimens, two n -type and two p -type.

* CP-4 is a mixture of 15 ml glacial acetic acid, 15 ml HF, 25 ml conc. HNO_3 , and a few drops of bromine. A 0.1% solution of potassium hydroxide in distilled water was used in the electrolytic etching; the current density was about 50 ma/cm² and the electrolysis was continued for 2 min. The antimony oxychloride “long life” treatment consisted essentially of making the specimen anodic in a suspension of hydrolyzed Sb Cl_3 for 8 min, at 1½ v.

as measured with the filter in place again. This increase persists after the filter is replaced but V_x decreases toward the original value over a period of hours or days. Fig. 5 shows how a specimen behaved over a period of several days. Each time the specimen was exposed to unfiltered light (as indicated by the arrows) V_x increased, as measured with the filter in place again, and then slowly decreased with time although it usually did not return completely in the waiting period. This effect was also produced by heating in an oven at 70°-100°C. The same type of behavior was observed with a *p*-type specimen. Haynes and Hornbeck (9) had observed that recombination velocity was increased by heating to temperatures of less than 100°C in other lifetime measurements on germanium; it was therefore thought that the increase in V_x in the P.E.M. measurements was due to an increase in S .

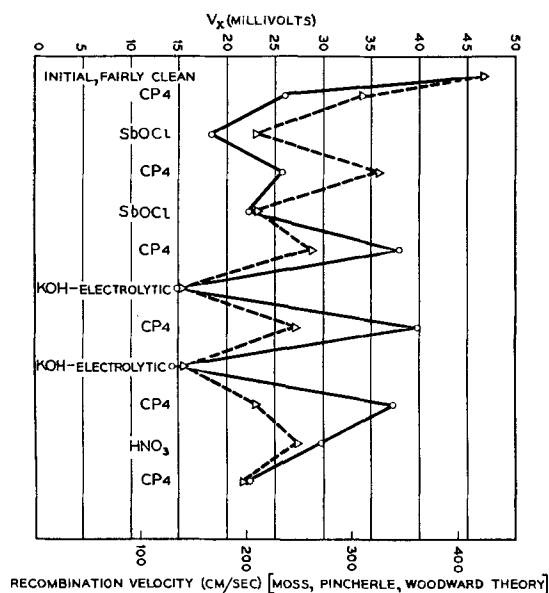


FIG. 4. Change of V_x as two *p*-type germanium specimens received a series of surface treatments. Δ Specimen A, *p*-type 13 ohm-cm; $^\circ$ Specimen B, (*p*-type) 13 ohm-cm.

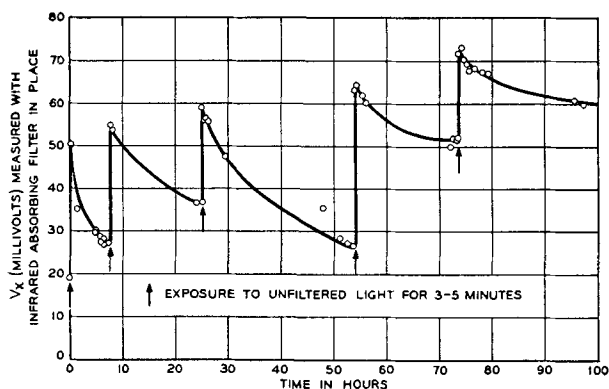


FIG. 5. Effect of heating by exposure to intense unfiltered light. *n*-Type germanium, 11 ohm-cm. Measurements by photoelectromagnetic method in room air at ~ 45% R.H.

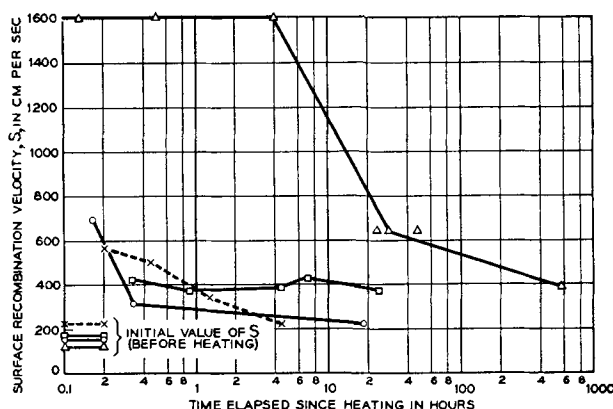


FIG. 6. Effect of heating on recombination velocity of germanium. Recombination velocity calculated from diffusion length measurement of filament lifetime. $^\circ$ Specimen A (*n*-type) exposed to intense light for 5 min (as in photoelectromagnetic experiments). \times , Specimen A illuminated again. Δ , Specimen A heated in oven at 100°C for 15 min. \square , Specimen B (*n*-type) heated in oven at 100°C for 15 min.

To check this, the effect of heating was followed by diffusion length measurements of lifetime on thin rods of *n*-type germanium. This method has been described by Goucher (10). The results are shown in Fig. 6 in which S , computed from diffusion length, is plotted against time elapsed since heating. It is seen that the recombination velocity increased each time a specimen was heated, either by exposure to the unfiltered light used in the photoelectromagnetic experiments or by heating in an oven. There was considerable variation in the magnitude of the effect, possibly because of differences in atmospheric contamination during heating.

Parallel effects were also observed in few unprotected diodes and in an *n-p-n* grown junction transistor. In the diodes heating to 100°C for a total of 30 min caused an increase at room temperature of 30-50% in the reverse saturation current while the transistor exhibited an increase in $1-\alpha$ of over 60%.

In all cases the effect seemed to be temporary, disappearing gradually on standing in air. The heat effect experiments described were all carried out in room air usually controlled at 50% relative humidity or less. As yet the authors have no definite explanation for this behavior, although differences due to changing the ambient atmosphere have been noticed.

ACKNOWLEDGMENT

The authors gratefully acknowledge the help of Mr. T. F. Donovan in constructing equipment and making measurements, and Mr. R. Enz who made the diffusion length measurements.

Any discussion of this paper will appear in a Discussion Section to be published in the June 1956 JOURNAL.

REFERENCES

1. W. SHOCKLEY, "Electrons and Holes in Semiconductors," pp. 318-325, D. Van Nostrand and Co., New York (1950).
2. T. S. MOSS, L. PINCHERLE, AND A. M. WOODWARD, *Proc. Phys. Soc.*, **B66**, 743 (1953).
3. I. K. KIKOIN AND M. M. NOSKOV, *Physik. Seits. fur Sov. Union*, **5**, 586 (1934).
4. P. AIGRAIN AND H. BULLIARD, *Compt. rend.*, **236**, 595, 672 (1953).
5. P. AIGRAIN, *Annales de Radioelectricité*, **9**, pp. 219-226, July 1954.
6. H. BULLIARD, *Phys. Rev.*, **94**, 1564 (1954).
7. B. H. SCHULTZ, International Conference on Semiconductors, Amsterdam, June 29-July 3, 1954. To be published.
8. R. KEYES AND T. G. MAPLE, in a paper presented at Detroit Meeting of American Physical Society, March 1954, reported that a dip in HF produces, temporarily, a very high recombination velocity on germanium.
9. J. R. HAYNES AND J. A. HORNBECK, Bell Telephone Laboratories, Private communication.
10. F. S. GOUCHER, *Phys. Rev.*, **81**, 475 (1951).

Electrodeposition of Titanium on Base Metals¹

M. E. SIBERT AND M. A. STEINBERG

Horizons Incorporated, Cleveland, Ohio

ABSTRACT

A method for electrodeposition of protective titanium coatings on steel and other base metals is described. The procedure involves electrolysis of potassium titanium fluoride dissolved in alkali or alkaline earth halides under an inert atmosphere. Graphite or titanium metal anodes are employed.

Adherent titanium coatings up to 0.005 in. (0.127 mm) thick are produced. Coatings are essentially pure titanium. Underlying the coating is a base metal-titanium alloy layer producing a firm metal-metal bond. Coatings so prepared possess the corrosion resistance of titanium metal. Layers heavier than 0.005 in. (0.127 mm) may be prepared by repeating the process.

Equipment and materials used, conditions of operation, and properties of the electrodeposited titanium are described completely.

INTRODUCTION

Titanium is a useful corrosion resistant material under many conditions. However, its use is limited because of its relatively high cost. In many cases, a thin protective layer of titanium over a base metal would be adequate. At present, there are no methods available for application of such coatings other than pressure-roll-diffusion cladding which also suffers from a relatively high cost disadvantage.

A research program was initiated with the goal of developing methods for electrodeposition of titanium on steel and other base metals. The work was confined to fused salt electrolysis since it is doubtful that titanium can be isolated in aqueous or other oxygen containing media. Previous work has characterized titanium as a highly oxyphilic element. For this reason, all work was carried out under an inert atmosphere.

There are few recorded attempts to deposit titanium electrolytically on base metals. Most electrodeposition work has been done in aqueous media, and as such is open to question. Attempts have been made to duplicate some of this experimental work, but these efforts have been unsuccessful in terms of reported results.

Gratsianskii and Vovkogan (3) reported deposition of titanium films 1μ thick on copper from solutions of sulfanilic acid and titanium hydroxide. Platinum and zinc-titanium anodes were used. Cathode current densities of 0.1 amp/dm^2 at 20°C were recommended.

Haissinsky and Emmanuel-Zavissiano (4) claimed

deposition of thin black titanium films from titanium dioxide in sulfuric acid and $\text{Na}_2\text{SO}_4 \cdot 10\text{H}_2\text{O}$ at a pH of 1.2–1.6. Such coatings contained $0.1\text{--}0.2 \text{ mg Ti/cm}^2$. They were produced using a lead cathode and platinum anode with a cathode current density of $1.5\text{--}2.0 \text{ amp/dm}^2$. Higher currents were said to precipitate titanium(IV) hydroxide. Similar plates were obtained on zinc and antimony, but results were negative with nickel and platinum. They also reported a plating method using titanium(III) sulfate solutions (5).

Pokorny and Schneider (7) obtained a patent on electroplating of titanium from a strongly alkaline solution of titanium dioxide or titanium(IV) hydroxide on iron or copper cathodes.

Leutz (6) obtained a patent on a process for electrolytically forming protective layers on base metals by anodic treatment in a bath containing a colloidal suspension of silicon, zinc, titanium, aluminum, or rare earth oxide and acid. An anion capable of forming an insoluble salt with the metal to be treated must be present.

Russell (8) reported a method of depositing titanium on noble metals by battery action which he also claimed to be valid for uranium, tungsten, and molybdenum. Acidified solutions of a salt of the metal to be plated are shaken with the noble metal. Mercury is specifically mentioned as a noble metal.

Gratsianskii and Vovkogan (3) also reported electrodeposition of titanium as a zinc alloy from a bath of aluminum chloride-sodium chloride-sodium fluoride. A 60-40 zinc-titanium alloy surface on iron or copper was produced at 300°C under 0.5 amp/dm^2 current density using a zinc-titanium anode.

Fischer and Dorsch were granted a patent on a fused salt titanium electroplating process (2). Again, alloys were produced by electrolysis of fused mix-

¹ Manuscript received April 7, 1955. This paper was prepared for delivery before the Cincinnati Meeting, May 1-5, 1955, and is based in part on work carried out by Horizons Incorporated for the Aeronautical Research Laboratory, Wright Air Development Center, United States Air Forces, under Contract Number AF-33(616)-393.

tures of alkali or alkaline earth halides and titanium halides. Such baths were operated above the melting point of the alloy to be formed and below the melting point of the alloying cathode metal.

Recently, Brenner and Senderoff (1) reported formation of 0.5 mil adherent layers of titanium on tungsten by electrolysis of titanium(III) chloride in a mixture of sodium chloride and potassium chloride. Such layers were formed at 900°C and at 30 amp/dm².

Schlechten, Straumanis, and Gill (9) have described the deposition of titanium coatings from pyrosols of titanium. The pyrosols were formed from titanium metal and fused alkali or alkaline earth chlorides. Coatings up to 7 mils were obtained on copper and iron, but these were essentially alloys.

There are several choices of procedure: a titanium bearing material may be electrolytically decomposed; a soluble metal anode might be used with a carrier salt; or a pyrosol might be used. The first approach was used in this investigation.

The choice of a source electrolyte was reasonably limited due to the assumed requirement for a stable anhydrous, oxygen and nitrogen free salt. It must also be a good electrical conductor, thus ionic in nature. A common source material meeting these requirements is potassium titanium fluoride. It is readily prepared by standard chemical techniques and may be handled in air, although it is readily oxidized at elevated temperatures.

In order to obtain a melt at reasonable temperature, the source electrolyte is diluted, preferably with another halide. Furthermore, the double fluoride is not readily reduced as a pure melt.

In this process, a suitable melt of K₂TiF₆ dissolved in a second halide is electrolyzed to reduce the K₂TiF₆ and cathodically deposit thin layers of titanium on steel parts. The process is a rapid, high current procedure resulting in an adherent diffusion bonded titanium layer. Details of the procedure are given below.

EXPERIMENTAL

The Electrolytic Cell

Titanium was electrodeposited in a cell specifically constructed for high temperature inert atmosphere electrolysis. The cell takes a salt charge of 5 lb in a crucible 4 in. (10.2 cm) in diameter x 8 in. (20.3 cm) deep. Equipment of similar design has been previously described in detail (10).

Electrolytic Procedure

The process was essentially an electrolysis of a K₂TiF₆-NaCl melt with the material to be plated used as a cathode. The salt bath was chosen on the

basis of favorable operating characteristics. Pure K₂TiF₆ was not readily electrolytically reduced to metal because of the high titanium ion concentration and consequent ease of reoxidation. However, when the salt was dissolved in melts of alkali or alkaline earth fluorides and chlorides, the reduction proceeded with varying degrees of success. Fluorides were not generally suitable because of their insolubility. Some of the salt bath adhered to the cathode and was best removed by aqueous washing. Alkaline earth chlorides were undesirable because of their hygroscopic nature and the difficulty in drying them. Considering both chemical and economic aspects, lithium chloride, sodium chloride, and potassium chloride were the most useful bath materials. Since sodium chloride was readily available in pure anhydrous form and also behaved well electrolytically, it was employed for most of the work.

All salts were of AR grade or equivalent. The K₂TiF₆ was twice recrystallized and usually vacuum dried to remove residual moisture.

Cathodes to be plated were, for the most part, machined from ingot iron. In some cases cold rolled steel was used. Cathodes were in the form of bars, cylinders, or truncated cones. To further insure a clean surface, the cathodes were washed in carbon tetrachloride, then pickled in 20% hydrochloric acid -10% nitric acid for 20 min, followed by rinsing and drying.

The cell, in clean condition, was first heated to 850°-950°C with a thorough argon flushing. The salts were then charged and melted over a period of 30-45 min.

After the temperature had been adjusted, any additional desired bath purification was carried out. A low voltage pre-electrolysis may be used to remove residual moisture and/or other impurities. Graphite or steel cathodes may be used; any deposit is discarded.

The cathode assembly was then lowered into the melt. Cathodes were generally attached to nickel rods by means of welding or clamping. The rod, in turn, was protected with a graphite sleeve. The current was then applied, voltage adjusted, and electrolysis carried out for the desired number of ampere hours, during which time some chlorine was evolved anodically.

For most of the work a 15-17% K₂TiF₆ concentration in sodium chloride was employed as the melt. This gave a mixture melting at about 720°C and having a convenient fluidity at the usual electrolysis temperature range of 850°-950°C. Such a bath provided available titanium (approximately 68 g) for a large number of cathodes. It was possible, however, to operate successfully a bath containing between 5-25% K₂TiF₆.

TABLE I. Operating conditions for titanium electroplating of steel

Run	Type K ₂ TiF ₆	Other agents	Temp. °C	Current density amp/dm ²	Volts	Amp hr	Time min	Cathode	Results	Remarks
1-4	Recryst. (wet)	H ₂ O	905	86	6.1	67	80	<i>in. ingot iron</i> ¼ × 1 × 3½	Good clad 0.002 in. (0.051 mm)	<i>Run on bath</i> Fourth
2-6	Recryst.	—	910	81	5.7	67	80	¼ × 1 × 3¾	Excellent 0.003 in. (0.076 mm)	Sixth
3-2	Recryst. vac. dried	1% TiO ₂	810	475	—	67	20	¼ × 1 × 2½	Very good 0.004 in. (0.102 mm)	Second
4-1	Recryst. vac. dried	1% TiO ₂	810	345	13.5	67	20	¼ × 1 × 3½	Very thin	First
5-1	Recryst.	H ₂ O	770	345	14	67	20	¼ × 1 × 3½	Spotty	First
6-3	Recryst. vac. dried	—	885	480	8.3	93	20	¼ × 1 × 3½	None	Third

After electrolysis, the cathode was withdrawn from the melt with voltage on it to prevent solution of the titanium electroplate. It was then allowed to cool in the argon atmosphere above the bath or in a cooling chamber (argon filled) which may be used as a cell accessory. The cathode was washed in water to remove the salt coating and some crystalline metal. A typical washed plated specimen has a bright finish and resembles common electroplated materials.

Electrolysis Experimentation

A variety of conditions have been imposed on the basic process in order to elucidate the optimum conditions of operation. Almost from the first run, evidences of cladding were detected, but results were sporadic and nonuniform. Temperature, voltage, current, and type of titanium source electrolyte were varied and studied.

In this process, voltage, type of cell feed, and temperature were the principal contributing factors. Data for typical runs illustrating operating conditions are given in Table I. The first three runs illustrate satisfactory deposition conditions. The fourth run was unsatisfactory due to excessive voltage and consequent codeposition of sodium. The fifth run was poor from this same standpoint and also was operated at too low a temperature. In the last run, the cathode was not properly cleaned, and the voltage was somewhat high.

In each electrolytic run, plating took place early in the run and the process terminated. Continued electrolysis produced a porous crystalline deposit around the cathode, but no further electroplating. However, if the cathode was cleaned and the process repeated, the thickness of the coating was increased.

In a typical multiple electrolysis, a bar 0.246 in. (6.24 mm) thick was plated at 5.7 v and 95 amp/dm² at 910°C using a 16% K₂TiF₆-NaCl melt. After one run the thickness was 0.252 in. (6.35 mm). The bar was withdrawn, washed, and replated four times until the thickness was 0.262 in. (6.65 mm).

This yielded a total plate 0.008 in. (0.20 mm) thick or an average of 0.0016 in. (0.04 mm)/pass.

The presence of impurities in the melt was a factor of some significance. It was indicated initially that small additions of titanium dioxide or the use of incompletely dried K₂TiF₆ (which would yield oxides on melting) improved the characteristics of the titanium electrodeposition process.

A small amount of titanium oxide, either titanium dioxide or Ti₂O₃, was helpful and possibly necessary to obtain successful electrocladding. It was known that all melts contained some moisture initially as contributed both by the K₂TiF₆ and sodium chloride. This averaged about 0.01–0.02% by weight. Thus, some oxide was undoubtedly present in all such runs and as such was a contributing factor. It was also demonstrated that such oxides are not reduced to metal or to titanium monoxide in a melt of sodium chloride and K₂TiF₆. It is probable, therefore, that Ti₂O₃ or titanium dioxide present initially remained in the melt over a substantial period of time through a cycling redox process, even when low voltage purification electrolyses were carried out. Therefore, it was quite possible for oxides, either initially in the melt or deliberately added, to play a part in the electrocladding process.

It was possible that oxygen here played somewhat

TABLE II. Effect of cell feed on titanium electrodeposition

Run No.	Treatment K ₂ TiF ₆	Bath Additives	Thickness of Ti Coating	Remarks
1	Recryst. no drying	—	0.003 in. (0.076 mm)	H ₂ O—0.1% in melt after run
2	Commercial vac. dried	—	0.003 in. (0.076 mm)	245 Amp-hr run
3	Bath from 6 (see below)	—	0.0025 in. (0.064 mm)	0.13% H ₂ O at start electrolysis
4	Recryst. air dried	1% TiO ₂	0.002 in. (0.051 mm)	150 Amp-hr low voltage electrolysis
5	Recryst. vac. dried	—	0.001 in. (0.025 mm)	
6	Recryst. (wet—from filter)	20% H ₂ O start	Spotty	
7	Commercial vac. dried	—	None	

TABLE III. *Effect of bath temperature on electrodeposition of titanium*

Run	Temp °C	Volts	Current density amp/dm ²	Total amp-hr/dm ²	Cathode type	Cladding results	Remarks
1	765	3.0	120	40	Mild steel truncated cone	None	Bath pre-electrolyzed
2	755	6.6	485-240	640	Mild steel truncated cone	None	
3	770	14	345	115	Ingot iron bar	Spotty	Wet K ₂ TiF ₆ —1st run
4	875	3.0	120	29	Truncated cone	Thin	
5	885	6.3	485	198	Truncated cone	Good	TiO ₂ in bath
6	900	—	345	345	Ingot iron bar	Heavy	Wet K ₂ TiF ₆ —3rd run
7	905	5.9	86	115	Ingot iron bar	Excellent	Wet K ₂ TiF ₆

the same role as sulfur in electroplating processes. Additives in the form of sulfonates are frequently made to plating baths to produce fine grained smooth deposits. Indications are that deposits produced in such a manner contain appreciable sulfur; maximum sulfur concentrations are noted at the points of high current density, indicating that the additive may deposit at such points and divert the current to other areas, thus producing a uniform smooth deposit. Since oxygen has a similar electronic configuration to that of sulfur, it may be that a comparable action took place in titanium electrodeposition.

The data in Table II illustrate the effects of adding titanium dioxide and moisture to the salt melts. Runs are arranged in approximate decreasing order of effectiveness of the cell feed. The use of commercial or recrystallized K₂TiF₆ in a freshly dried state (runs 5 and 7) produced poor deposition or none at all; however, after one run on a bath and its subsequent standing overnight, which exposed it to some back diffusion of air and normal cell leakage, the second run (run 2) produced good results. Runs 1 and 4 are illustrative of results obtained by adding nominal amounts of moisture and titanium dioxide to the melt.

Temperature had a definite effect upon the process. The fluotitanate was reduced to metal over a considerable temperature range, but poor plating was obtained below 800°C. Coatings were not continuous and were subject to peeling. Plates obtained at 800°–900°C had a diffusion bond of titanium and base metal between the base metal and titanium layers. This bonding area was high in base metal content, and, in the case of iron, gave a typical stabilization of the β titanium phase in this area. The layer over this bonding area was normal α titanium. Such a bond is highly desirable from an adherence standpoint, and it is apparent that temperatures of the order of 800°C are required to produce this type of bonding. Evidence indicates that plating took place at lower temperatures, but that the diffusion rate of iron into titanium was not sufficiently rapid to effect a good bond, so the plates tended to flake off in

the relatively corrosive atmosphere of the K₂TiF₆-NaCl melt.

Voltage was important in its relation to the decomposition voltages of the bath constituents. No titanium was produced at less than 1.8 v in this cell. The decomposition voltage of sodium chloride is about 3.1 v at 850°C, but as long as an appreciable titanium concentration (0.5 % or more) existed in the bath, no sodium was produced up to 5.5–6.0 v. Thus, the bath was operated at about 3–6 v. Current density did not seem to be an important variable between the limits of 50–500 amp/dm².

Table III gives a tabulation of typical runs showing effects of temperature. It is noted from these runs that no particular effects are evident from voltage and current variation, cathode geometry, and time within the stated limits.

It is evident from the data in Table III that the higher temperatures were requisite for successful operation of the process. At temperatures under 800°C, variations in voltage, current, and type of cathode produced either poorly coated specimens or no coating. On the other hand, well clad specimens resulted at the higher temperatures regardless of current, voltage, and type of cathode.

As a final check on the process, electrodeposition of titanium on standard nuts and bolts was attempted. These were welded or bolted to standard nickel cathode rods and the process carried out as for other cathodes. Some difficulty was experienced in

TABLE IV. *Electrocladding of commercial bolts*

Run	Cathode	Voltage	Current Amp	Temp °C	Ti coating	Remarks
1	Cold-rolled ½ in. bolt	3.0	50	955	Poor	Rusted in brine
2	Cold-rolled ½ in. bolt	5.6	200	977	Coated	Some alloying
3	Cold-rolled ½ in. bolt	5.5	200	855	Coated	
4	Cold-rolled ¼ in. bolt	2.6	20	845	None	
5	Cold-rolled ⅜ in. bolt	2.5	35	855	Good	No attack 20% HNO ₃

getting good coatings inside the threads, presumably due to the differential in current density over the ridges. Coated specimens were obtained, but results were not entirely consistent. Typical runs are listed in Table IV.

Corrosion Testing of Cathodes

Most of the various coated specimens produced (rods, bars, cones, and bolts) have been corrosion tested by several methods: 20% and concentrated nitric acid, 20% and concentrated hydrochloric acid, concentrated sulfuric acid, and 20% sodium chloride solution.

In general, all cathodes which appeared evenly coated were comparable to titanium metal in their resistance to all acid and basic media for periods up to 3 months. In some instances, thin spots were revealed by the brine test, particularly in the case of threads on the bolts. Fully coated bolts, however, were obtained.

This is a case where a large adjustment in current density might have had some effect. The ridges of the threads were well covered, these being the points of maximum current density, but the troughs were coated only thinly or not at all.

One corrosion test which is representative of electrodeposited bar specimens involved soaking in a 20% nitric acid solution for 27 days (648 hr). A washed cathode specimen was selected measuring 0.751 in. (1.91 cm) wide x 0.268 in. (0.68 cm) thick. After 27 days, there was no detectable change in measurement of the sample.

Physical Examination

A large number of titanium coated specimens were examined metallographically. This conclusively established the nature of the process and the type of bonding obtained. It was a measure of the uniformity and thickness of the titanium coatings prepared.

Fig. 1 is illustrative of a typical electrodeposited titanium layer. A section of the cathode is shown under polarized light delineating the transition structures. From the surface are the α titanium area (where grains are evident), β titanium high in iron, a thin intermetallic area (probably TiFe), and a high iron alloy bond merging with the matrix.

Identification of these phases was confirmed by x-ray analysis. Fig. 2A is an x-ray reflection pattern from the surface of the specimen in Fig. 1 showing an α titanium structure. Fig. 2B is from a thin deposit and shows β titanium lines. The pattern in Fig. 2C contains both α and β titanium lines as shown by a coating of medium thickness. For comparison, the pattern of commercially pure titanium is shown as Fig. 2D.

The electrodeposits in Fig. 3-5 were all prepared

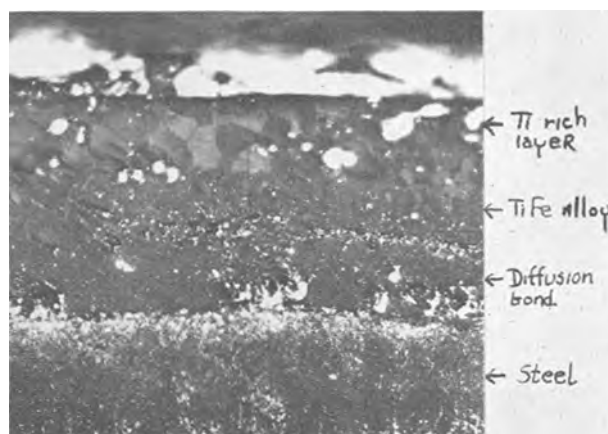


FIG. 1. Typical titanium electrodeposit on mild steel. (250 \times before reduction for publication)

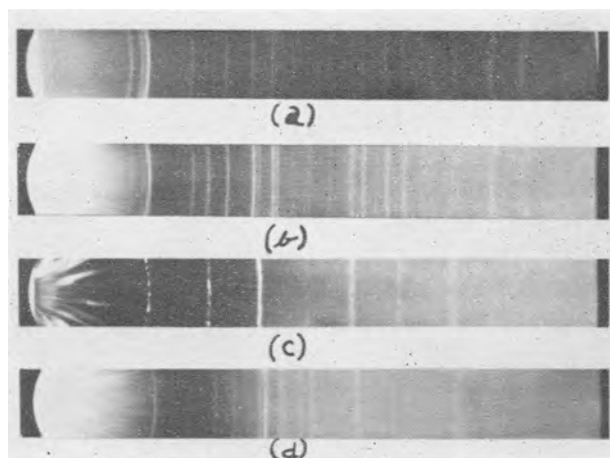


FIG. 2. X-ray patterns of electrodeposited titanium. (a) Surface of specimen in Fig. 2. (b) Thin coating showing β titanium lines. (c) Intermediate coating showing α and β lines. (d) Commercial titanium pattern.

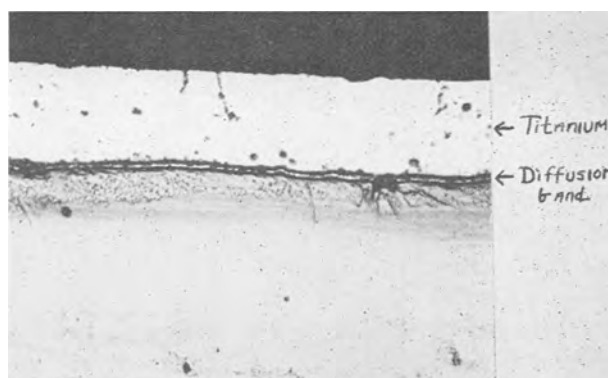


FIG. 3. Heavy coating on ingot iron bar. Etched in HF-HNO₃-glycerine. (500 \times before reduction for publication)

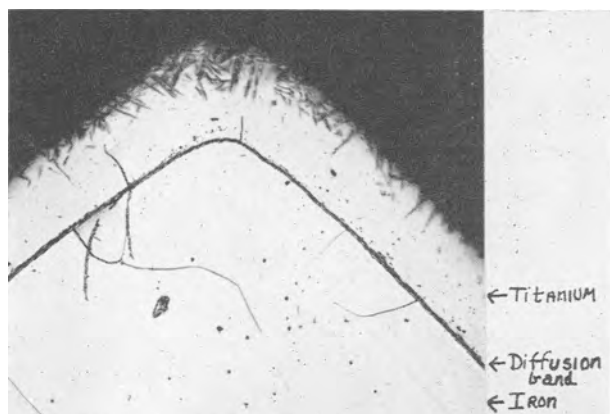


FIG. 4. Thin coating (<0.001 in.) on ingot iron bar; corner of sample; etched HF-HNO₃-glycerine. (250 \times before reduction for publication)

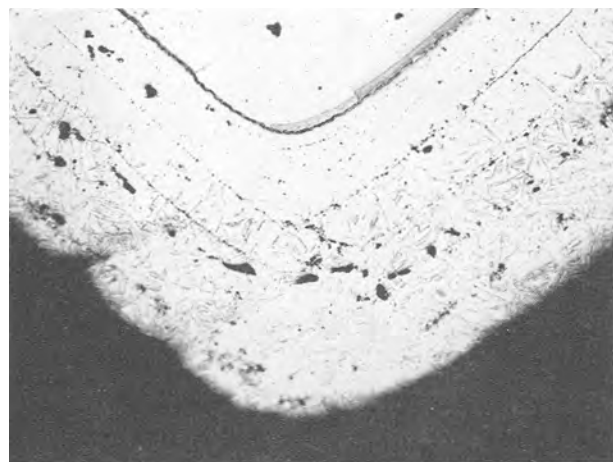


FIG. 5. Corner view of five titanium layers electrodeposited on ingot iron. (250 \times before reduction for publication)

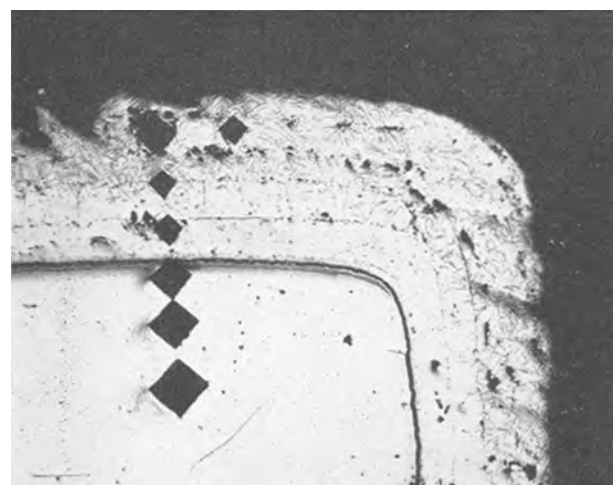


FIG. 6. Multiple layer specimen showing microhardness impressions. Etched in HF-HNO₃-glycerine. (250 \times before reduction for publication)

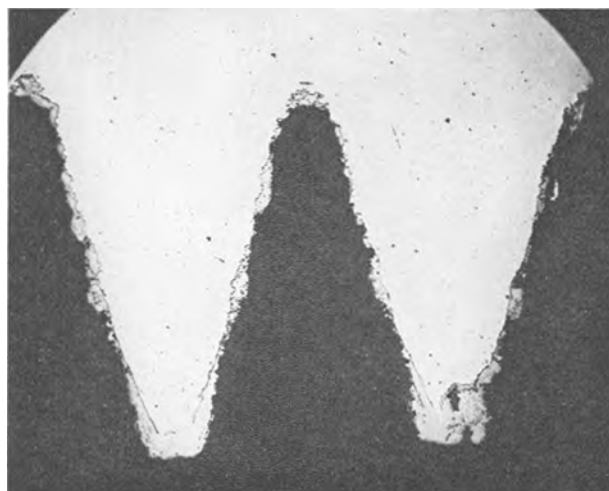


FIG. 7. Titanium electrodeposit on threaded bolt section

at 800°–950°C and show an iron-titanium interface stabilizing the β titanium phase. There is some variation in porosity in such a group of specimens, but the porosity is never continuous through the deposit to base metal. Fig. 3 and 4 illustrate the variation in thickness of deposit which may be obtained. Characteristics of the bond and surfaces are the same.

Fig. 4 and 5 illustrate the uniformity of deposits obtained at the corners of specimens.

Fig. 5 is of particular interest, illustrating five separate layers produced from five separate repetitive runs. The thickness of each individual layer is evident from the faint lines in the coating parallel to the surface. Fig. 6 is the same specimen showing microhardness impressions taken on various layers of the sample. A Vickers pyramid with a 25 g load was used for these measurements. From surface to the center, readings of 352, 383, and 340 VPN were obtained for the titanium and 167, 119, and 80 VPN for the iron.

In comparing Fig. 1 with Fig. 3, it is observed that a coating applied to mild steel has a thicker boundary phase than for ingot iron. This layer is thought to be a titanium carbide or perhaps an oxycarbide, since it is associated with decarburization of the base metal.

Fig. 7 is a longitudinal section of a threaded bolt electrodeposited with titanium. The coating is less uniform than those obtained on bars or cylinders, but does provide corrosion protection to the threads.

DISCUSSION OF RESULTS

It was established that steel can be plated by electrolytic means, and consistently good results were obtained on simple surfaces. A fused bath of sodium chloride and K₂TiF₆ was satisfactory; lithium chloride or potassium chloride could be used

with equal success in place of sodium chloride. A protective atmosphere was a requirement as was an inert container for the melt.

A low voltage pre-electrolysis to remove impurities was of no special advantage to the process, i.e., it did not guarantee a successful run. Presumably, pre-electrolysis did assist in removal of excess moisture and other minor impurities which had decomposition voltages under that of K_2TiF_6 . It is doubtful that such a procedure effectively removed titanium dioxide or Ti_2O_3 from a $NaCl-K_2TiF_6$ melt.

An increase in temperature up to $950^\circ C$ benefited the electrodeposition action. Temperatures much greater than this caused incipient melting rather than a diffusion bonded electroplate. Voltage was not a critical factor and was varied between 3 and 6. Current density was even less significant, good runs resulting at 50–500 amp/dm².

Bath concentration was not extensively investigated, but it is known that the system $NaCl-K_2TiF_6$ is operable as an electrolyte in the range 5–25% K_2TiF_6 . Sixteen per cent K_2TiF_6 produced a mixture of convenient melting range and provided a metal/bath weight ratio of 3/100, making any one bath suitable for treatment of a large total area of base metal surface.

The exact time required for deposition at a given current was not well established, but it is known to be relatively short. If a cathode was left in the bath for longer than 10–15 min at 80 amp/dm², a heavy build-up of crystalline titanium resulted. A $3\frac{3}{4}$ in. x 1 in. x $\frac{1}{4}$ in. (9.52 cm x 2.54 cm x 0.64 cm) steel bar was coated at 35 amp-hr in 10 min.

Heavier coatings were prepared by removing the cathode, cleaning it, and repeating the process. It was not shown why the plating process stopped after a relatively short time and was succeeded by crystalline deposition. However, the fact that the plating could be continued after cleaning was indicative that such behavior was associated with either the cathode surface or the area immediately adjacent to the cathode. A small volume of salt was removed with the cathode and discarded during the washing. This may have served to deplete the cathode area of a high concentration of depositing ions, enabling further plating rather than dendritic crystal growth. Similarly, such a cleaning procedure might remove codepositing impurities which could serve as nuclei for crystal growth on the cathode surface.

Hard, adherent, titanium coatings were produced by this method. There was no tendency toward peeling or exfoliation. The coatings were ductile enough to permit rolling or working of the original cathode.

Bend tests were conducted on coated samples having a 1 in. x $\frac{1}{4}$ in. (2.54 cm x 0.64 cm) cross section,

and the titanium surface layer cracked after very slight plastic extensions of approximately 1%. However, it was noted in these tests that the adherence of titanium to the ingot iron base material was excellent. In free bend tests no peeling of the coating occurred after bending specimens flat upon themselves (bend radius of about $\frac{1}{2}$ the thickness of the sample). These films were generally 0.001–0.003 in. (0.025–0.076 mm) thick, but could be increased by repeated electrolysis.

SUMMARY

A process was developed whereby thin titanium layers were bonded to steel or other base metals by fused salt electrolysis involving the use of a fused $NaCl-K_2TiF_6$ mixture. It was a rapid, inexpensive process, since high currents and voltages were employed and only a small amount of titanium was involved. The electroplated layer completely protected the coated article with all the corrosion resistance properties of titanium itself. The titanium layer was firmly bonded to the base metal by an alloy interface.

Consistently good results were achieved using cathodes of simple geometry. Articles such as nuts and bolts were more difficult because of the areas of varying current density, but this can be overcome.

ACKNOWLEDGMENT

The authors are grateful to the Wright Air Development Center for support of this work and permission to publish the results.

The authors also acknowledge the work of the following in carrying out this research effort: G. J. Franke, R. H. Baskey, F. C. Wagner, and B. C. Raynes, all of Horizons Incorporated.

Any discussion of this paper will appear in a discussion section to be published in the June 1956 JOURNAL.

REFERENCES

1. A. BRENNER AND S. SENDEROFF, *This Journal*, **99**, 223C (1952).
2. H. FISCHER AND K. DORSCH, German Pat. 615,951, July 16, 1935.
3. N. N. GRATIANSKII AND A. P. VOVKOGON, *Zapiski Inst. Khim. Akad. Nauk, U. R. S. S.*, **7**, 173 (1940).
4. M. HAISSINSKY AND H. EMMANUEL-ZAVISSIANO, *Compt. rend.*, **204**, 759 (1937).
5. M. HAISSINSKY AND H. EMMANUEL-ZAVISSIANO, *J. chim. phys.*, **34**, 641 (1937).
6. R. H. LEUTZ, German Pat. 741,670, September 30, 1943.
7. E. POKORNY AND K. SCHNEIDER, German Pat. 582,528, April 22, 1934; 605,551, November 13, 1934.
8. A. S. RUSSELL, *Nature*, **127**, 273 (1931).
9. A. W. SCHLECHTEN, M. E. STRAUMANIS, AND C. B. GILL, *This Journal*, **102**, 81 (1955).
10. M. A. STEINBERG, M. E. SIBERT, AND E. WAINER, *ibid.*, **101**, 63 (1954).

Liquidus Curves for Aluminum Cell Electrolyte

I. Cryolite-Alumina¹

N.W.F. PHILLIPS, R. H. SINGLETON,² AND E. A. HOLLINGSHEAD

Aluminium Laboratories Limited, Arvida, Quebec, Canada

ABSTRACT

Liquidus curves for the system cryolite-alumina up to 1050°C and 16% alumina were determined by means of cooling curves and visual examination of the cooling melt. The freezing point of pure cryolite was 1009° ± 1°C, and the cryolite-alumina eutectic point was at 962°C and 10% alumina (weight per cent). On the alumina side of the eutectic point, crystallization was sluggish, and there was no break in the cooling curve corresponding to the first appearance of crystals in the melt.

INTRODUCTION

Aluminum is produced commercially by the electrolysis of alumina dissolved in molten cryolite with minor additions of other salts. Therefore, it is useful to know the primary freezing points of these solutions. The object of this work was to determine accurate liquidus curves for the binary system cryolite-alumina. Those previously published are in disagreement with each other, and the present and other investigators have not been able to dissolve nearly as much alumina in molten cryolite at a given temperature as the curves indicate.

The primary freezing points were determined for those parts of the system molten at 1050°C by thermal analysis and by visual examination of the cooling melt.

MATERIALS

Hand-picked natural cryolite containing no visible impurities was crushed to pass 150 mesh. It had 0.06% loss on ignition at 700°C and contained 0.02% iron, 0.03% silicon, 0.02% magnesium, and 0.01% lead. The alumina was Linde fine abrasive alpha alumina, which had a loss on ignition at 1000°C of 0.24% and contained 0.02% sodium, 0.01% silicon, and 0.01% lead.

APPARATUS

The sample was contained in a covered 10% rhodium-platinum crucible, which fitted inside an insulating firebrick box of 13 mm wall thickness. This was supported in a crucible furnace heated by a flat 80-14-6 nickel-chromium-iron resistor and lined with insulating firebrick. The platinum, 10% rhodium-platinum thermocouple was in a 5 mm protection tube, also of 10% rhodium-platinum.

¹ Manuscript received May 31, 1955. This paper was prepared for delivery before the Cincinnati Meeting, May 1 to 5, 1955.

² Present address: National Research Corporation, Cambridge, Mass.

This alloy was used for the stirrer as well, in preference to pure platinum, because of its greater rigidity. The light beam of an arc lamp was directed into the crucible, and the melt was observed through a telescope with a magnification of twenty diameters.

A controller, used when taking cooling curves, regulated the furnace temperature so as to maintain a constant differential thermocouple voltage across the wall of the refractory box. This device (1) gives a nearly constant heat loss from the crucible and sharper arrests in the cooling curve. The controller was of the proportional position type with a continuously variable transformer to supply the furnace transformer. When the furnace temperature became too high, the power input was stepped down 15%, then reduced gradually; when it became too low, the reverse took place. An on-off controller maintained the furnace temperature for melting the sample, and, with periodic manual settings, gave the very slow rates of cooling required for the determination of primary freezing points by the visual method.

The cold junction of the measuring thermocouple was in cracked ice in a vacuum flask, and it was connected to a Rubicon Type B potentiometer. A special recorder, also supplied by the Rubicon Company, Philadelphia, registered the difference between the thermocouple output and a suitable voltage set on the potentiometer. This difference, usually in the 200 μv range, was multiplied to an appropriate level for a modified Brown Electronik strip-chart recorder by means of an external conversion unit. The balancing mechanism of this recorder was actuated by the amplifier of a photoelectric galvanometer in the microvolt circuit. The conversion unit had six ranges of 0-20 to 0-1000 μv and included a potentiometer with a range of -10 to +10 μv for testing and compensation of thermal emf's.

METHOD

The 150 g samples were made up by weight and heated at 1050° or 1100°C with stirring until a clear

melt was obtained. Then, for alumina contents up to 10% by weight, the melt was cooled with stirring at the rate of 1–3°C/min, and the primary freezing point determined from the cooling curve. Supercooling of up to 5°C took place. The cooling melts were observed through the telescope, and the first appearance of crystals corresponded with the primary break in the cooling curve.

For alumina contents higher than 10% there was no break in the cooling curve corresponding with the first appearance of crystals in the melt, and the primary break occurred at an appreciably lower temperature. This behavior is attributed to the sluggishness with which the crystals form and to the steepness of the liquidus curve. In this range the temperature at which crystals first appeared was taken as the primary freezing point. To minimize the effect of slow crystallization, final determinations by this visual method were made with cooling rates of less than 0.1°C/min.

The thermocouples were checked regularly at the freezing point of reagent-grade sodium chloride. This was found to be $801^\circ \pm 0.5^\circ\text{C}$ using a thermocouple calibrated in pure silver and in samples of aluminum and copper certified by the National Bureau of Standards. The calibration was made in pure alumina crucibles using pure alumina thermocouple protection tubes and carbon powder over the molten metal.

RESULTS

The freezing point of the cryolite, determined with a calibrated thermocouple, was found to be $1009^\circ \pm 1^\circ\text{C}$. Molten cryolite is slightly unstable, and on holding in the covered crucible for four hours at 1050°C , the freezing point decreased one degree.

Results for the system cryolite-alumina are shown graphically in Fig. 1 along with those of some of the investigations previously reported. The eutectic point is at 962°C and 10% alumina (weight per cent). The liquidus curve on the alumina side rises steeply to 1050°C at 16% alumina. The primary crystals which form on the alumina side of the eutectic point are hexagonal, but it was not definitely established that they are alpha alumina. Results on the cryolite side of the eutectic point, which were obtained by the cooling curve method, are not in error by more than 2°C . The limit of error on the alumina side, where the visual method was used, is estimated to be 5°C ; the results will tend to be low because it is not possible to make a correction for supercooling with this method. Duplicate results by a skilled observer did not differ by more than 2 or 3°C . When a clear melt 2 or 3°C above its primary freezing point was seeded with alpha alumina, crystallization did not begin, nor did the added crystals dissolve. The loss

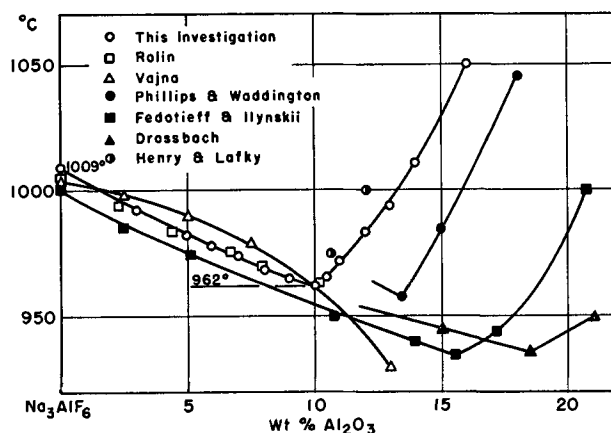


FIG. 1. Liquidus diagram for cryolite-alumina

in weight by evaporation from a melt containing 14% alumina was 1% after seven hours at 1050°C .

Rolin's data (2), which extend only to 10% alumina, do not differ from those of the present investigation by more than 3°C , while others differ by up to 10°C in this range. Above 10% alumina, the nearest other results are those of Henry and Lafky (3), who determined the percentage of alumina which would dissolve in cryolite on prolonged stirring at a given temperature. Phillips and Waddington used the cooling curve method, with a rate of $2^\circ\text{C}/\text{min}$, and observed that crystals formed in the melt before the primary break occurred. Their data, briefly reported in the discussion of Vajna's paper (4), and those of Henry and Lafky, became available after the present investigation was made. There are still greater differences between the present results and those of Fedotieff and Ilynskii (5), Drossbach (6), and other earlier investigators. They used the cooling curve method with higher rates of cooling. This method has been shown to be inadequate on the alumina side of the eutectic point.

ACKNOWLEDGMENT

The authors wish to acknowledge the assistance of Miss Anne Fischer and Mr. Leon Villeneuve who carried out many of the measurements.

Any discussion of this paper will appear in a Discussion Section to be published in the June 1956 JOURNAL.

REFERENCES

1. C. S. SMITH, *Trans. Am. Inst. Mining Met. Engrs.*, **137**, 236 (1940).
2. M. ROLIN, *Ann. Phys.*, **6**, 970 (1951).
3. J. L. HENRY AND W. M. LAFKY, Paper presented at the 126th Nat. Meeting of the American Chemical Society, New York, 1954.
4. A. VAJNA, *Alluminio*, **22**, 635 (1953).
5. P. P. FEDOTIEFF AND V. ILYNSKII, *Z. anorg. Chem.*, **80**, 113 (1913).
6. P. DROSSBACH, *Z. Elektrochem.*, **42**, 65 (1936).

The Vapor Pressure of Rhenium¹

E. M. SHERWOOD, D. M. ROSENBAUM, J. M. BLOCHER, JR., AND I. E. CAMPBELL

Battelle Memorial Institute, Columbus, Ohio

ABSTRACT

The vapor pressure of rhenium was determined over a temperature range of 2220°–2725°C. At 2500°C, the vapor pressure of rhenium is approximately one and one-half times that of tantalum. Estimates were made of the boiling point of rhenium (5630°C) and of the vapor pressure of liquid rhenium. The computed ΔH° of sublimation of rhenium is 187 kcal.

INTRODUCTION

Rhenium, with a melting point of 3180°C and a density of 21, is a relatively rare and quite expensive metal which, nevertheless, offers attractive possibilities as a material for electronic and other specialized applications. Its high resistance to attack in the so-called "water cycle" (hundreds of times better than tungsten, under certain conditions) (1) is of particular advantage in electron-tube applications. However, in order to evaluate fully the potential importance of rhenium in such a field of use, it was desirable to have information concerning its vapor pressure.

To obtain the required information, the Langmuir weight-loss method, which has been used previously in determining the vapor pressure of such metals as titanium (2), was employed. The validity of the data was checked by thermodynamic calculations, and both the boiling point of the metal and the vapor pressure of liquid metal were estimated.

DESCRIPTION OF THE TEST METHOD

The Langmuir weight-loss method (3) involves heating a wire of the desired material in a good vacuum (10^{-5} mm Hg, or less) at a constant temperature, for a measured time interval, and determining the loss in weight as a result of evaporation of metal from the wire. The following relationships, (I) and (II), are then used to compute the vapor pressure.

$$\log p_{\text{atm}} = \log m - \frac{1}{2} \log M + \frac{1}{2} \log T - 1.647 \quad (\text{I})$$

where p_{atm} = vapor pressure, atmospheres,² M = gram molecular weight of the vapor, T = temperature, degrees Kelvin, and m = rate of evaporation, g/cm²/sec.

$$\text{Further, } m = \left(\frac{\rho}{\pi}\right)^{1/2} \cdot \left(\frac{W_o^{1/2} - W^{1/2}}{t}\right) \quad (\text{II})$$

¹ Manuscript received April 11, 1955.

² Strictly, $\alpha \cdot p_{\text{atm}} = m \cdot \text{const} \cdot T^{1/2} \cdot M^{1/2}$, the familiar Knudsen equation. As is usually valid for metals, α , the accommodation coefficient, is assumed equal to unity (4).

where ρ = computed density at temperature of run, g/cc, W_o = initial weight/unit length of wire, g/cm, W = final weight/unit length of wire, g/cm, and t = time of run, sec.

Test Specimens

The specimens used in the experimental work were in the form of wires, about 0.050 in. in diameter by 6 in. long. These wires were made by cold pressing minus 325-mesh rhenium powder at 30 tons/in.² into the form of bars $\frac{1}{4} \times \frac{1}{4} \times 6$ in. in size. Stearic acid in ether was used as a die lubricant. The density of the pressed bars was 35–40% of the theoretical value. The bars were presintered in a vacuum of 10^{-6} mm Hg for 2 hr at 1200°C to improve their strength. A 5% increase in density was secured at this step. Subsequent sintering of the bars in hydrogen at 2700°C for 1 hr produced densities 85–93% of theoretical.

The following fabrication schedule was used, with appropriate intermediate anneals in hydrogen for 2 hr at 1750°C: (a) careful hand hammering of corners of bars; (b) cold rolling of the corners to produce bars of octagonal cross section; (c) cold swaging, at 20% reduction per pass, until the diameter was reduced to 0.060 in.; (d) cold wire drawing, at 10% reduction, to the finished size of approximately 0.050 in.

Fig. 1 is a photomicrograph of a longitudinal section of a typical wire specimen in its condition prior to test.

Test Equipment

The test specimen was supported in a horizontal position by two split molybdenum clamping blocks, each 0.5 in. in diameter by 1.5 in. long. Each of these blocks was provided with a tapped hole so that it could be screwed onto the 0.25-in. diameter tungsten supporting electrode. This assembly was mounted in a 100-mm Pyrex bulb with the ends of the tungsten electrodes protruding from the bulb and sealed to it by uranium glass (Fig. 2).

A 45-mm Pyrex tube, with an optically flat Pyrex

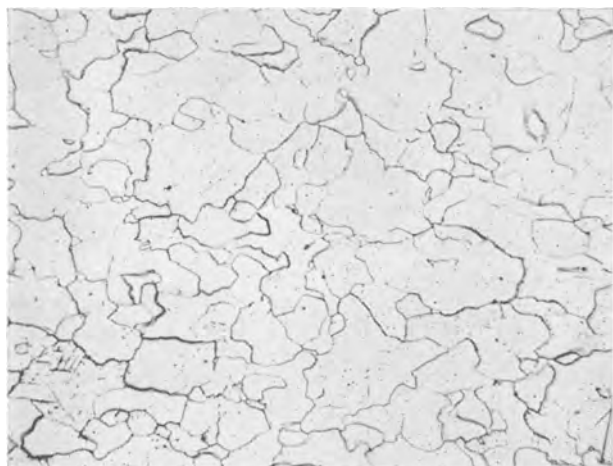


FIG. 1. Longitudinal section of typical rhenium-wire specimen (250 magnification, electrolytic oxalic acid etch).

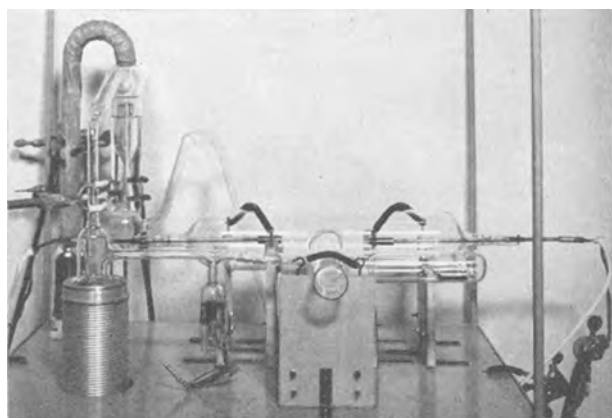


FIG. 2. Experimental equipment

plate sealed in its free end, was joined at right angles to the bulb, and perpendicular to the test specimen at its center. The temperature of the wire was determined by a L&N optical pyrometer, which had been calibrated, with the flat Pyrex sight window in place, against a N.B.S. standard tungsten-ribbon lamp. The observed temperatures (accuracy of observation about $\pm 10^\circ\text{K}$) were corrected for the emissivity of rhenium. Over the temperature range used in these determinations ($2500^\circ\text{--}3000^\circ\text{K}$), the emissivity at 0.655μ varies between 0.39 and 0.36. The "true" temperature was obtained from a previously determined³ calibration curve showing the relation between black-body temperature and brightness temperature for rhenium. A magnetically operated glass shutter was placed in the line of sight between the test wire and the optical window to prevent condensation of evaporated rhenium on the window. The shutter was maintained in this position except when temperature determinations were being made.

³ Unpublished work at Battelle Memorial Institute.

Fig. 2 illustrates the complete vacuum system (except for the mechanical fore pump), which includes an ionization gauge, liquid-nitrogen trap, and three-stage mercury diffusion pump.

In all test runs the pressure was less than 10^{-5} mm of Hg.

Procedure

With the specimen in place, the system was evacuated to about 10^{-5} mm and then filled with high-purity helium as a purge. Next, the system was re-evacuated to 10^{-5} mm, or lower, and the rhenium was electrically heated, with stabilized a-c power, to the desired temperature as rapidly as possible. Wire temperature was maintained constant by adjusting the applied voltage so that the product of the cube root of the current and the voltage was constant. Test runs were terminated when it was judged that sufficient metal had been evaporated from the surface of the wire to permit accurate weight-loss determination.

RESULTS

Table I lists the results of the experiments. High temperature densities, calculated from extrapolated linear coefficient of thermal expansion data,³ were used in equation (II). Density values ranged from 19.73 to 19.93 g/cc. Owing to the cooling effect of the molybdenum clamping blocks, a sharp temperature gradient existed adjacent to the blocks. To compensate for this gradient, an effective wire length, $\frac{1}{2}$ in. less than the free length of the wire between the blocks, was used in the computations.

An empirical expression for the vapor pressure of rhenium was calculated from the experimental determinations, using the method of least squares. For the temperature range covered, equation (III) is a valid representation of the vapor pressure of rhenium:

$$\log_{10} p_{\text{atm}} = 7.5237 - 40865/T \quad (\text{III})$$

or

$$\log_{10} p_{\text{mm}} = 10.4038 - 40865/T$$

TABLE I. Experimental values of vapor pressure for rhenium

Corrected temperature		Duration of run, sec	Rate of evaporation, g/cm ² /sec	Vapor pressure	
$^\circ\text{C}$	$^\circ\text{K}$			Atmosphere	mm Hg
2221	2494	259,200	1.54×10^{-8}	1.24×10^{-9}	9.39×10^{-7}
2250	2523	151,200	3.23×10^{-8}	2.61×10^{-9}	1.98×10^{-6}
2332	2650	30,600	7.35×10^{-8}	6.04×10^{-9}	4.59×10^{-6}
2475	2748	54,000	6.96×10^{-7}	5.56×10^{-8}	4.23×10^{-5}
2480	2753	23,400	4.67×10^{-7}	3.93×10^{-8}	2.99×10^{-5}
2606	2879	7,200	2.77×10^{-6}	2.38×10^{-7}	1.81×10^{-4}
2726	2999	1,560	8.41×10^{-6}	7.37×10^{-7}	5.60×10^{-4}

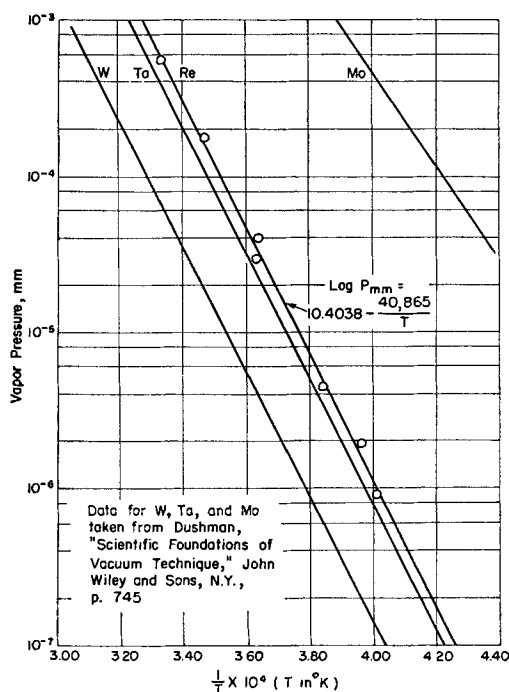


FIG. 3. Vapor pressure of rhenium and other refractory metals as a function of reciprocal temperature.

The vapor pressure of rhenium, so determined, is about ten times greater than that of tungsten and about one and one-half that of tantalum. This is illustrated in Fig. 3, in which data for molybdenum are given as well.

Thermodynamic Treatment

The following important relationship forms the basis for the thermodynamic calculations presented in this section:

$$\begin{aligned} -R \ln p_{\text{atm}} &= [(F^\circ - H^\circ_0)/T]_g - [(F^\circ - H^\circ_0)/T]_{c,1} \\ &\quad + \Delta H^\circ_0/T, \\ &= \Delta[(F^\circ - H^\circ_0)/T] + \Delta H^\circ_0/T \quad (\text{IV}) \end{aligned}$$

where R = the universal gas constant, 1.987 cal/mole, $[(F^\circ - H^\circ_0)/T]_g$ = the free-energy function for the vapor, $[(F^\circ - H^\circ_0)/T]_{c,1}$ = the free-energy function for liquids or crystalline solids, ΔH°_0 = the heat of sublimation at absolute zero, in cal/mole.

$$\Delta[(F^\circ - H^\circ_0)/T] = [(F^\circ - H^\circ_0)/T]_g - [(F^\circ - H^\circ_0)/T]_{c,1} \quad (\text{V})$$

$[(F^\circ - H^\circ_0)/T]_g$ can be determined from spectroscopic data, $[(F^\circ - H^\circ_0)/T]_{c,1}$ can be evaluated when the thermal variation of C_p , the heat capacity, is known and appropriate account is taken of phase changes.

The source of the spectroscopic data used in the calculation of the free-energy function for rhenium vapor was Klinkenberg (6).

TABLE II. ΔH°_0 of sublimation for rhenium

T, °K	$-[(F^\circ - H^\circ_0)/T]_g$	$-[(F^\circ - H^\circ_0)/T]_c$	Vapor pressure, atm	ΔH°_0 , cal
2494	50.735	16.172	1.24×10^{-9}	187,826
2523	50.793	16.254	2.61×10^{-9}	186,218
2605	50.953	16.481	6.04×10^{-9}	188,013
2748	51.222	16.865	5.56×10^{-8}	185,622
2753	51.231	16.878	3.93×10^{-8}	187,848
2879	51.458	17.203	2.38×10^{-7}	185,860
2999	51.670	17.505	7.37×10^{-7}	186,601
Average				186,855 ± 1015

The thermal variation of the specific heat of rhenium from 0° to 300°K was computed using Seitz (7).

Since this paper was presented, Cobble, Oliver, and Smith (8) have presented experimental data for C_p over this temperature range. The computed values used in this work are only a few per cent lower than those of the above published work.

The data of Jaeger and Rosenbohm (9) were used over the range 300°–1500°K, and were extrapolated to the melting point.

A discontinuous increase in C_p of 0.9 cal/mole/° was assumed at the melting point. The heat capacity for liquid rhenium was assumed constant up to the boiling point.

Vapor pressure of the solid.—Equation (IV) was used first to assess the quantitative accuracy of the experimental data; i.e., ΔH°_0 was computed for each of the experimental temperatures, using the corresponding measured values of the vapor pressure. Table II lists the results of these computations. Although the standard deviation from the mean is 1015 calories, somewhat higher than might be desired, no over-all trend upward or downward is indicated. The value 187,000 calories has been taken as ΔH°_0 of sublimation for rhenium.

Next, $\Delta[(F^\circ - H^\circ_0)/T]$ was expanded as a quadratic function of T over the range of experimental data, using the values for $\Delta[(F^\circ - H^\circ_0)/T]$ from Table II and at the melting point, i.e.,

$$\begin{aligned} \Delta[(F^\circ - H^\circ_0)/T] &= a + bT + cT^2 \quad (\text{V}) \\ &= -37.327 + 14.258 \times 10^{-4} T \\ &\quad - 1.257 \times 10^{-7} T^2 \end{aligned}$$

Equation (IV) becomes

$$\begin{aligned} -R \ln p_{\text{atm}} &= -37.327 + 14.528 \times 10^{-4} T \\ &\quad - 1.257 \times 10^{-7} T^2 + 187,000/T \\ -\log p_{\text{atm}} &= (1/4.5753) \cdot (-37.327 + 14.258 \\ &\quad \times 10^{-4} T - 1.257 \times 10^{-7} T^2 \\ &\quad + 187,000/T) \quad (\text{VI}) \end{aligned}$$

TABLE III. Vapor pressure of liquid rhenium

$T, ^\circ K$	$-[(F_o - H_o^\circ)/T]$	Computed vapor pressure of liquid rhenium, atm
3453 (mp)	33.846	3.64×10^{-5}
3500	33.784	5.09×10^{-5}
4000	33.177	1.08×10^{-3}
4500	32.663	1.14×10^{-2}
5000	32.238	7.44×10^{-2}
5500	31.906	0.349
5900 (bp)*	31.702	1.000

* (mp) = melting point; (bp) = boiling point.

The vapor pressure of solid rhenium then can be calculated from equation (VI) for the experimental temperatures.

Vapor-pressure values, determined experimentally, were compared with those calculated from both equation (III) and equation (VI). In general, good agreement was obtained in both cases, the average difference between experimental and calculated values being about 16%. For the highest temperature at which tests were run (2999°K), equation (III) failed to give a good approximation, and the calculated value was too high. Further departure of the values computed using equation (III) from those made using equation (VI) occurred at still higher temperatures. However, it should be noted that the value of the vapor pressure at the melting point (3.83×10^{-5} atm), calculated using equation (VI), was quite close to the value obtained using equation (VII) (3.64×10^{-5} atm).

Vapor pressure of liquid rhenium.—After a reasonable value for ΔH_o° was obtained, equation (IV) was used to compute the vapor pressure of liquid rhenium at various temperatures above the melting point. These computed values are, in reality, estimates, since no data are available for the heat capacity of liquid rhenium. Brewer (10) has estimated the entropy of fusion of rhenium as 2.3 eu, and this value was used in computation of the free energy function of liquid rhenium, above the melting point (3180°C). The heat capacity of liquid rhenium was assumed to be 10.8 cal/mole/°. As was done for the solid, $\Delta[(F_o - H_o^\circ)/T]$ was expanded as a function of T from the melting point upward to give:

$$\Delta[(F_o - H_o^\circ)/T] = -40.582 + 25.807 \times 10^{-4}T - 1.824 \times 10^{-7}T^2 \quad (\text{VII})$$

Using equations (IV) and (VII), the values of Table III were computed.

If p_{atm} is set = 1 in equation (IV), then its logarithm is zero, and, by a method of successive approximation, T_{bp} can be calculated. The value

so obtained is 5900°K (5630°C), as indicated in the table.

DISCUSSION OF RESULTS

The reliability of the data appears to be good. The chief source of possible error lies in the assumption that the temperature of the wire test specimen was uniform except for about $\frac{1}{4}$ in. at each end near the clamping electrodes.

Measurement of temperature variation over the length of the resistively heated specimen indicates that the effective length adopted was accurate to within 10%.

The absence of volatile impurities was evidenced by the fact that runs made at successively lower temperatures with the same wire checked runs made at successively higher temperatures.

No evidence of metal-film formation was detected on the sight-window, indicating that the glass shutter performed satisfactorily.

Lack of information on the heat capacity of rhenium from about 1200°C to the boiling point offered the most serious handicap in arriving at good estimates of the boiling point of rhenium and the vapor pressure of liquid rhenium. Since these estimates were made (11), tests have been run, over the temperature range 1500°–2700°K, which indicate both the manner in which C_p for rhenium varies and the relative value of C_p for rhenium compared to that for tungsten. It is believed that estimated values in this temperature range are within less than 10% of the true values. For example, the recently measured value of C_p at 2700°K was about 9.5 cal/mole/°, whereas the assumed value was about 9.1 cal/mole/°.

Finally, still better estimates of the vapor pressure of liquid rhenium and of the boiling point could have been made if experimental data on the heat of fusion of rhenium were available.

ACKNOWLEDGMENT

This work was done at the Battelle Memorial Institute under an Air Force Contract (No. AF 33(616)-232) on "Uses of Rhenium" with the Aeronautical Research Laboratory, Wright Air Development Center. Appreciative thanks are due the Air Force for permission to present and publish this paper.

Any discussion of this paper will appear in a Discussion Section to be published in the June 1956 JOURNAL.

REFERENCES

1. Unpublished Information, Battelle Memorial Institute.

2. J. M. BLOCHER, JR., AND I. E. CAMPBELL, *J. Am. Chem. Soc.*, **71**, 4040 (1949).
3. I. LANGMUIR, *Phys. Rev.*, 2329 (1913).
4. H. L. JOHNSTON AND A. L. MARSHALL, *J. Am. Chem. Soc.*, **62**, 1382 (1940).
5. W. F. GIAUQUE, *ibid.*, **52**, 4808 (1930).
6. P. F. A. KLINKENBERG, *Physica*, **14** (5), 271 (1948).
7. F. SEITZ, "Modern Theory of Solids," p. 137, McGraw-Hill Book Co., New York (1940).
8. J. W. COBBLE, G. D. OLIVER, AND W. T. SMITH, *J. Am. Chem. Soc.*, **75**, 5875 (1953).
9. F. JAEGER AND E. ROSENBOHM, *Proc. Acad. Sci. Amsterdam*, **36**, 787 (1933).
10. L. BREWER, "The Chemistry and Metallurgy of Miscellaneous Materials—Thermodynamics," edited by L. L. Quill, p. 29, McGraw-Hill Book Co., Inc., New York (1950).
11. Unpublished Information, Battelle Memorial Institute.

The Kinetics of Formation of Anodic Ta₂O₅— Further Studies¹

D. A. VERMILYEA

General Electric Research Laboratory, Schenectady, New York

ABSTRACT

A new investigation of the kinetics of formation of anodic Ta₂O₅ films showed that data reported previously are in error. The new data show that the activation energy for the process is not a single linear function of the applied electric field, and that the pre-exponential factor is also a function of the applied field. Possible mechanisms are considered, but none explains the results adequately.

INTRODUCTION

In a previous paper (1) data obtained from measurements of the growth of anodic oxide films on tantalum were presented. It was found possible to describe the data by an equation of the type

$$\dot{X} = A \exp (BE - Q/kT) \quad (\text{I})$$

where \dot{X} is the rate of film growth, A and B are constants, E is the electric field strength, and Q is an experimental activation energy. More extensive measurements with improved techniques suggest a better interpretation of the data. This paper presents the results of these recent measurements.

EXPERIMENTAL

All of the equipment used, which consisted of a constant voltage power supply, constant temperature bath, an automatic timing circuit, and a calibrated optical step gauge for measuring thickness, were described previously (1). The absolute accuracy of the step gauge was checked by a direct measurement of film thickness (see Appendix), and thicknesses measured with the step gauge were found to be within at least 10% of the true thickness.

In the previous paper the major emphasis was placed on experiments conducted with a constant current power supply. The range of electric field strengths available by this method is limited by the long times required at very low currents and by heating of the specimen at high currents. On the other hand, when constant voltage experiments were made it was necessary to correct the recorded times because it was not possible to start with zero film thickness at zero time. The correction for initial conditions involved an extrapolation, and errors were introduced because of the short total time range over which the extrapolation was made. In

addition, it is now known that polarization at the cathode was overcompensated for in the first constant voltage experiments.

In the experiments reported in the present paper only the constant voltage method was used. A small cathode of about 0.5 cm² was used so that cathode polarization would always reach its maximum value in a time which was shorter by a factor of at least 10² than the time of voltage application. In the earlier experiments a large cathode prevented the polarization from rising quickly enough. All of the experiments were conducted using 2% nitric acid for the electrolyte and a constant voltage of 100 volts.²

The method of obtaining data was as follows. An oxide film was formed on the specimen to a thickness such that about 250 ma would be passed through the cell when 100 v was applied at the desired temperature. The voltage drop due to polarization plus resistance in the cell was measured at 250 ma using a platinum anode, and the value obtained was added to 100 v. This total voltage was then applied to the tantalum for 0.1 sec, after which the specimen was removed and the oxide film thickness measured. This process was repeated, using longer time intervals as the current decreased, corrections for polarization and resistive voltage drops being made for each expected current.

Once the data were obtained, plots were made of thickness vs. the logarithm of the time. On these plots the original thickness was included by adding 0.1 sec to all measured times. Next, several electric field strengths were selected and the thickness at each field calculated; the rate of film growth at that thickness was obtained for each temperature by dividing the slope of the appropriate thickness vs. log time plot by the time required to reach that thickness. Activation energies were then obtained by the method of least squares for each field strength selected.

² 100 volts is the true voltage after correction for reaction voltage as described in reference (1).

¹ Manuscript received September 22, 1954. This paper was prepared for delivery at the Cincinnati Meeting, May 1 to 5, 1955.

RESULTS AND DISCUSSION

Fig. 1 and 2 show thickness vs. log time plots for 0° and 99°C, respectively. The curve for 0°C is linear to about 4×10^5 sec, while the curve for 99°C

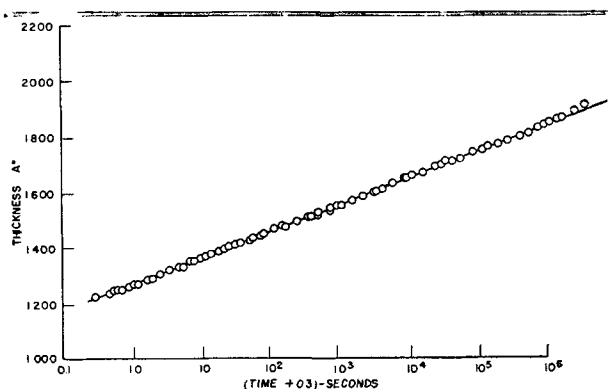


FIG. 1. Thickness vs. log time for a run made at 0°C

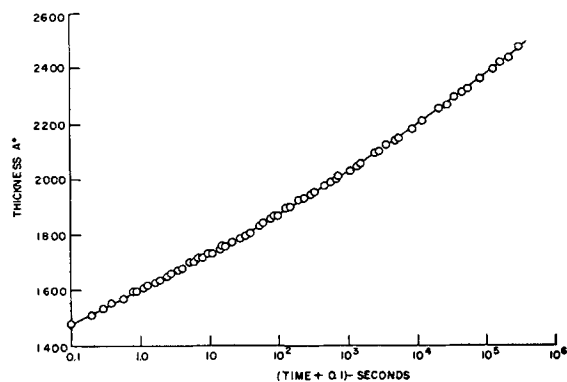


FIG. 2. Thickness vs. log time for a run made at 99°C

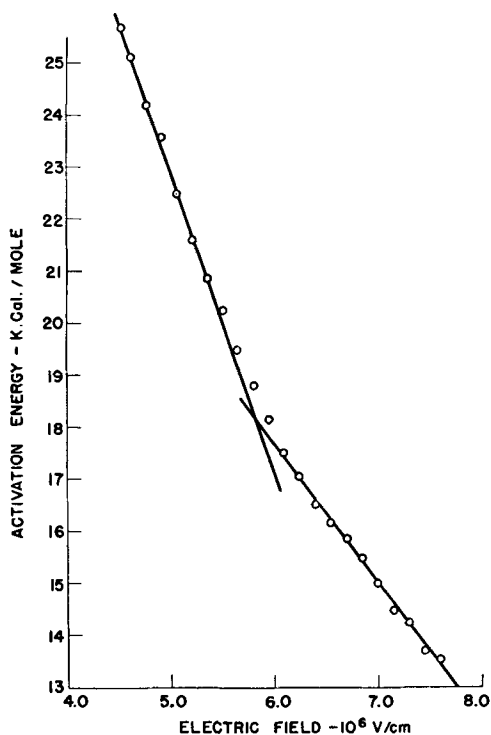


FIG. 3. Activation energy as a function of applied field

is nowhere linear. Intermediate temperatures give plots which varied gradually from nearly all linear at lower temperatures to nearly all curved at higher temperatures. Fig. 3 shows a plot of activation energy vs. electric field strength, while Fig. 4 shows the variation with field strength of the intercepts at $T = 0^\circ\text{K}$ of the activation energy plots.

Fig. 5 shows plots of the data obtained in the present investigation and in the earlier investigation at 19°C as well as a replot of data reported by Young (2) from experiments at 20°C. Earlier data obtained from constant current experiments agree well at low fields with the later data obtained from

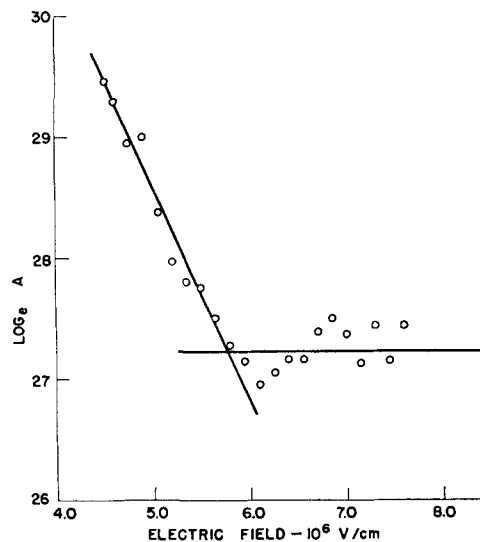


FIG. 4. Pre-exponential factor as a function of applied field.

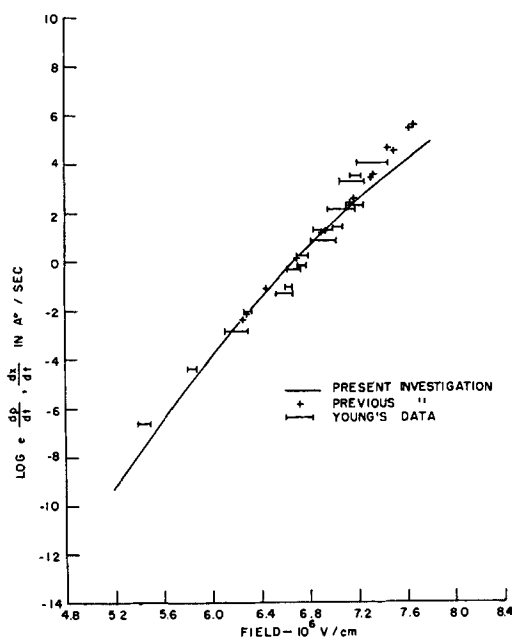


FIG. 5. Log rate as a function of applied field for this and previous investigations.

constant voltage experiments, but, at high fields, rates of film growth at a given field are greater in earlier data. It is believed that this discrepancy results from heating the oxide film above the bath temperature in the earlier experiments. In the previous paper a calculation was made of the temperature rise which a specimen would undergo when a specific current density was passed for a few seconds, and it was found that the expected temperature rise was a few degrees centigrade. The estimated temperature rise was probably low, because the boundary conditions, which assumed constant rate of heat input to one face of an infinite piece of metal, were not exactly those of the experiment. It would be difficult to make an exact calculation of the actual temperature rise which occurred in the earlier experiments, but it was certainly enough to influence the results seriously. In the present investigation, where at high current densities the time of voltage application was only 0.1 sec, such heating was negligible.

It may be seen from Fig. 5 that the data reported by Young agree well with the earlier data obtained by Vermilyea (1). Young employed a constant current method for obtaining data, and his results were also probably influenced by heating the specimen at high formation rates.

According to the mechanism proposed by Mott and Cabrera (3), a plot of activation energy vs. applied field should give a straight line of slope $q\lambda/kT$, where q is the charge on the diffusing ion and λ is the distance from the position of equilibrium in the metal to the top of the energy barrier opposing entrance into the oxide. This mechanism assumes that the rate-controlling step consists of moving an ion from the metal into the oxide, and that once the ion is in the oxide it moves rapidly to the outer interface and reacts to form oxide.

It is apparent from Fig. 3 that one straight line cannot be drawn through the points, but two straight lines seem to fit the data fairly well except for a transition region. At the present time no mechanism which accounts satisfactorily for this behavior has been found. One plausible hypothesis which was examined proposed that the curve of Fig. 3 resulted from the presence of two successive barriers to the motion of ions, one effective at low and one at high electric fields. Evidence presented in a previous publication (4) indicates that tantalum is the mobile ion during anodic oxidation. If it is assumed that the charge on the tantalum is +5, the heights of the two barriers in the absence of an applied field would be 2.17 and 1.47 electron volts, while the corresponding half widths would be 4.8 Å and 2.4 Å. The larger barrier might be thought to

be the one at the metal-oxide interface with the smaller one opposing motion within the film.

One difficulty with such a proposal is that, at high fields when the controlling step is within the film, a space charge would develop which would result in a nonuniform field. Dewald (5) has suggested that space charges may be important in determining the kinetics of anodic oxidation, but it has been shown (6) that any space charge must be very small. There is the possibility, however, that any space charge formed in the film might be negligible except at the metal-oxide interface, so that the field in the oxide film might be linear except for a small boundary layer. That this is *not* a possible explanation of the observed results may be shown as follows. Consider a constant current experiment conducted at constant temperature. The flux of ions past the metal-oxide interface is given by

$$J_I = C_I A_I \exp^{-\Delta H_I/kT} \exp^{q\lambda_I E_I/kT} \quad (\text{II})$$

while at any plane in the oxide a distance X from the interface the flux will be

$$J_X = C_X A_X \exp^{-\Delta H_X/kT} \exp^{q\lambda_X E_X/kT} \quad (\text{III})$$

where C_I, C_X = concentration of diffusing species at the metal-oxide interface and in the film, respectively. A_I, A_X = frequency factors at the interface and in the film. These frequency factors consist of the product of a vibrational frequency, an entropy of activation, and a lattice constant. $\Delta H_I, \Delta H_X$ = heats of activation at the interface and in the oxide. q = charge on diffusing ion. λ_I, λ_X = half widths of the barriers opposing diffusion at the interface and in the oxide. E_I, E_X = electric field intensity at the interface and in the oxide. $\Delta H_X, \lambda_X$, and A_X are assumed to be constant throughout the film. Assuming that the fluxes are divergence free,

$$J_I = J_X \quad (\text{IV})$$

The concentration of ions at any plane is therefore:

$$\begin{aligned} C_X &= \frac{C_I A_I \exp(-\Delta H_I/kT) \exp q\lambda_I E_I/kT}{A_X \exp(-\Delta H_X/kT) \exp q\lambda_X E_X/kT} \\ &= B \exp q/kT(\lambda_I E_I - \lambda_X E_X) \end{aligned} \quad (\text{V})$$

where B is a constant at any one temperature. Poisson's equation for one-dimension states that

$$\frac{dE}{dX} = \frac{4\pi\rho}{\kappa} \quad (\text{VI})$$

where ρ is the charge density and κ is the dielectric constant. Substituting the value of C_X from equation (V) in equation (VI) gives:

$$\exp\left(\frac{q\lambda_X}{kT} E_X\right) dE = \left(\frac{4\pi q e}{\kappa}\right) B \exp\left(\frac{q\lambda_I}{kT} E_I\right) dX \quad (\text{VII})$$

TABLE I. Calculated field as a function of distance in the film

X = distance from oxide-metal interface Å	Field v/Å	Average field in a film of thickness X v/Å
0	0.0626	—
100	0.0629	0.0627
500	0.0635	0.0631
1000	0.0642	0.0635
1500	0.0648	0.0639
2000	0.0654	0.0642
3000	0.066	0.0647
4000	0.0665	0.0651
5000	0.0669	0.0654

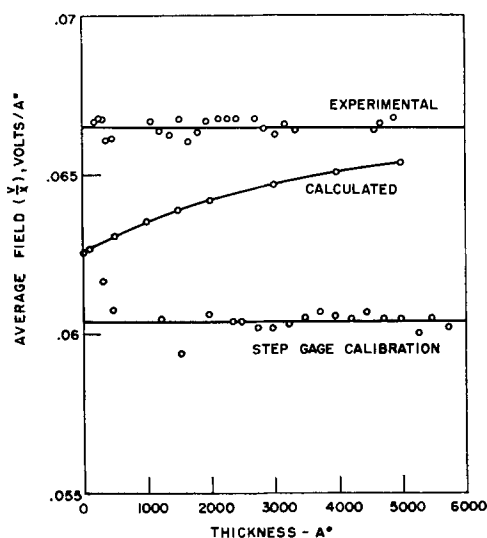


FIG. 6. Average field vs. film thickness. The calculated and experimental values are for anodization at 0.815 Å/sec at 19°C.

where z = the valence of the diffusing ion, and e = the electronic charge. Integrating and solving for E_x gives:

$$E_x = \frac{kT}{q\lambda_x} \ln \left\{ \frac{q\lambda_x}{kT} \cdot \left[\frac{4\pi ze}{\kappa} B \exp \left(\frac{q\lambda_I E_I}{kT} \right) X + D \right] \right\} \quad (\text{VIII})$$

where D is a constant of integration. Solving for D subject to the boundary condition $E_x = E_I$ at $X = 0$, and substituting again in equation (VIII), the final expression for E_x is:

$$E_x = \frac{kT}{q\lambda_x} \ln \left[\frac{q\lambda_x}{kT} \frac{4\pi ze B}{\kappa} \exp \left(\frac{q\lambda_I E_I}{kT} \right) X + \exp \left(\frac{q\lambda_x E_I}{kT} \right) \right] \quad (\text{IX})$$

In order to calculate E_x as a function of distance in the film it is necessary to evaluate the constant

B , which involves some assumptions regarding vibrational frequency and entropy of activation. It will be assumed that the vibrational frequency is 10^{13} and that the entropy of activation is 20 cal/degree. These values are both probably somewhat too large. They were deliberately chosen in this way to minimize the concentration of ions in transit required to give the observed pre-exponential factor. If the resultant space charge distorts the field in the film too much when the concentration is low, it may be concluded that the mechanism is invalid.

From Fig. 4, the pre-exponential factor at fields in which control is assumed to be in the film is 6×10^{11} , if the growth rate, \dot{X} , is expressed in Å/second, and it will be assumed that the value is the same for processes in the film and at the interface. The ion flux $C_I A_I$ corresponding to 6×10^{11} Å/sec is 1.43×10^{26} ions/cm²/sec. The quantity A_x is given by $2\lambda_x \nu \exp(\Delta S/R)$, where ν is the vibration frequency. Taking $2\lambda_x = 4.76 \times 10^{-8}$ from Fig. 3, $A_x = 1.114 \times 10^{10}$. Using the values for heats of activation at zero field obtained from Fig. 3, $B = 7.9 \times 10^{-3}$ at $T = 19^\circ\text{C}$.

Consider now a constant-current experiment conducted at 19°C and a rate of 0.815 Å/sec. The field required at the metal-oxide interface to produce an ion flux equivalent to this rate is found from the data in Fig. 3 to be 6.26×10^6 v/cm. Using this value for E_I , assuming $q = 5$, $K = 25$, and taking $\lambda_I = 4.8$ Å, E_x was calculated for different values of X with the results shown in Table I. From a plot of field vs. thickness, the average field was calculated by graphical integration, and these values are also included in Table I.

The increase in average field thickness is about 4% over the thickness range from 100 to 5000 Å. In order to determine whether such an increase actually occurs, a specimen was anodized under the conditions for which the calculation was made, the thickness and voltage being measured periodically. The average field at each thickness was then calculated by dividing the voltage by the thickness.³ Fig. 6 shows a plot of the calculated and experimental values of the average field for these conditions. It may be seen that the experimental field is constant with thickness, and that the increase in the calculated field is large compared to the experimental uncertainty. Also, the calculated fields are less than the experimental fields at all thicknesses.

Since the thicknesses were measured by comparison with the optical thickness step gauge, it was necessary to be certain that there was no com-

³ The applied voltage must be corrected for the voltage of the electrochemical reaction (7).

pensating error in the step gauge. The data of Fig. 4, reference (1), are replotted in Fig. 6 to show that the average field in the specimens used to calibrate the step gauge does not change with film thickness. The scatter at small thicknesses is a result of the poorer sensitivity of the measurement for thinner films.

It is concluded on the basis of these calculations that the observed results are not to be explained on the basis of the two postulated energy barriers. Another possible explanation of the observed results is that the field changes the activation energy by changing the nature of the film. It has been observed that the dielectric constant of the film and the rate of solution of the film in hydrofluoric acid are functions of the formation field, and perhaps the activation energy for ion movement is also. An investigation of these effects is now in progress.

CONCLUSIONS

1. The activation energy for the rate-determining step during anodic oxidation of tantalum is not a single linear function of the applied electric field.

2. The pre-exponential factor in the equation for the rate of growth of the film is a function of the applied electric field. The factor is nearly constant above a certain field but increases at lower fields.

3. Because the accumulation of a space charge in the oxide film results in nonlinearity of the thickness-voltage plot at constant formation rate while such plots are actually linear, mechanisms involving the accumulation of large space charges in the film are not in agreement with experiment.

ACKNOWLEDGMENT

Contributions to the interpretation of the data presented in this paper were made by E. W. Hart, C. P. Bean, and D. Turnbull in many interesting discussions. These discussions and the helpful criticisms of the manuscript which were made by D. Turnbull are gratefully acknowledged. The author is also indebted to Dr. J. F. Dewald, of the Bell Telephone Laboratories, for a stimulating discussion on the effects of space charges.

Any discussion of this paper will appear in a Discussion Section to be published in the June 1956 JOURNAL.

REFERENCES

1. D. A. VERMILYEA, *Acta Met.*, **1**, 282 (1953).
2. L. YOUNG, *Trans. Faraday Soc.*, **50**, 153 (1954).
3. N. F. MOTT AND N. CABRERA, *Repts. Progr. Phys.*, **12**, 163 (1948-49).
4. D. A. VERMILYEA, *Acta Met.*, **2**, 482 (1954).
5. J. F. DEWALD, *Acta Met.*, **2**, 340 (1954).
6. D. A. VERMILYEA, *Acta Met.*, **3**, 106 (1954).
7. D. A. VERMILYEA, *This Journal*, **101**, 389 (1954).

APPENDIX

A measurement of the true thickness of an oxide film was made by stripping the film from the metal, mounting a very small flake of the film in the electron microscope, turning the flake until it was as nearly as possible parallel to the electron beam as evidenced by the smallest possible shadow on the fluorescent screen, and measuring the width of the resulting shadow. A film which was estimated to be 5000 Å thick by comparison with the optical step gauge was found by the electron microscope method to be 5200 Å ± 250 Å. The agreement is very good, especially when it is considered that the measurement with the electron microscope would tend to be slightly high because of charging of the flake by the electron beam.



Surface Contamination of Copper by Phosphate Ion During Electropolishing—Use of P³²*

N. H. SIMPSON¹ AND NORMAN HACKERMAN

Department of Chemistry, University of Texas, Austin, Texas

In the course of an investigation on surface migration of copper ion on the surface of single crystals of copper it was necessary to electropolish. This was done in a phosphate bath and it was desirable to know whether the surface retained any of the phosphate.

Both single crystal copper and polycrystalline copper specimens were used. Work hardened material was removed by etching in 20% nitric acid and the specimens were then hand polished (holding them with soft paper tissue) with No. 2, 3, and 4 metallographic emery paper in succession. The paper was laid on plate glass. Polishing² was carried out by stroking in a given direction until all markings ran in the same direction. The specimen was then rotated 90° and the process was repeated. Grit particles were removed from the surface, between each type of emery paper used, with soft paper tissue.

After mechanical polishing, a piece of copper wire was wound around the crystal to serve as a means of handling the specimen thereafter. Loose particles were again removed from the surface with soft tissue and the specimen was then rinsed in distilled water, in ethyl alcohol, and in ether to remove both grease and water soluble contaminants. This process was then reversed, with the final rinse in distilled water. All specimens were repolished between experiments.

The specimen was then suspended in a solution made of equal volumes of 85% H₃PO₄ (analytically pure) and distilled water. The solution was pre-electrolyzed between copper electrodes. This "ageing" step was necessary since its omission led to nonuniform polishing and to pitting. Probably the step raises the copper ion activity in solution and this, in turn, increases the dissolution potential enough so that copper dissolves more rapidly on the raised portions of the surface.

* Manuscript received April 15, 1955.

¹ Present address: Chief, Engineering Test Laboratory, Convair, Fort Worth, Texas.

² The method was described in private communication with S. V. Cathcart and P. Smith of the Oak Ridge National Laboratories, Oak Ridge, Tennessee.

The specimen to be polished was made the anode in the solution after treatment as described, and 99.90% copper sheet served as the cathode. Approximately one volt was applied across the cell, and a current of approximately one ampere flowed. The voltage was maintained low enough to prevent formation of gas bubbles on the specimen since

TABLE I. Data from phosphate retention test

Experiment No.	Treatment after electropolishing	Phosphate remaining, calculated as molecular layers
Polycrystalline		
1	Rinsed 5 min in tap H ₂ O, 5 min in dist. H ₂ O, room temperature	0.70
2	Rinsed 6 min 50°C tap H ₂ O, 4 min dist. H ₂ O, room temperature	0.29
Single Crystals		
3	Rinsed 6 min 50°C tap H ₂ O, 4 min in dist. H ₂ O, room temperature	0.14
4	Rinsed 6 min in 19°C tap H ₂ O, 4 min in dist. H ₂ O	1.20
5	Rinsed 10 min room temperature in dist. H ₂ O	1.20
6	Rinsed 6 min in boiling tap H ₂ O, 4 min in boiling dist. H ₂ O	<0.06
7	Rinsed 6 min in boiling tap H ₂ O, 4 min in boiling dist. H ₂ O	0.09
8	Boiling dist. H ₂ O for 10 min	0.35

pits formed beneath them. If bubbles did form the specimen was removed, rewashed, and mechanically repolished before continuing the electropolishing. The proper polishing voltage could be maintained by keeping it within the range where a slight pulsation was apparent. This pulsation may have been caused by a monomolecular build-up of a hydrated

copper phosphate coating followed by its dissolution or sloughing off. The specimen was allowed to polish in this range for approximately 30 min. If conditions were right, an exceedingly high polish was obtained on the surface of the copper.

The amount of phosphate retained was determined by using $\text{H}_3\text{P}^{32}\text{O}_4$.³ After distilling until a silver nitrate test showed no chloride ion the tagged phosphoric acid was diluted with 85% analytically pure H_3PO_4 . Enough of the $\text{H}_3\text{P}^{32}\text{O}_4$ was used to produce a count of approximately $1 \times 10^7/\text{minute}/\mu\text{l}$. This solution was diluted to twice its volume with distilled water and after ageing with copper, as explained above, was used in the electropolishing experiments.

³ Obtained from Oak Ridge National Laboratory, Isotope Division.

Data for both a polycrystalline specimen and a single crystal are given in Table I.

It is apparent that some phosphate was retained even after thorough rinsing. The amount left decreased with increasing temperature of the wash. The effect is noticeably greater for tap water than for distilled water. In fact, the amount left after treatment with boiling tap water (plus distilled water) is not significant, i.e., it is within experimental error. The more complete removal by boiling tap water, as compared to boiling distilled water, may be caused by the pH difference.

It was concluded that since oxidation occurs in the boiling water system, the optimum condition for removal of phosphate from polished copper surfaces is that given by experiment 3 in Table I.

Any discussion of this paper will appear in a Discussion Section to be published in the June 1956 JOURNAL.

The Effect of Alloying Elements in Iron on Hydrogen Overvoltage and Corrosion Rate in Acid Environments¹

MILTON STERN²

Corrosion Laboratory, Massachusetts Institute of Technology, Cambridge, Massachusetts

ABSTRACT

Alloying elements commonly found in steel were added to pure iron to establish their effect on hydrogen overvoltage and corrosion rate in 0.1M citric acid (pH 2.06), 0.1M malic acid (pH 2.24), and 4% sodium chloride at pH 1 and 2. Sulfur, phosphorus, and carbon proved detrimental to corrosion resistance. Copper and manganese were effective in decreasing the detrimental influence of sulfur. Hydrogen overvoltage data are used to explain the particular influences found for various addition elements.

INTRODUCTION

In a previous paper (1) the electrochemical behavior of pure iron in various oxygen-free acid environments was reported. In this investigation, small amounts of various elements were added to pure iron in an effort to establish their effect on both hydrogen overvoltage and corrosion characteristics.

In oxygen-containing neutral solutions, such factors as composition, cold-work, and heat-treatment have little effect on the corrosion rate of iron and steels (2). The reason for this becomes obvious when one considers that the reaction, under these conditions, is cathodically controlled, and the corrosion current is essentially determined by the limiting diffusion current for oxygen reduction. In acid media, however, particularly when oxygen-free, the effect of the above factors may be pronounced. This is true because the metal is under mixed control in such an environment, and the corrosion rate is determined by both the anodic polarization characteristics and the hydrogen overvoltage behavior of the material. At present, there is no reason to believe that the local anodic polarization behavior of a steel is independent of composition. Hoar and Havenhand (3) have reported that local anodic polarization is the most important factor in determining corrosion rates of various steels in acid environments, but their conclusion is not completely supported by the present work. Their tests, unfortunately, were conducted in the presence of oxygen. Although the major anodic reaction is $\text{Fe (metal)} \rightarrow \text{Fe}^{++} + 2 \text{ electrons}$, activation polarization for this anodic reaction could be quite different for different iron base alloys. For example, the site of the reaction should play a significant role, depending on whether dissolution occurs at grain bound-

aries, at specific crystallographic planes, or at various surface imperfections.³ Anodic concentration polarization would probably be about the same for a variety of iron-base alloys and again would be roughly independent of composition and heat-treatment. Cathodic polarization (activation hydrogen overvoltage), on the other hand, should depend on metal structure and composition, and on impurities and depolarizers in solution (5).

It becomes obvious, therefore, that many factors influence the final corrosion rate of iron-base alloys in acids, but that all of these can be resolved into shifts and changes in local cell polarization behavior.

PROCEDURE

Using pure iron, which was the same material reported previously (1), alloys with the following composition were prepared: 0.11% copper, 0.08% silicon, 0.017% phosphorus, 0.02% sulfur, 0.11% manganese, 0.11% carbon, 0.11% manganese with 0.032% sulfur, 0.08% copper with 0.022% sulfur, and 0.10% copper with 0.028% phosphorus.

Alloys were melted in a vacuum induction furnace similar to that illustrated by Seybolt and Burke (6). The furnace was arranged so that additions to the melt could be made by magnetically moving a small pure iron cup containing the alloy addition down a Vycor chute into a pure alumina crucible containing molten iron.

Phosphorus was added as Bureau of Standards ferrophosphorus, while the carbon alloy was made by gas carburizing pure iron and adding a known quantity of the resultant material to molten iron. Other alloy additions were made with the purest elemental materials commercially available.

The 1 lb heats were cast in an iron mold using the stopper-rod bottom-pouring technique. The 1 in.

¹ Manuscript received March 17, 1955. This paper was prepared for delivery before the Pittsburgh Meeting, October 9 to 13, 1955.

² Present address: Metals Research Laboratories, Electro Metallurgical Company, Niagara Falls, New York.

³ Hoar and Holliday (4) present an excellent discussion of the part surface structure plays on iron solution in acid media.

TABLE I. Corrosion rates, corrosion currents, and hydrogen overvoltage constants in 0.1M citric acid (pH 2.06) at 25° C

Alloy	Observed corrosion rate (mdd)	Corrosion potential E_{corr} (overvoltage scale)*	Tafel slope β	Exchange current i_o ($\mu\text{A}/\text{cm}^2$)	Corrosion current	
					i_{corr} ($\mu\text{A}/\text{cm}^2$)	
					Calculated	Observed
Pure Fe	29	-0.172	0.084	9.3×10^{-2}	10.4	11.5
0.11% Cu	41	-0.175	0.081	1.0×10^{-1}	15.0	16.3
0.08% Si	45	-0.185	0.112	3.5×10^{-1}	15.6	18
0.017% P	165	-0.160	0.080	7.0×10^{-1}	70	66
0.11% Mn	18	-0.180	0.085	3.7×10^{-2}	5.0	7.2
0.015% S	706	-0.240	0.066	5.9×10^{-2}	258	282
0.11% C	710	-0.152	0.058	7.4×10^{-1}	310	284
0.11% Mn + 0.032% S	260	-0.225	0.086	2.9×10^{-1}	119	104
0.08% Cu + 0.022% S	32	-0.206	0.061	4.0×10^{-3}	9.6	12.9
0.10% Cu + 0.028% P	376	-0.141	0.021	3.0×10^{-5}	158	150

* Potential difference between alloy and hydrogen electrode in the same solution.

diameter ingots were machined smooth, cold-swaged to $\frac{1}{2}$ in., and cold-rolled to $\frac{3}{16}$ in.⁴ The materials were then annealed 1 hr at 950°C, air-cooled, and machined into appropriate samples.

The procedures and equipment for determining corrosion potential, hydrogen overvoltage, and corrosion rate are the same as those reported previously (1). It is worth re-emphasizing here that, except where otherwise indicated, the data reported are steady-state values often obtained after waiting well over 100 hr.

RESULTS

An earlier paper (1) discussed the cathodic behavior of pure iron in oxygen-free acid media. The role of both activation and concentration polarization was illustrated, and conditions necessary for elimination of concentration polarization were defined. The information which follows was accumulated under conditions where concentration polarization is negligible.

The earlier communication also discussed a method for calculating corrosion rates from electrochemical measurements alone. Briefly, this method is based on the assumption that corroding iron may be considered as a cathodically polarized hydrogen electrode with its own particular hydrogen overvoltage constants. The overvoltage constants and the corrosion potential define the local action current. The equation for local cathodic activation polarization as a function of current density is expressed

$$\eta_a = -\beta \log \frac{i_x + i_{la}}{i_o} \quad (\text{I})$$

where η_a = hydrogen overvoltage (activation), β = constant (slope of the Tafel region), i_x = exter-

nal applied current density, i_{la} = local action current density, i_o = exchange current density.

With no external applied current (when the metal corrodes freely) the equation reduces to

$$E_{\text{corr}} = -\beta \log i_{\text{corr}}/i_o \quad (\text{II})$$

or

$$\log i_{\text{corr}} = \log i_o - E_{\text{corr}}/\beta \quad (\text{III})$$

where i_{corr} = corrosion current density and E_{corr} = corrosion potential on the overvoltage scale, i.e., difference in potential between an iron electrode and a hydrogen electrode in the same solution. (As used here, the potential is given a negative sign.)

Equation (III) reveals that an experimental determination of the corrosion potential, exchange current, and slope in the Tafel overvoltage region permits calculation of the corrosion current, i_{corr} .⁵ Furthermore, equation (III) illustrates how various electrochemical factors affect the corrosion rate. High exchange current values, small β values, and active corrosion potentials contribute toward increasing the corrosion rate. As shown later, no one factor is more important than another in determining the final corrosion rate.

0.1M Citric acid (pH 2.06).—Table I gives corrosion data and overvoltage constants for the experi-

⁵ For materials with very high corrosion rates, considerable current is necessary to polarize the electrode into the Tafel region to obtain β and i_o values. This sometimes gives difficulty from concentration polarization and resistance polarization effects. Where these difficulties were encountered, solutions were stirred with hydrogen gas to eliminate local surface pH increases. The resistance drop effect was corrected by progressively moving the salt bridge probe farther away from the electrode and extrapolating the IR drop thus obtained to zero distance. This procedure was checked by noting whether the resulting corrected data fell on a Tafel plot which is an extension of the straight line obtained in the lower current region where resistance drop is negligible.

⁴ The sulfur and manganese-sulfur alloys were too brittle to roll in this manner. The sulfur alloy was used as-cast, while the manganese-sulfur alloy was swaged to $\frac{3}{4}$ in. and rolled only to $\frac{3}{8}$ in.

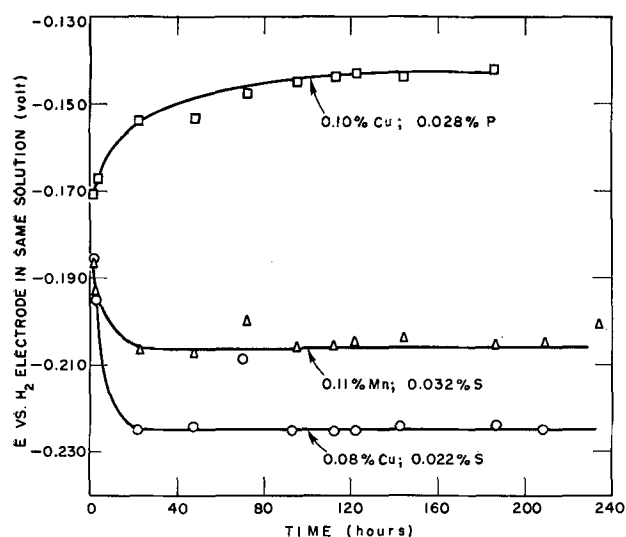


FIG. 1. Typical potential-time relationship for three steels in 0.1M citric acid (pH 2.06).

mental alloys in 0.1M citric acid. Also included is a comparison of corrosion currents calculated in the above manner and corrosion currents determined from actual rate measurements. The corrosion rate expressed in milligrams/square decimeter per day (mdd) is divided by 2.5 to obtain corrosion current in microamperes per square centimeter. It is evident that the electrochemical method appears to give reasonable checks with measured corrosion currents.⁶ Overvoltage constants are markedly different for the various alloys, no one electrochemical factor being most important in influencing the rate.

Although electrochemical data presented in Table I are sufficient to describe the cathodic behavior of the alloys, detailed information for three of the materials is discussed below and may be considered typical. Fig. 1 and 2 illustrate the potential-time and weight loss-time curves for the copper-phosphorus, copper-sulfur, and manganese-sulfur alloys. Many of the alloys appeared to reach a steady corrosion rate after about 10 hr as was the case for the copper-sulfur alloy illustrated. The alloy containing sulfur alone never did quite reach a steady corrosion rate, the value increasing with time for reasons discussed later. The corrosion rate for the sulfur alloy reported in Table I is that determined at the time the cathodic polarization measurement was conducted—235 hr after the specimen was immersed.

Fig. 3 shows the overvoltage curves obtained for the above alloys and is used to illustrate how the various electrochemical factors influence the corro-

⁶ For 22 experiments with corrosion rates between 1 and 100 mdd, the average deviation between the two methods was found to be 12%. However, neglecting four runs with deviations greater than 20%, the average deviation becomes 7.8%.

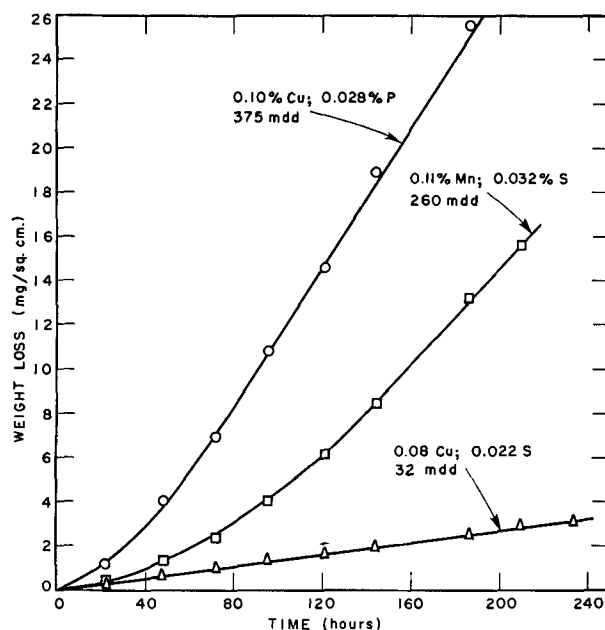


FIG. 2. Typical weight loss-time behavior of three steels in 0.1M citric acid (pH 2.06).

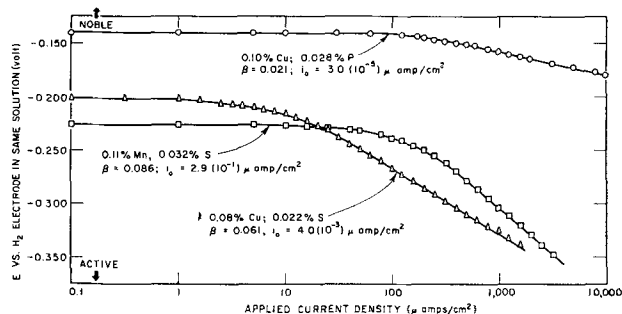


FIG. 3. Typical hydrogen overvoltage curves for three steels in 0.1M citric acid (pH 2.06).

sion rate. It is well known that the corrosion rate is determined by the intersection of a local cathodic and a local anodic polarization curve. With this in mind, it becomes evident that shifting the local cathodic polarization curve to the right results in an intersection of local curves at a higher current value, producing a greater corrosion rate. This process is equivalent to increasing the exchange current, i_0 . Further, if the local cathodic curve is made less steep, a higher corrosion rate results. This is equivalent to decreasing β in equation (I). Finally, a change in local anodic polarization behavior may cause either an increase or a decrease in corrosion rate; a decreased rate corresponds to a shift in corrosion potential in the noble direction, while an increased rate is accompanied by a potential shift in the active direction. Changes in local cathodic polarization behavior (changes in i_0 and β) also affect the corrosion potential, and it becomes quite evident that there is no direct relation between corrosion potential

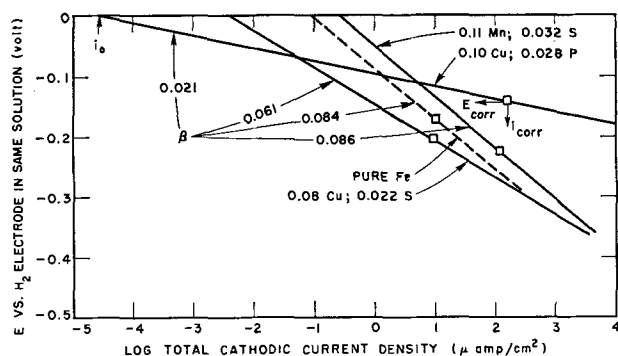


FIG. 4. Local cathodic polarization curves for three steels and pure iron illustrating the influence of the exchange current, i_0 , and the Tafel slope, β , on the corrosion rate in 0.1M citric acid (pH 2.06).

TABLE II. Corrosion rates, corrosion currents, and hydrogen overvoltage constants in 0.1M malic acid (pH 2.24) at 25°C

Alloy	Observed corrosion rate (mdd)	Corrosion potential E_{corr} (over-voltage scale)*	Tafel slope β	Exchange current i_0 ($\mu a/cm^2$)	Corrosion current i_{corr} ($\mu a/cm^2$)	
					Calculated	Observed
Pure Fe	3.0	-0.158	0.083	1.5×10^{-2}	1.2	1.2
0.11% Cu	0.9	-0.163	0.086	3.3×10^{-3}	0.26	0.36
0.08% Si	0.9	-0.176	0.088	2.2×10^{-3}	0.22	0.36
0.017% P	4.8	-0.168	0.097	3.7×10^{-2}	2.0	1.9

* Potential difference between alloy and hydrogen electrode in the same solution.

and corrosion rate for a series of alloys with different local polarization characteristics (Table I).

The overvoltage constants shown on Fig. 3 may be used further to illustrate how β and i_0 affect rates. The copper-phosphorus alloy has an abnormally low exchange current, $3 \times 10^{-5} \mu a/cm^2$. Unfortunately, this advantage is more than compensated by a very low β value, 0.021. The net result is that the corrosion rate is still high. A comparison between the manganese-sulfur and copper-sulfur alloys shows that the manganese-containing material has the advantage of a high β value. However, this is overcome by the low i_0 value of the copper-bearing material so that the corrosion rate for the latter alloy is lower.

Fig. 4 shows the local cathodic polarization curves⁷ for these same alloys along with that of pure

⁷ Throughout the literature, reference is made to the fact that hydrogen overvoltage is a linear function of current at potentials only slightly removed from the reversible hydrogen potential. This is true if one plots overvoltage against applied current. For a hydrogen electrode, applied current is equivalent to the difference between the total rate of reduction of hydrogen ions and the total rate of oxidation of

iron for comparison purposes. These local curves are constructed from the overvoltage data of Table I. Fig. 4 illustrates the various effects β and i_0 have on the rate. The corrosion potentials are also indicated on this figure to illustrate a very important point. If the local anodic polarization curve for all of the alloys shown in Table I were the same, and the only difference between them were hydrogen overvoltage, then this one local anodic curve ought to intersect the various local cathodic curves in such a manner that the resulting corrosion potentials would fall on some smooth curve. This is not the case. The four points plotted in Fig. 4 are sufficient to illustrate this. Had all the data from Table I been put on this figure, it would be even more obvious that the corrosion potential is not a simple function of corrosion rate. Hoar and Havenhand (3) actually reported that various steels corrode at different rates in acids because the local anodic curves are different. Data reported here, however, actually show that both local anodic and cathodic polarization vary for different compositions.

0.1M Malic acid (pH 2.24).—Electrochemical data were obtained for only three of the alloys in 0.1M malic acid. This information is shown in Table II which includes data for pure iron reported previously. With few exceptions, the corrosion rates of the various alloys are considerably less in 0.1M malic acid than in either 0.1M citric acid or 4% sodium chloride at almost comparable pH values. Table II reveals that exchange currents in malic acid are considerably lower than in citric acid. This alone can account for a considerable portion of the rate decrease as explained earlier.

4% Sodium chloride (pH 1 and 2).—Table III gives electrochemical data for three alloys at pH 1 and 2. The alloys do not behave in the same manner as pure iron. The pure material appears to be practically independent of pH . For the alloys, however, both the Tafel slope and the exchange current are functions of pH . Table IV shows how the corrosion rate varies with pH for all of the alloys. No obvious explanation is available for the differences in behavior between pure iron and its alloys. Considerable research in the field of hydrogen overvoltage mechanisms is still necessary to explain such data.

DISCUSSION

The corrosion data of Table IV should be supplemented by some visual observations. The carbon

hydrogen gas. However, when one considers only the total cathodic current—equivalent to the total rate of hydrogen reduction—hydrogen overvoltage and a logarithmic function are so plotted in Fig. 4. A discussion of hydrogen electrode kinetics is given by Bockris (7).

TABLE III. Corrosion rates, corrosion currents, and hydrogen overvoltage constants in 4% sodium chloride at pH 1 and 2

Alloy	Observed corrosion rate (mdd)	Corrosion potential E_{corr} (overvoltage scale)*	Tafel slope β	Exchange current i_0 ($\mu\text{a}/\text{cm}^2$)	Corrosion current i_{corr} ($\mu\text{a}/\text{cm}^2$)	
					Calculated	Observed
pH 1						
Pure Fe	30	-0.203	0.100	1.0×10^{-1}	10.5	11.1
0.11% Cu	390	-0.230	0.084	2.8×10^{-1}	154	156
0.08% Si	725	-0.230	0.089	6.7×10^{-1}	270	290
0.017% P	1000	-0.190	0.068	6.3×10^{-1}	390	400
pH 2						
Pure Fe	30	-0.201	0.100	1.1×10^{-1}	11	11.3
0.11% Cu	98	-0.233	0.093	1.3×10^{-1}	42	39
0.08% Si	89	-0.230	0.090	7.1×10^{-2}	28	36
0.017% P	480	-0.175	0.084	1.8	220	192

* Potential difference between alloy and hydrogen electrode in the same solution.

TABLE IV. Corrosion rates of various alloys in oxygen-free acids at 25°C

Alloy	NaCl pH 1	NaCl pH 2	0.1M Citric pH 2.06	0.1M Malic pH 2.24
Pure Fe	30	30	29	3.0
0.11% Cu	390	98	41	0.9
0.08% Si	725	89	45	0.9
0.017% P	1000	480	165	4.8
0.11% Mn	115	41	18	14.1
0.015% S	2830	244	706	151
0.11% C	562	220	710	488
0.11% Mn + 0.032% S	222	142	260	6.2
0.08% Cu + 0.022% S	186	162	32	168
0.10% Cu + 0.028% P	606	394	376	339

alloy corrodes by pitting; the sulfur alloy corrodes both intergranularly and at grain centers by pitting; and the samples of manganese-sulfur alloy pitted in 4 or 5 spots in all the environments except malic acid. The mechanical properties and the pitting tendency of this latter alloy indicate that all the sulfur was not completely combined with manganese. The copper alloy builds up a surface deposit of copper in sodium chloride solutions, while the phosphorus-containing materials corrode with a resultant black granular surface precipitate which was not identified. This black coating is not magnetite and was unstable when exposed to oxygen-containing distilled water, slowly turning to a white flocculent precipitate with traces of brown ferric hydroxide.

These results confirm earlier reports (3, 8, 9) on the detrimental effect that both phosphorus and sulfur have on corrosion rates in acids. Although early investigators unfortunately disregarded the important influence of oxygen in acid environments, their data still showed clearly the beneficial effect of copper in sulfur-bearing materials.

The overvoltage constants give some insight into

why these elements affect the rate as they do. Phosphorus alone increases the exchange current. Sulfur functions by decreasing the Tafel slope, by changing the local anodic polarization characteristics, and by changing the anode to cathode area ratio. (This alloy pits.) Copper eliminates the detrimental effect of sulfur by lowering the exchange current. Both the sulfur and carbon alloys have two-phase structures which partly explains their pitting tendencies. Hoar (3) has reported that massive cementite is detrimental to acid corrosion resistance.

The effect of cation differences probably resides partly in their ability to complex iron and the added alloying elements. However, the significant differences in overvoltage constants for the same material in different environments indicates the cations or undissociated acid molecules play some role in the hydrogen reduction reaction.

In general, study of the various electrochemical constants shows the complex way in which the alloying elements affect overvoltage factors. Since only one composition of each alloy has been investigated and the interactions between various elements have not been fully explored, these data cannot be justifiably extrapolated to compositional effects in mild steel with normal quantities of foreign elements. Considerable additional information concerning the effects of various amounts of alloying elements and interactions between elements is important. Also, a study of the significance of hydrogen overvoltage measurements on a two-phase structure would be very helpful in interpreting data obtained on such complex metal surfaces.

ACKNOWLEDGMENT

This program was supported by a Postdoctoral Fellowship established by the Weirton Steel Company. The discussions and guidance of Professor H.

H. Uhlig were invaluable throughout the course of the work.

Any discussion of this paper will appear in a Discussion Section to be published in the June 1956 JOURNAL.

REFERENCES

1. M. STERN, *This Journal*, **102**, 609 (1955).
2. H. H. UHLIG, *Corrosion*, **5**, 169 (1949).
3. T. P. HOAR AND D. HAVENHAND, *J. Iron Steel Inst.*, **133**, 239P (1936).
4. T. P. HOAR AND R. D. HOLLIDAY, *J. Appl. Chem.*, **3**, 502 (1953).
5. J. O'M. BOCKRIS, "Electrical Phenomena at Interfaces," p. 155, The MacMillan Company, New York (1951).
6. A. U. SEYBOLT AND J. E. BURKE, "Experimental Metallurgy," p. 182, J. Wiley and Sons, New York (1953).
7. J. O'M. BOCKRIS, National Bureau of Standards Circular 524, p. 243 (1951).
8. C. A. EDWARDS, D. L. PHILLIPS, AND D. F. THOMAS, *J. Iron Steel Inst.*, **137**, 223P (1938).
9. J. E. STEAD, *ibid.*, **94**, 5 (1916).

An Electronic Self-Balancing Zero-Resistance Ammeter¹

DONALD R. MAKAR AND HOWARD T. FRANCIS

Armour Research Foundation of Illinois Institute of Technology, Chicago, Illinois

ABSTRACT

A relatively simple electronic device is described which permits continuous observation of the short-circuit current flowing in a galvanic corrosion cell. The device is particularly useful for measuring currents from low-resistance cells, where the internal resistance of a micro- or milliammeter would be excessive. The corrosion cell current is automatically held at that value which maintains the cell voltage at $0 \pm 0.00005\text{v}$ ($50 \mu\text{v}$).

INTRODUCTION

Measurement of short-circuit currents in galvanic corrosion cells has always posed a problem, since use of a series meter always introduces some additional resistance in the metallic circuit. This difficulty is not serious in high-resistance cells, since the additional resistance of a current meter is usually sufficiently low to be negligible. In low-resistance cells, however, introduction of a milliammeter or microammeter is frequently impractical.

The usual solution to this problem is the use of a so-called "zero-resistance" ammeter. The principle of the device has been presented by Brown and Mears (1). More recently, Godard (2) described a self-balancing zero-resistance ammeter which employed a relay-controlled, motor-driven potentiometric circuit, so arranged that the cell current was maintained at that value which produced zero voltage at the electrode terminals. Thus, IR drop in the entire metallic circuit was compensated exactly by an external voltage source.

The device to be described operates on the same basic principle as any zero resistance ammeter, but is felt to be considerably simpler than Godard's while retaining all the advantages of automatic balancing. In addition, the voltage-sensing system placed across the galvanic cell has a much higher input resistance than the sensitive relay used in Godard's meter. Thus, even high-resistance cells can be handled with no sacrifice of sensitivity at the balance point.

DESCRIPTION OF APPARATUS

Fig. 1 shows the basic circuit of a zero-resistance ammeter. To simulate short-circuit conditions, the current flow is adjusted to that value which produces zero voltage at the cell terminals. Such adjustment may be made by variation of R or of E . Godard's device operates by automatic adjustment of R ; the device described herein operates by adjustment of E .

Fig. 2 shows the complete circuit diagram of the electronic zero-resistance ammeter. The basic cell circuit is at the lower left, and consists of a multi-

range ammeter (with a reversing switch), resistors R_1 and R_2 , and terminals for an external recording meter (shorted when not in use), all connected in series. The voltage across R_1 is arranged to oppose the corrosion cell, while the voltage appearing across R_2 augments the cell. The remaining circuits are (a) a three-stage amplifier (top), (b) a phase detector (5963) which operates the relay, (c) parallel 6AK6's (bottom center) whose cathode resistor is R_2 , and (d) a conventional power supply (lower right).

The operation of the device is as follows. When the current passing through the cell is such that the cell voltage is not zero, the 60-cycle chopper puts a pulsed signal on the grid of the first amplifier stage. This signal is amplified and applied to the grids of the 5963 phase detector. Depending on the polarity of the cell voltage, the signal will cause one or the other of the 5963 triode sections to conduct more heavily, depending on the phase relation between the signal and the a-c plate voltage. It should be noted that the voltages supplied to the two plates are 180° out of phase.

Depending on which triode conducts, a voltage is produced between the cathodes which moves the relay arm to the left or to the right. If it moves to the left, the control grids of the parallel 6AK6's are made more negative (toward cutoff); if it moves to the right, the grids are brought toward ground potential (increasing the tube current). As the 6AK6 plate current changes, the voltage drop across the cathode resistor (R_2) varies accordingly, thus increasing or decreasing the corrosion cell current, whichever is required to bring the cell voltage toward zero.

The amplifier gain is such that the device will hold the cell voltage at $0 \pm 0.00005\text{ v}$ and will accommodate cell currents up to 20 ma.

Certain features of the circuit justify further comment. In order to compensate for the phase shift inherent in the chopper, its coil is placed in series with the 28 mfd condenser shown. This value was determined experimentally and was selected to make the point of switching coincide with the zero-voltage point in the 60 cycle a-c supply, thus providing maximum sensitivity in the phase detector.

¹ Manuscript received March 23, 1955.

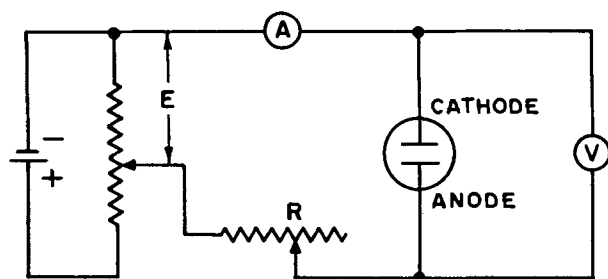


FIG. 1. Elementary zero-resistance ammeter

The 6.8 M and 10 M resistors in the grid circuit of the 6AK6's are not critical, but were selected to give reasonable rates of charge and discharge of the 1 mfd condenser. Smaller values of resistance would give a more rapid approach to the balance point, but would cause relay oscillation.

The purpose of the resistor R_1 and its associated circuit is to provide a fixed d-c voltage against which the 6AK6 cathode resistor can operate when only a very small voltage is required to drive the corrosion cell. Thus, the 6AK6 tubes always operate well above zero plate current, regardless of the actual corrosion current. This feature has the added advantage that cells whose polarity may reverse during a test can be observed continuously.

Resistors R_3 and R_4 in the cathode circuit of the 5963 are coarse and fine controls, respectively, for centering the relay position to correspond to zero corrosion cell voltage. Once set, no further adjustment is necessary.

The diodes of the 6AV6 amplifier tubes are unused; this tube was selected for the high amplification factor of its triode section. Type 12AX7 (dual triodes) should be equally satisfactory.

The chopper is a Model A-175, manufactured by the Airpax Products Company, which mounts in a 7-pin miniature socket. Its coil is operated from the 6.3 v heater supply.

The relay is a Model 534, manufactured by the

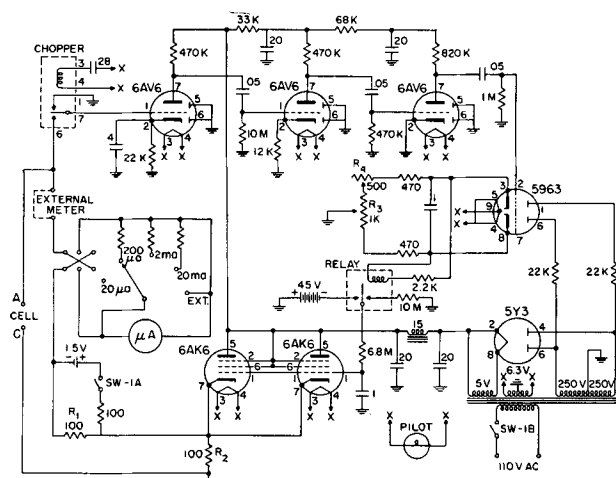


FIG. 2. Electronic self-balancing zero-resistance ammeter.

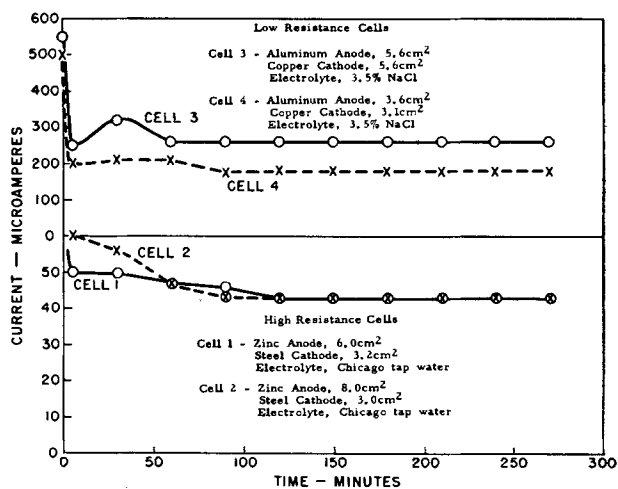


FIG. 3. Current flow in typical high- and low-resistance cells.

Weston Electrical Instrument Corporation; it has a sensitivity of $-7.5 \mu\text{a} - +7.5 \mu\text{a}$, with a coil resistance of 1100 ohms.

The microammeter is a Triplet 321-T, with a range of $0-20 \mu\text{a}$ and a resistance of 2050 ohms. The range is extended by selection of the appropriate shunt resistor, as shown in Fig. 2. When an external recording meter is used, the internal meter may be shorted to minimize the total resistance of the cell circuit, if necessary. The exact values of the shunt resistors should be determined experimentally to insure accurate calibration of each current range.

TYPICAL DATA

To illustrate the operation of the device, a number of corrosion cells were made up and their current-time curves prepared. The results, together with the cell descriptions, are shown in Fig. 3.

While the range of currents embraced by the instrument could be extended above 20 ma if desired, this range seems adequate for most laboratory scale work.

Since most corrosion couples have open-circuit potentials in the order of many millivolts, the $50 \mu\text{v}$ sensitivity of the balancing circuit assures negligible departure from short-circuit conditions.

ACKNOWLEDGMENT

The work described above was a part of a project on Stress Corrosion of Aircraft Alloys, carried out at Armour Research Foundation under the sponsorship of the National Advisory Committee for Aeronautics. The authors thank the Committee for its support and for permission to publish this article.

Any discussion of this paper will appear in a Discussion Section to be published in the June 1956 JOURNAL.

REFERENCES

1. R. H. BROWN AND R. B. MEARS, *Trans. Electrochem. Soc.*, **74**, 510 (1938).
2. H. P. GODARD, *Corrosion*, **7**, 93 (March 1951).

Factors Affecting the Formation of Anodic Oxide Coatings in Sulfuric Acid Electrolytes¹

RALPH B. MASON

Aluminum Research Laboratories, New Kensington, Pennsylvania

ABSTRACT

The amount of sulfate found in anodic coatings formed on pure aluminum anodes in sulfuric acid electrolytes increased as the current density and concentration of acid increased, but decreased as the temperature was raised. Chemical analysis showed that the coatings consisted substantially of Al_2O_3 and SO_3 with practically no water.

Factors affecting solubility of the coatings, such as heat developed within the coating, and time of immersion, were investigated. Rapid changes in current and voltage, which occurred in the first 15 sec after application of current, gave certain clues as to the possible mechanism of pore formation.

INTRODUCTION

In a paper by Norden (1) published only a few years after electrolytic aluminum became available in commercial quantities, the composition of sulfuric acid anodic coatings and the efficiency of the over-all electrochemical reaction were discussed. While some of the conclusions of that work are now considered to be in error, it was indicated even then that the oxide coatings formed in dilute sulfuric acid electrolytes contain about 13% SO_3 as determined by classical analytical methods.

Most investigators have recognized the presence of appreciable amounts of sulfate in anodic coatings formed in the sulfuric acid electrolytes. One aim of this paper is to show that the sulfate is an important minor constituent of the sulfuric acid anodic coating, and that the coating composition can be changed by varying the electrochemical conditions of formation.

Heat generated in an aluminum anode during coating, especially at high current densities, and the rapid changes in voltage and current which take place when the current is first applied to a clean aluminum anode in a sulfuric acid electrolyte were also investigated.

EXPERIMENTAL

Composition of Coatings

Specimens of 1095 aluminum, which had been pre-anodized in sulfuric acid, stripped in phosphoric-chromic acid, and weighed, were anodically coated in 15% sulfuric acid under varying conditions of time, current density, and temperature. They were then dried, weighed, and the coating removed in 50

ml of phosphoric-chromic acid stripping solution (2, 3). The water used to rinse each specimen was added to the stripping solution which was then diluted to exactly 100 ml. By weighing the specimens after stripping, it was possible to obtain by subtraction the exact weight of coating dissolved in the solution. Al_2O_3 and SO_3 were precisely determined in the same stripping solution containing an accurately known weight of coating.²

Conditions of forming the anodic oxide coatings, as well as the results of the analytical determinations, are shown in Table I. In the case of the 10-min coatings, three individual specimens were prepared and the oxide coatings removed in the same 50 ml of stripping solution. The 100 panels with the 5-sec coatings were formed individually and were weighed 10 at a time, but were all stripped in a single portion (50 ml) of stripping solution. It was necessary to concentrate the wash water by evaporation before adding to the stripping solution and diluting to 100 ml. For the control sample (or analysis blank), a volume of distilled water equal to the wash water was evaporated to slightly less than 50 ml and added to the stripping solution before diluting to the final 100 ml.

The Al_2O_3 and SO_3 content of the anodic oxide coatings prepared in 15% sulfuric acid at 70°, 50°, or 34°F (21.1°, 10.0°, or 1.1°C) accounted for practically the total coating weight. This meant that there could be little water present, at the most about 1%. Some coatings prepared at 50°F (10°C) were not dried at 105°C before stripping; consequently, they may have contained a small amount

² The chromium was removed from an aliquot portion of the stripping solution in a mercury cathode cell before determining the aluminum. The sulfate was determined in the usual way from another portion of the stripping solution after reducing the chromate with alcohol.

¹ Manuscript received March 19, 1955. This paper was prepared for delivery before the Pittsburgh Meeting, October 9 to 13, 1955.

TABLE I. Composition of anodic oxide coatings on pure aluminum (1095)

C.D.		Range volts	Time	No. panels	Panel area cm ²	Temperature		Total wt. coating g	Al ₂ O ₃ %	SO ₃ %	Total %
Amp/ dm ²	Amp/ ft ²					°C	°F				
1.3	12	23-23	30 Min.	1	77.4	1.1	34	0.2751	84.3	15.0	99.3
2.6	24	24-25	30 Min.	1	38.7	1.1	34	0.2834	84.4	15.9	100.3
3.9	36	25-27	30 Min.	1	25.8	1.1	34	0.2869	84.0	16.4	100.4
5.2	48	26-32	30 Min.	1	19.4	1.1	34	0.2946	83.3	16.8	100.1
7.8	72	27-42	30 Min.	1	12.9	1.1	34	0.3188	83.3	17.1	100.4
1.3	12		5.0 Sec.	100	77.4	10.0	50	0.0897*	88.6	13.9	102.5
1.3	12	20-20	10 Min.	3	77.4	10.0	50	0.2642*	86.0	13.7	99.7
1.3	12	20-20	10 Min.	1	77.4	10.0	50	0.0873*	85.3	13.6	98.9
1.3	12	20-20	30 Min.	1	77.4	10.0	50	0.2630*	85.3	14.1	99.4
1.3	12	20-20	30 Min.	1	77.4	10.0	50	0.2621	85.3	13.7	99.0
1.3	12	20-21	60 Min.	1	38.7	10.0	50	0.2625*	84.9	14.0	98.9
2.6	24	21-21	10 Min.	3	38.7	10.0	50	0.2741*	84.4	15.0	99.4
2.6	24	21-23	30 Min.	1	38.7	10.0	50	0.2727*	84.3	14.8	99.1
3.9	36	22-24	30 Min.	1	38.7	10.0	50	0.2769	84.0	15.3	99.3
5.2	48	23-23	10 Min.	3	19.4	10.0	50	0.2824*	83.4	15.9	99.3
5.2	48	23-27	30 Min.	1	19.4	10.0	50	0.2825*	83.9	15.9	99.8
7.8	72	24-26	10 Min.	3	12.9	10.0	50	0.2858	83.4	16.4	99.8
7.8	72	24-33	30 Min.	1	12.9	10.0	50	0.2968	82.5	16.8	99.3
7.8	72	23-37	30 Min.	1	12.9	10.0	50	0.2947	82.3	16.6	98.9
1.3	12	16-16	30 Min.	1	77.4	21.1	70	0.2395	86.1	12.4	98.5
2.6	24	19-20	30 Min.	1	38.7	21.1	70	0.2522	84.9	14.0	98.9
3.9	36	21-23	30 Min.	1	25.8	21.1	70	0.2596	84.7	14.8	99.5
5.2	48	21-23	30 Min.	1	19.4	21.1	70	0.2628	84.0	15.1	99.1
7.8	72	22-29	30 Min.	1	12.9	21.1	70	0.2712	83.3	16.0	99.3

Note: Electrolyte = 15% H₂SO₄.

* Coating not dried at 105°C before weighing and stripping.

of water sorbed on the surface. Oxide coatings prepared in sulfuric acid when only air dried contained a surprisingly small amount of water. Small analytical errors in the Al₂O₃ and SO₃ contents of the coatings formed at 34°F (1.1°C) are indicated, since the combined weights are slightly over 100%. The weight of aluminum reacting was no greater than

that demanded by Faraday's law, and the possibility of suboxide formation was considered. However, there was no reduction of the chromic acid in the stripping solutions that could be detected by the usual analytical methods.

Under corresponding conditions, the SO₃ content was higher at 34°F (1.1°C) than at 50° or 70°F (10° or 21.1°C). At a given current density, the percentage of SO₃ remained fairly constant as the thickness or weight of coating increased with time of treatment. When a higher current density was employed the SO₃ content rose.

Values for the 30-min coatings in Table I were plotted in Fig. 1 to show the uniform increase in SO₃ content with current density increase. Under corresponding conditions of current density, there was about 1.0% more SO₃ in the coatings produced at 34°F (1.1°C) than in those formed at 50°F (10°C).

Since the major constituents of the anodic coating formed in sulfuric acid on 1095 aluminum were (by chemical analysis) Al₂O₃ and SO₃, the weight ratio of Al₂O₃ to SO₃ was plotted against current density in Fig. 2. This type of plot minimized any error introduced by water sorbed on the oxide surface. At a weight ratio of 5.1 the composition corresponded to

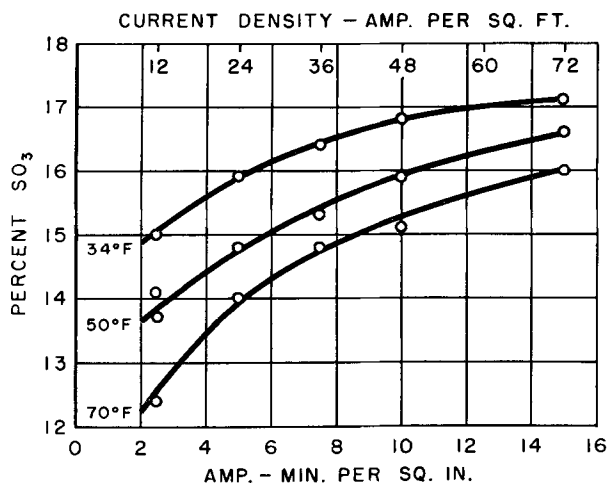


FIG. 1. Variation of SO₃ content with current density and temperature.

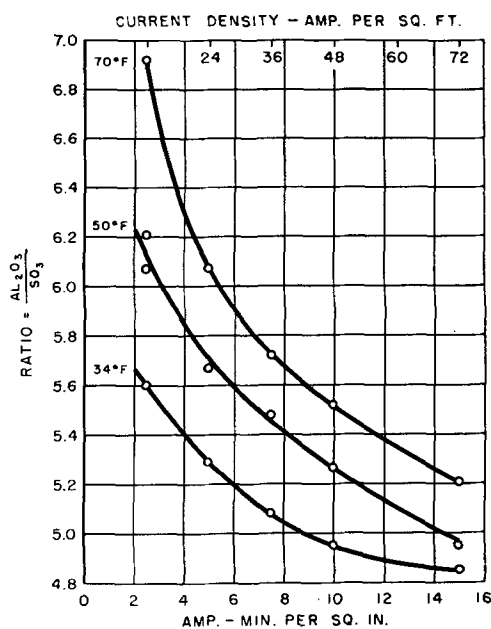


FIG. 2. Variation of the $\text{Al}_2\text{O}_3:\text{SO}_3$ ratio with current density and temperature.

$4\text{Al}_2\text{O}_3 \cdot \text{SO}_3$ or $\text{Al}_2(\text{SO}_4)_3 \cdot 11\text{Al}_2\text{O}_3$. However, the coating composition varied with the conditions of formation, and in most cases simple molecular formulas could not be assigned.

In Fig. 1 and 2, it should be pointed out that as the current density doubled, the thickness of the coating also approximately doubled. If the data for the coatings at 50°F other than the 30-min coatings in Table I were plotted in curve 1 according to the current densities employed, it would be found that the points would fall on or very near the curve already drawn. Therefore, it is concluded that current density and not thickness of coating controlled the SO_3 content of anodic coatings formed in sulfuric acid at a given temperature.

Oxide coatings formed on 1095 aluminum in 25% sulfuric acid at 50°F (10°C) had an appreciably higher SO_3 content than those formed in the 15% sulfuric acid. If plotted as the data of Fig. 1, the curve would lie slightly above the one for 34°F (1.1°C). In the case of coatings formed in an electrolyte of 12% sulfuric acid + 1% oxalic acid at 50°F (10°C), the SO_3 content was practically the same as that found for the 15% sulfuric acid electrolyte, but the coatings also contained about 0.2 to 0.4% oxalic acid. The higher value was obtained at the lowest current density, 12 amp/ft² (1.3 amp/dm²).

The sulfate incorporated in the oxide coating could not be removed by boiling in water or by the more drastic electroendosmosis treatment to an extent of more than about 2% of the total sulfate present. Only the sulfate actually exposed on the surface could be fixed as barium sulfate, and this

TABLE II. Heat effects at the aluminum anode

Current density		Temperature rise			
		With agitation		Without agitation	
		°F	°C	°F	°C
amp/ft ²	amp/dm ²				
12	1.3	1.8	1.0	9.5	5.3
24	2.6	3.8	2.1	17.1	9.5
48	5.2	8.2	4.5	27.5	15.3

again amounted to only 2% of the total amount present.

The sulfate content was a distinctive component of anodic coatings formed in sulfuric acid electrolytes.

Heat Effects

In order to show that considerable heat developed in certain cases at the oxide-aluminum interface, a copper-constantan thermocouple was placed between two pieces of aluminum foil (1050) which were then cemented together. The cold junction of the thermocouple was placed in the 15% sulfuric acid bath at 50°F (10°C). Current was applied and a temperature reading made as soon as the voltage and current were constant. Temperature readings were made when there was good agitation of the electrolyte and when there was no agitation. Table II shows that, as the current density doubled, the temperature rise was about twice as great. It was also very evident that rapid agitation of the electrolyte was necessary for more effective removal of heat through the oxide surface.

As the time of anodic treatment at constant current increased, the voltage also rose, especially when high current densities were used. Two series of measurements are recorded in Table III to show how the temperature of the aluminum anode in these partic-

TABLE III. Increase in temperature with time of treatment

Current density		Time, min	Cell volts	Temperature rise	
				°F	°C
amp/ft ²	amp/dm ²				
48	5.2	1.5	24.0	7.9	4.4
		5	25.0	8.3	4.6
		10	26.0	8.5	4.7
		15	27.5	9.2	5.1
		20	30.0	10.7	5.9
72	7.8	1	25.0	8.6	4.8
		5	26.5	9.2	5.1
		11	33.0	11.8	6.5
		15	40.0	14.7	8.2
		20	48.5	18.1	10.1
		25	57.0	21.3	11.8
		30	68.5	27.4	15.2
		35	83.5	33.1	18.4
		40	110.0	42.9	23.8

ular experiments varied at constant current with time of treatment and voltage in the 15% sulfuric acid electrolyte at 50°F (10°C) with good agitation.

Results given in Table III show why it is impractical to treat a thin specimen, especially of 1050 metal, for a long time at a high current density even though good agitation of the electrolyte is used. Heat is developed very rapidly in the oxide coating and it can be removed only slowly by the electrolyte. Metallic aluminum is a good conductor of heat, and diffusion of heat takes place rapidly within the aluminum. By using a heavier gauge aluminum sheet as anode, the temperature within the oxide coating can be reduced. Some investigators have recommended internal cooling, but in many cases this is not a practical solution to the problem. If only a small area of a larger piece of aluminum is to be coated at 50°F (10°C), a resist can be used on the parts not to be coated, but the whole specimen should be immersed in the bath. If the part is exposed to the air at 70°F (21.1°C), heat will be carried into the specimen from without. The use of extra heavy insulated aluminum contacts or fins aids in the removal of heat from within the specimen.

Variations of Current and Voltage with Time

Although there are numerous references (4, 5) in the literature on oxide coatings showing the rapid changes in current and voltage which take place when a potential is applied to an aluminum anode immersed in a sulfuric acid bath, this work was repeated using the coating conditions employed for this paper.

Specimens of 1095 aluminum sheet, having the correct area to give the desired current density with 1 amp of current flowing, were suspended by tanta-

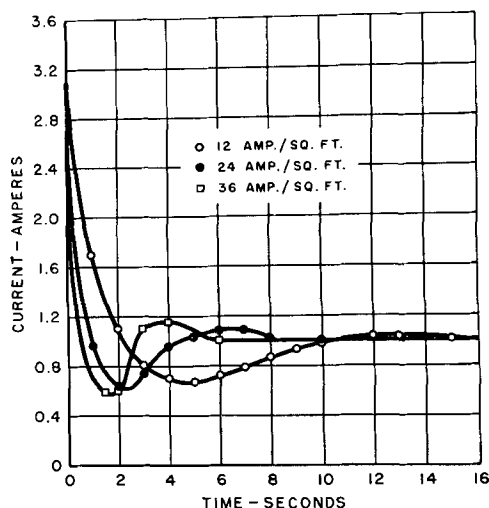


FIG. 3. Changes in current with time at the beginning of anodic oxidation. Current density values are for the steady state.

TABLE IV. Variation of maximum and minimum voltages with current density

Current density		Volts		
		Maximum	Minimum	Constant
amp/ft ²	amp/dm ²			
12	1.3	22.1 at 5 sec.	19.6 at 12 sec.	20.1
24	2.6	23.4 at 2-3 sec.	21.4 at 6 sec.	21.7
36	3.9	24.5 at 1-2 sec.	22.2 at 4+ sec.	22.5

Electrolyte temperature—50°F (10°C).

lum clips midway between two lead cathodes in the vigorously stirred bath of 15% sulfuric acid at 50°F (10°C). A potentiometer across a bank of storage batteries was adjusted to give a final steady current of exactly 1 amp with a test specimen. A freshly cleaned specimen was then placed in the bath and the current applied. Readings were made at 1-sec intervals. About 10 freshly cleaned specimens were required for each curve, since only two or three points could be determined on one specimen. The average results of the current measurements were plotted against time in Fig. 3.

At the instant a potential was applied to a specimen, tested as above, there was a surge of current of about 3.3 amp. The current rapidly decreased to a minimum value of about 0.6 to 0.7 amp, the time required to reach the minimum value being dependent on the current density at the steady state. The current rapidly increased to a second maximum slightly greater than 1 amp and then fell to the steady current of 1 amp for which the potentiometer was originally set. The heights of the second maximum appear to be proportional to the current density. If agitation of the electrolyte was not used, the first portion of the curve was approximately the same, but the second maximum and the final steady current were higher.

When voltage readings were made as above, the voltage quickly reached a maximum corresponding to the time of the minimum current value and quickly decreased to a minimum voltage at the point where the current reaches the second maximum. The voltage then increased to a steady value corresponding to the steady current state.

The maximum and minimum voltages obtained for the aluminum-lead cell were recorded in Table IV.

The first portion of the 12 amp/ft² curve of Fig. 3, where the current decreased rapidly while the voltage rose, represented the formation of a fairly uniform film of increasing thickness and resistance. At this stage, the efficiency of oxide formation was less than 100% by the amount of oxide dissolved uniformly from the exposed outer surface by the sulfuric acid electrolyte. After about 4-5 sec the

formation of definite pores (4) started and continued with some adjustments in distribution until the steady state was reached in about 15 sec. At higher current densities the steady state was reached more rapidly and so the times given here are only relative, being dependent on the particular current source and potentiometer used.

The oxide coating composition was dependent on the current density, temperature, and composition of the electrolyte. The coating composition did not appreciably change after the initial 5 sec, provided the current density and temperature remained constant (see Table I).

After the pore pattern has been established, the solution of the oxide coating by the sulfuric acid is believed to be concentrated at the bottom of the pores, which all together represent an area of about one-ninth the apparent surface.³ Because of the concentration of the sulfuric acid attack, the oxide at the bottom of the pores should be dissolved at a much more rapid rate—up to 9 times as fast. Part of the increased rate of solution at the bottom of the pores is believed to be the result of an increase in temperature. A more important factor may well be the more rapid solution rate of the electrolyte caused by discharged SO_4 ions or the products of this action. Regardless of the exact mechanism, the rate of solution of oxide at the bottom of the pores approximately equals the rate of oxide formation and the pore remains extending practically through the oxide coating. The outer portion of the coating, after the pore pattern is once established, is subjected only to the chemical solution action of the sulfuric acid at the average bath temperature. The efficiency of over-all oxide formation is always less than 100% by the amount of oxide dissolved in forming the pores and the small amount of oxide dissolved from the outer surface by chemical solu-

³ The pore volume of a coating made under the above conditions is about 11%.

tion action of the sulfuric acid at the average bath temperature.

SUMMARY

Oxide coatings formed in sulfuric acid were practically anhydrous but always contained an appreciable amount of combined sulfur. The composition of the coating may be represented as $\text{Al}_2\text{O}_3 \cdot X\text{SO}_3$ where X varies from about 0.18 to 0.26 depending on the conditions of formation.

Considerable heat was developed at the base of the pores, especially when high current densities were used. Unless this heat was removed rapidly through the oxide coating by suitable agitation of the electrolyte or by other means, the coating is dissolved at a more rapid rate.

The rapid changes in current and voltage that took place as the current was applied to an aluminum anode in sulfuric acid can be used to explain certain problems in regard to pore formation and the rapid solution of the anodic coating at the base of the pores.

ACKNOWLEDGMENT

Acknowledgment is made to Mr. Richard Unangst of the Aluminum Research Laboratories for his careful and painstaking analysis of the oxide coatings and to Miss Phyllis Fowle for the preparation of many of the specimens.

Any discussion of this paper will appear in a Discussion Section to be published in the June 1956 JOURNAL.

REFERENCES

1. K. NORDEN, *Z. Elektrochem.*, **6**, 159, 188 (1899).
2. J. D. EDWARDS, *Am. Soc. Testing Materials, Proc.*, **40**, 959 (1940).
3. R. B. MASON AND C. J. SLUNDER, *Ind. Eng. Chem.*, **39**, 1602 (1947).
4. W. BAUMANN, *Z. Physik*, **111**, 708 (1939).
5. V. H. WILSDORF, *Z. angew. Physik*, **2**, 17 (1950).

Modified Calcium Pyrophosphate Phosphors¹

D. E. KINNEY

Chemical Products Plant, Lamp Division, General Electric Company, Cleveland, Ohio

ABSTRACT

The preparation and optical properties of $(\text{Ca}, \text{Na}_2)_2\text{P}_2\text{O}_7:\text{Sb}$ and $(\text{Ca}, \text{Na}_2)_2\text{P}_2\text{O}_7:\text{Sb}:\text{Mn}$ phosphors are described. The partial substitution of sodium for calcium has been found to increase markedly the efficiency of the luminescent emission. The enhancement of luminescence as a result of this modification is attributed to compensation of valence: Sb^{+3} and Na^{+1} compensating for two Ca^{+2} in the lattice. The doubly activated phosphor provides an example of "sensitized luminescence." $(\text{Ca}, \text{Na}_2)_2\text{P}_2\text{O}_7:\text{Sb}$ fluoresces in the deep blue. The observed fluorescence of $(\text{Ca}, \text{Na}_2)_2\text{P}_2\text{O}_7:\text{Sb}:\text{Mn}$ may vary between blue-white and pink-white depending upon the manganese concentration.

INTRODUCTION

In recent years phosphors having an alkaline earth phosphate matrix have received considerable attention in the literature. Butler (1) described calcium orthophosphate activated by tin alone or by tin and manganese in combination. The study also included mixed orthophosphates of other alkaline earth elements. Froelich and Margolis (2) reported in detail on calcium orthophosphate doubly activated by cerium and manganese, and Froelich (3) studied magnesium pyrophosphate activated by combinations of cerium, thorium, and manganese. In the former case, sodium was found to enhance thermal stability; it did not contribute directly toward increased efficiency. Strontium orthophosphate activated by tin and manganese has been investigated by Botden (4). McKeag and Ranby (5) described calcium pyrophosphate activated by antimony, samarium, tin, or manganese, and Henderson and Ranby (6) developed an unusual phosphor, barium pyrophosphate activated by titanium in high concentrations. Huniger and Panke (7) surveyed a host of phosphate phosphors approximating metaphosphate proportions.

This paper describes the unusual effects obtained by the substitution of sodium for a minor portion of the calcium in calcium pyrophosphate phosphors activated by antimony alone or by antimony and manganese in combination.

PHOSPHOR PREPARATION AND COMPOSITION

Efficient $(\text{Ca}, \text{Na}_2)_2\text{P}_2\text{O}_7$ phosphors are conventionally prepared by a solid-state reaction involving firing an intimate mixture of (a) calcium monohydrogen phosphate (or the pyrophosphate), (b) a sodium compound such as the carbonate or a halide,

(c) the activator compounds, and (d) enough ammonium phosphate to slightly more than compensate, on a molar basis, for the added sodium and activator ions. Treating a suspension of calcium and sodium carbonates and the activator compounds with phosphoric acid, drying and then firing the entire mass produces equally efficient phosphors.

Firing is carried out in an electrically heated furnace in open, fused silica trays. Generally, temperatures of from 850° to 875°C are employed, but the sodium concentration in the batch material governs the exact temperature: relatively high sodium requires relatively lower temperatures to avoid sintered products. The phosphors are white in body color with the exception that extremely high manganese concentrations produce a slightly pink powder.

Raw materials of at least reagent quality were used throughout the investigation. Calcium pyrophosphate phosphors appear to be comparable to the calcium halophosphates in sensitivity to the common "killer" impurities. The activators were generally introduced as Sb_2O_3 and MnCO_3 , although any oxide-producing compound will serve, with the reservation that the products of decomposition do not contain metallic elements other than the specific activator elements.

As is true of many oxide-type phosphors, modified calcium pyrophosphate phosphors exhibit maximum efficiency when the composition departs from that of a stoichiometric compound. While generally described as pyrophosphates, maximum luminescence is only obtained when an excess of phosphate ion is present. If the base-to-acid ratio is defined as

$$\frac{\text{moles CaO} + \frac{1}{2} \text{ moles Na}_2\text{O} + \frac{1}{3} \text{ moles Sb}_2\text{O}_3}{\text{moles P}_2\text{O}_5}$$

then maximum luminescence occurs when this ratio falls between 1.85 and 1.95, as shown in Fig. 1.

Phosphors prepared without sodium are but

¹ Manuscript received June 27, 1955. This paper was prepared for delivery before the Chicago Meeting, May 2 to 6, 1954.

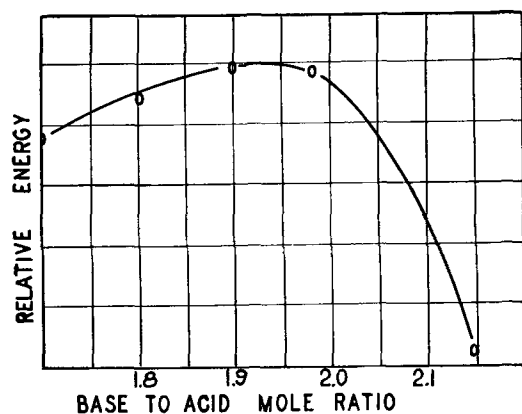


FIG. 1. Effect of base-to-acid ratio on relative energy output of $(\text{Ca}, \text{Na}_2)_2\text{P}_2\text{O}_7:\text{Sb}$ under 2537 \AA excitation.

weakly luminescent. Incorporation of a trace amount of sodium has a marked effect on the efficiency of the phosphor. Results show (Fig. 2) that the efficiency increases rapidly with increasing sodium, and less rapidly at about 0.5 mole % Na_2O . The optimum concentration is found to be about 0.8% Na_2O . Above the optimum, the brightness decreases only slightly; even at about 7% Na_2O , although highly sintered, the phosphor is still reasonably bright. The introduction of sodium has no effect on the color of the emission.

Antimony is incorporated in concentrations from about 0.1 to 1.5 mole % Sb_2O_3 , although the more narrow range from 0.3 to 1% is preferred and about 0.7% gives maximum efficiency. Fig. 3 shows the effect of antimony concentration on relative efficiency of $(\text{Ca}, \text{Na}_2)_2\text{P}_2\text{O}_7:\text{Sb}$. The phosphors having a "white" emission, i.e., with manganese as well as antimony, generally require the same antimony concentration as do the singly activated blue-emitting phosphors. If manganese is added to the phosphor, its concentration should be controlled with some degree of accuracy in order to obtain the desired color (the reason for this is apparent from the data in Table III). The efficiency of the manganese band increases with concentration up to contents corresponding to 4.5 mole % MnCO_3 . Higher concentrations reduce the intensity of the emission.

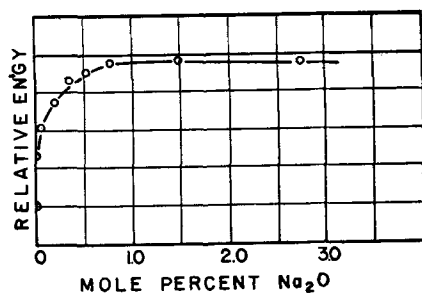


FIG. 2. Effect of sodium concentration on relative energy output of $(\text{Ca}, \text{Na}_2)_2\text{P}_2\text{O}_7:\text{Sb}$ under 2537 \AA excitation.

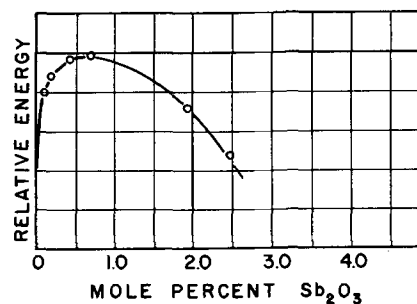


FIG. 3. Effect of antimony concentration on relative energy output of $(\text{Ca}, \text{Na}_2)_2\text{P}_2\text{O}_7:\text{Sb}$.

Table I gives representative formulations for three phosphors of varied emission spectra.

The sodium may, instead, be introduced as one of the halides or as any compound of sodium which converts to the oxide at the firing temperatures employed. The anion associated with the sodium cation has little effect on the optical characteristics of the phosphor.

Chemical analyses have shown that the only phosphor constituent lost during firing is antimony; generally about 10% of the added amount is volatilized. Virtually all of the antimony is present in the trivalent state, but a small amount is present in some acid-insoluble form, presumably a calcium antimonate.

Examination of x-ray diffraction patterns of $(\text{Ca}, \text{Na}_2)_2\text{P}_2\text{O}_7:\text{Sb}$ phosphors has shown that sodium has no effect on the calcium pyrophosphate lattice. Antimony has been found to lower substantially the temperature of the beta to alpha inversion. Those phosphors having optimum composition and fired at temperatures which lead to high efficiency contain two phases: alpha and beta calcium pyrophosphate in approximately a 1:3 ratio. Firing temperatures of 1250°C lead to alpha modification pyrophosphate phosphors; these are mentioned below.

EMISSION SPECTRA-OPTICAL CHARACTERISTICS

$(\text{Ca}, \text{Na}_2)_2\text{P}_2\text{O}_7:\text{Sb}$ phosphors are excited by short wave-length ultraviolet radiation (primarily 2537 \AA Hg) to give a deep blue emission which has a peak wave length of 4150 \AA . The position of this band in the spectrum is not affected by sodium concentra-

TABLE I. Formulations of representative phosphors

Component	Blue	Blue-white	Pink-white
	g	g	g
CaHPO_4	136.1	134.7	127.8
$(\text{NH}_4)_2\text{HPO}_4$	5.8	7.2	13.6
Na_2CO_3	1.3	1.3	1.3
Sb_2O_3	3.5	3.5	3.5
MnCO_3	0	1.1	6.9

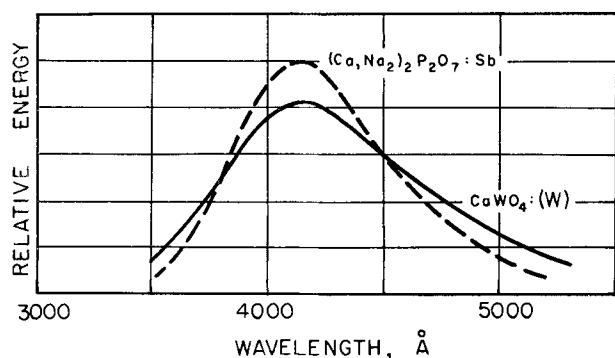


FIG. 4. Spectral energy distribution curves of $(\text{Ca}, \text{Na}_2)_2\text{P}_2\text{O}_7:\text{Sb}$ and $\text{CaWO}_4:(\text{W})$ under identical conditions of excitation.

tion, nor by antimony concentration. The relative efficiency of the 4150 Å band, as influenced by the sodium concentration, is shown in Fig. 2. Fig. 4 shows the spectral energy distribution for the antimony-activated phosphor compared to self-activated CaWO_4 as excited by 2537 Å ultraviolet of the same intensity. The spectral energy distribution curves were obtained using a General Electric recording spectroradiometer.

The introduction of manganese, in addition to antimony, into the matrix gives rise to a new emission band with peak wave length of 5750 Å. At a fixed antimony concentration, with increasing manganese, the 5750 Å band continues to develop at the expense of the 4150 Å. Manganese alone produces a cathodoluminescent phosphor which fails to respond to 2537 Å ultraviolet. In Fig. 5 are shown the spectral energy distribution curves of several $(\text{Ca}, \text{Na}_2)_2\text{P}_2\text{O}_7:\text{Sb}:\text{Mn}$ phosphors of variable manganese content. For comparison, a typical calcium halophosphate (about 1% manganese) is also shown. All the phosphors were excited by 2537 Å ultraviolet of equal intensity. Fig. 6 gives a portion of the I.C.I.

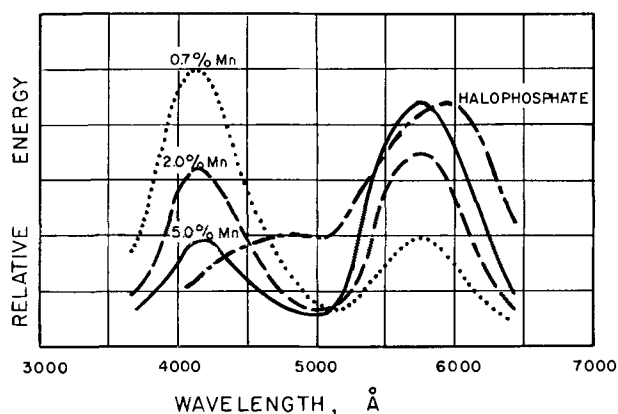


FIG. 5. Spectral energy distribution curves of $(\text{Ca}, \text{Na}_2)_2\text{P}_2\text{O}_7:\text{Sb}:\text{Mn}$ phosphors of variable manganese concentration and a calcium halophosphate (1% Mn) under identical conditions of excitation.

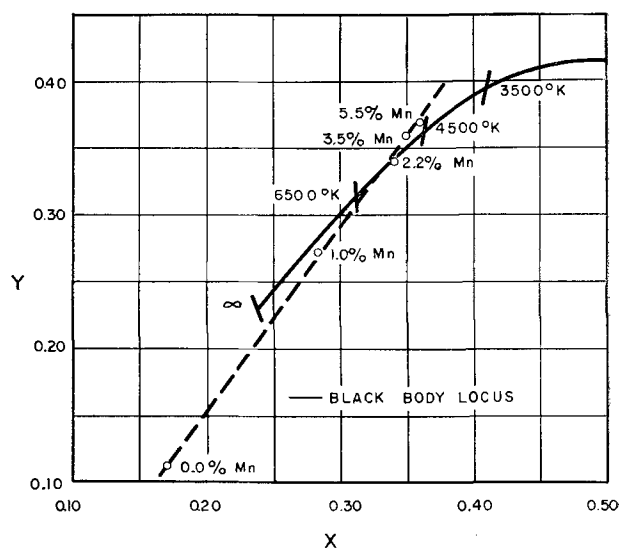


FIG. 6. I.C.I. coordinates x and y , for fluorescent lamps coated with various modified calcium pyrophosphate phosphors.

chromaticity diagram on which are plotted the trichromatic coefficients, x and y , for 40-watt fluorescent lamps coated with phosphors containing various concentrations of manganese. The values plotted are the average values for several lamps. The 100-hr luminous efficiency of these lamps varies between 13 lpw for the deep-blue-emitting $(\text{Ca}, \text{Na}_2)_2\text{P}_2\text{O}_7:\text{Sb}$ and 42 lpw for $(\text{Ca}, \text{Na}_2)_2\text{P}_2\text{O}_7:\text{Sb}:\text{Mn}$ prepared with about 2.5 mole % MnCO_3 .

With cathode ray excitation the antimony (4150 Å) band of the singly activated phosphor is observed with moderate efficiency; the manganese (5750 Å) band of the doubly activated phosphor is excited more efficiently. Thus, the phosphor containing 2 mole % manganese and 1 mole % antimony is "white" under 2537 Å ultraviolet excitation, but a pronounced yellow-orange under cathode ray excitation.

The phosphorescence of the antimony emission decays at a faster rate than that of the manganese emission. Individual rates of decay are of the same order of magnitude as found for the respective emission bands in halophosphate phosphors.

SUBSTITUTIONS FOR CALCIUM

Substitutions of other divalent elements for calcium in $(\text{Ca}, \text{Na}_2)_2\text{P}_2\text{O}_7:\text{Sb}$ phosphors shift the observed color toward longer wave lengths, but at a sacrifice of efficiency. With substitutions of the order of 10% of the calcium atoms, the shift is observed as a broadening of the long wave-length side of the 4150 Å band. When the ratio of atoms of substitute to atoms of calcium approaches unity, a new emission band becomes evident. Sodium is essential here to obtain optimum luminescence.

The introduction of cadmium gives rise to an emission band at 4600 Å which is detectable when 40% of the calcium atoms have been replaced. The relative efficiency of this band is about 50% of the original 4150 Å band, but the phosphor is 50% brighter due to increased eye-sensitivity in the 4600 Å region of the spectrum.

Similar observations were made for barium, strontium, zinc, and magnesium substitutions. Strontium, substituted for 60% of the calcium atoms, shows a rather weak band with a peak wave length of about 5000 Å. Barium gives a weak band with a peak wave length of about 5100 Å when 40% of the calcium atoms have been replaced. Magnesium and zinc substitutions both produce extremely weak emission bands.

These substitutions in $(\text{Ca}, \text{Na}_2)_2\text{P}_2\text{O}_7:\text{Sb}:\text{Mn}$ phosphors serve to shift manganese emission toward longer wave lengths with lower efficiency. Magnesium, strontium, and zinc all reduce the efficiency so far as to be undesirable and the products of a barium substitution are nonluminescent, due to the insolubility of manganese in the presence of barium. Only cadmium produces a shift in peak wave length which results in practical efficiencies. When 25% of the calcium atoms have been replaced by cadmium, the manganese band has a peak wave length of 5850 Å.

SENSITIZED LUMINESCENCE

The $(\text{Ca}, \text{Na}_2)_2\text{P}_2\text{O}_7:\text{Sb}:\text{Mn}$ phosphors are an example of "sensitized luminescence," a phenomenon recently afforded considerable treatment in the literature, in particular by Botden (4), Schulman (8), Ginther (9), and Fonda (10) on specific luminescent systems, and by Dexter (11) on some theoretical aspects. Measurements of quantum outputs of the sensitizer and activator emission bands relative to the quantum output of magnesium tungstate which has been shown (12) to have a conversion efficiency of 100% were made for phosphors of variable antimony and manganese contents. Table II summarizes the effects of variations in antimony concentration on the quantum outputs of the two emission bands

TABLE II. *Effect of Sb_2O_3 concentration on quantum outputs*

Mole % Sb_2O_3	Quantum output Sb	Quantum output Mn	Total Quantum output	Ratio quantum output Mn/Sb
0.01	5.0	8.4	13.4	1.68
0.06	12.9	25.2	38.1	1.95
0.26	19.7	32.4	52.1	1.65
0.55	20.4	37.3	57.7	1.83
0.96	19.9	35.1	55.0	1.77
1.20	18.7	33.9	52.6	1.82
2.46	16.2	32.5	48.7	2.00

TABLE III. *Effect of MnCO_3 concentration on quantum outputs*

Mole % MnCO_3	Quantum output Sb	Quantum output Mn	Total quantum output
0	55.4	0	55.4
0.04	43.5	13.0	56.5
0.50	38.0	21.0	59.0
1.28	31.6	31.6	63.2
2.36	23.5	40.0	63.5
4.27	15.7	44.0	59.7
6.90	11.7	38.5	50.2
9.53	8.7	28.8	37.5

for phosphors containing a fixed activator content of 2.6 mole % as manganese carbonate. Under the same conditions of excitation, magnesium tungstate is arbitrarily assigned a quantum output of 100.

The effects of increasing manganese content on the quantum outputs of the two emission bands, at a fixed sensitizer content of 0.4 mole % antimony trioxide, are given in Table III.

It is apparent that the quantum outputs of both the sensitizer and activator emission bands rise with increasing sensitizer content until an optimum is reached, in this case about 0.7 mole % Sb_2O_3 . With increasing activator content, the quantum output of the sensitizer emission falls continuously, whereas the quantum output of the activator emission rises to an optimum at about 4.5 mole % MnCO_3 .

Critical concentrations of sensitizer and activator for optimum output of the phosphor system are about 0.7 and 5 mole %, respectively. At these concentrations phosphors have been prepared with total quantum outputs of about 65. The best phosphors have absolute absorptions for short wave-length ultraviolet of about 77%. The internal quantum efficiency (conversion of absorbed short wave-length ultraviolet to emitted visible radiation) is therefore about 80%, based on magnesium tungstate having 95% absolute absorption and an internal quantum efficiency of 100%. The singly activated phosphor has an internal quantum efficiency of about 80% also.

If the ratio of the quantum outputs of the activator and sensitizer emissions as a function of sensitizer concentration is considered (Table II), this ratio is found to be independent, within the limits of experimental error, of the sensitizer concentration. This is taken as evidence that the transfer of energy from an excited sensitizer center to an activator center is a direct, one-step process. The transfer of energy to an activator center takes place only when activator centers are in close proximity to sensitizer centers. Maximum quantum output occurs when the ratio of activator concentration to sensitizer concentration is high; in this case 7:1. This direct transfer process

is identical to that found in $\text{CaF}_2:\text{Ce}:\text{Mn}$ phosphors (9) where maximum efficiency of the process occurs at an activator to sensitizer ratio of 10:1. This is in contrast to the character of the energy transfer in $\text{Ca}_3(\text{PO}_4)_2:\text{Ce}:\text{Mn}$ (4) and $3 \text{Ca}_3(\text{PO}_4)_2:\text{CaF}_2:\text{Sb}:\text{Mn}$ (10) where the ratio of the quantum output of the activator to that of the sensitizer increases with sensitizer concentration. This is interpreted as denoting that the transfer may involve a succession of sensitizer centers before the energy is eventually transferred to an activator center. In these latter cases, the ratio of the critical concentrations of activator to sensitizer approximates unity. The distinctive differences among sensitized phosphors are treated fully by Botden (4).

The range of transfer of energy from sensitizer to activator may be calculated according to the relationship (4, 8, 9)

$$\frac{\text{Quantum Output Mn}}{\text{Quantum Output Sb}} = \frac{1 - (1 - X_{\text{Mn}})^k}{(1 - X_{\text{Mn}})^k}$$

where X_{Mn} is the activator concentration. Assuming an average value for the ratio of quantum outputs of 1.8 and a concentration of activator equal to 2.6 mole % MnCO_3 , the range over which energy is transferred, K , is 39 atoms. This is in agreement with experimentally determined values for other systems (4, 8, 9) as well as the theoretically predicted value (11).

DISCUSSION

Substitution of a minor portion of the calcium by sodium in calcium pyrophosphate phosphors activated by antimony alone or by antimony and manganese in combination has been shown to increase greatly the efficiency of these phosphors. The role that sodium plays in producing the observed effects is not fully understood and can, at best, only be subjected to hypothesis.

On the basis of Kroeger's (13) explanation for the function of halide in $\text{ZnS}:\text{Ag}$ phosphors, it is suggested that monovalent sodium ions fill the lattice vacancies that would ordinarily arise from the replacement of divalent calcium ions by trivalent antimony ions. Thus, one monovalent sodium ion and one trivalent antimony ion replace two divalent calcium ions in the lattice, and electroneutrality is

preserved. Maximum luminescent efficiency should then occur when the number of antimony ions and sodium ions is equal. This has been shown to be the case. That high efficiency is maintained when sodium ions are present well in excess of the number required for electroneutrality is ascribed to a fluxing action, in the true sense, on the part of the sodium ions. It is quite probable that additional sodium ions occupy interstitial sites. Sodium oxide or a sodium halide might well exist in solid solution in calcium pyrophosphate, particularly in fairly low concentrations.

It might be supposed that any monovalent cation could function in the manner described for sodium. The size of the other alkali metal ions, relative to divalent calcium, precludes their filling the lattice vacancies without considerable effect on the lattice dimensions and the lattice position of the antimony centers, or, possibly, their ionic radii are so divergent that they are insoluble in the lattice. It is also an observed fact that lithium and potassium do not bring about the pronounced increase in luminous output that sodium does. Table IV gives the ionic radii (due to Goldschmidt or Pauling) of several pertinent elements.

The addition of manganese to the system presents no problem since Mn^{+2} and Ca^{+2} are mutually interchangeable.

While $\text{Ca}_2\text{P}_2\text{O}_7:\text{Sb}$ phosphors absorb a fair amount of short wave-length ultraviolet, they are not efficient. The introduction of sodium, however, greatly increases the absorption and the resulting light output. $(\text{Ca}, \text{Na}_2)_2\text{P}_2\text{O}_7$ is not a good absorber and does not exhibit luminescence.

Kroeger and co-workers (14) have noted that the position of the emission band for $\text{Ca}_2\text{P}_2\text{O}_7:\text{Mn}$ under cathode ray excitation depends on the temperature of preparation. These investigators report that the beta modification, obtained by firing below 1150°C , has an emission with peak wave length of about 5650 \AA , and the alpha modification, obtained by firing above 1150°C , has an emission with peak wave length of about 6000 \AA . In the present investigation, phosphors were generally prepared at temperatures well below the range from 1150° to 1270°C , the range of reported temperatures for the transition from beta to alpha calcium pyrophosphate. The peak wave length of the manganese emission in $(\text{Ca}, \text{Na}_2)_2\text{P}_2\text{O}_7:\text{Sb}:\text{Mn}$ phosphors, excited either by short wave-length ultraviolet radiation or by cathode rays, is 5750 \AA or slightly higher than Kroeger's value. This is attributed to the presence of some alpha pyrophosphate in a predominately beta system as has been shown by x-ray analyses.

$(\text{Ca}, \text{Na}_2)_2\text{P}_2\text{O}_7:\text{Sb}:\text{Mn}$ phosphors fired at temper-

TABLE IV. Ionic radii of elements

Monovalent		Divalent		Trivalent	
\AA		\AA		\AA	
Li	0.60	Mn	0.90	Sb	0.90
Na	0.98	Ca	0.99		
K	1.33	Cd	0.97		

atures of about 1250°C exhibit emission bands with peak wave lengths of 4400 Å and 6000 Å for the antimony and manganese bands, respectively. These phosphors are badly sintered and not as efficient as those prepared at 850°-875°C.

ACKNOWLEDGMENT

The author wishes to thank Shannon Jones and Dr. Gorton R. Fonda for their many helpful discussions. He wishes to acknowledge the interest and encouragement of Walter P. Cartun, Richard S. Mackie, and the late P. R. Dickinson. Finally, the author is indebted to his colleagues in various departments of the Lamp Division and in the Research Laboratories of the General Electric Company for their varied contributions and assistance without which this investigation would not have been possible.

Any discussion of this paper will appear in a Discussion Section to be published in the June 1956 JOURNAL.

REFERENCES

1. K. H. BUTLER, *This Journal*, **100**, 250 (1953).
2. H. C. FROELICH AND J. M. MARGOLIS, *ibid.*, **98**, 400 (1951).
3. H. C. FROELICH, *ibid.*, **95**, 255 (1949).
4. TH. P. J. BOTDEN, *Philips Research Rpts.*, **7**, 197 (1952).
5. A. K. McKEAG AND P. W. RANBY (To General Electric Co., Ltd.) British Pat. Spec. 578,272, June 21, 1946.
6. S. T. HENDERSON AND P. W. RANBY, *This Journal*, **98**, 479 (1951).
7. M. HUNIGER AND H. PANKE (To General Electric Co.), U.S. Pats. 2,241,950, May 13, 1941; 2,241,951, May 13, 1941; 2,270,124, Jan. 13, 1942.
8. J. H. SCHULMAN, R. J. GINTHER, AND C. C. KLICK, *This Journal*, **97**, 123 (1950).
9. R. J. GINTHER, *ibid.*, **101**, 248 (1954).
10. G. R. FONDA, *Brit. J. Appl. Phys.*, Supplement No. 4, 69S (1955).
11. D. L. DEXTER, *J. Chem. Phys.*, **21**, 836 (1953).
12. G. R. FONDA, *J. Phys. Chem.*, **49**, 303 (1944).
13. F. A. KROEGER AND J. A. M. DIKHOFF, *Physica*, **16**, 297 (1950).
14. F. A. KROEGER, J. TH. G. OVERBEEK, J. GORRISON, AND J. VAN DEN BOOMGAARD, *This Journal*, **96**, 132 (1949).

The Enhancement Effect of Electric Fields on Some X-Ray Excited Phosphors¹

GEORGES DESTRIAU,² JOSEPH MATTLER,² MICHEL DESTRIAU, AND HANS ECKARD GÜMLICH

Faculté des Sciences, Paris, France

ABSTRACT

Further experiments are reported on the enhancement of phosphor output by the application of an electric field. This new and permanent enhancement of the light emitted by phosphors irradiated by x-rays is different from the momentary illumination observed in the Gudden and Pohl effect. Many factors have been studied, such as field strength, frequency, and temperature.

INTRODUCTION

Some years ago it was reported (1) that electric fields could produce a quenching of light emitted by some phosphors (such as ZnS:Cu, ZnSCdS:Ag, ZnSCdS:Cu) when these phosphors were irradiated either by x-rays or by ultraviolet radiations. Since that time, many additional results have been published on this phenomenon which is observed when the phosphor powder, embedded in an insulator, is suitably excited between two electrodes, one of which is transparent (conducting glass).

More recently (2) an opposite phenomenon was reported. It was observed when some ZnSCdS:Mn phosphors were irradiated by a beam of x-rays. It also occurred with some ZnS:Mn phosphors, but to a lesser degree. When the field was applied simultaneously with irradiation by x-rays, the light emitted by this phosphor was greater than when no field was applied.

DESCRIPTION OF PHENOMENON

Schematically, when no field was applied, the brightness, excited only by the action of a constant beam of x-rays, increased with time following curve I or *OAB* (Fig. 1). If, simultaneously with the x-ray irradiation, an alternating field was applied (not a constant field in order to avoid polarization effects), the brightness increased, following curve II which lies higher than curve I.

Let B_0 and B_1 be, respectively, the constant brightness reached after a certain time when no field is applied (curve I) and when the field is applied (curve II). The ratio $r = B_1/B_0$ is then called the "sensitizing ratio." It can reach values higher than 3.

¹ Manuscript received March 17, 1955.

² Consultant, Lamp Division, Westinghouse Electric Corporation, Bloomfield, New Jersey.

If the phosphor was irradiated from time zero, but the field was not applied until time t_1 , the brightness first increased following the part *OA* of curve I, at time t_1 it rose suddenly following *AM*, and then it decreased slowly toward the plateau of curve II. If the field was then removed at time t_2 , one again observed a sudden rise *PQ* and the brightness then fell again slowly toward the plateau of curve I. The small peaks *M* and *Q* must be ascribed to a small Gudden and Pohl effect (3).

The phenomena were quite different when the above phosphors were irradiated by ultraviolet radiations instead of x-rays. In this case the usual quenching effect was observed, that is to say a curve II below curve I.

Cusano (4) recently found a similar phenomenon of enhancement when thin transparent layers of some phosphors, but not powders, were placed between two electrodes in contact with the sensitive layer. With such a device Cusano observed that there was always an enhancement of the emission when a direct field was applied, irradiation being either by x-rays or by ultraviolet radiations.

All experiments reported here were made on powders embedded in an insulator and subjected to an alternating field.

Field dependence of the sensitizing ratio.—Very low fields, even 200 v/cm, were able to give a noticeable effect. The sensitizing ratio first increased with the field strength and then passed through a maximum at about 15,000–20,000 v/cm (Fig. 2). On the same figure are shown, for the same phosphor, the variations of the "quenching ratio" when irradiation is made by ultraviolet radiation instead of x-rays.

Effect of frequency and x-ray beam intensity.—Experiments have been made between 10 and 5,000 cps. In this range, the sensitizing ratio was not dependent on the frequency of the applied field.

Similarly, the sensitizing ratio was not dependent on the intensity of the exciting beam. Using an x-ray

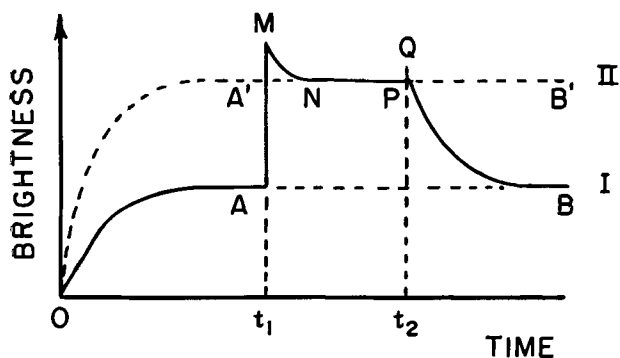


FIG. 1. General behavior of the enhancement effect. Curve I (OAB) when no field is applied; Curve II (OA'B') when a field is applied, from time zero, simultaneously with x-ray irradiation. If the field is applied at time t_1 a sudden rise AM is obtained and another small rise PQ when the field is removed.

half-wave generator (80,000 v applied to the tube), the sensitizing ratio varied only 6% when the tube current was varied from 0.1 to 1 ma.

Effect of temperature.—When the temperature was raised from 18° to 54°C, the brightness B_0 and B_1 (the plateaus of curves I and II, respectively) both decreased, but the sensitizing ratio, r , remained almost constant. Table I gives data on one representative sample. In this narrow temperature range the variations of r are near the limit of the experimental error.

Brightness Waves

It has been shown (5) that, in the quenching effect, brightness waves (instantaneous output as a function of time during a cycle of field variation) were deeply disturbed, chiefly by the appearance of a secondary and transient peak at the time when, in each cycle, the field passed through zero. In the enhancement effect, however, although the height of

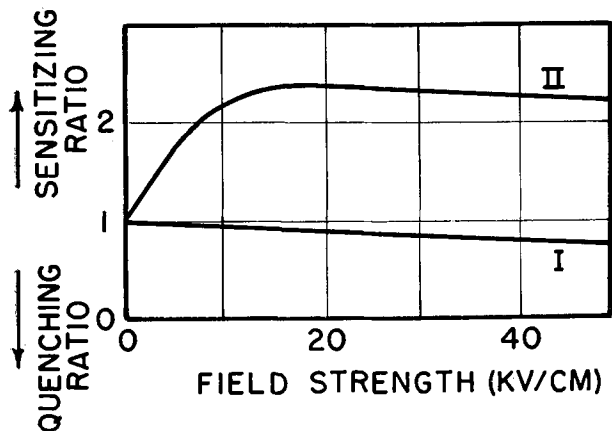


FIG. 2. Variations of the quenching ratio (curve I) as a function of field strength when irradiation is made by ultraviolet radiation, and variations of the sensitizing ratio (curve II) when irradiation is made by x-rays. The phosphor sample is the same in both cases.

TABLE I

Temperature °C	B_0 (arbitrary units)	B_1 (arbitrary units)	Sensitizing ratio r
18	115	172	1.50
23	107	160	1.50
29	99	147	1.48
37	82.5	125	1.51
42	80	118	1.48
45	75	112	1.49
49	70.5	104	1.48
52	71.5	105	1.47
54	67.5	99	1.47

each peak is increased, the shape of the brightness wave was generally only very weakly disturbed, and with some samples there was no disturbance. With other samples which showed some very small disturbances of the brightness waves in the enhancement effect, however, the same behavior of a transient but very small secondary peak on the decreasing side was found; this peak always occurred at the time when the field, in each cycle, passed through zero (Fig. 3).

Identical phenomena occurred when the half-wave x-ray generator was operated at a frequency twice that applied to the electroluminescent cell in order to obtain one emission of light in each half-cycle of the field variation.

With doubly activated phosphors (for example, Cu and Mn activated ZnSCdS) a Gudden-Pohl effect can be superimposed on the normal enhancement effect (Fig. 4), but this flash lasts only a very short time. It is thus quite different from the permanent phenomenon described above.

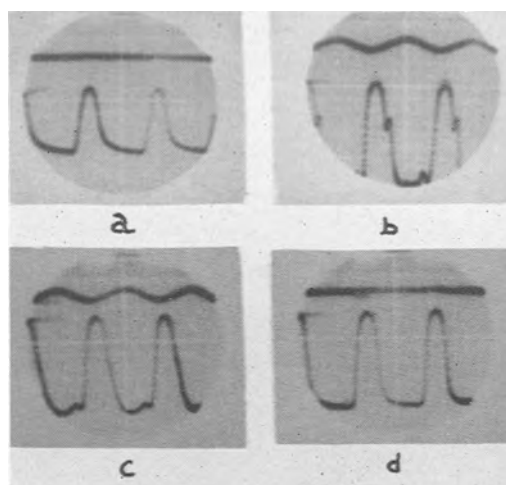


FIG. 3. Brightness waves for sample No. 1 of low sensitivity; simultaneous recordings of sinusoidal field wave and brightness wave (upper trace in each is sinusoidal field): (a) without any field; (b) at the time of the greatest disturbance (with secondary peak); (c) after a long time; (d) when the field is removed.

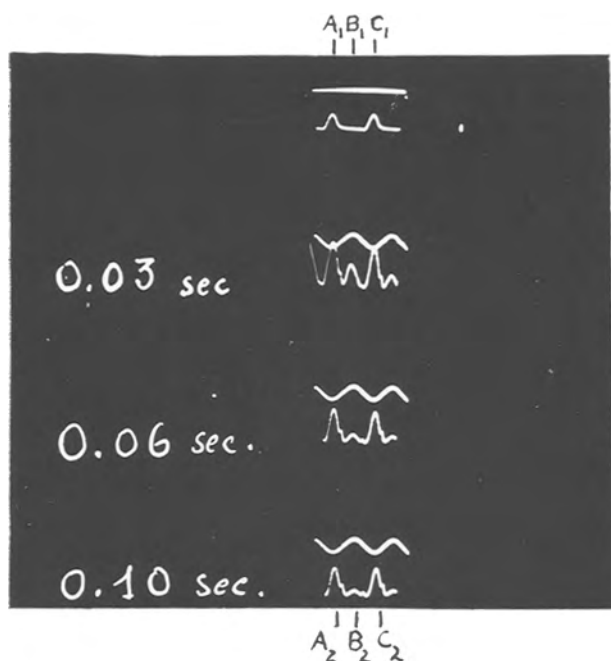


FIG. 4. Mn and Cu activated ZnSCdS. Superimposition of a Gudden and Pohl effect on the enhancement effect. Beam of x-rays emitted from a half-wave x-ray generator. Upper recording: brightness wave just before field application; second recording: 0.03 sec after field application; third recording: 0.06 sec after field application; fourth recording: 0.10 sec after field application. On vertical lines A_1A_2 and C_1C_2 brightness waves of an enhancement effect plus a quickly decreasing Gudden and Pohl effect. On vertical lines B_1B_2 only the brightness wave of the Gudden and Pohl effect, the intensity of which vanishes quickly.

Effect of a Constant Field

When a direct potential is applied to such a cell without contact between the crystals and the electrodes, the internal field strength starts from a certain value E and then decays following an exponential law with time constant

$$\theta = 4\pi/K\rho$$

where K is the dielectric constant and ρ is the resistivity of the phosphor. Similarly, at the removal of the direct potential, the internal field immediately starts from the same value E and then decays following the same exponential law.

In both cases, i.e., when the constant potential is

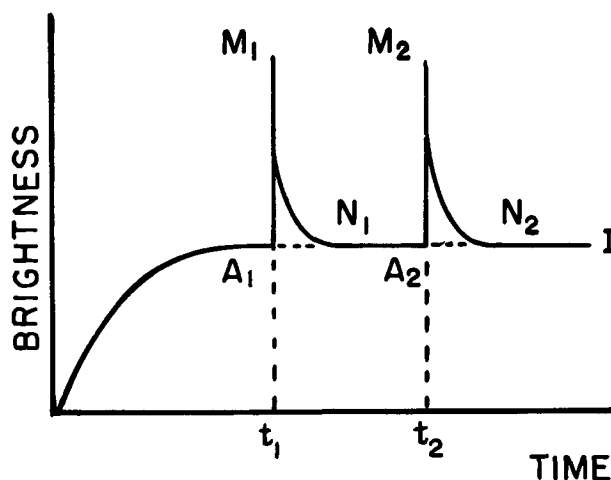


FIG. 5. Effect of a constant electric field upon the brightness of a phosphor excited by x-rays. Only a flash occurs at time t_1 when a d-c potential is applied, and another flash at time t_2 when the field is removed.

applied or removed, the internal field, which is the effective field in the crystals, starts from the same value and quickly falls toward zero. With such a device, one can obviously obtain only a momentary enhancement when the constant potential is removed as well as when it is applied (Fig. 5).

CONCLUSIONS

The light emitted by some Mn-activated ZnSCdS and also by some Mn-activated ZnS irradiated by x-rays is enhanced under the action of an electric field, while the light emitted is quenched by the field when irradiation is made with ultraviolet radiation. This phenomenon of permanent enhancement is quite different from the flash of momentary illumination observed in the Gudden and Pohl effect.

Any discussion of this paper will appear in a Discussion Section to be published in the June 1956 JOURNAL.

REFERENCES

1. G. DESTRIAU, *J. phys. radium*, **4**, 32 (1943).
2. G. DESTRIAU AND M. DESTRIAU, paper presented at ECS Chicago Meeting, Abstract 45, May 2-6, 1954.
3. B. GUDDEN AND R. W. POHL, *Z. Physik.*, **2**, 192 (1920).
4. D. A. CUSANO, paper presented at meeting of the American Physical Society, New York City, Abstract LA6, January 1955.
5. G. DESTRIAU, *J. Appl. Phys.*, **25**, 67 (1954).

Influence of the K Absorption Edges of Cadmium and Silver on the X-ray Diffraction Patterns of Some Cadmium Compounds¹

R. J. ROBINSON AND F. SCHOSSBERGER

Armour Research Foundation of Illinois Institute of Technology, Chicago, Illinois

ABSTRACT

On x-ray powder and single-crystal rotation photographs of CdS, CdSe, and CdO, certain low-angle spots and lines were observed. Analysis of the absorption conditions of the general radiation showed that the unique closeness of the K absorption edges of Cd in the sample and Ag in the film emulsion could form a spectral line. The low-angle lines thus appear as Bragg reflections of the crystals of these substances produced by an average wave length $\lambda = 0.475 \text{ \AA}$.

INTRODUCTION

X-ray powder and single-crystal rotation photographs of CdS obtained by Ni-filtered $\text{CuK}\alpha$ radiation show relatively sharp lines or spots in the low-angle region in addition to the pattern of hexagonal CdS. In a previous paper (1) the low-angle diffraction effects of the two substances were tentatively related to one of the following: presence of an unknown modification, stacking faults, or deformation faulting in the crystals.

Observations of discontinuities due to absorption effects on the x-ray diffraction photographs of Mo and Sb (2) suggested that similar conditions could affect Cd compounds. In general, the white radiation of the Cu target x-ray tube which passed through the Ni filter produced only a continuous background on the film, i.e., the Ag absorption edge was usually masked. Absorption of radiation in the sample, however, caused discontinuities at the particular wave lengths which corresponded to the absorption edges characteristic for the elements in the sample material (3).

An abrupt change of the reflected intensity occurred in the band of white radiation for the wave length corresponding to a K absorption edge, where the absorption coefficient changed in the ratio of approximately 8:1. Bragg reflections of single crystals or crystal powders were thus caused by the white radiation and were reflected to definite angles, which introduced steps in the background of the film. As a rule, such discontinuities on the film did not have the appearance of a single crystal spot or a Debye-Scherrer line, but they looked like bands (4). Furthermore, the prominence of the steps was reduced by scattered radiation from all parts of the x-ray equipment and by Compton scattering of the

sample. However, if the sample contained elements having a K absorption edge close to that of the Ag grain in the emulsion, an additional absorption effect contributed to the contrast of the steps. The Cd (at. no. = 48) K absorption edge at 0.4641 \AA lay very close to that of Ag (at. no. = 47), $\lambda_K = 0.4858 \text{ \AA}$. At the Ag edge, a sudden increase of the sensitivity of the photographic emulsion occurred for the remaining part of the white radiation band reflected by the crystallographic planes of the Cd-containing sample but not absorbed by the Cd in the sample. Cd in the sample and Ag in the film emulsion therefore formed a selective filter so that only a thin band was observed with an average wave length of 0.475 \AA . Because of the unique closeness of the K absorption edges of the two elements, the spectral width of the band appearing on the film was very narrow (0.022 \AA). The resulting effect, in a sense, was comparable to a Ross filter (5, 6) utilizing two filters composed of two elements of adjacent atomic number whose thicknesses were adjusted so that the transmitted spectra were identical for all wave lengths except for the narrow band between the respective K absorption edges. Therefore, relatively sharp Bragg reflections of each crystallographic plane became possible in the low-angle region in addition to the reflections caused by the characteristic $\text{K}\alpha$ radiation of the tube. These low-angle reflections repeated the powder pattern or single crystal spots given by the characteristic radiation, but at spacings on the film corresponding to the average wave length of the narrow band between the above-mentioned K absorption edges.

In the first column of Table I, the d -values of the low-angle lines of α -Cds were calculated for $\text{Cu K}\alpha$ radiation ($\lambda = 1.541 \text{ \AA}$) since they were obtained in powder diagrams using Ni filtered radiation from a Cu tube (Fig. 1). This follows the procedure used in

¹ Manuscript received April 20, 1955.

TABLE I. *d*-Values of the low-angle lines of CdS caused by absorption of part of the white radiation in the sample and film emulsion

<i>d</i> in Å* $\lambda = 1.541\text{Å}$	Observed relative intensity	<i>d</i> in Å† $\lambda = 0.475\text{Å}$	Indices	Hexagonal α -CdS <i>d</i> in Å	Observed relative intensity
11.5	3	3.54	10 $\bar{1}$ 0	3.55	8
10.5	7	3.23	0002	3.33	4
			10 $\bar{1}$ 1	3.13	9
7.98	3	2.45	10 $\bar{1}$ 2	2.43	5
6.75	5	2.08	11 $\bar{2}$ 0	2.06	10
6.19	4	1.91	10 $\bar{1}$ 3	1.89	7
—	—	—	20 $\bar{2}$ 0	1.782	5
5.70	4	1.754	11 $\bar{2}$ 2	1.755	7
5.32	-1	1.64	20 $\bar{2}$ 1	1.723	5
—	—	—	0004	1.673	-1
—	—	—	20 $\bar{2}$ 2	1.575	3
4.92	-1	1.515	10 $\bar{1}$ 4	1.516	1
4.58	1	1.41	20 $\bar{2}$ 3	1.396	5
—	—	—	21 $\bar{3}$ 0	1.351	4
—	—	—	21 $\bar{3}$ 1	1.323	6
—	—	—	11 $\bar{2}$ 4	1.299	2
4.11	1	1.265	10 $\bar{1}$ 5	1.263	-1
—	—	—	21 $\bar{3}$ 2	1.255	6
—	—	—	20 $\bar{2}$ 4	1.225	-1
—	—	—	30 $\bar{3}$ 0	1.191	4
3.74	1	1.151	21 $\bar{3}$ 3	1.156	6

* The *d*-values of the observed low-angle lines as determined for $\lambda_{CuK\alpha}$.

† The *d*-values of the same lines as determined for an average wave length between the K absorption edges of Cd and Ag.

the previous paper (1). In the third column, however, the same low-angle lines of α -CdS (Ni filtered radiation from a copper tube) were calculated using a wave length of 0.475 Å. The *d*-values obtained with this average wave length can be compared with the *d*-values of hexagonal α -CdS which are shown in the fifth column. A comparison shows that the low-angle lines can be indexed by the hexagonal unit cell dimensions of α -CdS if the correct wave length is used.

The layer lines appearing in the low-angle region of single crystal rotation photographs (1) could be explained by the same effect. In general, there was good agreement between the *d*-values for all observed lines, although the relationship of the intensities did not seem to be maintained in all cases. This variation and the deviation of the position of (20 $\bar{2}$ 1) in the low-angle region were probably caused by other overlapping diffraction effects (3) in this region of the film. The intensity changes may also have been a result of the change in value of the atomic scattering factor of Cd near the absorption edge.

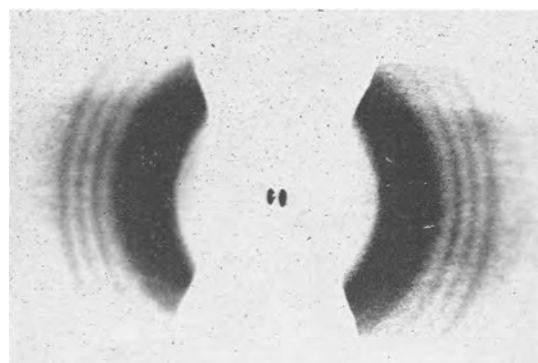


FIG. 1. Low-angle lines in a powder diagram of α -CdS caused by absorption effects of the white radiation in the sample and film emulsion.

At 24 kv the minimum wave length in the emission spectrum of the x-ray tube is above 0.5 Å and the low-angle diffraction effects should disappear. This phenomenon was verified on a sample which had shown the effect at 40 kv. Similar calculations made on the position of the low-angle lines in x-ray diagrams of CdSe and CdO showed the same agreement between the calculated and observed *d*-values. The occurrence of the low-angle diffraction effects on photographic films also could be avoided by first reflecting the characteristic radiation of the tube on a crystal monochromator.

Differences in intensities and sharpness of the low-angle lines (1) were probably caused by changes in the radiation condition of the x-ray tube and by variation of the amount of sample in the camera, which explains the absence of the effect in some of the reported diagrams. No other polymorphic modification or stacking faults, as discussed tentatively in a previous communication, seemed to be present in the vapor-phase-grown CdS crystals. Mechanical deformation faulting, observed by grinding, should change the appearance of the pattern equally in the low-angle region and in the part produced by the characteristic Cu radiation.

Any discussion of this paper will appear in a Discussion Section to be published in the June 1956 JOURNAL.

REFERENCES

1. F. SCHOSSBERGER, *This Journal*, **102**, 22 (1955).
2. H. P. KLUG AND L. E. ALEXANDER, "X-Ray Diffraction Procedure," p. 381, J. Wiley & Sons, Inc., New York (1954).
3. A. BAXTER AND J. C. M. BRENTANO, *Phil. Mag.* **24**, 473 (1937).
4. R. BROOKS, *Brit. J. Appl. Phys.*, **2**, 76 (1951).
5. P. A. ROSS, *Phys. Rev.*, **28**, 425 (1926).
6. P. KIRPATRICK, *Rev. Sci. Inst.*, **10**, 186 (1939); *ibid.*, **15**, 223 (1944).

Preparation of High-Purity Thorium by the Iodide Process¹

N. D. VEIGEL, E. M. SHERWOOD, AND I. E. CAMPBELL

Battelle Memorial Institute, Columbus, Ohio

ABSTRACT

Preparation of massive thorium of high-purity, in lots of several hundred grams each, by the van Arkel-de Boer (iodide) process is described. Substantial reduction in the nonmetallic content of the deposits over that of the feed material was obtained. Optimum conditions for deposition were determined.

INTRODUCTION

The object of this work was the preparation of massive thorium metal² of high purity and, more particularly, of metal low in nonmetallic constituents. Although a number of processes³ described in the literature yield metal low in metallic impurities, few of these processes lead to the freedom from nonmetallic impurities that is attainable by the iodide method. In the van Arkel-de Boer method, as described in this paper, thorium metal of high purity was prepared in lots of several hundred grams. By using a feed material low in metallic impurities and employing the iodide process to remove a substantial amount of the nonmetallics, a high-purity product was obtained.

EXPERIMENTAL

Preparation of Feed Material

In the work reported here, thorium, furnished by the AEC, was used as a feed material. Heavy chips were cut from sections of an ingot or rolled plate, using a shaper without lubrication of the tool. Prior to use, the feed was degreased, washed with distilled water, and dried. Approximately 4 kg of cleaned thorium chips was placed in the annular space be-

tween the inner wall of a Pyrex deposition bulb (Fig. 1B) and a perforated molybdenum retainer.

Preparation of Deposition Vessel

A V-shaped "starting filament" of iodide-thorium wire, 0.64 mm in diameter and about 115 cm in overall length, was attached to 1/4-in. diameter tungsten supporting electrodes by means of molybdenum tie wires. In order to prevent premature burnout of the filament during the deposition operation, sufficient tie wire was provided to insure a tapered junction between starting wire and electrode. A bridged quartz ring was attached to the lower end of the filament by means of fine tungsten wire. This ring served the dual functions of keeping the filament under slight tension and of preventing it from coming in contact with the metal feed retainer. With the tied filament (Fig. 1A) centrally located in the deposition vessel, the Pyrex electrode cap was sealed to the bulb. The sealed deposition bulb (Fig. 1C) was next attached to an all-glass vacuum system through a short length of constricted tubulation.

Outgassing and Iodination

The deposition vessel was outgassed at 510°C for 24 hr. At the end of this period, the residual pressure in the bulb was usually of the order of 10⁻⁴ mm of mercury. During outgassing, a side arm, containing about 10 g crushed, resublimed iodine, was kept under refrigeration. The outgassed deposition unit and the attached side arm containing the iodine were sealed off from the vacuum system and the bulb was cooled to 260°C, the temperature at which iodination was carried out. The arm containing the iodine was allowed to warm to room temperature and the iodine was slowly vaporized into the deposition vessel by gentle heating with a gas torch. The product of the iodination reaction was canary yellow thorium tetraiodide, observable on the bulb walls and feed after the vessel had cooled to room temperature. Subsequent to iodination, the exhaust tubulation was sealed off at the constriction, and the

¹ Manuscript received March 20, 1955. This paper was prepared for delivery before the Chicago Meeting, May 2 to 6, 1954. Work on the paper was performed under AEC Contract (W-7405-eng-92).

² Thorium, a metal of possible interest as a nuclear fuel, is relatively nonreactive when freshly prepared, being silvery in appearance when cut or polished. Although its natural radioactivity is somewhat greater than that of ordinary uranium, it has never been considered dangerous. Thorium compounds, principally the oxide, are used industrially in such applications as luminous gas mantles, for special purpose refractories, and in electron-tube cathodes. The fine metal powder is sometimes used in electron tubes as a getter. While some fires have occurred, owing to the pyrophoric nature of the powder, thorium is generally considered to be nonhazardous to work with.

³ W. C. Lilliendahl, "Rare Metals Handbook," Chapter 23, (C. A. Hampel, Editor), Reinhold Publishing Corporation, New York (1954). A description of the Ames Process for the preparation of thorium is not available.

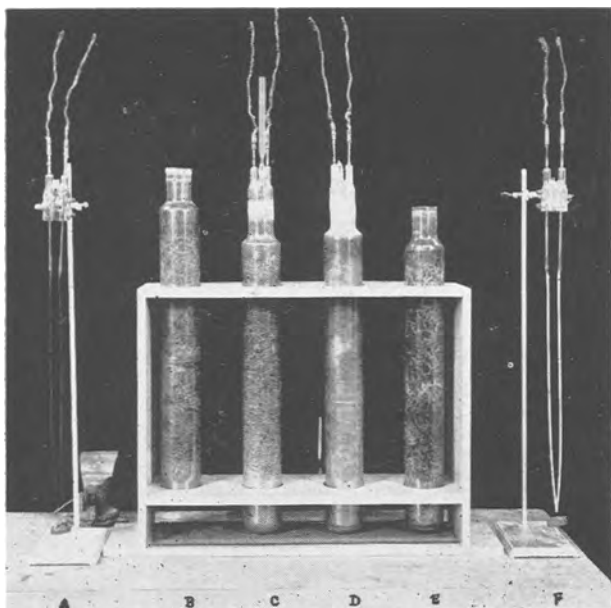


FIG. 1. Iodide thorium at various stages of processing

finished bulb (Fig. 1D) was placed in the deposition furnace.

Deposition

It was found that deposition took place most readily when the externally measured bulb temperature was in the range 455°–485°C. Hence, the deposition furnace was provided with sectionalized windings which could be controlled individually to maintain the desired temperature range. Radiation-shielded thermocouples were attached to the deposition vessel at the center of each furnace section. A cooling coil, made of thin-walled copper tubing, was embedded in the furnace insulation in order to remove the large amount of heat developed in the central portion of the bulb during the later stages of the run as the power input to the filament increased.

Sixty-cycle a-c power was supplied to heat the filament. Voltage leads were attached to the electrodes at the supply-lead junctions.

Since it was difficult to determine the temperature of the filament, correct operating conditions were reached by an indirect means. The voltage applied to the filament was increased in steps until onset of deposition was indicated by an increase in current while the voltage was held at a particular value. On the assumptions (a) that the emissivity and resistivity of the filament remain constant, and (b) that no heat is lost from the filament by conduction through the supporting electrodes, it can be shown that the filament temperature remains constant as the symmetrical cross section increases uniformly, if the following relation is satisfied:

$$I^{1/3}E = K$$

where I = current (amp), E = applied voltage (v), and K = a constant.

It was found that deposition would usually begin if E and I were such that $K = 0.43/\text{cm}$ of filament length, and that burnout of the filament rarely occurred if K was equal to or less than $0.63/\text{cm}$. Hence, initially, E and I were adjusted to give $K = 0.43/\text{cm}$ and then the voltage was maintained at a constant value until $K = 0.63/\text{cm}$ was reached. Subsequently, the voltage was decreased as the current increased in order to maintain constant " K ." Runs were terminated when the current reached values of the order of 100 amp, since the bulb temperatures could not be restricted to the desired level at higher current owing to the large amount of heat radiated from the filament.

After termination of deposition, the electrode-cap seal was cracked with a hot wire, the finished filament was removed (Fig. 1E and 1F) and trimmed, and the feed was washed with tap and distilled water, and dried prior to the succeeding run. The cap was cleaned, the old tie-sections were removed, and a new filament was attached to the supporting electrodes.

Factors Influencing Deposition and Characteristics of Iodide Thorium

A representative V-shaped thorium "crystal bar" prepared during the course of the work is shown in Fig. 1F. This filament was 0.62 cm in diameter and 112 cm in over-all length. Approximately 200–250 g of metal was prepared per run, depending on the conditions under which deposition took place. The average deposition rate was about 10 g/hr for this length of filament. The deposited metal consisted of bright, rather loosely to well-knit, columnar grains, which extended radially from the center to the outside of the bar. The cross sections of the grains varied from a fraction of a square millimeter to several square millimeters in area. Individual grains

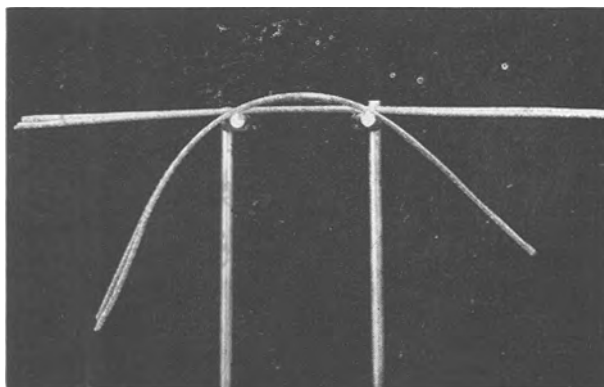


FIG. 2. Comparison of rapidly (straight) vs. less rapidly (curved) deposited iodide thorium crystal bar.

were quite ductile and could be bent sharply through an angle of 180° without fracture.

In general, it can be said that rapidly deposited iodide metal tends to be more closely knit and has somewhat smaller grain size than does metal deposited less rapidly, even though the apparent temperature of the bar is the same in the two cases. Fig. 2 illustrates the degree of compactness achieved in two crystal bars, one of which was deposited at a considerably greater rate than the other, and, hence, possessed greater stiffness.

Similar experiments with other refractory metals have shown that smoother deposits could be obtained if the filament temperature is high enough. However, the low tensile strength of thorium precluded operation at sufficiently elevated filament temperatures to achieve such results. Thus, larger crystal bars tend to pull apart under their own weight during deposition and possess rough, rather coarsely crystalline surfaces.

As in the case of both titanium and zirconium, one of the most important single factors influencing the deposition rate of thorium in the van Arkel-de Boer process was the temperature of the deposition vessel and its effect on the vapor pressure and stability of the iodides. At the iodination temperature used in this work (260°C), thorium tetraiodide was formed. The tetraiodide was relatively stable in the presence of excess metal at any temperature below about 500°C. At temperatures above 500°C, however, it reacted with excess metal to form the less volatile lower iodides. In the preparation of thorium metal by the van Arkel-de Boer process, prolonged operation at high bulb temperatures resulted in the tie-up of iodine as relatively nonvolatile lower iodides. The rate of filament growth decreased as the feed material was covered with a film of lower iodides, and deposition ultimately stopped. This could be avoided by operating at bulb temperatures in excess of 600°–610°C, at which temperatures the lower iodides disproportionate. However, Pyrex glass softens in this temperature range; thus, deposition of thorium from the lower iodides in Pyrex equipment was not feasible.

Since the deposition rate increased with the bulb temperature, up to the temperatures at which the formation of lower iodides took place, there was an optimum bulb temperature for Pyrex apparatus. This optimum was found experimentally to be in the range 455°–485°C.

When using Vycor, silica, or metal deposition vessels, it was possible to raise the bulb temperature sufficiently to secure deposition from the lower iodides. In some deposition runs in Pyrex, radiation

TABLE I. Comparison of impurity levels of thorium feed metal and iodide thorium prepared from this feed

Material	Element, % by wt		
	Carbon	Oxygen	Nitrogen
Thorium feed metal	0.115	0.110	0.029
Thorium crystal bar	0.020	<0.01	<0.01

TABLE II. Comparison of room temperature mechanical properties of AEC and iodide thorium

Property	AEC thorium	Iodide thorium
Hardness, VHN	80	40
Ultimate tensile strength, psi	30,000	20,000
Reduction in area, %	48	60

from the filament was sufficient to permit local overheating which led to the formation of lower iodides, as evidenced by black lustrous deposits on the walls of the deposition vessel. For this reason, also, it became necessary to terminate the runs when the crystal bars had grown to an appropriate diameter.

DISCUSSION

The extent of reduction of nonmetallic impurities afforded by the iodide process is illustrated in Table I, which shows the carbon content reduced to about $\frac{1}{6}$ that of the feed, oxygen to less than $\frac{1}{10}$, and nitrogen to less than $\frac{1}{3}$.

The mechanical properties of thorium were considerably influenced by the nonmetallic impurity content. Decreasing hardness, increasing ductility, and lower tensile strength usually go hand in hand with increasing purity.

As further evidence of the reduction in the nonmetallic content which the iodide process gives, Table II indicates comparative values for the hardness, tensile strength, and reduction in area of both the AEC-feed material and the iodide thorium prepared from it. The hardness value is markedly lower.

It should be pointed out that thorium is apparently less sensitive to oxygen and nitrogen than are titanium and zirconium, two other Group IV metals frequently prepared by the iodide process. Although the reduced oxygen and nitrogen content undoubtedly has some effect on the mechanical properties of iodide thorium, other work has shown that lower carbon content is primarily responsible for the observed decrease in hardness.

Any discussion of this paper will appear in a Discussion Section to be published in the June 1956 JOURNAL.

Liquidus Curves for Aluminum Cell Electrolyte

II. Ternary Systems of Cryolite-Alumina with Sodium Fluoride, Sodium Chloride, and Aluminum Fluoride¹

N. W. F. PHILLIPS, R. H. SINGLETON,² AND E. A. HOLLINGSHEAD

Aluminium Laboratories Limited, Arvida, Quebec, Canada

ABSTRACT

Liquidus curves for those parts of the systems molten at 1050°C have been determined by means of cooling curves and visual examination of the cooling melt. The system cryolite-alumina-aluminum fluoride is incomplete due to the high volatility of the latter component. The binary systems of cryolite with sodium fluoride, sodium chloride, and aluminum fluoride gave, respectively: eutectic point at 882°C, 40% sodium fluoride; eutectic point at 734°C, 68.5% sodium chloride; peritectic point at 734°C, 30% aluminum fluoride; and eutectic point at 693°C, 40% aluminum fluoride (compositions in weight per cent). Diagrams for the three ternary systems have been made.

INTRODUCTION

In a previous paper (1) liquidus curves for the binary system cryolite-alumina were reported and compared with earlier data. The object of this paper is to present liquidus curves for the ternary systems cryolite-alumina with sodium fluoride, sodium chloride, and aluminum fluoride. Only scanty data on these systems were available, and they were obtained solely by the cooling curve method, which gives erroneous results for the binary system on the alumina side of the eutectic point.

Primary freezing points were determined for those parts of the systems molten at 1050°C by the cooling curve method and by visual examination of the cooling melt.

MATERIALS

Hand-picked natural cryolite containing no visible impurities was crushed to pass 150 mesh. It contained 0.02% iron, 0.03% silicon, 0.02% magnesium, and 0.01% lead. The alumina was Alcoa A-10, which had a loss on ignition at 1000°C of 0.17% and contained 0.06% sodium, 0.04% iron, and 0.03% silicon. The aluminum fluoride was produced by vacuum distillation from Baker's reagent-grade hydrate. It contained 0.09% iron, 0.02% silicon, 0.03% manganese, and 99% aluminum fluoride (based on total fluorine content). The sodium fluoride, which contained no free alkali, and the sodium chloride were Baker's reagent-grade.

METHOD

The apparatus and methods used in this investigation were as described for the system cryolite-

alumina (1). As for this system, primary freezing points were determined by the cooling curve method when the first appearance of crystals, as observed through a telescope, corresponded with the primary break in the cooling curve. This was so for the three binary systems of cryolite with sodium fluoride, sodium chloride, and aluminum fluoride, and for the corresponding ternary systems containing alumina on the cryolite side of the eutectic line. Cooling rates of 1–3°C/min were used.

On the alumina side of the eutectic line in the ternary systems there was no break in the cooling curve corresponding to the first appearance of crystals in the melt, and the primary break occurred at an appreciably lower temperature. Here the primary freezing points were obtained by the visual method, i.e., by determining the temperature at which crystals first appeared in the slowly cooling melt. For final determinations, rates of cooling of less than 0.1°C/min were used. The failure to obtain a corresponding break in the cooling curve is attributed to the sluggishness with which the crystals form and to the steepness of the liquidus curves.

The platinum, 10% rhodium-platinum thermocouples were checked regularly at the freezing point of pure sodium chloride. With melts containing aluminum fluoride the determinations were made as rapidly as possible to minimize changes in composition due to evaporation.

ACCURACY

Results obtained by the cooling curve method for the binary and ternary systems containing sodium fluoride or sodium chloride are not in error by more than 3°C. The limit of error for results obtained by the visual method on these ternary systems, i.e., on the alumina side of the eutectic line, is estimated to be 5°C. No significant error due to changes in

¹ Manuscript received May 31, 1955. This paper was prepared for delivery before the Cincinnati Meeting, May 1 to 5, 1955.

² Present address: National Research Corporation, Cambridge, Mass.

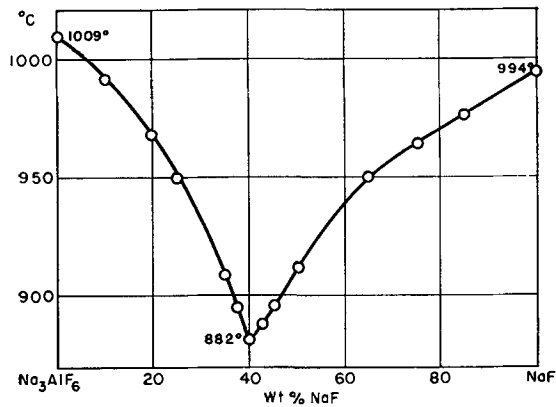


FIG. 1. Liquidus diagram for cryolite-sodium fluoride

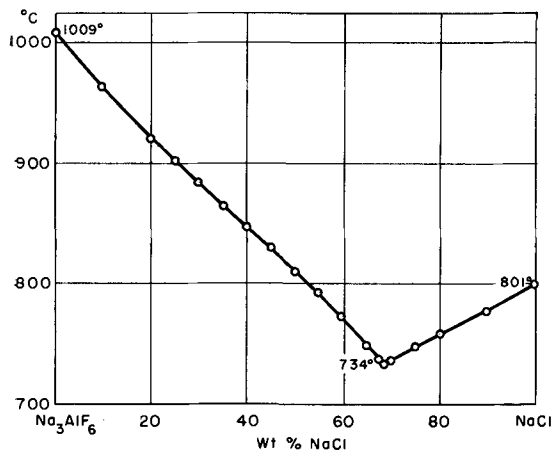


FIG. 2. Liquidus diagram for cryolite-sodium chloride

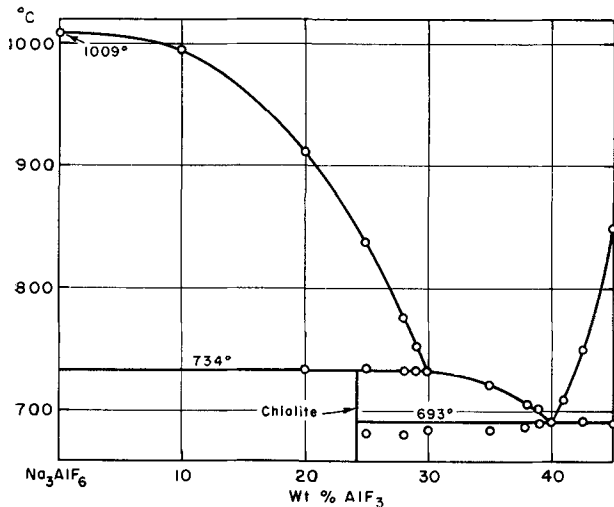


FIG. 3. Liquidus diagram for cryolite-aluminum fluoride

composition was revealed by repeated measurements on the same melt or by weight loss.

For the system cryolite-aluminum fluoride, the loss by evaporation during a determination was less than 1% for aluminum fluoride contents up to 40%, and the limit of error of the results in this range is 3°C. This applies also to the system cryolite-

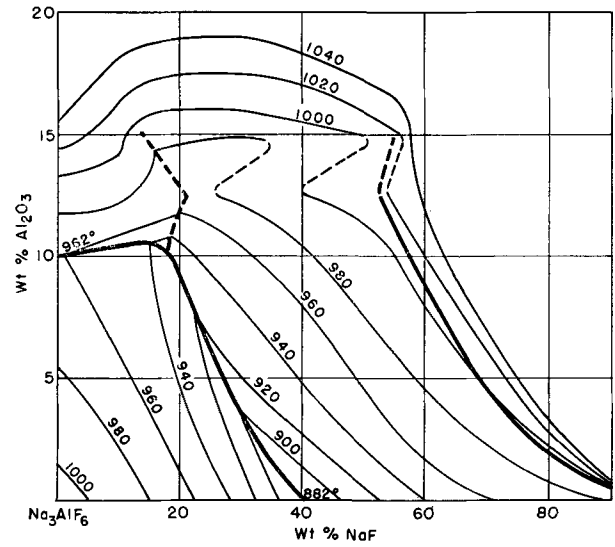


FIG. 4. Liquidus diagram for cryolite-alumina-sodium fluoride.

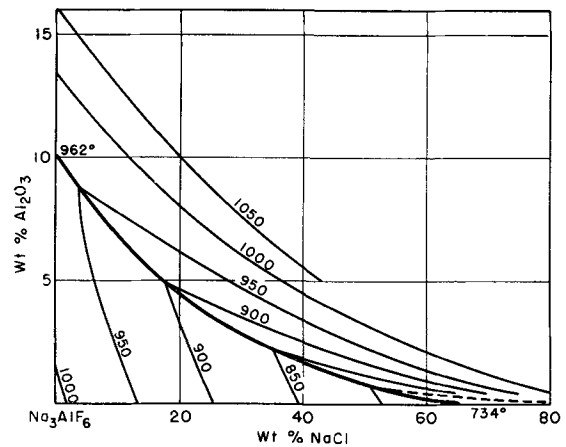


FIG. 5. Liquidus diagram for cryolite-alumina-sodium chloride.

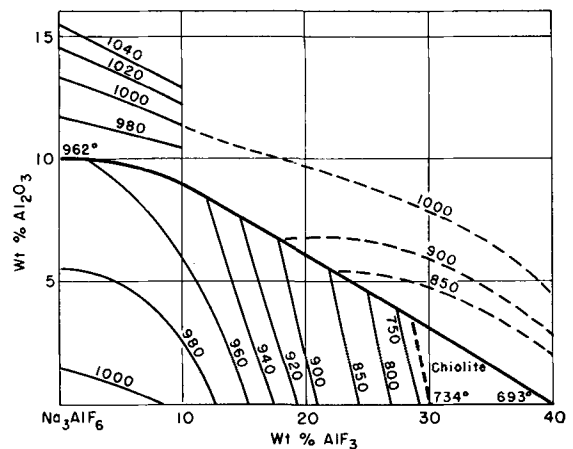


FIG. 6. Liquidus diagram for cryolite-alumina-aluminum fluoride.

alumina-aluminum fluoride on the cryolite side of the eutectic line. On the alumina side of the eutectic line at 10% aluminum fluoride, the estimated limit of error is 5°C. The other results for these two systems are less reliable.

In the course of the measurements reported here, the freezing points of sodium chloride, cryolite, and sodium fluoride were found to be 800°, 1006°, and 991°C, respectively. Subsequent measurements with a thermocouple calibrated at the freezing points of pure silver and samples of aluminum and copper certified by the National Bureau of Standards gave slightly higher values, namely $801^\circ \pm 0.5^\circ$, $1009^\circ \pm 1^\circ$, and $994^\circ \pm 1^\circ$, respectively. Hence the results reported for the binary and ternary systems are believed to be slightly low.

RESULTS

The liquidus diagram for cryolite-sodium fluoride (Fig. 1) has a eutectic point at 882°C and 40% sodium fluoride (weight per cent). The early results of Fedotieff and Ilyinskii (2), and of Lorenz and co-workers (3), which are not shown, are in fair agreement with those of the present work. Petit (4) reports 885°C for the eutectic temperature. Cryolite-sodium chloride (Fig. 2) has a eutectic point at 734°C and 68.5% sodium chloride. No data have been published previously on this system. Cryolite-aluminum fluoride (Fig. 3) has a peritectic point in the liquidus curve at 734°C and 30% aluminum fluoride, corresponding to the peritectic melting of the compound chiolite. There is a eutectic point at 693°C and 40% aluminum fluoride. The results of Fedotieff and Ilyinskii are in fair agreement.

The liquidus diagram for cryolite-alumina-sodium fluoride (Fig. 4) is based on those for cryolite-alumina (1) and cryolite-sodium fluoride, and on sections taken at 1, 5, 10, 12.5, 15, and 17.5% sodium fluoride. Pure sodium fluoride would dissolve 0.01% alumina, but not 0.05%, at 1100°C. There is a eutectic line joining the eutectic points of the two binary systems. Another eutectic line joins it at 18% sodium fluoride, but its position is only tentatively established. A peritectic line runs from 15% alumina, 55% sodium fluoride to the sodium fluoride corner. The data of Vajna (5), covering sodium fluoride contents up to 15%, were obtained by the cooling

method only and did not reveal the eutectic line. Those of Fedotieff and Ilyinskii, for solutions of alumina in the cryolite-sodium fluoride eutectic mixture, are in error for the same reason.

The liquidus diagram for cryolite-alumina-sodium chloride (Fig. 5) is based on those for the corresponding binary systems, and on sections taken at 0.5, 2, 5, and 10% alumina and at 10 and 20% sodium chloride. Pure sodium chloride would not dissolve 0.01% alumina at 1100°C. There is a eutectic line joining the eutectic points of the two binary systems. The only other data on this system are those of Henry and Lafky (6), who determined the percentage of alumina which would dissolve in cryolite containing up to 20% sodium chloride on prolonged stirring at a given temperature. They are in only rough agreement with those of the present investigation.

The liquidus diagram for cryolite-alumina-aluminum fluoride (Fig. 6), which has been only partially determined, is based on those for cryolite-alumina and cryolite-aluminum fluoride, and on sections at 5% alumina and 10% aluminum fluoride, respectively. There is a eutectic line joining the eutectic points of the two binary systems and a peritectic line corresponding to the decomposition of chiolite. The data of Vajna covering aluminum fluoride contents up to 15% are in approximate agreement on the cryolite side of the eutectic line.

ACKNOWLEDGMENT

The authors wish to acknowledge the assistance of Miss Anne Fischer and Mr. Leon Villeneuve who carried out many of the measurements.

Any discussion of this paper will appear in a Discussion Section to be published in the June 1956 JOURNAL.

REFERENCES

1. N. W. F. PHILLIPS, R. H. SINGLETON, AND E. A. HOLLINGSHEAD, *This Journal*, **102**, 648 (1955).
2. P. P. FEDOTIEFF AND VL. ILYINSKII, *Z. anorg. Chem.*, **80**, 113 (1912).
3. R. LORENZ, A. JABS, AND W. EITEL, *ibid.*, **83**, 39 (1913).
4. G. PETIT, *Compt. rend.*, **234**, 1281 (1952).
5. A. VAJNA, *Alluminio*, **22**, 635 (1953).
6. J. L. HENRY AND W. M. LAFKY, Paper presented at the American Chemical Society Meeting, New York (1954).

Discussion Section



OXIDATION OF IRON-MOLYBDENUM AND NICKEL-MOLYBDENUM ALLOYS (pp. 7-15)

CATASTROPHIC OXIDATION OF SOME MOLYBDENUM-CONTAINING ALLOYS

(pp. 16-21)

S. S. Brenner

N. J. GRANT¹: Unfortunately, the author was entirely unaware of the research conducted on the mechanism of this type of oxidation and published elsewhere.²

There has been considerable duplication of effort; fortunately, the mechanism proposed by Mr. Brenner agrees in substance with that proposed in the two papers cited and therefore strengthens the prior theoretical considerations.

A high concentration of the contaminating element (Mo, V, W, Bi, or Pb) was also found at the metal-oxide interface by x-ray and chemical analysis in these publications. The oxidation reaction was determined to take place at the metal-oxide interface and atmospheric oxygen was shown to have direct contact with this interface. In addition, it was found necessary to have a liquid oxide present for accelerated oxidation to occur. The temperature increase at the interface as a result of the oxidation reaction which is hypothesized by the author was actually measured and recorded.

Based on this evidence, a mechanism of accelerated oxidation had been proposed in which the liquid oxide reacted with the metal to form the metal oxide plus a suboxide and was illustrated by means of x-ray diffraction studies of the oxide present. The suboxide is subsequently regenerated by atmospheric oxygen which has direct contact with the metal-oxide interface and the accelerated oxidation process continues.

S. S. BRENNER: I presume Dr. Grant refers mainly to the paper on catastrophic oxidation. I cannot agree with him that there was a considerable degree of duplication of effort, although there was necessarily some overlapping. The main purposes of the paper were: (a) to show the effect of stepwise changes of composition on the oxidation of some prepared molybdenum alloys, (b) to show how catastrophic oxidation is initiated in these alloys, and (c) to clarify further the growth of the bulk oxide which is separated from the metal surface by the liquid oxide phase.

The author was aware of the publications hypothesizing a liquid oxide layer at the metal-oxide interface and the

This Discussion Section includes discussion of papers appearing in the *JOURNAL* of The Electrochemical Society, **102**, No. 1-6 (January-June 1955). Discussion not available for this issue will appear in the Discussion Section of the June 1956 *JOURNAL*.

¹ Dept. of Metallurgy, Massachusetts Institute of Technology, Cambridge, Mass.

² F. C. MONKMAN AND N. J. GRANT, *Corrosion*, **9**, 460 (1953); also, A. DE S. BRASUNAS AND N. J. GRANT, *Trans. Am. Soc. Metals*, **44**, 1117 (1952).

accompanying oxidation-reduction process. References to some of these publications were made at the beginning of the paper. Similarly the temperature increase at the liquid oxide-metal interface was not presented as an hypothesis by the author but was used rather to clarify the growth process of the bulk oxide.

Perhaps more detailed references would have avoided this misunderstanding.

THE ELECTRIC ARC AS A CIRCUIT ELEMENT

T. E. Browne, Jr. (pp. 27-37)

GEORGE W. VINAL³: The paper by T. E. Browne, Jr., recalls to mind the series of papers on the electric arc by Professor Walter G. Cady and several of his graduate students, including H. D. Arnold and myself. These are not mentioned by Dr. Browne. In some particulars these earlier papers, published in 1907 to 1909, anticipate results reported by Dr. Browne. As an example, Fig. 1 in his paper is practically identical with Fig. 1 in the paper "On the Electric Arc Between Metallic Electrodes" by Cady and Vinal⁴ and its translation.⁵ Other papers of Professor Cady's series on the arc appeared in these journals.

T. E. BROWNE, JR.: No attempt was made to present a complete bibliography with this paper, but the author appreciates the mention by Dr. Vinal of the additional early papers on the subject.

POLARIZATION STUDIES OF COPPER, NICKEL, TITANIUM, AND SOME COPPER AND NICKEL ALLOYS IN THREE PER CENT SODIUM CHLORIDE

H. B. Bomberger, F. H. Beck, and M. G. Fontana (pp. 53-58)

CECIL V. KING⁶: The authors call attention to the reduction of oxygen in aerated solutions and of hydrogen ions in all solutions as responsible for the cathodic polarization observed. It may be of interest to make quantitative calculation of the oxygen diffusion current and the hydrogen ion concentration polarization to be expected.

The reversible potential, vs. the saturated calomel cell (SCE), for oxygen reduction, is given by

$$E = 1.228 - 0.246 - 0.06 \text{ pH} + 0.015 \log p_{\text{O}_2} \quad (\text{I})$$

with $p_{\text{O}_2} = 0.2$ atm and $\text{pH} = 7$, $E = +0.55$ v; if $\text{pH} = 11$, $E = +0.31$ v. Oxygen is reduced at less positive and all negative potentials, hence, at any potential considered here.

The oxygen diffusion current is given by

$$i_a = 4FDc/\delta \text{ amp/cm}^2 \quad (\text{II})$$

³ 12 E. Stanworth Drive, Princeton, N. J.

⁴ W. G. CADY AND G. W. VINAL, *Am. J. Sci.*, **23**, 89 (1909).

⁵ *Physik. Z.*, **10**, 569 (1909).

⁶ Dept. of Chemistry, New York University, New York, N. Y.

at the cathode become depleted during galvanic corrosion (or also during local cell corrosion) the corrosion current will almost certainly decrease temporarily, thereby permitting oxygen to diffuse from the bulk of the solution back to the solution/cathode interface. This will tend to maintain a higher concentration of oxygen in the region of the cathodes to reduce cathodic polarization. Evidently the same sequence of events can occur during determination of polarization curves using the emf of the galvanic couple as the potential source.

Therefore, it should be realized that both local-cell corrosion and galvanic corrosion are self-regulating processes, whereas determination of cathodic polarization curves by means of the application of constant applied currents from an external emf is not. Although the authors attribute the difference between their measured and calculated current values for the copper-steel couple to contamination of the copper cathode by iron corrosion products, it should be realized that these two experiments were performed under two entirely different sets of conditions.

M. G. FONTANA: Dr. Pryor correctly notes that the use of constant currents from an external source does not yield information as applicable for galvanic cell studies as is obtained in the direct study of specific galvanic cells, since the current in a galvanic cell has a tendency to change. Changes in current imply nonsteady-state conditions that can be due to a number of variables, such as, polarization of the partner electrode, film growth, and temperature and environmental changes. In a carefully controlled experiment a corrosion cell should eventually acquire and maintain a constant current so that the polarization of its cathode should be quite similar to that of another cathode polarized with constant current under otherwise identical conditions. Any differences that may exist then can be attributable to surface conditions acquired during the unsteady-state history of the cells.

This, of course, is difficult to demonstrate. In such a study, sufficient time must be allowed and skill exercised to develop steady-state conditions. The choice of accompanying anodes is important since their polarization characteristics will affect the behavior of the test cathode, and contamination of the solution by salts from the anode must be avoided.

Constant currents from an external emf can be used to advantage in polarization studies, depending on the specific objectives. For example, data can be obtained under conditions that are readily defined, and the polarization characteristics of the electrode under study are not influenced by the peculiarities of the accompanying electrode; this gives information that should be more fundamental to the material under study.

NITRIDES OF CHROMIUM AND CHROMIUM-TITANIUM ALLOYS

New Film-Type Resistance Elements

E. R. Olson, E. H. Layer, and A. E. Middleton
(pp. 73-76)

DONALD CAPLAN AND MALCOLM J. FRASER¹²: After treating Cr powder in ammonia, x-ray diffraction analysis

¹² Dept. of Metallurgical Engineering, Rensselaer Polytechnic Institute, Troy, N. Y.

by the authors showed the presence of Cr₂N and CrN. This indicates that each granule consisted of a case of CrN surrounding a core of Cr₂N which means, in turn, that equilibrium had not been attained in the ten-min treating time. Otherwise, the powder would have been entirely CrN. It is most probable, however, that the evaporated films of Cr, since they were only 200 to 1500 Å thick (approximately 80 to 600 atomic distances) were totally converted to CrN. (We have found, for instance, that, even in specimens three orders of magnitude thicker, the nitride layer thickens at a rate in excess of 10⁴ Å/10 min at 1050°C.) It follows that in all cases the authors were examining single-phase films and, therefore, their suggestion that Cr₂N has a lower resistivity than CrN is not justified. The variation in electrical characteristics of the film observed by the authors might be related to variations with treating temperature of the Cr/N ratio in the CrN.

We have found, as did the authors, that, in the temperature range 950° to 1250°C, Cr is nitrided to CrN by ammonia. Single-phase films of the lower nitride, Cr₂N, could be prepared, if required, in an atmosphere of dissociated ammonia over this same temperature range.

E. R. OLSON: We appreciate the interest of and comments by Mr. Caplan and Mr. Fraser on our studies. We have been following their work with great interest and consider their findings of considerable value to our work.

The questionable presence of Cr₂N in our resistor films was brought to our attention some time ago through examination by electron diffraction methods of films nitrided at 1100° and 900°C. The studies revealed the presence of CrN and Cr but no Cr₂N. Investigations are currently getting under way in which correlation of electrical properties with Cr/N ratio will be studied. Preparation of both Cr₂N and CrN-type structures will be attempted to establish the effects of structure variations as well as nitrogen content on the electrical characteristics.

Incidentally, although it was not specifically stated in the article, the nitriding time for the powders was 60 min. Even this, however, may not have been sufficient time to reach equilibrium.

THE CRYSTALLOGRAPHIC DEPENDENCE OF THE OXIDATION POTENTIAL OF SOLID COPPER

W. E. Tragert and W. D. Robertson (pp. 86-94)

M. E. STRAUMANIS¹³: The results obtained on copper by the authors agree with those obtained on zinc some decades ago¹⁴: no appreciable differences in equilibrium potentials, as measured on different single Zn crystal planes, could be detected, and, under hydrogen, the potential of the single planes was equal to that of zinc amalgam. If there were some small differences then they were due to reasons of secondary nature. However, crystal planes dissolving in the electrolyte showed different dissolution potentials.¹⁵ This behavior of metallic crystals can be explained well.¹⁶

The plane of electrolytic growth of Cu-crystals is the

¹³ Dept. of Metallurgy, School of Mines and Metallurgy, Rolla, Mo.

¹⁴ M. STRAUMANIS, *Z. physik. Chem. A*, **147**, 161, Table I (1930).

¹⁵ M. STRAUMANIS, *ibid.*, **147**, 161, Table II (1930).

¹⁶ M. STRAUMANIS, *ibid.*, **156**, 150 (1931).

111-plane.¹⁷ This again agrees very well with the authors' statement that the plane with the most stable potential is the 111-plane. Thus, single Cu-crystals are electrolytically built up and decomposed over the 111-plane.

RESISTANCE AND POLARIZATION IN A STORAGE BATTERY

E. Willihnganz (pp. 99-101)

J. J. LANDER¹⁸: When the negative plate of the lead-acid cell is discharged, an unusual polarization curve is observed. This consists of a very rapid drop occurring in times which may be measured in fractions of a second, followed by a gradual recovery which may take seconds or minutes. This was explained by Dr. Willihnganz¹⁹ as being due to supersaturation of the solution in the neighborhood of the electrode with lead ions which are being discharged into solution. The voltage recovery occurs because the supersaturation is at least partially relieved by precipitation of lead sulfate on the electrode.

That such a process is quite possible is very easily demonstrated by mixing two solutions which will produce a solution supersaturated with lead sulfate and observing the time for turbidity to occur. Moreover, such an explanation is consistent with data which have been accumulated in our laboratory in studies of negative plate polarization.

During the time that the lead ion is establishing supersaturation in the surface layer and before the rate of precipitation becomes appreciable, diffusion into the body of the solution can take place and this process will limit, initially, the build-up in lead ion concentration at the surface. Therefore, using the equation for linear diffusion

$$\Delta C = \frac{2It^{\frac{1}{2}}}{\pi^{\frac{1}{2}}\eta FAD^{\frac{1}{2}}}$$

and assuming the applicability of the Nernst equation, the build-up in polarization at the discharging lead electrode can be calculated. Results are shown in Table I as a function of current density. For comparison, the last column shows how polarization would build up if the polarization process resulted from the depletion of the sulfate ion concentration at the surface of the electrode.

TABLE I. Polarization in volts

log <i>t</i> *	Current Density			
	170 ma/cm ²	1.7	0.16	170 (SO ₄ ²⁻ depletion)
-6.0	0.07	0.01		
-4.0	0.10	0.038	0.012	
-2.0	0.13	0.066	0.040	
0		0.095	0.068	0.001
+1.0				0.005
+2.0				0.032

* *t* in seconds.

¹⁷ G. TAMMANN AND M. STRAUMANIS, *Z. anorg. Chem.*, **175**, 131, 135 (1928).

¹⁸ Naval Research Lab., Washington, D. C.

¹⁹ E. WILLIHNGANZ, *Trans. Electrochem. Soc.*, **79**, 253 (1941).

The interesting feature of this table is the extreme rapidity with which polarization values of some magnitude can be established, and this for a Faradaic process at quite ordinary current densities. Obviously, this results from the very low concentration of lead ions in solution at the start (about 9×10^{-9} moles/cc), so that the passage of but fractions of coulombs can result in a manyfold increase in the lead ion concentration in the surface layer. If the supersaturation process actually occurs in the discharge of the lead electrode, then it must be reckoned with in making polarization measurements and interpreting them. For example, one can readily see that the usual methods of making resistance measurements would result in high values.

Dr. Willihnganz is probably quite correct in ascribing his high apparent resistances at the lower frequencies to a "pseudocapacitance." It seems questionable, however, that his results must be disassociated from changes in the lead ion activity and that, therefore, the negative plate reaction must take place in two steps.

It has already been indicated for one of his experimental conditions, namely the pulse discharge with the cell at rest, that the lead ion concentration could be important. Because he is directing his attention to the electrode surface rather than the solution layer, he concludes that the size and duration of the pulse is sufficient to cause only a minor disturbance in the double layer. That is to say, if the Nernst theory is applicable here, it is the change in concentration of ions in the solution layer which determines the voltage change. It can readily be calculated, using his estimated area and measured current and time, that, if the lead ions produced were constrained to remain in a 10 Å thick layer in the surface electrolyte, the concentration would be increased sixtyfold. This is equivalent to a polarization of 50 mv. Of course, diffusion must occur and, if the linear diffusion equation is applied to the same data, the concentration change in the solution at the electrode surface is calculated to result in a polarization of 1.2 mv which is somewhat greater than the measured value of 0.5 mv but is obviously large enough to account for it. With the cell at rest, it is practically immaterial whether this is a charge or discharge pulse because, for a charge pulse where concentration at the electrode surface is limited by diffusion of lead ions to the surface, a polarization of 1.35 mv is calculated. Therefore, it is possible that two of the experimental conditions can be explained on the basis of lead ion activity changes.

It may be argued that, because the cell was given a 2% discharge, sufficient lead sulfate nuclei were present to allow rapid crystallization of the lead sulfate and so the supersaturation effect would be eliminated. Our data show that the effect is indeed reduced when lead sulfate crystals are present to start with, but it requires something like 50% discharge of a flat plate to eliminate the effect entirely.

For the conditions where the pulse is superimposed on a charge or a discharge current, the situation seems much less clear. However, the argument, that, because a million-fold change in lead ion activity is apparently involved, the change in lead ion activity cannot be responsible for the polarization voltage, does not seem to be justified, be-

cause, inasmuch as a pseudocapacitance is involved, the same argument clearly can be leveled at any other mechanism of the same type which might be proposed. In view of the foregoing and the remarkable similarity of the traces, it seems just as reasonable to say that the lead ion concentration is responsible for the polarization in all cases. Furthermore, in the search for another mechanism it would be necessary to find a Faradaic process the polarization characteristics of which would be as sensitive to minute quantities of current as is the straightforward reaction. If such were found, then the original explanation for the negative plate polarization on discharge would be in considerable doubt, to say the least.

The millionfold figure does not seem to be unquestionable. It is not stated exactly in the paper to what the 0.1 and -0.1 v polarization values correspond. Presumably they are the steady-state differences in voltage between the cell on charge or on discharge vs. the open circuit voltage, i.e., the sum of the polarization at both plates and the internal resistance drop. The value of -0.1 would be about right for a discharge at the 4-hr rate (25 amp). If so, then, on discharge, 0.025 v of the total is due to internal resistance. Our data indicate that the polarization at the positive plate is greater than that at the negative after the negative has settled down, but, even if the polarization were equal at both plates, the value at the negative would be only 0.037. This means that the change in concentration at the negative under these discharge conditions would be seventeenfold. A similar condition at the charging overvoltage of 0.1 v would result in a total change of 17×40 , or about seven hundredfold.

E. WILLIHNGANZ: The comments of J. J. Lander show a difference of opinion concerning the presence of a concentration gradient of lead ions at the surface of a lead electrode when current is flowing. We did not mean to imply that such a gradient does not exist, or that it is not important. We did try to eliminate this gradient as completely as possible so that we could measure the internal resistance of a storage battery and get a number which meant actual electrical resistance. Consequently, our experimental conditions were considerably different from those usually encountered in studying electrode reactions.

For example, these test conditions are considerably different from those used in polarography. In a polarographic analysis, conditions are chosen to emphasize the importance of the diffusion gradient, while we tried to minimize it.

Where the mechanism of an electrode reaction is being studied, there is certainly a possibility that the concentration gradient is the end result of a series of reactions. It is the steps which precede the establishment of a concentration gradient which we feel are not clearly understood, and our pulse discharge data were merely an attempt to point out the possible existence of a problem.

Mr. Lander's criticism concerning the omission of an IR correction from the calculation is correct, but not important. The term "polarization" is used in the following fashion: A polarization of -0.1 v is the difference in potential between a negative plate equilibrium in sulfuric acid and a similar electrode when current is flowing at a constant rate. With a discharge current of 25 amp, with

a cell resistance of 0.001 ohm, and on the assumption that half of this resistance can be ascribed to the negative plate, the 0.1 v figure we used should be corrected to 0.088 v, while, during charge at 1 amp, the corrected polarization becomes 0.0995 v. If these values now are inserted in the Nernst equation and if it is assumed that at equilibrium the electrolyte contains 9×10^{-9} moles/cc of lead ions, we find that during charge the lead ion concentration has dropped to 1.5×10^{-12} , while during discharge it has increased to 2.2×10^{-5} .

The pulse polarization amounts to about 0.5 mv for either of the above lead concentrations. Again applying the Nernst equation, this corresponds to a 4% change in concentration of lead ions. This leads to a discrepancy. It seems impossible for a 0.01 microcoulomb/cm² pulse to produce a 4% change in concentration at the interface, irrespective of whether the initial concentration was 10^{-5} or 10^{-12} moles/cm². This is one of the reasons for believing that the pulse voltage is not controlled by the concentration of lead ions in solution, but rather by the composition of the double layer on the lead surface.

Mr. Lander's calculations of polarization voltages, using Fick's law and assuming a concentration gradient, can be criticized from two standpoints. First, he is talking about a different order of magnitude of current density from our work; second, he is using a figure for the surface area in a battery which we feel is not reliable within an order of magnitude. We estimated the effective electrode area of the sponge lead in a storage battery from the measurements of Falk and Lange. This was merely an approximation to learn the order of magnitude of the disturbance of the electrode surface. The use of this estimate of area to calculate diffusion gradients and voltages seems to put more trust in the estimate than it deserves.

Our major reason for suspecting something other than a diffusion gradient lies in the measurements of Falk and Lange at high frequencies. In the range of 1000 to 20,000 cycles, their values for the apparent capacitance and parallel resistance do not appear to fit the rather simple picture of a double-layer capacitance and a concentration gradient. For this reason, we believe that the lead electrode deserves further study to work out the charge and discharge mechanism.

THE EXTRACTIVE METALLURGY OF ZIRCONIUM BY THE ELECTROLYSIS OF FUSED SALTS

III. Expanded Scale Process Development of the Electrolytic Production of Zirconium from K_2ZrF_6

Bertram C. Raynes, Edward L. Thellmann,
Morris A. Steinberg, and Eugene Wainer
(pp. 137-144)

JAMES C. SCHAEFFER²⁰: You said that the graphite middle section of your cathode extended beneath the surface of the molten bath. Some zirconium probably deposits on the graphite section and, if so, suggests the possibility of the formation of ZrC by interaction of the Zr deposited with the graphite. Have you found any evidence of such taking place?

²⁰ Republic Steel Corp., Cleveland, Ohio.

MORRIS A. STEINBERG: Some zirconium does deposit on the graphite section of the cathode which extends into the melt. This portion of the deposit is contaminated with carbon and ZrC to some extent and is generally discarded. However, this amounts to only 1–2% of the total deposit.

ROBERT C. WADE²¹: 1. How much K_2ZrF_6 is lost by washing out the salts in the cathode deposit? What is the yield of Zr based on K_2ZrF_6 ?

2. How many washes are necessary to get a halide-free product?

3. What is the halide content (%) of the final powder?

MORRIS A. STEINBERG: 1. The deposits contain about 1–2% by weight of zirconium as salts. This is equivalent to 2–4% of the total available Zr. The average yield of metal based on K_2ZrF_6 is 85–90%.

2. For a deposit containing 4000 g Zr, 90–100 l of water in about 20 washes were used. This volume may be reduced by one half or more by recycling the wash water.

3. No accurate data are available on halide contents of the powder. However, the final wash water gives no detectable precipitate on addition of $AgNO_3$.

PRELIMINARY INVESTIGATION OF HAFNIUM METAL BY THE KROLL PROCESS

H. L. Gilbert and M. M. Barr (pp. 243–245)

G. M. BUTLER²²: 1. Carborundum Metals Company is faced with reduction of several thousand pounds of HfO_2 to sponge. I asked if the authors' observation, that $HfCl_4$ reacted more readily with H_2O than did $ZrCl_4$, could be due to the small scale and relatively crude nature of the small chlorinator used.

Mr. F. E. Block²³ said that the difference was real and troublesome— $HfCl_4$ being more reactive and harder to treat to remove.

2. I commented that preliminary Hf sponge production experiments at Carborundum Metals Company tended to confirm the authors' observation that buttons melted from the sponge were quite hard and difficult to machine. Purity requirements were not as high as for reactor-grade zirconium.

H. L. GILBERT: Mr. Butler's question concerning the reactivity of hafnium tetrachloride with water is one which has been given much thought and effort in our laboratory. We believe from our experience that there is greater initial reactivity in the case of hafnium tetrachloride and can state that, when zirconium and hafnium tetrachlorides are subjected to the same purification step of vacuum treatment and sublimation, the zirconium tetrachloride is transferred in the pure anhydrous form while hafnium tetrachloride seems to be associated with a series of oxygen-containing compounds which either transfer by sublimation or decompose and reform with the net result that the sublimed hafnium tetrachloride is not oxygen free. These compounds are active over an extended range from below to considerably above the sublimation temperature of hafnium tetrachloride. Our most exacting laboratory effort has not produced an oxygen-free hafnium tetrachloride.

²¹ Metal Hydrides Inc., Beverly, Mass.

²² The Carborundum Co., Niagara Falls, N. Y.

²³ Nonferrous Metals Branch, Northwest Electrodevelopment Lab., U. S. Bureau of Mines, Albany, Oreg.

S. J. MORANA²⁴: Has any particular difficulty been observed in maintaining a constant briquet level by using the closed feeding system described in the slide?

H. L. GILBERT: Mr. Morana's question concerning the maintenance of the proper briquet level in the chlorinator is quite in order. We found it necessary to determine the briquet level at least once during each shift, by inserting a graphite probe through the chlorinator top.

RESISTANCE STUDIES ON VARIOUS TYPES OF DRY CELLS

Richard Glicksman and C. K. Morehouse (pp. 273–278)

The authors make the following correction of an error in their original paper. On p. 275, under the heading *Discussion*, the first sentence should read: "Vinal (1) has pointed out that, as far back as 1885, Preece found that the resistance of a cell was less when measured at high current drains than when measured at low current drains."

J. J. COLEMAN²⁵: This paper, like all others that I know on the subject of the internal resistance of dry cells, ignores a basic difficulty. Whatever the "equivalent circuit" is for a dry cell, it certainly is not a simple resistor. In fact, a condenser in parallel with a resistor is probably not sufficiently complex to represent a dry cell—or even one of the electrodes.

To make clear what recognition of a dry cell as a complex network means, I invite your attention to what happens if the experimenter replaces the dry cell with an assembly consisting of a dry cell in parallel with a condenser. This adds one more complication to an already complicated network. In other words this assembly is not much more complicated than the dry cell itself. Suppose that the experimenter makes his measurements on this assembly. What conclusions can he draw?

In the first place, it is apparent that any determination of the impedance of this assembly by alternating current of a single frequency will tell us nothing about the internal resistance of the dry cell. Speaking crudely we can say the difficulty is that we do not know how much current goes through the dry cell and how much goes through the condenser.

In recognition of this problem various experimenters have measured the "instantaneous" potential drop which results in a direct current being sent through the cell. Turning our attention to the dry cell in parallel with a condenser again, it is clear that this provides no solution. While the condenser does not affect the flow of current after a steady state is reached, it is an important factor during the first few milliseconds of discharge.

A very short pulse of direct current has many of the aspects of alternating current. It will, for example, pass through a condenser.

Moreover, it is easy to demonstrate that we are concerned with a real, practical difficulty. After prolonged discharge the bobbin in a dry cell is permeated throughout with a hard mass of dry crystals. Obviously, the resistance of the web of electrolyte has increased tremendously.

In such a cell, alternating current or a pulse of direct current can travel to the edge of the bobbin entirely as an

²⁴ The Beryllium Corp., Reading, Pa.

²⁵ Burgess Battery Co., Freeport, Ill.

electronic current and can be converted into an ionic current at the surface of the bobbin by an action which is analogous to that of a condenser, or a storage battery, or both. No prolonged flow of direct current, on the other hand, can be maintained in this way.

Perhaps a quantitative example will be helpful. Suppose that the web of black has a resistance of 1 ohm and the web of electrolyte has the same resistance in an undischarged cell. One would guess that the resistance of the bobbin would be $\frac{1}{2}$ ohm and this turns out to be a very good approximation. Suppose now that the resistance of the web of electrolyte goes to infinity. A flow of direct current lasting several minutes is impossible. So far as any practical use of the cell is concerned, this one factor—without regard to the condition of the manganese dioxide or zinc—is sufficient to prevent the flow of useful current. Practically speaking, it is meaningful to say that the internal resistance itself has risen to infinity.

On the other hand, the resistance to alternating current or to a pulse of direct current is 1 ohm.

Any experimenter who ignores these difficulties is likely to conclude that the increase of internal resistance plays a minor role in the fall of potential during discharge. In some cases such a conclusion would be correct, but in many cases it is wrong, and in no cases can it be proven by the method described in the present paper.

RICHARD GLUCKSMAN AND C. K. MOREHOUSE: It is true, as Dr. Coleman says, that a dry cell cannot be simply represented as a resistor; however, his suggestion that it would be better represented as a capacitor in parallel with a resistor, as shown in Fig. 1a, does not fully explain the experimental results.

A dry cell with such an equivalent circuit would give an oscillographic curve similar to that shown in Fig. 1b when it goes from a closed to open circuit condition, i.e., the cell voltage would increase exponentially as soon as the current was interrupted. However, our measurements show an oscillographic curve with a large discontinuity (Fig. 1d), indicating that the major portion of the resistance is not effectively bridged by a capacitor. This would correspond more closely to the equivalent circuit pictured in Fig. 1c.

The fact that the discontinuity represents over 80% of the total increase indicates that the capacity could only effectively parallel a small part of the resistance. Furthermore, a substantial part of the remaining 20% voltage increase with time is probably due to the decay of concentration and activation polarization processes which would give a voltage-time curve similar to the exponential recovery curve of a capacitor. Therefore, we would conclude that the capacitance parallels only an inappreciable part of the resistance, and that we are getting a fairly accurate measurement of the internal resistance of a dry cell.

Dr. Coleman also suggests the possibility of the electrolyte being converted into dry crystals as a result of prolonged discharge. This condition may exist in completely run-down cells, but it does not apply here, where D-size cells were discharged at a 0.200-amp constant current drain for 8 hr. The cell is by no means dry after such a discharge, and we believe that the resistance of the electrolyte increases only slightly during the course of normal discharge, and its value is certainly finite.

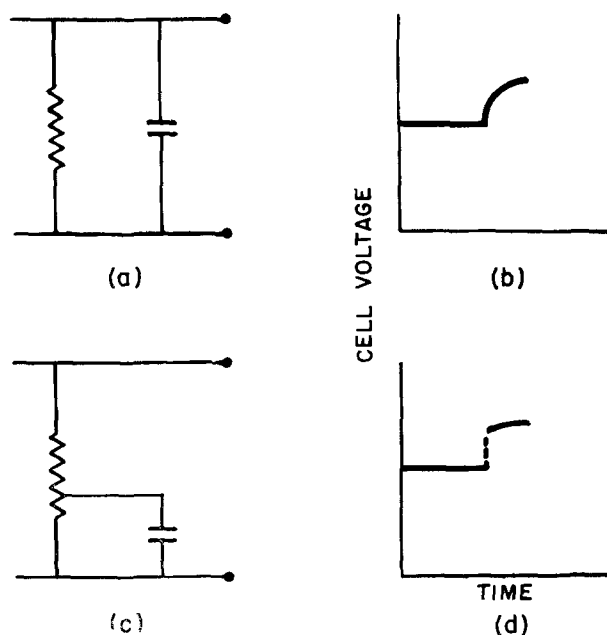


FIG. 1. Possible equivalent circuits and potential recovery curves of a Leclanché dry cell.

Although there are many difficulties involved in measuring the internal resistance of dry cells, it is believed that the results obtained from our measurements are valid. They show that the change in internal resistance as a cell is discharged accounts for only a small percentage of the total voltage drop and that other factors are more important in contributing to the gradual fall of potential with time in the Leclanché cell.

RECENT INNOVATIONS IN THE CONTROL AND OPERATION OF ZIRCONIUM REDUCTION FURNACES

F. E. Block and A. D. Abraham (pp. 311-315)

MORRIS EISENBERG²⁶: Have you or your group attempted to work out the mechanism and chemical kinetics for the Mg-ZrCl₄ reaction on the basis of the operational data for the batch process?

F. E. BLOCK: The reaction rates discussed in this paper are actually average rates since the reaction is nonuniform in nature. Actually, the reaction occurs at small centers around the inside edge of the crucible and it may shift rapidly to one or more different locations. Also, the rate of zirconium chloride sublimation is nonuniform and the concentration of chloride vapors in the retort atmosphere varies throughout the reaction. For these reasons kinetic data could not be calculated on the basis of the batch operation.

A METALLURGICAL EVALUATION OF IODIDE CHROMIUM

D. J. Maykuth, W. D. Klopp, R. I. Jaffee, and H. B. Goodwin (pp. 316-331)

W. H. SMITH²⁷: This paper is a welcomed contribution to those engaged in a study of the metallurgy of chromium.

²⁶ Stanford Research Institute, Stanford, Calif.

²⁷ Research Lab., General Electric Co., Schenectady, N. Y.

Several of the statements made by the authors, however, conflict with results obtained at this laboratory and elsewhere. The first is in regard to the effect of nitrogen on the room temperature ductility of chromium. Our work indicates that the ductility of chromium is more adversely affected by small amounts of nitrogen than any other single impurity. It has been found that less than 0.01% by weight of nitrogen in annealed chromium can raise the bend transition temperature well above room temperature. Slightly more, 0.02% nitrogen, can be tolerated in cold-worked chromium before the bend transition temperature exceeds room temperature. These findings confirm those of Wain, Henderson, and Johnston²⁸ who set the limit of nitrogen in cold-worked metal at 0.02% and a limit of 0.001% in annealed material if room temperature ductility is to be maintained. I do not believe that any data presented in your paper are specific enough to warrant the conclusion that nitrogen contents up to 0.032% have no apparent effect on bend ductility.

Regarding your conclusions on the effect of sulfur, I should like to make the following comments. Alloys of chromium containing 0.1% sulfur prepared by arc melting have been bend tested in the as-cast condition. The transition temperature was less than 100°C which is in the range expected for the base composition used, without sulfur. We have not tried to fabricate these alloys. Your poor results on rolling suggest that sulfur may render chromium hot short. It would be interesting to know if the authors found any adverse effects of sulfur on the bend ductility of as-cast chromium.

D. J. MAYKUTH: Our work did not include a study of the specific effects of nitrogen on the ductility of chromium. With the exception of a single sample, each of the chromium sheets evaluated contained 0.005% nitrogen or less, and, as noted in our paper, variations in nitrogen content below this value had no apparent effect on the room temperature ductility of chromium. However, one ingot of commercial electrolytic chromium, which contained 0.032% nitrogen, 0.26% oxygen, 0.005% carbon, and

²⁸ H. L. WAIN, F. HENDERSON, AND S. F. M. JOHNSTON, *J. Inst. Metals*, **83**, 133 (1954).

0.014% sulfur, was fabricated to sheet and evaluated in bend tests in the wrought condition. Samples of this sheet showed an average ductile-to-brittle transition temperature of -15°C , a temperature which compares favorably with iodide chromium sheet containing about the same amount of carbon and sulfur, but appreciably less nitrogen and oxygen. Our statement that nitrogen variations from 0.001 to 0.032% have no apparent effect on bend ductility was based on these observations.

The results of Mr. Smith's bend tests on as-cast chromium-sulfur alloy samples were noted with interest. Since we did not investigate the as-cast bend ductility of any of our samples, we are not able to offer any additional information on this subject.

PREPARATION OF TITANIUM BY FLUORIDE ELECTROLYSIS

M. A. Steinberg, S. Carlton, M. E. Sibert, and E. Wainer (pp. 332-340)

JAMES C. SCHAEFER²⁹: 1. You spoke of recrystallizing the K_2TiF_6 from hot water. Are you sure that some $\text{Ti}(\text{OH})_4$ does not form by hydrolysis and contaminate your salt?

2. You also spoke of a low efficiency, but had no explanation for same. Don't you think that there is a reaction between the Ti and some of the Cl_2 that is liberated, and also have you considered the solubility of Ti in such a molten bath?

M. E. SIBERT: 1. The K_2TiF_6 was recrystallized from hot water, but the solution was distinctly acid, making hydrolysis negligible. Any $\text{Ti}(\text{OH})_4$ so formed would appear as an insoluble phase (TiO_2). No difficulty was experienced in obtaining insoluble contents of less than 0.1%.

2. Chlorination of deposited titanium is negligible as evidenced by the type of crystal growth obtained. A more tenable explanation for efficiency losses is anodic reoxidation of reduced [Ti(II) and Ti(III)] ion species. Titanium is soluble in the K_2TiF_6 -NaCl melt, but this is also a minor factor in this case.

²⁹ Republic Steel Corp., Cleveland, Ohio.



A Rapid Test for Sulfation¹

C. C. Rose²

Abstract

Lead-acid storage batteries are subject to early failure by operation or storage in a condition of partial discharge. This type of failure is commonly called "sulfation." It has not been defined accurately and has been difficult to produce and evaluate in the laboratory. A method is proposed which is fairly rapid, consistent, and significant, and which measures the contribution of various factors involved.

Lead-acid storage batteries in automotive service fail generally from three principal causes: overcharge, undercharge, or mechanical defects. Cycling failure of positive plates is seldom encountered in this service any longer. Normal failure in batteries which last at least their guarantee life is generally positive grid corrosion.

The modern battery of proper size, in normal service, with proper voltage regulator setting to provide full charge gravity in the battery with a minimum of overcharge, is capable of lasting from 50,000-100,000 miles of driving. One of the most serious causes of damage is undercharge, which often results in premature battery failure because of "sulfation." This is easily recognized, chiefly by the condition of the negative plate. Even after being carefully recharged, such negatives tend to be hard and dense when scratched instead of showing the soft gray metallic luster of good sponge lead. They are often sandy or gritty, particularly if they have been subjected to high acid gravity and high temperatures, and most characteristically they do not show a reverse cadmium reading even when fully charged. This is not because the plates are sulfated, but rather is a symptom of antimony contamination of negative active material and an indication that such plates will sulfate rapidly on open circuit.

This condition results in a high open circuit loss of three or more points per day in gravity and often a loss of 75% or more of cold starting capacity. There is no practical or economically feasible method of restoring such batteries to a normal healthy condition. Sodium and magnesium sulfates or other battery dopes do not help. Sulfation is distinct from the simple condition of discharge, or sulfation brought about by short circuits through battery separators, or the result of complete battery breakdown.

Sulfation does not "account for 70% of all battery failures" as has been stated, or any appreciable fraction thereof. Scrap battery surveys indicate that only about 18% had sulfated negatives even though most of them had given normal life. Of some 4000 batteries which failed prematurely for one reason or another and were returned for adjustment, approximately 13% were judged sulfation failures or neglect failures. There is no good way of translating this figure to total production, but assuming 1% returns, it represents not over 0.13% of the total. There is no reason then to say that sulfation is a major cause for battery failure, although it

still is a major weakness of the lead-acid battery and it generally causes failure before normal life is attained.

The real importance of this characteristic is that it limits the stand-by time of lead-acid batteries either in stock or vehicle storage. It has been a difficult situation to understand clearly and even more difficult to explain and prevent. This is because a lead-acid battery stands a great deal of abuse and neglect without suffering permanent damage.

For this reason a simple and practical test for sulfation is in order. Strangely enough, no test has been devised or at least agreed on to date to do this, and such a test procedure is not too obvious. It is felt that neglect in keeping batteries fully charged while in stock, particularly in hot weather, is a factor contributing to sulfation failure. This is especially harmful when such batteries are installed in service without being fully charged, and it is almost certain to be fatal when such service continues to provide inadequate input, and the undercharged condition is allowed to prevail.

Admitting this, it was still not possible to explain all that was happening in the field or to duplicate it in the laboratory. Quite by accident the additional factor or a combination of factors contributing to the condition was found, and a rapid, consistent, and significant test for measuring the influence of the various battery components involved has been devised.

The Sulfation Test

The basis of the test is high temperature open circuit stand and high temperature charge. Whether the latter condition is critical or not, it ties in with field conditions, and it does seem to accelerate the test. Readings taken on batteries under the hood in cars parked in the sun have shown temperatures as high as 165°F. At these temperatures with normal regulator settings charging rates are high because battery voltage is low. Under such conditions it is hard to anticipate battery failure from sulfation except that self discharge is extremely high both day and night while the car is idle. Water loss is also very high resulting in low levels and high gravity which again is extremely harmful to negative plates. Thus, a test devised to include charge and open circuit stand at 150°F seems reasonable and practical for laboratory purposes.

The exact times, sequence, and rate of capacity measurement, etc., for such a test are not too critical. Several different schedules have been tried including recharge and capacity testing at 80°F. Such procedure slowed up the testing and showed no advantage. Also it may be found that one or more of the discharge cycles in the proposed schedule can be eliminated and yet here again it may be said that such a cycle is not unfavorable to a battery normally and that it further simulates operating conditions.

¹ Manuscript received November 12, 1954. This paper was prepared for delivery before the Boston Meeting, October 3 to 7, 1954.

² Automotive Division, Electric Storage Battery Company, Cleveland, Ohio.

TABLE I. Test schedule 150°F water bath temperature

Friday	9:00 A.M.	Batteries begin open circuit stand.
Saturday		On open circuit.
Sunday		On open circuit.
Monday		On open circuit.
Tuesday	9:00 A.M.	Catchout. Discharge at 40 amp to 1.7 volts per cell.
	11:00 A.M.	On charge at 5 amp.
Wednesday	9:00 A.M.-10:00 A.M.	Discharge at 40 amp.
	10:00 A.M.-3:00 P.M.	Charge at 10 amp.
	3:00 P.M.	On open circuit.
Thursday	9:00 A.M.-9:30 A.M.	Discharge at 40 amp.
	9:30 A.M.-3:30 P.M.	Charge at 10 amp.
	3:30 P.M.-4:00 P.M.	Discharge at 40 amp.
	4:00 P.M.	On charge at 5 amp.
Friday	9:00 A.M.	Stop charge.

The recommended schedule (Table I, S-40 Test) is workable in any battery laboratory with S.A.E. cycling circuits plus a simple water bath to maintain temperature. The comparison of residual capacity after O.C. stand is just as accurately measured by the 40 amp discharge normal to cycle testing as it is at higher rates. Results are consistent and significant and are available in 10-12 weeks. Tests were all run on 100 amp-hr S.L.I. batteries.

Fig. 1 indicates the effect of electrolyte gravity on negative sulfation. That this has been recognized by the industry is shown by the change to high level lower gravity in many batteries now offered, although it is doubtful that many of these manufacturers know the exact effect of this change. The change from 1.280 to 1.260 practically doubled the resistance of a battery to sulfation failure, all other factors being equal, with still further improvement possible at 1.240 gravity.

In Fig. 2 the combined effect of insulation and of positive grid alloy is shown. Rubber insulation is outstanding in all comparisons and the indication is that improved types of glass fiber and diatomaceous earth can approach rubber in this characteristic. These batteries ran 34 or more weeks, failed apparently from positive grid corrosion plus some loss of active material and with negatives still showing good negative cadmium readings at the end of life. The function here is apparently a filtering or sequestering action protecting the negative from the antimony dissolved from the positive. That this is so is clearly indicated in the direct comparison of the 11% and 6% positive alloys with wood insulation, the high antimony alloy failing much more rapidly than the low. Comparison of the wood and rubber insulation with the low antimony alloy is quite obviously in favor of rubber again at a favorable low 1.260 gravity.

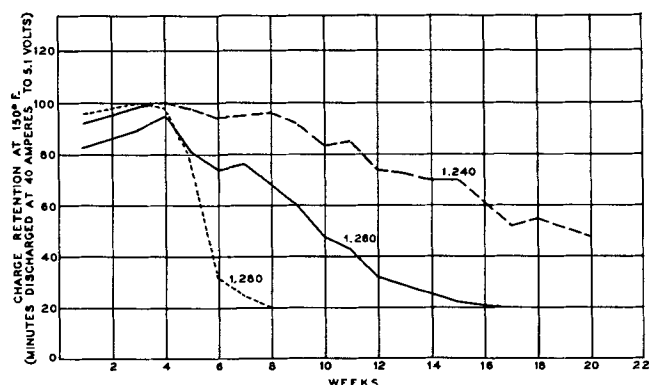


FIG. 1. Effect of full charge specific gravity on sulfation life; 6% Sb positive grid alloy; mechanical insulation.

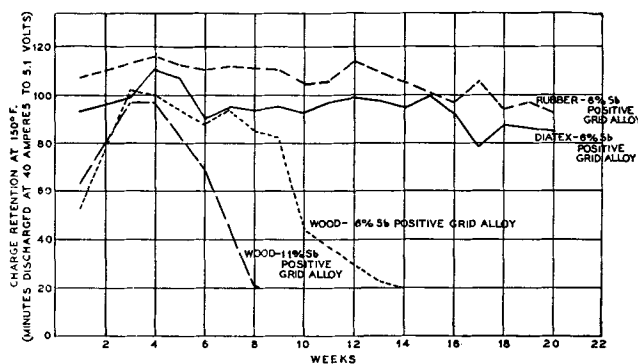


FIG. 2. Effect of separator and alloy on sulfation life; specific gravity, 1.260.

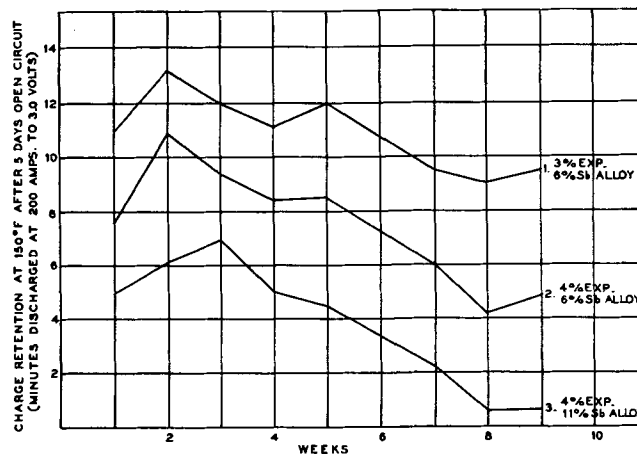


FIG. 3. Effect of expander and positive grid alloy on sulfation; 1.285 specific gravity; rubber insulation.

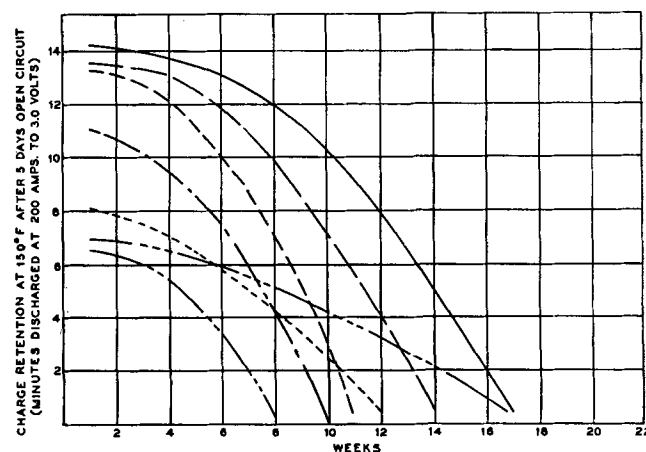


FIG. 4. Comparison of competitive batteries on sulfation test.

This test may be used to advantage in testing the new mechanical separators as well. By mechanical separators is meant those other than wood or rubber, made from cellulose, or glass fibers plus diatomaceous earth filler, and bonded with some kind of plastic acid resisting resin. A distinct difference in resistance to sulfation is shown which cannot be predicted from appearance or from other normal battery or separator tests. It was found that the particular brand of separators which showed up weakest on this sulfation test corresponded with field returns from this same cause of failure.

In Fig. 3 two variables are involved. The principal variable was expander which governs the activity of the negative plate and the difference between 3% and 4% is quite ap-

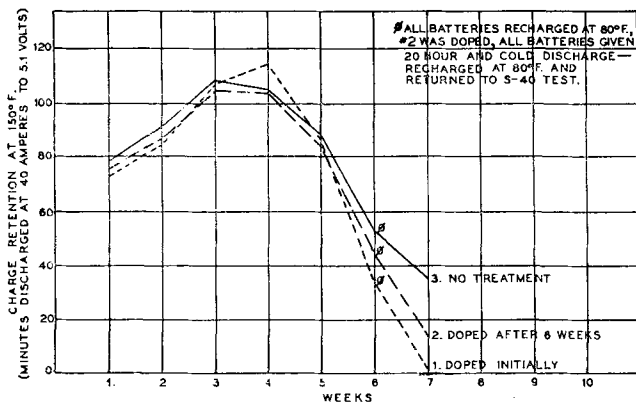


FIG. 5. Effect of battery dope on high temperature sulfation life. 11% Sb positive alloy; wood insulation; 1.285 specific gravity.

preciable. This test was run with rubber insulation, which is favorable and eliminates the separator variable, but at high gravity to accelerate testing. Also the discharge was run at 200 amp instead of 40 and is recorded on a somewhat different scale, which does not affect the shape of the curves. The effect of grid alloy is again shown and it is apparent that these factors are cumulative.

Fig. 4 is a comparison of commercial batteries all of the same ampere-hour capacity, of different makes, and as purchased on the open market. It is evident that all of these batteries are subject to this type of failure and that the benefits gained by proper selection of expander, grid alloy, and acid gravity are cumulative. The top curve represents a favorable combination of these variables.

The difference in the position of the curves at the start is not a significant part of this comparison since it probably is caused largely by their difference in age and care in stock. However, it certainly does indicate what happens to batteries not properly maintained prior to installation in service.

Fig. 5 represents the results of a test carefully designed to determine the effect of a battery dope on sulfation. Three identical batteries were built and one of them was doped just before starting this test. This is battery No. 1. At the end of six weeks this battery had definitely failed with the other two not far behind. At this point the second battery was

TABLE II

Battery No.	1	2	3
Additional treatment.....	None	Doped	None
Twenty-hour discharge			
Specific gravity (80°F).....	1.276	1.280	1.272
Capacity (hr).....	<18	<18	18.7
Cold discharge			
Specific gravity (80°F).....	1.289	1.293	1.282
Neg. cadmium.....	+ .04	+ .04	+ .02
5 sec volts.....	4.20	4.40	4.50
Minutes.....	0.82	1.00	1.21
Recharge 80°F returned to sulfation test			

TABLE III

Battery No.	1	2	3
Sulfation cycle #7 (min).....	0	13.1	36.2
Twenty-hour discharge (hr).....	<12	<12	<12
Open circuit at 95°F (14 days)			
Start specific gravity (80°F).....	1.237	1.258	1.247
Finish specific gravity (80°F)....	1.188	1.192	1.173
Loss.....	.049	.066	.074
Twenty-hour capacity (hr).....	0.0	0.2	2.0
Cold capacity			
Minutes.....	0.49	0.66	0.85
5 sec volts.....	4.00	4.03	4.25
Twenty-hour capacity (hr).....	11.8	13.2	16.7

doped to determine whether a dope could salvage a battery otherwise sound but in a sulfated condition. This was battery No. 2.

At this point a 20 hr and a 300 amp discharge at 0°F were run not only to measure the capacity of the batteries but to favor the dope by at least three careful and complete recharges at 80°F. Results are indicated in Table II.

The batteries were returned to the sulfation test where continued deterioration was clearly indicated. They were again removed and final data obtained as indicated in Table III. Capacity after open circuit stand was practically nil although the comparison distinctly favors the undoped battery. It is interesting to note that gravity loss did not indicate the true capacity loss at this point and that it actually favored the doped batteries. Full charge cold capacity likewise had been lost almost completely in the doped batteries—certainly it was not better than in the undoped one.

Final inspection of the elements indicated a slight but significant difference in the appearance of the negatives. Those in the doped batteries were hard, lacked good metallic luster, and the outside negatives were partially washed out. The positive plates also showed a similar slight difference in favor of the undoped battery, with less sulfate and better appearing active material. The positive plates of the doped batteries had not lost active material as was expected, probably explained by the fact that this was not a cycling test.

Conclusions

The proposed test results in a definite negative plate failure which duplicates in appearance and electrochemical characteristics that encountered in service. Test results are not complicated by the failure of other components of the battery as is often the case in other storage battery tests. The effect of the contributing factors, such as acid gravity, positive grid alloy, expander, and separators, is clearly indicated both singly and collectively. The test indicates very definitely that battery dopes do not prevent negative plate failure, i.e., sulfation, nor can they restore batteries in this condition. The combination of rubber insulation, 1.260 or lower acid gravity, 6% antimony lead positive grids, and minimum expander results in a battery with the least tendency to failure from sulfation.

Review of High Temperature Metal-Ceramic Seals¹

Hayne Palmour, III²

Abstract

A technical review of the development of metal-ceramic seals is presented, with emphasis on methods devised for high temperature brazing of metals to low-loss technical ceramics for electronic applications. Basic mechanisms of metal-ceramic bonding are discussed briefly, as are the problems resulting from mis-match between thermal expansivities of metals and ceramics. Illustrations of feasible design types are shown, and comparative data on electrical and mechanical properties of various technical ceramics (including glass) are listed.

Today's demand for high temperature hermetically sealed metal-ceramic assemblies is an outgrowth of the constant push by the electronics industry toward higher operating frequencies and miniaturized components with resultant high power ratings and high temperatures for components and systems alike.

If we were to reduce the complex requirements of modern electronic design to extremely simple terms, we might come up with the idea that all circuits are composed of appropriately chosen conductors, semiconductors, and nonconductors, operating in suitable environments. In these simple terms, this paper shall be particularly concerned with the matter of effecting combinations of appropriate metal conductors and ceramic nonconductors to isolate and control an environment, like the atmosphere within a vacuum tube.

One of the earliest and most useful man-made nonconductors was glass, and the development of vacuum tight glass-to-metal seals near the end of the last century made the incandescent light a practical commodity; the same glass seals, with some refinements in materials and techniques, helped to launch the infant radio industry on its way with adequate vacuum tubes in glass envelopes.

But as the radio industry grew into an electronics industry and began to add words like "radar" and "microwave" to our common vocabulary, the usefulness of glass as a nonconductor dropped in more or less direct ratio to the frequencies and temperatures involved because of its inherent high dielectric losses at elevated temperatures and its poor heat shock resistance (Table I).

Fortunately, there is available a group of dense, essentially crystalline ceramics which demonstrate superior low-loss properties at high frequencies and high temperatures (Table I). In addition, these low-loss ceramics offer higher mechanical strength and generally better thermal shock behavior than can be expected from glass. While they do not always lend themselves to fabrication in the complex shapes which are possible with plastic molten glass, they are amenable to fabrication in a broad range of useful shapes to close dimensional tolerances. Consequently, these low-loss ceramics might be expected to solve many of the problems which have heretofore bedeviled the tube designer restricted to working with glass. Low-loss ceramic materials have not been limited to vacuum tubes alone, but have found wide use in many other electronic components.

For the low-loss ceramics to become useful in the full range of electronic applications, there must first be the counterpart of the glass-to-metal seal—a metal-to-ceramic seal to bond

the conductor and nonconductor together into a mechanically strong, pressure-, vacuum-, or water-tight unit.

A metal-ceramic seal, or more precisely, a hermetically sealed metal-ceramic assembly, is composed of at least one metal unit, in conjunction with one or more ceramic units, or of several ceramic units sharing metallic bonding interfaces; the ceramic, the metal, and the bond areas must be impervious to the passage of liquids or gases. Obviously, the ceramic may function as a nonconductor, as a structural member, or as both. Likewise, the metal may be only a structural or bonding member, an electrical conductor, or both.

There are two general uses of metal-ceramic seals. One is in the production of ceramic envelopes and "windows" for electron tubes, and, because sealing in this case constitutes assembly, the sealing operation is generally accomplished by the tube manufacturer.

The second use is a broader one, where there is an increasing demand for ready-sealed metal-ceramic units, such as feed-through insulators for hermetic-sealed transformers, capacitors, and the like, which the manufacturer solders or brazes into his product.

It should be pointed out that metal-to-ceramic seals represents a special case of a more general, and much older matter—that of metal-to-ceramic bonding. The ceramic field is a very broad one, including glass, porcelain enameling, ordinary dinnerware, decorative pottery, and other inorganic, nonmetallic materials which are processed at high temperatures.

The ceramics which are of interest in electronics, usually called "technical ceramics," are among the most recent developments in a ceramic technology which extends back over a history of several thousand years. During a great part of that long history ceramic-to-metal bonding has played an important part in the aesthetic appeal and usefulness of ceramic materials.

Metal-to-ceramic bonds fall into three general categories, based in large part on the mechanism by which the required intimacy of contact at the ceramic-metal interface is obtained.

The first of these utilizes a molten ceramic wetting a relatively more refractory metal. Porcelain enamel on metal is of this type, and so are the glass bonded decorative metals applied to pottery and glass. Another application of this type of bond is found in the glass-to-metal seals commonly used in electronic work. Since this bond employs a molten or glassy ceramic phase, the finished unit displays many of the brittle properties of glass. Fairly low melting ceramic compositions are required, so the bond is generally restricted to low temperature operations.

The reverse situation is found in type two, where the metal provides the fluid phase to wet a relatively more refractory ceramic. Examples of this sort may be found in certain classes

¹ Manuscript received October 21, 1954. This paper was prepared for delivery before the Chicago Meeting, May 2 to 6, 1954.

² Research Department, American Lava Corporation, Chattanooga, Tennessee.

of cermets, and in the "hard solder" metal-to-ceramic seals which are of particular interest in this discussion.

The third type of bonding comes about in solid-state reactions. The intimacy of contact is provided mechanically by pressure, spraying, dipping, or painting, or granular mixing techniques, and solid-state reactions occur during firing at a temperature slightly below the melting point of either metal or ceramic. This reaction is typical of refractory cermets.

In each of these categories, a mechanism for obtaining intimate contact between the metal and ceramic components has been described. The actual nature of the bond, and the resultant bond strength, are dependent on more complex factors.

There can be a simple mechanical bond, deriving its strength from interlocking particles, or from penetration of the liquid phase into surface pores and grain boundaries at the refractory interface, or from van der Waals forces.

There can be a chemical bonding which depends on solvent action, transferring constituents from the solid phase into the liquid phase. In this case there is the possibility that new solid phases may form within the matrix to produce a crystal-line bridging structure across the interface.

There may be a chemical bonding when an active metal constituent, either in a melt, or by solid-stage change, undergoes a valence shift toward a metalloid or nonmetallic state, progressing continuously from metal to suboxide to oxide across the interface, becoming finally an integral part of the refractory ceramic structure.

Certain metals, because of their atomic size and chemical properties, exhibit an affinity for chemical bonding with ceramics. They share the common property of relatively easy oxidation, yielding refractory oxides which are compatible with the oxides normally used in ceramic compositions. The active metals, titanium and zirconium from Group IV of the atomic chart; the transition metals, iron, cobalt, and nickel; chromium and molybdenum in Group VI; and manganese in Group VII are useful in this respect.

It is extremely difficult to observe directly or measure quantitatively conditions at a bond interface. Pineus (1) has described a tapered sectioning technique to produce a cross section of the bond having an apparent thickness 10 times greater than the width, as an aid to microscopic examination. Kingery (2) has reported on studies of the relationship between bond strength and interfacial contact angles, using a sessile drop of molten metal on a ceramic surface, where good bonding is always accompanied by very low contact angles.

The matter of thermal expansion is an essential consideration in any metal-to-ceramic bond. The expansion characteristics of metals and ceramics are inherently dissimilar, and where the bonding material is nonductile over a considerable temperature range, careful selection of metal and ceramic and proper design of the unit, to utilize high compressive strength of the ceramic rather than the much weaker tensile strength, determine whether or not the bond will be successful.

The mechanisms of bonding constitute a major field of investigation and study beyond the scope of this review. However, the subject is well covered in the literature, particularly under the heading of porcelain enamelling on metals, and in the field of cermets (3-5).

There are four basic techniques for developing metal bonds suitable for ceramic-to-metal seals. The first technique, that of using glass as a bond between metal and ceramic, fails to meet the most stringent requirements of high temperature, high-frequency electronic service. For this reason, and because

TABLE I. *Comparative electrical and mechanical properties of glasses and ceramics*

	Soft glass	Hard glass	Alumina ceramic
Safe temperature at continuous heat.....	Below 450°C	Below 450°C	1100°C
Thermal shock resistance.....	Poor	Fair	Excellent
Tensile strength.....	Low	Low	Good
Compressive strength.....	Good	Good	Excellent
Te value.....	300°C	300°C	800°C
Power factor at 1 mc room temperature.....	0.0090	0.0040	0.0007
Dielectric constant.....	7.0	4.7	8.3

the various methods are well understood and well covered in the literature, glass bonded seals will be excluded from this discussion.

The remaining three are similar in that each technique utilizes one or more of the metals which exhibit an affinity for ceramic bonding as the "active ingredient," and in the fact that a reducing or inert atmosphere is necessary during firing to prevent excessive oxidation of the metal before it can seal with the ceramic. They are commonly known as the moly-manganese process, the titanium hydride process, and the active metals process.

The present day moly-manganese process is the outgrowth of the first successful high temperature seals, developed in Germany, near the beginning of World War II (6). The Telefunken process utilized an initial coating of molybdenum powder with admixtures of iron and nickel painted on a steatite ceramic, which was fired on in hydrogen atmosphere to develop a strong bond at a temperature near the softening point of the ceramic. There was little knitting of the moly particles with each other, so the initial layer was augmented with nickel powder painted on and fired in hydrogen to alloy with the moly and produce a bright metal surface which could subsequently be silver brazed. The final assembly of the metallized ceramic with metal parts which had also been nickel alloyed was made in hydrogen with silver solder. Telefunken produced acceptable radar tubes, but experienced considerable variations in the quality of bonding with the moly-iron-nickel mixture (7).

Nolte and Spurek (8) have since modified the process to utilize manganese rather than nickel and iron to promote bonding with the ceramic, and substituted electrodeposited nickel and copper in the alloying operation. The moly-manganese bond is less sensitive to slight process and kiln atmosphere variables than was the case with nickel-iron-moly used in the Telefunken process.

The moly-manganese process appears to have these advantages: strong bond; good reproducibility; and excellent dimensional control of metallized areas.

Disadvantages are: multistep process (3 firings); hydrogen firing tends to discolor ceramics and glazes and may impair electrical properties.

Bondley, in 1947, introduced the use of titanium hydride in conjunction with silver solder, copper, or silver (9). The area to be metallized is painted with titanium hydride; the ceramic and metal parts are assembled with silver solder wire in contact with the hydride area to provide the fill material. One firing in vacuum or inert atmosphere completes the seal, at a temperature just above the melting temperature of the solder. The hydride dissociates during the early stage of firing to leave a thin layer of finely divided active metal. The

TABLE II. Mechanical and electrical properties of dense, low loss ceramics

Property	Forsterite 2MgO·SiO ₂	Alumina 85% Al ₂ O ₃	Alumina 97% Al ₂ O ₃
Specific gravity, g/cc.	2.8	3.4	Above 3.6
Safe temperature at continuous heat, °C.....	1000	1100	1500
Hardness, Mohs' scale.....	7.5	9.0	9.0
Coefficient of thermal expansion			
25°-100°C.....	9.1×10^{-6}	5.8×10^{-6}	5.0×10^{-6}
25°-700°C.....	10.6×10^{-6}	7.5×10^{-6}	7.8×10^{-6}
Tensile strength, psi..	10,000	20,000	25,000
Compressive strength, psi.....	85,000	140,000	170,000
Heat shock resistance.	Fair	Excellent	Excellent
Impact resistance, (Charpy).....	4.0	6.3	8.2
Dielectric strength, v/mil.....	240	250	260
Dielectric constant, 1 mc.....	6.20	8.30	9.85
Power factor, 1 mc....	0.0004	0.0007	0.0003
Loss factor, 1 mc....	0.0020	0.0060	0.0029

hydrogen given off is credited with a beneficial cleaning action to further condition the metal and ceramic sealing surfaces.

Later work by Pearsall and Zingesser demonstrated the suitability of other hydrides, notably zirconium, and also showed that the active metals themselves produced comparable results (10).

We may list these advantages for the hydride technique: strong bond, excellent reproducibility; only one firing operation; vacuum or inert atmosphere rather than hydrogen; firing temperatures well below the softening point of the body; use with silver, copper, silver solder, lead and soft solders.

Disadvantages include: high fluidity of the solder at the alloying temperature, which may make dimensional control of the metallized area difficult; and application of the hydride involves hand work of considerable skill to achieve product uniformity.

Pearsall and Zingesser's work (10) opened up several new avenues of approach, which might be grouped together and called the active metal techniques.

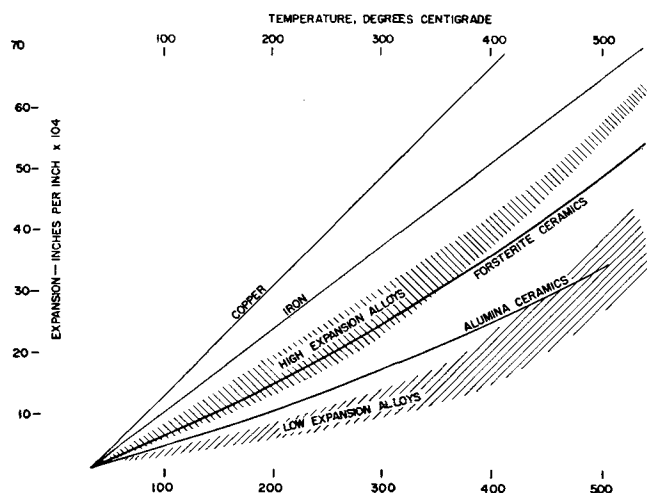


FIG. 1. Expansion characteristics of metals and ceramics.

Briefly, they found that active metals, particularly titanium and zirconium, could be used to produce excellent seals in the form of an alloy with silver, copper, or silver solder, or in powder form used much like the hydrides, or as a sandwiched thin layer between sheets of solder (7).

A titanium cored silver solder is now commercially produced in wire form, available with 3%, 5%, or 8% titanium (11). The cored wire, in preformed rings or other shapes, is assembled with the metal and ceramic, or with ceramics alone, and fired in vacuum or inert gases, such as helium and argon. The silver-copper eutectic solder melts at 760°C, and with further heating to 950°C, alloys with the titanium core and wets the ceramic and metal parts to effect the seal.

It is the simplest technique yet devised for metal-ceramic brazing, but there are several design limitations which are necessary to control the flow of the superheated solder.

It seems to be most applicable where the sealing zone is almost totally enclosed between matching parts of the assembly, where the length of the flow is relatively short, and where the final brazed zone is quite thin.

Advantages are: strong bond, excellent reproducibility with proper design configurations; simple mechanical assembly; and only one firing in vacuum, helium, or argon.

Disadvantages are: design limitations; and flow difficult to control.

There is some evidence that the titanium-cored wire technique may be improved by using high silver content solders, rather than the rapidly melting eutectic composition. With sterling silver, for example, the solder is plastic rather than fluid from 760° almost to the alloying temperature at 950°C, and does not tend to flow away from the titanium core. Consequently, alloying is more uniform, and the flow is more easily controlled.

The processes already described are most appropriate for direct assembly with formed metal parts. There are many applications where a bare metallized pattern on ceramics is desirable. Paintable powder mixes of silver solder with active metals may be used where a metallized band or other configurations to close dimensional tolerances are required on ceramics (12). Controlled flow, excellent wetting, and strong bonds have been obtained using eutectic silver solder with 8% titanium metal, suitably suspended and applied by brushing, and fired to about 850°C in vacuum. These metallized ceramics can be silver brazed in protective atmospheres. If precautions are taken to avoid heat shock, they may be brazed with a torch using a reducing flame.

There are certain other techniques which have promise, although there are certain inherent difficulties in processing which make them less attractive, at the present time, than the methods mentioned.

Knecht (12) has described a solid-state bonding of metal and ceramic powders formed under high pressures in layered zones, somewhat like powder metallurgy practice, and matured at elevated temperatures in protective atmospheres.

Strong bonds can be developed on alumina ceramics with vapor-deposited Inconel-copper films, which can then be silver brazed with fair success.³ Processing offers real technical problems, including suitable means of masking, rotating the work, and controlling deposition rates, to achieve uniformly metallized areas, to close dimensions, on a great variety of sizes and shapes.

Selection of metals and ceramics for these high temperature seal applications is of great importance. As mentioned earlier,

³ Author's experimental work.

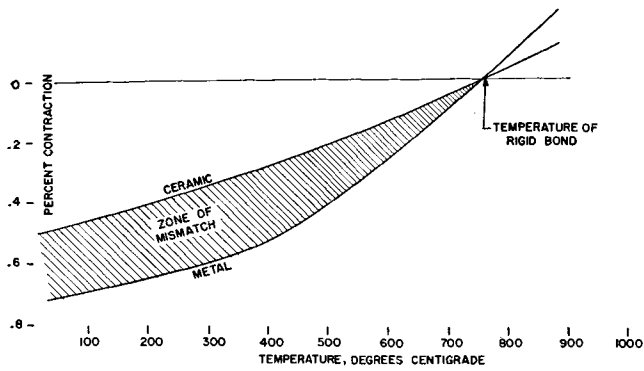


FIG. 2. Stresses on cooling below melting point of silver solder.

thermal expansion differences between metal and ceramic create the most difficult technical problems in sealing practice.

Three ceramic body types are most desirable from the standpoint of electrical and mechanical properties for use in high temperature seals. They are Forsterite, $2\text{MgO} \cdot \text{SiO}_2$; 85% alumina; and the 95-97% alumina bodies (Table II).

Forsterite has relatively high thermal expansion characteristics, making the choice of matching metals somewhat easier, but it is inferior to the alumina ceramics in mechanical strength and particularly in heat shock resistance. Low expansion metals of the Kovar type, nickel-cobalt-iron alloys, provide a fairly satisfactory match with the aluminas.

Metals for sealing purposes must first of all be adequately workable, and must possess reasonable electrical characteristics, but the thermal expansion characteristics are generally determining factors in selecting a suitable metal. Copper would be highly desirable, were its thermal expansion not so very much higher than any of the usable ceramics (Fig. 1).

The chrome-iron and nickel-iron alloys, and the nickel-cobalt-iron alloy developed for glass sealing cover a fairly wide expansion range between room temperature and the annealing point of glass at about 400°C , but above that temperature there is a sharp inflection toward much higher expansion rates. The conductivity of these sealing alloys is considerably lower than copper, which, in some cases, makes them unsatisfactory for the intended electrical use, or requires an excessively large wire size.

Fig. 2 illustrates the contraction experienced on cooling a seal between an alumina ceramic and the best available metal alloy.

The silver solder, which makes the seal, becomes rigid and nonductile at about 700°C above room temperature, and the

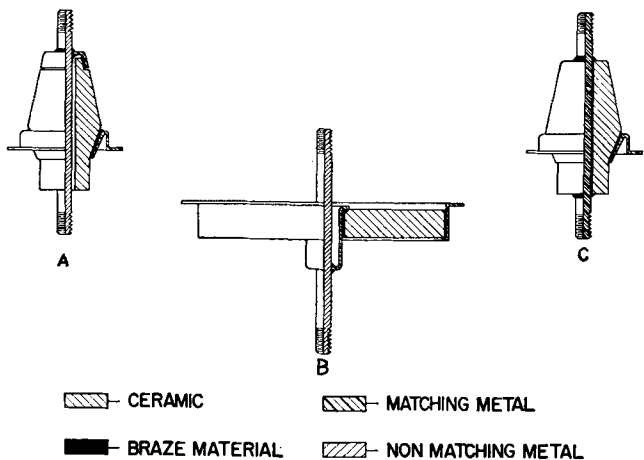


FIG. 3. Three types of feed-through insulators

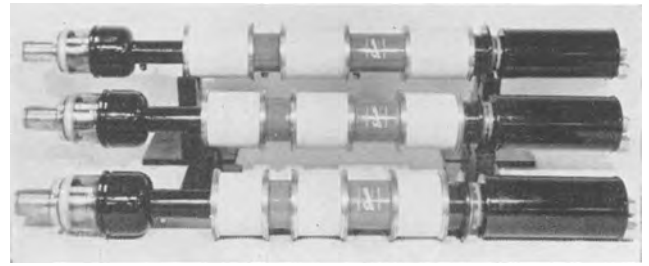


FIG. 4. Large metal-ceramic sealed klystrons

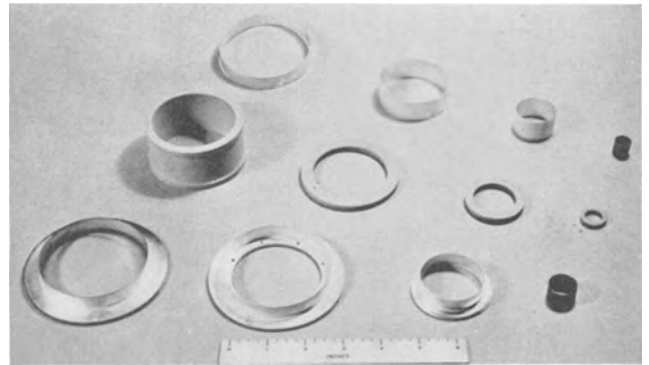


FIG. 5. Component metal and ceramic parts of experimental tetrode prior to assembly.

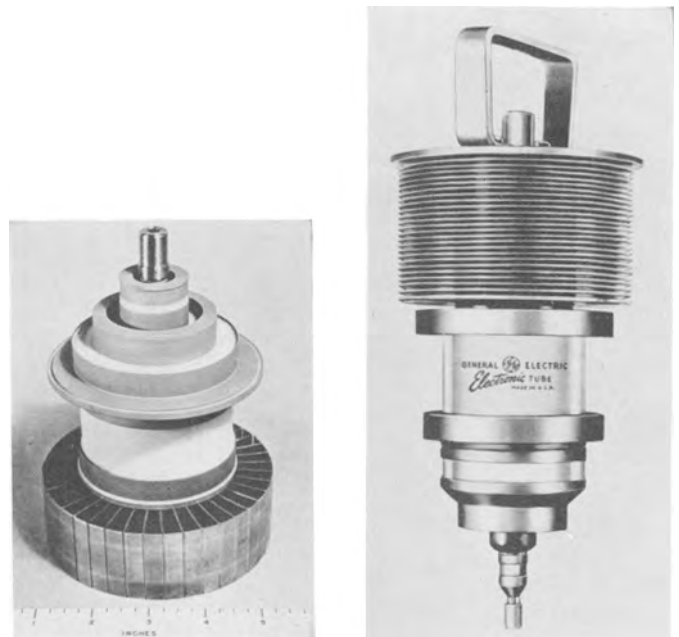


FIG. 6. (left) Assembled tetrode

FIG. 7. (right) High-frequency triode with metal-ceramic envelope.

mismatch in contraction rates, must result in stresses which under certain conditions may be disruptive. There are no metals available which really match ceramics in expansivity and careful design to achieve a safe distribution of stresses is required. Thus, the resolution of expansion mismatches is the chief aspect, the basic function, of the specialized design configurations which are employed in making high temperature seals.

From the mechanical standpoint, there are two distinctly different types of seals. The outside seal has a band of metal surrounding the ceramic, generally giving compressive stresses

in the ceramic. The inside seal has the ceramic surrounding the metal and gives rise to tensile stresses, usually considered dangerous.

Three types of feed-through insulators will serve to indicate the basic principles of design (Fig. 3). In the first example, (Fig. 3a), outside seals of matching or compatible metals are employed in both positions, and the center conductor, which may be nonmatching, is brazed to the upper cup to complete the seal. Where mechanical stresses or electrical requirements demand that the center conductor be completely sealed within the ceramic, a matching metal is mandatory, and the dimensional tolerances should insure a close fit to limit the solder to a thin film (Fig. 3b).

A tapered mounting ring is preferred over straight cylindrical shapes to avoid sudden discontinuities in the ceramic. The shape and thinness of the metal stock prevent excessive loading which might rupture the ceramic, particularly under thermal shock conditions.

The ceramic wafer (Fig. 3c) illustrates another condition where a nonmatching center conductor must be used, and the shape will not allow an outside seal. A thin walled cup of a matching metal is used, with the hope that the tensile stresses it transmits do not exceed the tensile strength of the ceramic.

By careful design, very intricate assemblies are now being commercially produced by several manufacturers.

High-frequency klystrons with low-loss ceramic envelopes and high temperature seals of the moly-manganese type are commercially produced as are various types of triodes and tetrodes for radar and other high frequency uses (Fig. 4, 5, 6, and 7).

Conclusion

The future for these seals is bright, and the demand for them is increasingly urgent. Those who are working with them wish hopefully that the expansion characteristics of available

ceramics could be ideally matched over a broad temperature range with new metal alloys. Electronics designers should be acquainted with the particular problems of metal-ceramic sealing so that cooperative designing could aid in eliminating some of these problems. But the fact remains that, with existing metals and ceramics, there are enough techniques, methods and design stratagems now available to produce high quality, high temperature seals which should amply satisfy high-frequency electronic requirements.

REFERENCES

1. A. G. PINCUS, *J. Am. Ceram. Soc.*, **36**, 152 (1953).
2. W. D. KINGERY, *et al.*, *J. Am. Ceram. Soc.*, **36**, 363, 403 (1953); *ibid.*, **37**, 18, 42 (1954).
3. A. I. ANDREWS, "Enamels," Twin City Printing Co., Champaign, Ill. (1935).
4. J. A. STAVROLAKIS, *et al.*, WADC Technical Report 53-356, October (1953) (Armour Research Foundation, Illinois Institute of Technology).
5. "Proceedings of the WADC Ceramic Conference on Ceramics, 6-8 October, 1952," WADC Technical Report 52-327. Restricted.
6. "German Centimeter & Decimeter Tubes," Intelligence Report (TUB-1) Office of the Theater, Chief Signal Officer, APO 887 (1945).
7. L. NAVIAS, General Electric Research Laboratory Report RL-833, April (1953).
8. H. J. NOLTE AND R. F. SPURCK, *Television Eng.*, **1**, 14 (1950).
9. R. J. BONDLEY, *Electronics*, **20** (7), 97 (1947); *Ceramic Age*, **58** (1), 15 (1951).
10. C. S. PEARSALL AND P. K. ZINGESER, Technical Report #104, Research Laboratory of Electronics, Massachusetts Institute of Technology (1949).
11. H. BENDER, *Ceramic Age*, **63** (4), 15, 46 (1954).
12. W. KNECHT, Air Force Technical Report No. 6101, February (1950).
13. W. H. KOHL, "Materials Technology in Vacuum Tubes," Reinhold Publishing Co., New York (1951).



Report of the Chlor-Alkali Committee of the Industrial Electrolytic Division for the Year 1954¹

William C. Gardiner,² Morton S. Kircher,³ and Warren D. Sherrow⁴

Production in 1954

The production of chlorine set a new record of 2,895,100 tons in 1954, an increase of 3.4% over 1953. Daily capacity is now estimated to be 10,600 tons so that the average production was 75% of the installed capacity. The year started with a low average of 7350 tons per day in January and gradually improved to 8400 tons per day which held for October, November, and December.

Caustic soda production was 3,393,900 tons, of which 14% was by the lime-soda process.

Changes in the Industry

The new plant of the Hooker Electrochemical Company at Montague, Mich., started in April and the chemical chlorine process plant of Hercules Powder at Brunswick, Ga., was started. International Minerals and Chemical Corporation expanded their caustic potash and chlorine facilities at Niagara Falls, N. Y. The Wichita, Kan., plant of Frontier Chemical Company expanded and a further expansion has been announced.

The Muscle Shoals caustic-soda chlorine plant was sold to Diamond Alkali in October and was expected to be in production early in 1955.

The Dominion Alkali Plant at Beauharnois, Quebec, has been sold to Columbia-Southern.

West Virginia Pulp and Paper Company shut down their plants at Covington, Va. and Tyrone, Pa., and are expanding their plant at Luke, Md., by replacing the Hargreaves-Bird cells with Hooker cells.

Dow Chemical Company built a plant to convert NaOH to Na₂CO₃ at Freeport, Texas.

General Aniline and Film Corporation announced their decision to build a 50 ton chlorine plant at Linden, N. J., using Mathieson cells.

Weyerhaeuser Timber Company has indicated that they will build a plant of 110 tons capacity at Longview, Wash. This will be the sixteenth paper mill with a captive chlorine plant.

Canadian Industries Limited announced that they would abandon their chlorine plant at Sandwich, Ont., which was partially destroyed when it sank into a brine well cavity. Expansion at Cornwall, Ont., will make up for the loss.

The price of mercury hurt mercury cell operators. Starting at \$187-\$189 per flask (\$2.46-\$2.49/lb), every price change was up until it reached an unprecedented \$325-\$330/flask (\$4.28-\$4.35/lb) in October. The year closed with the price at \$318-\$320 (\$4.19-\$4.21). In July the General Services Administration announced a three year guaranteed-price program which calls for buying a maximum of 125,000 flasks

¹ Prepared for delivery before the Cincinnati Meeting, May 1 to 5, 1955.

² Olin Mathieson Chemical Corporation, Niagara Falls, N. Y.

³ Hooker Electrochemical Company, Niagara Falls, N. Y.

⁴ Great Lakes Carbon Corporation, Niagara Falls, N. Y.

of domestic mercury and 75,000 flasks of Mexican metal at \$225 per flask. The program also provides for contracts with producers in other countries. Mercury cells use about 5% of the total U. S. consumption.

Oldbury Electrochemical Company started their sodium chlorate plant in Columbus, Miss.

Joshua Szechtman has announced his invention of a cell to produce metallic sodium, sodium-lead alloy, or caustic soda. It is still a paper development but is based on the old Acker process, also German work before and during World War II with the electrolysis of fused salt in a cell with a cathode of molten lead.⁵ Szechtman's idea is to use a modern mercury cell design and substitute a thin stream of molten lead for mercury with fused salt as electrolyte. The sodium-lead alloy could be used directly for tetraethyl lead production. Sodium metal would be recovered by distillation or secondary electrolysis. Caustic soda would be made by blowing steam through the sodium-lead alloy.

Chlorine End Use

The end use pattern of chlorine for 1953 was published in *Chemical and Engineering News*, March 22, 1954, as follows:

Ethylene oxide and glycol	17.0
Pulp and paper	14.2
Carbon tetrachloride	6.8
Trichlorethylene	6.2
Tetraethyl lead fluid	5.6
Monochlorobenzene	5.0
Vinyl chloride	4.4
Direct treatment of water and sewage	4.0
Perchloroethylene	3.8
Propylene glycol	2.3
All other consumers	30.7
	100.0

During 1954 certain chlorinated solvents, plastics (vinyl chloride), and propellants (for aerosol bombs) made gains, while pesticides and herbicides (2-4D, 2-4-5T, etc.) and automotive fluids dropped slightly. Other uses remained about the same.

Literature

Three articles of interest to the chlor-alkali industry were published during 1954 in the *JOURNAL OF THE ELECTRO-CHEMICAL SOCIETY*:

"Diaphragm Type Amalgam Caustic-Chlorine Cell" by Chas. Potter and A. L. Bisio, p. 158.

"The pH in Chlorine-Caustic Electrolysis by the Mercury Cell Process" by Lars Barr, p. 497.

"Explosive Limits of Hydrogen-Chlorine Mixtures" by A. W. Umland, p. 626.

An excellent chapter on chlor-alkali technology was written by Dr. Karl Hass in Ullmanns "Encyklopädie der technischen Chemie," Urban and Schwarzenberg, München-Berlin (1954).

⁵ Field Intelligence Agency Technical Report No. 830.



The Lithium Industry

P. E. Landolt¹

In recent years many articles have been published on lithium, so that reference to the literature will serve to acquaint those interested with the progress made in lithium technology and to justify the designation "Industry."

While the element lithium was discovered in 1807 by Arfvedsen in Sweden, little was done with it for nearly fifty years when Bunsen, Matthiesen, and others produced this element in metallic form. As early as 1817, Sir Humphrey Davy isolated a minute amount of metallic lithium.

With the advent of World War I, the Germans used lithium as a substitute material in lead bearings, "B-Metal," and in a light, strong aluminum alloy, "Scleron." In World War II lithium hydride was used principally as a source of hydrogen for air-borne sea-rescue work. After World War II interest in lithium and its compounds increased and a diverse number of uses followed: e.g., ceramics, pharmaceuticals, low temperature greases, air conditioning, metallurgical uses including fluxes for brazing and welding, alkaline storage batteries, etc.

Within the past few years, recognition of the stability of lithium hydride and of lithium isotope 6 as a source of tritium has made the element important in nuclear developments.

Growth of the Industry in the United States

Prior to World War II there was one principal producer of lithium products, Maywood Chemical Works, owning a rich source of raw materials in South Dakota and a chemical plant with a capacity of approximately 1,000,000 lb lithium carbonate per annum from which its various lithium products were made, including lithium metal.

During World War II, additional facilities were developed, increasing the over-all U. S. capacity to 4,000,000 lb lithium carbonate per annum. Prior to and during the war, American Potash and Chemical Corporation produced a by-product, lithium sodium phosphate, containing the equivalent of 1,000,000–1,500,000 lb per annum of lithium carbonate which was sold to Maywood Chemical Works and Foote Mineral Company. Immediately following the war, consumption of lithium products was reduced to the prewar figure of approximately 400,000–500,000 lb per annum (as carbonate).

This consumption steadily increased until it reached a figure of approximately 5,000,000 lb in 1954, with American Potash producing and selling its own lithium carbonate.

During 1954 Foote opened up and operated mining facilities at Kings Mountain, North Carolina, acquired from Solvay Division, Allied Chemical & Dye Corporation, and a new large chemical plant at Sunbright, Virginia.

Also during the past year, Lithium Corporation of America, in addition to its plant at St. Louis Park, Minnesota, completed a large plant adjacent to mining facilities at Bessemer City, North Carolina.

American Potash is now building a large plant at San Antonio, Texas, using raw materials from Northern Rhodesia.

Therefore, by the end of 1955, or certainly in 1956, there

will be a total production capacity in the States of nearly 50,000,000 lb lithium carbonate or its equivalent per annum.

In 1955, it is expected that the consumption of lithium products will be of the order 12,000,000–15,000,000 lb (as carbonate), possibly more (see below).

The rest of the world, so far as it can be estimated, consumes less than 25% of this amount.

Raw Materials

Lithium occurs primarily in nature as complex aluminum silicates: spodumene $\text{LiAl}(\text{SiO}_3)_2$, lepidolite (a lithia mica), and petalite, a modified spodumene. It also occurs in lesser quantities as a fluophosphate, amblygonite LiAlFPO_4 . It is also recovered from desert brines as a lithium sodium phosphate (20–22% Li_2O). The greatest quantities of lithium are recovered from spodumene.

Major Processes of Recovery

There are three principal methods practiced.

1. *Base exchange with alkali.*—This method was developed largely by Wadman² and von Girsowald.³ In these methods ground spodumene or lepidolite is mixed with potassium sulfate or bisulfate (1:1) and heated to a high temperature (close to the fusion point). The mix is then cooled and leached to extract lithium sulfate and the excess potassium sulfate. This method is relatively expensive, being a batch operation and requiring potassium carbonate to precipitate lithium carbonate.

Similar methods using sodium sulfate have been suggested, but they are comparatively complicated and expensive.

2. *Roasting with lime.*—Spodumene concentrates mixed with CaO or CaCO_3 (1:2) are heated nearly to the fusion point. This reaction produces, after leaching, a solution of lithium hydroxide. Such methods are particularly attractive where lithium hydroxide is the desired end product. However, due to the limited solubility of lithium hydroxide, over-all recoveries of lithium are only fair.

A modification of this method was developed by Fraas and Ralston⁴ in which a mix was prepared for portland cement manufacture, with lithium silicate minerals substituted for clay or shale, and to which CaCl_2 was added to convert and volatilize lithium as chloride.

This necessitated the simultaneous production of good cement clinker, free of alkali, and recovered the lithium as an impure chloride, very difficult to purify. It required operations of a magnitude great enough to produce cement competitively (at least 1000 bbl/24 hr). About 20% of the mix would be spodumene concentrates. It was never carried out on a commercial scale.

3. *Roasting with sulfuric acid.*—This process was developed by Ellestad and Leute.⁵ Spodumene concentrates are first decrepitated at approximately 1100°C to convert alpha- to beta-spodumene. The material is then ground and mixed with

² U. S. Pat. 847,856 (1906).

³ U. S. Pat. 1,710,155 (1929).

⁴ U. S. Bureau of Mines RI 3344 (1937).

⁵ U. S. Pat. 2,516,109 (1950).

¹ Consulting Engineer, 36 West 44th Street, New York, N. Y.

H₂SO₄ (66°B) and heated to about 250°C. The material is then leached to extract lithium sulfate, which is then purified and treated with soda ash to precipitate and remove lithium carbonate.⁶

This method is being applied to the treatment of spodumene concentrates (4–6% Li₂O) and to mined ore (1–1.5% Li₂O).

Production of Lithium Metal (Electrolytic)

The starting materials for electrolysis are lithium chloride and potassium chloride. Various types of cells have been tried, but, in present practice, the type of cell developed for magnesium electrolysis is best adapted.

The cell is heated externally by gas or oil and the salt mixture (approximately a eutectic mixture) is fused. The anodes are graphite and the cathodes steel. Current is applied and molten lithium metal is formed, rising to the surface of the bath and collecting in an adjacent reservoir from which it is removed and cast in ingots, approximately 8.75 cm in diameter x 15 cm long (3.5 in. x 6 in.), weighing about 450 g (1 lb).

Chlorine forms at the anode and is vented from the cell and recovered. Five pounds of chlorine are produced for each pound of metallic lithium made. The bath temperature is approximately 550°C. About 20–22 kwh of electrical energy are required for each pound of lithium produced. Voltage required in the cell is 6–10 v. Multiple cells can be operated, reducing labor costs to a minimum.

Lithium Hydride Production

Lithium hydride is produced by introducing dry hydrogen into an autoclave (electrically heated) in which metallic lithium is placed. The reaction is carried on just above the melting point of the hydride, 630°C. Lithium hydride is a salt-like material, which when fused and electrolyzed releases hydrogen at the anode. Yields are close to theoretical values.

Lithium amide (LiNH₂) may be produced from lithium metal or lithium hydride, introducing ammonia into the reaction chamber held at a suitable temperature to produce the amide. Yields are close to theoretical values.

Research Outline for Lithium

One of the interesting factors in lithium developments is the large number of uses to which it may be put. These uses may be summarized as follows: ceramics; air conditioning; brazing and welding fluxes; all purpose lubricating greases; catalysis; metal refining and foundry operations; alloys; organic synthesis; pharmaceuticals; alkaline storage batteries; heat transfer; and nuclear phenomena.

This diverse use suggests possibilities of extended research in many of these fields. In fact, intensive research work is being carried on at present in many of these fields. Fundamental research on the properties of metallic lithium is also important, e.g., specific heats, conductivity, coefficient of expansion, etc.

Unique Properties of Lithium

Lithium has become important largely because of its unique properties. As an alkali element, it generally conforms to the expected properties of its group. However, it exhibits many properties that would appear to be more in common with the elements of the alkaline earth group; for example: lithium fluoride—insoluble in water; lithium carbonate—slightly soluble in water; lithium phosphate—insoluble in water;

lithium hydroxide monohydrate—solubility 22 g in 100 g H₂O; lithium stearate—insoluble in water.

Lithium metal is extremely reactive: it combines with nitrogen, hydrogen, oxygen, sulfur, and several other elements.

Lithium and its ion are of especial interest to the electrochemist. The standard electrode potential (–3.02 v) is higher than that of any other metal, with the possible exception of cesium. In water the ion has exceptionally low mobility, in

TABLE I. Consumption of lithium products (exact breakdown not available)

	Annual demand in the U. S. (as equiv. Li ₂ CO ₃)		Req'd raw material as 5% Li ₂ O concen- trates (65% recovery)
	lb		tons
Prior to World War II	Min.	400,000	2,500
	Max.	750,000	4,700
World War II	Min.	2,000,000	12,500
	Max.	3,000,000	18,750
Postwar 1946–1950	Avg.	1,100,000	6,875
Expected demand—1955 1956–1960	In excess	10,000,000	62,500
	In excess	30,000,000	187,500

TABLE II. Growth of lithium metal consumption

Prior to 1914	Experimental lots for research purposes
World production 1914–1942	Less than 5,000 lb/annum
U. S. 1942–1946	Less than 100,000 lb/annum
U. S. 1947–1952	Less than 30,000 lb/annum
U. S. 1955	Over 100,000 lb/annum
Potential demand	1,000,000± lb/annum

TABLE III. Growth of industry capacity in the U.S. (as equiv. Li₂CO₃), in lb

	1946	1954	1955	1956 Estimated
Lithium Corp. of America	3,000,000	3,000,000	12–15,000,000	20,000,000
Maywood Chemical Works	1,000,000 app.	1,000,000+	1,000,000	1,000,000
American Potash & Chemical Corp. est.	1,250,000	1,500,000	1,800,000	10,000,000
(jointly to Maywood and Foote Mineral Co.)				
Foote Mineral Co. est.	1,000,000±	6,000,000	12–15,000,000	15,000,000
Total	5,000,000 app.	11,500,000	30,000,000	46,000,000

TABLE IV. Consumption by use

	1951 (as equiv. carbonate)		Est. 1955	
	000 lb	%	000 lb	%
Lubricating greases.....	816	27	3,300	39
Ceramics.....	779	26	1,600	19
Welding and brazing.....	287	9	1,100	13
Air conditioning.....	320	11	1,100	13
Alkaline storage.....	393	13	610	7
Pharmaceuticals.....	33	1	30	—
Defense and miscellaneous.....	393	13	760	9
	3,021	100	8,500	100

(Chem. Week, Nov. 8, 1952).

The 1955 consumption may be of the order of 20,000,000 lb Li₂CO₃ or its equivalent.

⁶ See *Ind. Eng. Chem.*, **43**, 2636 (1951).

molten salts exceptionally high mobility. Lithium salts are used to lower the melting point and increase the fluidity of molten mixtures. The salts such as carbonate and chloride are quite stable at high temperatures.

Lithium has two isotopes in nature with mass numbers of 6 and 7 (approximate ratio 1 to 10). Radioactive Li^8 has a very short half-life. Lithium 6 is an interesting source of tritium (H^3), which is produced by slow neutron irradiation:



Economics of Lithium

Production Statistics

Figures represented by the U. S. Bureau of Mines are presented on mined material. Some portion of such raw material, particularly lepidolite and petalite, is used directly in special glass manufacture. Tables I, II, III, and IV give information on consumption of lithium and growth of the industry.

Cost of Lithium Metal

The prime factor in the cost of lithium metal is in the raw material converted to useful salts. Therefore, if the cost of mineral concentrates necessary to ultimately produce lithium metal is known, it can be equated to the cost of metal as follows:

Raw material cost per unit Li_2O	Raw material cost/lb Li
@ \$4.50	0.50
6.00	0.75
8.00	1.00
10.00	1.25
12.00	1.50

To this must be added the chemical extraction cost and the cost of producing lithium chloride. To these costs must be added labor, power, and maintenance for the production of metal, and depreciation, overhead, and profit. The price of the metal will be of the order of 10–15 times the raw material cost, depending on the output of metal produced.

Capital costs including working capital will be in the range

of \$5.00 to \$8.00 per pound per annum production, including all operations from chemical extraction of the ore to metal.

SELECTED BIBLIOGRAPHY

- P. ASSMANN, *Z. Metallkunde*, **18**, 256 (1926); *C. A.*, **20**, 1585, 3424 (1926).
- A. BURCKHARDT, AND G. SACHS, *Metallwirtschaft*, **11**, 239 (1932).
- G. H. CHAMBERS, AND E. G. ENCK, *Footprints*, **7**, No. 1, 1 (June 1934); *Chem. Ind.*, **34**, 405 (1934).
- D. K. CRAMPTON, *Trans. Am. Inst. Mining Met. Engrs.*, **104**, 164 (1933).
- J. CZOCHRALSKI AND G. WELTER, U. S. Pat. 1,620,081 and 1,620,082.
- W. FRANKENBURGER, *Z. Elektrochem.*, **32**, 481 (1926).
- C. VON GIRSEWALD AND H. WEIDMANN, German Pat. 413,721, U. S. Pat. 1,515,001.
- J. A. HEDVAL, *Z. Elektrochem.*, **36**, 853 (1930).
- F. HESS, U. S. Bureau of Mines R. I. 3040 (1938).
- E. KOCH, U. S. Pat. 1,926,545.
- W. KROLL, German Pat. 537,716.
- P. E. LANDOLT, *Mining Eng.*, **3**, 1045 (1951).
- P. E. LANDOLT AND F. R. PYNE, *Foundry*, **77**, 90 (1949).
- P. E. LANDOLT, "Rare Metals Handbook," C. A. Hampel, Editor, Chap. 1, Reinhold Publishing Corp., New York (1954).
- K. M. LEUTE AND R. S. ELLESTAD, U. S. Pat. 2,516,109.
- P. D. FROST, J. H. JACKSON, A. C. LOONAM, AND C. H. LORIG, *J. Metals*, **188**, 1171 (1950).
- G. MASING AND G. TAMMANN, *Z. anorg. u. allgem. Chem.*, **67**, 183 (1910).
- G. MASING AND C. HASSE, *Wiss. Veröffentl.-Siemens-Korzern*, **7**, 321 (1928).
- Metalloy Corp., Div. Lithium Corp. of America, Inc., Bibliography—Organo-lithium Compounds (1950), (1951), (1953).
- H. MOISSAN, *Compt. rend.*, **135**, 652 (1902).
- H. OSBORG, *Trans. Electrochem Soc.*, **66**, 91 (1934).
- O. C. RALSTON AND F. FRAAS, U. S. Bureau of Mines R. I. 3344 (1937).
- E. E. SCHUMACHER, W. C. ELLIS, AND J. F. ECKEL, Bell Telephone System, Tech. Publ. B. 515, Oct. 1930.
- W. C. SMITH, U. S. Pat. 1,812,992; 1,812,993; 1,923,955.
- P. F. WINTERITZ, U. S. Pat. 2,488,485.
- A. L. DE SY, *Am. Foundryman*, **15**, 60 (1949); **15**, 838 (1949).
- O. SMALLEY, *Iron Age*, **164**, 68 (1949).